

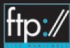


ANALYSIS OF
**MULTICONDUCTOR
TRANSMISSION LINES**

SECOND EDITION



CLAYTON R. PAUL



ANALYSIS OF MULTICONDUCTOR TRANSMISSION LINES

Second Edition

CLAYTON R. PAUL

Professor of Electrical and Computer Engineering
Mercer University
Macon, GA 31207

and

Emeritus Professor of Electrical Engineering
University of Kentucky
Lexington, KY 40506



IEEE PRESS



WILEY-INTERSCIENCE
A JOHN WILEY & SONS, INC., PUBLICATION

Copyright © 2008 by John Wiley & Sons, Inc. All rights reserved

Published by John Wiley & Sons, Inc., Hoboken, New Jersey
Published simultaneously in Canada

No part of this publication may be reproduced, stored in a retrieval system, or transmitted in any form or by any means, electronic, mechanical, photocopying, recording, scanning, or otherwise, except as permitted under Section 107 or 108 of the 1976 United States Copyright Act, without either the prior written permission of the Publisher, or authorization through payment of the appropriate per-copy fee to the Copyright Clearance Center, Inc., 222 Rosewood Drive, Danvers, MA 01923, (978) 750-8400, fax (978) 750-4470, or on the web at www.copyright.com. Requests to the Publisher for permission should be addressed to the Permissions Department, John Wiley & Sons, Inc., 111 River Street, Hoboken, NJ 07030, (201) 748-6011, fax (201) 748-6008, or online at <http://www.wiley.com/go/permission>.

Limit of Liability/Disclaimer of Warranty: While the publisher and author have used their best efforts in preparing this book, they make no representations or warranties with respect to the accuracy or completeness of the contents of this book and specifically disclaim any implied warranties of merchantability or fitness for a particular purpose. No warranty may be created or extended by sales representatives or written sales materials. The advice and strategies contained herein may not be suitable for your situation. You should consult with a professional where appropriate. Neither the publisher nor author shall be liable for any loss of profit or any other commercial damages, including but not limited to special, incidental, consequential, or other damages.

For general information on our other products and services or for technical support, please contact our Customer Care Department within the United States at (800) 762-2974, outside the United States at (317) 572-3993 or fax (317) 572-4002.

Wiley also publishes its books in a variety of electronic formats. Some content that appears in print may not be available in electronic formats. For more information about Wiley products, visit our web site at <http://www.wiley.com>.

Library of Congress Cataloging-in-Publication Data

Paul, Clayton R.

Analysis of multiconductor transmission lines / by Clayton R. Paul. – 2nd ed.
p. cm.

ISBN 978-0-470-13154-1 (cloth)

1. Multiconductor transmission lines. 2. Electric circuit analysis—Data processing. I. Title.

TK7872.T74P38 2008

621.319'2—dc22

2007013722

Printed in the United States of America

10 9 8 7 6 5 4 3 2 1

This textbook is dedicated to the humane and compassionate treatment of animals

A man is truly ethical only when he obeys the compulsion to help all life which he is able to assist, and shrinks from injuring anything that lives.

Albert Schweitzer

It ill becomes us to invoke in our daily prayers the blessings of God, the compassionate, if we in turn will not practice elementary compassion towards our fellow creatures.

Gandhi

We can judge the heart of man by his treatment of animals.

Immanuel Kant

CONTENTS

| | |
|--|-------------|
| Preface | xvii |
| 1 Introduction | 1 |
| 1.1 Examples of Multiconductor Transmission-Line Structures | 5 |
| 1.2 Properties of the TEM Mode of Propagation | 8 |
| 1.3 The Transmission-Line Equations: A Preview | 18 |
| 1.3.1 Unique Definition of Voltage and Current for the TEM Mode of Propagation | 19 |
| 1.3.2 Defining the Per-Unit-Length Parameters | 22 |
| 1.3.3 Obtaining the Transmission-Line Equations from the Transverse Electromagnetic Field Equations | 28 |
| 1.3.4 Properties of the Per-Unit-Length Parameters | 30 |
| 1.4 Classification of Transmission Lines | 32 |
| 1.4.1 Uniform versus Nonuniform Lines | 33 |
| 1.4.2 Homogeneous versus Inhomogeneous Surrounding Media | 35 |
| 1.4.3 Lossless versus Lossy Lines | 36 |
| 1.5 Restrictions on the Applicability of the Transmission-Line Equation Formulation | 37 |
| 1.5.1 Higher Order Modes | 38 |
| 1.5.1.1 The Infinite, Parallel-Plate Transmission Line | 38 |
| | vii |

| | | |
|----------|---|------------|
| 1.5.1.2 | The Coaxial Transmission Line | 43 |
| 1.5.1.3 | Two-Wire Lines | 44 |
| 1.5.2 | Transmission-Line Currents versus Antenna Currents | 45 |
| 1.6 | The Time Domain versus the Frequency Domain | 47 |
| 1.6.1 | The Fourier Series and Transform | 50 |
| 1.6.2 | Spectra and Bandwidth of Digital Waveforms | 52 |
| 1.6.3 | Computing the Time-Domain Response of Transmission Lines Having Linear Terminations Using Fourier Methods and Superposition | 56 |
| | Problems | 61 |
| | References | 69 |
| 2 | The Transmission-Line Equations for Two-Conductor Lines | 71 |
| 2.1 | Derivation of the Transmission-Line Equations from the Integral Form of Maxwell's Equations | 71 |
| 2.2 | Derivation of the Transmission-Line Equations from the Per-Unit-Length Equivalent Circuit | 77 |
| 2.3 | Properties of the Per-Unit-Length Parameters | 78 |
| 2.4 | Incorporating Frequency-Dependent Losses | 79 |
| 2.4.1 | Properties of the Frequency-Domain Per-Unit-Length Impedance $\hat{z}(\omega)$ and Admittance $\hat{y}(\omega)$ | 81 |
| | Problems | 85 |
| | References | 88 |
| 3 | The Transmission-Line Equations for Multiconductor Lines | 89 |
| 3.1 | Derivation of the Multiconductor Transmission-Line Equations from the Integral Form of Maxwell's Equations | 89 |
| 3.2 | Derivation of the Multiconductor Transmission-Line Equations from the Per-Unit-Length Equivalent Circuit | 99 |
| 3.3 | Summary of the MTL Equations | 101 |
| 3.4 | Incorporating Frequency-Dependent Losses | 102 |
| 3.5 | Properties of the Per-Unit-Length Parameter Matrices \mathbf{L} , \mathbf{C} , \mathbf{G} | 103 |
| | Problems | 108 |
| | References | 109 |
| 4 | The Per-Unit-Length Parameters for Two-Conductor Lines | 110 |
| 4.1 | Definitions of the Per-Unit-Length Parameters l , c , and g | 111 |

| | | |
|----------|--|------------|
| 4.2 | Lines Having Conductors of Circular, Cylindrical Cross Section (Wires) | 113 |
| 4.2.1 | Fundamental Subproblems for Wires | 113 |
| 4.2.1.1 | The Method of Images | 118 |
| 4.2.2 | Per-Unit-Length Inductance and Capacitance for Wire-Type Lines | 119 |
| 4.2.3 | Per-Unit-Length Conductance and Resistance for Wire-Type Lines | 130 |
| 4.3 | Lines Having Conductors of Rectangular Cross Section (PCB Lands) | 144 |
| 4.3.1 | Per-Unit-Length Inductance and Capacitance for PCB-Type Lines | 145 |
| 4.3.2 | Per-Unit-Length Conductance and Resistance for PCB-Type Lines | 148 |
| | Problems | 156 |
| | References | 158 |
| 5 | The Per-Unit-Length Parameters for Multiconductor Lines | 160 |
| 5.1 | Definitions of the Per-Unit-Length Parameter Matrices L , C , and G | 161 |
| 5.1.1 | The Generalized Capacitance Matrix \mathcal{C} | 167 |
| 5.2 | Multiconductor Lines Having Conductors of Circular, Cylindrical Cross Section (Wires) | 171 |
| 5.2.1 | Wide-Separation Approximations for Wires in Homogeneous Media | 171 |
| 5.2.1.1 | $n + 1$ Wires | 173 |
| 5.2.1.2 | n Wires Above an Infinite, Perfectly Conducting Plane | 173 |
| 5.2.1.3 | n Wires Within a Perfectly Conducting Cylindrical Shield | 174 |
| 5.2.2 | Numerical Methods for the General Case | 176 |
| 5.2.2.1 | Applications to Inhomogeneous Dielectric Media | 181 |
| 5.2.3 | Computed Results: Ribbon Cables | 187 |
| 5.3 | Multiconductor Lines Having Conductors of Rectangular Cross Section | 189 |
| 5.3.1 | Method of Moments (MoM) Techniques | 190 |
| 5.3.1.1 | Applications to Printed Circuit Boards | 199 |
| 5.3.1.2 | Applications to Coupled Microstrip Lines | 211 |
| 5.3.1.3 | Applications to Coupled Striplines | 219 |

| | | |
|----------|--|------------|
| 5.4 | Finite Difference Techniques | 223 |
| 5.5 | Finite-Element Techniques | 229 |
| | Problems | 237 |
| | References | 239 |
| 6 | Frequency-Domain Analysis of Two-Conductor Lines | 240 |
| 6.1 | The Transmission-Line Equations in the Frequency Domain | 241 |
| 6.2 | The General Solution for Lossless Lines | 242 |
| 6.2.1 | The Reflection Coefficient and Input Impedance | 244 |
| 6.2.2 | Solutions for the Terminal Voltages and Currents | 247 |
| 6.2.3 | The SPICE (PSPICE) Solution for Lossless Lines | 250 |
| 6.2.4 | Voltage and Current as a Function of Position on the Line | 252 |
| 6.2.5 | Matching and VSWR | 255 |
| 6.2.6 | Power Flow on a Lossless Line | 256 |
| 6.3 | The General Solution for Lossy Lines | 258 |
| 6.3.1 | The Low-Loss Approximation | 260 |
| 6.4 | Lumped-Circuit Approximate Models of the Line | 265 |
| 6.5 | Alternative Two-Port Representations of the Line | 269 |
| 6.5.1 | The Chain Parameters | 270 |
| 6.5.2 | Approximating Abruptly Nonuniform Lines with the Chain-Parameter Matrix | 273 |
| 6.5.3 | The Z and Y Parameters | 275 |
| | Problems | 278 |
| 7 | Frequency-Domain Analysis of Multiconductor Lines | 282 |
| 7.1 | The MTL Transmission-Line Equations in the Frequency Domain | 282 |
| 7.2 | The General Solution for An $(n + 1)$ -Conductor Line | 284 |
| 7.2.1 | Decoupling the MTL Equations by Similarity Transformations | 284 |
| 7.2.2 | Solution for Line Categories | 291 |
| 7.2.2.1 | Perfect Conductors in Lossy, Homogeneous Media | 292 |
| 7.2.2.2 | Lossy Conductors in Lossy, Homogeneous Media | 293 |
| 7.2.2.3 | Perfect Conductors in Lossless, Inhomogeneous Media | 296 |
| 7.2.2.4 | The General Case: Lossy Conductors in Lossy, Inhomogeneous Media | 298 |
| 7.2.2.5 | Cyclic-Symmetric Structures | 298 |

| | | |
|----------|---|------------|
| 7.3 | Incorporating the Terminal Conditions | 305 |
| 7.3.1 | The Generalized Thevenin Equivalent | 305 |
| 7.3.2 | The Generalized Norton Equivalent | 308 |
| 7.3.3 | Mixed Representations | 310 |
| 7.4 | Lumped-Circuit Approximate Characterizations | 312 |
| 7.5 | Alternative $2n$ -Port Characterizations | 314 |
| 7.5.1 | Analogy of the Frequency-Domain MTL Equations to State-Variable Equations | 314 |
| 7.5.2 | Characterizing the Line as a $2n$ -Port with the Chain-Parameter Matrix | 316 |
| 7.5.3 | Properties of the Chain-Parameter Matrix | 318 |
| 7.5.4 | Approximating Nonuniform Lines with the Chain-Parameter Matrix | 322 |
| 7.5.5 | The Impedance and Admittance Parameter Matrix Characterizations | 323 |
| 7.6 | Power Flow and the Reflection Coefficient Matrix | 327 |
| 7.7 | Computed and Experimental Results | 332 |
| 7.7.1 | Ribbon Cables | 332 |
| 7.7.2 | Printed Circuit Boards | 335 |
| | Problems | 338 |
| | References | 342 |
| 8 | Time-Domain Analysis of Two-Conductor Lines | 343 |
| 8.1 | The Solution for Lossless Lines | 344 |
| 8.1.1 | Wave Tracing and the Reflection Coefficients | 346 |
| 8.1.2 | Series Solutions and the Difference Operator | 356 |
| 8.1.3 | The Method of Characteristics and a Two-Port Model of the Line | 361 |
| 8.1.4 | The SPICE (PSPICE) Solution for Lossless Lines | 365 |
| 8.1.5 | The Laplace Transform Solution | 368 |
| 8.1.5.1 | Lines with Capacitive and Inductive Loads | 370 |
| 8.1.6 | Lumped-Circuit Approximate Models of the Line | 373 |
| 8.1.6.1 | When is the Line Electrically Short in the Time Domain? | 374 |
| 8.1.7 | The Time-Domain to Frequency-Domain (TDFD) Transformation Method | 375 |
| 8.1.8 | The Finite-Difference, Time-Domain (FDTD) Method | 379 |
| 8.1.8.1 | The Magic Time Step | 385 |

| | | |
|----------|--|------------|
| 8.1.9 | Matching for Signal Integrity | 392 |
| 8.1.9.1 | When is Matching Required? | 398 |
| 8.1.9.2 | Effects of Line Discontinuities | 399 |
| 8.2 | Incorporation of Losses | 406 |
| 8.2.1 | Representing Frequency-Dependent Losses | 408 |
| 8.2.1.1 | Representing Losses in the Medium | 408 |
| 8.2.1.2 | Representing Losses in the Conductors and Skin Effect | 410 |
| 8.2.1.3 | Convolution with Frequency-Dependent Losses | 415 |
| 8.2.2 | The Time-Domain to Frequency-Domain (TDFD) Transformation Method | 421 |
| 8.2.3 | The Finite-Difference, Time-Domain (FDTD) Method | 423 |
| 8.2.3.1 | Including Frequency-Independent Losses | 423 |
| 8.2.3.2 | Including Frequency-Dependent Losses | 427 |
| 8.2.3.3 | Prony's Method for Representing a Function | 431 |
| 8.2.3.4 | Recursive Convolution | 434 |
| 8.2.3.5 | An Example: A High-Loss Line | 439 |
| 8.2.3.6 | A Correction for the FDTD Errors | 443 |
| 8.2.4 | Lumped-Circuit Approximate Characterizations | 447 |
| 8.2.5 | The Use of Macromodels in Modeling the Line | 450 |
| 8.2.6 | Representing Frequency-Dependent Functions in the Time Domain Using Pade Methods | 453 |
| | Problems | 461 |
| | References | 467 |
| 9 | Time-Domain Analysis of Multiconductor Lines | 470 |
| 9.1 | The Solution for Lossless Lines | 470 |
| 9.1.1 | The Recursive Solution for MTLs | 471 |
| 9.1.2 | Decoupling the MTL Equations | 476 |
| 9.1.2.1 | Lossless Lines in Homogeneous Media | 478 |
| 9.1.2.2 | Lossless Lines in Inhomogeneous Media | 479 |
| 9.1.2.3 | Incorporating the Terminal Conditions via the SPICE Program | 482 |
| 9.1.3 | Lumped-Circuit Approximate Characterizations | 487 |
| 9.1.4 | The Time-Domain to Frequency-Domain (TDFD) Transformation Method | 488 |
| 9.1.5 | The Finite-Difference, Time-Domain (FDTD) Method | 488 |
| 9.1.5.1 | Including Dynamic and/or Nonlinear Terminations in the FDTD Analysis | 490 |
| 9.2 | Incorporation of Losses | 496 |
| 9.2.1 | The Time-Domain to Frequency-Domain (TDFD) Method | 498 |

| | | |
|-----------|--|------------|
| 9.2.2 | Lumped-Circuit Approximate Characterizations | 498 |
| 9.2.3 | The Finite-Difference, Time-Domain (FDTD) Method | 499 |
| 9.2.4 | Representation of the Lossy MTL with the Generalized Method of Characteristics | 501 |
| 9.2.5 | Model Order Reduction (MOR) Methods | 512 |
| 9.2.5.1 | Pade Approximation of the Matrix Exponential | 512 |
| 9.2.5.2 | Asymptotic Waveform Evaluation (AWE) | 515 |
| 9.2.5.3 | Complex Frequency Hopping (CFH) | 518 |
| 9.2.5.4 | Vector Fitting | 518 |
| 9.3 | Computed and Experimental Results | 524 |
| 9.3.1 | Ribbon Cables | 526 |
| 9.3.2 | Printed Circuit Boards | 530 |
| | Problems | 537 |
| | References | 541 |
| 10 | Literal (Symbolic) Solutions for Three-Conductor Lines | 544 |
| 10.1 | The Literal Frequency-Domain Solution for a Homogeneous Medium | 548 |
| 10.1.1 | Inductive and Capacitive Coupling | 554 |
| 10.1.2 | Common-Impedance Coupling | 556 |
| 10.2 | The Literal Time-Domain Solution for a Homogeneous Medium | 558 |
| 10.2.1 | Explicit Solution | 560 |
| 10.2.2 | Weakly Coupled Lines | 562 |
| 10.2.3 | Inductive and Capacitive Coupling | 564 |
| 10.2.4 | Common-Impedance Coupling | 567 |
| 10.3 | Computed and Experimental Results | 567 |
| 10.3.1 | A Three-Wire Ribbon Cable | 568 |
| 10.3.2 | A Three-Conductor Printed Circuit Board | 569 |
| | Problems | 575 |
| | References | 576 |
| 11 | Incident Field Excitation of Two-Conductor Lines | 578 |
| 11.1 | Derivation of the Transmission-Line Equations for Incident Field Excitation | 578 |
| 11.1.1 | Equivalence of Source Representations | 585 |
| 11.2 | The Frequency-Domain Solution | 586 |
| 11.2.1 | Solution of the Transmission-Line Equations | 586 |

| | | |
|-----------|---|------------|
| 11.2.2 | Simplified Forms of the Excitations | 592 |
| 11.2.3 | Incorporating the Line Terminations | 594 |
| 11.2.4 | Uniform Plane-Wave Excitation of the Line | 598 |
| 11.2.4.1 | Special Cases | 602 |
| 11.2.4.2 | One Conductor Above a Ground Plane | 606 |
| 11.2.5 | Comparison with Predictions of Method of Moments Codes | 610 |
| 11.3 | The Time-Domain Solution | 611 |
| 11.3.1 | The Laplace Transform Solution | 611 |
| 11.3.2 | Uniform Plane-Wave Excitation of the Line | 620 |
| 11.3.3 | A SPICE Equivalent Circuit | 625 |
| 11.3.4 | The Time-Domain to Frequency-Domain (TDFD) Transformation | 628 |
| 11.3.5 | The Finite-Difference, Time-Domain (FDTD) Solution Method | 628 |
| 11.3.6 | Computed Results | 635 |
| | Problems | 638 |
| | References | 639 |
| 12 | Incident Field Excitation of Multiconductor Lines | 641 |
| 12.1 | Derivation of the MTL Equations for Incident Field Excitation | 642 |
| 12.1.1 | Equivalence of Source Representations | 648 |
| 12.2 | Frequency-Domain Solutions | 650 |
| 12.2.1 | Solution of the MTL Equations | 651 |
| 12.2.2 | Simplified Forms of the Excitations | 653 |
| 12.2.3 | Incorporating the Line Terminations | 655 |
| 12.2.3.1 | Lossless Lines in Homogeneous Media | 658 |
| 12.2.4 | Lumped-Circuit Approximate Characterizations | 660 |
| 12.2.5 | Uniform Plane-Wave Excitation of the Line | 660 |
| 12.3 | The Time-Domain Solution | 667 |
| 12.3.1 | Decoupling the MTL Equations | 668 |
| 12.3.2 | A SPICE Equivalent Circuit | 674 |
| 12.3.3 | Lumped-Circuit Approximate Characterizations | 681 |
| 12.3.4 | The Time-Domain to Frequency-Domain (TDFD) Transformation | 681 |
| 12.3.5 | The Finite-Difference, Time-Domain (FDTD) Solution Method | 682 |

| | |
|--|------------|
| 12.4 Computed Results | 686 |
| Problems | 691 |
| References | 692 |
| 13 Transmission-Line Networks | 693 |
| 13.1 Representation of Lossless Lines with the SPICE Model | 696 |
| 13.2 Representation with Lumped-Circuit Approximate Models | 699 |
| 13.3 Representation via the Admittance or Impedance $2n$ -Port Parameters | 699 |
| 13.4 Representation with the BLT Equations | 712 |
| 13.5 Direct Time-Domain Solutions in Terms of Traveling Waves | 721 |
| 13.6 A Summary of Methods for Analyzing Multiconductor Transmission Lines | 726 |
| Problems | 727 |
| References | 728 |
| Publications by the Author Concerning Transmission Lines | 729 |
| Appendix A. Description of Computer Software | 736 |
| A.1 Programs for the Calculation of the Per-Unit-Length Parameters | 738 |
| A.1.1 Wide-Separation Approximations for Wires: WIDSEPP . FOR | 738 |
| A.1.2 Ribbon Cables: RIBBON . FOR | 740 |
| A.1.3 Printed Circuit Boards: PCB . FOR | 743 |
| A.1.4 Coupled Microstrip Structures: MSTRP . FOR | 745 |
| A.1.5 Coupled Stripline Structures: STRPLINE . FOR | 746 |
| A.2 Frequency-Domain Analysis | 747 |
| A.2.1 General: MTL . FOR | 747 |
| A.3 Time-Domain Analysis | 748 |
| A.3.1 Time-Domain to Frequency-Domain Transformation: TIMEFREQ . FOR | 748 |
| A.3.2 Branin's Method Extended to Multiconductor Lines: BRANIN . FOR | 748 |
| A.3.3 Finite Difference-Time Domain Method: FINDIF . FOR | 749 |
| A.3.4 Finite-Difference-Time-Domain Method: FDTDLOSS . FOR | 749 |

| | | |
|--|--|----------------|
| A.4 | SPICE/PSPICE Subcircuit Generation Programs | 749 |
| A.4.1 | General Solution, Lossless Lines: SPICEMTL.FOR | 750 |
| A.4.2 | Lumped-Pi Circuit, Lossless Lines: SPICELPI.FOR | 750 |
| A.4.3 | Inductive-Capacitive Coupling Model: SPICELC.FOR | 751 |
| A.5 | Incident Field Excitation | 752 |
| A.5.1 | Frequency-Domain Program: INCIDENT.FOR | 752 |
| A.5.2 | SPICE/PSPICE Subcircuit Model: SPICEINC.FOR | 753 |
| A.5.3 | Finite-Difference, Time-Domain (FDTD) Model: FDTDINC.FOR | 754 |
| | References | 755 |
| Appendix B. A SPICE (PSPICE) Tutorial | | 756 |
| B.1 | Creating the SPICE or PSPICE Program | 757 |
| B.2 | Circuit Description | 758 |
| B.3 | Execution Statements | 763 |
| B.4 | Output Statements | 765 |
| B.5 | Examples | 767 |
| B.6 | The Subcircuit Model | 769 |
| | References | 771 |
| | Index | 773 |

PREFACE

This is the second edition of a textbook that is intended for a senior or graduate-level course in an electrical engineering (EE) curriculum on the subject of the analysis of multiconductor transmission lines (MTLs). It will also serve as a useful reference for industry professionals. The term MTL typically refers to a set of $n + 1$ parallel conductors that serve to transmit electrical signals between two or more points, for example, a source and a load. The dominant mode of propagation on an MTL is the transverse electromagnetic (TEM) mode of propagation, where the electric and magnetic fields surrounding the conductors lie solely in the transverse plane orthogonal to the line axis. This structure is capable of guiding waves whose frequencies range from dc to where the line cross-sectional dimensions become a significant fraction of a wavelength. At higher frequencies, higher order modes coexist with the TEM mode, and other guiding structures such as waveguides and antennas are more practical structures for transmitting the signal between a source and a load. There are many applications for this wave-guiding structure. High-voltage power transmission lines are intended to transmit 60-Hz sinusoidal waveforms and the resulting power. In addition to this low-frequency power signal, there may exist other higher frequency components of the transmitted signal such as when a fault occurs on the line or a circuit breaker opens and recloses. The waveforms on the line associated with these events have high-frequency spectral content. Cables in modern electronic systems such as aircraft, ships, and vehicles serve to transmit power as well as signals throughout the system. These cables consist of a large number of individual wires that are packed into bundles for neatness and space conservation. The electromagnetic fields surrounding these closely spaced individual wires interact with each other and induce signals in all the other adjacent circuits. This is unintended and is referred to as *crosstalk*. This crosstalk can cause functional degradation of the circuits at the ends of the cable. The prediction of crosstalk will be one of the major objectives in this text.

There are numerous other similar transmission-line structures. A printed circuit board (PCB) consists of a planar dielectric board on which rectangular cross-section conductors (lands) serve to interconnect digital devices as well as analog devices. Crosstalk can be a significant functional problem with these PCBs as can the degra-

duction of the intended signal transmission through attenuation, time delay, and other effects. Signal degradation, time delay, and crosstalk can create significant functional problems in today's high-speed digital circuits so that it is important to understand and predict this effect. Digital systems constitute the primary type of electronic system today and will no doubt dominate in the future. Clock speeds and data transfer rates are accelerating at an astounding rate. Personal computers today have clock speeds on the order of 3GHz. The spectral content of these high-speed digital waveforms extends well into the lower GHz frequency range. This means that crosstalk as well as unintended radiated emissions are presenting performance problems in digital systems that were unheard of a decade ago. This will no doubt increase in the future. As recent as 15 years ago, many of the signal connection conductors such as wires and PCB lands were electrically short enough at the highest significant frequency of the digital signals that the effect of those interconnection conductors could generally be ignored. Today, most of the PCB lands must be treated as a transmission line, and the matching of those lines is no longer an option in the design of a digital system. Distributed-parameter properties of these conductors can no longer be ignored. Hence, there is a growing need for digital design engineers to be able to understand the concepts and design principles of a transmission line. The objective of this text is to examine various methods for solving the transmission-line equations for multiconductor lines as well as to develop an understanding of the general properties of wave propagation on the lines.

The analysis of transmission lines consisting of two parallel conductors of uniform cross section has traditionally been a fundamental subject in electrical engineering. Prior to the introduction of digital computer engineering topics into the undergraduate EE curricula, all EE undergraduates were required to complete a course on two-conductor transmission lines. However, because of the introduction of computer engineering courses into an already crowded 4-year undergraduate degree program, the transmission-line course(s) in many EE programs has been relegated to a senior technical elective if offered at all. Unfortunately, the increasing use of high-speed digital technology requires that all EEs must have a working knowledge of transmission lines. In addition, the use of MTLs consisting of more than two conductors is becoming more widespread because of the increasing need for high-volume and high-speed data and signal transmission. Signal integrity (the effect of the transmission line on the signal transmission) is becoming a critical aspect of high-speed digital system performance. This text is intended to fill the need for a structured course on transmission lines in an EE program.

This text is the second edition of a previous text concerning the analysis of MTLs. The text has undergone a significant reorganization with the emphasis given toward a university textbook for a senior/graduate textbook on transmission lines. In the first edition the two-conductor and MTL discussions were combined into a single chapter. In this second edition, each broad analysis topic, for example, per-unit-length parameters, frequency-domain analysis, time-domain analysis, and incident field excitation, now has a chapter concerning two-conductor lines followed immediately by a chapter on MTLs for that topic. This allows the instructor to choose his or her emphasis either on two-conductor lines or on MTLs, or on both. This organization also makes

it easier for the reader to understand the analysis of MTLs. The analysis of MTLs is very similar to that of two-conductor lines except that the detail is considerably increased. However, with the aid of matrix symbology and techniques, most of the MTL topics are straightforward extensions of the corresponding two-conductor line topics. Hence, by devoting a separate chapter to each two-conductor line topic and then following that with a chapter on the corresponding MTL topic, the MTL material can be more readily understood.

In addition to this significant reorganization of the material, the text now contains important developments in analysis methods that have been developed in the intervening 13 years since the first edition was published. Digital technology has virtually taken over the field of electronics. The clock and data speeds in those digital systems have accelerated at an astonishing rate, meaning that the spectral content of those signals that are propagating along the interconnect lands now extends into and, in some high-end servers, above the 20-GHz region. This has caused most of the signal interconnects in those systems, which were inconsequential from a standpoint of transmission-line effects 13 years ago, to now become critical to the functionality of those systems. The transmission-line behavior of those interconnects can no longer be ignored. In addition, the number and density of those interconnects have increased dramatically so that the analysis of their effects is now a serious computational problem. Hence, the current emphasis is on the development of macromodels and on “model order reduction” or (MOR) for the time-domain analysis of these high-density interconnects. Generation of macromodels that compactly describe these interconnects from a port standpoint requires the determination of the transfer functions representing those interconnects. Typical distributed-parameter interconnects have an enormous number of poles such that the transfer functions are ratios of very high order polynomials in the Laplace transform variable s . The current analysis methods focus on MOR methods that seek to determine a highly reduced number of dominant poles of those transfer functions, thereby simplifying the analysis. MOR methods such as recursive convolution, complex frequency hopping (CFH), Pade, asymptotic waveform expansion (AWE), and vector fitting (VF) as well as the synthesis of lumped-circuit models are the current methods of choice. Chapters 8 and 9, which cover the time-domain analysis of two-conductor lines and MTLs, respectively, have been considerably expanded to now include those topics among many others that have been developed in the intervening years.

The second edition of this text is now divided into 13 chapters, whereas the first edition only had eight chapters. Considerable thought has gone into the reorganization of the text. The author is of the strong opinion that organization of subject material into a logical and well thought-out form is perhaps the most important pedagogical technique in a reader’s learning process. This logical organization is one of the important attributes of the text. Chapter 1 discusses the background and rationale for the use of MTLs. The general properties of the TEM mode of propagation are discussed, and the transmission-line equations are derived for two-conductor lines using several methods. The various classifications of MTLs (uniform, lossless, and homogeneous medium) are discussed along with the restrictions on the use of the TEM model. An important addition to this chapter has been made in the second edition: the discussion

of the time domain versus the frequency domain. This is a crucial aspect of any EE's ability to design electronic systems. The chapter presents a very useful method for the time-domain analysis of a linear system such as an MTL having linear terminations by computing the frequency-domain transfer function, decomposing the periodic or nonperiodic input signal into its Fourier spectral components, passing those through the system, and recombining in time at the output. This allows a straightforward incorporation of frequency-dependent losses of the conductors and the surrounding medium. These frequency-dependent losses complicate, as we will see, the direct time-domain solution of the transmission-line equations.

Chapter 2 provides a derivation of the two-conductor transmission-line equations along with the general properties of the per-unit-length parameters in those equations. Chapter 3 discusses these topics for MTLs.

Chapter 4 discusses the derivation of the per-unit-length parameters of inductance, capacitance, resistance, and conductance for two-conductor lines, whereas Chapter 5 repeats this for MTLs. In both chapters, numerical methods for the determination of these important per-unit-length parameters are discussed in detail.

Chapter 6 discusses the frequency-domain solution of the transmission-line equations, and Chapter 7 repeats this for MTLs. The discussion of two-conductor transmission lines in Chapter 6 has been expanded considerably over the first edition coverage and now constitutes a traditional undergraduate coverage.

Chapter 8 discusses the time-domain analysis of two-conductor lines, and Chapter 9 repeats this for MTLs. Again, the time-domain solution for two-conductor lines in Chapter 8 is considerably expanded over the first edition coverage and now constitutes a traditional undergraduate coverage. In addition, Chapter 8 now includes an extensive discussion of methods for achieving signal integrity (SI) in high-speed digital interconnects. The finite-difference, time-domain (FDTD) solution method is developed as is the time-domain to frequency-domain transformation (TDFD) method. Both of these allow the inclusion of frequency-dependent losses. Detailed discussions of recursive convolution and MOR techniques such as Pade methods are now included in Chapter 8. Chapter 9 on the time-domain analysis of MTLs now includes extensive discussion of MOR methods such as the generalized method of characteristics, Pade methods, asymptotic waveform expansion, complex frequency hopping, and vector fitting. In addition, Chapter 9 now includes the development of the FDTD method for dynamic terminations.

Chapter 10 gives the symbolic or literal solution of perhaps the only MTL that admits a closed-form solution in terms of symbols: a three-conductor lossless line in a homogeneous medium. This chapter is virtually the same as in the first edition although it has been revised.

Chapter 11 gives the frequency-domain and time-domain solutions for two-conductor lines with incident field illumination. Chapter 12 repeats that for MTLs. The emphasis is on uniform plane-wave excitation as from a distant antenna or a lightning stroke.

Finally, Chapter 13 discusses the analysis of interconnected transmission-line networks such as branched cables. There is not enough difference between the methods for two-conductor lines and MTLs to warrant splitting this chapter into two chapters.

Appendix A contains the descriptions of numerous FORTRAN computer codes that implement all the techniques in this text. Numerous experimental results are included in this text ranging from cables to PCBs in order to illustrate real-world problems. These codes are used to provide the predictions for these experimental results. The codes can be downloaded from the Wiley ftp site at ftp://ftp.wiley.com/public/sci_tech_med/multiconductor_transmission/.

Appendix B is new to this edition and contains a brief but thorough tutorial on the SPICE/PSPICE circuit analysis program.

Many of the author's colleagues have contributed substantially to the advancement of this subject. Professors Antonio Orlandi and Frederick M. Tesche along with the late Albert A. Smith Jr. are among those to whom the author owes a debt of gratitude for many insightful discussions on this subject.

*Clayton R. Paul
Macon, Georgia*

1

INTRODUCTION

This text concerns the analysis of transmission-line structures that serve to guide electromagnetic (EM) waves between two or more points. The analysis of transmission lines consisting of two parallel conductors of uniform cross section has traditionally been a fundamental subject in electrical engineering (EE) [A.1,A.3,A.6]. Prior to the introduction of digital computer engineering topics into the undergraduate EE curricula, all EE undergraduates were required to complete a course on two-conductor transmission lines. However, because of the introduction of computer engineering courses into an already crowded 4-year undergraduate degree program, the transmission-line course in many EE programs has been relegated to a senior technical elective if offered at all. Unfortunately, the increasing use of high-speed digital technology requires that all EE undergraduates must have a working knowledge of transmission lines. In addition, the use of multiconductor transmission lines (MTLs) consisting of more than two conductors is becoming more widespread because of the increasing need for high-volume and high-speed data and signal transmission. Signal integrity, the effect of the transmission line on the signal transmission, is becoming a critical aspect of high-speed digital system performance.

This text is the second edition of a previous text concerning the analysis of MTLs. It has been reorganized with the emphasis given toward a university textbook for a senior/graduate textbook on transmission lines. The text has been reorganized so that each broad analysis topic, for example, per-unit-length parameters, frequency-domain analysis, time-domain analysis, incident field excitation, and transmission-line networks, has a chapter concerning two-conductor lines followed immediately by

a chapter on MTLs for that topic. This allows the instructors to choose their emphasis either on two-conductor lines or on MTLs, or on both. This organization also makes it easier for the reader to understand the analysis of MTLs. The analysis of MTLs is very similar to that of two-conductor lines except that the detail is considerably increased. However, with the aid of matrix symbology and techniques most of the MTL topics are straightforward extensions of the corresponding two-conductor line topics. Hence by devoting a separate chapter to each two-conductor line topic and then following that with a chapter on the corresponding MTL topic, the MTL material can be more readily understood.

The analysis of MTLs is somewhat more difficult than the analysis of two-conductor lines, but the applications cover a broad frequency spectrum and encompass a wide variety of transmission lines ranging from power transmission lines to microwave circuits [B.4, Refs. 1–16]. However, matrix methods and notation provide a straightforward extension of many, if not most, of the aspects of two-conductor lines to MTLs. Many of the concepts and performance measures of two-conductor lines require more elaborate concepts when extended to MTLs. For example, in order to eliminate reflections at terminations on a two-conductor line, we simply terminate it in a matched load, that is, a load resistance that equals the (real) characteristic impedance of the line. In the case of MTLs, we must terminate the line in a *characteristic impedance matrix* or network of resistances in order to eliminate all reflections. It is not sufficient to simply insert a resistance between each conductor and the reference conductor; there must also be resistances between every pair of conductors. In order to describe the degree of mismatch of a particular load impedance on a two-conductor line, we compute a scalar reflection coefficient. In the case of an MTL, we can obtain the analogous quantity, but it becomes a *reflection coefficient matrix*.

On a two-conductor line there is a forward- and a backward-traveling wave each traveling in opposite directions with velocity v . In the case of an MTL consisting of $n + 1$ conductors, there exist n forward- and n backward-traveling waves each with its own velocity. Each pair of forward- and backward-traveling waves is referred to as a *mode*. If the MTL is immersed in a homogeneous medium, each mode velocity is identical to the phase velocity of light in that medium. The mode velocities of an MTL that is immersed in an inhomogeneous medium (such as wires with dielectric insulations or printed circuit boards (PCBs)) will, in general, be different.

The governing transmission-line equations for a two-conductor line will be a coupled set of two first-order partial differential equations for the line voltage $V(z, t)$ and line current $I(z, t)$, where the line conductors are parallel to the z axis and time is denoted as t . In the case of an MTL consisting of $n + 1$ conductors parallel to the z axis, the corresponding governing equations are a coupled set of $2n$ first-order *matrix* partial differential equations relating the n line voltages $V_i(z, t)$ and n line currents $I_i(z, t)$ for $i = 1, 2, \dots, n$. The number of conductors may be quite large, for example, $n + 1 = 100$, in which case efficiency of solution of the $2n$ MTL equations becomes an important consideration. The ease of solution of the MTL equations depends upon the assumptions or approximations one is willing to make about the line, for example, uniform line versus nonuniform line, lossless line versus lossy line, a homogeneous

surrounding medium versus an inhomogeneous surrounding media, and so on, as well as the solution technique chosen. Although it is tempting to dismiss the analysis of MTLs as simply being a special case of two-conductor lines and thereby not requiring scrutiny, this is not the case. In addition to a thorough discussion of two-conductor lines, we will examine the methods for solution of MTLs. Numerous experimental results will be compared to the predictions of the transmission-line equations, for both two-conductor lines and MTLs, in order to show their accuracy as well as the relative influence of the line parameters.

The analysis of an MTL for the resulting n line voltages $V_i(z, t)$ and n line currents $I_i(z, t)$ is in general, a three-step process:

Step 1: *Determine the per-unit-length parameters of inductance, capacitance, conductance, and resistance for the given line.* All cross-sectional information about the particular line such as conductor cross sections, wire radii, conductor separations, and so on that distinguishes it from some other line is contained in these per-unit-length parameters and nowhere else. In the case of an two-conductor line, these parameters are scalars. In the case of an MTL consisting of $n + 1$ conductors, these parameters are contained in matrices that are of dimension $n \times n$. The MTL equations are identical in form for all lines: only the per-unit-length parameters are different. Without the determination of the per-unit-length parameters for the specific line, one cannot solve the resulting MTL equations because the coefficients in those equations (the per-unit-length parameters) will be unknown.

Step 2: *Determine the general solution of the resulting MTL equations.* For a two-conductor line, the general solution consists of the sum of a forward- and a backward-traveling wave. In the case where the sources driving the line are general excitation waveforms, these waves are represented by *two unknown functions* that are functions of position along the line z and time t . In the case of sinusoidal steady-state excitation of the line, there are *two complex-valued undetermined constants*. For an MTL consisting of $n + 1$ conductors, the general solution consists of the sum of n forward- and n backward-traveling waves. In the case where the sources driving the line are general excitation waveforms, these waves are represented by *2n unknown functions* that are functions of position along the line z and time t . In the case of sinusoidal steady-state excitation of the line, there are *2n complex-valued undetermined constants*.

Step 3: *Incorporate the terminal conditions to determine the unknown functions or unknown coefficients in the general form of the solution.* A transmission line will have terminations at the left and right ends consisting of independent voltage and/or current sources and lumped elements such as resistors, capacitors, inductors, diodes, transistors, and so on. These *terminal constraints* provide the additional $2n$ equations (n for the left termination and n for the right termination), which can be used to explicitly determine the $2n$ undetermined functions or the $2n$ coefficients in the general form of the MTL equation solution that was obtained in step 2.

The above sequence of steps is referred to as the *direct method*. There are also other methods of solution that avoid these individual steps. These are *numerical* methods that seek to directly integrate the transmission-line differential equations and at the same time include the terminal constraint relations at the two ends of the line. An example of such a method that we will investigate is the finite-difference, time-domain (FDTD) method.

The excitation sources for the MTL will have several forms. Independent lumped sources within the two termination networks are one method of exciting the line. Each source is intended to be coupled to the endpoint of the line to which it is attached. However, the electromagnetic fields associated with the current and voltage on that line interact with neighboring lines inducing signals at those endpoints. This coupling is *unintentional* and is referred to as *crossstalk*. Another method of exciting a line is with an incident electromagnetic field such as radio, radar, or TV signals, or a lightning pulse. This form of unintended excitation produces sources that are distributed along the line and will also induce unintentional signals at the line endpoints that may cause *interference*. Lumped sources can occur at discrete points along the line as with the direct attachment of a lightning stroke. The effect of incident fields distributed either along the line or at discrete points can be included in the MTL equations. In order to obtain the complete solution for the line voltages and currents via the direct solution method, *each of the above three steps must be performed* and in the above order. Throughout our discussions, this sequence of solution steps should be kept in mind.

Electromagnetic fields are, in reality, distributed throughout space. If a structure's largest dimension is electrically small, that is, much less than a wavelength, we can approximately lump the EM effects into circuit elements as in lumped-circuit theory and represent the line with a lumped equivalent circuit, thereby avoiding a direct solution of the transmission-line equations. The transmission-line formulation that we will use to analyze the line views the line as a distributed-parameter structure along the line axis and thereby extends the lumped-circuit analysis techniques to structures that are electrically large in this dimension. However, the cross-sectional dimensions, for example, conductor separations, must be electrically small in order for the analysis to yield valid results. The fundamental assumption for all transmission-line formulations and analyses whether it be for a two-conductor line or an MTL is that the electromagnetic field surrounding the conductors has a transverse electromagnetic (TEM) structure. A TEM field structure is one in which the electric and magnetic fields in the space surrounding the line conductors are transverse or perpendicular to the line axis. In other words, the TEM field structure has no components of the electric or magnetic fields directed along the line axis. The electric and magnetic fields in the space around the line conductors propagate along the line as waves and are said to propagate in the TEM mode. One of the important consequences of the TEM mode of propagation is to allow the unique definition of line voltages and currents. Voltage and current are normally definable only for dc or static fields [A.1]. For the TEM field structure, voltage between the line conductors and currents flowing on those conductors can be uniquely defined even though the fields are varying with time. There are certain nonideal aspects of an MTL, such as imperfect line conductors and/or an inhomogeneous surrounding medium, that, theoretically, invalidate the

TEM mode, transmission-line equation description. However, we will include these nonideal properties in the transmission-line equation formulation of the ideal TEM mode on the assumption that their effects are small. This is referred to as the quasi-TEM mode assumption. In addition to the TEM mode of propagation, there may exist other higher order modes of propagation [17–19]. These higher order modes generally have cutoff frequencies below which they are highly attenuated and for all practical purposes do not propagate. The TEM mode has a cutoff frequency of dc. For typical transmission-line structures such as cables and PCBs, the higher order modes are cutoff (or highly attenuated) for frequencies up to the lower gigahertz frequency range. Consequently using the TEM mode, transmission-line equation formulation to analyze typical lines will provide an accurate analysis of the line for frequencies of excitation well into the lower gigahertz frequency range. An important consequence of the TEM mode, MTL equation formulation is that the sum of the line currents at any cross section of the line is zero. In this sense we say that one of the conductors, the *reference conductor*, is the return for the other n currents. Even though the line cross section is electrically small, it may not be true that the currents sum to zero at any cross section; there may be other currents in existence on the line conductors [20–23]. Presence of nearby conductors or other metallic structures that are not included in the formulation may cause these additional currents [24]. Asymmetries in the physical terminal excitation such as offset source positions (which are implicitly ignored in the terminal representation) can also create these non-TEM currents [24]. It is important to understand these restrictions on the applicability of the transmission-line equation representation and the validity of the results obtained from it.

Although there is a voluminous base of references for this topic, important ones will be referenced, where appropriate, by [x]. These are grouped into two categories—those by the author (grouped by category) and other references. References consisting of publications on this topic by the author are listed at the end of the text and are grouped by category. Additional references will be listed at the end of each chapter.

1.1 EXAMPLES OF MULTICONDUCTOR TRANSMISSION-LINE STRUCTURES

There are a number of examples of wave-guiding structures that may be viewed as “transmission lines.” Figure 1.1 shows examples of $(n + 1)$ -conductor, wire-type lines consisting of parallel wires. Throughout this text, we will refer to conductors that have circular–cylindrical cross sections as *wires*. The conductors are parallel to the line axis, which is the z axis of a rectangular coordinate system. One of the conductors is designated as the 0 (zero) conductor or *reference conductor*. The line voltages $V_i(z, t)$ are defined between each of the other n conductors and this reference conductor. The currents flowing on the other n conductors, $I_i(z, t)$, “return” along this reference conductor. The voltages and currents are functions of position along the line, z , and time t . Figure 1.1(a) shows an example of $n + 1$ wires, where the reference conductor is another wire. Typical examples of such lines are ribbon

cables used to interconnect electronic systems. Figure 1.1(b) shows n wires above an infinite, perfectly conducting ground plane (the reference conductor). Typical examples are cables that have a metallic structure as a return or high-voltage power distribution lines. Figure 1.1(c) shows n wires within an overall cylindrical shield (the reference conductor). Shields are often placed around groups of wires in order to prevent or reduce the coupling of electromagnetic fields to the wires from adjacent wires (crosstalk) or from distant sources such as radar transmitters or radio and television transmitters. Normally, all wires are surrounded by circular–cylindrical dielectric insulations. However, these insulations are omitted from these figures and, in some cases, may be ignored in the analysis of such lines. Hence the surrounding medium is said to be *homogeneous* in that the permittivity ϵ and permeability μ of the surrounding dielectric medium are constants and are independent of position. Hence, the wire structures of Figure 1.1 are said to constitute lines in a *homogeneous medium*. For the lines in Figure 1.1(a) and (b), the only logical homogeneous medium of infinite extent would be free space with parameters of *permittivity* ϵ_0 and *permeability* μ_0 . For the line within an overall shield in Figure 1.1(c), the fields are contained within the shield that may be a homogeneous dielectric other than free space with parameters $\epsilon = \epsilon_r \epsilon_0$ and $\mu = \mu_0$. The permeability of all dielectrics is that of free space, whereas the permittivity is characterized by a relative permittivity (relative to that of free space) of ϵ_r . Thus dielectrics affect electric fields and do not affect magnetic fields. The wires in each of these structures are also shown as being of *uniform cross section* along their length and parallel to each other (as well as the

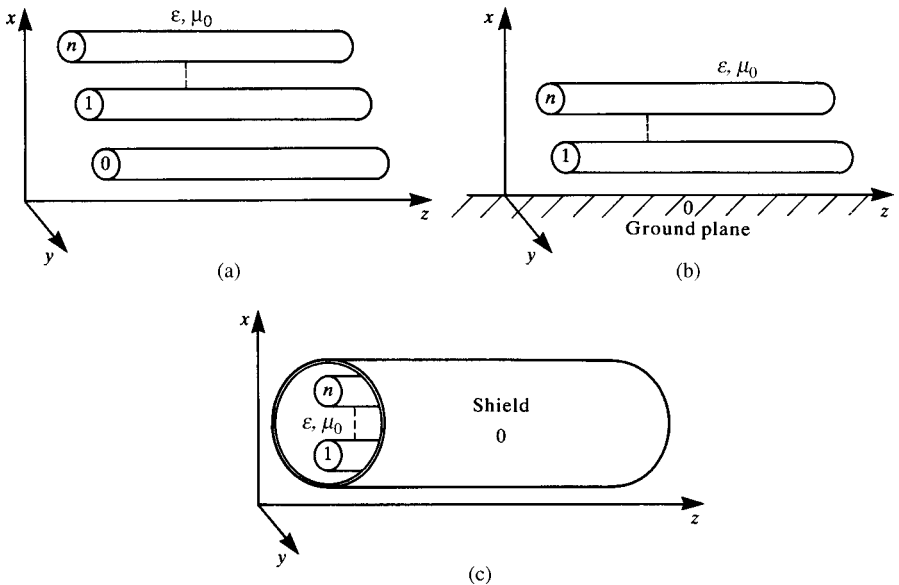


FIGURE 1.1 Multiconductor lines in homogeneous media: (a) $(n+1)$ -wire line, (b) n wires above a ground plane, and (c) n wires within a cylindrical shield.

ground plane in Fig. 1.1(b) and the shield axis in Fig. 1.1(c)). Such lines are said to be *uniform lines*. Nonuniform lines in which the conductors either are not of uniform cross section along their length or are not parallel arise from either nonintentional or intentional reasons. For example, the conductors of a high-voltage power distribution line, because of their weight, sag and are not parallel to the ground. Tapered lines are intentionally designed to give certain desirable characteristics in microwave filters.

Figure 1.2 shows examples of lines wherein the conductors have rectangular cross sections. Figure 1.2(a) shows a structure having n conductors of rectangular cross

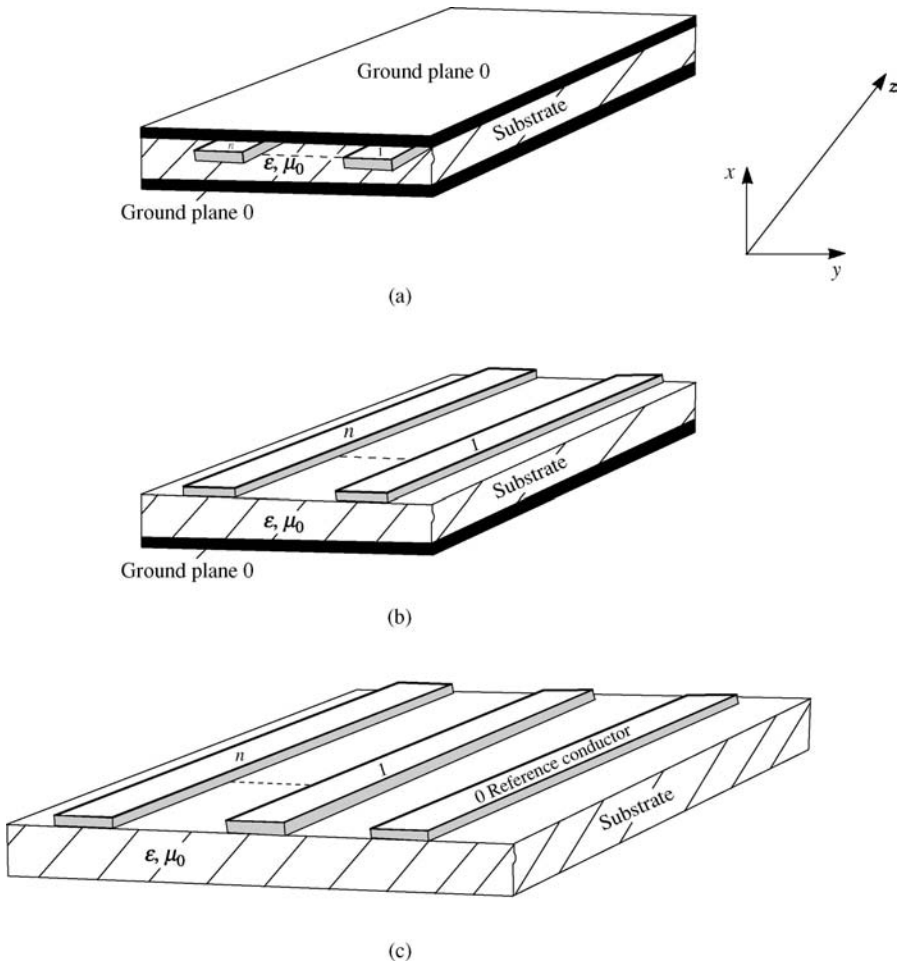


FIGURE 1.2 Multiconductor lines consisting of conductors of rectangular cross section (lands): (a) an n -conductor coupled stripline (homogeneous medium), (b) an n -conductor coupled microstrip line (inhomogeneous medium), and (c) n lands on a PCB (inhomogeneous medium).

section (*lands*) imbedded in a dielectric substrate. This type of structure is referred to as a *coupled stripline*. Infinite ground planes are on either side of the substrate and constitute the reference conductor(s). This structure represents the case of innerplanes in PCBs. Multiple layers of interconnected lands are buried in a single board and allow for “wiring” the board without taking up a large surface area. “Vias” connect lands on each level. Figure 1.2(b) shows n lands on one side of a dielectric substrate and an infinite ground plane, the reference conductor, on the other side. This is referred to in microwave literature as a *coupled microstrip* and is used to construct microwave filters. This structure also represents the outer layer of a printed circuit board that has innerplanes. Figure 1.2(c) shows $n + 1$ lands on one side of the dielectric substrate. One of those lands constitutes the reference conductor to which all the other line voltages are referenced. This type of structure is common on PCBs in low-cost electronic circuits that do not contain innerplanes. The stripline of Figure 1.2(a) has the fields contained between the two ground planes much like the shielded cable of Figure 1.1(c). Hence, the dielectric is homogeneous with permittivity $\varepsilon = \varepsilon_r \varepsilon_0$ and permeability $\mu = \mu_0$. The structures of Figure 1.2(b) and (c) constitute lines in an inhomogeneous medium in that the electric field lines will exist partly in the substrate and partly in the surrounding air.

The structures in Figure 1.1, as well as the coupled stripline in Figure 1.2(a), are, by implication, immersed in a homogeneous medium. Therefore, the velocity of propagation of the waves on those lines is equal to that of the medium in which they are immersed or $v = 1/\sqrt{\mu\varepsilon}$, where μ is the *permeability* of the surrounding medium and ε is the *permittivity* of the surrounding medium. For free space, these become $\mu_0 = 4\pi \times 10^{-7}$ H/m and $\varepsilon_0 \cong 1/36\pi \times 10^{-9}$ F/m. The velocity of propagation in free space is $v_0 = 1/\sqrt{\mu_0\varepsilon_0} = 2.99792458 \times 10^8$ m/s. For the structures shown in Figure 1.2(b) and (c), which are immersed in an *inhomogeneous medium* (the fields exist partly in free space and partly in the substrate), there are n waves or *modes* whose velocities are, in general, different. This complicates the analysis of such structures as we will see.

1.2 PROPERTIES OF THE TEM MODE OF PROPAGATION

As mentioned previously, the fundamental assumption in any transmission-line formulation is that the electric field intensity vector $\mathcal{E}(x, y, z, t)$ and the magnetic field intensity vector $\mathcal{H}(x, y, z, t)$ satisfy the TEM field structure, that is, they lie in a plane (the x - y plane) transverse or perpendicular to the line axis (the z axis). Therefore, it is appropriate to examine the general properties of this TEM mode of propagation or field structure.

Consider a rectangular coordinate system shown in Figure 1.3 illustrating a propagating TEM wave in which the field vectors are assumed to lie in a plane (the x - y plane) that is transverse to the direction of propagation (the z axis). These field vectors are denoted with a t subscript to denote that they lie in the *transverse* (x - y) plane. It is assumed that the medium is homogeneous, linear, and isotropic and is characterized by the scalar parameters of permittivity ε , permeability μ , and conductivity σ .

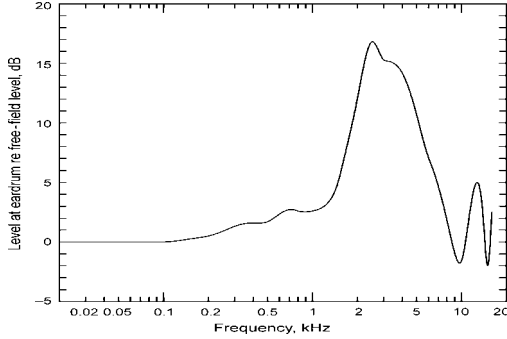


FIGURE 1.3 Illustration of the electromagnetic field structure of the TEM mode of propagation.

Maxwell's equations in differential or point form are [A.1,A.3,A.6]:

$$\nabla \times \vec{\mathcal{E}}_t = -\mu \frac{\partial \vec{\mathcal{H}}_t}{\partial t} \quad (1.1a)$$

$$\nabla \times \vec{\mathcal{H}}_t = \sigma \vec{\mathcal{E}}_t + \varepsilon \frac{\partial \vec{\mathcal{E}}_t}{\partial t} \quad (1.1b)$$

Equation (1.1a) is Faraday's law, and Eq. (1.1b) is Ampere's law. The del operator ∇ can be broken into two components: one component, ∇_z , in the z direction and the other component, ∇_t , in the transverse plane, as in [A.1]

$$\nabla = \nabla_t + \nabla_z \quad (1.2a)$$

where

$$\nabla_t = \vec{a}_x \frac{\partial}{\partial x} + \vec{a}_y \frac{\partial}{\partial y} \quad (1.2b)$$

$$\nabla_z = \vec{a}_z \frac{\partial}{\partial z} \quad (1.2c)$$

and \vec{a}_x , \vec{a}_y , and \vec{a}_z are unit vectors pointing in the appropriate directions. Applying (1.2) to (1.1) gives

$$(\nabla_t + \nabla_z) \times \vec{\mathcal{E}}_t = \underbrace{\nabla_t \times \vec{\mathcal{E}}_t}_{z \text{ directed}} + \underbrace{\nabla_z \times \vec{\mathcal{E}}_t}_{\text{in the transverse plane}} = -\mu \frac{\partial \vec{\mathcal{H}}_t}{\partial t} \quad (1.3a)$$

$$(\nabla_t + \nabla_z) \times \vec{\mathcal{H}}_t = \underbrace{\nabla_t \times \vec{\mathcal{H}}_t}_{z \text{ directed}} + \underbrace{\nabla_z \times \vec{\mathcal{H}}_t}_{\text{in the transverse plane}} = \sigma \vec{\mathcal{E}}_t + \varepsilon \frac{\partial \vec{\mathcal{E}}_t}{\partial t} \quad (1.3b)$$

Matching those components on both sides of (1.3) in the z direction and in the transverse plane gives

$$\vec{a}_z \times \frac{\partial \vec{\mathcal{E}}_t}{\partial z} = -\mu \frac{\partial \vec{\mathcal{H}}_t}{\partial t} \quad (1.4a)$$

$$\vec{a}_z \times \frac{\partial \vec{\mathcal{H}}_t}{\partial z} = \sigma \vec{\mathcal{E}}_t + \varepsilon \frac{\partial \vec{\mathcal{E}}_t}{\partial t} \quad (1.4b)$$

$$\nabla_t \times \vec{\mathcal{E}}_t = 0 \quad (1.4c)$$

$$\nabla_t \times \vec{\mathcal{H}}_t = 0 \quad (1.4d)$$

Equations (1.4a) and (1.4b) show that the electric and magnetic field intensity vectors are orthogonal (perpendicular to each other) [A.1]. Equations (1.4c) and (1.4d) are identical in the transverse plane to those for *static fields* [A.1]. This shows that the electric and magnetic fields of a TEM field distribution satisfy a static distribution in the transverse plane. In other words, the electric and magnetic fields in the transverse plane are identical in structure to those for dc excitation, even though they vary with time. This is an extremely important consequence of the TEM field structure in that (a) voltages and currents that are ordinarily definable only for static (dc) excitation can be uniquely defined for this problem in the transverse plane even though the fields are time varying, and (b) we can determine important transmission-line parameters such as per-unit-length capacitance, inductance, and conductance by using only static field analysis methods in the transverse (x - y) plane, which greatly simplifies their determination.

An important vector identity is that the curl of the gradient of some scalar field $f(x, y, z)$ is always zero: $\nabla \times \nabla f(x, y, z) = 0$ [A.1]. In the transverse plane, this identity translates to

$$\nabla_t \times \nabla_t f(x, y) = 0 \quad (1.5)$$

where ∇_t is the transverse del operator given in (1.2b). Because of (1.4c), (1.4d), and this identity, we may define each of the transverse field vectors as the transverse gradients of some auxiliary scalar fields or *potential functions*, $\phi(x, y)$ and $\psi(x, y)$,

which lie in the transverse plane as [A.1]

$$\vec{\mathcal{E}}_t = e(z, t) \nabla_t \phi(x, y) \quad (1.6a)$$

$$\vec{\mathcal{H}}_t = h(z, t) \nabla_t \psi(x, y) \quad (1.6b)$$

Note that the field vectors are separable into the product of functions of z and t and functions of the transverse plane coordinates x and y . This is permissible in the rectangular coordinate system [A.1]. Because the transverse electric and magnetic field vectors are orthogonal, according to (1.6) the gradient fields $\nabla_t \phi(x, y)$ and $\nabla_t \psi(x, t)$ are also orthogonal in the transverse plane. Hence, the scalar field lines for $\phi = \text{constant}$ are everywhere in the transverse plane orthogonal to the scalar field lines for $\psi = \text{constant}$. Gauss' laws in the transverse plane become [A.1]

$$\nabla_t \cdot \vec{\mathcal{E}}_t = 0 \quad (1.7a)$$

$$\nabla_t \cdot \vec{\mathcal{H}}_t = 0 \quad (1.7b)$$

Applying (1.7) to (1.6) gives

$$\nabla_t \cdot \nabla_t \phi(x, y) = \nabla_t^2 \phi(x, y) = 0 \quad (1.8a)$$

$$\nabla_t \cdot \nabla_t \psi(x, y) = \nabla_t^2 \psi(x, y) = 0 \quad (1.8b)$$

where

$$\nabla_t^2 \phi(x, y) = \frac{\partial^2 \phi(x, y)}{\partial^2 x} + \frac{\partial^2 \phi(x, y)}{\partial^2 y} = 0 \quad (1.9a)$$

$$\nabla_t^2 \psi(x, y) = \frac{\partial^2 \psi(x, y)}{\partial^2 x} + \frac{\partial^2 \psi(x, y)}{\partial^2 y} = 0 \quad (1.9b)$$

are Laplace's equations in the transverse plane [A.1]. Equations (1.9) show that the auxiliary scalar potential functions satisfy Laplace's equation in any transverse plane, as is the case for static (dc) fields. This again shows that the electric and magnetic field structure in the transverse plane for the TEM mode of propagation is identical to that of a static (dc) distribution. As we will show later, there are numerous static field methods to compute this static field distribution.

Now suppose we take the cross product of the z -directed unit vector with (1.4a) and (1.4b). This gives

$$\vec{a}_z \times \left[\vec{a}_z \times \frac{\partial \vec{\mathcal{E}}_t}{\partial z} \right] = -\mu \left[\vec{a}_z \times \frac{\partial \vec{\mathcal{H}}_t}{\partial t} \right] \quad (1.10a)$$

$$\vec{a}_z \times \left[\vec{a}_z \times \frac{\partial \vec{\mathcal{H}}_t}{\partial z} \right] = \sigma(\vec{a}_z \times \vec{\mathcal{E}}_t) + \varepsilon \left[\vec{a}_z \times \frac{\partial \vec{\mathcal{E}}_t}{\partial t} \right] \quad (1.10b)$$

However,

$$\vec{a}_z \times \left[\vec{a}_z \times \frac{\partial \vec{\mathcal{E}}_t}{\partial z} \right] = -\frac{\partial \vec{\mathcal{E}}_t}{\partial z} \quad (1.11a)$$

$$\vec{a}_z \times \left[\vec{a}_z \times \frac{\partial \vec{\mathcal{H}}_t}{\partial z} \right] = -\frac{\partial \vec{\mathcal{H}}_t}{\partial z} \quad (1.11b)$$

as illustrated in Figure 1.4. Therefore, Eqs. (1.10) become

$$-\frac{\partial \vec{\mathcal{E}}_t}{\partial z} = -\mu \left[\vec{a}_z \times \frac{\partial \vec{\mathcal{H}}_t}{\partial t} \right] \quad (1.12a)$$

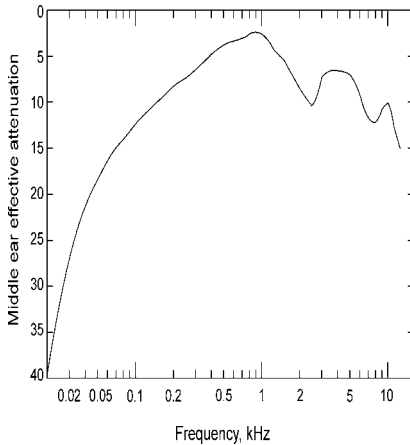


FIGURE 1.4 Illustration of the identity $\vec{a}_z \times (\vec{a}_z \times \vec{\mathcal{E}}_t) = -\vec{\mathcal{E}}_t$.

$$-\frac{\partial \vec{\mathcal{H}}_t}{\partial z} = \sigma(\vec{a}_z \times \vec{\mathcal{E}}_t) + \varepsilon \left[\vec{a}_z \times \frac{\partial \vec{\mathcal{E}}_t}{\partial t} \right] \quad (1.12b)$$

Taking the partial derivative of both sides of (1.12) with respect to z , taking the partial derivative of both sides of (1.4a) and (1.4b) with respect to t , and substituting gives the second-order *vector* partial differential equations that the transverse field vectors must satisfy:

$$\frac{\partial^2 \vec{\mathcal{E}}_t}{\partial z^2} = \mu\sigma \frac{\partial \vec{\mathcal{E}}_t}{\partial t} + \mu\varepsilon \frac{\partial^2 \vec{\mathcal{E}}_t}{\partial t^2} \quad (1.13a)$$

$$\frac{\partial^2 \vec{\mathcal{H}}_t}{\partial z^2} = \mu\sigma \frac{\partial \vec{\mathcal{H}}_t}{\partial t} + \mu\varepsilon \frac{\partial^2 \vec{\mathcal{H}}_t}{\partial t^2} \quad (1.13b)$$

Substituting (1.6) into (1.13) yields the second-order *scalar* partial differential equations in terms of the scalar functions $e(z, t)$ and $h(z, t)$ as

$$\frac{\partial^2 e(z, t)}{\partial z^2} = \mu\sigma \frac{\partial e(z, t)}{\partial t} + \mu\varepsilon \frac{\partial^2 e(z, t)}{\partial t^2} \quad (1.14a)$$

$$\frac{\partial^2 h(z, t)}{\partial z^2} = \mu\sigma \frac{\partial h(z, t)}{\partial t} + \mu\varepsilon \frac{\partial^2 h(z, t)}{\partial t^2} \quad (1.14b)$$

Once (1.14) are solved for the scalar functions $e(z, t)$ and $h(z, t)$, we can determine the transverse field vectors by solving for the scalar potential functions in the transverse plane, $\nabla_t \phi(x, y)$ and $\nabla_t \psi(x, y)$, and taking the products as in (1.6). This second problem, solving for the scalar potential functions in the transverse plane, depends only on the cross-sectional dimensions of the transmission line.

Now let us consider the case where the medium is *lossless*, that is, $\sigma = 0$. In this case, Eqs. (1.14) reduce to

$$\frac{\partial^2 e(z, t)}{\partial z^2} = \mu\varepsilon \frac{\partial^2 e(z, t)}{\partial t^2} \quad (1.15a)$$

$$\frac{\partial^2 h(z, t)}{\partial z^2} = \mu\varepsilon \frac{\partial^2 h(z, t)}{\partial t^2} \quad (1.15b)$$

The general solutions of these consist of waves traveling in the $+z$ and $-z$ directions as in [A.1]

$$e(z, t) = e^+ \left(t - \frac{z}{v} \right) + e^- \left(t + \frac{z}{v} \right) \quad (1.16a)$$

$$h(z, t) = h^+ \left(t - \frac{z}{v} \right) + h^- \left(t + \frac{z}{v} \right) \quad (1.16b)$$

where the velocity of propagation is

$$v = \frac{1}{\sqrt{\mu\varepsilon}} \quad (1.17)$$

Observe that in these solutions, the variables z and t can only appear together as $t \pm (z/v)$. The function $e^+(t - (z/v))$ represents a *forward-traveling wave* since as t progresses, z must increase to keep the argument constant and track corresponding points on the waveform. Similarly, the function $e^-(t + (z/v))$ represents a *backward-traveling wave* traveling in the $-z$ direction. The solutions for the electric and magnetic field vectors may be obtained by substituting (1.16a) and (1.16b) into (1.6) to yield

$$\vec{\mathcal{E}}_t(x, y, z, t) = \underbrace{e^+ \left(t - \frac{z}{v} \right) \nabla_t \phi(x, y)}_{\vec{\mathcal{E}}_t^+} + \underbrace{e^- \left(t + \frac{z}{v} \right) \nabla_t \phi(x, y)}_{\vec{\mathcal{E}}_t^-} \quad (1.18a)$$

$$\begin{aligned} \vec{\mathcal{H}}_t(x, y, z, t) &= \underbrace{h^+ \left(t - \frac{z}{v} \right) \nabla_t \psi(x, y)}_{\vec{\mathcal{H}}_t^+} + \underbrace{h^- \left(t + \frac{z}{v} \right) \nabla_t \psi(x, y)}_{\vec{\mathcal{H}}_t^-} \\ &= \frac{1}{\eta} e^+ \left(t - \frac{z}{v} \right) [\vec{a}_z \times \nabla_t \phi(x, y)] - \frac{1}{\eta} e^- \left(t + \frac{z}{v} \right) [\vec{a}_z \times \nabla_t \phi(x, y)] \end{aligned} \quad (1.18b)$$

where the *intrinsic impedance* of the medium is

$$\eta = \sqrt{\frac{\mu}{\varepsilon}} \quad (1.19)$$

These may be proven by direct substitution into (1.12) and recalling that $\vec{a}_z \times [\vec{a}_z \times \nabla_t \phi] = -\nabla_t \phi$ and $\vec{a}_z \times [\vec{a}_z \times \nabla_t \psi] = -\nabla_t \psi$. Hence we may write the transverse fields as

$$\vec{\mathcal{E}}_t(x, y, z, t) = \vec{\mathcal{E}}_t^+(x, y, z, t) + \vec{\mathcal{E}}_t^-(x, y, z, t) \quad (1.20a)$$

$$\begin{aligned} \vec{\mathcal{H}}_t(x, y, z, t) &= \vec{\mathcal{H}}_t^+(x, y, z, t) + \vec{\mathcal{H}}_t^-(x, y, z, t) \\ &= \frac{1}{\eta} \vec{a}_z \times \vec{\mathcal{E}}_t^+(x, y, z, t) - \frac{1}{\eta} \vec{a}_z \times \vec{\mathcal{E}}_t^-(x, y, z, t) \end{aligned} \quad (1.20b)$$

Consequently, we may indicate the vector relation between the forward- and backward-traveling electric and magnetic field components as

$$\vec{\mathcal{H}}_t^\pm = \pm \frac{1}{\eta} \vec{a}_z \times \vec{\mathcal{E}}_t^\pm \quad (1.21)$$

with the sign depending on whether we are considering the backward- or forward-traveling wave component.

If the time variation of the field vectors is sinusoidal, we use phasor notation [A.2,A.5]:

$$\vec{\mathcal{E}}_t(x, y, z, t) = \text{Re}\left\{\vec{\hat{E}}_t(x, y, z)e^{j\omega t}\right\} \quad (1.22a)$$

$$\vec{\mathcal{H}}_t(x, y, z, t) = \text{Re}\left\{\vec{\hat{H}}_t(x, y, z)e^{j\omega t}\right\} \quad (1.22b)$$

where the phasor transverse field vectors are complex valued and denoted as $\vec{\hat{E}}_t$ and $\vec{\hat{H}}_t$. We will denote complex-valued quantities with a caret ($\hat{\cdot}$) over the quantity. In terms of the scalar functions $e(z, t)$ and $h(z, t)$, these become

$$e(z, t) = \text{Re}\{\hat{e}(z)e^{j\omega t}\} \quad (1.23a)$$

$$h(z, t) = \text{Re}\{\hat{h}(z)e^{j\omega t}\} \quad (1.23b)$$

Replacing time derivatives with $\frac{\partial}{\partial t} = j\omega$ in (1.15) gives the *phasor form* of the differential equations for a lossless medium, $\sigma = 0$, as

$$\frac{d^2\hat{e}(z)}{dz^2} = -\omega^2\mu\varepsilon\hat{e}(z) \quad (1.24a)$$

$$\frac{d^2\hat{h}(z)}{dz^2} = -\omega^2\mu\varepsilon\hat{h}(z) \quad (1.24b)$$

The solutions to these equations are [A.1]

$$\hat{e}(z) = \hat{e}^+e^{-j\beta z} + \hat{e}^-e^{j\beta z} \quad (1.25a)$$

$$\hat{h}(z) = \hat{h}^+e^{-j\beta z} + \hat{h}^-e^{j\beta z} \quad (1.25b)$$

where the complex undetermined constants are denoted as \hat{e}^\pm and \hat{h}^\pm , and the phase constant is denoted as

$$\beta = \omega\sqrt{\mu\varepsilon} \quad (\text{rad/m}) \quad (1.26)$$

The terms $e^{\pm j\beta z} = 1\mathcal{L}(\pm\beta z)$ represent a phase shift as the single-frequency, sinusoidal waves propagate in the z direction. Substituting (1.25) into (1.6) gives the phasor field

vectors:

$$\vec{E}_t(x, y, z) = \underbrace{\hat{e}^+ \nabla_t \phi(x, y)}_{\vec{E}^+(x, y)} e^{-j\beta z} + \underbrace{\hat{e}^- \nabla_t \phi(x, y)}_{\vec{E}^-(x, y)} e^{j\beta z} \quad (1.27a)$$

$$\begin{aligned} \vec{H}_t(x, y, z) &= \underbrace{\hat{h}^+ \nabla_t \psi(x, y)}_{\vec{H}^+(x, y)} e^{-j\beta z} + \underbrace{\hat{h}^- \nabla_t \psi(x, y)}_{\vec{H}^-(x, y)} e^{j\beta z} \\ &= \frac{1}{\eta} \hat{e}^+ \vec{a}_z \times \nabla_t \phi(x, y) e^{-j\beta z} - \frac{1}{\eta} \hat{e}^- \vec{a}_z \times \nabla_t \phi(x, y) e^{j\beta z} \end{aligned} \quad (1.27b)$$

and once again

$$\vec{H}^\pm = \pm \frac{1}{\eta} \vec{a}_z \times \vec{E}^\pm \quad (1.28)$$

The time-domain expressions are obtained by multiplying (1.27) by $e^{j\omega t}$ and taking the real part of the result according to (1.22) [A.1]. For example, the x component of the transverse electric field vector and the y component of the magnetic field vector are

$$\mathcal{E}_x(x, y, z, t) = E_{mx}^+ \cos(\omega t - \beta z + \theta_x^+) + E_{mx}^- \cos(\omega t + \beta z + \theta_x^-) \quad (1.29a)$$

$$\mathcal{H}_y(x, y, z, t) = \frac{1}{\eta} E_{mx}^+ \cos(\omega t - \beta z + \theta_x^+) - \frac{1}{\eta} E_{mx}^- \cos(\omega t + \beta z + \theta_x^-) \quad (1.29b)$$

where the x components of the undetermined complex field components are functions of x and y and are denoted as $\hat{E}_x^\pm(x, y) = E_{mx}^\pm \angle \theta_x^\pm$. The phase velocity of the waves is obtained by setting the argument of each cosine in (1.29) to a constant (in order to follow a point on the waveform) and differentiating to yield $\omega dt - \beta dz = 0$ or $v = (dz/dt) = (\omega/\beta)$. Substituting (1.26) gives the wave constant phase velocity as

$$\begin{aligned} v &= \frac{\omega}{\beta} \\ &= \frac{1}{\sqrt{\mu\epsilon}} \end{aligned} \quad (1.30)$$

The phase constant β has the unit of rad/m and represents a phase shift as the wave propagates through the medium. A *wavelength*, denoted as λ , is the distance (in meters) a single-frequency, sinusoidal wave must travel to change phase by 2π radians or 360° . Hence, $\beta\lambda = 2\pi$ and therefore

$$\lambda = \frac{2\pi}{\beta} = \frac{v}{f} \quad (1.31)$$

If we now consider adding conductive losses to the medium, $\sigma \neq 0$, this adds a transverse conductive current term, $\vec{J}_t = \sigma \vec{\mathcal{E}}_t$, to Ampere's law given in Eq. (1.1b). Replacing time derivatives with $j\omega$ in the second-order differential equations in (1.14) gives the corresponding phasor differential equations for the case of a lossy medium as

$$\begin{aligned} \frac{d^2 \hat{e}(z)}{dz^2} &= j\omega\mu\sigma \hat{e}(z) + (j\omega)^2(\mu\varepsilon) \hat{e}(z) \\ &= j\omega\mu(\sigma + j\omega\varepsilon) \hat{e}(z) \\ &= \hat{\gamma}^2 \hat{e}(z) \end{aligned} \quad (1.32a)$$

$$\begin{aligned} \frac{d^2 \hat{h}(z)}{dz^2} &= j\omega\mu\sigma \hat{h}(z) + (j\omega)^2(\mu\varepsilon) \hat{h}(z) \\ &= j\omega\mu(\sigma + j\omega\varepsilon) \hat{h}(z) \\ &= \hat{\gamma}^2 \hat{h}(z) \end{aligned} \quad (1.32b)$$

where the *propagation constant* is

$$\begin{aligned} \hat{\gamma} &= \sqrt{j\omega\mu(\sigma + j\omega\varepsilon)} \\ &= \alpha + j\beta \end{aligned} \quad (1.33)$$

The solutions to these equations are [A.1]

$$\hat{e}(z) = \hat{e}^+ e^{-\alpha z} e^{-j\beta z} + \hat{e}^- e^{\alpha z} e^{j\beta z} \quad (1.34a)$$

$$\hat{h}(z) = \hat{h}^+ e^{-\alpha z} e^{-j\beta z} + \hat{h}^- e^{\alpha z} e^{j\beta z} \quad (1.34b)$$

Hence, the phase constant is the imaginary part of the propagation constant and is no longer $\omega\sqrt{\mu\varepsilon}$, as was the case for a lossless medium, that is, $\beta \neq \omega\sqrt{\mu\varepsilon}$. In addition, the real part of the propagation constant, α , is said to be the *attenuation constant* and it represents losses in the medium as we will see later. The phasor solutions for the phasor field vectors for this case of a lossy medium, $\sigma \neq 0$, are

$$\vec{\hat{E}}_t(x, y, z) = \underbrace{\hat{e}^+ \nabla_t \phi(x, y)}_{\vec{\hat{E}}^+(x, y)} e^{-\alpha z} e^{-j\beta z} + \underbrace{\hat{e}^- \nabla_t \phi(x, y)}_{\vec{\hat{E}}^-(x, y)} e^{\alpha z} e^{j\beta z} \quad (1.35a)$$

$$\begin{aligned} \vec{\hat{H}}_t(x, y, z) &= \underbrace{\hat{h}^+ \nabla_t \psi(x, y)}_{\vec{\hat{H}}^+(x, y)} e^{-\alpha z} e^{-j\beta z} + \underbrace{\hat{h}^- \nabla_t \psi(x, y)}_{\vec{\hat{H}}^-(x, y)} e^{\alpha z} e^{j\beta z} \\ &= \frac{1}{\hat{\eta}} \hat{e}^+ \vec{a}_z \times \nabla_t \phi(x, y) e^{-\alpha z} e^{-j\beta z} - \frac{1}{\hat{\eta}} \hat{e}^- \vec{a}_z \times \nabla_t \phi(x, y) e^{\alpha z} e^{j\beta z} \end{aligned} \quad (1.35b)$$

where the intrinsic impedance now becomes complex as

$$\begin{aligned}\hat{\eta} &= \sqrt{\frac{j\omega\mu}{\sigma + j\omega\varepsilon}} \\ &= \eta \angle \theta_\eta \\ &= \eta e^{j\theta_\eta}\end{aligned}\tag{1.36}$$

and once again

$$\vec{\hat{H}}^\pm = \pm \frac{1}{\hat{\eta}} \vec{a}_z \times \vec{E}^\pm\tag{1.37}$$

Again, the time-domain expressions are obtained by multiplying (1.35a) and (1.35b) by $e^{j\omega t}$ and taking the real part of the result according to (1.22) [A.1]. For example, the x component of the transverse electric field vector and the y component of the magnetic field vector are

$$\mathcal{E}_x(x, y, z, t) = E_{mx}^+ e^{-\alpha z} \cos(\omega t - \beta z + \theta_x^+) + E_{mx}^- e^{\alpha z} \cos(\omega t + \beta z + \theta_x^-)\tag{1.38a}$$

$$\begin{aligned}\mathcal{H}_y(x, y, z, t) &= \frac{1}{\eta} E_{mx}^+ e^{-\alpha z} \cos(\omega t - \beta z + \theta_x^+ - \theta_\eta) \\ &\quad - \frac{1}{\eta} E_{mx}^- e^{\alpha z} \cos(\omega t + \beta z + \theta_x^- - \theta_\eta)\end{aligned}\tag{1.38b}$$

Thus, in addition to a phase shift represented by $e^{\pm j\beta z}$, the waves suffer an *attenuation* of their amplitudes as represented by $e^{\pm \alpha z}$. We will find these properties of the TEM mode of propagation arising in various guises throughout our examination of MTLs.

1.3 THE TRANSMISSION-LINE EQUATIONS: A PREVIEW

Consider a two-conductor transmission line that has two conductors of uniform cross section that are parallel to each other and the z axis as shown in Figure 1.5(a). The conductors are considered to be perfect conductors (lossless, $\sigma = \infty$), and the surrounding medium is homogeneous and lossy with parameters $\mu = \mu_0$, $\varepsilon = \varepsilon_r \varepsilon_0$, σ . The transverse electric and magnetic fields are shown in Figure 1.5(b) in the transverse x - y plane. In order to satisfy the boundary conditions on the surfaces of the perfect conductors, the electric fields must be normal to the conductor surfaces and the magnetic fields must be tangent to the conductor surfaces [A.1]. It should be noted that because these conductors are assumed to be perfect conductors, the boundary conditions also show that the magnetic field intensity vector $\vec{\mathcal{H}}$ must be tangent to the surfaces of these perfect conductors and induces a surface current to flow on these conductors [A.1]. Since the magnetic field lies in the transverse plane, these induced

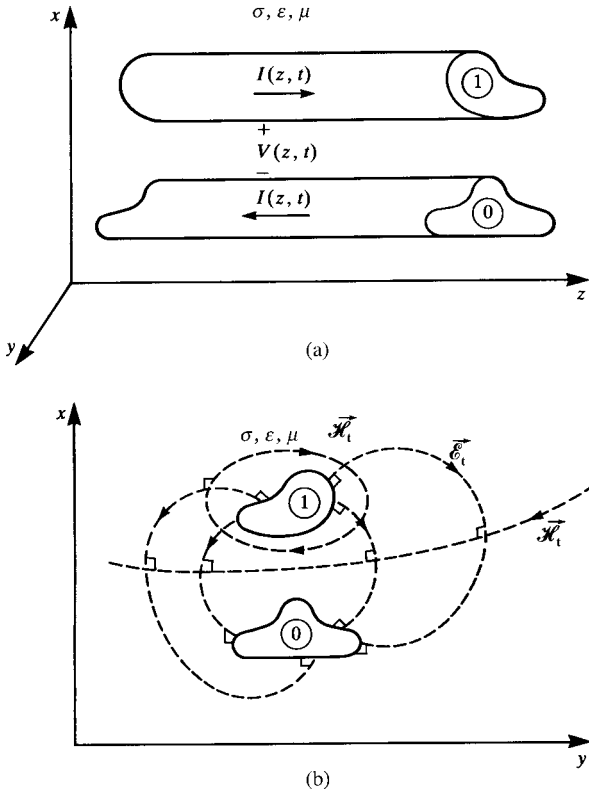


FIGURE 1.5 Illustration of (a) the current and voltage and (b) the TEM fields for a two-conductor line.

currents on the surfaces of the conductors are directed in the z direction [A.1]. These are the transmission-line currents. In addition, since the conductors are assumed to be perfect conductors, these boundary conditions show that the electric flux density vector $\vec{\mathcal{D}} = \epsilon \vec{\mathcal{E}}$ that is normal to the surfaces of the conductors induces a surface charge density on these conductors from which the transverse electric field vectors emanate [A.1]. In addition, the transverse electric and magnetic field lines are everywhere in this transverse plane orthogonal to each other.

1.3.1 Unique Definition of Voltage and Current for the TEM Mode of Propagation

In the previous section, it was shown that the electric and magnetic field vectors in the transverse (x - y) plane satisfy a static distribution. In other words, the electric and magnetic fields in the transverse plane have distributions identical to dc fields even though they vary with time. Hence we may uniquely define a voltage between the two conductors by integrating the component of the electric field tangent to a contour c in the

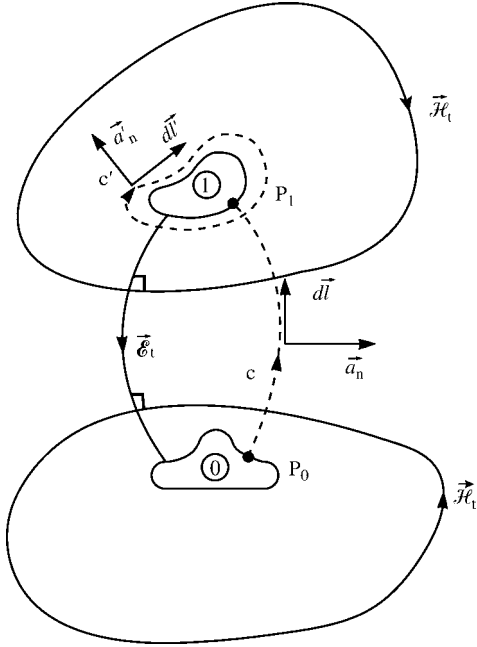


FIGURE 1.6 Illustrations of the contours and surfaces for the definitions of voltage and current for a two-conductor line.

transverse plane between two points on each conductor as shown in Figure 1.6 [A.1]:

$$\begin{aligned}
 V(z, t) &= - \int_c \vec{\mathcal{E}}_t \cdot d\vec{l} \\
 &= - \int_{P_0}^{P_1} \vec{\mathcal{E}}_t \cdot d\vec{l}
 \end{aligned}
 \tag{1.39}$$

This may be directly shown by substituting the relation between the transverse electric field and the scalar potential function in (1.6a):

$$\begin{aligned}
 V(z, t) &= - \int_{P_0}^{P_1} e(z, t) \nabla_t \phi(x, y) \cdot d\vec{l} \\
 &= -e(z, t) \int_{P_0}^{P_1} \nabla_t \phi(x, y) \cdot d\vec{l} \\
 &= -e(z, t) [\phi_1 - \phi_0]
 \end{aligned}
 \tag{1.40}$$

where ϕ_0 and ϕ_1 are the potentials on the surfaces of the two conductors in this transverse plane [A.1]. Because the conductors are assumed to be perfect conductors,

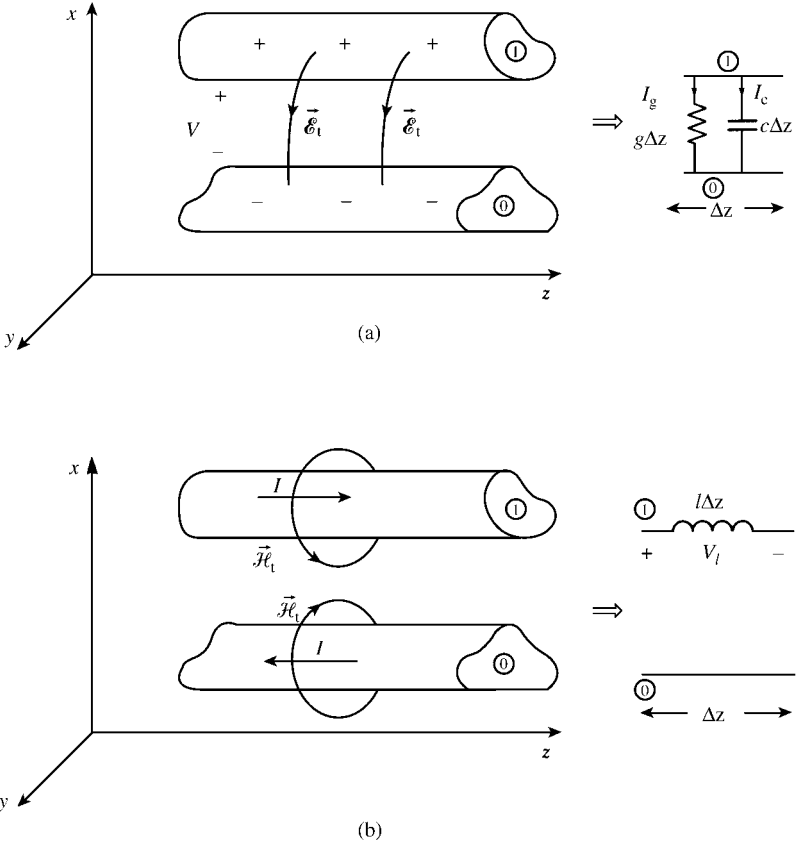


FIGURE 1.7 Illustrations of the intuitive meaning of the per-unit-length parameters.

the potentials are the same at all points on their surfaces, and because this transverse electric field is conservative, this integral is independent of path in the transverse plane and is therefore unique. Similarly, we can uniquely define current as the line integral of the transverse magnetic field around a closed path c' encircling the top conductor as shown in Figure 1.6 [A.1]:

$$I(z, t) = \oint_{c'} \vec{\mathcal{H}}_t \cdot d\vec{l}' \tag{1.41}$$

Since there is no component of the electric field in the z direction, there is no displacement current in the z direction and this reduces to Ampere's law for static conditions [A.1]. Hence, this result is independent of path taken around this conductor so long as it encircles only this conductor.

1.3.2 Defining the Per-Unit-Length Parameters

Figure 1.7 gives an intuitive view of the essential ingredients of the transmission-line equations: the per-unit-length parameters of the line. Figure 1.7(a) shows the effect of the transverse electric field \mathcal{E}_t that is directed from the top conductor to the bottom conductor. The transverse electric field lines begin on positive charge on the surface of the upper conductor and terminate on negative charge on the surface of the lower conductor. This transverse electric field will cause two currents in the surrounding dielectric in this transverse plane that are directed from the top conductor to the lower conductor:

$$\underbrace{I_t(z, t)}_{\text{transverse current}} = \underbrace{I_g(z, t)}_{\text{conduction current}} + \underbrace{I_c(z, t)}_{\text{displacement current}} \quad (1.42)$$

A transverse conduction current $\vec{J}_t = \sigma \vec{\mathcal{E}}_t$, is induced by this transverse electric field to flow in the lossy medium due to its conductivity σ from the top conductor to the bottom conductor in this transverse plane. This effect is represented for a section of line of length Δz by a conductance. For a uniform line, this effect is uniformly distributed along the line. Hence if a section of line of length Δz has a total conductance G , then a *per-unit-length conductance* g whose units are S/m, is given by

$$g = \underbrace{\lim}_{\Delta z \rightarrow 0} \frac{G}{\Delta z} \quad (\text{S/m}) \quad (1.43)$$

The transverse current flowing from the top conductor to the bottom conductor is related to the voltage between the two conductors by

$$I_g(z, t) = g \Delta z V(z, t) \quad (1.44)$$

In addition, since charge is stored on the top and bottom conductors, we essentially have a capacitance between the two conductors. If a section of line of length Δz has a total capacitance C , the charge is related to the voltage by $Q = CV$. For a uniform line, this effect is uniformly distributed along the line. Hence if a section of line of length Δz has a total capacitance C , then the *per-unit-length capacitance* c whose units are F/m, is given by

$$c = \underbrace{\lim}_{\Delta z \rightarrow 0} \frac{C}{\Delta z} \quad (\text{F/m}) \quad (1.45)$$

The (displacement) current flowing in the transverse plane from the top conductor to the bottom conductor is

$$I_c(z, t) = c \Delta z \frac{\partial V(z, t)}{\partial t} \quad (1.46)$$

Consider Figure 1.7(b). The current flowing along the top conductor and returning along the bottom conductor will generate a magnetic field intensity in the transverse plane, $\vec{\mathcal{H}}_t$. The transverse magnetic flux density is [A.1] $\vec{\mathcal{B}}_t = \mu \vec{\mathcal{H}}_t$ Wb/m². This produces a magnetic flux $\psi = \int_s \vec{\mathcal{B}}_t \cdot d\vec{s}$ through the surface that lies between the two conductors. A section of line will therefore have a total inductance L . For a uniform line, this effect is uniformly distributed along the line. Hence if a section of line of length Δz has a total inductance L , then a *per-unit-length inductance* l whose units are H/m, is given by

$$l = \underbrace{\lim}_{\Delta z \rightarrow 0} \frac{L}{\Delta z} \quad (\text{H/m}) \quad (1.47)$$

This will produce a longitudinal voltage drop around the loop contained by the two conductors of

$$V_l(z, t) = l \Delta z \frac{\partial I(z, t)}{\partial t} \quad (1.48)$$

Note that this inductance is a property of the loop formed by the two conductors and as such may be placed in either the top or the bottom conductor. It cannot be uniquely assigned to either conductor.

Adjacent to each of these figures is a lumped-circuit model of an electrically small Δz section. Figure 1.8(a) combines these into one model. The total line length is represented as a continuum of these, as shown in Figure 1.8(b). From the per-unit-length model of the line in Figure 1.8(a), we can obtain the transmission-line equations by using Kirchhoff's voltage (KVL) and current (KCL) laws [A.2,A.5]. Writing KVL at the left and right ends of this circuit gives

$$V(z + \Delta z, t) - V(z, t) = -l \Delta z \frac{\partial I(z, t)}{\partial t} \quad (1.49a)$$

and writing KCL at the top right node gives

$$I(z + \Delta z, t) - I(z, t) = -g \Delta z V(z + \Delta z, t) - c \Delta z \frac{\partial V(z + \Delta z, t)}{\partial t} \quad (1.49b)$$

Dividing (1.49) by Δz and taking the limit as $\Delta z \rightarrow 0$ yields the *transmission-line equations*:

$$\frac{\partial V(z, t)}{\partial z} = -l \frac{\partial I(z, t)}{\partial t} \quad (1.50a)$$

$$\frac{\partial I(z, t)}{\partial z} = -g V(z, t) - c \frac{\partial V(z, t)}{\partial t} \quad (1.50b)$$

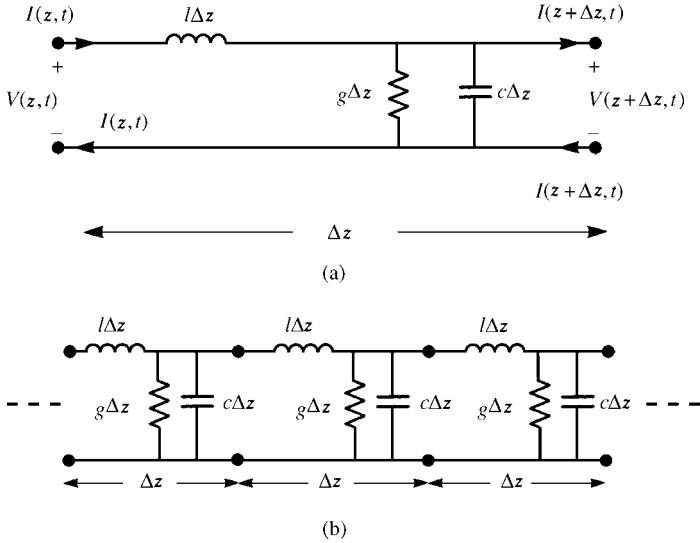


FIGURE 1.8 The per-unit-length equivalent circuit for a two-conductor line.

The above is an intuitive view of the per-unit-length line parameters. In order to compute values of these parameters, we need more precise definitions of them. First, we compute the per-unit-length inductance. We desire to compute the total magnetic flux through a surface between the two conductors that is of differential length along the line of Δz , and the surface is uniform along the line, that is, does not vary with z . The desired surface is shown in Figure 1.9(a) where the unit normal to the surface s is denoted as \vec{a}_n . A cross section in the transverse plane is shown in Figure 1.6. The magnetic flux density vector is $\vec{\mathcal{B}}_t = \mu \vec{\mathcal{H}}_t$ and the total magnetic flux through the surface is the surface integral of this over the surface:

$$\psi = \int_s \mu \vec{\mathcal{H}}_t \cdot \vec{a}_n ds \tag{1.51}$$

The total inductance is the ratio of the magnetic flux through this surface to the current that caused it:

$$l\Delta z = - \frac{\int_s \mu \vec{\mathcal{H}}_t \cdot \vec{a}_n ds}{I(z, t)} \tag{1.52}$$

where l is the per-unit-length inductance desired. We have defined the closed contour around the perimeter of this surface as c . The differential path length along this contour is denoted by $d\vec{l}$, and the normal to the surface is denoted as \vec{a}_n , as shown in Figure 1.6. The definition of the direction of the desired flux through this surface is according to the right-hand rule with respect to the current. Placing the thumb in the

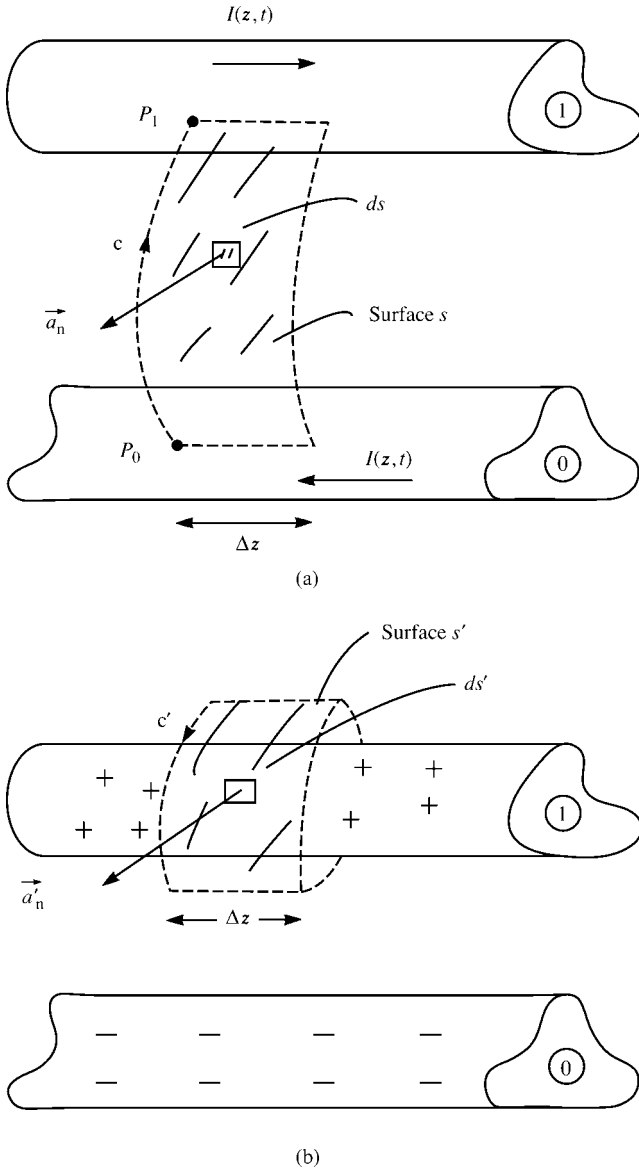


FIGURE 1.9 Contours and surfaces for the derivation of the transmission-line equations: (a) derivation of the voltage change equation, and (b) derivation of the current change equation.

direction of the current (into the page in the $+z$ direction for the top conductor and out of the page in the $-z$ direction for the bottom conductor) gives the direction of the desired flux as clockwise when looking in the $+z$ direction, as in Figure 1.6, which is opposite to the direction of the normal to the surface, \vec{a}_n . Hence, a minus sign is required in (1.52). For a length of the surface of Δz that is considered differentially

small, the flux through the surface does not vary with z . Hence we may remove this dimension from the integral in (1.52). Therefore, as we shrink the length of the surface to zero, the desired flux is obtained by simply integrating along the contour c to give

$$l\Delta z = -\frac{\Delta z\mu \int_c \vec{\mathcal{H}}_t \cdot \vec{a}_n dl}{I(z, t)} \quad (1.53a)$$

or

$$l = -\frac{\mu \int_c \vec{\mathcal{H}}_t \cdot \vec{a}_n dl}{I(z, t)} \quad (1.53b)$$

Substituting the definition of current given in (1.41) gives

$$l = -\mu \frac{\int_c \vec{\mathcal{H}}_t \cdot \vec{a}_n dl}{\oint_{c'} \vec{\mathcal{H}}_t \cdot d\vec{l}'} \quad (1.54)$$

Next, consider obtaining the per-unit-length capacitance c as illustrated in Figure 1.9(b). Charge of equal magnitude but opposite sign is distributed along each conductor and around their peripheries. We desire to compute the total charge contained on the top conductor along a differential length along the line of Δz . The electric flux density vector on the surface of the perfect conductor is $\vec{\mathcal{D}}_t = \varepsilon \vec{\mathcal{E}}_t$ and, according to the boundary conditions on the surface of this perfect conductor, is normal to the surface [A.1]. In order to determine the charge on the conductor surface, we surround it with a closed surface s' that is just off the surface of the conductor and determine the total electric flux through that surface. A cross section in the transverse plane is shown in Figure 1.6, where the unit normal to the surface s' is \vec{a}'_n . The total capacitance is the ratio of this total charge to the voltage between the two conductors:

$$c\Delta z = \frac{\varepsilon \oint_{s'} \vec{\mathcal{E}}_t \cdot \vec{a}'_n ds'}{V(z, t)} \quad (1.55)$$

where s' is the closed surface and c is the per-unit-length capacitance desired. We have defined the closed contour around the perimeter of this surface as c' . The differential path length along this contour is denoted by $d\vec{l}'$ and the normal to the surface is denoted as \vec{a}'_n . Note that these surfaces and contours are designated with primes to distinguish them from the surfaces and contours used to determine the inductance above. Since the transverse electric field and electric flux density vector is from the upper conductor to the lower conductor, it is directed out of this closed surface s' giving the enclosed

charge as positive. For a length of the surface of Δz that is considered differentially small, the flux through the surface does not vary with z . Hence we may remove this dimension from the integral in (1.55). Therefore, as we shrink the length of the surface to zero, the desired flux is obtained by simply integrating along the closed contour c' to give

$$c\Delta z = \frac{\Delta z \varepsilon \oint_{c'} \vec{\mathcal{E}}_t \cdot \vec{a}'_n dl'}{V(z, t)} \quad (1.56a)$$

or

$$c = \frac{\varepsilon \oint_{c'} \vec{\mathcal{E}}_t \cdot \vec{a}'_n dl'}{V(z, t)} \quad (1.56b)$$

Substituting the definition of voltage given in (1.39) gives

$$c = \varepsilon \frac{\oint_{c'} \vec{\mathcal{E}}_t \cdot \vec{a}'_n dl'}{- \int_c \vec{\mathcal{E}}_t \cdot d\vec{l}} \quad (1.57)$$

In order to determine the per-unit-length conductance g , we need to determine the transverse conduction current. The transverse conduction current is obtained by integrating $\sigma \vec{\mathcal{E}}_t$ over the closed surface s' as

$$g\Delta z = \frac{\sigma \oint_{s'} \vec{\mathcal{E}}_t \cdot \vec{a}'_n ds'}{V(z, t)} \quad (1.58)$$

Once again, we assume that the length of the surface along the line Δz is differentially small so that this dimension may be removed from the integral in (1.58), and the desired transverse current is obtained by simply integrating along the contour c' to give

$$g\Delta z = \frac{\Delta z \sigma \oint_{c'} \vec{\mathcal{E}}_t \cdot \vec{a}'_n dl'}{V(z, t)} \quad (1.59a)$$

or

$$g = \frac{\sigma \oint_{c'} \vec{\mathcal{E}}_t \cdot \vec{a}'_n dl'}{V(z, t)} \quad (1.59b)$$

Substituting the definition of voltage given in (1.39) gives

$$g = \frac{\oint \vec{\mathcal{E}}_t \cdot \vec{a}'_n dl'}{-\int_c \vec{\mathcal{E}}_t \cdot d\vec{l}} \quad (1.60)$$

In Section 1.3.4, we will show that the per-unit-length parameters satisfy the following relations:

$$lc = \mu\varepsilon \quad (1.61)$$

$$gl = \sigma\mu \quad (1.62)$$

Taking the ratio of (1.61) and (1.62) or the ratio of (1.60) and (1.57) gives another relation:

$$\frac{g}{c} = \frac{\sigma}{\varepsilon} \quad (1.63)$$

Hence for a *homogeneous* medium surrounding the conductors that is characterized by the parameters σ , ε , and μ , we only need to determine one of the three parameters. For example, if we determine the per-unit-length capacitance c , then the other two parameters are obtained in terms of c as $l = (\mu\varepsilon/c)$ and $g = (\sigma/\varepsilon)c$.

1.3.3 Obtaining the Transmission-Line Equations from the Transverse Electromagnetic Field Equations

In Section 1.2 we showed that, for the TEM mode, the transverse field vectors satisfy the relations in (1.12):

$$-\frac{\partial \vec{\mathcal{E}}_t}{\partial z} = -\mu \left[\vec{a}_z \times \frac{\partial \vec{\mathcal{H}}_t}{\partial t} \right] \quad (1.12a)$$

$$-\frac{\partial \vec{\mathcal{H}}_t}{\partial z} = \sigma(\vec{a}_z \times \vec{\mathcal{E}}_t) + \varepsilon \left[\vec{a}_z \times \frac{\partial \vec{\mathcal{E}}_t}{\partial t} \right] \quad (1.12b)$$

Integrating (1.12a) along contour c to define the line voltage as given in (1.39) gives

$$\frac{\partial V(z, t)}{\partial z} = -\mu \frac{\partial}{\partial t} \int_c (\vec{a}_z \times \vec{\mathcal{H}}_t) \cdot d\vec{l} \quad (1.64)$$

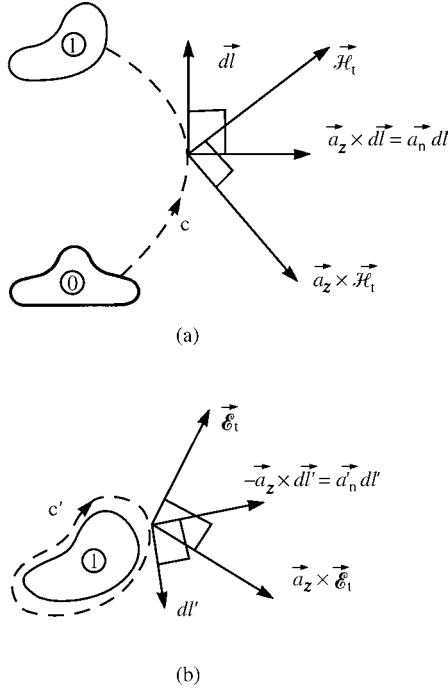


FIGURE 1.10 Illustration of the derivation of certain vector identities.

From Figure 1.10(a), we observe the identities:

$$\begin{aligned}
 (\vec{a}_z \times \vec{\mathcal{H}}_t) \cdot d\vec{l} &= -\vec{\mathcal{H}}_t \cdot (\vec{a}_z \times d\vec{l}) \\
 &= -\vec{\mathcal{H}}_t \cdot \vec{a}_n dl
 \end{aligned}
 \tag{1.65}$$

Substituting this into (1.64), we obtain

$$\frac{\partial V(z, t)}{\partial z} = \mu \frac{\partial}{\partial t} \int_c \vec{\mathcal{H}}_t \cdot \vec{a}_n dl
 \tag{1.66}$$

From the definition of the per-unit-length inductance in (1.53b), this becomes the first transmission-line equation:

$$\frac{\partial V(z, t)}{\partial z} = -l \frac{\partial I(z, t)}{\partial t}
 \tag{1.67}$$

Similarly, integrating (1.12b) around the closed contour c' to define the line currents as in (1.41) gives

$$\frac{\partial I(z, t)}{\partial z} = -\sigma \oint_{c'} (\vec{a}_z \times \vec{\mathcal{E}}_t) \cdot d\vec{l}' - \varepsilon \frac{\partial}{\partial t} \oint_{c'} (\vec{a}_z \times \vec{\mathcal{E}}_t) \cdot d\vec{l}' \quad (1.68)$$

From Figure 1.10(b), we observe the identities

$$\begin{aligned} (\vec{a}_z \times \vec{\mathcal{E}}_t) \cdot d\vec{l}' &= -\vec{\mathcal{E}}_t \cdot (\vec{a}_z \times d\vec{l}') \\ &= \vec{\mathcal{E}}_t \cdot \vec{a}'_n dl' \end{aligned} \quad (1.69)$$

Substituting this into (1.68) yields

$$\frac{\partial I(z, t)}{\partial z} = -\sigma \oint_{c'} \vec{\mathcal{E}}_t \cdot \vec{a}'_n dl' - \varepsilon \frac{\partial}{\partial t} \oint_{c'} \vec{\mathcal{E}}_t \cdot \vec{a}'_n dl' \quad (1.70)$$

Observing the definitions of the per-unit-length capacitance and conductance in (1.56b) and (1.59b), respectively, this gives the second transmission-line equation

$$\frac{\partial I(z, t)}{\partial z} = -gV(z, t) - c \frac{\partial V(z, t)}{\partial t} \quad (1.71)$$

1.3.4 Properties of the Per-Unit-Length Parameters

In this section, we will prove the important relations between the per-unit-length parameters given in (1.61) and (1.62):

$$lc = \mu\varepsilon \quad (1.61)$$

$$gl = \sigma\mu \quad (1.62)$$

which also give the relation

$$\frac{g}{c} = \frac{\sigma}{\varepsilon} \quad (1.63)$$

The first-order transmission-line differential equations in (1.67) and (1.71) are coupled in that V and I appear in each equation. They can be converted to uncoupled second-order equations by differentiating (1.67) with respect to z , differentiating (1.71) with respect to t , and then substituting and reversing the process to yield

$$\frac{\partial^2 V(z, t)}{\partial z^2} = gl \frac{\partial V(z, t)}{\partial t} + lc \frac{\partial^2 V(z, t)}{\partial t^2} \quad (1.72a)$$

$$\frac{\partial^2 I(z, t)}{\partial z^2} = gl \frac{\partial I(z, t)}{\partial t} + lc \frac{\partial^2 I(z, t)}{\partial t^2} \quad (1.72b)$$

The transverse field vectors were shown to satisfy the second-order differential equations given in (1.13):

$$\frac{\partial^2 \vec{\mathcal{E}}_t}{\partial z^2} = \mu\sigma \frac{\partial \vec{\mathcal{E}}_t}{\partial t} + \mu\varepsilon \frac{\partial^2 \vec{\mathcal{E}}_t}{\partial t^2} \quad (1.13a)$$

$$\frac{\partial^2 \vec{\mathcal{H}}_t}{\partial z^2} = \mu\sigma \frac{\partial \vec{\mathcal{H}}_t}{\partial t} + \mu\varepsilon \frac{\partial^2 \vec{\mathcal{H}}_t}{\partial t^2} \quad (1.13b)$$

Integrating these according to (1.39) and (1.41) in order to write them in terms of the line voltage and current gives

$$\frac{\partial^2 V(z, t)}{\partial z^2} = \mu\sigma \frac{\partial V(z, t)}{\partial t} + \mu\varepsilon \frac{\partial^2 V(z, t)}{\partial t^2} \quad (1.73a)$$

$$\frac{\partial^2 I(z, t)}{\partial z^2} = \mu\sigma \frac{\partial I(z, t)}{\partial t} + \mu\varepsilon \frac{\partial^2 I(z, t)}{\partial t^2} \quad (1.73b)$$

Comparing (1.73) to (1.72), we observe the important relations between the per-unit-length parameters:

$$gl = \mu\sigma \quad (1.74a)$$

$$lc = \mu\varepsilon \quad (1.74b)$$

Alternatively, we may obtain a direct proof of these relations between the per-unit-length parameters in the following manner. Write the product of the per-unit-length inductance and capacitance from their definitions in (1.54) and (1.57) as

$$lc = -\mu \frac{\int \vec{\mathcal{H}}_t \cdot \vec{a}_n dl}{\oint_{c'} \vec{\mathcal{H}}_t \cdot d\vec{l}'} \varepsilon \frac{\int \vec{\mathcal{E}}_t \cdot \vec{a}_n dl'}{-\int_c \vec{\mathcal{E}}_t \cdot d\vec{l}} \quad (1.75)$$

We showed in Section 1.2 that, for a lossless medium ($\sigma = 0$), the forward- and backward-traveling components of the waves are related by the intrinsic impedance of the medium as

$$\vec{\mathcal{E}}_t^\pm = \mp \eta (\vec{a}_z \times \vec{\mathcal{H}}_t^\pm) \quad (1.76a)$$

Taking the cross product of \vec{a}_z with both sides and using $\vec{a}_z \times (\vec{a}_z \times \vec{\mathcal{H}}_t) = -\vec{\mathcal{H}}_t$ yields

$$\vec{\mathcal{H}}_t^\pm = \pm \frac{1}{\eta} (\vec{a}_z \times \vec{\mathcal{E}}_t^\pm) \tag{1.76b}$$

Substituting these into (1.75) yields

$$lc = -\mu \frac{\int \pm \frac{1}{\eta} (\vec{a}_z \times \vec{\mathcal{E}}_t^\pm) \cdot \vec{a}_n dl \oint \mp \eta (\vec{a}_z \times \vec{\mathcal{H}}_t^\pm) \cdot \vec{a}'_n dl'}{\oint_{c'} \vec{\mathcal{H}}_t^\pm \cdot d\vec{l}'} \frac{\epsilon c'}{\oint_c \vec{\mathcal{E}}_t^\pm \cdot d\vec{l}} \tag{1.77}$$

From Figure 1.10 (replacing $\vec{\mathcal{E}}_t$ with $\vec{\mathcal{H}}_t$ and vice versa) we obtain the identities

$$(\vec{a}_z \times \vec{\mathcal{E}}_t^\pm) \cdot \vec{a}_n dl = \vec{\mathcal{E}}_t^\pm \cdot d\vec{l} \tag{1.78a}$$

and

$$(\vec{a}_z \times \vec{\mathcal{H}}_t^\pm) \cdot \vec{a}'_n dl' = -\vec{\mathcal{H}}_t^\pm \cdot d\vec{l}' \tag{1.78b}$$

Substituting these into (1.77) yields

$$lc = -\mu \frac{\pm \int_c \vec{\mathcal{E}}_t^\pm \cdot d\vec{l} \pm \oint_{c'} \vec{\mathcal{H}}_t^\pm \cdot d\vec{l}'}{\oint_{c'} \vec{\mathcal{H}}_t^\pm \cdot d\vec{l}'} \epsilon \frac{c'}{-\int_c \vec{\mathcal{E}}_t^\pm \cdot d\vec{l}} \tag{1.79}$$

$$= \mu \epsilon$$

Taking the ratio of the basic definitions of g in (1.60) and c in (1.57) gives the relation $g = (\sigma/\epsilon)c$. Substituting (1.79) into this gives the relation $gl = \sigma\mu$.

1.4 CLASSIFICATION OF TRANSMISSION LINES

One of the primary tasks in obtaining the complete solution for the voltage and current of a transmission line is the general solution of the transmission-line equations (Step 2). The type of line being considered significantly affects this solution. We are familiar with the difficulties in the solution of various ordinary differential equations encountered in the analysis of lumped circuits [A.2,A.5]. An example of an ordinary differential equation encountered in lumped-circuit analysis is

$$\frac{dV(t)}{dt} + aV(t) = b \sin(\omega t)$$

Although the equations to be solved for lumped systems are ordinary differential equations (there is only one independent variable, time t) and are somewhat simpler to solve than the transmission-line equations, which are partial differential equations (since the voltage and current are functions of two independent variables, time t and position along the line z), the type of circuit strongly affects the solution difficulty. For example, if any of the circuit elements are functions of time (a time-varying circuit), then the coefficients in the equation, for example, a , will be functions of the independent variable, t . An example is

$$\frac{dV(t)}{dt} + a(t)V(t) = b \sin(\omega t)$$

These equations, although linear, are said to be *nonconstant coefficient ordinary differential equations*, which are considerably more difficult to solve than constant coefficient ones [A.4]. Suppose one or more of the circuit elements are *nonlinear*; that is, the element voltage has a nonlinear relation to its current. In this case, the circuit differential equations become *nonlinear ordinary differential equations*, which are equally difficult to solve [A.4]. So the class of lumped circuit being considered drastically affects the difficulty of solution of the governing differential equations.

1.4.1 Uniform versus Nonuniform Lines

Solution of the transmission-line partial differential equations has similar parallels. We have been implicitly assuming that the per-unit-length parameters are independent of position along the line z and, of course, time t . The per-unit-length parameters contain all the cross-sectional structural dimensions of the line. If the cross-sectional dimensions of the line vary along the line axis, then the per-unit-length parameters will be functions of the position variable, z , for example, $g(z)$, $c(z)$, and $l(z)$. This makes the resulting transmission-line equations very difficult to solve because the coefficients, the per-unit-length parameters, will be functions of one of the independent variables in the same fashion as a nonconstant coefficient ordinary differential equation:

$$\frac{\partial V(z, t)}{\partial z} = -l(z) \frac{\partial I(z, t)}{\partial t}$$

$$\frac{\partial I(z, t)}{\partial z} = -g(z)V(z, t) - c(z) \frac{\partial V(z, t)}{\partial t}$$

Such transmission-line structures are said to be *nonuniform lines*. This includes both the cross-sectional dimensions of the line conductors and the cross-sectional dimensions of any inhomogeneous surrounding medium. If the cross-sectional dimensions of both the line conductors and the surrounding, perhaps inhomogeneous, medium are *constant along the line axis*, the line is said to be a *uniform line* whose resulting differential equations are simple to solve because the per-unit-length parameters l , c , and g are constants independent of z . An example of a nonuniform (in conductor cross

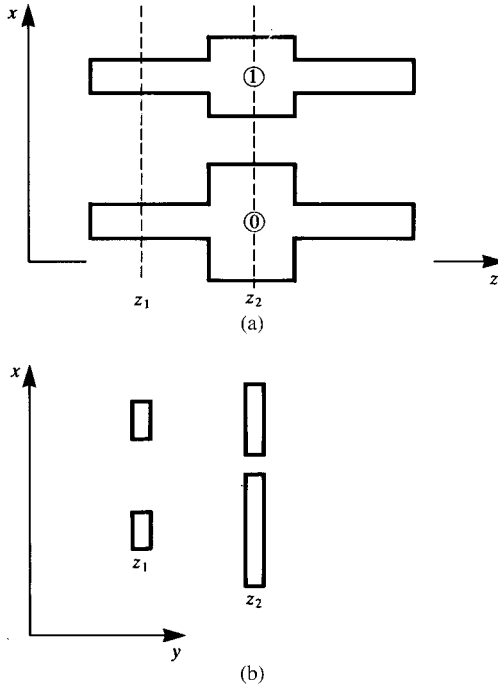


FIGURE 1.11 Illustration of a nonuniform line caused by variations in the conductor cross section.

section) line is shown in Figure 1.11. Figure 1.11(a) shows the view along the line axis, whereas Figure 1.11(b) shows the view in cross section. Because the conductor cross sections are different at z_1 and z_2 , the per-unit-length parameters will be functions of position z . This type of structure occurs frequently on printed circuit boards. A common way of handling this is to divide the line into three uniform sections and cascade the representations. This is an approximation since it neglects the fringing of the fields at the junctions. Figure 1.12 shows a nonuniform line where the nonuniformity is introduced by the inhomogeneous medium. A wire is surrounded by dielectric insulation. Along the two end segments, the medium is inhomogeneous since in one part of the region the fields exist in the dielectric insulation, ϵ_1, μ_0 , and in the other they exist in free space, ϵ_0, μ_0 . In the middle region, the dielectric insulation is also inhomogeneous consisting of regions containing $\epsilon_1, \mu_0, \epsilon_2, \mu_0$ and ϵ_0, μ_0 . However, because of this change in the properties of the surrounding medium from one section to the next, the total line is a *nonuniform* one and the resulting per-unit-length parameters will be functions of z . The resulting transmission-line equations for Figures 1.11 and 1.12 are very difficult to solve because of the nonuniformity of the line. Again, a common way of analyzing this type of problem is to partition the line into a cascade of uniform subsections. This is, again, an approximation since it neglects the fringing of the fields at the junctions.

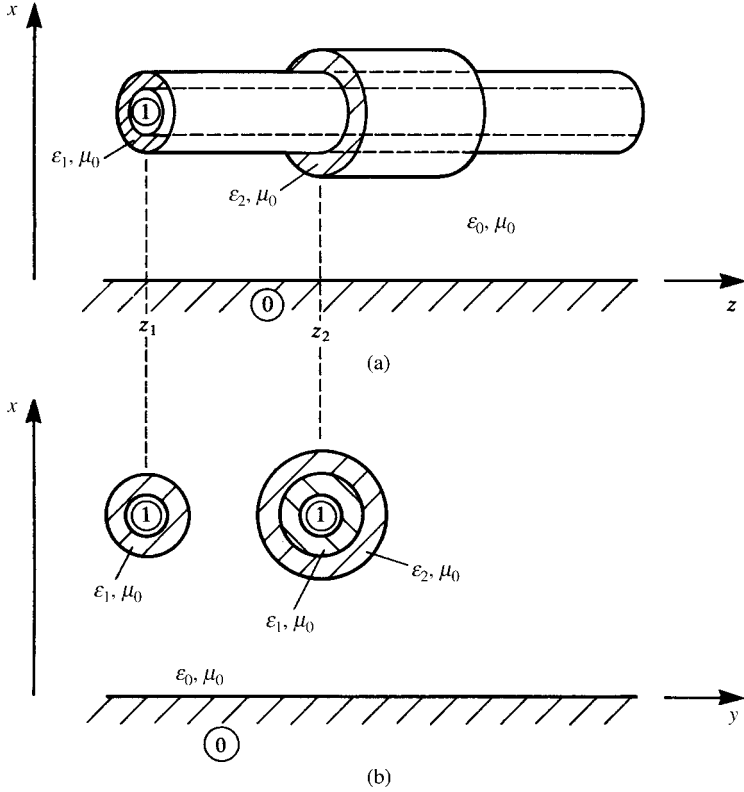


FIGURE 1.12 Illustration of a nonuniform line caused by variations in the surrounding medium cross section.

1.4.2 Homogeneous versus Inhomogeneous Surrounding Media

Figure 1.1 shows lines in a homogeneous medium; that is, there is one dielectric surrounding the conductors and hence the permittivity, conductivity, and permeability are independent of position in the space surrounding the conductors. Dielectric insulations surrounding wires such as in ribbon cables are examples of inhomogeneous media since the electric field lines will be partly in this dielectric insulation and partly in the remaining free space. The PCB structures in Figure 1.2(b) and (c) are also examples of lines in an inhomogeneous medium. The electric field lines will lie partly in the dielectric substrate and partly in the remaining free space. For structures in a homogeneous medium such as the wire-type structures in Figure 1.1 and the coupled stripline in Figure 1.2(a), all waves will travel at the same velocity. For lines consisting of $n + 1$ conductors in an inhomogeneous medium, there will be n waves each traveling with different velocities. This complicates the solution of the transmission-line equations as we will see later.

There are numerous combinations of these characterizations. A line may be in a homogeneous medium yet because of a change in the conductor cross sections along the line, it would be classified as a nonuniform line and would be very difficult to solve. A line may be in an inhomogeneous medium but because this inhomogeneity as well as the conductor cross sections do not change along the line axis, it would be classified as a uniform line. It would be relatively simple to solve. For these reasons, we will restrict the transmission lines that we will consider in this text to be *uniform lines*. They may, however, be in a *homogeneous or an inhomogeneous medium*. In either case, a *uniform line* has (a) conductor cross sections that do not vary with z and (b) surrounding dielectric properties that may be functions of x and y but do not vary with z .

Technically, an inhomogeneous surrounding medium, although uniform along the line (z) axis, invalidates the basic assumption of a TEM field structure. The reason for this is that a TEM field structure must have one and only one velocity of propagation of the waves in the medium. However, this cannot be the case for an inhomogeneous medium. If one portion of the inhomogeneous medium is characterized by ϵ_1, μ_0 and the other is characterized by ϵ_2, μ_0 , such as for the lines in Figure 1.2(b) and (c), the velocities of TEM waves in infinite, homogeneous regions characterized by these parameters will be $v_1 = 1/\sqrt{\epsilon_1\mu_0}$ and $v_2 = 1/\sqrt{\epsilon_2\mu_0}$, which will be different. Nevertheless, the transmission-line equations are usually solved in spite of this observation and are assumed to adequately represent the situation so long as these velocities are not substantially different. This is referred to as the *quasi-TEM assumption*.

1.4.3 Lossless versus Lossy Lines

All of the previous derivations include losses in the medium through a per-unit-length conductance parameter g . This loss in the surrounding (assumed homogeneous) medium does not invalidate the TEM field structure assumption. However, the previous derivations also assumed *perfect conductors*. In other words, the conductors were assumed to be lossless and to have no resistance properties along their z axes. Practical transmission lines are obviously constructed of imperfect conductors that have loss. However, in order that the transmission line be a useful guided wave structure, these conductor losses must be small. Nevertheless, how shall we include these losses and what will be their effect on the ideal assumption of a TEM field structure?

We may include the possibility of the line conductors being *imperfect conductors* with small losses through a per-unit-length resistance parameter r . Unlike losses in the surrounding medium, *lossy conductors implicitly invalidate the TEM field structure assumption*. Figure 1.13 shows why this is the case. The line current flowing through the imperfect line conductor generates a nonzero electric field along the conductor surface, $\mathcal{E}_z(z, t) = rI(z, t)$, which is directed in the z direction, thereby violating the basic assumption of the TEM field structure in the surrounding medium. The total electric field is the sum of the transverse component and this z -directed component.

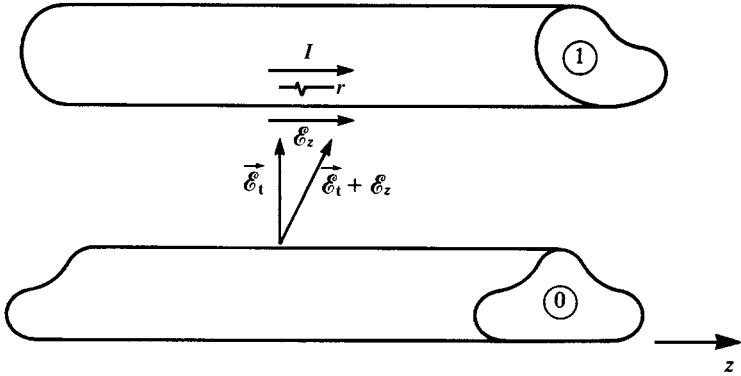


FIGURE 1.13 Illustration of the effect of conductor losses in creating non-TEM fields.

However, if the conductor losses are small, this resulting field structure is *almost similar to a TEM structure*. This is again referred to as the *quasi-TEM assumption* and, although the transmission-line equations are no longer valid, they are nevertheless assumed to represent the situation for small losses through the inclusion of the per-unit-length resistance parameter r . In the derivation of the transmission-line equations for an MTL, we will include this parameter.

In summary, the TEM field structure and mode of propagation characterization of a transmission line is valid only for uniform lines consisting of perfect conductors and surrounded by a homogeneous medium. Note that this medium may be lossy and not violate the TEM assumption so long as it is homogeneous (in σ , ϵ , and μ). Violations of these assumptions (lossy conductors and/or an inhomogeneous medium surrounding the conductors) are considered under the *quasi-TEM* assumption so long as they are not extreme [17, 18].

1.5 RESTRICTIONS ON THE APPLICABILITY OF THE TRANSMISSION-LINE EQUATION FORMULATION

There are some additional, implicit assumptions in the TEM transmission-line equation characterization. In the derivation of the transmission-line equations from the distributed-parameter lumped circuit of Figure 1.8, distributing the lumped elements along the line and allowing the section length to go to zero, $\lim_{\Delta z \rightarrow 0} \Delta z$, means that line lengths that are *electrically long*, that is, much greater than a wavelength λ , are properly handled with this lumped-circuit characterization. However, it was assumed that the line cross-sectional dimensions such as conductor separations were electrically small at the frequencies of excitation of the line. Structures whose cross-sectional dimensions are electrically large at the frequency of excitation will have, in addition to the TEM field structure and mode of propagation, other higher order

TE and TM field structures and modes of propagation simultaneously with the TEM mode [A.1, 17–19]. Therefore, the solution of the transmission-line equations does not give the complete solution in the range of frequencies where these non-TEM modes coexist on the line. A comparison of the predictions of the TEM transmission-line equation results with the results of a numerical code (which does not presuppose existence of only the TEM mode) for a two-wire line showed differences beginning with frequencies where the wire separations were as small as $\lambda/40$ [H.7]. Analytical solution of Maxwell's equations in order to consider the total effect of all modes is usually a formidable task. There are certain structures where an analytical solution is feasible, and we will discuss these in the next two sections.

1.5.1 Higher Order Modes

In the following two subsections, we analytically solve Maxwell's equations for two *closed structures* to obtain the complete solution and demonstrate that the TEM formulation is complete up to some frequency where the conductor separations are some significant fraction of a wavelength above which higher order modes begin to propagate.

1.5.1.1 The Infinite, Parallel-Plate Transmission Line Consider the *infinite, parallel-plate transmission line* shown in Figure 1.14. The two infinite and perfectly conducting plates lie in the y - z plane and are located at $x = 0$ and $x = a$. We will obtain the complete solutions for the fields in the space between the two plates, which is assumed to be homogeneous and lossless and characterized by ϵ and μ . Maxwell's equations for sinusoidal excitation become

$$\nabla \times \vec{E} = -j\omega\mu\vec{H} \quad (1.80a)$$

$$\nabla \times \vec{H} = j\omega\epsilon\vec{E} \quad (1.80b)$$

Expanding these and noting that the plates are infinite in extent in the y direction so that $\frac{\partial}{\partial y} = 0$ gives [A.1]

$$\begin{aligned} \frac{\partial E_y}{\partial z} &= j\omega\mu H_x \\ \frac{\partial E_x}{\partial z} - \frac{\partial E_z}{\partial x} &= -j\omega\mu H_y \\ \frac{\partial E_y}{\partial x} &= -j\omega\mu H_z \\ \frac{\partial H_y}{\partial z} &= -j\omega\epsilon E_x \\ \frac{\partial H_x}{\partial z} - \frac{\partial H_z}{\partial x} &= j\omega\epsilon E_y \\ \frac{\partial H_y}{\partial x} &= j\omega\epsilon E_z \end{aligned} \quad (1.81)$$

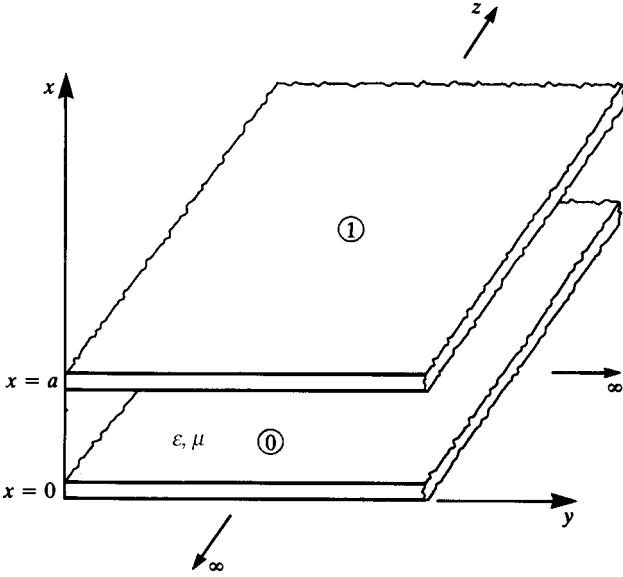


FIGURE 1.14 The infinite parallel-plate waveguide for demonstrating the effect of cross-sectional dimensions on higher order modes.

In addition, we have the *wave equations* [A.1]:

$$\begin{aligned} \nabla^2 \vec{E} + \omega^2 \mu \epsilon \vec{E} &= 0 \\ \nabla^2 \vec{H} + \omega^2 \mu \epsilon \vec{H} &= 0 \end{aligned} \tag{1.82}$$

Expanding these and recalling that the plates are infinite in the *y* dimension so that $\frac{\partial}{\partial y} = 0$ gives [A.1]

$$\begin{aligned} \frac{\partial^2 \vec{E}}{\partial x^2} + \frac{\partial^2 \vec{E}}{\partial z^2} + \omega^2 \mu \epsilon \vec{E} &= 0 \\ \frac{\partial^2 \vec{H}}{\partial x^2} + \frac{\partial^2 \vec{H}}{\partial z^2} + \omega^2 \mu \epsilon \vec{H} &= 0 \end{aligned} \tag{1.83}$$

Let us now look for waves propagating in the *+z* direction. To do so, we use the principle of *separation of variables*, where we separate the dependence on *x*, *y*, and *z* as

$$\vec{E}(x, y, z) = \vec{E}'(x, y)e^{-\gamma z} \tag{1.84}$$

where γ is the propagation constant (to be determined). Substituting this into (1.81) yields

$$\begin{aligned}
 \gamma E'_y &= -j\omega\mu H'_x \\
 -\gamma E'_x - \frac{\partial E'_z}{\partial x} &= -j\omega\mu H'_y \\
 \frac{\partial E'_y}{\partial x} &= -j\omega\mu H'_z \\
 \gamma H'_y &= j\omega\varepsilon E'_x \\
 -\gamma H'_x - \frac{\partial H'_z}{\partial x} &= j\omega\varepsilon E'_y \\
 \frac{\partial H'_y}{\partial x} &= j\omega\varepsilon E'_z
 \end{aligned} \tag{1.85}$$

and

$$\begin{aligned}
 \frac{\partial^2 \vec{E}'}{\partial x^2} + (\gamma^2 + \omega^2\mu\varepsilon)\vec{E}' &= 0 \\
 \frac{\partial^2 \vec{H}'}{\partial x^2} + (\gamma^2 + \omega^2\mu\varepsilon)\vec{H}' &= 0
 \end{aligned} \tag{1.86}$$

The equations in (1.85) can be manipulated to yield [A.1]

$$\begin{aligned}
 H'_x &= -\frac{\gamma}{h^2} \frac{\partial H'_z}{\partial x} \\
 E'_x &= -\frac{\gamma}{h^2} \frac{\partial E'_z}{\partial x} \\
 H'_y &= -\frac{j\omega\varepsilon}{h^2} \frac{\partial E'_z}{\partial x} \\
 E'_y &= \frac{j\omega\mu}{h^2} \frac{\partial H'_z}{\partial x} \\
 h^2 &= \gamma^2 + \omega^2\mu\varepsilon
 \end{aligned} \tag{1.87}$$

Observe that $E'(x, y)$ and $H'(x, y)$ are functions of x only since there can be no variation in the y direction due to the infinite extent of the plates in this direction and also the z variation has been assumed. Thus the partial derivatives in (1.85)–(1.87) can be replaced by ordinary derivatives. We now investigate the various modes of propagation.

The Transverse Electric (TE) Mode ($E_z = 0$) The TE mode of propagation assumes that the electric field is confined to the transverse or x – y plane so that $E_z = 0$. Therefore, from (1.87) we see that $E'_x = H'_y = 0$. The wave equations in (1.86) reduce to

$$\frac{d^2 E'_y}{dx^2} + h^2 E'_y = 0 \tag{1.88}$$

whose general solution is

$$E'_y = C_1 \sin(hx) + C_2 \cos(hx) \quad (1.89)$$

The boundary conditions are such that the electric field tangent to the surfaces of the plates is zero:

$$E_y = 0|_{x=0, x=a} \quad (1.90)$$

which, when applied to (1.89), yields $C_2 = 0$ and $ha = m$ for $m = 0, 1, 2, 3, \dots$. Thus, the solution becomes

$$E_y = C_1 \sin\left(\frac{m\pi x}{a}\right) e^{-\gamma z} \quad (1.91)$$

From (1.85) we obtain

$$\begin{aligned} H_z &= j \frac{1}{\omega\mu} \frac{\partial E_y}{\partial x} \\ &= j \frac{m\pi}{\omega\mu a} C_1 \cos\left(\frac{m\pi x}{a}\right) e^{-\gamma z} \end{aligned} \quad (1.92)$$

and

$$H_x = j \frac{\gamma}{\omega\mu} C_1 \sin\left(\frac{m\pi x}{a}\right) e^{-\gamma z} \quad (1.93)$$

Since

$$h = \frac{m\pi}{a} \quad (1.94)$$

the propagation constant becomes

$$\gamma = \sqrt{\left(\frac{m\pi}{a}\right)^2 - \omega^2 \mu \epsilon} \quad (1.95)$$

For the lowest order mode, $m = 0$, all field components vanish. The next higher order mode is the TE_1 mode for $m = 1$.

The Transverse Magnetic (TM) Mode ($H_z = 0$) The TM mode has the magnetic field confined to the transverse x - y plane so that $H_z = 0$. Carrying through a development similar to the above for this mode gives the nonzero field vectors as

$$\begin{aligned} H_y &= D_2 \cos\left(\frac{n\pi x}{a}\right) e^{-\gamma z} \\ E_x &= -j \frac{\gamma}{\omega\epsilon} D_2 \cos\left(\frac{n\pi x}{a}\right) e^{-\gamma z} \\ E_z &= j \frac{n\pi}{a\omega\epsilon} D_2 \sin\left(\frac{n\pi x}{a}\right) e^{-\gamma z} \end{aligned} \quad (1.96)$$

for $n = 0, 1, 2, \dots$. The propagation constant is again given by (1.95) with m replaced by n . In contrast to the TE modes, the lowest order TM mode is the TM_0 mode for $n = 0$. For this case, the propagation constant reduces to the familiar

$$\begin{aligned}\gamma &= j\omega\sqrt{\mu\varepsilon} \\ &= j\beta\end{aligned}\tag{1.97}$$

and the field vectors in (1.96) reduce to

$$\begin{aligned}H_y &= D_2 e^{-j\beta z} \\ E_x &= -j \frac{\gamma}{\omega\varepsilon} D_2 e^{-j\beta z} \\ &= \sqrt{\frac{\mu}{\varepsilon}} D_2 e^{-j\beta z} \\ E_z &= 0\end{aligned}\tag{1.98}$$

However, this is the TEM mode!

The transmission-line equations for this TEM mode can be obtained by differentiating (1.98) with respect to z to yield

$$\begin{aligned}\frac{dE_x}{dz} &= -j\omega\mu H_y \\ \frac{dH_y}{dz} &= -j\omega\varepsilon E_x\end{aligned}\tag{1.99}$$

We may write these in terms of voltage and current by integrating in the transverse plane:

$$\begin{aligned}V(z) &= - \int_{x=0}^{x=a} E_x dx \\ &= -aE_x\end{aligned}\tag{1.100a}$$

and

$$I(z) = -wH_y\tag{1.100b}$$

The result for the current in (1.100b) is due to the fact that the H field is tangent to the upper and lower plates that are assumed to be perfect conductors and hence produces a surface current on the plate $J_{sz} = -H_y|_{x=a}$ in A/m that is directed in the z direction. In a section of width w along the y dimension, the total current is $J_{sz}w = -H_y w$ A.

Hence (1.99) becomes

$$\begin{aligned}
 \frac{dV}{dz} &= j\omega\mu \int_{x=0}^{x=a} H_y dx \\
 &= -j\omega \underbrace{\left(\mu \frac{a}{w}\right)}_l \underbrace{(-H_y w)}_I \\
 \frac{dI}{dz} &= -j\omega \underbrace{\left(\varepsilon \frac{w}{a}\right)}_c V
 \end{aligned} \tag{1.101}$$

and the per-unit-length inductance and capacitance are then defined as

$$\begin{aligned}
 l &= \mu \frac{a}{w} \quad \text{H/m} \\
 c &= \varepsilon \frac{w}{a} \quad \text{F/m}
 \end{aligned} \tag{1.102}$$

Therefore, the lowest order TM mode, TM_0 , is equivalent to the TEM mode and the TE_0 mode is nonexistent. We must then ascertain when the next higher order modes begin to propagate, thus adding to the total picture. The propagation constant in (1.95) must be imaginary or at least have a nonzero imaginary part. Clearly, for $m = n = 0$, we have the propagation constant of a plane wave: $\gamma = j\omega\sqrt{\mu\varepsilon} = j\beta$. For higher order modes to propagate, we require from (1.95) that $\omega^2\mu\varepsilon \geq h^2$, giving

$$\omega \geq \frac{1}{\sqrt{\mu\varepsilon}} \frac{n\pi}{a} \tag{1.103}$$

The cutoff frequency for the lowest order TEM mode, TM_0 , is clearly dc. The cutoff frequencies of the next higher order modes, TE_1 and TM_1 , are from (1.103)

$$\begin{aligned}
 f_{\text{TE}_1, \text{TM}_1} &= \frac{1}{2\pi\sqrt{\mu\varepsilon}} \frac{\pi}{a} \\
 &= \frac{v}{2a}
 \end{aligned} \tag{1.104}$$

In terms of wavelength, $\lambda = v/f$, we find that the TEM mode will be the only possible mode so long as the plate separation a is less than one-half wavelength, that is,

$$a < \frac{\lambda}{2} \tag{1.105}$$

This illustrates that so long as the cross-sectional dimensions of the line are electrically small, only the TEM mode can propagate! This is illustrated in Figure 1.15.

1.5.1.2 The Coaxial Transmission Line Another *closed system* transmission line that is capable of supporting the TEM mode is the *coaxial transmission line* shown in

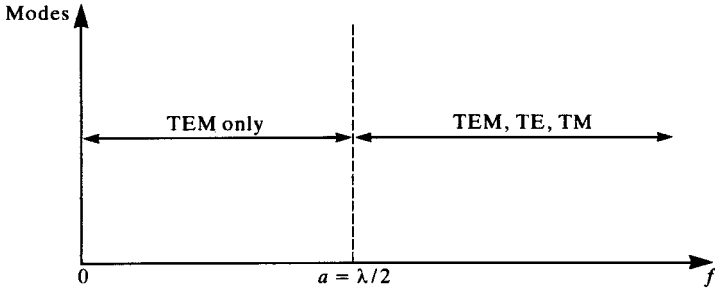


FIGURE 1.15 Illustration of the dependence of higher order modes on cross-sectional electrical dimensions for the parallel-plate transmission line.

Figure 1.16. The general solution to Maxwell’s equations for the fields and modes in the space between the inner wire and the outer shield was obtained in [1]. Clearly, this structure can support the TEM mode with a cutoff frequency of dc. The higher order TE and TM modes have the following cutoff properties. The lowest order TE mode is cutoff for frequencies such that the average circumference between the conductors is less than approximately a wavelength, that is,

$$2\pi \frac{(a + b)}{2} < \lambda \tag{1.106}$$

Similarly, the lowest order TM mode is cutoff for frequencies such that the difference between the two conductor radii is less than approximately one-half wavelength, that is,

$$(b - a) < \frac{\lambda}{2} \tag{1.107}$$

These results again support the notion that the TEM mode will be the only mode of propagation in closed systems so long as the conductor separation is electrically small.

1.5.1.3 Two-Wire Lines The previous two transmission-line structures are closed systems. For *open systems* such as the two-wire line, the issue of higher order modes is not so clear-cut. Numerical analysis of a two-wire line given in [H.7] showed that the predictions of the transmission-line formulation for the two-wire line began



FIGURE 1.16 The coaxial cable for illustrating the dependence of higher order modes on cross-sectional electrical dimensions.

to deviate from the complete solution when the cross-sectional dimensions such as wire separation are no longer electrically small. This supports our intuition. The problem was investigated in more detail in [19] where these notions are confirmed. Also certain other modes are capable of propagating with no clearly defined cutoff frequency. However, the TEM mode formulation and the resulting transmission-line equation representation for two-wire lines will be reasonably adequate so long as the wire separations are electrically small. Ordinarily, this is satisfied for practical transmission-line structures.

1.5.2 Transmission-Line Currents versus Antenna Currents

There is one remaining restriction on the completeness of the TEM mode, transmission-line representation that needs to be discussed. It can be shown that under the TEM transmission-line equation formulation for a two-conductor line, the currents so determined on the two conductors at any cross section must be equal in magnitude and oppositely directed (see Problem 1.3). Thus, the total current at any cross section is zero. This is the origin of the reference to the term that one of the conductors serves as a “return” for the current on the other conductor. On a transmission line, there may also be currents that do not sum to zero at any cross section. These so-called “antenna currents” or “common-mode currents” tend to go to zero at the line endpoints. Hence, their presence along the line does not substantially change the predictions of the terminal voltages and currents. Therefore, in the usual use of the transmission-line model to predict crosstalk and signal integrity on transmission lines, the TEM transmission-line equations give substantially the complete result.

Consider the pair of parallel wires shown in Figure 1.17(a) carrying, at the same cross section, currents I_1 and I_2 . In general, we may decompose or represent these as a linear combination of two other currents. The so-called *differential-mode currents* I_D are equal in magnitude at a cross section and are oppositely directed, as shown in Figure 1.17(b). These correspond to the TEM mode, transmission-line currents that will be predicted by the transmission-line model. The other currents are the so-called *common-mode currents* I_C which are equal in magnitude at a cross section but are directed in the same direction, as shown in Figure 1.17(c). These are sometimes referred to as “antenna-mode” currents [20, 21]. This decomposition can be obtained by writing, from Figure 1.17,

$$\begin{aligned} I_1 &= I_C + I_D \\ I_2 &= I_C - I_D \end{aligned} \tag{1.108}$$

In matrix form, these can be written as

$$\begin{bmatrix} I_1 \\ I_2 \end{bmatrix} = \begin{bmatrix} 1 & 1 \\ 1 & -1 \end{bmatrix} \begin{bmatrix} I_C \\ I_D \end{bmatrix} \tag{1.109}$$

Equation (1.109) represents a nonsingular transformation between the two sets of currents since the transformation matrix is nonsingular. Therefore, its inverse can be

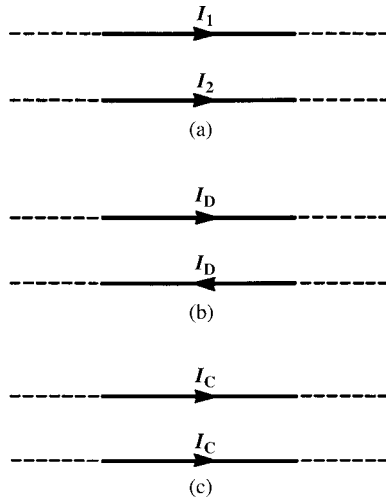


FIGURE 1.17 Illustration of the decomposition of total currents into differential-mode (transmission-line mode) and common-mode (antenna mode) components.

taken and the transformation reversed to yield

$$\begin{bmatrix} I_C \\ I_D \end{bmatrix} = \frac{1}{2} \begin{bmatrix} 1 & 1 \\ 1 & -1 \end{bmatrix} \begin{bmatrix} I_1 \\ I_2 \end{bmatrix} \quad (1.110)$$

This gives

$$\begin{aligned} I_C &= \frac{I_1 + I_2}{2} \\ I_D &= \frac{I_1 - I_2}{2} \end{aligned} \quad (1.111)$$

Note that $I_2 \cong -I_1$; that is, in a normal situation, one current “returns” to its source on the other conductor. Hence, $I_C \ll I_D$. Therefore, the common-mode currents are much smaller in magnitude than the differential-mode currents and so do not substantially affect the results of an analysis of currents and voltages of a transmission line. However, in the prediction of radiated emissions from this two-wire line, the common-mode currents are significant because the radiated electric fields from the differential-mode currents tend to subtract, but those from the common-mode currents tend to add. Thus, a “small” common-mode current can give the same order of magnitude of radiated emission as a much larger differential-mode current. This was confirmed for cables and PCBs in [A.3,22,23]. The significant point here is that if one bases a prediction of the *radiated emissions* from a two-conductor line on the currents obtained from a transmission-line equation analysis, the predicted emissions will generally lie far below those of the emissions due to the common-mode currents. On the contrary, the common-mode currents can generally be ignored in a near-field transmission-line analysis such as in determining *crossstalk*.

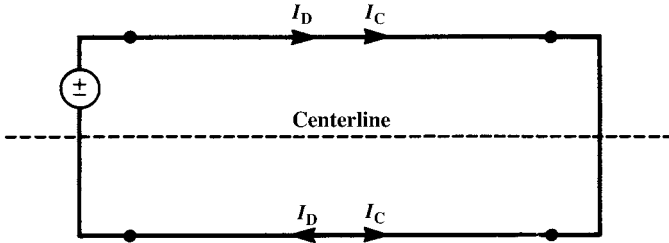


FIGURE 1.18 Illustration of an asymmetry that creates common-mode currents.

There are a number of ways through which these non-TEM mode currents can be created on a transmission line. Figure 1.18 illustrates one of these. It is important to remember that the TEM mode, transmission-line equation formulation only characterizes the line and assumes that the two (or more) conductors of the line continue indefinitely along the z axis. The analysis does not inherently consider the field effects of the eventual terminations for a finite-length line. This problem was investigated in [24]. It was found that *asymmetries* as well as the presence of nearby metallic structures create these “nonideal” currents. For example, consider the two-wire line shown in Figure 1.18, which is driven by a voltage source at the left end and terminated in a short circuit at the right end. This was analyzed using a numerical solution of Maxwell’s equations, commonly referred to as a method of moments (MoM). This analysis gives the complete solution for the currents without presupposing the existence of only the TEM mode. It was found that if the voltage source was situated and modeled as being centered in the left segment on the centerline, then $I_2 = -I_1$; in other words, the currents on the wires are only differential-mode currents. However, if the voltage source was placed asymmetrically to the centerline such as shown and the resulting currents decomposed as in (1.111), common-mode currents appeared. This asymmetrical placement of the source, which is not explicitly considered in the transmission-line equation formulation, was apparently the source.

The important point here is that the TEM mode, transmission-line equation formulation that we will consider in this text predicts only the differential-mode currents. If the line cross section is electrically small and one is interested only in predicting the currents and voltages on the line for the purposes of predicting signal distortion and *crosstalk* (the primary goal of this text), this prediction will be reasonably accurate. On the contrary, if one is interested in predicting the radiated electric field from this line, then the predictions of that field using only the currents predicted by the transmission-line equation formulation will most likely be inadequate since the contributions due to the common-mode currents typically are frequently the dominant contributors to radiated emissions [22, 23].

1.6 THE TIME DOMAIN VERSUS THE FREQUENCY DOMAIN

The two important domains that we will use throughout this text to analyze transmission-line structures are the *time domain* and the *frequency domain*. It is

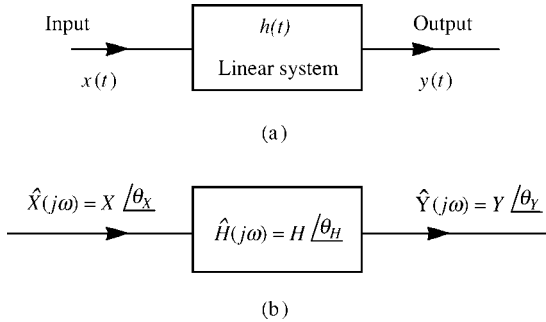


FIGURE 1.19 Illustration of the concept of a transfer function for a linear system.

critically important that we understand these two notions since they will form the heart of our analyses. First, let us discuss viewing the transmission-line problem as a *single-input, single-output* system as illustrated in Figure 1.19(a). This is a very standard way of viewing a system [A.2,A.5]. An input $x(t)$ is applied to the system (which we suppose here is a linear one) and produces the output $y(t)$. The system may be characterized by its *impulse response* $h(t)$. Analysis in the *time domain* refers to applying a signal or waveform that has some general shape and dependence on time t and determining the output or solution as a general waveform $y(t)$. Although not strictly required, we may obtain this solution in terms of the impulse response $h(t)$. The impulse response is the response when a unit impulse function is applied at the input; that is, if $x(t) = \delta(t)$, then $y(t) = h(t)$. The *time-domain solution* may be obtained with the *convolution integral* [A.2,A.5]:

$$y(t) = \int_0^t h(t - \tau)x(\tau)d\tau \quad (1.112)$$

Analysis in the *frequency domain* refers to applying a single-frequency sinusoidal waveform

$$x(t) = X \cos(\omega t + \theta_X) \quad (1.113)$$

and determining the output under the assumption that the system response has reached *steady state*. For a linear system, the response will be of the same form and the same frequency as the input signal but with a different amplitude and phase:

$$y(t) = Y \cos(\omega t + \theta_Y) \quad (1.114)$$

To analyze the response of the system, we move to the frequency domain by replacing time quantities with their complex-valued *phasor* equivalents [A.2,A.5]:

$$x(t) = X \cos(\omega t + \theta_X) \Rightarrow \hat{X}(j\omega) = X \angle \theta_X \quad (1.115a)$$

$$y(t) = Y \cos(\omega t + \theta_Y) \Rightarrow \hat{Y}(j\omega) = Y \angle \theta_Y \quad (1.115b)$$

as illustrated in Figure 1.19(b), and we write all complex-valued quantities with a caret ($\hat{\cdot}$) over them and $j = \sqrt{-1}$. The impulse response in the frequency domain is the familiar *transfer function* or *frequency response* that also has a magnitude and a phase:

$$h(t) \Rightarrow \hat{H}(j\omega) = H \angle \theta_H \quad (1.115c)$$

In order to obtain this frequency response, we apply a unit amplitude, zero phase input sinusoidal signal, sweep its frequency, and determine the response magnitude and phase at each applied frequency:

$$\hat{X} = 1 \angle 0^\circ \Rightarrow \hat{Y} = H \angle \theta_H \quad (1.116)$$

Then the solution process in the *frequency domain* is to obtain the magnitude and phase of the output using complex algebra as

$$Y \angle \theta_Y = H \angle \theta_H \times X \angle \theta_X \quad (1.117)$$

The result is obtained by multiplying magnitudes and adding angles in accordance with the rules of complex arithmetic [A.2.A.5]:

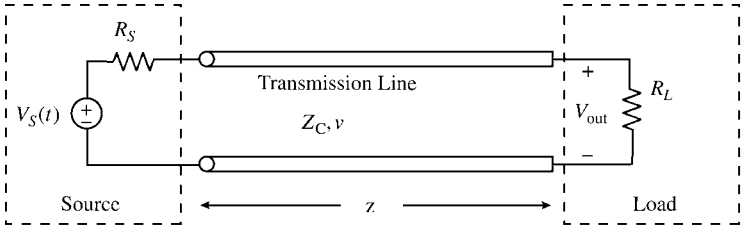
$$\hat{Y} = (HX) \angle (\theta_H + \theta_X) \quad (1.118)$$

Having done this, we return to the *time domain* by (a) multiplying the phasor result by $e^{j\omega t}$ and (b) taking the real part of the result:

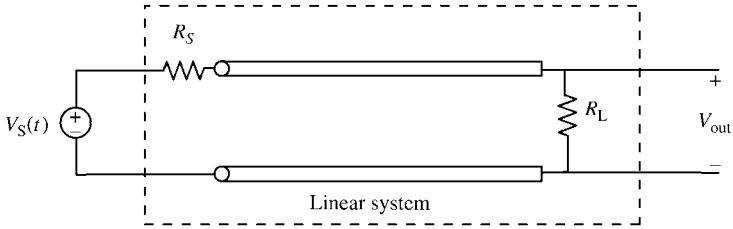
$$\begin{aligned} y(t) &= \text{Re}\{\hat{Y} e^{j\omega t}\} \\ &= HX \cos(\omega t + \theta_H + \theta_X) \end{aligned} \quad (1.119)$$

This phasor analysis method is virtually the heart of all analyses of electrical engineering systems as well as other dynamical systems.

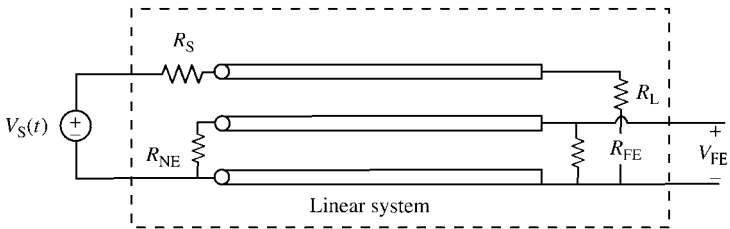
We may represent a two-conductor transmission-line problem in the form of a single-input, single-output system as shown in Figure 1.20. Consider a general source and load termination of a transmission line shown in Figure 1.20(a). The source consists of an open-circuit voltage source, $V_S(t)$, and a source resistance, R_S . The load represents, perhaps, the input to a device and is represented by the resistor R_L . We may be interested in determining, for example, the output voltage across the load, $V_{\text{out}}(t)$. In order to put this into the form of a single-input, single-output system as illustrated in Figure 1.19(a), we consider the input to the system to be the voltage source, $x(t) = V_S(t)$, and the output to be the voltage across the load resistor, $y(t) = V_{\text{out}}(t)$. Hence we imbed the line and the termination resistors in the system as shown in Figure 1.20(b). It is very important to observe that the “system” contains the termination resistors. Hence, nonlinear terminations render the problem a nonlinear one, and the phasor solution method is no longer valid. In the case of a multiconductor



(a)



(b)



(c)

FIGURE 1.20 Characterizing a transmission line as a single-input, single-output system.

line as shown in Figure 1.20(c), the input is again $x(t) = V_S(t)$ and the desired output may be, for example, the far-end crosstalk voltage, $y(t) = V_{FE}(t)$.

1.6.1 The Fourier Series and Transform

The primary reason we concentrate so much emphasis on the single-frequency sinusoidal response of a linear system via the frequency domain is that we can decompose any periodic time-domain waveform into its sinusoidal components via the Fourier series [A.2,A.3]. Hence we can represent any periodic waveform having period P as the infinite sum of sinusoids whose frequencies are multiples of the basic repetition frequency

$$f_0 = \frac{1}{P} \tag{1.120}$$

as [A.2,A.3]

$$x(t) = c_0 + \sum_{n=1}^{\infty} 2c_n \cos(n\omega_0 t + \angle c_n) \quad (1.121)$$

and $\omega_0 = 2\pi f_0 = 2\pi/P$. The Fourier expansion coefficients in (1.121) are obtained from [A.2,A.3]

$$\begin{aligned} \hat{c}_n &= \frac{1}{P} \int_{t_1}^{t_1+P} x(t) e^{-jn\omega_0 t} dt \\ &= c_n \angle c_n \end{aligned} \quad (1.122)$$

where \hat{c}_n is a complex number, and c_n and $\angle c_n$ are the magnitude and the phase, respectively, of it. In the frequency domain, we can determine the transfer function at each of these *harmonics* as

$$\hat{H}(jn\omega_0) = |\hat{H}(jn\omega_0)| \angle \hat{H}(jn\omega_0) \quad (1.123)$$

If the system (line and terminations) is linear, then we may employ *superposition* and pass each sinusoidal component of the input through the system and sum them at the output to obtain the Fourier series of the output $y(t)$ as illustrated in Figure 1.21:

$$y(t) = c_0 \hat{H}(0) + \sum_{n=1}^{\infty} 2c_n |\hat{H}(jn\omega_0)| \cos(n\omega_0 t + \angle c_n + \angle \hat{H}(jn\omega_0)) \quad (1.124)$$

This is an incredibly powerful result. It says that we can indirectly solve for the time-domain response of the output $y(t)$ by decomposing the input signal, $x(t)$, into its sinusoidal components with the Fourier series as in (1.121), solving for the frequency response of the system to these harmonics of the input signal, and then *summing these individual responses in time* as in (1.124). However, this will represent only the steady-state solution part of $y(t)$ and transients are not included. Theoretically, the Fourier series requires an infinite number of harmonics be summed to yield the time-domain function. In a practical sense, we only need to sum a finite number to arrive at a reasonable approximation to the output solution $y(t)$.

For waveforms that are not periodic, that is, consist of a single pulse, the Fourier transform provides a similar representation [A.2,A.3]. In this case, the discrete spectrum consisting of harmonics is replaced by a continuous spectrum. The discrete Fourier series coefficients are replaced by the Fourier transform, $\hat{X}(j\omega)$. The process described above is essentially unchanged.

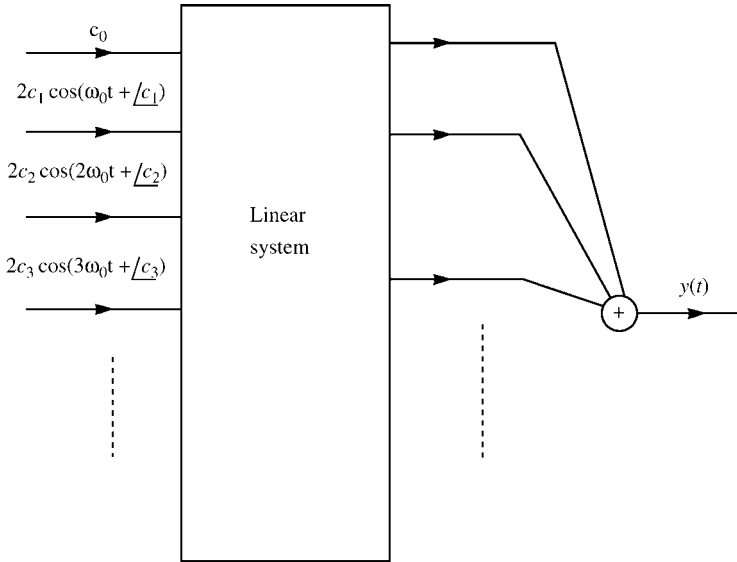


FIGURE 1.21 Illustration of using superposition and the Fourier series to indirectly obtain the time-domain output of a linear system.

1.6.2 Spectra and Bandwidth of Digital Waveforms

The methods and techniques for analyzing MTLs discussed in this text apply for source waveforms in the termination networks as well as incident fields that have any general time variation. However, because of the preponderance of digital methods and devices today, we will concentrate our examples on digital waveforms that represent clock and data signals. A digital clock signal is periodic and has a trapezoidal waveform shown in Figure 1.22. The pulse width τ is defined between the half-amplitude levels of the pulse, and τ_r and τ_f denote the 0–100 % rise and fall times of the pulse, respectively. The expansion coefficients in (1.122) were obtained in [A.3] and are

$$c_0 = A \frac{\tau}{P} \tag{1.125a}$$

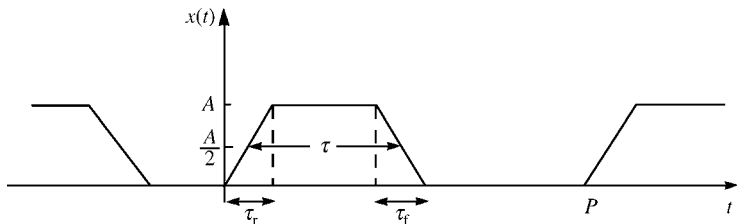


FIGURE 1.22 A periodic, trapezoidal pulse train representing a digital signal.

$$\hat{c}_n = -j \frac{A}{2\pi n} \left(\frac{\sin\left(\frac{n\pi\tau_r}{P}\right)}{\frac{n\pi\tau_r}{P}} e^{jn\pi\tau/P} - \frac{\sin\left(\frac{n\pi\tau_f}{P}\right)}{\frac{n\pi\tau_f}{P}} e^{-jn\pi\tau/P} \right) e^{-jn\pi\frac{(\tau+\tau_r)}{P}} \quad (1.125b)$$

In digital applications, it is usually desired to have the rise and fall times of the pulse equal. In this case, the expansion coefficients simplify to [A.3]

$$\hat{c}_n = A \frac{\tau}{P} \frac{\sin\left(\frac{n\pi\tau}{P}\right)}{\frac{n\pi\tau}{P}} \frac{\sin\left(\frac{n\pi\tau_r}{P}\right)}{\frac{n\pi\tau_r}{P}} e^{-jn\pi\frac{(\tau+\tau_r)}{P}}, \quad \tau_r = \tau_f \quad (1.126)$$

Observe that the dc component, c_0 in (1.125a), and the harmonic amplitudes involve the ratio of the pulse width to pulse period or the pulse *duty cycle*:

$$D = \frac{\tau}{P} \quad (1.127)$$

It is also generally desired to have the duty cycle to be 50 % or $D = 0.5$. Bounds on the spectral amplitudes can be developed for the case where the rise and fall times are equal [A.3]. These are shown in Figure 1.23. There are two break frequencies. Up to $f = 1/\pi\tau = f_0/\pi D$, the amplitudes are bounded by a 0 dB/decade slope and after that fall off at a rate of -20 dB/decade. Above the next break frequency of $f = 1/\pi\tau_r$, the harmonic amplitudes fall off at a rate of -40 dB/decade. Hence the high-frequency spectral content is primarily determined by the rise/fall times of the pulse.

This result can be derived for unequal rise/fall times if we assume a 50% duty cycle, that is, $D = \tau/P = 0.5$. The magnitudes of the coefficients for odd n and even n are

$$|\hat{c}_n| = \frac{A}{2\pi n} \left| \frac{\sin\left(\frac{n\pi\tau_r}{P}\right)}{\frac{n\pi\tau_r}{P}} + \frac{\sin\left(\frac{n\pi\tau_f}{P}\right)}{\frac{n\pi\tau_f}{P}} \right|, \quad n \text{ odd} \quad (1.128a)$$

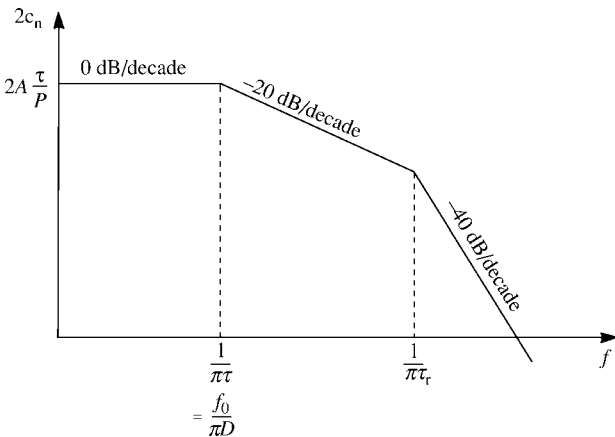


FIGURE 1.23 Spectral bounds for a periodic, trapezoidal pulse train.

and

$$|\hat{c}_n| = \frac{A}{2\pi n} \left| \frac{\sin\left(\frac{n\pi\tau_r}{P}\right)}{\frac{n\pi\tau_r}{P}} - \frac{\sin\left(\frac{n\pi\tau_f}{P}\right)}{\frac{n\pi\tau_f}{P}} \right|, \quad n \text{ even} \quad (1.128b)$$

Observe that for equal rise/fall times, the even harmonics are zero. However, plotting this in asymptotic form as in Figure 1.23 cannot be done since it is not in the form of a product of terms.

The important question of how many harmonics need be included in the sum in (1.121) in order to reasonably reproduce the pulse waveform with that sum can now be estimated for equal rise/fall times. Noting in Figure 1.23 that above the second break point the harmonic amplitudes are rolling off at -40 dB/decade, we might choose to stop the summation at some frequency above this second break point. Since this is a somewhat loose criterion, we might choose for convenience a frequency three times this break frequency. But this is approximately the inverse of the pulse rise time. Hence, we might choose an estimate of the *bandwidth* of a digital pulse as

$$\text{BW} \cong \frac{1}{\tau_r} \quad (1.129)$$

Interestingly, the second $(\sin x)/x$ function involving the rise/fall time in (1.126) goes to zero at this frequency. In order to illustrate the critical point that addition of each harmonic in time gives a point on the total time-domain waveform and we only need to sum harmonics up to the bandwidth of the pulse in order to obtain a reasonable reproduction of the waveform, we show in Figure 1.24 a 5-V, 100-MHz, 1-ns rise/fall time, 50% duty cycle periodic, trapezoidal pulse train. The bandwidth is, according to (1.129), $\text{BW} = 1$ GHz. Hence we should sum the first 10 harmonics. The amplitudes and phases of these first 10 harmonics are

| n | c_n | $\angle c_n$ (rad) |
|-----|---------|--------------------|
| 1 | 3.1310 | -1.8850 |
| 2 | 0 | 0 |
| 3 | -0.9108 | -5.6549 |
| 4 | 0 | 0 |
| 5 | 0.4053 | -9.4248 |
| 6 | 0 | 0 |
| 7 | -0.1673 | -13.1947 |
| 8 | 0 | 0 |
| 9 | 0.0387 | -16.9646 |
| 10 | 0 | 0 |

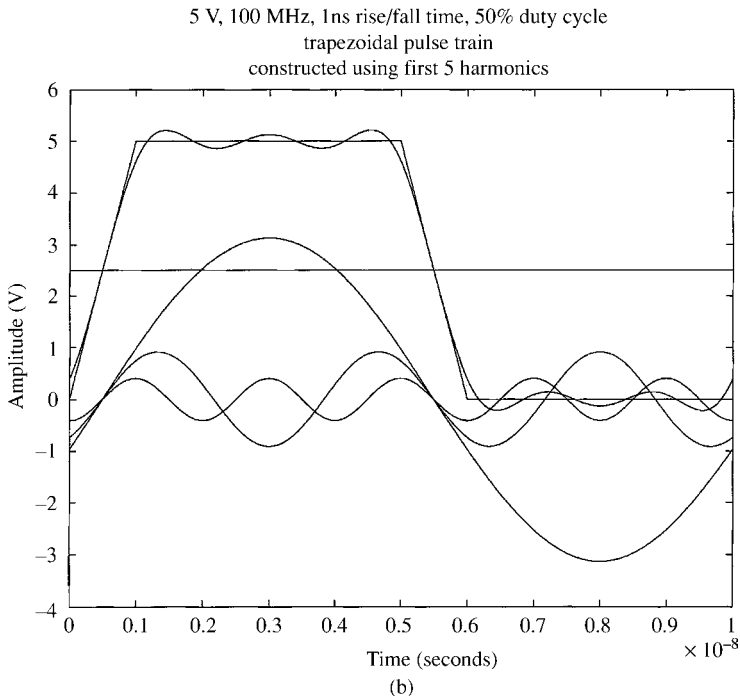
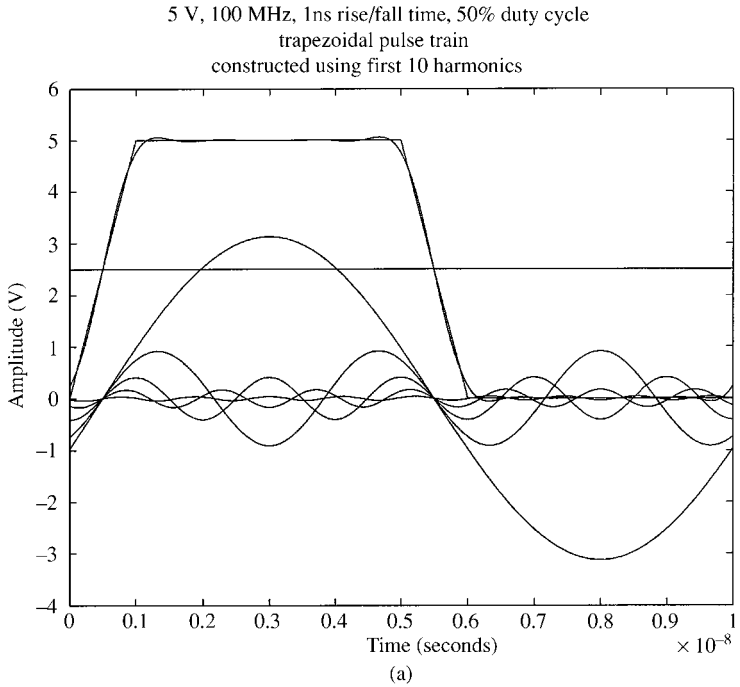


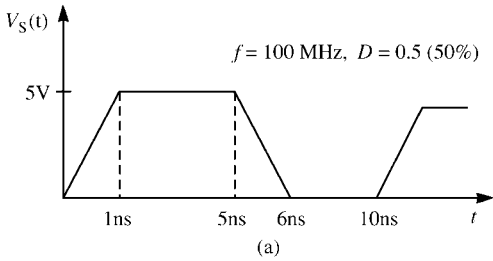
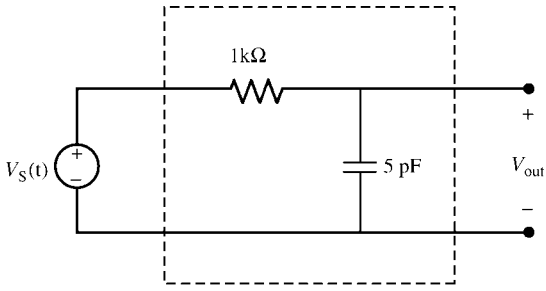
FIGURE 1.24 Reconstruction of a 5-V, 100-MHz, 1-ns rise/fall time, 50 % duty cycle trapezoidal pulse train (a) using the first 10 harmonics and (b) using the first five harmonics.

Rather than including the minus signs of the third and seventh harmonics in the angle, we have left them in the magnitude. Technically, this is not correct since a magnitude can have no sign, but it simplifies the result. Observe that the even harmonics are zero. This is a characteristic of a 50 % duty cycle waveform. Figure 1.24(a) shows the result of summing the first 10 harmonics. Although there is a small error at the corners, the overall representation is quite good. Figure 1.24(b) shows the result of summing only the first five harmonics. This is another criterion that is often cited for the bandwidth of a digital signal: $BW = 0.5/\tau_r$. Observe that the reconstruction with only five harmonics is not so good: there is considerable ringing on the waveform.

1.6.3 Computing the Time-Domain Response of Transmission Lines Having Linear Terminations Using Fourier Methods and Superposition

In this section, we will show a very simple but extremely powerful method of solution. It is called the time-domain to frequency-domain or TDFD transformation. A FORTRAN program, TIMEFREQ.FOR, described in Appendix A implements this powerful method. It may also be viewed as a “poor man’s inverse fast Fourier transform (FFT).” The basic idea was described earlier. Decompose the input signal into its sinusoidal harmonic components. Imbed the terminations into a single-input, single-output “black-box” system as illustrated in Figures 1.19 and 1.20. Determine by phasor methods the sinusoidal steady-state response of the transfer function of this single-input, single-output system at each of the harmonics of the input signal. Then pass each sinusoidal component through the system computing the sinusoidal response by phasor methods and sum in time these responses as illustrated in Figure 1.21 to give the time-domain output of the system. Although this gives (within the approximation of a finite number of Fourier components) the time-domain output signal without having to directly solve the differential equations relating the output to the input, there are two important restrictions. (1) In order for this method to be applicable, the system must be *linear* because we have used the principle of *superposition*. For transmission lines, this essentially means that the terminations must be linear because the transmission lines are, in general, linear. For example, if one line is terminated in a diode, then the entire system is nonlinear since this nonlinear termination is imbedded in, and is therefore a part of, the system. (2) This also assumes that the system has reached steady state; that is, the transient portion of the response has decayed to essentially zero. Hence if we apply a periodic waveform to the input as with a digital clock signal, we may have to wait several cycles (periods) or time constants of the system before we will have reached steady state.

As an example of this method, consider the low-pass filter in Figure 1.25(a) consisting of a 1-k Ω resistor and a 5-pF capacitor. A trapezoidal digital waveform with a frequency of 100 MHz (a period of 10 ns), 5 V amplitude, 50% duty cycle, and 1 ns rise/fall times is applied to the input. Figure 1.25(b) shows the exact output voltage across the capacitor obtained directly in the time domain with PSPICE (see Appendix B for a brief tutorial on the PSPICE program) using the program



Output Voltage of Low-Pass Filter for an Input of a
100-MHZ, 5-V 50% Duty Cycle, 1ns Rise/Fall Time Trapezoidal Pulse Train
Computed Directly With PSPICE

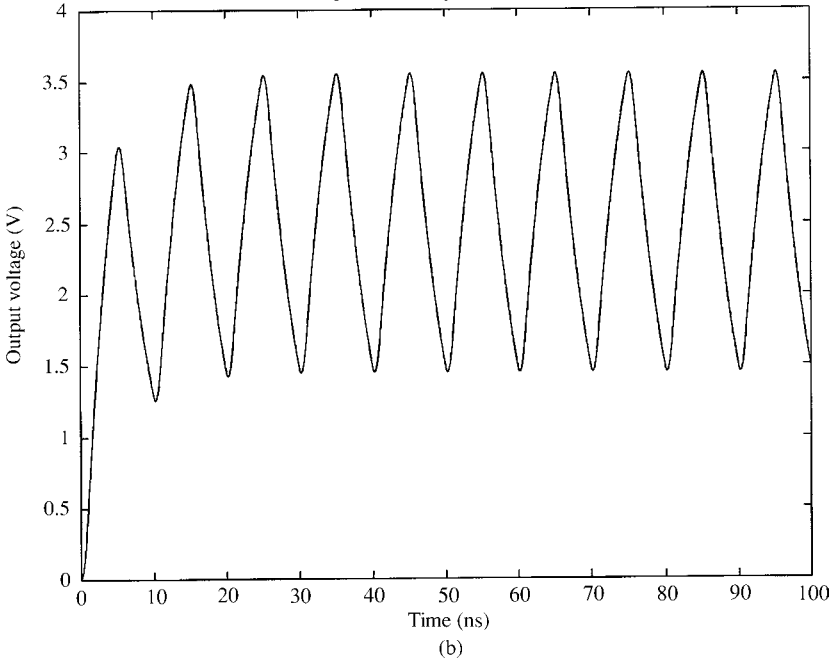


FIGURE 1.25 An electric circuit example illustrating the use of superposition to combine the responses to harmonics of the input signal: (a) the circuit, (b) the total response computed using PSPICE, and (c) the response by combining the responses to harmonics of the input waveform.

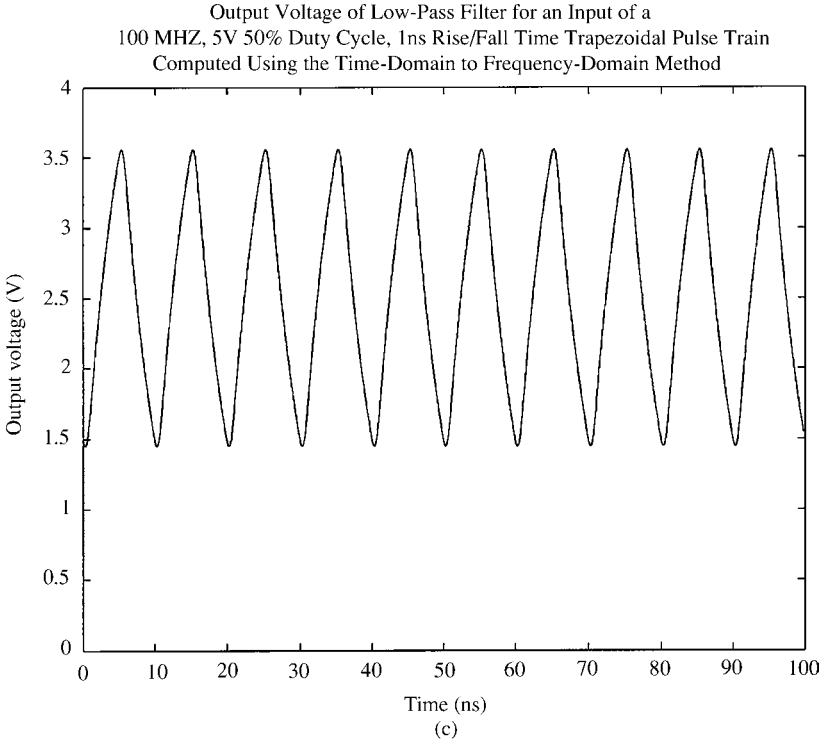


FIGURE 1.25 (Continued)

EXAMPLE

```
VS 1 0 PULSE(0 5 0 1N 1N 4N 10N)
R 1 2 1K
C 2 0 5P
.TRAN 0.1N 100N 0 0.1N
.PROBE
.PRINT TRAN V(2)
.END
```

Observe that there is a transient time interval at the beginning lasting approximately five time constants: $5RC = 25$ ns. Next, we compute the output using the TDFD method. Since the bandwidth of this signal is on the order of $BW \cong 1/\tau_r = 1$ GHz, we need to pass frequency components up to 1 GHz through the system. Figure 1.25(c) shows the result of passing the first 10 harmonics, 100 MHz, 200 MHz, 300 MHz, 400 MHz, 500 MHz, 600 MHz, 700 MHz, 800 MHz, 900 MHz and 1 GHz, through the system and summing their responses in time using the TDFD method and the FORTRAN program TIMEFREQ.FOR. Observe that this result shows no transient interval; it presupposes that steady state has been reached. Observe also that once the response has reached steady state, the two waveforms are virtually identical.

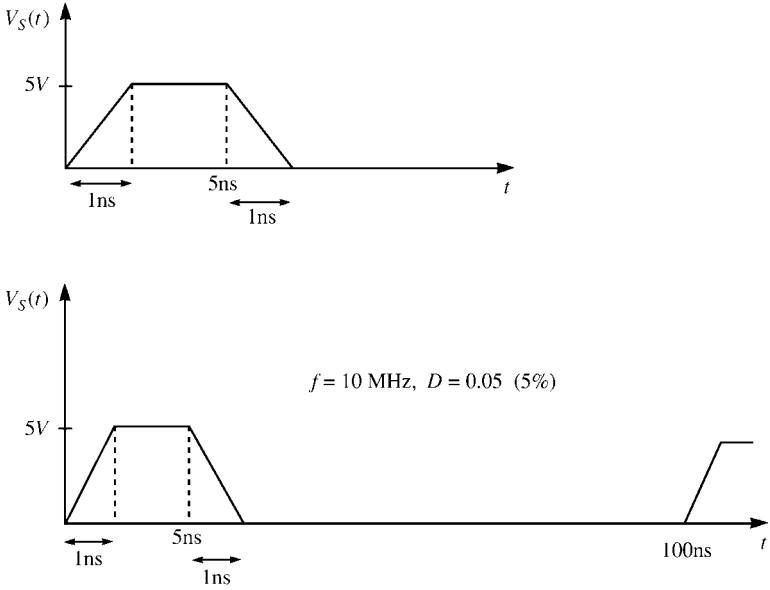
The method can also be used to compute the response to a single pulse. The basic idea is to use a periodic waveform that has the same shape over one period as the desired single pulse *but* choose the period sufficiently long (inverse of the repetition frequency that is chosen sufficiently small) so that the response to the single pulse has essentially reached steady state before the onset of the next pulse in this periodic waveform. For a single pulse that starts at a level of 0 (zero) at $t = 0$ and ends at a level of 0 at some later time, the steady-state response is also 0. Hence we choose a period that is sufficiently long so that the response has essentially decayed to zero before the onset of the next pulse. For example, suppose we apply a single pulse again having a rise/fall time of 1 ns, a pulse width of 5 ns, and a peak level of 5 V to the low-pass filter in Figure 1.25(a). If we choose the frequency of this periodic waveform long enough, say 100 ns or a frequency of 10 MHz, as shown in Figure 1.26(a), the response will probably have reached steady state before the onset of the next pulse at 100 ns because the time constant of this system is $RC = 5$ ns. If not, choose a lower frequency. Note that the duty cycle of this new pulse train in Figure 1.26(a) is no longer 50%: it is $D = 0.05$. This insures that there is a sufficient length of time after the pulse “turns off” to allow the response to settle down to its steady-state value of 0. Actually, we could choose the duty cycle to be 50% so long as the remaining time after the pulse has turned off, one-half the period, is much longer than the time constant of the system. The exact value of the frequency of this new waveform is not critical; its choice only requires that the system output has reached steady state before the onset of the next pulse in order to use this method to compute the response to a single pulse. The exact time-domain PSPICE simulation (for a single pulse) is obtained with

EXAMPLE

```
VS 1 0 PWL(0 0 1N 5 5N 5 6N 0)
R 1 2 1K
C 2 0 5P
.TRAN 0.05N 50N 0 0.05N
.PROBE
.PRINT TRAN V(2)
.END
```

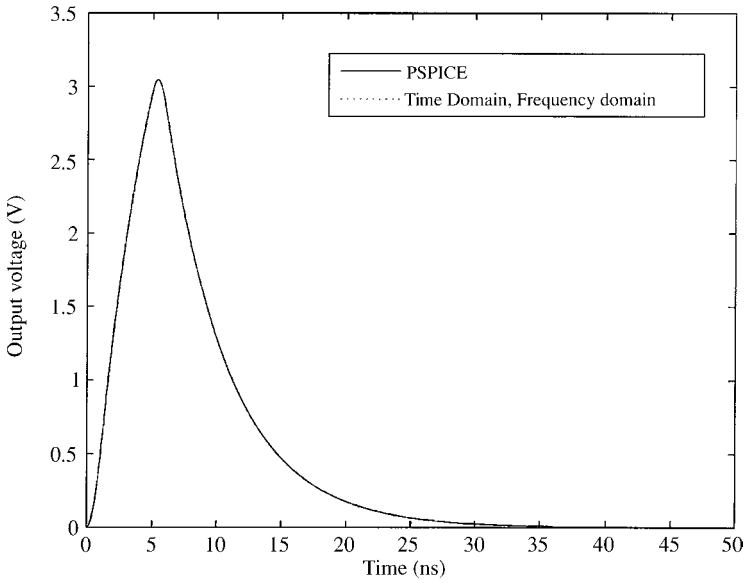
Figure 1.26(b) shows the comparison of the responses of the system to this pulse computed by PSPICE and that computed with the TDFD method using the FORTRAN program TIMEFREQ.FOR (for a 10-MHz pulse train having the same shape as the desired pulse but a duty cycle of $D = 0.05$ or 5%). The results are virtually identical.

An important advantage of using this method to obtain the time-domain response of a transmission line as opposed to solving the differential equations directly is that losses in the line (in the conductors and the surrounding medium) may be easily incorporated into the frequency-domain transfer function solution and hence into the final solution. The conductor losses above a certain frequency have a \sqrt{f} dependence due to *skin effect* [1]. This is quite difficult to incorporate into a direct time-domain solution, but it is simple to include in a frequency response calculation. When the terminations are nonlinear, however, we have no choice but to obtain the solution



(a)

Output Voltage of a Low-Pass Filter for a 5V, 5ns pulse width, 1ns Rise/Fall Time Pulse



(b)

FIGURE 1.26 Illustration of using a periodic waveform with a sufficiently long period to determine the response to a single pulse: (a) the pulse train, (b) computed responses using PSPICE and the TDFD transformation method.

directly in the time domain by solving the differential equations. Frequency-dependent losses then become a very difficult problem to include.

PROBLEMS

- 1.1** Two perfectly conducting circular plates are separated by a distance d as shown in Figure P1.1. The plates have very large radii with respect to d (ideally infinite) so that, in cylindrical coordinates, we may assume a “TEM-mode” field structure, $\vec{\mathcal{E}}(\rho, t) = \mathcal{E}_z(\rho, t)\vec{a}_z$ and $\vec{\mathcal{H}}(\rho, t) = \mathcal{H}_\phi(\rho, t)\vec{a}_\phi$. Define voltage and current as

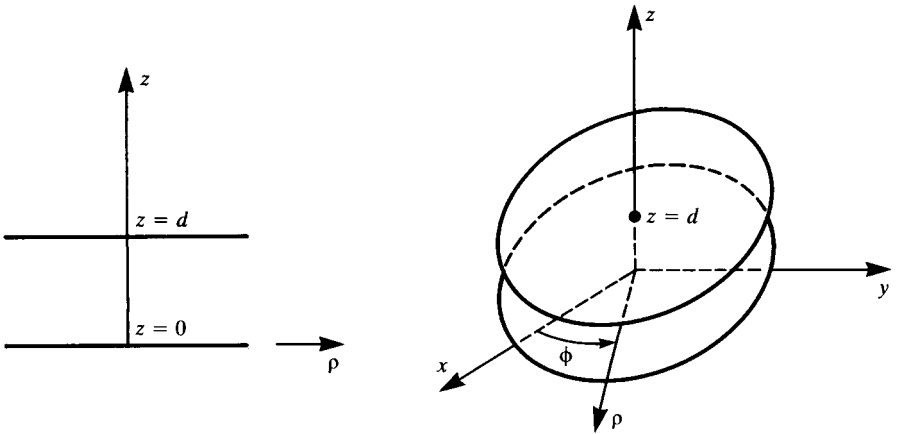


FIGURE P 1.1

$$V(\rho, t) = -\mathcal{E}_z(\rho, t)d$$

$$I(\rho, t) = 2\pi\rho\mathcal{H}_\phi(\rho, t)$$

Show, from Maxwell’s equations in cylindrical coordinates, that V and I satisfy the transmission-line equations

$$\frac{\partial V(\rho, t)}{\partial \rho} = -l \frac{\partial I(\rho, t)}{\partial t}$$

$$\frac{\partial I(\rho, t)}{\partial \rho} = -c \frac{\partial V(\rho, t)}{\partial t}$$

where l and c are static parameters defined by

$$l = \frac{\mu d}{2\pi\rho}$$

$$c = \frac{2\pi\varepsilon\rho}{d}$$

Would it be appropriate to classify this as a *nonuniform* line? Could the mode of propagation to which these equations apply be classified as a “TEM mode”?

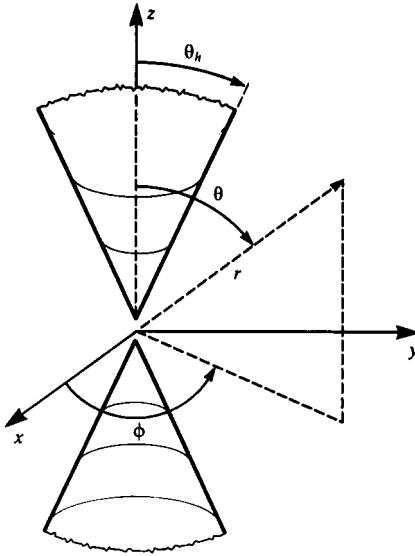


FIGURE P1.2

- 1.2 The infinite biconical transmission line consists of two perfectly conducting cones of half angle θ_h as shown in Figure P1.2. Solve Maxwell’s equations in spherical coordinates for this structure assuming that $\vec{\mathcal{E}}(r, \theta) = \mathcal{E}_\theta(r, \theta)\vec{a}_\theta$ and $\vec{\mathcal{H}}(r, \theta) = \mathcal{H}_\phi(r, \theta)\vec{a}_\phi$. Show that the following definitions of voltage and current are unique:

$$V(r, t) = \int_{\theta_h}^{\pi - \theta_h} \mathcal{E}_\theta r d\theta$$

$$I(r, t) = \int_0^{2\pi} \mathcal{H}_\phi r \sin(\theta) d\phi$$

where V and I satisfy the following transmission-line equations:

$$\frac{\partial V(r, t)}{\partial r} = -l \frac{\partial I(r, t)}{\partial t}$$

$$\frac{\partial I(r, t)}{\partial r} = -c \frac{\partial V(r, t)}{\partial t}$$

Show that

$$l = \frac{\mu}{\pi} \ln \left(\cot \frac{\theta_h}{2} \right)$$

$$c = \frac{\pi \epsilon}{\ln \left(\cot \frac{\theta_h}{2} \right)}$$

Would this be classified as a *uniform* or *nonuniform* line? Would it be appropriate to classify the propagation mode as TEM?

- 1.3 Show that, assuming a TEM field structure, the currents on the two conductors in Figure 1.5 are equal in magnitude and oppositely directed at any cross section.
- 1.4 Show that, assuming a TEM field structure, the charge per unit length on one conductor in Figure 1.5 is equal in magnitude and opposite in sign to the charge per unit length on the other conductor at any cross section.
- 1.5 Consider the coaxial cable in Figure 1.1(c) consisting of an exterior shield and an inner wire that is located on the axis of the shield. The dielectric interior to the shield has a relative permittivity of $\epsilon_r = 2.3$. Determine the velocity of propagation and the one-way time delay on the line, $T_D = \mathcal{L}/v$, for a line of total length $\mathcal{L} = 10$ m. [50.55 ns]

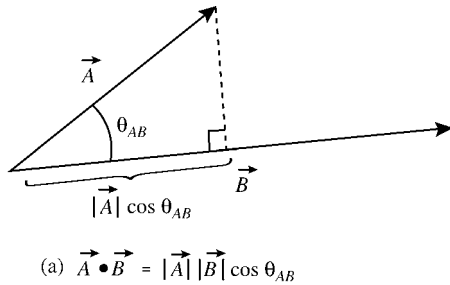


FIGURE P 1.7

- 1.6 Consider the stripline in Figure 1.2(a) consisting of one land between two infinite ground planes. The dielectric is glass epoxy with $\epsilon_r = 4.7$. Determine the velocity of propagation and the one-way time delay on the line, $T_D = \mathcal{L}/v$, for a line of total length $\mathcal{L} = 10$ in. [1.84 ns]
- 1.7 The *dot product* of two vectors is defined as $\vec{A} \cdot \vec{B} = |\vec{A}| |\vec{B}| \cos \theta_{AB}$, where $|\vec{A}|$ denotes the magnitude (length) of vector \vec{A} [A.1]. The dot product can be thought of as the product of the length of one vector and the projection of the other vector on this vector as illustrated in Figure P1.7. The dot product gives a *scalar* as the result. The dot product can be mechanically computed from $\vec{A} \cdot \vec{B} = A_x B_x + A_y B_y + A_z B_z$ [A.1]. For the two vectors $\vec{A} = 3\vec{a}_x + 2\vec{a}_y$, and

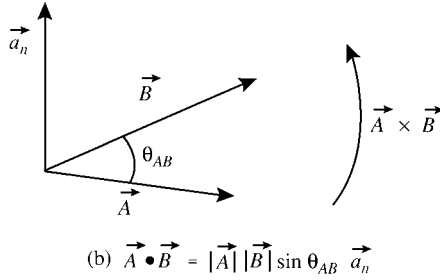


FIGURE P1.8

$\vec{B} = 2\vec{a}_x - 5\vec{a}_y$, determine the dot product of the two vectors (a) directly and (b) using the basic definition of the dot product. Repeat for $\vec{A} = 2\vec{a}_x - 3\vec{a}_y$ and $\vec{B} = 5\vec{a}_x$. [-4, 10]

- 1.8** The *cross product* of two vectors is defined as $\vec{A} \times \vec{B} = |\vec{A}| |\vec{B}| \sin \theta_{AB} \vec{a}_n$, where $|\vec{A}|$ denotes the magnitude (length) of vector \vec{A} and \vec{a}_n is a unit vector normal or perpendicular to the plane containing the vectors \vec{A} and \vec{B} [A.1]. There are two sides to this plane, so the unit vector \vec{a}_n direction is determined according to the *right-hand rule* as illustrated in Fig. P1.8. The cross product gives a *vector* as the result. The cross product can be mechanically computed from [A.1]

$$\vec{A} \times \vec{B} = (A_y B_z - A_z B_y) \vec{a}_x + (A_z B_x - A_x B_z) \vec{a}_y + (A_x B_y - A_y B_x) \vec{a}_z$$

For the vectors $\vec{A} = \vec{a}_z$ and $\vec{B} = E\vec{a}_x$, determine the cross product (a) directly and (b) from the basic definition of the cross product. (Set up a rectangular coordinate system and use your right hand.) Repeat this for $\vec{A} = \vec{a}_x$ and $\vec{B} = E\vec{a}_z$ and $\vec{A} = \vec{a}_y - \vec{a}_z$ and $\vec{B} = E\vec{a}_x$. [$E\vec{a}_y, -E\vec{a}_y, -E\vec{a}_y - E\vec{a}_z$]

- 1.9** The *divergence* of a vector field is given by [A.1]

$$\nabla \cdot \vec{\mathcal{E}}(x, y, z) = \frac{\partial \mathcal{E}_x}{\partial x} + \frac{\partial \mathcal{E}_y}{\partial y} + \frac{\partial \mathcal{E}_z}{\partial z}$$

The divergence of a vector field gives the net *outflow* of the vector field from a point and hence locates sources and sinks of the vector field. Determine the divergence of $\vec{\mathcal{E}} = E_0 \vec{a}_x$. Repeat for $\vec{\mathcal{E}} = x\vec{a}_x + y\vec{a}_y$. Interpret these results. [0, $x + y$]

- 1.10** The *curl* of a vector field in rectangular coordinates is given by [A.1]

$$\nabla \times \vec{\mathcal{E}} = \left(\frac{\partial \mathcal{E}_z}{\partial y} - \frac{\partial \mathcal{E}_y}{\partial z} \right) \vec{a}_x + \left(\frac{\partial \mathcal{E}_x}{\partial z} - \frac{\partial \mathcal{E}_z}{\partial x} \right) \vec{a}_y + \left(\frac{\partial \mathcal{E}_y}{\partial x} - \frac{\partial \mathcal{E}_x}{\partial y} \right) \vec{a}_z$$

The curl gives the net circulation of the field much like vortices or eddies in a river. Determine the curl of $\vec{\mathcal{E}} = E_0\vec{a}_y$. Repeat for $\vec{\mathcal{E}} = -y\vec{a}_x + x\vec{a}_y$. Interpret these results. $[0, 2\vec{a}_z]$

- 1.11** Demonstrate that the various components in (1.3) are in the indicated directions. (Draw a rectangular coordinate system and use your right hand.)
- 1.12** Demonstrate the identity in (1.5), where the gradient is defined as [A.1]

$$\nabla f(x, y, z) = \frac{\partial f}{\partial x}\vec{a}_x + \frac{\partial f}{\partial y}\vec{a}_y + \frac{\partial f}{\partial z}\vec{a}_z$$

- 1.13** Demonstrate the identity in (1.11).
- 1.14** Demonstrate the result in (1.13).
- 1.15** Show that the general solutions in (1.16) satisfy the equations in (1.15).
- 1.16** Power flow in an electromagnetic field is given by the Poynting vector [A.1] as

$$\vec{S} = \vec{\mathcal{E}} \times \vec{\mathcal{H}}$$

Show that the forward- and backward-traveling waves in (1.20) give the proper direction of power flow. (Draw a rectangular coordinate system and use your right hand.)

- 1.17** Show that (1.25) satisfy the phasor differential equations in (1.24).
- 1.18** Show that (1.34) satisfy the phasor differential equations in (1.32).
- 1.19** Show that the voltage definition in (1.40) reduces as shown.
- 1.20** Derive the transmission-line equations from each of the circuits in Figure P1.20 in the limit as $\Delta z \rightarrow 0$. Observe that the total inductance (capacitance) in each structure is $l\Delta z(c\Delta z)$. This shows that the structure of the per-unit-length equivalent circuit is not important in obtaining the transmission-line equations from it so long as the total per-unit-length inductance and capacitance is contained in the structure and we let $\Delta z \rightarrow 0$.
- 1.21** Demonstrate the identities in (1.65) and (1.69).
- 1.22** Derive the second-order transmission-line equations in (1.72).
- 1.23** A coaxial cable shown in Figure P1.23 has an interior dielectric that is defined in annuli as ϵ_1, μ_0 for $r_w < r < a$ and ϵ_2, μ_0 for $a < r < r_s$. Is this a uniform transmission line? Is the medium homogeneous or inhomogeneous? How would you compute the per-unit-length capacitance for this transmission line? (Recall that capacitors in series add like resistors in parallel and capacitors in parallel add like resistors in series.)

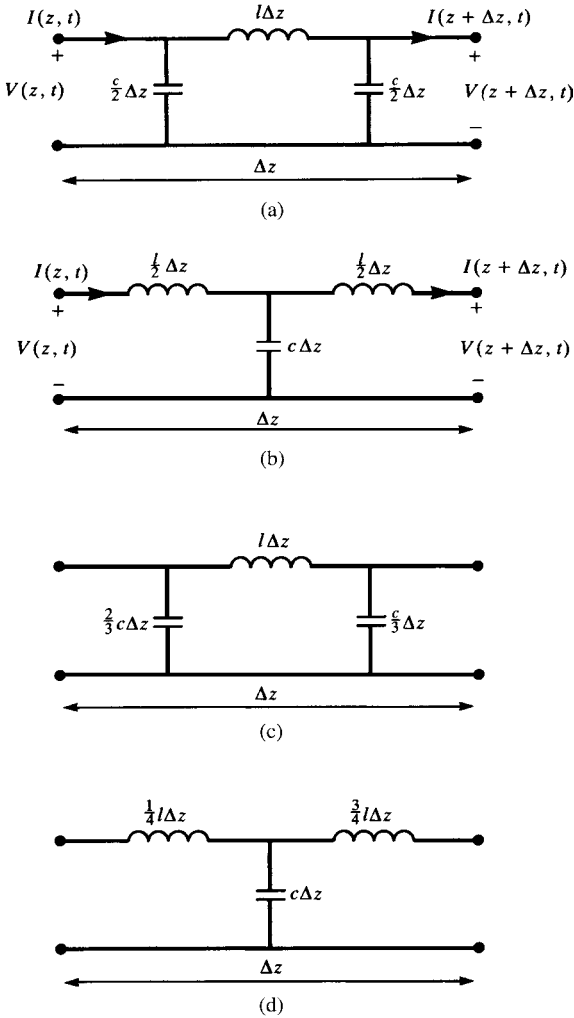


FIGURE P 1.20

- 1.24** A stripline shown in Figure P1.24 has a dielectric that is defined in planes of thickness a and b as ϵ_1, μ_0 and ϵ_2, μ_0 . Is this a uniform transmission line? Is the medium homogeneous or inhomogeneous? How would you compute the per-unit-length capacitance for this transmission line? (Recall that capacitors in series add like resistors in parallel, and capacitors in parallel add like resistors in series.)
- 1.25** Demonstrate the relations in (1.81) and (1.85).
- 1.26** Demonstrate the relations in (1.87).

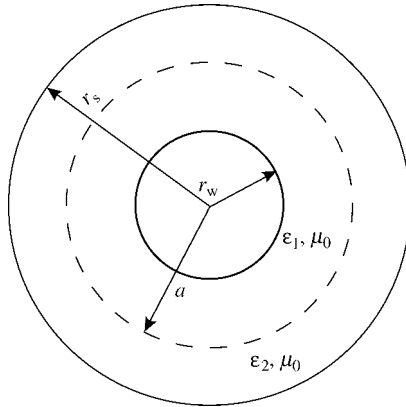


FIGURE P 1.23

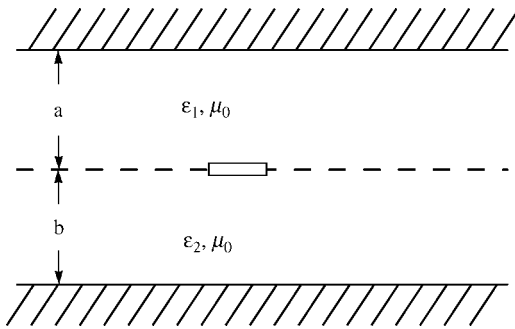


FIGURE P 1.24

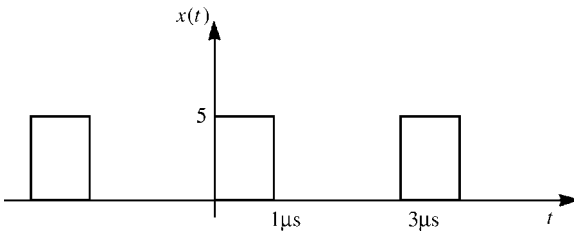


FIGURE P 1.28

- 1.27** Demonstrate the per-unit-length parameters of the parallel-plate line in (1.102).
- 1.28** Determine the Fourier coefficients in (1.122) for the square-wave waveform in Figure P1.28. [$\hat{c}_n = (5/3)(\sin(n\pi/3))/(n\pi/3)\angle -n\pi/3$].
- 1.29** Determine the Fourier coefficients in (1.122) for the full-wave rectified waveform in Figure P1.29. [$\hat{c}_n = (2A/\pi(1 - 4n^2))$]

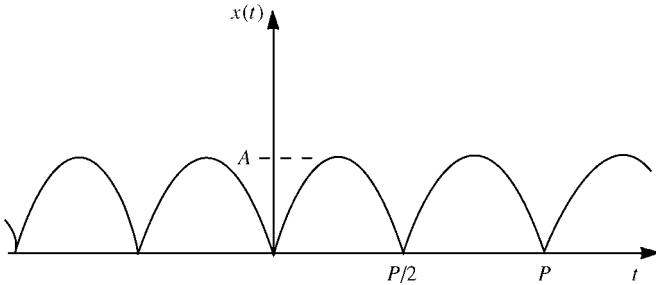


FIGURE P 1.29

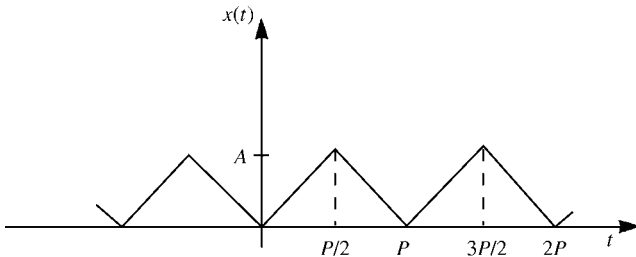


FIGURE P 1.30

- 1.30** Determine the Fourier coefficients in (1.122) for the triangular waveform in Figure P1.30. [$c_0 = (A/2)$, $\hat{c}_n = -(2A/(n\pi)^2)$ n odd]
- 1.31** Use MATLAB or PSPICE to recombine the first 10 harmonics of the waveform in Figure P1.28 to give an approximation to the time-domain waveform.

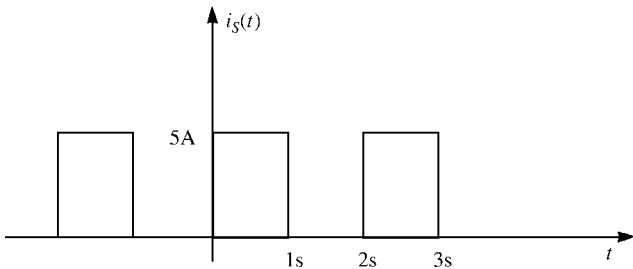
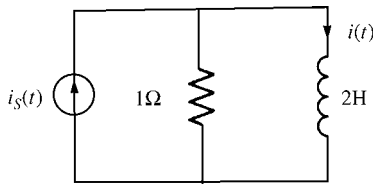


FIGURE P 1.34

- 1.32** Use MATLAB or PSPICE to recombine the first 10 harmonics of the waveform in Figure P1.29 to give an approximation to the time-domain waveform.
- 1.33** Use MATLAB or PSPICE to recombine the first 10 harmonics of the waveform in Figure P1.30 to give an approximation to the time-domain waveform.
- 1.34** The square-wave current source in Figure P1.34 is applied to the associated circuit as shown. Determine the resulting output current through the inductor, $i(t)$, in the form

$$i(t) = I_0 + \sum_{n=1}^7 I_n \cos(n\omega_0 t + \theta_n)$$

Use PSPICE and TIMEFREQ.FOR to determine the output current of this linear system and compare the approximation using a finite number of Fourier components (seven for TIMEFREQ.FOR) to the exact result (using PSPICE). [$I_0 = 2.5$, $I_1 = 0.5$, $\theta_1 = -80.96^\circ$, $I_2 = 0$, $I_3 = 0.0562$, $\theta_3 = -86.96^\circ$, $I_4 = 0$, $I_5 = 0.0203$, $\theta_5 = -88.17^\circ$, $I_6 = 0$, $I_7 = 0.0103$, $\theta_7 = -88.7^\circ$]

REFERENCES

- [1] S. Ramo, J.R. Whinnery, and T. VanDuzer, *Fields and Waves in Communication Electronics*, 2nd edition, John Wiley & Sons, New York, 1984.
- [2] R.B. Adler, L.J. Chu, and R.M. Fano, *Electromagnetic Energy Transmission and Radiation*, John Wiley, New York, 1963.
- [3] S. Frankel, *Multiconductor Transmission Line Analysis*, Artech House, Dedham, MA, 1977.
- [4] H. Uchida, *Fundamentals of Coupled Lines and Multiwire Antennas*, Sasaki Publishing Co, Sendai, Japan, 1967.
- [5] S. Hayashi, *Surges on Transmission Systems*, Denki-Shoin, Kyoto, Japan, 1955.
- [6] W.C. Johnson, *Transmission Lines and Networks*, McGraw-Hill, New York, 1950.
- [7] L.V. Bewley, *Traveling Waves on Transmission Systems*, 2nd edition, John Wiley & Sons, New York, 1951.
- [8] P.I. Kuznetsov and R.L. Stratonovich, *The Propagation of Electromagnetic Waves in Multiconductor Transmission Lines*, Macmillan, New York, 1964.
- [9] P.C. Magnuson, *Transmission Lines and Wave Propagation*, Allyn & Bacon, Newton, MA, 1970.
- [10] R.E. Collin, *Field Theory of Guided Waves*, 2nd edition, IEEE Press, New York, 1991.
- [11] J. Zaborsky and J.W. Rittenhouse, *Electric Power Transmission*, Ronald Press, New York, 1954.
- [12] R.E. Matlick, *Transmission Lines for Digital and Communication Networks*, McGraw-Hill, New York, 1969.

- [13] L. Young (ed.), *Parallel Coupled Lines and Directional Couplers*, Artech House, Dedham, MA, 1972.
- [14] T. Itoh (ed.), *Planar Transmission Line Structures*, IEEE Press, New York, 1987.
- [15] W.T. Weeks, Multiconductor transmission line theory in the TEM approximation, *IBM Journal of Research and Development*, 604–611, 1972.
- [16] K.D. Marx, Propagation modes, equivalent circuits and characteristic terminations for multiconductor transmission lines with inhomogeneous dielectrics, *IEEE Transactions on Microwave Theory and Techniques*, **21**, 450–457, 1973.
- [17] A.F. dos Santos and J.P. Figanier, The method of series expansion in the frequency domain applied to multiconductor transmission lines, *IEEE Transactions on Microwave Theory and Techniques*, **23**(9), 753–756, 1975.
- [18] I.V. Lindell, On the quasi-TEM modes in inhomogeneous multiconductor transmission lines, *IEEE Transactions on Microwave Theory and Techniques*, **29**(8), 812–817, 1981.
- [19] Y. Leviatan and A.T. Adams, The response of a two-wire transmission line to incident field and voltage excitation, including the effects of higher order modes, *IEEE Transactions on Antennas and Propagation*, **30**(5), 998–1003, 1982.
- [20] K.S.H. Lee, Two parallel terminated conductors in external fields, *IEEE Transactions on Electromagnetic Compatibility*, **20**, 288–295, 1978.
- [21] S. Frankel, Forcing functions for externally excited transmission lines, *IEEE Transactions on Electromagnetic Compatibility*, **22**, 210, 1980.
- [22] C.R. Paul and D.R. Bush, Radiated emissions from common-mode currents, *Proceedings of the 1987 IEEE International Symposium on Electromagnetic Compatibility*, Atlanta, GA, (September 1987).
- [23] C.R. Paul, A comparison of the contributions of common-mode and differential-mode currents in radiated emissions, *IEEE Transactions on Electromagnetic Compatibility*, **31**, 189–193, 1989.
- [24] K.B. Hardin, Decomposition of radiating structures to directly predict asymmetric-mode radiation, PhD dissertation, University of Kentucky, 1991.

2

THE TRANSMISSION-LINE EQUATIONS FOR TWO-CONDUCTOR LINES

In this chapter, we will show the derivation of the transmission-line equations for two-conductor lines from two points of view. First, they will be derived from the integral form of Maxwell's equations, and second they will be derived from the per-unit-length distributed parameter equivalent circuit. Both methods allow the incorporation of conductor losses. In Chapter 3, we will repeat this for a general $(n + 1)$ -conductor multiconductor transmission line (MTL). The process will be identical to that for a two-conductor line, but the details will be a bit more tedious. Nevertheless, the transmission-line equations for an MTL, written using matrix notation, will be identical in *form* to those for a two-conductor line.

2.1 DERIVATION OF THE TRANSMISSION-LINE EQUATIONS FROM THE INTEGRAL FORM OF MAXWELL'S EQUATIONS

Recall Faraday's law in integral form [A.1,A.6]:

$$\oint_c \vec{\mathcal{E}} \cdot d\vec{l} = -\mu \frac{d}{dt} \int_s \vec{\mathcal{H}} \cdot d\vec{s} \quad (2.1)$$

This is illustrated in Figure 2.1. The differential path length around the closed contour c that bounds the open surface s is denoted by $d\vec{l}$. A differential surface area of surface

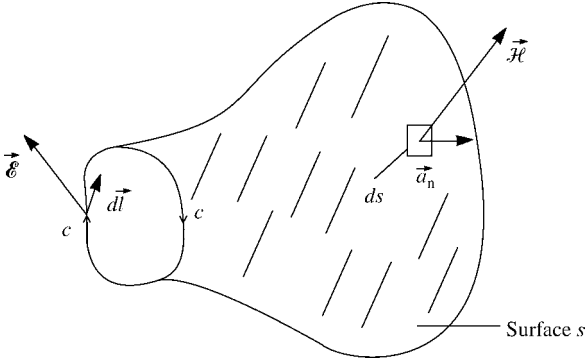


FIGURE 2.1 Illustration of the relation of the contour and surface in Faraday’s law.

s is denoted by $d\vec{s} = ds \vec{a}_n$, where \vec{a}_n is a unit normal to the surface. The direction of the contour c and the normal to the open surface it surrounds are related in Faraday’s law by the right-hand rule [A.1,A.6]. In other words, if we place the fingers of our right hand in the direction of c , the thumb will point in the direction of \vec{a}_n , which gives the direction “out of this open surface.”

Figure 2.2(a) shows a general two-conductor line. We have shown an open surface s between the two conductors that is uniform in cross section along the longitudinal or z direction, which is the axis of the line. (The surface is considered to be flat for simplicity as illustrated in Figure 2.2(b), although any open surface will yield the same result so long as its cross section in the z or longitudinal direction is uniform, that is, independent of z .) The surface is bounded by the closed contour c . Writing Faraday’s law around this contour yields

$$\int_a^{a'} \vec{\mathcal{E}}_t \cdot d\vec{l} + \int_{a'}^{b'} \vec{\mathcal{E}}_l \cdot d\vec{l} + \int_{b'}^b \vec{\mathcal{E}}_t \cdot d\vec{l} + \int_b^a \vec{\mathcal{E}}_l \cdot d\vec{l} = \mu \frac{d}{dt} \int_s \vec{\mathcal{H}}_t \cdot \vec{a}_n ds \quad (2.2)$$

where $\vec{\mathcal{E}}_t$ denotes the transverse electric field (in the x - y cross-sectional plane) and $\vec{\mathcal{E}}_l$ denotes the *longitudinal* or z -directed electric field (along the surfaces of the conductors). Observe that in Figure 2.2 the unit normal to this surface, \vec{a}_n , is opposite the direction for Faraday’s law since the contour c is defined in the clockwise direction, and hence the minus sign on the right-hand side of (2.1) is absent here. Here, we are including losses of the conductors as an approximation in that this longitudinal electric field produced along the conductor surfaces by the imperfect conductors is assumed not to significantly perturb the field structure from a transverse electromagnetic (TEM) one. As discussed in Chapter 1, the assumption of a TEM field structure allows us to *uniquely* define a voltage between the top conductor and the bottom conductor

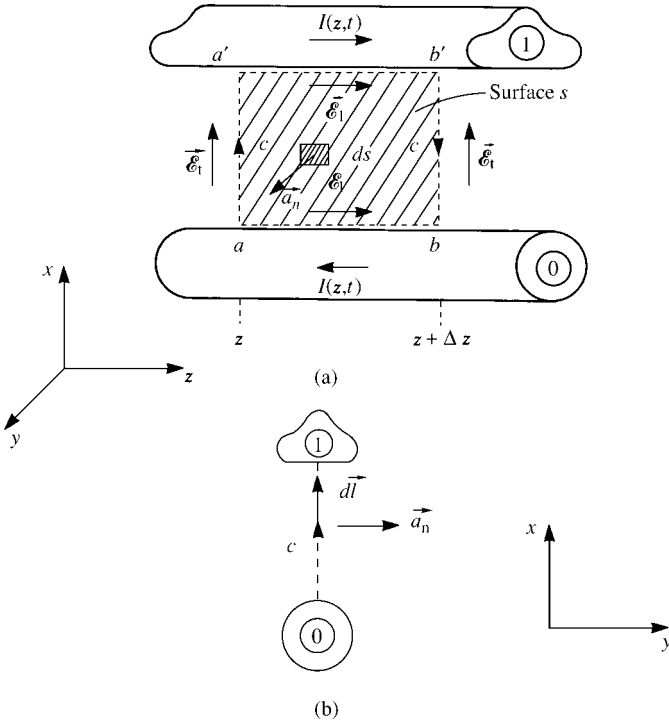


FIGURE 2.2 Definition of the contour c and associated surface s for derivation of the first transmission-line equation: (a) longitudinal view (along the z line axis) and (b) in the transverse x - y plane looking in the direction of increasing z .

(positive at the top conductor) as

$$V(z, t) = - \int_a^{a'} \vec{\mathcal{E}}_1(x, y, z, t) \cdot d\vec{l} \quad (2.3a)$$

$$V(z + \Delta z, t) = - \int_b^{b'} \vec{\mathcal{E}}_1(x, y, z + \Delta z, t) \cdot d\vec{l} \quad (2.3b)$$

To allow for imperfect conductors, we define the per-unit-length conductor resistance of each conductor as $r_1 \Omega/\text{m}$ and $r_0 \Omega/\text{m}$. Thus,

$$- \int_{a'}^{b'} \vec{\mathcal{E}}_1 \cdot d\vec{l} = -r_1 \Delta z I(z, t) \quad (2.4a)$$

$$- \int_b^a \vec{\mathcal{E}}_1 \cdot d\vec{l} = -r_0 \Delta z I(z, t) \quad (2.4b)$$

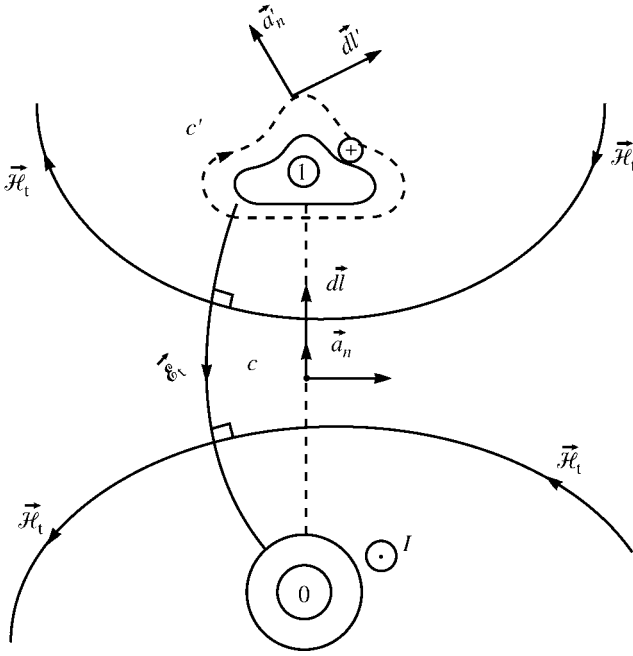


FIGURE 2.3 Illustration of the definitions of the contour c and surface s for determining the first transmission-line equation from Faraday’s law, and the definitions of the contour c' and surface s' for determining the second transmission-line equation from the equation of conservation of charge.

where, along the conductors, $\vec{\mathcal{E}}_1 = \mathcal{E}_z \vec{a}_z$ and $d\vec{l} = dz \vec{a}_z$. As discussed in Chapter 1, the current is *uniquely defined* for a TEM field structure as

$$I(z, t) = \oint_{c'} \vec{\mathcal{H}}_t \cdot d\vec{l} \tag{2.5}$$

and contour c' is a contour just off the surface of and encircling the top conductor in the transverse plane as shown in Figure 2.3. Hence, (2.2) becomes

$$-V(z, t) + r_1 \Delta z I(z, t) + V(z + \Delta z, t) + r_0 \Delta z I(z, t) = \mu \frac{d}{dt} \int_s \vec{\mathcal{H}}_t \cdot \vec{a}_n ds \tag{2.6}$$

Dividing both sides by Δz and rearranging gives

$$\frac{V(z + \Delta z, t) - V(z, t)}{\Delta z} = -r_1 I(z, t) - r_0 I(z, t) + \mu \frac{1}{\Delta z} \frac{d}{dt} \int_s \vec{\mathcal{H}}_t \cdot \vec{a}_n ds \tag{2.7}$$

As shown in Chapter 1, the magnetic flux penetrating the surface per unit of line length is, as shown in Figure 2.3,

$$\begin{aligned}\psi &= -\mu \lim_{\Delta z \rightarrow 0} \frac{1}{\Delta z} \int_s \vec{\mathcal{H}}_t \cdot \vec{a}_n ds \\ &= l I(z, t)\end{aligned}\quad (2.8)$$

where l is the per-unit-length inductance. Observe that a minus sign is required here because of the relative directions of $\vec{\mathcal{H}}_t$ and the normal to the surface, \vec{a}_n , as shown in Figure 2.3. Taking the limit of (2.7) as $\Delta z \rightarrow 0$ and substituting (2.8) yields the first transmission-line equation:

$$\frac{\partial V(z, t)}{\partial z} = -r I(z, t) - l \frac{\partial I(z, t)}{\partial t} \quad (2.9)$$

The total per-unit-length resistance of a Δz section of the line is the sum of the per-unit-length resistances of each conductor, r_1 and r_0 , and we denote this total resistance as $r = r_1 + r_0$.

In order to derive the second transmission-line equation, consider placing a closed surface s' around the top conductor and just off that conductor as shown in Figure 2.4. This is the same surface used to define current in (2.5). The portion of the surface over the end caps is denoted as s'_e , whereas the portion over the sides is denoted as s'_s . Recall the continuity equation or equation of conservation of charge [A.1]:

$$\oiint_{s'} \vec{\mathcal{J}} \cdot d\vec{s}' = -\frac{d}{dt} Q_{\text{enc}} \quad (2.10)$$

Over the end caps, we have

$$\iint_{s'_e} \vec{\mathcal{J}} \cdot d\vec{s}' = I(z + \Delta z, t) - I(z, t) \quad (2.11)$$

Over the sides of the surface, there are two currents penetrating it: a *conduction current* $\mathcal{I}_c = \sigma \mathcal{E}_t$ and a *displacement current* $\mathcal{I}_d = \varepsilon(\partial \mathcal{E}_t / \partial t)$, where the surrounding homogeneous medium is characterized by conductivity σ and permittivity ε . These notions can be extended to an inhomogeneous medium surrounding the conductors in a similar but approximate manner. This is an approximation since an inhomogeneous medium, uniform along the line or not, invalidates the TEM field structure assumption, which requires that all waves propagate with the same velocity. A portion of the left-hand side of (2.10) contains the *transverse conduction current* flowing between the

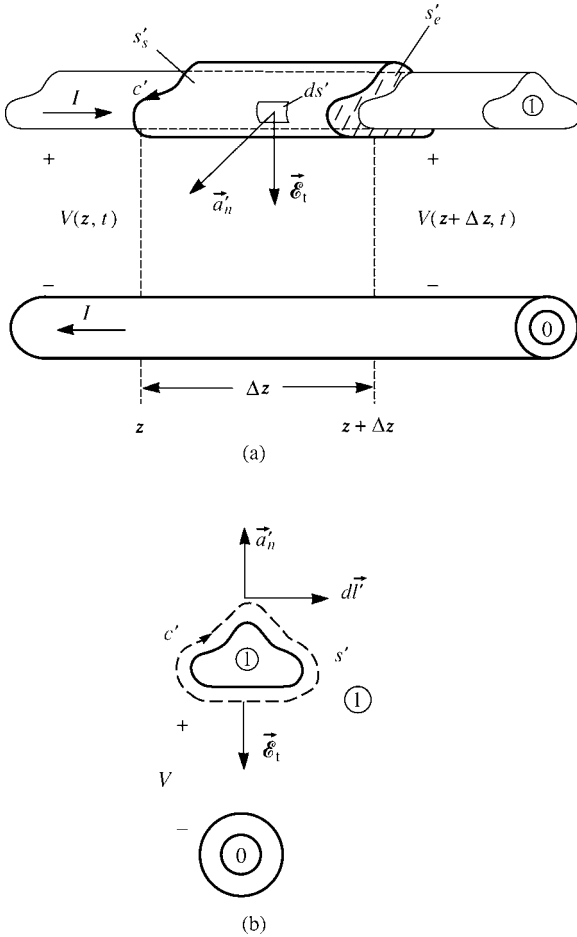


FIGURE 2.4 Definition of the contour c' and surface s' for derivation of the second MTL equation: (a) longitudinal view (along the z line axis) and (b) in the transverse x - y plane looking in the direction of increasing z .

conductors:

$$\iint_{s'_s} \vec{\mathcal{J}}_c \cdot d\vec{s}' = \sigma \iint_{s'_s} \vec{\mathcal{E}}_t \cdot d\vec{s}' \quad (2.12)$$

This can again be considered by defining a *per-unit-length conductance*, g S/m, between the two conductors as the ratio of conduction current flowing between the two conductors in the transverse plane to the voltage between the two conductors (see Figure 2.4(b)). Therefore,

$$gV(z, t) = \sigma \lim_{\Delta z \rightarrow 0} \frac{1}{\Delta z} \iint_{s'_s} \vec{\mathcal{E}}_t \cdot d\vec{s}' \quad (2.13)$$

Similarly, the charge enclosed by the surface (residing on the conductor surface) is, by Gauss' law,

$$Q_{\text{enc}} = \varepsilon \iint_{s'_s} \vec{\mathcal{E}}_t \cdot d\vec{s}' \quad (2.14)$$

The charge per unit of line length can be defined in terms of the *per-unit-length capacitance* c between the conductors as

$$c V(z, t) = \varepsilon \lim_{\Delta z \rightarrow 0} \frac{1}{\Delta z} \iint_{s'_s} \vec{\mathcal{E}}_t \cdot d\vec{s}' \quad (2.15)$$

Substituting (2.11), (2.12), and (2.14) into (2.10) and dividing both sides by Δz gives

$$\frac{I(z + \Delta z, t) - I(z, t)}{\Delta z} + \sigma \frac{1}{\Delta z} \iint_{s'_s} \vec{\mathcal{E}}_t \cdot d\vec{s}' = -\varepsilon \frac{1}{\Delta z} \frac{d}{dt} \iint_{s'_s} \vec{\mathcal{E}}_t \cdot d\vec{s}' \quad (2.16)$$

Taking the limit as $\Delta z \rightarrow 0$ and substituting (2.13) and (2.15) yields the second transmission-line equation:

$$\frac{\partial I(z, t)}{\partial z} = -g V(z, t) - c \frac{\partial V(z, t)}{\partial t} \quad (2.17)$$

2.2 DERIVATION OF THE TRANSMISSION-LINE EQUATIONS FROM THE PER-UNIT-LENGTH EQUIVALENT CIRCUIT

The per-unit-length equivalent circuit for a section of line of length Δz is shown in Figure 2.5. Writing Kirchhoff's voltage law (KVL) around the loop gives

$$V(z + \Delta z, t) - V(z, t) = -r \Delta z I(z, t) - l \Delta z \frac{\partial I(z, t)}{\partial t} \quad (2.18)$$

Dividing both sides by Δz and taking the limit as $\Delta z \rightarrow 0$ yields the first transmission-line equation:

$$\frac{\partial V(z, t)}{\partial z} = -r I(z, t) - l \frac{\partial I(z, t)}{\partial t} \quad (2.19)$$

Writing Kirchhoff's current law (KCL) at the upper node gives

$$I(z + \Delta z, t) - I(z, t) = -g \Delta z V(z + \Delta z, t) - c \Delta z \frac{\partial V(z + \Delta z, t)}{\partial t} \quad (2.20)$$

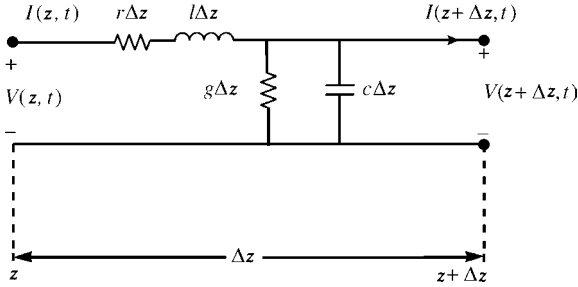


FIGURE 2.5 The per-unit-length equivalent circuit for derivation of the transmission-line equations.

Dividing both sides by Δz and taking the limit as $\Delta z \rightarrow 0$ yields the second transmission-line equation:

$$\frac{\partial I(z, t)}{\partial z} = -gV(z, t) - c \frac{\partial V(z, t)}{\partial t} \tag{2.21}$$

2.3 PROPERTIES OF THE PER-UNIT-LENGTH PARAMETERS

The per-unit-length parameters of inductance, l , capacitance, c , and conductance, g , were obtained in Chapter 1 under the assumptions of (1) *perfect line conductors* and (2) a *homogeneous* surrounding medium. The per-unit-length inductance is the ratio of the magnetic flux per unit of line length penetrating the loop between the two wires, ψ , and the current on the wires as

$$l = \frac{\psi}{I} \tag{2.22a}$$

The per-unit-length capacitance is the ratio of the per-unit-length charge distribution on the conductors, q , and the voltage between the two conductors as

$$c = \frac{q}{V} \tag{2.22b}$$

The per-unit-length conductance is the ratio of the current through the surrounding dielectric and flowing from one conductor to the other in the transverse plane, J_t , and the voltage between the two conductors as

$$g = \frac{J_t}{V} \tag{2.22c}$$

These parameters are related, *for a homogeneous medium*, as shown in Chapter 1, as

$$lc = \mu\varepsilon \quad (2.23a)$$

$$gl = \sigma\mu \quad (2.23b)$$

$$\frac{g}{c} = \frac{\sigma}{\varepsilon} \quad (2.23c)$$

It was assumed that the parameters of the surrounding *homogeneous* medium, permeability μ , permittivity ε , and conductivity σ , are constants. Numerical methods for obtaining the per-unit-length parameters of l , c , and g for an inhomogeneous surrounding medium will be obtained in Chapter 5.

2.4 INCORPORATING FREQUENCY-DEPENDENT LOSSES

As will be discussed in more detail in Chapter 4, these per-unit-length parameters will, in general, be *frequency dependent* and will depend to varying degrees on the frequency of excitation of the line, $\omega = 2\pi f$, which are denoted as $l(\omega)$, $c(\omega)$, $g(\omega)$, and $r(\omega)$. For perfect conductors, the line currents will reside on the surfaces of those conductors and therefore $r = 0$. For imperfect conductors, the currents will be uniformly distributed over the conductor cross sections at low frequencies, but at higher frequencies will, because of *skin effect*, migrate toward the surfaces of the conductors lying in a thickness on the order of a skin depth, $\delta = 1/\sqrt{\pi f \mu \sigma_c}$, where $\mu = \mu_0$ is the permeability of the conductor material and σ_c is its conductivity. This results in the per-unit-length resistances being a function of frequency, $r(\omega)$. As the frequency of excitation of the line increases, the resistance will increase at a rate of \sqrt{f} . Similarly, some of the magnetic flux will lie internal to the conductors giving a per-unit-length internal inductance that is also frequency dependent, $l_i(\omega)$. As the frequency of excitation increases and the currents migrate to the conductor surfaces, this internal inductance due to magnetic flux internal to the conductors will decrease at a rate of \sqrt{f} eventually going to zero as the frequency increases without bound. Hence, the total per-unit-length inductance will be the sum of this frequency-dependent internal inductance and the external inductance due to the magnetic flux external to the conductors, l_e , as $l = l_e + l_i(\omega)$. The per-unit-length inductance l discussed in Chapter 1 and given in (2.22a) is essentially this external inductance l_e , which is obtained as $f \rightarrow \infty$, that is, for perfect line conductors. We will henceforth denote l_e simply as l .

Similarly, the medium surrounding the conductors has an *effective conductivity* that is primarily due to bound charge in the dielectric and is frequency dependent, $\sigma_{\text{eff}}(\omega)$. Hence, the per-unit-length conductance will be frequency dependent, $g(\omega)$. The relative permittivity of many dielectrics, $\varepsilon_r(f)$, is not constant but is (mildly) a function of frequency decreasing with increasing frequency. Hence, the per-unit-length capacitance will be a (mild) function of frequency, $c(\omega)$.

It is much easier to include these frequency-dependent per-unit-length parameters when the transmission-line equations are written in phasor form in the frequency domain. Transforming the time-domain transmission-line equations with the Fourier transform yields the frequency-domain transmission-line equations. These may be obtained by simply replacing $\frac{\partial}{\partial t} \rightarrow j\omega$ to give

$$\begin{aligned}\frac{d\hat{V}(z, \omega)}{dz} &= -[r(\omega) + j\omega l_i(\omega)] \hat{I}(z, \omega) - j\omega l \hat{I}(z, \omega) \\ &= -\hat{z}(\omega) \hat{I}(z, \omega)\end{aligned}\quad (2.24a)$$

$$\begin{aligned}\frac{d\hat{I}(z, \omega)}{dz} &= -g(\omega) \hat{V}(z, \omega) - j\omega c(\omega) \hat{V}(z, \omega) \\ &= -\hat{y}(\omega) \hat{V}(z, \omega)\end{aligned}\quad (2.24b)$$

where the per-unit-length impedance and admittance, respectively, are

$$\hat{z}(\omega) = \underbrace{[r(\omega) + j\omega l_i(\omega)]}_{\hat{z}_i} + j\omega l \quad (2.25a)$$

$$\hat{y}(\omega) = g(\omega) + j\omega c(\omega) \quad (2.25b)$$

and $\hat{z}_i(\omega) = [r(\omega) + j\omega l_i(\omega)]$ is the per-unit-length internal impedance of the conductors. The fact that the per-unit-length parameters are generally functions of frequency presents no problems in the solution of these frequency-domain versions of the transmission-line equations. These equations are solvable at each frequency by evaluating the per-unit-length parameters at that frequency and including them as constants at that frequency. In the time domain, Eqs. (2.24) become convolutions [A.2.A.5]:

$$\begin{aligned}\frac{\partial V(z, t)}{\partial z} &= -z(t) * I(z, t) \\ &= -\int_0^t z(\tau) I(z, t - \tau) d\tau\end{aligned}\quad (2.26a)$$

$$\begin{aligned}\frac{\partial I(z, t)}{\partial z} &= -y(t) * V(z, t) \\ &= -\int_0^t y(\tau) V(z, t - \tau) d\tau\end{aligned}\quad (2.26b)$$

where $*$ denotes *convolution*, and $z(t)$ and $y(t)$ are the time-domain inverse Fourier transforms of $\hat{z}(\omega)$ and $\hat{y}(\omega)$:

$$\hat{z}(\omega) \Leftrightarrow z(t) \quad (2.27a)$$

$$\hat{y}(\omega) \Leftrightarrow y(t) \quad (2.27b)$$

Hence, frequency-dependent per-unit-length parameters can be easily included in the frequency-domain transmission-line equations, but their inclusion in the time-domain transmission-line equations presents significant computational problems because of the requirement to (1) obtain the time-domain per-unit-length parameters from the frequency-domain parameters and (2) perform the required convolution.

2.4.1 Properties of the Frequency-Domain Per-Unit-Length Impedance $\hat{z}(\omega)$ and Admittance $\hat{y}(\omega)$

The frequency-domain per-unit-length impedance parameter $\hat{z}(\omega)$ and admittance parameter $\hat{y}(\omega)$ cannot be specified arbitrarily. To show this, we first investigate the general properties of the Fourier transform (integral). The Fourier transform relates the frequency-domain function to the corresponding time-domain function as [1, 2]

$$\hat{F}(\omega) = \int_{-\infty}^{\infty} f(t) e^{-j\omega t} dt \quad (2.28)$$

Substituting Euler's identity

$$e^{j\theta} = \cos(\theta) + j \sin(\theta) \quad (2.29)$$

into (2.28) yields

$$\hat{F}(\omega) = \int_{-\infty}^{\infty} f(t) \cos(\omega t) dt - j \int_{-\infty}^{\infty} f(t) \sin(\omega t) dt \quad (2.30)$$

Hence, the Fourier transform can be written as the sum of a real part $F_R(\omega)$ and an imaginary part $F_I(\omega)$ as

$$\hat{F}(\omega) = F_R(\omega) + jF_I(\omega) \quad (2.31)$$

where $F_R(\omega)$ and $F_I(\omega)$ are real functions of $\omega = 2\pi f$ and f is the cyclic frequency, and the real and imaginary parts are given by

$$F_R(\omega) = \int_{-\infty}^{\infty} f(t) \cos(\omega t) dt \quad (2.32a)$$

and

$$F_I(\omega) = - \int_{-\infty}^{\infty} f(t) \sin(\omega t) dt \quad (2.32b)$$

If $f(t)$ is a real-valued function of t , then the Fourier transform must satisfy

$$\hat{F}(-\omega) = \hat{F}^*(\omega) \quad (2.33)$$

where the * superscript denotes the complex conjugate. To prove this, substitute $\omega \Rightarrow -\omega$ into (2.30) and use the trigonometric properties $\cos(-\omega t) = \cos(\omega t)$ and $\sin(-\omega t) = -\sin(\omega t)$. Hence, for $f(t)$ that are real-time functions, the real and imaginary parts of the Fourier transform are related as

$$F_R(\omega) = F_R(-\omega) \quad (2.34a)$$

and

$$F_I(\omega) = -F_I(-\omega) \quad (2.34b)$$

so that for real $f(t)$ the real part of the Fourier transform must be an even function of ω and the imaginary part must be an odd function of ω . The inverse Fourier transform is [1, 2]

$$f(t) = \frac{1}{2\pi} \int_{-\infty}^{\infty} \hat{F}(\omega) e^{j\omega t} d\omega \quad (2.35)$$

If $\hat{F}(-\omega) = \hat{F}^*(\omega)$, then

$$\begin{aligned} f(t) &= \frac{1}{2\pi} \int_0^{\infty} \hat{F}(\omega) e^{j\omega t} d\omega + \frac{1}{2\pi} \int_0^{\infty} \hat{F}(-\omega) e^{-j\omega t} d\omega \\ &= \frac{1}{\pi} \int_0^{\infty} [F_R(\omega) \cos(\omega t) - F_I(\omega) \sin(\omega t)] d\omega \\ &= \frac{1}{\pi} \operatorname{Re} \int_0^{\infty} \hat{F}(\omega) e^{j\omega t} d\omega \end{aligned} \quad (2.36)$$

and we have used the complex algebra property that $\hat{C} + \hat{C}^* = 2\operatorname{Re}[\hat{C}]$. Therefore, the necessary and sufficient condition for $f(t)$ to be a real function of t is that the Fourier transform satisfy (2.33) and therefore (2.34). Hence, the Fourier transforms of the per-unit-length impedance and admittance parameters must satisfy

$$\hat{z}(-\omega) = \hat{z}^*(\omega) \quad (2.37a)$$

$$\hat{y}(-\omega) = \hat{y}^*(\omega) \quad (2.37b)$$

or, equivalently,

$$z_R(\omega) = z_R(-\omega) \quad (2.38a)$$

$$z_I(\omega) = -z_I(-\omega) \quad (2.38b)$$

and

$$y_R(\omega) = y_R(-\omega) \quad (2.39a)$$

$$y_I(\omega) = -y_I(-\omega) \quad (2.39b)$$

Hence, the real parts of $\hat{z}(\omega)$ and $\hat{y}(\omega)$ must be *even functions of ω* and the imaginary parts must be *odd functions of ω* .

These general properties of the Fourier transform can also be used to show that the real and imaginary parts of the Fourier transform of the per-unit-length parameters in (2.25) cannot be specified independently but are related [1–3]. First, consider the general single-input, single-output linear system characterized by its time-domain impulse response, $h(t)$. The input is denoted by $x(t)$, and the output is denoted by $y(t)$. The output may be obtained in the time domain with the convolution integral as

$$\begin{aligned} y(t) &= h(t) * x(t) \\ &= \int_0^t h(t - \tau) x(\tau) d\tau \\ &= \int_0^t h(\tau) x(t - \tau) d\tau \end{aligned} \quad (2.40)$$

These forms of the convolution integral are valid for $x(t) = 0$ for $t < 0$ and $h(t) = 0$ for $t < 0$. The impulse response $h(t)$ is the response for a unit impulse input $x(t) = \delta(t)$ as $y(t) = h(t)$. We assume that the system is *causal*, that is,

$$h(t) = 0, \quad t < 0 \quad (2.41)$$

which means that we cannot have an output response before the input is applied. Causality is obviously a general requirement for all physical systems and also applies to $z(t)$ and $y(t)$ in (2.26) and (2.27). It can be shown that for a *causal* $h(t)$, the real and imaginary parts of its transform are Hilbert transform pairs and must be related as [1–3]

$$H_R(\omega) = \frac{1}{\pi} \int_{-\infty}^{\infty} \frac{H_I(\omega')}{(\omega - \omega')} d\omega' \quad (2.42a)$$

and

$$H_I(\omega) = -\frac{1}{\pi} \int_{-\infty}^{\infty} \frac{H_R(\omega')}{(\omega - \omega')} d\omega' \quad (2.42b)$$

where the Fourier transform of $h(t)$ is

$$\hat{H}(\omega) = H_R(\omega) + j H_I(\omega) \quad (2.43)$$

and $H_R(\omega)$ and $H_I(\omega)$ are real valued. Hence, we conclude that, in order to satisfy causality, the real and imaginary parts of the per-unit-length impedance and admittance parameters in (2.25) must be related as in (2.42). Similar relations exist between the magnitude and phase of $\hat{H}(\omega) = H(\omega) \angle \theta(\omega)$:

$$\ln |H(\omega)| = \frac{1}{\pi} \int_{-\infty}^{\infty} \frac{\theta(\omega')}{\omega - \omega'} d\omega' \quad (2.44a)$$

$$\theta(\omega) = -\frac{1}{\pi} \int_{-\infty}^{\infty} \frac{\ln |H(\omega')|}{\omega - \omega'} d\omega' \quad (2.44b)$$

These relations can also be written, for real-valued $f(t)$, as

$$\begin{aligned} H_R(\omega) &= \frac{1}{\pi} \int_0^{\infty} \frac{H_I(\omega')}{\omega - \omega'} d\omega' + \frac{1}{\pi} \int_{-\infty}^0 \frac{H_I(\omega')}{\omega - \omega'} d\omega' \\ &= \frac{1}{\pi} \int_0^{\infty} \frac{H_I(\omega')}{\omega - \omega'} d\omega' + \frac{1}{\pi} \int_0^{\infty} \frac{H_I(-\omega')}{\omega + \omega'} d\omega' \\ &= \frac{2}{\pi} \int_0^{\infty} \frac{\omega' H_I(\omega')}{\omega^2 - \omega'^2} d\omega' \end{aligned} \quad (2.45a)$$

and

$$\begin{aligned} H_I(\omega) &= -\frac{1}{\pi} \int_0^{\infty} \frac{H_R(\omega')}{\omega - \omega'} d\omega' - \frac{1}{\pi} \int_{-\infty}^0 \frac{H_R(\omega')}{\omega - \omega'} d\omega' \\ &= -\frac{1}{\pi} \int_0^{\infty} \frac{H_R(\omega')}{\omega - \omega'} d\omega' - \frac{1}{\pi} \int_0^{\infty} \frac{H_R(-\omega')}{\omega + \omega'} d\omega' \\ &= -\frac{2\omega}{\pi} \int_0^{\infty} \frac{H_R(\omega')}{\omega^2 - \omega'^2} d\omega' \end{aligned} \quad (2.45b)$$

where we have made the assumption that $h(t)$ is a real-valued function of t and have therefore substituted the relations in (2.34):

$$H_R(\omega) = H_R(-\omega) \tag{2.46a}$$

and

$$H_I(\omega) = -H_I(-\omega) \tag{2.46b}$$

The results in (2.42) and (2.45) assume that $h(t)$ contains no impulses at $t = 0$ and hence assumes that $H(\omega) \rightarrow 0$ as $\omega \rightarrow \infty$. If the real part approaches a finite, nonzero constant as $\omega \rightarrow \infty$, $H_R(\infty)$, then (2.45) can be written

$$H_R(\omega) = H_R(\infty) + \frac{2}{\pi} \int_0^\infty \frac{\omega' H_I(\omega')}{\omega^2 - \omega'^2} d\omega' \tag{2.47a}$$

and

$$H_I(\omega) = -\frac{2\omega}{\pi} \int_0^\infty \frac{[H_R(\omega') - H_R(\infty)]}{\omega^2 - \omega'^2} d\omega' \tag{2.47b}$$

These important relations in (2.47) between the real and imaginary parts of the Fourier transform of a real and *causal* time function $h(t)$ are also known as the Kronig–Kramers relations [3]. These will be useful in relating the real and imaginary parts of the complex permittivity of a lossy dielectric in Chapter 4.

PROBLEMS

- 2.1 Demonstrate the result in (2.6).
- 2.2 Demonstrate the result in (2.16).
- 2.3 Derive the transmission-line equations from each of the circuits in Figure P2.3 in the limit as $\Delta z \rightarrow 0$. Observe that the total inductance (capacitance) in each structure is $l\Delta z(c\Delta z)$. This shows that the structure of the per-unit-length equivalent circuit is not important in obtaining the transmission-line equations from it so long as the total per-unit-length inductance and capacitance are contained in the structure and we let $\Delta z \rightarrow 0$.
- 2.4 Evaluate the convolution integral

$$\int_0^{t=4\text{ s}} f(\tau) I(z, t - \tau) d\tau$$

for the functions in Figure P2.4. $[(5/3) \times 10^{-3} \text{ V}]$

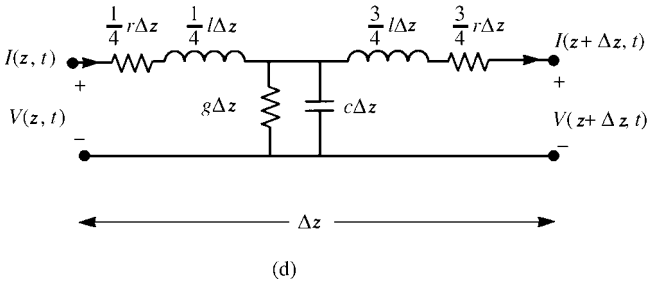
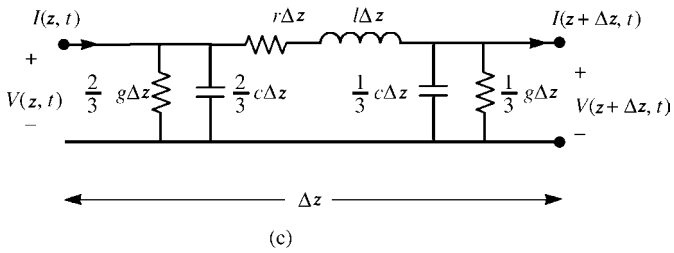
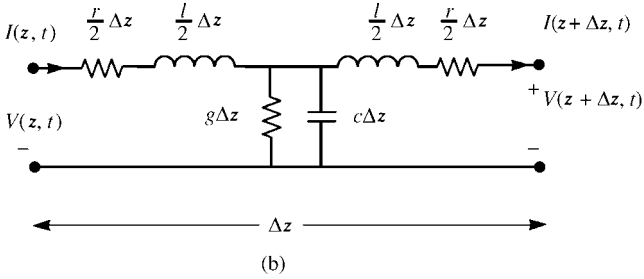
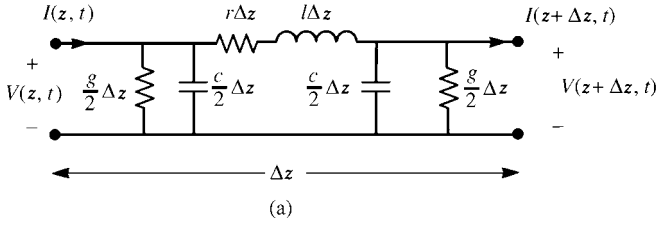


FIGURE P2.3

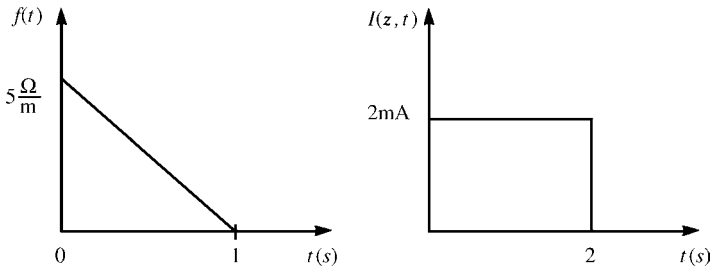


FIGURE P2.4

2.5 Evaluate the convolution integral

$$\int_0^{t=1 \text{ ns}} f(\tau) I(z, t - \tau) d\tau$$

for the functions in Figure P2.5. [$3.8 \mu\text{V}$]

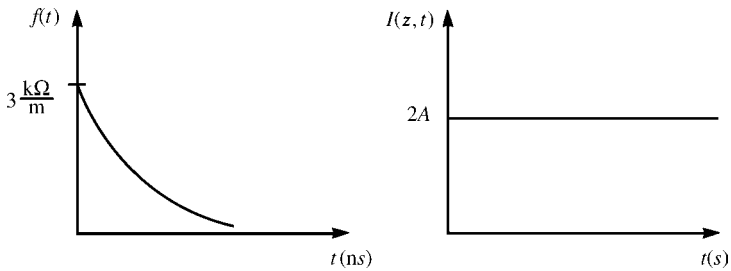


FIGURE P2.5

- 2.6 Demonstrate the result in (2.33).
- 2.7 Demonstrate the result in (2.36).
- 2.8 Demonstrate the result in (2.44).
- 2.9 Show that if a transform $\hat{F}(\omega)$ contains ω only as the product with $j = \sqrt{-1}$, that is, $j\omega$, then the transform represents a real-valued time function $f(t)$.
- 2.10 Show that if a transform $\hat{F}(\omega)$ contains ω only as $\sqrt{\omega}(1 + j)$, then the transform represents a real-valued time function $f(t)$. [Hint: Use the complex-variable identity $\sqrt{j\omega} = (\sqrt{\omega}/\sqrt{2})(1 + j)$.]
- 2.11 Show that $\hat{F}(\omega) = M\sqrt{j\omega}$ represents a causal time function $f(t)$. [Hint: Use the complex-variable identity $\sqrt{j\omega} = (\sqrt{\omega}/\sqrt{2})(1 + j)$, the results of Problem 2.10, and Eq. (2.45b).]
- 2.12 Suppose that the real part of $\hat{H}(\omega)$ is a unit impulse (in frequency) centered at the origin, $\omega = 0$, defined by $H_R(\omega) = \delta(\omega)$. Determine and sketch the imaginary part of $\hat{H}(\omega)$ in order that the time-domain function $h(t)$ is causal. [$H_I(\omega) = -1/(\pi\omega)$]
- 2.13 Suppose that the real part of $\hat{H}(\omega)$ is defined by $H_R(\omega) = 1$ for $-W < \omega < W$, and is zero elsewhere, i.e., $H_R(\omega) = 0$ for $\omega < -W$ for $\omega > W$. Determine and sketch the imaginary part of $\hat{H}(\omega)$ in order that the time-domain function $h(t)$ is causal. [$H_I(\omega) = (1/\pi) \ln |(\omega - W)/(\omega + W)|$]

REFERENCES

- [1] A. Papoulis, *The Fourier Integral and Its Applications*, McGraw-Hill, New York, 1962.
- [2] A.B. Carlson, *Communication Systems—An Introduction to Signals and Noise in Electrical Communication*, McGraw-Hill, New York, 1968.
- [3] S. Ramo, J.R. Whinnery, and T. VanDuzer, *Fields and Waves in Communication Electronics*, 2nd edition, John Wiley & Sons, New York, 1984.

3

THE TRANSMISSION-LINE EQUATIONS FOR MULTICONDUCTOR LINES

In Chapter 1, we discussed the general properties of all transmission-line equation characterizations. The transverse electromagnetic (TEM) field structure and associated mode of propagation is the fundamental, underlying assumption in the representation of a transmission-line structure with the transmission-line equations. These were developed in the previous chapter for two-conductor lines. In this chapter, we will extend those notions to *multiconductor transmission lines (MTLs)* consisting of $n + 1$ conductors.

The development and derivation of the MTL equations parallel the developments for two-conductor lines considered in the previous chapter. In fact, the developed MTL equations have, using matrix notation, a *form* identical to those equations. There are some new concepts concerning the important per-unit-length parameters that contain the cross-sectional dimensions of the particular line.

3.1 DERIVATION OF THE MULTICONDUCTOR TRANSMISSION-LINE EQUATIONS FROM THE INTEGRAL FORM OF MAXWELL'S EQUATIONS

Figure 3.1 shows the general $(n + 1)$ -conductor line to be considered. It consists of n conductors and a *reference conductor* (denoted as the zeroth conductor) to which the n line voltages will be referenced. This choice of the reference conductor is not unique. Applying Faraday's law to the contour c_i that encloses surface s_i shown between the

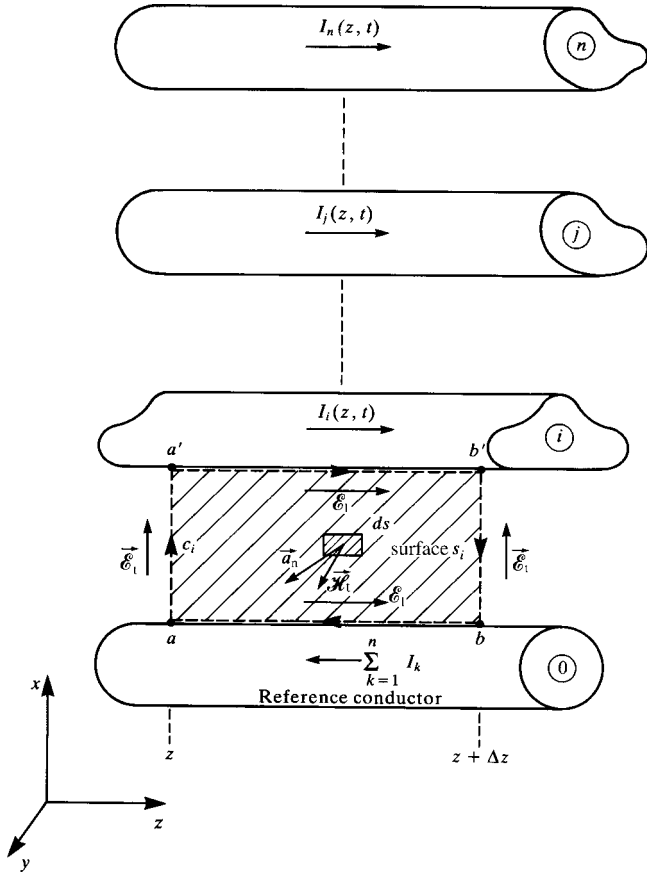


FIGURE 3.1 Illustration of the contour c_i and associated surface s_i for the derivation of the first transmission-line equation for the i th circuit.

reference conductor and the i th conductor gives

$$\int_a^{a'} \vec{\mathcal{E}}_t \cdot d\vec{l} + \int_{a'}^b \vec{\mathcal{E}}_1 \cdot d\vec{l} + \int_{b'}^b \vec{\mathcal{E}}_t \cdot d\vec{l} + \int_b^a \vec{\mathcal{E}}_1 \cdot d\vec{l} = \mu \frac{d}{dt} \int_{s_i} \vec{\mathcal{H}}_t \cdot \vec{a}_n ds \quad (3.1)$$

where, again, $\vec{\mathcal{E}}_t$ denotes the transverse electric field (in the x - y cross-sectional plane) and $\vec{\mathcal{E}}_1$ denotes the *longitudinal* or z -directed electric field (along the surfaces of the conductors). Observe, once again, that because of the choice of the direction of the contour, the direction of \vec{a}_n (out of the page), and the right-hand rule, the minus sign on the right-hand side of Faraday's law is absent in (3.1). Once again, because of the assumption of a TEM field structure, we may *uniquely* define a voltage between the

i th conductor and the reference conductor (positive on the i th conductor) as

$$V_i(z, t) = - \int_a^{a'} \vec{\mathcal{E}}_t(x, y, z, t) \cdot d\vec{l} \quad (3.2a)$$

$$V_i(z + \Delta z, t) = - \int_b^{b'} \vec{\mathcal{E}}_t(x, y, z + \Delta z, t) \cdot d\vec{l} \quad (3.2b)$$

We again define the per-unit-length conductor resistances as $r_i \Omega/\text{m}$, and the per-unit-length resistance of the reference conductor is denoted as $r_0 \Omega/\text{m}$. Thus,

$$- \int_a^{a'} \vec{\mathcal{E}}_t \cdot d\vec{l} = -r_i \Delta z I_i(z, t) \quad (3.3a)$$

$$- \int_b^{a'} \vec{\mathcal{E}}_t \cdot d\vec{l} = -r_0 \Delta z \sum_{k=1}^n I_k(z, t) \quad (3.3b)$$

The current of the i th conductor is

$$I_i(z, t) = \oint_{c'_i} \vec{\mathcal{H}}_t \cdot d\vec{l}' \quad (3.4)$$

where the contour c'_i surrounds the i th conductor just off its surface. For the TEM field structure assumption it can be shown, as was the case for two-conductor lines, that the sum of the currents on all $n + 1$ conductors in the z direction at any cross section is zero. This is the basis for saying that the currents of the n conductors *return through the reference conductor*. Substituting into (1) yields

$$-V_i(z, t) + r_i \Delta z I_i(z, t) + V_i(z + \Delta z, t) + r_0 \Delta z \sum_{k=1}^n I_k(z, t) = \mu \frac{d}{dt} \int_{s_i} \vec{\mathcal{H}}_t \cdot \vec{a}_n ds \quad (3.5)$$

Dividing both sides by Δz and rearranging gives

$$\begin{aligned} \frac{V_i(z + \Delta z, t) - V_i(z, t)}{\Delta z} &= -r_0 I_1 - r_0 I_2 - \cdots - (r_0 + r_i) I_i - \cdots - r_0 I_n \\ &+ \mu \frac{1}{\Delta z} \frac{d}{dt} \int_{s_i} \vec{\mathcal{H}}_t \cdot \vec{a}_n ds \end{aligned} \quad (3.6)$$

Before taking the limit as $\Delta z \rightarrow 0$, let us make some observations similar to the case of two-conductor lines. Clearly, the total magnetic flux penetrating the surface

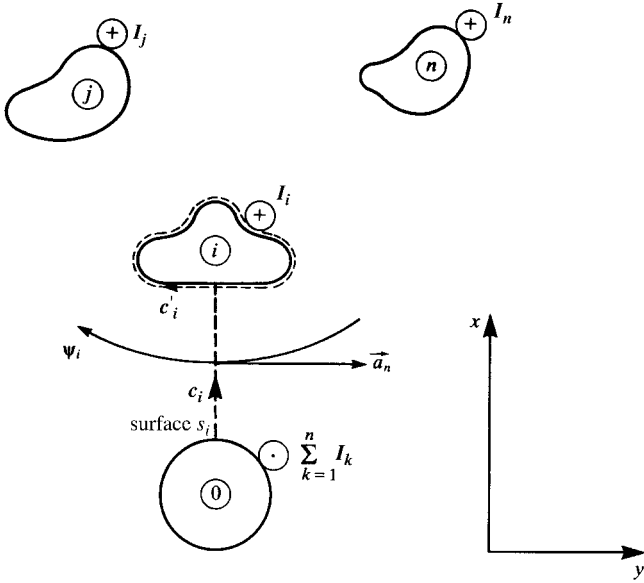


FIGURE 3.2 Cross-sectional illustration of the contour c_i and associated surface s_i for the derivation of the first transmission-line equation for the i th circuit.

s_i in Figure 3.1 will be a linear combination of the fluxes due to the currents on all the conductors. Consider a cross-sectional view of the line *looking in the direction of increasing z* shown in Figure 3.2. The currents of the n conductors are implicitly defined in the positive z direction according to (3.4) since the contour c'_i surrounding the i th conductor is defined in the clockwise direction. Therefore, the magnetic fluxes due to the currents of the n conductors will also be in the clockwise direction looking in the direction of increasing z . The per-unit-length magnetic flux ψ_i penetrating the surface s_i between the reference conductor and the i th conductor is therefore *defined* to be in this clockwise direction *when looking in the direction of increasing z* as shown in Figure 3.2. Therefore, this per-unit-length magnetic flux penetrating surface s_i can be written as

$$\begin{aligned} \psi_i &= -\mu \lim_{\Delta z \rightarrow 0} \frac{1}{\Delta z} \int_{s_i} \vec{\mathcal{H}}_t \cdot \vec{a}_n ds \\ &= l_{i1}I_1 + l_{i2}I_2 + \cdots + l_{ii}I_i + \cdots + l_{in}I_n \end{aligned} \tag{3.7}$$

Observe that a minus sign is again required in this flux expression. This is because the direction of the required flux, ψ_i , and the defined unit normal to the surface, \vec{a}_n , are in opposite directions. The l_{ii} term is the per-unit-length *self-inductance* of the i th circuit or loop, and the l_{ij} terms are the per-unit-length *mutual inductances* between this i th circuit and the j th circuit. Taking the limit of (3.6) as $\Delta z \rightarrow 0$ and substituting

(3.7) yields

$$\begin{aligned}
 \frac{\partial V_i(z, t)}{\partial z} = & -r_0 I_1(z, t) - r_0 I_2(z, t) - \dots - (r_0 + r_i) I_i(z, t) - \dots \\
 & -r_0 I_n(z, t) - l_{i1} \frac{\partial I_1(z, t)}{\partial t} - l_{i2} \frac{\partial I_2(z, t)}{\partial t} - \dots - l_{ii} \frac{\partial I_i(z, t)}{\partial t} - \dots \\
 & -l_{in} \frac{\partial I_n(z, t)}{\partial t}
 \end{aligned} \tag{3.8}$$

This first MTL equation can be written in a compact form using matrix notation as

$$\frac{\partial}{\partial z} \mathbf{V}(z, t) = -\mathbf{R}\mathbf{I}(z, t) - \mathbf{L} \frac{\partial}{\partial t} \mathbf{I}(z, t) \tag{3.9}$$

where the $n \times 1$ voltage and current vectors are defined as

$$\mathbf{V}(z, t) = \begin{bmatrix} V_1(z, t) \\ \vdots \\ V_i(z, t) \\ \vdots \\ V_n(z, t) \end{bmatrix} \tag{3.10a}$$

$$\mathbf{I}(z, t) = \begin{bmatrix} I_1(z, t) \\ \vdots \\ I_i(z, t) \\ \vdots \\ I_n(z, t) \end{bmatrix} \tag{3.10b}$$

The *per-unit-length inductance matrix* is defined from (3.7) as

$$\Psi = \mathbf{L}\mathbf{I} \tag{3.11a}$$

where Ψ is an $n \times 1$ vector containing the total magnetic fluxes per unit length, ψ_i , penetrating the i th circuit, which is the surface defined between the i th conductor and the reference conductor:

$$\Psi = \begin{bmatrix} \psi_1 \\ \vdots \\ \psi_i \\ \vdots \\ \psi_n \end{bmatrix} \tag{3.11b}$$

The flux through the circuit (loop), ψ_i , is directed in the clockwise direction when looking in the $+z$ direction (see Figure 3.2). The *per-unit-length inductance matrix* \mathbf{L} contains the individual per-unit-length self-inductances, l_{ii} , of the circuits and the per-unit-length mutual inductances between the circuits, l_{ij} . In Section 3.5, \mathbf{L} will be shown to be a symmetric matrix as

$$\mathbf{L} = \begin{bmatrix} l_{11} & l_{12} & \cdots & l_{1n} \\ l_{12} & l_{22} & \cdots & l_{2n} \\ \vdots & \vdots & \ddots & \vdots \\ l_{1n} & l_{2n} & \cdots & l_{nn} \end{bmatrix} \tag{3.11c}$$

Similarly, from (3.8) we define the *per-unit-length resistance matrix* as

$$\begin{aligned} \mathbf{R} &= \begin{bmatrix} (r_1 + r_0) & r_0 & \cdots & r_0 \\ r_0 & (r_2 + r_0) & \cdots & r_0 \\ \vdots & \vdots & \ddots & \vdots \\ r_0 & r_0 & \cdots & (r_n + r_0) \end{bmatrix} \\ &= \begin{bmatrix} r_1 & 0 & \cdots & 0 \\ 0 & r_2 & \cdots & 0 \\ \vdots & \vdots & \ddots & \vdots \\ 0 & 0 & \cdots & r_n \end{bmatrix} + \begin{bmatrix} r_0 & r_0 & \cdots & r_0 \\ r_0 & r_0 & \cdots & r_0 \\ \vdots & \vdots & \ddots & \vdots \\ r_0 & r_0 & \cdots & r_0 \end{bmatrix} \end{aligned} \tag{3.12}$$

Observe that this first transmission-line equation given in (3.9) is identical in form to the *scalar* first transmission-line equation for a two-conductor line given in (2.9) and (2.19) of Chapter 2.

This per-unit-length resistance matrix in (3.12) has a nice form but is restricted to reference conductors that are finite-sized conductors such as wires. In the case of a reference conductor being a large ground plane, each current returning in the ground plane will be concentrated beneath the “going down” conductor as illustrated in Figure 3.3. These currents spread out in the ground plane and cause the per-unit-

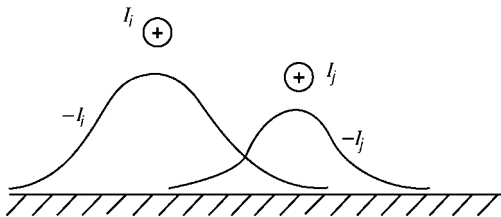


FIGURE 3.3 Illustration of “current spreading” in a ground plane and the principle that the return currents will concentrate beneath the associated “going-down” conductor.

length resistance matrix to be of the form

$$\begin{aligned}
 \mathbf{R} &= \begin{bmatrix} (r_1 + r_{11}) & r_{12} & \cdots & r_{1n} \\ r_{12} & (r_2 + r_{22}) & \cdots & r_{2n} \\ \vdots & \vdots & \ddots & \vdots \\ r_{1n} & r_{2n} & \cdots & (r_n + r_{nn}) \end{bmatrix} \\
 &= \begin{bmatrix} r_1 & 0 & \cdots & 0 \\ 0 & r_2 & \cdots & 0 \\ \vdots & \vdots & \ddots & \vdots \\ 0 & 0 & \cdots & r_n \end{bmatrix} + \begin{bmatrix} r_{11} & r_{12} & \cdots & r_{1n} \\ r_{12} & r_{22} & \cdots & r_{2n} \\ \vdots & \vdots & \ddots & \vdots \\ r_{1n} & r_{2n} & \cdots & r_{nn} \end{bmatrix} \tag{3.13}
 \end{aligned}$$

where r_{ij} are due to the resistance of the ground plane and are generally not equal.

In order to derive the second MTL equation, we place a closed surface s' around the i th conductor as shown in Figure 3.4. The portion of the surface over the end caps is denoted as s'_e , whereas the portion over the sides is denoted as s'_s . Recall the

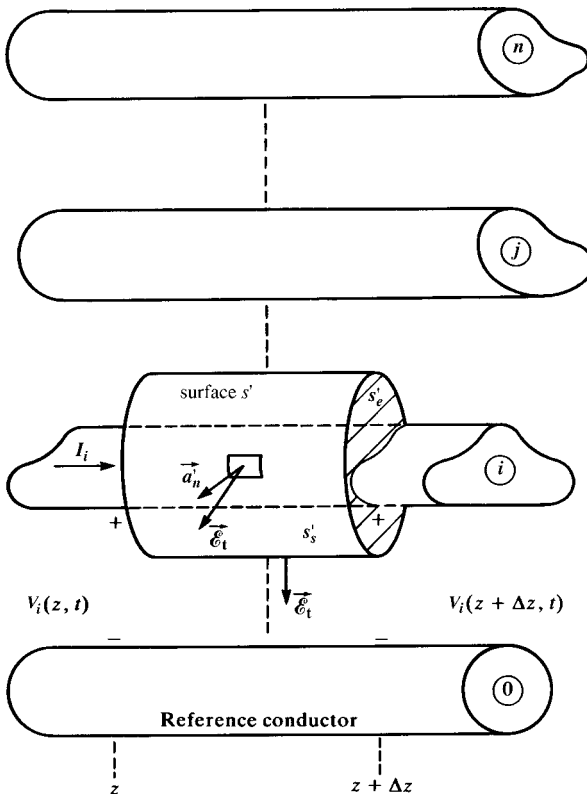


FIGURE 3.4 Illustration of the contour c'_i and associated surface s'_i for the derivation of the second transmission-line equation for the i th conductor.

continuity equation or equation of conservation of charge:

$$\oint_{s'} \vec{\mathcal{J}} \cdot d\vec{s}' = - \frac{d}{dt} Q_{\text{enc}} \quad (3.14)$$

Over the end caps, we have

$$\iint_{s'_e} \vec{\mathcal{J}} \cdot d\vec{s}' = I_i(z + \Delta z, t) - I_i(z, t) \quad (3.15)$$

Over the sides of the surface, there are again two currents: a *conduction current* $\vec{\mathcal{J}}_c = \sigma \vec{\mathcal{E}}_t$, and *displacement current* $\vec{\mathcal{J}}_d = \epsilon \frac{\partial \vec{\mathcal{E}}_t}{\partial t}$, where the surrounding homogeneous medium is characterized by conductivity σ and permittivity ϵ . Again, these notions can be extended to an inhomogeneous medium surrounding the conductors in a similar manner. A portion of the left-hand side of (3.14) contains the *transverse conduction current* flowing between the conductors:

$$\iint_{s'_s} \vec{\mathcal{J}}_c \cdot d\vec{s}' = \sigma \iint_{s'_s} \vec{\mathcal{E}}_t \cdot d\vec{s}' \quad (3.16)$$

This can again be considered by defining *per-unit-length conductances* g_{ij} S/m between each pair of conductors as the ratio of conduction current flowing between the two conductors in the transverse plane to the voltage between the two conductors. Therefore, as illustrated in Figure 3.5(a),

$$\begin{aligned} \sigma \lim_{\Delta z \rightarrow 0} \frac{1}{\Delta z} \iint_{s'_s} \vec{\mathcal{E}}_t \cdot d\vec{s}' &= g_{i1}(V_i - V_1) + \cdots + g_{ii}V_i + \cdots + g_{in}(V_i - V_n) \\ &= -g_{i1}V_1(z, t) - g_{i2}V_2(z, t) - \cdots + \sum_{k=1}^n g_{ik}V_k(z, t) \\ &\quad - \cdots - g_{in}V_n(z, t) \end{aligned} \quad (3.17)$$

Similarly, the charge enclosed by the surface (residing on the conductor surface) is, by Gauss' law,

$$Q_{\text{enc}} = \epsilon \iint_{s'_s} \vec{\mathcal{E}}_t \cdot d\vec{s}' \quad (3.18)$$

The charge per unit of line length can be defined in terms of the *per-unit-length capacitances* c_{ij} between each pair of conductors. Therefore, as illustrated in

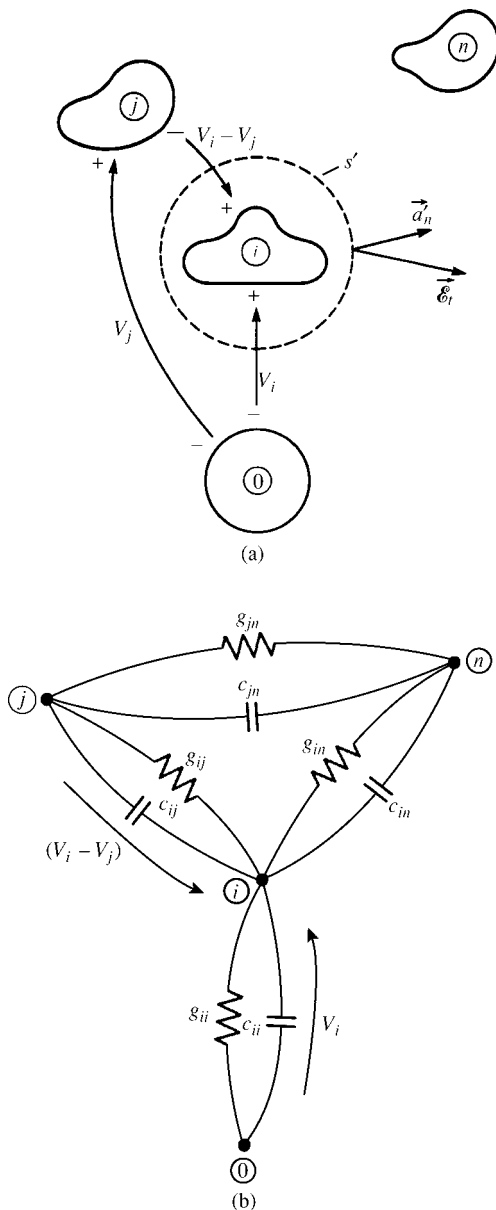


FIGURE 3.5 Cross-sectional illustration of (a) the contour c'_i and associated surface s'_i for the derivation of the second transmission-line equation for the i th conductor and (b) the equivalent per-unit-length conductances and capacitances.

Figure 3.5(a),

$$\begin{aligned} \varepsilon \lim_{\Delta z \rightarrow 0} \frac{1}{\Delta z} \iint_{s'_s} \vec{\mathcal{E}}_t \cdot d\vec{s}' &= c_{i1}(V_i - V_1) + \cdots + c_{ii}V_i + \cdots + c_{in}(V_i - V_n) \\ &= -c_{i1}V_1(z, t) - c_{i2}V_2(z, t) - \cdots + \sum_{k=1}^n c_{ik}V_k(z, t) \\ &\quad - \cdots - c_{in}V_n(z, t) \end{aligned} \quad (3.19)$$

These concepts are illustrated in cross section in Figure 3.5(b). Substituting (3.15), (3.16), and (3.18) into (3.14) and dividing both sides by Δz gives

$$\frac{I_i(z + \Delta z, t) - I_i(z, t)}{\Delta z} + \sigma \frac{1}{\Delta z} \iint_{s'_s} \vec{\mathcal{E}}_t \cdot d\vec{s}' = -\varepsilon \frac{1}{\Delta z} \frac{d}{dt} \iint_{s'_s} \vec{\mathcal{E}}_t \cdot d\vec{s}' \quad (3.20)$$

Taking the limit as $\Delta z \rightarrow 0$ and substituting (3.17) and (3.19) yields

$$\begin{aligned} \frac{\partial I_i(z, t)}{\partial z} &= g_{i1}V_1(z, t) + g_{i2}V_2(z, t) + \cdots - \sum_{k=1}^n g_{ik}V_k(z, t) + \cdots \\ &\quad + g_{in}V_n(z, t) + c_{i1} \frac{\partial}{\partial t} V_1(z, t) + c_{i2} \frac{\partial}{\partial t} V_2(z, t) + \cdots \\ &\quad - \sum_{k=1}^n c_{ik} \frac{\partial}{\partial t} V_k(z, t) + \cdots + c_{in} \frac{\partial}{\partial t} V_n(z, t) \end{aligned} \quad (3.21)$$

Equations (3.21) can be placed in compact form with matrix notation giving

$$\frac{\partial}{\partial z} \mathbf{I}(z, t) = -\mathbf{G} \mathbf{V}(z, t) - \mathbf{C} \frac{\partial}{\partial t} \mathbf{V}(z, t) \quad (3.22)$$

where \mathbf{V} and \mathbf{I} are defined by (3.10). The *per-unit-length conductance matrix* \mathbf{G} represents the conduction current flowing between the conductors in the transverse plane and is defined from (3.17) as

$$\mathbf{G} = \begin{bmatrix} \sum_{k=1}^n g_{1k} & -g_{12} & \cdots & -g_{1n} \\ -g_{12} & \sum_{k=1}^n g_{2k} & \cdots & -g_{2n} \\ \vdots & \vdots & \ddots & \vdots \\ -g_{1n} & -g_{2n} & \cdots & \sum_{k=1}^n g_{nk} \end{bmatrix} \quad (3.23)$$

The *per-unit-length capacitance matrix*, \mathbf{C} , represents the displacement current flowing between the conductors in the transverse plane and is defined from (3.19) as

$$\mathbf{C} = \begin{bmatrix} \sum_{k=1}^n c_{1k} & -c_{12} & \cdots & -c_{1n} \\ -c_{12} & \sum_{k=1}^n c_{2k} & \cdots & -c_{2n} \\ \vdots & \vdots & \ddots & \vdots \\ -c_{1n} & -c_{2n} & \cdots & \sum_{k=1}^n c_{nk} \end{bmatrix} \quad (3.24)$$

As will be shown in Section 3.5, both \mathbf{G} and \mathbf{C} are symmetric. Again observe that (3.22) is the matrix counterpart to the scalar second transmission-line equation for two-conductor lines given in (2.17) and (2.21) in Chapter 2. If we denote the total charge on the i th conductor per unit of line length as q_i , then the fundamental definition of \mathbf{C} is

$$\mathbf{Q} = \mathbf{C} \mathbf{V} \quad (3.25a)$$

where \mathbf{Q} is the $n \times 1$ vector of the total per-unit-length charges

$$\mathbf{Q} = \begin{bmatrix} q_1 \\ \vdots \\ q_i \\ \vdots \\ q_n \end{bmatrix} \quad (3.25b)$$

and \mathbf{V} is given by (3.10a). Similarly, the fundamental definition of \mathbf{G} is $\mathbf{I}_t = \mathbf{G}\mathbf{V}$, where \mathbf{I}_t is the $n \times 1$ vector containing the transverse conduction currents between the conductors per unit of line length.

The above per-unit-length parameter matrices once again contain all the cross-sectional dimension information that distinguishes one MTL structure from another.

3.2 DERIVATION OF THE MULTICONDUCTOR TRANSMISSION-LINE EQUATIONS FROM THE PER-UNIT-LENGTH EQUIVALENT CIRCUIT

As an alternative method, we derive the MTL equations from the *per-unit-length equivalent circuit* shown in Figure 3.6. Writing Kirchhoff's voltage law around the i th *circuit* consisting of the i th conductor and the reference conductor yields

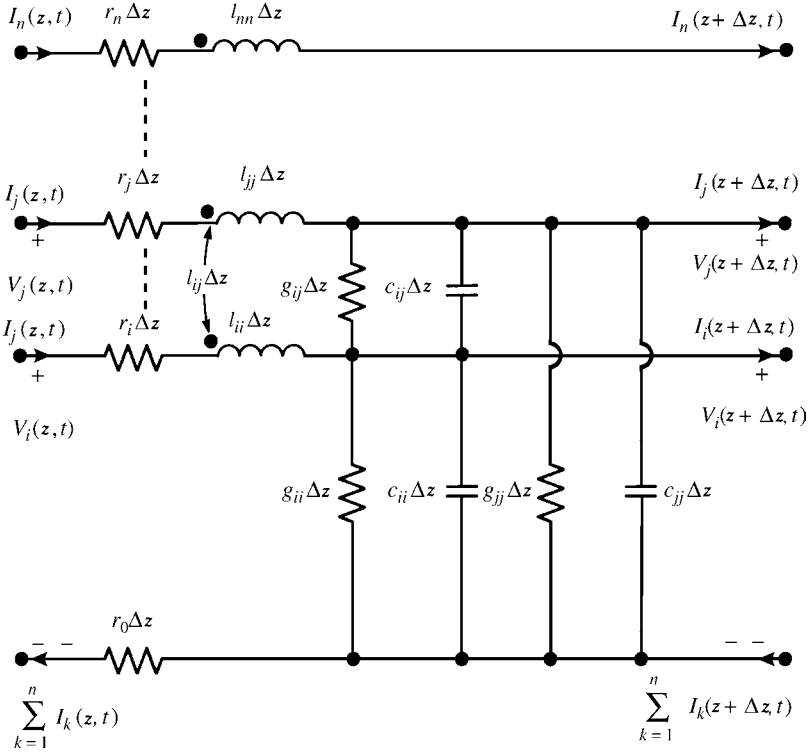


FIGURE 3.6 The per-unit-length equivalent circuit for derivation of the transmission-line equations.

$$\begin{aligned}
 -V_i(z, t) + r_i \Delta z I_i(z, t) + V_i(z + \Delta z, t) + r_0 \Delta z \sum_{k=1}^n I_k(z, t) &= -l_{i1} \Delta z \frac{\partial I_1(z, t)}{\partial t} \\
 -l_{i2} \Delta z \frac{\partial I_2(z, t)}{\partial t} - \dots - l_{ii} \Delta z \frac{\partial I_i(z, t)}{\partial t} - \dots - l_{in} \Delta z \frac{\partial I_n(z, t)}{\partial t} & \quad (3.26a)
 \end{aligned}$$

Dividing both sides by Δz and taking the limit as $\Delta z \rightarrow 0$ once again yields the first transmission-line equation given in (3.8) with the collection for all i given in matrix form in (3.9).

Similarly, the second MTL equation can be obtained by applying Kirchoff's current law to the i th conductor in the per-unit-length equivalent circuit in Figure 3.6 to yield

$$\begin{aligned}
 I_i(z + \Delta z, t) - I_i(z, t) &= -g_{i1} \Delta z (V_i - V_1) - \dots - g_{ii} \Delta z V_i - \dots \\
 -g_{in} \Delta z (V_i - V_n) - c_{i1} \Delta z \frac{\partial}{\partial t} (V_i - V_1) - \dots - c_{ii} \Delta z \frac{\partial}{\partial t} V_i - \dots \\
 -c_{in} \Delta z \frac{\partial}{\partial t} (V_i - V_n) & \quad (3.26b)
 \end{aligned}$$

Dividing both sides by Δz , taking the limit as $\Delta z \rightarrow 0$, and collecting terms once again yields the second transmission-line equation given in (3.21) with the collection for all i given in matrix form in (3.22).

3.3 SUMMARY OF THE MTL EQUATIONS

In summary, the *MTL equations* are given by the collection

$$\frac{\partial}{\partial z} \mathbf{V}(z, t) = -\mathbf{R} \mathbf{I}(z, t) - \mathbf{L} \frac{\partial}{\partial t} \mathbf{I}(z, t) \quad (3.27a)$$

$$\frac{\partial}{\partial z} \mathbf{I}(z, t) = -\mathbf{G} \mathbf{V}(z, t) - \mathbf{C} \frac{\partial}{\partial t} \mathbf{V}(z, t) \quad (3.27b)$$

The structures of the per-unit-length resistance matrix \mathbf{R} in (3.12) or (3.13), inductance matrix \mathbf{L} in (3.11c), conductance matrix \mathbf{G} in (3.23), and capacitance matrix \mathbf{C} in (3.24) are very important as are the definitions of the per-unit-length entries in those matrices. The precise definitions of these elements are rather intuitive and lead to many ways of computing them for a particular MTL type. These computational methods will be considered in detail in Chapters 4 and 5. The important properties of the per-unit-length parameter matrices will be obtained in Section 3.5. Again, these bear striking parallels to their scalar counterparts for the two-conductor line.

The MTL equations in (3.27) are a set of $2n$, *coupled, first-order, partial differential equations*. They may be put in a more compact form as

$$\frac{\partial}{\partial z} \begin{bmatrix} \mathbf{V}(z, t) \\ \mathbf{I}(z, t) \end{bmatrix} = - \begin{bmatrix} \mathbf{0} & \mathbf{R} \\ \mathbf{G} & \mathbf{0} \end{bmatrix} \begin{bmatrix} \mathbf{V}(z, t) \\ \mathbf{I}(z, t) \end{bmatrix} - \begin{bmatrix} \mathbf{0} & \mathbf{L} \\ \mathbf{C} & \mathbf{0} \end{bmatrix} \frac{\partial}{\partial t} \begin{bmatrix} \mathbf{V}(z, t) \\ \mathbf{I}(z, t) \end{bmatrix} \quad (3.28)$$

We will find this first-order form to be especially helpful when we set out to solve them in later chapters. If the conductors are perfect conductors, then $\mathbf{R} = \mathbf{0}$, whereas if the surrounding medium is lossless ($\sigma = 0$), then $\mathbf{G} = \mathbf{0}$. The line is said to be *lossless* if both the conductors and the medium are lossless in which case the MTL equations simplify to

$$\frac{\partial}{\partial z} \begin{bmatrix} \mathbf{V}(z, t) \\ \mathbf{I}(z, t) \end{bmatrix} = - \begin{bmatrix} \mathbf{0} & \mathbf{L} \\ \mathbf{C} & \mathbf{0} \end{bmatrix} \frac{\partial}{\partial t} \begin{bmatrix} \mathbf{V}(z, t) \\ \mathbf{I}(z, t) \end{bmatrix} \quad (3.29)$$

The first-order, coupled forms in (3.27) can be placed in the form of *second-order, uncoupled* equations by differentiating (3.27a) with respect to z and differentiating (3.27b) with respect to t to yield

$$\frac{\partial^2}{\partial z^2} \mathbf{V}(z, t) = -\mathbf{R} \frac{\partial}{\partial z} \mathbf{I}(z, t) - \mathbf{L} \frac{\partial^2}{\partial z \partial t} \mathbf{I}(z, t) \quad (3.30a)$$

$$\frac{\partial^2}{\partial z \partial t} \mathbf{I}(z, t) = -\mathbf{G} \frac{\partial}{\partial t} \mathbf{V}(z, t) - \mathbf{C} \frac{\partial^2}{\partial t^2} \mathbf{V}(z, t) \quad (3.30b)$$

In taking the derivatives with respect to z , we assume that the line is uniform; that is, the per-unit-length parameter matrices are independent of z . Substituting (3.30b) and (3.27b) into (3.30a) and reversing the process yields the *uncoupled, second-order equations*:

$$\frac{\partial^2}{\partial z^2} \mathbf{V}(z, t) = [\mathbf{R}\mathbf{G}] \mathbf{V}(z, t) + [\mathbf{R}\mathbf{C} + \mathbf{L}\mathbf{G}] \frac{\partial}{\partial t} \mathbf{V}(z, t) + \mathbf{L}\mathbf{C} \frac{\partial^2}{\partial t^2} \mathbf{V}(z, t) \quad (3.31a)$$

$$\frac{\partial^2}{\partial z^2} \mathbf{I}(z, t) = [\mathbf{G}\mathbf{R}] \mathbf{I}(z, t) + [\mathbf{C}\mathbf{R} + \mathbf{G}\mathbf{L}] \frac{\partial}{\partial t} \mathbf{I}(z, t) + \mathbf{C}\mathbf{L} \frac{\partial^2}{\partial t^2} \mathbf{I}(z, t) \quad (3.31b)$$

Observe that the various matrix products in (3.31) do not generally commute so that the proper order of multiplication must be observed.

3.4 INCORPORATING FREQUENCY-DEPENDENT LOSSES

We have so far neglected the important fact that, like the two-conductor case, the per-unit-length parameters in \mathbf{R} , \mathbf{L} , \mathbf{G} , and \mathbf{C} are generally frequency dependent, that is, $\mathbf{R}(\omega)$, $\mathbf{L}(\omega)$, $\mathbf{G}(\omega)$, and $\mathbf{C}(\omega)$. For perfect conductors, the currents reside on the surfaces of the conductors and $\mathbf{R} = \mathbf{0}$. For imperfect conductors, the currents, because of skin effect, will migrate toward the conductor surfaces as frequency is increased, and at high frequencies will be concentrated near the conductor surfaces in annuli of thickness equal to a skin depth: $\delta = 1/\sqrt{\pi f \sigma \mu}$. In addition, closely spaced conductors will cause the current distribution over the conductors to be nonuniformly distributed over the cross sections. The currents internal to the conductors will cause a per-unit-length internal inductance matrix $\mathbf{L}_i(\omega)$ that is also frequency dependent. This is due to the magnetic flux internal to the conductors. As frequency increases, this internal flux decreases as a rate of \sqrt{f} eventually decreasing to zero. This internal inductance matrix can be included in the total inductance as the sum with the external inductance matrix that is due to the magnetic flux external to the conductors, \mathbf{L} , which is substantially frequency independent. Similarly, the per-unit-length conductance matrix will be frequency dependent. This is because the dielectric will have a loss due to the incomplete alignment of the bound charges in it as frequency increases giving an effective conductivity that is frequency dependent, $\mathbf{G}(\omega)$. Similarly, the relative permittivity of the surrounding dielectric is (mildly) dependent on frequency giving a (mildly) frequency-dependent per-unit-length capacitance matrix $\mathbf{C}(\omega)$.

These frequency-dependent parameters can more readily be incorporated by writing the above MTL equations in the frequency domain by replacing $\frac{\partial}{\partial t} \rightarrow j\omega$ in (3.27) to give

$$\frac{d}{dz} \hat{\mathbf{V}}(z, \omega) = -\hat{\mathbf{Z}}(\omega) \hat{\mathbf{I}}(z, \omega) \quad (3.32a)$$

$$\frac{d}{dz} \hat{\mathbf{I}}(z, \omega) = -\hat{\mathbf{Y}}(\omega) \hat{\mathbf{V}}(z, \omega) \quad (3.32b)$$

where $\hat{\mathbf{Z}}(\omega)$ and $\hat{\mathbf{Y}}(\omega)$ are the per-unit-length impedance and admittance matrices, respectively, and are given by

$$\hat{\mathbf{Z}}(\omega) = \mathbf{R}(\omega) + j\omega\mathbf{L}_i(\omega) + j\omega\mathbf{L} \quad (3.33a)$$

$$\hat{\mathbf{Y}}(\omega) = \mathbf{G}(\omega) + j\omega\mathbf{C}(\omega) \quad (3.33b)$$

The second-order uncoupled equations are

$$\frac{d^2}{dz^2} \hat{\mathbf{V}}(z, \omega) = \hat{\mathbf{Z}}(\omega) \hat{\mathbf{Y}}(\omega) \hat{\mathbf{V}}(z, \omega) \quad (3.34a)$$

$$\frac{d^2}{dz^2} \hat{\mathbf{I}}(z, \omega) = \hat{\mathbf{Y}}(\omega) \hat{\mathbf{Z}}(\omega) \hat{\mathbf{I}}(z, \omega) \quad (3.34b)$$

Again, the matrices do not generally commute and the proper order of multiplication must be preserved.

In the time domain, the frequency-domain MTL equations in (3.32) become

$$\begin{aligned} \frac{\partial}{\partial z} \mathbf{V}(z, t) &= -\mathbf{Z}(t) * \mathbf{I}(z, t) \\ &= -\int_0^t \mathbf{Z}(\tau) \mathbf{I}(z, t - \tau) d\tau \end{aligned} \quad (3.35a)$$

$$\begin{aligned} \frac{\partial}{\partial z} \mathbf{I}(z, t) &= -\mathbf{Y}(t) * \mathbf{V}(z, t) \\ &= -\int_0^t \mathbf{Y}(\tau) \mathbf{V}(z, t - \tau) d\tau \end{aligned} \quad (3.35b)$$

where $*$ denotes convolution and the inverse Fourier transforms are denoted as

$$\mathbf{Z}(t) \Leftrightarrow \hat{\mathbf{Z}}(\omega) \quad (3.36a)$$

$$\mathbf{Y}(t) \Leftrightarrow \hat{\mathbf{Y}}(\omega) \quad (3.36b)$$

3.5 PROPERTIES OF THE PER-UNIT-LENGTH PARAMETER MATRICES \mathbf{L} , \mathbf{C} , \mathbf{G}

In Chapter 1 we showed that, for a two-conductor line immersed in a homogeneous medium characterized by permeability μ , conductivity σ , and permittivity ϵ , the per-

unit-length inductance l , conductance g , and capacitance c are related by $lc = \mu\epsilon$ and $lg = \mu\sigma$. For the case of an MTL consisting of $n + 1$ conductors immersed in a homogeneous medium characterized by permeability μ , conductivity σ , and permittivity ϵ , the per-unit-length parameter matrices are similarly related by

$$\mathbf{LC} = \mathbf{CL} = \mu\epsilon \mathbf{1}_n \quad (3.37a)$$

$$\mathbf{LG} = \mathbf{GL} = \mu\sigma \mathbf{1}_n \quad (3.37b)$$

where the $n \times n$ identity matrix is defined as having unity entries on the main diagonal and zeros elsewhere:

$$\mathbf{1}_n = \begin{bmatrix} 1 & 0 & \cdots & 0 & 0 \\ 0 & 1 & \cdots & 0 & 0 \\ \vdots & \vdots & \ddots & \vdots & \vdots \\ 0 & 0 & \cdots & 1 & 0 \\ 0 & 0 & \cdots & 0 & 1 \end{bmatrix} \quad (3.38)$$

Other important properties such as our logical assumption that these per-unit-length matrices are symmetric will also be shown.

Recall from Chapter 1 that the transverse electric and magnetic fields of the TEM field structure in a homogeneous medium characterized by ϵ , μ , and σ satisfy the following differential equations (see Eqs. (1.13) of Chapter 1):

$$\frac{\partial^2 \vec{\mathcal{E}}_t}{\partial z^2} = \mu\sigma \frac{\partial \vec{\mathcal{E}}_t}{\partial t} + \mu\epsilon \frac{\partial^2 \vec{\mathcal{E}}_t}{\partial t^2} \quad (3.39a)$$

$$\frac{\partial^2 \vec{\mathcal{H}}_t}{\partial z^2} = \mu\sigma \frac{\partial \vec{\mathcal{H}}_t}{\partial t} + \mu\epsilon \frac{\partial^2 \vec{\mathcal{H}}_t}{\partial t^2} \quad (3.39b)$$

Define voltage and current in the usual fashion as integrals in the transverse plane (see Fig. 2.3) as

$$V_i(z, t) = - \int_{c_i} \vec{\mathcal{E}}_t \cdot d\vec{l} \quad (3.40a)$$

$$I_i(z, t) = \oint_{c'_i} \vec{\mathcal{H}}_t \cdot d\vec{l}' \quad (3.40b)$$

Applying (3.40) to (3.39) yields

$$\frac{\partial^2}{\partial z^2} V_i(z, t) = \mu\sigma \frac{\partial}{\partial t} V_i(z, t) + \mu\epsilon \frac{\partial^2}{\partial t^2} V_i(z, t) \quad (3.41a)$$

$$\frac{\partial^2}{\partial z^2} I_i(z, t) = \mu\sigma \frac{\partial}{\partial t} I_i(z, t) + \mu\epsilon \frac{\partial^2}{\partial t^2} I_i(z, t) \quad (3.41b)$$

Collecting Eqs. (3.41) for all conductors in matrix form yields

$$\frac{\partial^2}{\partial z^2} \mathbf{V}(z, t) = \mu\sigma \frac{\partial}{\partial t} \mathbf{V}(z, t) + \mu\varepsilon \frac{\partial^2}{\partial t^2} \mathbf{V}(z, t) \quad (3.42a)$$

$$\frac{\partial^2}{\partial z^2} \mathbf{I}(z, t) = \mu\sigma \frac{\partial}{\partial t} \mathbf{I}(z, t) + \mu\varepsilon \frac{\partial^2}{\partial t^2} \mathbf{I}(z, t) \quad (3.42b)$$

Comparing (3.42) to (3.31) with $\mathbf{R} = \mathbf{0}$ gives the identities in (3.37). Because of the identities in (3.37), which are valid only for a homogeneous medium, we need to determine only one of the per-unit-length parameter matrices since (3.37) can be written, for example, as

$$\mathbf{L} = \mu\varepsilon \mathbf{C}^{-1} \quad (3.43a)$$

$$\begin{aligned} \mathbf{G} &= \frac{\sigma}{\varepsilon} \mathbf{C} \\ &= \mu\sigma \mathbf{L}^{-1} \end{aligned} \quad (3.43b)$$

$$\mathbf{C} = \mu\varepsilon \mathbf{L}^{-1} \quad (3.43c)$$

The previous relations in (3.37) and (3.43) are valid *only for a homogeneous surrounding medium*. In the remainder of this chapter, we will address the general case where the dielectric medium surrounding the $n + 1$ conductors may be *inhomogeneous*. Throughout this text, we will assume that any medium surrounding the line conductors (homogeneous or inhomogeneous) is not ferromagnetic and therefore has a permeability of free space, $\mu = \mu_0$. Designate the capacitance matrix with the surrounding medium (homogeneous or inhomogeneous) removed and replaced by free space having permeability ε_0 and permeability μ_0 as \mathbf{C}_0 . Since inductance depends on the permeability of the surrounding medium and does not depend on the permittivity of the medium, and the permeability of dielectrics is that of free space, μ_0 , the inductance matrix \mathbf{L} can be obtained from \mathbf{C}_0 using the relations for a homogeneous medium (in this case, free space) given in (3.43a) as

$$\mathbf{L} = \mu_0\varepsilon_0\mathbf{C}_0^{-1} \quad (3.44)$$

Therefore, for an inhomogeneous medium, we may determine these per-unit-length parameter matrices by (1) computing the capacitance matrix with the inhomogeneous medium present, \mathbf{C} , (2) computing the per-unit-length capacitance matrix with the inhomogeneous medium removed and replaced with free space, \mathbf{C}_0 , and then (3) computing \mathbf{L} from (3.44). It turns out that we will also develop in Chapters 4 and 5 a method for computing \mathbf{G} for an inhomogeneous medium from a modified capacitance calculation. Hence, we will only have to construct a capacitance solver in order to determine the per-unit-length parameter matrices of \mathbf{L} , \mathbf{C} , and \mathbf{G} for the general case of an inhomogeneous medium. In Chapter 5, we will examine numerical methods for computing the entries in these per-unit-length matrices for an inhomogeneous medium surrounding the conductors.

The identities in (3.37) and (3.43) are *valid only for a homogeneous surrounding medium* as is the assumption of a TEM field structure and the resulting MTL equations. We will often extend the MTL equation representation, in an approximate manner, to include *inhomogeneous media* as well as imperfect conductors under the *quasi-TEM assumption*. In the case of a surrounding medium that is either *homogeneous or inhomogeneous*, the per-unit-length parameter matrices \mathbf{L} , \mathbf{C} , and \mathbf{G} have several important properties. The primary ones are that they are *symmetric* and *positive-definite* matrices. As an illustration, we will prove that \mathbf{C} is symmetric. The proof that \mathbf{C} is a symmetric matrix (regardless of whether the surrounding medium is homogeneous or inhomogeneous) can be accomplished from energy considerations [A.1,1]. The basic relation for \mathbf{C} is given in (3.25). Suppose we invert this relation to give

$$\mathbf{V} = \mathbf{PQ} \tag{3.45a}$$

where $\mathbf{P} = \mathbf{C}^{-1}$ or, in expanded form,

$$\begin{aligned} V_1 &= p_{11}q_1 + \cdots + p_{1n}q_n \\ &\vdots \\ V_n &= p_{n1}q_1 + \cdots + p_{nn}q_n \end{aligned} \tag{3.45b}$$

If we can prove that $p_{ij} = p_{ji}$, then it follows that $c_{ij} = c_{ji}$. Suppose all conductors *except* the i th and j th are connected to the reference conductor (grounded) and all conductors are initially uncharged. Suppose we start charging the i th conductor to a final per-unit-length charge of q_i . Charging the i th conductor to an incremental charge q results in a voltage of the conductor, from (3.45b), of $V_i = p_{ii}q$. The incremental energy required to do this is $dW = V_i dq$. The total energy required to place the

charge q_i on the i th conductor is $W = \int_0^{q_i} p_{ii}q \, dq = (p_{ii}q_i^2/2)$. Now if we charge

the j th conductor to an incremental charge of q in the presence of the charged i th conductor, the voltage of the j th conductor is $V_j = p_{ji}q_i + p_{jj}q$ and the incremental energy required is $dW = (p_{ji}q_i + p_{jj}q) dq$. The total energy required to charge the

j th conductor to a charge of q_j becomes $W = \int_0^{q_j} dW dq = p_{ji}q_i q_j + (p_{jj}q_j^2/2)$. Thus,

the total energy required to charge conductor i to q_i and conductor j to q_j is

$$W_{\text{total}} = p_{ji}q_i q_j + \frac{p_{ii}q_i^2}{2} + \frac{p_{jj}q_j^2}{2}$$

If we reverse this process charging conductor j to q_j and then charging conductor i to q_i , we obtain

$$W_{\text{total}} = p_{ij}q_j q_i + \frac{p_{jj}q_j^2}{2} + \frac{p_{ii}q_i^2}{2}$$

Since the total energies must be the same regardless of the sequence in which the conductors are charged, we see, by comparing these two energy expressions, that

$$P_{ij} = P_{ji}$$

Therefore, it follows that

$$c_{ij} = c_{ji}$$

and therefore the capacitance matrix \mathbf{C} is *symmetric*.

Recall that this proof of symmetry relied on energy considerations and therefore is valid for *inhomogeneous media*. Because of the relation in (3.44), $\mathbf{L} = \mu_0 \epsilon_0 \mathbf{C}_0^{-1}$, it is clear that the per-unit-length inductance matrix is also symmetric. The proof that \mathbf{C} , \mathbf{L} , and \mathbf{G} are symmetric matrices (regardless of whether the surrounding medium is homogeneous or inhomogeneous) can also be obtained from a more general relation called Green's reciprocity theorem [2]. This relation relies on the important assumption that the surrounding medium is *isotropic*. This means that the parameters of permittivity, permeability, and conductivity are scalars. An anisotropic medium is one in which these parameters are matrices relating the three components of the vectors \mathbf{E} , \mathbf{D} , \mathbf{B} , \mathbf{H} , and \mathbf{J}_t , where \mathbf{J}_t is the vector of transverse currents flowing through the surrounding medium [A.1]. We also, of course, assume that the surrounding medium is *linear*.

We next set out to prove that \mathbf{L} , \mathbf{C} , and \mathbf{G} are *positive definite*. The energy stored in the electric field per unit of line length is [2]

$$\begin{aligned} w_e &= \frac{1}{2} \sum_{k=1}^n q_k V_k \\ &= \frac{1}{2} \mathbf{Q}^t \mathbf{V} \end{aligned} \quad (3.46)$$

where the *transpose* of a matrix \mathbf{M} is denoted by \mathbf{M}^t . The vector \mathbf{Q} contains the per-unit-length charges on the conductors and is given in (3.25b). Substituting the relation for \mathbf{C} in (3.25a), $\mathbf{Q} = \mathbf{C}\mathbf{V}$, into (3.46) gives

$$w_e = \frac{1}{2} \mathbf{V}^t \mathbf{C} \mathbf{V} > 0 \quad (3.47)$$

where we have used the matrix property that $\mathbf{Q}^t = [\mathbf{C}\mathbf{V}]^t = \mathbf{V}^t \mathbf{C}^t$ along with the previously proven property that \mathbf{C} is symmetric, that is, $\mathbf{C}^t = \mathbf{C}$. This total energy stored in the electric field must be positive and nonzero for all nonzero choices of the voltages (positive or negative). Thus, we say that \mathbf{C} is *positive definite* if

$$\mathbf{V}^t \mathbf{C} \mathbf{V} > 0 \quad (3.48)$$

for all possible nonzero values of the entries in \mathbf{V} . It turns out that this implies that all of the *eigenvalues* of \mathbf{C} must be *positive* and *nonzero*, a property we will find very useful in our later developments [3].

Similarly, the energy stored in the magnetic field per unit of line length is [2]

$$\begin{aligned} w_m &= \frac{1}{2} \sum_{k=1}^n \psi_k I_k \\ &= \frac{1}{2} \Psi^t \mathbf{I} \end{aligned} \quad (3.49)$$

where Ψ is the $n \times 1$ vector of magnetic fluxes through the respective circuits and is given in (3.11b). Substituting the relation for \mathbf{L} given in (3.11a) gives

$$w_m = \frac{1}{2} \mathbf{I}^t \mathbf{L} \mathbf{I} > 0 \quad (3.50)$$

where $\Psi^t = [\mathbf{L}\mathbf{I}]^t = \mathbf{I}^t \mathbf{L}$, and we use the property that \mathbf{L} is symmetric, $\mathbf{L}^t = \mathbf{L}$. Since the stored magnetic energy must always be greater than zero, we see that \mathbf{L} is positive definite also:

$$\mathbf{I}^t \mathbf{L} \mathbf{I} > 0 \quad (3.51)$$

Again, this means that the eigenvalues of \mathbf{L} are all positive and nonzero.

Matrices \mathbf{C} and \mathbf{G} have the unique property that the sum of all elements in any row is greater than zero (see (3.23) and (3.24)). Such a matrix is said to be *hyperdominant*. It can be shown that any hyperdominant matrix form is always positive definite (see Problem 3.11). Hence, \mathbf{G} is also positive definite and therefore its eigenvalues are all positive and nonzero.

PROBLEMS

- 3.1 Demonstrate the result in (3.8).
- 3.2 Demonstrate the form of \mathbf{R} given in (3.12).
- 3.3 Demonstrate the result in (3.21).
- 3.4 Demonstrate the form of \mathbf{G} in (3.23).
- 3.5 Demonstrate the form of \mathbf{C} in (3.24).
- 3.6 Derive the MTL equations for the per-unit-length equivalent circuit of a four-conductor line shown in Figure P3.6.
- 3.7 Demonstrate the result in (3.31).
- 3.8 A four-conductor line immersed in free space has the following per-unit-length inductance matrix:

$$\mathbf{L} = \begin{bmatrix} 8 & 3 & 2 \\ 3 & 6 & 1 \\ 2 & 1 & 4 \end{bmatrix} \frac{\text{nH}}{\text{m}}$$

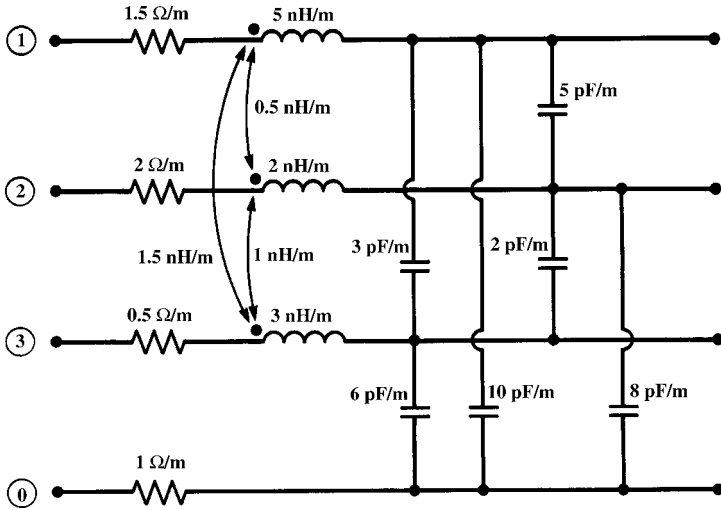


FIGURE P3.6

Determine the per-unit-length capacitance matrix. If the surrounding medium is homogeneous with conductivity $\sigma = 10^{-3}$ S/m, determine the per-unit-length conductance matrix.

- 3.9** Demonstrate the result in (3.42).
- 3.10** Show that the criterion for positive definiteness of a real, symmetric matrix is that its eigenvalues are all positive and nonzero. (*Hint:* Transform the matrix to another equivalent one with a transformation matrix that diagonalizes it as $\mathbf{T}^{-1}\mathbf{M}\mathbf{T} = \Lambda$, where Λ is diagonal with its eigenvalues on the main diagonal. It is always possible to diagonalize any real, symmetric matrix such that $\mathbf{T}^{-1} = \mathbf{T}^t$, where \mathbf{T}^t is the transpose of \mathbf{T} .) Show that the per-unit-length inductance matrix in Problem 3.8 is positive definite.
- 3.11** A matrix with the structure of \mathbf{G} in (3.23) or \mathbf{C} in (3.24) whose off-diagonal terms are negative and the sum of the elements in a row or column is positive is said to be *hyperdominant*. Show that a hyperdominant matrix is always positive definite.

REFERENCES

- [1] R.Plonsey and R.E. Collin, *Principles and Applications of Electromagnetic Fields*, 2nd edition, McGraw-Hill, New York, 1982.
- [2] M. Javid and P.M. Brown, *Field Analysis and Electromagnetics*, McGraw-Hill, New York, 1963.
- [3] F.E. Hohn, *Elementary Matrix Algebra*, 2nd edition, Macmillan, New York, 1964.

4

THE PER-UNIT-LENGTH PARAMETERS FOR TWO-CONDUCTOR LINES

The per-unit-length parameters of inductance, capacitance, resistance, and conductance are essential ingredients in the determination of the transmission-line voltages and currents from the solution of the transmission-line equations. All of the cross-sectional dimension information about the specific line being investigated is contained in these parameters and nowhere else. Hence, without a determination of these for the transmission line under consideration, solution of the transmission-line equations cannot be completed as the per-unit-length parameters in them are unknown. It is important to recall that, under the fundamental transverse electromagnetic (TEM) field structure assumption, the per-unit-length parameters of inductance, capacitance, and conductance are determined as a static (dc) solution to Laplace's equation, for example, $\nabla^2\phi(x, y) = 0$, in the two-dimensional cross-sectional (x, y) plane of the line. Therefore, the per-unit-length inductance (external), capacitance, and conductance are governed by the fields external to the line conductors and are determined as static field solutions in the transverse plane for perfect conductors that have conductivities of $\sigma = \infty$. The per-unit-length resistances and internal inductances are computed from the currents and magnetic fields internal to the conductors. We will consider only *uniform* lines where the conductor cross sections and the cross sections of any inhomogeneous surrounding media are constant along the line. Hence, these per-unit-length parameters are independent of the line axis variable z .

The purpose of this chapter is to investigate methods for determining these per-unit-length parameters of inductance, l , capacitance, c , conductance, g , and resistance, r , for two-conductor lines. In the following chapter, we will similarly investigate

the determination of the entries in the $n \times n$ per-unit-length parameter matrices \mathbf{L} , \mathbf{C} , \mathbf{G} , and \mathbf{R} . We will divide the determination of these parameters into those for wire-type lines and those for conductors of rectangular cross section (lands) that are typical of printed circuit boards (PCBs). In the case of wire-type lines consisting of two wires (circular, cylindrical cross sections) where the surrounding medium is homogeneous, we can obtain *exact solutions* for the per-unit-length parameters of l , g , and c . The *exact solution* for the per-unit-length resistance r of wires is also obtainable. When we add circular dielectric insulations as is typical of wires, we can no longer obtain exact, closed-form solutions for g and c , and must use numerical approximation methods [C.1,C.2]. In the case of two-conductor lines where the conductors have rectangular cross sections such as are typical of PCBs, there exist approximate formulas for the per-unit-length parameters of l , g , and c . However, we must use approximate, numerical methods to determine the per-unit-length resistance r for conductors of rectangular cross section. A similar discussion will apply to the entries in the per-unit-length parameter matrices of a multiconductor transmission line (MTL). So the determination of the per-unit-length parameters can be simple or very difficult depending on (1) whether the cross sections of the conductors are circular or rectangular and (2) whether the conductors are surrounded by a homogeneous or an inhomogeneous dielectric medium.

In summary, there are very few transmission lines for which the cross-sectional fields can be solved, analytically, in order to give simple formulas for the per-unit-length parameters of inductance, conductance, and capacitance, contrary to what many handbooks imply. We will show a few important special cases for which formulas for these parameters exist. For the remaining cases, we have no alternative but to employ approximate, numerical methods. These can be somewhat tedious but are not difficult, conceptually.

4.1 DEFINITIONS OF THE PER-UNIT-LENGTH PARAMETERS l , c , AND g

An intuitive definition of these per-unit-length parameters was given in Chapter 1. First, it is important to designate the *reference conductor* for the line voltage as illustrated in Figure 4.1(a). Once this is done, the currents on the conductors are equal and oppositely directed at any cross section, and the current on the conductor that is at the assumed positive voltage goes down that conductor in the positive z direction and “returns” along the reference conductor in the $-z$ direction. The per-unit-length inductance l is the ratio of the magnetic flux penetrating the cross-sectional surface between the two conductors per unit of line length, ψ , and the current along the conductors that produced it:

$$l = \frac{\psi}{I} \quad (4.1)$$

In determining this inductance, we usually place a current on the conductors, going down one and returning on the reference conductor, and determine the resulting

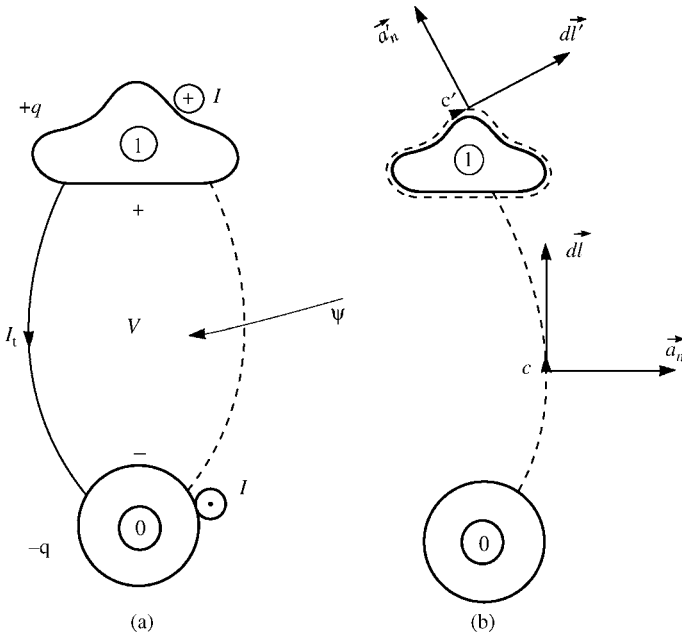


FIGURE 4.1 Cross-sectional illustration of (a) definitions of charge, current, voltage, magnetic flux, and transverse current, and (b) the contours and surfaces to be used in their formal definitions.

magnetic flux. Hence, the direction for the desired magnetic flux through the surface between the conductors is clockwise when looking in the $+z$ direction. The per-unit-length capacitance c is the ratio of the charge per unit of line length, q , and the voltage between the two conductors that induced it:

$$c = \frac{q}{V} \tag{4.2}$$

In determining this capacitance, we usually place a positive per-unit-length charge on the positive voltage conductor and an equal but opposite charge on the reference conductor and determine the resulting voltage induced between the two conductors. The per-unit-length conductance g is the ratio of the per-unit-length conduction current I_t flowing in the transverse, $x - y$, plane from the positive conductor to the reference conductor through a lossy dielectric surrounding the conductors and the voltage between the two conductors:

$$g = \frac{I_t}{V} \tag{4.3}$$

There are many clever ways of computing these static (dc) parameters in the $x - y$ plane. Formal definitions of each of these parameters for a *homogeneous medium* characterized by μ , ϵ , and σ were obtained in Chapter 1 with reference to Figure 4.1(b) as

$$l = -\mu \frac{\int \vec{\mathcal{H}}_t \cdot \vec{a}_n dl}{\oint_{c'} \vec{\mathcal{H}}_t \cdot d\vec{l}} \quad (4.4)$$

$$c = \varepsilon \frac{\oint \vec{\mathcal{E}}_t \cdot \vec{a}'_n dl'}{-\int_c \vec{\mathcal{E}}_t \cdot d\vec{l}} \quad (4.5)$$

$$g = \sigma \frac{\oint \vec{\mathcal{E}}_t \cdot \vec{a}'_n dl'}{-\int_c \vec{\mathcal{E}}_t \cdot d\vec{l}} \quad (4.6)$$

4.2 LINES HAVING CONDUCTORS OF CIRCULAR, CYLINDRICAL CROSS SECTION (WIRES)

In this section, we will determine the per-unit-length parameters for lines consisting of two conductors having circular, cylindrical cross sections. These are referred to as *wires*.

4.2.1 Fundamental Subproblems for Wires

In order to determine simple relations for the per-unit-length parameters of wires, we need to discuss the following important subproblems [A.3.B.4,1,2].

Consider an infinitely long wire carrying a dc current I that is uniformly distributed over its cross section as shown in Figure 4.2. The transverse magnetic field intensity $\vec{\mathcal{H}}_t$ is directed in the circumferential direction by symmetry. Enclosing the wire and current by a cylinder of radius r and applying Ampere's law for the TEM field [A.1]:

$$\oint_c \vec{\mathcal{H}}_t \cdot d\vec{l} = I \quad (4.7)$$

gives

$$\mathcal{H}_t = \frac{I}{2\pi r} \quad (4.8)$$

This result is due to the observation that (1) $\vec{\mathcal{H}}_t$ is tangent to $d\vec{l}$ and therefore the dot product can be removed from (4.7) and the vectors replaced with their magnitudes,

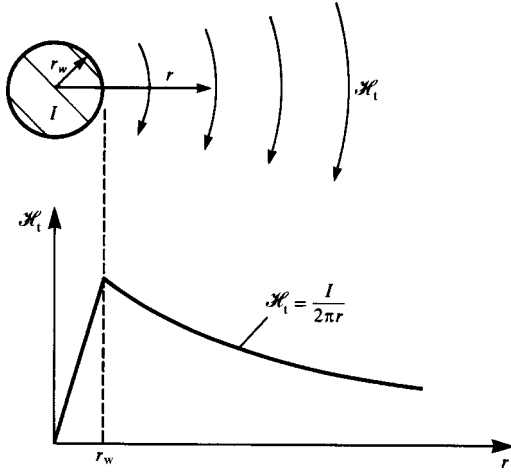


FIGURE 4.2 The low-frequency magnetic field intensity vector about a current-carrying wire.

and (2) $\vec{\mathcal{H}}_t$ is constant around the contour of radius r and so may be removed from the integral.

Now consider determining the magnetic flux from this current that penetrates a surface s that is parallel to the wire and of uniform cross section along the wire length as shown in Figure 4.3(a). The edges of the surface are at distances R_1 and R_2 from the wire. Next consider this problem in cross section as shown in Figure 4.3(b). Consider the closed, wedge-shaped surface consisting of the original surface along with surfaces s_1 and s_2 . Surface s_1 is the flat surface extending radially along R_1 to a radius of R_2 , and surface s_2 is a cylindrical surface of constant radius R_2 that joins surfaces s and s_1 . Gauss' law provides that there are no isolated sources of the magnetic field. Thus, the total magnetic flux through a closed surface must be zero [A.1]:

$$\oiint_s \vec{\mathcal{B}} \cdot d\vec{s} = 0 \tag{4.9}$$

where $\vec{\mathcal{B}}$ is the *magnetic flux density vector* and is related for linear, homogeneous, isotropic media to the magnetic field intensity vector $\vec{\mathcal{H}}$ as $\vec{\mathcal{B}} = \mu\vec{\mathcal{H}}$. From (4.9), the total magnetic flux through the wedge-shaped surface of Figure 4.3(b) is the sum of the fluxes through the original surface s and surfaces s_1 and s_2 since no flux is directed through the end caps because of the transverse nature of the magnetic field. But the flux through s_2 is also zero because the magnetic field is tangent to it. Thus, the total magnetic flux penetrating the original surface s is the same as the flux penetrating surface s_1 , as shown in Figure 4.3(c). But the problem of Figure 4.3(c) is simpler than the original problem because the magnetic field is orthogonal to the surface. Thus,

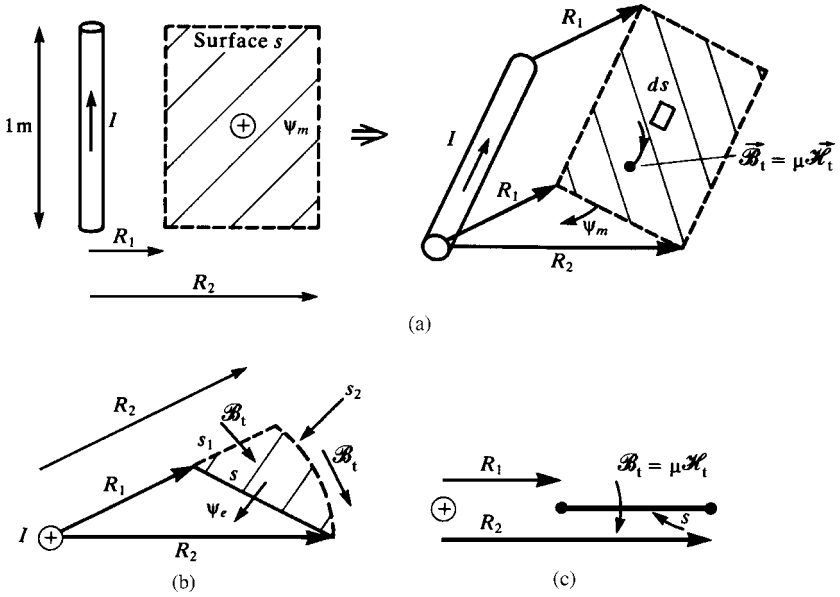


FIGURE 4.3 Illustration of the fundamental subproblem for determination of the flux through a surface due to a current-carrying wire by the computation of a simpler problem.

the total magnetic flux through either surface is

$$\begin{aligned}
 \iint_{s_1} \vec{\mathcal{B}}_t \cdot d\vec{s} &= \Delta z \int_{R_1}^{R_2} \frac{\mu I}{2\pi r} dr \\
 &= \Delta z \frac{\mu I}{2\pi} \ln\left(\frac{R_2}{R_1}\right)
 \end{aligned} \tag{4.10}$$

where we have assumed that $R_2 > R_1$ to give the indicated direction of ψ . The magnetic flux per unit of line length is

$$\psi = \frac{\mu I}{2\pi} \ln\left(\frac{R_2}{R_1}\right) \quad (\text{Wb/m}) \tag{4.11}$$

We will find the results of this subproblem to be of considerable utility in our future developments.

The above derivation has been made with two important assumptions: (1) the wire is infinitely long and (2) the current is uniformly distributed over the wire cross section and is symmetrical about its axis. The first assumption allows us to assume that the magnetic field is invariant along the direction of the wire axis. The second assumption means that we may replace the wire with a *filamentary current* at its axis on which all

the current I is concentrated and implicitly assumes that there are no closely spaced currents to disturb this symmetry. The effects of this infinitely long filament of current on the flux penetrating the above surface will be the same as the original current.

We next consider the dual problem of determining the voltage between two points due to a filament of charge. Consider a very long wire carrying a charge per unit of length q C/m, as shown in Figure 4.4(a). We assume that the charge is either uniformly distributed around the periphery of the wire or concentrated as a filament of charge. In this case, the electric field intensity \mathcal{E} will be radially directed in a direction transverse to the wire. Gauss' law provides that the total electric flux penetrating a closed surface is equal to the net positive charge enclosed by that surface [A.1]:

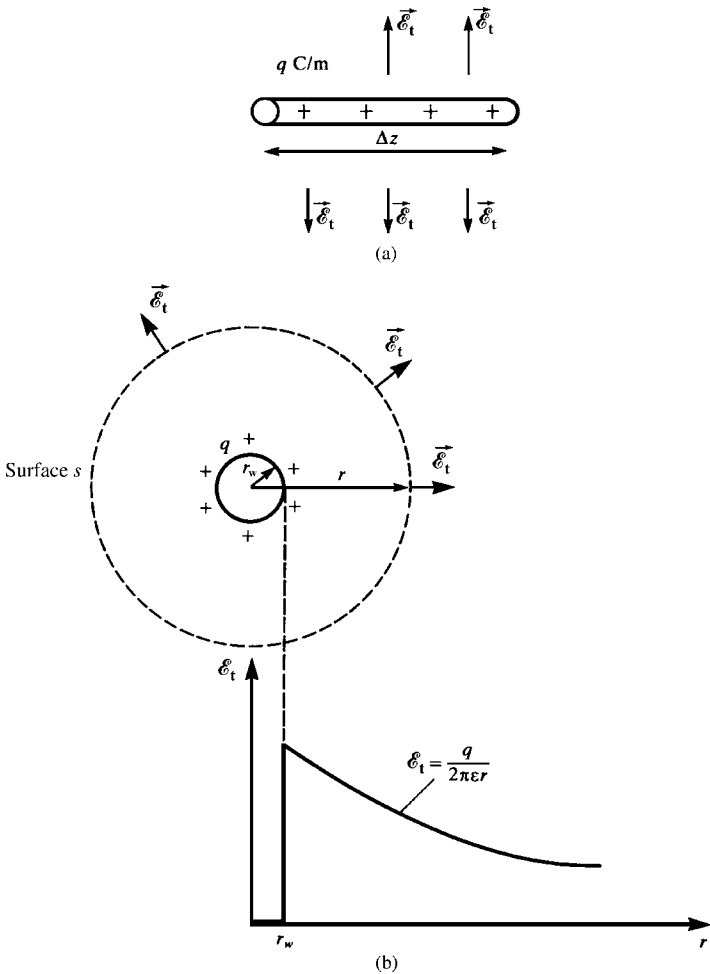


FIGURE 4.4 Illustration of the electric field intensity vector about a charge-carrying wire.

$$\oiint_s \vec{\mathcal{D}} \cdot d\vec{s} = Q_{\text{enc}} \tag{4.12}$$

where $\vec{\mathcal{D}}$ is the *electric flux density vector*. For linear, homogeneous, and isotropic media, this is related to the electric field intensity vector by $\vec{\mathcal{D}} = \epsilon \vec{\mathcal{E}}$. Consider enclosing the charge-carrying wire with a cylinder of radius r , as shown in Figure 4.4(b). The electric field is obtained by applying (4.12) to that closed surface to yield

$$\epsilon \oiint_s \vec{\mathcal{E}}_t \cdot d\vec{s} = q \Delta z \tag{4.13}$$

The dot product may be removed and the vectors replaced with their magnitudes since the electric field is orthogonal to the sides of the surface and no electric field is directed through the end caps of the surface. Furthermore, the electric field may be removed from the integral since it is constant in value over the sides of the surface. This gives a simple expression for the electric field away from the filament:

$$\mathcal{E}_t = \frac{q}{2\pi\epsilon r} \quad (\text{V/m}) \tag{4.14}$$

Next consider the problem of determining the voltage between two points away from the filament as shown in Figure 4.5(a). The points are at radii R_1 and R_2 from the filament. The voltage is defined as (uniquely because of the transverse nature of the electric field)

$$V_{ab} = - \int_c \vec{\mathcal{E}}_t \cdot d\vec{l} \tag{4.15}$$

A simpler problem is illustrated in Figure 4.5(b). Contour c_1 extends along a radial line from the end of R_1 to a distance R_2 , and contour c_2 is of constant radius R_2

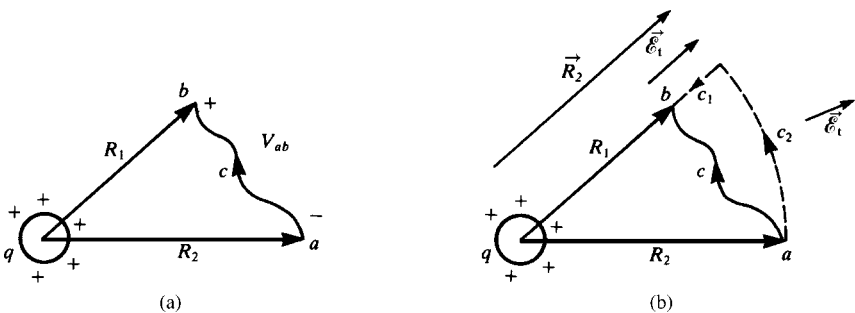


FIGURE 4.5 Illustration of the calculation of voltage between two points from a charge-carrying wire (a) directly and (b) from a simpler problem.

and extends from that end to the beginning of the original contour. Thus, since the definition of voltage in (4.15) is independent of the path taken between the two points, we may alternatively compute

$$\begin{aligned}
 V_{ab} &= - \int_{c_1} \vec{\mathcal{E}}_t \cdot d\vec{l} - \int_{c_2} \vec{\mathcal{E}}_t \cdot d\vec{l} \\
 &= - \int_{R_2}^{R_1} \frac{q}{2\pi\epsilon r} dr \\
 &= \frac{q}{2\pi\epsilon} \ln\left(\frac{R_2}{R_1}\right) \tag{4.16}
 \end{aligned}$$

where we assume $R_2 > R_1$. This result was made possible by the observation that over c_2 the electric field is orthogonal to the contour so that the second integral is zero, and over c_1 the electric field is tangent to the contour. We will also find this result to be of considerable utility in our future work.

Once again, this simple result implicitly assumes that (1) the wire is infinitely long and (2) the charge is uniformly distributed around its periphery. The first assumption ensures that the electric field will not vary along the line length. The second assumption means that we may replace the wire with a filament of charge and implicitly assumes that there are no closely spaced charge distributions to disturb this symmetry.

4.2.1.1 The Method of Images The remaining principle that we will employ is the *method of images*. Consider a point charge Q situated a height h above an infinite, perfectly conducting plane as shown in Figure 4.6(a). We can replace the infinite plane with an equal but negative charge $-Q$ at a distance h below the previous location of the surface of the plane, and the resulting fields will be identical in the space above the plane's surface [A.1]. The negative charge is said to be the *image* of the positive charge. We can similarly image currents. Consider a current I parallel to and at a height h above an infinite, perfectly conducting plane shown in Figure 4.6(b). If the plane is replaced with an equal but oppositely directed current at a distance h below the position of the plane surface, all the fields above the plane's surface will be identical in both problems [A.1]. This can be conveniently remembered using the following mnemonic device. Consider the current I as producing positive charge at one endpoint and negative at the other (denoted by circles with enclosed polarity signs). Imaging these "point charges" as above gives the correct image current direction. A vertically directed current is similarly imaged as shown in Figure 4.6(c). Current directions that are neither vertical nor horizontal can be resolved into their horizontal and vertical components, and the above results can be used to give the correct image current distribution [A.1].

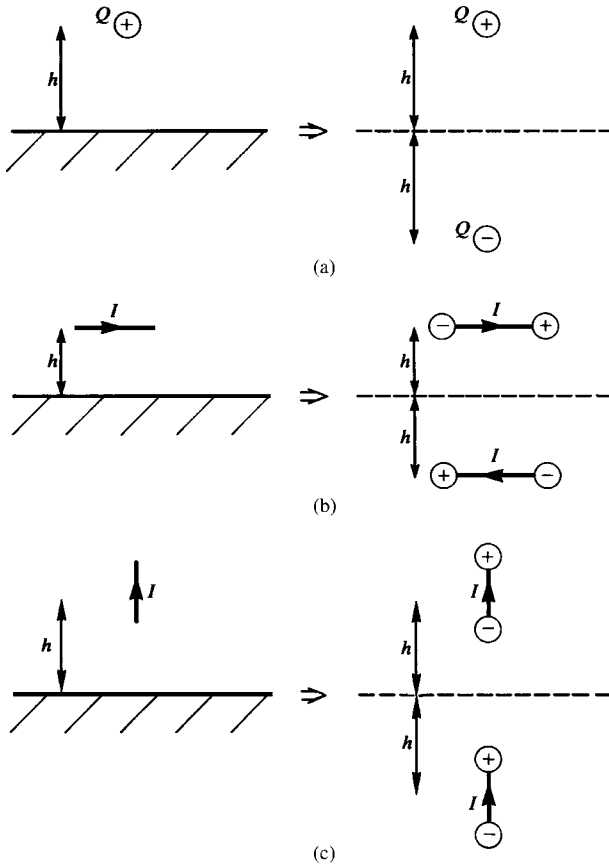


FIGURE 4.6 The method of images: (a) charge above a perfectly conducting plane, (b) current parallel to a perfectly conducting plane, and (c) current perpendicular to a perfectly conducting plane.

4.2.2 Per-Unit-Length Inductance and Capacitance for Wire-Type Lines

There exist few transmission-line structures for which the per-unit-length parameters can be determined *exactly*. The class of two-conductor lines of circular, cylindrical cross section (wires) in a homogeneous medium characterized by μ_0 , ϵ , and σ considered in this section represents a significant portion of such lines. In the case that the wires are surrounded by circular dielectric insulations, the surrounding medium is inhomogeneous in ϵ (air and the dielectric). The per-unit-length inductance l is not affected by this inhomogeneous medium since dielectrics have $\mu = \mu_0$. Hence, l is the same as for wires surrounded by a homogeneous medium, that being free space. However, for this case of an inhomogeneous medium, closed-form formulas for the per-unit-length capacitance c are not obtainable, and approximate, numerical methods must be used to determine this parameter [C.1,C.2]. We will reserve discussion of

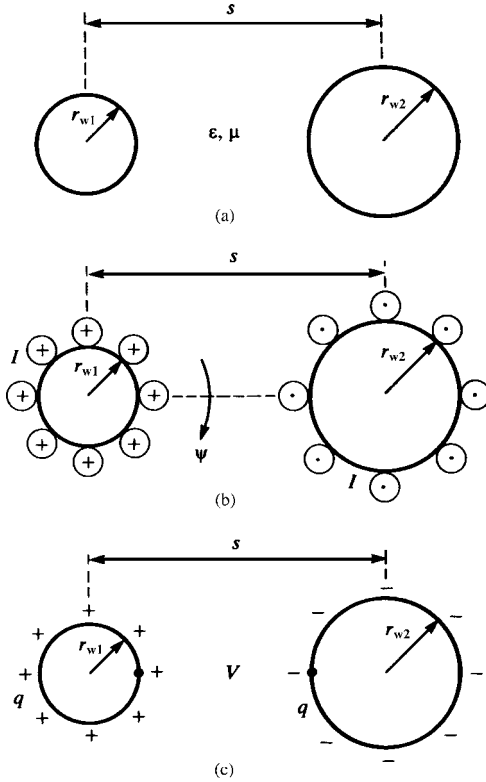


FIGURE 4.7 Illustration of (a) a two-wire line, and calculation of (b) the per-unit-length inductance and (c) the per-unit-length capacitance.

these numerical methods and inhomogeneous surrounding media until we consider multiconductor lines in Chapter 5. For the present, we will assume that the wires are immersed in a homogeneous medium.

Consider the case of two perfectly conducting wires of radii r_{w1} and r_{w2} that are separated by a distance s in a homogeneous medium as shown in Figure 4.7(a). Let us assume that the currents (which, for perfect conductors, must reside on the surface) are uniformly distributed around the wire peripheries as shown in Figure 4.7(b). Using the above result for the magnetic flux from a filament of current in (4.11), we obtain the total flux passing between the two wires as

$$\begin{aligned}
 \psi &= \frac{\mu I}{2\pi} \ln\left(\frac{s - r_{w2}}{r_{w1}}\right) + \frac{\mu I}{2\pi} \ln\left(\frac{s - r_{w1}}{r_{w2}}\right) \\
 &= \frac{\mu I}{2\pi} \ln\left(\frac{(s - r_{w2})(s - r_{w1})}{r_{w1}r_{w2}}\right)
 \end{aligned}
 \tag{4.17}$$

where $\mu = \mu_0$. This result assumes that the current is uniformly distributed around each wire periphery. This will not be the case if the wires are closely separated since one current will interact and cause a nonuniform distribution of the other current (this is referred to as *proximity effect*). In order to make this result valid, we must require that the wires be *widely separated*. The necessary ratio of separation to wire radius to make this valid will be investigated when we determine the exact solution. Therefore, because of the necessity to have the wires widely separated, the separation must be much larger than either of the wire radii so that (4.17) simplifies to

$$l = \frac{\psi}{I} \cong \frac{\mu}{2\pi} \ln \left(\frac{s^2}{r_{w1}r_{w2}} \right) \quad (\text{H/m}) \quad (4.18)$$

In the practical case of the wire radii being equal, $r_{w1} = r_{w2} = r_w$, this reduces to

$$l \cong \frac{\mu}{\pi} \ln \left(\frac{s}{r_w} \right) \quad (\text{H/m}) \quad (4.19)$$

The per-unit-length capacitance will be similarly determined in an approximate manner. Consider the two wires carrying charge uniformly distributed around each wire periphery as shown in Figure 4.7(c). The voltage between the wires can similarly be obtained by superimposing the voltages due to the two equal but opposite charge distributions using (4.16) as

$$\begin{aligned} V &= \frac{q}{2\pi\epsilon} \ln \left(\frac{(s - r_{w2})}{r_{w1}} \right) + \frac{q}{2\pi\epsilon} \ln \left(\frac{(s - r_{w1})}{r_{w2}} \right) \\ &= \frac{q}{2\pi\epsilon} \ln \left(\frac{(s - r_{w2})(s - r_{w1})}{r_{w1}r_{w2}} \right) \cong \frac{q}{2\pi\epsilon} \ln \left(\frac{s^2}{r_{w1}r_{w2}} \right) \end{aligned} \quad (4.20)$$

and we have used the necessary requirement that the wires be widely separated, that is, $s \gg r_{w1}, r_{w2}$, so that the charge is uniformly distributed around the wire peripheries. The per-unit-length capacitance is

$$\begin{aligned} c &= \frac{q}{V} \\ &\cong \frac{2\pi\epsilon}{\ln \left(\frac{s^2}{r_{w1}r_{w2}} \right)} \quad (\text{F/m}) \end{aligned} \quad (4.21)$$

For equal wire radii, this simplifies to

$$c \cong \frac{\pi\epsilon}{\ln \left(\frac{s}{r_w} \right)} \quad (\text{F/m}) \quad (4.22)$$

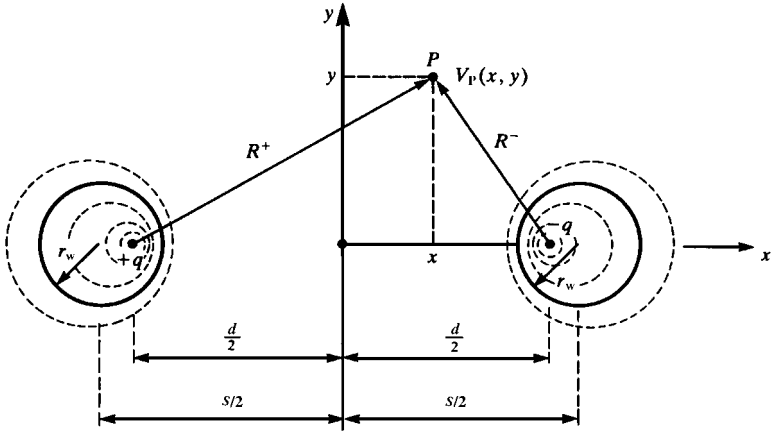


FIGURE 4.8 Illustration of the exact calculation of the per-unit-length capacitance of two wires.

We now turn to an *exact* derivation of the per-unit-length capacitance. The essence of the method is to place a charge per unit of line length, q , on filaments separated by a distance d , as shown in Figure 4.8. Then we determine the *equipotential contours* about these filaments and locate the actual wires on these contours that correspond to the voltage of the wires. This gives the equivalent spacing between the two wires, s , that carry the same charge per unit of line length. The voltage at a point P shown in Figure 4.8 due to the filaments of charge, one carrying q and the other carrying $-q$, with respect to the origin, $x = 0$ and $y = 0$, can be found using the previous basic subproblem as

$$\begin{aligned}
 V_P(x, y) &= -\frac{q}{2\pi\epsilon} \ln\left(\frac{R^+}{d/2}\right) + \frac{q}{2\pi\epsilon} \ln\left(\frac{R^-}{d/2}\right) \\
 &= \frac{q}{2\pi\epsilon} \ln\left(\frac{R^-}{R^+}\right)
 \end{aligned}
 \tag{4.23}$$

Thus, points on equipotential contours are such that the ratio

$$\begin{aligned}
 \frac{R^-}{R^+} &= e\left(\frac{2\pi\epsilon V_P}{q}\right) \\
 &= K
 \end{aligned}
 \tag{4.24}$$

is constant, where K is that constant. Substituting the equations for R^+ and R^- :

$$R^+ = \sqrt{(x + d/2)^2 + y^2}
 \tag{4.25a}$$

$$R^- = \sqrt{(x - d/2)^2 + y^2} \tag{4.25b}$$

gives

$$\frac{(x - d/2)^2 + y^2}{(x + d/2)^2 + y^2} = K^2 \tag{4.26}$$

Expanding this gives

$$x^2 + xd \frac{(K^2 + 1)}{(K^2 - 1)} + \left(\frac{d}{2}\right)^2 + y^2 = 0 \tag{4.27}$$

In order to determine the location of the circular equipotential surfaces that define the equivalent conductors and their radii, we write this in the equation of a circle located at $x = -s/2$ and having a radius of r_w :

$$\left(x + \frac{s}{2}\right)^2 + y^2 = r_w^2 \tag{4.28}$$

Expanding this gives

$$x^2 + xs + \left(\frac{s}{2}\right)^2 - r_w^2 + y^2 = 0 \tag{4.29}$$

Comparing (4.29) to (4.27) gives

$$\frac{s}{2} = \frac{d}{2} \frac{K^2 + 1}{K^2 - 1} \tag{4.30a}$$

and

$$r_w = \frac{Kd}{K^2 - 1} \tag{4.30b}$$

The constant K can be eliminated by taking the difference of the squares of (4.30a) and (4.30b) to give

$$\frac{d}{2} = \sqrt{\left(\frac{s}{2}\right)^2 - r_w^2} \tag{4.31}$$

Dividing (4.30a) by (4.30b) eliminates d , giving a quadratic equation in K :

$$K^2 - \frac{s}{r_w} K + 1 = 0 \tag{4.32}$$

Solving for K gives

$$K = \frac{s}{2r_w} \pm \sqrt{\left(\frac{s}{2r_w}\right)^2 - 1} \quad (4.33)$$

Substituting this into (4.23) and (4.24) gives the voltage as

$$V_P = \frac{q}{2\pi\epsilon} \ln \left[\frac{s}{2r_w} \pm \sqrt{\left(\frac{s}{2r_w}\right)^2 - 1} \right] \quad (4.34)$$

Recall that this is the voltage of the point *with respect to the origin of the coordinate system*, which is located midway between the two wires. Thus, the voltage between the two wires that are separated by a distance s is

$$V = 2V_P = \frac{q}{\pi\epsilon} \ln \left[\frac{s}{2r_w} + \sqrt{\left(\frac{s}{2r_w}\right)^2 - 1} \right] \quad (4.35)$$

and the per-unit-length capacitance becomes

$$\begin{aligned} c &= \frac{q}{V} \\ &= \frac{\pi\epsilon}{\ln \left[\frac{s}{2r_w} + \sqrt{\left(\frac{s}{2r_w}\right)^2 - 1} \right]} \quad (\text{F/m}) \end{aligned} \quad (4.36)$$

This can be defined in terms of the inverse hyperbolic cosine as

$$\cosh^{-1}(x) = \ln \left[x + \sqrt{x^2 - 1} \right] \quad (4.37)$$

to give

$$c = \frac{\pi\epsilon}{\cosh^{-1} \left(\frac{s}{2r_w} \right)} \quad (\text{F/m}) \quad (4.38)$$

If the wire radii are not equal, the corresponding *exact result* for the per-unit-length capacitance is derived in [3] and becomes

$$c = \frac{2\pi\epsilon}{\cosh^{-1} \left(\frac{s^2 - r_{w1}^2 - r_{w2}^2}{2r_{w1}r_{w2}} \right)} \quad (\text{F/m}) \quad (4.39)$$

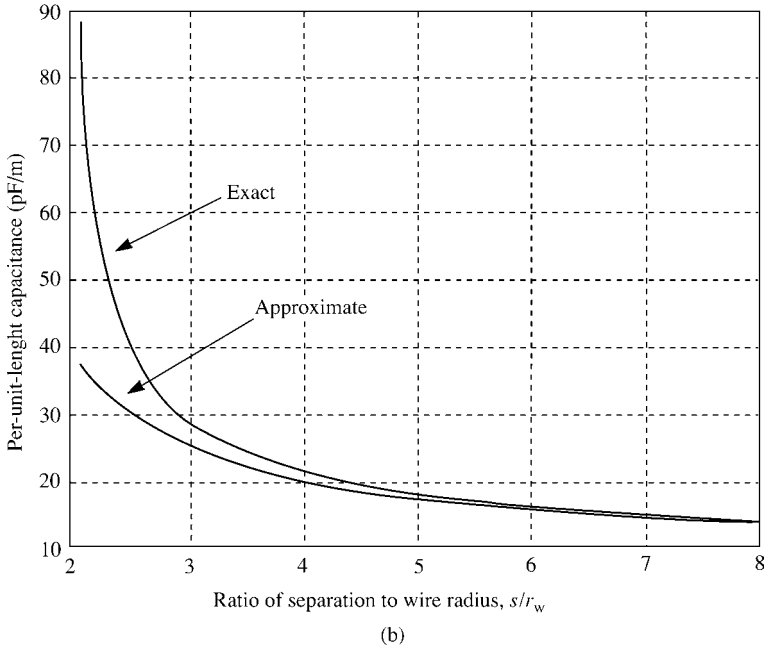
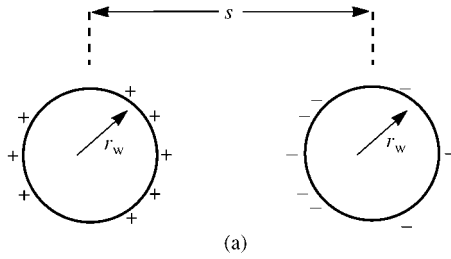


FIGURE 4.9 A comparison of the exact and approximate formulas for the per-unit-length capacitance of two wires.

The *exact* result in (4.36) or (4.38) simplifies for widely spaced wires. For example, suppose $s \gg r_w$. The exact result in (4.36) reduces to the approximate result derived earlier and given in (4.22). The error for a ratio $s/r_w = 5$ is only 2.7%. A ratio of separation to wire radius of 4 would mean that another wire of the same radius would just fit between the two original wires. For this very small separation, the error between the approximate expression (4.22) and the exact expression (4.36) is only 5.3%. So the *wide-separation approximation* given in (4.22) is quite adequate for practical wire separations. Figure 4.9 shows the comparison between the approximate relation in (4.22) and the exact relation in (4.38).

In Chapter 1, it was shown that for lines in a homogeneous medium characterized by μ , ϵ , and σ , the per-unit-length parameters are related as

$$lc = \mu\epsilon \quad (4.40a)$$

$$lg = \mu\sigma \quad (4.40b)$$

and

$$\frac{g}{c} = \frac{\sigma}{\epsilon} \quad (4.40c)$$

The per-unit-length inductance can be obtained from this result, assuming that the surrounding medium is *homogeneous* in ϵ and μ as

$$\begin{aligned} l &= \mu\epsilon c^{-1} \\ &= \frac{\mu}{\pi} \cosh^{-1} \left(\frac{s}{2r_w} \right) \quad (\text{H/m}) \end{aligned} \quad (4.41)$$

Similarly, if the medium is lossy and *homogeneous* in σ we can obtain

$$\begin{aligned} g &= \frac{\sigma}{\epsilon} c \\ &= \frac{\pi\sigma}{\cosh^{-1} \left(\frac{s}{2r_w} \right)} \quad (\text{S/m}) \end{aligned} \quad (4.42)$$

Next, consider the case of one wire at a height h above and parallel to an infinite, perfectly conducting plane (sometimes referred to as a *ground plane*) as shown in Figure 4.10(a). By the method of images, we may replace the plane with its image located at an equal distance h below the position of the plane as shown in Figure 4.10(b). The desired capacitance is between each wire and the position of the plane. But, as capacitances in series add like resistors in parallel, we see that this problem can be related to the problem of the previous section as

$$c_{\text{two-wire}} = \frac{c_{\text{one wire above ground}}}{2} \quad (4.43)$$

Therefore, the capacitance of one wire above an infinite, perfectly conducting plane becomes, substituting $h = s/2$ in (4.38),

$$c = \frac{2\pi\epsilon}{\cosh^{-1} \left(\frac{h}{r_w} \right)} \quad (\text{F/m}) \quad (4.44)$$

or, approximately, for $h \gg r_w$:

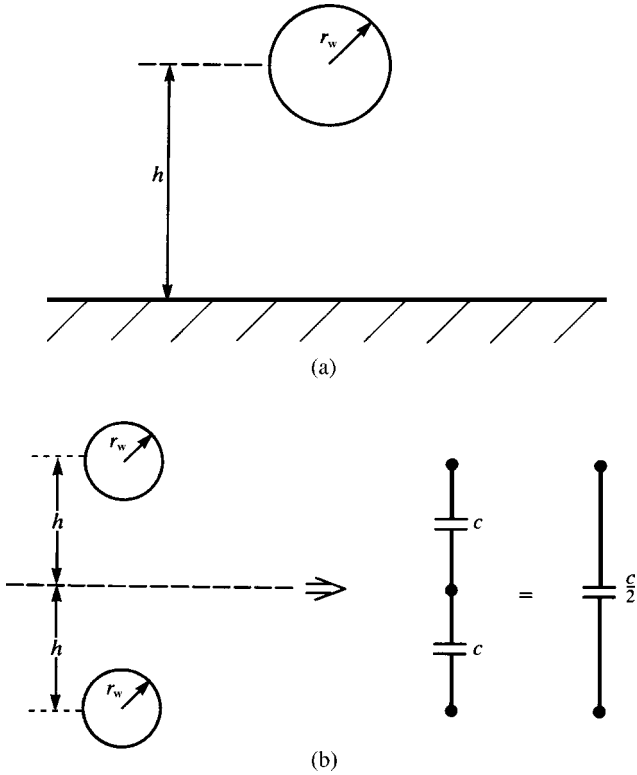


FIGURE 4.10 Illustration of the calculation of the per-unit-length capacitance of one wire above a conducting plane from the corresponding capacitance of two wires via the method of images.

$$c \cong \frac{2\pi\epsilon}{\ln\left(\frac{2h}{r_w}\right)} \quad (\text{F/m}) \tag{4.45}$$

The inductance can be obtained for this *homogeneous medium* from this result as

$$\begin{aligned} l &= \mu\epsilon c^{-1} \\ &= \frac{\mu}{2\pi} \cosh^{-1}\left(\frac{h}{r_w}\right) \quad (\text{H/m}) \\ &\cong \frac{\mu}{2\pi} \ln\left(\frac{2h}{r_w}\right) \end{aligned} \tag{4.46}$$

Similarly, if the medium is lossy and *homogeneous* in σ , we can obtain

$$\begin{aligned}
 g &= \frac{\sigma}{\varepsilon} c \\
 &= \frac{2\pi\sigma}{\cosh^{-1}\left(\frac{h}{r_w}\right)} \quad (\text{S/m}) \\
 &\cong \frac{2\pi\sigma}{\ln\left(\frac{2h}{r_w}\right)} \quad (4.47)
 \end{aligned}$$

Finally, consider the *coaxial cable* shown in Figure 4.11 consisting of a wire of radius r_w within and centered on the axis of a shield of inner radius r_s . The medium between the wire and the shield is assumed to be homogeneous. The case of an inhomogeneous medium can be solved so long as the inhomogeneity exists in annuli symmetric about the shield axis. If we place a total charge q per unit of line length on the inner conductor, a negative charge of equal magnitude will be induced on the interior of the shield. Observe that, by symmetry, the charge distributions will be uniformly distributed around the conductor peripheries regardless of the conductor separations. We earlier obtained the result for the electric field due to the charge q per

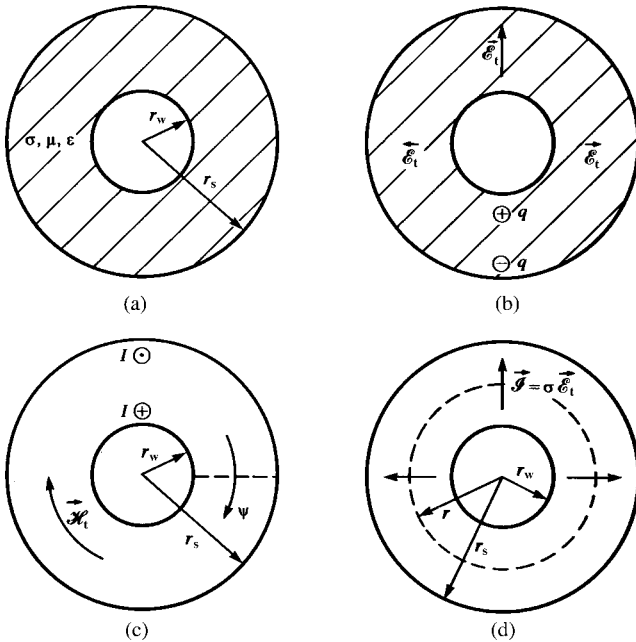


FIGURE 4.11 Illustration of the direct calculation of the per-unit-length parameters for a coaxial cable: (a) the general structure, (b) the per-unit-length capacitance, (c) the per-unit-length inductance, and (d) the per-unit-length conductance.

unit of line length on the inner wire as

$$\vec{\mathcal{E}}_t = \frac{q}{2\pi\epsilon r} \vec{a}_r, \quad r_w \leq r \leq r_s \quad (4.48)$$

Observe that the field will be directed in the radial (transverse) direction. The voltage between the two conductors can be obtained as

$$\begin{aligned} V &= - \int_{r_s}^{r_w} \frac{q}{2\pi\epsilon r} dr \\ &= \frac{q}{2\pi\epsilon} \ln\left(\frac{r_s}{r_w}\right) \end{aligned} \quad (4.49)$$

The capacitance per unit of line length is therefore

$$\begin{aligned} c &= \frac{q}{V} \\ &= \frac{2\pi\epsilon}{\ln\left(\frac{r_s}{r_w}\right)} \quad (\text{F/m}) \end{aligned} \quad (4.50)$$

Observe that, because of symmetry, the charge distributions will be uniform around the conductor peripheries regardless of conductor separation so that this result is *exact*. The per-unit-length inductance can be derived directly or by using

$$\begin{aligned} l &= \mu\epsilon c^{-1} \\ &= \frac{\mu}{2\pi} \ln\left(\frac{r_s}{r_w}\right) \quad (\text{H/m}) \end{aligned} \quad (4.51)$$

Similarly, the per-unit-length conductance is

$$\begin{aligned} g &= \frac{\sigma}{\epsilon} c \\ &= \frac{2\pi\sigma}{\ln\left(\frac{r_s}{r_w}\right)} \quad (\text{S/m}) \end{aligned} \quad (4.52)$$

The per-unit-length inductance can be derived directly. Consider placing a flat surface of length Δz between the inner and outer conductors as shown in Figure 4.11(c). The desired magnetic flux passes through this surface. Clearly, the flux will be in the circumferential direction since, due to symmetry, the current will be uniformly distributed around the periphery of the inner wire and the inside surface of the shield.

Thus, we may use the fundamental result derived earlier to give

$$\begin{aligned}
 l &= \frac{\psi}{I} \\
 &= \frac{\mu}{2\pi} \ln\left(\frac{r_s}{r_w}\right)
 \end{aligned}
 \tag{4.53}$$

The per-unit-length conductance can similarly be obtained directly from Figure 4.11(d) by finding the ratio of the transverse current to the voltage using (4.48) and (4.49):

$$\begin{aligned}
 g &= \frac{\int_{\phi=0}^{2\pi} \sigma \mathcal{E}_t r d\phi}{V} \\
 &= \frac{2\pi\sigma}{\ln\left(\frac{r_s}{r_w}\right)}
 \end{aligned}
 \tag{4.54}$$

4.2.3 Per-Unit-Length Conductance and Resistance for Wire-Type Lines

In the preceding section, we have represented the losses in a *homogeneous medium* by conductivity σ . The conductivity σ represents losses in the medium that are due to free charge in the dielectric. There is another loss mechanism that usually dominates the resistive losses in a dielectric. This is due to the polarization of the dielectric that is due to *bound charge* in the dielectric. Figure 4.12 illustrates this. Within the dielectric are dipoles of charge consisting of equal but opposite-sign charges that are tightly bound together. Some materials such as water consist of permanent dipoles that are randomly oriented so that the material has no net polarization. Dipoles are created in other materials when an external electric field slightly deforms the atoms

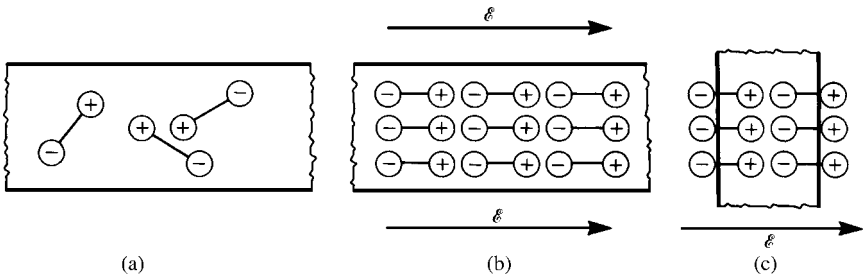


FIGURE 4.12 Illustration of the effects of bound (polarization) charge: (a) microscopic dipoles, (b) alignment of the dipoles with an applied electric field, and (c) creation of a bound surface charge.

creating microscopic separations of the positive and negative charge centers. When an electric field is applied, these dipoles attempt to align with that field as shown in Figure 4.12(b). This creates a bound surface charge appearing on the opposite faces of a block of the dielectric, as illustrated in Figure 4.12(c). This process accounts for the increase in capacitance of a parallel-plate capacitor when a dielectric other than air is inserted between the plates [A.1].

As the frequency of the applied electric field increases, the alignment of these dipoles with the changing direction of the field increasingly lags behind, thereby creating a loss in the dielectric. This is represented by a frequency-dependent effective conductivity of the dielectric. Polarization loss is represented by a complex permittivity of the dielectric as [A.1]

$$\hat{\epsilon} = \epsilon - j\epsilon_p \quad (4.55)$$

Both ϵ and ϵ_p are frequency dependent [6]. The real and imaginary parts of this complex permittivity are not independent but are related by the Kronig–Kramers relations given in (2.47) of Chapter 2 [4]. Ampere’s law for sinusoidal excitation is modified as

$$\begin{aligned} \nabla \times \vec{H} &= \sigma \vec{E} + j\omega \hat{\epsilon} \vec{E} \\ &= \underbrace{(\sigma + \omega\epsilon_p)}_{\sigma_{\text{eff}}} \vec{E} + j\omega \epsilon \vec{E} \end{aligned} \quad (4.56)$$

and σ represents the conduction current losses due to free charge in the dielectric (which is usually very small and generally negligible in comparison with the effects of bound charge). Hence, the effective conductivity, representing conductive and polarization losses, is

$$\sigma_{\text{eff}} = (\sigma + \omega\epsilon_p) \quad (4.57)$$

An alternative way of representing both these losses is with the *loss tangent*. The loss tangent is the ratio of the real part of (4.56) to the imaginary part [A.1]:

$$\begin{aligned} \tan \delta &= \frac{(\sigma + \omega\epsilon_p)}{\omega\epsilon} \\ &\cong \frac{\epsilon_p}{\epsilon} \end{aligned} \quad (4.58)$$

The polarization losses will dominate the resistive losses in typical dielectrics of practical interest. Handbooks tabulate this loss tangent for various dielectric materials at various frequencies [5]. Therefore, the effective conductivity of a dielectric is related to the loss tangent as

$$\sigma_{\text{eff}} = \omega\epsilon \tan \delta \quad (4.59)$$

Hence, in a *homogeneous medium*, the per-unit-length conductance is related to the per-unit-length capacitance as

$$g = \frac{\sigma_{\text{eff}}}{\varepsilon} c = \omega \tan \delta c \quad (4.60)$$

The loss tangent, $\tan \delta$, is not frequency independent, and hence the per-unit-length conductance does not increase linearly with frequency as (4.60) seems to imply. For typical dielectric materials used to construct transmission lines, the variation of the loss tangent with frequency is relatively constant over certain frequency ranges [6]. For other dielectrics, the frequency variation of the loss tangent is more pronounced. For FR4 (glass epoxy), which is a common dielectric substrate used to construct PCBs, the loss tangent achieves a maximum value on the order of 0.02 in the range of 1–100 MHz and decreases on either side of this frequency range. For some materials, ε is mildly frequency dependent. For example, polyvinyl chloride, which is a typical insulation for wires, has a permittivity $\varepsilon = \varepsilon_r \varepsilon_0$, which is frequency dependent with ε_r decreasing from 4.3 at 10 kHz to 3 at 100 MHz [6]. Molecular resonances in the microwave frequency range can lead to resonances in the loss tangent over certain frequency bands [6]. For sinusoidal excitation, the total per-unit-length admittance between the two conductors is the sum of the per-unit-length conductance and the per-unit-length capacitive reactance as

$$\begin{aligned} \hat{y} &= g + j\omega c \\ &= j\omega c(1 - j \tan \delta) \end{aligned} \quad (4.61)$$

For FR4 in PCBs, $\tan \delta \cong 0.02$ in the frequency range of 1–100 MHz, and the conductance is a factor of 50 smaller than the capacitive reactance.

For the case of lines in an *inhomogeneous* surrounding medium such as the case of wires that are surrounded by circular dielectric insulations (the inhomogeneity is caused by the surrounding dielectric and air), the relation in (4.60) for the per-unit-length conductance, of course, does not apply since each region has its own loss tangent and these loss tangents are not the same. However, it is possible to incorporate losses in the inhomogeneous medium in the following manner [A.1,B.4,7]. Write Ampere's law as

$$\begin{aligned} \nabla \times \vec{H} &= \sigma \vec{E} + j\omega \hat{\varepsilon} \vec{E} \\ &= (\sigma + \omega \varepsilon_p) \vec{E} + j\omega \varepsilon \vec{E} \\ &= j\omega \underbrace{\varepsilon(1 - j \tan \delta)}_{\hat{\varepsilon}} \vec{E} \end{aligned} \quad (4.62)$$

Hence, we can incorporate losses in the medium by determining only the capacitance and using a complex permittivity in that calculation as

$$\hat{\varepsilon} = \varepsilon(1 - j \tan \delta) \quad (4.63)$$

As we will see later in this chapter, for lines surrounded by an inhomogeneous medium such as wires with circular dielectric insulations, we must use approximate, numerical methods to solve for the per-unit-length capacitance [C.1,C.2]. Losses can be readily incorporated into that capacitance solver by using complex permittivities as in (4.63) for each region instead of real permittivities to give a complex capacitance as [B.4,7]

$$\hat{c} = c_R + j c_I \quad (4.64)$$

where c_R and c_I are the real and imaginary parts, respectively, of the complex capacitance. Hence, the complex admittance is

$$\begin{aligned} \hat{y} &= j\omega\hat{c} \\ &= j\omega(c_R + jc_I) \\ &= -\omega c_I + j\omega c_R \\ &= g + j\omega c \end{aligned} \quad (4.65)$$

and we identify the effective per-unit-length conductance as

$$g = -\omega c_I \quad (4.66a)$$

and the per-unit-length capacitance is obtained as

$$c = c_R \quad (4.66b)$$

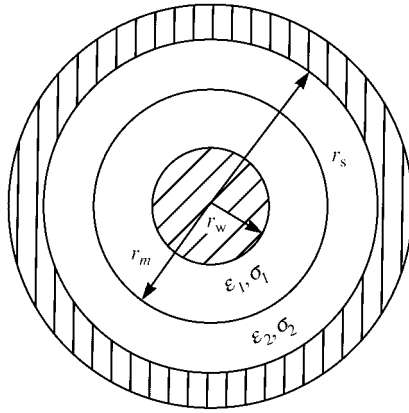
As an example, consider the case of a coaxial cable having two different dielectric regions as shown in Figure 4.13(a). Two dielectrics occupy annuli between the two conductors. The inner wire is of radius r_w and the overall shield is of interior radius r_s . The inhomogeneous medium is characterized by

$$\varepsilon_1, \tan\delta_1, \quad r_w < r < r_m \quad (4.67a)$$

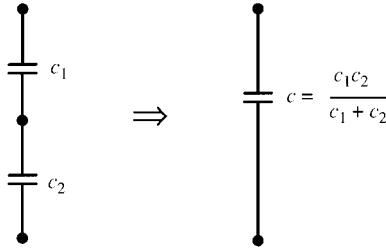
$$\varepsilon_2, \tan\delta_2, \quad r_m < r < r_s \quad (4.67b)$$

First, let us ignore loss. The surface between the two dielectrics located at $r = r_m$ is an equipotential surface and hence the net per-unit-length capacitance is that of the capacitances of each region in series as shown in Figure 4.13(b). Since capacitors in series combine like resistances in parallel, the net capacitance is

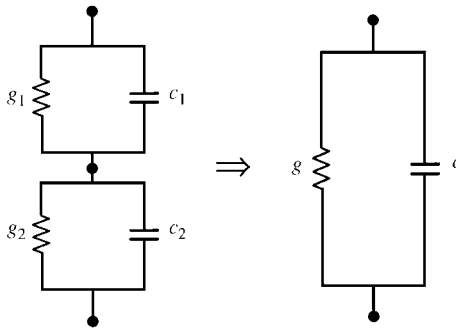
$$c = \frac{c_1 c_2}{c_1 + c_2} \quad (4.68a)$$



(a)



(b)



(c)

FIGURE 4.13 Calculation of the per-unit-length capacitance and conductance for a coaxial cable having an inhomogeneous medium in the form of concentric annuli: (a) the general structure, (b) representing the two regions in terms of per-unit-length capacitances in series, and (c) representing loss in the medium in terms of per-unit-length conductances.

where, from our previous results,

$$c_1 = \frac{2\pi \epsilon_1}{\ln\left(\frac{r_m}{r_w}\right)} \tag{4.68b}$$

and

$$c_2 = \frac{2\pi \epsilon_2}{\ln\left(\frac{r_s}{r_m}\right)} \tag{4.68c}$$

Hence, the overall capacitance is

$$c = \frac{2\pi \epsilon_1 \epsilon_2}{\epsilon_1 \ln\left(\frac{r_s}{r_m}\right) + \epsilon_2 \ln\left(\frac{r_m}{r_w}\right)} \tag{4.69}$$

We will examine a numerical example having the dimensions of a RG58U coaxial cable. Suppose that the desired frequency is $f = 100$ MHz, and the dimensions are $r_w = 16$ mils, $r_m = 35$ mils, $r_s = 58$ mils, $\epsilon_1 = 2\epsilon_0$, $\epsilon_2 = 6\epsilon_0$, $\tan\delta_1 = 0.01$, and $\tan\delta_2 = 0.04$. The per-unit-length capacitance neglecting loss in the medium is

$$\begin{aligned} c &= \frac{2\pi \epsilon_1 \epsilon_2}{\epsilon_1 \ln\left(\frac{r_s}{r_m}\right) + \epsilon_2 \ln\left(\frac{r_m}{r_w}\right)} \\ &= 1.168 \times 10^{-10} \text{ (F/m)} \end{aligned} \tag{4.70}$$

To include losses, we use a complex permittivity for each region as shown in (4.63), and (4.70) becomes

$$\begin{aligned} \hat{c} &= \frac{2\pi \hat{\epsilon}_1 \hat{\epsilon}_2}{\hat{\epsilon}_1 \ln\left(\frac{r_s}{r_m}\right) + \hat{\epsilon}_2 \ln\left(\frac{r_m}{r_w}\right)} \\ &= 1.168 \times 10^{-10} - j1.788 \times 10^{-12} \end{aligned} \tag{4.71}$$

where $\hat{\epsilon}_1 = \epsilon_1(1 - j\tan\delta_1)$ and $\hat{\epsilon}_2 = \epsilon_2(1 - j\tan\delta_2)$. Hence, from this we obtain, according to (4.66),

$$\begin{aligned} g &= -\omega c_1 \\ &= 1.123 \times 10^{-3} \text{ (S/m)} \end{aligned} \tag{4.72a}$$

and

$$\begin{aligned}
 c &= c_R \\
 &= 1.168 \times 10^{-10} \quad (\text{F/m})
 \end{aligned}
 \tag{4.72b}$$

We may check these results by observing that the equivalent circuit becomes as shown in Figure 4.13(c), where c_1 and c_2 are as given in (4.68b) and (4.68c) and

$$g_1 = \frac{2\pi \sigma_1}{\ln\left(\frac{r_m}{r_w}\right)}
 \tag{4.73a}$$

and

$$g_2 = \frac{2\pi \sigma_2}{\ln\left(\frac{r_s}{r_m}\right)}
 \tag{4.73b}$$

and, according to (4.59),

$$\sigma_1 = \omega \varepsilon_1 \tan \delta_1
 \tag{4.74a}$$

and

$$\sigma_2 = \omega \varepsilon_2 \tan \delta_2
 \tag{4.74b}$$

From Figure 4.13(c), the complex per-unit-length admittance is

$$\begin{aligned}
 \hat{y} &= \frac{(g_1 + j\omega c_1)(g_2 + j\omega c_2)}{(g_1 + j\omega c_1) + (g_2 + j\omega c_2)} \\
 &= g + j\omega c \\
 &= 1.123 \times 10^{-3} + j7.341 \times 10^{-2}
 \end{aligned}
 \tag{4.75}$$

This confirms our previous calculation that $g = 1.123 \times 10^{-3}$ and $\omega c = 7.341 \times 10^{-2}$, giving $c = 1.168 \times 10^{-10}$. The equivalence of $j\omega \hat{c}$ in (4.71) and (4.75) can also be proven analytically.

We now turn to the determination of the per-unit-length resistance of wires. The current density and the electric and magnetic fields in good conductors are governed by the *diffusion equation*. Ampere’s law relates the curl of the magnetic field to the sum of conduction current and displacement current. For sinusoidal excitation, this becomes

$$\nabla \times \vec{H} = \underbrace{\sigma \vec{E}}_{\text{conduction current}} + \underbrace{j\omega \varepsilon \vec{E}}_{\text{displacement current}}
 \tag{4.76}$$

A good conductor is one in which the conduction current, greatly exceeds the displacement current, which is satisfied for most metallic conductors and frequencies of reasonable interest. Thus, Ampere's law within the conductor becomes approximately

$$\nabla \times \vec{H} \cong \vec{J} = \sigma \vec{E} \quad (4.77a)$$

Similarly, Faraday's law is

$$\nabla \times \vec{E} = -j\omega\mu \vec{H} \quad (4.77b)$$

Taking the curl of Faraday's law gives [A.1]

$$\begin{aligned} \nabla \times \nabla \times \vec{E} &= \nabla \left(\nabla \cdot \vec{E} \right) - \nabla^2 \vec{E} \\ &= -j\omega\mu \nabla \times \vec{H} \end{aligned} \quad (4.78)$$

Substituting Gauss' law

$$\nabla \cdot \varepsilon_0 \vec{E} = 0 \quad (4.79)$$

gives

$$\nabla^2 \vec{E} = j\omega\mu\sigma \vec{E} \quad (4.80)$$

Since the current density is related to the electric field in the conductor as $\vec{J} = \sigma \vec{E}$, we arrive at the *diffusion equation*

$$\nabla^2 \vec{J} = j\omega\mu\sigma \vec{J} \quad (4.81)$$

Consider a semi-infinite, conducting half space with parameters σ , ε , and μ , whose surface lies in the x - y plane as shown in Figure 4.14 [4]. Assume that the electric field and associated conduction current density are directed in the z direction. The diffusion equation in terms of this z -directed electric field becomes

$$\frac{d^2 \hat{E}_z}{dx^2} = j\omega\mu\sigma \hat{E}_z \quad (4.82)$$

Similar equations govern the magnetic field \hat{H}_y and the current density \hat{J}_z . The solutions are

$$\hat{E}_z = \hat{E}_0 e^{-x/\delta} e^{-jx/\delta} \quad (4.83a)$$

$$\hat{H}_y = \hat{H}_0 e^{-x/\delta} e^{-jx/\delta} \quad (4.83b)$$

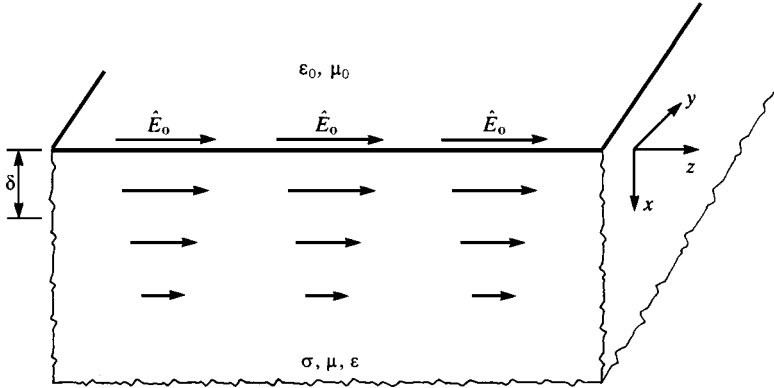


FIGURE 4.14 Diffusion of currents and fields into a semi-infinite conductive half space.

$$\hat{J}_z = \hat{J}_0 e^{-x/\delta} e^{-jx/\delta} \tag{4.83c}$$

where the familiar *skin depth* is

$$\delta = \frac{1}{\sqrt{\pi f \mu \sigma}} \tag{4.84}$$

and \hat{E}_0 , \hat{H}_0 , and \hat{J}_0 are the appropriate quantities at the surface ($x = 0$). This result shows that the fields and current density decay rapidly in the conductor and are essentially confined to layers at the surface of thickness equal to a few skin depths.

The *surface impedance* can be defined as the ratio of the z -directed electric field at the surface and total current density:

$$\hat{Z}_s = \frac{\hat{E}_0}{\hat{J}_T} \tag{4.85}$$

The total current in the conductor can be obtained by integrating the current density given in (4.83c) throughout the conductor:

$$\begin{aligned} \hat{J}_T &= \int_0^\infty \hat{J}_z dx \\ &= \frac{\hat{J}_0 \delta}{(1 + j)} \end{aligned} \tag{4.86}$$

Substituting into (4.85) gives ($\hat{J}_0 = \sigma \hat{E}_0$)

$$\hat{Z}_s = R_s + j\omega L_i \tag{4.87}$$

where

$$R_s = \frac{1}{\sigma\delta} = \sqrt{\frac{\pi f\mu}{\sigma}} \quad (\Omega/\text{square}) \quad (4.88a)$$

$$\omega L_i = R_s \quad (4.88b)$$

This surface impedance is the impedance of an area of the surface of unit width and unit length so that we use the term ohms/square. The term R_s is referred to as the surface resistance, and the term L_i is referred to as the internal inductance. Observe that the surface resistance *increases* as \sqrt{f} , whereas the internal inductance *decreases* as \sqrt{f} so that the internal inductive reactance *increases* as \sqrt{f} . Observe also that the surface resistance in (4.88a) could have been more easily calculated by assuming the current density to be *constant* in a thickness equal to one skin depth of the surface and zero elsewhere. Equivalently, the surface impedance can be written as

$$\hat{Z}_s = \sqrt{\frac{j\omega\mu}{\sigma}} \quad (4.89)$$

Essentially, we could have obtained the same result from the *intrinsic impedance* of the conductor [A.1]:

$$\hat{\eta} = \sqrt{\frac{j\omega\mu}{\sigma + j\omega\epsilon}} \quad (4.90)$$

by observing that within the conductor the conduction current dominates the displacement current, that is, $\sigma \gg \omega\epsilon$.

Next we consider the *resistance* and *internal inductance* of circular-cylindrical conductors (wires). The resistance and internal inductance are again due to the wire conductance being finite. In the case of perfect conductors, the currents flow on the surfaces of the conductors. Resistance and internal inductance result from the current and magnetic flux internal to the imperfect conductors in a fashion similar to the case of the surface impedance of a plane conductor and can be computed in a straightforward fashion if we know the current distribution over the wire cross section. The internal inductance results from magnetic flux internal to the conductor that links the current, whereas the external inductance results from the magnetic flux that is external to the conductors that penetrates the area between the conductor and the reference conductor as discussed previously.

The determination of these parameters for wires is very straightforward *if we assume the current is symmetric about the axis of the wire* [4, 8]. At dc the current is uniformly distributed over the cross section, whereas at higher frequencies the current crowds to the surface being concentrated in a thickness on the order of a skin depth. This observation leads to a useful equivalent circuit representing this skin effect, which attempts to mimic this phenomenon [9]. Essentially, this assumption of current symmetry about the wire axis means that we assume there are no nearby currents

close enough to upset this symmetry (proximity effect) [10]. Neighboring conductors also affect this current distribution for conductors of rectangular cross section [11]. Determination of these parameters when other currents are close enough to upset this symmetry is considerably more difficult, and for typical wire radii and spacings the symmetrical current distribution assumption is adequate. For example, reference [4] gives the exact per-unit-length *high-frequency* resistance for a two-wire line in a homogeneous medium consisting of two identical wires of radii r_w separated by s as

$$r = \frac{2R_s}{2\pi r_w} \left[\frac{\frac{s}{2r_w}}{\sqrt{\left(\frac{s}{2r_w}\right)^2 - 1}} \right] \quad (\Omega/\text{m})$$

where the surface resistance R_s is given in (4.88a).

$$R_s = \frac{1}{\sigma\delta} = \sqrt{\frac{\pi f\mu}{\sigma}}$$

is the surface resistance of the conductor. For $s = 4r_w$ such that one wire exactly fits between the two wires, the resistance is 15% higher than that obtained by assuming the current is symmetric about the axis of the wire; that is, the wire separation is sufficient so that proximity effect is not pronounced.

Internal to the conductor, the conduction current dominates the displacement current so that the diffusion equation again describes the conduction current distribution internal to the wire. Let us assume that this current density is z directed (along the wire axis) and is symmetric about the axis of the wire and write the diffusion equation in cylindrical coordinates. We orient the wire about the z axis of a cylindrical coordinate system. Because of the assumed symmetry, the current density is independent of z and ϕ but is a function of the radius r from the wire axis so that the diffusion equation reduces to [A.1]

$$\frac{d^2 \hat{J}_z}{dr^2} + \frac{1}{r} \frac{d\hat{J}_z}{dr} + k^2 \hat{J}_z = 0 \tag{4.91}$$

where

$$\begin{aligned} k^2 &= -j\omega\mu\sigma \\ &= -j \frac{2}{\delta^2} \end{aligned} \tag{4.92}$$

The solution to this equation is [A.1,4,8]

$$\hat{J}_z = \hat{J}_0 \frac{\text{ber}(\sqrt{2}r/\delta) + j\text{bei}(\sqrt{2}r/\delta)}{\text{ber}(\sqrt{2}r_w/\delta) + j\text{bei}(\sqrt{2}r_w/\delta)} \tag{4.93}$$

where $\text{ber}(x)$ and $\text{bei}(x)$ are the real and imaginary parts, respectively, of the Bessel function of the first kind of a complex argument (4,8,12). The term \hat{J}_0 is the current density at the outer radius of the wire, $r = r_w$.

It now remains to determine the total internal impedance (per unit length) of the wire. The total current in the wire can be found by integrating Ampere's law around the wire surface (assuming that displacement current within the wire is much less than the conduction current):

$$\begin{aligned}\hat{I} &= \oint \vec{H} \cdot d\vec{l} \\ &= 2\pi r_w \hat{H}_\phi|_{r=r_w}\end{aligned}\quad (4.94)$$

The magnetic field can be obtained from Faraday's law multiplied by the wire conductivity:

$$\nabla \times \vec{J} = -j\omega\mu\sigma \vec{H} \quad (4.95)$$

Substituting the result for curl in cylindrical coordinates [A.1] and recalling that the current density is z directed and dependent only on r and the magnetic field is ϕ directed gives

$$\frac{d\hat{J}_z}{dr} = j\omega\mu\sigma \hat{H}_\phi \quad (4.96)$$

Substituting this into (4.94) and using (4.93) gives the total current in terms of the current at the wire surface. The per-unit-length internal impedance becomes

$$\begin{aligned}\hat{z}_{\text{int}} &= \frac{\hat{E}_z|_{r=r_w}}{\hat{I}} \\ &= \frac{j\omega\mu\sigma}{2\pi r_w \sigma} \frac{\hat{J}_z|_{r=r_w}}{\frac{d\hat{J}_z}{dr}|_{r=r_w}} \\ &= \frac{1}{\sqrt{2}\pi r_w \sigma \delta} \left[\frac{\text{ber}(q) + j\text{bei}(q)}{\text{bei}'(q) - j\text{ber}'(q)} \right] \quad (\Omega/\text{m})\end{aligned}\quad (4.97a)$$

where

$$\begin{aligned}\text{ber}'(q) &= \frac{d}{dq} \text{ber}(q) \\ \text{bei}'(q) &= \frac{d}{dq} \text{bei}(q)\end{aligned}$$

and

$$q = \sqrt{2} \frac{r_w}{\delta} \quad (4.97b)$$

Writing this total internal impedance in terms of its real and imaginary parts as

$$\hat{z}_{\text{int}} = r + j\omega l_i \quad (4.98)$$

gives the conductor resistance and internal inductance as

$$\frac{r}{r_{\text{dc}}} = \frac{q}{2} \left[\frac{\text{ber}(q)\text{bei}'(q) - \text{bei}(q)\text{ber}'(q)}{(\text{bei}'(q))^2 + (\text{ber}'(q))^2} \right] \quad (4.99)$$

$$\frac{l_i}{l_{i,\text{dc}}} = \frac{4}{q} \left[\frac{\text{bei}(q)\text{bei}'(q) + \text{ber}(q)\text{ber}'(q)}{(\text{bei}'(q))^2 + (\text{ber}'(q))^2} \right] \quad (4.100)$$

where

$$r_{\text{dc}} = \frac{1}{\sigma\pi r_w^2} \quad (\Omega/\text{m}) \quad (4.101)$$

$$l_{i,\text{dc}} = \frac{\mu_0}{8\pi} = 0.5 \times 10^{-7} \quad (\text{H}/\text{m}) \quad (4.102)$$

are the dc per-unit-length resistance and internal inductance, respectively, of the wire [A.1].

Although the results in (4.99) and (4.100) are exact assuming a current distribution that is *symmetric* about the wire axis, they are somewhat complicated. Reasonable simplifications can be obtained depending on whether the frequency is such that the wire radius is greater than or less than a skin depth. Figure 4.15 shows the ratio of the per-unit-length resistance and the dc resistance of (4.99) plotted as a function of the ratio of the wire radius and a skin depth, r_w/δ . Observe that the transition to \sqrt{f} frequency dependence commences around the point where the wire radius is two skin depths, $r_w = 2\delta$. Similarly, Figure 4.16 shows the ratio of the per-unit-length internal inductance and the dc internal inductance of (4.100) plotted as a function of the ratio of wire radius to skin depth. The transition to $1/\sqrt{f}$ frequency dependence commences at the same point as for the resistance. Consequently, the exact results can be approximated by

$$\left. \begin{aligned} r &= \frac{1}{\sigma\pi r_w^2} \quad (\Omega/\text{m}) \\ l_i &= \frac{\mu_0}{8\pi} = 0.5 \times 10^{-7} \quad (\text{H}/\text{m}) \end{aligned} \right\} r_w < 2\delta \quad (4.103a)$$

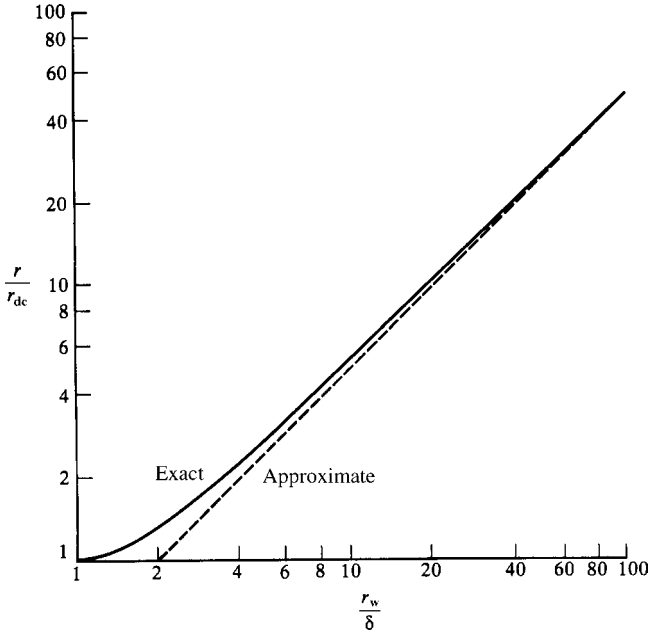


FIGURE 4.15 Frequency dependence of the per-unit-length resistance of a wire as a function of the ratio of wire radius to skin depth.

$$\left. \begin{aligned} r &= \frac{1}{2\pi r_w \sigma \delta} = \frac{1}{2r_w} \sqrt{\frac{\mu}{\pi\sigma}} \sqrt{f} \quad (\Omega/\text{m}) \\ l_i &= \frac{1}{4\pi r_w} \sqrt{\frac{\mu}{\pi\sigma}} \frac{1}{\sqrt{f}} \quad (\text{H}/\text{m}) \end{aligned} \right\} r_w > 2\delta \quad (4.103b)$$

Observe that the *low-frequency resistance* for $r_w < 2\delta$ in (4.103a) could have been computed by assuming that the current is uniformly distributed over the cross section as illustrated in Figure 4.17(a), as is the case at dc. Similarly, the *high-frequency resistance* for $r_w > 2\delta$ in (4.103b) could have been computed by assuming that the current is uniformly distributed over an annulus at the wire surface of thickness equal to one skin depth as illustrated in Figure 4.17(b), which satisfies our intuition based on the plane conductor case. Considering the complexity of the exact results, we will use these approximations in our future work.

Also observe an important point from (4.103b). For *high frequencies*, that is, $r_w \gg 2\delta$, the resistance and internal *inductive reactance* are equal. In other words,

$$z_{\text{int}} = r + j\omega l_i \quad (4.104a)$$

and

$$r = \omega l_i, \quad r_w \gg 2\delta \quad (4.104b)$$

This fact will prove to be very beneficial in our future results.

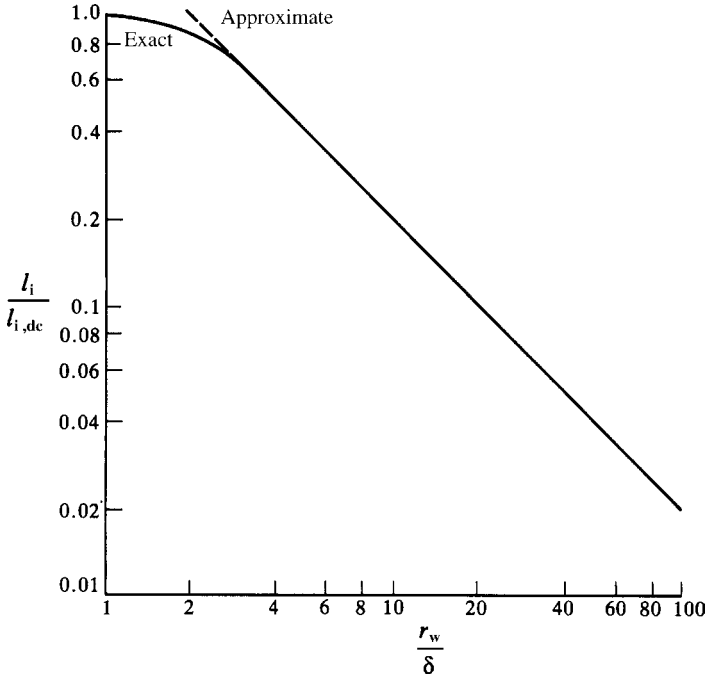


FIGURE 4.16 Frequency dependence of the per-unit-length internal inductance of a wire as a function of the ratio of wire radius to skin depth.

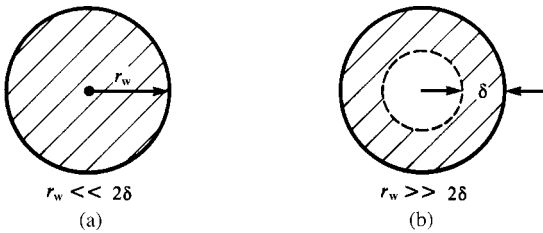


FIGURE 4.17 Illustration of the cross-sectional current distribution of a wire for (a) low frequencies and (b) high frequencies.

4.3 LINES HAVING CONDUCTORS OF RECTANGULAR CROSS SECTION (PCB LANDS)

In this section, we will consider lines composed of conductors of rectangular cross section (lands). These represent typical transmission lines found on PCBs.

4.3.1 Per-Unit-Length Inductance and Capacitance for PCB-Type Lines

There are very few closed-form equations for the per-unit-length inductance and capacitance of transmission lines consisting of parallel conductors having rectangular cross sections. Most are approximate relations, and references [13–19] provide the following. These structures are usually characterized by their characteristic impedance:

$$Z_C = \sqrt{\frac{l}{c}} \tag{4.105a}$$

and velocity of propagation:

$$\begin{aligned} v &= \frac{1}{\sqrt{lc}} \\ &= \frac{1}{\sqrt{\epsilon'_r \epsilon_0 \mu_0}} = \frac{v_0}{\sqrt{\epsilon'_r}} \end{aligned} \tag{4.105b}$$

where ϵ'_r is the *effective relative permittivity* of the surrounding (possibly inhomogeneous) medium. From these, we can therefore obtain the per-unit-length inductance and capacitance as

$$l = \frac{Z_C}{v} \tag{4.106a}$$

and

$$c = \frac{1}{Z_C v} \tag{4.106b}$$

Figure 4.18 shows the three such primary lines: the stripline, the microstrip line, and the PCB line. The *stripline* shown in Figure 4.18(a) consists of a perfectly conducting strip of rectangular cross section of width w and thickness t situated midway between two infinite, perfectly conducting planes that are separated by a distance s . This configuration represents lands that are buried in an innerplane PCB. The dielectric medium between the planes is *homogeneous* and is characterized by $\epsilon = \epsilon_r \epsilon_0$ and $\mu = \mu_0$. Assuming a zero-thickness strip ($t = 0$), the per-unit-length inductance is

$$l = \frac{30\pi}{v_0} \frac{1}{\left[\frac{w_e}{s} + 0.441 \right]} \tag{4.107a}$$

and the effective width of the conductor is

$$\frac{w_e}{s} = \begin{cases} \frac{w}{s}, & \frac{w}{s} \geq 0.35 \\ \frac{w}{s} - \left(0.35 - \frac{w}{s}\right)^2, & \frac{w}{s} \leq 0.35 \end{cases} \tag{4.107b}$$

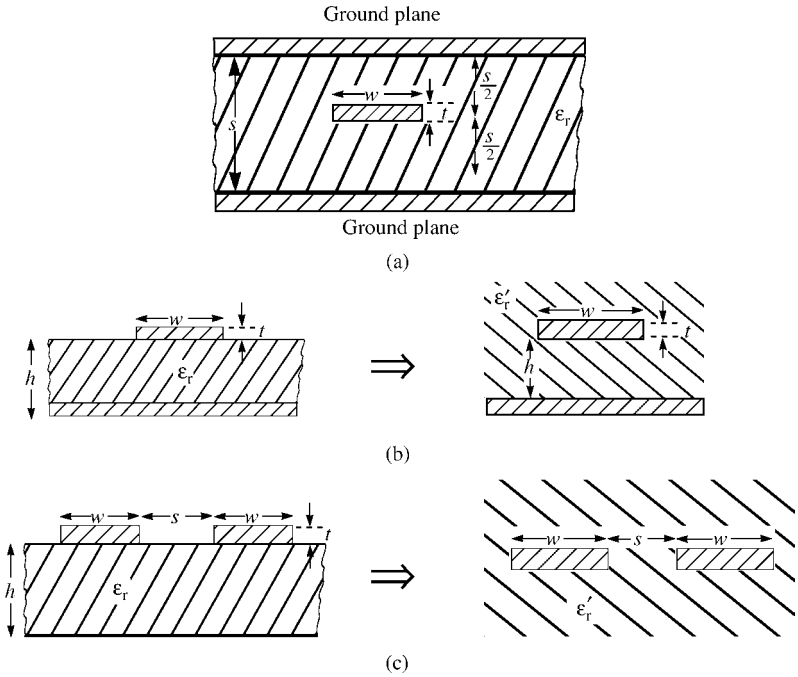


FIGURE 4.18 Cross-sectional dimensions of lines composed of conductors of rectangular cross section: (a) the stripline, (b) the microstrip line, and (c) the printed circuit board.

The per-unit-length capacitance is

$$c = \frac{\epsilon_r}{30\pi v_0} \left[\frac{w_e}{s} + 0.441 \right] \tag{4.107c}$$

The *microstrip line* shown in Figure 4.18(b) is typical of the outer layers on an innerplane PCB. A land of width w is placed on a board of thickness h that has a perfectly conducting plane on the opposite side. The board has a relative permittivity ϵ_r . Assuming the land thickness is zero ($t = 0$), the per-unit-length inductance is

$$l = \begin{cases} \frac{60}{v_0} \ln \left[\frac{8h}{w} + \frac{w}{4h} \right], & \frac{w}{h} \leq 1 \\ \frac{120\pi}{v_0} \left[\frac{w}{h} + 1.393 + 0.667 \ln \left(\frac{w}{h} + 1.444 \right) \right]^{-1}, & \frac{w}{h} \geq 1 \end{cases} \tag{4.108a}$$

and the effective relative permittivity is

$$\epsilon'_r = \frac{\epsilon_r + 1}{2} + \frac{\epsilon_r - 1}{2} \frac{1}{\sqrt{1 + 12 \frac{h}{w}}} \tag{4.108b}$$

This effective relative permittivity accounts for the fact that the electric field lines are partly in air and partly in the substrate dielectric. If this inhomogeneous medium (air and the dielectric) is replaced with a homogeneous one having an effective relative permittivity of ϵ'_r as shown in Figure 4.18(b), all properties of the line remain unchanged. The per-unit-length capacitance is

$$c = \begin{cases} \frac{\epsilon'_r}{60v_0 \ln \left[\frac{8h}{w} + \frac{w}{4h} \right]}, & \frac{w}{h} \leq 1 \\ \frac{\epsilon'_r}{120\pi v_0} \left[\frac{w}{h} + 1.393 + 0.667 \ln \left(\frac{w}{h} + 1.444 \right) \right], & \frac{w}{h} \geq 1 \end{cases} \quad (4.108c)$$

The PCB shown in Figure 4.18(c) has two lands of width w placed on one side of the board and separated edge to edge by a distance s . The board has a thickness h and a relative permittivity ϵ_r . Assuming the land thickness is zero ($t = 0$), the per-unit-length inductance is

$$l = \begin{cases} \frac{120}{v_0} \ln \left(2 \frac{1 + \sqrt{k}}{1 - \sqrt{k}} \right), & \frac{1}{\sqrt{2}} \leq k \leq 1 \\ \frac{377\pi}{v_0 \ln \left(2 \frac{1 + \sqrt{k'}}{1 - \sqrt{k'}} \right)}, & 0 \leq k \leq \frac{1}{\sqrt{2}} \end{cases} \quad (4.109a)$$

where k is

$$k = \frac{s}{s + 2w} \quad (4.109b)$$

and $k' = \sqrt{1 - k^2}$. The effective relative permittivity is

$$\epsilon'_r = \frac{\epsilon_r + 1}{2} \left\{ \tanh \left[0.775 \ln \left(\frac{h}{w} \right) + 1.75 \right] + \frac{kw}{h} [0.04 - 0.7k + 0.01(1 - 0.1\epsilon_r)(0.25 + k)] \right\} \quad (4.109c)$$

which again accounts for the fact that the electric field lines are partly in air and partly in the substrate dielectric. If this inhomogeneous medium (air and the dielectric) is replaced with a homogeneous one having an effective relative permittivity of ϵ'_r as shown in Figure 4.18(c), all properties of the line remain unchanged. The per-unit-length capacitance is

$$c = \begin{cases} \frac{\epsilon'_r}{120v_0 \ln\left(2 \frac{1 + \sqrt{k}}{1 - \sqrt{k}}\right)}, & \frac{1}{\sqrt{2}} \leq k \leq 1 \\ \frac{\epsilon'_r \ln\left(2 \frac{1 + \sqrt{k'}}{1 - \sqrt{k'}}\right)}{377\pi v_0}, & 0 \leq k \leq \frac{1}{\sqrt{2}} \end{cases} \quad (4.109d)$$

4.3.2 Per-Unit-Length Conductance and Resistance for PCB-Type Lines

For the case of a homogeneous medium such as the stripline shown in Figure 4.18(a), the per-unit-length conductance g is obtained from the per-unit-length capacitance c as before:

$$\begin{aligned} g &= \frac{\sigma_{\text{eff}}}{\epsilon} c \\ &= \omega \tan \delta c \end{aligned} \quad (4.110)$$

where $\tan \delta$ is the loss tangent of the homogeneous dielectric medium. For the case of an inhomogeneous medium such as the microstrip line shown in Figure 4.18(b) or the PCB shown in Figure 4.18(c), it is not possible to use (4.110) because the loss tangents for the various regions are different. However, the previously discussed method of using a numerical solver for the determination of the per-unit-length capacitance c but using in that solver complex permittivities in terms of the loss tangents for each region as

$$\hat{\epsilon}_i = \epsilon_i(1 - j \tan \delta_i) \quad (4.111)$$

to give an overall, complex capacitance as

$$\hat{c} = c_R + jc_I \quad (4.112)$$

can be used. From this complex capacitance, the effective per-unit-length conductance and capacitance of this *inhomogeneous medium* can be determined as before as

$$g = -\omega c_I \quad (4.113a)$$

and

$$c = c_R \quad (4.113b)$$

The per-unit-length resistance and internal inductance for conductors of rectangular cross section (a land) have not been obtained in closed form, and numerical approximation methods must be used. Unlike wires, analytical solutions for the resistance and internal inductance are complicated by the fact that we do not know the current distribution over the cross section. As frequency increases, skin effect causes

the current distribution to move toward the outer surface of the conductor tending to be concentrated at the corners when skin effect is well developed [C.9–C.11]. Early works consisted of measured results for the skin effect [20, 21]. Wheeler developed a simple “incremental inductance rule” for computing the high-frequency impedance of a conductor when skin effect is well developed [22]. Wheeler’s incremental inductance rule requires that the conductor resistance and internal inductive reactance must be equal at high frequencies where skin effect is well developed. This is the case for conductors of circular cross section $r = \omega l_{int}$ (see 4.103b). However, it should not be used for conductors of rectangular cross section, because, as we will see later in this section, the resistance and internal inductive reactance are not equal. The direct solution for the resistance and internal inductance of conductors of rectangular cross section can be obtained using a variety of methods for solving the diffusion equation in the two-dimensional transverse plane for infinitely long conductors [23–31, C.9–C.11].

The partial element equivalent circuit (PEEC) method can be used to solve the problem numerically by dividing the rectangular bar into rectangular subbars as shown in Figure 4.19(a) [32, 33]. The method uses the concepts of partial inductance [A.3,33–36]. Figure 4.19(a) shows a bar of length L , width w , and thickness t . If we assume the current to be uniformly distributed over the cross section, the total

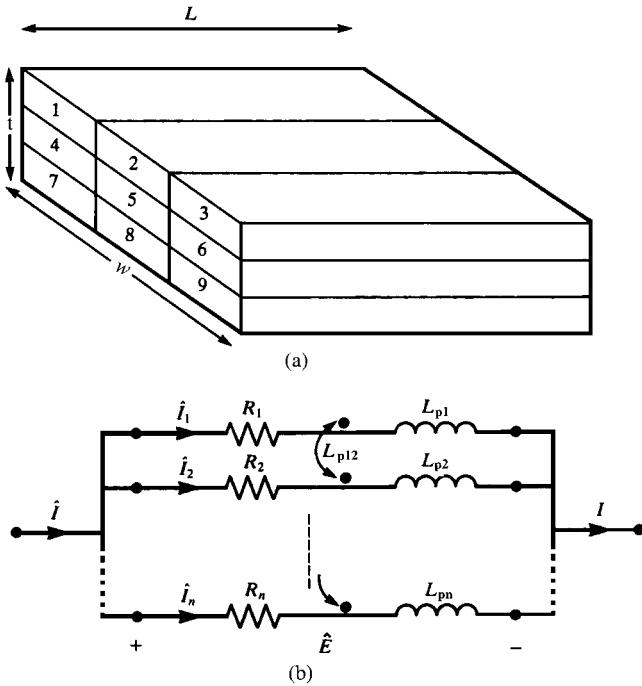


FIGURE 4.19 Representation of a rectangular bar having a nonuniform current distribution over the cross section in terms of subbars having constant current distributions and the resulting circuit model.

bar resistance can be determined as

$$R = \frac{L}{\sigma wt} \quad (\Omega) \quad (4.114)$$

The self partial inductance of the bar, L_p , can be similarly determined for uniform current distribution over the cross section [33–36]. This notion can be extended to bars that have nonuniform current distributions over their cross section by dividing the bar into N subbars of rectangular cross section over which we assume the current to be uniformly distributed but whose level is unknown. This essentially approximates the actual current distribution over the cross section as a piecewise-constant approximation. The voltage across each subbar is

$$\hat{E} = R_i \hat{I}_i + j\omega L_{pi} \hat{I}_i + j\omega \sum_{\substack{k=1 \\ k \neq i}}^N (L_{pik} \hat{I}_k) \quad (4.115)$$

where R_i is the resistance of each subbar, L_{pi} is the self partial inductance of the subbar, and L_{pik} is the mutual partial inductance between the i th and k th subbars. Formulas for these mutual partial inductances between conductors of rectangular cross section having uniformly distributed currents over their cross section are available in [33–35]. Arranging (4.115) for all subbars gives

$$\begin{bmatrix} \hat{E} \\ \hat{E} \\ \vdots \\ \hat{E} \end{bmatrix} = \begin{bmatrix} (R_1 + j\omega L_{p1}) & j\omega L_{p12} & \cdots & j\omega L_{p1N} \\ j\omega L_{p12} & (R_2 + j\omega L_{p2}) & \ddots & j\omega L_{p2N} \\ \vdots & \vdots & \ddots & \vdots \\ j\omega L_{p1N} & j\omega L_{p2N} & \cdots & (R_N + j\omega L_{pN}) \end{bmatrix} \begin{bmatrix} \hat{I}_1 \\ \hat{I}_2 \\ \vdots \\ \hat{I}_N \end{bmatrix} \quad (4.116a)$$

or

$$\hat{\mathbf{E}} = \hat{\mathbf{Z}} \hat{\mathbf{I}} \quad (4.116b)$$

for N subbars. The sum of the subbar currents equals the total current for the bar, and the voltages across all subbars are equal to the voltage across the bar as illustrated in Figure 4.19(b). These constraints can be imposed to give the total resistance and partial inductance of the overall bar by inverting $\hat{\mathbf{Z}}$ in (4.116b) to yield

$$\hat{\mathbf{I}} = \hat{\mathbf{Z}}^{-1} \hat{\mathbf{E}} \quad (4.116c)$$

The first constraint that the total current of the bar is the sum of the currents of the subbars is imposed by summing the entries in the rows of $\hat{\mathbf{Z}}^{-1}$, and the second constraint that the voltages across the subbars must be equal is imposed by summing the entries in the columns of $\hat{\mathbf{Z}}^{-1}$ to give the effective admittance

$$\hat{Y}(f) = \sum_{i=1}^N \sum_{j=1}^N [\hat{Z}^{-1}]_{ij} \tag{4.117a}$$

The impedance of the complete bar including skin effect is obtained by inverting this admittance as

$$\hat{Z}(f) = \frac{1}{\sum_{i=1}^N \sum_{j=1}^N [\hat{Z}^{-1}]_{ij}} \tag{4.117b}$$

The real part of this resulting composite impedance is the resistance $R(f)$ and includes the effect of nonuniform current distribution over the bar cross section. The imaginary part includes the internal inductance (due to flux internal to the conductor) as well as the effect of flux external to the conductor.

A similar numerical method described in [C.10] allows the computation of the internal inductance as well. Figure 4.20 shows the current distribution across the conductor cross section for a 1.4-mil-thick (1 ounce copper cladding) and 15-mil-wide land, where 1 mil = 0.001 inch. These are shown for frequencies of 100kHz, 10MHz, 100MHz, and 1GHz. This shows the previously mentioned phenomenon that the current distribution tends to peak at the sharp corners of the land cross section. Figure 4.21 shows plots of the per-unit-length resistance and internal

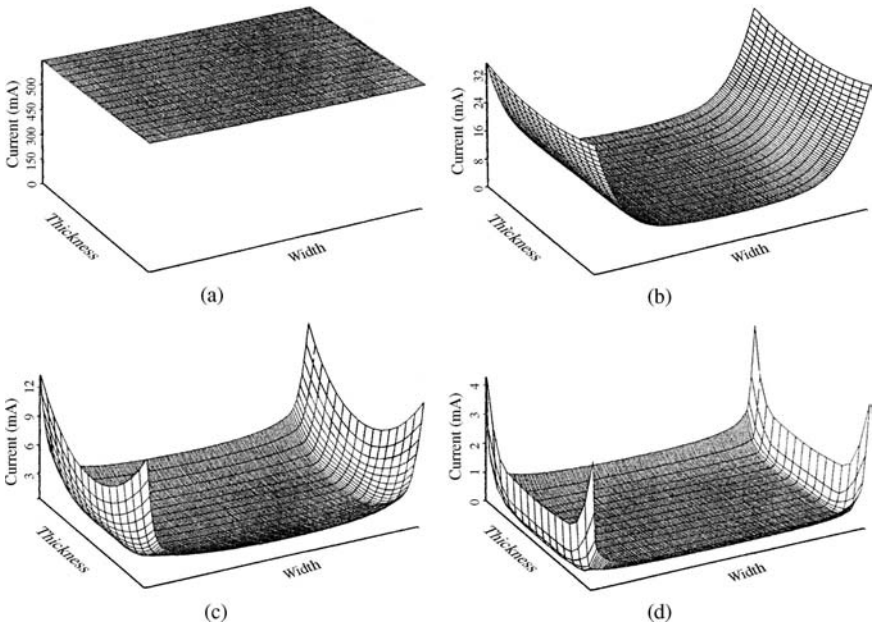


FIGURE 4.20 Current distribution over the rectangular cross section of a 1.4 mil × 15 mil land at (a) 100 kHz, (b) 10 MHz, (c) 100 MHz, and (d) 1 GHz.

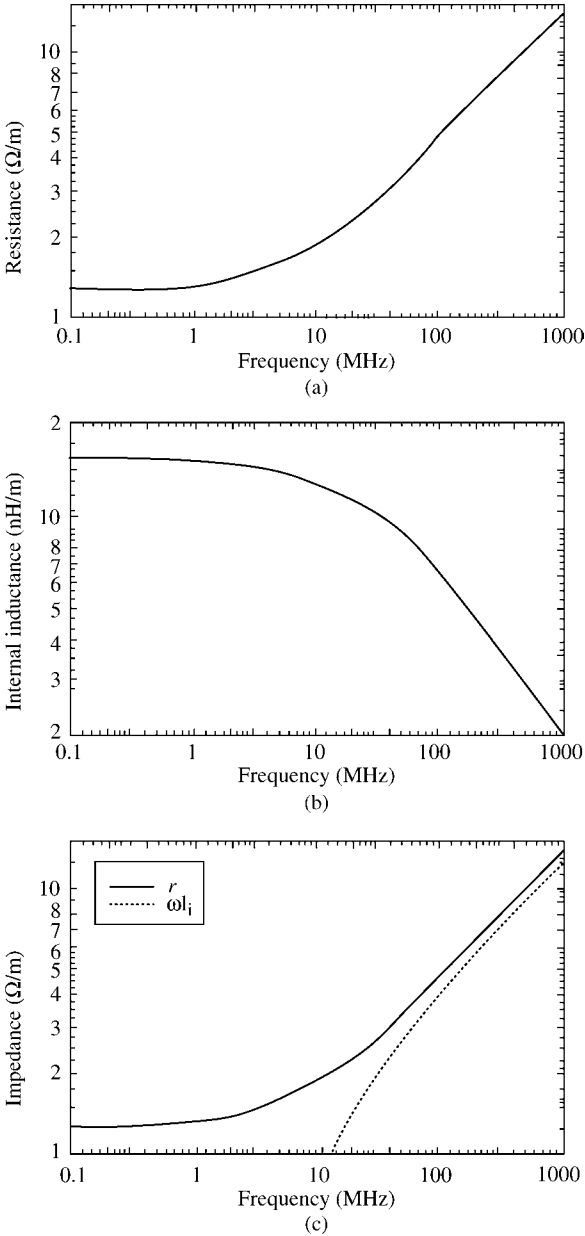


FIGURE 4.21 The per-unit-length internal impedance of a 1.4 mil \times 15 mil land: (a) resistance, (b) internal inductance, and (c) resistance versus internal inductive reactance.

inductance for this case of a 1.4-mil-thick and 15-mil-wide copper land as a function of frequency. This shows that above approximately 10 MHz, the per-unit-length resistance increases at a rate of 10 dB/decade or \sqrt{f} symbolizing that skin effect is becoming well developed above this frequency. Similarly, the per-unit-length internal inductance decreases above 10 MHz at a rate of 10 dB/decade or $1/\sqrt{f}$. Figure 4.21(c) compares the per-unit-length resistance to the per-unit-length internal inductive reactance, ωl_i . Observe that when skin effect is well developed, the resistance and internal inductive reactance ωl_i are not equal. The difference for these bar dimensions is on the order of 10%. This is slightly different from the case of a circular cross-section conductor (wire) where the per-unit-length resistance and internal inductive reactance are equal (see the results for wires in (4.103b)). Figure 4.22(a) shows this comparison for a $50 \mu\text{m} \times 50 \mu\text{m}$ copper land, and Figure 4.22(b) shows the comparison for a $4.62 \text{ mm} \times 4.62 \text{ mm}$ copper land. For these latter cases, the

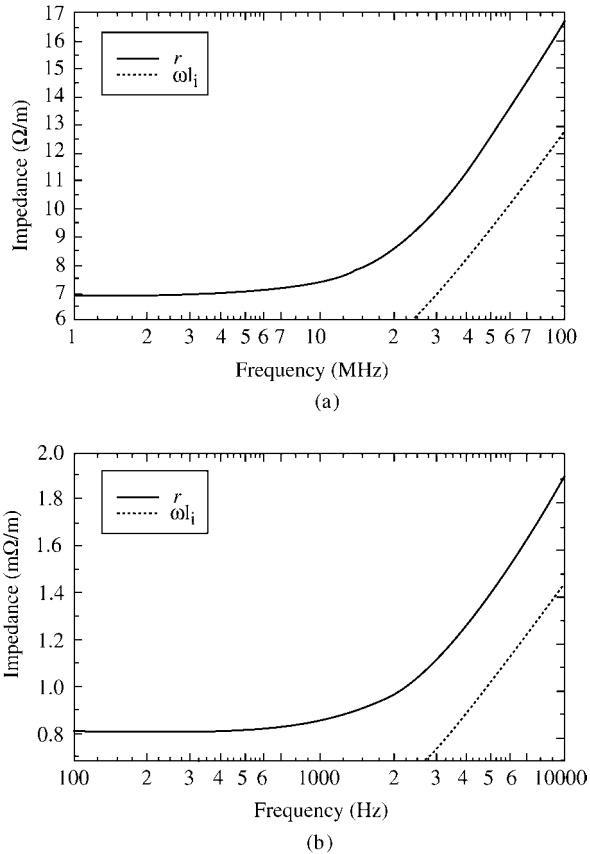


FIGURE 4.22 Comparison of the per-unit-length resistance and high-frequency internal inductive reactance for (a) a $50 \mu\text{m} \times 50 \mu\text{m}$ land and (b) a $4.62 \text{ mm} \times 4.62 \text{ mm}$ land.

difference between the resistance and internal inductive reactance is on the order of 30%. It appears that for bars with high aspect ratios, that is, $w \gg t$, the high-frequency resistance r_{hf} and the high-frequency internal inductive reactance $\omega l_{i,hf}$ are approximately equal as was the case for round wires.

The above methods, although quite accurate if the number of subbars is chosen sufficiently large, are computationally intensive. A simple but approximate method that parallels the notions for a round wire is to approximate the resistance for the two cases where the bar dimensions are much less than or much greater than a skin depth. In the case where the bar dimensions are much less than a skin depth, the current can be approximated as being uniform over the bar cross section as illustrated in Figure 4.23(a). Thus, the low-frequency, dc per-unit-length resistance can simply be calculated as

$$r_{dc} = \frac{1}{\sigma wt} \quad (\Omega/m) \tag{4.118}$$

For higher frequencies where the bar dimensions are much greater than a skin depth, that is, $w, t \gg \delta$ and skin effect is well developed, we assume that the current distribution over the bar is uniformly distributed over strips of thickness that is proportional to a skin depth, that is, $k\delta/2$, and zero elsewhere as illustrated in Figure 4.23(b). Actually

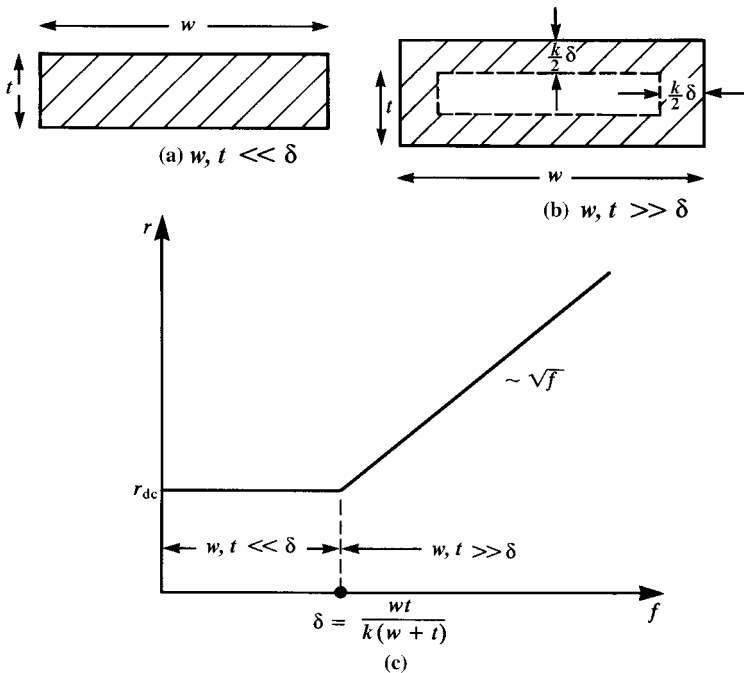


FIGURE 4.23 An approximate frequency-dependent model for a land: (a) low frequency, $w, t \ll \delta$, (b) high frequency, $w, t \gg \delta$, and (c) asymptotes for the resistance frequency response.

this is not correct since, as is shown in Figure 4.20, the current tends to concentrate first along the short edge, the thickness, and then along the long edge, the width. Also, as was shown previously, the current peaks at the corners of the bar when skin effect is well developed, but this effect is ignored here. This gives the approximate high-frequency per-unit-length resistance as

$$\begin{aligned}
 r_{\text{hf}} &\cong \frac{1}{\sigma(k\delta t + k\delta w)} \\
 &= \frac{1}{k\sigma\delta(w + t)}
 \end{aligned}
 \tag{4.119}$$

which increases as \sqrt{f} . Numerical calculations show that k is some constant whose value lies between 1 and 2, $1 < k < 2$. The high-frequency resistance formula in (4.119) assumes that the widths of the current concentrations are the same. The plots of the current distribution shown in Figure 4.20 show that the current first tends to crowd to the edge of one dimension where that dimension becomes on the order of a skin depth and then crowds toward the edge of the other dimension when that dimension becomes on the order of a skin depth at a higher frequency. Setting the dc and high-frequency asymptotes in (4.118) and (4.119) equal gives

$$\delta = \frac{1}{k} \frac{wt}{(w + t)}
 \tag{4.120}$$

as shown in Figure 4.23(c). Figure 4.24 illustrates the comparison of this approximation to the method of subbars described previously for various divisions of the bar (w/NW , t/NT). The resistance of the bar is the real part of \tilde{Z} computed as in (4.117b). The bar is typical of a land on the surface of a printed circuit board and has $t = 1.4$ mils and $w = 15$ mils. The results were computed for bar lengths of 1 and 10 in., and the per-unit-length resistance obtained by dividing the total resistance by the bar length was virtually identical for the two lengths. The break frequency in (4.120) occurs around 7 MHz for $k = 1.3$, where the dimension $wt/(w + t)$ in (4.120) is 1.3δ . For this dimension, the thickness of each current concentration is 0.65δ . The computed results are plotted in Figure 4.24 and indicate very close correlation for $k = 1.3$. For $k = 2$, the break frequency in (4.120) occurs around 16.5 MHz, where the dimension $wt/(w + t)$ in (4.120) is 2δ . For this dimension, the thickness of each current concentration is one skin depth: $k/2 = \delta$. The results of the subbar method shown in Figure 4.24 indicate that the true resistance in the high-frequency region is some 50% higher than that predicted by the approximate method for $k = 2\delta$. This error is evidently due to the omission of the peaking of the current at the corners in the approximation. For the data shown in Figure 4.22(a) for a square bar of side dimensions of 50 μm , the value of k to provide close prediction of the high-frequency asymptote at 100 MHz of 16.5 Ω/m is $k = 1.58$. For the data shown in Figure 4.22(b) for a square bar of side dimensions of 4.62 mm, the value of k to provide close prediction of the high-frequency asymptote at 10 kHz of 1.9×10^{-3} Ω/m is $k = 1.486$.

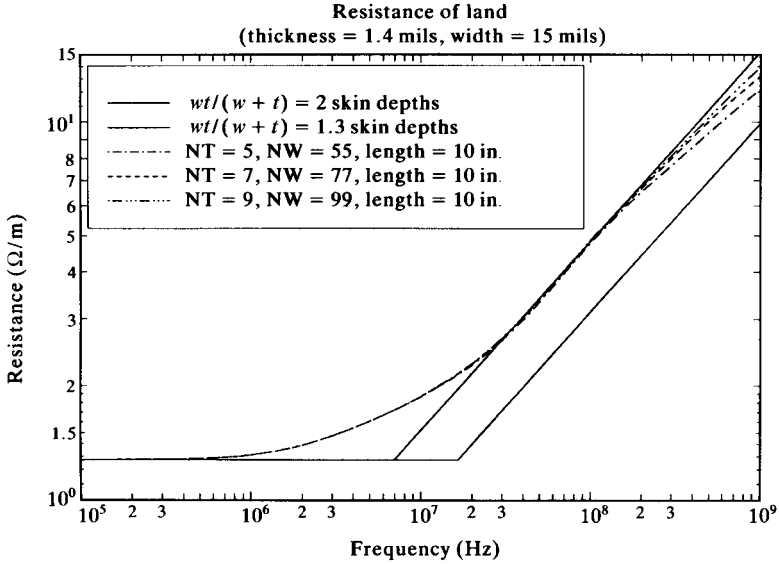


FIGURE 4.24 Results of the computation of the per-unit-length resistance of a land via the method of subbars for a thickness of 1.4 mils and a width of 15 mils.

PROBLEMS

- 4.1 Write the equation for the per-unit-length inductance of two widely spaced identical wires in (4.19) in terms of nH/in. $[10.16 \ln(s/r_w)]$
- 4.2 Determine the exact and approximate values for the per-unit-length inductance and capacitance of a two-wire ribbon cable consisting of two #28 gauge stranded wires ($r_w = 7.5$ mils, 1 mil = 0.001 in.) that are separated by 50 mils. Determine the ratio of wire separation to wire radius. [Exact: $0.75 \mu\text{H/m} = 19.04 \text{ nH/in.}$, $14.82 \text{ pF/m} = 0.3765 \text{ pF/in.}$, approximate: $0.759 \mu\text{H/m} = 19.27 \text{ nH/in.}$, $14.64 \text{ pF/m} = 0.372 \text{ pF/in.}$ The ratio of wire separation to wire radius is 6.7.]
- 4.3 Determine the exact and approximate values for the per-unit-length capacitance and inductance of one #20 gauge solid wire of radius 16 mils at a height of 1 cm above an infinite ground plane. Determine the ratio $2h/r_w$. [Exact: $14.26 \text{ pF/m} = 0.36 \text{ pF/in.}$, $0.779 \mu\text{H/m} = 19.79 \text{ nH/in.}$; approximate: $14.26 \text{ pF/m} = 0.36 \text{ pF/in.}$, $0.779 \mu\text{H/m} = 19.79 \text{ nH/in.}$ The ratio $2h/r_w$ is 49.]
- 4.4 A RG58U coaxial cable consists of a #20 gauge solid wire ($r_w = 16$ mils), a shield having an inner radius of 58 mils. The interior dielectric is polyethylene ($\epsilon_r = 2.3$). Determine the per-unit-length capacitance and inductance as well as the velocity of propagation as a percentage of the speed of light. [$0.2576 \mu\text{H/m} = 6.54 \text{ nH/in.}$, $99.2 \text{ pF/m} = 2.52 \text{ pF/in.}$, 66%]

- 4.5** Determine the per-unit-length capacitance and inductance of a stripline having dimensions $s = 20$ mils, $w = 5$ mils, and a dielectric having $\epsilon_r = 4.7$. [113.2 pF/m = 2.88 pF/in., 0.461 μ H/m = 11.7 nH/in.]
- 4.6** Determine the per-unit-length capacitance and inductance of a microstrip line having dimensions of $h = 50$ mils, $w = 5$ mils, and $\epsilon_r = 4.7$. [38.26 pF/m = 0.972 pF/in., 0.877 μ H/m = 22.3 nH/in., 3.018]
- 4.7** Determine the per-unit-length capacitance and inductance of a PCB configuration having dimensions $s = 15$ mils, $w = 15$ mils, $h = 62$ mils, and $\epsilon_r = 4.7$. [38.53 pF/m = 0.979 pF/in., 0.804 μ H/m = 20.42 nH/in.]
- 4.8** Two bare #20 gauge (radius = 16 mils) wires are separated center to center by 50 mils. Determine the exact and approximate values of the per-unit-length capacitance and inductance. [Exact: 27.33 pF/m, 0.4065 μ H/m; approximate: 24.38 pF/m, 0.4558 μ H/m. The ratio of separation to wire radius is only 3.13, which is not sufficient for the approximate results to be valid.]
- 4.9** One bare #12 gauge (radius = 40 mils) is suspended at a height of 80 mils above its return path, which is a large ground plane. Determine the exact and approximate values of the per-unit-length capacitance and inductance. [Exact: 42.18 pF/m, 0.2634 μ H/m; approximate: 40.07 pF/m, 0.2773 μ H/m. The ratio of wire height above ground to wire radius is only 2.0, which is not sufficient for the approximate results to be valid although the error is only about 5%.]
- 4.10** A typical coaxial cable is RG-6U, which has an interior #18 gauge (radius 20.15 mils) solid wire, an interior shield radius of 90 mils, and an inner insulation of foamed polyethylene having a relative permittivity of 1.45. Determine the per-unit-length capacitance, inductance, and the velocity of propagation relative to that of free space. [53.83 pF/m, 0.3 μ H/m. The velocity of propagation relative to free space is $v/v_0 = 1/\sqrt{\epsilon_r} = 0.83$.]
- 4.11** Typical dimensions for striplines in multilayer PCBs are a plate separation of 10 mils, a conductor width of 5 mils, and $\epsilon_r = 4.7$. Determine the per-unit-length capacitance and inductance for this structure. [156.4 pF/m and 0.334 μ H/m]
- 4.12** A microstrip line is constructed on a FR-4 board having a relative permittivity of 4.7. The board thickness is 64 mils and the land width is 10 mils. Determine the per-unit-length capacitance and inductance as well as the effective relative permittivity. [0.7873 μ H/m, 43.18 pF/m and $\epsilon'_r = 3.06$]
- 4.13** A PCB has land widths of 5 mils and an edge-to-edge separation of 5 mils. The board is glass epoxy having a relative permittivity of 4.7 and a thickness of 47 mils. Determine the per-unit-length capacitance and inductance as well as the effective relative permittivity. [0.8038 μ H/m, 39.06 pF/m, and $\epsilon'_r = 2.825$]
- 4.14** Determine the per-unit-length dc resistance of a #28 gauge solid wire ($r_w = 6.3$ mils) and a #28 gauge stranded wire consisting of seven strands of #36 gauge wire ($r_w = 2.5$ mils). [214.3 m Ω /m, 194.4 m Ω /m]
- 4.15** Determine the frequency where the resistance of a #20 gauge solid wire ($r_w = 16$ mils) begins to increase due to skin effect. [105.8 kHz] Determine the resistance of the wire at 100 MHz. [1.022 Ω /m]

- 4.16** Determine the resistance of a 6-in. PCB land of width 5 mils at 1 MHz and at 40 MHz. [0.59Ω , 0.776Ω]
- 4.17** A current is at a certain distance above a perfectly conducting, infinite ground plane, which lies in the x - y plane. If the vector current is given by $-3\mathbf{a}_x - 5\mathbf{a}_y + 2\mathbf{a}_z$, determine the image current that is at the same distance below the location of the ground plane. [$3\mathbf{a}_x + 5\mathbf{a}_y + 2\mathbf{a}_z$]

REFERENCES

- [1] W.B. Boast, *Vector Fields*, Harper & Row, New York, 1964.
- [2] E. Weber, *Electromagnetic Fields*, vol. I, John Wiley & Sons, New York, 1950.
- [3] W.R. Smythe, *Static and Dynamic Electricity*, 3rd edition, McGraw-Hill, New York, 1968.
- [4] S. Ramo, J.R. Whinnery, and T. Van Duzer, *Fields and Waves in Communication Electronics*, 2nd edition, John Wiley & Sons, New York, 1984.
- [5] A.R. von Hippel, *Dielectric Materials and Applications*, MIT Press and Wiley, New York, 1954.
- [6] R.E. Matick, *Transmission Lines for Digital and Communication Networks*, McGraw-Hill, New York, 1969.
- [7] R.F. Harrington and C. Wei, Losses in multiconductor transmission lines in multilayered dielectric media, *IEEE Transactions on Microwave Theory and Techniques*, **32** (7), 705–710, 1984.
- [8] W.C. Johnson, *Transmission Lines and Networks*, McGraw-Hill, New York, 1950.
- [9] C. Yen, Z. Fazarinc, and R.L. Wheeler, time-domain skin-effect model for transient analysis of lossy transmission lines, *Proceedings of IEEE*, **70** (7), 750–757, 1982.
- [10] V. Belevitch, Theory of the proximity effect in multiwire cables, *Philips Research Reports*, **32** (Part I), 16–43, (Part II), 96–177, 1977.
- [11] M.E. Hellman and I. Palocz, The effect of neighboring conductors on the currents and fields in plane parallel transmission lines, *IEEE Transactions on Microwave Theory and Techniques*, **17** (5), 254–258, 1969.
- [12] H.B. Dwight, *Tables of Integrals and Other Mathematical Data*, 4th edition, Macmillan, New York, 1961.
- [13] S.B. Cohn, Problems in strip transmission lines, *IEEE Transactions on Microwave Theory and Techniques*, **3**, 119–126, 1955.
- [14] K.C. Gupta, R. Garg, and R. Chadha, *Computer-Aided Design of Microwave Circuits*, Artech House, Dedham, MA, 1981.
- [15] K.C. Gupta, R. Garg, and I.J. Bahl, *Microstrip Lines and Slotlines*, Artech House, Dedham, MA, 1979.
- [16] R.E. Collin, *Field Theory of Guided Waves*, 2nd edition, IEEE Press, New York, 1991.
- [17] T.C. Edwards, *Foundations for Microstrip Engineering*, Wiley, New York, 1981.
- [18] H.R. Kaupp, Characteristics of microstrip transmission lines, *IEEE Transactions on Electronic Computers*, **16**, 186–193, 1967.

- [19] H.A. Wheeler, Transmission-line properties of parallel strips separated by a dielectric sheet, *IEEE Transactions on Microwave Theory and Techniques*, **13**, 172–185, 1965.
- [20] J.D. Cockcroft, Skin effect in rectangular conductors at high frequencies, *Proceedings of the Royal Society*, **122** (A 790), 533–542, 1929.
- [21] S.J. Haefner, Alternating current resistance of rectangular conductors, *Proceeding of IRE*, **25**, 434–447, 1937.
- [22] H.A. Wheeler, Formulas for the skin-effect, *Proceeding of IRE*, **30**, 412–424, 1942.
- [23] P. Silvester, Modal theory of skin effect in flat conductors, *Proceedings of IEEE*, **54** (9), 1147–1151, 1966.
- [24] P. Silvester, The accurate calculation of skin effect of complicated shape, *IEEE Transactions on Power Apparatus and Systems*, **87**, 735–742, 1968.
- [25] M.J. Tsuk, and J.A.Kong, A hybrid method for the calculation of the resistance and inductance of transmission lines with arbitrary cross sections, *IEEE Transactions on Microwave Theory and Techniques*, **39** (8), 1338–1347, 1991.
- [26] F. Olyslager, N. Fache, and D. De Zutter, A fast and accurate line parameter calculation of general multiconductor transmission lines in multilayered media, *IEEE Transactions on Microwave Theory and Techniques*, **39** (6), 901–909, 1991.
- [27] P. Waldow and I. Wolff, The skin-effect at high frequencies, *IEEE Transactions on Microwave Theory and Techniques*, **33** (10), 1076–1081, 1985.
- [28] H. Lee and T. Itoh, Phenomenological loss equivalence method for planar quasi-TEM transmission lines with a thin normal conductor or superconductor, *IEEE Transactions on Microwave Theory and Techniques*, **37** (12), 1904–1909, 1989.
- [29] G.I. Costache, Finite element method applied to skin-effect problems in strip transmission lines, *IEEE Transactions on Microwave Theory and Techniques*, **35** (11), 1009–1013, 1987.
- [30] T. Itoh, (ed.) *Planar Transmission Line Structures*, IEEE Press, New York, 1987.
- [31] E.L. Barsotti, E.F. Kuester, and J.M. Dunn, A simple method to account for edge shape in the conductor loss in microstrip, *IEEE Transactions on Microwave Theory and Techniques*, **39** (1), 98–105, 1991.
- [32] W.T. Weeks, L.L. Wu, M.F. McAlister, and A. Singh, Resistive and inductive skin effect in rectangular conductors, *IBM Journal of Research and Development*, **23** (6), 652–660.
- [33] A.E. Ruehli, Inductance calculations in a complex integrated circuit environment, *IBM Journal of Research and Development*, **16** (5), 470–481, 1972.
- [34] F.W. Grover, *Inductance Calculations*, Dover Publications, New York, 1946.
- [35] C. Hoer, and C. Love, Exact inductance equations for rectangular conductors with applications to more complicated geometries, *Journal of the Research of the National Bureau of Standards-C. Engineering and Instrumentation*, **69C** (2), 127–137, 1965.
- [36] A.W. Barr, Calculation of frequency-dependent impedance for conductors of rectangular cross section, *AMP Journal of Technology*, **1**, 91–100, 1991.

5

THE PER-UNIT-LENGTH PARAMETERS FOR MULTICONDUCTOR LINES

In this chapter, we will extend the notions developed for two-conductor lines in the previous chapter to multiconductor lines. In general, the concepts are identical but the details are more involved. We will find that numerical approximate methods must generally be employed to compute the entries in the per-unit-length parameter matrices \mathbf{L} , \mathbf{C} , and \mathbf{G} . The entries in the per-unit-length resistance matrix \mathbf{R} are grouped as shown in Chapter 3, Eqs. (3.12) and (3.13), and are computed, as an approximation, for the isolated conductors. Hence, the entries in \mathbf{R} are the same as were obtained for two-conductor lines in the previous chapter; that is, we disregard proximity effect in the resistance calculation.

In the case of multiconductor transmission lines (MTLs), the situation is somewhat similar except that the details become more involved. In the case of a MTL where the conductors have circular, cylindrical cross sections such as wires and the surrounding medium is homogeneous, we can obtain approximate closed-form solutions for the entries in the per-unit-length parameter matrices \mathbf{L} , \mathbf{C} , and \mathbf{G} under the assumption that the conductors are widely separated from each other. This condition of being widely separated is not very restrictive for typical dimensions of wire-type lines such as ribbon cables. However, dielectric insulations are usually present around the conductors of wire-type lines such as ribbon cables, and therefore wire-type MTLs generally require the use of numerical methods to compute the entries in the per-unit-length parameter matrices. For the case of MTLs having conductors of rectangular cross sections such as lands on printed circuit boards (PCBs), approximate numerical methods must always be used regardless of whether the surrounding medium is homogeneous (as is the case

for the coupled stripline) or inhomogeneous (as for the case of the coupled microstrip and the case of a general PCB).

5.1 DEFINITIONS OF THE PER-UNIT-LENGTH PARAMETER MATRICES \mathbf{L} , \mathbf{C} , AND \mathbf{G}

We first review the fundamental definitions of the per-unit-length parameter matrices of inductance, \mathbf{L} , capacitance, \mathbf{C} , and conductance, \mathbf{G} . Recall that these per-unit-length parameters are determined as *static field solutions* in the transverse plane for perfect line conductors. As opposed to two-conductor lines, there are only a few closed-form solutions for MTLs. Generally, approximate numerical methods must be used for the computation of the entries in the per-unit-length parameter matrices \mathbf{L} , \mathbf{C} , and \mathbf{G} . In any event, we showed in Chapter 3 that \mathbf{L} , \mathbf{C} , and \mathbf{G} are symmetric and positive-definite matrices. Again, we will restrict our discussions to *uniform lines*. As discussed previously, computation of the entries in \mathbf{R} is identical to those calculations for two-conductor lines given previously; that is, we will neglect proximity effect and compute these entries for isolated conductors.

The entries in the per-unit-length inductance matrix \mathbf{L} relate *the total magnetic flux* penetrating the i th circuit, per unit of line length, to all the line currents producing it as

$$\Psi = \mathbf{L} \mathbf{I} \quad (5.1a)$$

or, in expanded form,

$$\begin{bmatrix} \psi_1 \\ \psi_2 \\ \vdots \\ \psi_n \end{bmatrix} = \begin{bmatrix} l_{11} & l_{12} & \cdots & l_{1n} \\ l_{12} & l_{22} & \cdots & l_{2n} \\ \vdots & \vdots & \ddots & \vdots \\ l_{1n} & l_{2n} & \cdots & l_{nn} \end{bmatrix} \begin{bmatrix} I_1 \\ I_2 \\ \vdots \\ I_n \end{bmatrix} \quad (5.2b)$$

If we interpret the above relations in a manner similar to the n -port parameters [A.2], we obtain the following relations for the entries in \mathbf{L} :

$$l_{ii} = \left. \frac{\psi_i}{I_i} \right|_{I_1 = \cdots = I_{i-1} = I_{i+1} = \cdots = I_n = 0} \quad (5.2a)$$

$$l_{ij} = \left. \frac{\psi_i}{I_j} \right|_{I_1 = \cdots = I_{j-1} = I_{j+1} = \cdots = I_n = 0} \quad (5.2b)$$

The entries l_{ii} are the *self-inductances* of the i th circuit, and the entries l_{ij} with $i \neq j$ are the *mutual inductances* between the i th and the j th circuits. Thus, we can compute these inductances by placing a current on one conductor (and returning it on the reference conductor), setting the currents on all other conductors to zero, and determining the magnetic flux, per unit of line length, penetrating the other *circuit*. The definition of

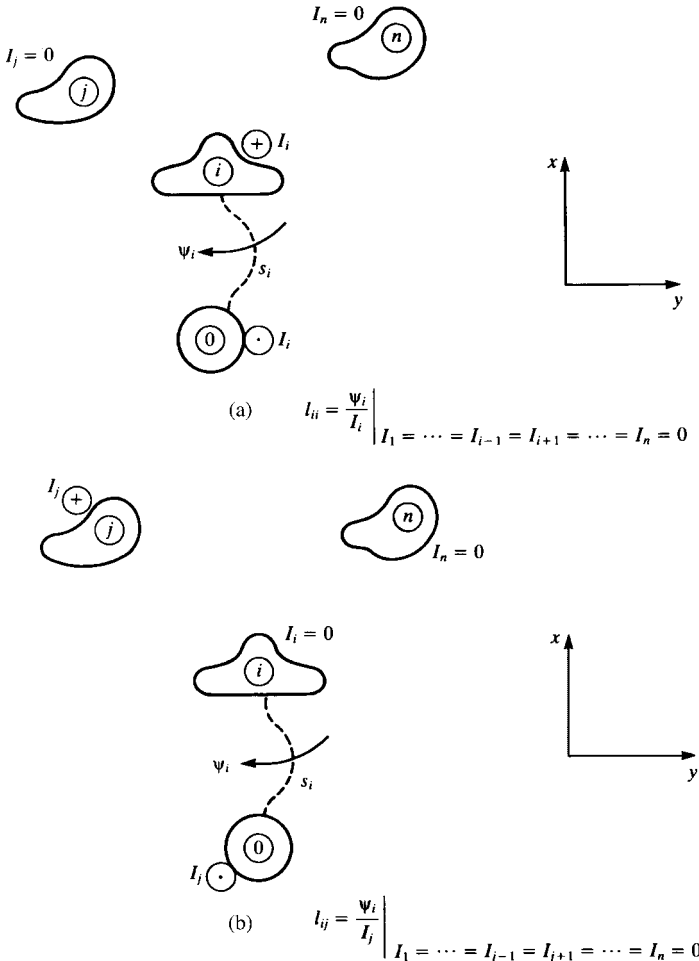


FIGURE 5.1 Illustration of the definitions of flux through a circuit for determination of the per-unit-length inductances: (a) self-inductances l_{ii} and (b) mutual inductances l_{ij} .

the i th circuit is critically important in obtaining the correct value and sign of these elements. This important concept is illustrated in Figure 5.1. The i th circuit is the *surface* between the i th conductor and the reference conductor. This surface is of arbitrary shape but is uniform along the line. This surface shape may be a flat surface or some other shape so long as this shape is uniform along the line. The magnetic flux per unit length penetrating this surface (circuit) is *defined* as being in the *clockwise direction* around the i th conductor when looking in the direction of increasing z . In other words, *the flux direction* Ψ_i through surface s_i is the direction in which magnetic flux would be generated by the current of the i th conductor. Figure 5.1(a) shows the calculation of l_{ii} , and Figure 5.1(b) shows the calculation of l_{ij} .

In order to illustrate this important concept further, consider a three-conductor line consisting of three wires lying in a plane where the middle wire is chosen, arbitrarily, as the reference conductor as shown in Figure 5.2(a). This resembles a ribbon cable without dielectric insulations. The surfaces and individual configurations for computing l_{11} , l_{22} , and l_{12} are shown in the remaining figures. Observe that the surface for Ψ_2 is between conductor 2 and the reference conductor, but observe the desired direction of this flux; it is chosen with respect to the magnetic flux that would be produced by current I_2 on conductor 2. So, the flux direction for the i th circuit is defined by the direction of the current on the i th conductor and the right-hand rule when looking in the direction of increasing z .

The entries in the per-unit-length capacitance matrix C relate the *total charge* on the i th conductor per unit of line length to all of the line voltages producing it as

$$\mathbf{Q} = \mathbf{C} \mathbf{V} \tag{5.3a}$$

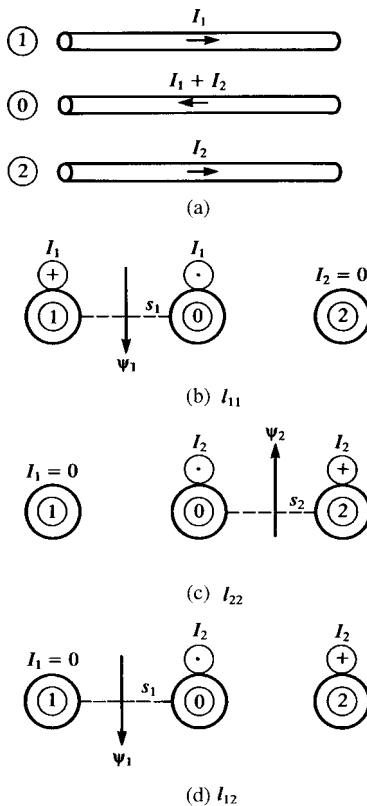


FIGURE 5.2 Illustrations of the derivation of the per-unit-length inductances for a three-wire ribbon cable with the center wire as the reference conductor.

or, in expanded form,

$$\begin{bmatrix} q_1 \\ q_2 \\ \vdots \\ q_n \end{bmatrix} = \begin{bmatrix} \sum_{k=1}^n c_{1k} & -c_{12} & \cdots & -c_{1n} \\ -c_{12} & \sum_{k=1}^n c_{2k} & \cdots & -c_{2n} \\ \vdots & \vdots & \ddots & \vdots \\ -c_{1n} & -c_{2n} & \cdots & \sum_{k=1}^n c_{nk} \end{bmatrix} \begin{bmatrix} V_1 \\ V_2 \\ \vdots \\ V_n \end{bmatrix} \quad (5.3b)$$

The particular form for the entries in \mathbf{C} in (5.3b) was derived in Chapter 3. If we denote the entries in \mathbf{C} in the i th row and j th column as $[\mathbf{C}]_{ij}$, these can be obtained by interpreting (5.3b) as an n -port relation and applying the usual constraints of setting all voltages except the j th voltage V_j to zero (“grounding” them to the reference conductor) and determining the charge q_i on the i th conductor (and $-q_i$ on the reference conductor) to give $[\mathbf{C}]_{ij}$:

$$[\mathbf{C}]_{ii} = \left. \frac{q_i}{V_i} \right|_{V_1 = \cdots = V_{i-1} = V_{i+1} = \cdots = V_n = 0} \quad (5.4a)$$

$$[\mathbf{C}]_{ij} = \left. \frac{q_i}{V_j} \right|_{V_1 = \cdots = V_{j-1} = V_{j+1} = \cdots = V_n = 0} \quad (5.4b)$$

This amounts to several two-conductor capacitance calculations where the other $n - 1$ conductors are connected with short circuits to the reference conductor.

Although the above method of setting all but one voltage to zero and determining the resulting per-unit-length charge on the other conductors is straightforward, an alternative and simpler method is to apply a per-unit-length charge q_j on the j th conductor, the negative of this, $-q_j$, on the reference conductor, and zero charge on the other conductors and then determining the resulting voltage between the i th conductor and the reference conductor. In order to do this, we invert (5.3) to give

$$\mathbf{V} = \mathbf{PQ} \quad (5.5a)$$

or, in expanded form,

$$\begin{bmatrix} V_1 \\ V_2 \\ \vdots \\ V_n \end{bmatrix} = \begin{bmatrix} p_{11} & p_{12} & \cdots & p_{1n} \\ p_{12} & p_{22} & \cdots & p_{2n} \\ \vdots & \vdots & \ddots & \vdots \\ p_{1n} & p_{2n} & \cdots & p_{nn} \end{bmatrix} \begin{bmatrix} q_1 \\ q_2 \\ \vdots \\ q_n \end{bmatrix} \quad (5.5b)$$

where

$$\mathbf{C} = \mathbf{P}^{-1} \quad (5.5c)$$

The entries in \mathbf{P} are referred to as the *coefficients of potential*. Once the entries in \mathbf{P} are obtained, \mathbf{C} is obtained via (5.5c). The coefficients of potential are obtained from (5.5b) as

$$p_{ii} = \frac{V_i}{q_i} \bigg|_{q_1 = \dots = q_{i-1} = q_{i+1} = \dots = q_n = 0} \quad (5.6a)$$

$$p_{ij} = \frac{V_i}{q_j} \bigg|_{q_1 = \dots = q_{j-1} = q_{j+1} = \dots = q_n = 0} \quad (5.6b)$$

These relationships show that to determine p_{ij} we place a per-unit-length charge q_j on conductor j with no charge on the other conductors (but $-q_j$ on the reference conductor) and determine the resulting voltage V_i of conductor i (between it and the reference conductor with the voltage positive at the i th conductor). These concepts are illustrated in Figure 5.3. Once \mathbf{P} is obtained in this fashion, \mathbf{C} is obtained as the inverse of \mathbf{P} as shown in (5.5c). It is important to point out that the self-capacitance between the i th conductor and the reference conductor, c_{ii} , is not simply the entry in the i th row and i th column of \mathbf{C} . Observe the form of the entries in \mathbf{C} given in (5.3b). The off-diagonal entries are the negatives of the mutual capacitances between the pairs of conductors whereas the main-diagonal entries are the sum of the self-capacitance and the mutual capacitances in that row (or column). Therefore, to obtain the self-capacitance c_{ii} , we sum the entries in the i th row (or column) of \mathbf{C} .

The per-unit-length conductance matrix \mathbf{G} relates the *total transverse conduction current* passing between the conductors per unit of line length to all the line voltages producing it as

$$\mathbf{I}_t = \mathbf{G} \mathbf{V} \quad (5.7a)$$

or, in expanded form,

$$\begin{bmatrix} I_{t1} \\ I_{t2} \\ \vdots \\ I_{tn} \end{bmatrix} = \begin{bmatrix} \sum_{k=1}^n g_{1k} & -g_{12} & \cdots & -g_{1n} \\ -g_{12} & \sum_{k=1}^n g_{2k} & \cdots & -g_{2n} \\ \vdots & \vdots & \ddots & \vdots \\ -g_{1n} & -g_{2n} & \cdots & \sum_{k=1}^n g_{nk} \end{bmatrix} \begin{bmatrix} V_1 \\ V_2 \\ \vdots \\ V_n \end{bmatrix} \quad (5.7b)$$

The particular forms of the entries in \mathbf{G} in (5.7b) were obtained in Chapter 3.

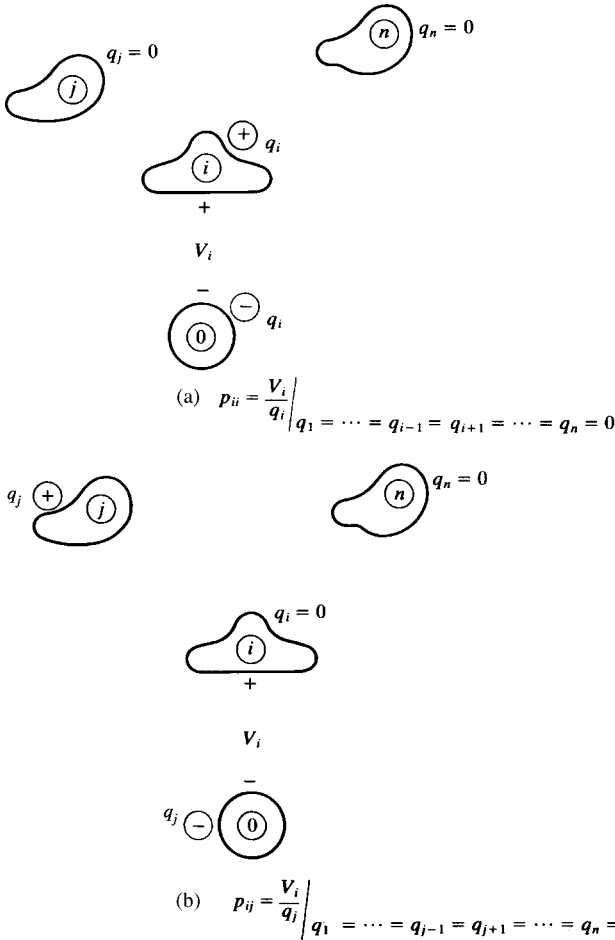


FIGURE 5.3 Illustrations of the determination of the per-unit-length coefficients of potential: (a) self terms p_{ii} and (b) mutual terms p_{ij} .

Once again, the entries in \mathbf{G} can be determined as several subproblems by interpreting (5.7b) as an n -port. For example, to determine the entry in \mathbf{G} in the i th row and j th column, which is denoted as $[\mathbf{G}]_{ij}$, we could enforce a voltage between the j th conductor and the reference conductor, V_j , with all other conductor voltages set to zero (“grounding” them to the reference conductor), $V_1 = \dots = V_{j-1} = V_{j+1} = \dots = V_n = 0$, and determine the per-unit-length transverse current I_{ti} flowing between the i th conductor and the reference conductor. Denoting each of the entries in \mathbf{G} as $[\mathbf{G}]_{ij}$ gives these entries in \mathbf{G} as

$$[\mathbf{G}]_{ii} = \frac{I_{ti}}{V_i} \Big|_{V_1 = \dots = V_{i-1} = V_{i+1} = \dots = V_n = 0} \tag{5.8a}$$

$$[\mathbf{G}]_{ij} = \left. \frac{I_{ti}}{V_j} \right|_{V_1 = \dots = V_{j-1} = V_{j+1} = \dots = V_n = 0} \quad (5.8b)$$

In order to numerically determine the entries in \mathbf{L} , \mathbf{C} , and \mathbf{G} , we *need only a capacitance solver*. First, we solve for the scalar capacitance matrix with the dielectric(s) surrounding the conductors *removed* and replaced with free space that is denoted as \mathbf{C}_0 . The per-unit-length inductance matrix can be obtained from

$$\mathbf{L} = \mu_0 \varepsilon_0 \mathbf{C}_0^{-1} \quad (5.9)$$

In order to obtain the per-unit-length capacitance and conductance matrices, we could, as an alternative to the direct method outlined before, use the capacitance solver with each dielectric replaced by its complex permittivity:

$$\hat{\varepsilon}_i = \varepsilon_i (1 - j \tan \delta_i) \quad (5.10)$$

where $\tan \delta_i$ is the loss tangent (at the particular frequency of interest) of the i th dielectric layer and $\tan \delta_i = (\sigma_{\text{eff},i} / \varepsilon_i)$. This will give a complex-valued capacitance matrix as

$$\hat{\mathbf{C}} = \mathbf{C}_R + j\mathbf{C}_I \quad (5.11)$$

Then, as discussed in the previous chapter, we obtain the per-unit-length capacitance and conductance matrices as

$$\mathbf{C} = \mathbf{C}_R \quad (5.12a)$$

and

$$\mathbf{G} = -\omega \mathbf{C}_I \quad (5.12b)$$

and $\omega = 2\pi f$ is the radian frequency of interest.

5.1.1 The Generalized Capacitance Matrix $\hat{\mathbf{C}}$

The above definitions as well as the derivation of the MTL equations assume that we (arbitrarily) select one of the $n + 1$ conductors as the *reference conductor* to which all the n voltages V_i are referenced. Once the reference conductor is chosen, all the per-unit-length parameter matrices must be computed for that choice consistently. Although the choice of reference conductor is arbitrary, choosing one of the $n + 1$ conductors over another as reference may facilitate the computation of the per-unit-length parameters. For example, if one of the $n + 1$ conductors is an infinite, perfectly conducting plane, choosing the plane as the reference conductor simplifies the calculation of the per-unit-length parameters. However, choice of this plane as reference is not mandatory; we could instead choose one of the other n

conductors as the reference conductor. In this section, we describe a technique for computing a certain per-unit-length parameter matrix, the *generalized capacitance matrix* \mathcal{C} , without regard to the choice of the reference conductor. The dimensions of this generalized capacitance matrix are $(n + 1) \times (n + 1)$. We will show that a transmission-line capacitance \mathbf{C} which is of dimensions $n \times n$, for any conductor chosen as reference conductor can be easily obtained from this generalized capacitance matrix. If a different choice of the reference conductor is made, we can readily obtain the transmission-line capacitance matrix \mathbf{C} for this new choice of reference conductor from the generalized capacitance matrix using simple algebraic relations without repeating the time-consuming calculation of the per-unit-length generalized capacitance. The generalized capacitance matrix for the line with the surrounding medium removed and replaced by free space, \mathcal{C}_0 , and the generalized capacitance matrix with the permittivities replaced by their complex-valued permittivities given in (5.10) as $\hat{\mathcal{C}} = \mathcal{C}_R + \mathcal{C}_I$ can similarly be obtained. The transmission-line capacitance matrix \mathbf{C}_0 and the complex transmission-line capacitance matrix $\hat{\mathbf{C}} = \mathbf{C}_R + j\mathbf{C}_I$ can then be easily obtained from these corresponding generalized capacitance matrices. Then other transmission-line per-unit-length matrices \mathbf{L} , \mathbf{C} , and \mathbf{G} can then be easily obtained from these as

$$\mathbf{L} = \mu_0 \varepsilon_0 \mathbf{C}_0^{-1} \quad (5.13)$$

and

$$\mathbf{C} = \mathbf{C}_R \quad (5.14a)$$

and

$$\mathbf{G} = -\omega \mathbf{C}_I \quad (5.14b)$$

Hence, the major computational effort is in determining the generalized capacitance matrices.

The n MTL voltages V_i are defined to be between each conductor and the chosen reference conductor. We may also define the potentials ϕ_i of each of the $n + 1$ conductors with respect to some reference point or line that is parallel to the z axis [C.4]. The total charge per unit of line length, q_i , of each of the $n + 1$ conductors can be related to their potentials ϕ_i for $i = 0, 1, 2, \dots, n$ with the $(n + 1) \times (n + 1)$ generalized capacitance matrix \mathcal{C} as

$$\mathbf{Q}' = \mathcal{C}\Phi \quad (5.15a)$$

or, in expanded form, as

$$\underbrace{\begin{bmatrix} q_0 \\ q_1 \\ \vdots \\ q_n \end{bmatrix}}_{\mathbf{Q}} = \underbrace{\begin{bmatrix} \epsilon_{00} & \epsilon_{01} & \cdots & \epsilon_{0n} \\ \epsilon_{10} & \epsilon_{11} & \cdots & \epsilon_{1n} \\ \vdots & \vdots & \ddots & \vdots \\ \epsilon_{n0} & \epsilon_{n1} & \cdots & \epsilon_{nn} \end{bmatrix}}_{\mathcal{C}} \underbrace{\begin{bmatrix} \phi_0 \\ \phi_1 \\ \vdots \\ \phi_n \end{bmatrix}}_{\Phi} \quad (5.15b)$$

Observe that \mathcal{C} is $(n+1) \times (n+1)$, whereas the previous per-unit-length parameter matrices \mathbf{L} , \mathbf{C} , and \mathbf{G} are $n \times n$. Also the generalized capacitance matrix, like the transmission-line capacitance matrix, is symmetric, that is, $\epsilon_{ij} = \epsilon_{ji}$, for similar reasons. It can be shown that for a charge-neutral system, as is the case for the MTL, the reference potential terms for the choice of reference point for these potentials, ϕ_i , vanish as the reference point recedes to infinity so that the choice of reference point does not affect the determination of the generalized capacitance matrix [B.4,C.1,C.4,C.7].

Suppose that \mathcal{C} has been computed and we select a reference conductor. Without loss of generality, let us select the reference conductor as the zeroth conductor. In order to obtain the $n \times n$ capacitance matrix \mathbf{C} from \mathcal{C} , define the MTL line voltages, with respect to this zeroth reference conductor, as

$$V_i = \phi_i - \phi_0 \quad (5.16)$$

for $i = 1, 2, \dots, n$. We assume that the entire system of $n+1$ conductors is charge neutral:

$$q_0 + q_1 + q_2 + \cdots + q_n = 0 \quad (5.17a)$$

Therefore, the charge (per unit of line length) on the zeroth conductor can be written in terms of the charges on the other n conductors as

$$q_0 = -\sum_{k=1}^n q_k \quad (5.17b)$$

Denote the entries in the i th row and j th column of the per-unit-length capacitance matrix \mathbf{C} , with the zeroth conductor chosen as reference conductor, as C_{ij} :

$$\begin{bmatrix} q_1 \\ q_2 \\ \vdots \\ q_n \end{bmatrix} = \begin{bmatrix} C_{11} & C_{12} & \cdots & C_{1n} \\ C_{12} & C_{22} & \cdots & C_{2n} \\ \vdots & \vdots & \ddots & \vdots \\ C_{1n} & C_{2n} & \cdots & C_{nn} \end{bmatrix} \begin{bmatrix} V_1 \\ V_2 \\ \vdots \\ V_n \end{bmatrix} \quad (5.18)$$

Comparing (5.18) to (5.3b), we observe that $C_{ii} = \sum_{k=1}^n c_{ik}$ and $C_{ij} = -c_{ij}$. Substituting (5.16) and (5.17) into (5.15) and expanding gives ($\phi_i = V_i + \phi_0$)

$$\begin{aligned} -\sum_{k=1}^n q_k &= \epsilon_{01} V_1 + \epsilon_{02} V_2 + \cdots + \epsilon_{0n} V_n + \left(\sum_{m=0}^n \epsilon_{0m} \right) \phi_0 \\ q_1 &= \epsilon_{11} V_1 + \epsilon_{12} V_2 + \cdots + \epsilon_{1n} V_n + \left(\sum_{m=0}^n \epsilon_{1m} \right) \phi_0 \\ &\vdots \\ q_n &= \epsilon_{n1} V_1 + \epsilon_{n2} V_2 + \cdots + \epsilon_{nn} V_n + \left(\sum_{m=0}^n \epsilon_{nm} \right) \phi_0 \end{aligned} \quad (5.19)$$

Adding all equations in (5.19) gives

$$\begin{aligned} 0 &= \left(\sum_{m=0}^n \epsilon_{m1} \right) V_1 + \left(\sum_{m=0}^n \epsilon_{m2} \right) V_2 + \cdots + \left(\sum_{m=0}^n \epsilon_{mn} \right) V_n \\ &\quad + \left(\sum_{m=0}^n \epsilon_{0m} + \sum_{m=0}^n \epsilon_{1m} + \cdots + \sum_{m=0}^n \epsilon_{nm} \right) \phi_0 \end{aligned} \quad (5.20a)$$

or

$$\phi_0 = -\frac{\sum_{k=1}^n [(\sum_{m=0}^n \epsilon_{mk}) V_k]}{\sum_{l=0}^n [\sum_{m=0}^n \epsilon_{lm}]} \quad (5.20b)$$

Substituting (5.20b) into the last n equations in (5.19) yields the entries in the per-unit-length capacitance matrix \mathbf{C} , given in (5.18) as [C.4]

$$C_{ij} = \epsilon_{ij} - \frac{(\sum_{k=0}^n \epsilon_{ik}) (\sum_{m=0}^n \epsilon_{mj})}{(\sum \mathcal{E})} \quad (5.21)$$

The first summation in the numerator of (5.21) is the sum of all the elements in the i th row of \mathcal{E} , whereas the second summation in the numerator of (5.21) is the sum of all the elements in the j th column of \mathcal{E} . The denominator summation $\sum \mathcal{E}$ is the sum of all the elements in \mathcal{E} .

In the case of two conductors, the result in (5.21) gives per-unit-length capacitance between the two conductors and reduces to

$$c = \frac{\epsilon_{11}\epsilon_{00} - \epsilon_{01}\epsilon_{10}}{\epsilon_{00} + \epsilon_{01} + \epsilon_{10} + \epsilon_{11}} \quad (5.22)$$

The generalized capacitance matrix, like the transmission-line capacitance, is symmetric so that $\epsilon_{01} = \epsilon_{10}$. Eliminating the potential reference node (or line) and observing that capacitors in series (parallel) combine like resistors in parallel (series), one can directly obtain the result in (5.22) from the equivalent circuit of Figure 5.4(a).

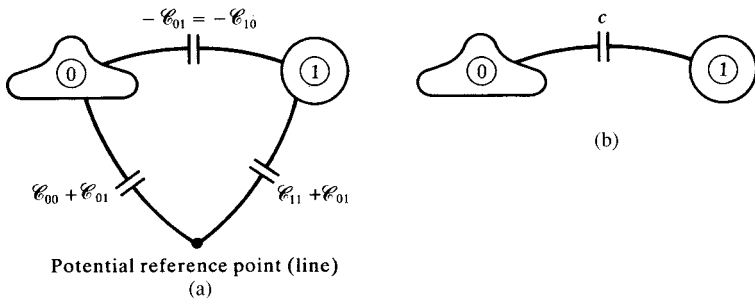


FIGURE 5.4 Illustration of (a) the meaning of the per-unit-length generalized capacitance matrix for a two-conductor line and (b) the elimination of the reference line to yield the capacitance between the conductors.

Therefore, we can obtain the per-unit-length generalized capacitance matrix \mathcal{C} , then choose a reference conductor, and then easily compute \mathbf{C} for that choice of reference conductor from \mathcal{C} using the relation in (5.21). If the surrounding medium is inhomogeneous in ϵ , we similarly compute the generalized capacitance matrix with the dielectric removed (replaced with free space), \mathcal{C}_0 , and from that compute the per-unit-length capacitance matrix with the dielectric removed, \mathbf{C}_0 , with the above method. Once \mathbf{C}_0 is computed in this fashion, we may then compute $\mathbf{L} = \mu_0 \epsilon_0 \mathbf{C}_0^{-1}$. Computing the complex generalized capacitance matrix using a complex permittivity for each homogeneous region as in (5.10), $\hat{\mathcal{C}} = \mathcal{C}_R + j\mathcal{C}_I$, we can obtain the complex transmission-line matrix as $\hat{\mathbf{C}} = \mathbf{C}_R + j\mathbf{C}_I$ and from that we can obtain the transmission-line capacitance matrix as $\mathbf{C} = \mathbf{C}_R$ and the conductance matrix as $\mathbf{G} = -\omega \mathbf{C}_I$ as shown in (5.12).

5.2 MULTICONDUCTOR LINES HAVING CONDUCTORS OF CIRCULAR, CYLINDRICAL CROSS SECTION (WIRES)

Conductors having cross sections that are circular–cylindrical are referred to as *wires*. These types of conductors are frequently found in cables that interconnect electronic circuitry and form an important class of MTLs.

5.2.1 Wide-Separation Approximations for Wires in Homogeneous Media

The results for two-conductor lines in a homogeneous medium obtained in the previous chapter are exact. For similar lines consisting of more than two conductors, exact, closed-form solutions cannot be obtained, in general. However, if the wires are relatively widely spaced, we can obtain some simple but approximate closed-form solutions using the fundamental subproblems derived in Section 4.2.1 of the previous chapter [B.4]. These results assume that the currents and charges are symmetric about the wire axes, which implicitly assumes that the wires are widely spaced. In other words we assume that proximity effect is not

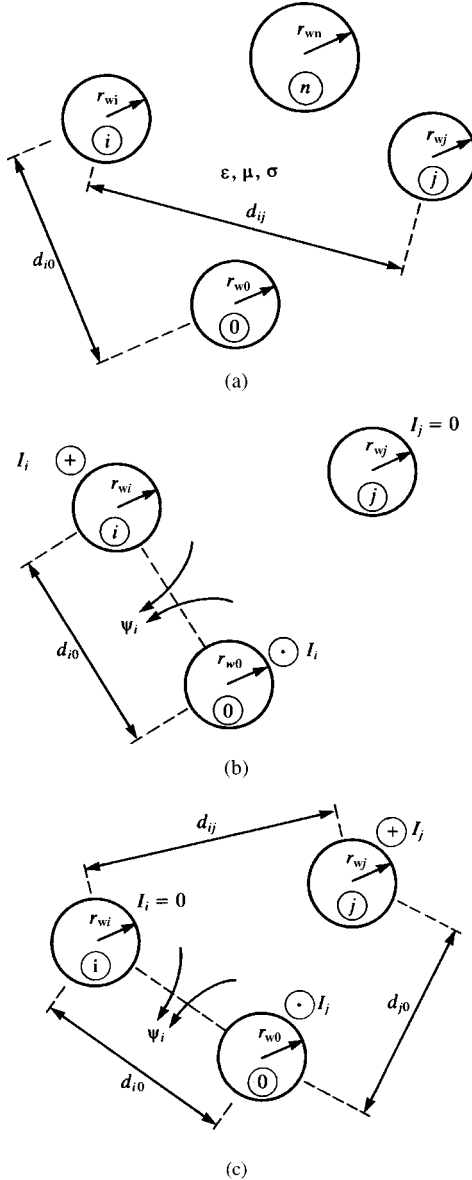


FIGURE 5.5 Illustration of the calculation of per-unit-length inductances using the wide-separation approximations for $n + 1$ wires: (a) the cross-sectional structure, (b) self-inductance, and (c) mutual inductance.

pronounced. As we saw in the case of two-wire lines, the requirement of *widely spaced wires* is not overly restrictive. The following wide-separation approximations for wires are implemented in the FORTRAN program WIDSESEP.FOR described in Appendix A.

5.2.1.1 $n+1$ Wires Consider the case of $n + 1$ wires in a homogeneous medium as shown in Figure 5.5(a). The entries in the per-unit-length inductance matrix are defined in (5.1) and (5.2). If the wires are widely separated, we can use the fundamental subproblems derived in Section 4.2.1 of the previous chapter to give these entries. The self-inductance is obtained from Figure 5.5(b) and the mutual inductance is obtained as in Figure 5.5(c) as

$$\begin{aligned}
 l_{ii} &= \left. \frac{\psi_i}{I_i} \right|_{I_1 = \dots = I_{i-1} = I_{i+1} = \dots = I_n = 0} \\
 &= \frac{\mu}{2\pi} \ln \left(\frac{d_{i0}}{r_{w0}} \right) + \frac{\mu}{2\pi} \ln \left(\frac{d_{i0}}{r_{wi}} \right) \\
 &= \frac{\mu}{2\pi} \ln \left(\frac{d_{i0}^2}{r_{w0} r_{wi}} \right) \tag{5.23a}
 \end{aligned}$$

$$\begin{aligned}
 l_{ij} &= \left. \frac{\psi_i}{I_j} \right|_{I_1 = \dots = I_{j-1} = I_{j+1} = \dots = I_n = 0} \\
 &= \frac{\mu}{2\pi} \ln \left(\frac{d_{j0}}{d_{ij}} \right) + \frac{\mu}{2\pi} \ln \left(\frac{d_{i0}}{r_{w0}} \right) \\
 &= \frac{\mu}{2\pi} \ln \left(\frac{d_{i0} d_{j0}}{d_{ij} r_{w0}} \right) \tag{5.23b}
 \end{aligned}$$

The entries in the per-unit-length capacitance and conductance matrices for this assumed *homogeneous* surrounding medium can be obtained from this result as before:

$$\mathbf{C} = \mu \varepsilon \mathbf{L}^{-1} \tag{5.24a}$$

$$\begin{aligned}
 \mathbf{G} &= \frac{\sigma}{\varepsilon} \mathbf{C} \\
 &= \sigma \mu \mathbf{L}^{-1} \tag{5.24b}
 \end{aligned}$$

5.2.1.2 n Wires Above an Infinite, Perfectly Conducting Plane Consider the case of n wires above and parallel to an infinite, perfectly conducting plane shown in Figure 5.6. Replacing the plane with the image currents and using the fundamental result derived in Section 4.2.1 of the previous chapter yields

$$\begin{aligned}
 l_{ii} &= \left. \frac{\psi_i}{I_i} \right|_{I_1 = \dots = I_{i-1} = I_{i+1} = \dots = I_n = 0} \\
 &= \frac{\mu}{2\pi} \ln \left(\frac{h_i}{r_{wi}} \right) + \frac{\mu}{2\pi} \ln \left(\frac{2h_i}{h_i} \right) \\
 &= \frac{\mu}{2\pi} \ln \left(\frac{2h_i}{r_{wi}} \right) \tag{5.25a}
 \end{aligned}$$

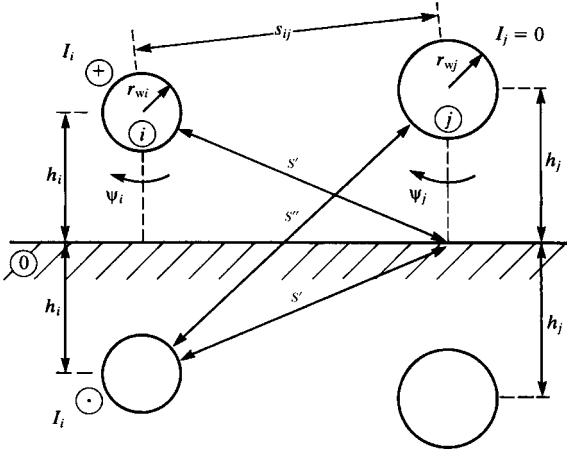


FIGURE 5.6 Illustration of the calculation of per-unit-length inductances using the wide-separation approximations for n wires above a ground plane.

$$\begin{aligned}
 l_{ij} &= l_{ji} = \frac{\psi_j}{I_i} \Big|_{I_1 = \dots = I_{i-1} = I_{i+1} = \dots = I_n = 0} \\
 &= \frac{\mu}{2\pi} \ln \left(\frac{s'}{s_{ij}} \right) + \frac{\mu}{2\pi} \ln \left(\frac{s''}{s'} \right) \\
 &= \frac{\mu}{2\pi} \ln \left(\frac{\sqrt{s_{ij}^2 + 4h_i h_j}}{s_{ij}} \right) \\
 &= \frac{\mu}{4\pi} \ln \left[1 + \frac{4h_i h_j}{s_{ij}^2} \right]
 \end{aligned}
 \tag{5.25b}$$

This is again a problem of a homogeneous medium, and therefore the entries in the per-unit-length capacitance and conductance matrices can then be found from these results using (5.24).

5.2.1.3 n Wires Within a Perfectly Conducting Cylindrical Shield Consider n wires of radii r_{wi} within a perfectly conducting circular-cylindrical shield shown in Figure 5.7(a). The interior radius of the shield is denoted by r_S and the distances of the wires from the shield axis are denoted by d_i , whereas the angular separations are denoted by θ_{ij} . The perfectly conducting shield may be replaced by image currents located at radial distances from the shield center of r_S^2/d_i as shown in Figure 5.7(b) [B.1, 1, 2]. The directions of the desired magnetic fluxes are as shown. Assuming that the wires are widely separated from each other and the shield, we may assume that the currents are uniformly distributed around the wire and shield peripheries. Thus, we may use the basic results of Section 4.2.1 of the previous

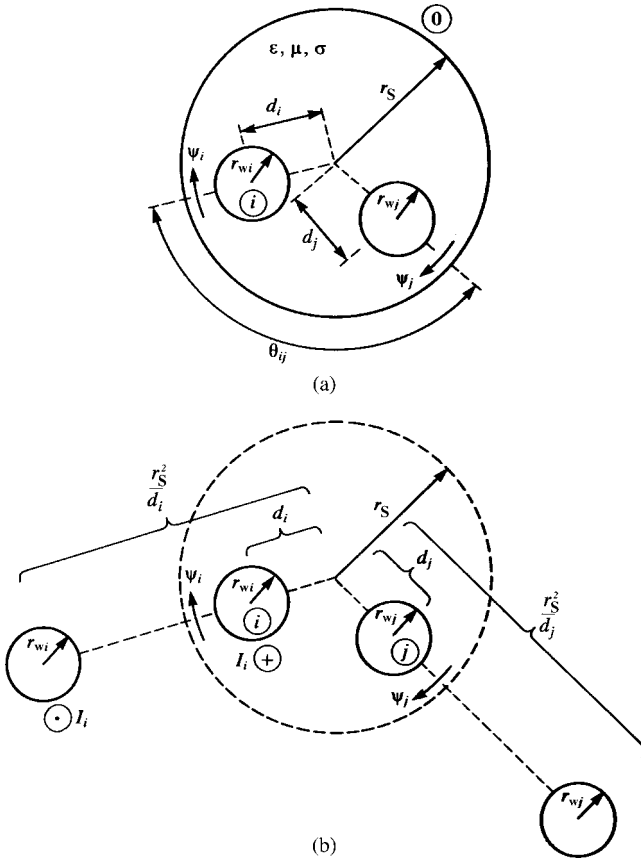


FIGURE 5.7 Illustration of the calculation of per-unit-length inductances using the wide-separation approximations for n wires within a cylindrical shield: (a) the cross-sectional structure and (b) replacement with images.

chapter to give [B.1]

$$\begin{aligned}
 l_{ii} &= \frac{\psi_i}{I_i} \Big|_{I_1 = \dots = I_{i-1} = I_{i+1} = \dots = I_n = 0} \\
 &= \frac{\mu}{2\pi} \ln \left(\frac{r_S - d_i}{r_{wi}} \right) + \frac{\mu}{2\pi} \ln \left(\frac{\frac{r_S^2}{d_i} - d_i}{\frac{r_S^2}{d_i} - r_S} \right) \\
 &= \frac{\mu}{2\pi} \ln \left(\frac{r_S^2 - d_i^2}{r_S r_{wi}} \right)
 \end{aligned} \tag{5.26a}$$

$$\begin{aligned}
 l_{ij} = l_{ji} &= \frac{\psi_j}{I_i} \Big|_{I_1 = \dots = I_{i-1} = I_{i+1} = \dots = I_n = 0} \\
 &= \frac{\mu}{2\pi} \ln \left(\frac{d_j}{r_s} \sqrt{\frac{(d_i d_j)^2 + r_s^4 - 2d_i d_j r_s^2 \cos \theta_{ij}}{(d_i d_j)^2 + d_j^4 - 2d_i d_j^3 \cos \theta_{ij}}} \right) \quad (5.26b)
 \end{aligned}$$

The entries in the per-unit-length capacitance and conductance matrices for this homogeneous medium can be obtained using the relations in (5.24).

5.2.2 Numerical Methods for the General Case

The results in the previous three subsections give simple formulas for the entries in the per-unit-length parameter matrices of **L**, **C**, and **G** for n wires and a reference conductor for three cases: (1) $n + 1$ wires, (2) n wires above an infinite, perfectly conducting “ground” plane, and (3) n wires within an overall circular–cylindrical shield. There are two important restrictions on their applicability. These are that (1) the wires must be *widely separated* and (2) the dielectric medium surrounding the wires must be *homogeneous*; that is, circular dielectric insulations are ignored. The wide-separation assumption provides the simplification that the charge distributions around the wire peripheries are approximately uniform. This assumption was made so that we may use the fundamental subproblems for wires derived in Section 4.2.1 of the previous chapter to obtain those results. The charge distributions around closely spaced wires will be nonuniform around their peripheries but will be approximately uniform for ratios of wire separation to wire radius of 4 and higher (see Fig. 4.9). However, a significant restriction on the utility of those results is that they assume a homogeneous surrounding dielectric medium. Practical wire-type cables have circular–cylindrical insulating dielectrics surrounding them, which creates an *inhomogeneous* medium (air and the dielectric insulation). In this section, we will obtain a numerical technique that can be used to obtain accurate results for multiwire lines having an inhomogeneous surrounding medium as well as closely spaced conductors. The following method is described in [C.1–C.7] and is implemented for the practical case of a *ribbon cable* in a FORTRAN computer program RIBBON.FOR described in Appendix A.

First, consider an $(n + 1)$ -wire line in a homogeneous medium. If the wires are closely spaced, proximity effect will cause the charge distributions to be nonuniform around the wire peripheries. In the case of wires that are closely spaced, the charge distributions will tend to concentrate on the adjacent surfaces (*proximity effect*) (see Fig. 4.9). In order to model this effect, we will assume a *form* of the charge distribution around the i th wire periphery in the form of a Fourier series as a function of the peripheral angle θ_i as

$$\rho_i(\theta_i) = a_{i0} + \sum_{k=1}^{A_i} a_{ik} \cos(k\theta_i) + \sum_{k=1}^{B_i} b_{ik} \sin(k\theta_i) \quad (\text{C/m}^2) \quad (5.27)$$

This Fourier series representation for the i th wire contains a total number of unknowns of $N_i = 1 + A_i + B_i$. For a line consisting of $n + 1$ wires, there will be a total

of $N = \sum_{i=0}^n N_i$ unknowns to be determined. The coefficients of each expansion, a_{i0} , a_{ik} , and b_{ik} , are to be determined such that the boundary conditions are satisfied. These boundary conditions are that the potential at points on each conductor *due to all charge distributions* equals the potential of that conductor. (Since we assume perfect conductors for the computation of \mathbf{L} , \mathbf{C} , and \mathbf{G} , the potentials of all points on a conductor are the same.) The charge distribution in (5.27) has dimensions of C/m^2 since it gives the distribution around the wire periphery per unit of line length. Once the expansion coefficients in (5.27) are determined to satisfy the boundary conditions, the total charge on the i th conductor *per unit of line length* is obtained by integrating (5.27) around the wire periphery to yield

$$\begin{aligned}
 q_i &= \int_{\theta_i=0}^{2\pi} \rho_i(\theta_i) r_{wi} d\theta_i \\
 &= 2\pi r_{wi} a_{i0} \quad (C/m)
 \end{aligned}
 \tag{5.28}$$

Hence, the charge per unit of line length is determined solely by the constant term in the expansion. However, the other terms affect this constant term. This simple result is due to the fact that $\int_{\theta_i=0}^{2\pi} \cos(k\theta_i) d\theta_i = \int_{\theta_i=0}^{2\pi} \sin(k\theta_i) d\theta_i = 0$.

We now determine the potential at an arbitrary point in the transverse plane at a position r_p, θ_p from each of these charge distributions, that is, $\phi_i(r_p, \theta_p)$, as illustrated in Figure 5.8. This can be obtained by assuming that the charge distribution around the periphery of the i th conductor is composed of filaments of per-unit-length charge $\rho_i r_{wi} d\theta_i$ C/m, each of whose amplitudes are weighted by the particular distribution, that is, $1, \cos(k\theta_i)$, and $\sin(k\theta_i)$. Then we use the previous fundamental subproblem result given in Eq. (4.16) for the voltage between two points. With reference to Figure (5.8), we obtain

$$\phi_i(r_p, \theta_p) - \phi_0(r_0, \theta_0) = -\frac{\rho_i r_{wi} d\theta_i}{2\pi\epsilon} \ln\left(\frac{s_p}{s_0}\right)
 \tag{5.29}$$

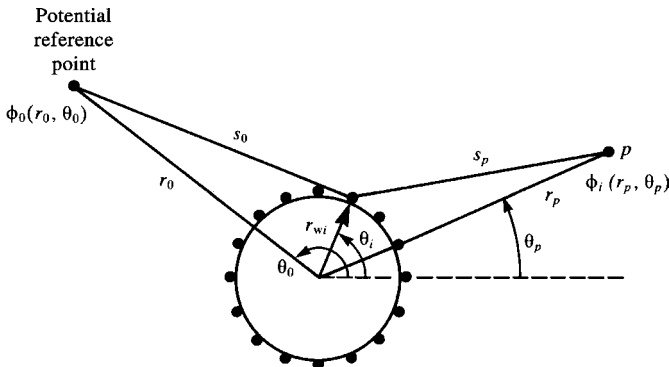


FIGURE 5.8 Determination of the potential of a charge-carrying wire having various circumferential distributions by replacement of the charge with weighted filaments of charge.

It was shown in [C.7] that the *potential* of the reference point, $\phi_0(r_0, \theta_0)$, can be omitted if the system of conductors is electrically neutral, that is, the net charge per unit of line length is zero. Since this is satisfied for our MTL systems, we will henceforth omit the reference potential term. Thus, the differential contribution to the potential due to a filamentary component of the charge distribution is

$$d\phi_i(r_p, \theta_p) = -\frac{\rho_i r_{wi} d\theta_i}{2\pi\epsilon} \ln(s_p) \quad (5.30)$$

The distance from the filament to the point is (according to the law of cosines) given by

$$s_p = \sqrt{r_p^2 + r_{wi}^2 - 2r_p r_{wi} \cos(\theta_i - \theta_p)} \quad (5.31)$$

Substituting this along with the form for the charge distribution given in (5.27) into (5.30) and integrating around the conductor periphery gives the total contribution to the potential due to the charge distributions:

$$\begin{aligned} \phi_i(r_p, \theta_p) &= a_{i0} \int_{\theta_i=0}^{2\pi} I(\theta_i) r_{wi} d\theta_i \\ &+ \sum_{k=1}^{A_i} a_{ik} \int_{\theta_i=0}^{2\pi} I(\theta_i) \cos(k\theta_i) r_{wi} d\theta_i \\ &+ \sum_{k=1}^{B_i} b_{ik} \int_{\theta_i=0}^{2\pi} I(\theta_i) \sin(k\theta_i) r_{wi} d\theta_i \end{aligned} \quad (5.32a)$$

where

$$\begin{aligned} I(\theta_i) &= -\frac{1}{2\pi\epsilon} \ln\left(\sqrt{r_p^2 + r_{wi}^2 - 2r_p r_{wi} \cos(\theta_i - \theta_p)}\right) \\ &= -\frac{1}{4\pi\epsilon} \ln\left(r_p^2 + r_{wi}^2 - 2r_p r_{wi} \cos(\theta_i - \theta_p)\right) \end{aligned} \quad (5.32b)$$

Each of the integrals in (5.32a) can be evaluated in closed form giving [B.4]

$$\begin{aligned} \phi_i(r_p, \theta_p) &= \alpha_{i0} \left(-\frac{r_{wi} \ln(r_p)}{\epsilon} \right) + \sum_{k=1}^{A_i} a_{ik} \left(\frac{r_{wi}^{k+1} \cos(k\theta_p)}{2k\epsilon r_p^k} \right) \\ &+ \sum_{k=1}^{B_i} b_{ik} \left(\frac{r_{wi}^{k+1} \sin(k\theta_p)}{2k\epsilon r_p^k} \right) \end{aligned} \quad (5.33)$$

Therefore, the contributions to the potential from each of these charge distributions are given in Table 5.1.

TABLE 5.1

| Charge distribution | Contribution to the potential $\phi(r_p, \theta_p)$ |
|---------------------|--|
| 1 | $-\frac{r_w \ln(r_p)}{\epsilon}$ |
| $\cos(m\theta)$ | $\frac{r_w^{m+1} \cos(m\theta_p)}{2 \epsilon m r_p^m}$ |
| $\sin(m\theta)$ | $\frac{r_w^{m+1} \sin(m\theta_p)}{2 \epsilon m r_p^m}$ |

Satisfaction of the boundary conditions is obtained if we choose a total of

$$\begin{aligned}
 N &= \sum_{i=0}^n N_i \\
 &= (n + 1) + \sum_{i=0}^n A_i + \sum_{i=0}^n B_i
 \end{aligned}
 \tag{5.34}$$

points on the wires at which we enforce the potential of the wire due to all the charge distributions on this conductor and all of the other conductors as illustrated in Figure 5.9. This leads to a set of N simultaneous equations that must be solved for the expansion coefficients, written in matrix form, as

$$\Phi = \mathbf{D} \mathbf{A}
 \tag{5.35a}$$

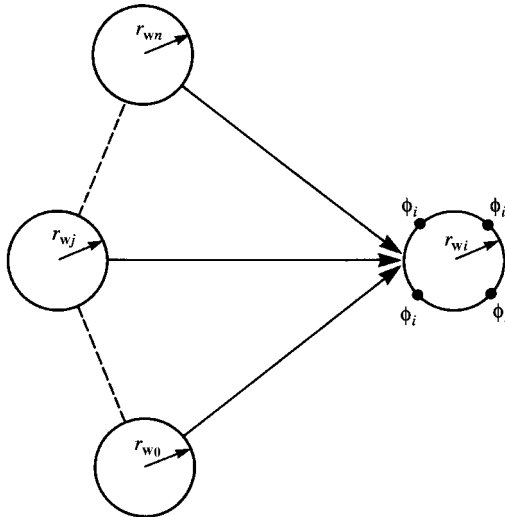


FIGURE 5.9 Determination of the total potential at a point due to all charge distributions.

or, in expanded form,

$$\begin{bmatrix} \Phi_0 \\ \vdots \\ \Phi_i \\ \vdots \\ \Phi_n \end{bmatrix} = \begin{bmatrix} \mathbf{D}_{00} & \cdots & \mathbf{D}_{0j} & \cdots & \mathbf{D}_{0n} \\ \vdots & \vdots & \vdots & \vdots & \vdots \\ \mathbf{D}_{i0} & \cdots & \mathbf{D}_{ij} & \cdots & \mathbf{D}_{in} \\ \vdots & \vdots & \vdots & \vdots & \vdots \\ \mathbf{D}_{n0} & \cdots & \mathbf{D}_{nj} & \cdots & \mathbf{D}_{nn} \end{bmatrix} \begin{bmatrix} \mathbf{A}_0 \\ \vdots \\ \mathbf{A}_j \\ \vdots \\ \mathbf{A}_n \end{bmatrix} \quad (5.35b)$$

The vector of potentials at the match points on the i th conductor is denoted as

$$\Phi_i = \begin{bmatrix} \phi_i \\ \vdots \\ \phi_i \\ \vdots \\ \phi_i \end{bmatrix} \quad (5.35c)$$

and the vector of expansion coefficients of the charge distribution on the i th conductor is denoted as

$$\mathbf{A}_i = \begin{bmatrix} a_{i0} \\ a_{i1} \\ \vdots \\ a_{iA_i} \\ b_{i1} \\ \vdots \\ b_{iB_i} \end{bmatrix} \quad (5.35d)$$

and \mathbf{A}_i denotes the expansion coefficients associated with the i th conductor according to (5.27). Each \mathbf{A}_i will have $N_i = 1 + A_i + B_i$ rows as will Φ_i . Each \mathbf{D}_{ij} will have dimension of $N_i \times N_j$. Inverting (5.35) gives the expansion coefficients in terms of a linear combination of the potentials of each conductor:

$$\mathbf{A} = \mathbf{D}^{-1} \Phi \quad (5.36a)$$

or, in expanded form,

$$\begin{bmatrix} \mathbf{A}_0 \\ \vdots \\ \mathbf{A}_i \\ \vdots \\ \mathbf{A}_n \end{bmatrix} = \begin{bmatrix} \mathbf{B}_{00} & \cdots & \mathbf{B}_{0j} & \cdots & \mathbf{B}_{0n} \\ \vdots & \vdots & \vdots & \vdots & \vdots \\ \mathbf{B}_{i0} & \cdots & \mathbf{B}_{ij} & \cdots & \mathbf{B}_{in} \\ \vdots & \vdots & \vdots & \vdots & \vdots \\ \mathbf{B}_{n0} & \cdots & \mathbf{B}_{nj} & \cdots & \mathbf{B}_{nn} \end{bmatrix} \begin{bmatrix} \Phi_0 \\ \vdots \\ \Phi_j \\ \vdots \\ \Phi_n \end{bmatrix} \quad (5.36b)$$

The generalized capacitance matrix \mathcal{C} described in Section 5.1.1 can be obtained from (5.36), using (5.28), as [C.1–C.7]

$$\mathcal{C}_{ij} = 2\pi r_{wi} \sum_{\text{first row}} \mathbf{B}_{ij} \tag{5.37}$$

This simple result is due to the fact that according to (5.28) we need only to determine a_{i0} , and each submatrix in (5.36) relates

$$\begin{bmatrix} a_{i0} \\ a_{i1} \\ \vdots \\ a_{iA_i} \\ b_{i1} \\ \vdots \\ b_{iB_i} \end{bmatrix} = \begin{bmatrix} \phantom{a_{i0}} \\ \phantom{a_{i1}} \\ \\ \mathbf{B}_{ij} \\ \phantom{a_{i0}} \\ \phantom{a_{i1}} \\ \end{bmatrix} \begin{bmatrix} \phi_j \\ \vdots \\ \vdots \\ \phi_j \\ \vdots \\ \vdots \\ \phi_j \end{bmatrix} \tag{5.38}$$

or, in expanded form,

$$\begin{aligned} a_{i0} &= [\mathbf{B}_{ij}]_{11} \phi_j + \cdots + [\mathbf{B}_{ij}]_{1k} \phi_j + \cdots + [\mathbf{B}_{ij}]_{1N_j} \phi_j \\ &= \left\{ [\mathbf{B}_{ij}]_{11} + \cdots + [\mathbf{B}_{ij}]_{1k} + \cdots + [\mathbf{B}_{ij}]_{1N_j} \right\} \phi_j \end{aligned} \tag{5.39}$$

where $[\mathbf{B}_{ij}]_{mn}$ denotes the entry in row m and column n of \mathbf{B}_{ij} . Hence, \mathcal{C}_{ij} involves the sum of the entries in the first row of \mathbf{B}_{ij} .

5.2.2.1 Applications to Inhomogeneous Dielectric Media This method can be extended to handle inhomogeneous media such as circular–cylindrical dielectric insulations around the wires. Observe that for each wire and dielectric insulation of that wire there are two surfaces that contain charge and each distribution must be expanded into a Fourier series with respect to the angle around that boundary θ_i . These two surfaces are the conductor–dielectric surface and the dielectric–free-space surface.

As previously discussed in Chapter 4, dielectric media consist of microscopic dipoles of *bound charge* as illustrated in Figure 5.10(a). Application of an external

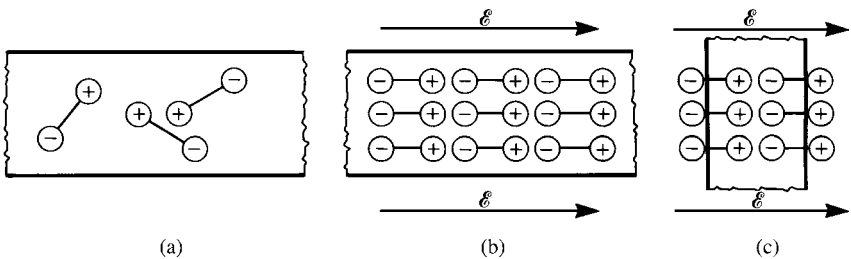


FIGURE 5.10 Illustration of the effects of bound (polarization) charge: (a) microscopic dipoles, (b) alignment of the dipoles with an applied electric field, and (c) creation of a bound surface charge.

electric field causes these microscopic dipoles of bound charge to align with the field as illustrated in Figure 5.10(b). If a slab of dielectric is immersed in an electric field, a bound charge density will appear on the surfaces of the dielectric as illustrated in Figure 5.10(c).

Charge consists of two types: *free charge* is the charge that is free to move and *bound charge* is the charge appearing on the surfaces of dielectrics in response to an applied electric field as shown in Figure 5.10(c). At the interface between two dielectric surfaces, the boundary condition is that the components of the *electric flux density vector* $\vec{\mathcal{D}}$ that are normal to the interface must be continuous, that is, $\mathcal{D}_{1n} = \epsilon_1 \mathcal{E}_{1n} = \epsilon_2 \mathcal{E}_{2n} = \mathcal{D}_{2n}$. A simple way of handling inhomogeneous dielectric media is to replace the dielectrics with free space having bound charge at the interface [C.1–C.7,1,2]. At places where the dielectric is adjacent to a perfect conductor, we have both free charge and bound charge, and the free charge density on the surface of the conductor is equal to the component of the electric flux density vector that is normal to the conductor surface, \mathcal{D}_n (C/m²) [A.1]. Of course, the component of the electric field intensity vector that is tangent to a boundary is continuous across the boundary for an interface between two dielectrics, $\mathcal{E}_{t1} = \mathcal{E}_{t2}$, and is zero at the surface of a perfect conductor.

In order to adapt the above numerical method to wires that have circular, cylindrical dielectric insulations, we describe the charge (bound plus free) around the wire periphery as a Fourier series in the peripheral angle, θ_i , as in (5.27):

$$\rho_{if}(\theta_i) - \rho_{ib}(\theta_i) = a_{i0} + \sum_{k=1}^{A_i} a_{ik} \cos(\theta_i) + \sum_{k=1}^{B_i} b_{ik} \sin(\theta_i) \quad (\text{C/m}^2) \quad (5.40)$$

In (5.40), ρ_{if} denotes the *free charge distribution* on the *i*th conductor periphery and ρ_{ib} denotes the *bound charge distribution* on the dielectric periphery facing the conductor as shown in Figure 5.11. At the dielectric periphery facing the free-space region, there is only bound charge that we similarly expand in a Fourier series in peripheral angle θ_i as

$$\rho'_{ib}(\theta_i) = a'_{i0} + \sum_{k=1}^{A'_i} a'_{ik} \cos(\theta_i) + \sum_{k=1}^{B'_i} b'_{ik} \sin(\theta_i) \quad (\text{C/m}^2) \quad (5.41)$$

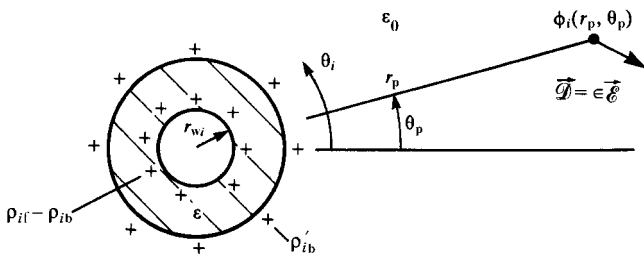


FIGURE 5.11 The general problem of the determination of the potential of a dielectric-insulated wire due to free and bound charge distributions at the two interfaces.

In (5.40), we have anticipated that the bound charge distribution at the conductor periphery will be opposite in sign to the bound charge distribution around the dielectric–free-space boundary. Also, we denote the bound charge distribution at the dielectric–free-space boundary in (5.41) with a prime, whereas the bound charge distribution at the conductor–dielectric boundary in (5.40) is denoted without a prime. This is because, although the *total* bound charge per unit length at each boundary must be the same, the distributions around the peripheries are different since the boundary radii are different. For each dielectric-insulated wire, there are a total of N_i unknown expansion coefficients, $N_i = 1 + A_i + B_i$, for the free plus bound charge on the conductor peripheries and a total of N'_i unknown expansion coefficients, $N'_i = 1 + A'_i + B'_i$, for the bound charge on the outer dielectric periphery. For a total of $n + 1$ wires, this gives a total number of unknowns of $N + N'$, where

$$\begin{aligned}
 N &= \sum_{i=0}^n N_i \\
 &= (n + 1) + \sum_{i=0}^n A_i + \sum_{i=0}^n B_i
 \end{aligned} \tag{5.42a}$$

$$\begin{aligned}
 N' &= \sum_{i=0}^n N'_i \\
 &= (n + 1) + \sum_{i=0}^n A'_i + \sum_{i=0}^n B'_i
 \end{aligned} \tag{5.42b}$$

unknowns. Observe that the total bound charge at the dielectric–conductor boundary per unit of line length must equal the total bound charge per unit of line length at the dielectric–free-space boundary but their distributions will not be the same. To determine the total charge on each surface per unit of line length, we integrate the charge distribution in (5.40) and (5.41) to yield

$$\begin{aligned}
 q_{if} - q_{ib} &= \int_0^{2\pi} (\rho_{if} - \rho_{ib}) r_{wi} d\theta_i \\
 &= 2\pi r_{wi} a_{i0} \text{ (C/m)}
 \end{aligned} \tag{5.43a}$$

and

$$\begin{aligned}
 q_{ib} &= \int_0^{2\pi} (\rho'_{ib}) (r_{wi} + t_i) d\theta_i \\
 &= 2\pi (r_{wi} + t_i) a'_{i0} \text{ (C/m)}
 \end{aligned} \tag{5.43b}$$

where t_i is the thickness of the dielectric for the i th wire.

In order to enforce the boundary conditions, we choose points on each conductor periphery at which to enforce the conductor potential ϕ_i and points on each dielectric–free-space periphery at which to enforce the continuity of the normal components of the electric flux density vector due to all these charge distributions. This

gives a set of $N + N'$ simultaneous equations of a form similar to (5.35):

$$\begin{bmatrix} \Phi \\ \mathbf{0} \end{bmatrix} = \begin{bmatrix} \mathbf{D}_{11} & \mathbf{D}_{12} \\ \mathbf{D}_{21} & \mathbf{D}_{22} \end{bmatrix} \begin{bmatrix} \mathbf{A} \\ \mathbf{A}' \end{bmatrix} \tag{5.44}$$

The first $N = \sum_{i=0}^n N_i$ rows enforce the conductor potentials, and the second $N' = \sum_{i=0}^n N'_i$ rows enforce the continuity of the normal components of the electric flux density vector across the dielectric–free-space interfaces. The vector \mathbf{A} contains the $N = \sum_{i=0}^n N_i$ expansion coefficients of the free plus bound charge at the conductor peripheries, and the vector \mathbf{A}' contains the $N' = \sum_{i=0}^n N'_i$ expansion coefficients of the bound charge at the dielectric–free-space peripheries. The match points around the two peripheries are not chosen to be evenly spaced but are chosen with a scheme that avoids giving a singular matrix in (5.44) [C.3].

The entries in (5.44) can be obtained by considering a cylindrical boundary of radius r_b of infinite length shown in Figure 5.12, which supports the charge distributions 1 , $\cos(m\theta_b)$, and $\sin(m\theta_b)$ around its periphery. This is identical to the problem of free charge around a conductor periphery considered in the previous section, but here the charge distribution can represent free or bound charge distributions. Proceeding as in the previous section by modeling the charge distributions as weighted filaments of charge gives the potential both inside and outside the boundary. Similarly, the electric field due to these charge distributions can be obtained from the gradient of these potential solutions [A.1]:

$$\begin{aligned} \vec{E}(r_p, \theta_p) &= -\nabla\phi \\ &= -\frac{\partial\phi}{\partial r}\vec{a}_r - \frac{1}{r_p}\frac{\partial\phi}{\partial\theta}\vec{a}_\theta \end{aligned} \tag{5.45}$$

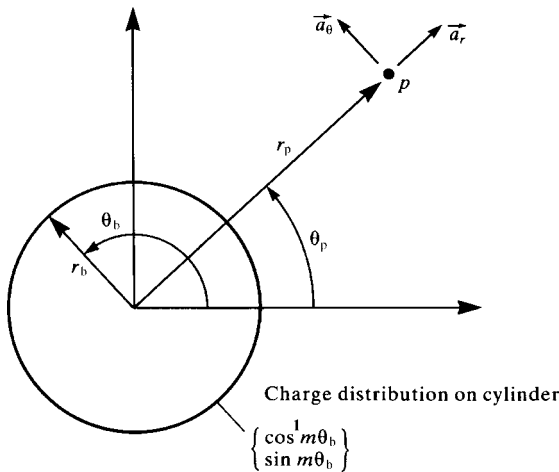


FIGURE 5.12 The general problem of determining the potential inside and outside a charge distribution.

which becomes

$$\begin{bmatrix} \mathbf{A}_0 \\ \vdots \\ \mathbf{A}_i \\ \vdots \\ \mathbf{A}_n \\ \cdots \\ \mathbf{A}'_0 \\ \vdots \\ \mathbf{A}'_i \\ \vdots \\ \mathbf{A}'_n \end{bmatrix} = \begin{bmatrix} \mathbf{B}_{00} & \cdots & \mathbf{B}_{0j} & \cdots & \mathbf{B}_{0n} \\ \vdots & \vdots & \vdots & \vdots & \vdots \\ \mathbf{B}_{i0} & \cdots & \mathbf{B}_{ij} & \cdots & \mathbf{B}_{in} \\ \vdots & \vdots & \vdots & \vdots & \vdots \\ \mathbf{B}_{n0} & \cdots & \mathbf{B}_{nj} & \cdots & \mathbf{B}_{nn} \\ \cdots & \cdots & \cdots & \cdots & \cdots \\ \mathbf{B}'_{00} & \cdots & \mathbf{B}'_{0j} & \cdots & \mathbf{B}'_{0n} \\ \vdots & \vdots & \vdots & \vdots & \vdots \\ \mathbf{B}'_{i0} & \cdots & \mathbf{B}'_{ij} & \cdots & \mathbf{B}'_{in} \\ \vdots & \vdots & \vdots & \vdots & \vdots \\ \mathbf{B}'_{n0} & \cdots & \mathbf{B}'_{nj} & \cdots & \mathbf{B}'_{nn} \end{bmatrix} \begin{bmatrix} \Phi_0 \\ \vdots \\ \Phi_j \\ \vdots \\ \Phi_n \end{bmatrix} \tag{5.46b}$$

Recall that the charge at the conductor–dielectric interface consists of *free charge plus bound charge*, $\rho_{if} - \rho_{ib}$. The entries in the generalized capacitance matrix relate the *free charge* on the conductors to the conductor potentials. Therefore, according to (5.43a) and (5.43b), we must add the total (bound) charge at the dielectric–free-space surface to the total (bound plus free) charge at the conductor–dielectric surface in order to obtain the free charge on the conductor to give the total per-unit-length free charge for each wire as

$$\begin{aligned} q_{if} &= (q_{if} - q_{ib}) + q_{ib} \\ &= 2\pi r_{wi} a_{i0} + 2\pi (r_{wi} + t_i) a'_{i0} \end{aligned} \tag{5.47}$$

Thus, in a fashion similar to the bare conductor case above, the entries in the generalized capacitance matrix can be obtained from (5.47) as

$$\begin{aligned} \epsilon_{ij} &= \left. \frac{q_{if}}{\phi_j} \right|_{\phi_0 = \cdots = \phi_{j-1} = \phi_{j+1} = \cdots = \phi_n = 0} \\ &= 2\pi r_{wi} \sum_{\text{first row}} \mathbf{B}_{ij} + 2\pi (r_{wi} + t_i) \sum_{\text{first row}} \mathbf{B}'_{ij} \end{aligned} \tag{5.48}$$

where $\sum_{\text{first row}} \mathbf{B}_{ij}$ denotes the sum of the elements in the first row of the submatrix \mathbf{B}_{ij} of (5.46b) relating the coefficients of the bound plus free charge at the i th conductor interface to the potential of the j th conductor, ϕ_j , and $\sum_{\text{first row}} \mathbf{B}'_{ij}$ denotes the sum of the elements in the first row of the submatrix \mathbf{B}'_{ij} of (5.46b) relating the coefficients of the bound charge at the dielectric–free-space interface for the i th conductor to the potential of the j th conductor, ϕ_j .

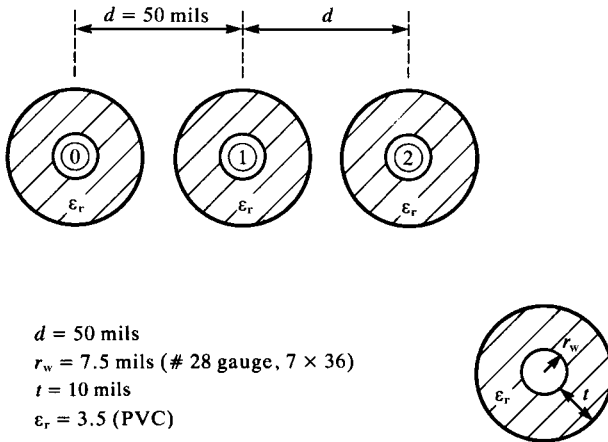


FIGURE 5.13 Dimensions of a three-wire ribbon cable for illustration of numerical results.

5.2.3 Computed Results: Ribbon Cables

As an illustration of the numerical results, consider the three-wire ribbon cable shown in Figure 5.13. The outside wire is chosen for the reference conductor. The center-to-center separations of the wires are 50 mils (1 mil = 0.001 inch). The wires are identical and are composed of # 28 gauge (7 × 36) stranded wires with radii of $r_w = 7.5$ mils and polyvinyl chloride (PVC) insulations of thickness $t = 10$ mils and relative dielectric constant $\epsilon_r = 3.5$. The results are computed using the RIBBON.FOR computer program described in Appendix A, which implements the method described in this section for ribbon cables. The generalized capacitance matrix was computed using 10 Fourier coefficients around each wire surface (the constant term and nine cosine terms) and 10 Fourier coefficients around each dielectric-free-space surface and the results are shown in Table 5.4.

The per-unit-length transmission-line capacitance matrices \mathbf{C} and \mathbf{C}_0 become as shown in Table 5.5. The last column of Table 5.5 shows the effective dielectric constant (relative permittivity) as $\epsilon'_r = [\mathbf{C}]_{ij} / [\mathbf{C}_0]_{ij}$. The per-unit-length inductances shown in

TABLE 5.4 The generalized capacitances for the three-wire ribbon cable with and without the dielectric insulations.

| Entry | With dielectric (pF/m) \mathcal{C} | Without dielectric (pF/m) \mathcal{C}_0 |
|--------------------|--------------------------------------|---|
| \mathcal{C}_{00} | 26.2148 | 17.6900 |
| \mathcal{C}_{01} | -18.0249 | -10.5205 |
| \mathcal{C}_{02} | -5.03325 | -4.22544 |
| \mathcal{C}_{11} | 37.8189 | 22.9694 |
| \mathcal{C}_{12} | -18.0249 | -10.5205 |
| \mathcal{C}_{22} | 26.2148 | 17.6901 |

TABLE 5.5 The transmission-line capacitances for the three-wire ribbon cable with and without the insulation dielectrics.

| Entry | With dielectric (pF/m) C | Without dielectric (pF/m) C ₀ | Effective dielectric constant, ε' _r |
|-----------------|--------------------------|--|--|
| C ₁₁ | 37.432 | 22.494 | 1.664 |
| C ₁₂ | -18.716 | -11.247 | 1.664 |
| C ₂₂ | 24.982 | 16.581 | 1.507 |

TABLE 5.6 The transmission-line inductances for the three-wire ribbon cable computed exactly and using the wide-separation approximations.

| Entry | Exact (μH/m) | Wide-separation approximation (μH/m) | Percent error (%) |
|-----------------|--------------|--------------------------------------|-------------------|
| L ₁₁ | 0.74850 | 0.75885 | 1.38 |
| L ₁₂ | 0.50770 | 0.51805 | 2.04 |
| L ₂₂ | 1.0154 | 1.0361 | 2.04 |

Table 5.6 were computed exactly as $\mathbf{L} = \mu_0 \epsilon_0 \mathbf{C}_0^{-1}$, and using the wide-separation approximations.

The wide-separation approximations are computed from (5.23) using the FORTRAN program WIDSESEP.FOR described in Appendix A as

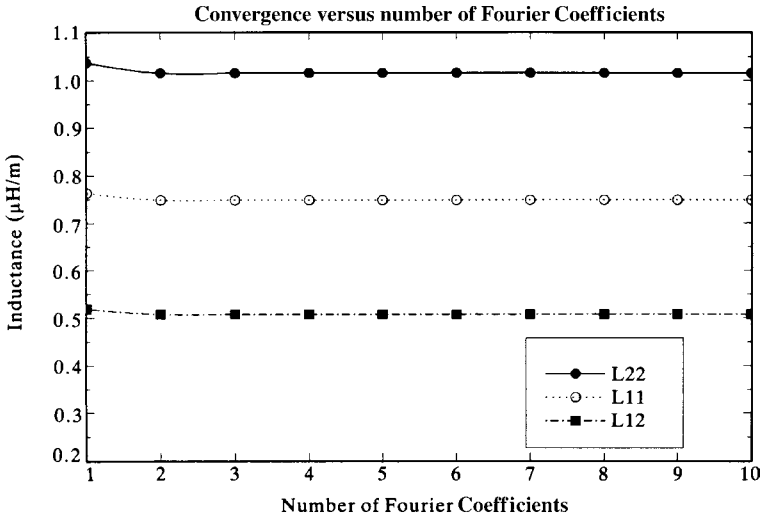
$$l_{11} = \frac{\mu_0}{\pi} \ln \left(\frac{d}{r_w} \right)$$

$$l_{12} = \frac{\mu_0}{2\pi} \ln \left(\frac{2d}{r_w} \right)$$

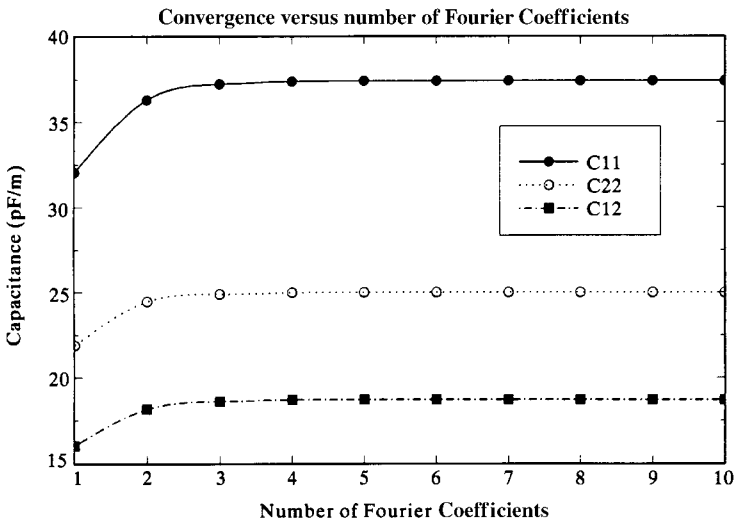
$$l_{22} = \frac{\mu_0}{\pi} \ln \left(\frac{2d}{r_w} \right)$$

Once again, the wide-separation approximations give results for the entries in the per-unit-length inductance matrix that are within some 2 % of the values computed from $\mathbf{L} = \mu_0 \epsilon_0 \mathbf{C}_0^{-1}$. The ratio of adjacent wire separation to wire radius is 6.67, so we would expect this.

Figure 5.14 illustrates the convergence of the method for the three-wire ribbon cable. The per-unit-length inductances and per-unit-length capacitances are plotted versus the number of Fourier coefficients around the wire and dielectric boundaries in Figure 5.14(a) and (b), respectively. Observe that the inductances converge to accurate values after about two Fourier coefficients per boundary, whereas the capacitances require on the order of three or four Fourier coefficients per boundary for convergence.



(a)



(b)

FIGURE 5.14 Convergence of the per-unit-length parameters of the three-wire ribbon cable versus number of expansion coefficients: (a) inductances and (b) capacitances.

5.3 MULTICONDUCTOR LINES HAVING CONDUCTORS OF RECTANGULAR CROSS SECTION

The basic solution problem in determining the entries in the per-unit-length parameter matrices \mathbf{L} , \mathbf{C} , and \mathbf{G} remains the same as before. The per-unit-length parameters of inductance, capacitance, and conductance are all obtained as the static (dc) solution of the fields in the transverse x - y plane for perfect conductors. Essentially, this

means that we need to solve Laplace's or Poisson's equation in the two-dimensional transverse plane [A.1]:

$$\nabla^2\phi(x, y) = \frac{\partial^2\phi}{\partial x^2} + \frac{\partial^2\phi}{\partial y^2} = \rho(x, y) \quad (5.49)$$

There are various methods for solving this equation. The method we will use determines an approximate solution using various numerical techniques that we will discuss in this section.

5.3.1 Method of Moments (MoM) Techniques

MoM techniques essentially solve integral equations where the unknown is in the integrand. An example is the integral form of Poisson's equation in the transverse x - y plane:

$$\phi(x, y) = \frac{1}{4\pi\epsilon} \iint_s \frac{\rho(x', y')}{r} ds \quad (5.50)$$

where a charge distribution in the x - y plane, ρ , is distributed over some surface s . Ordinarily, we know or prescribe the potential at points in the region (e.g., on perfectly conducting bodies) and wish to determine the charge distribution that produces it. Thus, we need to solve an integral equation for the integrand [A.1, 2–5].

The problems of interest here are the perfect conductors in the two-dimensional plane that are infinite in length (in the z direction) and the i th conductor that has some unknown surface charge density, $\rho_i(x, y)$ (C/m^2), residing on its surface as illustrated in Figure 5.15. Observe that the units of this charge distribution are per square meter: One dimension is along the z axis and the other dimension is

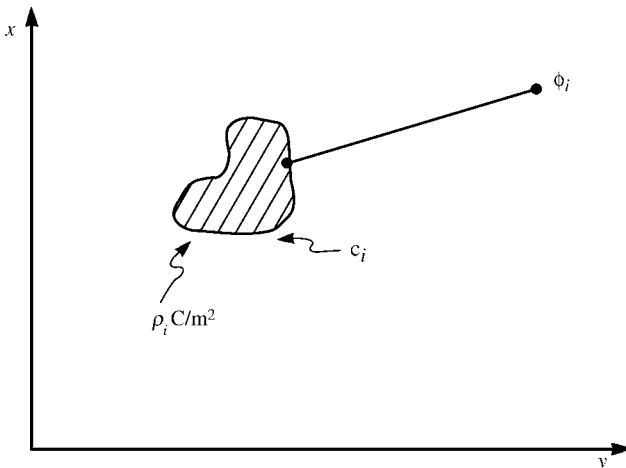


FIGURE 5.15 Illustration of the solution of Poisson's equation in two dimensions.

around the conductor surface in the transverse x - y plane. One common way of doing this, which we used for the ribbon cable, is to approximate the charge distribution around the two-dimensional conductor periphery as infinitely long filaments of charge in the z direction (C/m) and use the basic problem of the potential of an infinitesimal line charge that was developed in Section 4.2.1. This forms the basis for numerical techniques that are used to analyze these two-dimensional structures of infinite length for determining the per-unit-length parameters [2–5]. Thus, we initially solve the problem of the potential of an infinitely long filament of charge carrying a per-unit-length charge in the z direction, which is uniformly distributed in the z direction. The potential at a point is the sum of the potentials of each line charge that makes up the desired charge distribution around the conductor periphery.

A more general way is to represent the charge distribution over the i th conductor surface as a linear combination of *basis functions*, ρ_{ik} , as

$$\begin{aligned} \rho_i(x, y) &= \alpha_{i1}\rho_{i1}(x, y) + \alpha_{i2}\rho_{i2}(x, y) + \cdots + \alpha_{iN_i}\rho_{iN_i}(x, y) \\ &= \sum_{k=1}^{N_i} \alpha_{ik}\rho_{ik}(x, y) \end{aligned} \quad (5.51)$$

Entire domain expansions use basis functions that are nonzero over the entire contour of the surface in the same manner as a Fourier series represents a time-domain function using basis functions defined over the time interval encompassing one complete period. This was the technique used earlier to expand the charge distributions around the wire and dielectric insulation peripheries of ribbon cables. *Subdomain expansions* seek to represent the charge distribution over discrete segments of the surface contour [C.1,C.2]. Each of the expansion basis functions, ρ_{ik} , are defined over the discrete segments of the contour, c_{ik} , and are zero over the other segments. We will concentrate on the subdomain expansion method. There are many ways of choosing the expansion functions over the segments. One of the simplest ways is to represent the charge distribution as a “staircase function,” where the charge distribution is constant over the segments of the contour:

$$\rho_{ik} = \begin{cases} 1, & \in c_{ik} \\ 0, & \notin c_{ik} \end{cases} \quad (5.52)$$

This is illustrated in Figure 5.16 and is referred to as the *pulse expansion method*. The charge distribution is assumed to be constant over the segments c_{ik} of the surface, but the levels α_{ik} are unknown as yet. Hence, we are making a “staircase” approximation to the true distribution. This is the essence of the MoM method that we will use for PCBs. More elaborate approximations such as triangular distributions may be made with corresponding increase in difficulty of analysis.

In order to illustrate the method as applied to PCB structures, consider a PCB shown in Figure 5.17(a) where three infinitesimally thin lands (flat, perfect conductors) reside on the surface of a dielectric substrate having a relative permittivity of ϵ_r . Each land is at potential ϕ_i and carries a per-unit-length charge distribution q_i (C/m). This charge

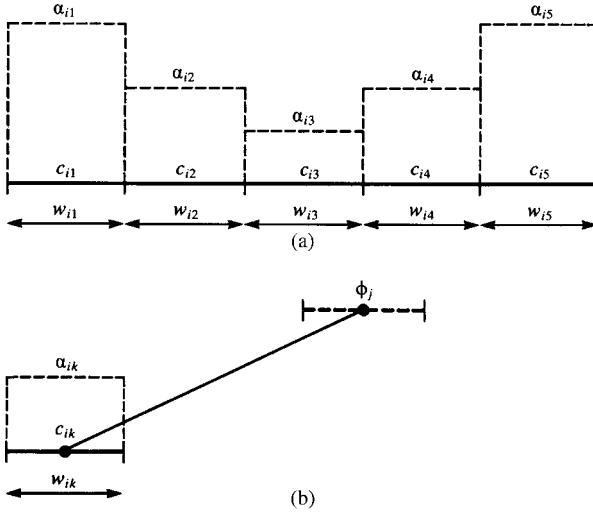


FIGURE 5.16 Illustration of the pulse expansion of a charge distribution on a flat strip.

distribution q_i is the total charge on the land per unit of line length in the z direction. Figure 5.17(b) shows an important distinction between the case of PCB lands and the case of round wires; the charge distributions across the land widths on PCB lands, ρ_i (C/m^2), tend to peak at the edges of the lands [6]. In order to determine the per-

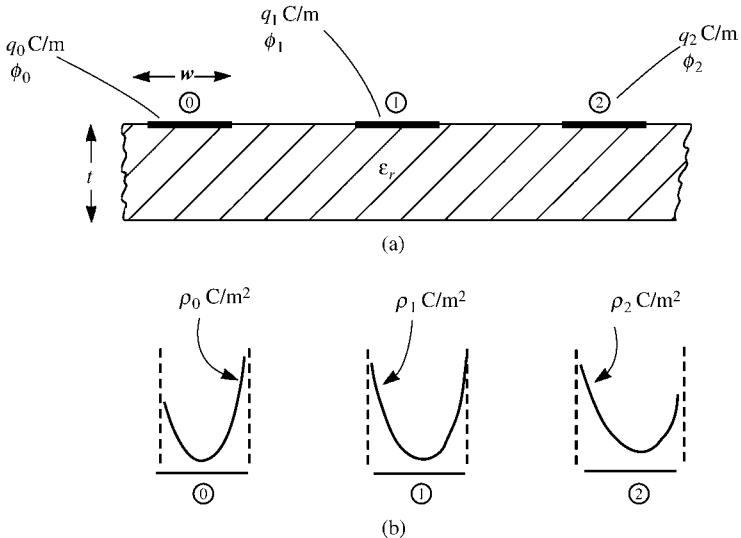


FIGURE 5.17 Illustration of the charge distributions over the lands of a PCB.

unit-length capacitance matrix for this structure we must relate these per-unit-length charge distributions q_i to the conductor potentials ϕ_i , with the generalized capacitance matrix \mathcal{C} as

$$\underbrace{\begin{bmatrix} q_0 \\ q_1 \\ q_2 \end{bmatrix}}_{\mathbf{Q}} = \underbrace{\begin{bmatrix} \epsilon_{00} & \epsilon_{01} & \epsilon_{02} \\ \epsilon_{10} & \epsilon_{11} & \epsilon_{12} \\ \epsilon_{20} & \epsilon_{21} & \epsilon_{22} \end{bmatrix}}_{\mathcal{C}} \underbrace{\begin{bmatrix} \phi_0 \\ \phi_1 \\ \phi_2 \end{bmatrix}}_{\Phi} \tag{5.53}$$

We represent this charge distribution over each land as in (5.51) with the staircase approximation or pulse expansion method given in (5.52) as illustrated in Figure 5.18(a). The α_{ik} unknown levels of the charge distributions are to be determined to satisfy the boundary condition that the potential over the i th conductor is ϕ_i as illustrated in Figure 5.18(b). The total charge (per unit length in the z direction) in

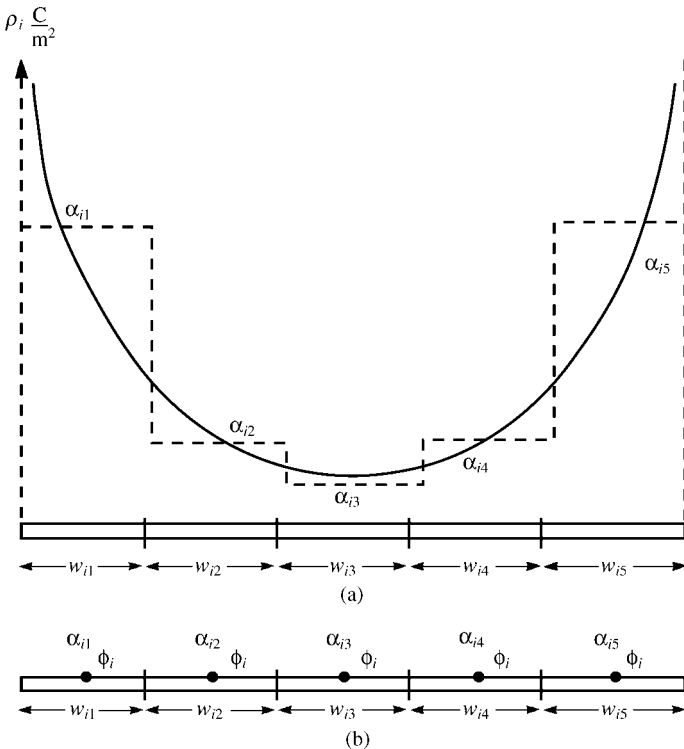


FIGURE 5.18 Illustration of (a) approximating the charge distribution over a land with piecewise-constant expansion functions and (b) matching the potential at the center of each strip.

C/m is obtained by summing the charges of the subsections of that conductor:

$$q_i = \sum_{k=1}^{N_i} \alpha_{ik} \int_{c_i} \rho_{ik} dc_i \quad (\text{C/m}) \quad (5.54)$$

In the case of the pulse expansion method, this simplifies to

$$\begin{aligned} q_i &= \alpha_{i1} w_{i1} + \alpha_{i2} w_{i2} + \cdots + \alpha_{iN_i} w_{iN_i} \\ &= \sum_{k=1}^{N_i} \alpha_{ik} w_{ik} \quad (\text{C/m}) \end{aligned} \quad (5.55)$$

where w_{ik} is the width of the k th segment of the i th conductor. The potential at a point on the i th conductor due to this representation will be due to the contributions from all the unknown charge distributions and can therefore be written as a linear combination of them as

$$\phi_i(x, y) = \sum_{k=1}^{N_i} K_{ik} \alpha_{ik} \quad (5.56)$$

Each coefficient K_{ik} is determined as the contribution to the potential due to each basis function alone:

$$K_{ik} = \phi_i |_{\alpha_{ik}=1, \alpha_{i1}, \dots, \alpha_{ik-1}, \alpha_{ik+1}, \dots, \alpha_{iN_i}=0} \quad (5.57)$$

There are many ways of generating the required equations. One rather simple technique is the method of *point matching*. For illustration consider a system of $n + 1$ conductors each having a prescribed potential of ϕ_i for $i = 0, 1, \dots, n$. We next enforce the potential of each conductor, ϕ_i , due to all charge distributions in the system to be the potential of that conductor at the center of each subsection of the conductor. Typical resulting equations are of the form

$$\phi_i = \sum_{k=1}^{N_0} K_{0k} \alpha_{0k} + \cdots + \sum_{k=1}^{N_i} K_{ik} \alpha_{ik} + \cdots + \sum_{k=1}^{N_n} K_{nk} \alpha_{nk} \quad (5.58)$$

Choosing a total of

$$N = \sum_{k=0}^n N_k \quad (5.59)$$

points on the conductors gives the following set of N simultaneous equations in terms of the expansion coefficients:

$$\Phi = \mathbf{D} \mathbf{A} \quad (5.60a)$$

or, in expanded form,

$$\begin{bmatrix} \Phi_0 \\ \vdots \\ \Phi_i \\ \vdots \\ \Phi_n \end{bmatrix} = \begin{bmatrix} \mathbf{D}_{00} & \cdots & \mathbf{D}_{0j} & \cdots & \mathbf{D}_{0n} \\ \vdots & \vdots & \vdots & \vdots & \vdots \\ \mathbf{D}_{i0} & \cdots & \mathbf{D}_{ij} & \cdots & \mathbf{D}_{in} \\ \vdots & \vdots & \vdots & \vdots & \vdots \\ \mathbf{D}_{n0} & \cdots & \mathbf{D}_{nj} & \cdots & \mathbf{D}_{nn} \end{bmatrix} \begin{bmatrix} \mathbf{A}_0 \\ \vdots \\ \mathbf{A}_j \\ \vdots \\ \mathbf{A}_n \end{bmatrix} \quad (5.60b)$$

The vector of potentials at the match points on the i th conductor is denoted as

$$\Phi_i = \begin{bmatrix} \phi_i \\ \vdots \\ \phi_i \\ \vdots \\ \phi_i \end{bmatrix} \quad (5.60c)$$

and the vector of expansion coefficients of the charge distribution on the i th conductor is denoted as

$$\mathbf{A}_i = \begin{bmatrix} \alpha_{i1} \\ \vdots \\ \alpha_{ik} \\ \vdots \\ \alpha_{iN_i} \end{bmatrix} \quad (5.60d)$$

Inverting (5.60) gives

$$\mathbf{A} = \mathbf{D}^{-1} \Phi \quad (5.61a)$$

or, in expanded form,

$$\begin{bmatrix} \mathbf{A}_0 \\ \vdots \\ \mathbf{A}_i \\ \vdots \\ \mathbf{A}_n \end{bmatrix} = \begin{bmatrix} \mathbf{B}_{00} & \cdots & \mathbf{B}_{0j} & \cdots & \mathbf{B}_{0n} \\ \vdots & \vdots & \vdots & \vdots & \vdots \\ \mathbf{B}_{i0} & \cdots & \mathbf{B}_{ij} & \cdots & \mathbf{B}_{in} \\ \vdots & \vdots & \vdots & \vdots & \vdots \\ \mathbf{B}_{n0} & \cdots & \mathbf{B}_{nj} & \cdots & \mathbf{B}_{nn} \end{bmatrix} \begin{bmatrix} \Phi_0 \\ \vdots \\ \Phi_j \\ \vdots \\ \Phi_n \end{bmatrix} \quad (5.61b)$$

Once the expansion coefficients are obtained from (5.61), the total charge (per unit of length in the z direction in C/m) can be obtained from (5.55). The generalized capacitance matrix \mathcal{C} can then be obtained. In the case of point matching and pulse expansion functions as with flat conductors, the entries in the generalized capacitance

matrix can be directly obtained from (5.61) as

$$\mathcal{C}_{ij} = w_{i1} \sum_{\text{row } 1} B_{ij} + w_{i2} \sum_{\text{row } 2} B_{ij} + \cdots + w_{iN_i} \sum_{\text{row } N_i} B_{ij} \quad (5.62)$$

where w_{ik} is the width of the k th subsection of the i th conductor. This simple result is obtained from (5.55):

$$\begin{aligned} q_i &= \alpha_{i1}w_{i1} + \alpha_{i2}w_{i2} + \cdots + \alpha_{iN_i}w_{iN_i} \\ &= \sum_{k=1}^{N_i} \alpha_{ik}w_{ik} \quad (\text{C/m}) \end{aligned} \quad (5.55)$$

and is due to the fact that a submatrix of (5.61b) relates

$$\begin{bmatrix} \alpha_{i1} \\ \vdots \\ \alpha_{ik} \\ \vdots \\ \alpha_{iN_i} \end{bmatrix} = \begin{bmatrix} & & & & \\ & & & & \\ & & \mathbf{B}_{ij} & & \\ & & & & \\ & & & & \end{bmatrix} \begin{bmatrix} \phi_j \\ \vdots \\ \phi_j \\ \vdots \\ \phi_j \end{bmatrix} \quad (5.63a)$$

Expanding this gives the expansion coefficients as

$$\alpha_{ik} = \left\{ \sum_{\text{row } k} \mathbf{B}_{ij} \right\} \phi_j \quad (5.63b)$$

If the widths of all conductor segments are chosen to be the same and designated as w , then the elements of the generalized capacitance matrix are simplified as

$$\mathcal{C}_{ij} = w \sum \mathbf{B}_{ij} \quad (5.64)$$

where $\sum \mathbf{B}_{ij}$ is the sum of all the elements in the submatrix \mathbf{B}_{ij} .

Thus, the basic subproblem is determining K_{ik} in (5.57), that is, determining the potential at the center of a segment due to a constant charge distribution of unit value, $\alpha_{ik} = 1(\text{C/m}^2)$, over some other segment where that segment can be associated with another conductor. In order to illustrate this, consider the infinitesimally thin conducting strip of width w and infinite length supporting a charge distribution $\rho(\text{C/m}^2)$ that is constant along the strip cross section as shown in Figure 5.19. If we treat this as an array of wire filaments each of which bears a charge per unit of filament length of $\rho dx \text{ C/m}$, then we may determine the potential at a point as the sum of the potentials of these filaments again using the basic result for the potential of a filament given in

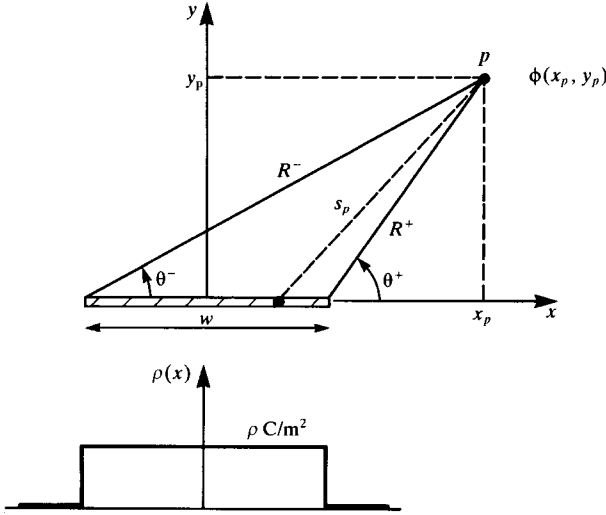


FIGURE 5.19 Calculation of the potential due to a constant charge distribution on a flat strip.

(4.16) or (5.30) [2, 5]:

$$\begin{aligned}
 \phi(w, x_p, y_p) &= -\frac{\rho}{2\pi\epsilon} \int_{x=-\frac{w}{2}}^{\frac{w}{2}} \ln \left(\sqrt{(x_p - x)^2 + (y_p)^2} \right) dx \\
 &= -\frac{\rho}{4\pi\epsilon} \left[\left(x_p + \frac{w}{2} \right) \ln \left(\left(x_p + \frac{w}{2} \right)^2 + y_p^2 \right) \right. \\
 &\quad - \left(x_p - \frac{w}{2} \right) \ln \left(\left(x_p - \frac{w}{2} \right)^2 + y_p^2 \right) \\
 &\quad \left. - 2w + 2y_p \left(\tan^{-1} \left(\frac{x_p + \frac{w}{2}}{y_p} \right) - \tan^{-1} \left(\frac{x_p - \frac{w}{2}}{y_p} \right) \right) \right] \tag{5.65}
 \end{aligned}$$

This integral is evaluated using [7]. This may be simplified somewhat if we denote the distances from the edges of the strip as R^+ and R^- and the angles as θ^+ and θ^- , as shown in Figure 5.19. In terms of these (5.65) becomes

$$\phi(w, x_p, y_p) = \frac{\rho}{2\pi\epsilon} \left[x_p \ln \left(\frac{R^+}{R^-} \right) - \frac{w}{2} \ln (R^+ R^-) + w - y_p (\theta^+ - \theta^-) \right] \tag{5.66}$$

In the case where the field or observation point lies at the midpoint of the strip in question, this becomes

$$\phi(w) = \frac{\rho}{2\pi\epsilon} w \left[1 - \ln \left(\frac{w}{2} \right) \right] \tag{5.67}$$

The electric field due to this charge distribution will be needed for problems that involve dielectric interfaces. The electric field can be computed from this result as [A.1]

$$\vec{E} = -\frac{\partial\phi}{\partial x}\vec{a}_x - \frac{\partial\phi}{\partial y}\vec{a}_y \tag{5.68}$$

As an illustration of this method, consider the rectangular conducting box shown in Figure 5.20. The four walls are insulated from one another and are maintained at potentials of $\phi_1 = 0$, $\phi_2 = 10$ V, $\phi_3 = 20$ V, and $\phi_4 = 30$ V. Suppose we divide the two vertical conductors into four segments each and the horizontal members into three segments each. Using pulse expansion functions for each segment and point matching gives 14 equations in 14 unknowns (the levels of the assumed constant charge distributions over each segment). Using the above results gives the potentials at the six interior points as shown in Table 5.7.

The *exact* results were obtained via a direct solution of Laplace’s equation using separation of variables. In terms of the general parameters denoted in Figure 5.20,

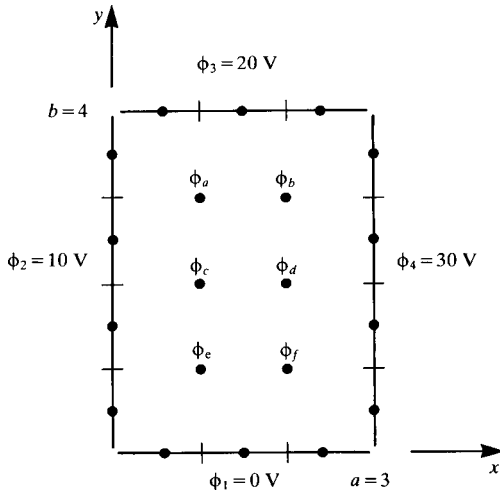


FIGURE 5.20 A two-dimensional problem for demonstration of the solution of Laplace’s equation via the pulse expansion–point matching method.

TABLE 5.7

| | MoM | Exact |
|------------------------|--------|---------|
| $\phi_a(x = 1, y = 3)$ | 16.433 | 16.4784 |
| $\phi_b(x = 2, y = 3)$ | 21.834 | 21.8499 |
| $\phi_c(x = 1, y = 2)$ | 14.130 | 14.1575 |
| $\phi_d(x = 2, y = 2)$ | 20.514 | 20.4924 |
| $\phi_e(x = 1, y = 1)$ | 9.527 | 9.60942 |
| $\phi_f(x = 2, y = 1)$ | 14.934 | 14.9810 |

the solution is [8]

$$\phi(x, y) = \sum_{\substack{n=1 \\ n \text{ odd}}}^{\infty} \left\{ \frac{4}{n\pi} \frac{\sin(n\pi y/b)}{\sinh(n\pi a/b)} \left[\phi_4 \sinh\left(\frac{n\pi x}{b}\right) + \phi_2 \sinh\left(\frac{n\pi}{b}(a-x)\right) \right] \right. \\ \left. + \frac{4}{n\pi} \frac{\sin(n\pi x/a)}{\sinh(n\pi a/b)} \left[\phi_3 \sinh\left(\frac{n\pi y}{a}\right) + \phi_1 \sinh\left(\frac{n\pi}{a}(b-y)\right) \right] \right\}$$

where $a = 3$, $b = 4$, and $\phi_1 = 0$, $\phi_2 = 10 \text{ V}$, $\phi_3 = 20 \text{ V}$, and $\phi_4 = 30 \text{ V}$. The solution using finite-difference and finite-element methods will be given in subsequent subsections.

The pulse expansion–point matching technique described above is particularly simple to implement in a digital computer program. Achieving convergence generally requires a rather large computational expense since the conductor subsections must be chosen sufficiently small to give an accurate representation of the charge distributions. This is particularly true in the case of lands on PCBs where the charge distribution peaks at the edges of each land. There are other choices of expansion functions such as triangles or piecewise sinusoidal functions, but the programming complexity also increases. For this reason, we will use the pulse expansion–point matching method for PCBs.

5.3.1.1 Applications to Printed Circuit Boards The above MoM method can be adapted to the computation of the per-unit-length capacitances of conductors with rectangular cross sections as occur on PCBs. Consider a typical PCB shown in Figure 5.21(a) having infinitesimally thin conducting lands on the surface of a dielectric board of thickness t and relative dielectric constant of ϵ_r . The widths of the lands are denoted as w_i and the edge-to-edge separations are denoted as s_{ij} . A direct approach would be to subsection each land into N_i segments of length w_{ik} . The charge on each subsection could be represented using the pulse expansion method as being constant over that segment with unknown level of α_{ik} . We could similarly subsection the surface of the dielectric and represent the bound charge on that surface with pulse expansions. A more direct way would be to imbed the dielectric in the basic *Green's*

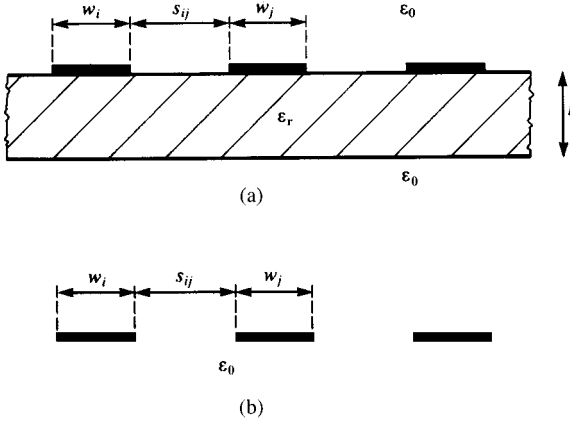


FIGURE 5.21 A PCB for illustration of the determination of the per-unit-length capacitances.

function. We will choose to do this. Thus, the problem becomes one of subsectioning the conductors immersed in free space as illustrated in Figure 5.21(b).

First, we consider solving the problem with the board removed as in Figure 5.21(b) and then we will consider adding the board. Consider the subproblem of a strip of width w representing one of the subsections of a land shown in Figure 5.22. We need to determine the potential at a point a distance d from the strip center and in the plane of the strip. This basic subproblem was solved earlier, and the results of (5.65) and (5.67) specialized to this case are as follows. For a point at the center of the strip, that is, $d = 0$, the self-potential is given by (5.67):

$$\begin{aligned}
 \phi_{\text{self}}(w) &= \frac{1}{2\pi\epsilon_0} \left[w - w \ln \left(\frac{w}{2} \right) \right] \\
 &= \frac{w}{2\pi\epsilon_0} \left[1 - \ln \left(\frac{w}{2} \right) \right]
 \end{aligned}
 \tag{5.69a}$$

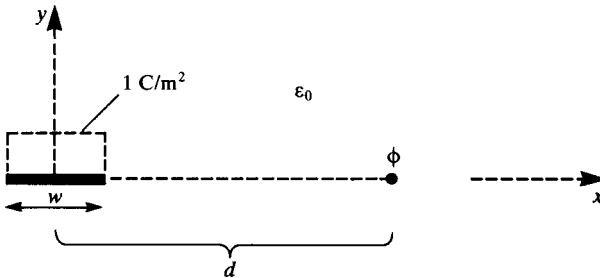


FIGURE 5.22 Illustration of the determination of the potential due to a constant charge distribution on a flat strip via point matching.

For the potential on another segment where $d \neq 0$ and generally $d > w/2$, the potential is

$$\begin{aligned} \phi(w, d) &= \frac{1}{2\pi\epsilon_0} \left[w + \left(d - \frac{w}{2}\right) \ln\left(d - \frac{w}{2}\right) - \left(d + \frac{w}{2}\right) \ln\left(d + \frac{w}{2}\right) \right] \\ &= \phi_{\text{self}}(w) + \frac{w}{2\pi\epsilon_0} \left[\frac{1}{2} (2D - 1) \ln(2D - 1) - \frac{1}{2} (2D + 1) \ln(2D + 1) \right] \end{aligned} \tag{5.69b}$$

The mutual result in (5.69b) is written in terms of the self term in (5.69a) and the ratio of the subsection separation to subsection width:

$$D = \frac{d}{w} \tag{5.69c}$$

Next consider incorporating the dielectric board into these basic results. The first problem that needs to be solved is that of an infinite (in the z direction) line charge of q C/m situated at a height h above the plane interface between two dielectric media as shown in Figure 5.23. The upper half space has free-space permittivity ϵ_0 , and the lower half space has permittivity $\epsilon = \epsilon_r \epsilon_0$. This classic problem allows one to compute the potential in each region by images in the same fashion as though the lower region were a perfect conductor [1, 9]. The solution can be obtained by visualizing lines of electric flux density, ψ , emanating from the line charge. For an infinite line charge carrying a per-unit-length charge density of q C/m, the electric flux density at a distance r from the line charge is [A.1]

$$\begin{aligned} \psi &= D \\ &= \frac{q}{2\pi r} \end{aligned} \tag{5.70}$$

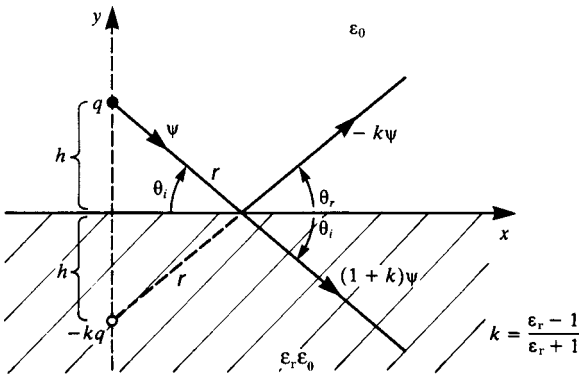


FIGURE 5.23 Illustration of the method of images for a point charge above an infinite dielectric half space.

In a region of permittivity ϵ , the electric field intensity E is related to D as $D = \epsilon E$. Consider one such flux line emanating from the line charge that is incident on the interface at some angle θ_i . Some of this flux can be visualized as passing through the interface as $(1 + k)\psi$, whereas some is reflected at an angle θ_r as $-k\psi$. The boundary conditions at the interface require that the normal components of the electric flux density be continuous or

$$\psi \sin \theta_i + k\psi \sin \theta_r = (1 + k)\psi \sin \theta_i \tag{5.71a}$$

This shows that the angles of incidence and reflection are the same (Snell's law), $\theta_i = \theta_r$ [A.1]. Similarly, the tangential components of the electric field must be continuous across the interface giving

$$\frac{1}{\epsilon_0} \psi \cos \theta_i - \frac{1}{\epsilon_0} k\psi \cos \theta_r = \frac{1}{\epsilon_r \epsilon_0} (1 + k)\psi \cos \theta_i \tag{5.71b}$$

Recalling that $\theta_i = \theta_r$ gives

$$k = \frac{\epsilon_r - 1}{\epsilon_r + 1} \tag{5.72a}$$

and

$$(1 + k) = \frac{2\epsilon_r}{\epsilon_r + 1} \tag{5.72b}$$

We will find the following combinations of k arising later:

$$\begin{aligned} (1 - k) &= \frac{2}{\epsilon_r + 1} \\ &= \frac{1}{\epsilon_{r,\text{eff}}} \end{aligned} \tag{5.73a}$$

and

$$\begin{aligned} (1 - k^2) &= \frac{2}{\epsilon_r + 1} (1 + k) \\ &= \frac{1}{\epsilon_{r,\text{eff}}} (1 + k) \end{aligned} \tag{5.73b}$$

and

$$\epsilon_{r,\text{eff}} = \frac{\epsilon_r + 1}{2} \tag{5.73c}$$

We have written (5.73) in terms of an effective relative permittivity, $(\epsilon_r + 1)/2$. This would be the effective permittivity for the half space in Figure 5.23 as the average of the two permittivities.

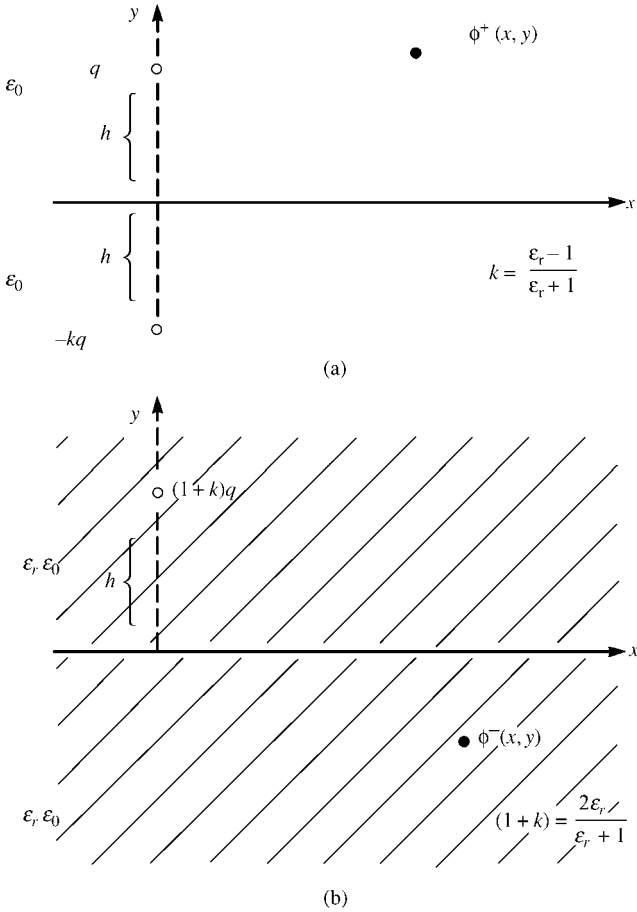


FIGURE 5.24 Solution for the potential in each half space in Figure 5.23.

The potential in each half space can be determined as two complementary problems illustrated in Figure 5.24. The potential in a region of permittivity ϵ at a distance d from an infinite line charge bearing a charge distribution of q C/m is [A.1]

$$\begin{aligned} \phi(d) &= -\frac{q}{2\pi\epsilon} \ln(d) \\ &= -\frac{q}{4\pi\epsilon} \ln(d^2) \end{aligned} \tag{5.74}$$

This omits the reference potential. The potential in the upper half space ($y > 0$) is as though it were due to the original charge q at the original height h and an image charge $-kq$ with the dielectric removed and at a distance h below the interface as

shown in Figure 5.24(a):

$$\phi^+(x, y) = -\frac{q}{4\pi\epsilon_0} \ln [x^2 + (y - h)^2] + \frac{kq}{4\pi\epsilon_0} \ln [x^2 + (y + h)^2] \quad (5.75a)$$

The potential below the interface ($y < 0$) is computed as though it is due to a line charge $(1 + k)q$ located at a height h above the interface with the upper free-space region replaced by the dielectric as shown in Figure 5.24(b):

$$\phi^-(x, y) = -\frac{(1 + k)q}{4\pi\epsilon_r\epsilon_0} \ln [x^2 + (y - h)^2] \quad (5.75b)$$

The problem of imaging across a dielectric boundary can be visualized as reflection of the electric flux density vector at the interface similar to optics as shown in Figure 5.25. For a source in the region of permittivity ϵ_0 crossing a boundary into a region of permittivity $\epsilon_r\epsilon_0$ as shown in Figure 5.25(a), the reflected and transmitted electric flux densities are as shown. On the contrary, for a source in the region of permittivity $\epsilon_r\epsilon_0$ crossing a boundary into a region of permittivity ϵ_0 as shown in Figure 5.25(b), the reflected and transmitted electric flux densities are as shown. The reflected ray is the incident ray, instead of being multiplied by $-k$ is multiplied by k . The transmitted ray is

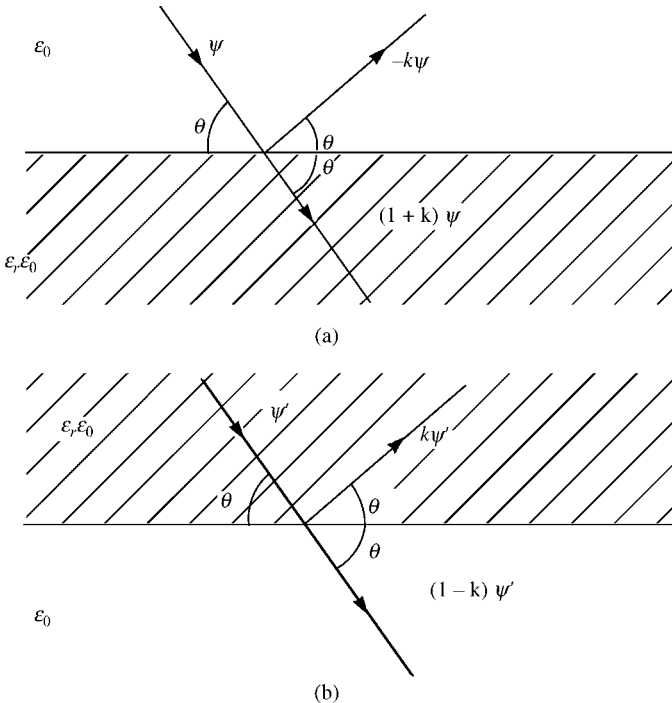


FIGURE 5.25 Solution of the half-space dielectric problem in Figure 5.23 in terms of fluxes.

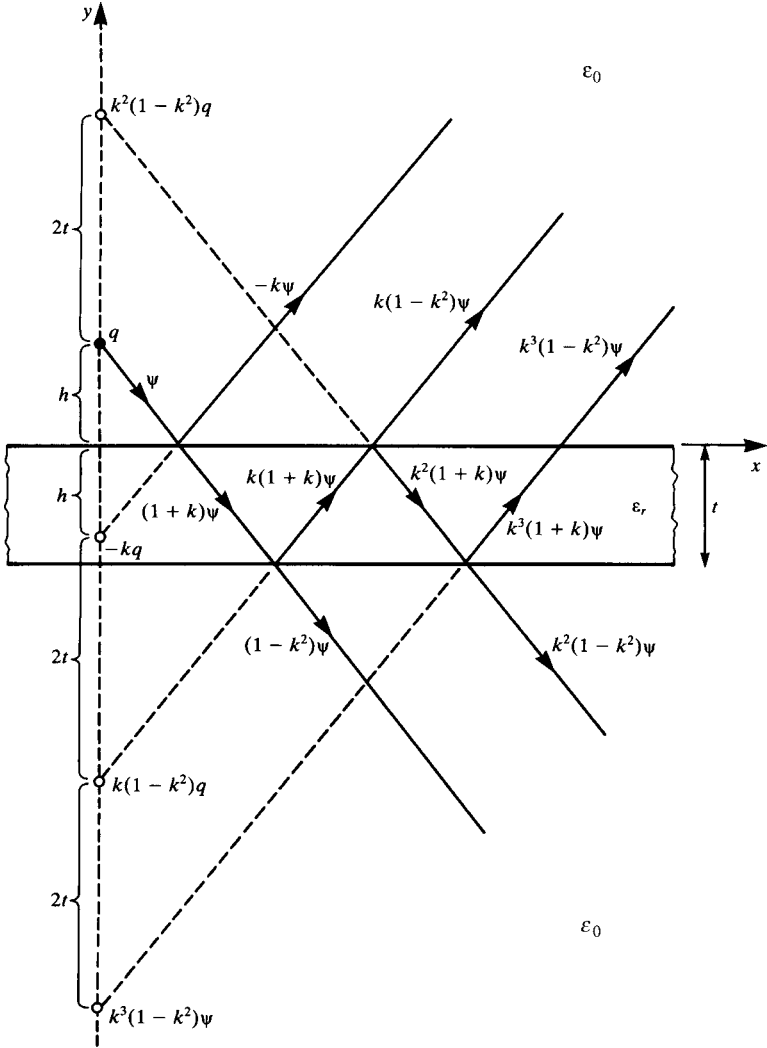


FIGURE 5.26 Images of a point charge above a dielectric slab of finite thickness.

the incident ray, instead of being multiplied by $(1 + k)$ is multiplied by $(1 - k)$. Hence, for the case of two dielectric boundaries representing a PCB dielectric substrate such as shown in Figure 5.26, we can easily successively image across both boundaries using this idea. This then gives an infinite set of images.

The problem now of interest for the PCB is a line charge on the surface of a dielectric slab (the PCB board) of relative permittivity ϵ_r and thickness t shown in Figure 5.27(a). We wish to find the potential at a point on the board at a distance d from the line charge. Specializing the results of Figure 5.26 for $h = 0$ gives the images

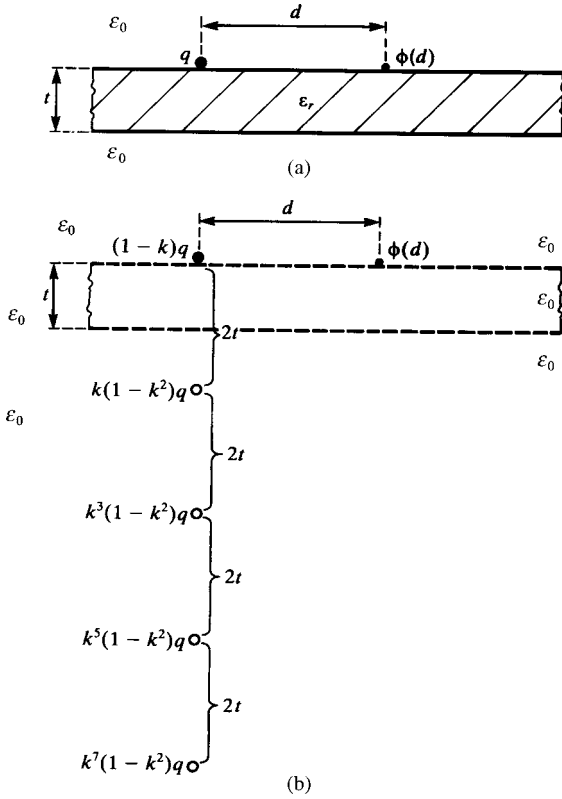


FIGURE 5.27 Illustration of the replacement of a dielectric slab of finite thickness with images to be used in modeling a PCB.

shown in Figure 5.27(b) where, for the purposes of computing the potential above the board, the board is replaced with free space. Utilizing 5.74, the potential then is of the form of a series:

$$\begin{aligned}
 \phi(d) &= -\frac{q}{4\pi\epsilon_0} (1 - k) \ln [d^2] - \frac{q}{4\pi\epsilon_0} (1 - k^2) \sum_{n=1}^{\infty} k^{(2n-1)} \ln [d^2 + (2nt)^2] \\
 &= -\frac{q}{4\pi\epsilon_0\epsilon_{r,\text{eff}}} \ln [d^2] - \frac{q}{4\pi\epsilon_0\epsilon_{r,\text{eff}}} (1 + k) \sum_{n=1}^{\infty} k^{(2n-1)} \ln [d^2 + (2nt)^2]
 \end{aligned}
 \tag{5.76}$$

and we have replaced items with those given in 5.73. This series converges rapidly as

$$k = \frac{(\epsilon_r - 1)}{(\epsilon_r + 1)} < 1$$

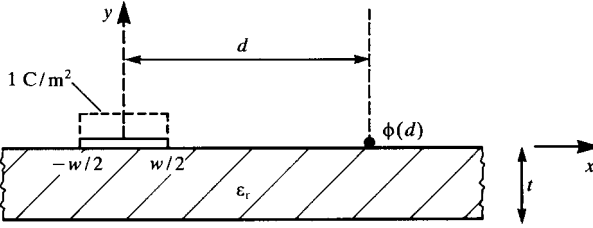


FIGURE 5.28 Illustration of the determination of the per-unit-length capacitances for a PCB by point matching.

Applying this result for a line charge to a infinitesimally thin strip on a dielectric slab by representing the charge distribution (pulse expansion function) as a set of 1 C/m line charges as shown in Figure 5.28 requires performing the following integral:

$$\begin{aligned} \phi(d) = & -\frac{1}{4\pi\epsilon_0\epsilon_{r,\text{eff}}} \int_{-\frac{w}{2}}^{\frac{w}{2}} \ln [(x+d)^2] dx \\ & -\frac{1}{4\pi\epsilon_0\epsilon_{r,\text{eff}}} (1+k) \sum_{n=1}^{\infty} k^{(2n-1)} \int_{-\frac{w}{2}}^{\frac{w}{2}} \ln [(x+d)^2 + (2nt)^2] dx \end{aligned} \tag{5.77}$$

For a point at the center of the strip, that is, $d = 0$, the self-potential is given by

$$\begin{aligned} \phi_{\text{self}}(w) = & \frac{1}{2\pi\epsilon_0\epsilon_{r,\text{eff}}} \left[w - w \ln \left(\frac{w}{2} \right) \right] + \frac{1}{2\pi\epsilon_0\epsilon_{r,\text{eff}}} (1+k) \sum_{n=1}^{\infty} k^{(2n-1)} \times \\ & \left\{ w - \frac{w}{2} \ln \left[\left(\frac{w}{2} \right)^2 + (2nt)^2 \right] - (4nt) \tan^{-1} \left(\frac{w}{4nt} \right) \right\} \end{aligned} \tag{5.78a}$$

For the potential on another segment where $d \neq 0$ and generally $d > w/2$, the potential is

$$\begin{aligned} \phi(w, d) = & \frac{1}{2\pi\epsilon_0\epsilon_{r,\text{eff}}} \left[w + \left(d - \frac{w}{2} \right) \ln \left(d - \frac{w}{2} \right) - \left(d + \frac{w}{2} \right) \ln \left(d + \frac{w}{2} \right) \right] \\ & + \frac{1}{2\pi\epsilon_0\epsilon_{r,\text{eff}}} (1+k) \sum_{n=1}^{\infty} k^{(2n-1)} \left\{ w + \frac{1}{2} \left(d - \frac{w}{2} \right) \ln \left[\left(d - \frac{w}{2} \right)^2 + (2nt)^2 \right] \right. \\ & - \frac{1}{2} \left(d + \frac{w}{2} \right) \ln \left[\left(d + \frac{w}{2} \right)^2 + (2nt)^2 \right] \\ & \left. + (2nt) \left[\tan^{-1} \left(\frac{d - \frac{w}{2}}{2nt} \right) - \tan^{-1} \left(\frac{d + \frac{w}{2}}{2nt} \right) \right] \right\} \end{aligned} \tag{5.78b}$$

These results can be simplified and written as

$$\phi_{\text{self}}(w) = \frac{w}{2\pi\epsilon_0\epsilon_{r,\text{eff}}} \left[1 - \ln\left(\frac{w}{2}\right) \right] + \frac{w}{2\pi\epsilon_0\epsilon_{r,\text{eff}}} (1+k) \sum_{n=1}^{\infty} k^{(2n-1)} \left\{ 1 - \ln\left(\frac{w}{2}\right) - \frac{1}{2} \ln\left[1 + (4nT)^2\right] - (4nT) \tan^{-1}\left(\frac{1}{4nT}\right) \right\} \quad (5.79a)$$

and

$$\begin{aligned} \phi(w, d) = & \frac{w}{2\pi\epsilon_0\epsilon_{r,\text{eff}}} \left[1 - \ln\left(\frac{w}{2}\right) + \frac{1}{2}(2D-1) \ln(2D-1) - \frac{1}{2}(2D+1) \ln(2D+1) \right] \\ & + \frac{w}{2\pi\epsilon_0\epsilon_{r,\text{eff}}} (1+k) \sum_{n=1}^{\infty} k^{(2n-1)} \\ & \times \left\{ 1 - \ln\left(\frac{w}{2}\right) + \frac{1}{4}(2D-1) \ln\left[(2D-1)^2 + (4nT)^2\right] \right. \\ & - \frac{1}{4}(2D+1) \ln\left[(2D+1)^2 + (4nT)^2\right] \\ & \left. + (2nT) \left[\tan^{-1}\left(\frac{2D-1}{4nT}\right) - \tan^{-1}\left(\frac{2D+1}{4nT}\right) \right] \right\} \quad (5.79b) \end{aligned}$$

The results have been written in terms of the ratios of the subsection separation to subsection width, D , and board thickness to land width, T :

$$D = \frac{d}{w} \quad (5.80a)$$

and

$$T = \frac{t}{w} \quad (5.80b)$$

Recall that

$$\epsilon_{r,\text{eff}} = \frac{(\epsilon_r + 1)}{2} \quad (5.80c)$$

denotes the effective dielectric constant as the board thickness becomes infinite, $t \rightarrow \infty$, such that it fills the lower half space so that half the electric field lines would exist in air and the other half in the infinite half space occupied by the board. These results are used in the FORTRAN program PCB.FOR described in Appendix A to compute the entries in the per-unit-length capacitance matrix \mathbf{C} of a PCB. The per-unit-length inductance matrix \mathbf{L} is computed with the board removed from the basic relationship derived earlier:

$$\mathbf{L} = \mu_0\epsilon_0\mathbf{C}_0^{-1} \quad (5.81)$$

where \mathbf{C}_0 is the per-unit-length capacitance matrix with the board removed.

As an example consider the three-conductor PCB shown in Figure 5.29 consisting of three conductors of equal width w and identical edge-to-edge separations s . The

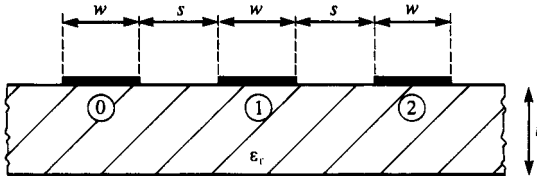


FIGURE 5.29 A PCB consisting of identical conductors with identical separations for the computation of numerical results.

following computed results are obtained with the FORTRAN program PCB.FOR (pulse expansion functions and point matching). The results will be computed for typical board parameters: $\epsilon_r = 4.7$ (glass epoxy), $t = 47$ mils, $w = s = 10$ mils. Choosing the left-most conductor as the reference conductor, Figure 5.30(a) compares the elements of the per-unit-length inductance matrix \mathbf{L} , Figure 5.30(b) compares the elements of the per-unit-length capacitance matrix \mathbf{C} , and Figure 5.30(c) compares the elements of the per-unit-length capacitance without the board, \mathbf{C}_0 , computed for various numbers of land subdivisions. Observe that convergence is achieved for about 20–30 subdivisions of each land. As a check on these results, observe that $L_{22} > L_{11}$ as it should be since the loop area between the reference conductor and the second conductor is larger than the loop area between the reference conductor and the first conductor. Similarly, in the capacitance plots observe that $C_{11} > C_{22}$ and $C_{011} > C_{022}$ since the first conductor is closer to the reference conductor. Figure 5.31 shows the convergence for the capacitances for various numbers of land subdivisions with \mathbf{C} , and without, \mathbf{C}_0 , the board. If one takes the ratios of the corresponding capacitance with and without the board, we see that the effective relative dielectric constant is on the order of 2.6–2.8 for this land width, land separation, and board thickness. This is on the order of the effective dielectric constant

$$\epsilon_{r,\text{eff}} = \frac{\epsilon_r + 1}{2} = 2.85$$

if the board occupied the infinite half space such that half the electric field lines would reside in free space and the other half in the board. We would expect this to be the case for (a) moderately thick boards and (b) closely spaced lands. For wide land separations, more of the electric field lines exit the bottom of the board and are more important than for closely spaced lands.

There are no known closed-form solutions for this problem, but we may compare the computed results of PCB.FOR to the approximate relations of Chapter 4 for two-conductor PCBs. For example, the results for a two-conductor PCB are given in Eqs. (4.109) of Chapter 4. For example, consider a two-conductor PCB having $\epsilon_r = 4.7$, $w = s = 15$ mils and $t = 62$ mils. Equations (4.109) give $l = 0.804 \mu\text{H/m}$ and $c = 38.53 \text{ pF/m}$. PCB.FOR using 30 divisions per land gives $l = 0.809 \mu\text{H/m}$ and $c = 38.62 \text{ pF/m}$, a difference of 0.2–0.6 %. For a PCB having $\epsilon_r = 4.7$, $w = s = 5$ mils and $t = 47$ mils, the formulas in (4.109) of Chapter 4 give

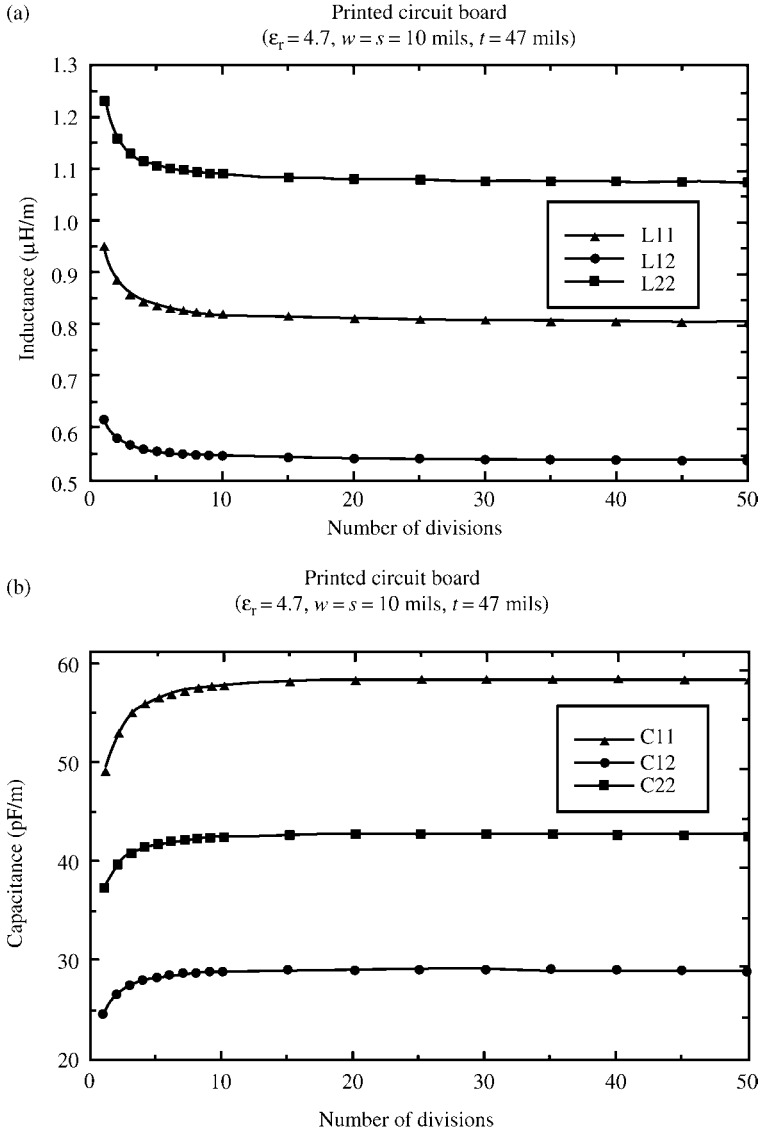


FIGURE 5.30 Illustration of the per-unit-length (a) inductances, (b) capacitances, and (c) capacitances with the board removed for various numbers of divisions of each land for $\epsilon_r = 4.7$, land width = separation = 10 mils, and board thickness = 47 mils.

$l=0.804 \mu\text{H}/\text{m}$ and $c = 39.06 \text{ pF}/\text{m}$, whereas PCB. FOR using 30 divisions per land gives $l = 0.809 \mu\text{H}/\text{m}$ and $c = 39.07 \text{ pF}/\text{m}$, a difference of 0.03–0.6 %.

And finally, we will compute the entries in **C** and **L** for a PCB that will be used in later crosstalk analyses: $\epsilon_r = 4.7$ (glass epoxy), $t = 47$ mils, $w = 15$ mils, and

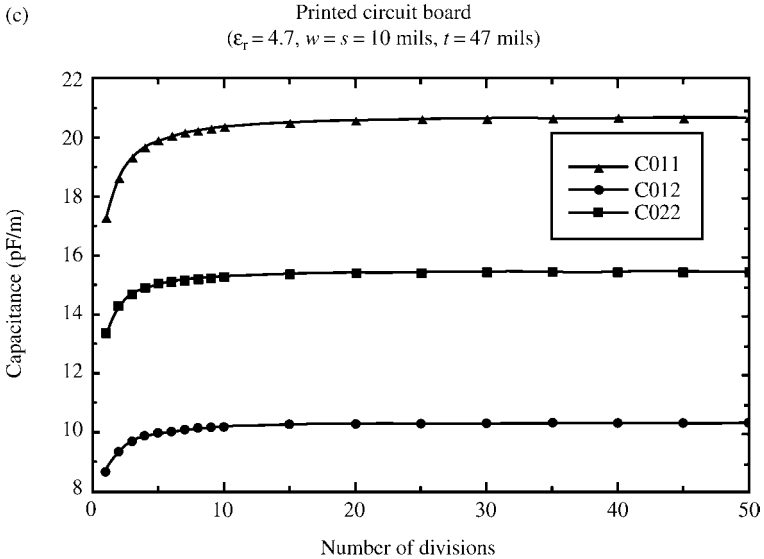


FIGURE 5.30 (Continued).

$s = 45$ mils. This separation is such that exactly three lands could be placed between any two adjacent lands. The results for the pulse expansion function, point matching method for 50 divisions per land computed using PCB . FOR are

$$\mathbf{L} = \begin{bmatrix} 1.10515 & 0.690613 \\ 0.690613 & 1.38123 \end{bmatrix} (\mu\text{H}/\text{m})$$

$$\mathbf{C} = \begin{bmatrix} 40.5985 & -20.2992 \\ -20.2992 & 29.7378 \end{bmatrix} (\text{pF}/\text{m})$$

5.3.1.2 Applications to Coupled Microstrip Lines Next, we consider applying this technique to the *coupled microstrip* consisting of lands (of zero thickness) on a dielectric substrate of thickness t and relative permittivity ϵ_r with an infinite ground plane on the other side shown in Figure 5.32. The ground plane will serve as the reference or zeroth conductor so that the computation of the generalized capacitance matrix will not be necessary for this case: We directly compute the transmission-line capacitance matrix with the dielectric present, \mathbf{C} , and with the dielectric removed, \mathbf{C}_0 . This is implemented in the FORTRAN computer code `MSTRP . FOR` described in Appendix A. We will assume that all lands are of equal width, w , and edge-to-edge separation, s . Although only three lands are shown, the code will handle any number of lands with the appropriate dimensioning of the arrays in `MSTRP . FOR`. This problem will represent a PCB with innerplanes, that is, the outer surface of the PCB and the underlying innerplane.

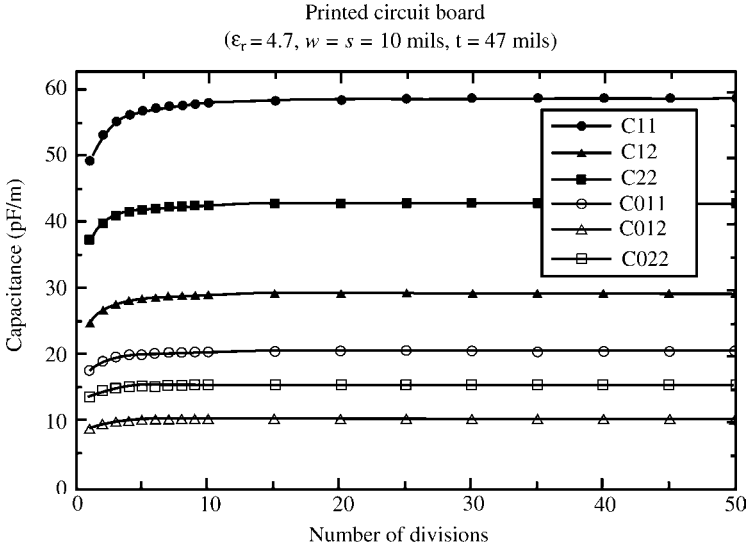


FIGURE 5.31 Comparison of the capacitances with and without the dielectric board versus the number of divisions per land from Figure 5.30(b) and (c).

The first and most basic subproblem we must address is the case of an infinitely long (in the z direction) filament carrying a per-unit-length charge of q C/m on the surface of the board and the determination of the potential on the board at a distance d away as shown in Figure 5.33(a). The sequence of images is shown in Figure 5.33(b) with their sequence number shown. With regard to Figures 5.25 and 5.26, we start with the original charge q and its image across the upper surface that gives a total of $(1 - k)q$ on the surface of the dielectric with that removed. Then, we image this across the ground plane in order to remove the ground plane giving the second image of $-(1 - k)q$ located at a distance t below the original position of the ground plane or a distance $2t$ below the first charge. Next, we image this charge across the

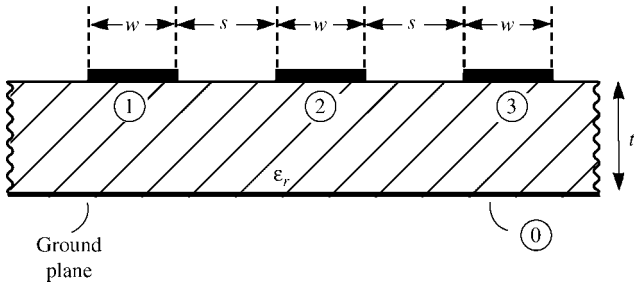


FIGURE 5.32 The three-conductor coupled microstrip line with equal land widths and separations.

upper surface of the dielectric according to Figure 5.25(b) by multiplying by k to give an image charge of $-k(1 - k)q$ located at a distance of $2t$ above the dielectric surface. Then, this is imaged across the ground plane to give an image charge of $k(1 - k)q$ located at a distance $3t$ below the ground plane or a distance of $4t$ below the first charge. Successive imaging across the ground plane and the dielectric gives the sequence of image charges shown in Figure 5.33(b). This allows the computation of the potential on the surface of the dielectric at a distance d from the original charge

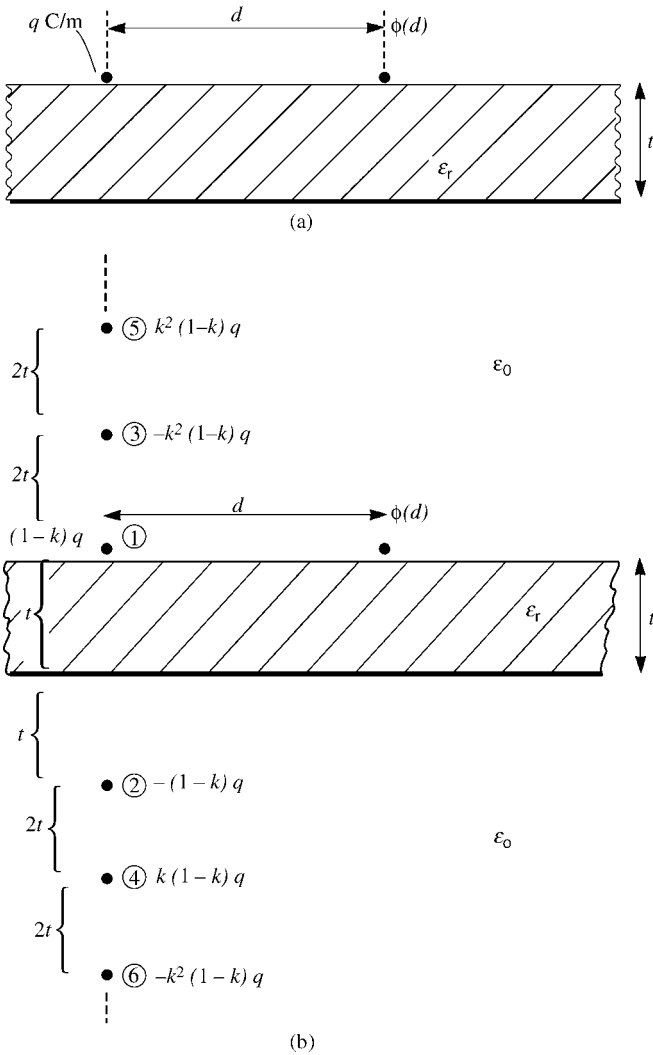


FIGURE 5.33 Determination of (a) the potential on a microstrip due to a line charge by (b) imaging across the boundaries.

with the dielectric and the ground plane removed. Hence, we have the simple problem of computing the potential of an infinite set of line charges in free space. The basic potential for each of these is

$$\begin{aligned} \phi(x) &= -\frac{q}{2\pi\epsilon_0} \ln(x) \\ &= -\frac{q}{4\pi\epsilon_0} \ln(x^2) \end{aligned} \tag{5.82}$$

Applying this to the sequence of images in Figure 5.33(b) gives

$$\begin{aligned} \phi(d) &= -\frac{(1-k)q}{4\pi\epsilon_0} \ln[d^2] + \frac{(1-k)q}{4\pi\epsilon_0} \ln[d^2 + (2t)^2] + \frac{k(1-k)q}{4\pi\epsilon_0} \ln[d^2 + (2t)^2] \\ &\quad - \frac{k(1-k)q}{4\pi\epsilon_0} \ln[d^2 + (4t)^2] - \frac{k^2(1-k)q}{4\pi\epsilon_0} \ln[d^2 + (4t)^2] \\ &\quad + \frac{k^2(1-k)q}{4\pi\epsilon_0} \ln[d^2 + (6t)^2] + \frac{k^3(1-k)q}{4\pi\epsilon_0} \ln[d^2 + (6t)^2] + \dots \end{aligned} \tag{5.83}$$

This can be written as

$$\begin{aligned} \phi(d) &= -\frac{(1-k)q}{4\pi\epsilon_0} \ln[d^2] - \frac{(1-k^2)q}{4\pi\epsilon_0} \sum_{n=1}^{\infty} (-1)^n k^{(n-1)} \ln[d^2 + (2nt)^2] \\ &= -\frac{q}{4\pi\epsilon_0\epsilon_{r,\text{eff}}} \ln[d^2] - \frac{q}{4\pi\epsilon_0\epsilon_{r,\text{eff}}} (1+k) \sum_{n=1}^{\infty} (-1)^n k^{(n-1)} \ln[d^2 + (2nt)^2] \end{aligned} \tag{5.84}$$

where we have substituted $(1+k)(1-k) = (1-k^2)$ and we have written this in terms of the effective dielectric constant where the board thickness goes to infinity, that is, $t \rightarrow \infty$:

$$\begin{aligned} \epsilon_{r,\text{eff}} &= \frac{\epsilon_r + 1}{2} \\ &= \frac{1}{(1-k)} \end{aligned} \tag{5.85}$$

Comparing (5.84) to the same basic subproblem solution for the PCB given in (5.76) shows that we may easily modify the PCB code by simply replacing the summation $\sum_{n=1}^{\infty} k^{(2n-1)}$ in the PCB .FOR program results for the potential with the board present given in (5.78) and (5.79) with $\sum_{n=1}^{\infty} (-1)^n k^{(n-1)}$:

$$\underbrace{\sum_{n=1}^{\infty} k^{(2n-1)}}_{\text{PCB}} \Leftrightarrow \underbrace{\sum_{n=1}^{\infty} (-1)^n k^{(n-1)}}_{\text{MSTRP}} \tag{5.86}$$

Hence, we can make a simple modification of PCB .FOR. In addition, we remove the generalized capacitance calculation from that code as we will be directly computing the transmission-line capacitance matrix since the reference conductor, the ground plane, is already designated.

There is one final but subtle difference. Note that the first term in the summation in (5.84) for $n = 1$ is nonzero even with the board absent, that is, $k = 0$. This is the

term representing the first image across the ground plane. Hence, the self-potential of a land ($d = 0$) with *the board removed* is, from (5.79a) ($\epsilon_r = 1$, $k = 0$),

$$\begin{aligned}\phi_{\text{self}}(w) &= \frac{w}{2\pi\epsilon_0} \left[1 - \ln\left(\frac{w}{2}\right) \right] - \frac{w}{2\pi\epsilon_0} \left\{ 1 - \ln\left(\frac{w}{2}\right) - \frac{1}{2} \ln[1 + (4T)^2] - 4T \tan^{-1}\left(\frac{1}{4T}\right) \right\} \\ &= \frac{w}{2\pi\epsilon_0} \left\{ \frac{1}{2} \ln[1 + (4T)^2] + 4T \tan^{-1}\left(\frac{1}{4T}\right) \right\}\end{aligned}\quad (5.87a)$$

and we have written this in terms of the ratio of dielectric thickness t to land subsection width w :

$$T = \frac{t}{w} \quad (5.88)$$

Similarly, the potential *with the board removed* but $d \neq 0$ and generally $d > w/2$ becomes, from (5.79b),

$$\begin{aligned}\phi(w, d) &= \frac{w}{2\pi\epsilon_0} \frac{1}{2} \left\{ (2D - 1) \ln(2D - 1) - (2D + 1) \ln(2D + 1) \right. \\ &\quad - \frac{1}{2} (2D - 1) \ln[(2D - 1)^2 + (4T)^2] \\ &\quad + \frac{1}{2} (2D + 1) \ln[(2D + 1)^2 + (4T)^2] \\ &\quad \left. + T \left[\tan^{-1}\left(\frac{2D + 1}{4T}\right) - \tan^{-1}\left(\frac{2D - 1}{4T}\right) \right] \right\}\end{aligned}\quad (5.87b)$$

and we have written this in terms of (5.88) and the ratio of distance to the potential point, d , to land subsection width w :

$$D = \frac{d}{w} \quad (5.89)$$

The potentials with the board present are obtained from (5.79a) and (5.79b) by substituting (5.86). For the self-potential term, $d = 0$, we obtain

$$\begin{aligned}\phi_{\text{self}}(w) &= -\frac{w}{2\pi\epsilon_0\epsilon_r\epsilon_{r,\text{eff}}} (1 + k) \sum_{n=1}^{\infty} (-1)^n k^{(n-1)} \\ &\quad \times \left\{ \frac{1}{2} \ln \left[1 + (4nT)^2 \right] + (4nT) \tan^{-1} \left(\frac{1}{4nT} \right) \right\}\end{aligned}\quad (5.90a)$$

In reducing this result, we have used the summation $(1 - k + k^2 - k^3 + \dots) = 1/(1 + k)$. For $d \neq 0$, the potential becomes, from (5.79b) substituting (5.86),

$$\begin{aligned} \phi(w, d) = & \frac{w}{2\pi\epsilon_0\epsilon_{r,\text{eff}}} \left[\frac{1}{2} (2D - 1) \ln (2D - 1) - \frac{1}{2} (2D + 1) \ln (2D + 1) \right] \\ & + \frac{w}{2\pi\epsilon_0\epsilon_{r,\text{eff}}} (1 + k) \sum_{n=1}^{\infty} (-1)^n k^{(n-1)} \\ & \times \left\{ \frac{1}{4} (2D - 1) \ln \left[(2D - 1)^2 + (4nT)^2 \right] \right. \\ & - \frac{1}{4} (2D + 1) \ln \left[(2D + 1)^2 + (4nT)^2 \right] \\ & \left. + (2nT) \left[\tan^{-1} \left(\frac{2D - 1}{4nT} \right) - \tan^{-1} \left(\frac{2D + 1}{4nT} \right) \right] \right\} \end{aligned} \tag{5.90b}$$

As an example consider a two-conductor coupled microstrip line consisting of two conductors of equal width w over a ground plane. The following computed results are obtained with the FORTRAN program MSTRP.FOR (pulse expansion functions and point matching). The results will be computed for typical board parameters: $\epsilon_r = 4.7$ (glass epoxy), $t = 47$ mils, and $w = s = 10$ mils. Figure 5.34(a) compares the elements of the per-unit-length inductance matrix \mathbf{L} , Figure 5.34(b) compares the elements of the per-unit-length capacitance matrix \mathbf{C} , and Figure 5.34(c) compares the elements of the per-unit-length capacitance without the board, \mathbf{C}_0 , computed for various numbers of land subdivisions. Observe that convergence is achieved for about 20–30 subdivisions of each land. Also observe that the capacitances on the main diagonal of \mathbf{C} and \mathbf{C}_0 , C_{11} and C_{22} as well as C_{011} and C_{022} , are equal as they should be by symmetry. Similarly, $L_{11} = L_{22}$ as should be the case by symmetry. Figure 5.35 shows the convergence for the capacitances for various numbers of land subdivisions. If one takes the ratios of the corresponding capacitance with and without the board, we see that the effective relative dielectric constant is on the order of 2.6–3.1 for this land width, land separation, and board thickness. This is on the order of the effective dielectric constant

$$\epsilon_{r,\text{eff}} = \frac{\epsilon_r + 1}{2} = 2.85$$

if the board occupied the infinite half space such that half the electric field lines would reside in free space and the other half in the board. We would expect this to be the case for (a) moderately thick boards and (b) closely spaced lands. For wide land separations, more of the electric field lines will be influenced by the ground plane at the bottom of the board and are more important than for closely spaced lands.

We may compare the computed results of MSTRP.FOR to the approximate relations of Chapter 4. For example, the results for a microstrip line consisting of one land of width w above a ground plane are given in Eqs. (4.108) of Chapter 4. For example, consider a microstrip line having $\epsilon_r = 4.7$, $w = 5$ mils, and $t = 50$ mils. Equations (4.108) give $l = 0.8765 \mu\text{H/m}$ and $c = 38.26 \text{ pF/m}$. MSTRP.FOR using 30 divisions per land gives $l = 0.879 \mu\text{H/m}$ and $c = 39.03 \text{ pF/m}$, a difference of 0.3–2%. For a

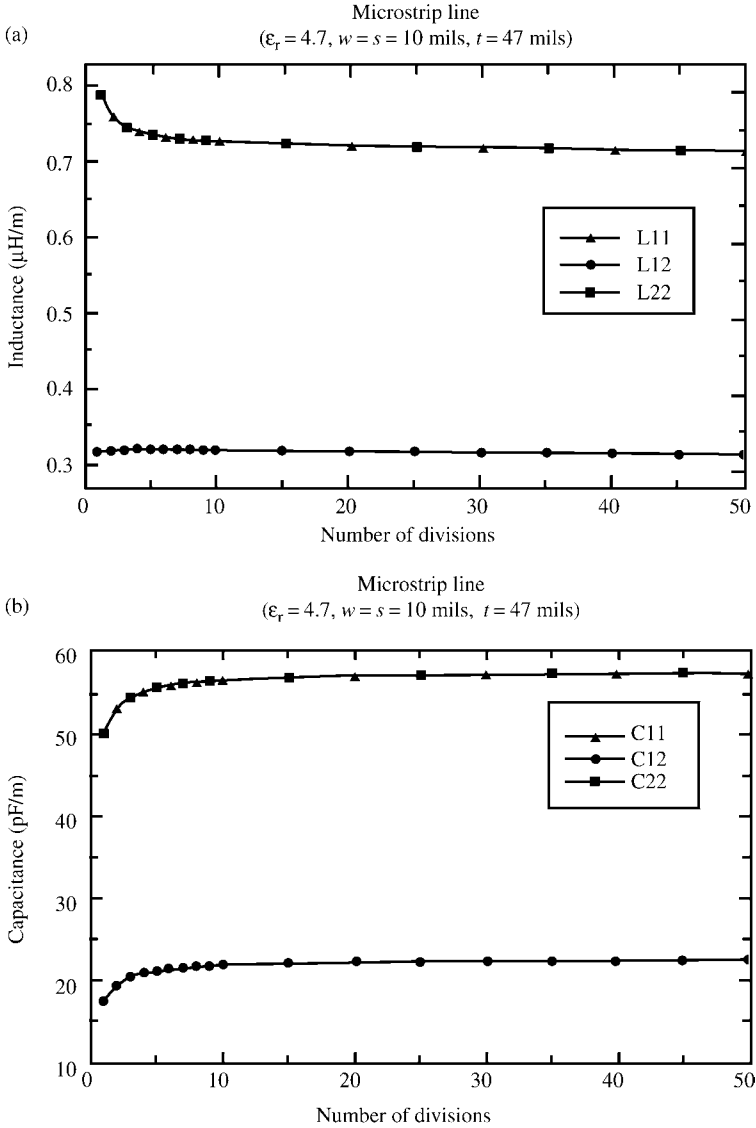


FIGURE 5.34 Determination of (a) inductances, (b) capacitances, and (c) capacitances with the board removed for a two-conductor coupled microstrip with $\epsilon_r = 4.7$, land width = separation = 10 mils, and board thickness = 47 mils.

microstrip line having $\epsilon_r = 4.7$, $w = 100$ mils, and $t = 62$ mils, the formulas in (4.108) of Chapter 4 give $l = 0.335 \mu\text{H/m}$ and $c = 115.7 \text{ pF/m}$, whereas MSTRP . FOR using 30 divisions per land gives $l = 0.336 \mu\text{H/m}$ and $c = 115.2 \text{ pF/m}$, a difference of 0.3–0.4 %.

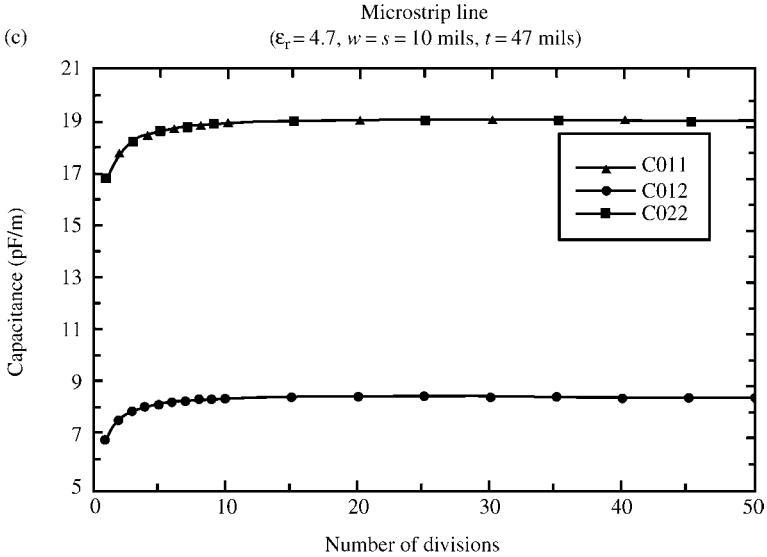


FIGURE 5.34 (Continued).

And finally, we will compute the entries in **C** and **L** for a coupled microstrip line that will be used in later crosstalk analyses: $\epsilon_r = 4.7$ (glass epoxy), $t = 62$ mils, $w = 100$ mils, and $s = 100$ mils. The results for the pulse expansion function, point matching method for 50 divisions per land computed using

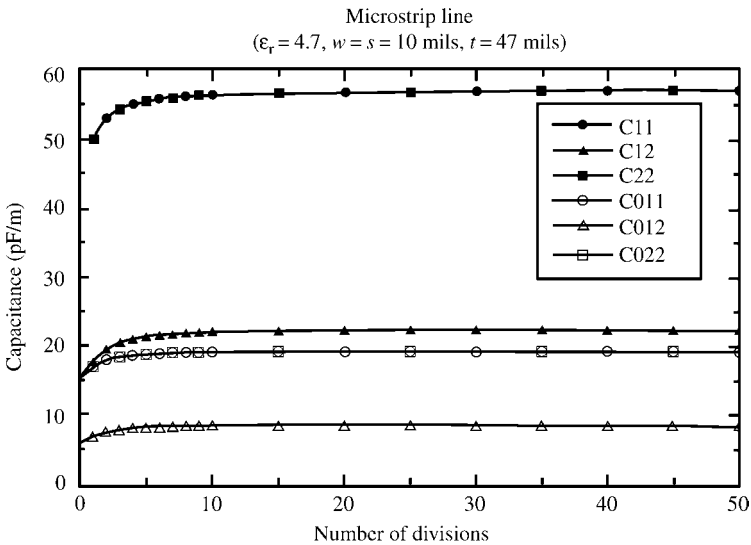


FIGURE 5.35 Comparison of the capacitances with and without the dielectric board versus the number of divisions per land from Figure 5.34 (b) and (c).

MSTRP . FOR are

$$\mathbf{L} = \begin{bmatrix} 0.334497 & 0.0372044 \\ 0.0372044 & 0.334497 \end{bmatrix} (\mu\text{H/m})$$

$$\mathbf{C} = \begin{bmatrix} 115.844 & -4.96916 \\ -4.96916 & 115.844 \end{bmatrix} (\text{pF/m})$$

5.3.1.3 Applications to Coupled Striplines Next, we consider applying this technique to the *coupled stripline* consisting of lands (of zero thickness) embedded in a dielectric substrate of thickness t and relative permittivity ϵ_r with infinite ground planes on both sides as shown in Figure 5.36. The ground planes will serve as the reference or zeroth conductor so that the computation of the generalized capacitance matrix will not be necessary for this case: We directly compute the transmission-line capacitance matrix with the dielectric present, \mathbf{C} , and with the dielectric removed, \mathbf{C}_0 . This is implemented in the FORTRAN computer code STRPLINE . FOR described in Appendix A. We will assume that all lands are of equal width, w , with equal edge-to-edge separations, s , and the lands are located midway between the ground planes. Although only three lands are shown, the code will handle any number of lands with the appropriate dimensioning of the arrays in STRPLINE . FOR . This problem will represent a PCB with innerplanes where lands are buried between the innerplanes.

The first and most basic subproblem we must address is the case of an infinitely long (in the z direction) filament carrying a per-unit-length charge of 1 (C/m) located midway between the ground planes, and we need to determine the potential at a point also midway between the ground planes and a distance d from the line charge as shown in Figure 5.37(a). This is a somewhat canonical problem that is solved in Collin [6]

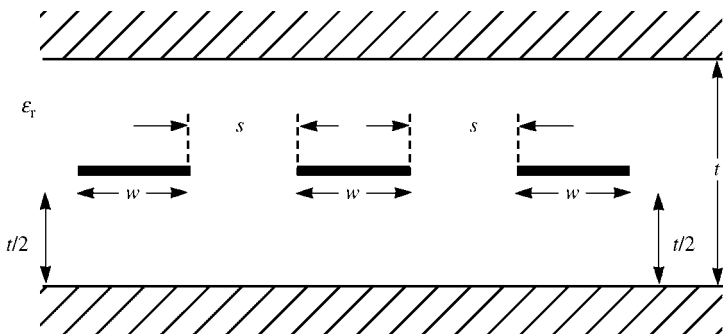


FIGURE 5.36 The three-conductor coupled stripline with equal land widths and separations.

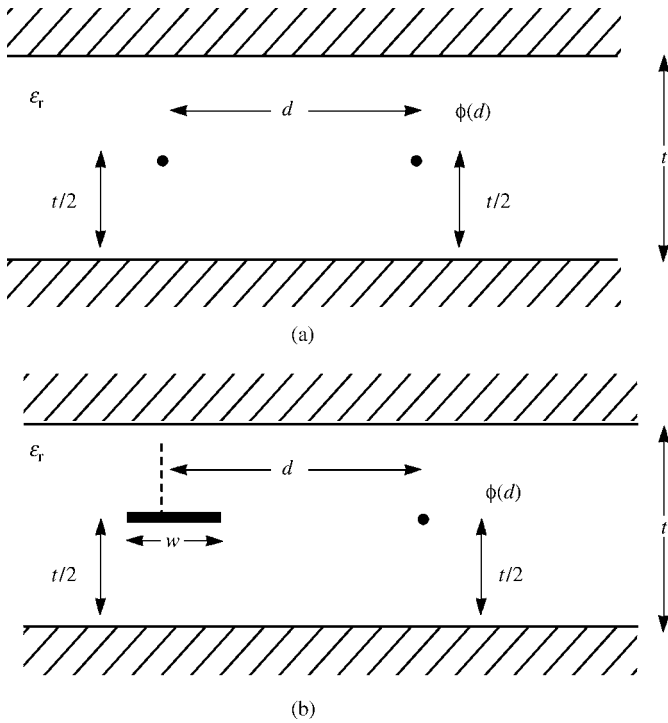


FIGURE 5.37 Illustration of the basic determination of the potential of a stripline for (a) a line charge and (b) a land with constant charge distribution.

and Smythe [1]. The potential specialized to this case is [6].

$$\begin{aligned} \phi(d) &= \frac{1}{\pi\epsilon_0\epsilon_r} \tanh^{-1} \left(e^{-\frac{\pi|d|}{t}} \right) \\ &= \frac{1}{2\pi\epsilon_0\epsilon_r} \ln \left(\frac{1 + e^{-\frac{\pi|d|}{t}}}{1 - e^{-\frac{\pi|d|}{t}}} \right) \end{aligned} \tag{5.91}$$

Smythe also gives an equivalent form as

$$\phi(d) = \frac{1}{2\pi\epsilon_0\epsilon_r} \tanh^{-1} \left(\frac{1}{\cosh \left(\frac{\pi d}{t} \right)} \right) \tag{5.92}$$

The final subproblem is a strip of zero thickness and width w carrying a charge distribution of 1 C/m^2 shown in Figure 5.37(b). The strip is parallel to the ground planes and is located midway between them. The desired potential is located midway between the planes and is a distance d from the midpoint of the strip. Treating the strip as a sequence of charge filaments $dx \text{ (C/m)}$, we sum the contributions to the potential as

$$\phi(d) = \frac{1}{\pi\epsilon} \int_{-w/2}^{w/2} \tanh^{-1} \left(e^{-\frac{\pi|d-x|}{t}} \right) dx \tag{5.93}$$

This can be integrated by making a change of variables as $u = e^{-(\pi d/t)} e^{(\pi x/t)}$ so that $du = (\pi/t)u \, dx$. Substituting into (5.93) gives

$$\phi(d) = \frac{t}{\pi^2\epsilon} \int_{e^{-\frac{\pi}{t}(d+\frac{w}{2})}}^{e^{-\frac{\pi}{t}(d-\frac{w}{2})}} \frac{\tanh^{-1}(u)}{u} du \tag{5.94}$$

This integrates to (see Dwight [7] integral 735.1)

$$\begin{aligned} \phi(d) = \frac{t}{\pi^2\epsilon} \left[\left(E_m + \frac{E_m^3}{9} + \frac{E_m^5}{25} + \frac{E_m^7}{49} + \dots \right) \right. \\ \left. - \left(E_p + \frac{E_p^3}{9} + \frac{E_p^5}{25} + \frac{E_p^7}{49} + \dots \right) \right] \end{aligned} \tag{5.95a}$$

where

$$E_m = e^{-\frac{\pi}{t}(d-\frac{w}{2})} \tag{5.95b}$$

and

$$E_p = e^{-\frac{\pi}{t}(d+\frac{w}{2})} \tag{5.95c}$$

Each of these two series converges rapidly as for a match point on another strip, $d > w/2$. For the case where the match point is at the center of the charge-bearing strip, that is, $d = 0$, we require

$$\phi_{\text{self}}(0) = \frac{2}{\pi\epsilon} \int_0^{\frac{w}{2}} \tanh^{-1} \left(e^{-\frac{\pi x}{t}} \right) dx \tag{5.96}$$

This may also be integrated by making the substitution $u = e^{-(\pi x/t)}$ and $du = -(\pi/t)u dx$ to give

$$\begin{aligned} \phi_{\text{self}}(0) &= -\frac{2t}{\pi^2 \epsilon} \int_1^{e^{-\frac{\pi w}{2t}}} \frac{\tanh^{-1} u}{u} du \\ &= \frac{2t}{\pi^2 \epsilon} \left[\left(1 + \frac{1}{9} + \frac{1}{25} + \frac{1}{49} + \dots \right) - \left(E + \frac{E^3}{9} + \frac{E^5}{25} + \dots \right) \right] \end{aligned} \tag{5.97a}$$

where

$$E = e^{-\frac{\pi w}{2t}} \tag{5.97b}$$

Again, both series converge rapidly and the first series converges to (see Dwight [7] # 48.12)

$$1 + \frac{1}{9} + \frac{1}{25} + \frac{1}{49} + \dots = \frac{\pi^2}{8} \tag{5.97c}$$

We can essentially adapt the program MSTRP.FOR directly to this case by simply changing the computation subroutine for determining $\phi(d)$ and $\phi(0)$ to the above results.

As an example, consider the coupled stripline consisting of two conductors between ground planes where $t = 47$ mils, $w = s = 10$ mils, and $\epsilon_r = 4.7$. The results obtained with STRPLINE.FOR are shown in the following figures. Figure 5.38(a) compares the elements of the per-unit-length inductance matrix \mathbf{L} and Figure 5.38(b) compares the elements of the per-unit-length capacitance matrix, \mathbf{C} , computed for various numbers of land subdivisions. It is not necessary to show the corresponding results with the board replaced by free space, \mathbf{C}_0 , since for this homogeneous medium $\mathbf{C} = \epsilon_r \mathbf{C}_0$. Observe that convergence is achieved for about 20–30 subdivisions of each land. Also observe that the capacitances on the main diagonal of \mathbf{C} , C_{11} and C_{22} , are equal as they should be by symmetry. Similarly, $L_{11} = L_{22}$ as should be the case by symmetry.

We may compare the computed results of STRPLINE.FOR to the approximate relations of Chapter 4. For example, the results for a stripline line consisting of one land of width w midway between the ground planes are given in Eqs. (4.107) of Chapter 4. For example, consider a stripline line having $\epsilon_r = 4.7$, $w = 5$ mils, and $t = 50$ mils. Equations (4.107) give $l = 0.6566 \mu\text{H/m}$ and $c = 79.54 \text{ pF/m}$. STRPLINE.FOR using 60 divisions per land gives $l = 0.6515 \mu\text{H/m}$ and $c = 80.27 \text{ pF/m}$, a difference of 0.8–0.9 %. For a stripline line having $\epsilon_r = 4.7$, $w = 5$ mils, and $t = 10$ mils, the formulas in (4.107) of Chapter 4 give $l = 0.334 \mu\text{H/m}$ and $c = 156.4 \text{ pF/m}$, whereas STRPLINE.FOR using 60 divisions per land gives $l = 0.3362 \mu\text{H/m}$ and $c = 155.53 \text{ pF/m}$, a difference of 0.6–0.7 %.

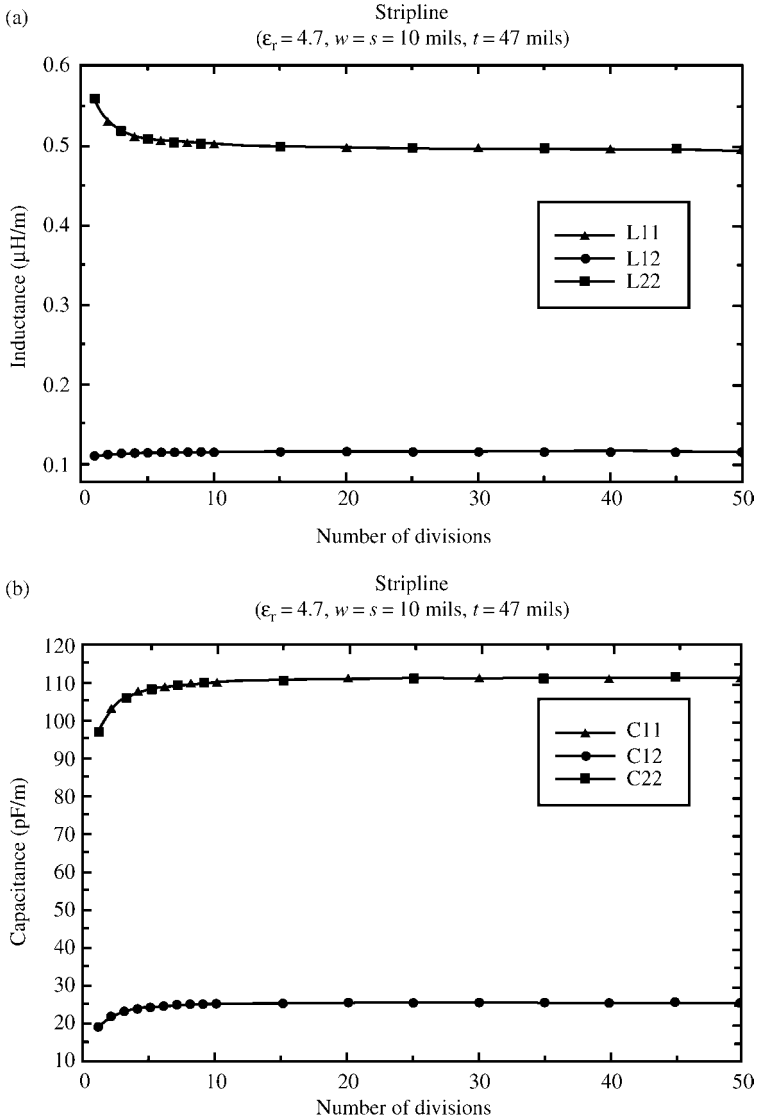


FIGURE 5.38 Determination of (a) inductances and (b) capacitances for a two-conductor coupled stripline with $\epsilon_r = 4.7$, land width = separation = 10 mils, and board thickness = 47 mils.

5.4 FINITE DIFFERENCE TECHNIQUES

Recall that the entries in the per-unit-length inductance, capacitance, and conductance matrices are determined as a static (dc) solution for the fields in the transverse (x - y) plane. Essentially, the transverse fields are such that the potential in the space

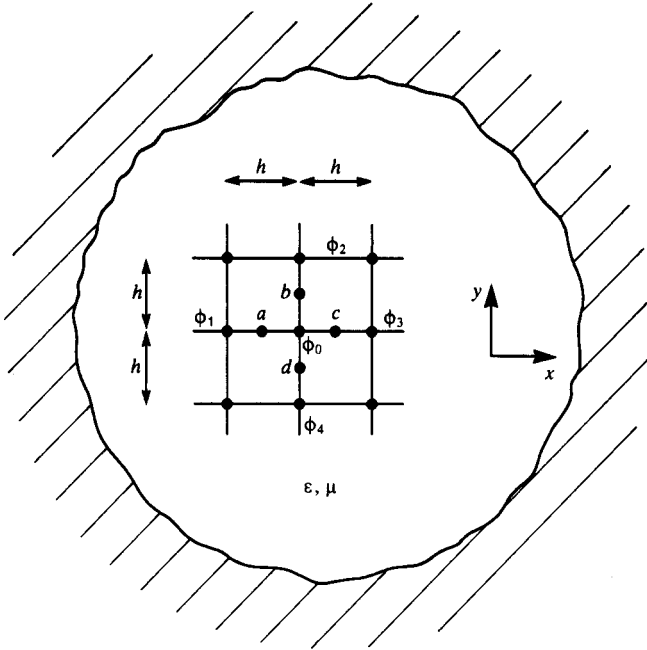


FIGURE 5.39 The finite-difference grid.

surrounding the conductors, $\phi(x,y)$, again satisfies Laplace’s equation in the transverse plane:

$$\nabla^2 \phi(x, y) = \frac{\partial^2 \phi(x, y)}{\partial x^2} + \frac{\partial^2 \phi(x, y)}{\partial y^2} = 0 \tag{5.98}$$

Finite-difference techniques approximate these spatial partial derivatives in a discrete fashion in the space surrounding the conductors. For example, consider the closed region shown in Figure 5.39. The space is gridded into cells of length and width h . First-order approximations to the first partial derivatives at the interior cell points a , b , c , and d are [A.1.4]

$$\left. \frac{\partial \phi}{\partial x} \right|_a = \frac{\phi_0 - \phi_1}{h} \tag{5.99a}$$

$$\left. \frac{\partial \phi}{\partial x} \right|_c = \frac{\phi_3 - \phi_0}{h} \tag{5.99b}$$

$$\left. \frac{\partial \phi}{\partial y} \right|_b = \frac{\phi_2 - \phi_0}{h} \quad (5.99c)$$

$$\left. \frac{\partial \phi}{\partial y} \right|_d = \frac{\phi_0 - \phi_4}{h} \quad (5.99d)$$

The second-order derivatives are similarly approximated using these results as

$$\begin{aligned} \left. \frac{\partial^2 \phi}{\partial x^2} \right|_0 &= \frac{1}{h} \left(\left. \frac{\partial \phi}{\partial x} \right|_c - \left. \frac{\partial \phi}{\partial x} \right|_a \right) \\ &= \frac{(\phi_3 - \phi_0) - (\phi_0 - \phi_1)}{h^2} \end{aligned} \quad (5.100a)$$

$$\begin{aligned} \left. \frac{\partial^2 \phi}{\partial y^2} \right|_0 &= \frac{1}{h} \left(\left. \frac{\partial \phi}{\partial y} \right|_b - \left. \frac{\partial \phi}{\partial y} \right|_d \right) \\ &= \frac{(\phi_2 - \phi_0) - (\phi_0 - \phi_4)}{h^2} \end{aligned} \quad (5.100b)$$

This amounts to a *central difference* expression for the partial derivatives [4]. Substituting these results into (5.98) gives a discrete approximation to Laplace's equation:

$$\begin{aligned} \frac{\partial^2 \phi(x, y)}{\partial x^2} + \frac{\partial^2 \phi(x, y)}{\partial y^2} &= 0 \\ &= \frac{\phi_1 + \phi_2 + \phi_3 + \phi_4 - 4\phi_0}{h^2} \end{aligned} \quad (5.101)$$

or

$$\phi_0 = \frac{1}{4} [\phi_1 + \phi_2 + \phi_3 + \phi_4] \quad (5.102)$$

Thus, the potential at a point is the average of the potentials of the surrounding four points in the mesh. Equation (5.102) is to be satisfied at all mesh points. Typically, this is accomplished by prescribing the potentials of the mesh points on the conductor surfaces, initially prescribing zero potential to the interior points and then recursively applying (5.102) at all the interior points until the change is less than some predetermined amount at which point the iteration is terminated.

An example of the application of the method is shown in Figure 5.40, which was solved earlier using a MoM method and a direct solution of Laplace's equation with those results given in Table 5.8. A rectangular box having the four conducting walls at different potentials is shown. The potentials of the interior mesh points obtained iteratively are shown. Observe that, even with this relatively course mesh, the potentials of the mesh points converge rather rapidly.

This method could also be solved in a direct fashion rather than iteratively. Enforcement of the potential via (5.102) at the six interior mesh points gives

TABLE 5.8

| | Direct method | Iteration | Exact |
|----------|---------------|-----------|---------|
| ϕ_a | 16.44 | 16.41 | 16.4784 |
| ϕ_b | 21.66 | 21.63 | 21.8499 |
| ϕ_c | 14.10 | 14.07 | 14.1575 |
| ϕ_d | 20.19 | 20.16 | 20.4924 |
| ϕ_e | 9.77 | 9.76 | 9.60942 |
| ϕ_f | 14.99 | 14.98 | 14.9810 |

$$\begin{bmatrix} 4 & -1 & -1 & 0 & 0 & 0 \\ -1 & 4 & 0 & -1 & 0 & 0 \\ -1 & 0 & 4 & -1 & -1 & 0 \\ 0 & -1 & -1 & 4 & 0 & -1 \\ 0 & 0 & -1 & 0 & 4 & -1 \\ 0 & 0 & 0 & -1 & -1 & 4 \end{bmatrix} \begin{bmatrix} V_a \\ V_b \\ V_c \\ V_d \\ V_e \\ V_f \end{bmatrix} = \begin{bmatrix} 30 \\ 50 \\ 10 \\ 30 \\ 10 \\ 30 \end{bmatrix} \tag{5.103}$$

Solving this gives the potentials of the interior mesh points compared to those obtained by iteration in Figure 5.40 as shown in Table 5.8. The exact results were obtained from an analytical solution of Laplace’s equation given previously [8].

The solution for the potentials via this method is only one part of the process of determining the per-unit-length generalized capacitance matrix. In order to compute the generalized capacitance matrix, we need to determine the total charge on the conductors (per unit of line length). To implement this calculation, recall Gauss’s law:

$$Q = \oiint_s \vec{\mathcal{D}} \cdot d\vec{s} \tag{5.104}$$

that provides that the charge enclosed by a surface is equal to the integral of the normal component of the electric flux density vector over that surface. For a linear, homogeneous, isotropic medium,

$$\vec{\mathcal{D}} = \epsilon \vec{\mathcal{E}} = \epsilon \frac{\partial \phi}{\partial n} \vec{a}_n \tag{5.105}$$

where \vec{a}_n is the unit vector normal to the surface. In order to apply this to the problem of computing the charge on the surface of a conductor, consider Figure 5.41. Applying (5.104) and (5.105) to a strip along the conductor surface between the conductor and the first row of mesh points just off the surface gives

$$q = \oint_l \vec{\mathcal{D}} \cdot d\vec{l} = \oint_l \epsilon \frac{\partial \phi}{\partial n} dl \tag{5.106}$$

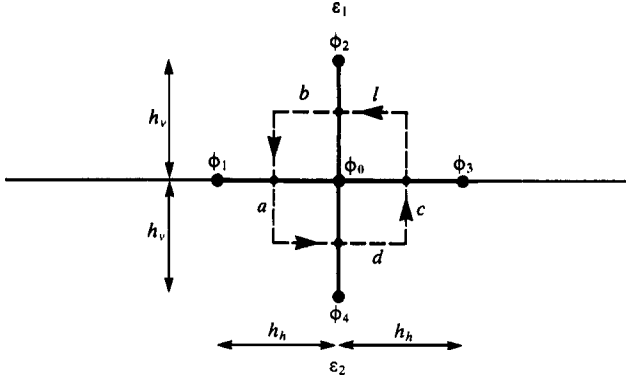


FIGURE 5.42 Illustration of the implementation of the finite-difference method for multiple dielectrics.

Using the potentials computed at the interior mesh points, we can obtain the charge on the surface by applying (5.106) in discrete form as

$$\begin{aligned}
 q = & \dots + \varepsilon \frac{(\phi_i - \phi_a)}{h_v} h_h + \varepsilon \frac{(\phi_i - \phi_b)}{h_v} h_h \\
 & + \varepsilon \frac{(\phi_i - \phi_c)}{h_v} h_h + \varepsilon \frac{(\phi_i - \phi_d)}{h_v} h_h + \varepsilon \frac{(\phi_i - \phi_e)}{h_v} h_h + \varepsilon \frac{(\phi_i - \phi_f)}{h_v} h_h + \dots
 \end{aligned}
 \tag{5.107}$$

where h_v denotes the “vertical” length of the mesh perpendicular to the conductor surface and h_h denotes the “horizontal” length of the mesh parallel to the conductor surface. Once the charges on the conductors are obtained in this fashion, the generalized capacitance matrix can be formed and from it the per-unit-length capacitances can be obtained.

Dielectric inhomogeneities can be handled in a similar fashion with this method. Gauss’s law requires that, in the absence of any free charge intentionally placed at an interface between two dielectrics, there can be no net charge on the surface. Consider the interface between two dielectrics shown in Figure 5.42, where a mesh has been assigned at the boundary. Applying Gauss’s law to the surface surrounding the center point of the mesh shown as a dashed line gives

$$\begin{aligned}
 0 = & \oint_l \vec{\mathcal{D}} \cdot d\vec{l} = \oint_l \varepsilon \frac{\partial \phi}{\partial n} dl \\
 = & \varepsilon_1 \frac{(\phi_2 - \phi_0)}{h_v} h_h + \varepsilon_1 \frac{(\phi_1 - \phi_0)}{h_h} \frac{h_v}{2} + \varepsilon_2 \frac{(\phi_1 - \phi_0)}{h_h} \frac{h_v}{2} \\
 & + \varepsilon_2 \frac{(\phi_4 - \phi_0)}{h_v} h_h + \varepsilon_2 \frac{(\phi_3 - \phi_0)}{h_h} \frac{h_v}{2} + \varepsilon_1 \frac{(\phi_3 - \phi_0)}{h_h} \frac{h_v}{2}
 \end{aligned}
 \tag{5.108}$$

Finite-difference methods are particularly adapted to *closed systems*. For *open systems* where the space extends to infinity in all directions, a method must be employed to terminate the mesh. A rather simple but computationally intensive technique is to extend the mesh to a large but finite distance from the conductors and terminate it in zero potential. To check the sufficiency of this, extend the mesh slightly larger and recompute the results.

5.5 FINITE-ELEMENT TECHNIQUES

The third important numerical method for solving (approximately) Laplace's equation is the *finite-element method* or FEM. The FEM approximates the region and its potential distribution by dividing the region into subregions (finite elements) and representing the potential distribution over that subregion. We will restrict our discussion to the most commonly used finite element, the triangle surface shown in Figure 5.43(a). Higher order elements are discussed in [4, 9]. Figure 5.43(b) illustrates the approximation of a 2D region using these triangular elements. The triangle element has three nodes at which the potentials are prescribed (known). The potential distribution over the element is a polynomial approximation in the x, y coordinates:

$$\phi(x, y) = a + bx + cy \quad (5.109)$$

Evaluating this equation at the three nodes gives

$$\begin{bmatrix} \phi_1 \\ \phi_2 \\ \phi_3 \end{bmatrix} = \begin{bmatrix} 1 & x_1 & y_1 \\ 1 & x_2 & y_2 \\ 1 & x_3 & y_3 \end{bmatrix} \begin{bmatrix} a \\ b \\ c \end{bmatrix} \quad (5.110)$$

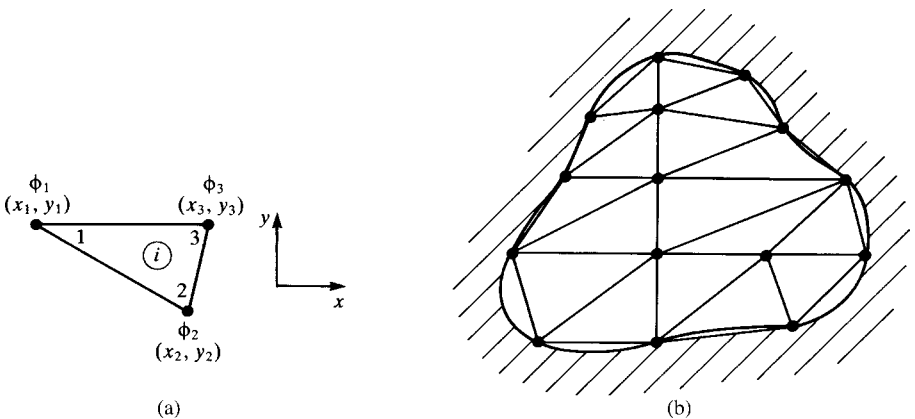


FIGURE 5.43 Illustration of (a) the finite-element triangular element and (b) its use in representing two-dimensional problems.

Solving this for the coefficients gives

$$a = \frac{1}{2A} [K_1\phi_1 + K_2\phi_2 + K_3\phi_3] \tag{5.111a}$$

$$b = \frac{1}{2A} [Y_1\phi_1 + Y_2\phi_2 + Y_3\phi_3] \tag{5.111b}$$

$$c = -\frac{1}{2A} [X_1\phi_1 + X_2\phi_2 + X_3\phi_3] \tag{5.111c}$$

where

$$\begin{aligned} K_1 &= (x_2y_3 - x_3y_2) \\ K_2 &= (x_3y_1 - x_1y_3) \\ K_3 &= (x_1y_2 - x_2y_1) \end{aligned} \tag{5.111d}$$

$$\begin{aligned} Y_1 &= (y_2 - y_3) \\ Y_2 &= (y_3 - y_1) \\ Y_3 &= (y_1 - y_2) \end{aligned} \tag{5.111e}$$

$$\begin{aligned} X_1 &= (x_2 - x_3) \\ X_2 &= (x_3 - x_1) \\ X_3 &= (x_1 - x_2) \end{aligned} \tag{5.111f}$$

and the area of the element is

$$\begin{aligned} A &= \frac{1}{2} \begin{vmatrix} 1 & x_1 & y_1 \\ 1 & x_2 & y_2 \\ 1 & x_3 & y_3 \end{vmatrix} \\ &= \frac{1}{2} [K_1 + K_2 + K_3] \end{aligned} \tag{5.112}$$

Observe the cyclic ordering of the subscripts in (5.111) as $1 \rightarrow 2 \rightarrow 3$. Given the node potentials, the potential at points on the element surface can be found from (5.109) using (5.111) and (5.112). The electric field over the surface of the element is constant:

$$\begin{aligned} \vec{E} &= -\nabla\phi \\ &= -b\vec{a}_x - c\vec{a}_y \end{aligned} \tag{5.113}$$

Observe that when a surface is approximated by these triangular elements as in Figure 5.43(b), the potential is guaranteed to be continuous across the common boundaries between any adjacent elements.

The key feature in insuring a solution of Laplace's equation by this method is that the solution is such that the total energy in the field distribution in the region is a minimum [4, 9]. The total energy in the system is the sum of the energies of the elements:

$$W = \sum_{i=1}^{N_e} W^{(i)} \quad (5.114)$$

The minimum energy requirement is that the derivatives with respect to all *free nodes* (nodes where the potential is unknown) are zero:

$$\left. \frac{\partial W}{\partial \phi_i} \right|_{\text{all free nodes}} = 0 \quad (5.115)$$

The energy of the *i*th element is

$$\begin{aligned} W^{(i)} &= \frac{1}{2} \int_{s_i} \varepsilon_i |\vec{E}_i|^2 ds_i \\ &= \frac{\varepsilon_i}{2} \int_{s_i} (b_i^2 + c_i^2) ds_i \\ &= \frac{\varepsilon_i}{2} (b_i^2 + c_i^2) A_i \\ &= \frac{\varepsilon_i}{8A_i} \left[(Y_{i1}^2 + X_{i1}^2) \phi_1^{(i)} \phi_1^{(i)} + 2(Y_{i1}Y_{i2} + X_{i1}X_{i2}) \phi_1^{(i)} \phi_2^{(i)} \right. \\ &\quad + (Y_{i2}^2 + X_{i2}^2) \phi_2^{(i)} \phi_2^{(i)} + 2(Y_{i1}Y_{i3} + X_{i1}X_{i3}) \phi_1^{(i)} \phi_3^{(i)} \\ &\quad \left. + (Y_{i3}^2 + X_{i3}^2) \phi_3^{(i)} \phi_3^{(i)} + 2(Y_{i2}Y_{i3} + X_{i2}X_{i3}) \phi_2^{(i)} \phi_3^{(i)} \right] \end{aligned} \quad (5.116)$$

where $\phi_k^{(i)}$ is the potential of node *k* (*k* = 1, 2, 3) for the *i*th element. This can be written in matrix notation as a *quadratic form* as

$$W^{(i)} = \frac{1}{2} \phi^{(i)t} \mathbf{C}^{(i)} \phi^{(i)} \quad (5.117a)$$

where

$$\phi^{(i)} = \begin{bmatrix} \phi_1^{(i)} \\ \phi_2^{(i)} \\ \phi_3^{(i)} \end{bmatrix} \quad (5.117b)$$

and superscript *t* denotes transpose. The matrix

$$\mathbf{C}^{(i)} = \begin{bmatrix} C_{11}^{(i)} & C_{12}^{(i)} & C_{13}^{(i)} \\ C_{12}^{(i)} & C_{22}^{(i)} & C_{23}^{(i)} \\ C_{13}^{(i)} & C_{23}^{(i)} & C_{33}^{(i)} \end{bmatrix} \quad (5.117c)$$

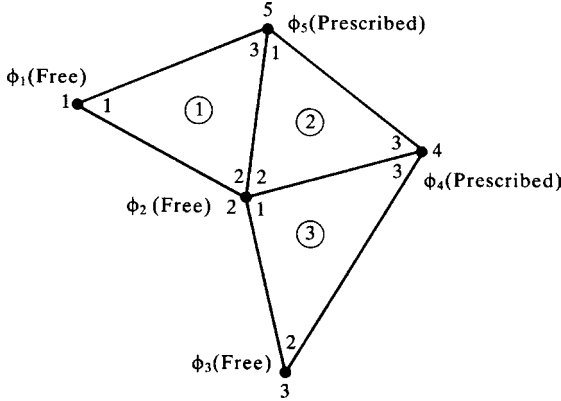


FIGURE 5.44 An example to illustrate the use of the FEM.

is referred to as the *local coefficient matrix* with entries

$$C_{mn}^{(i)} = \frac{\epsilon_i}{4A_i} (Y_{im}Y_{in} + X_{im}X_{in}) \tag{5.117d}$$

Now, we must assemble the total energy expression for a system that is approximated by finite elements according to (5.114). In order to illustrate this, consider the example of a region that is represented by three finite elements shown in Figure 5.44. The node numbers inside the elements are the *local node numbers* as used above. The *global node numbers* are shown uniquely for the five nodes. Nodes 1, 2, and 3 are *free nodes* whose potential is to be determined to satisfy Laplace’s equation in the region. Nodes 4 and 5 are *prescribed nodes* whose potentials are fixed (known). The total energy expression can be written in terms of the global nodes as

$$W = \sum_{i=1}^{N_e} W^{(i)} = \frac{1}{2} \phi^t C \phi \tag{5.118a}$$

where the vector of global node potentials is

$$\phi = \begin{bmatrix} \phi_1 = \phi_1^{(1)} \\ \phi_2 = \phi_2^{(1)} = \phi_2^{(2)} = \phi_1^{(3)} \\ \phi_3 = \phi_2^{(3)} \\ \phi_4 = \phi_3^{(2)} = \phi_3^{(3)} \\ \phi_5 = \phi_3^{(1)} = \phi_1^{(2)} \end{bmatrix} \tag{5.118b}$$

and

$$\mathbf{C} = \begin{bmatrix} C_{11} & C_{12} & C_{13} & C_{14} & C_{15} \\ C_{12} & C_{22} & C_{23} & C_{24} & C_{25} \\ C_{13} & C_{23} & C_{33} & C_{34} & C_{35} \\ C_{14} & C_{24} & C_{34} & C_{44} & C_{45} \\ C_{15} & C_{25} & C_{35} & C_{45} & C_{55} \end{bmatrix} \quad (5.118c)$$

This *global coefficient matrix* \mathbf{C} , like the local coefficient matrix, can be shown to be symmetric by energy considerations [9]. The entries in the global coefficient matrix can be assembled quite easily from the local coefficient matrix (whose entries are computed for the isolated elements independent of their future connection) with the following observation. For each element write the global coefficient matrix as

$$W^{(1)} = \phi^t \begin{bmatrix} C_{11}^{(1)} & C_{12}^{(1)} & 0 & 0 & C_{13}^{(1)} \\ C_{12}^{(1)} & C_{22}^{(1)} & 0 & 0 & C_{23}^{(1)} \\ 0 & 0 & 0 & 0 & 0 \\ 0 & 0 & 0 & 0 & 0 \\ C_{13}^{(1)} & C_{23}^{(1)} & 0 & 0 & C_{33}^{(1)} \end{bmatrix} \phi \quad (5.119a)$$

$$W^{(2)} = \phi^t \begin{bmatrix} 0 & 0 & 0 & 0 & 0 \\ 0 & C_{22}^{(2)} & 0 & C_{23}^{(2)} & C_{12}^{(2)} \\ 0 & 0 & 0 & 0 & 0 \\ 0 & C_{23}^{(2)} & 0 & C_{33}^{(2)} & C_{13}^{(2)} \\ 0 & C_{12}^{(2)} & 0 & C_{13}^{(2)} & C_{11}^{(2)} \end{bmatrix} \phi \quad (5.119b)$$

$$W^{(3)} = \phi^t \begin{bmatrix} 0 & 0 & 0 & 0 & 0 \\ 0 & C_{11}^{(3)} & C_{12}^{(3)} & C_{13}^{(3)} & 0 \\ 0 & C_{12}^{(3)} & C_{22}^{(3)} & C_{23}^{(3)} & 0 \\ 0 & C_{13}^{(3)} & C_{23}^{(3)} & C_{33}^{(3)} & 0 \\ 0 & 0 & 0 & 0 & 0 \end{bmatrix} \phi \quad (5.119c)$$

Assembling these according to (5.118) gives the total energy

$$\begin{aligned}
 W &= W^{(1)} + W^{(2)} + W^{(3)} \\
 &= \phi^t \begin{bmatrix} C_{11}^{(1)} & C_{12}^{(1)} & 0 & 0 & C_{13}^{(1)} \\ C_{12}^{(1)} & C_{22}^{(1)} + C_{22}^{(2)} + C_{11}^{(3)} & C_{12}^{(3)} & C_{23}^{(2)} + C_{13}^{(3)} & C_{23}^{(1)} + C_{12}^{(2)} \\ 0 & C_{12}^{(3)} & C_{22}^{(3)} & C_{23}^{(3)} & 0 \\ 0 & C_{23}^{(2)} + C_{13}^{(3)} & C_{23}^{(3)} & C_{33}^{(2)} + C_{33}^{(3)} & C_{13}^{(2)} \\ C_{13}^{(1)} & C_{23}^{(1)} + C_{12}^{(2)} & 0 & C_{13}^{(2)} & C_{33}^{(1)} + C_{11}^{(2)} \end{bmatrix} \phi
 \end{aligned} \tag{5.120}$$

A very simple rule for assembling this global coefficient matrix can be developed from this example. The main diagonal terms are the sums of the main diagonal terms of the local coefficient matrices for those elements that connect to this global node. The off-diagonal terms are the sums of the off-diagonal terms of the local coefficient matrices whose sides connect the two global nodes. Observe that the off-diagonal terms will have at most two entries, whereas the main diagonal terms will be the sum of a number of terms equal to the number of elements that share the global node.

Now it remains to differentiate this result with respect to the free nodes to insure minimum energy of the system thereby satisfying Laplace’s equation. To that end, let us number the global nodes by numbering the free nodes first and then numbering the prescribed (fixed potential) nodes last. The above energy expression can then be written in partitioned form as

$$\begin{aligned}
 W &= \frac{1}{2} [\phi_f^t \ \phi_p^t] \begin{bmatrix} \mathbf{C}_{ff} & \mathbf{C}_{fp} \\ \mathbf{C}_{pf} & \mathbf{C}_{pp} \end{bmatrix} \begin{bmatrix} \phi_f \\ \phi_p \end{bmatrix} \\
 &= \frac{1}{2} [\phi_f^t \mathbf{C}_{ff} \phi_f + \phi_f^t \mathbf{C}_{fp} \phi_p + \phi_p^t \mathbf{C}_{pf} \phi_f + \phi_p^t \mathbf{C}_{pp} \phi_p]
 \end{aligned} \tag{5.121}$$

Differentiating this with respect to the free node potentials and setting the result to zero gives the final equations to be solved:

$$\mathbf{C}_{ff} \phi_f = -\mathbf{C}_{fp} \phi_p \tag{5.122}$$

Solving this matrix equation for the free node potentials is referred to as the *direct method* of solving the FEM equations.

Observe from the example of Figure 5.44 that the global coefficient matrix \mathbf{C} has a number of zero entries. This is quite evident as only those (two) elements that contain the nodes for this entry will contribute a nonzero term. Thus, the coefficient matrices in (5.122) will be *sparse*. Although there exist sparse matrix solution routines that efficiently take advantage of this, FEM problems, particularly large ones, are generally solved more efficiently using the *iterative method*. This is similar to the iterative method for the finite-difference technique in that the free nodes are initially

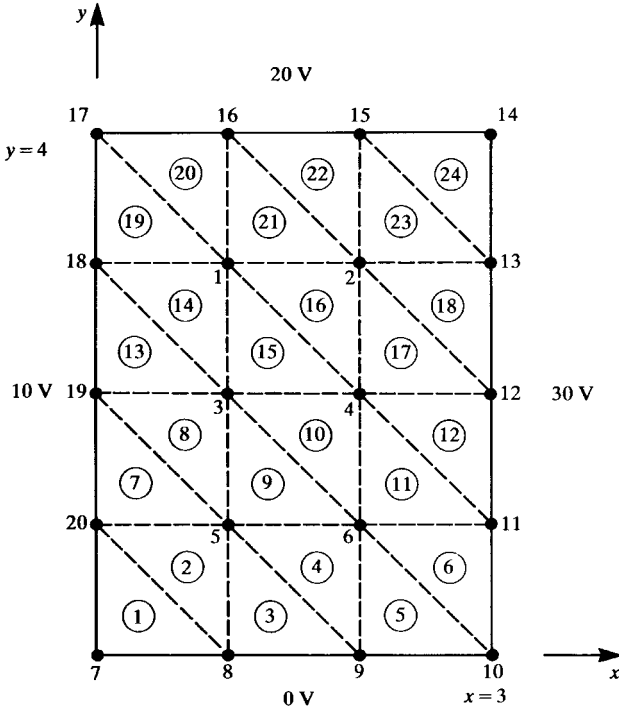


FIGURE 5.45 Illustration of the FEM applied to a previously solved problem.

prescribed some starting value (such as zero) and the new values of the free node potentials are computed. The process continues until the change in the free node potentials between iteration steps is less than some value. Writing out (5.122) for the example of Figure 5.44 gives

$$\begin{bmatrix} C_{11} & C_{12} & C_{13} \\ C_{12} & C_{22} & C_{23} \\ C_{13} & C_{23} & C_{33} \end{bmatrix} \begin{bmatrix} \phi_1 \\ \phi_2 \\ \phi_3 \end{bmatrix} + \begin{bmatrix} C_{14} & C_{15} \\ C_{24} & C_{25} \\ C_{34} & C_{35} \end{bmatrix} \begin{bmatrix} \phi_4 \\ \phi_5 \end{bmatrix} = \begin{bmatrix} 0 \\ 0 \\ 0 \end{bmatrix} \quad (5.123)$$

Writing this in terms of each free potential with respect to the other free potentials and the prescribed potentials gives

$$\phi_f^{\text{new}} = - \begin{bmatrix} 0 & C_{12}/C_{11} & C_{13}/C_{11} \\ C_{12}/C_{22} & 0 & C_{23}/C_{22} \\ C_{13}/C_{33} & C_{23}/C_{33} & 0 \end{bmatrix} \phi_f^{\text{old}} + \begin{bmatrix} C_{14}/C_{11} & C_{15}/C_{11} \\ C_{24}/C_{22} & C_{25}/C_{22} \\ C_{34}/C_{33} & C_{35}/C_{33} \end{bmatrix} \phi_p \quad (5.124a)$$

TABLE 5.9

| | Direct method | Iteration | Exact |
|----------|---------------|-----------|---------|
| ϕ_1 | 16.4389 | 16.4389 | 16.4784 |
| ϕ_2 | 21.6563 | 21.6563 | 21.8499 |
| ϕ_3 | 14.0994 | 14.0994 | 14.1575 |
| ϕ_4 | 20.1863 | 20.1863 | 20.4924 |
| ϕ_5 | 9.77226 | 9.77224 | 9.60942 |
| ϕ_6 | 14.9896 | 14.9896 | 14.9810 |

where

$$\phi = \begin{bmatrix} \phi_1 \\ \phi_2 \\ \phi_3 \end{bmatrix} \quad (5.124b)$$

$$\phi_p = \begin{bmatrix} \phi_4 \\ \phi_5 \end{bmatrix} \quad (5.124c)$$

As a numerical illustration of the method, consider the problem of a rectangular region of side lengths 4 and 3 with prescribed potentials of 0 V, 10 V, 20 V, and 30 V as shown in Figure 5.20. This was solved earlier with the MoM technique and the finite-difference technique. In order to compare this with the finite-difference technique, we will again choose six interior nodes and approximate the space between these nodes with 24 finite elements as shown in Figure 5.45. Observe that the potentials at nodes 7, 10, 14, and 17 are not known since there are gaps between the adjacent conductors. We will prescribe these potentials as the average of the adjacent conductor potentials or 5 V, 15 V, 25 V, and 15 V. The solution for the six interior node potentials via the direct and the iterative method become as shown in Table 5.9. The iterative method converged after 15 iterations.

Some of the important features of the FEM are that it can handle irregular boundaries as well as inhomogeneous media. Inhomogeneous media are handled by ensuring that the region is subdivided such that each finite element covers (approximately) a homogeneous subregion. The permittivities of the finite elements, ϵ_i , are contained in the $C_{mn}^{(i)}$ local node coefficients.

Once again, as with the finite-difference method, the finite-element method is most suited to closed systems. For open systems whose boundaries extend to infinity, an infinite mesh method can be developed [4] or the mesh can be extended sufficiently far from the main areas of interest and artificially terminated in zero potential thereby forming a (artificial) closed system.

The FEM is a highly versatile method for solving Laplace's equation as well as other electromagnetic fields problems [4, 9]. Other parameters of interest such as capacitances can be determined in the usual fashion by determining the resulting

charge on the conductors as the normal component of the displacement vector just off the conductor surfaces.

PROBLEMS

- 5.1** Demonstrate the generalized capacitance relations in (5.21).
- 5.2** Show the result in (5.22).
- 5.3** Demonstrate the result in (5.23) for $(n + 1)$ widely spaced wires.
- 5.4** Determine the per-unit-length inductances for a three-wire ribbon cable where the center wire is chosen as the reference conductor. $[l_{11} = l_{22} = (\mu_0/\pi)\ln(d/r_w), l_{12} = (\mu_0/2\pi)\ln(d/2r_w)]$ Evaluate these for a center-to-center wire spacing of 50 mils and #28 gauge stranded wires having wire radii of $r_w = 7.5$ mils. $[l_{11} = l_{22} = 0.759\mu\text{H/m} = 19.3\text{ nH/in.}, l_{12} = 0.24\mu\text{ H/m} = 6.1\text{ nH/in.}]$. Determine the per-unit-length capacitances (neglecting the wire insulations) from these. $[c_{11} = c_{22} = 11.1\text{ pF/m} = 0.28\text{ pF/in.}, c_{12} = 5.17\text{ pF/m} = 0.13\text{ pF/in.}]$
- 5.5** Repeat the calculations of problem 5.4 using WIDSESEP.FOR. $[l_{11} = l_{22} = 0.7588\mu\text{H/m}, l_{12} = 0.2408\mu\text{ H/m}, c_{11} = c_{22} = 11.13\text{ pF/m}, c_{12} = 5.174\text{ pF/m}]$
- 5.6** Demonstrate the relations in (5.25) for n wires above an infinite, perfectly conducting ground plane.
- 5.7** Determine the per-unit-length inductances for two wires at an equal height above a ground plane and separation s . $[l_{11} = l_{22} = (\mu_0/2\pi)\ln(2h/r_w), l_{12} = (\mu_0/4\pi)\ln(1+4(h^2/s^2))]$ Evaluate these for a center-to-center wire spacing of 2 cm, a height of 2 cm and #20 gauge solid wires having wire radii of $r_w = 16$ mils. $[l_{11} = l_{22} = 0.918\mu\text{ H/m} = 23.3\text{ nH/in.}, l_{12} = 0.161\mu\text{ H/m} = 4.09\text{ nH/in.}]$. Determine the per-unit-length capacitances (neglecting the wire insulations) from these. $[c_{11} = c_{22} = 10.3\text{ pF/m}, c_{12} = 2.19\text{ pF/m}]$
- 5.8** Repeat the calculations of problem 5.7 using WIDSESEP.FOR. $[l_{11} = l_{22} = 0.9178\mu\text{ H/m}, l_{12} = 0.1609\mu\text{ H/m}, c_{11} = c_{22} = 10.314\text{ pF/m}, c_{12} = 2.193\text{ pF/m}]$
- 5.9** Demonstrate the relations in (5.26) for n wires within an overall shield.
- 5.10** Determine the per-unit-length inductances for two wires within an overall shield where the wires are #28 gauge stranded having wire radii of $r_w = 7.5$ mils. The wires are separated by 180° , the shield radius is $r_S = 4r_w$, and the distance of each wire from the center is two wire radii. This is typical for shielded pairs of wires where the wire insulation thicknesses are equal to the wire radii. $[l_{11} = l_{22} = 0.22\mu\text{H/m}, l_{12} = 44.6\text{ nH/m}]$

- 5.11** Repeat the calculations of Problem 5.10 using `WIDSESEP.FOR`. [$l_{11} = l_{22} = 0.2197\mu\text{H/m}$, $l_{12} = 44.63\text{nH/m}$, $c_{11} = c_{22} = 42.1\text{pF/m}$, $c_{12} = 10.73\text{pF/m}$]
- 5.12** Demonstrate the results in Table 5.1.
- 5.13** Demonstrate the results in Tables 5.2 and 5.3.
- 5.14** Demonstrate the results in (5.48).
- 5.15** Determine, using `RIBBON.FOR`, the results in Tables 5.5 and 5.6 for a three-wire ribbon cable consisting of #28 gauge stranded wires ($r_w = 7.5$ mils) with insulation thicknesses of 10 mils and $\epsilon_r = 3.5$ and separations of 50 mils but with the center wire chosen as the reference conductor. [$l_{11} = l_{22} = 0.7485\mu\text{H/m}$, $l_{12} = 0.2408\mu\text{H/m}$, $c_{11} = c_{22} = 24.98\text{pF/m}$, $c_{12} = 6.266\text{pF/m}$]
- 5.16** Demonstrate the relations in (5.65) and (5.67).
- 5.17** Demonstrate the relations in (5.75) and (5.76).
- 5.18** Demonstrate the relations in (5.78).
- 5.19** Determine the per-unit-length inductances and capacitances for a three-conductor PCB having land widths of 25 mils, a board thickness of 30 mils, and an edge-to-edge separation of 10 mils and $\epsilon_r = 4.7$ using `PCB.FOR`. Use 30 divisions per land and choose the reference conductor to be the center land. [$l_{11} = l_{22} = 0.626\mu\text{H/m}$, $l_{12} = 0.1812\mu\text{H/m}$, $c_{11} = c_{22} = 38.35\text{pF/m}$, $c_{12} = 11.197\text{pF/m}$]
- 5.20** Demonstrate the relations in (5.83).
- 5.21** Determine the per-unit-length inductances and capacitances for a two-conductor coupled microstrip having land widths of 25 mils, a board thickness of 30 mils, and an edge-to-edge separation of 10 mils and $\epsilon_r = 4.7$ using `MSTRP.FOR`. Use 30 divisions per land and choose the reference conductor to be the center land. [$l_{11} = l_{22} = 0.4484\mu\text{H/m}$, $l_{12} = 0.1543\mu\text{H/m}$, $c_{11} = c_{22} = 65.26\text{pF/m}$, $c_{12} = 22.92\text{pF/m}$]
- 5.22** Demonstrate the relations in (5.95) and (5.97).
- 5.23** Determine the per-unit-length inductances and capacitances for a two-conductor coupled stripline having land widths of 25 mils, a separation between the two ground planes of 30 mils, and an edge-to-edge separation of 10 mils and $\epsilon_r = 4.7$ using `STRPLINE.FOR`. Use 30 divisions per land and choose the reference conductor to be the center land. [$l_{11} = l_{22} = 0.2466\mu\text{H/m}$, $l_{12} = 21.6\text{nH/m}$, $c_{11} = c_{22} = 195\text{pF/m}$, $c_{12} = 18.72\text{pF/m}$]
- 5.24** Demonstrate the relation for the finite-difference method in (5.102).
- 5.25** Reproduce the results in Table 5.8 for the finite-difference method.

- 5.26 Demonstrate the relations in (5.111) for the finite-element method.
- 5.27 Demonstrate the relation in (5.116) for the finite-element method.
- 5.28 Reproduce the results in Table 5.9 for the finite-element method.

REFERENCES

- [1] W.R. Smythe, *Static and Dynamic Electricity*, 3rd edition, McGraw-Hill, New York, 1968.
- [2] A.T. Adams, *Electromagnetics for Engineers*, Ronald Press, New York, 1971.
- [3] R.F. Harrington, *Field Computation by Moment Methods*, Macmillan, New York, 1968.
- [4] M.N. O. Sadiku, *Numerical Techniques in Electromagnetics*, CRC Press, Boca Raton, FL, 1992.
- [5] W.T. Weeks, Calculation of coefficients of capacitance of multiconductor transmission lines in the presence of a dielectric interface, *IEEE Transactions on Microwave Theory and Techniques*, **18** (1), 35–43, 1970.
- [6] R.E. Collin, *Field Theory of Guided Waves*, 2nd edition, IEEE Press, New York, 1991.
- [7] H.B. Dwight, *Tables of Integrals and Other Mathematical Data*, 4th edition, Macmillan, New York, 1961.
- [8] M.Javid, and P.M. Brown, *Field Analysis and Electromagnetics*, McGraw-Hill, New York, 1963.
- [9] P.P. Sylvestor, and R.L. Ferrari, *Finite Elements for Electrical Engineers*, 2nd Edition, Cambridge University Press, New York, 1990.

6

FREQUENCY-DOMAIN ANALYSIS OF TWO-CONDUCTOR LINES

In this chapter, we will examine the solution of the transmission-line equations for two-conductor lines, where the line is excited by a single-frequency sinusoidal signal and is in steady state. The analysis method is the familiar phasor technique of electric circuit analysis [A.2, A.5]. The excitation sources for the line are single-frequency sinusoidal waveforms such as $x(t) = X\cos(\omega t + \theta_X)$. Again, as explained in Chapter 1, the reason we invest so much time and interest in this form of line excitation is that we may decompose any other *periodic* waveform into an infinite sum of sinusoidal signals that have frequencies that are multiples of the basic repetition frequency of the signal via the Fourier series. We may then obtain the response to the original waveform as the superposition of the responses to those single-frequency harmonic components of the (nonsinusoidal) periodic input signal (see Figure 1.21 of Chapter 1). In the case of a nonperiodic waveform, we may similarly decompose the signal into a continuum of sinusoidal components via the Fourier transform and the analysis process remains unchanged. An additional reason for the importance of the frequency-domain method is that losses (of the conductors and the surrounding dielectric) can easily be handled in the frequency domain, whereas their inclusion in a time-domain analysis is problematic as we will see in Chapters 8 and 9. The per-unit-length resistance of the line conductors at high frequencies increases as the square root of the frequency, \sqrt{f} , because of skin effect, whereas the per-unit-length conductance of a homogeneous surrounding dielectric is also frequency dependent. In the frequency domain, we simply evaluate these at the frequency of interest and treat them as constants throughout the analysis.

For the phasor method, we replace the excitation signal with its phasor equivalent as

$$x(t) \Leftrightarrow \hat{X}(j\omega) \quad (6.1a)$$

where

$$\begin{aligned} \hat{X}(j\omega) &= X \angle \theta_X \\ &= X e^{j\theta_X} \end{aligned} \quad (6.1b)$$

We return to the time domain using Euler's identity by (1) multiplying the phasor result by $e^{j\omega t}$ and (2) taking the real part of the result:

$$\begin{aligned} x(t) &= X \cos(\omega t + \theta_X) \\ &= \operatorname{Re} \left\{ \underbrace{X \angle \theta_X}_{\hat{X}} e^{j\omega t} \right\} \end{aligned} \quad (6.2)$$

6.1 THE TRANSMISSION-LINE EQUATIONS IN THE FREQUENCY DOMAIN

We form the phasor or *frequency-domain* differential equations by replacing all time derivatives with $j\omega$ as

$$\frac{\partial}{\partial t} \Leftrightarrow j\omega \quad (6.3)$$

In the case of a *lossless line*, this reduces the time-domain partial differential transmission-line equations to their frequency-domain equivalent as

$$\frac{\partial}{\partial z} V(z, t) = -l \frac{\partial}{\partial t} I(z, t) \Leftrightarrow \frac{d}{dz} \hat{V}(z) = -j\omega l \hat{I}(z) \quad (6.4a)$$

$$\frac{\partial}{\partial z} I(z, t) = -c \frac{\partial}{\partial t} V(z, t) \Leftrightarrow \frac{d}{dz} \hat{I}(z) = -j\omega c \hat{V}(z) \quad (6.4b)$$

Observe that the frequency-domain or phasor transmission-line equations become ordinary differential equations because they are functions of only one variable, the line axis variable z . This is another important reason we go to the frequency domain: the solution of the transmission-line equations is simpler. Once we solve the phasor transmission-line ordinary differential equations in (6.4) and incorporate the terminal constraints at the left and right ends of the line, we return to the time domain by (1) multiplying the phasor solutions $\hat{V}(z)$ and $\hat{I}(z)$ by $e^{j\omega t}$ and (2) taking the real

part of that result as

$$\begin{aligned} V(z, t) &= \operatorname{Re} \left\{ \underbrace{V \angle \theta_V}_{\hat{V}(z)} e^{j\omega t} \right\} \\ &= V(z) \cos(\omega t + \theta_V(z)) \end{aligned} \quad (6.5a)$$

and

$$\begin{aligned} I(z, t) &= \operatorname{Re} \left\{ \underbrace{I \angle \theta_I}_{\hat{I}(z)} e^{j\omega t} \right\} \\ &= I(z) \cos(\omega t + \theta_I(z)) \end{aligned} \quad (6.5b)$$

Losses of the line are incorporated via the per-unit-length resistance of the conductors, $r(\sqrt{f})$, and the per-unit-length conductance of the surrounding medium, $g(f)$. The frequency-domain transmission-line equations in (6.4) are amended to

$$\frac{d}{dz} \hat{V}(z) = - \underbrace{(r + j\omega l)}_{\hat{z}} \hat{I}(z) \quad (6.6a)$$

$$\frac{d}{dz} \hat{I}(z) = - \underbrace{(g + j\omega c)}_{\hat{y}} \hat{V}(z) \quad (6.6b)$$

We will first examine the solution for a lossless line and then easily modify that solution for a lossy line.

6.2 THE GENERAL SOLUTION FOR LOSSLESS LINES

The transmission-line equations for a *lossless* line are given in (6.4) and repeated here:

$$\frac{d}{dz} \hat{V}(z) = -j\omega l \hat{I}(z) \quad (6.7a)$$

$$\frac{d}{dz} \hat{I}(z) = -j\omega c \hat{V}(z) \quad (6.7b)$$

These coupled first-order differential equations can be converted to uncoupled second-order differential equations in the usual manner by differentiating each with respect to z and substituting the other to yield ($j^2 = -1$)

$$\frac{d^2}{dz^2} \hat{V}(z) = -\omega^2 lc \hat{V}(z) \quad (6.8a)$$

$$\frac{d^2}{dz^2} \hat{I}(z) = -\omega^2 lc \hat{I}(z) \quad (6.8b)$$

The general solution to these coupled second-order equations is again [A.1, A.6]

$$\hat{V}(z) = \hat{V}^+ e^{-j\beta z} + \hat{V}^- e^{j\beta z} \quad (6.9a)$$

and

$$\hat{I}(z) = \frac{\hat{V}^+}{Z_C} e^{-j\beta z} - \frac{\hat{V}^-}{Z_C} e^{j\beta z} \quad (6.9b)$$

where the phase constant is again denoted as

$$\begin{aligned} \beta &= \omega \sqrt{lc} \\ &= \frac{\omega}{v} \text{ (rad/m)} \end{aligned} \quad (6.10)$$

and the phase velocity of propagation is

$$\begin{aligned} v &= \omega / \beta \\ &= 1 / \sqrt{lc} \end{aligned} \quad (6.11)$$

If the line is immersed in a *homogeneous medium* characterized by permittivity ε and permeability μ , then $lc = \mu\varepsilon$ and $v = 1/\sqrt{\mu\varepsilon}$. Hence, these TEM waves travel at the speed of light in that medium. The phase constant β represents a *phase shift* as the waves propagate along the line. The quantities \hat{V}^+ and \hat{V}^- are, as yet, undetermined constants. These will be determined by the specific load and source parameters. The line *characteristic impedance* is denoted as

$$Z_C = \sqrt{l/c} \quad (6.12)$$

The source and load configurations at $z = 0$ and at $z = \mathcal{L}$ are shown in Figure 6.1. In the frequency-domain representation, we may easily include inductors and

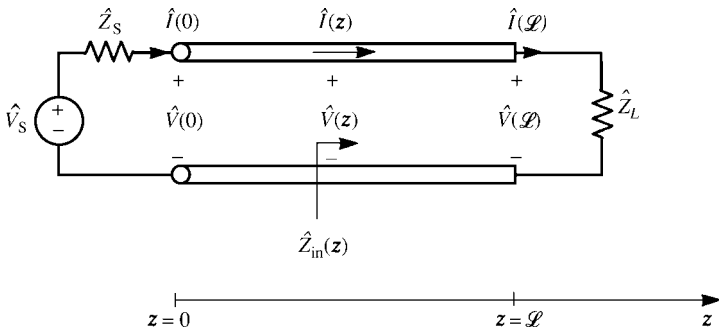


FIGURE 6.1 Definition of the parameters of a two-conductor line in the frequency domain.

capacitors in those complex-valued impedances, \hat{Z}_S and \hat{Z}_L . Once we incorporate the source and load terminal constraints into the general solution in (6.9) and determine the complex-valued constants \hat{V}^+ and \hat{V}^- , we can return to the time domain in the usual fashion by (1) multiplying the phasor result by $e^{j\omega t}$ and (2) taking the real part of the result to yield

$$\begin{aligned} V(z, t) &= \text{Re}\{V^+ e^{j\theta^+} e^{-j\beta z} e^{j\omega t} + V^- e^{j\theta^-} e^{j\beta z} e^{j\omega t}\} \\ &= \underbrace{V^+ \cos(\omega t - \beta z + \theta^+)}_{\substack{\text{forward-traveling} \\ +z \text{ wave}}} + \underbrace{V^- \cos(\omega t + \beta z + \theta^-)}_{\substack{\text{backward-traveling} \\ -z \text{ wave}}} \end{aligned} \quad (6.13a)$$

and

$$\begin{aligned} I(z, t) &= \text{Re}\left\{\frac{V^+}{Z_C} e^{j\theta^+} e^{-j\beta z} e^{j\omega t} - \frac{V^-}{Z_C} e^{j\theta^-} e^{j\beta z} e^{j\omega t}\right\} \\ &= \underbrace{\frac{V^+}{Z_C} \cos(\omega t - \beta z + \theta^+)}_{\substack{\text{forward-traveling} \\ +z \text{ wave}}} - \underbrace{\frac{V^-}{Z_C} \cos(\omega t + \beta z + \theta^-)}_{\substack{\text{backward-traveling} \\ -z \text{ wave}}} \end{aligned} \quad (6.13b)$$

where the undetermined constants are, in general, complex as $\hat{V}^\pm = V^\pm \angle \theta^\pm = V^\pm e^{j\theta^\pm}$. Observe that the characteristic impedance is the ratio of the voltage and current in the forward-traveling wave and the ratio of the voltage and current in the backward-traveling wave. Also, observe from (6.13) that since $\beta = \omega/v$, we may write

$$(\omega t \pm \beta z) \Leftrightarrow \omega(t \pm z/v)$$

This shows that the phase-shift term in the frequency-domain representation, $e^{\pm j\beta z}$, is equivalent in the time domain to a *time delay* ($t \pm z/v$).

6.2.1 The Reflection Coefficient and Input Impedance

In order to incorporate the source and load into the general solution, we define a voltage reflection coefficient as the ratio of the (phasor) voltages in the backward-traveling and forward-traveling waves:

$$\begin{aligned} \hat{\Gamma}(z) &= \frac{\hat{V}^- e^{j\beta z}}{\hat{V}^+ e^{-j\beta z}} \\ &= \frac{\hat{V}^-}{\hat{V}^+} e^{j2\beta z} \end{aligned} \quad (6.14)$$

The general solution in (6.9) for the phasor voltage and current along the line can be written in terms of the reflection coefficient at that point by substituting (6.14):

$$\hat{V}(z) = \hat{V}^+ e^{-j\beta z} [1 + \hat{\Gamma}(z)] \quad (6.15a)$$

and

$$\hat{I}(z) = \frac{\hat{V}^+}{Z_C} e^{-j\beta z} [1 - \hat{\Gamma}(z)] \quad (6.15b)$$

Evaluating the general expression for the reflection coefficient anywhere along the line given in (6.14) at the load, $z = \mathcal{L}$, gives

$$\hat{\Gamma}_L = \frac{\hat{V}^-}{\hat{V}^+} e^{j2\beta\mathcal{L}} \quad (6.16)$$

At the load, the phasor voltage and current are related by Ohm's law as

$$\hat{V}(\mathcal{L}) = \hat{Z}_L \hat{I}(\mathcal{L}) \quad (6.17)$$

Substituting (6.15) evaluated at the load, $z = \mathcal{L}$, gives

$$\hat{Z}_L = Z_C \frac{1 + \hat{\Gamma}_L}{1 - \hat{\Gamma}_L} \quad (6.18)$$

Solving this gives reflection coefficient at the load:

$$\hat{\Gamma}_L = \frac{\hat{Z}_L - Z_C}{\hat{Z}_L + Z_C} \quad (6.19)$$

Substituting (6.16) into (6.14) gives an expression for the reflection coefficient at any point along the line in terms of the load reflection coefficient, which can be directly calculated via (6.19):

$$\hat{\Gamma}(z) = \hat{\Gamma}_L e^{j2\beta(z-\mathcal{L})} \quad (6.20)$$

Substituting the explicit relation for the reflection coefficient in terms of the load reflection coefficient given in (6.20) into (6.15) gives a general expression for the phasor voltage and current anywhere on the line as

$$\hat{V}(z) = \hat{V}^+ e^{-j\beta z} \left[1 + \hat{\Gamma}_L e^{j2\beta(z-\mathcal{L})} \right] \quad (6.21a)$$

and

$$\hat{I}(z) = \frac{\hat{V}^+}{Z_C} e^{-j\beta z} \left[1 - \hat{\Gamma}_L e^{j2\beta(z-\mathcal{L})} \right] \quad (6.21b)$$

An important parameter of the line is the input impedance to the line at any point on the line. The input impedance is the ratio of the total voltage and current at that

point as shown in Figure 6.1:

$$\begin{aligned}\hat{Z}_{\text{in}}(z) &= \frac{\hat{V}(z)}{\hat{I}(z)} \\ &= Z_C \frac{[1 + \hat{\Gamma}(z)]}{[1 - \hat{\Gamma}(z)]}\end{aligned}\quad (6.22)$$

where we have substituted (6.15). The process for determining the input impedance is to (1) compute the load reflection coefficient from (6.19), (2) compute the reflection coefficient at the desired point from (6.20), and (3) then substitute that result into (6.22).

An important position to calculate the input impedance is at the input to the entire line, $z = 0$. The reflection coefficient at the input to the line is obtained from (6.20):

$$\hat{\Gamma}(0) = \hat{\Gamma}_L e^{-j2\beta \mathcal{L}} \quad (6.23)$$

Hence, the input impedance to a line of length \mathcal{L} is

$$\begin{aligned}\hat{Z}_{\text{in}}(0) &= Z_C \frac{[1 + \hat{\Gamma}(0)]}{[1 - \hat{\Gamma}(0)]} \\ &= Z_C \frac{[1 + \hat{\Gamma}_L e^{-j2\beta \mathcal{L}}]}{[1 - \hat{\Gamma}_L e^{-j2\beta \mathcal{L}}]}\end{aligned}\quad (6.24)$$

An explicit formula for this input impedance to the line can be obtained as [A.1, A.6]

$$\hat{Z}_{\text{in}}(0) = Z_C \frac{\hat{Z}_L + jZ_C \tan(\beta \mathcal{L})}{Z_C + j\hat{Z}_L \tan(\beta \mathcal{L})} \quad (6.25)$$

A *matched line* is one in which the load impedance is equal to the characteristic impedance, $\hat{Z}_L = Z_C$. Hence, from (6.25) or (6.24) with $\hat{\Gamma}_L = 0$, the input impedance to a matched line is equal to the characteristic impedance at all points along the line and is purely resistive. Observe that for a lossless line the characteristic impedance $Z_C = \sqrt{l/c}$ is a real number. Hence, in order to match a lossless line the load impedance can only be purely resistive. A few other interesting facts may be observed from (6.25). Substituting $\beta = 2\pi/\lambda$, where the wavelength at the frequency of excitation of the line is $\lambda = v/f$, yields

$$\hat{Z}_{\text{in}}(0) = Z_C \frac{\hat{Z}_L + jZ_C \tan\left(\frac{2\pi \mathcal{L}}{\lambda}\right)}{Z_C + j\hat{Z}_L \tan\left(\frac{2\pi \mathcal{L}}{\lambda}\right)} \quad (6.26)$$

For a line that is one-quarter wavelength long, that is, $\mathcal{L} = \lambda/4$, (6.26) becomes

$$\hat{Z}_{\text{in}}(0) = \frac{Z_C^2}{\hat{Z}_L}, \quad \mathcal{L} = \lambda/4 \quad (6.27)$$

If the load is an open circuit, $\hat{Z}_L = \infty$, then the input impedance to a quarter-wavelength section is a short circuit, $\hat{Z}_{in}(0) = 0$. Conversely, if the load is a short circuit, $\hat{Z}_L = 0$, then the input impedance to a quarter-wavelength section is an open circuit, $\hat{Z}_{in}(0) = \infty$. Also, (6.26) shows that for lengths of line that are a multiple of a half wavelength, that is, $\mathcal{L} = n(\lambda/2)$ for $n = 1, 2, 3, \dots$, the input impedance replicates, that is,

$$\begin{aligned}\hat{Z}_{in}(0) &= Z_C \frac{\hat{Z}_L + jZ_C \tan(n\pi)}{Z_C + j\hat{Z}_L \tan(n\pi)} \\ &= Z_L, \quad \mathcal{L} = n(\lambda/2)\end{aligned}\quad (6.28)$$

and

$$\hat{Z}_{in}\left(z \pm n\frac{\lambda}{2}\right) = \hat{Z}_{in}(z) \quad (6.29)$$

This result applies even if the line is not matched.

6.2.2 Solutions for the Terminal Voltages and Currents

In general, we will only be interested in determining the current and voltage at the input and output of the line. Evaluating (6.15) at $z = 0$ and $z = \mathcal{L}$ gives

$$\hat{V}(0) = \hat{V}^+ [1 + \hat{\Gamma}(0)] \quad (6.30a)$$

$$\hat{I}(0) = \frac{\hat{V}^+}{Z_C} [1 - \hat{\Gamma}(0)] \quad (6.30b)$$

and

$$\hat{V}(\mathcal{L}) = \hat{V}^+ e^{-j\beta\mathcal{L}} [1 + \hat{\Gamma}_L] \quad (6.31a)$$

$$\hat{I}(\mathcal{L}) = \frac{\hat{V}^+}{Z_C} e^{-j\beta\mathcal{L}} [1 - \hat{\Gamma}_L] \quad (6.31b)$$

If we can determine the undetermined constant \hat{V}^+ , then we can determine the source and load voltages and currents by substituting into (6.30) and (6.31).

In order to determine this undetermined constant, a convenient position to evaluate it is at the input to the line, $z = 0$. At the line input, the line can be replaced by the input impedance to the line as shown in Figure 6.2. The input voltage to the line can be determined by voltage division as

$$\hat{V}(0) = \frac{\hat{Z}_{in}(0)}{\hat{Z}_S + \hat{Z}_{in}(0)} \hat{V}_S \quad (6.32)$$

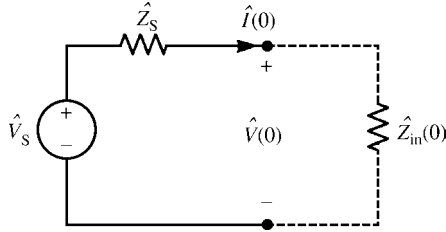


FIGURE 6.2 Determination of the phasor input voltage of the line.

Hence, the undetermined constant is determined from (6.30a) as

$$\hat{V}^+ = \frac{\hat{V}(0)}{[1 + \hat{\Gamma}(0)]} \tag{6.33}$$

The process of determining the input and output voltages and currents to the line is

1. Determine the load reflection coefficient $\hat{\Gamma}_L$ from (6.19)
2. Determine the input reflection coefficient $\hat{\Gamma}(0)$ from (6.23)
3. Determine the input impedance to the line, $\hat{Z}_{in}(0)$, from (6.24) or (6.25)
4. Determine the input voltage $\hat{V}(0)$ from (6.32)
5. Determine the undetermined constant \hat{V}^+ from (6.33)
6. Substitute this into (6.30) and (6.31) to determine the source and load voltages and currents.

A more direct way of determining these terminal voltages and currents is as follows. First, write the source relation in terms of a Thevenin equivalent relation as

$$\hat{V}(0) = \hat{V}_S - \hat{Z}_S \hat{I}(0) \tag{6.34}$$

Next, write the load terminal relation similarly as

$$\hat{V}(\mathcal{L}) = \hat{Z}_L \hat{I}(\mathcal{L}) \tag{6.35}$$

Substitute the general solution in (6.9) evaluated at $z = 0$ and at $z = \mathcal{L}$ into (6.34) and (6.35) to yield

$$\hat{V}^+ + \hat{V}^- = \hat{V}_S - \frac{\hat{Z}_S}{Z_C} (\hat{V}^+ - \hat{V}^-) \tag{6.36a}$$

$$\hat{V}^+ e^{-j\beta\mathcal{L}} + \hat{V}^- e^{j\beta\mathcal{L}} = \frac{\hat{Z}_L}{Z_C} (\hat{V}^+ e^{-j\beta\mathcal{L}} - \hat{V}^- e^{j\beta\mathcal{L}}) \tag{6.36b}$$

Rearranging these gives

$$\begin{bmatrix} (Z_C + \hat{Z}_S) & (Z_C - \hat{Z}_S) \\ (Z_C - \hat{Z}_L) e^{-j\beta\mathcal{L}} & (Z_C + \hat{Z}_L) e^{j\beta\mathcal{L}} \end{bmatrix} \begin{bmatrix} \hat{V}^+ \\ \hat{V}^- \end{bmatrix} = \begin{bmatrix} Z_C \hat{V}_S \\ 0 \end{bmatrix} \quad (6.37)$$

Solve these two simultaneous equations for the two undetermined constants \hat{V}^+ and \hat{V}^- and substitute them into the general solutions in (6.9) to determine the line voltage and current anywhere on the line and, in particular, at the source and the load. This general method of solution will be used in a virtually identical fashion for multiconductor transmission lines (MTLs) in the next chapter.

For the simple case of a two-conductor line, (6.37) can be solved by hand in literal fashion (symbols instead of numbers) to give general expressions for \hat{V}^+ and \hat{V}^- . These can then be written in closed form in terms of the reflection coefficients at the source and the load:

$$\hat{\Gamma}_S = \frac{\hat{Z}_S - Z_C}{\hat{Z}_S + Z_C} \quad (6.38a)$$

$$\hat{\Gamma}_L = \frac{\hat{Z}_L - Z_C}{\hat{Z}_L + Z_C} \quad (6.38b)$$

to give general expressions for the line voltage and current anywhere on the line as

$$\hat{V}(z) = \frac{1 + \hat{\Gamma}_L e^{-j2\beta\mathcal{L}} e^{j2\beta z}}{1 - \hat{\Gamma}_S \hat{\Gamma}_L e^{-j2\beta\mathcal{L}}} \frac{Z_C}{Z_C + \hat{Z}_S} \hat{V}_S e^{-j\beta z} \quad (6.39a)$$

$$\hat{I}(z) = \frac{1 - \hat{\Gamma}_L e^{-j2\beta\mathcal{L}} e^{j2\beta z}}{1 - \hat{\Gamma}_S \hat{\Gamma}_L e^{-j2\beta\mathcal{L}}} \frac{1}{Z_C + \hat{Z}_S} \hat{V}_S e^{-j\beta z} \quad (6.39b)$$

A considerable amount of information can be gleaned from these informative expressions. For example, the source and load voltages and currents become

$$\hat{V}(0) = \frac{1 + \hat{\Gamma}_L e^{-j2\beta\mathcal{L}}}{1 - \hat{\Gamma}_S \hat{\Gamma}_L e^{-j2\beta\mathcal{L}}} \frac{Z_C}{Z_C + \hat{Z}_S} \hat{V}_S \quad (6.40a)$$

$$\hat{I}(0) = \frac{1 - \hat{\Gamma}_L e^{-j2\beta\mathcal{L}}}{1 - \hat{\Gamma}_S \hat{\Gamma}_L e^{-j2\beta\mathcal{L}}} \frac{1}{Z_C + \hat{Z}_S} \hat{V}_S \quad (6.40b)$$

and

$$\hat{V}(\mathcal{L}) = \frac{1 + \hat{\Gamma}_L}{1 - \hat{\Gamma}_S \hat{\Gamma}_L e^{-j2\beta\mathcal{L}}} \frac{Z_C}{Z_C + \hat{Z}_S} \hat{V}_S e^{-j\beta\mathcal{L}} \quad (6.41a)$$

$$\hat{I}(\mathcal{L}) = \frac{1 - \hat{\Gamma}_L}{1 - \hat{\Gamma}_S \hat{\Gamma}_L e^{-j2\beta\mathcal{L}}} \frac{1}{Z_C + \hat{Z}_S} \hat{V}_S e^{-j\beta\mathcal{L}} \quad (6.41b)$$

If the line is matched at the load, that is, $\hat{Z}_L = Z_C$, so that the load reflection coefficient is zero, $\hat{\Gamma}_L = 0$, these reduce to

$$\hat{V}(0) = \frac{Z_C}{Z_C + \hat{Z}_S} \hat{V}_S, \quad \hat{\Gamma}_L = 0 \tag{6.42a}$$

$$\hat{I}(0) = \frac{1}{Z_C + \hat{Z}_S} \hat{V}_S, \quad \hat{\Gamma}_L = 0 \tag{6.42b}$$

and

$$\hat{V}(\mathcal{L}) = \frac{Z_C}{Z_C + \hat{Z}_S} \hat{V}_S e^{-j\beta\mathcal{L}}, \quad \hat{\Gamma}_L = 0 \tag{6.43a}$$

$$\hat{I}(\mathcal{L}) = \frac{1}{Z_C + \hat{Z}_S} \hat{V}_S e^{-j\beta\mathcal{L}}, \quad \hat{\Gamma}_L = 0 \tag{6.43b}$$

Observe that these results are sensible because the line input looks like $\hat{Z}_L = Z_C$, the magnitude of the voltage and current is constant all along the line, and the load and source voltage and current differ only by the phase shift of the line, $e^{-j\beta\mathcal{L}}$.

6.2.3 The SPICE (PSPICE) Solution for Lossless Lines

SPICE (or PSPICE) can be used to solve these phasor transmission-line problems for *lossless lines*. The SPICE or its personal computer version, PSPICE, computer program contains a model that is an *exact solution of the transmission-line equations for a lossless two-conductor transmission line*. See Appendix B for a tutorial on the use of SPICE/PSPICE. This exact model will be derived in Chapter 8. It is invoked by the following statement:

$$\text{TXXX N1 N2 N3 N4 Z0 = } Z_C \text{ TD = } T_D$$

where $Z_C = \sqrt{l/c}$ is the characteristic impedance of the line and $T_D = (\mathcal{L}/v)$ is the one-way time delay for propagation from one end of the line to the other. The name of the element, TXXX, denotes the model and XXX is the name of that specific model given by the user. The line and model are connected between nodes N1–N2 and N3–N4 as shown in Figure 6.3. Normally, nodes N2 and N4 are chosen to be the universal reference or ground node, the zero node: N2 = 0 and N4 = 0.

An example is shown in Figure 6.4(a). A 100-MHz voltage source having a magnitude of 10 V and an angle of 30° is attached to a two-conductor lossless line having a characteristic impedance of 50 Ω, a velocity of propagation of 200 m/μs, and a line length of 2.7 m. This gives a one-way time delay of $T_D = \mathcal{L}/v = 13.5$ ns. The source impedance is $\hat{Z}_S = 100 - j50 \Omega$ and the load impedance is $\hat{Z}_L = 100 + j200 \Omega$. The PSPICE node numbering is shown in Figure 6.4(b). SPICE requires *R*, *L*, and *C* circuit elements, so we have synthesized equivalent circuits for the source and

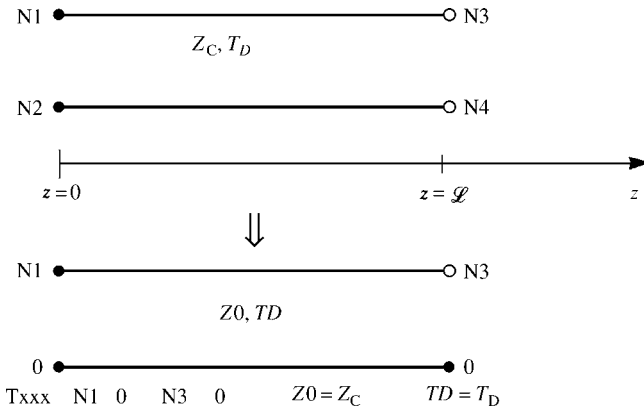


FIGURE 6.3 Representing a lossless transmission line with the SPICE (PSPICE) equivalent circuit.

load impedances as shown, which, at a frequency of 100 MHz, will give the desired complex impedances. The PSPICE program is

EXAMPLE

```
VS 1 0 AC 10 30
RS 1 2 100
CS 2 3 31.8P
T 3 0 4 0 Z0=50 TD=13.5N
RL 4 5 100
LL 5 0 0.318U
.AC DEC 1 1E8 1E8
.PRINT AC VM(3) VP(3) VM(4) VP(4)
.END
```

The `.AC` command causes the program to calculate the result from a starting frequency of 100 MHz to an ending frequency of 100 MHz in steps of one frequency per decade. In other words, the solutions are obtained at only 100 MHz. The `.PRINT` statement requests that the results be printed to a file with the magnitude of the node voltage at node 3 denoted as `VM(3)` and the phase denoted as `VP(3)`. The results are

$$\begin{aligned}\hat{V}(0) &= \text{VM}(3) \angle \text{VP}(3) \\ &= 2.136 \angle 120.1^\circ\end{aligned}$$

and

$$\begin{aligned}\hat{V}(L) &= \text{VM}(4) \angle \text{VP}(4) \\ &= 4.926 \angle -49.1^\circ\end{aligned}$$

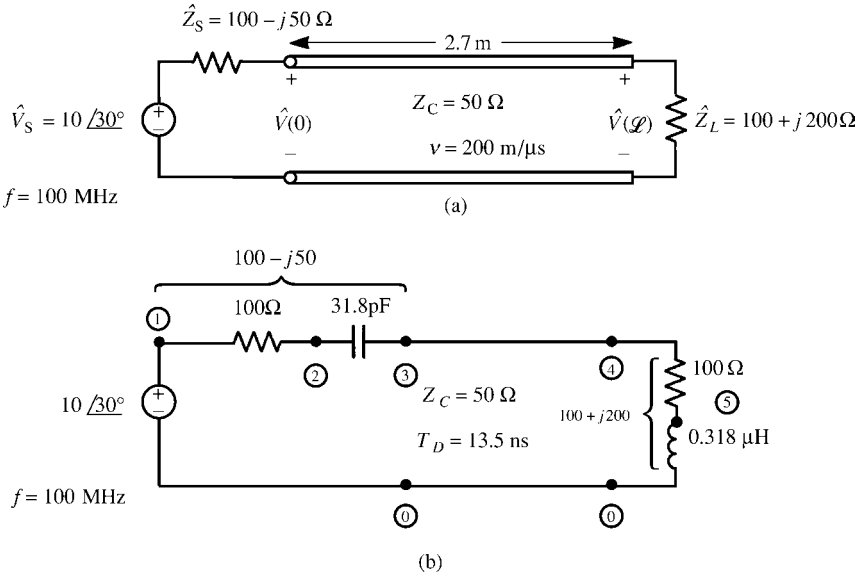


FIGURE 6.4 An example for computing the phasor terminal voltages of a lossless transmission line: (a) the problem statement and (b) the SPICE coding diagram.

These compare favorably with those computed directly by hand with the earlier results of

$$\hat{V}(0) = 2.14 \angle 120.13^\circ$$

and

$$\hat{V}(\mathcal{L}) = 4.93 \angle -409.12^\circ$$

Observe that the load voltage angle of -409.12° is equivalent to -49.12° .

6.2.4 Voltage and Current as a Function of Position on the Line

We have been primarily interested in determining the voltages and currents at the endpoints of the line. In this section, we will investigate and provide plots of the magnitudes of the phasor line voltage and current at various points along the line. We will plot the *magnitude* of these for distances $d = \mathcal{L} - z$ away from the load. Recall the expressions for the voltage and current at various positions along the line in (6.21). Substituting $z = \mathcal{L} - d$ into (6.21) and taking the magnitude gives

$$|\hat{V}_d| = |\hat{V}^+| \left| 1 + \hat{\Gamma}_L e^{-j2\beta d} \right| \tag{6.44a}$$

and

$$|\hat{I}_d| = \frac{|\hat{V}^+|}{Z_C} \left| 1 - \hat{\Gamma}_L e^{-j2\beta d} \right| \quad (6.44b)$$

There are three important cases of special interest that we will investigate: (1) the load is a short circuit, $\hat{Z}_L = 0$, (2) the load is an open circuit, $\hat{Z}_L = \infty$, and (3) the load is matched, $\hat{Z}_L = Z_C$.

For the case where the load is a short circuit, $\hat{Z}_L = 0$, the load reflection coefficient is $\hat{\Gamma}_L = -1$. Equations (6.44) reduce to

$$\begin{aligned} |\hat{V}_d| &= |\hat{V}^+| \left| 1 - e^{-j2\beta d} \right| \\ &= |\hat{V}^+| \underbrace{\left| e^{-j\beta d} \right|}_1 \underbrace{\left| e^{j\beta d} - e^{-j\beta d} \right|}_{|2j \sin(\beta d)|} \\ &\propto |\sin(\beta d)| \\ &= \left| \sin \left(2\pi \frac{d}{\lambda} \right) \right| \end{aligned} \quad (6.45a)$$

and

$$\begin{aligned} |\hat{I}_d| &= \frac{|\hat{V}^+|}{Z_C} \left| 1 + e^{-j2\beta d} \right| \\ &= \frac{|\hat{V}^+|}{Z_C} \underbrace{\left| e^{-j\beta d} \right|}_1 \underbrace{\left| e^{j\beta d} + e^{-j\beta d} \right|}_{|2 \cos(\beta d)|} \\ &\propto |\cos(\beta d)| \\ &= \left| \cos \left(2\pi \frac{d}{\lambda} \right) \right| \end{aligned} \quad (6.45b)$$

and we have written the result in terms of the distance from the load, d , in terms of wavelengths. These are plotted in Figure 6.5(b). Observe that the voltage is zero at the load and at distances from the load that are multiples of a half wavelength. The current is maximum at the load and is zero at distances from the load that are odd multiples of a quarter wavelength. Further, observe that corresponding points are separated by one-half wavelength. We will find this to be an important property for all other loads.

For the case where the load is an open circuit, $\hat{Z}_L = \infty$, the load reflection coefficient is $\hat{\Gamma}_L = 1$. Equations (6.44) reduce to

$$\begin{aligned} |\hat{V}_d| &= |\hat{V}^+| \left| 1 + e^{-j2\beta d} \right| \\ &\propto |\cos(\beta d)| \\ &= \left| \cos \left(2\pi \frac{d}{\lambda} \right) \right| \end{aligned} \quad (6.46a)$$

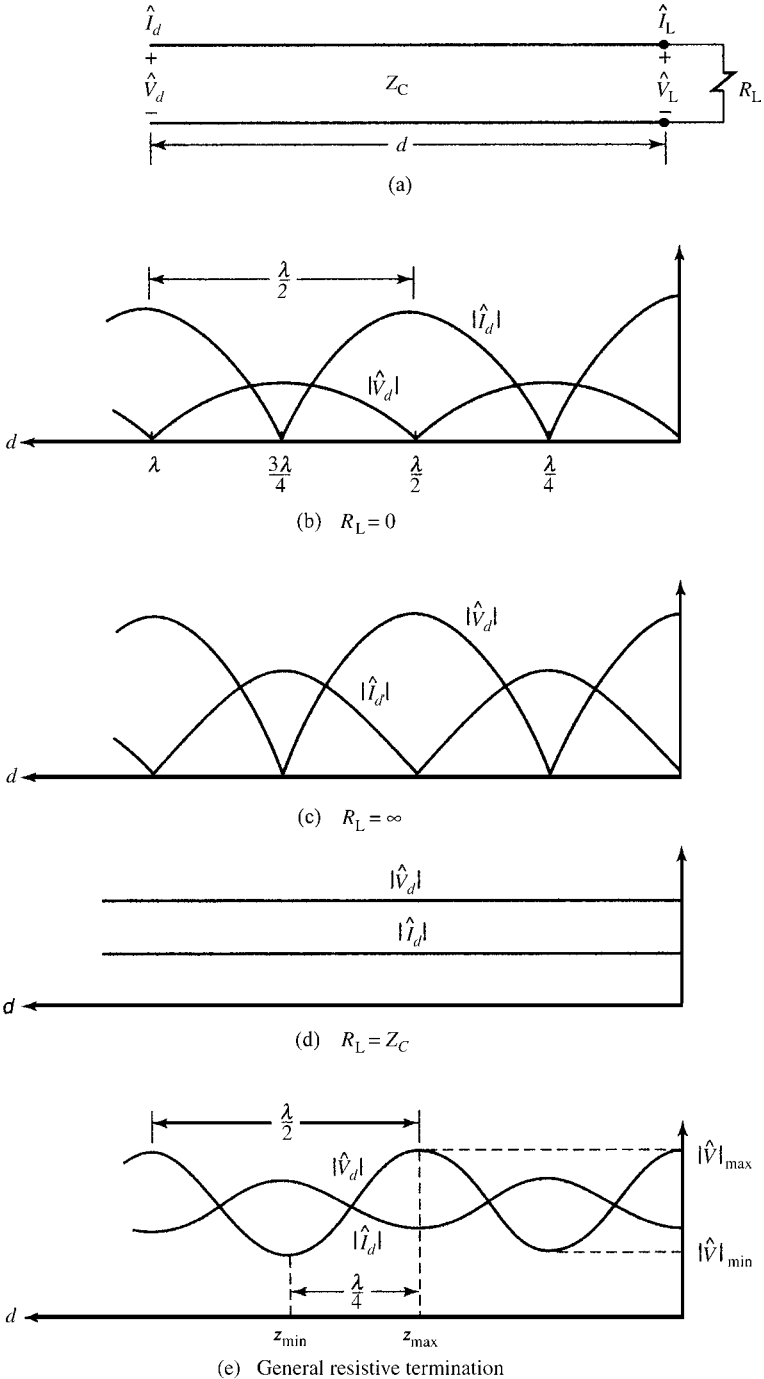


FIGURE 6.5 Illustration of the variation of the magnitudes of the line voltage and current for (b) a short-circuit load, $R_L = 0$, (c) an open-circuit load, $R_L = \infty$, (d) a matched load, $R_L = Z_C$ and (e) a general resistive termination.

and

$$\begin{aligned}
 |\hat{I}_d| &= \left| \frac{\hat{V}^+}{Z_C} \right| \left| 1 - e^{-j2\beta d} \right| \\
 &\propto |\sin(\beta d)| \\
 &= \left| \sin\left(2\pi \frac{d}{\lambda}\right) \right|
 \end{aligned} \tag{6.46b}$$

and we have again written the result in terms of the distance from the load, d , in terms of wavelengths. These are plotted in Figure 6.5(c). Observe that the current is zero at the load and at distances from the load that are multiples of a half wavelength. The voltage is maximum at the load and is zero at distances from the load that are odd multiples of a quarter wavelength. This is the reverse of the short-circuit load case. Further, again observe that corresponding points are separated by one-half wavelength.

And finally, we investigate the case of a *matched* load, $\hat{Z}_L = Z_C$. For this case, the load reflection coefficient is zero, $\hat{\Gamma}_L = 0$, so that the results in (6.44) show that the voltage and current are constant in magnitude along the line as shown in Figure 6.5(d). This is an important reason to match a line. Although the magnitudes of the voltage and current are constant along the line, they suffer a phase shift $e^{-j\beta z}$ as they propagate along it.

The general case is sketched in Figure 6.5(e). The locations of the voltage and current maxima and minima are determined by the actual load impedance, but adjacent corresponding points on each waveform are separated by one-half wavelength. This is an important and general result and can be proved from the general expressions in (6.44). In those expressions, the only dependence on the distance from the load, d , is in the phase term $e^{-j2\beta d}$. Substituting $\beta = 2\pi/\lambda$ and distances that are multiples of a half wavelength, $d \Rightarrow d \pm n(\lambda/2)$, we obtain

$$e^{-j2\beta\left(d \pm \frac{n\lambda}{2}\right)} = e^{-j2\beta d} \underbrace{e^{\mp j2n\pi}}_{+1} \tag{6.47}$$

Hence, we obtain the important result that *corresponding points on the magnitude of the line voltage and line current are separated by one-half wavelength in distance.*

6.2.5 Matching and VSWR

Figure 6.5 illustrates how the magnitudes of the voltage and current vary with position on the line. In the matched case shown in Figure 6.5(d), the magnitudes of the voltage and current do not vary with position, but in the cases of a short-circuit or an open-circuit load (severely mismatched), the magnitudes of the voltage and current vary drastically with position achieving minima of zero. Observe that the *maximum and the adjacent minimum are separated by one-quarter wavelength*. This variation of the voltage and current along the line for a mismatched load is very undesirable as it can cause spots along the line where large voltages can occur that may damage insulation or produce load voltages and currents that are radically different from the

input voltage to the line. Ideally, we would like the line to have no effect on the signal transmission (other than a phase shift or time delay) as will occur for the matched load.

Although we ideally always would like to match the line, there are many practical cases where we cannot exactly match the line. If $\hat{Z}_L \neq Z_C$, the line is mismatched but how do we quantitatively measure this degree of “mismatch”? A useful measure of this mismatch is the voltage standing wave ratio (VSWR). The VSWR is the ratio of the maximum voltage on the line to the minimum voltage on the line:

$$\text{VSWR} = \frac{|\hat{V}|_{\max}}{|\hat{V}|_{\min}} \tag{6.48}$$

These maximum and minimum voltages will be separated by one-quarter wavelength. Observe that for the extreme cases of a short-circuit load, $\hat{Z}_L = 0$, or an open-circuit load, $\hat{Z}_L = \infty$, the minimum voltage is zero and hence the VSWR is infinite:

$$\text{VSWR} = \begin{cases} \infty, & \hat{Z}_L = 0 \\ \infty, & \hat{Z}_L = \infty \end{cases} \tag{6.49}$$

but the VSWR is unity for a matched load:

$$\text{VSWR} = 1, \quad \hat{Z}_L = Z_C \tag{6.50}$$

The VSWR must therefore lie between these two bounds:

$$1 \leq \text{VSWR} < \infty \tag{6.51}$$

Industry considers a line to be “matched” if $\text{VSWR} < 1.2$

We can derive a quantitative result for the VSWR from (6.44a), which shows that the voltage at some distance d is proportional to $|\hat{V}_d| \propto |1 + \hat{\Gamma}_L e^{-j2\beta d}|$. The maximum will be proportional to $|\hat{V}|_{\max} \propto 1 + |\hat{\Gamma}_L|$ and the minimum will be proportional to $|\hat{V}|_{\min} \propto 1 - |\hat{\Gamma}_L|$. Hence, the VSWR is

$$\text{VSWR} = \frac{1 + |\hat{\Gamma}_L|}{1 - |\hat{\Gamma}_L|} \tag{6.52}$$

6.2.6 Power Flow on a Lossless Line

We now investigate the power flow on a lossless line. The forward- and backward-traveling voltage and current waves carry power. The average power flowing to the right (+z) at a point on the line can be determined in terms of the total voltage and current at that point in the same fashion as for a lumped circuit as

$$P_{AV} = \frac{1}{2} \text{Re} \left\{ \hat{V}(z) \hat{I}^*(z) \right\} \tag{6.53}$$

where * denotes the complex conjugate. Substituting the general expressions for voltage and current given in (6.21) gives

$$\begin{aligned}
 P_{AV} &= \frac{1}{2} \operatorname{Re} \left\{ \hat{V}(z) \hat{I}^*(z) \right\} \\
 &= \frac{1}{2} \operatorname{Re} \left\{ \hat{V}^+ e^{-j\beta z} \left[1 + \hat{\Gamma}_L e^{j2\beta(z-\mathcal{L})} \right] \frac{\hat{V}^{+*}}{Z_C} e^{j\beta z} \left[1 - \hat{\Gamma}_L^* e^{-j2\beta(z-\mathcal{L})} \right] \right\} \\
 &= \frac{1}{2} \operatorname{Re} \left\{ \frac{\hat{V}^+ \hat{V}^{+*}}{Z_C} \left[1 + \underbrace{\left(\hat{\Gamma}_L e^{j2\beta(z-\mathcal{L})} - \hat{\Gamma}_L^* e^{-j2\beta(z-\mathcal{L})} \right)}_{\text{imaginary}} - \hat{\Gamma}_L \hat{\Gamma}_L^* \right] \right\} \\
 &= \frac{|\hat{V}^+|^2}{2Z_C} \left[1 - |\hat{\Gamma}_L|^2 \right]
 \end{aligned} \tag{6.54}$$

and we have used the complex algebra result that the product of a complex number and its conjugate is the magnitude squared of that complex number. This result confirms that if the load is a short circuit, $\hat{\Gamma}_L = -1$, or an open circuit, $\hat{\Gamma}_L = 1$, then the net power flow in the +z direction is zero. Clearly, an open circuit or a short circuit can absorb no power. Essentially, then the power in the forward-traveling wave is equal to the power in the backward-traveling wave and all the incident power is reflected.

This can be confirmed by separately computing the average power flow in the individual waves. The power flowing to the right in the forward-traveling wave is

$$\begin{aligned}
 P_{AV}^+ &= \frac{1}{2} \operatorname{Re} \left\{ \left(\hat{V}^+ e^{-j\beta z} \right) \left(\frac{\hat{V}^{+*}}{Z_C} e^{j\beta z} \right) \right\} \\
 &= \frac{|\hat{V}^+|^2}{2Z_C}
 \end{aligned} \tag{6.55a}$$

and the power flowing to the left in the backward-traveling wave is

$$\begin{aligned}
 P_{AV}^- &= \frac{1}{2} \operatorname{Re} \left\{ \left(\hat{V}^- e^{j\beta z} \right) \left(-\frac{\hat{V}^{-*}}{Z_C} e^{-j\beta z} \right) \right\} \\
 &= -\frac{|\hat{V}^-|^2}{2Z_C} \\
 &= -\frac{|\hat{V}^+|^2}{2Z_C} |\hat{\Gamma}_L|^2
 \end{aligned} \tag{6.55b}$$

The sum of (6.55a) and (6.55b) gives (6.54). The ratio of reflected power to incident power is $|\hat{\Gamma}_L|^2$. For a matched load, $\hat{Z}_L = Z_C$, $\hat{\Gamma}_L = 0$ and all the power in the forward-traveling wave is absorbed in the (matched) load.

6.3 THE GENERAL SOLUTION FOR LOSSY LINES

The transmission-line equations for lossy lines include the per-unit-length resistance of the conductors, $r(\sqrt{f})$, and the per-unit-length conductance of the lossy surrounding medium, $g(f)$. The frequency-domain equations are

$$\frac{d}{dz} \hat{V}(z) = -\hat{z} \hat{I}(z) \quad (6.56a)$$

$$\frac{d}{dz} \hat{I}(z) = -\hat{y} \hat{V}(z) \quad (6.56b)$$

where the per-unit-length impedance and admittance are

$$\hat{z} = r + j\omega l \quad (6.57a)$$

and

$$\hat{y} = g + j\omega c \quad (6.57b)$$

Differentiating one equation with respect to z and substituting the other, and vice versa, gives the uncoupled second-order differential equations

$$\frac{d^2}{dz^2} \hat{V}(z) = \underbrace{\hat{z}\hat{y}}_{\hat{\gamma}^2} \hat{V}(z) \quad (6.58a)$$

$$\frac{d^2}{dz^2} \hat{I}(z) = \underbrace{\hat{y}\hat{z}}_{\hat{\gamma}^2} \hat{I}(z) \quad (6.58b)$$

and the propagation constant is

$$\begin{aligned} \hat{\gamma} &= \sqrt{\hat{z}\hat{y}} \\ &= \alpha + j\beta \end{aligned} \quad (6.59)$$

The real part, α , is the attenuation constant and the imaginary part, β , is the phase constant. Observe that for a lossy line, $\beta \neq \omega\sqrt{lc}$, as was the case for the lossless line. Furthermore, the phase velocity of propagation along the line is $v = \omega/\beta \neq 1/\sqrt{lc}$.

The general solution to (6.58) is [A.1]

$$\hat{V}(z) = \hat{V}^+ e^{-\alpha z} e^{-j\beta z} + \hat{V}^- e^{\alpha z} e^{j\beta z} \quad (6.60a)$$

$$\hat{I}(z) = \frac{\hat{V}^+}{\hat{Z}_C} e^{-\alpha z} e^{-j\beta z} - \frac{\hat{V}^-}{\hat{Z}_C} e^{\alpha z} e^{j\beta z} \quad (6.60b)$$

where the characteristic impedance now becomes complex as

$$\begin{aligned}\hat{Z}_C &= \sqrt{\frac{\hat{z}}{\hat{y}}} \\ &= Z_C \angle \theta_{Z_C} \\ &= Z_C e^{j\theta_{Z_C}}\end{aligned}\quad (6.61)$$

The time-domain result is obtained in the usual fashion by (1) multiplying the phasor quantity by $e^{j\omega t}$ and (2) taking the real part of the result:

$$V(z, t) = V^+ e^{-\alpha z} \cos(\omega t - \beta z + \theta^+) + V^- e^{\alpha z} \cos(\omega t + \beta z + \theta^-) \quad (6.62a)$$

$$I(z, t) = \frac{V^+}{Z_C} e^{-\alpha z} \cos(\omega t - \beta z + \theta^+ - \theta_{Z_C}) - \frac{V^-}{Z_C} e^{\alpha z} \cos(\omega t + \beta z + \theta^- - \theta_{Z_C}) \quad (6.62b)$$

Again, the general solution consists of the sum of a forward-traveling wave (+ z direction) and a backward-traveling wave ($-z$ direction). Observe that there are only two differences between the lossless line solution and the lossy line solution. First, the voltage and current amplitudes are attenuated as shown by the terms $e^{\pm\alpha z}$. Second, the characteristic impedance is no longer real but has a phase angle. Hence, the voltage and current are no longer in time phase but are out of phase by θ_{Z_C} , which is at most 45° .

Hence, we can directly modify the results obtained for the lossless line to include losses by replacing $j\beta$ in those results with $\hat{\gamma} = \alpha + j\beta$. For example, we define the load reflection coefficient as

$$\hat{\Gamma}_L = \frac{\hat{Z}_L - \hat{Z}_C}{\hat{Z}_L + \hat{Z}_C} \quad (6.63)$$

and the reflection coefficient anywhere on the line can be written in terms of the load reflection coefficient as

$$\begin{aligned}\hat{\Gamma}(z) &= \hat{\Gamma}_L e^{2\hat{\gamma}(z-\mathcal{L})} \\ &= \hat{\Gamma}_L e^{2\alpha(z-\mathcal{L})} e^{j2\beta(z-\mathcal{L})}\end{aligned}\quad (6.64)$$

The phasor general solution in (6.60) becomes

$$\hat{V}(z) = \hat{V}^+ e^{-\alpha z} e^{-j\beta z} (1 + \hat{\Gamma}(z)) \quad (6.65a)$$

$$\hat{I}(z) = \frac{\hat{V}^+}{\hat{Z}_C} e^{-\alpha z} e^{-j\beta z} (1 - \hat{\Gamma}(z)) \quad (6.65b)$$

Hence, the input impedance of the line at a point along the line is the ratio of (6.65a) and (6.65b):

$$\hat{Z}_{\text{in}}(z) = \hat{Z}_C \frac{(1 + \hat{\Gamma}(z))}{(1 - \hat{\Gamma}(z))} \quad (6.66)$$

The input impedance to the entire line at $z = 0$ is

$$\hat{Z}_{\text{in}}(z) = \hat{Z}_C \frac{(1 + \hat{\Gamma}_L e^{-2\alpha\mathcal{L}} e^{-j2\beta\mathcal{L}})}{(1 - \hat{\Gamma}_L e^{-2\alpha\mathcal{L}} e^{-j2\beta\mathcal{L}})} \quad (6.67)$$

This can be written in an alternative form as

$$\hat{Z}_{\text{in}}(0) = \hat{Z}_C \frac{\hat{Z}_L + \hat{Z}_C \tanh(\hat{\gamma}\mathcal{L})}{\hat{Z}_C + \hat{Z}_L \tanh(\hat{\gamma}\mathcal{L})} \quad (6.68)$$

The solution process for determining the terminal voltages and currents of the line is virtually unchanged from the lossless case. The direct solution for the undetermined constants in (6.60) and given in (6.37) for the lossless case becomes

$$\begin{bmatrix} (\hat{Z}_C + \hat{Z}_S) & (\hat{Z}_C - \hat{Z}_S) \\ (\hat{Z}_C - \hat{Z}_L) e^{-\hat{\gamma}\mathcal{L}} & (\hat{Z}_C + \hat{Z}_L) e^{\hat{\gamma}\mathcal{L}} \end{bmatrix} \begin{bmatrix} \hat{V}^+ \\ \hat{V}^- \end{bmatrix} = \begin{bmatrix} \hat{Z}_C \hat{V}_S \\ 0 \end{bmatrix} \quad (6.69)$$

The explicit solution for the line voltage and current anywhere on the line given for the lossless line in (6.39) becomes for the lossy line

$$\hat{V}(z) = \frac{1 + \hat{\Gamma}_L e^{-2\hat{\gamma}\mathcal{L}} e^{2\hat{\gamma}z}}{1 - \hat{\Gamma}_S \hat{\Gamma}_L e^{-2\hat{\gamma}\mathcal{L}}} \frac{\hat{Z}_C}{\hat{Z}_C + \hat{Z}_S} \hat{V}_S e^{-\hat{\gamma}z} \quad (6.70a)$$

$$\hat{I}(z) = \frac{1 - \hat{\Gamma}_L e^{-2\hat{\gamma}\mathcal{L}} e^{2\hat{\gamma}z}}{1 - \hat{\Gamma}_S \hat{\Gamma}_L e^{-2\hat{\gamma}\mathcal{L}}} \frac{1}{\hat{Z}_C + \hat{Z}_S} \hat{V}_S e^{-\hat{\gamma}z} \quad (6.70b)$$

6.3.1 The Low-Loss Approximation

Typically, losses are small at the significant range of frequencies for typical high-speed digital signals and for typical boards. For example, for a stripline with plate separation of 20 mils and a land of width 5 mils in FR4 ($\epsilon_r = 4.7$) we compute, from Eqs. (4.107) in Section 4.3.1 of Chapter 4 , $c = 113.2$ pF/m and $l = 0.461$ μ H/m. The characteristic impedance for this lossless stripline is $Z_C = \sqrt{l/c} = 63.8$ Ω and the velocity of propagation is $v = 1/\sqrt{l/c} = 1.38 \times 10^8$ m/s. Using Eq. (4.60) of Chapter 4 , the per-unit-length conductance is given by

$$g = \omega \tan \delta c \quad (6.71)$$

where $\tan \delta$ is the loss tangent of this (homogeneous) surrounding medium. For FR4 glass epoxy that is typical of PCBs, the loss tangent is approximately 0.02 in the low to high MHz range. Hence, for this board we obtain $g = 14.2 \times 10^{-12}$ f S/m. The high-frequency resistance in (4.119) dominates the dc resistance in (4.118) above a

frequency given in (4.120). For this problem and assuming that the constant $k = 2$, the frequency is 23 MHz. Hence, for frequencies above 23 MHz, the per-unit-length resistance of the land (thickness of 1.38 mils for 1 ounce copper) is computed from the high-frequency equation in (4.119) giving $r = 8.05 \times 10^{-4} \sqrt{f} \Omega/\text{m}$. By low loss we mean

$$r \ll \omega l \tag{6.72a}$$

$$g \ll \omega c \tag{6.72b}$$

For this stripline problem, r is less than ωl for $f > 1.34$ MHz and g is less than ωc for all frequencies. Observe that since $g = \omega \tan \delta c$, g is less than ωc by the loss tangent, which for FR4 is on the order of 0.02 in the low to high MHz range. (The loss tangent goes to zero at dc and at very high frequencies.)

Let us consider obtaining a simple formula for the characteristic impedance and the attenuation constant. The propagation constant is given in (6.59). Rewriting this,

$$\begin{aligned} \hat{\gamma} &= \alpha + j\beta \\ &= \sqrt{(r + j\omega l)(g + j\omega c)} \\ &= \sqrt{(j\omega l)(j\omega c) \left(1 + \frac{r}{j\omega l}\right) \left(1 + \frac{g}{j\omega c}\right)} \\ &= j\omega\sqrt{lc} \sqrt{\left(1 - \frac{rg}{\omega^2 lc}\right) - j\left(\frac{r}{\omega l} + \frac{g}{\omega c}\right)} \\ &\cong j\omega\sqrt{lc} \sqrt{1 - j\left(\frac{r}{\omega l} + \frac{g}{\omega c}\right)} \left\{ \begin{array}{l} r \ll \omega l \\ g \ll \omega c \end{array} \right\} \end{aligned} \tag{6.73}$$

We now apply the Taylor’s series to expand this:

$$(1 + x)^n = 1 + \frac{nx}{1!} + \frac{n(n-1)x^2}{2!} + \dots, \quad |x| < 1$$

to give

$$\hat{\gamma} \cong j\omega\sqrt{lc} \left[1 - j\left(\frac{r}{2\omega l} + \frac{g}{2\omega c}\right) \right] \tag{6.74}$$

from which we identify the attenuation and phase constants as

$$\alpha \cong \frac{1}{2} \left(\frac{r}{Z_C} + gZ_C \right) \tag{6.75a}$$

$$\beta \cong \omega\sqrt{lc} \tag{6.75b}$$

In a similar fashion, we obtain

$$\begin{aligned}
 Z_C &= \sqrt{\frac{r + j\omega l}{g + j\omega c}} \\
 &\cong \sqrt{\frac{l}{c}} \left\{ \begin{array}{l} r \ll \omega l \\ g \ll \omega c \end{array} \right\}
 \end{aligned}
 \tag{6.76}$$

Hence for a low-loss line where $r \ll \omega l$ and $g \ll \omega c$, the characteristic impedance and the velocity of propagation are independent of frequency and are essentially the same as for a lossless line. Figure 6.6 shows the magnitude and angle of the characteristic impedance versus frequency from 10 kHz to 1 GHz for the stripline considered previously, where the land is of width 5 mils and the plate separation is 20 mils. Observe that above about 5 MHz the characteristic impedance approaches the lossless value of $Z_C = 63.8 \Omega$. Figure 6.7(a) shows the attenuation constant and Figure 6.7(b) shows the velocity of propagation, $v = \omega/\beta$. The velocity of propagation approaches the lossless value of $v = 1.38 \times 10^8$ m/s above about 5 MHz. The value of the attenuation constant computed from the approximation in (6.75a) at 100 MHz is $\alpha = 1.085 \times 10^{-1}$, whereas the value computed directly from the exact expression in (6.59) is the same. Hence for typical board dimensions, the low-loss region where the above approximations apply is above about 5 MHz. Hence for today's digital signals, all of their sinusoidal components lie in the low-loss frequency range.

Consider a lossy line that is matched so that there are only forward-traveling waves on the line. The voltage and current, according to (6.60), are attenuated according to $e^{-\alpha z}$ as they travel along the line. Hence, the power loss in a line of length \mathcal{L} is $e^{-2\alpha \mathcal{L}}$ [A.1,A.3]. In dB, this becomes [A.3]

$$\begin{aligned}
 \text{Loss}_{\text{dB}} &= 10 \log_{10}(e^{2\alpha \mathcal{L}}) \\
 &= 8.686 \alpha \mathcal{L}
 \end{aligned}
 \tag{6.77}$$

For the above stripline at a frequency of 1 GHz, we obtain

$$\begin{aligned}
 Z_C &= 63.8 \Omega \\
 r &= 25.46 \Omega/\text{m} \\
 g &= 1.423 \times 10^{-2} \text{ S/m} \\
 \alpha &= 0.653
 \end{aligned}$$

The resistive loss is

$$\begin{aligned}
 \text{Loss}_r &= 4.343 \frac{r}{Z_C} \mathcal{L} \\
 &= 1.73 \mathcal{L} \text{ dB}
 \end{aligned}
 \tag{6.78a}$$

and the loss in the surrounding medium is

$$\begin{aligned}
 \text{Loss}_g &= 4.343 g Z_C \mathcal{L} \\
 &= 3.93 \mathcal{L} \text{ dB}
 \end{aligned}
 \tag{6.78b}$$

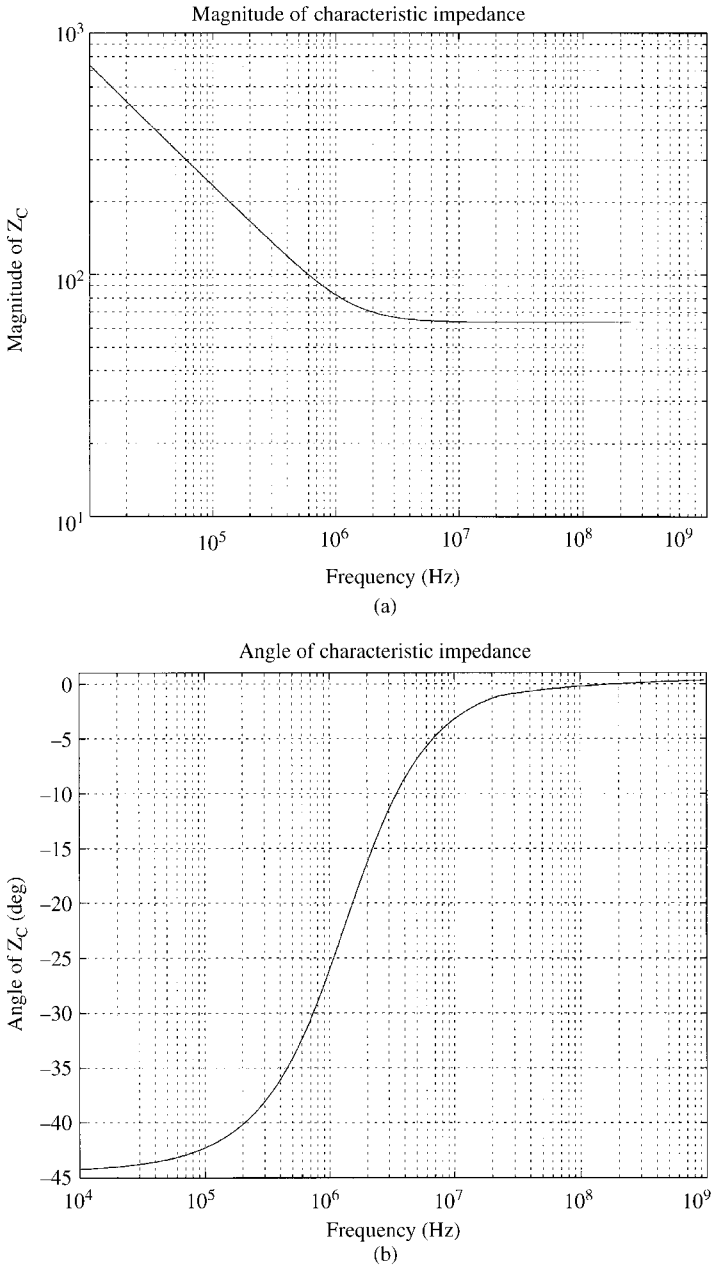
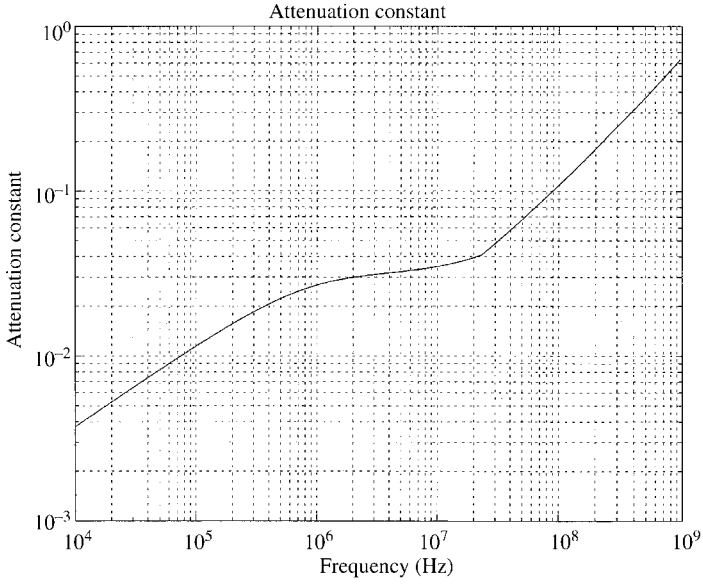
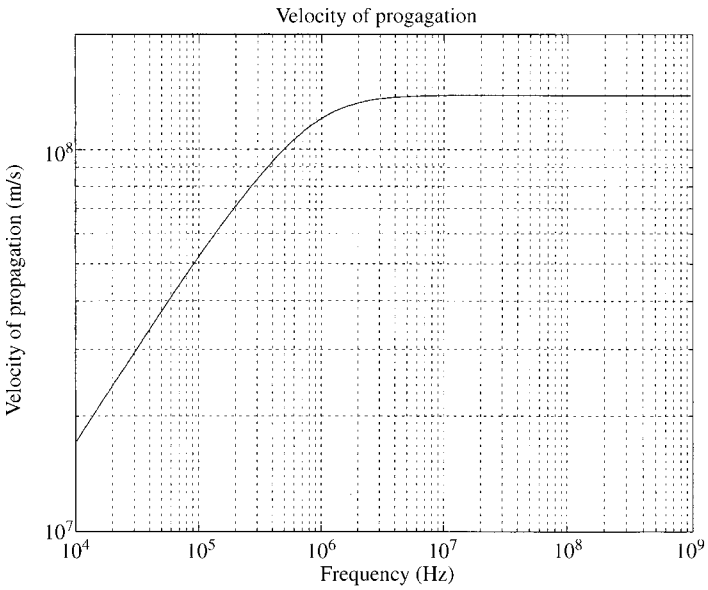


FIGURE 6.6 Plot of (a) the magnitude and (b) the phase of the line characteristic impedance for a low-loss line versus frequency.



(a)



(b)

FIGURE 6.7 Plot of (a) the attenuation constant and (b) the velocity of propagation for a low-loss line versus frequency.

The total loss is the sum of these. For a 6-in. length of this stripline, the total loss at 1 GHz is 0.86 dB. This says that the amplitude of a 1-GHz sine wave, which varies as $e^{-\alpha z}$, is reduced by about 1 dB; that is, the input level is reduced to about 90% at the output when traversing a line length of 6 in. Observe that above 1 GHz, the dielectric loss dominates the conductor loss.

6.4 LUMPED-CIRCUIT APPROXIMATE MODELS OF THE LINE

Although SPICE/PSPICE contains a model representing the *exact* solution of the transmission-line equations for a two-conductor *lossless* line, a frequently used alternative is a lumped-circuit approximate representation. The basic idea is to represent the line or segments of it as lumped circuits. Two common such models are the lumped-Pi and lumped-T models shown in Figure 6.8, named so for their topological appearance. In order for these to adequately represent the line, the line length must be electrically short at the excitation frequency; that is, $\mathcal{L} < (1/10)\lambda$. In some

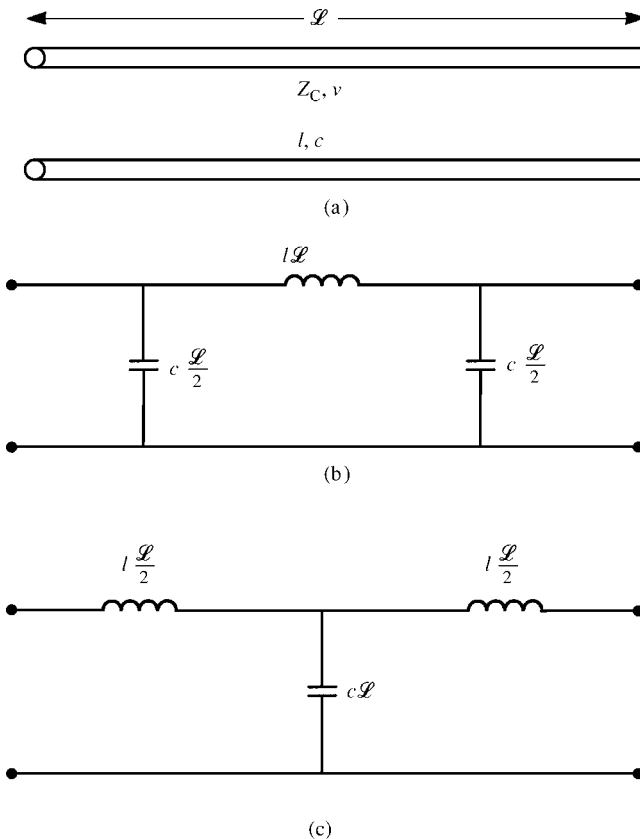


FIGURE 6.8 Illustration of lumped-circuit approximate models: (b) the lumped-Pi model and (c) the lumped-T model.

cases the line must be much shorter than this, electrically, say, $\mathcal{L} < (1/20)\lambda$, in order for lumped-circuit models to characterize what is truly a distributed-parameter phenomenon. If the total line length exceeds this criterion, then it is divided into a sequence of smaller segments, each of which is electrically short. Observe that in each of these lumped circuits, the total capacitance is $c\mathcal{L}$ and the total inductance is $l\mathcal{L}$. For example, in the lumped-Pi circuit in Figure 6.8(b), the total line capacitance is split and put on either side of the total inductance. This gives the lumped circuit a reciprocal property that the actual line possesses. Similarly, the lumped-T model in Figure 6.8(c) has all the capacitance placed in the middle of the line, and the total inductance is split and placed on either side. This gives reciprocal structures.

In order to investigate the adequacy of these approximate models, consider a two-conductor line of length 1 m and characterized by $l = 0.5 \mu\text{H}/\text{m}$ and $c = 200 \text{pF}/\text{m}$ shown in Figure 6.9(a). The characteristic impedance is 50Ω and the velocity of

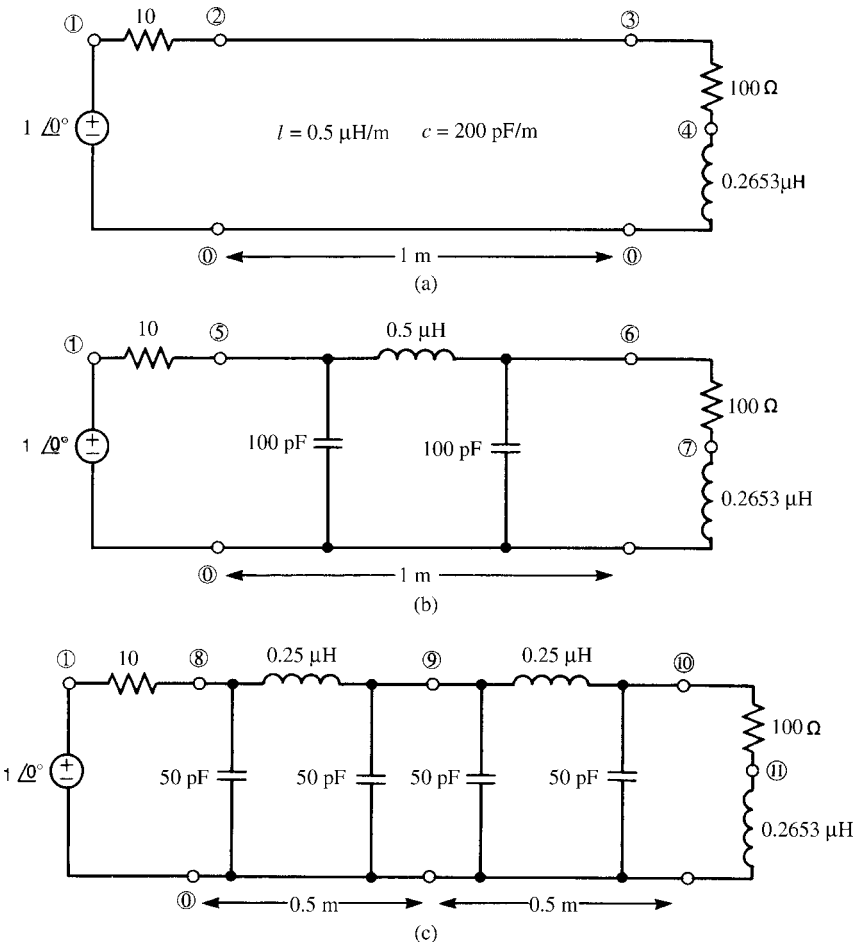


FIGURE 6.9 SPICE simulation of the frequency-response of (a) the transmission-line model, (b) a one-section lumped-Pi model, and (c) a two-section lumped-Pi model.

propagation is 1×10^8 m/s, giving a one-way time delay of 10 ns. The node numbering for the exact transmission-line model representation is shown in Figure 6.9(a). Figure 6.9(b) shows a one-section lumped-Pi model of the line along with the PSPICE node numbering. Figure 6.9(c) shows the line being broken in half and modeled with two lumped-Pi sections along with the PSPICE node numbering. The line is $\lambda/10$ at 10 MHz. Combining these three models into one program using one voltage source gives

```

EXAMPLE
VS 1 0 AC 1
* TRANSMISSION LINE MODEL
RS1 1 2 10
T 2 0 3 0 Z0=50 TD=10N
RL1 3 4 100
LL1 4 0 0.2653U
* ONE-PI SECTION
RS2 1 5 10
C11 5 0 100P
L11 5 6 0.5U
C12 6 0 100P
RL2 6 7 100
LL2 7 0 0.2653U
* TWO-PI SECTIONS
RS3 1 8 10
C21 8 0 50P
L21 8 9 0.25U
C22 9 0 50P
C23 9 0 50P
L22 9 10 0.25U
C24 10 0 50P
RL3 10 11 100
LL3 11 0 0.2653U
.AC DEC 50 1E6 100E6
.PRINT AC VM(2) VP(2) VM(3) VP(3) VM(5) VP(5)
+      VM(6) VP(6) VM(8) VP(8) VM(10) VP(10)
.PROBE
.END

```

Plots of the input and output voltages of the line resulting from these three models are shown in Figure 6.10. Observe that for frequencies below where the line is $\lambda/10$, that is, 10 MHz, all three models give the same result. The lumped-Pi model consisting of two sections extends this prediction range slightly higher. Previous work has shown that increasing the number of sections does not significantly increase the prediction range of the lumped-circuit model to make the increased complexity of the circuit worth it [B.15].

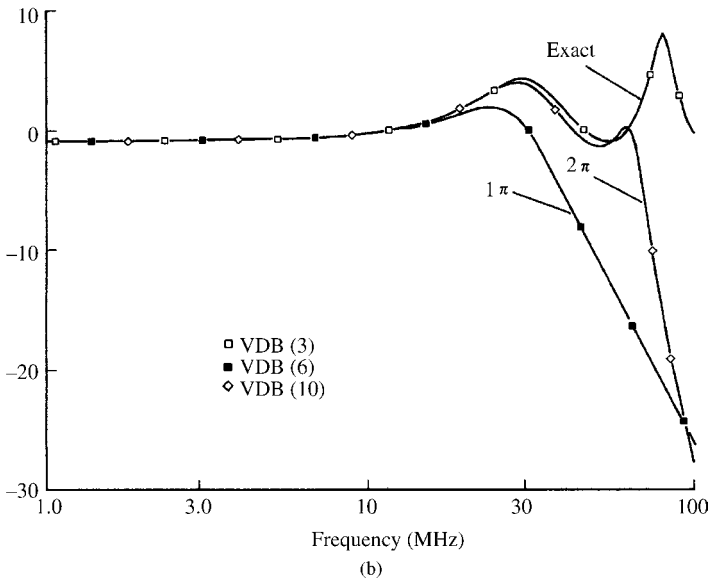
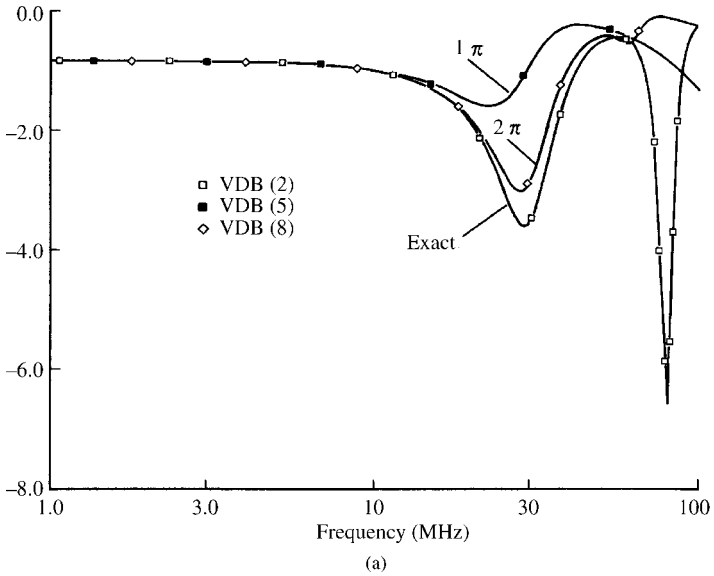


FIGURE 6.10 Plots of the SPICE-computed magnitudes of the circuits of Figure 6.9 for (a) the source voltages and (b) the load voltages.

Lossy lines can also be modeled with these lumped-circuit approximations. The line can similarly be modeled with lumped- Π or lumped- T sections but with the line per-unit-length resistance and conductance added as shown in Figure 6.11. Again, observe that the totals are $r\mathcal{L}$ and $g\mathcal{L}$. However, these per-unit-length parameters

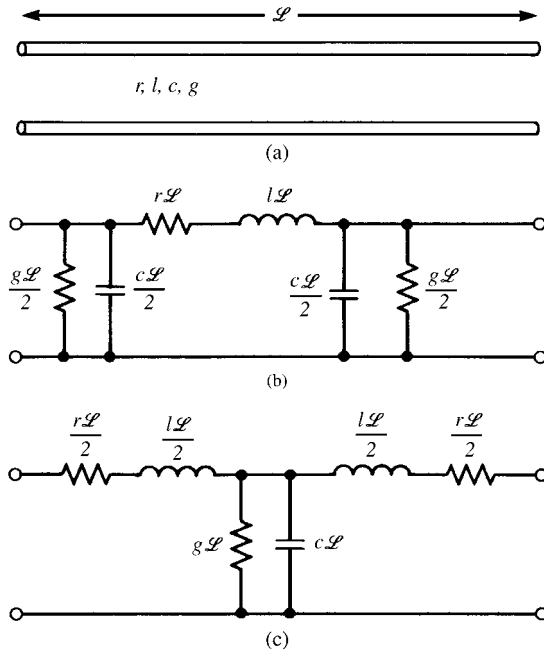


FIGURE 6.11 Illustration of the inclusion of losses into (b) the lumped-Pi and (c) the lumped-T equivalent circuits.

of resistance and conductance are frequency dependent as discussed in Sections 4.2.3 and 4.3.2 of Chapter 4. In the case of lossy lines excited at one frequency, these approximate models have a useful role since these per-unit-length parameters can be evaluated at the frequency of excitation and included in these models as a constant value element. However, in modeling time-domain excitation of the line such as the line driven by digital pulse waveforms, there is a significant problem. The digital pulse waveforms contain a continuum of sinusoidal components. Yet the per-unit-length resistance and conductance are frequency dependent. Hence, we should not use these lumped-circuit approximate models to model lines that are excited by general waveforms unless we ignore the frequency-dependant losses.

6.5 ALTERNATIVE TWO-PORT REPRESENTATIONS OF THE LINE

Since we are generally not interested in the line voltages and currents at points along the line other than at the terminations, we can imbed the line as a two-port as shown in Figure 6.12 and relate the terminal voltages and currents with two-port parameters.

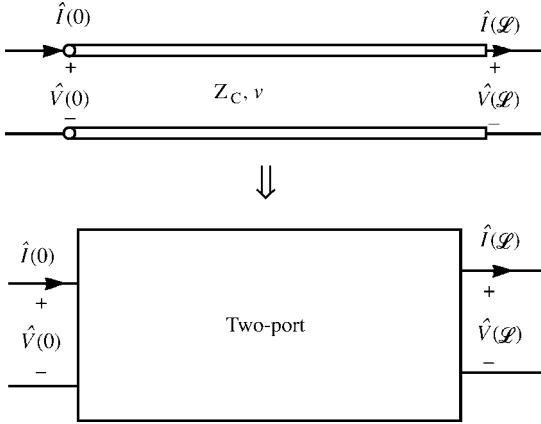


FIGURE 6.12 Characterization of a transmission line as a two-port.

6.5.1 The Chain Parameters

One of the most useful forms of two-port parameters for a transmission line is the *chain-parameter matrix* representation. This relates the terminal voltages and currents as

$$\begin{bmatrix} \hat{V}(\mathcal{L}) \\ \hat{I}(\mathcal{L}) \end{bmatrix} = \underbrace{\begin{bmatrix} \hat{\phi}_{11} & \hat{\phi}_{12} \\ \hat{\phi}_{21} & \hat{\phi}_{22} \end{bmatrix}}_{\hat{\Phi}(\mathcal{L})} \begin{bmatrix} \hat{V}(0) \\ \hat{I}(0) \end{bmatrix} \tag{6.79}$$

These can be straightforwardly obtained by evaluating the general solutions for a lossless line given in (6.9) at $z = 0$ and $z = \mathcal{L}$ to give

$$\begin{bmatrix} \hat{V}(0) \\ \hat{I}(0) \end{bmatrix} = \begin{bmatrix} 1 & 1 \\ \frac{1}{Z_C} & -\frac{1}{Z_C} \end{bmatrix} \begin{bmatrix} \hat{V}^+ \\ \hat{V}^- \end{bmatrix} \tag{6.80a}$$

$$\begin{bmatrix} \hat{V}(\mathcal{L}) \\ \hat{I}(\mathcal{L}) \end{bmatrix} = \begin{bmatrix} e^{-j\beta\mathcal{L}} & e^{j\beta\mathcal{L}} \\ \frac{1}{Z_C} e^{-j\beta\mathcal{L}} & -\frac{1}{Z_C} e^{j\beta\mathcal{L}} \end{bmatrix} \begin{bmatrix} \hat{V}^+ \\ \hat{V}^- \end{bmatrix} \tag{6.80b}$$

Inverting (6.80a) gives

$$\begin{bmatrix} \hat{V}^+ \\ \hat{V}^- \end{bmatrix} = \frac{1}{2} \begin{bmatrix} 1 & Z_C \\ 1 & -Z_C \end{bmatrix} \begin{bmatrix} \hat{V}(0) \\ \hat{I}(0) \end{bmatrix} \tag{6.81}$$

Substituting this into (6.80b) gives

$$\begin{aligned}
 \begin{bmatrix} \hat{V}(\mathcal{L}) \\ \hat{I}(\mathcal{L}) \end{bmatrix} &= \begin{bmatrix} e^{-j\beta\mathcal{L}} & e^{j\beta\mathcal{L}} \\ \frac{1}{Z_C} e^{-j\beta\mathcal{L}} & -\frac{1}{Z_C} e^{j\beta\mathcal{L}} \end{bmatrix} \frac{1}{2} \begin{bmatrix} 1 & Z_C \\ 1 & -Z_C \end{bmatrix} \begin{bmatrix} \hat{V}(0) \\ \hat{I}(0) \end{bmatrix} \\
 &= \underbrace{\begin{bmatrix} \cos(\beta\mathcal{L}) & -jZ_C \sin(\beta\mathcal{L}) \\ -j\frac{\sin(\beta\mathcal{L})}{Z_C} & \cos(\beta\mathcal{L}) \end{bmatrix}}_{\hat{\Phi}(\mathcal{L})} \begin{bmatrix} \hat{V}(0) \\ \hat{I}(0) \end{bmatrix}
 \end{aligned} \tag{6.82}$$

Hence, for a lossless line the chain parameters are

$$\hat{\phi}_{11} = \cos(\beta\mathcal{L}) \tag{6.83a}$$

$$\hat{\phi}_{12} = -jZ_C \sin(\beta\mathcal{L}) \tag{6.83b}$$

$$\hat{\phi}_{21} = -j\frac{\sin(\beta\mathcal{L})}{Z_C} \tag{6.83c}$$

$$\hat{\phi}_{22} = \cos(\beta\mathcal{L}) \tag{6.83d}$$

Observe some interesting properties of the chain-parameter matrix for a lossless line. If the line length is one quarter of a wavelength, $\beta\mathcal{L} = 2\pi(\mathcal{L}/\lambda) = \pi/2$ and the chain-parameter matrix becomes

$$\hat{\Phi}(\mathcal{L}) = \begin{bmatrix} 0 & -jZ_C \\ -j\frac{1}{Z_C} & 0 \end{bmatrix}, \quad \mathcal{L} = \frac{\lambda}{4} \tag{6.84a}$$

Conversely, if the line length is one-half wavelength, the chain-parameter matrix becomes

$$\hat{\Phi}(\mathcal{L}) = \begin{bmatrix} -1 & 0 \\ 0 & -1 \end{bmatrix}, \quad \mathcal{L} = \frac{\lambda}{2} \tag{6.84b}$$

If the line length is three quarters of a wavelength, the chain-parameter matrix becomes

$$\hat{\Phi}(\mathcal{L}) = \begin{bmatrix} 0 & jZ_C \\ j\frac{1}{Z_C} & 0 \end{bmatrix}, \quad \mathcal{L} = \frac{3\lambda}{4} \tag{6.84c}$$

If the line is one wavelength, the chain-parameter matrix becomes the identity matrix:

$$\hat{\Phi}(\mathcal{L}) = \begin{bmatrix} 1 & 0 \\ 0 & 1 \end{bmatrix}, \quad \mathcal{L} = \lambda \tag{6.84d}$$

which means that the input and output voltages are equal as are the input and output currents.

These are obtained for a lossless line. To obtain the chain parameters for a lossy line, we simply replace $\cos(\beta\mathcal{L}) \Rightarrow \cosh(\hat{\gamma}\mathcal{L})$ and replace $j\sin(\beta\mathcal{L}) \Rightarrow \sinh(\hat{\gamma}\mathcal{L})$ along with $Z_C \Rightarrow \hat{Z}_C$. Hence, for a lossy line, the chain parameters become

$$\begin{aligned}\hat{\phi}_{11} &= \cosh(\hat{\gamma}\mathcal{L}) \\ &= \frac{e^{\hat{\gamma}\mathcal{L}} + e^{-\hat{\gamma}\mathcal{L}}}{2}\end{aligned}\quad (6.85a)$$

$$\begin{aligned}\hat{\phi}_{12} &= -\hat{Z}_C \sinh(\hat{\gamma}\mathcal{L}) \\ &= -\hat{Z}_C \frac{e^{\hat{\gamma}\mathcal{L}} - e^{-\hat{\gamma}\mathcal{L}}}{2}\end{aligned}\quad (6.85b)$$

$$\begin{aligned}\hat{\phi}_{21} &= -\frac{1}{\hat{Z}_C} \sinh(\hat{\gamma}\mathcal{L}) \\ &= -\frac{1}{\hat{Z}_C} \frac{e^{\hat{\gamma}\mathcal{L}} - e^{-\hat{\gamma}\mathcal{L}}}{2}\end{aligned}\quad (6.85c)$$

$$\begin{aligned}\hat{\phi}_{22} &= \cosh(\hat{\gamma}\mathcal{L}) \\ &= \frac{e^{\hat{\gamma}\mathcal{L}} + e^{-\hat{\gamma}\mathcal{L}}}{2}\end{aligned}\quad (6.85d)$$

The chain parameters only relate the voltage and current at one end of the line to the voltage and current at the other end of the line. They do not explicitly determine those voltages and currents until we incorporate the terminal conditions. In order to incorporate the terminal conditions, we write the terminal conditions in the form of Thevenin equivalents. For example, for the typical terminations shown in Figure 6.1, these become

$$\hat{V}(0) = \hat{V}_S - \hat{Z}_S \hat{I}(0) \quad (6.86a)$$

and

$$\hat{V}(\mathcal{L}) = \hat{Z}_L \hat{I}(\mathcal{L}) \quad (6.86b)$$

Writing out the chain-parameter representation in (6.79) and substituting (6.86) gives

$$\hat{V}(\mathcal{L}) = \hat{Z}_L \hat{I}(\mathcal{L}) = \hat{\phi}_{11} [\hat{V}(0) = \hat{V}_S - \hat{Z}_S \hat{I}(0)] + \hat{\phi}_{12} \hat{I}(0) \quad (6.87a)$$

$$\hat{I}(\mathcal{L}) = \hat{\phi}_{21} [\hat{V}(0) = \hat{V}_S - \hat{Z}_S \hat{I}(0)] + \hat{\phi}_{22} \hat{I}(0) \quad (6.87b)$$

Substituting (6.87b) into (6.87a) yields.

$$[\hat{\phi}_{12} - \hat{\phi}_{11} \hat{Z}_S - \hat{Z}_L \hat{\phi}_{22} + \hat{Z}_L \hat{\phi}_{21} \hat{Z}_S] \hat{I}(0) = [\hat{Z}_L \hat{\phi}_{21} - \hat{\phi}_{11}] \hat{V}_S \quad (6.88a)$$

and

$$\hat{I}(\mathcal{L}) = \hat{\phi}_{21} \hat{V}_S + [\hat{\phi}_{22} - \hat{\phi}_{21} \hat{Z}_S] \hat{I}(0) \quad (6.88b)$$

Once (6.88a) is solved for the current at $z = 0$, (6.88b) can be solved for the current at $z = \mathcal{L}$. Then the voltages can be obtained from the terminal relations in (6.86).

6.5.2 Approximating Abruptly Nonuniform Lines with the Chain-Parameter Matrix

The chain-parameter matrix relates the voltage and current at the right end of the line to the voltage and current at the left end of the line. Hence, the overall chain-parameter matrix of several such lines that are *cascaded* in series can be obtained as the product of the chain-parameter matrices of the sections (in the proper order). For example, consider the cascade of N lines or sections of lines having chain-parameter matrices $\Phi(\Delta z_i)$, each of length Δz_i for $i = 1, 2, 3, \dots, N$ as shown in Figure 6.13(a). In other words, the overall chain-parameter matrix is

$$\begin{aligned} \hat{\Phi}(\mathcal{L}) &= \hat{\Phi}_N(\Delta z_N) \times \cdots \times \hat{\Phi}_i(\Delta z_i) \times \cdots \times \hat{\Phi}_1(\Delta z_1) \\ &= \prod_{k=1}^N \hat{\Phi}_{N-k+1}(\Delta z_{N-k+1}) \end{aligned} \quad (6.89)$$

It is important to observe the proper order of multiplication of the individual chain-parameter matrices in this product. This is a result of the definition of the chain-parameter matrices as

$$\begin{bmatrix} \hat{V}(z_{k+1}) \\ \hat{I}(z_{k+1}) \end{bmatrix} = \hat{\Phi}_{k+1}(\Delta z_{k+1}) \begin{bmatrix} \hat{V}(z_k) \\ \hat{I}(z_k) \end{bmatrix} \quad (6.90a)$$

and

$$\begin{bmatrix} \hat{V}(z_k) \\ \hat{I}(z_k) \end{bmatrix} = \hat{\Phi}_k(\Delta z_k) \begin{bmatrix} \hat{V}(z_{k-1}) \\ \hat{I}(z_{k-1}) \end{bmatrix} \quad (6.90b)$$

Figure 6.13(b) and (c) shows that the chain-parameter representation can be used to model nonuniform lines. For example, the twisted pair of wires shown in Figure 6.13(b) is truly a bifilar helix, but we can approximate it as a sequence of loops lying in the page with an abrupt interchange at the junctions. The chain-parameter matrices of the uniform sections are then multiplied together along with chain-parameter matrices that give an interchange of the voltages and currents at the junctions. If the lengths of the sections are assumed to be identical, then the overall chain-parameter

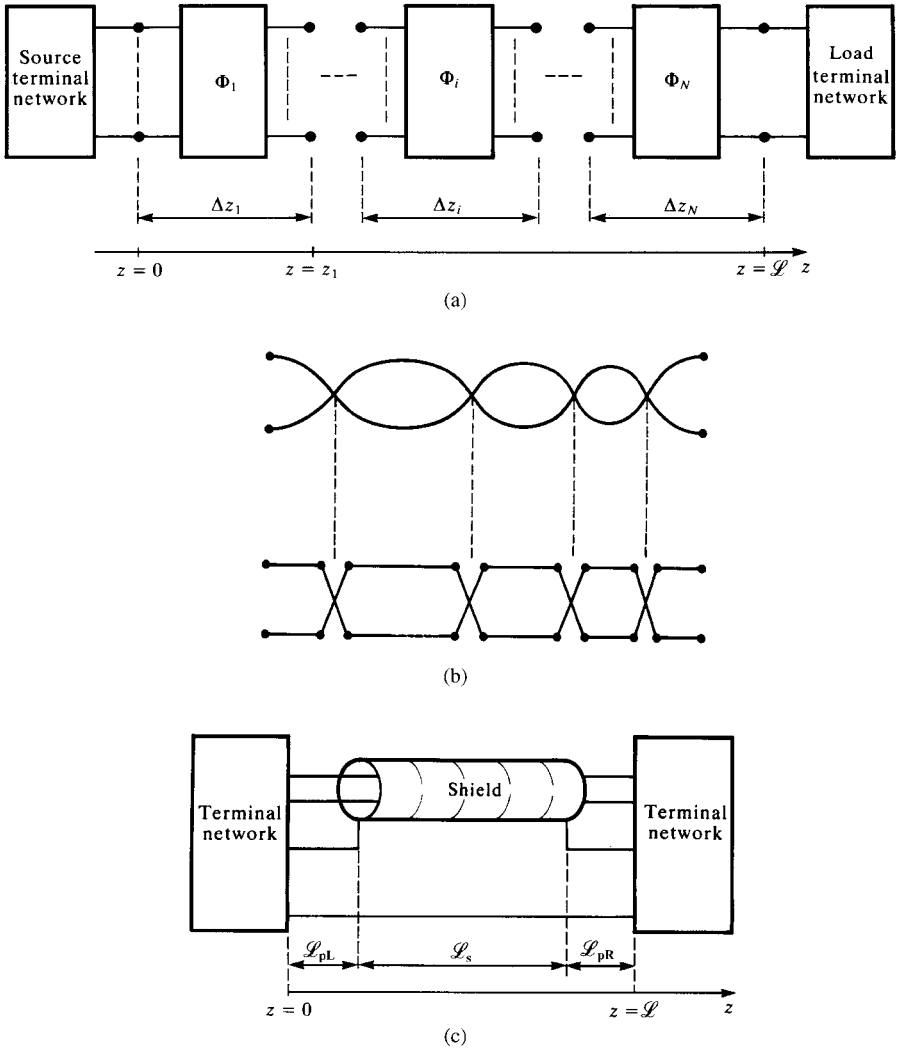


FIGURE 6.13 Representing abruptly nonuniform lines as (a) a cascade of uniform subsections, and applications to (b) twisted pairs and (c) shielded wires with pigtailed sections.

matrix is the N th power of the chain-parameter matrix of each section (that includes the interchange chain-parameter matrix). This can be computed quite efficiently using, for example, the Cayley–Hamilton theorem for powers of a matrix [A.2, G.1, G.6, G.7].

Figure 6.13(c) shows another application for shielded cables. Shielded cables often have exposed sections at the ends to facilitate connection of the shield to the terminal networks [F.1–F.6]. The shield is connected to the terminations via a “pigtail” wire over the exposed sections. The overall chain-parameter matrix can then

be obtained as the product of the chain-parameter matrices for the pigtail sections of length \mathcal{L}_{pL} and \mathcal{L}_{pR} and the chain-parameter matrix of the shielded section of length \mathcal{L}_S as

$$\hat{\Phi}(\mathcal{L}) = \hat{\Phi}_{pR}(\mathcal{L}_{pR}) \times \hat{\Phi}_S(\mathcal{L}_S) \times \hat{\Phi}_{pL}(\mathcal{L}_{pL}) \quad (6.91)$$

Once the overall chain-parameter matrix is obtained, the terminal constraints at the left and right ends of the line can be incorporated to solve for the terminal voltages and currents as described previously.

6.5.3 The Z and Y Parameters

The Z (impedance) parameters have the units of ohms and relate the voltages to the currents. These are defined as

$$\begin{bmatrix} \hat{V}(0) \\ \hat{V}(\mathcal{L}) \end{bmatrix} = \underbrace{\begin{bmatrix} \hat{Z}_{11} & \hat{Z}_{12} \\ \hat{Z}_{21} & \hat{Z}_{22} \end{bmatrix}}_{\hat{\mathbf{Z}}} \begin{bmatrix} \hat{I}(0) \\ -\hat{I}(\mathcal{L}) \end{bmatrix} \quad (6.92)$$

For the Z and Y parameters, the currents are defined to be directed into the two-port. Hence, we use $-\hat{I}(\mathcal{L})$ in this matrix representation. For a lossless line, the impedance parameters are again obtained by eliminating \hat{V}^+ and \hat{V}^- from the basic solution in (6.9) to yield

$$\begin{bmatrix} \hat{V}(0) \\ \hat{V}(\mathcal{L}) \end{bmatrix} = \underbrace{\begin{bmatrix} \frac{Z_C \cos(\beta\mathcal{L})}{j \sin(\beta\mathcal{L})} & \frac{Z_C}{Z_C \cos(\beta\mathcal{L})} \\ \frac{Z_C}{j \sin(\beta\mathcal{L})} & \frac{Z_C \cos(\beta\mathcal{L})}{j \sin(\beta\mathcal{L})} \end{bmatrix}}_{\hat{\mathbf{Z}}} \begin{bmatrix} \hat{I}(0) \\ -\hat{I}(\mathcal{L}) \end{bmatrix} \quad (6.93)$$

The Z-parameter matrix is symmetric, so we may write it as

$$\begin{bmatrix} \hat{V}(0) \\ \hat{V}(\mathcal{L}) \end{bmatrix} = \underbrace{\begin{bmatrix} \hat{Z}_s & \hat{Z}_m \\ \hat{Z}_m & \hat{Z}_s \end{bmatrix}}_{\hat{\mathbf{Z}}} \begin{bmatrix} \hat{I}(0) \\ -\hat{I}(\mathcal{L}) \end{bmatrix} \quad (6.94a)$$

where

$$\begin{aligned} \hat{Z}_s &= \frac{Z_C \cos(\beta\mathcal{L})}{j \sin(\beta\mathcal{L})} \\ &= Z_C \frac{1}{j \tan(\beta\mathcal{L})} \end{aligned} \quad (6.94b)$$

$$\hat{Z}_m = \frac{Z_C}{j \sin(\beta\mathcal{L})} \quad (6.94c)$$

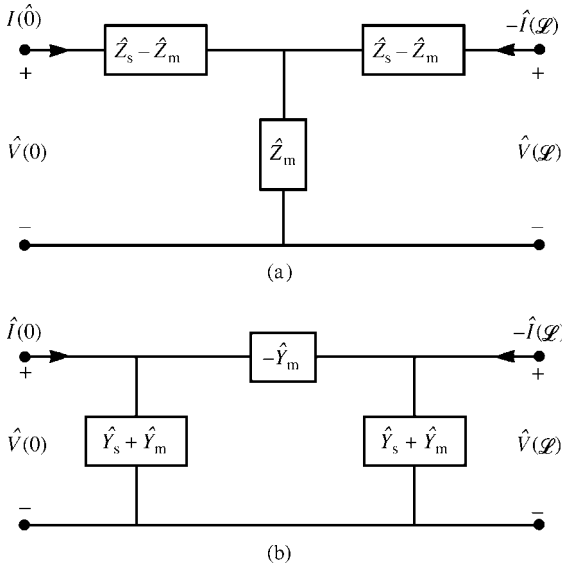


FIGURE 6.14 Equivalent circuits for (a) the Z parameters and (b) the Y parameters.

An (exact) equivalent circuit for the Z-parameter representation is shown in Figure 6.14(a).

Similarly, the Y (admittance) parameters relate the terminal currents to the terminal voltages and have the units of siemens and are defined as

$$\begin{bmatrix} \hat{I}(0) \\ -\hat{I}(\mathcal{L}) \end{bmatrix} = \underbrace{\begin{bmatrix} \hat{Y}_{11} & \hat{Y}_{12} \\ \hat{Y}_{21} & \hat{Y}_{22} \end{bmatrix}}_{\hat{\mathbf{Y}}} \begin{bmatrix} \hat{V}(0) \\ \hat{V}(\mathcal{L}) \end{bmatrix} \tag{6.95}$$

The Y-parameter matrix is the inverse of the Z-parameter matrix, $\mathbf{Y} = \mathbf{Z}^{-1}$, so that

$$\begin{bmatrix} \hat{I}(0) \\ -\hat{I}(\mathcal{L}) \end{bmatrix} = \underbrace{\begin{bmatrix} \frac{\cos(\beta\mathcal{L})}{jZ_C \sin(\beta\mathcal{L})} & -\frac{1}{jZ_C \sin(\beta\mathcal{L})} \\ -\frac{1}{jZ_C \sin(\beta\mathcal{L})} & \frac{\cos(\beta\mathcal{L})}{jZ_C \sin(\beta\mathcal{L})} \end{bmatrix}}_{\hat{\mathbf{Y}}} \begin{bmatrix} \hat{V}(0) \\ \hat{V}(\mathcal{L}) \end{bmatrix} \tag{6.96}$$

The Y-parameter matrix is symmetric, so we may write it as

$$\begin{bmatrix} \hat{I}(0) \\ -\hat{I}(\mathcal{L}) \end{bmatrix} = \underbrace{\begin{bmatrix} \hat{Y}_s & \hat{Y}_m \\ \hat{Y}_m & \hat{Y}_s \end{bmatrix}}_{\hat{\mathbf{Y}}} \begin{bmatrix} \hat{V}(0) \\ \hat{V}(\mathcal{L}) \end{bmatrix} \tag{6.97a}$$

where

$$\begin{aligned}\hat{Y}_s &= \frac{\cos(\beta\mathcal{L})}{jZ_C\sin(\beta\mathcal{L})} \\ &= \frac{1}{jZ_C\tan(\beta\mathcal{L})}\end{aligned}\quad (6.97b)$$

$$\hat{Y}_m = -\frac{1}{jZ_C\sin(\beta\mathcal{L})}\quad (6.97c)$$

An (exact) equivalent circuit for the Y -parameter representation is shown in Figure 6.14(b). Observe that the Z - and Y -parameter matrices are singular when the line length is a multiple of a half wavelength, that is, $\mathcal{L} = n(\lambda/2)$, because $\sin(\beta\mathcal{L}) = \sin(2\pi(\mathcal{L}/\lambda))$ is zero. The chain-parameter matrix on the contrary is never singular.

These are obtained for a lossless line. To obtain the Z or Y parameters for a lossy line, we again simply replace $\cos(\beta\mathcal{L}) \Rightarrow \cosh(\hat{\gamma}\mathcal{L})$ and replace $j\sin(\beta\mathcal{L}) \Rightarrow \sinh(\hat{\gamma}\mathcal{L})$ along with $Z_C \Rightarrow \hat{Z}_C$. Hence, for a lossy line the Z parameters become

$$\begin{aligned}\hat{Z}_s &= \hat{Z}_C \frac{1}{\tanh(\hat{\gamma}\mathcal{L})} \\ &= \hat{Z}_C \frac{e^{\hat{\gamma}\mathcal{L}} + e^{-\hat{\gamma}\mathcal{L}}}{e^{\hat{\gamma}\mathcal{L}} - e^{-\hat{\gamma}\mathcal{L}}}\end{aligned}\quad (6.98a)$$

$$\begin{aligned}\hat{Z}_m &= \hat{Z}_C \frac{1}{\sinh(\hat{\gamma}\mathcal{L})} \\ &= \hat{Z}_C \frac{2}{e^{\hat{\gamma}\mathcal{L}} - e^{-\hat{\gamma}\mathcal{L}}}\end{aligned}\quad (6.98b)$$

and the Y parameters become

$$\begin{aligned}\hat{Y}_s &= \hat{Y}_C \frac{1}{\tanh(\hat{\gamma}L)} \\ &= \hat{Y}_C \frac{e^{\hat{\gamma}L} + e^{-\hat{\gamma}L}}{e^{\hat{\gamma}L} - e^{-\hat{\gamma}L}}\end{aligned}\quad (6.99a)$$

$$\begin{aligned}\hat{Y}_m &= -\hat{Y}_C \frac{1}{\sinh(\hat{\gamma}L)} \\ &= -\hat{Y}_C \frac{2}{e^{\hat{\gamma}L} - e^{-\hat{\gamma}L}}\end{aligned}\quad (6.99b)$$

and $\hat{Y}_C = \frac{1}{\hat{Z}_C}$.

As was the case for the chain parameters, the Z and Y parameters only relate the voltages at each end of the line to the currents at each end of the line; they do not

explicitly determine them. As was the case for the chain parameters, the terminal conditions in (6.86) can be combined with the Z or Y parameters to give equations to explicitly solve for the terminal voltages and currents.

PROBLEMS

- 6.1** Show by direct substitution that (6.9) satisfy (6.8).
- 6.2** Show that (6.25) and (6.24) are equivalent.
- 6.3** For the transmission line shown in Figure 6.1, $f = 5$ MHz, $v = 3 \times 10^8$ m/s, $\mathcal{L} = 78$ m, $Z_C = 50 \Omega$, $\hat{V}_S = 50 \angle 0^\circ$, $\hat{Z}_S = 20 - j30 \Omega$, $\hat{Z}_L = 200 + j500 \Omega$. Determine (a) the line length as a fraction of a wavelength, (b) the voltage reflection coefficient at the load and at the input to the line, (c) the input impedance to the line, (d) the time-domain voltages at the input to the line and at the load, (e) the average power delivered to the load, and (f) the VSWR. [(a) 1.3, (b) $0.9338 \angle 9.866^\circ$, $0.9338 \angle 153.9^\circ$, (c) $11.73 \angle 81.16^\circ$, (d) $20.55 \cos(10\pi \times 10^6 t + 121.3^\circ)$, $89.6 \cos(10\pi \times 10^6 t - 50.45^\circ)$, (e) 2.77 W, and (f) 29.21]
- 6.4** For the transmission line shown in Figure 6.1, $f = 200$ MHz, $v = 3 \times 10^8$ m/s, $\mathcal{L} = 2.1$ m, $Z_C = 100 \Omega$, $\hat{V}_S = 10 \angle 60^\circ$, $\hat{Z}_S = 50 \Omega$, and $\hat{Z}_L = 10 - j50 \Omega$. Determine (a) the line length as a fraction of a wavelength, (b) the voltage reflection coefficient at the load and at the input to the line, (c) the input impedance to the line, (d) the time-domain voltages at the input to the line and at the load, (e) the average power delivered to the load, and (f) the VSWR. [(a) 1.4, (b) $0.8521 \angle -126.5^\circ$, $0.8521 \angle -54.5^\circ$, (c) $192 \angle -78.83^\circ$, (d) $9.25 \cos(4\pi \times 10^8 t + 46.33^\circ)$, $4.738 \cos(4\pi \times 10^8 t - 127^\circ)$, (e) 43 mW, and (f) 12.52]
- 6.5** For the transmission line shown in Figure 6.1, $f = 1$ GHz, $v = 1.7 \times 10^8$ m/s, $\mathcal{L} = 11.9$ cm, $Z_C = 100 \Omega$, $\hat{V}_S = 5 \angle 0^\circ$, $\hat{Z}_S = 20 \Omega$, and $\hat{Z}_L = -j160 \Omega$. Determine (a) the line length as a fraction of a wavelength, (b) the voltage reflection coefficient at the load and at the input to the line, (c) the input impedance to the line, (d) the time-domain voltages at the input to the line and at the load, (e) the average power delivered to the load, and (f) the VSWR. [(a) 0.7, (b) $1 \angle -64.1^\circ$, $1 \angle 152^\circ$, (c) $24.94 \angle 90^\circ$, (d) $3.901 \cos(2\pi \times 10^9 t + 38.72^\circ)$, $13.67 \cos(2\pi \times 10^9 t + 38.72^\circ)$, (e) 0 W, and (f) ∞]
- 6.6** For the transmission line shown in Figure 6.1, $f = 600$ MHz, $v = 2 \times 10^8$ m/s, $\mathcal{L} = 53$ cm, $Z_C = 75 \Omega$, $\hat{V}_S = 20 \angle 40^\circ$, $\hat{Z}_S = 30 \Omega$ and $\hat{Z}_L = 100 - j300 \Omega$. Determine (a) the line length as a fraction of a wavelength, (b) the voltage reflection coefficient at the input to the line and at the load, (c) the input impedance to the line, (d) the time-domain voltages at the input to the line and at the load, (e) the average power delivered to the load, and (f) the VSWR. [(a) 1.59, (b) $0.8668 \angle -25.49^\circ$, $0.8668 \angle -90.29^\circ$, (c) $74.62 \angle -81.84^\circ$, (d) $17.71 \cos(12\pi \times 10^8 t + 19.37^\circ)$, $24.43 \cos(12\pi \times 10^6 t - 163.8^\circ)$, (e) 0.298 W, and (f) 14.02]

6.7 For the transmission line shown in Figure 6.1, $f = 1 \text{ MHz}$, $v = 3 \times 10^8 \text{ m/s}$, $\mathcal{L} = 108 \text{ m}$, $Z_C = 300 \Omega$, $\hat{V}_S = 100 \angle 0^\circ$, $\hat{Z}_S = 50 + j50 \Omega$, and $\hat{Z}_L = 100 - j100 \Omega$. Determine (a) the line length as a fraction of a wavelength, (b) the voltage reflection coefficient at the load and at the input to the line, (c) the input impedance to the line, (d) the time-domain voltages at the input to the line and at the load, (e) the average power delivered to the load, and (f) the VSWR. [(a) 0.36, (b) $0.5423 \angle -139.4^\circ$, $0.5423 \angle -38.6^\circ$, (c) $657.1 \angle -43.79^\circ$, (d) $99.2 \cos(2\pi \times 10^6 t - 6.127^\circ)$, $46.5 \cos(2\pi \times 10^6 t - 153.3^\circ)$, (e) 5.41 W, and (f) 3.37]

6.8 Confirm the input and load voltages for Problem 6.3 using SPICE.

6.9 Confirm the input and load voltages for Problem 6.4 using SPICE.

6.10 Confirm the input and load voltages for Problem 6.5 using SPICE.

6.11 Confirm the input and load voltages for Problem 6.6 using SPICE.

6.12 Confirm the input and load voltages for Problem 6.7 using SPICE.

6.13 A half-wavelength dipole antenna is connected to a 100-MHz source with a 3.6-m length of 300- Ω transmission line (twin lead, $v = 2.6 \times 10^8 \text{ m/s}$) as shown in Figure P6.13. The source is represented by an open-circuit voltage of 10 V and source impedance of 50 Ω , whereas the input to the dipole antenna is represented by a 73- Ω resistance in series with an inductive reactance of 42.5 Ω . The average power dissipated in the 73- Ω resistance is equal to the power radiated into space by the antenna. Determine the average power radiated by the antenna with and without the transmission line and the VSWR on the line. [91.14 mW, 215.53 mW, 4.2]

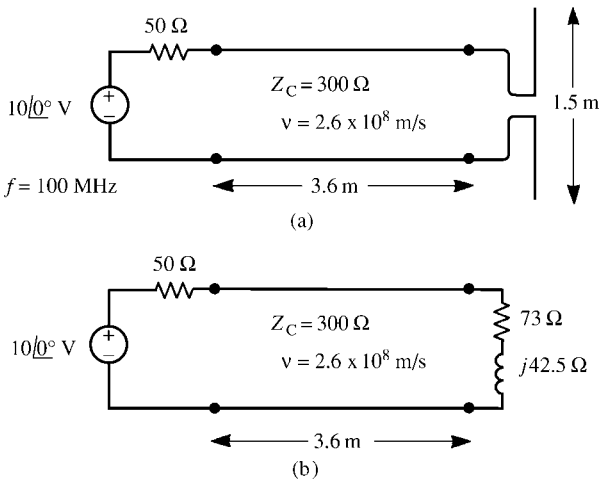


FIGURE P6.13

6.14 Two identical half-wavelength dipole antennas are connected in parallel and fed from one 300-MHz source as shown in Figure P6.14. Determine the average

power delivered to each antenna. *Hint:* Determine the electrical lengths of the transmission lines. [115 mW]

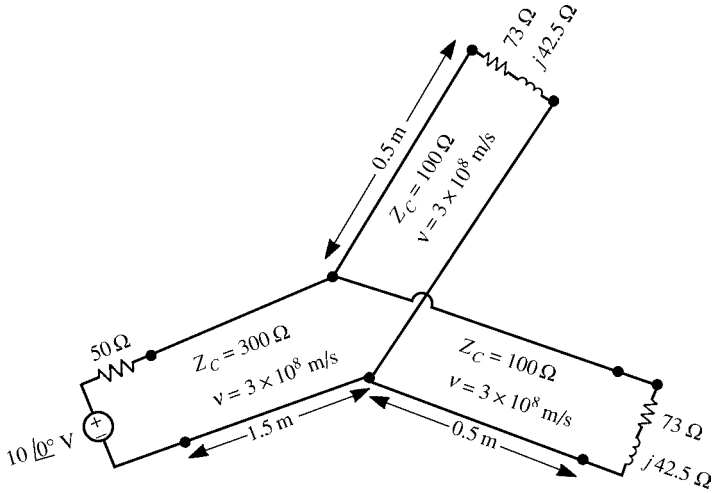


FIGURE P 6.14

- 6.15 Demonstrate the incorporation of terminal impedances in (6.37).
- 6.16 Demonstrate the formula for the voltage and current anywhere on the line in (6.39).
- 6.17 Demonstrate the power flow relation in (6.54).
- 6.18 Show, by direct substitution, that (6.60) satisfies (6.58).
- 6.19 Demonstrate the results in (6.75).
- 6.20 A low-loss coaxial cable has the following parameters: $\hat{Z}_C \cong (75 + j0) \Omega$, $\alpha = 0.05$, and $v = 2 \times 10^8 \text{ m/s}$. Determine the input impedance to a 11.175-m length of the cable at 400 MHz if the line is terminated in (a) a short circuit, (b) an open circuit, and (c) a $300\text{-}\Omega$ resistor. [(a) $90.209 \angle -34.86^\circ \Omega$, (b) $62.355 \angle 34.06^\circ \Omega$, and (c) $66.7 \angle 21.2^\circ \Omega$]
- 6.21 An air-filled line ($v = 3 \times 10^8 \text{ m/s}$) having a characteristic impedance of 50Ω is driven at a frequency of 30 MHz and is 1 m in length. The line is terminated in a load of $\hat{Z}_L = (200 - j200) \Omega$. Determine the input impedance using (a) the transmission-line model and (b) the approximate lumped-Pi model. Use PSPICE to compute both results. [(a) $(12.89 - j51.49) \Omega$, and (b) $(13.76 - j52.25) \Omega$]
- 6.22 A lossless coaxial cable ($v = 2 \times 10^8 \text{ m/s}$) having a characteristic impedance of 100Ω is driven at a frequency of 4 MHz and is 5 m in length. The line is terminated in a load of $\hat{Z}_L = (150 - j50) \Omega$ and the source is $\hat{V}_S = 10 \angle 0^\circ \text{ V}$ with $\hat{Z}_S = 25 \Omega$. Determine the input and output voltages to the line using (a) the transmission-line model, and (b) the approximate lumped-Pi model. Use PSPICE to compute both results. [Exact: $\hat{V}(0) = 7.954 \angle -6.578^\circ$, $\hat{V}(\mathcal{L}) =$

$10.25\angle -33.6^\circ$; approximate: $\hat{V}(0) = 7.959\angle -5.906^\circ$, $\hat{V}(\mathcal{L}) = 10.27\angle -35.02^\circ$

- 6.23** Verify the chain-parameter relations in (6.82).
6.24 Verify the Z parameters in (6.93).
6.25 Verify the Y parameters in (6.96).
6.26 Verify the equivalent circuits for the Z and Y parameters in Figure 6.14.

7

FREQUENCY-DOMAIN ANALYSIS OF MULTICONDUCTOR LINES

In this chapter, we consider the *frequency-domain* solution of the MTL (multi-conductor transmission lines) equations for an $(n + 1)$ -conductor line where the excitation sources are sinusoids that have been applied for a sufficient length of time so that the line voltages and currents are in *steady state*. We will find that, using matrix notation, the solutions to these phasor MTL equations bear a striking similarity to the solutions for two-conductor lines obtained in the previous chapter. The primary method we will use to solve these phasor MTL equations is to decouple them with a similarity transformation [A.4, 1–4]. This frequency-domain solution of the MTL equations has a long history [5–10].

7.1 THE MTL TRANSMISSION-LINE EQUATIONS IN THE FREQUENCY DOMAIN

We assume that the time variation of the line excitation sources is sinusoidal and the line is in steady state. Therefore, the line voltages and currents are also sinusoidal having a magnitude and a phase angle and the same frequency as the sources. Thus, the n line voltages and n line currents in the time domain are obtained from their *phasor* form in the usual fashion as

$$V_i(z, t) = \text{Re}\{\hat{V}_i(z) e^{j\omega t}\} \quad (7.1a)$$

$$I_i(z, t) = \text{Re}\{\hat{I}_i(z) e^{j\omega t}\} \quad (7.1b)$$

where $\text{Re}\{\cdot\}$ denotes the *real part* of the enclosed complex quantity, and the *phasor* voltages and currents have a magnitude and a phase angle as

$$\begin{aligned}\hat{V}_i(z) &= V_i(z)\angle\theta_i(z) \\ &= V_i(z)e^{j\theta_i(z)}\end{aligned}\tag{7.2a}$$

$$\begin{aligned}\hat{I}_i(z) &= I_i(z)\angle\phi_i(z) \\ &= I_i(z)e^{j\phi_i(z)}\end{aligned}\tag{7.2b}$$

The radian frequency of excitation (as well as the radian frequency of the resulting line voltages and currents) is denoted by ω , where $\omega = 2\pi f$ and f is the cyclic frequency of excitation. Inserting (7.2) into (7.1) gives the resulting *time-domain* forms of the n line voltages and n line currents as

$$V_i(z, t) = V_i(z)\cos(\omega t + \theta_i(z))\tag{7.3a}$$

$$I_i(z, t) = I_i(z)\cos(\omega t + \phi_i(z))\tag{7.3b}$$

Replacing all time derivatives in the time-domain MTL equations with $j\omega$, the frequency-domain (phasor) MTL equations are given, in matrix form, in Eq. (3.32) of Chapter 3:

$$\frac{d}{dz}\hat{\mathbf{V}}(z) = -\hat{\mathbf{Z}}\hat{\mathbf{I}}(z)\tag{7.4a}$$

$$\frac{d}{dz}\hat{\mathbf{I}}(z) = -\hat{\mathbf{Y}}\hat{\mathbf{V}}(z)\tag{7.4b}$$

where the $n \times 1$ column vectors $\hat{\mathbf{V}}(z)$ and $\hat{\mathbf{I}}(z)$ contain the n line voltages $\hat{V}_i(z)$ and n currents $\hat{I}_i(z)$ as

$$\hat{\mathbf{V}}(z) = \begin{bmatrix} \hat{V}_1(z) \\ \vdots \\ \hat{V}_i(z) \\ \vdots \\ \hat{V}_n(z) \end{bmatrix}\tag{7.5a}$$

$$\hat{\mathbf{I}}(z) = \begin{bmatrix} \hat{I}_1(z) \\ \vdots \\ \hat{I}_i(z) \\ \vdots \\ \hat{I}_n(z) \end{bmatrix}\tag{7.5b}$$

The $n \times n$ per-unit-length *impedance*, $\hat{\mathbf{Z}}$, and *admittance*, $\hat{\mathbf{Y}}$, matrices are given by

$$\hat{\mathbf{Z}} = \mathbf{R} + j\omega \mathbf{L} \quad (7.6a)$$

$$\hat{\mathbf{Y}} = \mathbf{G} + j\omega \mathbf{C} \quad (7.6b)$$

and contain the $n \times n$ per-unit-length resistance \mathbf{R} , inductance (containing both internal and external inductance) $\mathbf{L} = \mathbf{L}_i + \mathbf{L}_e$, conductance \mathbf{G} , and capacitance \mathbf{C} matrices. Since \mathbf{R} , \mathbf{L} , \mathbf{C} , and \mathbf{G} are symmetric matrices, $\hat{\mathbf{Z}}$ and $\hat{\mathbf{Y}}$ are also symmetric. The resulting equations in (7.4) are a set of *coupled, first-order ordinary differential equations with complex coefficients*.

Alternatively, the coupled, first-order phasor MTL equations in (7.4) can be placed in the form of *uncoupled, second-order ordinary differential equations* by differentiating one with respect to line position z and substituting the other, and vice versa, to yield.

$$\frac{d^2}{dz^2} \hat{\mathbf{V}}(z) = \hat{\mathbf{Z}} \hat{\mathbf{Y}} \hat{\mathbf{V}}(z) \quad (7.7a)$$

$$\frac{d^2}{dz^2} \hat{\mathbf{I}}(z) = \hat{\mathbf{Y}} \hat{\mathbf{Z}} \hat{\mathbf{I}}(z) \quad (7.7b)$$

Ordinarily, the per-unit-length parameter matrices $\hat{\mathbf{Z}}$ and $\hat{\mathbf{Y}}$ do not commute, that is, $\mathbf{ZY} \neq \mathbf{YZ}$, so that the proper order of multiplication in (7.7) must be observed. In differentiating (7.4) with respect to line position z , we have assumed that the per-unit-length parameter matrices \mathbf{R} , \mathbf{L} , \mathbf{G} , and \mathbf{C} are independent of z . Thus, we have assumed that the cross-sectional line dimensions and surrounding media properties are invariant along the line (independent of z) or, in other words, the line is a *uniform* line. Both the first-order coupled forms of the MTL equations given in (7.4) and the second-order uncoupled forms given in (7.7) will be useful in obtaining the final solution.

7.2 THE GENERAL SOLUTION FOR AN $(n + 1)$ -CONDUCTOR LINE

In the previous chapter, we discussed the well-known solutions for a two-conductor line. In this section, we begin our study of the solutions for an $(n + 1)$ -conductor line or MTL. In many cases, the results and properties of the solution for a two-conductor line carry over, with matrix notation, to an MTL.

7.2.1 Decoupling the MTL Equations by Similarity Transformations

As was the case for two-conductor lines, we concentrate on solving the *second-order* differential equations given in (7.7). Notice that the equations in (7.7) are coupled together because \mathbf{ZY} and \mathbf{YZ} are full matrices; that is, each set of voltages and currents,

$\hat{V}_i(z)$ and $\hat{I}_i(z)$, affects all the other sets of voltages and currents, $\hat{V}_j(z)$ and $\hat{I}_j(z)$. The essential idea in the solution method that we will use is to *decouple* them with a *similarity transformation* [1–4]. We will use a *change of variables* to decouple the second-order differential equations in (7.7) by putting them into the form of n separate equations describing n isolated two-conductor lines. Apply the solution techniques in the previous chapter to these individual two-conductor lines and then use the change of variables to return to the original voltages and currents. This method of using a *change of variables* is perhaps the most frequently used technique for generating the general solution to the MTL equations. A complete discussion of this technique for the phasor MTL equations is given in [B.25].

In implementing this method, we transform to *mode quantities* as

$$\hat{\mathbf{V}}(z) = \hat{\mathbf{T}}_V \hat{\mathbf{V}}_m(z) \quad (7.8a)$$

$$\hat{\mathbf{I}}(z) = \hat{\mathbf{T}}_I \hat{\mathbf{I}}_m(z) \quad (7.8b)$$

The $n \times n$ complex matrices $\hat{\mathbf{T}}_V$ and $\hat{\mathbf{T}}_I$ define a change of variables between the actual phasor line voltages and currents, $\hat{\mathbf{V}}$ and $\hat{\mathbf{I}}$, and the *mode* voltages and currents, $\hat{\mathbf{V}}_m$ and $\hat{\mathbf{I}}_m$. In order for this to be valid, these $n \times n$ matrices must be nonsingular; that is, $\hat{\mathbf{T}}_V^{-1}$ and $\hat{\mathbf{T}}_I^{-1}$ must exist, where we denote the inverse of an $n \times n$ matrix \mathbf{M} as \mathbf{M}^{-1} in order to go between both sets of variables. Substituting these into the second-order MTL equations in (7.7) gives

$$\begin{aligned} \frac{d^2}{dz^2} \hat{\mathbf{V}}_m(z) &= \hat{\mathbf{T}}_V^{-1} \hat{\mathbf{Z}} \hat{\mathbf{Y}} \hat{\mathbf{T}}_V \hat{\mathbf{V}}_m(z) \\ &= \hat{\gamma}^2 \hat{\mathbf{V}}_m(z) \end{aligned} \quad (7.9a)$$

$$\begin{aligned} \frac{d^2}{dz^2} \hat{\mathbf{I}}_m(z) &= \hat{\mathbf{T}}_I^{-1} \hat{\mathbf{Y}} \hat{\mathbf{Z}} \hat{\mathbf{T}}_I \hat{\mathbf{I}}_m(z) \\ &= \hat{\gamma}^2 \hat{\mathbf{I}}_m(z) \end{aligned} \quad (7.9b)$$

The objective is to decouple these second-order equations by finding a $\hat{\mathbf{T}}_V$ and a $\hat{\mathbf{T}}_I$ that simultaneously *diagonalize* $\hat{\mathbf{Z}} \hat{\mathbf{Y}}$ and $\hat{\mathbf{Y}} \hat{\mathbf{Z}}$ via *similarity transformations* as

$$\hat{\mathbf{T}}_V^{-1} \hat{\mathbf{Z}} \hat{\mathbf{Y}} \hat{\mathbf{T}}_V = \hat{\gamma}^2 \quad (7.10a)$$

$$\hat{\mathbf{T}}_I^{-1} \hat{\mathbf{Y}} \hat{\mathbf{Z}} \hat{\mathbf{T}}_I = \hat{\gamma}^2 \quad (7.10b)$$

where $\hat{\gamma}^2$ is an $n \times n$ diagonal matrix:

$$\hat{\gamma}^2 = \begin{bmatrix} \hat{\gamma}_1^2 & 0 & \cdots & 0 \\ 0 & \hat{\gamma}_2^2 & \ddots & \vdots \\ \vdots & \ddots & \ddots & 0 \\ 0 & \cdots & 0 & \hat{\gamma}_n^2 \end{bmatrix} \quad (7.10c)$$

The mode equations in (7.9) will therefore be decoupled. This will yield the n propagation constants $\hat{\gamma}_i$ of the n modes.

This is the classic *eigenvalue/eigenvector* problem of matrices [A.2, A.4, B.1, 1–4]. This classic problem can be summarized by the following. Suppose we wish to find an $n \times n$ nonsingular matrix \mathbf{T} that diagonalizes an $n \times n$ matrix \mathbf{M} as

$$\mathbf{T}^{-1} \mathbf{M} \mathbf{T} = \Lambda \tag{7.11}$$

where Λ is an $n \times n$ diagonal matrix with Λ_i on the main diagonal and zeros elsewhere. Multiplying both sides of (7.11) by \mathbf{T} yields

$$\mathbf{M} \mathbf{T} - \mathbf{T} \Lambda = \mathbf{0} \tag{7.12}$$

where $\mathbf{0}$ is the $n \times n$ zero matrix. The n columns of \mathbf{T} , \mathbf{T}_i , are the *eigenvectors* of \mathbf{M} and the n values Λ_i are the *eigenvalues* of \mathbf{M} . Equation (7.12) gives n equations for the n eigenvectors as [A.4, 1–4]

$$(\mathbf{M} - \Lambda_i \mathbf{1}_n) \mathbf{T}_i = \mathbf{0}, \quad i = 1, \dots, n \tag{7.13}$$

where $\mathbf{0}$ is the $n \times 1$ zero vector that contains all zeros and the $n \times 1$ column vectors of the eigenvectors \mathbf{T}_i contain the unknowns to be solved for. Equations (7.13) are a set of n homogeneous, algebraic equations. As such, they have [A.4, 1–4]

1. the unique solution $\mathbf{T}_i = \mathbf{0}$ or
2. an infinite number of solutions for \mathbf{T}_i .

Clearly, we want to determine the nontrivial solution (solution 2), which will exist only if the determinants of the coefficient matrices of (7.13) are zero [A.4, 1–4]:

$$|\mathbf{M} - \Lambda_i \mathbf{1}_n| = 0 \tag{7.14}$$

This gives the n th-order *characteristic equation* whose roots are the eigenvalues of \mathbf{M} .

From this discussion and a comparison with (7.10), it is clear that the columns of $\hat{\mathbf{T}}_V$ are the *eigenvectors* of $\hat{\mathbf{Z}}\hat{\mathbf{Y}}$ and the columns of $\hat{\mathbf{T}}_I$ are the *eigenvectors* of $\hat{\mathbf{Y}}\hat{\mathbf{Z}}$. The entries in $\hat{\gamma}^2$, $\hat{\gamma}_i^2$ for $i = 1, \dots, n$, are the *eigenvalues* of $\hat{\mathbf{Z}}\hat{\mathbf{Y}}$ and of $\hat{\mathbf{Y}}\hat{\mathbf{Z}}$. That the eigenvalues of $\hat{\mathbf{Z}}\hat{\mathbf{Y}}$ and $\hat{\mathbf{Y}}\hat{\mathbf{Z}}$ are the same follows from the fact that the eigenvalues of a matrix \mathbf{M} and its transpose \mathbf{M}^t are the same, which is clear from (7.14) because the determinant of a matrix and its transpose are the same [A.4, 1–4]. Taking the transpose of $\hat{\mathbf{Z}}\hat{\mathbf{Y}}$ yields $(\hat{\mathbf{Z}}\hat{\mathbf{Y}})^t = \hat{\mathbf{Y}}^t\hat{\mathbf{Z}}^t = \hat{\mathbf{Y}}\hat{\mathbf{Z}}$, where we have used the fact that $\hat{\mathbf{Z}}$ and $\hat{\mathbf{Y}}$ are symmetric, that is, $\hat{\mathbf{Z}}^t = \hat{\mathbf{Z}}$ and $\hat{\mathbf{Y}}^t = \hat{\mathbf{Y}}$. Hence, the transpose of $\hat{\mathbf{Z}}\hat{\mathbf{Y}}$ is $\hat{\mathbf{Y}}\hat{\mathbf{Z}}$, thus showing that they have the same eigenvalues. Observe that this property relies only on $\hat{\mathbf{Z}}$ and $\hat{\mathbf{Y}}$ being symmetric matrices. Hence, in order to decouple the second-order MTL equations, we only need to find a $\hat{\mathbf{T}}_V$ that diagonalizes the product of $\hat{\mathbf{Z}}\hat{\mathbf{Y}}$ as in (7.10a) or a $\hat{\mathbf{T}}_I$ that diagonalizes the product $\hat{\mathbf{Y}}\hat{\mathbf{Z}}$ as in (7.10b).

In order to diagonalize $\hat{\mathbf{Z}}\hat{\mathbf{Y}}$ or $\hat{\mathbf{Y}}\hat{\mathbf{Z}}$ as in (7.10), we must be able to find a linearly independent set of n eigenvectors. A sufficient condition for this is that all n eigenvalues be distinct. There are important cases where some of the eigenvalues are repeated, yet a linearly independent set of n eigenvectors can be found such that $\hat{\mathbf{Z}}\hat{\mathbf{Y}}$ can be diagonalized as in (7.10). In the case of repeated eigenvalues, the arrangement of the columns of $\hat{\mathbf{T}}_V$ and/or $\hat{\mathbf{T}}_I$ corresponding to those repeated eigenvalues is clearly not unique. Structures that exhibit certain types of symmetry can result in repeated eigenvalues and hence give rise to this nonunique assignment of the columns of $\hat{\mathbf{T}}_V$ or $\hat{\mathbf{T}}_I$. The nonunique assignment of these columns of $\hat{\mathbf{T}}_V$ or $\hat{\mathbf{T}}_I$ will not affect the diagonalization of the second-order equations in (7.7). We will assume in this chapter that $\hat{\mathbf{Z}}\hat{\mathbf{Y}}$ and $\hat{\mathbf{Y}}\hat{\mathbf{Z}}$ can be diagonalized as in (7.10). See [B.25] for a more complete discussion of this diagonalization problem for MTLs.

The transformations $\hat{\mathbf{T}}_V$ and $\hat{\mathbf{T}}_I$ are related [B.25]. Taking the transpose of both sides of (7.10) yields

$$\hat{\mathbf{T}}_V^t \hat{\mathbf{Y}}\hat{\mathbf{Z}} \left(\hat{\mathbf{T}}_V^{-1}\right)^t = \hat{\gamma}^2 = \hat{\mathbf{T}}_I^{-1} \hat{\mathbf{Y}}\hat{\mathbf{Z}} \hat{\mathbf{T}}_I \tag{7.15a}$$

$$\hat{\mathbf{T}}_I^t \hat{\mathbf{Z}}\hat{\mathbf{Y}} \left(\hat{\mathbf{T}}_I^{-1}\right)^t = \hat{\gamma}^2 = \hat{\mathbf{T}}_V^{-1} \hat{\mathbf{Z}}\hat{\mathbf{Y}} \hat{\mathbf{T}}_V \tag{7.15b}$$

and we have used the matrix algebra properties that the transpose of a product of matrices is the product of the transposes in reverse order, that is, $(\mathbf{AB})^t = \mathbf{B}^t\mathbf{A}^t$, and that $\hat{\mathbf{Z}}$ and $\hat{\mathbf{Y}}$ are symmetric, that is, $\hat{\mathbf{Z}}^t = \hat{\mathbf{Z}}$ and $\hat{\mathbf{Y}}^t = \hat{\mathbf{Y}}$, along with the fact that $\hat{\gamma}^2$ is diagonal, so it equals its transpose, that is, $(\hat{\gamma}^2)^t = \hat{\gamma}^2$. This indicates that $\hat{\mathbf{T}}_V$ and $\hat{\mathbf{T}}_I$ can be chosen such that they satisfy [B.25]

$$\hat{\mathbf{T}}_V = \hat{\mathbf{T}}_I^{-1} \tag{7.16a}$$

$$\hat{\mathbf{T}}_I = \hat{\mathbf{T}}_V^{-1} \tag{7.16b}$$

or

$$\begin{aligned} \hat{\mathbf{T}}_V^t \hat{\mathbf{T}}_I &= \mathbf{1}_n \\ &= \hat{\mathbf{T}}_I^t \hat{\mathbf{T}}_V \end{aligned} \tag{7.17}$$

where $\mathbf{1}_n$ is the $n \times n$ identity matrix with 1s on the main diagonal and zeros elsewhere, that is,

$$\mathbf{1}_n = \begin{bmatrix} 1 & 0 & \ddots & 0 & 0 \\ 0 & 1 & 0 & \ddots & 0 \\ \ddots & 0 & \ddots & 0 & \ddots \\ 0 & \ddots & 0 & 1 & 0 \\ 0 & 0 & \ddots & 0 & 1 \end{bmatrix} \tag{7.18}$$

Reference [B.25] gives a rigorous proof of this.

Thus, the equations governing the mode voltages and currents in (7.9) are *decoupled* and have the simple solution

$$\hat{\mathbf{V}}_m(z) = \mathbf{e}^{-\hat{\gamma}z} \hat{\mathbf{V}}_m^+ + \mathbf{e}^{\hat{\gamma}z} \hat{\mathbf{V}}_m^- \quad (7.19a)$$

$$\hat{\mathbf{I}}_m(z) = \mathbf{e}^{-\hat{\gamma}z} \hat{\mathbf{I}}_m^+ - \mathbf{e}^{\hat{\gamma}z} \hat{\mathbf{I}}_m^- \quad (7.19b)$$

where the *matrix exponentials* are defined as

$$\mathbf{e}^{\pm\hat{\gamma}z} = \begin{bmatrix} e^{\pm\hat{\gamma}_1 z} & 0 & \cdots & 0 \\ 0 & e^{\pm\hat{\gamma}_2 z} & \ddots & \vdots \\ \vdots & \ddots & \ddots & 0 \\ 0 & \cdots & 0 & e^{\pm\hat{\gamma}_n z} \end{bmatrix} \quad (7.20)$$

and $\hat{\mathbf{V}}_m^\pm$ and $\hat{\mathbf{I}}_m^\pm$ are $n \times 1$ vectors of (as yet) undetermined constants associated with the forward/backward-traveling waves of the modes:

$$\hat{\mathbf{V}}_m^\pm = \begin{bmatrix} \hat{V}_{m1}^\pm \\ \hat{V}_{m2}^\pm \\ \vdots \\ \hat{V}_{mn}^\pm \end{bmatrix}, \quad \hat{\mathbf{I}}_m^\pm = \begin{bmatrix} \hat{I}_{m1}^\pm \\ \hat{I}_{m2}^\pm \\ \vdots \\ \hat{I}_{mn}^\pm \end{bmatrix} \quad (7.21)$$

Transforming back to the actual line voltages and currents via (7.8) gives

$$\hat{\mathbf{V}}(z) = \hat{\mathbf{T}}_V \left(\mathbf{e}^{-\hat{\gamma}z} \hat{\mathbf{V}}_m^+ + \mathbf{e}^{\hat{\gamma}z} \hat{\mathbf{V}}_m^- \right) \quad (7.22a)$$

$$\hat{\mathbf{I}}(z) = \hat{\mathbf{T}}_I \left(\mathbf{e}^{-\hat{\gamma}z} \hat{\mathbf{I}}_m^+ - \mathbf{e}^{\hat{\gamma}z} \hat{\mathbf{I}}_m^- \right) \quad (7.22b)$$

Therefore, if we can find a transformation that diagonalizes *either* $\hat{\mathbf{Z}}\hat{\mathbf{Y}}$ or $\hat{\mathbf{Y}}\hat{\mathbf{Z}}$, then the decoupling of the equations is assured and the general solution of the MTL equations can be readily obtained.

The general solutions for the line voltages and currents given in (7.22) contain a total of $4n$ undetermined constants in the $n \times 1$ vectors $\hat{\mathbf{V}}_m^+$, $\hat{\mathbf{V}}_m^-$, $\hat{\mathbf{I}}_m^+$, and $\hat{\mathbf{I}}_m^-$. We will now relate those by defining the characteristic impedance matrix, thereby reducing the number of undetermined constants to $2n$. Substituting (7.22b) into (7.4b) yields

$$\begin{aligned} \hat{\mathbf{V}}(z) &= -\hat{\mathbf{Y}}^{-1} \frac{d}{dz} \hat{\mathbf{I}}(z) \\ &= \hat{\mathbf{Y}}^{-1} \hat{\mathbf{T}}_I \hat{\gamma} \left(\mathbf{e}^{-\hat{\gamma}z} \hat{\mathbf{I}}_m^+ + \mathbf{e}^{\hat{\gamma}z} \hat{\mathbf{I}}_m^- \right) \\ &= \underbrace{\hat{\mathbf{Y}}^{-1} \hat{\mathbf{T}}_I \hat{\gamma} \hat{\mathbf{T}}_I^{-1}}_{\hat{\mathbf{Z}}_C} \hat{\mathbf{T}}_I \left(\mathbf{e}^{-\hat{\gamma}z} \hat{\mathbf{I}}_m^+ + \mathbf{e}^{\hat{\gamma}z} \hat{\mathbf{I}}_m^- \right) \end{aligned} \quad (7.23)$$

If we define the characteristic impedance matrix as

$$\hat{\mathbf{Z}}_C = \hat{\mathbf{Y}}^{-1} \hat{\mathbf{T}}_I \hat{\gamma} \hat{\mathbf{T}}_I^{-1} \quad (7.24)$$

then

$$\hat{\mathbf{V}}(z) = \hat{\mathbf{Z}}_C \hat{\mathbf{T}}_I \left(\mathbf{e}^{-\hat{\gamma}z} \hat{\mathbf{I}}_m^+ + \mathbf{e}^{\hat{\gamma}z} \hat{\mathbf{I}}_m^- \right) \quad (7.25a)$$

$$\hat{\mathbf{I}}(z) = \hat{\mathbf{T}}_I \left(\mathbf{e}^{-\hat{\gamma}z} \hat{\mathbf{I}}_m^+ - \mathbf{e}^{\hat{\gamma}z} \hat{\mathbf{I}}_m^- \right) \quad (7.25b)$$

and the number of unknowns is reduced to the $2n$ unknowns in the $n \times 1$ vectors $\hat{\mathbf{I}}_m^+$ and $\hat{\mathbf{I}}_m^-$. An alternative form of the characteristic impedance matrix can be obtained from (7.10b):

$$\hat{\mathbf{Y}}^{-1} \hat{\mathbf{T}}_I = \hat{\mathbf{Z}} \hat{\mathbf{T}}_I \hat{\gamma}^{-2} \quad (7.26)$$

Substituting this into (7.24) yields an alternative form for the characteristic impedance matrix:

$$\hat{\mathbf{Z}}_C = \hat{\mathbf{Z}} \hat{\mathbf{T}}_I \hat{\gamma}^{-1} \hat{\mathbf{T}}_I^{-1} \quad (7.27)$$

Similarly, substituting (7.22a) into (7.4a) yields

$$\begin{aligned} \hat{\mathbf{I}}(z) &= -\hat{\mathbf{Z}}^{-1} \frac{d}{dz} \hat{\mathbf{V}}(z) \\ &= \hat{\mathbf{Z}}^{-1} \hat{\mathbf{T}}_V \hat{\gamma} \left(\mathbf{e}^{-\hat{\gamma}z} \hat{\mathbf{V}}_m^+ - \mathbf{e}^{\hat{\gamma}z} \hat{\mathbf{V}}_m^- \right) \\ &= \underbrace{\hat{\mathbf{Z}}^{-1} \hat{\mathbf{T}}_V \hat{\gamma} \hat{\mathbf{T}}_V^{-1}}_{\hat{\mathbf{Y}}_C} \hat{\mathbf{T}}_V \left(\mathbf{e}^{-\hat{\gamma}z} \hat{\mathbf{V}}_m^+ - \mathbf{e}^{\hat{\gamma}z} \hat{\mathbf{V}}_m^- \right) \end{aligned} \quad (7.28)$$

If we define the characteristic admittance matrix as

$$\hat{\mathbf{Y}}_C = \hat{\mathbf{Z}}^{-1} \hat{\mathbf{T}}_V \hat{\gamma} \hat{\mathbf{T}}_V^{-1} \quad (7.29)$$

then

$$\hat{\mathbf{V}}(z) = \hat{\mathbf{T}}_V \left(\mathbf{e}^{-\hat{\gamma}z} \hat{\mathbf{V}}_m^+ + \mathbf{e}^{\hat{\gamma}z} \hat{\mathbf{V}}_m^- \right) \quad (7.30a)$$

$$\hat{\mathbf{I}}(z) = \hat{\mathbf{Y}}_C \hat{\mathbf{T}}_V \left(\mathbf{e}^{-\hat{\gamma}z} \hat{\mathbf{V}}_m^+ - \mathbf{e}^{\hat{\gamma}z} \hat{\mathbf{V}}_m^- \right) \quad (7.30b)$$

TABLE 7.1 Characteristic impedance/admittance matrix relations

| $\hat{\mathbf{Z}}_C$ | $\hat{\mathbf{Y}}_C$ |
|---|---|
| $\hat{\mathbf{Y}}^{-1} \hat{\mathbf{T}}_I \hat{\gamma} \hat{\mathbf{T}}_I^{-1}$ | $\hat{\mathbf{Z}}^{-1} \hat{\mathbf{T}}_V \hat{\gamma} \hat{\mathbf{T}}_V^{-1}$ |
| $\hat{\mathbf{Z}} \hat{\mathbf{T}}_I \hat{\gamma}^{-1} \hat{\mathbf{T}}_I^{-1}$ | $\hat{\mathbf{Y}} \hat{\mathbf{T}}_V \hat{\gamma}^{-1} \hat{\mathbf{T}}_V^{-1}$ |
| $\hat{\mathbf{T}}_V \hat{\gamma}^{-1} \hat{\mathbf{T}}_V^{-1} \hat{\mathbf{Z}}$ | $\hat{\mathbf{T}}_I \hat{\gamma}^{-1} \hat{\mathbf{T}}_I^{-1} \hat{\mathbf{Y}}$ |
| $\hat{\mathbf{T}}_V \hat{\gamma} \hat{\mathbf{T}}_V^{-1} \hat{\mathbf{Y}}^{-1}$ | $\hat{\mathbf{T}}_I \hat{\gamma} \hat{\mathbf{T}}_I^{-1} \hat{\mathbf{Z}}^{-1}$ |
| $\hat{\mathbf{Y}}^{-1} (\hat{\mathbf{T}}_V^t)^{-1} \hat{\gamma} \hat{\mathbf{T}}_V^t$ | $\hat{\mathbf{Z}}^{-1} (\hat{\mathbf{T}}_I^t)^{-1} \hat{\gamma} \hat{\mathbf{T}}_I^t$ |
| $\hat{\mathbf{Z}} (\hat{\mathbf{T}}_V^t)^{-1} \hat{\gamma}^{-1} \hat{\mathbf{T}}_V^t$ | $\hat{\mathbf{Y}} (\hat{\mathbf{T}}_I^t)^{-1} \hat{\gamma}^{-1} \hat{\mathbf{T}}_I^t$ |

and the number of unknowns is reduced to the $2n$ unknowns in the $n \times 1$ vectors $\hat{\mathbf{V}}_m^+$ and $\hat{\mathbf{V}}_m^-$. An alternative form of the characteristic admittance matrix can be obtained from (7.10a):

$$\hat{\mathbf{Z}}^{-1} \hat{\mathbf{T}}_V = \hat{\mathbf{Y}} \hat{\mathbf{T}}_V \hat{\gamma}^{-2} \tag{7.31}$$

Substituting this into (7.29) yields an alternative form for the characteristic admittance matrix:

$$\hat{\mathbf{Y}}_C = \hat{\mathbf{Y}} \hat{\mathbf{T}}_V \hat{\gamma}^{-1} \hat{\mathbf{T}}_V^{-1} \tag{7.32}$$

Additional relations for the characteristic impedance/admittance matrix can be similarly obtained and are given in Table 7.1 [B.25].

To summarize, the general solution to the MTL equations is given by

$$\hat{\mathbf{V}}(z) = \hat{\mathbf{T}}_V \left(\mathbf{e}^{-\hat{\gamma}z} \hat{\mathbf{V}}_m^+ + \mathbf{e}^{\hat{\gamma}z} \hat{\mathbf{V}}_m^- \right) \tag{7.33a}$$

$$\begin{aligned} \hat{\mathbf{I}}(z) &= \hat{\mathbf{Y}} \hat{\mathbf{T}}_V \hat{\gamma}^{-1} \left(\mathbf{e}^{-\hat{\gamma}z} \hat{\mathbf{V}}_m^+ - \mathbf{e}^{\hat{\gamma}z} \hat{\mathbf{V}}_m^- \right) \\ &= \hat{\mathbf{Y}}_C \hat{\mathbf{T}}_V \left(\mathbf{e}^{-\hat{\gamma}z} \hat{\mathbf{V}}_m^+ - \mathbf{e}^{\hat{\gamma}z} \hat{\mathbf{V}}_m^- \right) \end{aligned} \tag{7.33b}$$

where

$$\hat{\mathbf{T}}_V^{-1} \hat{\mathbf{Z}} \hat{\mathbf{Y}} \hat{\mathbf{T}}_V = \hat{\gamma}^2 \tag{7.33c}$$

and the characteristic admittance matrix is given by

$$\hat{\mathbf{Y}}_C = \hat{\mathbf{Y}} \hat{\mathbf{T}}_V \hat{\gamma}^{-1} \hat{\mathbf{T}}_V^{-1} \tag{7.33d}$$

An alternative form is

$$\begin{aligned} \hat{\mathbf{V}}(z) &= \hat{\mathbf{Z}} \hat{\mathbf{T}}_I \hat{\gamma}^{-1} \left(\mathbf{e}^{-\hat{\gamma}z} \hat{\mathbf{I}}_m^+ + \mathbf{e}^{\hat{\gamma}z} \hat{\mathbf{I}}_m^- \right) \\ &= \hat{\mathbf{Z}}_C \hat{\mathbf{T}}_I \left(\mathbf{e}^{-\hat{\gamma}z} \hat{\mathbf{I}}_m^+ + \mathbf{e}^{\hat{\gamma}z} \hat{\mathbf{I}}_m^- \right) \end{aligned} \tag{7.34a}$$

$$\hat{\mathbf{I}}(z) = \hat{\mathbf{T}}_I \left(\mathbf{e}^{-\hat{\gamma}z} \hat{\mathbf{I}}_m^+ - \mathbf{e}^{\hat{\gamma}z} \hat{\mathbf{I}}_m^- \right) \tag{7.34b}$$

where

$$\hat{\mathbf{T}}_I^{-1} \hat{\mathbf{Y}} \hat{\mathbf{Z}} \hat{\mathbf{T}}_I = \hat{\gamma}^2 \tag{7.34c}$$

and the characteristic impedance matrix is given by

$$\hat{\mathbf{Z}}_C = \hat{\mathbf{Z}} \hat{\mathbf{T}}_I \hat{\gamma}^{-1} \hat{\mathbf{T}}_I^{-1} \tag{7.34d}$$

Although either form of solution is acceptable, we will consistently use throughout the remainder of this text the form in (7.34) that requires diagonalization of $\hat{\mathbf{Y}} \hat{\mathbf{Z}}$.

7.2.2 Solution for Line Categories

The solution process for determining the general solutions to the MTL equations described previously *assumes* that one can find an $n \times n$ nonsingular transformation matrix $\hat{\mathbf{T}}_I$ that *diagonalizes* the product of per-unit-length parameter matrices, $\hat{\mathbf{Y}} \hat{\mathbf{Z}}$, via a *similarity transformation* as

$$\hat{\mathbf{T}}_I^{-1} \hat{\mathbf{Y}} \hat{\mathbf{Z}} \hat{\mathbf{T}}_I = \hat{\gamma}^2 \tag{7.35a}$$

where $\hat{\gamma}^2$ is diagonal as

$$\hat{\gamma}^2 = \begin{bmatrix} \hat{\gamma}_1^2 & 0 & \dots & 0 \\ 0 & \hat{\gamma}_2^2 & \ddots & \vdots \\ \vdots & \ddots & \ddots & 0 \\ 0 & \dots & 0 & \hat{\gamma}_n^2 \end{bmatrix} \tag{7.35b}$$

The columns of $\hat{\mathbf{T}}_I$, $[\hat{\mathbf{T}}_I]_i$, are said to be the *eigenvectors* of the matrix $\hat{\mathbf{Y}} \hat{\mathbf{Z}}$ and the items $\hat{\gamma}_i^2$ are its *eigenvalues* as discussed previously [A.4]. Thus, the question becomes whether we can find n *linearly independent eigenvectors of $\hat{\mathbf{Y}} \hat{\mathbf{Z}}$ that will diagonalize it as in (7.35)*. We now set out to investigate when this is possible and computational methods.

There are a number of known cases of $n \times n$ matrices $\hat{\mathbf{M}}$ whose diagonalization is assured via a similarity transformation as $\hat{\mathbf{T}}^{-1} \hat{\mathbf{M}} \hat{\mathbf{T}}$. These are [A.4,1–4]

1. All eigenvalues of $\hat{\mathbf{M}}$ are *distinct*
2. $\hat{\mathbf{M}}$ is *real* and *symmetric*
3. $\hat{\mathbf{M}}$ is *complex* but *normal*; that is, $\hat{\mathbf{M}} \hat{\mathbf{M}}^* = \hat{\mathbf{M}}^* \hat{\mathbf{M}}$, where we denote the transpose of a matrix by \mathbf{t} and its conjugate by $*$
4. $\hat{\mathbf{M}}$ is *complex* and *Hermitian*; that is, $\hat{\mathbf{M}} = \hat{\mathbf{M}}^{\mathbf{t}*}$

For *normal* or *Hermitian* $\hat{\mathbf{M}}$, the transformation matrix can be found such that $\hat{\mathbf{T}}^{-1} = \hat{\mathbf{T}}^{t*}$, which is said to be a *unitary transformation*. For a *real, symmetric* \mathbf{M} , the real transformation matrix can be found such that $\mathbf{T}^{-1} = \mathbf{T}^t$, which is said to be an *orthogonal transformation*. There are very efficient and stable computer routines that determine this orthogonal transformation matrix for a *real, symmetric matrix* [4]. The Jacobi algorithm is one such method [4]. For other types of matrices, we are not assured that a nonsingular transformation can be found that diagonalizes it.

The matrix product to be diagonalized is expanded as

$$\begin{aligned}\hat{\mathbf{Y}}\hat{\mathbf{Z}} &= (\mathbf{G} + j\omega\mathbf{C})(\mathbf{R} + j\omega\mathbf{L}) \\ &= \mathbf{GR} + j\omega\mathbf{CR} + j\omega\mathbf{GL} - \omega^2\mathbf{CL}\end{aligned}\quad (7.36)$$

There exist digital computer subroutines that find the eigenvalues and eigenvectors of a general complex matrix and can be used to diagonalize $\hat{\mathbf{Y}}\hat{\mathbf{Z}}$. However, because the number of conductors, n , of the MTL can be quite large, it is important to investigate the conditions under which we can obtain an *efficient and numerically stable* diagonalization. Furthermore, because the frequency-domain computations must be repeated in order to obtain the frequency response of the line, we desire a transformation that is *frequency independent*; that is, $\hat{\mathbf{T}}_V$ and $\hat{\mathbf{T}}_I$ are independent of frequency and need to be computed only once. The following subsections address this point.

7.2.2.1 Perfect Conductors in Lossy, Homogeneous Media Consider the case of perfect conductors for which $\mathbf{R} = \mathbf{0}$. The matrix product becomes

$$\begin{aligned}\hat{\mathbf{Y}}\hat{\mathbf{Z}} &= (\mathbf{G} + j\omega\mathbf{C})(j\omega\mathbf{L}) \\ &= j\omega\mathbf{GL} - \omega^2\mathbf{CL}\end{aligned}\quad (7.37)$$

If the surrounding medium is *homogeneous* with parameters σ , ε , and μ , then we have the important identities:

$$\mathbf{CL} = \mathbf{LC} = \mu\varepsilon \mathbf{1}_n \quad (7.38a)$$

$$\mathbf{GL} = \mathbf{LG} = \mu\sigma \mathbf{1}_n \quad (7.38b)$$

and $\hat{\mathbf{Y}}\hat{\mathbf{Z}}$ is already diagonal. The internal inductance is zero here, that is, $\mathbf{L} = \mathbf{L}_e$. In this case, we may choose

$$\hat{\mathbf{T}}_I = \mathbf{1}_n \quad (7.39a)$$

$$\hat{\mathbf{T}}_V = \mathbf{1}_n \quad (7.39b)$$

and all the eigenvalues are identical giving the propagation constants as

$$\begin{aligned}\hat{\gamma} &= \sqrt{j\omega\mu\sigma - \omega^2\mu\varepsilon} \\ &= \alpha + j\beta\end{aligned}\quad (7.39c)$$

and the characteristic impedance matrix becomes

$$\hat{\mathbf{Z}}_C = \frac{j\omega}{\hat{\gamma}} \mathbf{L} \quad (7.40a)$$

$$\hat{\mathbf{Z}}_C^{-1} = \frac{\hat{\gamma}}{j\omega} \mathbf{L}^{-1} = \frac{\hat{\gamma}}{j\omega\mu\varepsilon} \mathbf{C} \quad (7.40b)$$

If the medium, in addition to being homogeneous is also lossless, $\sigma = 0$, the propagation constants become

$$\hat{\gamma} = j\omega\sqrt{\mu\varepsilon} \quad (7.41)$$

so that the attenuation constant is zero, $\alpha = 0$, and the phase constant is $\beta = \omega\sqrt{\mu\varepsilon}$. The velocity of propagation becomes

$$\begin{aligned}v &= \frac{\omega}{\beta} \\ &= \frac{1}{\sqrt{\mu\varepsilon}}\end{aligned}\quad (7.42)$$

where the characteristic impedance becomes real, given by

$$\hat{\mathbf{Z}}_C = v\mathbf{L} \quad (7.43a)$$

$$\hat{\mathbf{Z}}_C^{-1} = v\mathbf{C} \quad (7.43b)$$

An example of the application of these results is the coupled stripline. This case of perfect conductors in a homogeneous medium (lossless or lossy) is the only case where we may have TEM waves on the line. In the following sections, we investigate the *quasi-TEM* mode of propagation wherein the conductors can be lossy and/or the medium may be inhomogeneous. For these cases, the TEM mode cannot exist, but we assume that the conductor losses and/or inhomogeneities of the medium do not significantly perturb the field structure from a TEM distribution.

7.2.2.2 Lossy Conductors in Lossy, Homogeneous Media Consider the case where we permit imperfect conductors, $\mathbf{R} \neq \mathbf{0}$, but assume a homogeneous medium.

The matrix product $\hat{\mathbf{Y}}\hat{\mathbf{Z}}$ in (7.36) becomes, using the identities for a homogeneous medium given in (7.38),

$$\begin{aligned}\hat{\mathbf{Y}}\hat{\mathbf{Z}} &= \mathbf{G}\mathbf{R} + j\omega\mathbf{C}\mathbf{R} + (j\omega\mu\sigma - \omega^2\mu\varepsilon)\mathbf{1}_n \\ &= \left(\frac{\sigma}{\varepsilon} + j\omega\right)\mathbf{C}\mathbf{R} + (j\omega\mu\sigma - \omega^2\mu\varepsilon)\mathbf{1}_n\end{aligned}\quad (7.44)$$

where we neglected the *internal inductance* of the conductors, $\mathbf{L}_i = \mathbf{0}$. Hence, we need to diagonalize only $\mathbf{C}\mathbf{R}$ as

$$\begin{aligned}\hat{\mathbf{T}}_I^{-1}\mathbf{C}\mathbf{R}\hat{\mathbf{T}}_I &= \Lambda^2 \\ &= \begin{bmatrix} \Lambda_1^2 & 0 & \cdots & 0 \\ 0 & \Lambda_2^2 & \ddots & \vdots \\ \vdots & \ddots & \ddots & 0 \\ 0 & \cdots & 0 & \Lambda_n^2 \end{bmatrix}\end{aligned}\quad (7.45)$$

The eigenvalues of $\hat{\mathbf{Y}}\hat{\mathbf{Z}}$ become

$$\hat{y}_i^2 = \left(\frac{\sigma}{\varepsilon} + j\omega\right)\Lambda_i^2 + (j\omega\mu\sigma - \omega^2\mu\varepsilon)\quad (7.46)$$

The key problem here is finding the transformation matrix that diagonalizes $\mathbf{C}\mathbf{R}$ as in (7.45). Thus, we need to diagonalize the product of two matrices. A numerically stable transformation can be found to accomplish this in the following manner. Recall that \mathbf{C} is *real, symmetric, and positive definite* and \mathbf{R} is *real and symmetric*. First, consider diagonalizing \mathbf{C} . As \mathbf{C} is real and symmetric, one can find a *real, orthogonal transformation* \mathbf{U} that diagonalizes \mathbf{C} , where $\mathbf{U}^{-1} = \mathbf{U}^t$ [B.1, 3, 4]:

$$\begin{aligned}\mathbf{U}^t\mathbf{C}\mathbf{U} &= \theta^2 \\ &= \begin{bmatrix} \theta_1^2 & 0 & \cdots & 0 \\ 0 & \theta_2^2 & \ddots & \vdots \\ \vdots & \ddots & \ddots & 0 \\ 0 & \cdots & 0 & \theta_n^2 \end{bmatrix}\end{aligned}\quad (7.47)$$

Since \mathbf{C} is real, symmetric, and *positive definite*, its eigenvalues θ_i^2 are all real, nonzero, and positive [B.1, 3]. Therefore, the square roots of these, $\theta_i = \sqrt{\theta_i^2}$, will be *real, nonzero numbers*. Next form the *real, symmetric* matrix product

$$\theta^{-1}\mathbf{U}^t\mathbf{C}\mathbf{U}\theta^{-1} = \mathbf{1}_n\quad (7.48)$$

Now form

$$\begin{aligned}\theta^{-1} \mathbf{U}^t \mathbf{C} \mathbf{R} \mathbf{U} \theta &= \underbrace{\theta^{-1} \mathbf{U}^t \mathbf{C} \mathbf{U} \theta^{-1}}_{\mathbf{1}_n} \theta \mathbf{U}^t \mathbf{R} \mathbf{U} \theta \\ &= \theta \mathbf{U}^t \mathbf{R} \mathbf{U} \theta\end{aligned}\quad (7.49)$$

The matrix $\theta \mathbf{U}^t \mathbf{R} \mathbf{U} \theta$ is real and symmetric, so it can also be diagonalized with a real, orthogonal transformation \mathbf{S} as

$$\begin{aligned}\mathbf{S}^t [\theta \mathbf{U}^t \mathbf{R} \mathbf{U} \theta] \mathbf{S} &= \mathbf{S}^t [\theta^{-1} \mathbf{U}^t \mathbf{C} \mathbf{R} \mathbf{U} \theta] \mathbf{S} \\ &= \Lambda^2\end{aligned}\quad (7.50)$$

This result shows that the desired transformations are

$$\mathbf{T}_I = \mathbf{U} \theta \mathbf{S} \quad (7.51a)$$

$$\mathbf{T}_V = \mathbf{U} \theta^{-1} \mathbf{S} \quad (7.51b)$$

Also

$$\begin{aligned}\mathbf{T}_I^{-1} &= \mathbf{S}^t \theta^{-1} \mathbf{U}^t \\ &= \mathbf{T}_V^t\end{aligned}\quad (7.52a)$$

$$\begin{aligned}\mathbf{T}_V^{-1} &= \mathbf{S}^t \theta \mathbf{U}^t \\ &= \mathbf{T}_I^t\end{aligned}\quad (7.52b)$$

This gives

$$\begin{aligned}\mathbf{T}_V^{-1} \hat{\mathbf{Z}} \mathbf{T}_I &= \mathbf{T}_V^{-1} (\mathbf{R} + j\omega \mathbf{L}) \mathbf{T}_I \\ &= \Lambda^2 + j\omega \mu \varepsilon \mathbf{1}_n\end{aligned}\quad (7.53a)$$

$$\begin{aligned}\mathbf{T}_I^{-1} \hat{\mathbf{Y}} \mathbf{T}_V &= \mathbf{T}_I^{-1} (\mathbf{G} + j\omega \mathbf{C}) \mathbf{T}_V \\ &= \left(\frac{\sigma}{\varepsilon} + j\omega \right) \mathbf{1}_n\end{aligned}\quad (7.53b)$$

Hence, the product $\hat{\mathbf{Y}} \hat{\mathbf{Z}}$ is diagonalized for this choice of the transformations as

$$\hat{\mathbf{T}}_I^{-1} \hat{\mathbf{Y}} \hat{\mathbf{Z}} \hat{\mathbf{T}}_I = \left(\frac{\sigma}{\varepsilon} + j\omega \right) \Lambda^2 + (j\omega \mu \sigma - \omega^2 \mu \varepsilon) \mathbf{1}_n \quad (7.54)$$

The inverse of \mathbf{T}_I is also $\mathbf{T}_I^{-1} = \mathbf{S}^t \theta^{-1} \mathbf{U}^t = \mathbf{T}_I^t \mathbf{C}^{-1}$. There are numerous digital computer subroutines that implement the diagonalization of the product of two real, symmetric matrices, one of which is positive definite in the above fashion [B.5]. Note that $\hat{\mathbf{T}}_V^t \hat{\mathbf{T}}_I = \mathbf{1}_n$, and hence the eigenvectors of $\hat{\mathbf{Z}} \hat{\mathbf{Y}}$ and $\hat{\mathbf{Y}} \hat{\mathbf{Z}}$ are *orthonormal*.

The entries in the per-unit-length resistance matrix \mathbf{R} are functions of the square root of frequency, \sqrt{f} , at high frequencies due to skin effect. This does not pose any problems in the phasor solution as we simply evaluate these at the frequency of interest and perform the above computation at that frequency. We will find in the next chapter that this dependence of \mathbf{R} on \sqrt{f} poses some significant problems in the time-domain analysis of MTLs.

An example of the application of these results is the case of a lossy, coupled stripline. If all n conductors are identical and we assume that the reference conductor (a ground plane) is lossless, then $\mathbf{R} = r \mathbf{1}_n$ and we only need to diagonalize \mathbf{C} . Hence, the transformation in this case is *independent of frequency* and is an orthogonal one such that we can choose $\mathbf{T}_I^{-1} \mathbf{C} \mathbf{T}_I = \theta^2$ as in (7.47) and $\hat{\mathbf{T}}_I = \hat{\mathbf{T}}_V = \mathbf{U}$ with $\hat{\mathbf{T}}_I^{-1} = \hat{\mathbf{T}}_I^t$. The eigenvalues of $\hat{\mathbf{Y}} \hat{\mathbf{Z}}$ are obtained by replacing Λ_i^2 in (7.46) with $r\theta_i^2$.

7.2.2.3 Perfect Conductors in Lossless, Inhomogeneous Media We next turn our attention to the diagonalization of the matrix product $\hat{\mathbf{Y}} \hat{\mathbf{Z}}$, where we assume perfect conductors, $\mathbf{R} = \mathbf{0}$, and lossless media, $\mathbf{G} = \mathbf{0}$. The surrounding, lossless medium may be *inhomogeneous* in which case we no longer have the fundamental identity in (7.38a), that is, $\mathbf{C} \mathbf{L} \neq \mu \varepsilon \mathbf{1}_n$. In fact, the product of the per-unit-length inductance and capacitance matrices is generally not diagonal. The matrix product to be diagonalized becomes

$$\hat{\mathbf{Y}} \hat{\mathbf{Z}} = -\omega^2 \mathbf{C} \mathbf{L} \quad (7.55)$$

Once again, \mathbf{C} and \mathbf{L} are real, symmetric and \mathbf{C} is positive definite. Therefore, we can diagonalize $\mathbf{C} \mathbf{L}$ as in the previous section with orthogonal transformations as

$$\begin{aligned} \hat{\mathbf{T}}_I^{-1} \mathbf{C} \mathbf{L} \hat{\mathbf{T}}_I &= \Lambda^2 \\ &= \begin{bmatrix} \Lambda_1^2 & 0 & \cdots & 0 \\ 0 & \Lambda_2^2 & \ddots & \vdots \\ \vdots & \ddots & \ddots & 0 \\ 0 & \cdots & 0 & \Lambda_n^2 \end{bmatrix} \end{aligned} \quad (7.56)$$

The transformations that accomplish this are real and given by

$$\mathbf{T}_I = \mathbf{U} \theta \mathbf{S} \quad (7.57a)$$

$$\mathbf{T}_V = \mathbf{U} \theta^{-1} \mathbf{S} \quad (7.57b)$$

where \mathbf{U} and \mathbf{S} are obtained from

$$\begin{aligned} \mathbf{U}^t \mathbf{C} \mathbf{U} &= \theta^2 \\ &= \begin{bmatrix} \theta_1^2 & 0 & \cdots & 0 \\ 0 & \theta_2^2 & \ddots & \vdots \\ \vdots & \ddots & \ddots & 0 \\ 0 & \cdots & 0 & \theta_n^2 \end{bmatrix} \end{aligned} \quad (7.58a)$$

$$\begin{aligned} \mathbf{S}^t [\theta \mathbf{U}^t \mathbf{L} \mathbf{U} \theta] \mathbf{S} &= \mathbf{S}^t [\theta^{-1} \mathbf{U}^t \mathbf{C} \mathbf{L} \mathbf{U} \theta] \mathbf{S} \\ &= \Lambda^2 \end{aligned} \quad (7.58b)$$

The inverse of \mathbf{T}_I is $\mathbf{T}_I^{-1} = \mathbf{S}^t \theta^{-1} \mathbf{U}^t = \mathbf{T}_I^t \mathbf{C}^{-1}$. The desired eigenvalues of $\hat{\mathbf{Y}}\hat{\mathbf{Z}}$ are

$$\hat{\gamma}_i^2 = -\omega^2 \Lambda_i^2 \quad (7.59)$$

Also

$$\begin{aligned} \mathbf{T}_I^{-1} &= \mathbf{S}^t \theta^{-1} \mathbf{U}^t \\ &= \mathbf{T}_V^t \end{aligned} \quad (7.60a)$$

$$\begin{aligned} \mathbf{T}_V^{-1} &= \mathbf{S}^t \theta \mathbf{U}^t \\ &= \mathbf{T}_I^t \end{aligned} \quad (7.60b)$$

This gives

$$\begin{aligned} \mathbf{T}_V^{-1} \hat{\mathbf{Z}} \mathbf{T}_I &= \mathbf{T}_V^{-1} (j\omega \mathbf{L}) \mathbf{T}_I \\ &= j\omega \Lambda^2 \end{aligned} \quad (7.61a)$$

$$\begin{aligned} \mathbf{T}_I^{-1} \hat{\mathbf{Y}} \mathbf{T}_V &= \mathbf{T}_I^{-1} (j\omega \mathbf{C}) \mathbf{T}_V \\ &= j\omega \mathbf{1}_n \end{aligned} \quad (7.61b)$$

Hence, $\hat{\mathbf{Y}}\hat{\mathbf{Z}}$ is diagonalized for this choice of the transformations as

$$\hat{\mathbf{T}}_I^{-1} \hat{\mathbf{Y}}\hat{\mathbf{Z}}\hat{\mathbf{T}}_I = -\omega^2 \Lambda^2 \quad (7.62)$$

The characteristic impedance matrix is real and becomes

$$\begin{aligned}
 \hat{\mathbf{Z}}_C &= \hat{\mathbf{Z}} \hat{\mathbf{T}}_I \gamma^{-1} \hat{\mathbf{T}}_I^{-1} \\
 &= j\omega \mathbf{L} \mathbf{U} \theta \mathbf{S} \frac{1}{j\omega} \Lambda^{-1} \mathbf{S}^t \theta^{-1} \mathbf{U}^t \\
 &= \mathbf{U} \theta^{-1} \mathbf{S} \Lambda \mathbf{S}^t \theta^{-1} \mathbf{U}^t
 \end{aligned} \tag{7.63}$$

Note that $\hat{\mathbf{T}}_V^t \hat{\mathbf{T}}_I = \mathbf{1}_n$ and therefore the eigenvectors of $\hat{\mathbf{Z}} \hat{\mathbf{Y}}$ and $\hat{\mathbf{Y}} \hat{\mathbf{Z}}$ are *orthonormal*. An example of the use of this method is the case of a coupled microstrip line.

7.2.2.4 The General Case: Lossy Conductors in Lossy, Inhomogeneous Media In the most general case wherein the line conductors and medium are lossy, $\mathbf{R} \neq \mathbf{0}$, $\mathbf{G} \neq \mathbf{0}$, and the medium is inhomogeneous so that $\mathbf{L} \mathbf{C} \neq \mu \varepsilon \mathbf{1}_n$, we have no other recourse but to seek a *frequency-dependent* transformation $\hat{\mathbf{T}}_I(\omega)$ such that

$$\hat{\mathbf{T}}_I^{-1}(\omega) \underbrace{(\mathbf{G} + j\omega \mathbf{C})}_{\hat{\mathbf{Y}}(\omega)} \underbrace{(\mathbf{R} + j\omega \mathbf{L})}_{\hat{\mathbf{Z}}(\omega)} \hat{\mathbf{T}}_I(\omega) = \hat{\gamma}^2(\omega) \tag{7.64}$$

The computational problem here is that the transformation matrix $\hat{\mathbf{T}}_I(\omega)$ is frequency dependent and *must be recomputed at each frequency*. Thus, an eigenvector–eigenvalue subroutine for complex matrices must be called repeatedly at each frequency, which can be quite time consuming if the responses at a large number of frequencies are desired. In order to provide for this general case, a general frequency-domain FORTRAN program MTL.FOR, which determines $\hat{\mathbf{T}}_I(\omega)$ via (7.64) and incorporates the terminal relations at the left and right ends of the line, is described in Appendix A .

7.2.2.5 Cyclic-Symmetric Structures The MTL structures considered in Sections 7.2.2.1–7.2.2.3 are such that the matrix product $\hat{\mathbf{Y}} \hat{\mathbf{Z}}$ can always be diagonalized with a numerically efficient and stable similarity transformation $\hat{\mathbf{T}}_I$, which, except in the case of Section 7.2.2.2, is *frequency independent*. In the general case, the transformation matrix $\hat{\mathbf{T}}_I(\omega)$ will be *frequency dependent* as was discussed in the previous section. This section discusses MTLs that have certain *structural symmetry* so that a numerically stable (and trivial) transformation $\hat{\mathbf{T}}_I$ can always be found that diagonalizes $\hat{\mathbf{Y}} \hat{\mathbf{Z}}$. Furthermore, this transformation is *frequency independent*, regardless of whether the line is lossy and/or the medium is inhomogeneous, that is, the general case.

Consider structures composed of n *identical conductors* and a reference conductor wherein the n conductors have structural symmetry with respect to the reference conductor so that the per-unit-length impedance and admittance matrices have the

following symmetry [B.1, 11]:

$$\hat{\mathbf{Z}} = \begin{bmatrix} \hat{Z}_1 & \hat{Z}_2 & \hat{Z}_3 & \cdots & \hat{Z}_3 & \hat{Z}_2 \\ \hat{Z}_2 & \hat{Z}_1 & \hat{Z}_2 & \hat{Z}_3 & \ddots & \hat{Z}_3 \\ \hat{Z}_3 & \hat{Z}_2 & \hat{Z}_1 & \hat{Z}_2 & \ddots & \vdots \\ \vdots & \hat{Z}_3 & \hat{Z}_2 & \ddots & \ddots & \hat{Z}_3 \\ \hat{Z}_3 & \ddots & \ddots & \ddots & \hat{Z}_1 & \hat{Z}_2 \\ \hat{Z}_2 & \hat{Z}_3 & \cdots & \hat{Z}_3 & \hat{Z}_2 & \hat{Z}_1 \end{bmatrix} \quad (7.65a)$$

$$\hat{\mathbf{Y}} = \begin{bmatrix} \hat{Y}_1 & \hat{Y}_2 & \hat{Y}_3 & \cdots & \hat{Y}_3 & \hat{Y}_2 \\ \hat{Y}_2 & \hat{Y}_1 & \hat{Y}_2 & \hat{Y}_3 & \ddots & \hat{Y}_3 \\ \hat{Y}_3 & \hat{Y}_2 & \hat{Y}_1 & \hat{Y}_2 & \ddots & \vdots \\ \vdots & \hat{Y}_3 & \hat{Y}_2 & \ddots & \ddots & \hat{Y}_3 \\ \hat{Y}_3 & \ddots & \ddots & \ddots & \hat{Y}_1 & \hat{Y}_2 \\ \hat{Y}_2 & \hat{Y}_3 & \cdots & \hat{Y}_3 & \hat{Y}_2 & \hat{Y}_1 \end{bmatrix} \quad (7.65b)$$

Examples of structures that result in these types of per-unit-length parameter matrices are shown in Figure 7.1. Observe that in order for the main diagonal terms to be equal, the n conductors must be identical and the surrounding media (which may be inhomogeneous) must also exhibit symmetry. For example, if the n conductors are dielectric-insulated wires, the dielectric insulations of the n wires must have identical permittivities ϵ and thicknesses. The reference conductor need not share this property. A general cyclic-symmetric matrix $\hat{\mathbf{M}}$ has the entries given by

$$[\hat{\mathbf{M}}]_{ij} = \hat{M}_{|i-j|+1} \quad (7.66a)$$

where

$$\hat{M}_{j\pm n} = \hat{M}_j \quad (7.66b)$$

$$\hat{M}_{n+2-j} = \hat{M}_j \quad (7.66c)$$

and indices greater than n or less than 1 are defined by the convention: $n + j = j$ and $n + i = i$ [B.1]. Because of this special structure of the per-unit-length matrices, they are *normal* matrices, $\hat{\mathbf{Z}}\hat{\mathbf{Z}}^{t*} = \hat{\mathbf{Z}}^{t*}\hat{\mathbf{Z}}$, and each can be diagonalized by the same transformation as [B.1, 1–4]

$$\hat{\mathbf{T}}^{-1} \hat{\mathbf{Z}} \hat{\mathbf{T}} = \hat{\gamma}_Z^2 \quad (7.67a)$$

$$\hat{\mathbf{T}}^{-1} \hat{\mathbf{Y}} \hat{\mathbf{T}} = \hat{\gamma}_Y^2 \quad (7.67b)$$

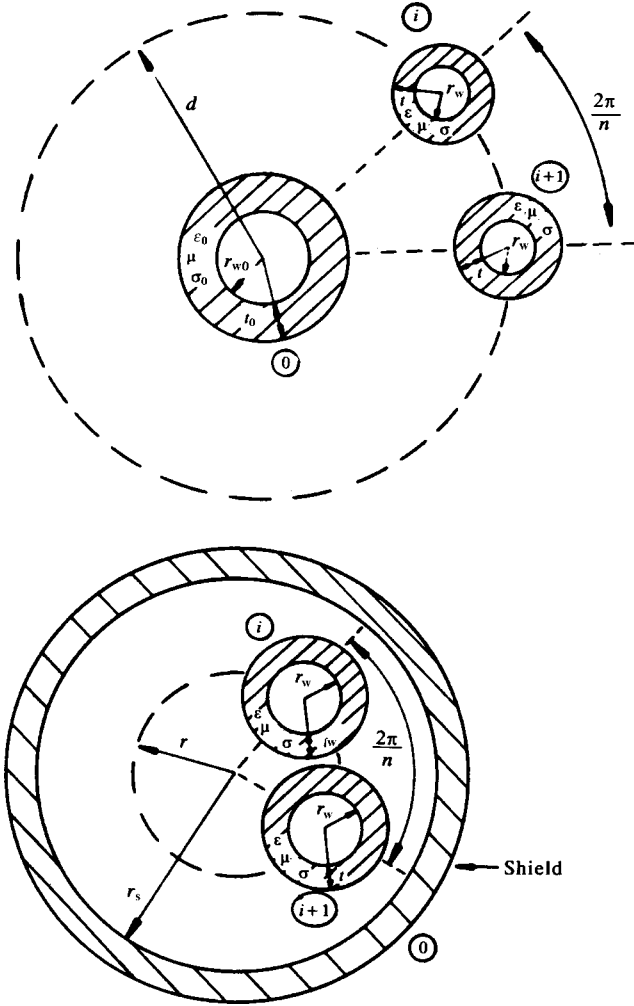


FIGURE 7.1 Cyclic-symmetric structures that are diagonalizable by a frequency-independent transformation.

where the $n \times n$ matrices $\hat{\gamma}_Z^2$ and $\hat{\gamma}_Y^2$ are *diagonal* and whose diagonal entries are given by [B.1]

$$[\hat{\gamma}_Z^2]_{ii} = \left[\sum_{p=1}^n [\hat{\mathbf{Z}}]_{1p} \angle \left\{ \frac{2\pi}{n} (p-1)(i-1) \right\} \right] \tag{7.68a}$$

$$[\hat{\gamma}_Y^2]_{ii} = \left[\sum_{q=1}^n [\hat{\mathbf{Y}}]_{1q} \angle \left\{ \frac{2\pi}{n} (q-1)(i-1) \right\} \right] \tag{7.68b}$$

In fact, the transformation is trivial to obtain [B.1]

$$[\hat{\mathbf{T}}]_{ij} = \frac{1}{\sqrt{n}} \angle \left\{ \frac{2\pi}{n} (i - 1)(j - 1) \right\} \tag{7.69}$$

and

$$\hat{\mathbf{T}}^{-1} = \hat{\mathbf{T}}^* \tag{7.70}$$

Therefore, $\hat{\mathbf{T}}$ is a unitary transformation. Similarly, the eigenvalues of $\hat{\mathbf{Y}}\hat{\mathbf{Z}}$ and $\hat{\mathbf{Z}}\hat{\mathbf{Y}}$ (the propagation constants) are easily determined as [B.1]

$$\begin{aligned} \hat{\gamma}_i^2 &= [\hat{\gamma}_Z^2]_{ii} [\hat{\gamma}_Y^2]_{ii} \\ &= \left[\sum_{p=1}^n [\hat{\mathbf{Z}}]_{1p} \angle \left\{ \frac{2\pi}{n} (p - 1)(i - 1) \right\} \right] \left[\sum_{q=1}^n [\hat{\mathbf{Y}}]_{1q} \angle \left\{ \frac{2\pi}{n} (q - 1)(i - 1) \right\} \right] \end{aligned} \tag{7.71}$$

Hence, we may choose

$$\hat{\mathbf{T}}_V = \hat{\mathbf{T}} \tag{7.72a}$$

$$\hat{\mathbf{T}}_I = \hat{\mathbf{T}} \tag{7.72b}$$

Note that $\hat{\mathbf{T}}_V^t \hat{\mathbf{T}}_I^* = \mathbf{1}_n$ and the eigenvectors of $\hat{\mathbf{Z}}\hat{\mathbf{Y}}$ and $\hat{\mathbf{Y}}\hat{\mathbf{Z}}$ are *orthonormal*.

As an illustration of these results, consider a four-conductor ($n = 3$), cyclic-symmetric structure line with

$$\hat{\mathbf{Z}} = \begin{bmatrix} \hat{Z}_s & \hat{Z}_m & \hat{Z}_m \\ \hat{Z}_m & \hat{Z}_s & \hat{Z}_m \\ \hat{Z}_m & \hat{Z}_m & \hat{Z}_s \end{bmatrix} \tag{7.73}$$

and $\hat{\mathbf{Y}}$ has a similar form. The transformation matrices become

$$\hat{\mathbf{T}}_V = \hat{\mathbf{T}}_I = \hat{\mathbf{T}} = \frac{1}{\sqrt{3}} \begin{bmatrix} 1 & 1 & 1 \\ 1 & e^{j2\pi/3} & e^{j4\pi/3} \\ 1 & e^{j4\pi/3} & e^{j2\pi/3} \end{bmatrix} \tag{7.74a}$$

$$\hat{\mathbf{T}}_V^{-1} = \hat{\mathbf{T}}_I^{-1} = \hat{\mathbf{T}}^* = \frac{1}{\sqrt{3}} \begin{bmatrix} 1 & 1 & 1 \\ 1 & e^{-j2\pi/3} & e^{-j4\pi/3} \\ 1 & e^{-j4\pi/3} & e^{-j2\pi/3} \end{bmatrix} \tag{7.74b}$$

The propagation constants become

$$\begin{aligned}\hat{\gamma}_1^2 &= \{\hat{Z}_s + \hat{Z}_m + \hat{Z}_m\} \{\hat{Y}_s + \hat{Y}_m + \hat{Y}_m\} \\ &= (\hat{Z}_s + 2\hat{Z}_m) (\hat{Y}_s + 2\hat{Y}_m)\end{aligned}\quad (7.75a)$$

$$\begin{aligned}\hat{\gamma}_2^2 &= \left\{ \hat{Z}_s \angle 0^\circ + \hat{Z}_m \angle \frac{2\pi}{3} + \hat{Z}_m \angle \frac{4\pi}{3} \right\} \left\{ \hat{Y}_s \angle 0^\circ + \hat{Y}_m \angle \frac{2\pi}{3} + \hat{Y}_m \angle \frac{4\pi}{3} \right\} \\ &= (\hat{Z}_s - \hat{Z}_m) (\hat{Y}_s - \hat{Y}_m)\end{aligned}\quad (7.75b)$$

$$\begin{aligned}\hat{\gamma}_3^2 &= \left\{ \hat{Z}_s \angle 0^\circ + \hat{Z}_m \angle \frac{4\pi}{3} + \hat{Z}_m \angle \frac{2\pi}{3} \right\} \left\{ \hat{Y}_s \angle 0^\circ + \hat{Y}_m \angle \frac{4\pi}{3} + \hat{Y}_m \angle \frac{2\pi}{3} \right\} \\ &= (\hat{Z}_s - \hat{Z}_m) (\hat{Y}_s - \hat{Y}_m)\end{aligned}\quad (7.75c)$$

and two of the propagation constants are equal. Define the characteristic impedances as

$$\hat{Z}_C^+ = \sqrt{(\hat{Z}_s + 2\hat{Z}_m) / (\hat{Y}_s + 2\hat{Y}_m)} \quad (7.76a)$$

$$\hat{Z}_C^- = \sqrt{(\hat{Z}_s - \hat{Z}_m) / (\hat{Y}_s - \hat{Y}_m)} \quad (7.76b)$$

The characteristic impedance matrix becomes

$$\begin{aligned}\hat{Z}_C &= \hat{Z} \hat{\Gamma}_I \hat{\gamma}^{-1} \hat{\Gamma}_I^{-1} \\ &= \frac{1}{3} \begin{bmatrix} (\hat{Z}_C^+ + 2\hat{Z}_C^-) & (\hat{Z}_C^+ - \hat{Z}_C^-) & (\hat{Z}_C^+ - \hat{Z}_C^-) \\ (\hat{Z}_C^+ - \hat{Z}_C^-) & (\hat{Z}_C^+ + 2\hat{Z}_C^-) & (\hat{Z}_C^+ - \hat{Z}_C^-) \\ (\hat{Z}_C^+ - \hat{Z}_C^-) & (\hat{Z}_C^+ - \hat{Z}_C^-) & (\hat{Z}_C^+ + 2\hat{Z}_C^-) \end{bmatrix}\end{aligned}\quad (7.77)$$

There are a number of cases where an MTL can be *approximated* as a cyclic-symmetric structure. A common case is a three-phase, high-voltage power transmission line consisting of three wires above earth. In order to reduce interference to neighboring telephone lines, the three conductors are often *transposed* at regular intervals. As an approximation, we may assume that each of the three (identical) wires occupies, at regular intervals, each of the three possible positions along the line (each of which is at the same height above earth, and the separation distance between adjacent wires is identical). With this assumption, the per-unit-length matrices \hat{Z} and \hat{Y} take on a cyclic-symmetric structure as in (7.73). Two of the propagation constants, $\hat{\gamma}_2$ and $\hat{\gamma}_3$, are equal and these are associated with the *aerial mode* of propagation. The third propagation constant, $\hat{\gamma}_1$, is associated with the *ground mode* of propagation.

This transformation is referred to in the power transmission literature as the *method of symmetrical components* [9, 10]. Such lines are said to be *balanced*. In the case of unbalanced lines where, for example, one phase may be shorted to ground, this transformation does not apply.

Other approximations of MTLs as cyclic-symmetric structures are useful. Cable harnesses carrying tightly packed insulated wires have been assumed to be cyclic-symmetric structures on the notion that all wires occupy, at some point along the line, all possible positions [11]. This leads to a cyclic-symmetric structure of the $n \times n$ per-unit-length impedance and admittance matrices that is similar to the special case of transposed power distribution lines where all off-diagonal terms are equal and, if we assume the conductors are identical, the main diagonal terms are equal:

$$[\hat{\mathbf{Z}}]_{ii} = \hat{Z}_s, \quad [\hat{\mathbf{Z}}]_{ij} = \hat{Z}_m \quad (7.78a)$$

$\underbrace{\hspace{1.5cm}}_{i \neq j}$

$$[\hat{\mathbf{Y}}]_{ii} = \hat{Y}_s, \quad [\hat{\mathbf{Y}}]_{ij} = \hat{Y}_m \quad (7.78b)$$

$\underbrace{\hspace{1.5cm}}_{i \neq j}$

The transformation matrices that diagonalize this structure are *real* and simple to obtain:

$$\mathbf{T}_I = \mathbf{T}_V = \frac{1}{\sqrt{n}} \begin{bmatrix} 1 & 1 & 1 & \cdots & 1 \\ 1 & (1 - n) & 1 & \cdots & 1 \\ 1 & 1 & (1 - n) & \cdots & 1 \\ \vdots & \vdots & \vdots & (1 - n) & \vdots \\ 1 & 1 & \cdots & 1 & (1 - n) \end{bmatrix} \quad (7.79a)$$

whose inverse is

$$\mathbf{T}_I^{-1} = \mathbf{T}_V^{-1} = \frac{1}{\sqrt{n}} \begin{bmatrix} 1 & 1 & 1 & \cdots & 1 \\ 1 & -1 & 0 & \cdots & 0 \\ 1 & 0 & -1 & \cdots & 0 \\ \vdots & \vdots & \vdots & -1 & 0 \\ 1 & 0 & \cdots & 0 & -1 \end{bmatrix} \quad (7.79b)$$

The eigenvalues are

$$\hat{\gamma}_1^2 = [\hat{Z}_s + (n - 1)\hat{Z}_m] [\hat{Y}_s + (n - 1)\hat{Y}_m] \quad (7.80a)$$

$$\hat{\gamma}_2^2 = \cdots = \hat{\gamma}_n^2 = [\hat{Z}_s - \hat{Z}_m] [\hat{Y}_s - \hat{Y}_m] \quad (7.80b)$$

Other common cases are the cyclic-symmetric, three-conductor lines shown in Figure 7.2. Two identical dielectric-insulated wires are suspended at equal heights

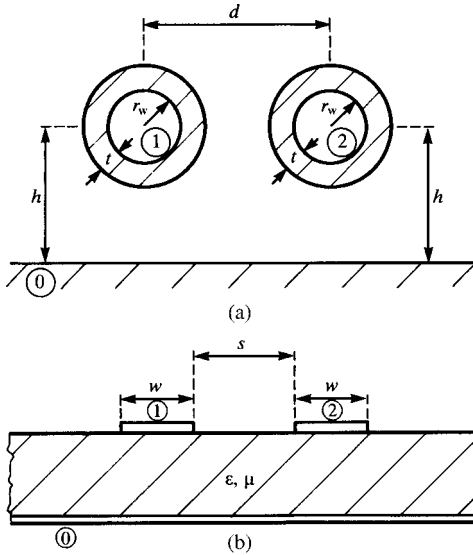


FIGURE 7.2 Certain three-conductor structures that are cyclic symmetric: (a) two identical wires at identical heights above a ground plane and (b) two identical lands of a coupled microstrip configuration.

above a ground plane as shown in Figure 7.2(a). The per-unit-length impedance and admittance matrices become

$$\hat{\mathbf{Z}} = \begin{bmatrix} \hat{Z}_s & \hat{Z}_m \\ \hat{Z}_m & \hat{Z}_s \end{bmatrix} \tag{7.81a}$$

$$\hat{\mathbf{Y}} = \begin{bmatrix} \hat{Y}_s & \hat{Y}_m \\ \hat{Y}_m & \hat{Y}_s \end{bmatrix} \tag{7.81b}$$

The transformation matrices simplify to

$$\mathbf{T}_I = \mathbf{T}_V = \frac{1}{\sqrt{2}} \begin{bmatrix} 1 & 1 \\ 1 & -1 \end{bmatrix} \tag{7.82a}$$

$$\mathbf{T}_I^{-1} = \mathbf{T}_V^{-1} = \frac{1}{\sqrt{2}} \begin{bmatrix} 1 & 1 \\ 1 & -1 \end{bmatrix} \tag{7.82b}$$

and the propagation constants become

$$\hat{\gamma}_1^2 = (\hat{Z}_s + \hat{Z}_m)(\hat{Y}_s + \hat{Y}_m) \tag{7.83a}$$

$$\hat{\gamma}_2^2 = (\hat{Z}_s - \hat{Z}_m)(\hat{Y}_s - \hat{Y}_m) \tag{7.83b}$$

Defining the characteristic impedances as

$$\hat{Z}_C^\pm = \sqrt{\frac{\hat{Z}_s \pm \hat{Z}_m}{\hat{Y}_s \pm \hat{Y}_m}} \quad (7.84)$$

we obtain the characteristic impedance matrix as

$$\hat{\mathbf{Z}}_C = \frac{1}{2} \begin{bmatrix} (\hat{Z}_C^+ + \hat{Z}_C^-) & (\hat{Z}_C^+ - \hat{Z}_C^-) \\ (\hat{Z}_C^+ - \hat{Z}_C^-) & (\hat{Z}_C^+ + \hat{Z}_C^-) \end{bmatrix} \quad (7.85)$$

This transformation is referred to in the microwave literature as the *even-odd mode* transformation and has been applied to the symmetrical, coupled microstrip line shown in Figure 7.2(b).

7.3 INCORPORATING THE TERMINAL CONDITIONS

The general solutions to the phasor MTL equations given in (7.34) involve $2n$ undetermined constants in the $n \times 1$ vectors $\hat{\mathbf{I}}_m^+$ and $\hat{\mathbf{I}}_m^-$:

$$\hat{\mathbf{V}}(z) = \hat{\mathbf{Z}}_C \hat{\mathbf{T}}_I \left(\mathbf{e}^{-\hat{\gamma}z} \hat{\mathbf{I}}_m^+ + \mathbf{e}^{\hat{\gamma}z} \hat{\mathbf{I}}_m^- \right) \quad (7.86a)$$

$$\hat{\mathbf{I}}(z) = \hat{\mathbf{T}}_I \left(\mathbf{e}^{-\hat{\gamma}z} \hat{\mathbf{I}}_m^+ - \mathbf{e}^{\hat{\gamma}z} \hat{\mathbf{I}}_m^- \right) \quad (7.86b)$$

Therefore, we need $2n$ additional constraint equations in order to evaluate these. These additional constraint equations are provided by the terminal conditions at $z = 0$ and $z = \mathcal{L}$ as illustrated in Figure 7.3. The driving sources and load impedances are contained in these terminal networks that are attached to the two ends of the line. The terminal constraint network at $z = 0$ shown in Figure 7.3(a) provides n equations relating the n phasor voltages $\hat{\mathbf{V}}(0)$ and n phasor currents $\hat{\mathbf{I}}(0)$. The terminal constraint network at $z = \mathcal{L}$ shown in Figure 7.3(b) provides n equations relating the n phasor voltages $\hat{\mathbf{V}}(\mathcal{L})$ and n phasor currents $\hat{\mathbf{I}}(\mathcal{L})$. The purpose of this section is to incorporate these terminal constraints to explicitly determine the terminal voltages and currents and complete this final but important last step in the solution process.

7.3.1 The Generalized Thevenin Equivalent

There are many ways of relating the voltages and currents at the terminals of an n -port. If the network is *linear*, this relationship will be a *linear combination* of the port voltages and currents. One obvious way is to generalize the Thevenin equivalent

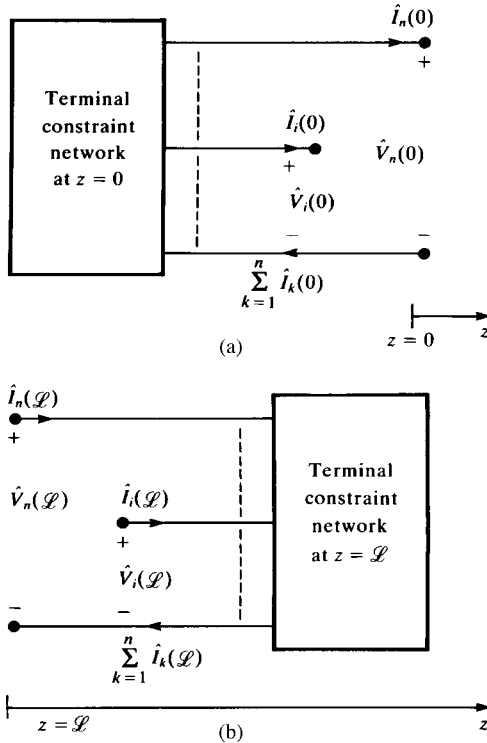


FIGURE 7.3 Modeling the terminal constraints of a $(n + 1)$ -conductor line.

representation of a one port as [A.2]

$$\hat{\mathbf{V}}(0) = \hat{\mathbf{V}}_S - \hat{\mathbf{Z}}_S \hat{\mathbf{I}}(0) \tag{7.87a}$$

$$\hat{\mathbf{V}}(L) = \hat{\mathbf{V}}_L + \hat{\mathbf{Z}}_L \hat{\mathbf{I}}(L) \tag{7.87b}$$

The $n \times 1$ vectors $\hat{\mathbf{V}}_S$ and $\hat{\mathbf{V}}_L$ contain the effects of the independent voltage and current sources in the termination networks at $z = 0$ and $z = L$, respectively. The $n \times n$ matrices $\hat{\mathbf{Z}}_S$ and $\hat{\mathbf{Z}}_L$ contain the effects of the impedances and any controlled sources in the terminal networks at $z = 0$ and $z = L$, respectively. In general, the impedance matrices $\hat{\mathbf{Z}}_S$ or $\hat{\mathbf{Z}}_L$ are *full*; that is, there is *cross coupling* between all ports of the network. However, the most common case will be terminal network configurations wherein these impedance matrices are diagonal and the coupling occurs only along the MTL. Figure 7.4 shows such a case wherein each line at $z = 0$ is terminated directly to the chosen reference conductor with an impedance and a voltage source, which represents a single Thevenin equivalent. In this case, the matrices in (7.87a)

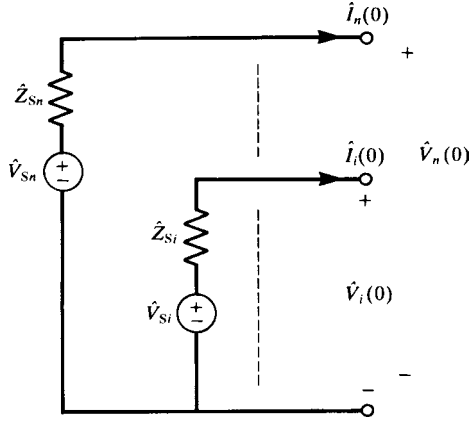


FIGURE 7.4 The generalized Thevenin representation of a termination with no cross coupling.

become

$$\hat{\mathbf{V}}_S = \begin{bmatrix} \hat{V}_{S1} \\ \vdots \\ \hat{V}_{Si} \\ \vdots \\ \hat{V}_{Sn} \end{bmatrix} \tag{7.88a}$$

$$\hat{\mathbf{Z}}_S = \begin{bmatrix} \hat{Z}_{S1} & 0 & \cdots & \cdots & 0 \\ 0 & \ddots & \ddots & \ddots & \vdots \\ \vdots & \ddots & \hat{Z}_{Si} & \ddots & \vdots \\ \vdots & \ddots & \ddots & \ddots & 0 \\ 0 & \cdots & \cdots & 0 & \hat{Z}_{Sn} \end{bmatrix} \tag{7.88b}$$

In order to solve for the $2n$ undetermined constants in $\hat{\mathbf{I}}_m^+$ and $\hat{\mathbf{I}}_m^-$, we evaluate the general forms of the solutions in (7.86) at $z = 0$ and $z = \mathcal{L}$ and substitute into the generalized Thevenin equivalent characterizations given in (7.87) to yield

$$\hat{\mathbf{Z}}_C \hat{\mathbf{T}}_I [\hat{\mathbf{I}}_m^+ + \hat{\mathbf{I}}_m^-] = \hat{\mathbf{V}}_S - \hat{\mathbf{Z}}_S \hat{\mathbf{T}}_I [\hat{\mathbf{I}}_m^+ - \hat{\mathbf{I}}_m^-] \tag{7.89a}$$

$$\hat{\mathbf{Z}}_C \hat{\mathbf{T}}_I [e^{-\hat{\gamma} \mathcal{L}} \hat{\mathbf{I}}_m^+ + e^{\hat{\gamma} \mathcal{L}} \hat{\mathbf{I}}_m^-] = \hat{\mathbf{V}}_L + \hat{\mathbf{Z}}_L \hat{\mathbf{T}}_I [e^{-\hat{\gamma} \mathcal{L}} \hat{\mathbf{I}}_m^+ - e^{\hat{\gamma} \mathcal{L}} \hat{\mathbf{I}}_m^-] \tag{7.89b}$$

Writing this in matrix form gives

$$\begin{bmatrix} (\hat{\mathbf{Z}}_C + \hat{\mathbf{Z}}_S) \hat{\mathbf{T}}_I & (\hat{\mathbf{Z}}_C - \hat{\mathbf{Z}}_S) \hat{\mathbf{T}}_I \\ (\hat{\mathbf{Z}}_C - \hat{\mathbf{Z}}_L) \hat{\mathbf{T}}_I e^{-\hat{\gamma}\mathcal{L}} & (\hat{\mathbf{Z}}_C + \hat{\mathbf{Z}}_L) \hat{\mathbf{T}}_I e^{\hat{\gamma}\mathcal{L}} \end{bmatrix} \begin{bmatrix} \hat{\mathbf{I}}_m^+ \\ \hat{\mathbf{I}}_m^- \end{bmatrix} = \begin{bmatrix} \hat{\mathbf{V}}_S \\ \hat{\mathbf{V}}_L \end{bmatrix} \quad (7.90)$$

Once this set of $2n$ simultaneous equations is solved for $\hat{\mathbf{I}}_m^+$ and $\hat{\mathbf{I}}_m^-$, the line voltages and currents are obtained at any z along the line by substitution into (7.86).

An alternative method for incorporating the terminal conditions is to substitute the generalized Thevenin equivalent characterizations in (7.87) into the chain-parameter matrix characterization of the line as a $2n$ -port, which was discussed in the previous chapter for two-conductor lines and is given for MTLs in Section 7.5.2 as

$$\hat{\mathbf{V}}(\mathcal{L}) = \hat{\Phi}_{11}(\mathcal{L})\hat{\mathbf{V}}(0) + \hat{\Phi}_{12}(\mathcal{L})\hat{\mathbf{I}}(0) \quad (7.91a)$$

$$\hat{\mathbf{I}}(\mathcal{L}) = \hat{\Phi}_{21}(\mathcal{L})\hat{\mathbf{V}}(0) + \hat{\Phi}_{22}(\mathcal{L})\hat{\mathbf{I}}(0) \quad (7.91b)$$

where each $\hat{\Phi}_{ij}(\mathcal{L})$ is $n \times n$ to yield [B.1]

$$[\hat{\Phi}_{12} - \hat{\Phi}_{11}\hat{\mathbf{Z}}_S - \hat{\mathbf{Z}}_L\hat{\Phi}_{22} + \hat{\mathbf{Z}}_L\hat{\Phi}_{21}\hat{\mathbf{Z}}_S] \hat{\mathbf{I}}(0) = \hat{\mathbf{V}}_L - [\hat{\Phi}_{11} - \hat{\mathbf{Z}}_L\hat{\Phi}_{21}] \hat{\mathbf{V}}_S \quad (7.92a)$$

$$\hat{\mathbf{I}}(\mathcal{L}) = \hat{\Phi}_{21}\hat{\mathbf{V}}_S + [\hat{\Phi}_{22} - \hat{\Phi}_{21}\hat{\mathbf{Z}}_S] \hat{\mathbf{I}}(0) \quad (7.92b)$$

Equations (7.92a) are a set of n simultaneous, algebraic equations, which can be solved for the n terminal currents at $z = 0$, $\hat{\mathbf{I}}(0)$. Once these are solved, the n terminal currents at $z = \mathcal{L}$, $\hat{\mathbf{I}}(\mathcal{L})$, can be obtained from (7.92b). The $2n$ terminal voltages $\hat{\mathbf{V}}(0)$ and $\hat{\mathbf{V}}(\mathcal{L})$ can be obtained from the terminal relations in (7.87).

7.3.2 The Generalized Norton Equivalent

The generalized Thevenin equivalent in the previous section is only one way of relating the terminal voltages and currents of a linear n -port. An alternative representation is the generalized Norton equivalent, wherein the voltages and currents are related by

$$\hat{\mathbf{I}}(0) = \hat{\mathbf{I}}_S - \hat{\mathbf{Y}}_S \hat{\mathbf{V}}(0) \quad (7.93a)$$

$$\hat{\mathbf{I}}(\mathcal{L}) = -\hat{\mathbf{I}}_L + \hat{\mathbf{Y}}_L \hat{\mathbf{V}}(\mathcal{L}) \quad (7.93b)$$

The $n \times 1$ vectors $\hat{\mathbf{I}}_S$ and $\hat{\mathbf{I}}_L$ again contain the effects of the independent voltage and current sources in the termination networks at $z = 0$ and $z = \mathcal{L}$, respectively. The $n \times n$ matrices $\hat{\mathbf{Y}}_S$ and $\hat{\mathbf{Y}}_L$ again contain the effects of the impedances and any controlled sources in the terminal networks at $z = 0$ and $z = \mathcal{L}$, respectively. Again, the admittance matrices $\hat{\mathbf{Y}}_S$ or $\hat{\mathbf{Y}}_L$ may be *full*; that is, there may be *cross coupling* between all ports of a terminal network. However, the most common case will be

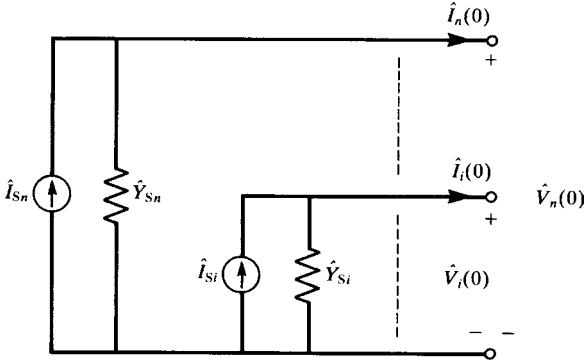


FIGURE 7.5 The generalized Norton representation of a termination with no cross coupling.

terminal network configurations wherein these admittance matrices are diagonal and the coupling occurs only along the MTL. Figure 7.5 shows such a case wherein each line is terminated directly at $z = 0$ to the chosen reference conductor with an admittance in parallel with a current source that represents a single Norton equivalent. In this case, the matrices in (7.93a) become

$$\hat{\mathbf{I}}_S = \begin{bmatrix} \hat{I}_{S1} \\ \vdots \\ \hat{I}_{Si} \\ \vdots \\ \hat{I}_{Sn} \end{bmatrix} \tag{7.94a}$$

$$\hat{\mathbf{Y}}_S = \begin{bmatrix} \hat{Y}_{S1} & 0 & \cdots & \cdots & 0 \\ 0 & \ddots & \ddots & \ddots & \vdots \\ \vdots & \ddots & \hat{Y}_{Si} & \ddots & \vdots \\ \vdots & \ddots & \ddots & \ddots & 0 \\ 0 & \cdots & \cdots & 0 & \hat{Y}_{Sn} \end{bmatrix} \tag{7.94b}$$

The $2n$ undetermined constants $\hat{\mathbf{I}}_m^+$ and $\hat{\mathbf{I}}_m^-$ in the general solution given in (7.86) are once again found by evaluating these solutions at $z = 0$ and $z = \mathcal{L}$ and substituting into the generalized Norton equivalent characterizations given in (7.93) to yield

$$\hat{\mathbf{T}}_I [\hat{\mathbf{I}}_m^+ - \hat{\mathbf{I}}_m^-] = \hat{\mathbf{I}}_S - \hat{\mathbf{Y}}_S \hat{\mathbf{Z}}_C \hat{\mathbf{T}}_I [\hat{\mathbf{I}}_m^+ + \hat{\mathbf{I}}_m^-] \tag{7.95a}$$

$$\hat{\mathbf{T}}_I \left[e^{-\hat{\gamma}\mathcal{L}} \hat{\mathbf{I}}_m^+ - e^{\hat{\gamma}\mathcal{L}} \hat{\mathbf{I}}_m^- \right] = -\hat{\mathbf{I}}_L + \hat{\mathbf{Y}}_L \hat{\mathbf{Z}}_C \hat{\mathbf{T}}_I \left[e^{-\hat{\gamma}\mathcal{L}} \hat{\mathbf{I}}_m^+ + e^{\hat{\gamma}\mathcal{L}} \hat{\mathbf{I}}_m^- \right] \tag{7.95b}$$

Writing this in matrix form gives

$$\begin{bmatrix} (\hat{\mathbf{Y}}_S \hat{\mathbf{Z}}_C + \mathbf{1}_n) \hat{\mathbf{T}}_I & (\hat{\mathbf{Y}}_S \hat{\mathbf{Z}}_C - \mathbf{1}_n) \hat{\mathbf{T}}_I \\ (\hat{\mathbf{Y}}_L \hat{\mathbf{Z}}_C - \mathbf{1}_n) \hat{\mathbf{T}}_I e^{-\hat{\gamma} \mathcal{L}} & (\hat{\mathbf{Y}}_L \hat{\mathbf{Z}}_C + \mathbf{1}_n) \hat{\mathbf{T}}_I e^{\hat{\gamma} \mathcal{L}} \end{bmatrix} \begin{bmatrix} \hat{\mathbf{I}}_m^+ \\ \hat{\mathbf{I}}_m^- \end{bmatrix} = \begin{bmatrix} \hat{\mathbf{I}}_S \\ \hat{\mathbf{I}}_L \end{bmatrix} \quad (7.96)$$

Once this set of $2n$ simultaneous equations is solved for $\hat{\mathbf{I}}_m^+$ and $\hat{\mathbf{I}}_m^-$, the line voltages and currents are obtained at any z along the line by substitution into (7.86).

An alternative method of incorporating the terminal conditions is to again substitute the generalized Norton equivalent terminal relations given in (7.93) into the chain-parameter representation given in (7.91) to yield [B.1]

$$[\hat{\Phi}_{21} - \hat{\Phi}_{22} \hat{\mathbf{Y}}_S - \hat{\mathbf{Y}}_L \hat{\Phi}_{11} + \hat{\mathbf{Y}}_L \hat{\Phi}_{12} \hat{\mathbf{Y}}_S] \hat{\mathbf{V}}(0) = -\hat{\mathbf{I}}_L - [\hat{\Phi}_{22} - \hat{\mathbf{Y}}_L \hat{\Phi}_{12}] \hat{\mathbf{I}}_S \quad (7.97a)$$

$$\hat{\mathbf{V}}(\mathcal{L}) = \hat{\Phi}_{12} \hat{\mathbf{I}}_S + [\hat{\Phi}_{11} - \hat{\Phi}_{12} \hat{\mathbf{Y}}_S] \hat{\mathbf{V}}(0) \quad (7.97b)$$

Equations (7.97a) are once again a set of n *simultaneous, algebraic equations*, which can be solved for the n terminal voltages at $z = 0$, $\hat{\mathbf{V}}(0)$. Once these are solved, the n terminal voltages at $z = \mathcal{L}$, $\hat{\mathbf{V}}(\mathcal{L})$, can be obtained from (7.97b). The $2n$ terminal currents $\hat{\mathbf{I}}(0)$ and $\hat{\mathbf{I}}(\mathcal{L})$ can be obtained from the terminal relations in (7.93).

7.3.3 Mixed Representations

There are some special cases where a termination cannot be represented as generalized Thevenin equivalents or as generalized Norton equivalents [F.10,G.3]. For example, suppose some of the conductors are terminated at $z = 0$ to the reference conductor in short circuits. In this case, the generalized Norton equivalent representation in (7.93a) does not exist for this termination since the termination admittance is infinite. However, the generalized Thevenin equivalent representation in (7.87a) does exist because the short circuit is equivalent to a load impedance of zero, which is a legitimate entry in $\hat{\mathbf{Z}}_S$. Shielded wires in which the shield (one of the MTL conductors) is “grounded” to the reference conductor represent such a case. Conversely, one of the conductors may be unterminated, that is, there is an open circuit between that conductor and the reference conductor. In this case, we must use the generalized Norton equivalent representation (the termination has zero admittance) since the generalized Thevenin equivalent representation does not exist (the termination has infinite impedance). An example of this is commonly found in *balanced* wire lines such as twisted pairs where neither wire is connected to the reference conductor [G.1–G.10]. This calls for a mixed representation of the terminal networks wherein one is represented with a generalized Thevenin equivalent and the other is represented with a generalized Norton equivalent.

We now obtain the equations to be solved for these mixed representations. Substituting (7.87a) and (7.93b) into the general solution in (7.86) yields

$$\begin{bmatrix} (\hat{\mathbf{Z}}_C + \hat{\mathbf{Z}}_S) \hat{\mathbf{T}}_I & (\hat{\mathbf{Z}}_C - \hat{\mathbf{Z}}_S) \hat{\mathbf{T}}_I \\ (\hat{\mathbf{Y}}_L \hat{\mathbf{Z}}_C - \mathbf{1}_n) \hat{\mathbf{T}}_I e^{-\hat{\gamma} \mathcal{L}} & (\hat{\mathbf{Y}}_L \hat{\mathbf{Z}}_C + \mathbf{1}_n) \hat{\mathbf{T}}_I e^{\hat{\gamma} \mathcal{L}} \end{bmatrix} \begin{bmatrix} \hat{\mathbf{I}}_m^+ \\ \hat{\mathbf{I}}_m^- \end{bmatrix} = \begin{bmatrix} \hat{\mathbf{V}}_S \\ \hat{\mathbf{I}}_L \end{bmatrix} \quad (7.98)$$

or, via the chain-parameter matrix,

$$[\hat{\Phi}_{22} - \hat{\Phi}_{21} \hat{\mathbf{Z}}_S - \hat{\mathbf{Y}}_L \hat{\Phi}_{12} + \hat{\mathbf{Y}}_L \hat{\Phi}_{11} \hat{\mathbf{Z}}_S] \hat{\mathbf{I}}(0) = -\hat{\mathbf{I}}_L - [\hat{\Phi}_{21} - \hat{\mathbf{Y}}_L \hat{\Phi}_{11}] \hat{\mathbf{V}}_S \quad (7.99a)$$

$$\hat{\mathbf{V}}(\mathcal{L}) = \hat{\Phi}_{11} \hat{\mathbf{V}}_S + [\hat{\Phi}_{12} - \hat{\Phi}_{11} \hat{\mathbf{Z}}_S] \hat{\mathbf{I}}(0) \quad (7.99b)$$

Similarly, substituting (7.93a) and (7.87b) into the general solution in (7.86) yields

$$\begin{bmatrix} (\hat{\mathbf{Y}}_S \hat{\mathbf{Z}}_C + \mathbf{1}_n) \hat{\mathbf{T}}_I & (\hat{\mathbf{Y}}_S \hat{\mathbf{Z}}_C - \mathbf{1}_n) \hat{\mathbf{T}}_I \\ (\hat{\mathbf{Z}}_C - \hat{\mathbf{Z}}_L) \hat{\mathbf{T}}_I e^{-\hat{\gamma} \mathcal{L}} & (\hat{\mathbf{Z}}_C + \hat{\mathbf{Z}}_L) \hat{\mathbf{T}}_I e^{\hat{\gamma} \mathcal{L}} \end{bmatrix} \begin{bmatrix} \hat{\mathbf{I}}_m^+ \\ \hat{\mathbf{I}}_m^- \end{bmatrix} = \begin{bmatrix} \hat{\mathbf{I}}_S \\ \hat{\mathbf{V}}_L \end{bmatrix} \quad (7.100)$$

or, using the chain-parameter matrix,

$$[\hat{\Phi}_{11} - \hat{\Phi}_{12} \hat{\mathbf{Y}}_S - \hat{\mathbf{Z}}_L \hat{\Phi}_{21} + \hat{\mathbf{Z}}_L \hat{\Phi}_{22} \hat{\mathbf{Y}}_S] \hat{\mathbf{V}}(0) = \hat{\mathbf{V}}_L - [\hat{\Phi}_{12} - \hat{\mathbf{Z}}_L \hat{\Phi}_{22}] \hat{\mathbf{I}}_S \quad (7.101a)$$

$$\hat{\mathbf{I}}(\mathcal{L}) = \hat{\Phi}_{22} \hat{\mathbf{I}}_S + [\hat{\Phi}_{21} - \hat{\Phi}_{22} \hat{\mathbf{Y}}_S] \hat{\mathbf{V}}(0) \quad (7.101b)$$

The above mixed representation can characterize termination networks wherein short-circuit terminations exist within one termination network and open-circuit terminations exist within the other termination network. Terminal networks wherein both short-circuit and open-circuit terminations exist within the same network can be handled with a more general formulation as

$$\hat{\mathbf{Y}}_S \hat{\mathbf{V}}(0) + \hat{\mathbf{Z}}_S \hat{\mathbf{I}}(0) = \hat{\mathbf{P}}_S \quad (7.102a)$$

$$\hat{\mathbf{Y}}_L \hat{\mathbf{V}}(\mathcal{L}) - \hat{\mathbf{Z}}_L \hat{\mathbf{I}}(\mathcal{L}) = \hat{\mathbf{P}}_L \quad (7.102b)$$

where $\hat{\mathbf{P}}_S$ and $\hat{\mathbf{P}}_L$ contain the effects of the independent sources in the terminations. Substituting the expressions for the line currents and voltages given in (7.86) yields

$$\begin{bmatrix} (\hat{\mathbf{Y}}_S \hat{\mathbf{Z}}_C + \hat{\mathbf{Z}}_S) \hat{\mathbf{T}}_I & (\hat{\mathbf{Y}}_S \hat{\mathbf{Z}}_C - \hat{\mathbf{Z}}_S) \hat{\mathbf{T}}_I \\ (\hat{\mathbf{Y}}_L \hat{\mathbf{Z}}_C - \hat{\mathbf{Z}}_L) \hat{\mathbf{T}}_I e^{-\hat{\gamma} \mathcal{L}} & (\hat{\mathbf{Y}}_L \hat{\mathbf{Z}}_C + \hat{\mathbf{Z}}_L) \hat{\mathbf{T}}_I e^{\hat{\gamma} \mathcal{L}} \end{bmatrix} \begin{bmatrix} \hat{\mathbf{I}}_m^+ \\ \hat{\mathbf{I}}_m^- \end{bmatrix} = \begin{bmatrix} \hat{\mathbf{P}}_S \\ \hat{\mathbf{P}}_L \end{bmatrix} \quad (7.103)$$

7.4 LUMPED-CIRCUIT APPROXIMATE CHARACTERIZATIONS

Lumped-circuit notions apply to circuits whose largest dimension is *electrically small*; that is, $\ll \lambda$, where $\lambda = v/f$ is the wavelength at the frequency of interest. This suggests another frequently used approximation of an MTL. Divide the line into N sections of length \mathcal{L}/N . If each of these section lengths is electrically short at the frequency of interest, $\mathcal{L}/N \ll \lambda$, then each section may be represented with a lumped model. These are referred to as *lumped, iterative* structures since the line must be more finely divided as frequency is increased.

Some typical lumped structures are shown in Figure 7.6 [B.1, 12]. Observe that the total parameter is the per-unit-length parameter multiplied by the section length, \mathcal{L}/N . These structures are named after the symbols their structures represent: the lumped-Pi or lumped-T structures. The chain-parameter matrices (discussed in Sec-

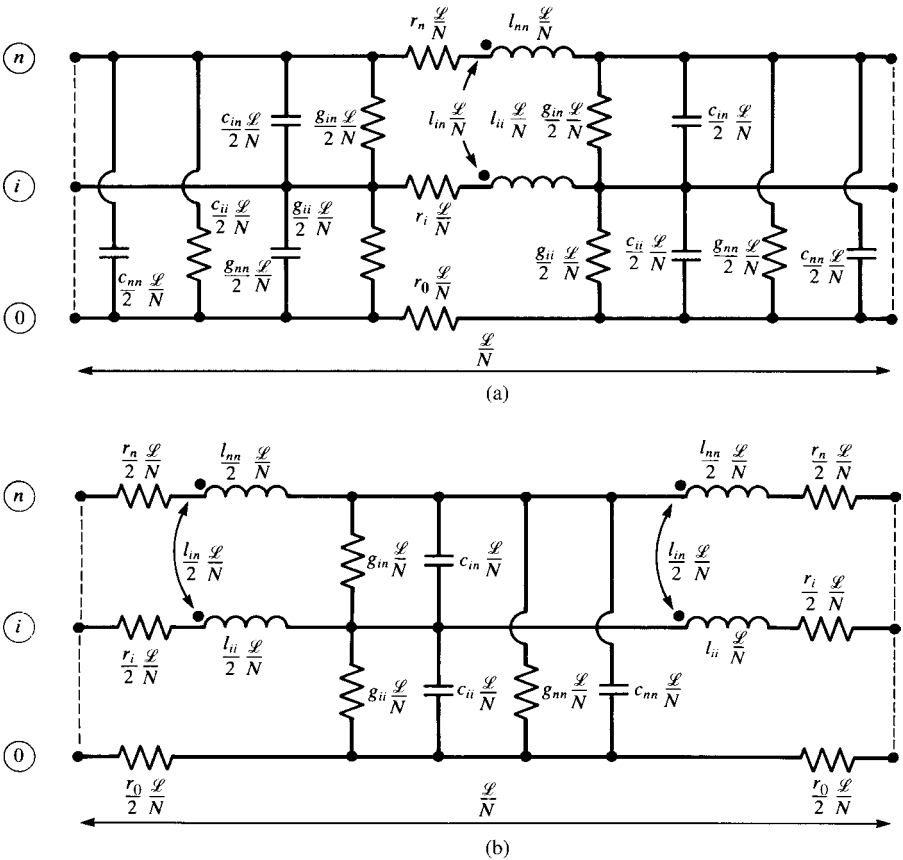


FIGURE 7.6 Lumped-circuit iterative approximate structures: (a) lumped Pi and (b) lumped T.

tion 7.5) of these structures can be derived in a straightforward fashion as [B.1]

$$\hat{\Phi}_{Pi} = \begin{bmatrix} \left\{ \mathbf{1}_n + \frac{1}{2} \hat{\mathbf{Z}} \hat{\mathbf{Y}} \left(\frac{\mathcal{L}}{N} \right)^2 \right\} & \left\{ -\hat{\mathbf{Z}} \frac{\mathcal{L}}{N} \right\} \\ \left\{ -\hat{\mathbf{Y}} \frac{\mathcal{L}}{N} - \frac{1}{4} \hat{\mathbf{Y}} \hat{\mathbf{Z}} \hat{\mathbf{Y}} \left(\frac{\mathcal{L}}{N} \right)^3 \right\} & \left\{ \mathbf{1}_n + \frac{1}{2} \hat{\mathbf{Y}} \hat{\mathbf{Z}} \left(\frac{\mathcal{L}}{N} \right)^2 \right\} \end{bmatrix} \quad (7.104a)$$

$$\hat{\Phi}_T = \begin{bmatrix} \left\{ \mathbf{1}_n + \frac{1}{2} \hat{\mathbf{Z}} \hat{\mathbf{Y}} \left(\frac{\mathcal{L}}{N} \right)^2 \right\} & \left\{ -\hat{\mathbf{Z}} \frac{\mathcal{L}}{N} - \frac{1}{4} \hat{\mathbf{Z}} \hat{\mathbf{Y}} \hat{\mathbf{Z}} \left(\frac{\mathcal{L}}{N} \right)^3 \right\} \\ \left\{ -\hat{\mathbf{Y}} \frac{\mathcal{L}}{N} \right\} & \left\{ \mathbf{1}_n + \frac{1}{2} \hat{\mathbf{Y}} \hat{\mathbf{Z}} \left(\frac{\mathcal{L}}{N} \right)^2 \right\} \end{bmatrix} \quad (7.104b)$$

The overall chain-parameter matrix of a line that is represented as a cascade of N such lumped sections is

$$\hat{\Phi} = \hat{\Phi}_{(Pi,T)}^N \quad (7.105)$$

Once this overall chain-parameter matrix is obtained, the terminal conditions are incorporated as described in the previous section to give the terminal voltages and currents of the MTL. Lumped-circuit analysis programs such as SPICE can be used to analyze the resulting lumped circuit as an alternative to obtaining the overall chain-parameter matrix via (7.105) and then incorporating the terminal conditions. Nonlinear terminations such as transistors and diodes can be readily incorporated into the terminations as these lumped-circuit programs include sophisticated models for them.

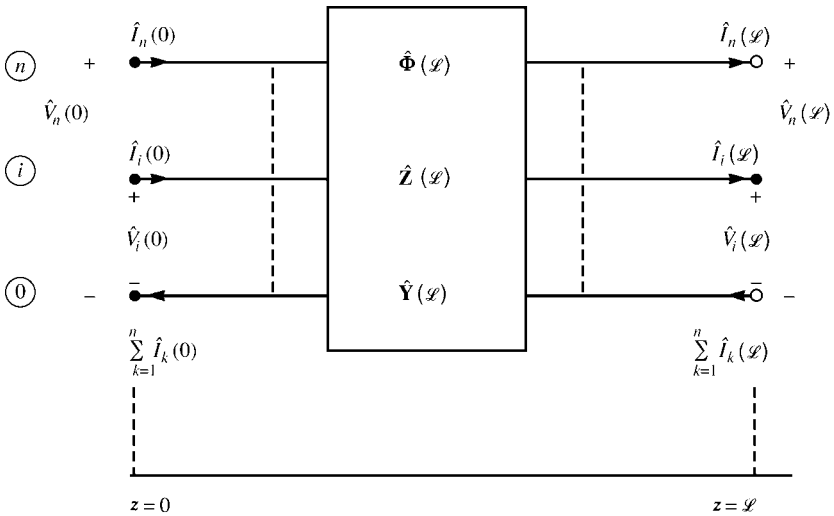


FIGURE 7.7 Representing an MTL as a 2n-port with its chain-parameter matrix Φ , its impedance matrix \mathbf{Z} , or its admittance matrix \mathbf{Y} .

7.5 ALTERNATIVE $2n$ -PORT CHARACTERIZATIONS

In this section, we will investigate the two-port characterization of an MTL using the chain-parameters, the Z parameters and the Y parameters. The MTL can be viewed as having $2n$ ports, n at the left and n at the right. Hence, we seek representations that relate the n voltages and n currents at $z = 0$, $\hat{\mathbf{V}}(0)$ and $\hat{\mathbf{I}}(0)$, to the n voltages and n currents at $z = \mathcal{L}$, $\hat{\mathbf{V}}(\mathcal{L})$ and $\hat{\mathbf{I}}(\mathcal{L})$, as illustrated in Figure 7.7.

7.5.1 Analogy of the Frequency-Domain MTL Equations to State-Variable Equations

Let us reconsider the phasor transmission-line equations for an $(n + 1)$ -conductor line given in (7.4). Writing these in compact matrix form gives

$$\frac{d}{dz} \hat{\mathbf{X}}(z) = \hat{\mathbf{A}} \hat{\mathbf{X}}(z) \tag{7.106a}$$

where

$$\hat{\mathbf{X}}(z) = \begin{bmatrix} \hat{\mathbf{V}}(z) \\ \hat{\mathbf{I}}(z) \end{bmatrix} \tag{7.106b}$$

$$\hat{\mathbf{A}} = \begin{bmatrix} \mathbf{0} & -\hat{\mathbf{Z}} \\ -\hat{\mathbf{Y}} & \mathbf{0} \end{bmatrix} \tag{7.106c}$$

These are first-order ordinary differential equations. As such, they are identical in form to the state-variable equations that describe automatic control systems and other linear systems [A.2, B.2, B.4, 1, 2]. In those characterizations, the independent variable is time t , whereas the independent variable for the MTL equations is the line axis variable z . Nevertheless, we may directly adapt the well-known solutions of those state-variable equations to the solution of the phasor MTL equations by simply replacing t in the state-variable formulation and solution with z .

Hence, the solution to the MTL phasor equations in (7.106) is [A.2, B.2, B.4, 1, 2]

$$\hat{\mathbf{X}}(z_2) = \hat{\Phi}(z_2 - z_1) \hat{\mathbf{X}}(z_1) \tag{7.107}$$

and the two position points on the line are such that $z_2 \geq z_1$. The $2n \times 2n$ matrix $\hat{\Phi}$ is called the *state-transition matrix*. In our terminology, $\hat{\Phi}$ is the *chain-parameter matrix*. Hence, we may write this out as

$$\underbrace{\begin{bmatrix} \hat{\mathbf{V}}(z_2) \\ \hat{\mathbf{I}}(z_2) \end{bmatrix}}_{\hat{\mathbf{X}}(z_2)} = \underbrace{\begin{bmatrix} \hat{\Phi}_{11}(z_2 - z_1) & \hat{\Phi}_{12}(z_2 - z_1) \\ \hat{\Phi}_{21}(z_2 - z_1) & \hat{\Phi}_{22}(z_2 - z_1) \end{bmatrix}}_{\hat{\Phi}(z_2 - z_1)} \underbrace{\begin{bmatrix} \hat{\mathbf{V}}(z_1) \\ \hat{\mathbf{I}}(z_1) \end{bmatrix}}_{\hat{\mathbf{X}}(z_1)} \tag{7.108}$$

where $\hat{\Phi}_{ij}$ are $n \times n$. If we choose $z_2 = \mathcal{L}$ and $z_1 = 0$, we essentially obtain the *chain-parameter matrix* $\hat{\Phi}$ for the overall line, which is $2n \times 2n$, as

$$\begin{aligned} \begin{bmatrix} \hat{\mathbf{V}}(\mathcal{L}) \\ \hat{\mathbf{I}}(\mathcal{L}) \end{bmatrix} &= \hat{\Phi}(\mathcal{L}) \begin{bmatrix} \hat{\mathbf{V}}(0) \\ \hat{\mathbf{I}}(0) \end{bmatrix} \\ &= \begin{bmatrix} \hat{\Phi}_{11}(\mathcal{L}) & \hat{\Phi}_{12}(\mathcal{L}) \\ \hat{\Phi}_{21}(\mathcal{L}) & \hat{\Phi}_{22}(\mathcal{L}) \end{bmatrix} \begin{bmatrix} \hat{\mathbf{V}}(0) \\ \hat{\mathbf{I}}(0) \end{bmatrix} \end{aligned} \quad (7.109)$$

Because of the direct analogy between the state-variable equations for a lumped system and the phasor MTL equations, we can immediately observe some important properties of the chain-parameter matrix that are directly taken from the same identities for the state-variable solution with t replaced with z [1, 2]:

$$\hat{\Phi}(0) = \mathbf{1}_{2n} \quad (7.110)$$

$$\hat{\Phi}^{-1}(\mathcal{L}) = \hat{\Phi}(-\mathcal{L}) \quad (7.111)$$

and

$$\begin{aligned} \hat{\Phi}(\mathcal{L}) &= \mathbf{e}^{\hat{\mathbf{A}}\mathcal{L}} \\ &= \mathbf{1}_{2n} + \frac{\mathcal{L}}{1!} \hat{\mathbf{A}} + \frac{\mathcal{L}^2}{2!} \hat{\mathbf{A}}^2 + \frac{\mathcal{L}^3}{3!} \hat{\mathbf{A}}^3 + \dots \end{aligned} \quad (7.112)$$

The property of the inverse of the chain-parameter matrix given in (7.111) is logical to expect because the inverse of (7.109) yields

$$\begin{aligned} \begin{bmatrix} \hat{\mathbf{V}}(0) \\ \hat{\mathbf{I}}(0) \end{bmatrix} &= \hat{\Phi}^{-1}(\mathcal{L}) \begin{bmatrix} \hat{\mathbf{V}}(\mathcal{L}) \\ \hat{\mathbf{I}}(\mathcal{L}) \end{bmatrix} \\ &= \hat{\Phi}(-\mathcal{L}) \begin{bmatrix} \hat{\mathbf{V}}(\mathcal{L}) \\ \hat{\mathbf{I}}(\mathcal{L}) \end{bmatrix} \end{aligned} \quad (7.113)$$

This follows as a simple reversal of the line axis scale (replacing z with $-z$) similar to the reversal in time for the state-transition matrix of lumped systems and the line is *reciprocal* (assuming the surrounding medium is linear and isotropic). We will find these properties to be important in obtaining insight into the interpretation of the MTL equation solution.

There is another powerful identity of the chain-parameter matrix. Suppose two sections of *identical lines*, each having lengths \mathcal{L}_1 and \mathcal{L}_2 , characterized by chain-parameter matrices as $\hat{\Phi}(\mathcal{L}_1)$ and $\hat{\Phi}(\mathcal{L}_2)$ are cascaded as shown in Figure 7.8. Clearly, the overall chain-parameter matrix is the product of these, in the proper order, as $\hat{\Phi}(\mathcal{L}_2)\hat{\Phi}(\mathcal{L}_1)$. But this is the chain-parameter matrix of a line whose total length is

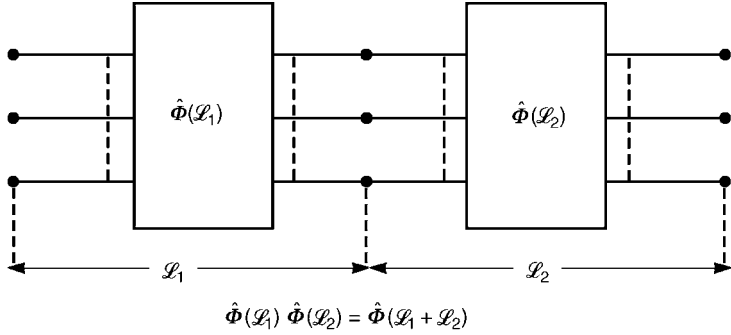


FIGURE 7.8 Illustration of a basic chain-parameter matrix identity.

$\mathcal{L}_1 + \mathcal{L}_2$. Hence, we arrive at another important matrix chain-parameter identity

$$\hat{\Phi}(\mathcal{L}_1 + \mathcal{L}_2) = \hat{\Phi}(\mathcal{L}_2)\hat{\Phi}(\mathcal{L}_1) \tag{7.114}$$

From this identity, we can establish the important identity concerning the inverse of the chain-parameter matrix in (7.111) as

$$\begin{aligned} \hat{\Phi}(\mathcal{L})\hat{\Phi}(-\mathcal{L}) &= \hat{\Phi}(\mathcal{L} + (-\mathcal{L})) \\ &= \hat{\Phi}(0) \\ &= \mathbf{1}_{2n} \end{aligned} \tag{7.111}$$

Observe that in order for the identity in (7.114) to be true, the $\hat{\Phi}$ must be the *exact solution* of the first-order differential equations characterizing the line voltages and currents given in (7.4). Hence the identity in (7.114) cannot be used in lieu of (7.105) to obtain the overall chain-parameter matrix of a line that is represented by lumped Pi or lumped T approximate models since these are *approximations* to the exact solution of (7.4).

7.5.2 Characterizing the Line as a $2n$ -Port with the Chain-Parameter Matrix

The phasor voltages and currents at the two ends of the line are related with the chain-parameter matrix as

$$\begin{aligned} \begin{bmatrix} \hat{\mathbf{V}}(\mathcal{L}) \\ \hat{\mathbf{i}}(\mathcal{L}) \end{bmatrix} &= \hat{\Phi}(\mathcal{L}) \begin{bmatrix} \hat{\mathbf{V}}(0) \\ \hat{\mathbf{i}}(0) \end{bmatrix} \\ &= \begin{bmatrix} \hat{\Phi}_{11}(\mathcal{L}) & \hat{\Phi}_{12}(\mathcal{L}) \\ \hat{\Phi}_{21}(\mathcal{L}) & \hat{\Phi}_{22}(\mathcal{L}) \end{bmatrix} \begin{bmatrix} \hat{\mathbf{V}}(0) \\ \hat{\mathbf{i}}(0) \end{bmatrix} \end{aligned} \tag{7.109}$$

This corresponds to viewing the $(n + 1)$ -conductor line as a $2n$ -port, as illustrated in Figure 7.7. The essential task in solving the phasor MTL equations is to determine the entries in the $n \times n$ submatrices $\hat{\Phi}_{ij}$. This section is devoted to that task.

The general solutions of the phasor MTL equations are given, via similarity transformations, in (7.86). Evaluating these at $z = 0$ and $z = \mathcal{L}$ and eliminating $\hat{\mathbf{I}}_m^\pm$ gives the chain-parameter submatrices as [B.1]

$$\begin{aligned}\hat{\Phi}_{11}(\mathcal{L}) &= \frac{1}{2} \hat{\mathbf{Y}}^{-1} \hat{\mathbf{T}}_I \left(\mathbf{e}^{\hat{\gamma} \mathcal{L}} + \mathbf{e}^{-\hat{\gamma} \mathcal{L}} \right) \hat{\mathbf{T}}_I^{-1} \hat{\mathbf{Y}} \\ &= \frac{1}{2} \hat{\mathbf{Z}}_C \hat{\mathbf{T}}_I \left(\mathbf{e}^{\hat{\gamma} \mathcal{L}} + \mathbf{e}^{-\hat{\gamma} \mathcal{L}} \right) \hat{\mathbf{T}}_I^{-1} \hat{\mathbf{Y}}_C\end{aligned}\quad (7.115a)$$

$$\begin{aligned}\hat{\Phi}_{12}(\mathcal{L}) &= -\frac{1}{2} \hat{\mathbf{Y}}^{-1} \hat{\mathbf{T}}_I \hat{\gamma} \left(\mathbf{e}^{\hat{\gamma} \mathcal{L}} - \mathbf{e}^{-\hat{\gamma} \mathcal{L}} \right) \hat{\mathbf{T}}_I^{-1} \\ &= -\frac{1}{2} \hat{\mathbf{Z}}_C \left[\hat{\mathbf{T}}_I \left(\mathbf{e}^{\hat{\gamma} \mathcal{L}} - \mathbf{e}^{-\hat{\gamma} \mathcal{L}} \right) \hat{\mathbf{T}}_I^{-1} \right]\end{aligned}\quad (7.115b)$$

$$\begin{aligned}\hat{\Phi}_{21}(\mathcal{L}) &= -\frac{1}{2} \hat{\mathbf{T}}_I \left(\mathbf{e}^{\hat{\gamma} \mathcal{L}} - \mathbf{e}^{-\hat{\gamma} \mathcal{L}} \right) \hat{\gamma}^{-1} \hat{\mathbf{T}}_I^{-1} \hat{\mathbf{Y}} \\ &= -\frac{1}{2} \left[\hat{\mathbf{T}}_I \left(\mathbf{e}^{\hat{\gamma} \mathcal{L}} - \mathbf{e}^{-\hat{\gamma} \mathcal{L}} \right) \hat{\mathbf{T}}_I^{-1} \right] \hat{\mathbf{Y}}_C\end{aligned}\quad (7.115c)$$

$$\hat{\Phi}_{22}(\mathcal{L}) = \frac{1}{2} \hat{\mathbf{T}}_I \left(\mathbf{e}^{\hat{\gamma} \mathcal{L}} + \mathbf{e}^{-\hat{\gamma} \mathcal{L}} \right) \hat{\mathbf{T}}_I^{-1} \quad (7.115d)$$

and $\hat{\mathbf{Y}}_C = \hat{\mathbf{Z}}_C^{-1}$. As a check on this result, observe that the identity in (7.110), $\hat{\Phi}(0) = \mathbf{I}_{2n}$, is satisfied.

Although (7.115) will be the primary method of computing the chain-parameter matrices, we may obtain an alternative form by evaluating (7.33a) and (7.33b) at $z = 0$ and $z = \mathcal{L}$ and eliminating $\hat{\mathbf{V}}_m^\pm$ to yield

$$\hat{\Phi}_{11}(\mathcal{L}) = \frac{1}{2} \hat{\mathbf{T}}_V \left(\mathbf{e}^{\hat{\gamma} \mathcal{L}} + \mathbf{e}^{-\hat{\gamma} \mathcal{L}} \right) \hat{\mathbf{T}}_V^{-1} \quad (7.116a)$$

$$\begin{aligned}\hat{\Phi}_{12}(\mathcal{L}) &= -\frac{1}{2} \hat{\mathbf{T}}_V \left(\mathbf{e}^{\hat{\gamma} \mathcal{L}} - \mathbf{e}^{-\hat{\gamma} \mathcal{L}} \right) \hat{\gamma}^{-1} \hat{\mathbf{T}}_V^{-1} \hat{\mathbf{Z}} \\ &= -\frac{1}{2} \left[\hat{\mathbf{T}}_V \left(\mathbf{e}^{\hat{\gamma} \mathcal{L}} - \mathbf{e}^{-\hat{\gamma} \mathcal{L}} \right) \hat{\mathbf{T}}_V^{-1} \right] \hat{\mathbf{Z}}_C\end{aligned}\quad (7.116b)$$

$$\begin{aligned}\hat{\Phi}_{21}(\mathcal{L}) &= -\frac{1}{2} \hat{\mathbf{Z}}^{-1} \hat{\mathbf{T}}_V \hat{\gamma} \left(\mathbf{e}^{\hat{\gamma} \mathcal{L}} - \mathbf{e}^{-\hat{\gamma} \mathcal{L}} \right) \hat{\mathbf{T}}_V^{-1} \\ &= -\frac{1}{2} \hat{\mathbf{Y}}_C \left[\hat{\mathbf{T}}_V \left(\mathbf{e}^{\hat{\gamma} \mathcal{L}} - \mathbf{e}^{-\hat{\gamma} \mathcal{L}} \right) \hat{\mathbf{T}}_V^{-1} \right]\end{aligned}\quad (7.116c)$$

$$\begin{aligned}\hat{\Phi}_{22}(\mathcal{L}) &= \frac{1}{2} \hat{\mathbf{Z}}^{-1} \hat{\mathbf{T}}_V \left(\mathbf{e}^{\hat{\gamma} \mathcal{L}} + \mathbf{e}^{-\hat{\gamma} \mathcal{L}} \right) \hat{\mathbf{T}}_V^{-1} \hat{\mathbf{Z}} \\ &= \frac{1}{2} \hat{\mathbf{Y}}_C \hat{\mathbf{T}}_V \left(\mathbf{e}^{\hat{\gamma} \mathcal{L}} + \mathbf{e}^{-\hat{\gamma} \mathcal{L}} \right) \hat{\mathbf{T}}_V^{-1} \hat{\mathbf{Z}}_C\end{aligned}\quad (7.116d)$$

7.5.3 Properties of the Chain-Parameter Matrix

In this section, we will define certain matrix analogies to the two-conductor solution [B.1, B.4]. These will place the results in a form directly analogous to the two-conductor case, which will simplify the notation and make the results easily remembered.

First, let us define the *square root of a matrix*. In scalar algebra, the square root is defined as *any quantity that when multiplied by itself gives the original quantity*, that is, $\sqrt{a}\sqrt{a} = a$. The square root of a matrix can similarly be defined as a matrix that when multiplied by itself gives the original matrix, that is, $\sqrt{\mathbf{M}}\sqrt{\mathbf{M}} = \mathbf{M}$. Recall the basic diagonalization:

$$\hat{\mathbf{T}}_I^{-1} \hat{\mathbf{Y}} \hat{\mathbf{Z}} \hat{\mathbf{T}}_I = \hat{\gamma}^2 \quad (7.117)$$

From this, we may define the square root of the matrix product as

$$\sqrt{\hat{\mathbf{Y}} \hat{\mathbf{Z}}} = \hat{\mathbf{T}}_I \hat{\gamma} \hat{\mathbf{T}}_I^{-1} \quad (7.118)$$

This can be verified by taking the product and using (7.117):

$$\begin{aligned} \sqrt{\hat{\mathbf{Y}} \hat{\mathbf{Z}}} \sqrt{\hat{\mathbf{Y}} \hat{\mathbf{Z}}} &= \hat{\mathbf{T}}_I \hat{\gamma} \hat{\mathbf{T}}_I^{-1} \hat{\mathbf{T}}_I \hat{\gamma} \hat{\mathbf{T}}_I^{-1} \\ &= \hat{\mathbf{T}}_I \hat{\gamma}^2 \hat{\mathbf{T}}_I^{-1} \\ &= \hat{\mathbf{Y}} \hat{\mathbf{Z}} \end{aligned} \quad (7.119)$$

The square root of the matrix product $\hat{\mathbf{Z}} \hat{\mathbf{Y}}$ can similarly be defined. Similarly, the transformation $\hat{\mathbf{T}}_V$ diagonalizes $\hat{\mathbf{Z}} \hat{\mathbf{Y}}$ as $\hat{\mathbf{T}}_V^{-1} \hat{\mathbf{Z}} \hat{\mathbf{Y}} \hat{\mathbf{T}}_V = \hat{\gamma}^2$. Hence, it is logical to define the square root of $\hat{\mathbf{Z}} \hat{\mathbf{Y}}$ as

$$\sqrt{\hat{\mathbf{Z}} \hat{\mathbf{Y}}} = \hat{\mathbf{T}}_V \hat{\gamma} \hat{\mathbf{T}}_V^{-1} \quad (7.120)$$

as multiplication by itself shows. From Table 7.1, we obtain $\hat{\mathbf{T}}_I \hat{\gamma} \hat{\mathbf{T}}_I^{-1} = \hat{\mathbf{Y}} \hat{\mathbf{T}}_V \hat{\gamma} \hat{\mathbf{T}}_V^{-1} \hat{\mathbf{Y}}^{-1}$ and $\hat{\mathbf{T}}_V \hat{\gamma} \hat{\mathbf{T}}_V^{-1} = \hat{\mathbf{Z}} \hat{\mathbf{T}}_I \hat{\gamma} \hat{\mathbf{T}}_I^{-1} \hat{\mathbf{Z}}^{-1}$. Hence, $\sqrt{\hat{\mathbf{Z}} \hat{\mathbf{Y}}}$ and $\sqrt{\hat{\mathbf{Y}} \hat{\mathbf{Z}}}$ are related as

$$\begin{aligned} \sqrt{\hat{\mathbf{Z}} \hat{\mathbf{Y}}} &= \hat{\mathbf{Y}}^{-1} \sqrt{\hat{\mathbf{Y}} \hat{\mathbf{Z}}} \hat{\mathbf{Y}} \\ &= \hat{\mathbf{Z}} \sqrt{\hat{\mathbf{Y}} \hat{\mathbf{Z}}} \hat{\mathbf{Z}}^{-1} \end{aligned} \quad (7.121)$$

which can again be confirmed by multiplication by itself. Therefore, from Table 7.1, the characteristic impedance matrix can be written, symbolically, as

$$\begin{aligned} \hat{\mathbf{Z}}_C &= \hat{\mathbf{Y}}^{-1} \sqrt{\hat{\mathbf{Y}} \hat{\mathbf{Z}}} = \hat{\mathbf{Z}} \left[\sqrt{\hat{\mathbf{Y}} \hat{\mathbf{Z}}} \right]^{-1} \\ &= \sqrt{\hat{\mathbf{Z}} \hat{\mathbf{Y}}} \hat{\mathbf{Y}}^{-1} = \left[\sqrt{\hat{\mathbf{Z}} \hat{\mathbf{Y}}} \right]^{-1} \hat{\mathbf{Z}} \end{aligned} \quad (7.122a)$$

and

$$\sqrt{\hat{\mathbf{Z}}\hat{\mathbf{Y}}} = \hat{\mathbf{Z}}_C \sqrt{\hat{\mathbf{Y}}\hat{\mathbf{Z}}} \hat{\mathbf{Y}}_C \quad (7.122b)$$

These results again reduce to the scalar characteristic impedance for two-conductor lines.

Additional symbolic definitions can be obtained for direct analogy to the two-conductor case by defining the matrix hyperbolic functions. First, define the matrix exponentials as

$$\mathbf{e}^{\hat{\gamma} \mathcal{L}} = \mathbf{1}_n + \frac{\mathcal{L}}{1!} \hat{\gamma} + \frac{\mathcal{L}^2}{2!} \hat{\gamma}^2 + \dots \quad (7.123a)$$

$$\mathbf{e}^{\sqrt{\hat{\mathbf{Y}}\hat{\mathbf{Z}}} \mathcal{L}} = \mathbf{1}_n + \frac{\mathcal{L}}{1!} \sqrt{\hat{\mathbf{Y}}\hat{\mathbf{Z}}} + \frac{\mathcal{L}^2}{2!} \left(\sqrt{\hat{\mathbf{Y}}\hat{\mathbf{Z}}} \right)^2 + \dots \quad (7.123b)$$

$$\mathbf{e}^{\sqrt{\hat{\mathbf{Y}}\hat{\mathbf{Z}}} \mathcal{L}} = \hat{\mathbf{T}}_I \mathbf{e}^{\hat{\gamma} \mathcal{L}} \hat{\mathbf{T}}_I^{-1} \quad (7.123c)$$

$$\mathbf{e}^{\sqrt{\hat{\mathbf{Z}}\hat{\mathbf{Y}}} \mathcal{L}} = \mathbf{1}_n + \frac{\mathcal{L}}{1!} \sqrt{\hat{\mathbf{Z}}\hat{\mathbf{Y}}} + \frac{\mathcal{L}^2}{2!} \left(\sqrt{\hat{\mathbf{Z}}\hat{\mathbf{Y}}} \right)^2 + \dots \quad (7.123d)$$

$$\mathbf{e}^{\sqrt{\hat{\mathbf{Z}}\hat{\mathbf{Y}}} \mathcal{L}} = \hat{\mathbf{T}}_V \mathbf{e}^{\hat{\gamma} \mathcal{L}} \hat{\mathbf{T}}_V^{-1} \quad (7.123e)$$

where we have used the relations in (7.118) and (7.120) for the matrix square roots $\sqrt{\hat{\mathbf{Y}}\hat{\mathbf{Z}}}$ and $\sqrt{\hat{\mathbf{Z}}\hat{\mathbf{Y}}}$. Substituting the relations in (7.121) and (7.122) yields

$$\begin{aligned} \mathbf{e}^{\sqrt{\hat{\mathbf{Z}}\hat{\mathbf{Y}}} \mathcal{L}} &= \hat{\mathbf{Y}}^{-1} \mathbf{e}^{\sqrt{\hat{\mathbf{Y}}\hat{\mathbf{Z}}} \mathcal{L}} \hat{\mathbf{Y}} \\ &= \hat{\mathbf{Z}}_C \mathbf{e}^{\sqrt{\hat{\mathbf{Y}}\hat{\mathbf{Z}}} \mathcal{L}} \hat{\mathbf{Y}}_C \end{aligned} \quad (7.124)$$

In terms of these matrix exponentials, we may define the matrix hyperbolic functions as

$$\begin{aligned} \cosh \left(\sqrt{\hat{\mathbf{Y}}\hat{\mathbf{Z}}} \mathcal{L} \right) &= \frac{1}{2} \left(\mathbf{e}^{\sqrt{\hat{\mathbf{Y}}\hat{\mathbf{Z}}} \mathcal{L}} + \mathbf{e}^{-\sqrt{\hat{\mathbf{Y}}\hat{\mathbf{Z}}} \mathcal{L}} \right) \\ &= \mathbf{1}_n + \frac{\mathcal{L}^2}{2!} \left(\sqrt{\hat{\mathbf{Y}}\hat{\mathbf{Z}}} \right)^2 + \frac{\mathcal{L}^4}{4!} \left(\sqrt{\hat{\mathbf{Y}}\hat{\mathbf{Z}}} \right)^4 + \dots \\ &= \frac{1}{2} \hat{\mathbf{T}}_I \left(\mathbf{e}^{\hat{\gamma} \mathcal{L}} + \mathbf{e}^{-\hat{\gamma} \mathcal{L}} \right) \hat{\mathbf{T}}_I^{-1} \end{aligned} \quad (7.125a)$$

$$\begin{aligned}
 \sinh \left(\sqrt{\hat{\mathbf{Y}}\hat{\mathbf{Z}}} \mathcal{L} \right) &= \frac{1}{2} \left(\mathbf{e}^{\sqrt{\hat{\mathbf{Y}}\hat{\mathbf{Z}}} \mathcal{L}} - \mathbf{e}^{-\sqrt{\hat{\mathbf{Y}}\hat{\mathbf{Z}}} \mathcal{L}} \right) \\
 &= \frac{\mathcal{L}}{1!} \sqrt{\hat{\mathbf{Y}}\hat{\mathbf{Z}}} + \frac{\mathcal{L}^3}{3!} \left(\sqrt{\hat{\mathbf{Y}}\hat{\mathbf{Z}}} \right)^3 + \dots \\
 &= \frac{1}{2} \hat{\mathbf{T}}_I \left(\mathbf{e}^{\hat{\gamma} \mathcal{L}} - \mathbf{e}^{-\hat{\gamma} \mathcal{L}} \right) \hat{\mathbf{T}}_I^{-1} \quad (7.125b)
 \end{aligned}$$

Similarly, as $\sqrt{\hat{\mathbf{Z}}\hat{\mathbf{Y}}} = \hat{\mathbf{Y}}^{-1} \sqrt{\hat{\mathbf{Y}}\hat{\mathbf{Z}}} \hat{\mathbf{Y}}$ and using the identities in Table 7.1,

$$\begin{aligned}
 \cosh \left(\sqrt{\hat{\mathbf{Z}}\hat{\mathbf{Y}}} \mathcal{L} \right) &= \frac{1}{2} \left(\mathbf{e}^{\sqrt{\hat{\mathbf{Z}}\hat{\mathbf{Y}}} \mathcal{L}} + \mathbf{e}^{-\sqrt{\hat{\mathbf{Z}}\hat{\mathbf{Y}}} \mathcal{L}} \right) \\
 &= \mathbf{1}_n + \frac{\mathcal{L}^2}{2!} \left(\sqrt{\hat{\mathbf{Z}}\hat{\mathbf{Y}}} \right)^2 + \frac{\mathcal{L}^4}{4!} \left(\sqrt{\hat{\mathbf{Z}}\hat{\mathbf{Y}}} \right)^4 + \dots \\
 &= \frac{1}{2} \hat{\mathbf{Y}}^{-1} \hat{\mathbf{T}}_I \left(\mathbf{e}^{\hat{\gamma} \mathcal{L}} + \mathbf{e}^{-\hat{\gamma} \mathcal{L}} \right) \hat{\mathbf{T}}_I^{-1} \hat{\mathbf{Y}} \\
 &= \frac{1}{2} \hat{\mathbf{Z}}_C \hat{\mathbf{T}}_I \left(\mathbf{e}^{\hat{\gamma} \mathcal{L}} + \mathbf{e}^{-\hat{\gamma} \mathcal{L}} \right) \hat{\mathbf{T}}_I^{-1} \hat{\mathbf{Y}}_C \\
 &= \hat{\mathbf{Z}}_C \cosh \left(\sqrt{\hat{\mathbf{Y}}\hat{\mathbf{Z}}} \mathcal{L} \right) \hat{\mathbf{Y}}_C \quad (7.126a)
 \end{aligned}$$

$$\begin{aligned}
 \sinh \left(\sqrt{\hat{\mathbf{Z}}\hat{\mathbf{Y}}} \mathcal{L} \right) &= \frac{1}{2} \left(\mathbf{e}^{\sqrt{\hat{\mathbf{Z}}\hat{\mathbf{Y}}} \mathcal{L}} - \mathbf{e}^{-\sqrt{\hat{\mathbf{Z}}\hat{\mathbf{Y}}} \mathcal{L}} \right) \\
 &= \frac{\mathcal{L}}{1!} \sqrt{\hat{\mathbf{Z}}\hat{\mathbf{Y}}} + \frac{\mathcal{L}^3}{3!} \left(\sqrt{\hat{\mathbf{Z}}\hat{\mathbf{Y}}} \right)^3 + \dots \\
 &= \frac{1}{2} \hat{\mathbf{Y}}^{-1} \hat{\mathbf{T}}_I \left(\mathbf{e}^{\hat{\gamma} \mathcal{L}} - \mathbf{e}^{-\hat{\gamma} \mathcal{L}} \right) \hat{\mathbf{T}}_I^{-1} \hat{\mathbf{Y}} \\
 &= \frac{1}{2} \hat{\mathbf{Z}}_C \hat{\mathbf{T}}_I \left(\mathbf{e}^{\hat{\gamma} \mathcal{L}} - \mathbf{e}^{-\hat{\gamma} \mathcal{L}} \right) \hat{\mathbf{T}}_I^{-1} \hat{\mathbf{Y}}_C \\
 &= \hat{\mathbf{Z}}_C \sinh \left(\sqrt{\hat{\mathbf{Y}}\hat{\mathbf{Z}}} \mathcal{L} \right) \hat{\mathbf{Y}}_C \quad (7.126b)
 \end{aligned}$$

In terms of these symbolic definitions, the chain-parameter submatrices in (7.115) can be written, symbolically, as

$$\begin{aligned}
 \hat{\Phi}_{11}(\mathcal{L}) &= \cosh \left(\sqrt{\hat{\mathbf{Z}}\hat{\mathbf{Y}}} \mathcal{L} \right) \\
 &= \hat{\mathbf{Y}}^{-1} \cosh \left(\sqrt{\hat{\mathbf{Y}}\hat{\mathbf{Z}}} \mathcal{L} \right) \hat{\mathbf{Y}} \\
 &= \hat{\mathbf{Z}}_C \cosh \left(\sqrt{\hat{\mathbf{Y}}\hat{\mathbf{Z}}} \mathcal{L} \right) \hat{\mathbf{Y}}_C \quad (7.127a)
 \end{aligned}$$

$$\begin{aligned}
 \hat{\Phi}_{12}(\mathcal{L}) &= -\hat{\mathbf{Z}}_C \sinh \left(\sqrt{\hat{\mathbf{Y}}\hat{\mathbf{Z}}} \mathcal{L} \right) \\
 &= -\sinh \left(\sqrt{\hat{\mathbf{Z}}\hat{\mathbf{Y}}} \mathcal{L} \right) \hat{\mathbf{Z}}_C \quad (7.127b)
 \end{aligned}$$

$$\begin{aligned}\hat{\Phi}_{21}(\mathcal{L}) &= -\hat{\mathbf{Y}}_C \sinh\left(\sqrt{\hat{\mathbf{Z}}\hat{\mathbf{Y}}}\mathcal{L}\right) \\ &= -\sinh\left(\sqrt{\hat{\mathbf{Y}}\hat{\mathbf{Z}}}\mathcal{L}\right)\hat{\mathbf{Y}}_C\end{aligned}\quad (7.127c)$$

$$\begin{aligned}\hat{\Phi}_{22}(\mathcal{L}) &= \cosh\left(\sqrt{\hat{\mathbf{Y}}\hat{\mathbf{Z}}}\mathcal{L}\right) \\ &= \hat{\mathbf{Y}} \cosh\left(\sqrt{\hat{\mathbf{Z}}\hat{\mathbf{Y}}}\mathcal{L}\right)\hat{\mathbf{Y}}^{-1} \\ &= \hat{\mathbf{Y}}_C \cosh\left(\sqrt{\hat{\mathbf{Z}}\hat{\mathbf{Y}}}\mathcal{L}\right)\hat{\mathbf{Z}}_C\end{aligned}\quad (7.127d)$$

Observe that these reduce to the scalar results obtained for the two-conductor line in the previous chapter.

The final chain-parameter identity is obtained using the inverse of the chain-parameter matrix given in (7.111). Multiplying the chain-parameter matrix by its inverse and using the identity for the inverse given in (7.111) gives

$$\begin{aligned}\hat{\Phi}(\mathcal{L})\hat{\Phi}^{-1}(\mathcal{L}) &= \mathbf{1}_{2n} \\ &= \hat{\Phi}(\mathcal{L})\hat{\Phi}(-\mathcal{L})\end{aligned}\quad (7.128a)$$

Substituting the form of the chain-parameter matrix gives

$$\begin{bmatrix} \hat{\Phi}_{11}(\mathcal{L}) & \hat{\Phi}_{12}(\mathcal{L}) \\ \hat{\Phi}_{21}(\mathcal{L}) & \hat{\Phi}_{22}(\mathcal{L}) \end{bmatrix} \begin{bmatrix} \hat{\Phi}_{11}(-\mathcal{L}) & \hat{\Phi}_{12}(-\mathcal{L}) \\ \hat{\Phi}_{21}(-\mathcal{L}) & \hat{\Phi}_{22}(-\mathcal{L}) \end{bmatrix} = \begin{bmatrix} \mathbf{1}_n & \mathbf{0} \\ \mathbf{0} & \mathbf{1}_n \end{bmatrix}\quad (7.128b)$$

Multiplying this gives the following identities for the chain-parameter submatrices:

$$\hat{\Phi}_{11}(\mathcal{L})\hat{\Phi}_{11}(-\mathcal{L}) + \hat{\Phi}_{12}(\mathcal{L})\hat{\Phi}_{21}(-\mathcal{L}) = \mathbf{1}_n\quad (7.129a)$$

$$\hat{\Phi}_{11}(\mathcal{L})\hat{\Phi}_{12}(-\mathcal{L}) + \hat{\Phi}_{12}(\mathcal{L})\hat{\Phi}_{22}(-\mathcal{L}) = \mathbf{0}\quad (7.129b)$$

$$\hat{\Phi}_{21}(\mathcal{L})\hat{\Phi}_{11}(-\mathcal{L}) + \hat{\Phi}_{22}(\mathcal{L})\hat{\Phi}_{21}(-\mathcal{L}) = \mathbf{0}\quad (7.129c)$$

$$\hat{\Phi}_{21}(\mathcal{L})\hat{\Phi}_{12}(-\mathcal{L}) + \hat{\Phi}_{22}(\mathcal{L})\hat{\Phi}_{22}(-\mathcal{L}) = \mathbf{1}_n\quad (7.129d)$$

Substituting the form of $\hat{\mathbf{A}}$ given in (7.106c) into the infinite series expansion of the chain-parameter matrix in (7.112) gives an infinite summation for the entries in the state-transition matrix as

$$\hat{\Phi}_{11}(\mathcal{L}) = \mathbf{1}_n + \frac{\mathcal{L}^2}{2!}\hat{\mathbf{Z}}\hat{\mathbf{Y}} + \frac{\mathcal{L}^4}{4!}[\hat{\mathbf{Z}}\hat{\mathbf{Y}}]^2 + \dots\quad (7.130a)$$

$$\hat{\Phi}_{12}(\mathcal{L}) = -\frac{\mathcal{L}}{1!}\hat{\mathbf{Z}} - \frac{\mathcal{L}^3}{3!}[\hat{\mathbf{Z}}\hat{\mathbf{Y}}]\hat{\mathbf{Z}} - \frac{\mathcal{L}^5}{5!}[\hat{\mathbf{Z}}\hat{\mathbf{Y}}]^2\hat{\mathbf{Z}} + \dots\quad (7.130b)$$

$$\hat{\Phi}_{21}(\mathcal{L}) = -\frac{\mathcal{L}}{1!}\hat{\mathbf{Y}} - \frac{\mathcal{L}^3}{3!}[\hat{\mathbf{Y}}\hat{\mathbf{Z}}]\hat{\mathbf{Y}} - \frac{\mathcal{L}^5}{5!}[\hat{\mathbf{Y}}\hat{\mathbf{Z}}]^2\hat{\mathbf{Y}} + \dots\quad (7.130c)$$

$$\hat{\Phi}_{22}(\mathcal{L}) = \mathbf{1}_n + \frac{\mathcal{L}^2}{2!} \hat{\mathbf{Y}} \hat{\mathbf{Z}} + \frac{\mathcal{L}^4}{4!} [\hat{\mathbf{Y}} \hat{\mathbf{Z}}]^2 + \dots \quad (7.130d)$$

From this series expansions of the chain-parameter submatrices, we see that

$$\hat{\Phi}_{11}(-\mathcal{L}) = \hat{\Phi}_{11}(\mathcal{L}) \quad (7.131a)$$

$$\hat{\Phi}_{12}(-\mathcal{L}) = -\hat{\Phi}_{12}(\mathcal{L}) \quad (7.131b)$$

$$\hat{\Phi}_{21}(-\mathcal{L}) = -\hat{\Phi}_{21}(\mathcal{L}) \quad (7.131c)$$

$$\hat{\Phi}_{22}(-\mathcal{L}) = \hat{\Phi}_{22}(\mathcal{L}) \quad (7.131d)$$

Substituting these into (7.129) yields the following identities for the chain-parameter submatrices:

$$\hat{\Phi}_{12}(\mathcal{L}) \hat{\Phi}_{22}(\mathcal{L}) \hat{\Phi}_{12}^{-1}(\mathcal{L}) \hat{\Phi}_{11}(\mathcal{L}) - \hat{\Phi}_{12}(\mathcal{L}) \hat{\Phi}_{21}(\mathcal{L}) = \mathbf{1}_n \quad (7.132a)$$

$$\hat{\Phi}_{21}(\mathcal{L}) \hat{\Phi}_{11}(\mathcal{L}) \hat{\Phi}_{21}^{-1}(\mathcal{L}) \hat{\Phi}_{22}(\mathcal{L}) - \hat{\Phi}_{21}(\mathcal{L}) \hat{\Phi}_{12}(\mathcal{L}) = \mathbf{1}_n \quad (7.132b)$$

$$\hat{\Phi}_{12}(\mathcal{L}) \hat{\Phi}_{22}(\mathcal{L}) \hat{\Phi}_{12}^{-1}(\mathcal{L}) = \hat{\Phi}_{11}(\mathcal{L}) \quad (7.132c)$$

$$\hat{\Phi}_{21}(\mathcal{L}) \hat{\Phi}_{11}(\mathcal{L}) \hat{\Phi}_{21}^{-1}(\mathcal{L}) = \hat{\Phi}_{22}(\mathcal{L}) \quad (7.132d)$$

$$\hat{\Phi}_{22}^{\dagger}(\mathcal{L}) = \hat{\Phi}_{11}(\mathcal{L}) \quad (7.132e)$$

The last identity follows from the series expansions in (7.130) and the fact that $\hat{\mathbf{Z}}$ and $\hat{\mathbf{Y}}$ are symmetric. These identities have proved to be of considerable value in reducing large matrix expressions that result from the solution of the MTL equations [B.1, B.2, B.4].

7.5.4 Approximating Nonuniform Lines with the Chain-Parameter Matrix

As discussed previously, nonuniform lines are lines whose cross-sectional dimensions (conductors and media) vary along the line axis [B.1, 13, 14]. For these types of lines, the per-unit-length parameter matrices will be functions of z , that is, $\mathbf{R}(z)$, $\mathbf{L}(z)$, $\mathbf{G}(z)$, and $\mathbf{C}(z)$. In this case, the MTL differential equations become *nonconstant-coefficient differential equations*. Although they remain linear (if the surrounding medium is linear), they are as difficult to solve as nonlinear differential equations. A simple but approximate way of solving the MTL equations for a nonuniform MTL is to approximate it as a *discretely uniform* MTL. This neglects any interaction between the sections, which may be due to fringing of the fields at the junctions between the uniform sections. To do this we break the line into a cascade of sections, each

of which can be modeled *approximately* as a uniform line characterized by a chain-parameter matrix $\hat{\Phi}_k$, as illustrated in Figure 6.13(a). The *overall chain-parameter matrix* of the entire line can be obtained as the product (in the appropriate order) of the chain-parameter matrices of the individual uniform sections as

$$\begin{aligned}\hat{\Phi}(\mathcal{L}) &= \hat{\Phi}_N(\Delta z_N) \times \cdots \times \hat{\Phi}_i(\Delta z_i) \times \cdots \times \hat{\Phi}_1(\Delta z_1) \\ &= \prod_{k=1}^N \hat{\Phi}_{N-k+1}(\Delta z_{N-k+1})\end{aligned}\quad (7.133)$$

Observe the important order of multiplication of the individual chain-parameter matrices. This is a result of the definitions of the chain-parameter matrices as

$$\begin{aligned}\begin{bmatrix} \hat{\mathbf{V}}(z_{k+1}) \\ \hat{\mathbf{I}}(z_{k+1}) \end{bmatrix} &= \hat{\Phi}_{k+1}(\Delta z_{k+1}) \begin{bmatrix} \hat{\mathbf{V}}(z_k) \\ \hat{\mathbf{I}}(z_k) \end{bmatrix} \\ \begin{bmatrix} \hat{\mathbf{V}}(z_k) \\ \hat{\mathbf{I}}(z_k) \end{bmatrix} &= \hat{\Phi}_k(\Delta z_k) \begin{bmatrix} \hat{\mathbf{V}}(z_{k-1}) \\ \hat{\mathbf{I}}(z_{k-1}) \end{bmatrix}\end{aligned}\quad (7.134)$$

Many nonuniform MTLs can be approximately modeled in this fashion. Once the overall chain-parameter matrix of the entire line is obtained as in (7.133), the terminal constraints at the ends of the line may be incorporated as described in Section 7.3 and the terminal voltages and currents solved for. Voltages and currents at interior points can also be determined from these terminal solutions by using the individual chain-parameter matrices of the uniform sections. For example, the voltages and currents at the right port of the second subsection can be obtained from the terminal voltages and currents as

$$\begin{bmatrix} \hat{\mathbf{V}}(z_2) \\ \hat{\mathbf{I}}(z_2) \end{bmatrix} = \hat{\Phi}_2(\Delta z_2) \times \hat{\Phi}_1(\Delta z_1) \begin{bmatrix} \hat{\mathbf{V}}(0) \\ \hat{\mathbf{I}}(0) \end{bmatrix}\quad (7.135)$$

7.5.5 The Impedance and Admittance Parameter Matrix Characterizations

The chain-parameter matrix is not the only way of relating the voltages and currents of the MTL viewed as a $2n$ -port. Other obvious ways are the *impedance parameters* [A.2]

$$\begin{bmatrix} \hat{\mathbf{V}}(0) \\ \hat{\mathbf{V}}(\mathcal{L}) \end{bmatrix} = \underbrace{\begin{bmatrix} \hat{\mathbf{Z}}_{11} & \hat{\mathbf{Z}}_{12} \\ \hat{\mathbf{Z}}_{21} & \hat{\mathbf{Z}}_{22} \end{bmatrix}}_{\hat{\mathbf{Z}}(\mathcal{L})} \begin{bmatrix} \hat{\mathbf{I}}(0) \\ -\hat{\mathbf{I}}(\mathcal{L}) \end{bmatrix}\quad (7.136)$$

and the *admittance parameters* [A.2]

$$\begin{bmatrix} \hat{\mathbf{I}}(0) \\ -\hat{\mathbf{I}}(\mathcal{L}) \end{bmatrix} = \underbrace{\begin{bmatrix} \hat{\mathbf{Y}}_{11} & \hat{\mathbf{Y}}_{12} \\ \hat{\mathbf{Y}}_{21} & \hat{\mathbf{Y}}_{22} \end{bmatrix}}_{\hat{\mathbf{Y}}(\mathcal{L})} \begin{bmatrix} \hat{\mathbf{V}}(0) \\ \hat{\mathbf{V}}(\mathcal{L}) \end{bmatrix}\quad (7.137)$$

The currents at both ends, $\hat{\mathbf{I}}(0)$ and $-\hat{\mathbf{I}}(\mathcal{L})$, are defined as being directed into the $2n$ -port in accordance with the usual convention. These alternative representations can be obtained from the chain-parameter submatrices. For example, the impedance parameter submatrices are defined, from (7.136), by setting currents equal to zero as

$$\hat{\mathbf{V}}(\mathcal{L}) = -\hat{\mathbf{Z}}_{22} \hat{\mathbf{I}}(\mathcal{L}) \Big|_{\hat{\mathbf{I}}(0)=\mathbf{0}} \quad (7.138a)$$

$$\hat{\mathbf{V}}(0) = -\hat{\mathbf{Z}}_{12} \hat{\mathbf{I}}(\mathcal{L}) \Big|_{\hat{\mathbf{I}}(0)=\mathbf{0}} \quad (7.138b)$$

$$\hat{\mathbf{V}}(\mathcal{L}) = \hat{\mathbf{Z}}_{21} \hat{\mathbf{I}}(0) \Big|_{\hat{\mathbf{I}}(\mathcal{L})=\mathbf{0}} \quad (7.138c)$$

$$\hat{\mathbf{V}}(0) = \hat{\mathbf{Z}}_{11} \hat{\mathbf{I}}(0) \Big|_{\hat{\mathbf{I}}(\mathcal{L})=\mathbf{0}} \quad (7.138d)$$

From the chain-parameter matrix, setting $\hat{\mathbf{I}}(0) = \mathbf{0}$, we obtain

$$\hat{\mathbf{V}}(\mathcal{L}) = \hat{\Phi}_{11} \hat{\mathbf{V}}(0) \Big|_{\hat{\mathbf{I}}(0)=\mathbf{0}} \quad (7.139a)$$

$$\hat{\mathbf{I}}(\mathcal{L}) = \hat{\Phi}_{21} \hat{\mathbf{V}}(0) \Big|_{\hat{\mathbf{I}}(0)=\mathbf{0}} \quad (7.139b)$$

from which we obtain

$$\begin{aligned} \hat{\mathbf{Z}}_{22} &= -\hat{\Phi}_{11} \hat{\Phi}_{21}^{-1} \\ &= -\hat{\Phi}_{21}^{-1} \hat{\Phi}_{22} \end{aligned} \quad (7.140a)$$

$$\hat{\mathbf{Z}}_{12} = -\hat{\Phi}_{21}^{-1} \quad (7.140b)$$

and we have used the chain-parameter identity given in (7.132d) in (7.140a). Similarly, setting $\hat{\mathbf{I}}(\mathcal{L}) = \mathbf{0}$ in the chain-parameter matrix gives

$$\hat{\mathbf{V}}(\mathcal{L}) = \hat{\Phi}_{11} \hat{\mathbf{V}}(0) + \hat{\Phi}_{12} \hat{\mathbf{I}}(0) \quad (7.141a)$$

$$\mathbf{0} = \hat{\Phi}_{21} \hat{\mathbf{V}}(0) + \hat{\Phi}_{22} \hat{\mathbf{I}}(0) \quad (7.141b)$$

from which we obtain

$$\begin{aligned} \hat{\mathbf{Z}}_{21} &= \hat{\Phi}_{12} - \hat{\Phi}_{11} \hat{\Phi}_{21}^{-1} \hat{\Phi}_{22} \\ &= -\hat{\Phi}_{21}^{-1} \end{aligned} \quad (7.142a)$$

$$\begin{aligned}\hat{\mathbf{Z}}_{11} &= -\hat{\Phi}_{21}^{-1}\hat{\Phi}_{22} \\ &= -\hat{\Phi}_{11}\hat{\Phi}_{21}^{-1}\end{aligned}\quad (7.142b)$$

We have used the matrix chain-parameter identities given in (7.132b) and (7.132d) to give equivalent forms of these impedance parameters, which demonstrate that the line is *reciprocal*, that is, $\hat{\mathbf{Z}}_{11} = \hat{\mathbf{Z}}_{22}$ and $\hat{\mathbf{Z}}_{12} = \hat{\mathbf{Z}}_{21}$. Substituting the relations for the various chain-parameter submatrices given in (7.115) and (7.127) yields

$$\begin{aligned}\hat{\mathbf{Z}}_{11} &= \hat{\mathbf{Z}}_{22} \\ &= \hat{\mathbf{Y}}^{-1}\hat{\mathbf{T}}_I\hat{\gamma}\left(\mathbf{e}^{\hat{\gamma}\mathcal{L}} - \mathbf{e}^{-\hat{\gamma}\mathcal{L}}\right)^{-1}\left(\mathbf{e}^{\hat{\gamma}\mathcal{L}} + \mathbf{e}^{-\hat{\gamma}\mathcal{L}}\right)\hat{\mathbf{T}}_I^{-1} \\ &= \hat{\mathbf{Z}}_C\left[\sinh\left(\sqrt{\hat{\mathbf{Y}}\hat{\mathbf{Z}}}\mathcal{L}\right)\right]^{-1}\cosh\left(\sqrt{\hat{\mathbf{Y}}\hat{\mathbf{Z}}}\mathcal{L}\right) \\ &= \cosh\left(\sqrt{\hat{\mathbf{Z}}\hat{\mathbf{Y}}}\mathcal{L}\right)\left[\sinh\left(\sqrt{\hat{\mathbf{Z}}\hat{\mathbf{Y}}}\mathcal{L}\right)\right]^{-1}\hat{\mathbf{Z}}_C\end{aligned}\quad (7.143a)$$

$$\begin{aligned}\hat{\mathbf{Z}}_{12} &= \hat{\mathbf{Z}}_{21} \\ &= 2\hat{\mathbf{Y}}^{-1}\hat{\mathbf{T}}_I\hat{\gamma}\left(\mathbf{e}^{\hat{\gamma}\mathcal{L}} - \mathbf{e}^{-\hat{\gamma}\mathcal{L}}\right)^{-1}\hat{\mathbf{T}}_I^{-1} \\ &= \hat{\mathbf{Z}}_C\left[\sinh\left(\sqrt{\hat{\mathbf{Y}}\hat{\mathbf{Z}}}\mathcal{L}\right)\right]^{-1} \\ &= \left[\sinh\left(\sqrt{\hat{\mathbf{Z}}\hat{\mathbf{Y}}}\mathcal{L}\right)\right]^{-1}\hat{\mathbf{Z}}_C\end{aligned}\quad (7.143b)$$

The admittance parameters can also be derived from the chain-parameters in a similar fashion or by realizing that the admittance parameter matrix is the inverse of the impedance parameter matrix. This yields

$$\begin{aligned}\hat{\mathbf{Y}}_{11} &= \hat{\mathbf{Y}}_{22} \\ &= -\hat{\Phi}_{12}^{-1}\hat{\Phi}_{11} \\ &= -\hat{\Phi}_{22}\hat{\Phi}_{12}^{-1} \\ &= \hat{\mathbf{T}}_I\left(\mathbf{e}^{\hat{\gamma}\mathcal{L}} - \mathbf{e}^{-\hat{\gamma}\mathcal{L}}\right)^{-1}\left(\mathbf{e}^{\hat{\gamma}\mathcal{L}} + \mathbf{e}^{-\hat{\gamma}\mathcal{L}}\right)\hat{\gamma}^{-1}\hat{\mathbf{T}}_I^{-1}\hat{\mathbf{Y}} \\ &= \left[\sinh\left(\sqrt{\hat{\mathbf{Y}}\hat{\mathbf{Z}}}\mathcal{L}\right)\right]^{-1}\cosh\left(\sqrt{\hat{\mathbf{Y}}\hat{\mathbf{Z}}}\mathcal{L}\right)\hat{\mathbf{Y}}_C \\ &= \hat{\mathbf{Y}}_C\cosh\left(\sqrt{\hat{\mathbf{Z}}\hat{\mathbf{Y}}}\mathcal{L}\right)\left[\sinh\left(\sqrt{\hat{\mathbf{Z}}\hat{\mathbf{Y}}}\mathcal{L}\right)\right]^{-1}\end{aligned}\quad (7.144a)$$

$$\begin{aligned}\hat{\mathbf{Y}}_{12} &= \hat{\mathbf{Y}}_{21} \\ &= \hat{\Phi}_{12}^{-1} \\ &= -2\hat{\mathbf{T}}_I\left(\mathbf{e}^{\hat{\gamma}\mathcal{L}} - \mathbf{e}^{-\hat{\gamma}\mathcal{L}}\right)^{-1}\hat{\gamma}^{-1}\hat{\mathbf{T}}_I^{-1}\hat{\mathbf{Y}} \\ &= -\left[\sinh\left(\sqrt{\hat{\mathbf{Y}}\hat{\mathbf{Z}}}\mathcal{L}\right)\right]^{-1}\hat{\mathbf{Y}}_C \\ &= -\hat{\mathbf{Y}}_C\left[\sinh\left(\sqrt{\hat{\mathbf{Z}}\hat{\mathbf{Y}}}\mathcal{L}\right)\right]^{-1}\end{aligned}\quad (7.144b)$$

The lumped-Pi and lumped-T circuits of Figure 7.6(a) and (b) can also be obtained from the impedance and admittance parameters. For example, write the impedance parameters as

$$\begin{aligned}\hat{\mathbf{V}}(0) &= (\hat{\mathbf{Z}}_{11} - \hat{\mathbf{Z}}_{12}) \hat{\mathbf{I}}(0) + \hat{\mathbf{Z}}_{12} (\hat{\mathbf{I}}(0) - \hat{\mathbf{I}}(\mathcal{L})) \\ \hat{\mathbf{V}}(\mathcal{L}) &= \hat{\mathbf{Z}}_{12} (\hat{\mathbf{I}}(0) - \hat{\mathbf{I}}(\mathcal{L})) + (\hat{\mathbf{Z}}_{22} - \hat{\mathbf{Z}}_{12}) (-\hat{\mathbf{I}}(\mathcal{L}))\end{aligned}\quad (7.145)$$

If the line is electrically short at the frequency of interest, we obtain

$$\begin{aligned}\hat{\mathbf{Z}}_{11} - \hat{\mathbf{Z}}_{12} &= \hat{\mathbf{Z}}_C \left[\sinh \left(\sqrt{\hat{\mathbf{Y}}\hat{\mathbf{Z}}} \mathcal{L} \right) \right]^{-1} \left\{ \cosh \left(\sqrt{\hat{\mathbf{Y}}\hat{\mathbf{Z}}} \mathcal{L} \right) - \mathbf{1}_n \right\} \\ &\cong \hat{\mathbf{Z}}_C \left[\sqrt{\hat{\mathbf{Y}}\hat{\mathbf{Z}}} \mathcal{L} \right]^{-1} \left\{ \frac{\mathcal{L}^2}{2} \left(\sqrt{\hat{\mathbf{Y}}\hat{\mathbf{Z}}} \right)^2 \right\} \\ &= \hat{\mathbf{Z}}_C \frac{\mathcal{L}}{2} \sqrt{\hat{\mathbf{Y}}\hat{\mathbf{Z}}} \\ &= \hat{\mathbf{Z}} \frac{\mathcal{L}^2}{2}\end{aligned}\quad (7.146a)$$

where we used the series expansions in (7.125) and the identity in (7.122a) and

$$\begin{aligned}\hat{\mathbf{Z}}_{12} &= \hat{\mathbf{Z}}_C \left[\sinh \left(\sqrt{\hat{\mathbf{Y}}\hat{\mathbf{Z}}} \mathcal{L} \right) \right]^{-1} \\ &\cong \hat{\mathbf{Z}}_C \left[\sqrt{\hat{\mathbf{Y}}\hat{\mathbf{Z}}} \mathcal{L} \right]^{-1} \\ &= \hat{\mathbf{Y}}^{-1} \mathcal{L}^{-1}\end{aligned}\quad (7.146b)$$

and we have used (7.125b) and (7.122a). Substituting (7.146) into (7.145) yields the lumped-T circuit shown in Figure 7.6(b) since the vertical branches have admittance of $\hat{\mathbf{Z}}_{12}^{-1} = \hat{\mathbf{Y}} \mathcal{L}$ and the horizontal branches have impedances of $\hat{\mathbf{Z}}_{11} - \hat{\mathbf{Z}}_{12} = \hat{\mathbf{Z}}_{22} - \hat{\mathbf{Z}}_{21} = \hat{\mathbf{Z}} \mathcal{L}/2$. Similarly, the admittance parameters in (7.137) can be written as

$$\begin{aligned}\hat{\mathbf{I}}(0) &= (\hat{\mathbf{Y}}_{11} + \hat{\mathbf{Y}}_{12}) \hat{\mathbf{V}}(0) - \hat{\mathbf{Y}}_{12} (\hat{\mathbf{V}}(0) - \hat{\mathbf{V}}(\mathcal{L})) \\ -\hat{\mathbf{I}}(\mathcal{L}) &= -\hat{\mathbf{Y}}_{12} (\hat{\mathbf{V}}(\mathcal{L}) - \hat{\mathbf{V}}(0)) + (\hat{\mathbf{Y}}_{22} + \hat{\mathbf{Y}}_{12}) \hat{\mathbf{V}}(\mathcal{L})\end{aligned}\quad (7.147)$$

Again, if the line is electrically short at the frequency of interest, we obtain

$$\begin{aligned}\hat{\mathbf{Y}}_{11} + \hat{\mathbf{Y}}_{12} &= \left[\sinh \left(\sqrt{\hat{\mathbf{Y}}\hat{\mathbf{Z}}} \mathcal{L} \right) \right]^{-1} \left\{ \cosh \left(\sqrt{\hat{\mathbf{Y}}\hat{\mathbf{Z}}} \mathcal{L} \right) - \mathbf{1}_n \right\} \hat{\mathbf{Y}}_C \\ &\cong \left[\sqrt{\hat{\mathbf{Y}}\hat{\mathbf{Z}}} \mathcal{L} \right]^{-1} \left\{ \frac{\mathcal{L}^2}{2} \left(\sqrt{\hat{\mathbf{Y}}\hat{\mathbf{Z}}} \right)^2 \right\} \hat{\mathbf{Y}}_C \\ &= \frac{\mathcal{L}}{2} \sqrt{\hat{\mathbf{Y}}\hat{\mathbf{Z}}} \hat{\mathbf{Y}}_C \\ &= \hat{\mathbf{Y}} \frac{\mathcal{L}}{2}\end{aligned}\quad (7.148a)$$

and

$$\begin{aligned}
 -\hat{\mathbf{Y}}_{12} &= \left[\sinh \left(\sqrt{\hat{\mathbf{Y}}\hat{\mathbf{Z}}} \mathcal{L} \right) \right]^{-1} \hat{\mathbf{Y}}_{\mathbf{C}} \\
 &\cong \left[\sqrt{\hat{\mathbf{Y}}\hat{\mathbf{Z}}} \mathcal{L} \right]^{-1} \hat{\mathbf{Y}}_{\mathbf{C}} \\
 &= \hat{\mathbf{Z}}^{-1} \mathcal{L}^{-1}
 \end{aligned} \tag{7.148b}$$

Substituting (7.148) into (7.147) yields the lumped-Pi circuit of Figure 7.6(a) as the horizontal branches have impedance of $\hat{\mathbf{Z}} \mathcal{L}$ and the vertical branches have admittances of $\hat{\mathbf{Y}}_{11} + \hat{\mathbf{Y}}_{12} = \hat{\mathbf{Y}}_{22} + \hat{\mathbf{Y}}_{21} = \hat{\mathbf{Y}} \mathcal{L}/2$.

7.6 POWER FLOW AND THE REFLECTION COEFFICIENT MATRIX

As a final analogy to the two-conductor line, let us define the *voltage reflection coefficient matrix* $\hat{\Gamma}_V(z)$ and investigate the flow of power on the line. The general solution for the phasor voltages and currents is written in the form of forward-traveling waves, $\hat{\mathbf{V}}^+(z)$ and $\hat{\mathbf{I}}^+(z)$, and backward-traveling waves, $\hat{\mathbf{V}}^-(z)$ and $\hat{\mathbf{I}}^-(z)$, from (7.34) as

$$\begin{aligned}
 \hat{\mathbf{V}}(z) &= \hat{\mathbf{V}}^+(z) + \hat{\mathbf{V}}^-(z) \\
 &= \hat{\mathbf{Z}}_{\mathbf{C}} (\hat{\mathbf{I}}^+(z) + \hat{\mathbf{I}}^-(z))
 \end{aligned} \tag{7.149a}$$

$$\hat{\mathbf{I}}(z) = \hat{\mathbf{I}}^+(z) - \hat{\mathbf{I}}^-(z) \tag{7.149b}$$

where

$$\hat{\mathbf{I}}^+(z) = \hat{\mathbf{T}}_I e^{-\hat{\gamma}z} \hat{\mathbf{I}}_m^+ \tag{7.150a}$$

$$\hat{\mathbf{I}}^-(z) = \hat{\mathbf{T}}_I e^{\hat{\gamma}z} \hat{\mathbf{I}}_m^- \tag{7.150b}$$

and

$$\hat{\mathbf{T}}_I^{-1} \hat{\mathbf{Y}} \hat{\mathbf{Z}} \hat{\mathbf{T}}_I = \hat{\gamma}^2 \tag{7.150c}$$

Hence, the forward- and backward-traveling voltage and current waves are related by the characteristic impedance matrix as

$$\hat{\mathbf{V}}^{\pm}(z) = \hat{\mathbf{Z}}_{\mathbf{C}} \hat{\mathbf{I}}^{\pm}(z) \tag{7.151}$$

Similarly, from (7.33)

$$\hat{\mathbf{V}}(z) = \hat{\mathbf{V}}^+(z) + \hat{\mathbf{V}}^-(z) \tag{7.152a}$$

$$\begin{aligned}\hat{\mathbf{I}}(z) &= \hat{\mathbf{I}}^+(z) - \hat{\mathbf{I}}^-(z) \\ &= \hat{\mathbf{Y}}_C (\hat{\mathbf{V}}^+(z) - \hat{\mathbf{V}}^-(z))\end{aligned}\quad (7.152b)$$

where

$$\hat{\mathbf{V}}^+(z) = \hat{\mathbf{T}}_V \mathbf{e}^{-\hat{\gamma}z} \hat{\mathbf{V}}_m^+ \quad (7.153a)$$

$$\hat{\mathbf{V}}^-(z) = \hat{\mathbf{T}}_V \mathbf{e}^{\hat{\gamma}z} \hat{\mathbf{V}}_m^- \quad (7.153b)$$

and

$$\hat{\mathbf{T}}_V^{-1} \hat{\mathbf{Z}} \hat{\mathbf{Y}} \hat{\mathbf{T}}_V = \hat{\gamma}^2 \quad (7.153c)$$

and $\hat{\mathbf{Y}}_C = \hat{\mathbf{Z}}_C^{-1}$. Let us define the *voltage reflection coefficient matrix* $\hat{\Gamma}_V(z)$ in a logical manner relating the reflected or backward-traveling voltage waves to the incident or forward-traveling voltage waves at any point on the line as

$$\hat{\mathbf{V}}^-(z) = \hat{\Gamma}_V(z) \hat{\mathbf{V}}^+(z) \quad (7.154a)$$

Substituting (7.151) yields

$$\hat{\mathbf{I}}^-(z) = \hat{\mathbf{Y}}_C \hat{\Gamma}_V(z) \hat{\mathbf{Z}}_C \hat{\mathbf{I}}^+(z) \quad (7.154b)$$

Hence, the *current reflection coefficient matrix* is related to the *voltage reflection coefficient matrix* as

$$\hat{\Gamma}_I(z) = -\hat{\mathbf{Y}}_C \hat{\Gamma}_V(z) \hat{\mathbf{Z}}_C \quad (7.155)$$

as the total backward-traveling current is $-\hat{\mathbf{I}}^-(z)$. Although (7.155) reduces to the scalar case for two-conductor lines, it is important to distinguish between the two reflection coefficient matrices in the MTL case since the products in (7.155) do not commute. Substituting (7.154a) and (7.155) into (7.152) gives

$$\begin{aligned}\hat{\mathbf{V}}(z) &= [\mathbf{1}_n + \hat{\Gamma}_V(z)] \hat{\mathbf{V}}^+(z) \\ &= [\mathbf{1}_n - \hat{\mathbf{Z}}_C \hat{\Gamma}_I(z) \hat{\mathbf{Y}}_C] \hat{\mathbf{V}}^+(z)\end{aligned}\quad (7.156a)$$

$$\begin{aligned}\hat{\mathbf{I}}(z) &= \hat{\mathbf{Y}}_C [\mathbf{1}_n - \hat{\Gamma}_V(z)] \hat{\mathbf{V}}^+(z) \\ &= \hat{\mathbf{Y}}_C [\mathbf{1}_n + \hat{\mathbf{Z}}_C \hat{\Gamma}_I(z) \hat{\mathbf{Y}}_C] \hat{\mathbf{V}}^+(z)\end{aligned}\quad (7.156b)$$

Similarly, substituting (7.154b) into (7.149) yields

$$\begin{aligned}\hat{\mathbf{V}}(z) &= \hat{\mathbf{Z}}_C [\mathbf{1}_n + \hat{\mathbf{Y}}_C \hat{\Gamma}_V(z) \hat{\mathbf{Z}}_C] \hat{\mathbf{I}}^+(z) \\ &= \hat{\mathbf{Z}}_C [\mathbf{1}_n - \hat{\Gamma}_I(z)] \hat{\mathbf{I}}^+(z)\end{aligned}\quad (7.157a)$$

$$\begin{aligned}\hat{\mathbf{I}}(z) &= [\mathbf{1}_n - \hat{\mathbf{Y}}_C \hat{\Gamma}_V(z) \hat{\mathbf{Z}}_C] \hat{\mathbf{I}}^+(z) \\ &= [\mathbf{1}_n + \hat{\Gamma}_I(z)] \hat{\mathbf{I}}^+(z)\end{aligned}\quad (7.157b)$$

The reflection coefficient matrices at two points z_2 and z_1 on the line can be related by substituting the general forms of forward- and backward-traveling voltages given in (7.153) into (7.154) to yield

$$\begin{aligned}\hat{\mathbf{V}}^-(z) &= \hat{\mathbf{T}}_V \mathbf{e}^{\hat{\gamma}z} \hat{\mathbf{V}}_m^- \\ &= \hat{\Gamma}_V(z) \hat{\mathbf{V}}^+(z) \\ &= \hat{\Gamma}_V(z) \hat{\mathbf{T}}_V \mathbf{e}^{-\hat{\gamma}z} \hat{\mathbf{V}}_m^+\end{aligned}\quad (7.158)$$

Evaluating these at $z = z_1$ and $z = z_2$ gives

$$\hat{\mathbf{T}}_V \mathbf{e}^{\hat{\gamma}z_2} \hat{\mathbf{V}}_m^- = \hat{\Gamma}_V(z_2) \hat{\mathbf{T}}_V \mathbf{e}^{-\hat{\gamma}z_2} \hat{\mathbf{V}}_m^+ \quad (7.159a)$$

and

$$\hat{\mathbf{T}}_V \mathbf{e}^{\hat{\gamma}z_1} \hat{\mathbf{V}}_m^- = \hat{\Gamma}_V(z_1) \hat{\mathbf{T}}_V \mathbf{e}^{-\hat{\gamma}z_1} \hat{\mathbf{V}}_m^+ \quad (7.159b)$$

Hence,

$$\mathbf{e}^{-\hat{\gamma}z_2} \hat{\mathbf{T}}_V^{-1} \hat{\Gamma}_V(z_2) \hat{\mathbf{T}}_V \mathbf{e}^{-\hat{\gamma}z_2} = \mathbf{e}^{-\hat{\gamma}z_1} \hat{\mathbf{T}}_V^{-1} \hat{\Gamma}_V(z_1) \hat{\mathbf{T}}_V \mathbf{e}^{-\hat{\gamma}z_1} \quad (7.160)$$

Solving gives

$$\hat{\Gamma}_V(z_2) = \hat{\mathbf{T}}_V \mathbf{e}^{\hat{\gamma}(z_2-z_1)} \hat{\mathbf{T}}_V^{-1} \hat{\Gamma}_V(z_1) \hat{\mathbf{T}}_V \mathbf{e}^{\hat{\gamma}(z_2-z_1)} \hat{\mathbf{T}}_V^{-1} \quad (7.161)$$

Substituting the identities in (7.123e) gives

$$\hat{\Gamma}_V(z_2) = \mathbf{e}^{\sqrt{\hat{\mathbf{Z}}\hat{\mathbf{Y}}(z_2-z_1)}} \hat{\Gamma}_V(z_1) \mathbf{e}^{\sqrt{\hat{\mathbf{Z}}\hat{\mathbf{Y}}(z_2-z_1)}} \quad (7.162)$$

Similarly, using (7.150) and (7.154), the current reflection coefficients are related as

$$\hat{\Gamma}_I(z_2) = \mathbf{e}^{\sqrt{\hat{\mathbf{Y}}\hat{\mathbf{Z}}(z_2-z_1)}} \hat{\Gamma}_I(z_1) \mathbf{e}^{\sqrt{\hat{\mathbf{Y}}\hat{\mathbf{Z}}(z_2-z_1)}} \quad (7.163)$$

Again, these reduce to the scalar results for a two-conductor line given in the previous chapter.

The *input impedance matrix* at any point on the line relates the total voltages and total currents at that point as

$$\hat{\mathbf{V}}(z) = \mathbf{Z}_{\text{in}}(z) \hat{\mathbf{I}}(z) \quad (7.164)$$

Substituting (7.156) and (7.157) into (7.164) yields

$$\begin{aligned}
 \hat{\mathbf{Z}}_{\text{in}}(z) &= [\mathbf{1}_n + \hat{\Gamma}_V(z)] [\mathbf{1}_n - \hat{\Gamma}_V(z)]^{-1} \hat{\mathbf{Z}}_C \\
 &= \hat{\mathbf{Z}}_C [\mathbf{1}_n + \hat{\mathbf{Y}}_C \hat{\Gamma}_V(z) \hat{\mathbf{Z}}_C] [\mathbf{1}_n - \hat{\mathbf{Y}}_C \hat{\Gamma}_V(z) \hat{\mathbf{Z}}_C]^{-1} \\
 &= \hat{\mathbf{Z}}_C [\mathbf{1}_n - \hat{\Gamma}_I(z)] [\mathbf{1}_n + \hat{\Gamma}_I(z)]^{-1}
 \end{aligned} \tag{7.165}$$

Similarly, the *voltage reflection coefficient matrix* can be written in terms of the input impedance matrix at a point on the line from (7.165) as

$$\begin{aligned}
 \hat{\Gamma}_V(z) &= \hat{\mathbf{Z}}_C [\hat{\mathbf{Z}}_{\text{in}}(z) + \hat{\mathbf{Z}}_C]^{-1} [\hat{\mathbf{Z}}_{\text{in}}(z) - \hat{\mathbf{Z}}_C] \hat{\mathbf{Y}}_C \\
 &= [\hat{\mathbf{Z}}_{\text{in}}(z) - \hat{\mathbf{Z}}_C] [\hat{\mathbf{Z}}_{\text{in}}(z) + \hat{\mathbf{Z}}_C]^{-1}
 \end{aligned} \tag{7.166}$$

Substituting (7.166) into the relation for the current reflection coefficient given by (7.155), we see that the *current reflection coefficient matrix* is

$$\begin{aligned}
 \hat{\Gamma}_I(z) &= -\hat{\mathbf{Y}}_C \hat{\Gamma}_V(z) \hat{\mathbf{Z}}_C \\
 &= -[\hat{\mathbf{Z}}_{\text{in}}(z) + \hat{\mathbf{Z}}_C]^{-1} [\hat{\mathbf{Z}}_{\text{in}}(z) - \hat{\mathbf{Z}}_C] \\
 &= -\hat{\mathbf{Y}}_C [\hat{\mathbf{Z}}_{\text{in}}(z) - \hat{\mathbf{Z}}_C] [\hat{\mathbf{Z}}_{\text{in}}(z) + \hat{\mathbf{Z}}_C]^{-1} \hat{\mathbf{Z}}_C
 \end{aligned} \tag{7.167}$$

If the line is terminated at $z = \mathcal{L}$ as

$$\hat{\mathbf{V}}(\mathcal{L}) = \hat{\mathbf{Z}}_L \hat{\mathbf{I}}(\mathcal{L}) \tag{7.168}$$

then the voltage reflection coefficient matrix at the load is

$$\begin{aligned}
 \hat{\Gamma}_V(\mathcal{L}) &= \hat{\mathbf{Z}}_C [\hat{\mathbf{Z}}_L + \hat{\mathbf{Z}}_C]^{-1} [\hat{\mathbf{Z}}_L - \hat{\mathbf{Z}}_C] \hat{\mathbf{Y}}_C \\
 &= [\hat{\mathbf{Z}}_L - \hat{\mathbf{Z}}_C] [\hat{\mathbf{Z}}_L + \hat{\mathbf{Z}}_C]^{-1}
 \end{aligned} \tag{7.169}$$

Similarly, the current reflection coefficient matrix at the load is obtained from (7.167) as

$$\begin{aligned}
 \hat{\Gamma}_I(\mathcal{L}) &= -[\hat{\mathbf{Z}}_L + \hat{\mathbf{Z}}_C]^{-1} [\hat{\mathbf{Z}}_L - \hat{\mathbf{Z}}_C] \\
 &= -\hat{\mathbf{Y}}_C [\hat{\mathbf{Z}}_L - \hat{\mathbf{Z}}_C] [\hat{\mathbf{Z}}_L + \hat{\mathbf{Z}}_C]^{-1} \hat{\mathbf{Z}}_C
 \end{aligned} \tag{7.170}$$

The voltage reflection coefficient at the input to the line $z = 0$ is given from (7.161) in terms of the voltage reflection coefficient at the load as

$$\hat{\Gamma}_V(0) = \hat{\mathbf{T}}_V \mathbf{e}^{-\hat{\gamma} \mathcal{L}} \hat{\mathbf{T}}_V^{-1} \hat{\Gamma}_V(\mathcal{L}) \hat{\mathbf{T}}_V \mathbf{e}^{-\hat{\gamma} \mathcal{L}} \hat{\mathbf{T}}_V^{-1} \tag{7.171}$$

These formulas reduce to the corresponding scalar results for a two-conductor line. From (7.169), we observe that in order to eliminate all reflections at the load, the line must be terminated in its characteristic impedance matrix, that is, $\hat{\mathbf{Z}}_L = \hat{\mathbf{Z}}_C$. This is the meaning of a *matched line* in the MTL case. It is not sufficient to simply place

impedances only between each line and the reference conductor. Impedances will need to be placed between all pairs of the n lines since the characteristic impedance is, in general, full.

The total average power transmitted on the MTL in the $+z$ direction is [A.2]

$$\begin{aligned}
 P_{\text{av}}(z) &= \frac{1}{2} \operatorname{Re} \{ \hat{\mathbf{V}}^t(z) \hat{\mathbf{I}}^*(z) \} \\
 &= \frac{1}{2} \operatorname{Re} \left\{ \begin{bmatrix} \hat{V}_1(z) & \hat{V}_2(z) & \cdots & \hat{V}_n(z) \end{bmatrix} \begin{bmatrix} \hat{I}_1^*(z) \\ \hat{I}_2^*(z) \\ \vdots \\ \hat{I}_n^*(z) \end{bmatrix} \right\} \\
 &= \frac{1}{2} \operatorname{Re} \{ \hat{V}_1(z) \hat{I}_1^*(z) + \hat{V}_2(z) \hat{I}_2^*(z) + \cdots + \hat{V}_n(z) \hat{I}_n^*(z) \} \quad (7.172)
 \end{aligned}$$

where the asterisk $*$ denotes the conjugate of the complex-valued quantity. Suppose the line is matched at its load, that is, $\hat{\mathbf{Z}}_L = \hat{\mathbf{Z}}_C$, so that the load reflection coefficient matrix is zero, that is, $\hat{\Gamma}_V(\mathcal{L}) = \mathbf{0}$. Equation (7.171) shows, as expected, that the reflection coefficient matrices are zero at all points on the line, that is, $\hat{\Gamma}_{V,I}(z) = \mathbf{0}$. Thus, there are only forward-traveling waves on the line, and there is no power flow in the $-z$ direction.

In terms of the mode voltages and currents, the average power flow on the line is

$$\begin{aligned}
 P_{\text{av}}(z) &= \frac{1}{2} \operatorname{Re} (\hat{\mathbf{V}}^t \hat{\mathbf{I}}^*) \\
 &= \frac{1}{2} \operatorname{Re} (\hat{\mathbf{V}}_m^t \hat{\mathbf{T}}_V^t \hat{\mathbf{T}}_I^* \hat{\mathbf{I}}_m^*) \quad (7.173)
 \end{aligned}$$

If $\hat{\mathbf{T}}_V$ and $\hat{\mathbf{T}}_I$ are such that

$$\hat{\mathbf{T}}_V^t \hat{\mathbf{T}}_I^* = \mathbf{1}_n \quad (7.174)$$

then

$$P_{\text{av}}(z) = \frac{1}{2} \operatorname{Re} (\hat{\mathbf{V}}_m^t \hat{\mathbf{I}}_m^*) \quad (7.175)$$

and the power is the sum of the powers of the individual modes. The condition in (7.174) is equivalent to stating that the voltage and current eigenvectors, the columns of $\hat{\mathbf{T}}_V$ and $\hat{\mathbf{T}}_I$, are orthonormal. In previous sections, we showed several cases for which the MTL equations are decoupleable and (7.174) is satisfied.

These properties are, of course, also directly analogous to the scalar, two-conductor line. The use of matrix notation allows a straightforward adaptation of the scalar results to the MTL case although there are some peculiarities unique to the MTL case.

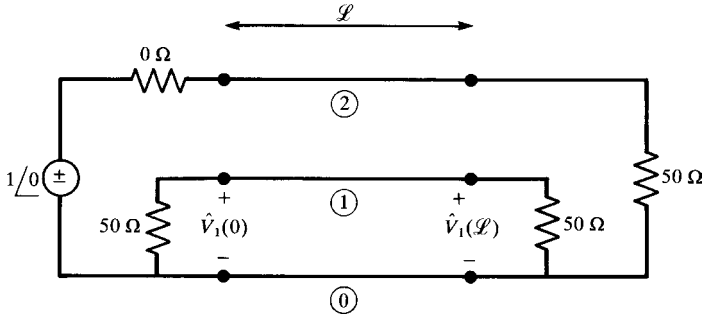


FIGURE 7.9 A three-conductor line for illustrating numerical results.

7.7 COMPUTED AND EXPERIMENTAL RESULTS

In this section, we will show some computed and experimental results that demonstrate the prediction methods of this chapter. The frequency-domain prediction model of this chapter is implemented in the computer program `MTL.FOR` described in Appendix A. This program determines the $2n$ undetermined constants in the general form of solution in (7.90): \mathbf{I}_m^\pm . The terminal configurations for both structures are shown in Figure 7.9. These are characterized as a generalized Thevenin equivalent as in (7.87) where

$$\begin{aligned} \hat{\mathbf{V}}_S &= \begin{bmatrix} 0 \\ 1 \angle 0^\circ \end{bmatrix} \\ \hat{\mathbf{Z}}_S &= \begin{bmatrix} 50 & 0 \\ 0 & 0 \end{bmatrix} \\ \hat{\mathbf{V}}_L &= \begin{bmatrix} 0 \\ 0 \end{bmatrix} \\ \hat{\mathbf{Z}}_L &= \begin{bmatrix} 50 & 0 \\ 0 & 50 \end{bmatrix} \end{aligned}$$

Two configurations of a three-conductor line ($n = 2$) are considered: a three-wire ribbon cable and a three-conductor printed circuit board. Experimentally determined frequency responses will be compared to the predictions of the MTL model as well as those of the lumped-Pi iterative approximation.

7.7.1 Ribbon Cables

The cross section of the three-wire ribbon cable is shown in Figure 7.10. The total line length is $\mathcal{L} = 2$ m. The per-unit-length parameters for this configuration were computed using the computer program `RIBBON.FOR` described in Appendix A and

are

$$\mathbf{L} = \begin{bmatrix} 0.7485 & 0.5077 \\ 0.5077 & 1.0154 \end{bmatrix} \mu\text{H/m}$$

$$\mathbf{C} = \begin{bmatrix} 37.432 & -18.716 \\ -18.716 & 24.982 \end{bmatrix} \text{pF/m}$$

The experimental results are compared to the predictions of the MTL model, with and without conductor losses, over the frequency range of 1 kHz to 100 MHz in Figure 7.11. Observe that below 100 kHz, losses in the line conductors are important and cannot be ignored. The dc resistance was computed for one of the #36 gauge strands ($r_w = 2.5$ mils) and dividing this result by the number of strands (7) to give $0.19444 \Omega/\text{m}$. Skin effect was included by determining the frequency where the radius of one of the #36 gauge strands equals two skin depths, $r_w = 2\delta = 2/\sqrt{\pi f_0 \mu \sigma}$ ($f_0 = 4.332$ MHz), and taking the resistance to vary as $r(f) = r_{dc} \sqrt{f/f_0}$ above this. Both the magnitude and the phase are well predicted. Observe that the line is one wavelength (ignoring the dielectric insulation) at 150 MHz. So the line is electrically short below, say, 15 MHz. Observe that the magnitude of the crosstalk for the lossless case (and a significant portion of the lossy case) increases directly with frequency or 20 dB/decade. We will find this to be a general result in Chapter 10.

Figure 7.12 shows the predictions of the lumped-Pi approximate model of Figure 7.6(a) using one and two Pi sections to represent the entire line. The wire resistances are assumed to be the dc values over the entire frequency range for these lumped-Pi models because skin effect (\sqrt{f}) dependency is difficult to model in the lumped-circuit program SPICE, which was used to solve the resulting circuit. Both one and two Pi

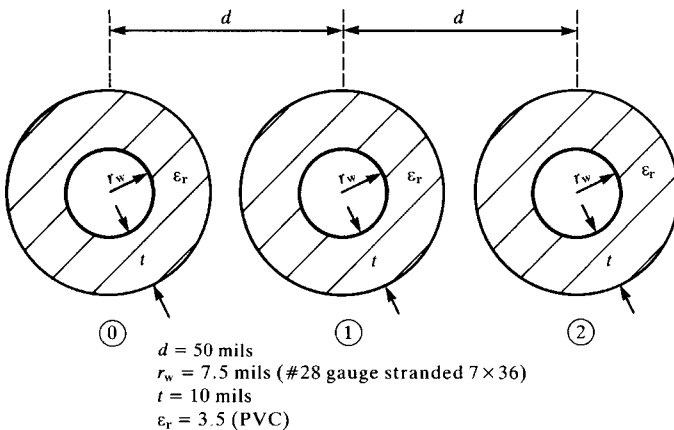


FIGURE 7.10 Dimensions of a three-conductor ribbon cable for illustrating numerical results.

sections give virtually identical predictions to the exact MTL model for frequencies below where the line is one tenth of a wavelength long. Observe that two Pi sections do not substantially extend the prediction accuracy frequency range even though the circuit complexity is double that for one Pi section.

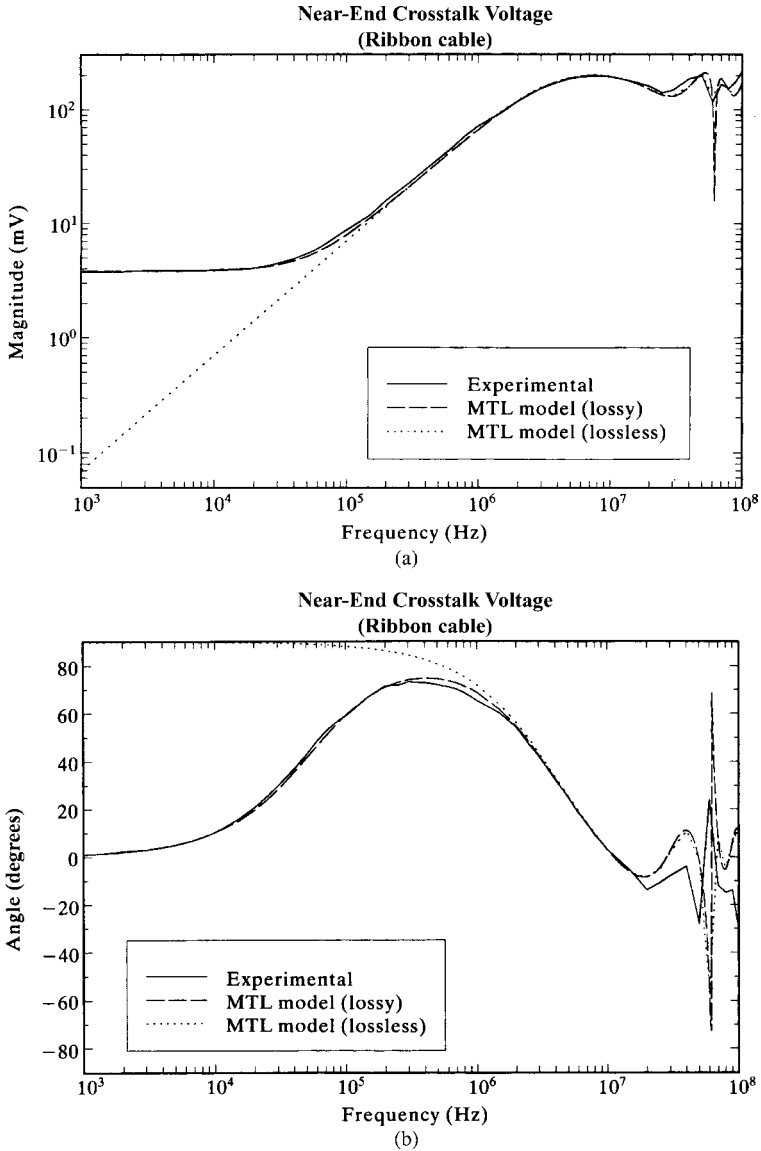


FIGURE 7.11 Comparison of the frequency response of the near-end crosstalk of the ribbon cable of Figure 7.10 determined experimentally and via the MTL model with and without losses: (a) magnitude and (b) phase.

7.7.2 Printed Circuit Boards

The next configuration is a three-conductor printed circuit board whose cross section is shown in Figure 7.13. The total line length is $\mathcal{L} = 10 \text{ in.} = 0.254 \text{ m}$. The per-unit-length parameters were computed using the computer program PCB.FOR described

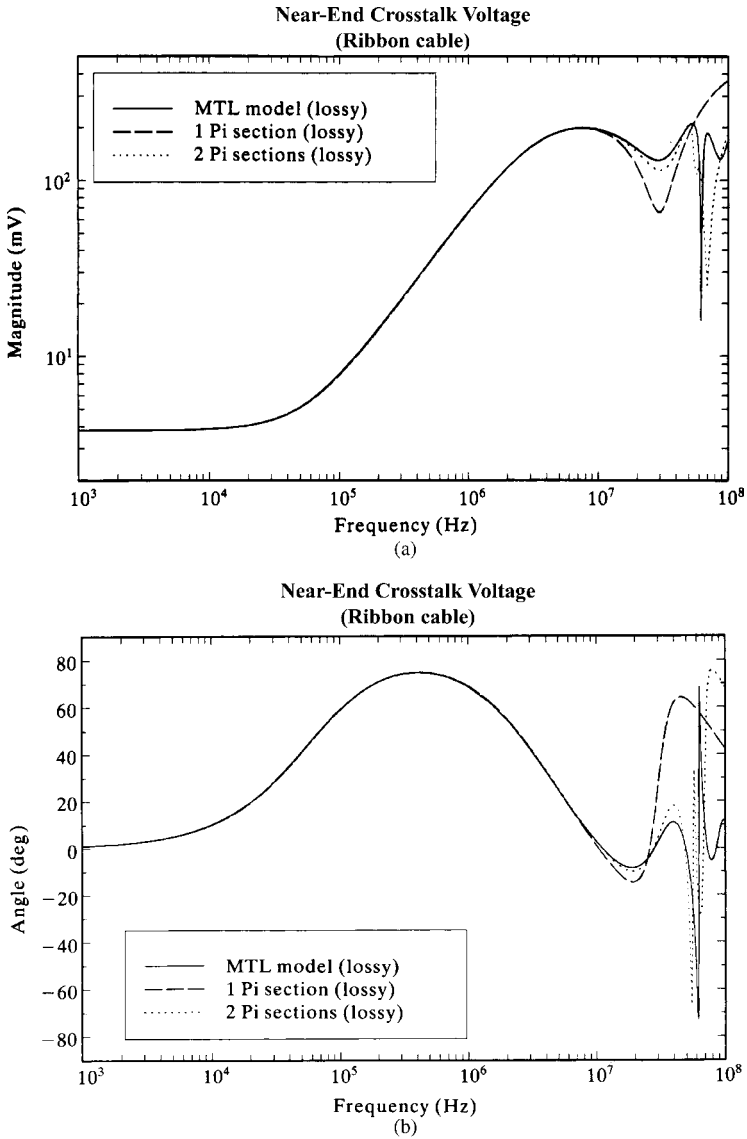


FIGURE 7.12 Comparison of the frequency response of the near-end crosstalk of the ribbon cable of Figure 7.10 determined via the MTL model with losses and via the lumped-Pi model with losses using one and two sections to represent the line: (a) magnitude and (b) phase.

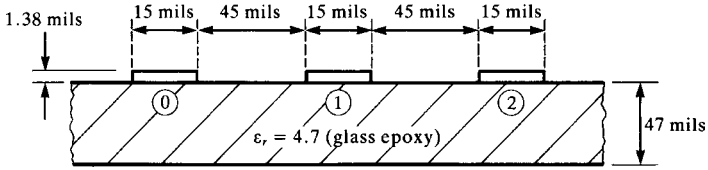


FIGURE 7.13 Dimensions of a three-conductor PCB for illustrating numerical results.

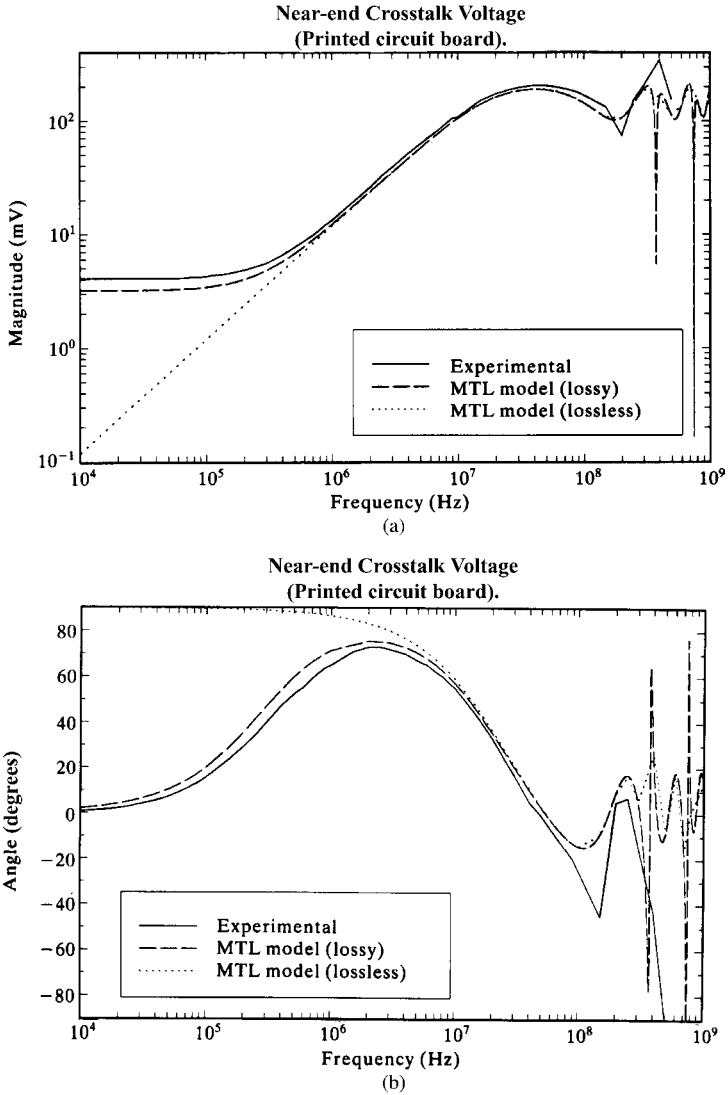


FIGURE 7.14 Comparison of the frequency response of the near-end crosstalk of the PCB of Figure 7.13 determined experimentally and via the MTL model with and without losses: (a) magnitude and (b) phase.

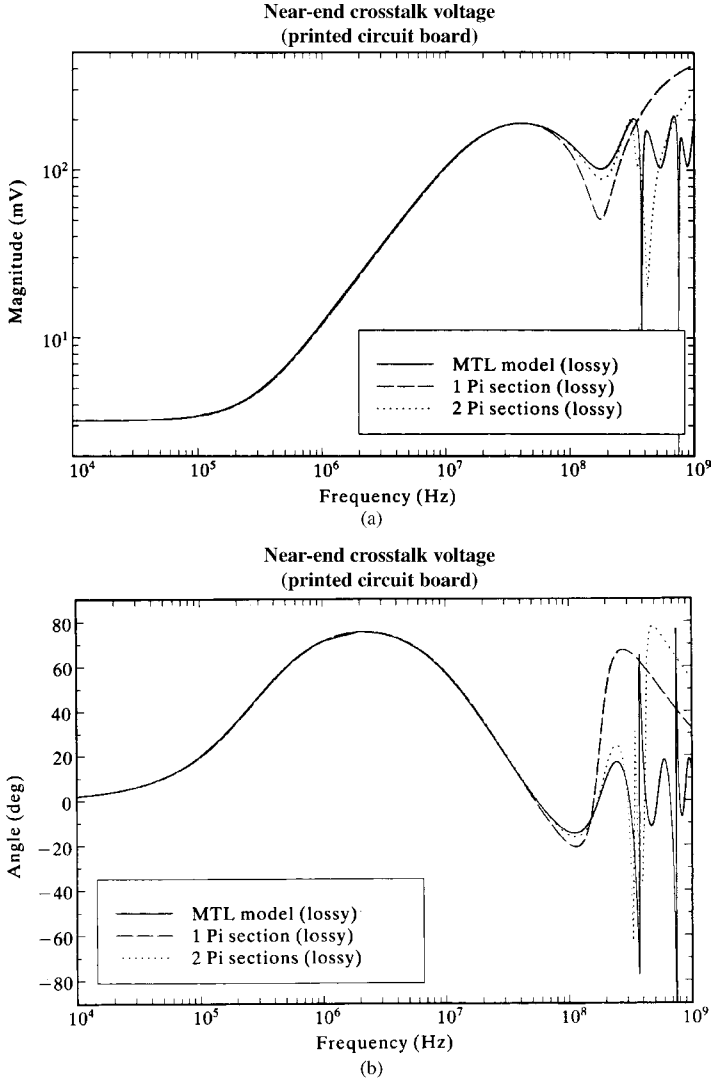


FIGURE 7.15 Comparison of the frequency response of the near-end crosstalk of the PCB of Figure 7.13 determined via the MTL model with losses and via the lumped-Pi model with losses using one and two sections to represent the line: (a) magnitude and (b) phase.

in Appendix A :

$$\mathbf{L} = \begin{bmatrix} 1.10515 & 0.690613 \\ 0.690613 & 1.38123 \end{bmatrix} \mu\text{H/m}$$

$$\mathbf{C} = \begin{bmatrix} 40.5985 & -20.2992 \\ -20.2992 & 29.7378 \end{bmatrix} \text{pF/m}$$

The experimentally obtained results are compared to the predictions of the MTL model with and without conductor losses over the frequency range of 10 kHz to 1 GHz in Figure 7.14. The conductor resistances were computed in a similar fashion to the ribbon cable. The dc resistance is $r_{dc} = 1/wt\sigma = 1.291 \Omega/\text{m}$, where w is the land width ($w = 15$ mils) and t is the land thickness for 1 ounce copper ($t = 1.38$ mils). The frequency where this transitions to a \sqrt{f} behavior was approximated as being where the land thickness equals two skin depths: $t = 2\delta$ or $f_0 = 14.218$ MHz. Observe that the frequency where the losses become important is on the order of 1 MHz. Both the magnitude and the phase are well predicted. The line is one wavelength (ignoring the board dielectric) at 1.18 GHz. Thus, the line can be considered to be electrically short for frequencies below some 100 MHz. Again note that the magnitude of the frequency response increases directly with frequency or 20 dB/decade, where the line is electrically short for the lossless case (and a significant portion of the lossy case).

Figure 7.15 shows the predictions of the lumped-Pi approximate model of Figure 7.6(a) using one and two Pi sections to represent the entire line. The wire resistances are again assumed to be the dc values over the entire frequency range for these lumped-Pi models because skin effect (\sqrt{f}) dependency is difficult to model in the lumped-circuit program SPICE, which was used to solve the resulting circuit. Both one and two Pi sections give virtually identical predictions to the exact MTL model for frequencies below where the line is one tenth of a wavelength long. Observe that, as in the case of the ribbon cable, two Pi sections do not substantially extend the prediction accuracy frequency range even though the circuit complexity is double that for one Pi section.

PROBLEMS

- 7.1 Verify the second-order phasor MTL equations in (7.7).
- 7.2 Verify the modal phasor MTL equations in (7.9).
- 7.3 Verify, by direct substitution, that (7.19) satisfy (7.9).
- 7.4 Verify, by direct substitution, that (7.33) and (7.34) satisfy (7.7).
- 7.5 Diagonalize the following matrix as $\mathbf{T}^{-1}\mathbf{M}\mathbf{T} = \Lambda$:

$$\mathbf{M} = \begin{bmatrix} 4 & 2 \\ 1 & 3 \end{bmatrix}$$

$$[T_{11} = 2, T_{12} = 1, T_{21} = 1, T_{22} = -1, \Lambda_1 = 5, \Lambda_2 = 2]$$

- 7.6 Determine the 2×2 matrices \mathbf{T} , which will diagonalize the following matrices:

$$\mathbf{M} = \begin{bmatrix} -4 & 2 \\ -1 & -1 \end{bmatrix}$$

$$\mathbf{M} = \begin{bmatrix} -2 & -1 \\ -1 & -2 \end{bmatrix}$$

$[T_{11} = 2, T_{12} = 1, T_{21} = 1, T_{22} = 1, \Lambda_1 = -3, \Lambda_2 = -2$ and $T_{11} = 1, T_{12} = 1, T_{21} = 1, T_{22} = -1, \Lambda_1 = -3, \Lambda_2 = -1]$

7.7 Diagonalize the following inductance matrix for a homogeneous medium via the method of Section 7.2.2.1:

$$\mathbf{L} = \begin{bmatrix} 5 & 1 \\ 1 & 3 \end{bmatrix} \quad (\mu\text{H/m})$$

[eigenvalues are $(4 + \sqrt{2}) \times 10^{-6} = 5.414 \times 10^{-6}$ and $(4 - \sqrt{2}) \times 10^{-6} = 2.586 \times 10^{-6}, T_{11} = T_{22} = 0.924, T_{21} = -T_{12} = 0.383]$

7.8 Demonstrate (7.52) and (7.53).

7.9 Demonstrate (7.60) and (7.61).

7.10 Show that a 2×2 real, symmetric matrix \mathbf{M} can be diagonalized with the orthogonal transformation:

$$\mathbf{T} = \begin{bmatrix} \cos \theta & -\sin \theta \\ \sin \theta & \cos \theta \end{bmatrix}$$

where

$$\tan 2\theta = \frac{2M_{12}}{M_{11} - M_{22}}$$

Show that the eigenvalues are

$$\begin{aligned} \Lambda_1^2 &= M_{11}\cos^2\theta + 2M_{12}\cos\theta\sin\theta + M_{22}\sin^2\theta \\ \Lambda_2^2 &= M_{11}\sin^2\theta - 2M_{12}\cos\theta\sin\theta + M_{22}\cos^2\theta \end{aligned}$$

7.11 Diagonalize the following product, \mathbf{CL} , where

$$\begin{aligned} \mathbf{C} &= \begin{bmatrix} 3 & -1 \\ -1 & 4 \end{bmatrix} \\ \mathbf{L} &= \begin{bmatrix} 2 & 1 \\ 1 & 3 \end{bmatrix} \end{aligned}$$

[eigenvalues are 5 and 11, $T_{11} = 3, T_{22} = 1, T_{21} = -1, T_{12} = 0]$

7.12 Demonstrate (7.66), (7.68), and (7.69).

7.13 Show that \mathbf{T} in (7.69) and its inverse in (7.70) diagonalize the following cyclic-symmetric matrix:

$$\mathbf{M} = \begin{bmatrix} 5 & 2 & 2 \\ 2 & 5 & 2 \\ 2 & 2 & 5 \end{bmatrix}$$

- 7.14 Demonstrate that the transformations in (7.79) and (7.82) diagonalize the cyclic-symmetric matrices.
- 7.15 Diagonalize the following matrix, which has cyclic-symmetric structure:

$$\mathbf{M} = \begin{bmatrix} 4 & 3 & 2 & 3 \\ 3 & 4 & 3 & 2 \\ 2 & 3 & 4 & 3 \\ 3 & 2 & 3 & 4 \end{bmatrix}$$

Show by direct calculation that the $\hat{\mathbf{T}}$ you obtain does in fact diagonalize this matrix and that $\hat{\mathbf{T}}^{-1} = \hat{\mathbf{T}}^*$. Verify from this that the eigenvalues are as expected according to (7.68).

- 7.16 Determine the generalized Thevenin equivalent representation, $\hat{\mathbf{V}}(0) = \hat{\mathbf{V}}_S - \hat{\mathbf{Z}}_S \hat{\mathbf{I}}(0)$, of the source termination network shown in Figure P7.16.

$$\left[\hat{\mathbf{V}}_S = \begin{bmatrix} V_{S1} \\ V_{S2} \end{bmatrix}, \hat{\mathbf{Y}}_S = \begin{bmatrix} (R_1 + R_3) & R_3 \\ R_3 & (R_1 + R_3) \end{bmatrix} \right]$$

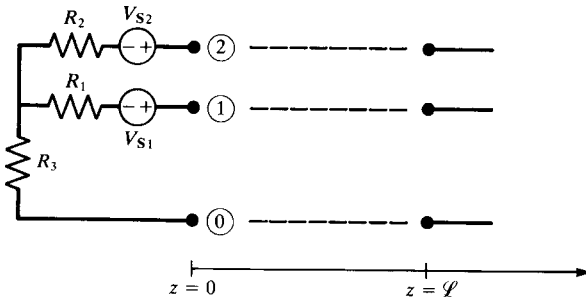


FIGURE P7.16

- 7.17 Determine the generalized Norton equivalent representation, $\hat{\mathbf{I}}(0) = \hat{\mathbf{I}}_S - \hat{\mathbf{Y}}_S \hat{\mathbf{V}}(0)$, of the source termination network shown in Figure P7.17.

$$\left[\hat{\mathbf{I}}_S = \begin{bmatrix} V_{S1}/R_1 \\ V_{S2}/R_2 \end{bmatrix}, \hat{\mathbf{Y}}_S = \begin{bmatrix} \left(\frac{1}{R_1} - \frac{1}{R_3} \right) & \frac{1}{R_3} \\ \frac{1}{R_3} & \left(\frac{1}{R_2} - \frac{1}{R_3} \right) \end{bmatrix} \right]$$

- 7.18 Characterize the source and load termination networks shown in Figure P7.18.

$$\left[\hat{\mathbf{I}}(0) = \hat{\mathbf{I}}_S - \hat{\mathbf{Y}}_S \hat{\mathbf{V}}(0), \hat{\mathbf{I}}_S = \frac{1}{R_S} \begin{bmatrix} -V_S \\ V_S \end{bmatrix}, \hat{\mathbf{Y}}_S = \frac{1}{R_S} \begin{bmatrix} -1 & 1 \\ 1 & -1 \end{bmatrix}, \right.$$

$$\left. \hat{\mathbf{V}}(\mathcal{L}) = \hat{\mathbf{V}}_L + \hat{\mathbf{Z}}_L \hat{\mathbf{I}}(\mathcal{L}), \hat{\mathbf{V}}_L = \mathbf{0}, \hat{\mathbf{Z}}_L = \begin{bmatrix} 0 & 0 \\ 0 & R_2 \end{bmatrix} \right]$$

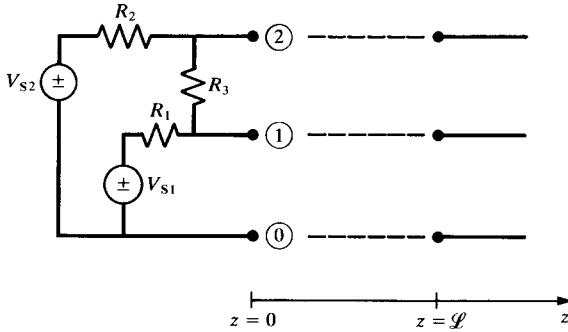


FIGURE P7.17

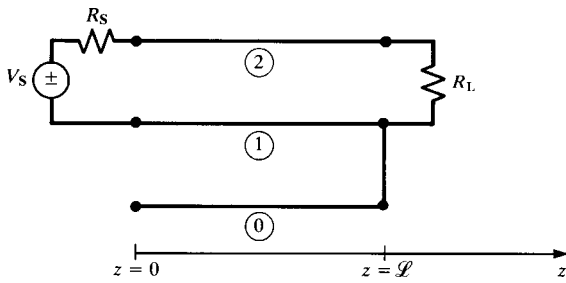


FIGURE P7.18

- 7.19 Verify the terminal relation incorporations using the chain-parameter matrices in (7.92), (7.97), and (7.101).
- 7.20 Verify the chain-parameter matrices for the lumped-circuit iterative structures given in (7.115).
- 7.21 Verify the chain-parameter matrix identities in (7.132).
- 7.22 Derive the relations for the impedance and admittance parameter submatrices in terms of the chain-parameter submatrices given in (7.140), (7.142), (7.144a), and (7.144b). Evaluate these for a lossless line in a homogeneous medium.
- 7.23 Use the FORTRAN code `MTL.FOR` to verify the results for the ribbon cable in Section 7.7.1 as shown in Figure 7.11.
- 7.24 Use the FORTRAN code `SPICELPI.FOR` to construct PSPICE subcircuit lumped-Pi models for the ribbon cable in Section 7.7.1 and verify the results in Figure 7.12.
- 7.25 Use the FORTRAN code `MTL.FOR` to verify the results for the PCB in Section 7.7.2 as shown in Figure 7.14.
- 7.26 Use the FORTRAN code `SPICELPI.FOR` to construct PSPICE subcircuit lumped-Pi models for the PCB in Section 7.7.2 and verify the results in Figure 7.15.

REFERENCES

- [1] K. Ogata, *State Space Analysis of Control Systems*, Prentice-Hall, Englewood Cliffs, NJ, 1967.
- [2] C.T. Chen, *Linear System Theory and Design*, Holt, Rinehart and Winston, New York, 1984.
- [3] F.E. Hohn, *Elementary Matrix Algebra*, 2nd edition, Macmillan, New York, 1964.
- [4] A. Ralston, *A First Course in Numerical Analysis*, McGraw-Hill, New York, 1965.
- [5] L.A. Pipes, Matrix theory of multiconductor transmission lines, *Philosophical Magazine*, **24**(159), 97–113, 1937.
- [6] S.O. Rice, Steady state solutions of transmission line equations, *Bell System Technical Journal*, **20**(2), 131–178, 1941.
- [7] L.A. Pipes, Steady-state analysis of multiconductor transmission lines, *Journal of Applied Physics*, **12**(11), 782–789, 1941.
- [8] L.A. Pipes, Direct computation of transmission matrices of electrical transmission lines, *Journal of the Franklin Institute, Part I*, **281**(4), 275–292, 1966; *Part II*, **281**(5), 387–405, 1966.
- [9] D.E. Hedman, Propagation on overhead transmission lines: I—Theory of modal analysis, and II—Earth conduction effects and practical results, *IEEE Transactions on Power Apparatus and Systems*, **84**, 200–211, 1965.
- [10] L.M. Wedepohl, Applications of matrix methods to the solution of traveling wave phenomena in polyphase systems, *Proceedings of IEE*, **110**(12), 2200–2212, 1963.
- [11] D.F. Strawe, Analysis of uniform symmetric transmission lines, The Boeing Company, Boeing Document D2-19734-1, August 1971.
- [12] W.I. Bowman and J.M. McNamee, Development of equivalent Pi and T matrix circuits for long untransposed transmission lines, *IEEE Transactions on Power Apparatus and Systems*, 625–632, 1964.
- [13] E.N. Protonotarios and O. Wing, Analysis and intrinsic properties of the general nonuniform transmission line, *IEEE Transactions on Microwave Theory and Techniques*, **15**(3), 142–150, 1967.
- [14] E.C. Bertnolli, Analysis of the N -wire exponential line, *Proceedings of IEEE*, 1225, 1967.

8

TIME-DOMAIN ANALYSIS OF TWO-CONDUCTOR LINES

The previous two chapters dealt with the solution of the transmission-line equations in the *frequency domain*, that is, for the case of *sinusoidal steady-state* excitation of the line. That is, the sources are sinusoids at a single frequency and are assumed to have been applied for a sufficiently long time such that all transients have decayed to zero leaving only the steady-state solution. In this and the following chapter, we will examine the solution of the transmission-line equations for sources that have any general time variation. This will include both the transient and the steady-state components of the solution and represents the solution in the *time domain*. Again, there will be striking parallels between the two-conductor solution methods given in this chapter and those for MTLs given in the following chapter.

We have seen in the previous chapters that incorporating line losses into the solution of the transmission-line equations is a very straightforward process in the frequency domain. We will see in this and the following chapter that the time-domain solution of the transmission-line equations for a *lossless line* is also a very simple and straightforward computational process for either two-conductor lines *or* multiconductor transmission lines (MTLs)! Line losses, however, introduce substantial complications in the solution of the transmission-line equations in the time domain. In addition to the low-frequency dc resistance and internal inductance, conductors exhibit a frequency-dependent resistance and internal inductance due to skin effect at high frequencies. This dependence on frequency is \sqrt{f} , which is difficult to characterize in the time domain. Incorporation of these losses into the frequency-domain solution is trivial; compute the resistances and internal inductive reactances of the line conductors at

the frequency of interest, include them as constants in the phasor transmission-line equations, and solve the resulting equations. For the next frequency of interest, recompute the resistances and internal inductive reactances of the conductors for this frequency and repeat the solution. The loss introduced by a nonzero conductivity of the surrounding media is also dependent on frequency and can likewise be easily incorporated into the frequency-domain solution. Although the inclusion of these losses does not significantly complicate the frequency-domain solution, it adds considerable complications to the general time-domain solution of the transmission-line equations.

We begin the discussion with a review of the solutions for two-conductor lossless lines. This serves to introduce the notion of traveling waves on the line and also introduces an important solution technique for numerical computation, the method of characteristics, which leads to the *exact solution* for a *lossless line* that is incorporated into the SPICE (PSPICE) computer program. Once these concepts and solution methods for lossless lines are discussed, we discuss methods for the incorporation of frequency-dependent losses. Frequency-dependent losses can be included in the solution via the time-domain to frequency-domain (TDFD) solution method whereby the input signal is resolved into its Fourier sinusoidal components and passed through the frequency-domain transfer function. The line losses are easily included when we compute the frequency-domain transfer function via the methods of Chapters 6 and 7. The output sinusoidal components are then summed over time to return to the time domain. This method requires that the line terminations be linear since superposition was used. An alternative method is the numerical finite-difference, time-domain (FDTD) method. This method approximates the derivatives in the transmission-line equations and solves the resulting difference equations in a recursive manner. The FDTD method will be first developed for the case of lossless lines and then extended to include frequency-dependent line losses. In the following chapter, all these methods will be extended to MTLs in a fashion that bears striking similarities to the two-conductor solution methods.

8.1 THE SOLUTION FOR LOSSLESS LINES

The scalar transmission-line equations for two-conductor lossless lines are

$$\frac{\partial V(z, t)}{\partial z} = -l \frac{\partial I(z, t)}{\partial t} \quad (8.1a)$$

$$\frac{\partial I(z, t)}{\partial z} = -c \frac{\partial V(z, t)}{\partial t} \quad (8.1b)$$

Differentiating one equation with respect to z and the other with respect to t and substituting yields the uncoupled second-order differential equations

$$\frac{\partial^2 V(z, t)}{\partial z^2} = lc \frac{\partial^2 V(z, t)}{\partial t^2} \quad (8.2a)$$

$$\frac{\partial^2 I(z, t)}{\partial z^2} = lc \frac{\partial^2 I(z, t)}{\partial t^2} \quad (8.2b)$$

The solutions to these equations are [A.1]

$$V(z, t) = \underbrace{V^+ \left(t - \frac{z}{v} \right)}_{\text{forward, } +z, \text{ traveling wave}} + \underbrace{V^- \left(t + \frac{z}{v} \right)}_{\text{backward, } -z, \text{ traveling wave}} \quad (8.3a)$$

$$\begin{aligned} I(z, t) &= \underbrace{I^+ \left(t - \frac{z}{v} \right)}_{\text{forward, } +z, \text{ traveling wave}} + \underbrace{I^- \left(t + \frac{z}{v} \right)}_{\text{backward, } -z, \text{ traveling wave}} \\ &= \frac{1}{Z_C} V^+ \left(t - \frac{z}{v} \right) - \frac{1}{Z_C} V^- \left(t + \frac{z}{v} \right) \end{aligned} \quad (8.3b)$$

where the *characteristic impedance* is

$$\begin{aligned} Z_C &= \sqrt{\frac{l}{c}} \\ &= vl \\ &= \frac{1}{vc} \end{aligned} \quad (8.4)$$

The waves V^+ and I^+ are traveling in the $+z$ direction as can be seen from their arguments; as t increases, z must also increase in order to track a point on the waveform. Hence, they are called forward-traveling waves. The waves V^- and I^- are similarly traveling in the $-z$ direction and are called backward-traveling waves. The characteristic impedance relates the voltage and current in the forward-traveling wave and in the backward-traveling wave as

$$V^+ \left(t - \frac{z}{v} \right) = Z_C I^+ \left(t - \frac{z}{v} \right) \quad (8.5a)$$

$$V^- \left(t + \frac{z}{v} \right) = -Z_C I^- \left(t + \frac{z}{v} \right) \quad (8.5b)$$

The *velocity of propagation* of the forward-traveling waves and the backward-traveling waves is

$$v = \frac{1}{\sqrt{lc}} \quad (8.6)$$

The functions of t and z , $V^+(t, z)$ and $V^-(t, z)$, are as yet unknown but have time and position related *only as* $t \pm z/v$.

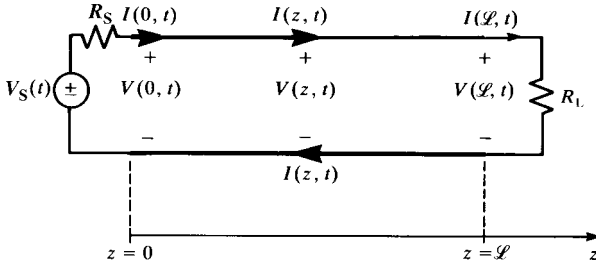


FIGURE 8.1 A two-conductor line in the time domain.

8.1.1 Wave Tracing and the Reflection Coefficients

Consider the two-conductor line of total length shown in Figure 8.1, where we assume resistive loads R_S and R_L . We will later extend this solution to include dynamic loads such as inductors and/or capacitors using the Laplace transform method or the SPICE solution. The SPICE solution method will also handle nonlinear loads. The forward- and backward-traveling waves are related at the load $z = L$ by the *load reflection coefficient* as [A.1]

$$\begin{aligned} \Gamma_L &= \frac{V^-(t + L/v)}{V^+(t - L/v)} \\ &= \frac{R_L - Z_C}{R_L + Z_C} \end{aligned} \tag{8.7}$$

Therefore, the reflected waveform at the load can be found from the incident wave using the load reflection coefficient as

$$V^-\left(t + \frac{L}{v}\right) = \Gamma_L V^+\left(t - \frac{L}{v}\right) \tag{8.8}$$

The reflection coefficient so defined applies to voltage waves only. A current reflection coefficient applying to the current waves can similarly be obtained and is the negative of the voltage reflection coefficient (due to the negative sign in (8.3b))

$$I^-\left(t + \frac{L}{v}\right) = -\Gamma_L I^+\left(t - \frac{L}{v}\right) \tag{8.9}$$

The reflection at the load is illustrated in Figure 8.2. The reflection process can be viewed as a mirror that produces, as a reflected V^- , a replica of V^+ that is “flipped around,” and all points on the V^- waveform are the corresponding points on the V^+ waveform multiplied by Γ_L . Note that the total voltage at the load, $V(L, t)$, is the *sum* of the individual waves present at the load at a particular time as shown by (8.3a).

Now let us consider the portion of the line at the source, $z = 0$, shown in Figure 8.3. When we initially connect the source to the line, we reason that a forward-traveling

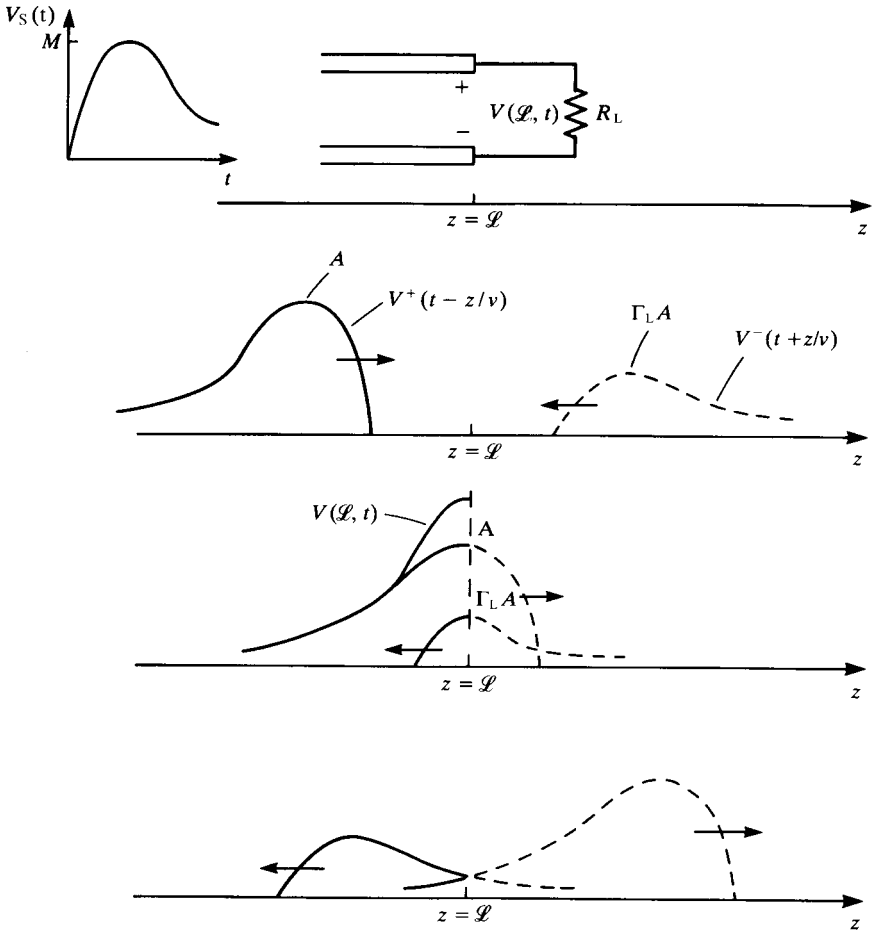


FIGURE 8.2 Illustration of reflections at a termination of a mismatched line.

wave will be propagated down the line. We would not expect a backward-traveling wave to appear on the line until this initial forward-traveling wave has reached the load, a time delay of

$$T_D = \mathcal{L}/v \tag{8.10}$$

since the incident wave will not have arrived to produce this reflected wave. The portion of the incident wave that is reflected at the load will require an additional time T_D to move back to the source. Therefore, for $0 \leq t \leq 2\mathcal{L}/v = 2T_D$, no backward-traveling waves will appear at $z = 0$, and for any time less than $2T_D$ the total voltage and current at $z = 0$ will consist only of forward-traveling waves V^+ and I^+ . Therefore,

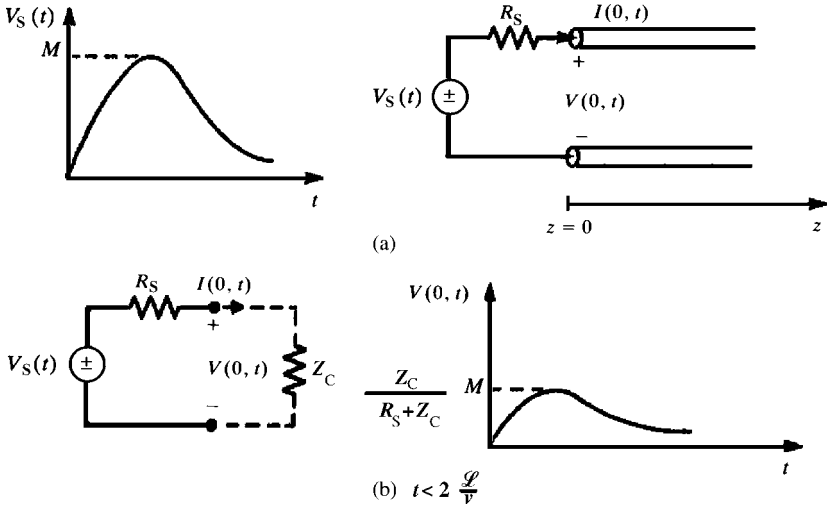


FIGURE 8.3 Characterization of the initially transmitted pulse.

from (8.3)

$$V(0, t) = V^+ \left(t - \frac{0}{v} \right) \tag{8.11a}$$

$$\begin{aligned}
 I(0, t) &= I^+ \left(t - \frac{0}{v} \right) \\
 &= \frac{V^+ \left(t - \frac{0}{v} \right)}{Z_C} \quad \text{for } 0 \leq t \leq 2T_D \tag{8.11b}
 \end{aligned}$$

Since the ratio of *total* voltage and *total* current on the line at the input to it is Z_C for $0 \leq t \leq 2T_D$, the line appears to have an input resistance of Z_C over this time interval. Thus, the forward-traveling voltage and current waves that are initially launched are related to the source voltage by (using voltage division)

$$V(0, t) = \frac{Z_C}{R_S + Z_C} V_S(t) \quad \text{for } 0 \leq t \leq 2T_D \tag{8.12a}$$

$$I(0, t) = \frac{1}{R_S + Z_C} V_S(t) \quad \text{for } 0 \leq t \leq 2T_D \tag{8.12b}$$

This initially launched wave has the same shape as the source voltage $V_S(t)$ (but is reversed; see Fig. 8.2).

The initially launched wave travels toward the load requiring a time $T_D = \mathcal{L}/v$ for the leading edge of the pulse to reach the load. When the pulse reaches the load, a reflected pulse is initiated, as shown in Figure 8.2. This reflected pulse requires an

additional time $T_D = \mathcal{L}/v$ for its leading edge to reach the source. At the source, we can similarly obtain a voltage reflection coefficient

$$\Gamma_S = \frac{R_S - Z_C}{R_S + Z_C} \quad (8.13)$$

as the ratio of the incoming incident wave (which is the wave that was reflected at the load) and the reflected portion of this incoming wave (which is sent back toward the load). A forward-traveling wave is therefore initiated at the source in the same fashion as at the load. This forward-traveling wave has the same shape as the incoming backward-traveling wave (which is the original pulse sent out by the source and reflected at the load), but corresponding points on the incoming wave are reduced by Γ_S . This process of repeated reflections continues as re-reflections at the source and the load. At any time, the total voltage (current) at any point on the line is the sum of all the individual voltage (current) waves existing on the line at that point and time, as shown by (8.3).

As an example, consider the transmission line shown in Figure 8.4(a). At $t = 0$, a 30-V battery with zero source resistance is attached to the line that has a total length of $\mathcal{L} = 400$ m, a velocity of propagation of $v = 200$ m/ μ s, and a characteristic impedance of $Z_C = 50 \Omega$. The line is terminated at the load in a 100 resistor so that the load reflection coefficient is

$$\begin{aligned} \Gamma_L &= \frac{100 - 50}{100 + 50} \\ &= \frac{1}{3} \end{aligned}$$

and the source reflection coefficient is

$$\begin{aligned} \Gamma_S &= \frac{0 - 50}{0 + 50} \\ &= -1 \end{aligned}$$

The one-way transit time is $T_D = \mathcal{L}/v = 2 \mu$ s. At $t = 0$, a 30-V pulse is sent down the line, and the line voltage is zero prior to the arrival of the pulse and 30 V after the pulse has passed. At $t = 2 \mu$ s, the pulse arrives at the load, and a backward-traveling pulse of magnitude $30\Gamma_L = 10$ V is sent back toward the source. When this reflected pulse arrives at the source, a pulse of magnitude Γ_S of the incoming pulse or $\Gamma_S\Gamma_L 30 = -10$ V is sent back toward the load. This pulse travels to the load, at which time a reflected pulse of Γ_L of this incoming pulse or $\Gamma_L\Gamma_S\Gamma_L 30 = -3.33$ V is sent back toward the source. At each point on the line, the total line voltage is the sum of the waves present on the line at that point and at that time.

The previous example has illustrated the process of sketching the line voltage at various points along the line and at discrete times. Generally, we are interested only in the voltage or current at the source end of the line, $V(0, t)$ and $I(0, t)$, and at the load

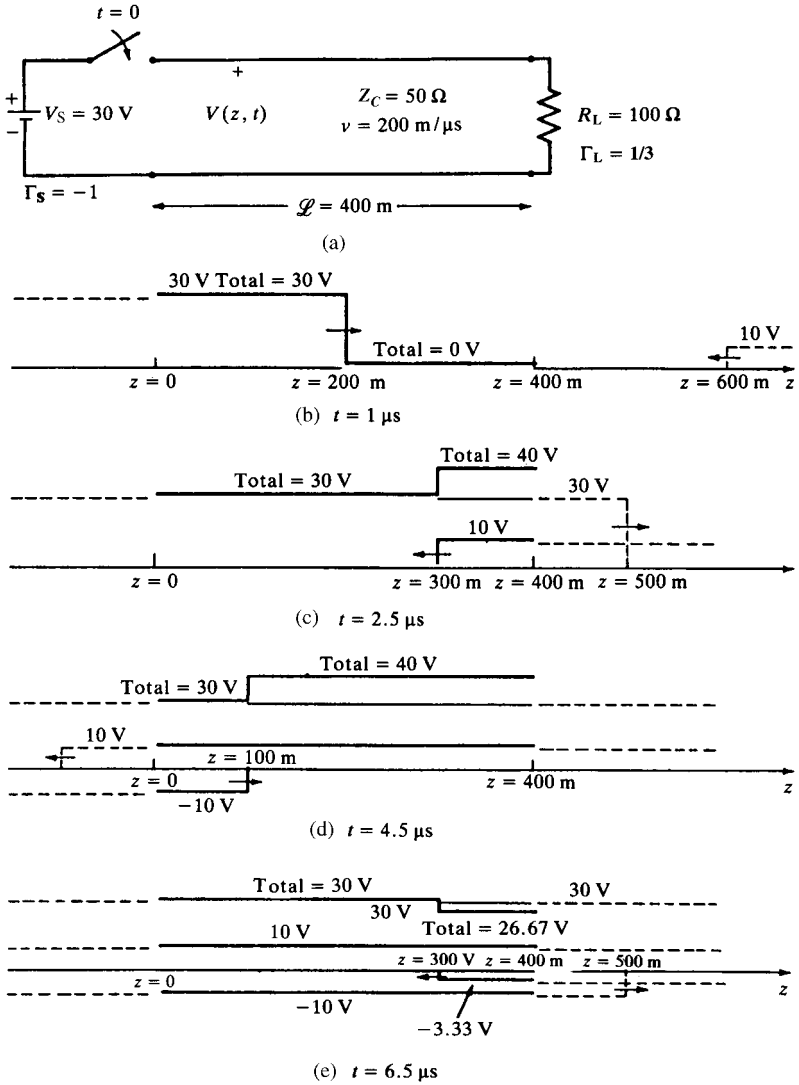


FIGURE 8.4 An example illustrating the computation of the line voltage at various points on the line.

end, $V(\mathcal{L}, t)$ and $I(\mathcal{L}, t)$ as functions of time and are not concerned with voltages and currents at interior points of the line. In order to illustrate this process, let us reconsider the previous example and sketch the voltage at the line output $z = \mathcal{L}$ as a function of time, as illustrated in Figure 8.5. At $t = 0$, a 30-V pulse is sent out by the source. The leading edge of this pulse arrives at the load at $t = 2 \mu\text{s}$. At this time, a pulse of $\Gamma_L 30 = 10 \text{ V}$ is sent back toward the source. This 10-V pulse arrives

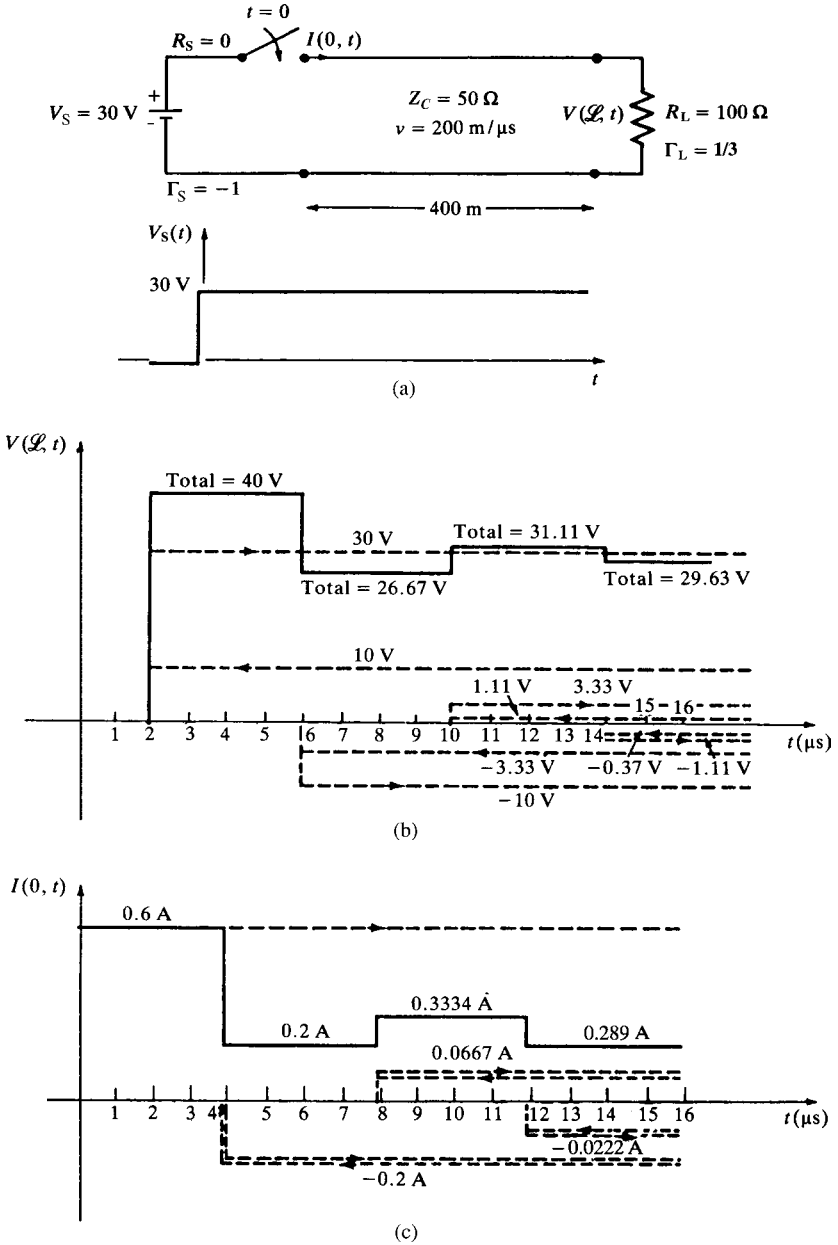


FIGURE 8.5 An example illustrating the computation of (a) the load voltage and (b) the source current as a function of time.

at the source at $t = 4 \mu\text{s}$, and a pulse of $\Gamma_S \Gamma_L 30 = -10 \text{ V}$ is returned to the load. This pulse arrives at the load at $t = 6 \mu\text{s}$, and a pulse of $\Gamma_L \Gamma_S \Gamma_L 30 = -3.33 \text{ V}$ is sent back toward the source. The contributions of these waves at $z = \mathcal{L}$ are shown in Figure 8.5(b) as dashed lines, and the total voltage is shown as a solid line. Arrows are placed on each component to indicate its direction of travel. Note that the load voltage oscillates about 30 V during the transient time interval, but asymptotically converges to the expected steady-state value of 30 V . If we had attached an oscilloscope across the load to display this voltage as a function of time, and the time scale were set to 1 ms per division, it would appear that the load voltage immediately assumed a value of 30 V . We would see the picture of Figure 8.5(b) only if the time scale of the oscilloscope were sufficiently reduced to, say, $1 \mu\text{s}$ per division. In order to sketch the load current $I(\mathcal{L}, t)$, we could divide the previously sketched load voltage by R_L . We could directly sketch the current at either end of the line by using current reflection coefficients (which are the negative of the voltage reflection coefficients) $\Gamma_S = 1$ and $\Gamma_L = -1/3$ and an initial current pulse of $30 \text{ V}/Z_C = 0.6 \text{ A}$ and combining the various forward- and backward-traveling current waves at each time point as was done for the voltages. The current at the input to the line, $I(0, t)$, is sketched in this fashion in Figure 8.5(c). Observe that the current oscillates about an expected steady-state value of $30 \text{ V}/R_L = 0.3 \text{ A}$.

The previous examples have illustrated sketching the voltage and current waveforms at the source and the load for sources that are dc (constant with time). The next example shows the effect of source voltage pulse width on the total voltages. Consider the example shown in Figure 8.6(a). The source voltage is a pulse of 100 V amplitude and $6 \mu\text{s}$ duration as shown in Figure 8.6(b). The line is specified by its per-unit-length capacitance and inductance of $c = 100 \text{ pF/m}$ and $l = 0.25 \mu\text{H/m}$. This corresponds to RG58U coaxial cable. The line therefore has a characteristic impedance of

$$\begin{aligned} Z_C &= \sqrt{\frac{l}{c}} \\ &= 50 \Omega \end{aligned}$$

and a velocity of propagation of

$$\begin{aligned} v &= \frac{1}{\sqrt{lc}} \\ &= 2 \times 10^8 \text{ m/s} \\ &= 200 \text{ m}/\mu\text{s} \end{aligned}$$

The source resistance is $R_S = 150 \Omega$ and the load is a short circuit with $R_L = 0 \Omega$. Hence, the source reflection coefficient is

$$\begin{aligned} \Gamma_S &= \frac{150 - 50}{150 + 50} \\ &= \frac{1}{2} \end{aligned}$$

and the load reflection coefficient is

$$\begin{aligned}\Gamma_L &= \frac{0 - 50}{0 + 50} \\ &= -1\end{aligned}$$

The one-way time delay is

$$\begin{aligned}T_D &= \frac{\mathcal{L}}{v} \\ &= 2 \mu\text{s}\end{aligned}$$

The initially sent out voltage pulse is

$$\frac{50}{50 + 150} \times 100 = 25 \text{ V}$$

The voltage at the input to the line, $V(0, t)$, is sketched in Figure 8.6(c). The incident and reflected voltage waveforms are again sketched with dashed lines with an arrow added to each to indicate whether they are associated with a forward-traveling or a backward-traveling wave. The initial voltage pulse of 25 V and 6 μs duration is sent to the load, arriving there after one time delay of 2 μs , where it is reflected as a pulse of -25 V. This pulse, reflected at the load, is inverted because of $\Gamma_L = -1$ and arrives at the source after an additional 2- μs time delay. This incoming pulse is reflected as -12.5 V and arrives at the load after 2 μs , where it is reflected as 12.5 V arriving at the source after another 2- μs delay. The process continues as shown. Adding all the incident and reflected pulses at the source at each time, we obtain the total voltage drawn with a solid line. Clearly, this total decays to zero as it should in steady state for this short-circuit load and the fact that the pulse turns off at $t = 6 \mu\text{s}$. Observe in this example, the pulse width of 6 μs is equivalent to three time delays. Hence, we see an overlap of the forward- and backward-traveling components, which creates an interesting result.

The current at the load, $I(\mathcal{L}, t)$, is similarly sketched in Figure 8.6(d). The reflection coefficients for the current are the negative of those for the voltage:

$$\begin{aligned}\Gamma_S &= -\frac{1}{2} \\ \Gamma_L &= +1\end{aligned}$$

and the initially sent out current pulse has a level of

$$\frac{100}{150 + 50} = \frac{1}{2} \text{ A}$$

Figure 8.6(d) shows the result that converges to the expected steady-state value of 0 A.

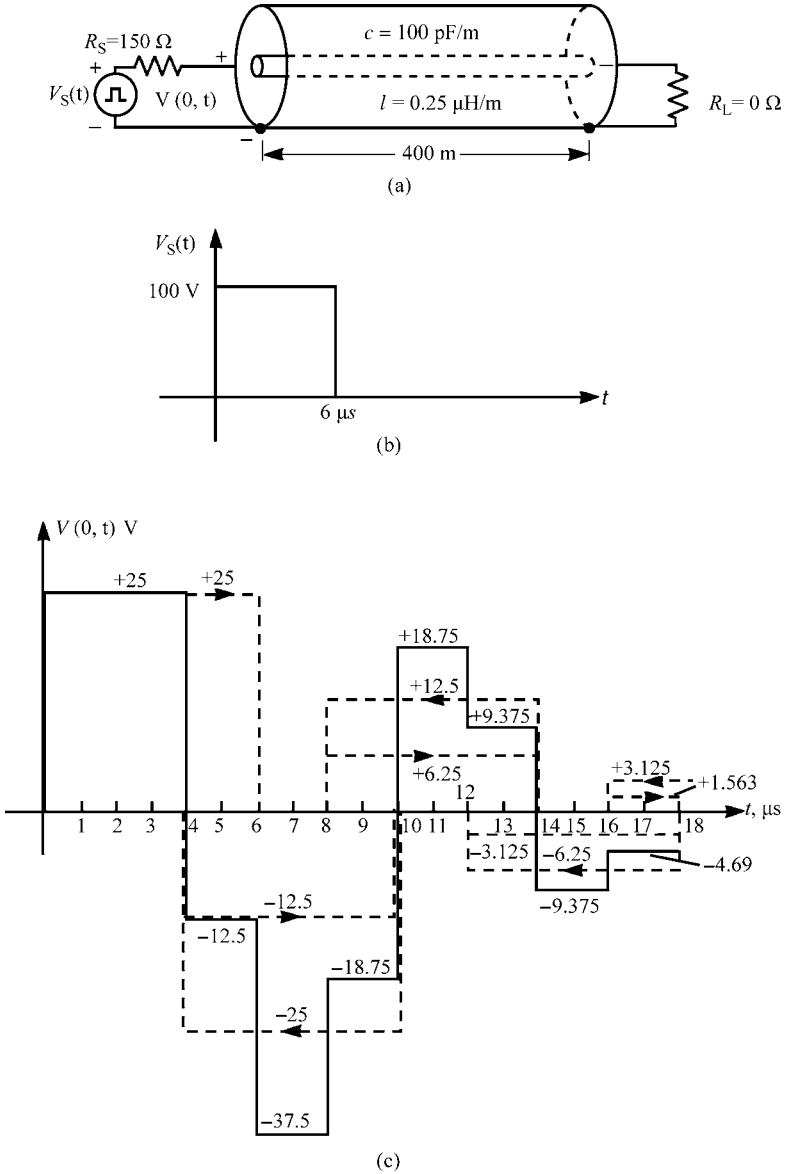


FIGURE 8.6 An example illustrating the computation of (c) the source voltage and (d) the load current for a pulse waveform illustrating the effect of pulse width, and (e) the effect of pulse shape.

In order to show the influence of the pulse *shape*, we reconsider this problem but with a pulse that rises steadily to 100 V in 6 μs as shown in Figure 8.6(e). The individual forward- and backward-traveling components are sketched with dashed lines and the total with a solid line. Observe that the waveforms at the end of the line

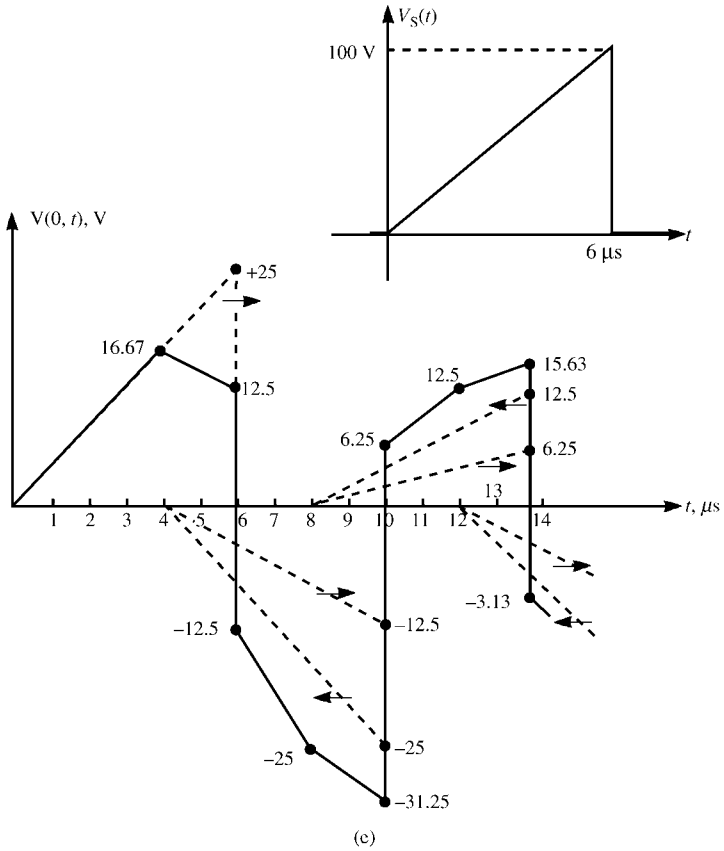
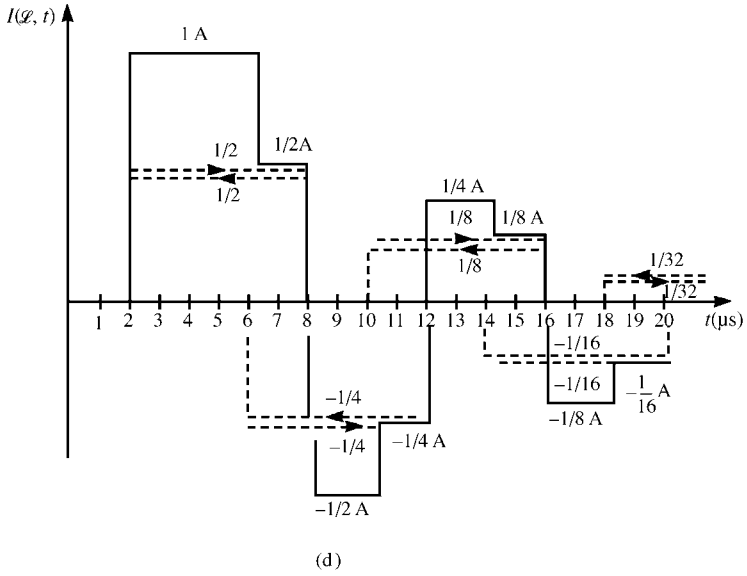


FIGURE 8.6 (Continued)

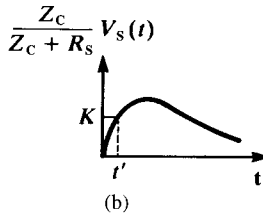
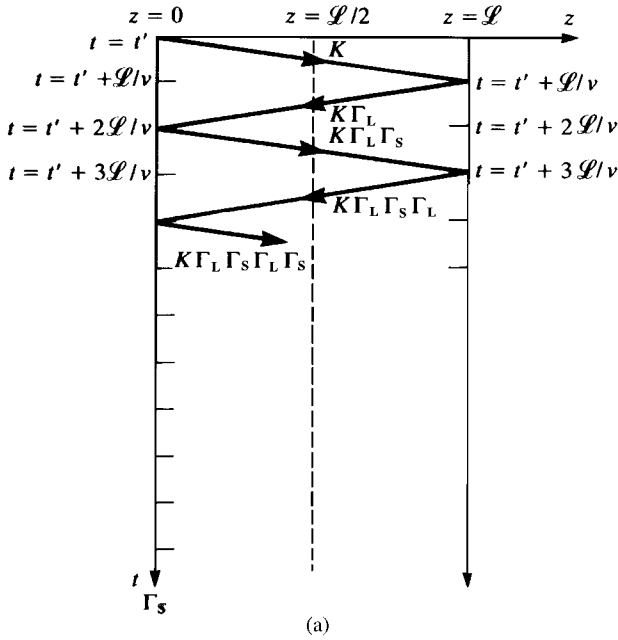


FIGURE 8.7 The lattice diagram.

have the same time shape in time as the source voltage. In other words, the first point to arrive at the source or load is the first point of $V_S(t)$ sent out at $t = 0$.

There are a number of other graphical methods that are equivalent to this graphical method. One of the more popular ones is referred to as the so-called lattice diagram [A.1]. This is illustrated in Figure 8.7(a). Position along the line is plotted along the upper horizontal axis and time is plotted vertically. The initial waveform applied to the line is $(Z_C/(Z_C + R_S))V_S(t)$, as shown in Figure 8.7(b). The lattice diagram simply tracks a particular point on this applied waveform, K at t' , as it travels back and forth along the line.

8.1.2 Series Solutions and the Difference Operator

An exact solution for this general result can be obtained for any $V_S(t)$ waveform by carrying through the above graphical method (or using the lattice diagram) in literal

form to yield

$$\begin{aligned}
 V(0, t) = \frac{Z_C}{Z_C + R_S} \{ & V_S(t) + (1 + \Gamma_S) \Gamma_L V_S(t - 2T_D) \\
 & + (1 + \Gamma_S) (\Gamma_S \Gamma_L) \Gamma_L V_S(t - 4T_D) \\
 & + (1 + \Gamma_S) (\Gamma_S \Gamma_L)^2 \Gamma_L V_S(t - 6T_D) + \dots \} \quad (8.14a)
 \end{aligned}$$

$$\begin{aligned}
 V(\mathcal{L}, t) = \frac{Z_C}{Z_C + R_S} \{ & (1 + \Gamma_L) V_S(t - T_D) + (1 + \Gamma_L) \Gamma_S \Gamma_L V_S(t - 3T_D) \\
 & + (1 + \Gamma_L) (\Gamma_S \Gamma_L)^2 V_S(t - 5T_D) + (1 + \Gamma_L) (\Gamma_S \Gamma_L)^3 V_S(t - 7T_D) + \dots \} \\
 = \frac{Z_C}{Z_C + R_S} (1 + \Gamma_L) \{ & V_S(t - T_D) + \Gamma_S \Gamma_L V_S(t - 3T_D) \\
 & + (\Gamma_S \Gamma_L)^2 V_S(t - 5T_D) + (\Gamma_S \Gamma_L)^3 V_S(t - 7T_D) + \dots \} \quad (8.14b)
 \end{aligned}$$

This succinct form of the solution gives the time-domain voltages explicitly as scaled versions of the input signal waveform $V_S(t)$, which are delayed by multiples of the line one-way delay T_D . To compute the total solution waveforms $V(0, t)$ and $V(\mathcal{L}, t)$, one simply draws the scaled and delayed $V_S(t)$ and adds the waveforms at corresponding time points according to (8.14).

Alternatively, this general result can be proved from an earlier frequency-domain exact solution given in Chapter 6 in (6.39a) for a lossless line. Substituting the relation for the phase constant in terms of the radian frequency and the velocity of propagation:

$$\beta = \omega/v$$

into that result yields

$$\hat{V}(z) = \frac{1 + \Gamma_L e^{-2j\omega T_D} e^{2j\omega z/v}}{1 - \Gamma_S \Gamma_L e^{-2j\omega T_D}} \frac{Z_C}{Z_C + R_S} \hat{V}_S e^{-j\omega z/v} \quad (8.15)$$

and we have substituted the line one-way time delay

$$T_D = \mathcal{L}/v$$

In terms of the Laplace transform variable s , we replace

$$s \iff j\omega$$

and (8.15) becomes, at the source, $z = 0$,

$$\hat{V}(0, s) = \left[\frac{1 + \Gamma_L e^{-2sT_D}}{1 - \Gamma_S \Gamma_L e^{-2sT_D}} \right] \frac{Z_C}{Z_C + R_S} \hat{V}_S(s) \quad (z = 0) \quad (8.16a)$$

and at the load, $z = \mathcal{L}$,

$$\hat{V}(\mathcal{L}, s) = \left[\frac{(1 + \Gamma_L) e^{-sT_D}}{1 - \Gamma_S \Gamma_L e^{-2sT_D}} \right] \frac{Z_C}{Z_C + R_S} \hat{V}_S(s) \quad (z = \mathcal{L}) \quad (8.16b)$$

Multiplying both sides of (8.16) by the common denominator gives

$$\left[1 - \Gamma_S \Gamma_L e^{-2sT_D} \right] \hat{V}(0, s) = \left[1 + \Gamma_L e^{-2sT_D} \right] \frac{Z_C}{Z_C + R_S} \hat{V}_S(s) \quad (8.17a)$$

$$\left[1 - \Gamma_S \Gamma_L e^{-2sT_D} \right] \hat{V}(\mathcal{L}, s) = (1 + \Gamma_L) e^{-sT_D} \frac{Z_C}{Z_C + R_S} \hat{V}_S(s) \quad (8.17b)$$

To put this into the time domain, we utilize the basic Laplace transform result of

$$e^{\pm smT_D} \hat{F}(s) \iff f(t \pm mT_D) \quad (8.18)$$

Hence, multiplication of a Laplace transformed function $\hat{F}(s)$ by $e^{\pm smT_D}$ gives the time-domain function advanced or delayed in time by mT_D . Using this result, (8.17) becomes

$$[V(0, t) - \Gamma_S \Gamma_L V(0, t - 2T_D)] = \frac{Z_C}{Z_C + R_S} [V_S(t) + \Gamma_L V_S(t - 2T_D)] \quad (8.19a)$$

$$[V(\mathcal{L}, t) - \Gamma_S \Gamma_L V(\mathcal{L}, t - 2T_D)] = \frac{Z_C}{Z_C + R_S} [1 + \Gamma_L] V_S(t - T_D) \quad (8.19b)$$

This represents a recursive solution. In other words, we obtain the present time solutions $V(0, t)$ and $V(\mathcal{L}, t)$ by using the solution at previous times that are two time delays before the present time, $V(0, t - 2T_D)$ and $V(\mathcal{L}, t - 2T_D)$ and the source voltage delayed by various time delays: $V_S(t)$, $V_S(t - T_D)$, and $V_S(t - 2T_D)$. So this recursive solution is obtained in a “bootstrapping” manner.

In order to obtain an explicit solution, we introduce the *time-shift* or *difference operator* D as

$$D^{\pm m} f(t) = f(t \pm mT_D) \quad (8.20)$$

In other words, the difference operator operates on a function of time to shift it ahead or backward in time. This difference operator obeys all the rules of algebra and can be manipulated as though it is an algebraic variable until it is used to return to the time domain using (8.20). We will have numerous occasions throughout this text to use this difference operator in solving *lossless* lines. Substituting this result into (8.19) gives

$$\left[1 - \Gamma_S \Gamma_L D^{-2} \right] V(0, t) = \frac{Z_C}{Z_C + R_S} [1 + \Gamma_L D^{-2}] V_S(t) \quad (8.21a)$$

$$\left[1 - \Gamma_S \Gamma_L D^{-2}\right] V(\mathcal{L}, t) = \frac{Z_C}{Z_C + R_S} \left[(1 + \Gamma_L) D^{-1}\right] V_S(t) \quad (8.21b)$$

Multiplying by D^2 gives

$$\left[D^2 - \Gamma_S \Gamma_L\right] V(0, t) = \frac{Z_C}{Z_C + R_S} [D^2 + \Gamma_L] V_S(t) \quad (8.22a)$$

$$\left[D^2 - \Gamma_S \Gamma_L\right] V(\mathcal{L}, t) = \frac{Z_C}{Z_C + R_S} [(1 + \Gamma_L) D] V_S(t) \quad (8.22b)$$

Dividing both sides by $[D^2 - \Gamma_S \Gamma_L]$ to put this in the form of a transfer function and using long division gives

$$\begin{aligned} V(0, t) &= \frac{Z_C}{Z_C + R_S} \left[\frac{D^2 + \Gamma_L}{D^2 - \Gamma_S \Gamma_L} \right] V_S(t) \\ &= \frac{Z_C}{Z_C + R_S} \left[1 + (1 + \Gamma_S) \Gamma_L D^{-2} + (1 + \Gamma_S) (\Gamma_S \Gamma_L) \Gamma_L D^{-4} \right. \\ &\quad \left. + (1 + \Gamma_S) (\Gamma_S \Gamma_L)^2 \Gamma_L D^{-6} + \dots \right] V_S(t) \end{aligned} \quad (8.23a)$$

$$\begin{aligned} V(\mathcal{L}, t) &= \frac{Z_C}{Z_C + R_S} \left[\frac{(1 + \Gamma_L) D}{D^2 - \Gamma_S \Gamma_L} \right] V_S(t) \\ &= \frac{Z_C}{Z_C + R_S} (1 + \Gamma_L) \left[D^{-1} + \Gamma_S \Gamma_L D^{-3} + (\Gamma_S \Gamma_L)^2 D^{-5} + \dots \right] V_S(t) \end{aligned} \quad (8.23b)$$

where we have used the long division result:

$$\frac{1}{D^2 - \Gamma_S \Gamma_L} = D^{-2} + \Gamma_S \Gamma_L D^{-4} + (\Gamma_S \Gamma_L)^2 D^{-6} + (\Gamma_S \Gamma_L)^3 D^{-8} + \dots \quad (8.24)$$

Operating on $V_S(t)$ with the various powers of D in the expansion using (8.20) returns to the time domain giving results that are identical to (8.14):

$$\begin{aligned} V(0, t) &= \frac{Z_C}{Z_C + R_S} \{V_S(t) + (1 + \Gamma_S) \Gamma_L V_S(t - 2T_D) \\ &\quad + (1 + \Gamma_S) (\Gamma_S \Gamma_L) \Gamma_L V_S(t - 4T_D) \\ &\quad + (1 + \Gamma_S) (\Gamma_S \Gamma_L)^2 \Gamma_L V_S(t - 6T_D) + \dots\} \end{aligned} \quad (8.14a)$$

$$\begin{aligned} V(\mathcal{L}, t) &= \frac{Z_C}{Z_C + R_S} (1 + \Gamma_L) \{V_S(t - T_D) \\ &\quad + \Gamma_S \Gamma_L V_S(t - 3T_D) + (\Gamma_S \Gamma_L)^2 V_S(t - 5T_D) \\ &\quad + (\Gamma_S \Gamma_L)^3 V_S(t - 7T_D) + \dots\} \end{aligned} \quad (8.14b)$$

Thus, for a two-conductor lossless line having resistive loads, one can immediately sketch the terminal voltage waveforms as scaled and delayed versions of the source voltage waveform $V_S(t)$.

A number of important results can be immediately seen from the general result in (8.14). For example, suppose the line is “matched” at the load, that is, $R_L = Z_C$. (Note that a matched line requires a completely resistive termination since Z_C for a lossless line is a real number.) For a matched line, the load reflection coefficient is zero, $\Gamma_L = 0$, and hence (8.14) reduce to

$$V(0, t) = \frac{Z_C}{Z_C + R_S} V_S(t) \quad (\text{for } R_L = Z_C) \quad (8.25a)$$

$$V(\mathcal{L}, t) = \frac{Z_C}{Z_C + R_S} V_S(t - T_D) \quad (\text{for } R_L = Z_C) \quad (8.25b)$$

This is the ideal case; the load voltage is identical to the initially sent out wave but scaled by the voltage division term and delayed by one time delay. Similarly, for a line that is matched at the source, that is, $R_S = Z_C$, (8.14) reduce to

$$V(0, t) = \frac{Z_C}{Z_C + R_S} [V_S(t) + \Gamma_L V_S(t - 2T_D)] \quad (\text{for } R_S = Z_C) \quad (8.26a)$$

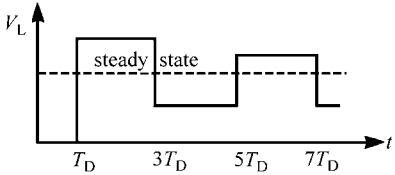
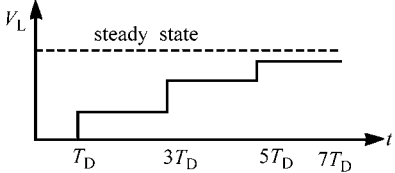
$$V(\mathcal{L}, t) = \frac{Z_C}{Z_C + R_S} (1 + \Gamma_L) V_S(t - T_D) \quad (\text{for } R_S = Z_C) \quad (8.26b)$$

With the line matched at the source but not at the load, the source voltage $V(0, t)$ is a combination of the initially sent out voltage and the voltage reflected at the load. No further reflections occur at the sources since it is matched. Similarly, with the line matched at the source but not at the load, the load voltage $V(\mathcal{L}, t)$ is the sum of the incoming wave and that immediately reflected at the load.

Mismatched lines $\Gamma_S \neq 0$ and $\Gamma_L \neq 0$ give rise to terminal voltages that do not immediately assume their steady-state voltages but converge to it in some fashion. Some of these converge by oscillating about the steady-state voltage, whereas others rise from zero to the steady-state value. Table 8.1 shows when this behavior occurs. Inspection of the load voltage expression in Eq. (8.14b) shows that the additional terms in this expression depend on the products of various powers of $(\Gamma_S \Gamma_L)$ and the initially sent out voltage wave. For the case where the source and reflection coefficients are of opposite sign, this product will be negative with its odd powers being negative but its even powers being positive. Hence, the waveform will oscillate about the steady-state value. On the contrary, if the source and reflection coefficients are of the same sign, all products will be positive and the load voltage waveform will rise steadily to the steady-state value. This behavior will explain how certain matching schemes achieve signal integrity, which will be considered in a later section.

The difference operator given in (8.20) is a powerful tool for *lossless lines*. Time shifting can be accomplished as a simple algebraic manipulation of this operator. We will have numerous occasions to use this powerful result.

TABLE 8.1 Effects of the signs of the reflection coefficients on the load voltage.

| Γ_S | Γ_L | Load voltage waveform |
|-------------|-------------|---|
| - | + |  |
| $R_S < Z_C$ | $R_L > Z_C$ | |
| + | - |  |
| $R_S > Z_C$ | $R_L < Z_C$ | |
| + | + | |
| $R_S > Z_C$ | $R_L > Z_C$ | |
| - | - | |
| $R_S < Z_C$ | $R_L < Z_C$ | |

8.1.3 The Method of Characteristics and a Two-Port Model of the Line

The previous sections have shown graphical and series methods for sketching the time-domain solution of the transmission-line equations for linear resistive loads. It is frequently desirable to have a numerical method that is suitable for a digital computer and will handle nonlinear as well as dynamic loads. The following method is referred to as the *method of characteristics*. The numerical implementation is attributed to Branin and was originally described in [1].

The method of characteristics seeks to transform the partial differential equations of the transmission line into ordinary differential equations that are easily integrable. To this end, we define the *characteristic curves* in the $z-t$ plane shown in Figure 8.8 as

$$\frac{dz}{dt} = \frac{1}{\sqrt{lc}} \tag{8.27a}$$

$$\frac{dz}{dt} = -\frac{1}{\sqrt{lc}} \tag{8.27b}$$

The differential changes in the line voltage and current are

$$dV(z, t) = \frac{\partial V(z, t)}{\partial z} dz + \frac{\partial V(z, t)}{\partial t} dt \tag{8.28a}$$

$$dI(z, t) = \frac{\partial I(z, t)}{\partial z} dz + \frac{\partial I(z, t)}{\partial t} dt \tag{8.28b}$$

Substituting the transmission-line equations in (8.1) into (8.28) gives

$$dV(z, t) = \left(-l \frac{\partial I(z, t)}{\partial t} \right) dz + \frac{\partial V(z, t)}{\partial t} dt \tag{8.29a}$$

$$dI(z, t) = \left(-c \frac{\partial V(z, t)}{\partial t} \right) dz + \frac{\partial I(z, t)}{\partial t} dt \quad (8.29b)$$

Along the forward characteristic defined by (8.27a), $dz = (1/\sqrt{lc}) dt$, these become

$$dV(z, t) = \left(-Z_C \frac{\partial I(z, t)}{\partial t} + \frac{\partial V(z, t)}{\partial t} \right) dt \quad (8.30a)$$

$$dI(z, t) = \left(-\frac{1}{Z_C} \frac{\partial V(z, t)}{\partial t} + \frac{\partial I(z, t)}{\partial t} \right) dt \quad (8.30b)$$

where we have substituted $Z_C = (\sqrt{l/c})$. Similarly, along the backward characteristic defined by (8.27b), $dz = -(1/\sqrt{lc}) dt$, these become

$$dV(z, t) = \left(Z_C \frac{\partial I(z, t)}{\partial t} + \frac{\partial V(z, t)}{\partial t} \right) dt \quad (8.31a)$$

$$dI(z, t) = \left(\frac{1}{Z_C} \frac{\partial V(z, t)}{\partial t} + \frac{\partial I(z, t)}{\partial t} \right) dt \quad (8.31b)$$

Multiplying (8.30b) by the characteristic impedance $Z_C = \sqrt{l/c}$ and adding the equations gives

$$dV(z, t) + Z_C dI(z, t) = 0 \quad (8.32a)$$

Similarly, multiplying (8.31b) by the characteristic impedance $Z_C = \sqrt{l/c}$ and subtracting the equations gives

$$dV(z, t) - Z_C dI(z, t) = 0 \quad (8.32b)$$

Equation (8.32a) holds along the characteristic curve defined by (8.27a) with phase velocity $v = 1/\sqrt{lc}$, whereas (8.32b) holds along the characteristic curve defined by (8.27b) with the same phase velocity. This is illustrated in Figure 8.8. These are directly integrable showing that the difference between two voltages at two points on a given characteristic is related to the difference between two currents on the same characteristic. Therefore, from Figure 8.8 we may obtain

$$[V(\mathcal{L}, t) - V(0, t - T_D)] = -Z_C [I(\mathcal{L}, t) - I(0, t - T_D)] \quad (8.33a)$$

$$[V(0, t) - V(\mathcal{L}, t - T_D)] = +Z_C [I(0, t) - I(\mathcal{L}, t - T_D)] \quad (8.33b)$$

where the one-way delay is $T_D = \mathcal{L}/v$.

A very useful two-port model of the line can be obtained by rewriting (8.33) as

$$[V(0, t) - Z_C I(0, t)] = [V(\mathcal{L}, t - T_D) - Z_C I(\mathcal{L}, t - T_D)] \quad (8.34a)$$

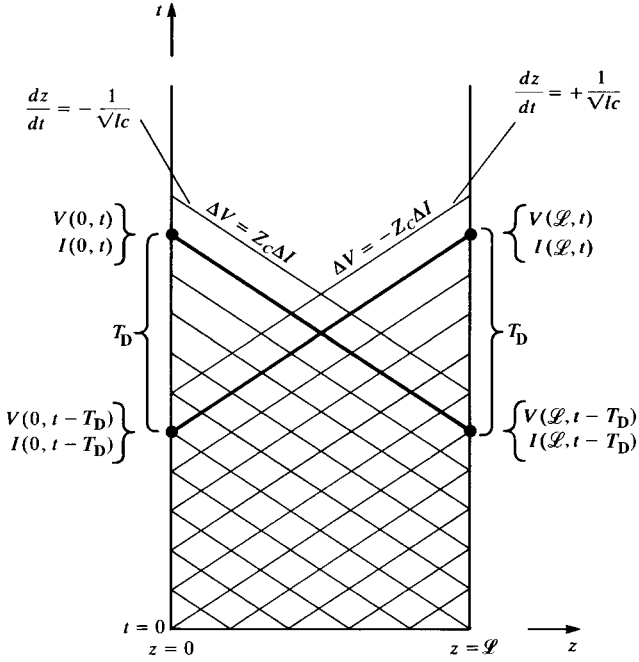


FIGURE 8.8 Illustration of characteristic curves for the method of characteristics.

$$[V(\mathcal{L}, t) + Z_C I(\mathcal{L}, t)] = [V(0, t - T_D) + Z_C I(0, t - T_D)] \quad (8.34b)$$

Hence, the voltage and current at one end of the line at some present time can be found from the voltage and current at the other end of the line at one time delay earlier. Hence, we obtain another recursive solution. This can be put in the form of an equivalent circuit by writing (8.34) as

$$V(0, t) = Z_C I(0, t) + E_0(\mathcal{L}, t - T_D) \quad (8.35a)$$

where

$$E_0(\mathcal{L}, t - T_D) = V(\mathcal{L}, t - T_D) - Z_C I(\mathcal{L}, t - T_D) \quad (8.35b)$$

and

$$V(\mathcal{L}, t) = -Z_C I(\mathcal{L}, t) + E_{\mathcal{L}}(0, t - T_D) \quad (8.36a)$$

where

$$E_{\mathcal{L}}(0, t - T_D) = V(0, t - T_D) + Z_C I(0, t - T_D) \quad (8.36b)$$

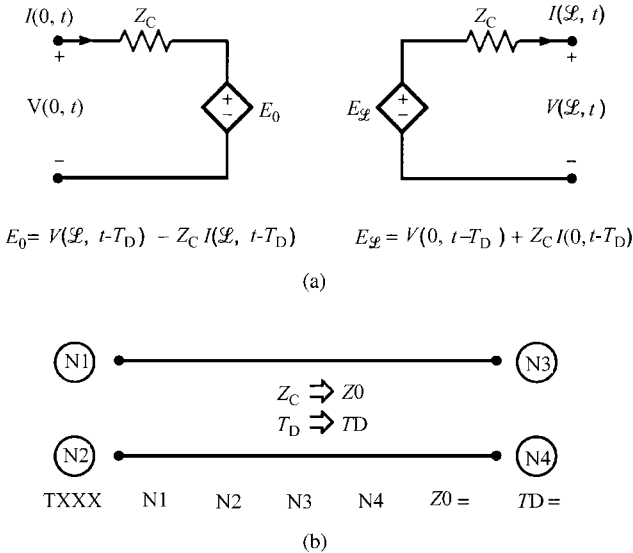


FIGURE 8.9 A time-domain equivalent circuit of a two-conductor line in terms of time-delayed controlled sources obtained from the method of characteristics (Bratin’s method) as implemented in SPICE.

Equations (8.35) and (8.36) suggest the equivalent circuit of the total line shown in Figure 8.9(a). The controlled source $E_\phi(0, t - T_D)$ is produced by the voltage and current at the input to the line at a time equal to a one-way transit delay earlier than the present time. Similarly, the controlled source $E_0(L, t - T_D)$ is produced by the voltage and current at the line output at a time equal to a one-way transit delay earlier than the present time.

Equations (8.34) can also be obtained in a simpler manner by manipulating the basic solutions given in (8.3) using the difference operator. Write (8.3) as

$$V(z, t) = V^+ \left(t - \frac{z}{v} \right) + V^- \left(t + \frac{z}{v} \right) \tag{8.37a}$$

$$Z_C I(z, t) = V^+ \left(t - \frac{z}{v} \right) - V^- \left(t + \frac{z}{v} \right) \tag{8.37b}$$

where we have multiplied (8.3b) by the characteristic impedance Z_C . Adding and subtracting these gives

$$V(z, t) + Z_C I(z, t) = 2V^+ \left(t - \frac{z}{v} \right) \tag{8.38a}$$

$$V(z, t) - Z_C I(z, t) = 2V^- \left(t + \frac{z}{v} \right) \tag{8.38b}$$

Evaluating these at $z = 0$ and $z = \mathcal{L}$ gives

$$V(0, t) + Z_C I(0, t) = 2V^+(t) \quad (8.39a)$$

$$V(0, t) - Z_C I(0, t) = 2V^-(t) \quad (8.39b)$$

$$V(\mathcal{L}, t) + Z_C I(\mathcal{L}, t) = 2V^+(t - T_D) = 2D^{-1}V^+(t) \quad (8.39c)$$

$$V(\mathcal{L}, t) - Z_C I(\mathcal{L}, t) = 2V^-(t + T_D) = 2D^{+1}V^-(t) \quad (8.39d)$$

Multiplying (8.39d) by D^{-1} (which amounts to time shifting the equation) and substituting into (8.39b) gives (8.34a):

$$[V(0, t) - Z_C I(0, t)] = [V(\mathcal{L}, t - T_D) - Z_C I(\mathcal{L}, t - T_D)] \quad (8.34a)$$

Similarly, multiplying (8.39a) by D^{-1} (which also amounts to time shifting the equation) and substituting into (8.39c) gives (8.34b):

$$[V(\mathcal{L}, t) + Z_C I(\mathcal{L}, t)] = [V(0, t - T_D) + Z_C I(0, t - T_D)] \quad (8.34b)$$

8.1.4 The SPICE (PSPICE) Solution for Lossless Lines

The equivalent circuit shown in Figure 8.9(a) is an exact solution of the transmission-line equations for a *lossless* two-conductor uniform transmission line. The circuit analysis program SPICE contains this *exact model* among its list of available circuit element models that the user may call [A.2, A.3, A.5, A.6]. The model is the TXXX element, where XXX is the model name chosen by the user. SPICE uses controlled sources having time delay to construct the equivalent circuit of Figure 8.9(a). The format of the SPICE command to invoke this model is given in Figure 8.9(b):

$$\text{TXXX N1 N2 N3 N4 ZO} = Z_C \quad \text{TD} = T_D$$

The user needs to input only the characteristic impedance of the line Z_C (SPICE refers to this parameter as ZO) and the one-way transit delay T_D (SPICE refers to this parameter as TD). Usually, nodes 2 and 4 are the SPICE universal ground node, that is, N2 = 0 and N4 = 0. Thus, SPICE will produce exact solutions of the transmission-line equations. Furthermore, nonlinear terminations such as diodes and transistors as well as dynamic terminations such as capacitors and inductors are easily handled with the SPICE code, whereas a graphical solution for these types of loads would be quite difficult. This author highly recommends the use of SPICE for the incorporation of two-conductor *lossless* transmission-line effects into any analysis of an electronic circuit. It is simple and straightforward to incorporate the transmission-line effects in any time-domain analysis of an electronic circuit, and, more importantly, models of the complicated, but typical, nonlinear loads such as diodes and transistors as well

as inductors and capacitors already exist in SPICE and can be called on by the user rather than the user needing to develop models for these devices.

As an example of the use of SPICE or the personal computer version PSPICE to model two-conductor lossless transmission lines in the time domain, consider the time-domain analysis of the circuit of Figure 8.5. The 30-V source is modeled with the PWL (piecewise linear) model (see Appendix B for a tutorial on SPICE) as transitioning from 0 to 30 V in 0.01 μs and remaining there throughout the analysis time interval of 20 μs as shown in Figure 8.10(a). The nodes are numbered as in Figure 8.10(a) and the SPICE (PSPICE) program is

```
FIGURE 8.5
VS 1 0 PWL(0 0 0.01U 30 20U 30)
TLINE 1 0 2 0 Z0=50 TD=2U
RL 2 0 100
.TRAN 0.01U 20U 0 0.01U
.PRINT TRAN V(2) I(VS)
.PROBE
.END
```

The results for the load voltage are plotted using the .PROBE option of the personal computer version PSPICE in Figure 8.10(b), and the input current to the line is plotted in Figure 8.10(c). Comparing these with the hand-calculated results shown in Figure 8.5 shows exact agreement.

The problem shown in Figure 8.6 is coded as shown in Figure 8.11(a). The source voltage is represented as having rise and fall times of 0.01 μs , as shown in Figure 8.11(a). The nodes are numbered in Figure 8.11(a), and the SPICE coding is

```
FIGURE 8.6
VS 1 0 PWL(0 0 0.01U 100 6U 100 6.01U 0)
RS 1 2 150
TLINE 2 0 3 0 Z0=50 TD=2U
RL 3 0 1E-6
.TRAN 0.01U 20U 0 0.01U
.PRINT TRAN V(2) I(RL)
.PROBE
.END
```

The solution for the input voltage V(2) is plotted in Figure 8.11(b) and is identical to the graphical solution in Figure 8.6(c). The solution for the load current I(RL) is shown in 8.11(c) and is identical to the graphical solution in Figure 8.6(d). For the other waveform shown in Figure 8.6(e), we need to change only the source specification to

```
VS 1 0 PWL(0 0 6U 100 6.01U 0)
```

The result is shown in Figure 8.11(d) and is identical to the graphical solution shown in Figure 8.6(e).

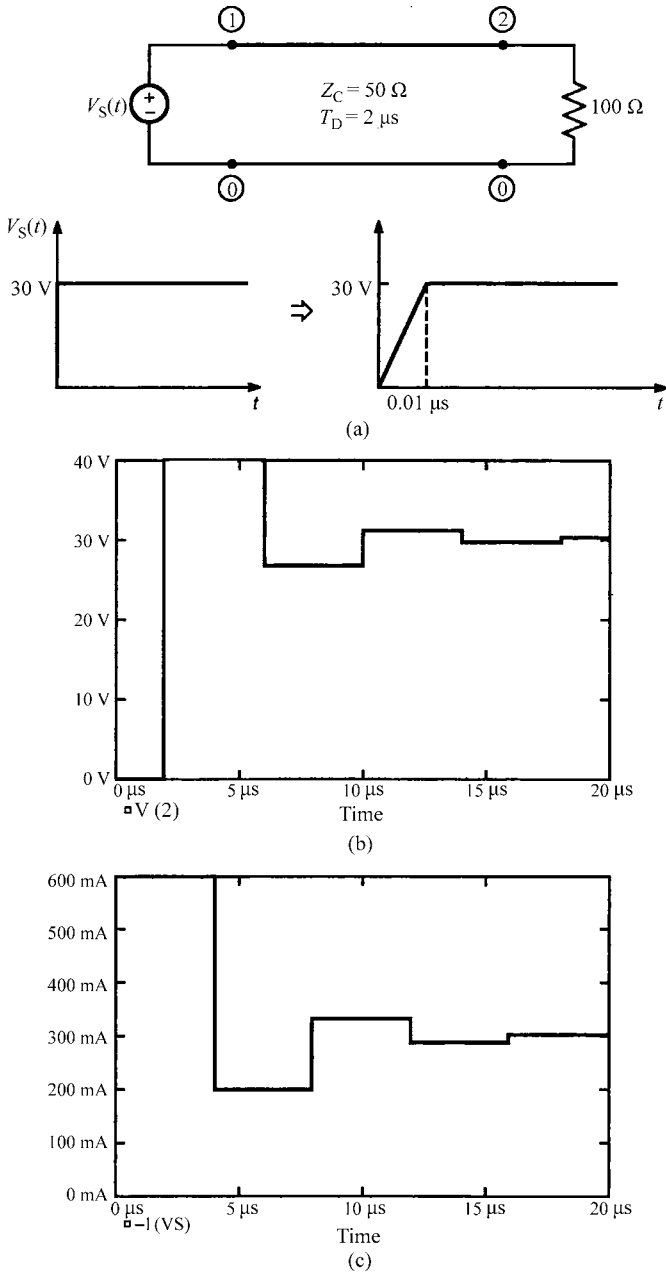


FIGURE 8.10 Results of the exact SPICE model for the problem of Figure 8.5.

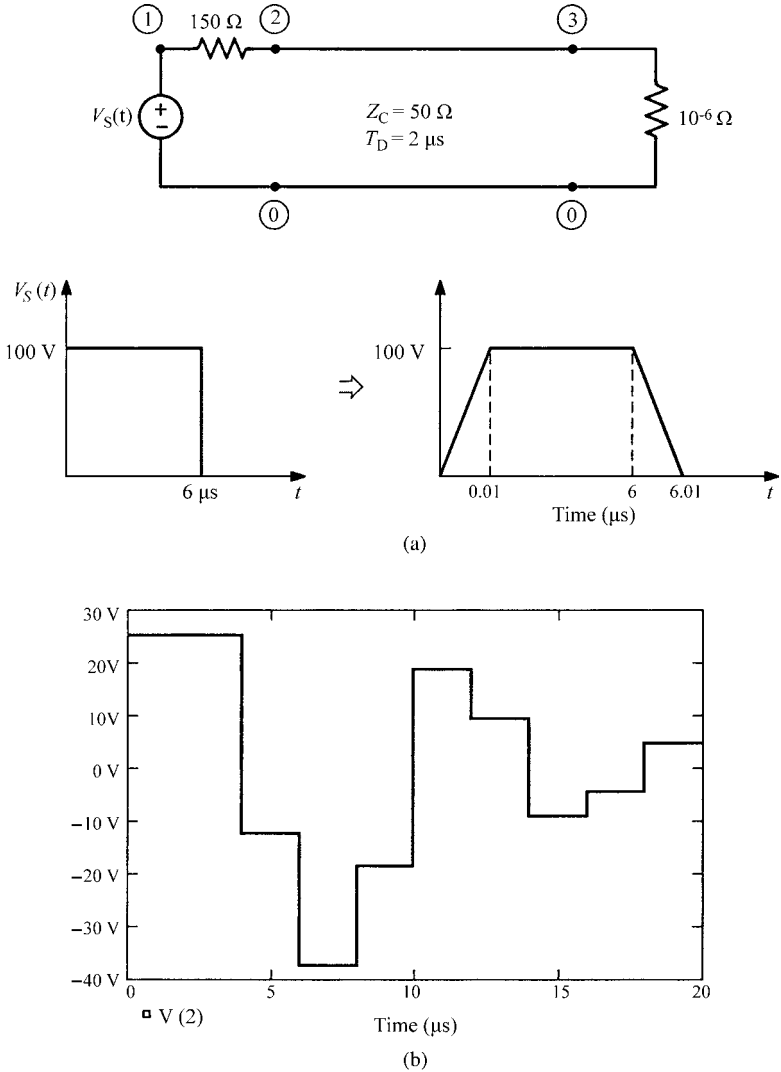


FIGURE 8.11 Results of the exact SPICE model for the problem of Figure 8.6(c)–(e).

8.1.5 The Laplace Transform Solution

An alternative method of solution of the transmission-line equations is the Laplace transform method. Taking the Laplace transform of the transmission-line equations in (8.1) with respect to time reduces these to ordinary differential equations as

$$\frac{d}{dz} \hat{V}(z, s) = -sI \hat{I}(z, s) \tag{8.40a}$$

$$\frac{d}{dz} \hat{I}(z, s) = -sC \hat{V}(z, s) \tag{8.40b}$$

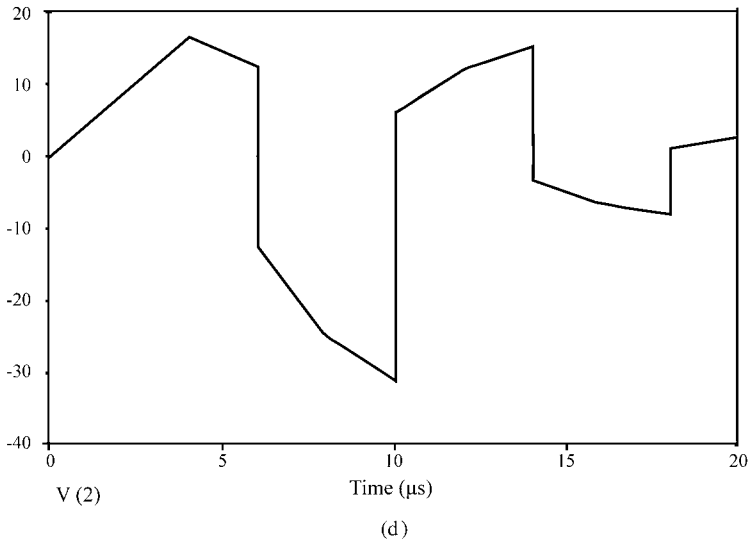
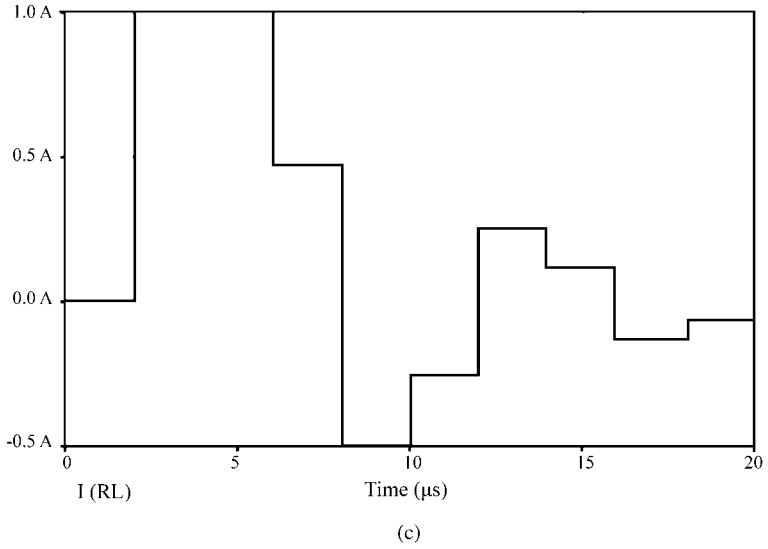


FIGURE 8.11 (Continued)

where s is the Laplace transform variable [A.2, A.5]. Differentiating each equation with respect to z and substituting the other gives the *uncoupled* second-order differential equations as

$$\frac{d^2}{dz^2} \hat{V}(z, s) = \frac{s^2}{v^2} \hat{V}(z, s) \tag{8.41a}$$

$$\frac{d^2}{dz^2} \hat{I}(z, s) = \frac{s^2}{v^2} \hat{I}(z, s) \tag{8.41b}$$

where $v = 1/\sqrt{lc}$ is the velocity of propagation of the waves on the line. The solution to these is simply [A.2, A.5]

$$\hat{V}(z, s) = e^{-sz/v} \hat{V}^+(s) + e^{sz/v} \hat{V}^-(s) \tag{8.42a}$$

$$\hat{I}(z, s) = \frac{1}{Z_C} e^{-sz/v} \hat{V}^+(s) - \frac{1}{Z_C} e^{sz/v} \hat{V}^-(s) \tag{8.42b}$$

where the characteristic impedance is $Z_C = \sqrt{l/c}$. Using the time shift property of the Laplace transform:

$$e^{\pm as} \hat{F}(s) = f(t \pm a) \tag{8.43}$$

gives the time-domain solution in (8.3).

8.1.5.1 Lines with Capacitive and Inductive Loads There are two advantages of using this Laplace transform method of solution. It allows a straightforward solution when the terminations contain dynamic elements, that is, inductive and/or capacitive elements. In addition, it also provides a method of including \sqrt{f} skin-effect losses as we will see later.

Sketching the source and load voltages on a line that has resistive terminations is quite simple. Sketching these voltages when one or both of the terminations are dynamic (capacitive or inductive) is a bit more complicated, but the use of the Laplace transform simplifies that process. Consider the situation shown in Figure 8.12(a), where the source resistance is $R_S = Z_C$ and hence the line is matched at the source. The load, however, is a capacitor representing, perhaps, the input to a CMOS logic gate. The source voltage is a pulse or step function rising to a level of V_0 volts and remaining there, that is, $V_S(t) = V_0 u(t)$, where $u(t)$ is the unit step function. This represents the transition from a logic 0 to a logic 1. In order to analyze this, we transform it with the Laplace transform, where s denotes the Laplace transform, variable as shown in Figure 8.12(b). The capacitor has an impedance of $Z_L = 1/sC$ [A.2, A.5]. The reflection coefficient at the source is zero as it is matched:

$$\Gamma_S = 0 \tag{8.44a}$$

and the reflection coefficient at the load is

$$\begin{aligned} \Gamma_L &= \frac{Z_L - Z_C}{Z_L + Z_C} \\ &= \frac{\frac{1}{sC} - Z_C}{\frac{1}{sC} + Z_C} \\ &= \frac{1 - sT_C}{1 + sT_C} \end{aligned} \tag{8.44b}$$

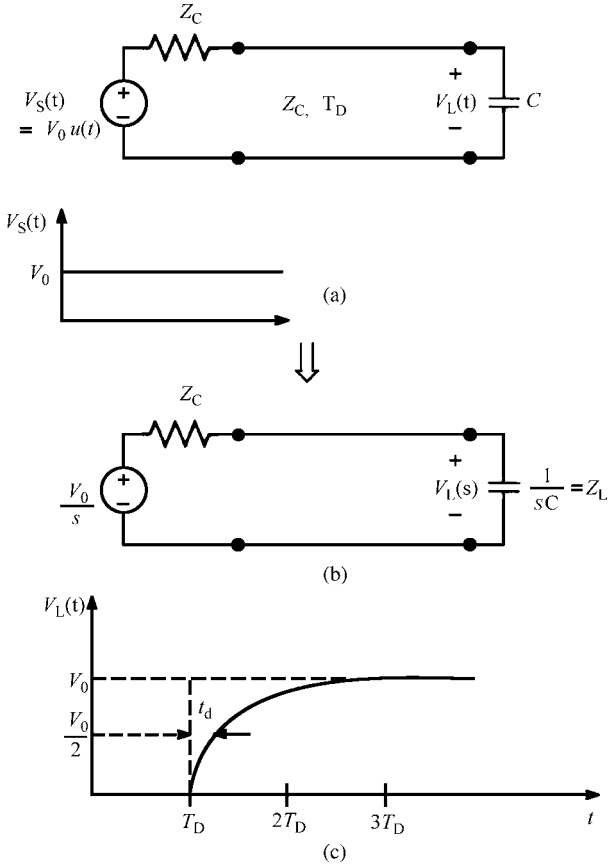


FIGURE 8.12 Illustration of the Laplace transform method of computing the load voltage time-domain response for a capacitive load.

and the time constant is denoted as [A.2, A.5]

$$T_C = Z_C C \tag{8.45}$$

Since the source is matched, we will only have a forward-traveling wave incident at the load and a reflected wave traveling back to the source. The load voltage is

$$V_L(t) = (1 + \Gamma_L) \frac{Z_C}{(R_S = Z_C) + Z_C} V_0 u(t - T_D) \tag{8.46}$$

Transforming this yields

$$V_L(s) = (1 + \Gamma_L(s)) \frac{1}{2} V_S(s) e^{-sT_D}$$

$$\begin{aligned}
 &= \frac{\frac{1}{T_C}}{\left(s + \frac{1}{T_C}\right)s} V_0 e^{-sT_D} \\
 &= \left[\frac{1}{s} - \frac{1}{\left(s + \frac{1}{T_C}\right)} \right] V_0 e^{-sT_D} \quad (8.47)
 \end{aligned}$$

The $1/2$ represents the voltage division factor for the initially sent out wave: $Z_C / ((R_S = Z_C) + Z_C) = 1/2$. The term e^{-sT_D} represents a one-way time delay of T_D . The final result has been expanded in partial fractions. Inverse transforming gives [A.2, A.5]

$$V_L(t) = V_0 u(t - T_D) - e^{-\frac{(t-T_D)}{T_C}} V_0 u(t - T_D) \quad (8.48)$$

This waveform is sketched in Figure 8.12(c). This result makes sense because the incoming traveling wave is a pulse with zero rise time. Initially, the capacitor looks like a short circuit gradually transitioning to an open circuit. Ideally (with an open-circuit load instead of a capacitor), the load voltage should rise abruptly to V_0 at $t = T_D$. The effect of the capacitor is to introduce a time delay (measured at the 50 % point) t_d , thereby giving the load voltage a rise time when the source had none. Evaluating (8.48) for $V_L(t) = 0.5V_0$ gives this time delay as

$$\begin{aligned}
 t_d &= 0.693T_C \\
 &= 0.693CZ_C \quad (8.49)
 \end{aligned}$$

For example, for a 50- Ω line and a 5-pF load capacitor, we would obtain a time delay of 0.173 ns in addition to the line one-way time delay of T_D .

Suppose we replace the capacitive load with an inductive one as shown in Figure 8.13(a). Carrying out the analysis of the previous section but with $Z_L = sL$ gives a similar result. The reflection coefficient at the source is again zero as it is matched:

$$\Gamma_S = 0 \quad (8.50a)$$

and the reflection coefficient at the load is

$$\begin{aligned}
 \Gamma_L &= \frac{Z_L - Z_C}{Z_L + Z_C} \\
 &= \frac{sL - Z_C}{sL + Z_C} \\
 &= \frac{sT_L - 1}{sT_L + 1} \quad (8.50b)
 \end{aligned}$$

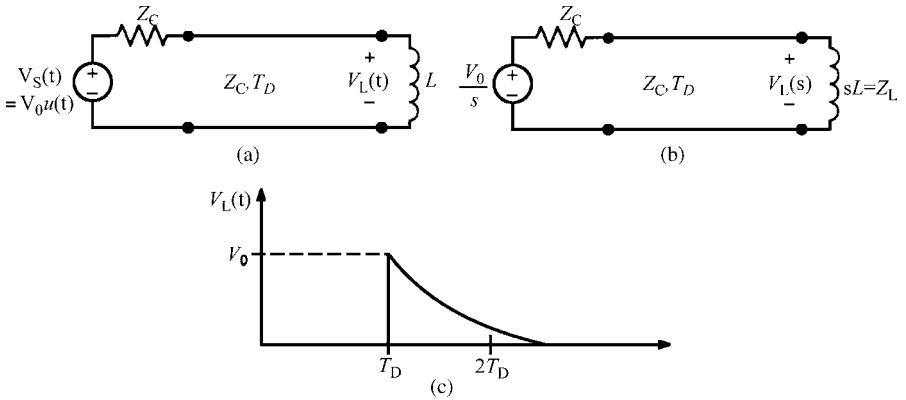


FIGURE 8.13 Illustration of the Laplace transform method of computing the load voltage time-domain response for an inductive load.

and the time constant is denoted as [A.2, A.5]

$$T_L = \frac{L}{Z_C} \tag{8.51}$$

The transformed load voltage is

$$\begin{aligned} V_L(s) &= (1 + \Gamma_L(s)) \frac{1}{2} V_S(s) e^{-sT_D} \\ &= \frac{1}{\left(s + \frac{1}{T_L}\right)} V_0 e^{-sT_D} \end{aligned} \tag{8.52}$$

Inverse transforming this gives [A.2, A.5]

$$V_L(t) = V_0 e^{-\frac{(t-T_D)}{T_L}} u(t - T_D) \tag{8.53}$$

which is plotted in Figure 8.13(c). This result makes sense because the incoming traveling wave at the load is a pulse with zero rise time. Initially, the inductor looks like an open circuit gradually becoming a short circuit.

8.1.6 Lumped-Circuit Approximate Models of the Line

As was the case for the frequency-domain analyses, the line may, under certain restrictions, be approximated with a lumped-circuit model as shown in Figure 8.14. Figure 8.14(b) shows the so-called lumped-Pi model, and Figure 8.14(c) shows the so-called lumped-T model. The lumped-Pi model extends the prediction frequency

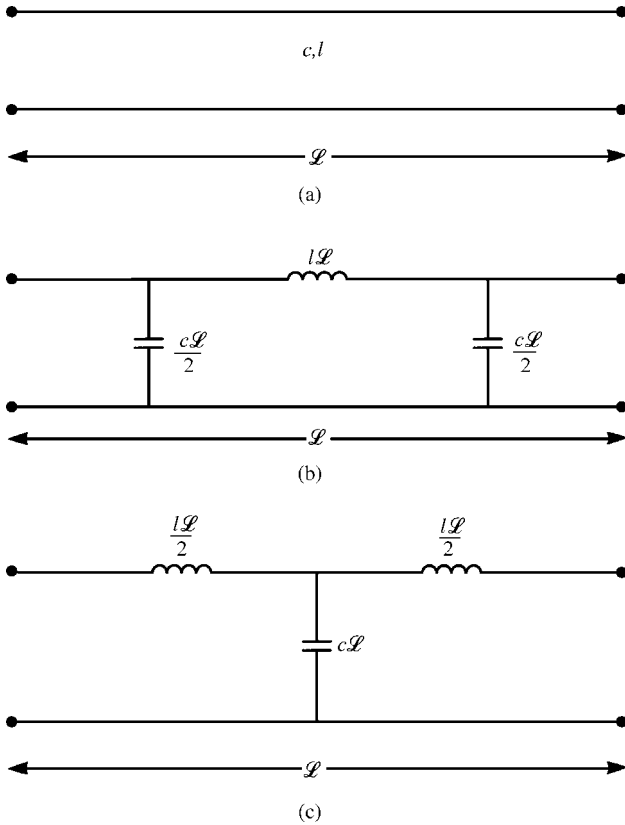


FIGURE 8.14 Illustration of (b) lumped-Pi and (c) lumped-T approximate time-domain circuits.

range slightly larger than that of the lumped-T model for high-impedance loads, that is, $R_S, R_L \gg Z_C$, and vice versa [B.15].

8.1.6.1 When is the Line Electrically Short in the Time Domain? In previous chapters, we noted that lumped-circuit models of a distributed parameter structure such as a transmission line are valid only so long as the line length is electrically short at the excitation frequency. For the time-domain analysis this presents problems because a time-domain waveform contains a continuum of sinusoidal frequency components according to Fourier analysis. However, if we specialize the analysis to the primary time-domain waveforms today, digital clock and data pulse trains, we can obtain a useful criterion for this. In Section 1.6.2 of Chapter 1, we showed that a reasonable criterion for the maximum significant spectral content of a digital waveform (its bandwidth) consisting of a periodic pulse train of trapezoidal pulses having equal rise

and fall times of τ_r is

$$\text{BW} = \frac{1}{\tau_r} \text{ Hz} \quad (8.54)$$

In order for the line to be electrically short at the highest significant frequency, we require that

$$\begin{aligned} \mathcal{L} &< \frac{1}{10} \lambda \\ &= \frac{1}{10} \frac{v}{f_{\max}} \end{aligned} \quad (8.55)$$

Substituting (8.54), $f_{\max} = 1/\tau_r$, yields

$$\tau_r > 10 T_D \quad (8.56)$$

In other words, the pulse rise and fall times must be greater than approximately 10 one-way time delays of the line in order for the line to be classified as “electrically short.” For example, for a pulse train having 100 ns rise and fall times and a line whose surrounding medium is free space, the total line length should not exceed 3 m. On the contrary, for a stripline representing a printed circuit board with innerplanes and a pulse train having 1 ns rise and fall times, the maximum line length should not exceed 1.4 cm (0.55 in.).

For today’s high-speed digital systems, the maximum length allowed in order for the line to be electrically short and the lumped-circuit models of Figure 8.14 to be valid often requires impractically short lengths of PCB lands. In order to extend the frequency range of validity of these lumped-circuit models, one might divide the total line length into sections that are electrically short and model each section with a lumped-Pi or lumped-T structure. This gives a progressively very large lumped circuit. It has been shown, however, that this process for such lines does not extend the frequency range enough to warrant the resulting complexity of the lumped circuit [B.15].

8.1.7 The Time-Domain to Frequency-Domain (TDFD) Transformation Method

The solution of a *lossless line* is virtually a trivial process using the SPICE (PSPICE) circuit analysis program and the *exact* model of a *lossless* line that is built into that program. Losses are not included in that model and are difficult to handle, as we will see in subsequent sections of this chapter. However, a simple technique for determining the time-domain response of a transmission line that will handle losses is known as the *time-domain to frequency-domain transformation* or TDFD method. This is a straightforward adaptation of a common analysis technique for lumped, linear circuits and systems that was described in Section 1.6.3 of Chapter 1 [A.2]. Here, we briefly

review that method. The only potential drawback to the method is that it is restricted to *linear loads* since the method inherently relies on the principle of superposition. However, it is an alternative technique for verifying other methods. Consider the *single-input, single-output lumped linear system* shown in Figure 8.15(a). The input to the system is denoted as $x(t)$, the output is denoted by $y(t)$, and the *unit impulse response* ($x(t) = \delta(t)$, $y(t) = h(t)$) is denoted by $h(t)$. The independent variable for the lumped system is time denoted by t . In the time domain, the response is obtained via the *convolution integral* [A.2, A.5]

$$y(t) = \int_0^t h(t - \tau) x(\tau) d\tau \tag{8.57a}$$

which is denoted as

$$y(t) = h(t) * x(t) \tag{8.57b}$$

In the *frequency domain*, this translates to

$$\hat{Y}(j\omega) = \hat{H}(j\omega)\hat{X}(j\omega) \tag{8.58}$$

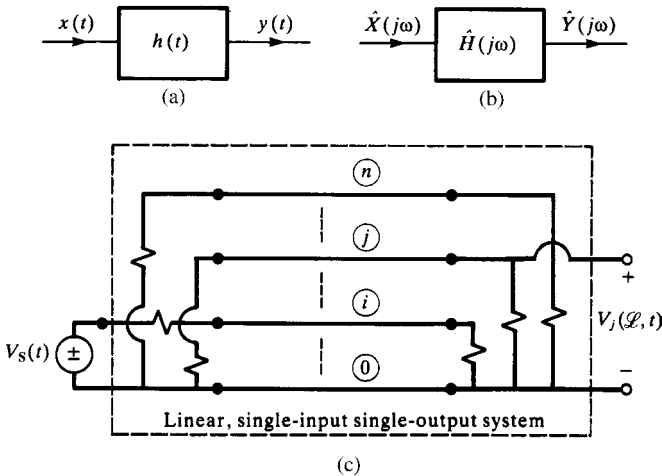


FIGURE 8.15 Illustration of the time-domain to frequency-domain transformation method of computing time-domain responses of *linear* MTLs: (a) a single-input, single-output linear system in the time domain, (b) a single-input, single-output linear system in the frequency domain, and (c) representation of an MTL as a single-input, single-output linear system.

where $\hat{H}(j\omega)$ is the *Fourier transform* of $h(t)$ and is called the *transfer function* of the system as illustrated in Figure 8.15(b) [A.2]. The frequency-domain transfer function $\hat{H}(j\omega)$ can be easily obtained by applying unit magnitude sinusoids to the input and computing the response using the usual *phasor* computational methods with the frequency of those sinusoids varied over the desired frequency range as illustrated in Figure 8.15(b). Once $\hat{H}(j\omega)$ is obtained in this manner, the time-domain impulse response is obtained as the *inverse Fourier transform* of $\hat{H}(j\omega)$: $h(t) = \mathcal{F}^{-1}\{\hat{H}(j\omega)\}$.

The method is a very intuitive one. Any time-domain waveform can be decomposed into its sinusoidal components with the Fourier series if it is periodic and the Fourier transform if it is not periodic [A.2]. A periodic waveform with period P has these frequency components appearing at discrete frequencies that are multiples of the basic repetition frequency: $f_0 = 1/P, 2f_0, 3f_0, \dots$. If the waveform is nonperiodic, these frequency components appear as a continuum. Nevertheless, the method for computing the time-domain response can be described quite simply in the following manner. Decompose the input signal via Fourier methods into its constituent sinusoidal components (magnitude and phase). Pass each component through the system and sum in time the time-domain responses at the output to each of these components by using phasor methods (See Figure 1.21 of Chapter 1.) The magnitudes of the output sinusoidal components are the products of the magnitudes of the input sinusoidal components multiplied by the magnitude of $\hat{H}(j\omega)$ at that frequency. The phases of the output sinusoidal components are the sums of the phases of the input sinusoidal components and the phases of $\hat{H}(j\omega)$ at that frequency. Therefore,

$$|\hat{Y}(j\omega_i)| = |\hat{H}(j\omega_i)| \times |\hat{X}(j\omega_i)| \quad (8.59a)$$

$$\angle \hat{Y}(j\omega_i) = \angle \hat{H}(j\omega_i) + \angle \hat{X}(j\omega_i) \quad (8.59b)$$

Clearly, a major restriction on the method is that the system be linear since we are implicitly applying the principle of superposition.

In the case of a periodic waveform with period P , these frequency components appear at discrete frequencies that are multiples of the basic repetition frequency $\omega_0 = 2\pi f_0 = 2\pi/P$, and $x(t)$ can be represented as the sum of these time-domain sinusoidal components with the Fourier series as [A.2, A.3]

$$x(t) = c_0 + \sum_{n=1}^{NH} c_n \cos(n\omega_0 t + \angle c_n) \quad (8.60)$$

where we have truncated the series to contain only NH harmonics. In the case of a periodic pulse train having trapezoidal pulses of peak magnitude X , duty cycle $D = \tau/P$, where τ is the pulse width (between 50% points), and equal rise/fall times

of τ_r , the items in (8.60) become [A.3]

$$c_0 = XD \quad (8.61a)$$

$$c_n = 2XD \frac{\sin(n\pi D)}{n\pi D} \frac{\sin(n\pi f_0 \tau_r)}{n\pi f_0 \tau_r} \quad (8.61b)$$

$$\angle c_n = -n\pi(D + f_0 \tau_r) \quad (8.61c)$$

For this case of a periodic waveform, we compute the frequency-domain transfer function at *each* of the NH harmonic frequencies with the methods of Chapters 6 and 7 (including skin-effect losses if we choose):

$$\hat{H}(jn\omega_0) = |\hat{H}(jn\omega_0)| \angle \hat{H}(jn\omega_0) \quad (8.62)$$

Then multiply each appropriate magnitude and add the angles to give the time-domain output as

$$y(t) = c_0 H(0) + \sum_{n=1}^{NH} c_n |\hat{H}(jn\omega_0)| \cos(n\omega_0 t + \angle c_n + \angle \hat{H}(jn\omega_0)) \quad (8.63)$$

In this way, we can include \sqrt{f} dependent skin-effect losses that are difficult to characterize directly in the time domain as we will discuss in Section 8.2.1, but again *this supposes a linear system*. This method is implemented in the FORTRAN program TIMEFREQ.FOR described in Appendix A. Actually, the periodic waveform results can be used for a nonperiodic waveform if we choose the pulse wave shape over a period to be that of the desired pulse and also choose a repetition frequency low enough that the response reaches its steady-state value before the onset of the next pulse.

Consider applying these concepts to an MTL. Suppose we apply a voltage source $V_S(t)$ to the i th conductor at $z = 0$ and desire the time-domain response of the j th line voltage, say, at the far end of the line $z = \mathcal{L}$, $V_j(\mathcal{L}, t)$. In order to view this problem as a single-input, single-output system, we *imbed* the transmission line *along with the terminations* into a two-port as illustrated in Figure 8.15(c) and extract the input to the system, $V_S(t)$, and the output of the system, $V_j(\mathcal{L}, t)$. The frequency-domain transfer function between these two ports, $\hat{H}_{ij}(j\omega)$, can be computed by the phasor methods of Chapters 6 and 7 wherein $V_S(t)$ is a sinusoid, $V_S(t) = \sin(\omega t)$. Once the frequency-domain transfer function is obtained in this fashion, the time-domain response can be determined for any time variation of $V_S(t)$ using the above summation of the responses to its sinusoidal components in (8.63), which amounts to the convolution integral of (8.57).

An important advantage is that this method can directly handle frequency-dependent losses such as skin-effect resistance of conductors. Another advantage is that only phasor computational methods are required; there is no need to numerically

integrate the time-domain transmission-line equations. A disadvantage is that the transmission line is assumed to be a *linear* line; that is, the line parameters *and* the terminations are assumed linear. For example, corona breakdown of the surrounding medium as well as nonlinear loads such as diodes and transistors *cannot* be handled with this method since it implicitly assumes a *linear system*. Nevertheless, the method is simple to implement for determining the time-domain response of a transmission line having *linear terminations*.

8.1.8 The Finite-Difference, Time-Domain (FDTD) Method

A numerical method for approximately determining the time-domain solution of the transmission-line equations is the Finite-Difference, Time-Domain or FDTD method [B.22–B.24, 2–5]. The derivatives in the transmission-line equations are discretized and approximated with various finite differences. In this method, the position variable z is discretized as Δz and the time variable t is discretized as Δt . There are many ways of approximating the derivatives $\partial/\partial z$ and $\partial/\partial t$ in those equations [2,6]. We used a particularly simple such discretization in the finite-difference method of solving Laplace's equation in two dimensions in Chapter 5 .

Consider a function of one variable, $f(t)$. Expanding this in a Taylor series in a neighborhood of a desired point t_0 gives

$$f(t_0 + \Delta t) = f(t_0) + \Delta t f'(t_0) + \frac{\Delta t^2}{2!} f''(t_0) + \frac{\Delta t^3}{3!} f'''(t_0) + \dots \quad (8.64)$$

where the primes denote the various derivatives with respect to t of the function. Solving this for the first derivative gives

$$f'(t_0) = \frac{f(t_0 + \Delta t) - f(t_0)}{\Delta t} - \frac{\Delta t}{2} f''(t_0) - \frac{\Delta t^2}{6} f'''(t_0) - \dots \quad (8.65)$$

Thus, the first derivative is approximated as

$$f'(t_0) = \frac{f(t_0 + \Delta t) - f(t_0)}{\Delta t} + \theta(\Delta t) \quad (8.66)$$

where $\theta(\Delta t)$ denotes that the error in truncating the series is on the order of Δt . So the first derivative may be approximated with the *forward difference*

$$f'(t_0) \cong \frac{f(t_0 + \Delta t) - f(t_0)}{\Delta t} \quad (8.67)$$

This amounts to approximating the derivative of $f(t)$ as with its slope about the region of the desired point. If we expand the Taylor's series as

$$f(t_0 - \Delta t) = f(t_0) - \Delta t f'(t_0) + \frac{\Delta t^2}{2!} f''(t_0) - \frac{\Delta t^3}{3!} f'''(t_0) + \dots \quad (8.68)$$

the first derivative can be approximated as

$$f'(t_0) = \frac{f(t_0) - f(t_0 - \Delta t)}{\Delta t} + \frac{\Delta t}{2} f''(t_0) - \frac{\Delta t^2}{6} f'''(t_0) + \dots \quad (8.69)$$

This gives the *backward difference*

$$f'(t_0) \cong \frac{f(t_0) - f(t_0 - \Delta t)}{\Delta t} \quad (8.70)$$

Other approximations known as *central differences* can be found by subtracting (8.68) from (8.64) to yield the first derivative *central difference* approximation

$$f'(t_0) \cong \frac{f(t_0 + \Delta t) - f(t_0 - \Delta t)}{2\Delta t} \quad (8.71)$$

with a truncation error on the order of Δt^2 . Similarly, the second derivative *central difference* is obtained by adding (8.64) and (8.68) to yield

$$f''(t_0) \cong \frac{f(t_0 + \Delta t) - 2f(t_0) + f(t_0 - \Delta t)}{\Delta t^2} \quad (8.72)$$

with a truncation error on the order of Δt^2 . The discretization of Laplace's equation in the finite-difference method of Chapter 3 amounts to a central difference approximation to Laplace's equation. The stability of the solution of Laplace's equation resulting from that discretization is assured unlike the stability of the discretizations of the transmission-line equations, which we now investigate.

Consider the discretization of the transmission-line equations in (8.1) for a two-conductor line:

$$\frac{\partial V(z, t)}{\partial z} + l \frac{\partial I(z, t)}{\partial t} = 0 \quad (8.73a)$$

$$\frac{\partial I(z, t)}{\partial z} + c \frac{\partial V(z, t)}{\partial t} = 0 \quad (8.73b)$$

We divide the line into NDZ sections, each of length Δz as shown in Figure 8.16. Similarly, we divide the total solution time into NDT segments of length Δt . In order to ensure stability of the discretization and to ensure second-order accuracy, we interlace the NDZ + 1 voltage points, $V_1, V_2, \dots, V_{\text{NDZ}}, V_{\text{NDZ}+1}$, and the NDZ current points, $I_1, I_2, \dots, I_{\text{NDZ}}$, as shown in Figure 8.17 [2,3,A.9]. Each voltage and adjacent current solution point is separated by $\Delta z/2$. In addition, the time points must also be interlaced and each voltage time point and adjacent current time point are separated by $\Delta t/2$, as illustrated in Figure 8.17. This sequencing diagram shown in Figure 8.17 is crucial for obtaining the correct discretization of the differential

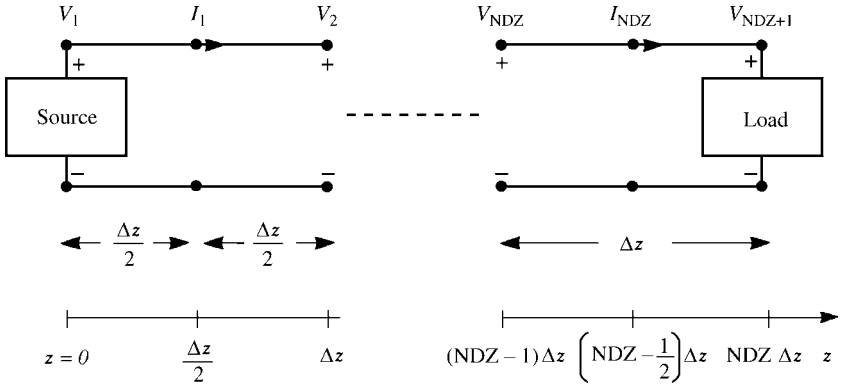


FIGURE 8.16 Discretization of the line into NDZ segments of length Δz for the FDTD analysis.

equations. The central difference approximations to (8.73) become

$$\frac{V_{k+1}^{n+1} - V_k^{n+1}}{\Delta z} + I \frac{I_k^{n+3/2} - I_k^{n+1/2}}{\Delta t} = 0 \tag{8.74a}$$

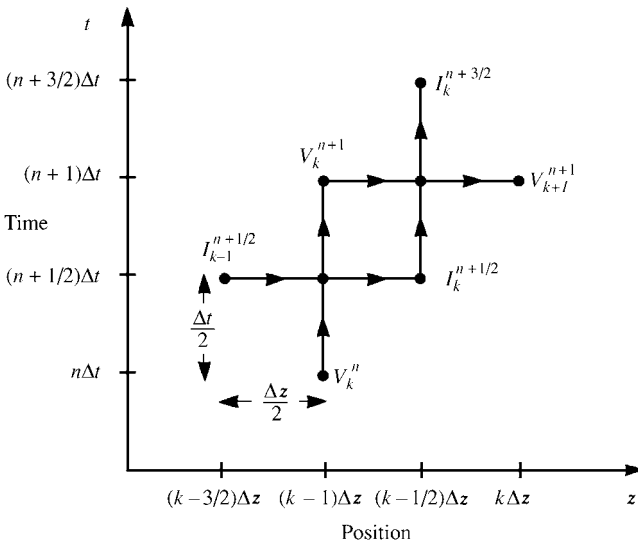


FIGURE 8.17 Interlacing the current and voltage solutions in space and time for the FDTD analysis.

for $k = 1, 2, \dots, \text{NDZ}$ and

$$\frac{I_k^{n+1/2} - I_{k-1}^{n+1/2}}{\Delta z} + c \frac{V_k^{n+1} - V_k^n}{\Delta t} = 0 \quad (8.74b)$$

for $k = 2, 3, \dots, \text{NDZ}$, where we denote

$$V_k^n \equiv V((k-1)\Delta z, n\Delta t) \quad (8.75a)$$

$$I_k^n \equiv I\left(\left(k - \frac{1}{2}\right)\Delta z, n\Delta t\right) \quad (8.75b)$$

The required recursion relations for the interior points on the line are obtained by solving Eqs. (8.74) giving

$$I_k^{n+3/2} = I_k^{n+1/2} - \frac{\Delta t}{\Delta z} I^{-1} \left(V_{k+1}^{n+1} - V_k^{n+1} \right) \quad (8.76a)$$

for $k = 1, 2, \dots, \text{NDZ}$ and

$$V_k^{n+1} = V_k^n - \frac{\Delta t}{\Delta z} c^{-1} \left(I_k^{n+1/2} - I_{k-1}^{n+1/2} \right) \quad (8.76b)$$

for $k = 2, 3, \dots, \text{NDZ}$. Equations (8.76) are solved in a leapfrog fashion. First, the voltages along the line are obtained, for a fixed time, from (8.76b) in terms of the previous solutions. Then the currents are obtained from (8.76a) in terms of the voltages obtained from (8.76b) as well as previously obtained values. The solution starts with an initially relaxed line having zero voltage and current values.

Next consider the incorporation of the terminal conditions. The essential problem in incorporating the terminal conditions is that the FDTD voltages and currents at each end of the line, V_1 , I_1 , and $V_{\text{NDZ}+1}$, I_{NDZ} , are not collocated in space or time, whereas the terminal conditions relate the voltage and current at the same position and at the same time. We will denote the current at the source ($z = 0$) as I_S and the current at the load ($z = \mathcal{L}$) as $I_{\mathcal{L}}$, as shown in Figure 8.18. The second transmission-line equation given in Eq. (8.73b) is discretized at the source by averaging the source currents I_S in order to obtain a value that is located in time at the same time point as $I_1^{n+1/2}$ as

$$\frac{1}{\Delta z/2} \left[I_1^{n+1/2} - \frac{\left(I_S^{n+1} + I_S^n \right)}{2} \right] + \frac{1}{\Delta t} c \left[V_1^{n+1} - V_1^n \right] = 0. \quad (8.77a)$$

Similarly, the second transmission-line equation, (8.73b), is discretized at the load by averaging the load currents $I_{\mathcal{L}}$ in order to obtain a value that is located in time at the

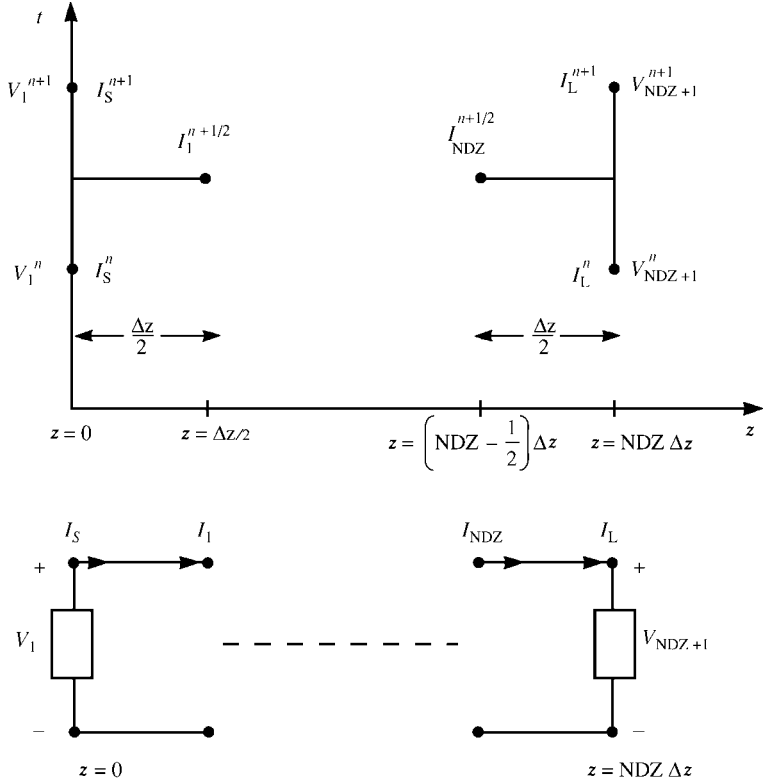


FIGURE 8.18 Discretizing the terminal voltages and currents of the line in order to incorporate the terminal constraints.

same time point as $I_{NDZ}^{n+1/2}$ as

$$\frac{1}{\Delta z/2} \left[\frac{(I_L^{n+1} + I_L^n)}{2} - I_{NDZ}^{n+1/2} \right] + \frac{1}{\Delta t} c \left[V_{NDZ+1}^{n+1} - V_{NDZ+1}^n \right] = 0 \quad (8.77b)$$

Equations (8.77) are solved to give the recursion relations at the source and the load:

$$V_1^{n+1} = V_1^n - \frac{2\Delta t}{\Delta z} c^{-1} I_1^{n+1/2} + \frac{\Delta t}{\Delta z} c^{-1} \left[I_S^{n+1} + I_S^n \right] \quad (8.78a)$$

$$V_{NDZ+1}^{n+1} = V_{NDZ+1}^n + \frac{2\Delta t}{\Delta z} c^{-1} I_{NDZ}^{n+1/2} - \frac{\Delta t}{\Delta z} c^{-1} \left[I_L^{n+1} + I_L^n \right] \quad (8.78b)$$

In the case of resistive terminations, the terminal characterizations are written in terms of a generalized Thevenin equivalent as

$$V_1 = V_S - R_S I_S \tag{8.79a}$$

$$V_{NDZ+1} = V_L + R_L I_L \tag{8.79b}$$

Inverting these gives

$$I_S = -G_S V_1 + G_S V_S \tag{8.80a}$$

$$I_L = G_L V_{NDZ+1} - G_L V_L \tag{8.80b}$$

Substituting (8.80) into Eqs. (8.78) gives the recursion relations for V_1 and V_{NDZ+1} :

$$V_1^{n+1} = \left(\frac{\Delta z}{\Delta t} R_{Sc} + 1 \right)^{-1} \left\{ \left(\frac{\Delta z}{\Delta t} R_{Sc} - 1 \right) V_1^n - 2R_S I_1^{n+1/2} + \left(V_S^{n+1} + V_S^n \right) \right\} \tag{8.81a}$$

and

$$V_{NDZ+1}^{n+1} = \left(\frac{\Delta z}{\Delta t} R_{Lc} + 1 \right)^{-1} \left\{ \left(\frac{\Delta z}{\Delta t} R_{Lc} - 1 \right) V_{NDZ+1}^n + 2R_L I_{NDZ}^{n+1/2} + \left(V_L^{n+1} + V_L^n \right) \right\} \tag{8.81b}$$

and the voltages at the interior points are determined from (8.76b):

$$V_k^{n+1} = V_k^n - \frac{\Delta t}{\Delta z} c^{-1} \left(I_k^{n+1/2} - I_{k-1}^{n+1/2} \right) \tag{8.81c}$$

for $k = 2, 3, \dots, NDZ$. Equations (8.81) are first solved for the voltages and then the currents are determined from those voltages using (8.76a) as

$$I_k^{n+3/2} = I_k^{n+1/2} - \frac{\Delta t}{\Delta z} t^{-1} \left(V_{k+1}^{n+1} - V_k^{n+1} \right) \tag{8.81d}$$

for $k = 1, 2, 3, \dots, NDZ$. For stability of the solution, the position and time discretizations must satisfy the Courant condition [2,3,6]

$$\Delta t \leq \frac{\Delta z}{v} \tag{8.82}$$

The Courant stability condition provides that for stability of the solution the time step must be no greater than the propagation time over each cell. The Δz discretization is

chosen sufficiently small such that each Δz section is *electrically small* at the significant spectral components of the source voltages $V_S(t)$ and $V_L(t)$. The FDTD method described in this section is implemented in the FORTRAN code `FINDIF.FOR`, which is described in Appendix A.

8.1.8.1 The Magic Time Step In order to ensure stability of the solution, we require that the time step Δt and spatial discretization Δz satisfy the Courant condition given in (8.82). Suppose we divide the total line length \mathcal{L} into NDZ sections of length

$$\Delta z = \frac{\mathcal{L}}{\text{NDZ}} \quad (8.83a)$$

and divide the total simulation run time, final solution time, into NDT intervals of length

$$\Delta t = \frac{\text{final solution time}}{\text{NDT}} \quad (8.83b)$$

The Courant stability condition in (8.82) requires that NDT and NDZ be related as

$$\text{NDT} \geq \text{NDZ} \times v \times \frac{\text{final solution time}}{\mathcal{L}} \quad (8.84)$$

Choosing the time step to give an equality in this relation is referred to as the “magic time step”:

$$\Delta t = \frac{\Delta z}{v} \quad (8.85a)$$

or

$$\text{NDT} = \text{NDZ} \times v \times \frac{\text{final solution time}}{\mathcal{L}} \quad (8.85b)$$

We will now prove that if the time step is chosen to be the magic time step, then the FDTD method gives an *exact solution* to the transmission-line equations with no approximation error!

In order to prove this amazing result, we will utilize the *exact* SPICE equivalent circuit of the line given in (8.35) and (8.36) and shown in Figure 8.9(a). Consider this representation for interior points along the line shown in Figure 8.19. The voltages and currents to be solved for in the finite-difference solution are V_k , I_k , and V_{k+1} . The currents and voltages I_A , V_A , and I_B are auxiliary variables that are to be eliminated. Each half of length $\Delta z/2$ is modeled with its own exact solution with reference to Figure 8.9(a) with a time delay of $\tau/2$, where

$$\tau = \frac{\Delta z}{v} \quad (8.86)$$

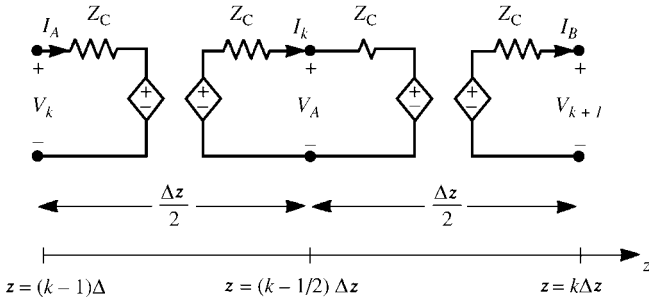


FIGURE 8.19 Use of Branim’s method to prove the exact FDTD discretization for interior current points for the magic time step.

In order to simplify the derivation, we again use the *difference operator*

$$D^{\pm m} f(t) = f(t \pm m\tau) \tag{8.87}$$

From Figure 8.19, we obtain

$$V_k = Z_C I_A + D^{-1/2} (V_A - Z_C I_k) \tag{8.88a}$$

$$V_A = -Z_C I_k + D^{-1/2} (V_k + Z_C I_A) \tag{8.88b}$$

$$V_A = Z_C I_k + D^{-1/2} (V_{k+1} - Z_C I_B) \tag{8.88c}$$

$$V_{k+1} = -Z_C I_B + D^{-1/2} (V_A + Z_C I_k) \tag{8.88d}$$

The objective is to eliminate \$V_A\$, \$I_A\$ and \$I_B\$ from these expressions. To do so, first subtract (8.88a) from (8.88d) giving

$$(V_{k+1} - V_k) = -Z_C (I_A + I_B) + 2Z_C D^{-1/2} I_k \tag{8.89}$$

Next, subtract (8.88b) from (8.88c) giving

$$0 = 2Z_C I_k + D^{-1/2} (V_{k+1} - V_k) - Z_C D^{-1/2} (I_A + I_B) \tag{8.90}$$

Multiplying (8.90) by \$D^{1/2}\$ gives

$$0 = 2Z_C D^{1/2} I_k + (V_{k+1} - V_k) - Z_C (I_A + I_B) \tag{8.91}$$

Subtracting (8.91) from (8.89) gives

$$(V_{k+1} - V_k) = -Z_C \left(D^{1/2} I_k - D^{-1/2} I_k \right) \tag{8.92}$$

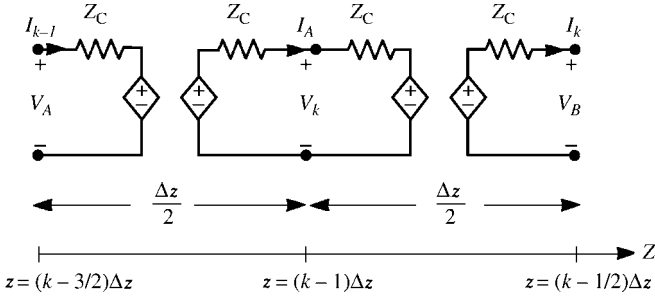


FIGURE 8.20 Use of Branim’s method to prove the exact FDTD discretization for interior voltage points for the magic time step.

Multiplying this by D and substituting the relation for the characteristic impedance $Z_C = vl$ gives

$$(DV_{k+1} - DV_k) = -vl \left(D^{3/2}I_k - D^{1/2}I_k \right) \tag{8.93}$$

Substituting the magic time step $\Delta t = \Delta z/v$ and rearranging gives

$$D^{3/2}I_k = D^{1/2}I_k - \frac{\Delta t}{\Delta z} l^{-1} (DV_{k+1} - DV_k) \tag{8.94}$$

which is the recursion relation for currents given in (8.81d).

Similarly, from Figure 8.20 we obtain

$$V_A = Z_C I_{k-1} + D^{-1/2} (V_k - Z_C I_A) \tag{8.95a}$$

$$V_k = -Z_C I_A + D^{-1/2} (V_A + Z_C I_{k-1}) \tag{8.95b}$$

$$V_k = Z_C I_A + D^{-1/2} (V_B - Z_C I_k) \tag{8.95c}$$

$$V_B = -Z_C I_k + D^{-1/2} (V_k + Z_C I_A) \tag{8.95d}$$

The objective is again to eliminate V_A , I_A , and V_B from these expressions. To do so, first add (8.95a) and (8.95d) giving

$$(V_A + V_B) = -Z_C (I_k - I_{k-1}) + 2D^{-1/2} V_k \tag{8.96}$$

Multiplying this by $D^{1/2}$ gives

$$D^{1/2} (V_A + V_B) = -Z_C \left(D^{1/2}I_k - D^{1/2}I_{k-1} \right) + 2V_k \tag{8.97}$$

Next, add (8.95b) and (8.95c) giving

$$2V_k = D^{-1/2} (V_A + V_B) - Z_C D^{-1/2} (I_k - I_{k-1}) \tag{8.98}$$

Multiplying (8.98) by $D^{1/2}$ gives

$$2D^{1/2}V_k = (V_A + V_B) - Z_C (I_k - I_{k-1}) \tag{8.99}$$

Adding (8.96) and (8.99) gives

$$\left(D^{1/2}V_k - D^{-1/2}V_k \right) = -Z_C (I_k - I_{k-1}) \tag{8.100}$$

Multiplying this by $D^{1/2}$ and substituting the relation for the characteristic impedance $Z_C = (1/vc)$ gives

$$(DV_k - V_k) = -\frac{1}{vc} \left(D^{1/2}I_k - D^{1/2}I_{k-1} \right) \tag{8.101}$$

Substituting the magic time step $\Delta t = \Delta z/v$, gives

$$DV_k = V_k - \frac{\Delta t}{\Delta z} c^{-1} \left(D^{1/2}I_k - D^{1/2}I_{k-1} \right) \tag{8.102}$$

which is the recursion relation for voltages given in (8.81c).

Next, consider the source termination along with the first half section shown in Figure 8.21. The relations are

$$V_1 = Z_C I_S + D^{-1/2} (V_A - Z_C I_1) \tag{8.103a}$$

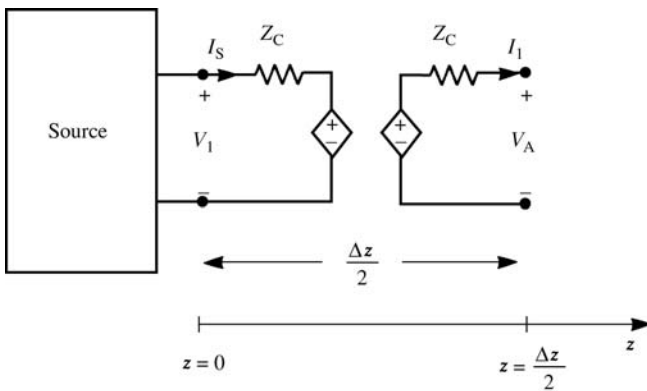


FIGURE 8.21 Use of Brainin’s method to prove the exact FDTD discretization for terminal voltage points at the left end of the line for the magic time step.

$$V_A = -Z_C I_1 + D^{-1/2} (V_1 + Z_C I_S) \tag{8.103b}$$

The objective is to eliminate V_A . To do so, we multiply (8.103a) by D and multiply (8.103b) by $D^{1/2}$ and add the equations to give

$$DV_1 - V_1 = -Z_C \left[2D^{1/2} I_1 - (DI_S + I_S) \right] \tag{8.104}$$

Substituting the relation for the characteristic impedance $Z_C = 1/vc$, along with the magic time step $\Delta t = \Delta z/v$ gives

$$\frac{1}{\Delta z/2} \left[D^{1/2} I_1 - \frac{(DI_S + I_S)}{2} \right] + c \frac{(DV_1 - V_1)}{\Delta t} = 0 \tag{8.105}$$

which is the source discretization relation given in (8.77a).

Similarly, consider the load termination along with the last half section shown in Figure 8.22. The relations are

$$V_B = Z_C I_{NDZ} + D^{-1/2} (V_{NDZ+1} - Z_C I_L) \tag{8.106a}$$

$$V_{NDZ+1} = -Z_C I_L + D^{-1/2} (V_B + Z_C I_{NDZ}) \tag{8.106b}$$

The objective is to eliminate V_B . To do so, we multiply (8.106a) by $D^{1/2}$ and multiply (8.106b) by D and add the equations to give

$$DV_{NDZ+1} - V_{NDZ+1} = -Z_C \left[(DI_L + I_L) - 2D^{1/2} I_{NDZ} \right] \tag{8.107}$$

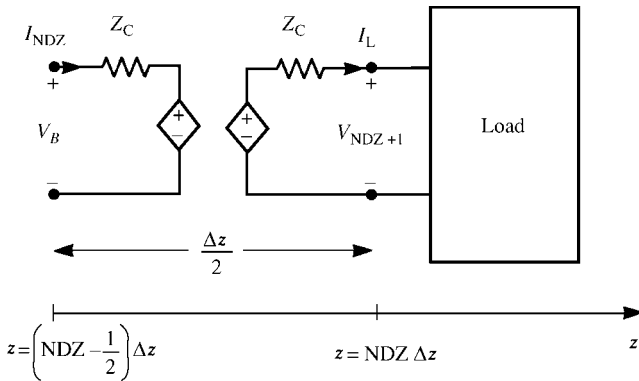


FIGURE 8.22 Use of Branin’s method to prove the exact FDTD discretization for terminal voltage points at the right end of the line for the magic time step.

Substituting the relation for the characteristic impedance, $Z_C = 1/vc$ along with the magic time step $\Delta t = \Delta z/v$ gives

$$\frac{1}{\Delta z/2} \left[\frac{(DI_L + I_L)}{2} - D^{1/2} I_{\text{NDZ}} \right] + c \frac{(DV_{\text{NDZ}+1} - V_{\text{NDZ}+1})}{\Delta t} = 0 \quad (8.108)$$

which is the load discretization relation given in (8.77b).

As an example, consider the two-conductor lossless line considered earlier and shown in Figure 8.5. The exact solution for the load voltage $V(\mathcal{L}, t)$ is sketched by hand in Figure 8.5(b), and the SPICE results (using a 30-V source voltage with a 0.01- μs rise time) are sketched in Figure 8.10(b). In the following computed results, we will designate

$$\Delta z = \frac{\mathcal{L}}{\text{NDZ}}$$

$$\Delta t = \frac{\text{final solution time}}{\text{NDT}}$$

The Courant condition given in (8.82) for stability of the FDTD solution translates to

$$\text{NDT} \geq \text{NDZ} \frac{v \times \text{final solution time}}{\mathcal{L}}$$

The magic time step occurs for an equality in this expression. Figure 8.23(a) shows the FDTD predictions for zero rise time and $\text{NDZ} = 200$ or $\Delta z = 2 \text{ m}$ and the magic time step of $\Delta t = \Delta z/v = 10 \text{ ns}$. For a final solution time of $20 \mu\text{s}$, this gives 2000 time steps or $\text{NDT} = 2000$. The results are *exactly* those for the hand calculations and the SPICE predictions. If we reduce the time step below that of the magic time step using 4000 time steps or $\Delta t = 5 \text{ ns}$, we observe considerable “ringing” on the leading edge of each transition. The FDTD solution for $\text{NDZ} = 1$ (dividing the line into only one section) and the “magic time step” of $\text{NDT} = 10$ or $\Delta t = 2 \mu\text{s}$ is denoted as X and gives the *exact solution* even for this course gridding of the line! Figure 8.23(b) shows the FDTD predictions for a 0.1 μs rise time and $\text{NDZ} = 200$ or $\Delta z = 2 \text{ m}$ and the magic time step of $\Delta t = \Delta z/v = 10 \text{ ns}$. Again, the results are *exactly* those for the SPICE predictions and the hand calculations. If we reduce the time step below that of the magic time step using 4000 time steps or $\Delta t = 5 \text{ ns}$, we observe less “ringing” on the leading edge of each transition than for the zero rise time solution. The spectrum of this 0.1- μs rise time pulse has a bandwidth of approximately $\text{BW} = 1/\tau_r = 10 \text{ MHz}$. So the section length Δz should be electrically short at this frequency requiring $\Delta z < (1/10)(v/f_{\text{max}}) = 2 \text{ m}$ ($f_{\text{max}} = 10 \text{ MHz}$, $v = 2 \times 10^8 \text{ m/s}$). Thus, if we do not wish to use the magic time step, we must further reduce Δz to eliminate this ringing. The results for the magic time step, $\text{NDZ} = 1$ and $\text{NDT} = 10$, are denoted with X and again give the *exact solution* even for this course gridding of the line!

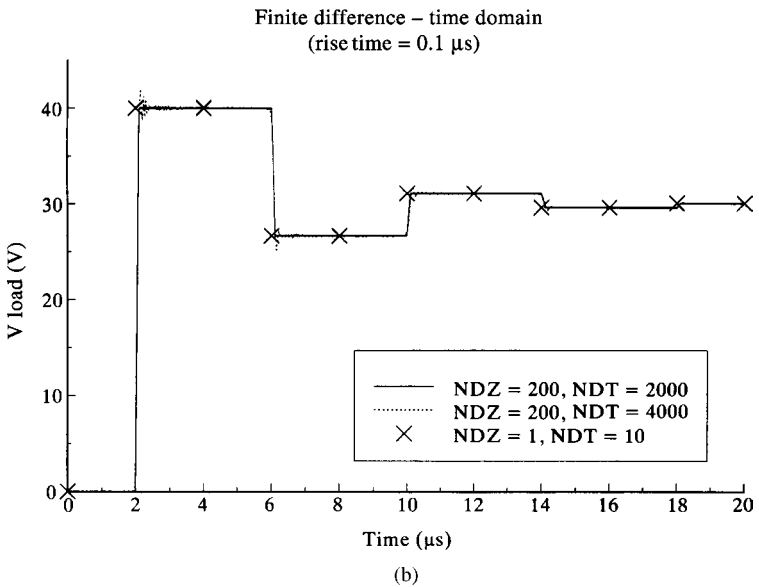
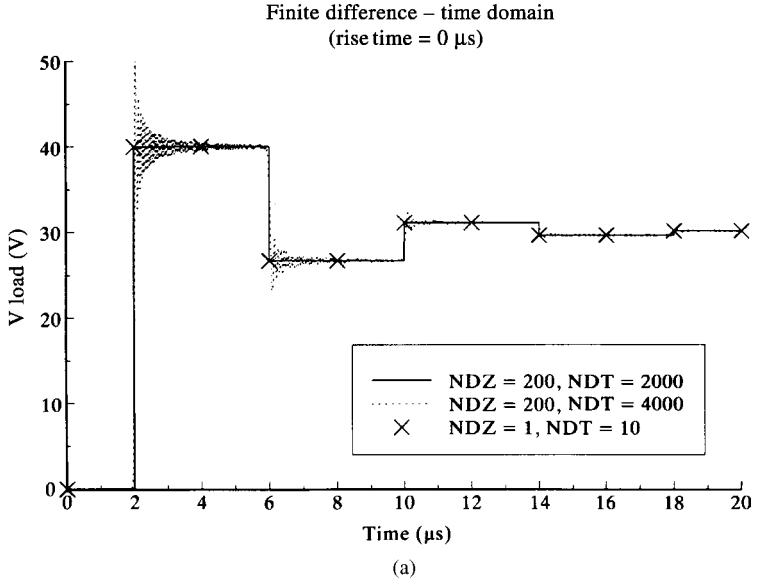


FIGURE 8.23 Illustration of the computation of the load voltage of Figure 8.5 using the FDTD method and comparison of the convergence to the choice of spatial and temporal discretization: (a) step response and (b) rise time of 0.1 μ s.

8.1.9 Matching for Signal Integrity

We have seen how mismatches at the source and/or load of a transmission line can cause the received voltage waveform to differ drastically from what was sent. In order to prevent logic errors, it is necessary that the received pulses have levels, shapes, and rise/fall times within certain allowable ranges. This is referred to as achieving *signal integrity*. Hence, mismatches affect signal integrity. In order to illustrate the detrimental effects of line mismatch, consider the typical line configuration shown in Figure 8.24(a). This approximates two CMOS inverters connected by a transmission

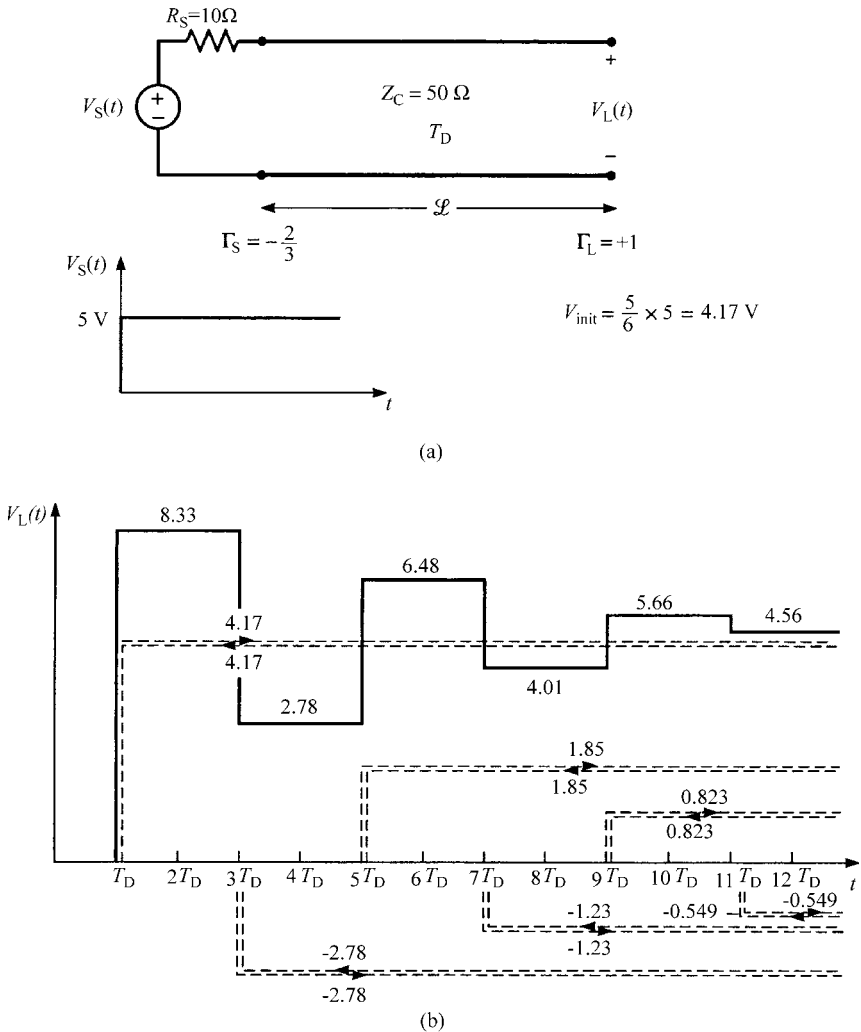


FIGURE 8.24 Illustration of “ringing” caused by mismatched lines in digital applications.

line. The driver has a very low output impedance of $10\ \Omega$ and an open-circuit voltage that rises to $5\ \text{V}$ with zero rise time. The load CMOS inverter is represented as an open circuit to facilitate graphing the waveform at its input. Typical CMOS devices have an input circuit that looks like a capacitance of some $5\text{--}15\ \text{pF}$. We will investigate the effect of actual device capacitance using SPICE in later results. The line is represented as having a characteristic impedance of $50\ \Omega$ and a general time delay. Sketching the load voltage, the input voltage to the CMOS receiver, is simple. The source reflection coefficient is $\Gamma_S = -2/3$, and the open-circuit load has a reflection coefficient of $\Gamma_L = +1$. The initially sent out voltage is $50/(50 + 10) \times 5 = 4.17\ \text{V}$. Figure 8.24(b) shows the resulting output voltage of the line. This illustrates “ringing” or overshoot common on such mismatched lines that can possibly cause logic errors (see Table 8.1).

It is common in digital circuits to eliminate this ringing using various matching schemes. The most common matching scheme is the *series match* shown in Figure 8.25(a). For typical CMOS gates, their source (output) resistances are less

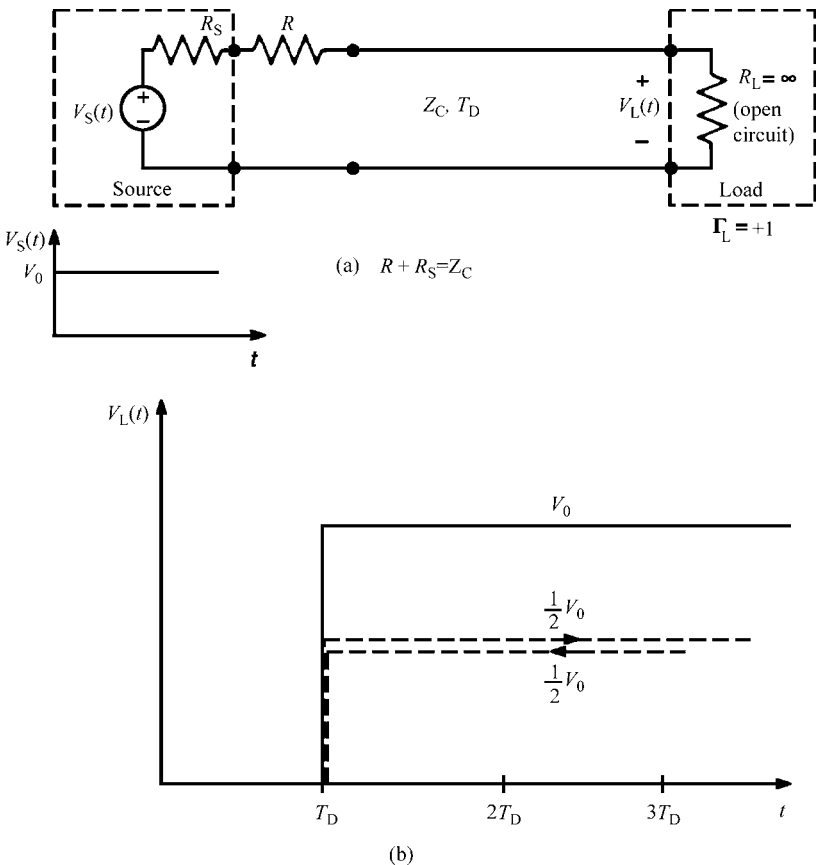


FIGURE 8.25 Illustration of how series matching eliminates ringing.

than the characteristic impedances of PCB lines. Hence, a resistor R is added to the input of the line (the output of the driving gate) such that

$$R_S + R = Z_C$$

This matches the line at the source. The initially sent out voltage wave will have a level half the source voltage level or $V_0/2$. Typically, the load is an open circuit or approximately so and hence the load reflection coefficient is $\Gamma_L = +1$. In this case the incident wave is completely reflected at the load giving a total of $V_0/2 + V_0/2 = V_0$ as illustrated in Figure 8.25(b). Hence, the load voltage rises to V_0 immediately giving perfect signal integrity. Another advantage of the series match is that, for an open-circuit load, no current flows in the line and hence the resistor R dissipates no power.

A second scheme for matching is the *parallel match* shown in Figure 8.26(a). Here, we place a resistor R in parallel with the load. We choose R such that the line

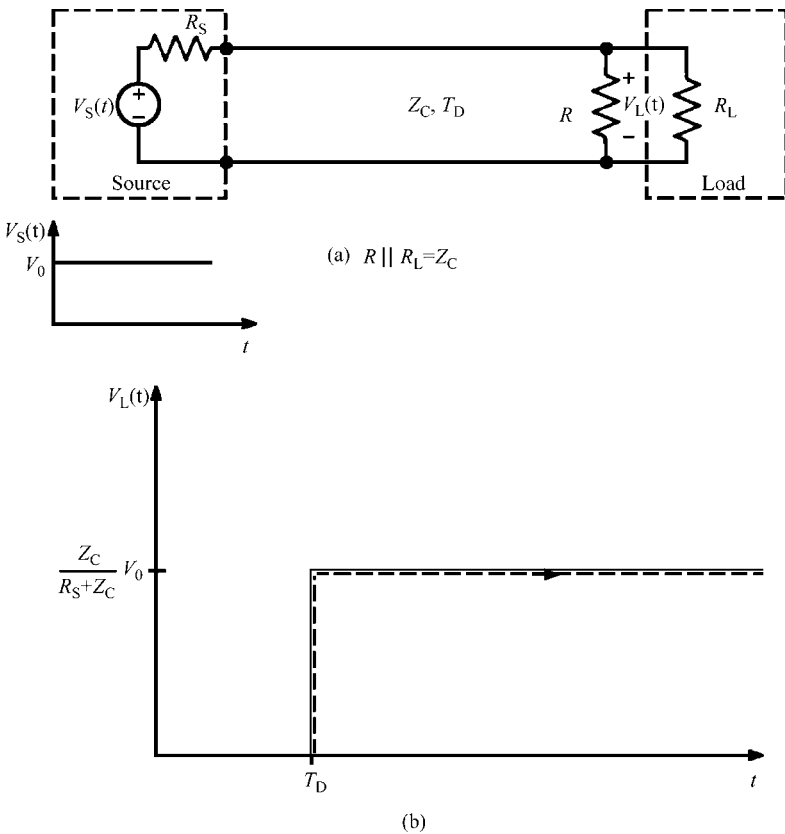


FIGURE 8.26 Illustration of how parallel matching eliminates ringing.

is matched at the load:

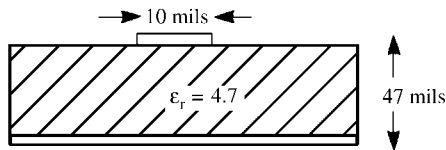
$$R \parallel R_L = \frac{RR_L}{R + R_L} = Z_C$$

The load voltage is plotted in Figure 8.26(b). Note that the initially sent out voltage has a level of

$$V_{\text{init}} = \frac{Z_C}{R_S + Z_C} V_0$$

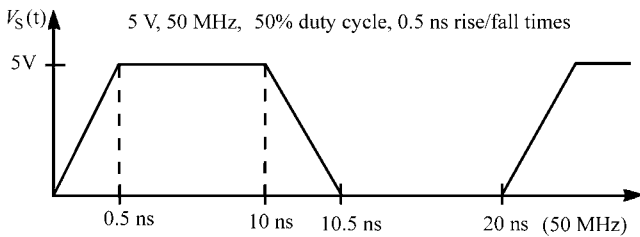
This incoming wave at the load is totally absorbed and there is no reflected wave. There are two disadvantages to the parallel match. First, the load voltage is always less than the source level of V_0 . For example, suppose $R_S = 25 \Omega$, $Z_C = 50 \Omega$, and $V_0 = 5 \text{ V}$. The load voltage level will be 3.33 V. In the parallel match case, we have no reflected wave to bring the load voltage up to the source voltage level. The second disadvantage of the parallel match case is that, even for an open-circuited load, the line will draw current when the source is in the high state. Hence, the matching resistor R will consume power.

As an example, consider a microstrip line shown in Figure 8.27(a) having glass epoxy ($\epsilon_r = 4.7$) as the substrate of thickness 47 mils and a land of width 10 mils. The characteristic impedance computed using the results of Chapter 4 is $Z_C = 124 \Omega$ and the effective relative permittivity is $\epsilon'_r = 3.09$. A line length of approximately 2 in.



| | | | |
|----------------------|--------------------|---------------------|------------------------|
| $\epsilon'_r = 3.09$ | $Z_C = 124 \Omega$ | $\mathcal{L} = 2''$ | $T_D = 0.3 \text{ ns}$ |
|----------------------|--------------------|---------------------|------------------------|

(a)



(b)

FIGURE 8.27 An example of a digital microstrip line.

would have a total one-way time delay of $T_D = 0.3$ ns. The source voltage waveform is as shown in Figure 8.27(b) consisting of a 5-V pulse train with a repetition frequency of 50 MHz and rise/fall times of 0.5 ns and a 50% duty cycle. The ideal case is shown in Figure 8.28, where the load voltage is identical to that sent out but with only a

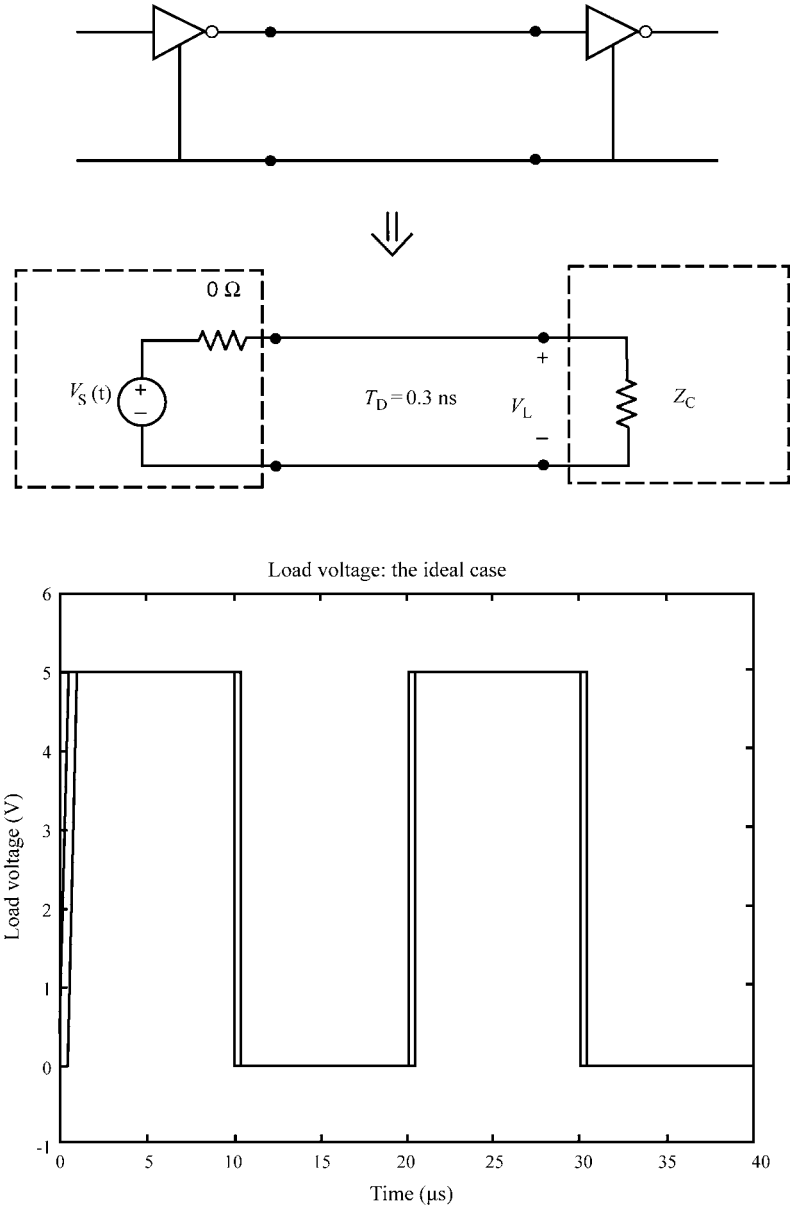


FIGURE 8.28 The ideal case of Figure 8.27 wherein the only effect of the line is a time delay.

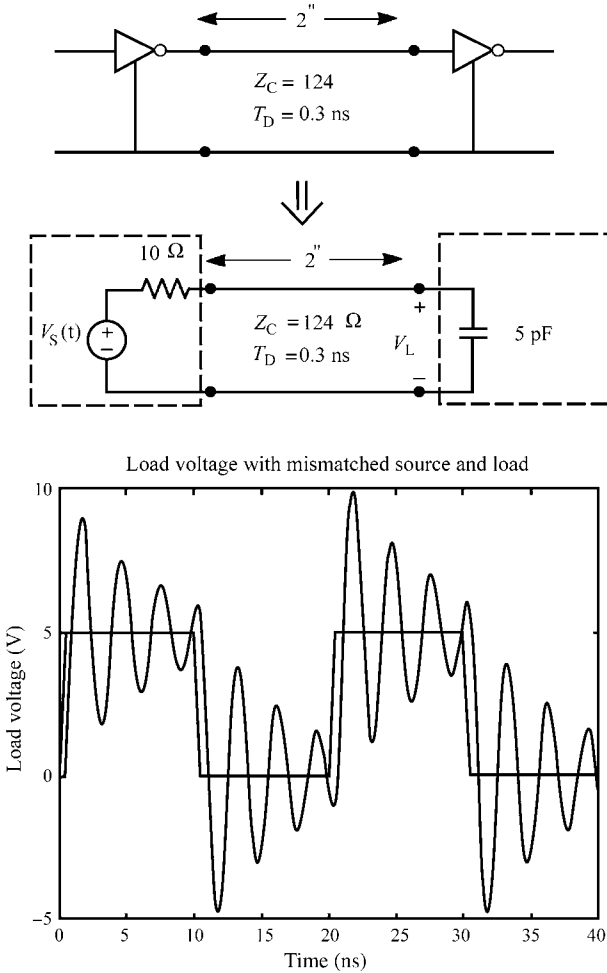


FIGURE 8.29 The mismatched case for a line connecting two CMOS inverters showing extreme ringing that has logic error ramifications.

0.3-ns delay. Figure 8.29 shows the SPICE simulation for the actual configuration illustrating a rather severe ringing even for this relatively short line. Logic errors will clearly result for this situation. Figure 8.30 shows the series matching case where a 114- Ω resistance is inserted in series with the source to provide series matching. The ringing is eliminated, but the load capacitance adds another time delay since the time constant is $Z_C C = 0.62$ ns. Figure 8.31 shows the case of a parallel match. Ringing here is not eliminated because the impedance of the capacitor dominates the parallel resistance at frequencies in the high-frequency portion of the spectrum giving a mismatch. The 124- Ω resistor in parallel with the 5-pF load capacitance has a break frequency of $f_c = 1/2\pi Z_C C = 257$ MHz, which is considerably below the

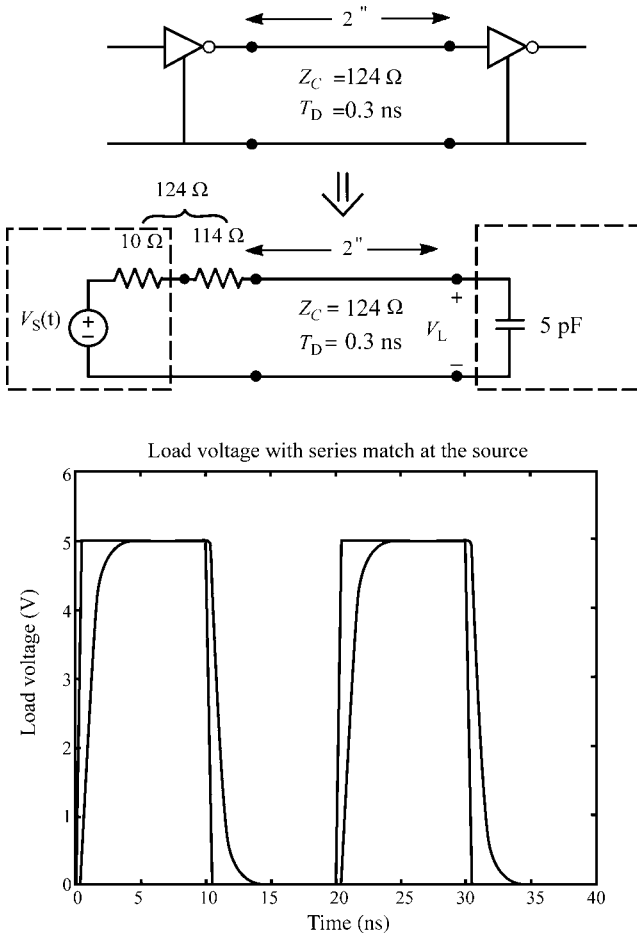


FIGURE 8.30 Series matching eliminates the ringing but the capacitive load imposes an additional time delay.

bandwidth of $BW = 1/\tau_r = 2\text{GHz}$. Hence, for frequencies above 257 MHz the line is not matched.

8.1.9.1 When is Matching Required? Matching a line is not always required in order that the voltage waveforms at the output of the line be approximately the same as the waveforms at the input to the line. Clearly, if the line is sufficiently short, matching will not be required. In general, we can obtain a time-domain criterion where the line is electrically short at the significant frequencies of the pulse spectrum. This was obtained in Section 8.1.6.1 in order to determine when a lumped-circuit model of the

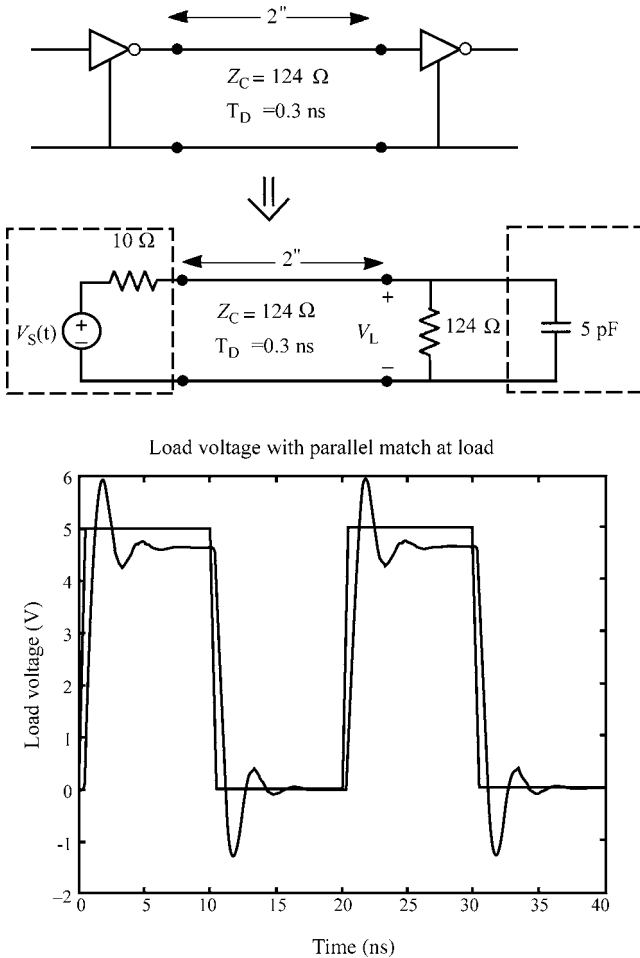


FIGURE 8.31 Parallel matching does not eliminate ringing because the load capacitance is not an open circuit and causes mismatch at the higher frequencies of the input pulse.

line was adequate. The same criterion applies here:

$$\tau_r > 10T_D \tag{8.109}$$

Hence, if the pulse rise time is greater than 10 one-way time delays of the line, the line and any mismatches should not significantly degrade the shape of the output waveform.

8.1.9.2 Effects of Line Discontinuities Until now there are no discontinuities along the line; that is, there are no changes in cross section along the line and there are no

terminations added along the line. In this section, we will investigate the effects of discontinuities along the line. A common discontinuity is where the line cross section changes, for example, the line width changes at some point as illustrated in Figure 8.32(a). Hence, the first portion has characteristic impedance Z_{C1} and the second portion has characteristic impedance Z_{C2} . First, consider a wave traveling on line 1 that is incident on the junction. A portion of the incident voltage, v_{i1} , is reflected back to the left and is given by $v_{r1} = \Gamma_{12}v_{i1}$ where the reflection coefficient is

$$\Gamma_{12} = \frac{Z_{C2} - Z_{C1}}{Z_{C2} + Z_{C1}} \quad (8.110a)$$

since the incoming wave essentially sees a termination impedance that is the characteristic impedance of the second line. In addition, a portion of the incident voltage, v_{i2} , is transmitted across the junction onto the second line and is given by $v_{t2} = T_{12}v_{i1}$. The total voltage on each side of the junction must be equal:

$$v_{i1} + v_{r1} = v_{t2} \quad (8.110b)$$

Hence, the reflection and transmission coefficients are related as

$$1 + \Gamma_{12} = T_{12} \quad (8.110c)$$

and the transmission coefficient is given by

$$T_{12} = \frac{2Z_{C2}}{Z_{C2} + Z_{C1}} \quad (8.110d)$$

This process is illustrated in Figure 8.32(b).

A similar process governs a wave on line 2 that is traveling to the left and strikes the junction as illustrated in Figure 8.32(c). A portion of the incident voltage, v_{i2} , is reflected back to the right and is given by $v_{r2} = \Gamma_{21}v_{i2}$, where the reflection coefficient is

$$\Gamma_{21} = \frac{Z_{C1} - Z_{C2}}{Z_{C1} + Z_{C2}} \quad (8.111a)$$

since the incoming wave essentially sees a termination impedance that is the characteristic impedance of the first line. In addition, a portion of the incident voltage, v_{i1} , is transmitted across the junction onto the first line and is given by $v_{t1} = T_{21}v_{i2}$. The total voltage on each side of the junction again must be equal:

$$v_{i2} + v_{r2} = v_{t1} \quad (8.111b)$$

Hence, the reflection and transmission coefficients are related as

$$1 + \Gamma_{21} = T_{21} \quad (8.111c)$$

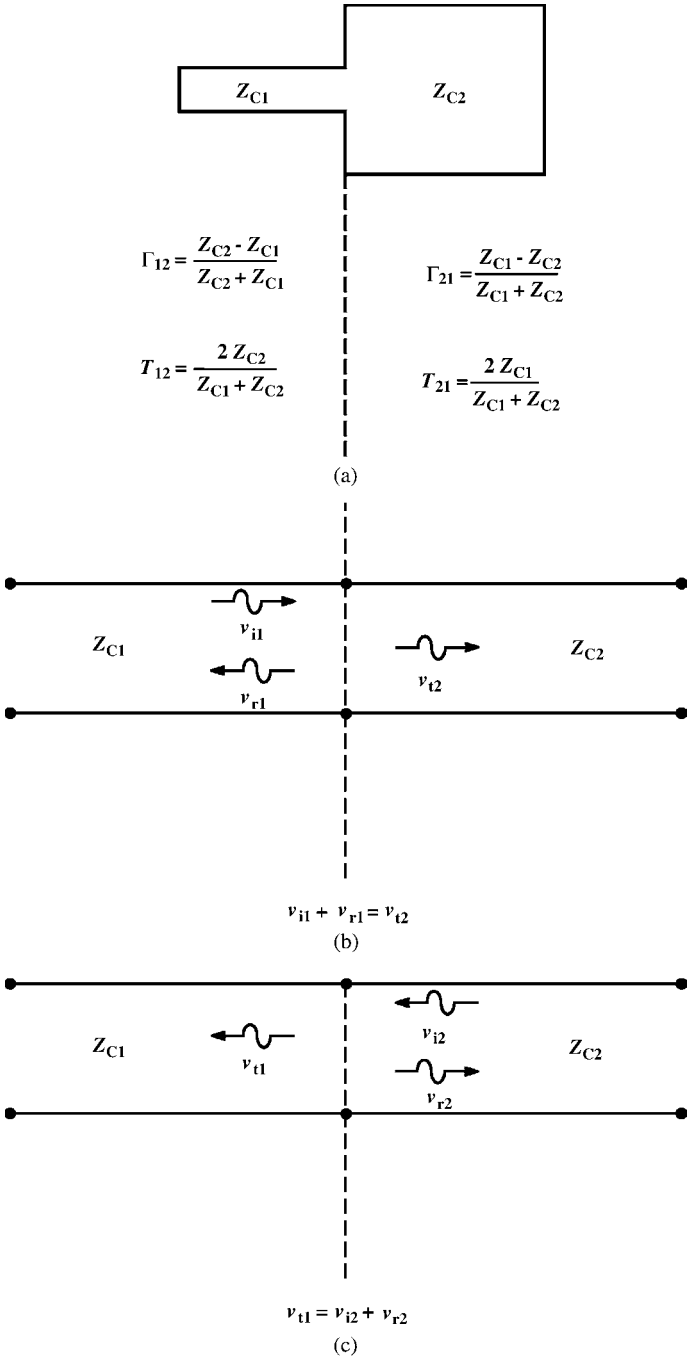


FIGURE 8.32 Reflections caused by a line discontinuity such as a change in line width.

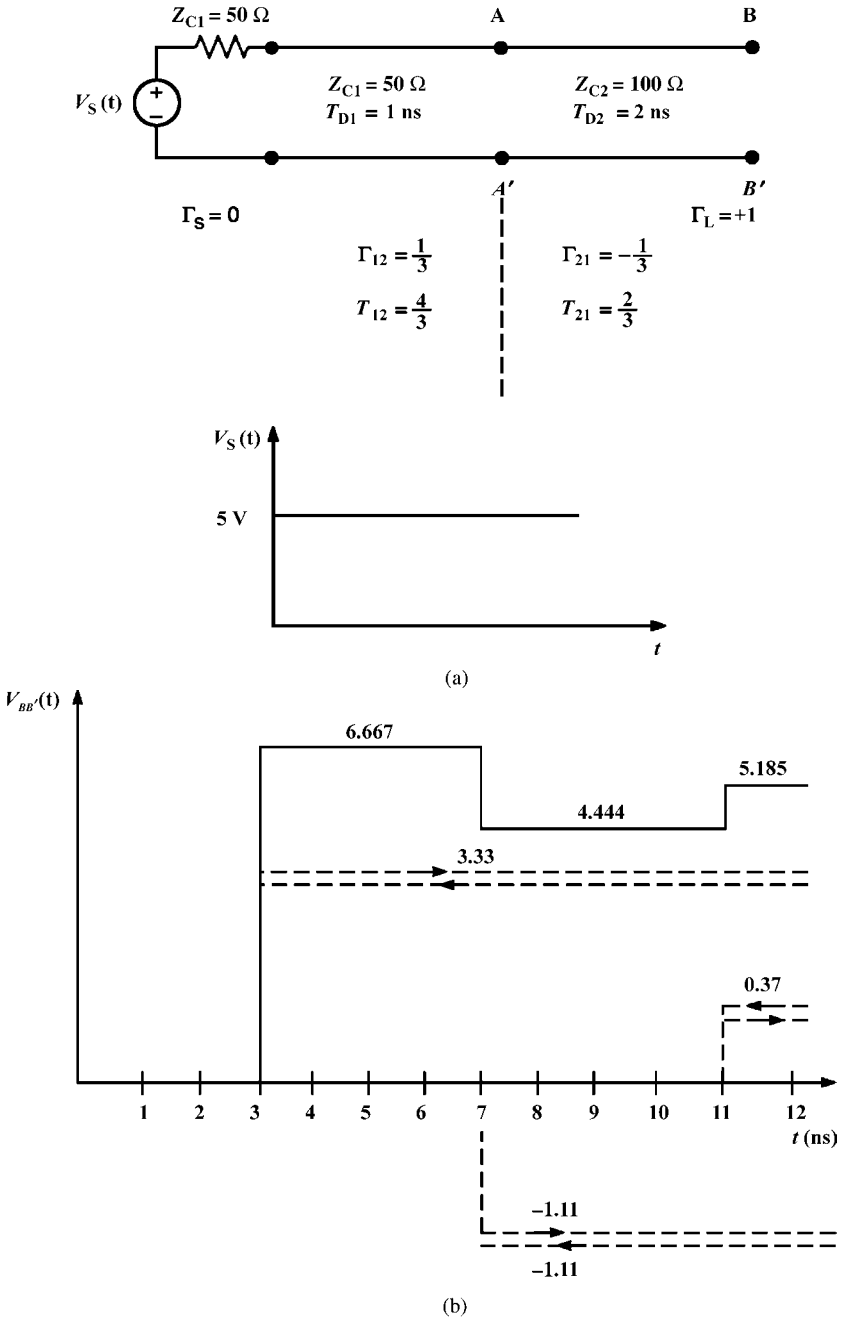
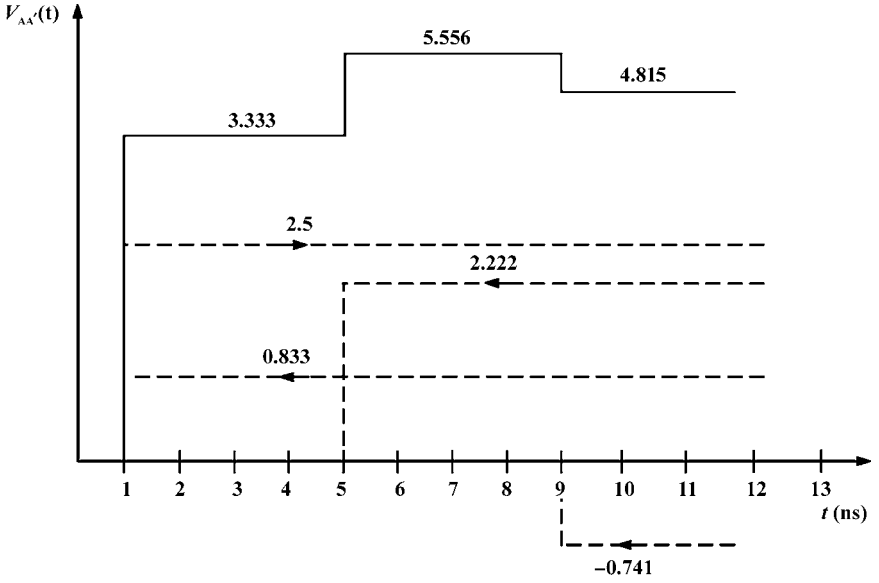
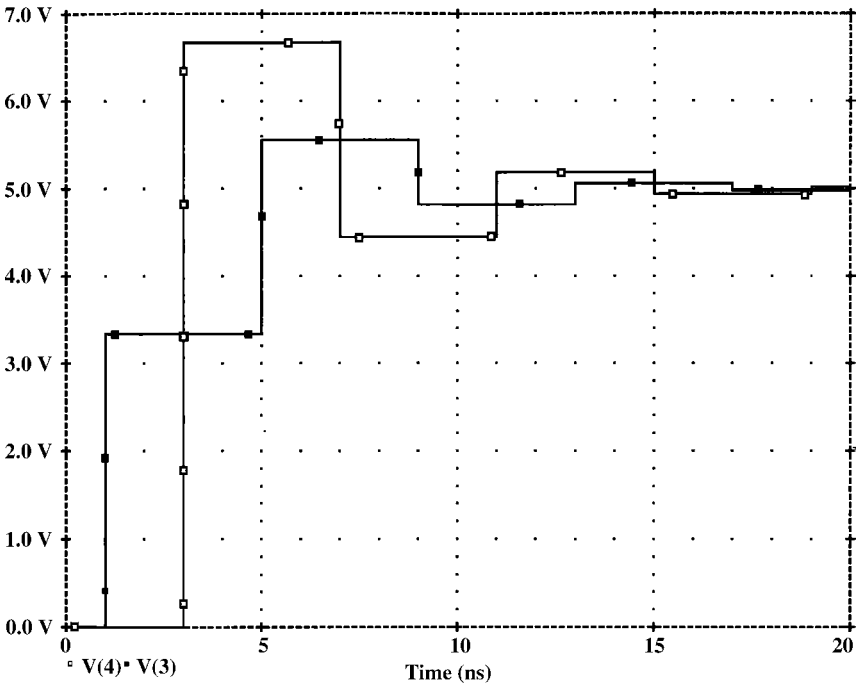


FIGURE 8.33 An example for calculating the effects of a line discontinuity: (a) the reflection and transmission coefficients, (b) plots of the midpoint and (c) terminal voltages, and (d) confirmation from a SPICE analysis.



(c)
Example



(d)

FIGURE 8.33 (Continued)

and the transmission coefficient is given by

$$T_{21} = \frac{2Z_{C1}}{Z_{C1} + Z_{C2}} \quad (8.111d)$$

This process is again illustrated in Figure 8.32(c).

We can again sketch the voltage waveforms at the load and at the junction by tracing the waves and using the above transmission and reflection coefficients while noting the direction of travel of the incident wave. For example, consider the series connection of two different lines illustrated in Figure 8.33(a). We wish to sketch the voltage at the load and at the junction. The line is series matched at the source and terminated in an open circuit. Line 1 has a total time delay of 1 ns and a characteristic impedance of 50Ω , whereas line 2 has a total time delay of 2 ns and a characteristic impedance of 100Ω . First, we compute the appropriate reflection and transmission coefficients for a wave incident on the junction from line 1 as shown:

$$\begin{aligned} \Gamma_{12} &= \frac{Z_{C2} - Z_{C1}}{Z_{C2} + Z_{C1}} \\ &= \frac{100 - 50}{100 + 50} \\ &= \frac{1}{3} \\ T_{12} &= \frac{2Z_{C2}}{Z_{C2} + Z_{C1}} \\ &= \frac{200}{100 + 50} \\ &= \frac{4}{3} \end{aligned}$$

Observe that $1 + \Gamma_{12} = T_{12}$. Similarly, for a wave incident on the junction from line 2, we obtain

$$\begin{aligned} \Gamma_{21} &= \frac{Z_{C1} - Z_{C2}}{Z_{C1} + Z_{C2}} \\ &= \frac{50 - 100}{50 + 100} \\ &= -\frac{1}{3} \\ T_{21} &= \frac{2Z_{C1}}{Z_{C1} + Z_{C2}} \\ &= \frac{100}{50 + 100} \\ &= \frac{2}{3} \end{aligned}$$

Again, observe that $1 + \Gamma_{21} = T_{21}$. The initial voltage sent out onto line 1 is

$$\begin{aligned} V_{\text{init}} &= \frac{Z_{C1}}{(R_S = Z_{C1}) + Z_{C1}} 5 \text{ V} \\ &= 2.5 \text{ V} \end{aligned}$$

Figure 8.33(b) shows the load voltage at the end of line 2. The initial voltage of 2.5 V is sent out and at one time delay of line 1, 1 ns, arrives at the junction. A voltage of $\Gamma_{12}2.5 \text{ V} = 0.833 \text{ V}$ is reflected to the left, arriving at the source after another 1 ns, where it is completely absorbed. A voltage of $T_{12}2.5 \text{ V} = 3.333 \text{ V}$ is transmitted across the junction onto line 2, arriving at the open-circuit load after 2 ns more or 3 ns. The open-circuited load had a reflection coefficient of +1, and hence 3.333 V is reflected. Thus, the total voltage is 6.667 V. This reflected voltage of 3.333 V arrives at the junction incident from the right after another 2 ns where $T_{21}3.333 \text{ V} = 2.222 \text{ V}$ is transmitted across the junction and after an additional 1 ns arrives at the source where it is completely absorbed. However, a reflected voltage of $\Gamma_{21}3.333 \text{ V} = -1.111 \text{ V}$ is reflected at the junction sending this back to the right, arriving at the load after 2 ns more or 7 ns. Since the load reflection coefficient is +1, this is totally reflected giving a total of 4.444 V. The process continues where the incoming (from the right) wave of 1 (reflected at the load) arrives at the junction after 2 ns more where $\Gamma_{21}(-1.111 \text{ V}) = +0.37 \text{ V}$ is reflected back to the load, arriving there after an additional 2 ns or 11 ns where it is completely reflected giving a total of 5.185 V.

Sketching the voltage at the junction is done in a similar process and is shown in Figure 8.33(c). The initially sent out voltage of 2.5 V arrives at the junction at 1 ns, where $\Gamma_{12}2.5 \text{ V} = 0.833 \text{ V}$ is reflected and $T_{12}2.5 \text{ V} = 3.333 \text{ V}$ is transmitted across the junction onto line 2. We can calculate the total voltage at the junction either as $v_{i1} + v_{r1} = 2.5 + 0.833 = 3.333 \text{ V}$ or as $v_{t2} = 3.333 \text{ V}$ since the voltages on either side of the junction must be equal. The reflected voltage of 0.833 V is totally absorbed at the matched source, but the transmitted voltage arrives at the load after an additional 2 ns and is totally reflected giving 3.333 V, arriving at the junction (as an incident wave from the right) after another 2 ns or a total of 1 ns + 2 ns + 2 ns = 5 ns. This is reflected as $\Gamma_{21}3.333 \text{ V} = -1.111 \text{ V}$ and transmitted as $T_{21}3.333 \text{ V} = 2.222 \text{ V}$. Since the total voltage on either side of the junction must be the same, we obtain either $(1 + \Gamma_{21})3.333 \text{ V} = 2.222 \text{ V}$ or $T_{21}3.333 \text{ V} = 2.222 \text{ V}$. Adding this to the voltage of 3.333 V already present gives a total voltage of 5.556 V. The 2.222 V is reflected and arrives at the load after another 2 ns, at which time it is completely reflected arriving at the junction after another 2 ns or a total of 9 ns. This is reflected as $\Gamma_{21}2.222 \text{ V} = -0.741 \text{ V}$. Adding this to the voltages present from previous reflections gives a total of 4.815 V. This is sketched in Figure 8.33(c).

PSPICE can be used to sketch both these voltages. The PSPICE code is

EXAMPLE

```
VS 1 0 PWL(0 0 1.0P 5 100N 5)
RS 1 2 50
```

```
T1 2 0 3 0 Z0=50 TD=1N
T2 3 0 4 0 Z0=100 TD=2N
RL 4 0 1E8
.TRAN 0.1N 20N 0 0.1N
.PROBE
.END
```

and we have used a rise time of 1 ps to simulate the step voltage. The voltages at the junction and at the load are sketched using PROBE in Figure 8.33(d), which confirm the hand-calculated plots.

In the previous example, series matching at the source does not eliminate reflections as evidenced in the computed results. This is due to the discontinuity. Reflections at the discontinuity that are sent back to the source are absorbed at the source because of matching, but a portion of the incident wave at the discontinuity is transmitted across the discontinuity and sent to the load. Because the load is not matched to the second part of the line, a reflection is transmitted back to the left, which is incident on the discontinuity and hence a portion is transmitted across it toward the source where it is absorbed. Consider the reverse, that is, suppose we parallel match at the load but do not series match at the source. A wave sent out by the source and incident on the discontinuity will create a reflection that is sent back to the source where it will be reflected. The portion of the incident wave that is transmitted across the discontinuity will be incident on the load but will be completely absorbed because the load is parallel matched. But the portion of the wave reflected at the source will again be incident on the discontinuity, and a portion will be transmitted across the discontinuity. This will again be incident on the load where it is absorbed. But we will have reflections at the source and at the discontinuity. Hence, in order to eliminate reflections we must series match at the source and parallel match at the load.

8.2 INCORPORATION OF LOSSES

Losses occur in the conductors and in the surrounding medium. Since these losses are, in general, frequency dependent, the frequency-domain representation of the transmission-line equations is the best way to represent them. Hence, the frequency-domain transmission-line equations are (see Chapter 2)

$$\begin{aligned} \frac{d\hat{V}(z, \omega)}{dz} &= - \underbrace{[r(\omega) + j\omega l_i(\omega)]}_{\hat{z}_i(\omega)} \hat{I}(z, \omega) - j\omega \hat{L}(z, \omega) \\ &= -\hat{z}(\omega) \hat{I}(z, \omega) \end{aligned} \tag{8.112a}$$

$$\begin{aligned} \frac{d\hat{I}(z, \omega)}{dz} &= -g(\omega) \hat{V}(z, \omega) - j\omega c \hat{V}(z, \omega) \\ &= -\hat{y}(\omega) \hat{V}(z, \omega) \end{aligned} \tag{8.112b}$$

where the per-unit-length impedance and admittance, respectively, are

$$\hat{z}(\omega) = \hat{z}_i(\omega) + j\omega l \quad (8.113a)$$

$$\hat{y}(\omega) = g(\omega) + j\omega c \quad (8.113b)$$

and the internal impedance of the conductors is

$$\hat{z}_i(\omega) = r(\omega) + j\omega l_i(\omega) \quad (8.113c)$$

The frequency-dependent per-unit-length (pul) resistance is denoted by $r(\omega)$, whereas the frequency-dependent pul internal inductance due to magnetic flux internal to the conductors is denoted by $l_i(\omega)$ and $\omega = 2\pi f$ is the radian frequency of excitation of the line. The frequency-dependent pul conductance due to losses in the surrounding dielectric is denoted by $g(\omega)$. The external pul parameters of inductance, l , and capacitance, c , are essentially independent of frequency up to frequencies in the lower GHz range. The relative permittivity ϵ_r of the surrounding dielectric medium may be a slight function of frequency, in which case c will be slightly frequency dependent. For example, polyvinyl chloride, a typical wire insulation material, has $\epsilon_r = 4.3$ at 10 kHz, but this decreases to $\epsilon_r = 3$ at 100 MHz [7]. The fact that some of the per-unit-length parameters are generally functions of frequency presents no problems in the solution of these frequency-domain versions of the transmission-line equations. These equations are solvable at each frequency by evaluating the per-unit-length parameters at that frequency and including them as constants at that frequency (see Chapter 6).

The Laplace transform of these equations is also a convenient and meaningful way to represent them. Replacing $s \iff j\omega$ yields

$$\begin{aligned} \frac{d\hat{V}(z, s)}{dz} &= -\hat{z}(s) \hat{I}(z, s) \\ &= -\hat{z}_i(s) \hat{I}(z, s) - s\hat{I}(z, s) \end{aligned} \quad (8.114a)$$

$$\begin{aligned} \frac{d\hat{I}(z, s)}{dz} &= -\hat{y}(s) \hat{V}(z, s) \\ &= -\hat{g}(s) \hat{V}(z, s) - s\hat{V}(z, s) \end{aligned} \quad (8.114b)$$

and the transform of the internal impedance is denoted as

$$\hat{z}_i(s) = r(s) + sl_i(s) \quad (8.115)$$

In the time domain, Eqs. (8.114) give convolutions:

$$\frac{\partial V(z, t)}{\partial z} = -z_i(t) * I(z, t) - l \frac{\partial I(z, t)}{\partial t} \quad (8.116a)$$

$$\frac{\partial I(z, t)}{\partial z} = -g(t) * V(z, t) - c \frac{\partial V(z, t)}{\partial t} \quad (8.116b)$$

where $*$ denotes *convolution* as [A.2, A.5]

$$z_i(t) * I(z, t) = \int_0^t z_i(\tau) I(z, t - \tau) d\tau \quad (8.117a)$$

$$g(t) * V(z, t) = \int_0^t g(\tau) V(z, t - \tau) d\tau \quad (8.117b)$$

and $z_i(t)$ and $g(t)$ are the inverse transforms of the pul internal impedance $\hat{z}_i(s)$ and the pul conductance $\hat{g}(s)$:

$$\hat{z}_i(s) \iff z_i(t) \quad (8.118a)$$

$$\hat{g}(s) \iff g(t) \quad (8.118b)$$

Hence, frequency-dependent per-unit-length parameters can be easily included in the frequency-domain transmission-line equations, but their inclusion in the time-domain transmission-line equations presents significant computational problems because of the requirement to (1) obtain the time-domain per-unit-length parameters from the frequency-domain parameters and (2) perform the required convolution.

8.2.1 Representing Frequency-Dependent Losses

Representation of these frequency-dependent losses in the frequency domain was discussed in Chapter 4. In this section, we will summarize those important concepts. In addition, we will investigate the implementation of convolution with these frequency-dependent loss parameters.

8.2.1.1 Representing Losses in the Medium The primary loss mechanism in dielectrics is due to polarization loss where the bound charges are represented by dipoles [A.1]. Their rotation to align with changes in an applied sinusoidally varying electric field lags behind and is not complete at the higher frequencies. This is represented by a complex permittivity as [7,8]

$$\hat{\epsilon} = \epsilon - j\epsilon_p \quad (8.119)$$

where ϵ_p is due to the lag in the rotation of the bound charge dipoles to align with the applied electric field with increasing frequencies. Dielectrics usually have a very small and generally negligible conductivity σ due to free charge in them. Substituting

(8.119) into Ampere's law gives

$$\begin{aligned}\nabla \times \vec{H} &= \sigma \vec{E} + j\omega \hat{\epsilon} \vec{E} \\ &= \underbrace{(\sigma + \omega \epsilon_p)}_{\sigma_{\text{eff}}} \vec{E} + j\omega \epsilon \vec{E}\end{aligned}\quad (8.120)$$

Hence, the effective conductivity representing conductive and polarization losses is

$$\sigma_{\text{eff}} = (\sigma + \omega \epsilon_p) \quad (8.121)$$

The *loss tangent* of the material is tabulated in handbooks at various frequencies [9] and is the ratio of the conduction current to the displacement current as

$$\begin{aligned}\tan \delta &= \frac{(\sigma + \omega \epsilon_p)}{\omega \epsilon} \\ &\cong \frac{\epsilon_p}{\epsilon}\end{aligned}\quad (8.122)$$

The polarization losses represented by $\omega \epsilon_p$ will dominate the resistive losses that are represented by σ in typical dielectrics of practical interest. Both ϵ and ϵ_p are functions of frequency. Hence, the loss tangent is frequency dependent. Therefore, the effective conductivity of a dielectric is frequency dependent and is related to the loss tangent as

$$\sigma_{\text{eff}} = \omega \epsilon \tan \delta \quad (8.123)$$

Hence, in a *homogeneous medium*, the per-unit-length conductance is related to the per-unit-length capacitance as

$$\begin{aligned}g &= \frac{\sigma_{\text{eff}}}{\epsilon} c \\ &= \omega \tan \delta c\end{aligned}\quad (8.124)$$

Since the loss tangent is a function of frequency, this does not imply that the per-unit-length conductance increases linearly with frequency.

The frequency-dependent complex permittivity in (8.119) can be represented over the frequency range of interest with the Debye model [7,8,10–12] as

$$\begin{aligned}\hat{\epsilon}(\omega) &= \epsilon(\omega) - j\epsilon_p(\omega) \\ &= \epsilon_{\text{hf}} + \sum_{i=1}^N \frac{K_i}{1 + j\omega\tau_i}\end{aligned}\quad (8.125)$$

and τ_i are the dipole relaxation time constants. At infinite frequency, $\lim_{f \rightarrow \infty} \epsilon_{\text{hf}} = \epsilon_0$ [7,11]. At dc, $\epsilon_r \epsilon_0 = \epsilon_{\text{hf}} + \sum_{i=1}^N K_i$. Noting that

$$\frac{K_i}{1 + j\omega\tau_i} \times \frac{1 - j\omega\tau_i}{1 - j\omega\tau_i} = \frac{K_i - jK_i\omega\tau_i}{1 + \omega^2\tau_i^2}$$

we obtain the real and imaginary parts of $\hat{\epsilon}(\omega)$ as

$$\epsilon(\omega) = \epsilon_{\text{hf}} + \sum_{i=1}^N \frac{K_i}{1 + \omega^2\tau_i^2} \tag{8.126a}$$

$$\epsilon_p(\omega) = \sum_{i=1}^N \frac{K_i\omega\tau_i}{1 + \omega^2\tau_i^2} \tag{8.126b}$$

The Debye model satisfies the Kronig–Kramers requirements for *causality* obtained in Section 2.4.1 of Chapter 2. Also, from Section 2.4.1 of Chapter 2, in order for the inverse transform to represent a real function of time, the real part of the complex permittivity must be an even function of frequency, that is, $\epsilon(\omega) = \epsilon(-\omega)$, and the imaginary part must be an odd function of frequency, that is, $\epsilon_p(\omega) = -\epsilon_p(-\omega)$, which (8.126) satisfy. The terms in the model, ϵ_{hf} , K_i , and τ_i , can be obtained by comparison with measured frequency response data [10]. Figure 8.34 illustrates a frequency response plot of the real and imaginary parts of the complex permittivity for typical dielectrics [7,11]. The real part decreases from the dc value of $\epsilon_r \epsilon_0$ to its value at high frequencies of $\epsilon_\infty = \epsilon_0$, exhibiting resonances at $\omega_i = 1/\tau_i$ much like a low-pass filter having several cutoff frequencies. The real part of the model in (8.126a) models this behavior but excludes the resonances shown. The imaginary part exhibits resonances at each $\omega_i = 1/\tau_i$ in a form like that of bandpass filters. Equation (8.126b) models this behavior of the imaginary part.

8.2.1.2 Representing Losses in the Conductors and Skin Effect As discussed in Chapter 4, as frequency increases, the currents in the conductors move to their surfaces, eventually residing in depths on the order of a skin depth

$$\delta = \frac{1}{\sqrt{\pi f \mu \sigma}} \tag{8.127}$$

For isolated conductors of circular cylindrical cross sections (wires), the current distribution at dc and at high frequencies where skin effect is well developed is illustrated in Figure 8.35. Hence, we can obtain approximations to that pul resistance as

$$\left. \begin{aligned} r_{\text{dc}} &= \frac{1}{\sigma\pi r_w^2} \text{ } \Omega/\text{m} \\ l_{i,\text{dc}} &= \frac{\mu_0}{8\pi} = 0.5 \times 10^{-7} \text{ H/m} \end{aligned} \right\} r_w < 2\delta \tag{8.128a}$$

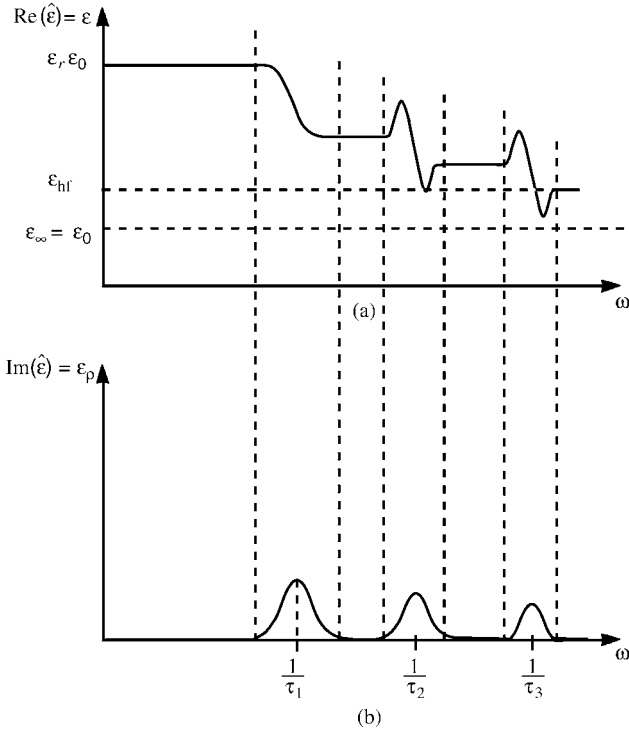


FIGURE 8.34 Illustration of the frequency response of the real and imaginary parts of the complex permittivity $\hat{\epsilon} = \epsilon - j\epsilon_p$ of a lossy dielectric.

$$\left. \begin{aligned}
 r_{hf} &= \frac{1}{2\pi r_w \sigma \delta} = \frac{1}{2r_w} \sqrt{\frac{\mu_0}{\pi \sigma}} \sqrt{f} \quad \Omega/\text{m} \\
 l_{i,hf} &= \frac{1}{4\pi r_w} \sqrt{\frac{\mu_0}{\pi \sigma}} \frac{1}{\sqrt{f}} \quad \text{H/m}
 \end{aligned} \right\} r_w > 2\delta \tag{8.128b}$$

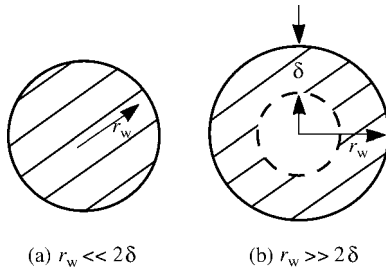


FIGURE 8.35 Illustration of skin effect for a solid wire.

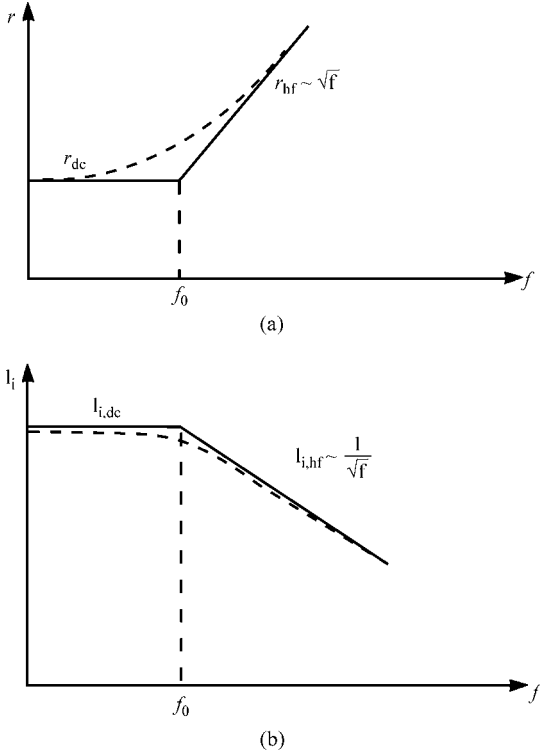


FIGURE 8.36 Asymptotic representation of the frequency response of the internal impedance of a wire.

Again, observe that the high-frequency resistance r_{hf} increases as the square root of frequency, \sqrt{f} , whereas the high-frequency internal inductance $l_{i,hf}$ decreases as the square root of frequency, $1/\sqrt{f}$. Hence we may, as a reasonable computational simplification, represent the pul resistance and internal inductance each with two asymptotes as illustrated in Figure 8.36. It was shown in Chapter 4 that for wires the asymptotes for the resistance and for the internal inductance join at the same frequency f_0 . In the case of an isolated wire, this break frequency is located where the wire radius is two skin depths, $r_w = 2\delta$, giving a break frequency of

$$f_0 = \frac{4}{\pi r_w^2 \mu_0 \sigma} \quad (r_w = 2\delta) \tag{8.129}$$

Also, observe that the high-frequency resistance and internal inductive reactance are equal, that is,

$$r_{hf} = \omega l_{i,hf} \tag{8.130}$$

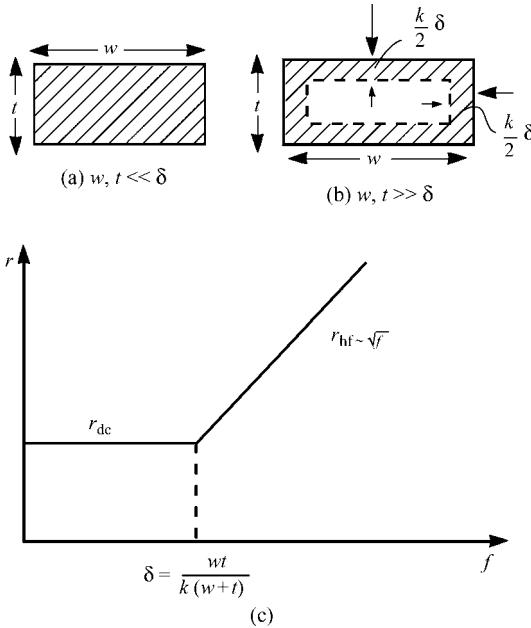


FIGURE 8.37 Asymptotic representation of the frequency response of the resistance of a PCB land.

The property in (8.130) is unique to wires but applies in an approximate fashion to conductors of rectangular cross section such as PCB lands.

Conductors of rectangular cross section such as PCB lands do not yield closed-form solutions for the pul resistance and internal inductance (see [13], Appendix III, for an approximate solution for the pul resistance of an isolated rectangular bar). Consider a conductor of rectangular cross section and width w and thickness t . Numerical solutions for the pul resistance and internal inductance were provided in Chapter 4. These computations show that at low frequencies where the width and thickness are much less than a skin depth, the current is again uniformly distributed over the cross section as illustrated in Figure 8.37(a). As frequency increases, the current crowds to the edges eventually lying substantially within a thickness of a few skin depths as illustrated in Figure 8.37(b). Numerical computations in Chapter 4 also showed a behavior unlike that of a wire; the current distribution over the PCB land cross section tends to peak at the corners. (See Figure 4.20 of Chapter 4 and Appendix III of [13]). This behavior complicates the characterization of the pul resistance and internal inductance of the land. Nevertheless, we will approximately characterize the resistance as shown in Figure 8.37(c) with two asymptotes that are joined at a frequency where

$$\delta = \frac{wt}{k(w+t)} \tag{8.131}$$

Numerical computations indicate that the constant k lies between 1 and 2, $1 < k < 2$. The dc resistance is, of course,

$$r_{\text{dc}} = \frac{1}{\sigma w t} \quad (\Omega/\text{m}) \quad (8.132\text{a})$$

and, referring to Figure 8.37(b), the high-frequency pul resistance is (approximately)

$$r_{\text{hf}} = \frac{1}{k\sigma\delta(w+t)} \quad (\Omega/\text{m}) \quad (8.132\text{b})$$

The computation of the pul internal inductance is not so simple. Numerical computations are shown in Figures 4.21 and 4.22 of Chapter 4. These indicate, as expected, that the high-frequency resistance, like that of a wire, increases as the square root of frequency, \sqrt{f} , and the high-frequency internal inductance decreases as the square root of frequency, $1/\sqrt{f}$. However, these figures show that, unlike the wire, the high-frequency resistance and high-frequency internal inductive reactance of an isolated conductor of rectangular cross section (PCB land) are not identical, that is, $r_{\text{hf}} \neq \omega l_{i,\text{hf}}$. However, for lands that have a high aspect ratio, that is, $w \gg t$, they are approximately equal, that is, $r_{\text{hf}} \cong \omega l_{i,\text{hf}}$. For example, for a land of width 15 mils and thickness 1.4 mils whose results are compared in Figure 4.21, the high-frequency resistance and internal inductive reactance differ by only about 10%. For square lands (see Figure 4.22), the high-frequency resistance and internal inductive reactance differ by about 30%. We can also represent the pul resistance and internal inductance with two asymptotes as for wires in Figure 8.36. However, the break frequency for the resistance and the break frequency for the internal inductance are not equal. We may make the approximation $r_{\text{hf}} = \omega l_{i,\text{hf}}$ for PCB lands because $l_{i,\text{hf}}$ is effectively added to the external inductance l in the transmission-line equations in (8.112a). The high-frequency internal inductance for practical line dimensions is orders of magnitude smaller than the external inductance and decreases with increasing frequency as \sqrt{f} . Hence, any approximation error in assuming $r_{\text{hf}} = \omega l_{i,\text{hf}}$ in the case of PCB lands is absorbed in and negligible with respect to the external inductance.

Hence for wires and PCB lands, we will approximate the frequency behavior with asymptotic representations shown in Figure 8.36. The break frequencies f_0 for both the resistance and the internal inductance are assumed equal for both wires and PCB lands. This will greatly simplify the characterization of these parameters. For example, because the two asymptotes join at the same frequency f_0 , we can write

$$r = \begin{cases} r_{\text{dc}}, & f < f_0 \\ r_{\text{dc}} \sqrt{\frac{f}{f_0}}, & f > f_0 \end{cases} \quad (8.133\text{a})$$

and

$$l_i = \begin{cases} l_{i,\text{dc}}, & f < f_0 \\ l_{i,\text{dc}} \sqrt{\frac{f_0}{f}}, & f > f_0 \end{cases} \quad (8.133\text{b})$$

We can also relate r_{dc} and $l_{i,\text{dc}}$. The high-frequency resistance and internal inductive reactance are also equal:

$$r_{\text{hf}} = \omega l_{i,\text{hf}} \quad (8.134)$$

The asymptotic approximate characterization in Figure 8.36 allows us to obtain a relation between the dc resistance r_{dc} and dc internal inductance $l_{i,\text{dc}}$. Substituting the high-frequency relations given in (8.133) into (8.134) gives, at $\omega_0 = 2\pi f_0$,

$$r_{\text{dc}} = \omega_0 l_{i,\text{dc}} \quad (8.135)$$

This can be verified for wires:

$$r_{\text{dc}} = \frac{1}{\pi r_w^2 \sigma} = 2\pi \underbrace{\frac{4}{\pi r_w^2 \mu_0 \sigma}}_{f_0} \times \underbrace{\frac{\mu_0}{8\pi}}_{l_{i,\text{dc}}} \quad (8.136)$$

which checks. Substituting (8.135) into (8.133) gives a simple approximation for the internal impedance of the conductors (which is true for wires and approximately true for PCB lands) as

$$\hat{z}_i(\omega) = r(\omega) + j\omega l_i(\omega) = \begin{cases} r_{\text{dc}} \left(1 + j \frac{f}{f_0} \right), & f < f_0 \\ r_{\text{dc}} \sqrt{\frac{f}{f_0}} (1 + j), & f > f_0 \end{cases} \quad (8.137)$$

These relations satisfy the requirement $\hat{z}_i(-\omega) = \hat{z}_i^*(\omega)$ derived in Section 2.4.1 of Chapter 2 for the transform to represent a real-valued function of time, $z_i(t)$. The relations in (8.137) require that we need only obtain (1) r_{dc} and (2) f_0 in order to characterize the complete frequency behavior with the asymptotic characterization in Figure 8.36. We can easily obtain the values for wires for r_{dc} (8.128a) and f_0 (8.129). We can approximately obtain these for PCB lands from (8.132a) and (8.131).

8.2.1.3 Convolution with Frequency-Dependent Losses The final task is to determine the time-domain form of the pul internal impedance, $\hat{z}_i(s)$, and conductance, $\hat{g}(s)$. Once this is done, we next address how to perform the convolutions $\hat{z}_i(s) * \hat{I}(z, s)$ and $\hat{g}(s) * \hat{V}(z, s)$.

First, consider the pul internal impedance given in asymptotic form in (8.137). The fact that the high-frequency internal impedance varies as the square root of frequency

makes this a very difficult task. There are some known inverse Laplace transforms of impedances that depend on square root of frequency [3,14,15]. The inverse Laplace transform of the square root of the Laplace transform variable is known [14]:

$$\frac{1}{\sqrt{s}} \iff \frac{1}{\sqrt{\pi}} \frac{1}{\sqrt{t}} \tag{8.138}$$

where s denotes the Laplace transform variable. We have the important complex variable relation [A.5]:

$$\begin{aligned} \sqrt{j\omega} &= \frac{\sqrt{\omega}}{\sqrt{2}} (1 + j) \\ &= \sqrt{\pi} \sqrt{f} (1 + j) \end{aligned} \tag{8.139}$$

This gives insight as to how we should go about obtaining frequency-domain functions that are transformable to the time domain. We need to write the frequency-domain function in the form of the square root of frequency multiplied by $(1 + j)$. Then transform that result to the Laplace domain by using (8.139), replace $j\omega \Rightarrow s$, and use (8.138). For example, the high-frequency surface impedance of plane conductors occurs frequently in electromagnetic scattering problems and is given by [3,15]

$$\begin{aligned} \hat{Z}(\omega) &= \sqrt{\frac{j\omega \mu}{\sigma}} \\ &= \sqrt{j\omega} \sqrt{\frac{\mu}{\sigma}} \end{aligned} \tag{8.140}$$

The Laplace transform of this is

$$\hat{Z}(s) = \sqrt{\frac{\mu}{\sigma}} \sqrt{s} \tag{8.141}$$

In order to utilize the inverse transform in (8.138), we multiply numerator and denominator by \sqrt{s} to yield

$$\begin{aligned} \hat{Z}(s) &= \sqrt{\frac{\mu}{\sigma}} \sqrt{s} \\ &= \sqrt{\frac{\mu}{\sigma}} \frac{1}{\sqrt{s}} s \end{aligned} \tag{8.142}$$

whose inverse transform is, according to (8.138),

$$Z(t) = \sqrt{\frac{\mu}{\pi\sigma}} \frac{1}{\sqrt{t}} \frac{\partial}{\partial t} \tag{8.143}$$

Hence, the convolution of this time-domain impedance with another function of time requires that we convolve this with the time derivative of that time function.

In the case of the line conductors of the transmission line, a simple way of obtaining this inverse transform of the conductor internal impedance is described in [16–18]. This relies on writing the Laplace transform of the conductor internal impedance in the form of $A + B\sqrt{s}$. The inverse transform of this result is, using (8.138),

$$A + B\sqrt{s} = A + B \frac{1}{\sqrt{s}} s \iff A + \frac{B}{\sqrt{\pi}} \frac{1}{\sqrt{t}} \frac{\partial}{\partial t} \quad (8.144)$$

This form can be achieved for conductors by simply adding the dc and high-frequency representations from (8.137) as

$$\hat{z}_i(\omega) = r_{dc} + r_{dc} \frac{\sqrt{\omega}}{\sqrt{\omega_0}} (1 + j) \quad (8.145)$$

We identify $A = r_{dc}$ and have omitted the dc internal inductance. This is a reasonable approximation since it is dominated by the external (loop) inductance of the line. The dc internal inductance $l_{i,dc}$ is (see (8.112a)) in series with the loop inductance l and is almost always negligible since it is much smaller than the loop inductance. Using (8.139) yields

$$\hat{z}_i(\omega) = r_{dc} + r_{dc} \frac{1}{\sqrt{\pi}\sqrt{f_0}} \sqrt{j\omega} \quad (8.146)$$

This relation satisfies the requirement $\hat{z}_i(-\omega) = \hat{z}_i^*(\omega)$ derived in Section 2.4.1 of Chapter 2 for the transform to represent a real-valued function of time, $z_i(t)$. The Laplace transform is

$$\begin{aligned} \hat{z}_i(s) &= r_{dc} + r_{dc} \frac{1}{\sqrt{\pi}\sqrt{f_0}} \sqrt{s} \\ &= r_{dc} + r_{dc} \frac{1}{\sqrt{\pi}\sqrt{f_0}} \frac{1}{\sqrt{s}} s \end{aligned} \quad (8.147)$$

We identify $A = r_{dc}$ and $B = \frac{r_{dc}}{\sqrt{\pi}\sqrt{f_0}}$. Hence, the inverse transform is

$$z_i(t) = r_{dc} + r_{dc} \frac{1}{\pi} \frac{1}{\sqrt{f_0}} \frac{1}{\sqrt{t}} \frac{\partial}{\partial t} \quad (8.148)$$

Next, we perform the required convolution given in (8.117a):

$$z_i(t) * I(z, t) = \int_0^t z_i(\tau) I(z, t - \tau) d\tau$$

$$= r_{dc} I(z, t) + r_{dc} \frac{1}{\pi} \frac{1}{\sqrt{f_0}} \int_0^t \frac{1}{\sqrt{\tau}} \frac{\partial I(z, t - \tau)}{\partial (t - \tau)} d\tau \quad (8.149)$$

We will show in Section 8.2.3 how to discretize this convolution and include it into a numerical analysis.

The representation $A + B\sqrt{s}$ essentially adds the dc and high-frequency asymptotes as shown in Figure 8.38. Observe in Figure 8.38(a) that adding the asymptotes for the resistance gives a reasonable approximation because below f_0 the dc resistance

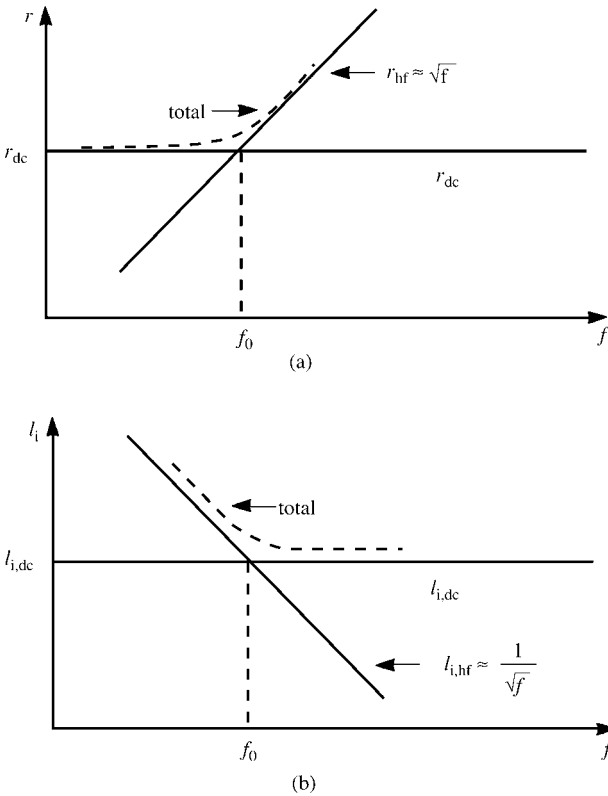


FIGURE 8.38 Illustration of the point that representing the conductor internal impedance as $A + B\sqrt{s}$ provides an error resulting from the high-frequency internal impedance being added to the low-frequency response.

asymptote dominates the high-frequency resistance asymptote as it should, giving the total as the dc resistance asymptote. Above f_0 , the high-frequency resistance asymptote dominates the dc resistance asymptote as it should, giving the total as the high-frequency asymptote. However, adding the internal inductance asymptotes as in Figure 8.38(b) causes some inaccuracy below f_0 since the high-frequency asymptote dominates the dc asymptote. (The approximation $A + B\sqrt{s}$ inherently omits the dc internal inductance, but this has little effect on the result because of the dominance of the high-frequency internal inductance in this region.) A method was given in [B.23] to rectify this problem. The $A + B\sqrt{s}$ model of the conductor impedance given in (8.145) can be modified to simulate the frequency-selective model given in (8.137) by multiplying the low-frequency impedance by a first-order low-pass filter and multiplying the high-frequency impedance by a first-order high-pass filter:

$$\begin{aligned} \hat{z}_i(\omega) &= \underbrace{r_{dc} \left(1 + j \frac{\omega}{\omega_0}\right)}_{\hat{z}_{i,dc}} \underbrace{\left(\frac{\omega_0}{\omega_0 + j\omega}\right)}_{\text{low-pass filter}} + \underbrace{r_{dc} \sqrt{\frac{\omega}{\omega_0}} (1 + j)}_{\hat{z}_{i,hf}} \underbrace{\left(\frac{j\omega}{\omega_0 + j\omega}\right)}_{\text{high-pass filter}} \\ &= r_{dc} + r_{dc} \left[\sqrt{\frac{2}{\omega_0}} \sqrt{j\omega} \left(\frac{j\omega}{\omega_0 + j\omega}\right) \right]. \end{aligned} \quad (8.150)$$

This relation satisfies the requirement $\hat{z}_i(-\omega) = \hat{z}_i^*(\omega)$ derived in Section 2.4.1 of Chapter 2 for the transform to represent a real-valued function of time, $z_i(t)$. Observe that this representation includes the dc internal inductance. Figure 8.39 shows the comparison between the frequency-selective representation of (8.137), the first-order filter representation of (8.150), a second-order filter representation, and the simple addition of $A + B\sqrt{s}$ given in (8.145). The first-order filter representation of (8.150) provides a reasonable approximation of the frequency-selective representation. The second-order filter improves this representation, but the computational implementation is considerably more complex than the first-order representation. In terms of the Laplace transform, (8.150) becomes

$$\hat{z}_i(s) = r_{dc} + r_{dc} \sqrt{\frac{2}{\omega_0}} \left(\frac{\sqrt{s}}{s + \omega_0}\right) s \quad (8.151)$$

The function in (8.151) has the inverse transform [14]

$$\frac{\sqrt{s}}{s + \omega_0} \iff \frac{1}{\sqrt{\pi t}} - \frac{2\sqrt{\omega_0}}{\sqrt{\pi}} e^{-\omega_0 t} \int_0^{\sqrt{\omega_0 t}} e^{-\lambda^2} d\lambda \quad (8.152)$$

Thus, the relevant convolution in (8.149) becomes

$$\begin{aligned} \hat{z}_i(s)I(z, s) &\iff z_i(t) * I(z, t) \\ &= r_{dc}I(z, t) + r_{dc}\sqrt{\frac{2}{\pi}} \left[\frac{1}{\sqrt{\alpha}} - 2e^{-\alpha} \int_0^{\sqrt{\alpha}} e^{\lambda^2} d\lambda \right] * \frac{\partial I(z, t)}{\partial t} \end{aligned} \tag{8.153a}$$

where

$$\alpha = \omega_0 t \tag{8.153b}$$

Note that the bracketed term in (8.153) may be computed in terms of α ; that is, it is independent of the specific break frequency of the conductor impedance ω_0 and is therefore independent of the specific problem. The integral in the second term in (8.153) can be approximated as

$$\begin{aligned} \int_0^{\sqrt{\alpha}} e^{\lambda^2} d\lambda &= \int_0^{\sqrt{\alpha}} \left[1 + \frac{\lambda^2}{1!} + \frac{\lambda^4}{2!} + \dots \right] d\lambda \\ &= \left[\alpha^{\frac{1}{2}} + \frac{\alpha^{\frac{3}{2}}}{3 \times 1!} + \frac{\alpha^{\frac{5}{2}}}{5 \times 2!} + \dots \right] \\ &= \sum_{n=0}^{\infty} \frac{\alpha^{n+\frac{1}{2}}}{(2n+1)n!} \end{aligned} \tag{8.154}$$

The frequency-dependent per-unit-length conductance $g(\omega)$ can be easily included in a convolution if we assume a *homogeneous medium*, for example, a stripline. It becomes a bit more detailed for a lossy inhomogeneous medium although, in principle, the method of calculating the pul capacitance using a complex permittivity discussed in Chapter 4 can be used to obtain $g(\omega)$ for an inhomogeneous medium at several frequencies and using curve fitting. For a homogeneous medium, the per-unit-length capacitance can be written as the product of the permittivity and a constant M as

$$\hat{c}(\omega) = \hat{\epsilon}(\omega)M \tag{8.155}$$

Substituting the Debye expression for $\hat{\epsilon}(\omega)$ given in (8.125) gives

$$\begin{aligned}\hat{c}(\omega) &= \left[\epsilon_{\text{hf}} + \sum_{i=1}^N \frac{K_i}{1 + j\omega\tau_i} \right] M \\ &= \left[\sum_{i=1}^N \frac{K_i}{1 + j\omega\tau_i} \right] M + c_{\text{hf}}\end{aligned}\quad (8.156)$$

and $c_{\text{hf}} = \epsilon_{\text{hf}}M$. Hence, the per-unit-length admittance is

$$\begin{aligned}\hat{y}(\omega) &= j\omega\hat{c}(\omega) \\ &= \left[\sum_{i=1}^N \frac{K_i}{1 + j\omega\tau_i} \right] j\omega M + j\omega c_{\text{hf}}\end{aligned}\quad (8.157)$$

Converting to the Laplace transform by substituting $j\omega \Rightarrow s$ yields

$$\hat{y}(s) = \left[\sum_{i=1}^N \frac{K_i}{1 + s\tau_i} \right] sM + sc_{\text{hf}}\quad (8.158)$$

The term $K_i/(1 + s\tau_i)$ has a simple inverse transform of $(K_i/\tau_i)e^{-t/\tau_i}$ [A.2,A.5]. Hence, the time-domain result is

$$y(t) = \left[\sum_{i=1}^N \frac{K_i}{\tau_i} e^{-t/\tau_i} \right] M \frac{\partial}{\partial t} + c_{\text{hf}} \frac{\partial}{\partial t}\quad (8.159)$$

The convolution $y(t) * V(t)$ in (8.116b) becomes

$$\begin{aligned}y(t) * V(t) &= \left[\sum_{i=1}^N M \frac{K_i}{\tau_i} e^{-t/\tau_i} \right] * \frac{\partial V(t)}{\partial t} + c_{\text{hf}} \frac{\partial V(t)}{\partial t} \\ &= M \sum_{i=1}^N \left[\frac{K_i}{\tau_i} \int_0^t e^{-\tau/\tau_i} \frac{\partial V(t-\tau)}{\partial(t-\tau)} d\tau \right] + c_{\text{hf}} \frac{\partial V(t)}{\partial t}\end{aligned}\quad (8.160)$$

The fact that the time-domain result $y(t)$ is the sum of exponentials makes the evaluation of the convolution $y(t) * V(z, t)$ in (8.116b) a simple task by using the method of *recursive convolution* to be described in Section 8.2.3.4.

8.2.2 The Time-Domain to Frequency-Domain (TDFD) Transformation Method

The TDFD transformation method described in Section 8.1.7 can easily incorporate frequency-dependent parameters since we need only to compute the

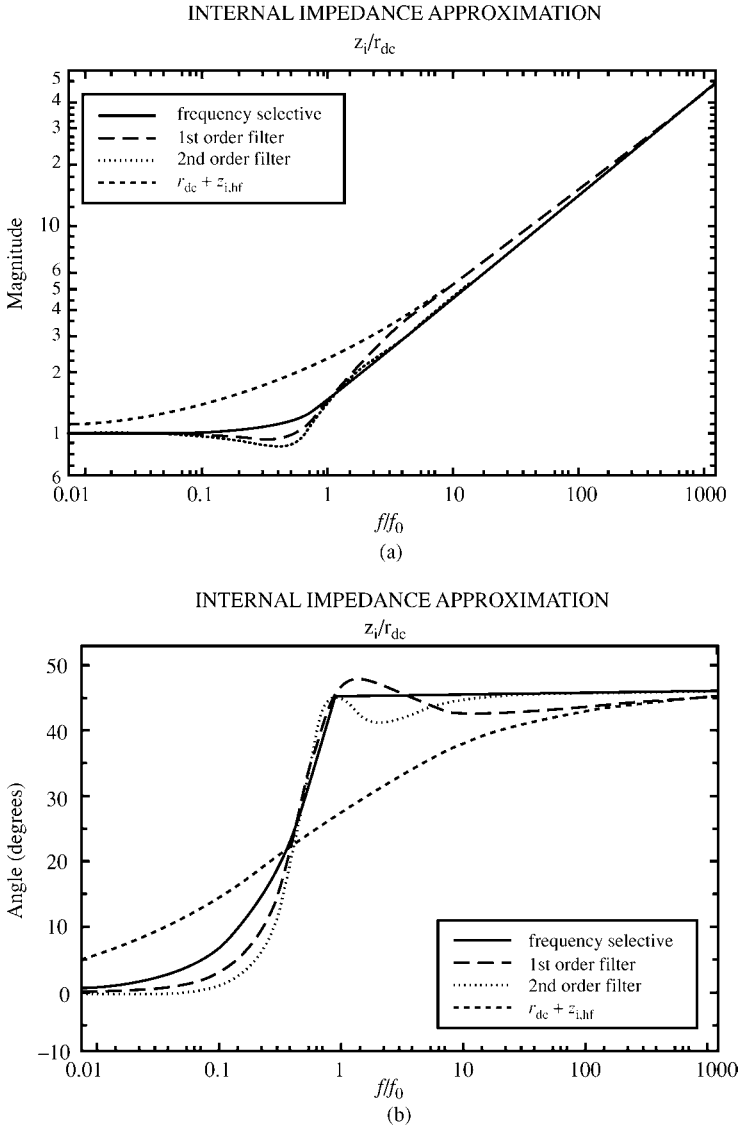


FIGURE 8.39 Plots of the magnitude and phase of the frequency-selective model of the conductor impedance, $A + B\sqrt{s}$, and the use of filters to eliminate the low-frequency error.

frequency-domain transfer function relating the source to the desired output (see Fig. 8.15). First, compute the Fourier series coefficients of the input waveform as

$$x(t) = c_0 + \sum_{n=1}^{NH} c_n \cos(n\omega_0 t + \angle c_n) \tag{8.161}$$

where the period of the input waveform is P and the fundamental frequency of the waveform is denoted by $\omega_0 = 2\pi f_0 = 2\pi/P$. Then compute the frequency-domain transfer function, including the frequency-dependent losses such as skin-effect losses and/or dielectric losses, at each harmonic frequency:

$$\hat{H}(jn\omega_0) = |\hat{H}(jn\omega_0)| \angle \hat{H}(jn\omega_0) \quad (8.162)$$

Then pass each component through this frequency-domain transfer function and recombine the time domain responses to each component in the time domain. To do this, we multiply each appropriate magnitude and add the angles to give the time-domain output as

$$y(t) = c_0 H(0) + \sum_{n=1}^{NH} c_n |\hat{H}(jn\omega_0)| \cos(n\omega_0 t + \angle c_n + \angle \hat{H}(jn\omega_0)) \quad (8.163)$$

In this way, we can include \sqrt{f} -dependent skin-effect losses that are difficult to characterize directly in the time domain. Again *this supposes a linear system*, that is, linear terminations on the line, but it gives us a simple way of verifying the accuracy of other solution methods. This method is implemented in the FORTRAN program TIMEFREQ.FOR described in Appendix A. The frequency-domain transfer function of the line can be computed including frequency-dependent skin-effect losses of the line conductors using the FORTRAN program MTL.FOR described in Appendix A.

8.2.3 The Finite-Difference, Time-Domain (FDTD) Method

The FDTD discretization of the time-domain transmission-line equations for lossy lines given in (8.116) can be accomplished in a virtually identical fashion to the case of lossless lines in Section 8.1.8 with reference to Figures 8.17 and 8.18. The only difference between the lossless and lossy line cases is in the discretization of the convolution terms in (8.117a) representing the frequency-dependent conductor losses and in (8.117b) representing the frequency-dependent dielectric losses.

8.2.3.1 Including Frequency-Independent Losses We have seen that the conductor loss per-unit-length parameters of resistance, $r(\omega)$, and internal inductance, $l_i(\omega)$, and the dielectric loss per-unit-length parameter of conductance, $g(\omega)$, are functions of frequency at high frequencies. At low frequencies, these are independent of frequency, that is, approximately their dc values. For today's high spectral content digital signals, this high-frequency dependence generally cannot be ignored. However, using the dc values of these parameters can give some reasonable approximations of the time-domain responses of the line as we will see in the computed results. In addition, this high-frequency dependence of these parameters complicates the formulation of the FDTD method. Hence, we will start this discussion of the FDTD method for lossy lines by formulating the FDTD recursion equations for a line that has only frequency-independent, that is, dc, values of these line loss parameters. This will also provide

a simplified introduction to the FDTD formulation, which will aid in understanding the more complicated result for frequency-dependent parameters in the next section. The transmission-line equations become

$$\frac{\partial V(z, t)}{\partial z} + rI(z, t) + l\frac{\partial I(z, t)}{\partial t} = 0 \quad (8.164a)$$

$$\frac{\partial I(z, t)}{\partial z} + gV(z, t) + c\frac{\partial V(z, t)}{\partial t} = 0 \quad (8.164b)$$

where we assume that the per-unit-length parameters r , l , g , and c are frequency independent, that is, constants. We discretize these as for the lossless case in Section 8.1.8 with reference to Figures 8.17 and 8.18 as

$$\frac{V_{k+1}^{n+1} - V_k^{n+1}}{\Delta z} + r\frac{I_k^{n+3/2} + I_k^{n+1/2}}{2} + l\frac{I_k^{n+3/2} - I_k^{n+1/2}}{\Delta t} = 0 \quad (8.165a)$$

for $k = 1, 2, \dots, \text{NDZ}$ and

$$\frac{I_k^{n+1/2} - I_{k-1}^{n+1/2}}{\Delta z} + g\frac{V_k^{n+1} + V_k^n}{2} + c\frac{V_k^{n+1} - V_k^n}{\Delta t} = 0 \quad (8.165b)$$

for $k = 2, 3, \dots, \text{NDZ}$, where we again denote

$$V_k^n \equiv V((k-1)\Delta z, n\Delta t) \quad (8.166a)$$

$$I_k^n \equiv I\left(\left(k - \frac{1}{2}\right)\Delta z, n\Delta t\right) \quad (8.166b)$$

Observe that we have averaged the current and voltage values about the discretization point in order to include the r and g parameters. This averaging amounts to the trapezoidal rule for numerical solution of ordinary differential equations [6]. The required recursion relations for the interior points on the line are obtained by solving Eqs. (8.165) giving

$$\left(\frac{\Delta z}{\Delta t}l + \frac{\Delta z}{2}r\right)I_k^{n+3/2} - \left(\frac{\Delta z}{\Delta t}l - \frac{\Delta z}{2}r\right)I_k^{n+1/2} = -\left(V_{k+1}^{n+1} - V_k^{n+1}\right) \quad (8.167a)$$

$$\left(\frac{\Delta z}{\Delta t}c + \frac{\Delta z}{2}g\right)V_k^{n+1} - \left(\frac{\Delta z}{\Delta t}c - \frac{\Delta z}{2}g\right)V_k^n = -\left(I_k^{n+1/2} - I_{k-1}^{n+1/2}\right) \quad (8.167b)$$

Note that the coefficients $(\Delta z/\Delta t)$ have the units of velocity, and hence $(\Delta z/\Delta t)l$ and $(\Delta z/\Delta t)c$ have the units of resistance and conductance, respectively. Similarly,

$(\Delta z/2)r$ and $(\Delta z/2)g$ have the units of resistance and conductance, respectively. Solving these and putting the voltage update equation first gives

$$\begin{aligned} V_k^{n+1} &= \left(\frac{\Delta z}{\Delta t} c + \frac{\Delta z}{2} g \right)^{-1} \left(\frac{\Delta z}{\Delta t} c - \frac{\Delta z}{2} g \right) V_k^n \\ &\quad - \left(\frac{\Delta z}{\Delta t} c + \frac{\Delta z}{2} g \right)^{-1} \left(I_k^{n+1/2} - I_{k-1}^{n+1/2} \right) \end{aligned} \quad (8.168a)$$

for $k = 2, 3, \dots, \text{NDZ}$ and

$$\begin{aligned} I_k^{n+3/2} &= \left(\frac{\Delta z}{\Delta t} l + \frac{\Delta z}{2} r \right)^{-1} \left(\frac{\Delta z}{\Delta t} l - \frac{\Delta z}{2} r \right) I_k^{n+1/2} \\ &\quad - \left(\frac{\Delta z}{\Delta t} l + \frac{\Delta z}{2} r \right)^{-1} \left(V_{k+1}^{n+1} - V_k^{n+1} \right) \end{aligned} \quad (8.168b)$$

for $k = 1, 2, \dots, \text{NDZ}$.

Next consider the incorporation of the terminal conditions. The essential problem in incorporating the terminal conditions is, as for the lossless case, that the FDTD voltages and currents at each end of the line, V_1, I_1 and $V_{\text{NDZ}+1}, I_{\text{NDZ}}$, are not collocated in space or time, whereas the terminal conditions relate the voltage and current at the same position and at the same time. We will again denote the current at the source ($z = 0$) as I_S and the current at the load ($z = \mathcal{L}$) as I_L , as shown in Figure 8.18. The second transmission-line equation given in Eq. (8.164b) is discretized at the source by averaging the source current I_S in order to obtain a value that is located in time at the same time point as $I_1^{n+1/2}$ as

$$\frac{1}{\Delta z/2} \left[I_1^{n+1/2} - \frac{(I_S^{n+1} + I_S^n)}{2} \right] + \frac{1}{2} g [V_1^{n+1} + V_1^n] + \frac{1}{\Delta t} c [V_1^{n+1} - V_1^n] = 0 \quad (8.169a)$$

Similarly, the second transmission-line equation, (8.164b), is discretized at the load by averaging the load current I_L in order to obtain a value that is located in time at the same time point as $I_{\text{NDZ}}^{n+1/2}$ as

$$\begin{aligned} \frac{1}{\Delta z/2} \left[\frac{(I_L^{n+1} + I_L^n)}{2} - I_{\text{NDZ}}^{n+1/2} \right] + \frac{1}{2} g [V_{\text{NDZ}+1}^{n+1} + V_{\text{NDZ}+1}^n] \\ + \frac{1}{\Delta t} c [V_{\text{NDZ}+1}^{n+1} - V_{\text{NDZ}+1}^n] = 0 \end{aligned} \quad (8.169b)$$

Equations (8.169) are solved to give the recursion relations for the voltages at the source and the load as

$$V_1^{n+1} = \left(\frac{\Delta z}{\Delta t}c + \frac{\Delta z}{2}g\right)^{-1} \left(\frac{\Delta z}{\Delta t}c - \frac{\Delta z}{2}g\right) V_1^n - 2\left(\frac{\Delta z}{\Delta t}c + \frac{\Delta z}{2}g\right)^{-1} I_1^{n+1/2} + \left(\frac{\Delta z}{\Delta t}c + \frac{\Delta z}{2}g\right)^{-1} [I_S^{n+1} + I_S^n] \tag{8.170a}$$

$$V_{\text{NDZ}+1}^{n+1} = \left(\frac{\Delta z}{\Delta t}c + \frac{\Delta z}{2}g\right)^{-1} \left(\frac{\Delta z}{\Delta t}c - \frac{\Delta z}{2}g\right) V_{\text{NDZ}+1}^n + 2\left(\frac{\Delta z}{\Delta t}c + \frac{\Delta z}{2}g\right)^{-1} I_{\text{NDZ}}^{n+1/2} - \left(\frac{\Delta z}{\Delta t}c + \frac{\Delta z}{2}g\right)^{-1} [I_L^{n+1} + I_L^n] \tag{8.170b}$$

In the case of resistive terminations, the terminal characterizations are written in terms of a generalized Thevenin equivalent as

$$V_1 = V_S - R_S I_S \tag{8.171a}$$

$$V_{\text{NDZ}+1} = V_L + R_L I_L \tag{8.171b}$$

Inverting these gives

$$I_S = -G_S V_1 + G_S V_S \tag{8.172a}$$

$$I_L = G_L V_{\text{NDZ}+1} - G_L V_L \tag{8.172b}$$

Substituting (8.172) into Eqs. (8.170) gives the recursion relations for V_1 and $V_{\text{NDZ}+1}$:

$$V_1^{n+1} = \left(\frac{\Delta z}{\Delta t}R_{Sc} + \frac{\Delta z}{2}R_{Sg} + 1\right)^{-1} \left\{ \left(\frac{\Delta z}{\Delta t}R_{Sc} - \frac{\Delta z}{2}R_{Sg} - 1\right) V_1^n - 2R_S I_1^{n+1/2} + (V_S^{n+1} + V_S^n) \right\} \tag{8.173a}$$

and

$$V_{\text{NDZ}+1}^{n+1} = \left(\frac{\Delta z}{\Delta t}R_{Lc} + \frac{\Delta z}{2}R_{Lg} + 1\right)^{-1} \left\{ \left(\frac{\Delta z}{\Delta t}R_{Lc} - \frac{\Delta z}{2}R_{Lg} - 1\right) V_{\text{NDZ}+1}^n + 2R_L I_{\text{NDZ}}^{n+1/2} + (V_L^{n+1} + V_L^n) \right\} \tag{8.173b}$$

and the voltages at the interior points are determined from (8.168a)

$$\begin{aligned}
 V_k^{n+1} = & \left(\frac{\Delta z}{\Delta t} c + \frac{\Delta z}{2} g \right)^{-1} \left(\frac{\Delta z}{\Delta t} c - \frac{\Delta z}{2} g \right) V_k^n \\
 & - \left(\frac{\Delta z}{\Delta t} c + \frac{\Delta z}{2} g \right)^{-1} \left(I_k^{n+1/2} - I_{k-1}^{n+1/2} \right)
 \end{aligned} \quad (8.173c)$$

for $k = 2, 3, \dots, \text{NDZ}$. Equations (8.173) are first for solved the voltages and then the currents are determined from those voltages using (8.168b) as

$$\begin{aligned}
 I_k^{n+3/2} = & \left(\frac{\Delta z}{\Delta t} l + \frac{\Delta z}{2} r \right)^{-1} \left(\frac{\Delta z}{\Delta t} l - \frac{\Delta z}{2} r \right) I_k^{n+1/2} \\
 & - \left(\frac{\Delta z}{\Delta t} l + \frac{\Delta z}{2} r \right)^{-1} \left(V_{k+1}^{n+1} - V_k^{n+1} \right)
 \end{aligned} \quad (8.168b)$$

for $k = 1, 2, 3, \dots, \text{NDZ}$. For stability of the solution, the position and time discretizations should again satisfy the Courant condition $\Delta t \leq \Delta z/v$.

8.2.3.2 Including Frequency-Dependent Losses First, consider the incorporation of the frequency-dependent conductor loss. Using the approximation $A + B\sqrt{s}$ for the conductor losses developed in Section 8.2.1.3, the time domain inverse Laplace transform of the conductor internal impedance is given, using the transform pair in (8.138), as

$$\hat{z}_i(s) = A + B\sqrt{s} = A + B\frac{1}{\sqrt{s}}s \iff A + B\frac{1}{\sqrt{\pi}}\frac{1}{\sqrt{t}}\frac{\partial}{\partial t} \quad (8.174)$$

From (8.148), we identify

$$A = r_{\text{dc}} \quad (8.175a)$$

$$B = \frac{r_{\text{dc}}}{\sqrt{\pi}\sqrt{f_0}} \quad (8.175b)$$

Hence, the required convolution given in (8.149) is

$$\begin{aligned}
 z_i(t) * I(z, t) &= \int_0^t z_i(\tau) I(z, t - \tau) d\tau \\
 &= AI(z, t) + B \frac{1}{\sqrt{\pi}} \int_0^t \frac{1}{\sqrt{\tau}} \frac{\partial I(z, t - \tau)}{\partial(t - \tau)} d\tau
 \end{aligned} \quad (8.176)$$

This convolution term can be discretized in the following fashion. Again divide the time axis into Δt segments. The discrete convolution can be approximated in the following manner, where $F(t)$ in the following represents the time derivative of the line current, $F(t) = (\partial/\partial t)I(z, t)$, which is approximated as being constant over the Δt segments [3]:

$$\begin{aligned} \int_0^t \frac{1}{\sqrt{\tau}} F(t - \tau) d\tau &\cong \int_0^{(n+1)\Delta t} \frac{1}{\sqrt{\tau}} F((n + 1)\Delta t - \tau) d\tau \\ &\cong \sum_{m=0}^n F^{n+1-m} \int_{m\Delta t}^{(m+1)\Delta t} \frac{1}{\sqrt{\tau}} d\tau \\ &= \sqrt{\Delta t} \sum_{m=0}^n F^{n+1-m} Z_0(m) \end{aligned} \tag{8.177a}$$

where

$$\begin{aligned} Z_0(m) &= \int_m^{(m+1)} \frac{1}{\sqrt{\xi}} d\xi \\ &= 2 \left[\sqrt{m + 1} - \sqrt{m} \right] \end{aligned} \tag{8.177b}$$

and we have made a change of variables in the integral in (8.177a) of $\tau = \Delta t \zeta$ in order to make this integral independent of the time discretization chosen for a specific problem. The derivation of this discrete convolution is illustrated in Figure 8.40 [A.2, A.5]. In this figure we see that

$$\begin{aligned} \int_0^{(n+1)\Delta t} \frac{1}{\sqrt{\tau}} F((n + 1)\Delta t - \tau) d\tau &\cong F^{n+1} \int_0^{\Delta t} \frac{1}{\sqrt{\tau}} d\tau + \dots \\ &+ F^3 \int_{(n-2)\Delta t}^{(n-1)\Delta t} \frac{1}{\sqrt{\tau}} d\tau + F^2 \int_{(n-1)\Delta t}^{n\Delta t} \frac{1}{\sqrt{\tau}} d\tau \\ &+ F^1 \int_{n\Delta t}^{(n+1)\Delta t} \frac{1}{\sqrt{\tau}} d\tau \\ &= \sum_{m=0}^n F^{n+1-m} \int_{m\Delta t}^{(m+1)\Delta t} \frac{1}{\sqrt{\tau}} d\tau \\ &= \sqrt{\Delta t} \sum_{m=0}^n F^{n+1-m} Z_0(m) \end{aligned} \tag{8.178}$$

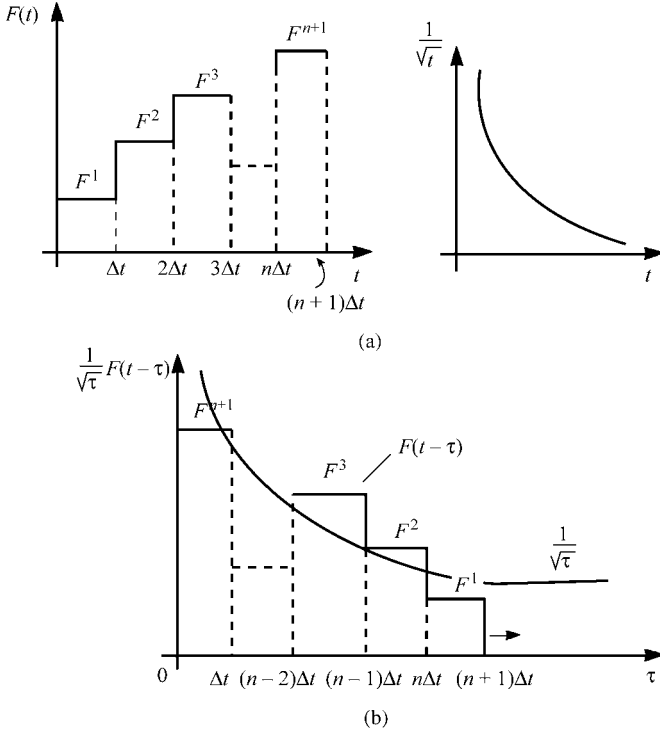


FIGURE 8.40 Illustration of the discrete convolution $\int_0^{(n+1)\Delta t} \frac{1}{\sqrt{\tau}} F(t - \tau) d\tau$.

Adapting this result to the discretization of the first transmission-line equation in (8.116a) using (8.149) gives, with reference to Figure 8.17,

$$\begin{aligned} & \frac{V_k^{n+1} - V_k^{n+1}}{\Delta z} + l \frac{I_k^{n+3/2} - I_k^{n+1/2}}{\Delta t} + A \frac{I_k^{n+3/2} + I_k^{n+1/2}}{2} \\ & + \frac{\sqrt{\Delta t}}{\sqrt{\pi}} B \sum_{m=0}^n \left[\frac{I_k^{n+3/2-m} - I_k^{n+1/2-m}}{\Delta t} \right] Z_0(m) = 0 \end{aligned} \quad (8.179a)$$

$$\frac{I_k^{n+1/2} - I_{k-1}^{n+1/2}}{\Delta z} + c \frac{V_k^{n+1} - V_k^n}{\Delta t} = 0 \quad (8.179b)$$

where $A = r_{dc}$ and $B = r_{dc}/\sqrt{\pi} \sqrt{f_0}$. Hence, the first equation, (8.74a) or (8.76a), has changed from the previous discretization for the case of perfect conductors.

Solving (8.179a) gives the recursion relation for this equation:

$$\begin{aligned}
 & \left(l \frac{\Delta z}{\Delta t} + A \frac{\Delta z}{2} + B \frac{1}{\sqrt{\pi}} \frac{\Delta z}{\sqrt{\Delta t}} Z_0(0) \right) I_k^{n+3/2} \\
 &= \left(l \frac{\Delta z}{\Delta t} - A \frac{\Delta z}{2} + B \frac{1}{\sqrt{\pi}} \frac{\Delta z}{\sqrt{\Delta t}} Z_0(0) \right) I_k^{n+1/2} \\
 &- B \frac{1}{\sqrt{\pi}} \frac{\Delta z}{\sqrt{\Delta t}} \sum_{m=1}^n \left[I_k^{n+3/2-m} - I_k^{n+1/2-m} \right] Z_0(m) - \left(V_{k+1}^{n+1} - V_k^{n+1} \right)
 \end{aligned} \tag{8.180}$$

or

$$\begin{aligned}
 I_k^{n+3/2} &= F^{-1} \left(l \frac{\Delta z}{\Delta t} - A \frac{\Delta z}{2} + B \frac{1}{\sqrt{\pi}} \frac{\Delta z}{\sqrt{\Delta t}} Z_0(0) \right) I_k^{n+1/2} \\
 &- F^{-1} B \frac{1}{\sqrt{\pi}} \frac{\Delta z}{\sqrt{\Delta t}} \sum_{m=1}^n \left[I_k^{n+3/2-m} - I_k^{n+1/2-m} \right] Z_0(m) \\
 &- F^{-1} \left(V_{k+1}^{n+1} - V_k^{n+1} \right)
 \end{aligned} \tag{8.181a}$$

for $k = 1, \dots, \text{NDZ}$ where

$$F = \left(l \frac{\Delta z}{\Delta t} + A \frac{\Delta z}{2} + B \frac{1}{\sqrt{\pi}} \frac{\Delta z}{\sqrt{\Delta t}} Z_0(0) \right) \tag{8.181b}$$

This replaces Eq. (8.76a) of the lossless case. For lossless dielectrics, $g = 0$, the voltage update equation in (8.76b) remains the same:

$$V_k^{n+1} = V_k^n - \frac{\Delta t}{\Delta z} c^{-1} \left(I_k^{n+1/2} - I_{k-1}^{n+1/2} \right) \tag{8.76b}$$

for $k = 2, 3, \dots, \text{NDZ}$. The terminal relations can again be included with reference to Figure 8.18 giving, for the case of a lossless dielectric, $g = 0$,

$$V_1^{n+1} = V_1^n - \frac{2\Delta t}{\Delta z} c^{-1} I_1^{n+1/2} + \frac{\Delta t}{\Delta z} c^{-1} \left[I_S^{n+1} + I_S^n \right] \tag{8.78a}$$

$$V_{\text{NDZ}+1}^{n+1} = V_{\text{NDZ}+1}^n + \frac{2\Delta t}{\Delta z} c^{-1} I_{\text{NDZ}}^{n+1/2} - \frac{\Delta t}{\Delta z} c^{-1} \left[I_L^{n+1} + I_L^n \right] \tag{8.78b}$$

where I_S and I_L are the line currents at the source and load ends, respectively. In the case of resistive terminations, the terminal characterizations are written in terms of a generalized Thevenin equivalent as

$$V_1 = V_S - R_S I_S \tag{8.79a}$$

$$V_{\text{NDZ}+1} = V_L + R_L I_L \tag{8.79b}$$

and these voltage update equations are unchanged from the lossless case since they were derived from the second transmission-line equation, which is unaffected by the conductor losses:

$$V_1^{n+1} = \left(\frac{\Delta z}{\Delta t} R_{Sc} + 1 \right)^{-1} \left\{ \left(\frac{\Delta z}{\Delta t} R_{Sc} - 1 \right) V_1^n - 2R_S I_1^{n+1/2} + \left(V_S^{n+1} + V_S^n \right) \right\} \quad (8.81a)$$

and

$$V_{NDZ+1}^{n+1} = \left(\frac{\Delta z}{\Delta t} R_{Lc} + 1 \right)^{-1} \left\{ \left(\frac{\Delta z}{\Delta t} R_{Lc} - 1 \right) V_{NDZ+1}^n + 2R_L I_{NDZ}^{n+1/2} + \left(V_L^{n+1} + V_L^n \right) \right\} \quad (8.81b)$$

The overall solution process is the same as for the lossless line case. First solve for the line voltages from (8.81) and (8.76b) and then obtain the line currents from (8.181).

8.2.3.3 Prony's Method for Representing a Function Unfortunately, the current update equation in (8.181a) requires storage of all past values of the currents, which presents a significant demand on storage requirements. A solution to this problem approximates $Z_0(m)$ as the sum of N exponential functions [3]:

$$\begin{aligned} Z_0(m) &= \int_m^{(m+1)} \frac{1}{\sqrt{\xi}} d\xi \\ &\cong \sum_{j=1}^N a_j e^{mb_j} \end{aligned} \quad (8.182)$$

In order to determine the $2N$ unknowns in this expansion, a_1, a_2, \dots, a_N and b_1, b_2, \dots, b_N , we can use Prony's method [19,20]. Prony's method approximates some general function of m , $f(m)$, at NS equally spaced sample points, $m = 0, T, 2T, \dots, (NS - 1)T$, over the complete interval of interest in terms of the sampling interval T ; where $NS \geq 2N$. These are denoted as

$$f(m = iT) \equiv f_i \quad \text{for } i = 0, 1, 2, \dots, NS - 1 \quad (8.183a)$$

and the first sample is at $m = 0$. Hence, the NS equally spaced samples are denoted as

$$\begin{aligned} f_0 &\equiv f(0) \\ f_1 &\equiv f(T) \\ f_2 &\equiv f(2T) \end{aligned}$$

$$\begin{aligned} & \vdots \\ f_{NS-1} & \equiv f((NS - 1)T) \end{aligned} \tag{8.183b}$$

Prony’s method approximates the function as a sum of exponentials as

$$\begin{aligned} f_i & \cong \sum_{j=1}^N a_j e^{ib_j T} \\ & = a_1 e^{ib_1 T} + a_2 e^{ib_2 T} + \dots + a_N e^{ib_N T} \\ & = a_1 z_1^i + a_2 z_2^i + \dots + a_N z_N^i \end{aligned} \tag{8.184a}$$

where we denote

$$z_j = e^{b_j T} \quad \text{for } j = 1, \dots, N \tag{8.184b}$$

Hence, we can write the Prony approximation as

$$f_i \cong \sum_{j=1}^N a_j z_j^i \quad \text{for } i = 0, 1, 2, \dots, NS - 1 \tag{8.184c}$$

If we determine z_j , we can recover the desired b_j from (8.184b) as

$$b_j = \frac{1}{T} \ln(z_j) \tag{8.185}$$

Matching (8.184a) at the NS equally spaced sample points gives a set of NS linear equations:

$$\begin{aligned} a_1 + a_2 + \dots + a_N & = f_0 \\ a_1 z_1 + a_2 z_2 + \dots + a_N z_N & = f_1 \\ a_1 z_1^2 + a_2 z_2^2 + \dots + a_N z_N^2 & = f_2 \\ & \vdots \\ a_1 z_1^{(NS-1)} + a_2 z_2^{(NS-1)} + \dots + a_N z_N^{(NS-1)} & = f_{NS-1} \end{aligned} \tag{8.186}$$

If we know z_j (or equivalently we know b_j so that we could determine z_j from (8.184b)), we could solve the first N of the equations in (8.186) for the values of the a_j . We could also solve all of the equations in (8.186) (an overdetermined set of NS equations in N unknowns) using the method of least squares [21,30]. (See Section 9.2.5.4 of Chapter 9 for a discussion of the method of least squares.) In order to determine z_j , we construct the following polynomial in terms of N auxiliary

coefficients β_i (which are to be determined):

$$\sum_{i=0}^N \beta_i z^i = \beta_0 + \beta_1 z + \beta_2 z^2 + \dots + \beta_{N-1} z^{N-1} + z^N = 0 \tag{8.187a}$$

and $\beta_N = 1$. If the β_i are determined, the polynomial in (8.187a) can be factored giving its roots as the desired z_j :

$$(z - z_1)(z - z_2) \dots (z - z_N) = 0 \tag{8.187b}$$

In order to obtain β_i , we write

$$\begin{aligned} \sum_{i=0}^N f_{k+i} \beta_i &= \sum_{i=0}^N \left\{ \sum_{j=1}^N a_j z_j^{k+i} \right\} \beta_i \\ &= \sum_{j=1}^N a_j z_j^k \underbrace{\left\{ \sum_{i=0}^N \beta_i z_j^i \right\}}_{=0} = 0 \quad \text{for } k = 0, 1, 2, \dots, NS - N - 1 \end{aligned} \tag{8.188}$$

This gives $NS - N$ linear equations in β_i :

$$\begin{aligned} f_0 \beta_0 + f_1 \beta_1 + \dots + f_{N-1} \beta_{N-1} + f_N &= 0 \\ f_1 \beta_0 + f_2 \beta_1 + \dots + f_N \beta_{N-1} + f_{N+1} &= 0 \\ &\vdots \\ f_{NS-N-1} \beta_0 + f_{NS-N} \beta_1 + \dots + f_{NS-2} \beta_{N-1} + f_{NS-1} &= 0 \end{aligned} \tag{8.189a}$$

where $\beta_N = 1$ or in matrix form

$$\begin{bmatrix} f_0 & f_1 & \dots & f_{N-1} \\ f_1 & f_2 & \dots & f_N \\ \vdots & \ddots & \ddots & \vdots \\ f_{NS-N-1} & f_{NS-N} & \dots & f_{NS-2} \end{bmatrix} \begin{bmatrix} \beta_0 \\ \beta_1 \\ \vdots \\ \beta_{N-1} \end{bmatrix} = \begin{bmatrix} -f_N \\ -f_{N+1} \\ \vdots \\ -f_{NS-1} \end{bmatrix} \tag{8.189b}$$

After the β_i are obtained from the solution of (8.189), the z_j can be obtained from the solution for the roots of the polynomial of (8.187). Then, the a_i can be found from the solution of the equations in (8.186). If the number of data points NS , is greater than the number of unknowns in the expansion, $NS > 2N$, the above simultaneous equations can be solved by the method of least squares [21,30]. (See Section 9.2.5.4 of Chapter 9 for a discussion of the method of least squares.)

Kunz showed that a reasonable Prony approximation to $Z_0(m)$ as in (8.182) can be obtained by using 10 terms, where the coefficients are given by [3]:

TABLE 8.2 Coefficients of the Prony approximation of $Z_0(m)$.

| i | a_i | b_i |
|-----|-----------------|------------------|
| 1 | 0.79098180E - 1 | -0.11484427E - 2 |
| 2 | 0.11543423E0 | -0.13818329E - 1 |
| 3 | 0.13435380E0 | -0.54037596E - 1 |
| 4 | 0.21870422E0 | -0.14216494E0 |
| 5 | 0.98229667E - 1 | -0.30128437E0 |
| 6 | 0.51360484E0 | -0.56142185E0 |
| 7 | -0.20962898E0 | -0.97117126E0 |
| 8 | 0.11974447E1 | -0.16338433E1 |
| 9 | 0.11225491E - 1 | -0.28951329E1 |
| 10 | -0.74425255E0 | -0.50410969E1 |

Observe from (8.177b) that $Z_0(0) = 2$. Adding the values of the expansion coefficients a_i in Table 8.2 gives $Z_0(0) = a_1 + a_2 + \dots + a_{10} = 1.41 \neq 2$. But this error does not substantially effect the problem since $Z_0(0)$ appears only in the term in (8.181b):

$$F = \left(l \frac{\Delta z}{\Delta t} + A \frac{\Delta z}{2} + B \frac{1}{\sqrt{\pi}} \frac{\Delta z}{\sqrt{\Delta t}} Z_0(0) \right) \tag{8.181b}$$

and a similar term in (8.181a). The term containing the per-unit-length inductance $l(\Delta z/\Delta t)$, dominates the other terms even for the high-loss line in the example in Section 8.2.3.5.

There are other ways of obtaining these coefficients in an exponential approximation as in (8.182). One is the Prony singular-value-decomposition (SVD) method [19]. The other is the matrix pencil (MP) method [22]. The coefficients of the exponential approximation of $Z_0(m)$ by all these methods are given in Table 8.3 [B.29].

The SVD method gives $Z_0(0) = 2.000000149$, whereas the MP method gives $Z_0(0) = 1.99994134$. The approximation error for each of these three methods is compared in Figure 8.41. Note that the MP method gives the best approximation, but all three methods give virtually the exact result for samples less than approximately 500.

8.2.3.4 Recursive Convolution The recursion relation for the currents in (8.181a) requires that we store all previous values of the currents. To obviate this need, we substitute (8.182) into (8.181a) to yield

$$I_k^{n+3/2} = F^{-1} \left(l \frac{\Delta z}{\Delta t} - A \frac{\Delta z}{2} + B \frac{\Delta z}{\sqrt{\pi \Delta t}} Z_0(0) \right) I_k^{n+1/2} - F^{-1} B \frac{\Delta z}{\sqrt{\pi \Delta t}} \sum_{i=1}^N \Psi_i^n - F^{-1} \left(V_{k+1}^{n+1} - V_k^{n+1} \right) \tag{8.190a}$$

TABLE 8.3

| i | Prony | | Prony-SVD | | Matrix Pencil | |
|-----|-----------------|------------------|------------------|------------------|-----------------|------------------|
| | a_i | b_i | a_i | b_i | a_i | b_i |
| 1 | 0.79098180E - 1 | -0.11484427E - 2 | 0.94437314E - 1 | -0.15821633E - 2 | 0.83141576 | -0.38772965E1 |
| 2 | 0.11543423 | -0.13818329E - 1 | 0.15665434 | -0.21821581E - 1 | 0.36307454 | -0.10222379E1 |
| 3 | 0.13435380 | -0.54037596E - 1 | 0.16504027 | -0.92157810E - 1 | 0.27397819 | -0.38821712 |
| 4 | 0.21870422 | -0.14216494 | 0.28881469 | -0.25144386 | 0.18917986 | -0.15317357 |
| 5 | 0.98229667E - 1 | -0.30128437 | 0.74258946E - 1 | -0.54918917 | 0.12665224 | -0.60535209E - 1 |
| 6 | 0.51360484 | -0.56142185 | 0.47247797 | -1.07005584 | 0.60012910E - 1 | -0.69394020E - 3 |
| 7 | -0.20962898 | -0.97117126 | -0.19950136E - 1 | -2.03571364 | 0.67810981E - 1 | -0.67863637E - 2 |
| 8 | 0.11974447E1 | -0.16338433E1 | 0.76826675 | -5.42397697 | 0.87875521E - 1 | -0.22711265E - 1 |
| 9 | 0.11225491E - 1 | -0.28951329E1 | | | | |
| 10 | -0.74425255 | -0.50410969E1 | | | | |

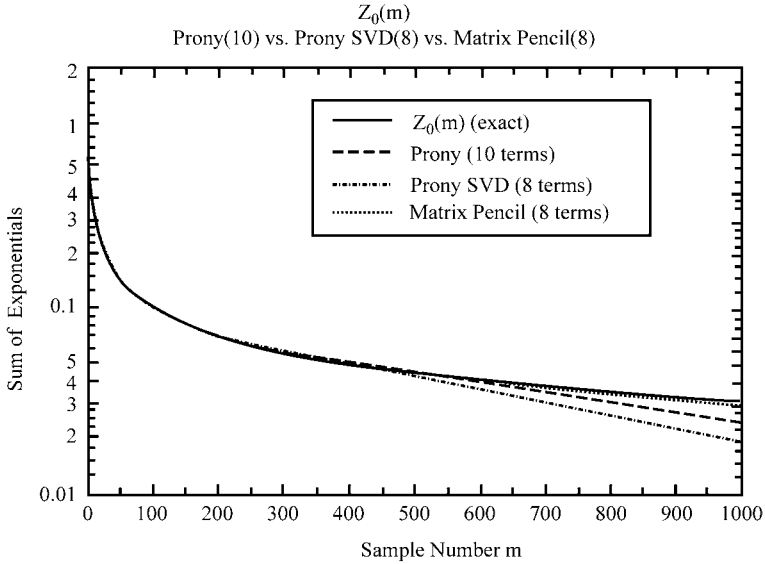


FIGURE 8.41 Comparison of the various representations of $Z_0(m) = \int_m^{m+1} \frac{1}{\sqrt{\xi}} d\xi$.

for $k = 1, \dots, NDZ$, where

$$\Psi_i^n = a_i e^{b_i} \left[I_k^{n+1/2} - I_k^{n-1/2} \right] + e^{b_i} \Psi_i^{n-1} \tag{8.190b}$$

The Ψ_i^n functions are updated via (8.190a) before evaluating (8.190a). Thus, only one additional past value of current, $I_k^{n-1/2}$, needs to be retained. The result in (8.190b) can be obtained by substituting the representation of $Z_0(m)$ as a sum of exponentials as shown in (8.182) into (8.181a) and expanding as

$$\begin{aligned} \sum_{m=1}^n Z_0(m) \left[I_k^{n+3/2-m} - I_k^{n+1/2-m} \right] &= \sum_{m=1}^n \sum_{i=1}^N a_i e^{mb_i} \left[I_k^{n+3/2-m} - I_k^{n+1/2-m} \right] \\ &= \sum_{i=1}^N a_i e^{b_i} \left[I_k^{n+1/2} - I_k^{n-1/2} \right] \\ &\quad + e^{b_i} \sum_{i=1}^N a_i e^{b_i} \left[I_k^{n-1/2} - I_k^{n-3/2} \right] \\ &\quad + e^{2b_i} \sum_{i=1}^N a_i e^{b_i} \left[I_k^{n-3/2} - I_k^{n-5/2} \right] \\ &\quad + \dots \end{aligned} \tag{8.191}$$

This method of representing a function as a sum of exponential terms as in (8.182) to avoid storage of previous values in the convolution is referred to as the method of *recursive convolution* [23,24]. It relies on the property of the exponential: $e^{(a+b)} = e^a e^b$. For example, suppose we wish to represent a function of t at discrete points t_i that are separated by $\Delta t = t_i - t_{i-1}$. Approximating the impulse response $h(t)$ as a sum of exponentials, the convolution $h(t) * x(t)$ gives

$$\begin{aligned}
 [h(t)*x(t)]|_{t=t_i} &= \int_0^{t_i} \underbrace{ae^{b\tau}}_{h(\tau)} x(t_i - \tau) d\tau \\
 &= \int_0^{t_i-t_{i-1}} ae^{b\tau} x(t_i - \tau) d\tau + \int_{t_i-t_{i-1}}^{t_i} ae^{b\tau} x(t_i - \tau) d\tau \\
 &= \int_0^{\Delta t} ae^{b\tau} x(t_i - \tau) d\tau + e^{b\Delta t} \int_0^{t_{i-1}} ae^{b\zeta} x(t_{i-1} - \zeta) d\zeta \\
 &= \int_0^{\Delta t} ae^{b\tau} x(t_i - \tau) d\tau + e^{b\Delta t} y(t_{i-1}) \tag{8.192}
 \end{aligned}$$

and we have used a change of variables $\zeta = \tau - (t_i - t_{i-1})$ in the second integral. Hence, the recursive convolution technique allows us to accumulate the values of the convolution at the previous time points as we proceed.

The FDTD equations in (8.76b), (8.81), and (8.190) that incorporate the frequency-dependent conductor loss are implemented in the FORTRAN program FDTDLOSS.FOR. (see Appendix A). This program does not include dielectric loss for which we now develop a recursion relation.

Recursive convolution can be used to provide a computationally efficient FDTD solution that also includes the dielectric losses for a *homogeneous* surrounding medium, for example, a stripline. The second transmission-line equation in the time domain contains the dielectric loss and is

$$\begin{aligned}
 \frac{\partial I(z, t)}{\partial z} &= -y(t) * V(z, t) \\
 &= -M \left[\sum_{i=1}^N \frac{K_i}{\tau_i} e^{-t/\tau_i} \right] * \frac{\partial V(z, t)}{\partial t} - c_{\text{hf}} \frac{\partial V(z, t)}{\partial t} \\
 &= -\sum_{i=1}^N M \frac{K_i}{\tau_i} \left[\int_0^t e^{-\tau/\tau_i} \frac{\partial V(z, t - \tau)}{\partial (t - \tau)} d\tau \right] - c_{\text{hf}} \frac{\partial V(z, t)}{\partial t} \tag{8.193}
 \end{aligned}$$

where we have substituted the previous result for the dielectric loss in a homogeneous medium given in (8.160). The convolution integral can be discretized as before to yield

$$\begin{aligned}
 \int_0^t e^{-\tau/\tau_i} \frac{\partial V(z, t - \tau)}{\partial(t - \tau)} d\tau &\cong \int_0^{(n+1)\Delta t} e^{-\tau/\tau_i} F((n+1)\Delta t - \tau) d\tau \\
 &= \sum_{m=0}^n F^{n+1-m} \int_{m\Delta t}^{(m+1)\Delta t} e^{-\tau/\tau_i} d\tau \\
 &= -\sum_{m=0}^n F^{n+1-m} \tau_i \left[e^{-(m+1)\Delta t/\tau_i} - e^{-m\Delta t/\tau_i} \right]
 \end{aligned}
 \tag{8.194}$$

where $F(t) = \partial V(z, t)/\partial t$. Hence, (8.193) can be discretized with reference to Figure 8.17 as

$$\begin{aligned}
 \frac{I_k^{n+1/2} - I_{k-1}^{n+1/2}}{\Delta z} + c_{\text{hf}} \frac{V_k^{n+1} - V_k^n}{\Delta t} \\
 = M \sum_{m=0}^n \sum_{i=1}^N K_i \left[\frac{V_k^{n+1-m} - V_k^{n-m}}{\Delta t} \right] \left[e^{-(m+1)\Delta t/\tau_i} - e^{-m\Delta t/\tau_i} \right]
 \end{aligned}
 \tag{8.195}$$

Solving this gives

$$\begin{aligned}
 V_k^{n+1} &= V_k^n - c_{\text{hf}}^{-1} \frac{\Delta t}{\Delta z} \left[I_k^{n+1/2} - I_{k-1}^{n+1/2} \right] \\
 &+ c_{\text{hf}}^{-1} M \sum_{m=0}^n \sum_{i=1}^N K_i \left[V_k^{n+1-m} - V_k^{n-m} \right] \left[e^{-(m+1)\Delta t/\tau_i} - e^{-m\Delta t/\tau_i} \right] \\
 &= V_k^n - H^{-1} c_{\text{hf}}^{-1} \frac{\Delta t}{\Delta z} \left[I_k^{n+1/2} - I_{k-1}^{n+1/2} \right] \\
 &+ H^{-1} c_{\text{hf}}^{-1} M \sum_{m=1}^n \sum_{i=1}^N K_i \left[V_k^{n+1-m} - V_k^{n-m} \right] \left[e^{-(m+1)\Delta t/\tau_i} - e^{-m\Delta t/\tau_i} \right]
 \end{aligned}
 \tag{8.196a}$$

where

$$H = \left[1 - c_{\text{hf}}^{-1} M \sum_{i=1}^N K_i \left(e^{-\Delta t/\tau_i} - 1 \right) \right]
 \tag{8.196b}$$

Writing this out and using the recursive convolution idea gives

$$V_k^{n+1} = V_k^n - H^{-1} c_{\text{hf}}^{-1} \frac{\Delta t}{\Delta z} \left[I_k^{n+1/2} - I_{k-1}^{n+1/2} \right] + H^{-1} c_{\text{hf}}^{-1} M \sum_{i=1}^N \Phi_i^n \quad (8.197a)$$

for $k = 2, \dots, \text{NDZ}$, where

$$\Phi_i^n = K_i e^{-\Delta t/\tau_i} \left[e^{-\Delta t/\tau_i} - 1 \right] \left[V_k^n - V_k^{n-1} \right] + e^{-\Delta t/\tau_i} \Phi_i^{n-1} \quad (8.197b)$$

Hence, only one additional past value, V_k^{n-1} , needs to be retained. In addition, the terminal voltage update equations in (8.78) and (8.81) were also derived from the second transmission-line equation and must likewise be discretized with reference to Figure 8.18.

8.2.3.5 An Example: A High-Loss Line In order to compare the predictions of these models, we will investigate a high-loss two-conductor transmission line shown in Figure 8.42. Two conductors of rectangular cross section of width $20 \mu\text{m}$ and thickness $10 \mu\text{m}$ are separated by $20 \mu\text{m}$ and placed on one side of a silicon substrate

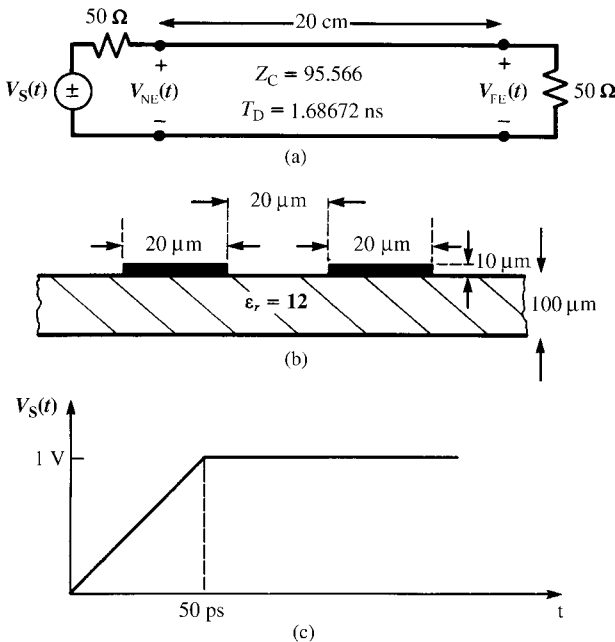


FIGURE 8.42 A lossy printed circuit board for illustration of numerical results: (a) line dimensions and terminations, (b) cross-sectional dimensions, and (c) representation of the open-circuit source voltage waveform.

($\epsilon_r = 12$) of thickness $100 \mu\text{m}$. The total line length is 20 cm and is terminated at the near and far ends in $50\text{-}\Omega$ resistors. The source is a ramp function rising to a level of 1 V with a rise time of 50 ps . The per-unit-length inductance and capacitance were computed as $l = 0.805969 \mu\text{H/m}$ and $c = 88.2488 \text{ pF/m}$. This gives a velocity of propagation in the lossless case of $v = 1.18573 \times 10^8 \text{ m/s}$ and a one-way time delay of $T_D = 1.68672 \text{ ns}$, which gives an effective dielectric constant of $\epsilon'_r = 6.4$ and a characteristic impedance of $Z_C = 95.566 \Omega$. The per-unit-length dc resistance is computed as $A = r_{dc} = 1/(\sigma wt) = 86.207 \Omega/\text{m}$. The break frequency where this transitions to the high-frequency resistance that varies as \sqrt{f} is computed from (8.131) with $k = 2$ as $f_0 = 393.06 \text{ MHz}$. The factor B is computed as described previously to be

$$B = \frac{1}{2(t+w)} \sqrt{\frac{\mu_0}{\sigma}} = \frac{r_{dc}}{\sqrt{\pi f_0}} = 2.45323 \times 10^{-3}.$$

Dielectric loss is not included in these calculations. Figure 8.43 shows the comparison of the SPICE (lossless) predictions, TDFD, and FDTD results for the near-end and far-end voltages. The TDFD transformation modeled the source as a 10-MHz periodic trapezoidal waveform with 50% duty cycle and rise/fall times of 50 ps . The code `TIMEFREQ.FOR` was used, which uses the frequency-domain transfer function obtained from `MTL.FOR`. The bandwidth of this signal is on the order of $1/\tau_r = 20 \text{ GHz}$, so 2000 harmonics were used in the computation of the frequency response via the

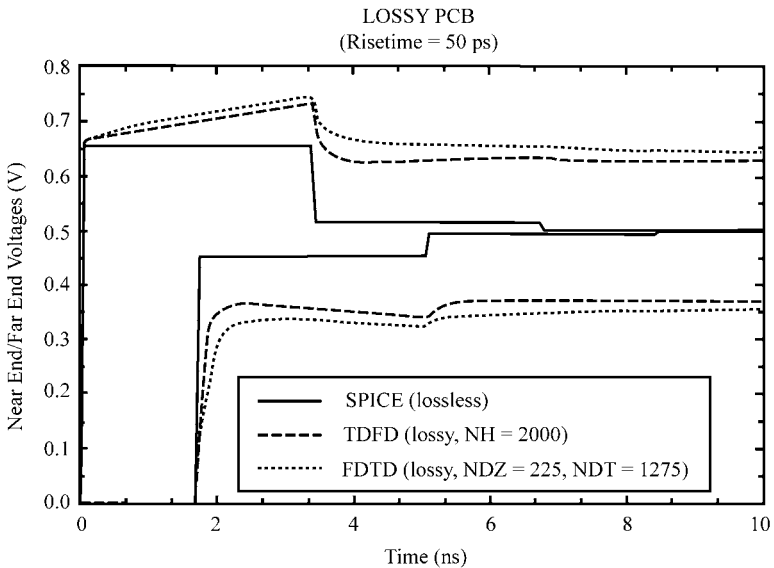


FIGURE 8.43 Source and load voltages of the two-conductor line of Figure 8.42 using the lossless SPICE model, the lossy FDTD model, and the time-domain to frequency-domain (TDFD) method including losses for a rise time of 50 ps .

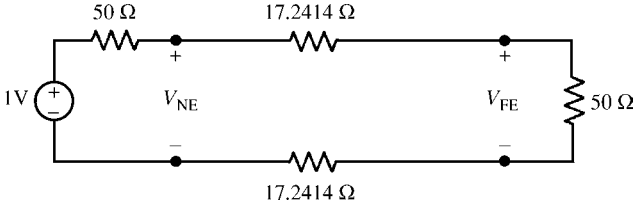


FIGURE 8.44 Model for computing the terminal voltages due to dc land resistance.

MTL.FOR code. The FDTD results were obtained with FDTDLOSS.FOR, which uses the Prony coefficients in Table 8.2 for approximating $Z_0(m)$ as in (8.182). The high-frequency spectrum rolls off at -40 dB/decade above $1/\pi\tau_r = 6.3662$ GHz. The spatial discretization for the FDTD results was chosen so that each cell was $\lambda/10$ at twice this break frequency giving $\text{NDZ} = 215$. The “magic time step” of $\Delta t = \Delta z/v$ for this spatial discretization and a total solution time of 10 ns is $\text{NDT} = 1275$. The TDFD results approach the steady-state limit obtained by replacing the line conductors with their total dc resistances of $r_{\text{dc}}\mathcal{L} = 17.2414 \Omega$ as shown in Figure 8.44 of $V_{\text{NE,ss}} = 0.628205$ V and $V_{\text{FE,ss}} = 0.371795$ V. The TDFD results at 10 ns are $V_{\text{NE}} = 0.6286$ V and $V_{\text{FE}} = 0.3719$ V, which converge rapidly to the steady-state values calculated from Figure 8.44. The FDTD results at 10 ns are $V_{\text{NE}} = 0.6436$ V and $V_{\text{FE}} = 0.3566$ V, and do not converge as rapidly to the steady-state values. However, the FDTD computations were recalculated to 40 ns, giving $V_{\text{NE}} = 0.6285$ V and $V_{\text{FE}} = 0.3715$ V. Hence, the FDTD results converge to the correct steady-state values but at a much slower rate than the TDFD predictions.

The effect of conductor loss is evident and significant, but the TDFD and the FDTD method give different results. This is due to the fact that the FDTD method simply adds the low-frequency dc resistance to the high-frequency impedance and models the total conductor impedances as

$$\begin{aligned}\hat{z}_i(\omega) &= A + B\sqrt{j\omega} \\ &= r_{\text{dc}} + r_{\text{hf}} + j\omega l_{i,\text{hf}} \\ &= r_{\text{dc}} + r_{\text{dc}}\sqrt{\frac{f}{f_0}}(1 + j)\end{aligned}\quad (8.198a)$$

The time-domain to frequency-domain method uses the frequency-domain transfer function computed with MTL.FOR, which uses the frequency-selective model of the conductor internal impedances:

$$\hat{z}_i(\omega) = \begin{cases} r_{\text{dc}} + j\omega l_{i,\text{dc}} = r_{\text{dc}}(1 + jf/f_0), & f \leq f_0 \\ r_{\text{hf}} + j\omega l_{i,\text{hf}} = r_{\text{dc}}\sqrt{f/f_0}(1 + j), & f \geq f_0 \end{cases}\quad (8.198b)$$

At the break frequency $f_0 = 393.06$ MHz, the FDTD value for $\hat{z}_i(\omega)$ is a factor of $\sqrt{2}$ larger than those of the frequency-selective TDFD method. The true value lies between

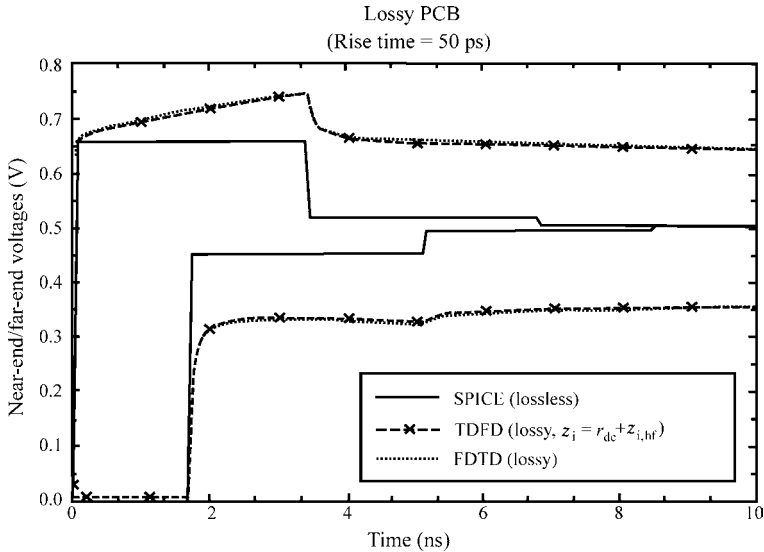


FIGURE 8.45 Recomputation of the results of Figure 8.43 but with the losses represented as $A + B\sqrt{s}$ in both the FDTD and the TDFD methods.

these two values (see Figs. 4.15 and 4.16 of Chapter 4). This break frequency lies in the -20 dB/decade region of the spectrum, which begins at $1/\pi\tau = 6.366$ MHz and ends at $1/\pi\tau_r = 6.366$ GHz [A.3]. Thus, we should expect a difference between the two model predictions. To verify that this is the case, the time-domain to frequency-domain transformation results were recomputed, wherein the low-frequency and high-frequency conductor impedances are added together in the frequency-domain transfer function as in the FDTD code rather than using a frequency-selective computation as described above. Figure 8.45 shows the results of this computation for the near-end and far-end voltages. These results confirm the hypothesis and additionally show that the FDTD code gives virtually identical results to the time-domain to frequency-domain transformation method when the same equations are being solved.

In the applications of the FDTD technique to electromagnetic scattering problems, a surface impedance boundary condition is frequently used. This condition essentially has a \sqrt{f} frequency dependence and requires no constant resistance [3,15]. This has led others to neglect r_{dc} in transmission-line problems. Numerous solutions of the transmission-line equations for lossy lines in the literature include only the high-frequency \sqrt{f} impedance of the line conductors and ignore their dc, constant resistance. We have included this dc resistance in the FDTD solution via the A term. The question is whether the dc resistance can be neglected and only the high-frequency \sqrt{f} impedance be used. Figure 8.46 shows the results of including only the dc resistance or only the high-frequency \sqrt{f} impedance of the conductors. Including only the dc resistance gives the correct late-time steady-state dc level of the responses, but the early-time results are not well predicted at the beginning of the transitions. Including only the high-frequency \sqrt{f} impedance of the conductors does not predict

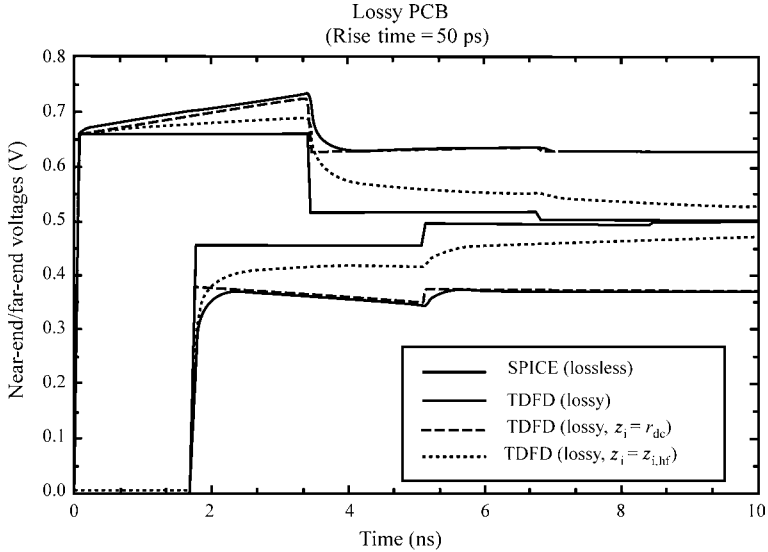


FIGURE 8.46 Recomputation of the TDFD results of Figure 8.43 but with losses represented as only their dc values or only their high-frequency values.

the correct late-time dc levels. Figure 8.47 shows the comparison between the TDFD and FDTD models using either only the dc resistance or only the high-frequency resistance. This again confirms the importance of including the dc resistance and additionally shows that the TDFD and FDTD models give virtually identical results when the same representations of the conductor impedances are used.

Observe in Figures 8.45–8.47 that there appears to be a violation of causality in the far-end computed results; that is, a response appears prior to one time delay of the lossless line of $T_D = \mathcal{L}\sqrt{lc} = 1.6867$ ns. Examining the plotted data, we find that all of the FDTD calculations for the far-end voltages in Figures 8.43 and 8.45–8.47 are, in fact, causal; that is, no response in the far-end voltages appears before $T_D = 1.6867$ ns. However, all of the TDFD computed results for the far-end voltages are noncausal to some degree. This may be a reconstruction error (aliasing) inherent in the TDFD recombination process.

8.2.3.6 A Correction for the FDTD Errors The difference in the TDFD and FDTD results is due to the different ways the two codes model the frequency-dependent internal impedance. The TDFD method uses a frequency-selective asymptote model given in (8.198b), whereas the FDTD method essentially adds the two asymptotes as in (8.198a). The actual result (at least for wires) lies between the two at the breakpoint f_0 (see Figs. 4.15 and 4.16 in Chapter 4). As discussed previously, the $A + B\sqrt{s}$ model in the FDTD code simply adds the low-frequency and high-frequency asymptotes. This has a representation problem because the high-frequency internal inductance dominates the dc internal inductance below the break frequency f_0 as illustrated in

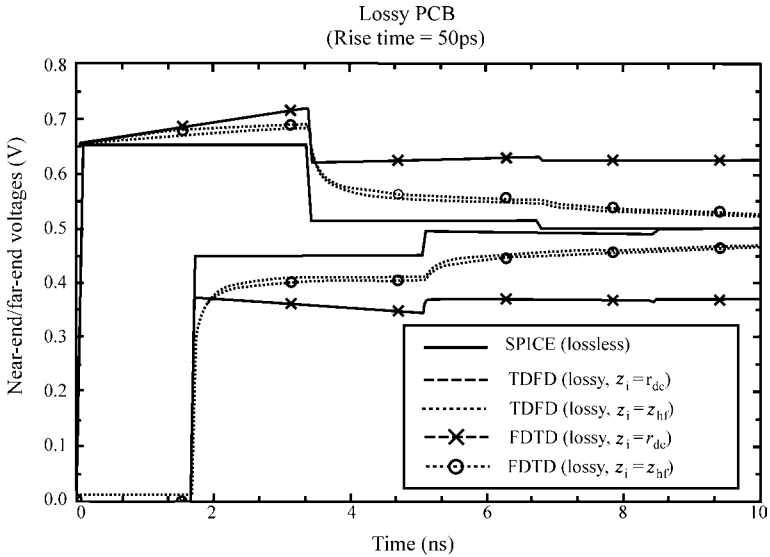


FIGURE 8.47 Recomputation of the FDTD and TDFD results of Figure 8.43 but with losses represented as only their dc values or only their high-frequency values.

Figure 8.38. This was remedied by multiplying the low-frequency impedance by a first-order low-pass filter and multiplying the high-frequency impedance by a first-order high-pass filter giving the representation in (8.150). The convolution term is then given by (8.153):

$$\begin{aligned}
 \hat{z}_i(s)I(z, s) &\iff z_i(t) * I(z, t) \\
 &= r_{dc}I(z, t) + r_{dc}\sqrt{\frac{2}{\pi}} \left[\frac{1}{\sqrt{\alpha}} - 2e^{-\alpha} \int_0^{\sqrt{\alpha}} e^{\lambda^2} d\lambda \right] * \frac{\partial I(z, t)}{\partial t}
 \end{aligned}
 \tag{8.153}$$

where

$$\alpha = \omega_0 t.
 \tag{8.154}$$

and the integral in the second term in (8.153) can be approximated as

$$\int_0^{\sqrt{\alpha}} e^{\lambda^2} d\lambda = \int_0^{\sqrt{\alpha}} \left[1 + \frac{\lambda^2}{1!} + \frac{\lambda^4}{2!} + \dots \right] d\lambda$$

$$\begin{aligned}
 &= \left[\frac{1}{\alpha^{\frac{1}{2}}} + \frac{\frac{3}{2}}{3 \times 1!} + \frac{\frac{5}{2}}{5 \times 2!} + \dots \right] \\
 &= \sum_{n=0}^{\infty} \frac{\alpha^{\frac{n+1}{2}}}{(2n+1)n!}.
 \end{aligned} \tag{8.155}$$

Evaluating the second term of (8.153) as before yields

$$\begin{aligned}
 &\int_0^t r_{dc} \sqrt{\frac{2}{\pi}} \left[\frac{1}{\sqrt{\alpha}} - 2e^{-\alpha} \int_0^{\sqrt{\alpha}} e^{\lambda^2} d\lambda \right] F(t - \tau) d\tau \\
 &\cong \int_0^{(n+1)\Delta t} r_{dc} \sqrt{\frac{2}{\pi}} \left[\frac{1}{\sqrt{\alpha}} - 2e^{-\alpha} \int_0^{\sqrt{\alpha}} e^{\lambda^2} d\lambda \right] F((n+1)\Delta t - \tau) d\tau \\
 &\cong r_{dc} \sqrt{\frac{2}{\pi}} \sum_{m=0}^n F^{n+1-m} \int_{m\Delta t}^{(m+1)\Delta t} \left[\frac{1}{\sqrt{\alpha}} - 2e^{-\alpha} \int_0^{\sqrt{\alpha}} e^{\lambda^2} d\lambda \right] d\tau \\
 &= r_{dc} \sqrt{\frac{2}{\pi}} \frac{1}{\omega_0} \sum_{m=0}^n F^{n+1-m} \int_{\omega_0 m \Delta t}^{\omega_0(m+1)\Delta t} \left[\frac{1}{\sqrt{\alpha}} - 2e^{-\alpha} \sum_{n=0}^{\infty} \frac{\alpha^{\frac{2n+1}{2}}}{(2n+1)n!} \right] d\alpha \\
 &= r_{dc} \sqrt{\frac{2}{\pi}} \frac{2}{\omega_0} \sum_{m=0}^n F^{n+1-m} \left[\sqrt{\alpha} - \sum_{n=0}^{\infty} G(n, \alpha) \right]_{\omega_0 m \Delta t}^{\omega_0(m+1)\Delta t}
 \end{aligned} \tag{8.199a}$$

where

$$G(n, \alpha) = \left\{ \begin{array}{ll} -\sqrt{\alpha} e^{-\alpha} + \frac{\sqrt{\pi}}{2} \int_0^{\sqrt{\alpha}} e^{\lambda^2} d\lambda & n = 0 \\ \left(\frac{2n-1}{2n} \right) G(n-1, \alpha) - \frac{1}{(2n+1)n!} \alpha^{\frac{2n+1}{2}} e^{-\alpha} & n \neq 0 \end{array} \right\}. \tag{8.199b}$$

In order to modify the previous development without these filters, define the quantity

$$K(\alpha) = \sqrt{\alpha} - \sum_{n=0}^{\infty} G(n, \alpha). \tag{8.200}$$

We may identify the quantity $Z_0(m)$ in the original development as

$$Z_0(m) = \frac{1}{\sqrt{\Delta t}} [K(\omega_0(m + 1)\Delta t) - K(\omega_0 m \Delta t)] \tag{8.201a}$$

and

$$B = r_{dc} \frac{2\sqrt{2}}{\sqrt{\pi}\omega_0}. \tag{8.201b}$$

Thus, the previous formulation may be modified if we obtain the appropriate representation for $Z_0(m)$.

The function $K(\alpha)$ can similarly be approximated with Prony’s method as

$$K(\alpha) \cong \sum_{i=1}^p a_i e^{\alpha b_i} \tag{8.202}$$

whose coefficients a_i and b_i are predetermined independent of the specific problem, that is, independent of ω_0 . The Ψ_i^n in (8.190b) are similarly modified using (8.201a) and this Prony representation. A reasonable approximation uses $p = 14$ terms in the Prony expansion with coefficients given in Table 8.4 [B.23].

TABLE 8.4 Coefficients of the Prony Approximation of $K(\alpha)$.

| i | a_i | b_i |
|-----|-----------------|-----------------|
| 1 | 2.1592880E - 2 | -1.1293984E0 |
| 2 | -3.4051657E - 2 | -1.6697772E0 |
| 3 | 4.8901666E0 | -5.0659628E - 1 |
| 4 | 1.1037285E2 | -2.5482929E0 |
| 5 | 6.3898279E - 2 | -6.8362799E0 |
| 6 | 1.6387213E - 1 | -2.6023629E - 1 |
| 7 | -9.3826731E + 1 | -1.7778543E0 |
| 8 | 7.0160068E - 1 | -1.4966650E - 1 |
| 9 | -6.0668061E - 1 | -1.2588752E + 1 |
| 10 | 1.3735503E + 3 | -2.1344676E0 |
| 11 | -1.6127498E - 1 | -5.1526627E - 2 |
| 12 | -1.3915974E + 3 | -2.1891200E0 |
| 13 | -3.7391617E0 | -3.9021096E - 1 |
| 14 | 1.5776220E - 1 | -1.0451770E - 2 |

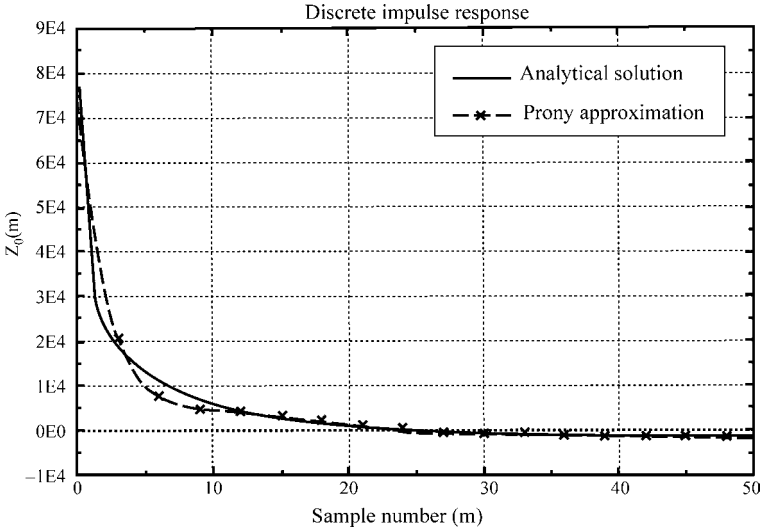


FIGURE 8.48 Prony representation of $Z_0(m)$ given in Eq. (8.201a).

Figure 8.48 compares the representation of $Z_0(m)$ given in (8.201a) using the Prony approximation of $K(\alpha)$ given in (8.202) to the exact result using (8.200). It should be noted that, although the Prony coefficients for $K(\alpha)$ can be predetermined independent of the problem, the representation error in $Z_0(m)$ depends on the specific structure since $Z_0(m)$ involves ω_0 and Δt . These values for the example previously considered are $\omega_0 = 2.47 \times 10^9$ and $\Delta t = 7.84$ ps.

Figure 8.49 compares the modified FDTD results to the TDFD results for the problem of Figure 8.42, which was considered previously. The FDTD errors in Figure 8.43 are now corrected illustrating the accuracy of the FDTD implementation of the first-order filter representation of conductor losses given in (8.150). Both results now give rapid convergence to the correct late-time steady-state limit obtained by replacing the line conductors with their total dc resistances of $r_{dc}\mathcal{L} = 17.2414 \Omega$ as shown in Figure 8.44 of $V_{NE,ss} = 0.628205 \Omega$ and $V_{FE,ss} = 0.371795 \Omega$. Although not shown, the TDFD results incorporating the filters as in (8.150) were compared to the FDTD results using these filters as implemented above and the results were virtually identical as they should be, further illustrating the accuracy of the Prony approximation.

8.2.4 Lumped-Circuit Approximate Characterizations

Perhaps the simplest way of including losses is via an approximate lumped-circuit model. The obvious structural choices are the lumped-Pi or lumped-T structures investigated previously. The advantage of these representations is that simple lumped-circuit analysis programs can be used to solve the line voltages either in the frequency domain or in the time domain. The primary difficulty with these approximations is that they do not correctly process certain of the high-frequency spectral components

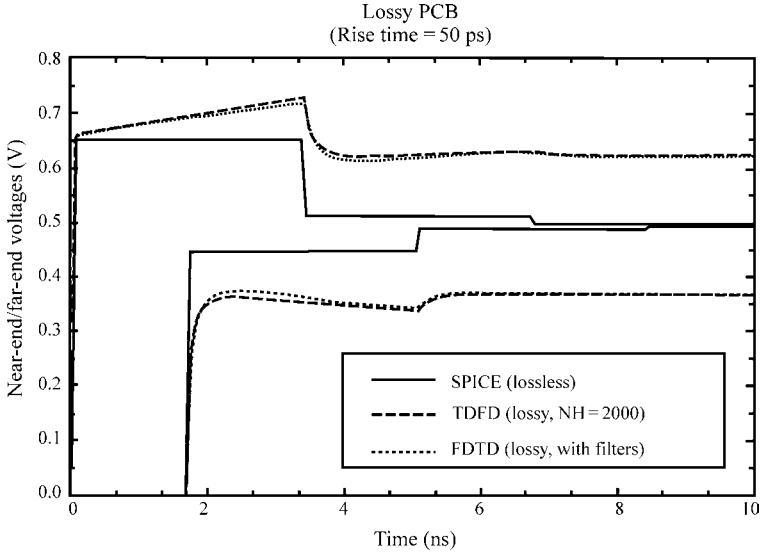


FIGURE 8.49 Recomputation of the results of Figure 8.43 but with the FDTD results represented using the corrected result in (8.153) using filters.

of the input signal because their validity is based on the assumption that they are electrically short at *all* frequencies of interest. Figure 8.50(a) shows a lumped-Pi representation of a section of the line. Typically, this type of representation requires a large number of such sections to represent the line for input signals having significant high-frequency spectral content. Implementation of this lumped-circuit approximation is straightforward if we omit consideration of the skin-effect \sqrt{f} behavior of the line resistance (and internal inductance) and only include the dc resistance and internal inductance, which can be represented as constant elements. We showed in the previous section that this would lead to errors in the early-time results.

A recurring problem is how we shall represent the \sqrt{f} skin-effect behavior in the time domain that is required in these lumped-circuit representations. A novel method of doing this is to simulate the physical process that occurs in the development of skin effect [25]. For a conductor of circular cross section, the current resides in annuli and is more strongly concentrated in the outer annuli as frequency is increased. Each of these annuli can be represented by a resistor and an inductor. The circuit representation of this process shown in Figure 8.50(b) serves to simulate this process. At dc, all resistors are in parallel giving the dc resistance. As frequency increases, each branch is successively removed from the circuit generating a \sqrt{f} frequency dependence. Of course, a larger number of branches are required to extend this \sqrt{f} behavior to higher frequencies. Another representation that is particularly useful for conductors of rectangular cross section is to simulate the representation of the conductor as numerous bars in parallel, as described in Chapter 4 and shown in Figure 4.19 . The current over each subbar is assumed constant but of unknown value, and the

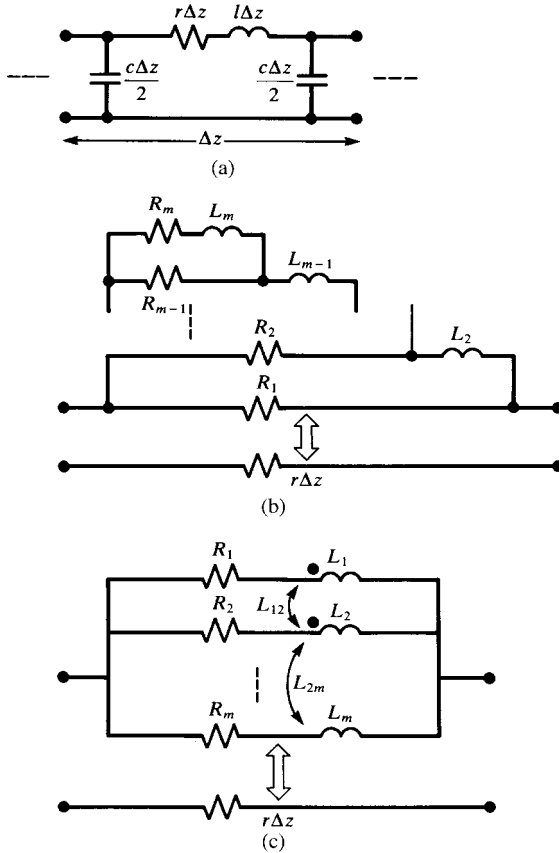


FIGURE 8.50 Methods of including frequency-dependent conductor losses into a lumped-circuit representation.

dc resistances and partial inductances of the individual subbars are used to give the circuit shown in Figure 8.50(c). This was implemented in [26–28]. Because of the interaction between the subbars via the mutual partial inductances, the currents in the subbars adjust to simulate the actual skin effect that occurs. Other methods of generating lumped-circuit models of the frequency-dependent skin-effect impedance are given in [B.17].

The FORTRAN code `SPICELPI.FOR` described in Appendix A generates a lumped-Pi SPICE subcircuit model for a *lossless line*. This can then be modified to include losses by adding either dc resistances or one of the skin effect simulations in Figure 8.50(b) or (c). In this way, only the line is modeled and nonlinear loads can be handled in the CAD code in which this model is imbedded. This is a simple approximation but suffers from the lengthy computation time, which a sufficiently large circuit model requires to model the very high-frequency spectral components of the input signal.

8.2.5 The Use of Macromodels in Modeling the Line

Macromodels of the line essentially represent the line as a two-port model at its input and output ports. An important part of the process in generating a macromodel is to convert the partial differential equations of the transmission line into ordinary differential equations that most CAD computer programs such as SPICE can handle. The SPICE equivalent circuit for a lossless line shown in Figure 8.9 is an example of a macromodel of the line. The effect of the terminal voltage and current at one port on the voltage and current at the other port is represented using time-delayed controlled sources. An additional advantage of a macromodel of the line occurs in modeling today's high-speed digital interconnect structures where, in many cases, line losses cannot be neglected. The solutions of the lossy transmission-line equations involve transcendental functions that have an infinite number of roots. Any transfer function of such a system will therefore have an infinite number of poles that characterize the time-domain response. Determining the inverse Laplace transforms of these in order to return to the time domain is an impossible task. If we can determine a macromodel of the line as a transfer function using a finite number of *dominant poles*, we can drastically reduce the simulation times. One method for doing this, the Pade method, will be discussed in this section. Other methods for model order reduction (MOR) for these dense, high-speed digital interconnects will be discussed in the next chapter.

A macromodel of a *lossy* line similar to that for a lossless line shown in Figure 8.9 can be obtained by using the *generalized method of characteristics* as follows [29]. First, we obtain the chain parameters of the lossy line in the frequency domain as

$$\begin{bmatrix} \hat{V}(\mathcal{L}) \\ \hat{I}(\mathcal{L}) \end{bmatrix} = \underbrace{\begin{bmatrix} \hat{\phi}_{11} & \hat{\phi}_{12} \\ \hat{\phi}_{21} & \hat{\phi}_{22} \end{bmatrix}}_{\hat{\Phi}(\mathcal{L})} \begin{bmatrix} \hat{V}(0) \\ \hat{I}(0) \end{bmatrix} \quad (8.203)$$

where the frequency-domain chain parameters are

$$\begin{aligned} \hat{\phi}_{11} &= \cosh(\hat{\gamma}\mathcal{L}) \\ &= \frac{e^{\hat{\gamma}\mathcal{L}} + e^{-\hat{\gamma}\mathcal{L}}}{2} \end{aligned} \quad (8.204a)$$

$$\begin{aligned} \hat{\phi}_{12} &= -\hat{Z}_C \sinh(\hat{\gamma}\mathcal{L}) \\ &= -\hat{Z}_C \frac{e^{\hat{\gamma}\mathcal{L}} - e^{-\hat{\gamma}\mathcal{L}}}{2} \end{aligned} \quad (8.204b)$$

$$\begin{aligned} \hat{\phi}_{21} &= -\frac{1}{\hat{Z}_C} \sinh(\hat{\gamma}\mathcal{L}) \\ &= -\frac{1}{\hat{Z}_C} \frac{e^{\hat{\gamma}\mathcal{L}} - e^{-\hat{\gamma}\mathcal{L}}}{2} \end{aligned} \quad (8.204c)$$

$$\begin{aligned}\hat{\phi}_{22} &= \cosh(\hat{\gamma}\mathcal{L}) \\ &= \frac{e^{\hat{\gamma}\mathcal{L}} + e^{-\hat{\gamma}\mathcal{L}}}{2}\end{aligned}\quad (8.204d)$$

The characteristic impedance is frequency dependent and is given by

$$\hat{Z}_C(\omega) = \sqrt{\frac{r(\omega) + j\omega l_1(\omega) + j\omega l}{g(\omega) + j\omega c}} \quad (8.205a)$$

The propagation constant is also frequency dependent and is given by

$$\hat{\gamma}(\omega) = \sqrt{[r(\omega) + j\omega l_1(\omega) + j\omega l][g(\omega) + j\omega c]} \quad (8.205b)$$

In terms of the Laplace transform variable s , these become

$$\hat{Z}_C(s) = \sqrt{\frac{r(s) + sl_1(s) + sl}{g(s) + sc}} \quad (8.206a)$$

and

$$\hat{\gamma}(s) = \sqrt{[r(s) + sl_1(s) + sl][g(s) + sc]} \quad (8.206b)$$

Writing out (8.203) and using the relations in (8.204) gives

$$\hat{V}(\mathcal{L}, s) = \left(\frac{e^{\hat{\gamma}(s)\mathcal{L}} + e^{-\hat{\gamma}(s)\mathcal{L}}}{2}\right) \hat{V}(0, s) - \hat{Z}_C(s) \left(\frac{e^{\hat{\gamma}(s)\mathcal{L}} - e^{-\hat{\gamma}(s)\mathcal{L}}}{2}\right) \hat{I}(0, s) \quad (8.207a)$$

$$\begin{aligned}\hat{Z}_C(s) \hat{I}(\mathcal{L}, s) &= -\left(\frac{e^{\hat{\gamma}(s)\mathcal{L}} - e^{-\hat{\gamma}(s)\mathcal{L}}}{2}\right) \hat{V}(0, s) \\ &\quad + \hat{Z}_C(s) \left(\frac{e^{\hat{\gamma}(s)\mathcal{L}} + e^{-\hat{\gamma}(s)\mathcal{L}}}{2}\right) \hat{I}(0, s)\end{aligned}\quad (8.207b)$$

Adding and subtracting these gives

$$\hat{V}(0, s) - \hat{Z}_C(s) \hat{I}(0, s) = e^{-\hat{\gamma}(s)\mathcal{L}} [\hat{V}(\mathcal{L}, s) - \hat{Z}_C(s) \hat{I}(\mathcal{L}, s)] \quad (8.208a)$$

$$\hat{V}(\mathcal{L}, s) + \hat{Z}_C(s) \hat{I}(\mathcal{L}, s) = e^{-\hat{\gamma}(s)\mathcal{L}} [\hat{V}(0, s) + \hat{Z}_C(s) \hat{I}(0, s)] \quad (8.208b)$$

These relations may be represented as shown in Figure 8.51(a), where

$$\hat{E}_0(s) = e^{-\hat{\gamma}(s)\mathcal{L}} [\hat{V}(\mathcal{L}, s) - \hat{Z}_C(s) \hat{I}(\mathcal{L}, s)] \quad (8.209a)$$

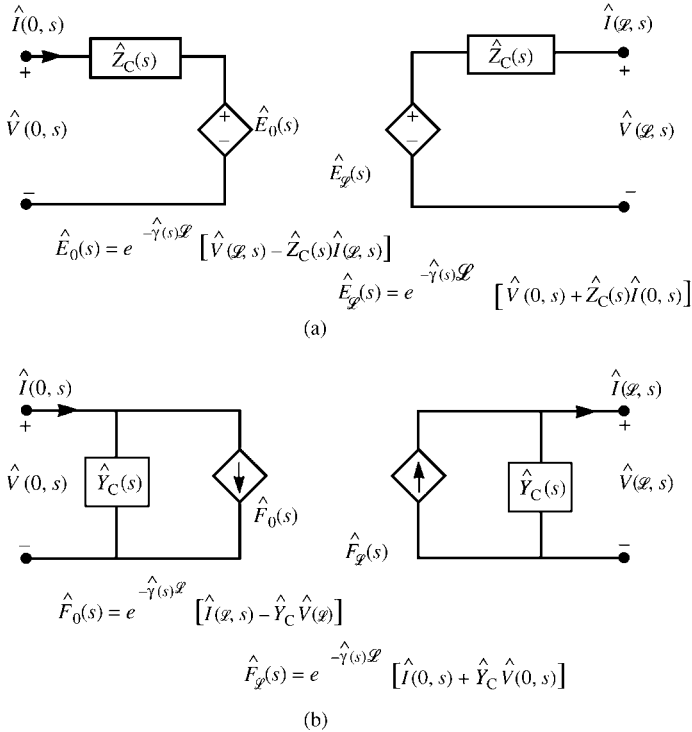


FIGURE 8.51 Two implementations of the generalized method of characteristics to represent lossy lines.

$$\hat{E}_{\mathcal{L}}(s) = e^{-\hat{\gamma}(s)\mathcal{L}} [\hat{V}(0, s) + \hat{Z}_C(s)\hat{I}(0, s)] \tag{8.209b}$$

or, alternatively,

$$\hat{E}_0(s) = e^{-\hat{\gamma}(s)\mathcal{L}} [2\hat{V}(\mathcal{L}, s) - \hat{E}_{\mathcal{L}}(s)] \tag{8.210a}$$

$$\hat{E}_{\mathcal{L}}(s) = e^{-\hat{\gamma}(s)\mathcal{L}} [2\hat{V}(0, s) - \hat{E}_0(s)] \tag{8.210b}$$

The results in (8.208) using either (8.209) or (8.210) give the equivalent macro-model shown in Figure 8.51(a), which is easily implementable in the frequency domain. For the time domain, the model in Figure 8.51(a) is problematic because of the need to develop the inverse transforms of

$$\hat{Z}_C(s) \iff z_C(t) \tag{8.211a}$$

$$e^{-\hat{\gamma}(s)\mathcal{L}} \iff h(t) \tag{8.211b}$$

where $h(t)$ is essentially the impulse response of a completely matched line. In the time domain, (8.208) become

$$V(0, t) - z_C(t) * I(0, t) = E_0(t) \quad (8.212a)$$

$$V(\mathcal{L}, t) + z_C(t) * I(\mathcal{L}, t) = E_{\mathcal{L}}(t) \quad (8.212b)$$

where

$$E_0(t) = h(t) * [V(\mathcal{L}, t) - z_C(t) * I(\mathcal{L}, t)] \quad (8.213a)$$

$$E_{\mathcal{L}}(t) = h(t) * [V(0, t) + z_C(t) * I(0, t)] \quad (8.213b)$$

or

$$E_0(t) = h(t) * [2V(\mathcal{L}, t) - E_{\mathcal{L}}(t)] \quad (8.214a)$$

$$E_{\mathcal{L}}(t) = h(t) * [2V(0, t) - E_0(t)] \quad (8.214b)$$

and $*$ denotes convolution. Hence, we are again faced with the difficult computational task of convolution.

An alternative form of the equivalent circuit macromodel (of the many that are possible) of the line can be obtained by multiplying both sides of (8.208a) and (8.208b) by the characteristic admittance $\hat{Y}_C(s) = 1/\hat{Z}_C(s)$ and rearranging to give

$$\hat{I}(0, s) - \hat{Y}_C(s)\hat{V}(0, s) = e^{-\hat{\gamma}(s)\mathcal{L}} [\hat{I}(\mathcal{L}, s) - \hat{Y}_C(s)\hat{V}(\mathcal{L}, s)] \quad (8.215a)$$

$$\hat{I}(\mathcal{L}, s) + \hat{Y}_C(s)\hat{V}(\mathcal{L}, s) = e^{-\hat{\gamma}(s)\mathcal{L}} [\hat{I}(0, s) + \hat{Y}_C(s)\hat{V}(0, s)] \quad (8.215b)$$

This may be represented by the equivalent circuit shown in Figure 8.51(b). In the time domain, these become

$$I(0, t) - y_C(t) * V(0, t) = h(t) * [I(\mathcal{L}, t) - y_C(t) * V(\mathcal{L}, t)] \quad (8.216a)$$

$$I(\mathcal{L}, t) + y_C(t) * V(\mathcal{L}, t) = h(t) * [I(0, t) + y_C(t) * V(0, t)] \quad (8.216b)$$

where $\hat{Y}_C(s) \iff y_C(t)$.

8.2.6 Representing Frequency-Dependent Functions in the Time Domain Using Pade Methods

The inverse Laplace transform time-domain forms in the macromodels in the previous section can be obtained using the Pade method [30–34]. The Laplace transform

function to be represented is modeled as a ratio of polynomials in s as

$$F(s) = \frac{N(s)}{D(s)} \quad (8.217)$$

Approximate the numerator and denominator polynomials $N(s)$ and $D(s)$ as N th order polynomials in s as

$$F(s) = F(0) \frac{1 + a_1s + \cdots + a_Ns^N}{1 + b_1s + \cdots + b_Ns^N} \quad (8.218)$$

where $F(0) = F(s)|_{s=0}$ is the dc response. Expanding this with partial fractions as [A.2, A.5]

$$F(s) = F(\infty) + \sum_{k=1}^N \frac{c_k}{s - p_k} \quad (8.219)$$

where $F(\infty) = F(s)|_{s \rightarrow \infty}$ is the steady-state response of the system and $F(\infty) = F(0)(a_N/b_N)$. p_k are the N poles of $F(s)$, and c_k are the N residues associated with the poles. The inverse Laplace transform becomes

$$f(t) = F(\infty)\delta(t) + \sum_{k=1}^N c_k e^{p_k t} \quad (8.220)$$

where $\delta(t)$ is the unit impulse function [A.2, A.5]. Hence, the time-domain representation can be represented as a sum of exponentials, thereby allowing the use of the recursive convolution procedure.

The $2N$ coefficients $a_1, \dots, a_N, b_1, \dots, b_N$ in (8.218) are determined by expanding $F(s)$ in terms of a power series in s or, in other words, the moments of $f(t)$, using a Maclaurin series about $s = 0$:

$$\begin{aligned} F(s) &= F(0) \left[1 + \sum_{k=1}^{\infty} m_k s^k \right] \\ &= F(0) \left[1 + m_1 s + m_2 s^2 + \cdots \right] \end{aligned} \quad (8.221)$$

The moments of $F(s)$ can be found by differentiating $F(s)$. Differentiating (8.221) gives m_k in terms of the derivatives of $F(s)$ as

$$m_k = \frac{1}{F(0)} \frac{1}{k!} \left. \frac{d^k F(s)}{ds^k} \right|_{s=0} \quad (8.222)$$

The term “moments” arises from the following. The Laplace transform of $F(s)$ is

$$\begin{aligned}
 F(s) &= \int_0^{\infty} f(t) e^{-st} dt \\
 &= \int_0^{\infty} f(t) \left[1 - \frac{st}{1!} + \frac{s^2 t^2}{2!} - \dots \right] dt \\
 &= \int_0^{\infty} f(t) dt - s \int_0^{\infty} t f(t) dt + s^2 \int_0^{\infty} \frac{t^2}{2!} f(t) dt - \dots \\
 &= k_0 + k_1 s + k_2 s^2 + \dots
 \end{aligned}
 \tag{8.223}$$

Hence, $k_i = F(0)m_i$ are said to be the *moments* of $f(t)$.

Equating (8.218) and (8.221), multiplying both sides by the denominator of (8.218), and grouping terms with like powers of s yields $2N$ equations that can be solved for the $2N$ coefficients $a_1, \dots, a_N, b_1, \dots, b_N$:

$$\begin{aligned}
 s : a_1 &= b_1 + m_1 \\
 s^2 : a_2 &= b_2 + m_1 b_1 + m_2 \\
 s^3 : a_3 &= b_3 + m_1 b_2 + m_2 b_1 + m_3 \\
 &\vdots \\
 s^{N-1} : a_{N-1} &= b_{N-1} + m_1 b_{N-2} + m_2 b_{N-3} + \dots + m_{N-1} \\
 s^N : a_N &= b_N + m_1 b_{N-1} + m_2 b_{N-2} + \dots + m_N
 \end{aligned}
 \tag{8.224a}$$

and

$$\begin{aligned}
 s^{N+1} : 0 &= m_1 b_N + m_2 b_{N-1} + \dots + m_N b_1 + m_{N+1} \\
 s^{N+2} : 0 &= m_2 b_N + m_3 b_{N-1} + \dots + m_{N+1} b_1 + m_{N+2} \\
 &\vdots \\
 s^{2N-1} : 0 &= m_{N-1} b_N + m_N b_{N-1} + \dots + m_{2N-2} b_1 + m_{2N-1} \\
 s^{2N} : 0 &= m_N b_N + m_{N+1} b_{N-1} + \dots + m_{2N-1} b_1 + m_{2N}
 \end{aligned}
 \tag{8.224b}$$

Representing these in matrix form gives the required $2N$ equations. The b_i coefficients for $i = 1, \dots, N$ can be obtained from (8.224b) as

$$\begin{bmatrix} m_1 & m_2 & m_3 & \dots & m_N \\ m_2 & m_3 & m_4 & \dots & m_{N+1} \\ m_3 & m_4 & m_5 & \dots & m_{N+2} \\ \vdots & \vdots & \vdots & \vdots & \vdots \\ m_N & m_{N+1} & m_{N+2} & \dots & m_{2N-1} \end{bmatrix} \begin{bmatrix} b_N \\ b_{N-1} \\ b_{N-2} \\ \vdots \\ b_1 \end{bmatrix} = - \begin{bmatrix} m_{N+1} \\ m_{N+2} \\ m_{N+3} \\ \vdots \\ m_{2N} \end{bmatrix}
 \tag{8.225a}$$

and the a_i coefficients for $i = 1, \dots, N$ can then be obtained from (8.224a) as

$$\begin{bmatrix} a_1 \\ a_2 \\ a_3 \\ \vdots \\ a_N \end{bmatrix} = \begin{bmatrix} 1 & 0 & 0 & \cdots & 0 \\ m_1 & 1 & 0 & \cdots & 0 \\ m_2 & m_1 & 1 & \cdots & 0 \\ \vdots & \vdots & \vdots & \ddots & \vdots \\ m_{N-1} & m_{N-2} & m_{N-3} & \cdots & 1 \end{bmatrix} \begin{bmatrix} b_1 \\ b_2 \\ b_3 \\ \vdots \\ b_N \end{bmatrix} + \begin{bmatrix} m_1 \\ m_2 \\ m_3 \\ \vdots \\ m_N \end{bmatrix} \quad (8.225b)$$

The N residues of the partial-fraction expansion in (8.219) can be found directly using the methods of [A.2, A.5] or in terms of the moments m_k [34]. First, obtain the N poles of the denominator polynomial $D(s)$ by factoring $D(s)$ using a root-finding algorithm as $D(s) = 1 + b_1s + \dots + b_Ns^N = b_N (s - p_1) \cdots (s - p_N)$. Differentiating (8.219) with respect to s and evaluating at $s = 0$ and comparing to (8.222) yields

$$m_k F(0) = - \sum_{i=1}^N \frac{c_i}{p_i^{k+1}} \quad (8.226)$$

hence we can obtain the residues indirectly from

$$\begin{bmatrix} \frac{1}{p_1^2} & \frac{1}{p_2^2} & \cdots & \frac{1}{p_N^2} \\ \frac{1}{p_1^3} & \frac{1}{p_2^3} & \cdots & \frac{1}{p_N^3} \\ \vdots & \vdots & \cdots & \vdots \\ \frac{1}{p_1^{N+1}} & \frac{1}{p_2^{N+1}} & \cdots & \frac{1}{p_N^{N+1}} \end{bmatrix} \begin{bmatrix} c_1 \\ c_2 \\ \vdots \\ c_N \end{bmatrix} = -F(0) \begin{bmatrix} m_1 \\ m_2 \\ \vdots \\ m_N \end{bmatrix} \quad (8.227)$$

and

$$F(\infty) - F(0) = \sum_{i=1}^N \frac{c_i}{p_i} \quad (8.228)$$

Unstable poles, that is, poles in the right-half plane, may be obtained rendering the representation unstable. Generally, these poles can be moved to the left-half plane resulting in a stable representation if we increase the order of the representation, N . However, the coefficient matrix in (8.225a), although a Toeplitz matrix, tends to be ill conditioned. Hence, care must be observed in increasing the order of the representation, N , and solving (8.225a). A LU decomposition method is recommended for use in solving (8.225a) along with some conditioning [30].

The Pade method of expanding the transfer function in moments about $s = 0$ described above is accurate in a region about $s = 0$ [30]. In the next chapter, we will discuss complex frequency hopping (CFH), which seeks to expand the region of convergence. References [31, 32] point out that it is generally preferable to expand

$F(s)$ about $s = \infty$ instead of about $s = 0$ and show examples to support this assertion. If we think about the frequency-domain meaning of $F(s)$, values around $s = \infty$ correspond to the high-frequency spectral content of the impulse response, whereas values around $s = 0$ correspond to the low-frequency spectral content. Predicting the low-frequency spectral content well means that our time-domain predictions of the impulse response will be most accurate for the late-time or steady-state part of that response. On the contrary, predicting the high-frequency spectral content well means that our time-domain predictions of the impulse response will be most accurate for the early-time or initial part of that response. In using this time-domain impulse response result in a convolution (the primary reason for using Pade), the early-time content of the impulse response is the most important aspect in the accurate prediction of the overall response. In performing the convolution, we virtually never use the steady-state response of the impulse response. To this end, we write the transfer function in terms of $z = 1/s$ as

$$\begin{aligned}
 F(s) &= F(\infty) \frac{s^N + A_1 s^{N-1} + \dots + A_N}{s^N + B_1 s^{N-1} + \dots + B_N} \\
 &= F(\infty) \frac{1 + A_1 z + \dots + A_N z^N}{1 + B_1 z + \dots + B_N z^N} \quad (z = 1/s)
 \end{aligned}
 \tag{8.229}$$

and $F(0) = F(\infty)(A_N/B_N)$. Again expand $F(s)$ in terms of moments by expanding about $s = \infty$ or, equivalently, about $z = 0$ as

$$\begin{aligned}
 F(s) &= F(\infty) \left[1 + \sum_{k=1}^{\infty} M_k z^k \right] \\
 &= F(\infty) \left[1 + M_1 z + M_2 z^2 + \dots \right]
 \end{aligned}
 \tag{8.230}$$

and the moments M_k are obtained from

$$M_k = \frac{1}{F(\infty)} \frac{1}{k!} \left. \frac{d^k F(s)}{dz^k} \right|_{z=0}
 \tag{8.231}$$

Equations (8.229) and (8.230) are of an identical form to (8.218) and (8.221) with $z \iff 1/s$. Hence, we may solve the $2N$ equations in (8.224) by replacing $a_i \implies A_i$, $b_i \implies B_i$, and $m_i \implies M_i$ and interchanging $F(0) \implies F(\infty)$. Alternatively, using the first $N - 1$ equations of (8.224a), the last equation of (8.224a), and the first $N - 1$ equations of (8.224b) yields an alternative set of $2N$ equations that can be solved for the $2N$ coefficients $A_1, \dots, A_{N-1}, B_1, \dots, B_N$ [31, 32]. The B_i coefficients for $i = 1, \dots, N$

can be obtained from

$$\begin{bmatrix} \left(1 - \frac{A_n}{B_n}\right) & M_1 & M_2 & \cdots & M_{N-1} \\ M_1 & M_2 & M_3 & \cdots & M_N \\ M_2 & M_3 & M_4 & \cdots & M_{N+1} \\ \vdots & \vdots & \vdots & \vdots & \vdots \\ M_{N-1} & M_N & M_{N+1} & \cdots & M_{2N-2} \end{bmatrix} \begin{bmatrix} B_N \\ B_{N-1} \\ B_{N-2} \\ \vdots \\ B_1 \end{bmatrix} = - \begin{bmatrix} M_N \\ M_{N+1} \\ M_{N+2} \\ \vdots \\ M_{2N-1} \end{bmatrix} \tag{8.232a}$$

and the A_i coefficients for $i = 1, \dots, N - 1$ can then be obtained from

$$\begin{bmatrix} A_1 \\ A_2 \\ A_3 \\ \vdots \\ A_{N-1} \end{bmatrix} = \begin{bmatrix} 1 & 0 & 0 & \cdots & 0 \\ M_1 & 1 & 0 & \cdots & 0 \\ M_2 & M_1 & 1 & \cdots & 0 \\ \vdots & \vdots & \vdots & \vdots & \vdots \\ M_{N-2} & M_{N-3} & M_{N-4} & \cdots & 1 \end{bmatrix} \begin{bmatrix} B_1 \\ B_2 \\ B_3 \\ \vdots \\ B_{N-1} \end{bmatrix} + \begin{bmatrix} M_1 \\ M_2 \\ M_3 \\ \vdots \\ M_{N-1} \end{bmatrix} \tag{8.232b}$$

and $A_N = B_N(F(0) / F(\infty))$. The rational function in (8.229) can again be expanded in partial fractions as

$$F(s) = F(\infty) + \sum_{k=1}^N \frac{d_k}{s - q_k} \tag{8.233}$$

where q_k are the N poles computed for this representation of $F(s)$ and d_k are the N residues associated with the poles. The poles and residues for this representation are generally different from those of the representation in (8.218). The time-domain result can again be written in terms of a sum of exponentials so that the method of recursive convolution can be used:

$$f(t) = F(\infty)\delta(t) + \sum_{k=1}^N d_k e^{q_k t} \tag{8.234}$$

Hence, the Prony method or the Pade method can be used to give exponential representations of $h(t)$ and $z_C(t)$ or $y_C(t)$ that can be used to implement the convolutions using the recursive convolution as described in Section 8.2.3.4. The Pade method has the advantage of using frequency-domain data. However, poles with nonnegative real parts may occur, thereby causing instabilities. Generally, these unstable poles can be moved to the left-half plane by increasing the order of the representation, N .

As an example, consider a lossy transmission line characterized by constant $r, l, g,$ and c per-unit-length parameters, that is, their dc values. The characteristic admittance

is written as [32]

$$\begin{aligned}
 \hat{Y}_C(s) &= \sqrt{\frac{g+sc}{r+sl}} \\
 &= \sqrt{\frac{c}{l}} \sqrt{\frac{1+\frac{g}{c}z}{1+\frac{r}{l}z}} \\
 &= \hat{Y}_C(\infty) \sqrt{\frac{1+\frac{g}{c}z}{1+\frac{r}{l}z}}
 \end{aligned} \tag{8.235}$$

where $z = 1/s$. Note that $\hat{Y}_C(\infty) = \sqrt{c/l}$. Expanding this in moments about $s = \infty$ or, equivalently, $z = 0$ gives

$$\sqrt{\frac{1+\frac{g}{c}z}{1+\frac{r}{l}z}} = 1 + M_1z + M_2z^2 + \dots + M_kz^k + \dots \tag{8.236}$$

and the moments are obtained as

$$M_k = \frac{1}{k!} \frac{d^k}{dz^k} \sqrt{\frac{1+\frac{g}{c}z}{1+\frac{r}{l}z}} \tag{8.237}$$

This differentiation, although tedious, can be performed symbolically giving exact expressions for the moments. Hence, $\hat{Y}_C(s)$ can be expanded in partial fractions as in (8.233) with the resulting time-domain expressions given in (8.234). Observe that the time-domain expression in (8.234) is in terms of a sum of exponentials. Hence, it can be used in a recursive convolution method to perform the convolutions in (8.216).

The propagation function $e^{-\hat{\gamma}(s)\mathcal{L}}$ can similarly be expanded to obtain $h(t)$. The propagation constant is

$$\begin{aligned}
 \hat{\gamma}(s) &= \sqrt{(r+sl)(g+sc)} \\
 &= s\sqrt{lc} \sqrt{\left(1+\frac{r}{l}z\right)\left(1+\frac{g}{c}z\right)} \\
 &= s\sqrt{lc} \left[1 + \sum_{k=1}^{\infty} M_k z^k \right]
 \end{aligned} \tag{8.238}$$

where we symbolically differentiate $\sqrt{(1 + (r/l)z)(1 + (g/c)z)}$ to obtain the moments M_k as

$$M_k = \frac{1}{k!} \frac{d^k \sqrt{(1 + \frac{r}{l}z)(1 + \frac{g}{c}z)}}{dz^k} \tag{8.239}$$

Hence, the propagation function $e^{-\hat{\gamma}(s)\mathcal{L}}$ is

$$\begin{aligned} e^{-\hat{\gamma}(s)\mathcal{L}} &= e^{-s\sqrt{lc}\mathcal{L}} e^{-s\sqrt{lc}\mathcal{L}} \sum_{k=1}^{\infty} M_k z^k \\ &= e^{-s\sqrt{lc}\mathcal{L}} e^{-M_1\sqrt{lc}\mathcal{L}} e^{-\sqrt{lc}\mathcal{L}} \sum_{k=1}^{\infty} (M_{k+1}/s^k) \\ &= e^{-sT_D} e^{-M_1T_D} e^{-\sum_{k=1}^{\infty} T_D (M_{k+1}/s^k)} \end{aligned} \tag{8.240}$$

where we denote the one-way time delay of the lossless line as $T_D = \sqrt{lc}\mathcal{L}$. Represent the last exponential with Pade methods as

$$\begin{aligned} e^{-\sum_{k=1}^{\infty} T_D (M_{k+1}/s^k)} &= 1 + \sum_{k=1}^{\infty} \frac{\beta_k}{s^k} \\ &= \frac{s^L + c_1s^{L-1} + \dots + c_L}{s^L + d_1s^{L-1} + \dots + d_L} \\ &= 1 + \sum_{i=1}^L \frac{K_i}{s - q_i} \end{aligned} \tag{8.241}$$

Using the infinite series expansion for the exponential gives recursion relations for β_k as [31,32]

$$\begin{aligned} \beta_1 &= \alpha_1 \\ \beta_2 &= \frac{1}{2} (2\alpha_2 + \alpha_1) = \frac{1}{2} (\alpha_1, 2\alpha_2) (\beta_1, 1) \\ \beta_3 &= \frac{1}{3} (\alpha_1, 2\alpha_2, 3\alpha_3) (\beta_2, \beta_1, 1) \\ &\vdots \\ \beta_k &= \frac{1}{k} (\alpha_1, 2\alpha_2, \dots, k\alpha_k) (\beta_{k-1}, \beta_{k-2}, \dots, 1) \end{aligned} \tag{8.242}$$

where we denote $\alpha_k = -T_D M_{k+1}$. Hence, we can write the propagation function as

$$e^{-\hat{\gamma}(s)\mathcal{L}} = e^{-sT_D} e^{-M_1 T_D} \left(1 + \sum_{i=1}^L \frac{K_i}{s - q_i} \right) \tag{8.243}$$

In the time domain, (8.243) gives

$$e^{-\hat{\gamma}(s)\mathcal{L}} F(s) \iff e^{-M_1 T_D} f(t - T_D) * \left(\delta(t) + \sum_{i=1}^L K_i e^{q_i t} \right) \tag{8.244}$$

Hence, we have the required representation in terms of exponentials to facilitate the recursive convolution scheme in performing the convolution. In order to include skin-effect losses, we use the previous representation of the internal impedance as $r + sl_i = A + B\sqrt{s}$ giving

$$\hat{Y}_C(s) = \sqrt{\frac{g + sc}{A + B\sqrt{s} + sl}} \tag{8.245a}$$

and

$$\hat{\gamma}(s) = \sqrt{(g + sc)(A + B\sqrt{s} + sl)} \tag{8.245b}$$

These are similarly symbolically differentiated to obtain their moments, and the Pade method yields the exponential representations as before. Other representations of these parameters using the Pade method are given in [33].

PROBLEMS

- 8.1** Show by direct substitution that the results in (8.3) satisfy (8.1) and (8.2).
- 8.2** Derive the voltage reflection coefficient in (8.7).
- 8.3** Show that the per-unit-length inductance and capacitance can be found from the characteristic impedance and velocity of propagation. [$l = (Z_C/v)$, $c = (1/vZ_C)$]
- 8.4** Sketch the load voltage $V(\mathcal{L}, t)$ and the input current to the line, $I(0, t)$, for the problem depicted in Figure P8.4 for $0 < t < 10$ ns. What should these plots converge to in the steady state? [$V(\mathcal{L}, t)$, $0 < t < 1$ ns, 0 V, $1 \text{ ns} < t < 3$ ns, 9.375 V, $3 \text{ ns} < t < 5$ ns, 8.203 V, $5 \text{ ns} < t < 7$ ns, 8.35 V, $7 \text{ ns} < t < 9$ ns, 8.331 V, $9 \text{ ns} < t < 11$ ns, 8.334 V, steady-state 8.333 V, and $I(0, t)$, $0 < t < 2$ ns, 0.125 A, $2 \text{ ns} < t < 4$ ns, 0.047A, $4 \text{ ns} < t < 6$ ns, 0.057 A, $6 \text{ ns} < t < 8$ ns, 0.055 A, $8 \text{ ns} < t < 10$ ns, 0.056 A, steady-state 0.056 A]

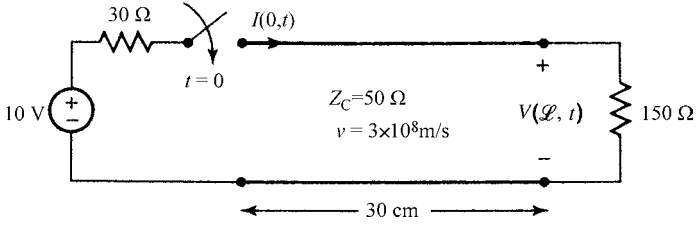


FIGURE P8.4

8.5 Sketch the load voltage $V(L, t)$, and the input voltage to the line, $V(0, t)$, for the problem depicted in Figure P8.5 for $0 < t < 20 \text{ ns}$. What should these plots converge to in the steady state? [$V(L, t)$, $0 < t < 2 \text{ ns}$, 0 V, $2 \text{ ns} < t < 6 \text{ ns}$, 6.667 V, $6 \text{ ns} < t < 10 \text{ ns}$, 4.444 V, $10 \text{ ns} < t < 14 \text{ ns}$, 5.185 V, $14 \text{ ns} < t < 18 \text{ ns}$, 4.938 V, $18 \text{ ns} < t < 22 \text{ ns}$, 5.021 V, steady-state 5 V, and $V(0, t)$, $0 < t < 4 \text{ ns}$, 3.33 V, $4 \text{ ns} < t < 8 \text{ ns}$, 5.556 V, $8 \text{ ns} < t < 12 \text{ ns}$, 4.815 V, $12 \text{ ns} < t < 16 \text{ ns}$, 5.062 V, $16 \text{ ns} < t < 20 \text{ ns}$, 4.979 V, steady-state 5 V]

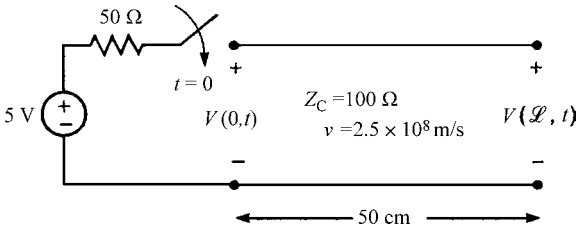


FIGURE P8.5

8.6 Sketch the input voltage to the line, $V(0, t)$, and the load current $I(L, t)$ for the problem depicted in Figure P8.6 for $0 < t < 10 \mu\text{s}$. What should these plots converge to in the steady state? [$V(0, t)$, $0 < t < 2 \mu\text{s}$, 66.67 V, $2 \mu\text{s} < t < 4 \mu\text{s}$, 22.22 V, $4 \mu\text{s} < t < 6 \mu\text{s}$, 7.407 V, $6 \mu\text{s} < t < 8 \mu\text{s}$, 2.469 V, $8 \mu\text{s} < t < 10 \mu\text{s}$, 0.823 V, steady-state 0 V and $I(L, t)$, $0 < t < 1 \mu\text{s}$, 0 V, $1 \mu\text{s} < t < 3 \mu\text{s}$, 1.33 A, $3 \mu\text{s} < t < 5 \mu\text{s}$, 1.778 A, $5 \mu\text{s} < t < 7 \mu\text{s}$, 1.926 A, $7 \mu\text{s} < t < 9 \mu\text{s}$, 1.975 A, $9 \mu\text{s} < t < 11 \mu\text{s}$, 1.992 A, steady-state 2 A]

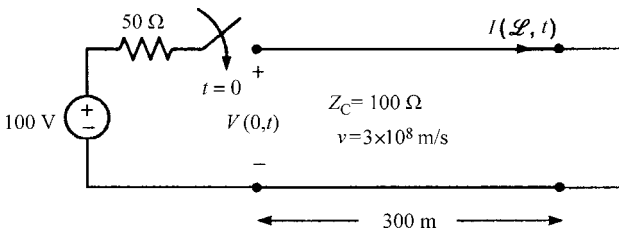


FIGURE P8.6

- 8.7 Sketch the input voltage to the line, $V(0, t)$, and the load voltage $V(\mathcal{L}, t)$ for the problem depicted in Figure P8.7 for $0 < t < 32$ ns. What should these plots converge to in the steady state? [$V(0, t)$, $0 < t < 8$ ns, 10 V, 8 ns $< t < 12$ ns, 5.556 V, 12 ns $< t < 16$ ns, -4.444 V, 16 ns $< t < 20$ ns, -3.951 V, 20 ns $< t < 24$ ns, 0.494 V, 24 ns $< t < 28$ ns, 0.439 V, 28 ns $< t < 32$ ns, -0.055 V steady-state 0 V, and $V(\mathcal{L}, t)$, $0 < t < 4$ ns, 0 V, 4 ns $< t < 12$ ns, 6.667 V, 12 ns $< t < 16$ ns, 5.926 V, 16 ns $< t < 20$ ns, -0.741 V, 20 ns $< t < 24$ ns, -0.658 V, 24 ns $< t < 28$ ns, 0.082 V, 28 ns $< t < 32$ ns, 0.073 V steady-state 0 V]

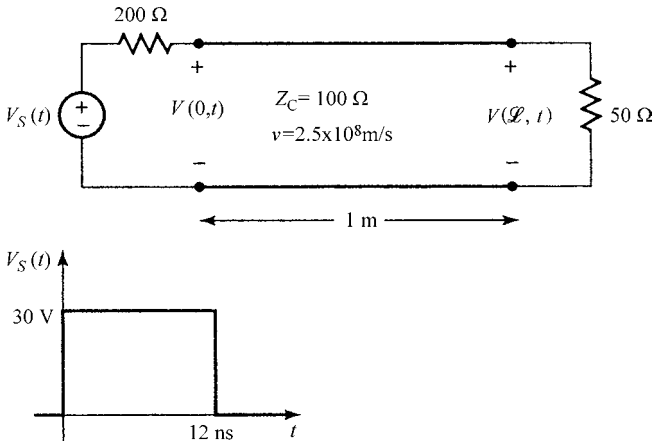


FIGURE P8.7

- 8.8 A time-domain reflectometer (TDR) is an instrument used to determine properties of transmission lines. In particular, it can be used to detect the locations of imperfections such as breaks in the line. The instrument launches a pulse down the line and records the transit time for that pulse to be reflected at some discontinuity and to return to the line input. Suppose a TDR having a source impedance of 50Ω is attached to a $50\text{-}\Omega$ coaxial cable having some unknown length and load resistance. The dielectric of the cable is Teflon ($\epsilon_r = 2.1$). The open-circuit voltage of the TDR is a pulse of duration $10 \mu\text{s}$. If the recorded

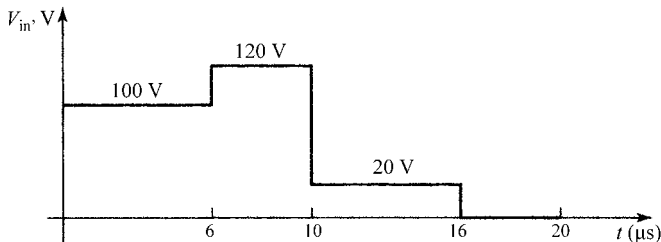


FIGURE P8.8

voltage at the input to the line is as shown in Figure P8.8, determine (a) the length of the line and (b) the unknown load resistance. [75Ω , 621.059 m]

- 8.9** A 12-V battery ($R_S = 0$) is attached to an unknown length of transmission line that is terminated in a resistance. If the input current to the line for $6 \mu\text{s}$ is as shown in Figure P8.9, determine (a) the line characteristic impedance and (b) the unknown load resistance. [$Z_C = 80 \Omega$, $R_L = 262.9 \Omega$]

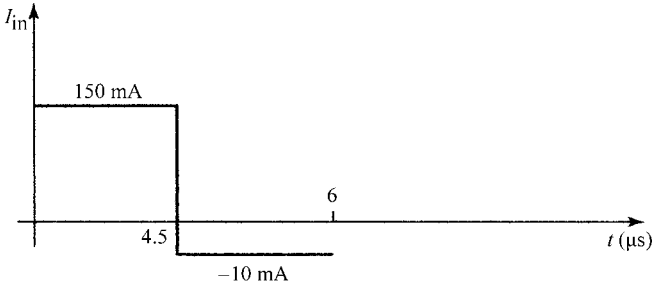


FIGURE P8.9

- 8.10** Digital clock and data pulses should ideally consist of rectangular pulses. Actual clock and data pulses, however, resemble pulses having a trapezoidal shape with certain rise and fall times. Depending on the ratio of the rise/fall time to the one-way transit time of the transmission line, the received voltage may oscillate about the desired value, possibly causing a digital gate at that end to switch falsely to an undesired state, and cause errors. Matching the line eliminates this problem because there are no reflections, but matching cannot always be accomplished. In order to investigate this problem, consider a line connecting two CMOS gates. The driver gate is assumed to have zero source resistance ($R_S = 0$), and the open-circuit voltage is a ramp waveform (simulating the leading edge of the clock/data pulse) given by $V_S(t) = 0$ for $t < 0$, $V_S(t) = 5(t/\tau_r)$ V for $0 \leq t \leq \tau_r$ and $V_S(t) = 5$ V for $t \geq \tau_r$, where τ_r is the pulse rise time. The input to a CMOS gate (the load on the line here) can be modeled as a capacitance of some 5–15pF. However, in order to simplify the problem, we will assume that the input to the load CMOS gate is an open circuit $R_L = \infty$. Sketch the load voltage of the line (the input voltage to the load CMOS gate) for line lengths having one-way transit times T such that (a) $\tau_r = (T_D/10)$, (b) $\tau_r = 2T_D$, (c) $\tau_r = 3T_D$, and (d) $\tau_r = 4T_D$. This example shows that in order to avoid problems resulting from mismatch, one should choose line lengths short enough such that $T_D \ll \tau_r$, that is, the line one-way delay is much less than the rise time of the clock/data pulses carried by the line.
- 8.11** Highly mismatched lines in digital products can cause what appears to be “ringing” on the signal output from the line. This is often referred to as “overshoot” or “undershoot” and can cause digital logic errors. To simulate this, we will investigate the problem shown in Figure P8.11. Two CMOS gates are connected by a transmission line as shown. A 5-V

step function voltage of the first gate is applied. Sketch the output voltage of the line (the input voltage to the load CMOS gate) for $0 < t < 9T_D$. [$0 < t < T_D$, 0 V, $T_D < t < 3 T_D$, 6.944 V, $3 T_D < t < 5 T_D$, 3.858 V, $5 T_D < t < 7 T_D$, 5.23 V, $7 T_D < t < 9 T_D$, 4.62 V. Steady state is 5 V]

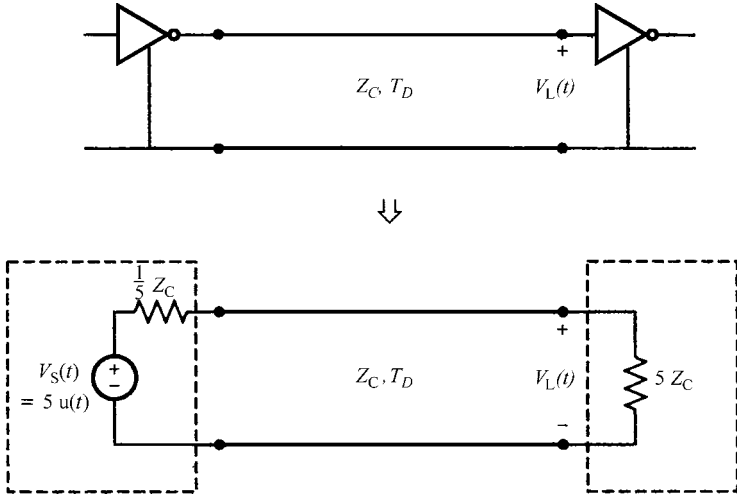


FIGURE P8.11

- 8.12** A transmission line of total length 200 m and velocity of propagation of $v = 2 \times 10^8$ (m/s) has $Z_C = 50 \Omega$, and $R_L = 20 \Omega$. It is driven by a source having $R_S = 100 \Omega$ and an open-circuit voltage that is a rectangular pulse of 6 V magnitude and 3 μ s duration. Sketch the input current to the line for a total time of 5 μ s. [$0 < t < 2 \mu$ s, 40 mA, 2μ s $< t < 3 \mu$ s, 51.43 mA, 3μ s $< t < 4 \mu$ s, 11.43 mA, 4μ s $< t < 5 \mu$ s, 9.796 mA, 5μ s $< t < 6 \mu$ s, -1.633 mA. Steady state is 0 A.]
- 8.13** Confirm the results of Problem 8.4 using SPICE (PSPICE).
- 8.14** Confirm the results of Problem 8.5 using SPICE (PSPICE).
- 8.15** Confirm the results of Problem 8.6 using SPICE (PSPICE).
- 8.16** Confirm the results of Problem 8.7 using SPICE (PSPICE).
- 8.17** Confirm the results of Problem 8.8 using SPICE (PSPICE).
- 8.18** Confirm the results of Problem 8.9 using SPICE (PSPICE).
- 8.19** Confirm the results of Problem 8.10 using SPICE (PSPICE).
- 8.20** Confirm the results of Problem 8.11 using SPICE (PSPICE).
- 8.21** Confirm the results of Problem 8.12 using SPICE (PSPICE).
- 8.22** One of the important advantages in using SPICE to solve transmission-line problems is that it will readily give the solution for problems that would be difficult to solve by hand. For example, consider the case of two CMOS inverter gates connected by a 5 cm length of 100- Ω transmission line as shown in Figure P8.22. The output of the driver gate is represented by a ramp waveform voltage

rising from 0 to 5 V in 1 ns and a 30-Ω internal source resistance. The receiving gate is represented at its input by 10 pF. Because of the capacitive load, this would be a difficult problem to do by hand. Use SPICE (PSPICE) to plot the output voltage of the line, $V_L(t)$, for $0 < t < 10$ ns. Observe in the solution that this output voltage varies rather drastically about the desired 5-V level going from 4.2 to 7 V before it stabilizes to 5 V well after 10 ns.

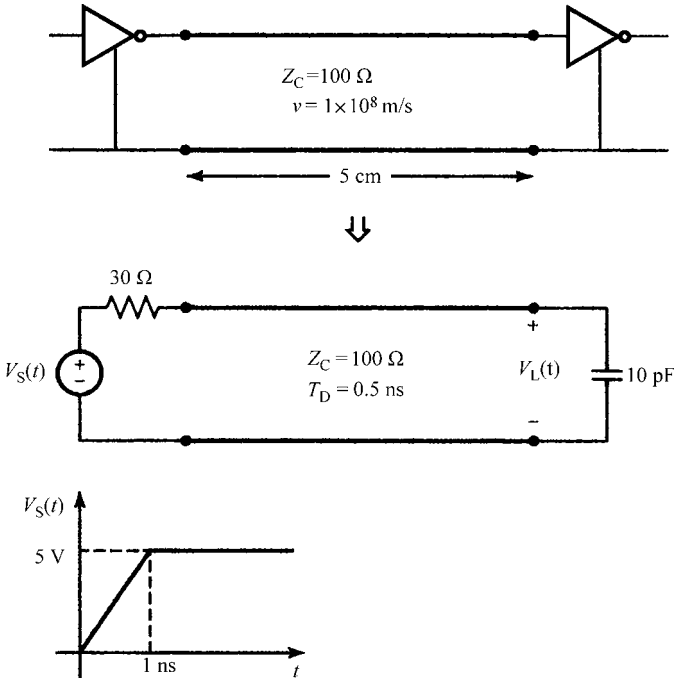


FIGURE P8.22

- 8.23 Demonstrate the series solutions in (8.14).
- 8.24 Derive the method of characteristics solution in (8.34).
- 8.25 Rederive the time-domain load voltage waveform for the line in Figure 8.12 but with a resistor R in parallel with the inductor C . Sketch the result. Does it make sense?

$$\left[V_L(t) = \frac{R}{R + Z_C} V_0 u(t - T_D) - \frac{R}{R + Z_C} e^{-\frac{R + Z_C}{CRZ_C}(t - T_D)} V_0 u(t - T_D) \right]$$

- 8.26 Rederive the time-domain load voltage waveform for the line in Figure 8.13 but with a resistor R in series with the inductor L . Sketch the result. Does it

make sense?

$$\left[V_L(t) = \frac{R}{R + Z_C} V_0 u(t - T_D) + \frac{Z_C}{R + Z_C} e^{-\frac{R + Z_C}{L}(t - T_D)} V_0 u(t - T_D) \right]$$

- 8.27** Verify the FDTD recursion relations for a lossless line with resistive loads given in (8.81).
- 8.28** Verify that the FDTD recursion relations for a lossless line in (8.76) and (8.78) give the exact solution of the transmission-line equations for the magic time step.
- 8.29** Use `FINDIF.FOR` described in Appendix A to verify the results in Figure 8.23.
- 8.30** Use `PSPICE` to verify the extreme results for a mismatched line shown in Figure 8.29.
- 8.31** Verify the results for a line discontinuity shown in Figure 8.33 by hand and by using `PSPICE`.
- 8.32** Use `MATLAB` to plot the real and imaginary parts of the Debye model given in (8.126).
- 8.33** Verify the FDTD recursion relations for a lossy line with dc losses given in (8.173) and (8.168).
- 8.34** Verify the FDTD recursion relations for a lossy line and resistive loads given in (8.181), (8.76), and (8.81).
- 8.35** Recompute the Prony coefficients in Table 8.1 using `MATLAB` and, if they are different, plot the result versus the exact value of $Z_0(m)$.
- 8.36** Use `TIMEFREQ.FOR`, `MTL.FOR`, and `FDTDLOSS.FOR` to confirm the results in Figure 8.43.
- 8.37** Derive the results for the Pade approximation given in (8.224).

REFERENCES

- [1] F.H. Branin, Jr., Transient analysis of lossless transmission lines, *Proceedings of IEEE*, **55**, 2012–2013, 1967.
- [2] M.N.O. Sadiku, *Numerical Techniques in Electromagnetics*, CRC Press, Boca Raton, FL, 1992.
- [3] K.S. Kunz and R.J. Luebbers, *The Finite Difference Time Domain Method in Electromagnetics*, CRC Press, Boca Raton, FL, 1993.
- [4] A.K. Agrawal, H.J. Price, and S.H. Gurbaxani, Transient response of multiconductor transmission lines excited by a nonuniform electromagnetic field, *IEEE Transactions on Electromagnetic Compatibility*, **22** (2), 119–129, 1980.

- [5] D.F. Higgins, Calculating transmission line transients on personal computers, *Proceedings of the IEEE International Symposium on Electromagnetic Compatibility, Atlanta, GA* August 25–27, 1987.
- [6] A. Ralston, *A First Course in Numerical Analysis*, McGraw-Hill, New York, 1965.
- [7] R.E. Matick, *Transmission Lines for Digital and Communication Networks*, McGraw-Hill, New York, 1969.
- [8] S. Ramo, J.R. Whinnery, and T. Van Duzer, *Fields and Waves in Communication Electronics*, 2nd edition, John Wiley & Sons, Inc., New York, 1984.
- [9] A.R. von Hippel, *Dielectric Materials and Applications*, MIT Press and Wiley, New York, 1954.
- [10] C. Gordan, T. Blazek, and R. Mittra, Time-domain simulation of multiconductor transmission lines with frequency-dependent losses, *IEEE Transactions on Microwave Theory and Techniques*, **11** (11), 1372–1387, 1992.
- [11] C. Kittel, *Introduction to Solid State Physics*, 2nd edition, John Wiley & Sons, Inc., New York, 1956.
- [12] K.M. Coperich Branch, J. Morsey, A.C. Cangellaris, and A.E. Ruehli, Physically consistent transmission line models for high-speed interconnects in lossy dielectrics, *IEEE Transactions on Advanced Packaging*, **25** (2), 129–135, 2002.
- [13] R.E. Collin, *Foundations for Microwave Engineering*, 2nd edition, McGraw-Hill, New York, 1992.
- [14] R.V. Churchill, *Operational Mathematics*, 2nd edition, McGraw-Hill, New York, 1958.
- [15] F.M. Tesche, On the inclusion of losses in time-domain solutions of electromagnetic interaction problems, *IEEE Transactions on Electromagnetic Compatibility*, **32** (1), 1–4, 1990.
- [16] R.L. Wiggington and N.S. Nahman, Transient analysis of coaxial cables considering skin effect, *Proceedings of IRE*, **45**, 166–174, 1957.
- [17] N.S. Nahman and D.R. Holt, Transient analysis of coaxial cables using the skin effect approximation $A + B\sqrt{s}$, *IEEE Transactions on Circuit Theory*, **19**, 443–451, 1972.
- [18] E.S. Mok and G.I. Costache, Skin-effect considerations on transient response of transmission line excited by an electromagnetic pulse *IEEE Transactions on Electromagnetic Compatibility*, **34**, 320–329, 1992.
- [19] F.B. Hildebrand, *Introduction to Numerical Analysis*, 2nd edition, Dover, New York, 1987.
- [20] L. Weiss and R.N. McDonough, Prony's method, Z-transforms, and Pade approximation, *SIAM Review*, **5** (2), 145–149, 1963.
- [21] C.L. Lawson and R. Hanson, *Solving Least Squares Problems*, Prentice-Hall, Englewood Cliffs, NJ, 1983.
- [22] T.K. Sarker and O. Pereira, Using matrix pencil method to estimate the parameters of a sum of complex exponentials, *IEEE Antennas and Propagation Magazine*, **37** (1), 48–55, 1995.
- [23] A. Semlyen and A. Dabuleanu, Fast and accurate switching transient calculations on transmission lines with ground return using recursive convolutions, *IEEE Transactions on Power Apparatus and Systems*, **94** (2), 561–571, 1975.
- [24] T.V. Nguyen, Recursive convolution and discrete time domain simulation of lossy coupled transmission lines, *IEEE Transactions on Computer-Aided Design of Integrated Circuits and Systems*, **13** (10), 1301–1305, 1994.

- [25] C. Yen, Z. Fazarinc, and R. L. Wheeler, Time-domain skin-effect model for transient analysis of lossy transmission lines, *Proceedings of IEEE*, **70**, 750–757, 1982.
- [26] T. Vu Dinh, B. Cabon, and J. Chilo, New skin-effect equivalent circuit, *Electronics Letters*, **26** (19), 1582–1584, 1990.
- [27] T. Vu Dinh, B. Cabon, and J. Chilo, Time domain analysis of skin effect on lossy interconnections, *Electronics Letters*, **26** (25), 2057–2058, 1990.
- [28] T. Vu Dinh, B. Cabon, and J. Chilo, SPICE simulation of lossy and coupled interconnection lines, *IEEE Transactions on Components, Packaging, and Manufacturing Technology—Part B: Advanced Packaging*, **17** (2), 134–146, 1994.
- [29] F.Y. Chang, The generalized method of characteristics for waveform relaxation analysis of lossy coupled transmission lines, *IEEE Transactions on Microwave Theory and Techniques*, **37** (12), 2028–2038, 1989.
- [30] W.H. Press, S.A. Teukolsky, W.T. Vetterling, and B.D. Flannery, *Numerical Recipes in FORTRAN*, 2nd edition, Cambridge University Press, New York, 1992.
- [31] F.Y. Chang, Transient simulation of frequency-dependent nonuniform coupled lossy transmission lines, *IEEE Transactions on Components, Packaging, and Manufacturing Technology—Part B: Advanced Packaging*, **17** (1), 3–14, 1994.
- [32] S. Lin and E.S. Kuh, Transient simulation of lossy interconnects based on the recursive convolution formulation, *IEEE Transactions on Circuits and Systems—I: Fundamental Theory and Applications*, **39** (11), 879–892, 1992.
- [33] F.Y. Chang, Waveform relaxation analysis of RLCG transmission lines, *IEEE Transactions on Circuits and Systems*, **37** (11), 1394–1415, 1990.
- [34] R. Achar and M.S. Nakhla, Simulation of high-speed interconnects *Proceedings of IEEE*, **89** (5), 693–728, 2001.

9

TIME-DOMAIN ANALYSIS OF MULTICONDUCTOR LINES

In the previous chapter, we examined the time-domain solution of the transmission-line equations and the incorporation of the terminal constraints for two-conductor lines. We will extend those results to the case of lines composed of more than two conductors or multiconductor transmission lines (MTLs) in this chapter. We will find that the results of the preceding chapter for two-conductor lines can be extended to the case of MTLs consisting of $n + 1$ conductors with $n > 1$ in a very straightforward manner using matrix notation.

9.1 THE SOLUTION FOR LOSSLESS LINES

In this section, we will examine the time-domain solution of the MTL equations for a *lossless line*:

$$\frac{\partial}{\partial z} \mathbf{V}(z, t) = -\mathbf{L} \frac{\partial}{\partial t} \mathbf{I}(z, t) \quad (9.1a)$$

$$\frac{\partial}{\partial z} \mathbf{I}(z, t) = -\mathbf{C} \frac{\partial}{\partial t} \mathbf{V}(z, t) \quad (9.1b)$$

where \mathbf{L} and \mathbf{C} are the per-unit-length inductance and capacitance matrices, respectively, and are of dimension $n \times n$. The line voltages and currents are contained in the $n \times 1$ vectors \mathbf{V} and \mathbf{I} . The uncoupled, second-order equations are

$$\frac{\partial^2}{\partial z^2} \mathbf{V}(z, t) = \mathbf{L} \mathbf{C} \frac{\partial^2}{\partial t^2} \mathbf{V}(z, t) \quad (9.2a)$$

$$\frac{\partial^2}{\partial z^2} \mathbf{I}(z, t) = \mathbf{C} \mathbf{L} \frac{\partial^2}{\partial t^2} \mathbf{I}(z, t) \quad (9.2b)$$

Note that the order of multiplication of \mathbf{L} and \mathbf{C} in these second-order equations must be strictly observed. The objective in this section is to determine the general solution of these equations and the incorporation of the terminal conditions. Some earlier works are represented by [1–9].

9.1.1 The Recursive Solution for MTLs

In the previous chapter, we developed a series solution for the terminal voltages of a lossless, two-conductor line. (See Eq. (8.14) in the previous chapter.) Branin's method was also developed for two-conductor lossless lines and expressed the terminal voltages at one end of the line in terms of the terminal voltages at the other end one-time delay earlier. This led to the SPICE exact solution model for two-conductor, lossless lines. The series solution can be extended in the following manner to *lossless* MTLs in *homogeneous media*. The following recursive solution cannot be readily extended to handle inhomogeneous media. Recall the *frequency-domain* chain parameter matrix as

$$\begin{bmatrix} \hat{\mathbf{V}}(\mathcal{L}) \\ \hat{\mathbf{I}}(\mathcal{L}) \end{bmatrix} = \begin{bmatrix} \hat{\Phi}_{11}(\mathcal{L}) & \hat{\Phi}_{12}(\mathcal{L}) \\ \hat{\Phi}_{21}(\mathcal{L}) & \hat{\Phi}_{22}(\mathcal{L}) \end{bmatrix} \begin{bmatrix} \hat{\mathbf{V}}(0) \\ \hat{\mathbf{I}}(0) \end{bmatrix} \quad (9.3)$$

where the submatrices are given in (7.115) of Chapter 7. Specializing these for a *lossless line* in a *homogeneous medium* gives

$$\hat{\Phi}_{11} = \cos(\beta \mathcal{L}) \mathbf{1}_n \quad (9.4a)$$

$$\hat{\Phi}_{12} = -j \sin(\beta \mathcal{L}) \mathbf{Z}_C \quad (9.4b)$$

$$\hat{\Phi}_{21} = -j \sin(\beta \mathcal{L}) \mathbf{Z}_C^{-1} \quad (9.4c)$$

$$\hat{\Phi}_{22} = \cos(\beta \mathcal{L}) \mathbf{1}_n \quad (9.4d)$$

where $\mathbf{1}_n$ is the $n \times n$ identity matrix with ones on the main diagonal and zeros elsewhere. The $n \times n$ characteristic impedance matrix is defined as

$$\mathbf{Z}_C = v \mathbf{L} \quad (9.5a)$$

$$\mathbf{Z}_C^{-1} = v \mathbf{C} \quad (9.5b)$$

and the velocity of propagation for this homogeneous medium is defined by

$$v = \frac{1}{\sqrt{\mu\epsilon}} \quad (9.6)$$

The phase constant in (9.4) is $\beta = \omega/v$.

The Laplace transform of the corresponding time-domain result can be obtained from this by substituting the Laplace transform variable s for $j\omega$, and replacing

$$j\beta \mathcal{L} = j\omega \frac{\mathcal{L}}{v} \Leftrightarrow sT_D \quad (9.7)$$

where the line one-way time delay is again denoted as

$$T_D = \frac{\mathcal{L}}{v} \quad (9.8)$$

The Laplace-transformed chain parameter matrices in (9.4) become

$$\hat{\Phi}_{11}(z, s) = \left(\frac{e^{sT_D} + e^{-sT_D}}{2} \right) \mathbf{1}_n \quad (9.9a)$$

$$\hat{\Phi}_{12}(z, s) = - \left(\frac{e^{sT_D} - e^{-sT_D}}{2} \right) \mathbf{Z}_C \quad (9.9b)$$

$$\hat{\Phi}_{21}(z, s) = - \left(\frac{e^{sT_D} - e^{-sT_D}}{2} \right) \mathbf{Z}_C^{-1} \quad (9.9c)$$

$$\hat{\Phi}_{22}(z, s) = \left(\frac{e^{sT_D} + e^{-sT_D}}{2} \right) \mathbf{1}_n \quad (9.9d)$$

Hence, taking the Laplace transform of the chain-parameter relation in (9.3) shows that the terminal voltages and currents are related as

$$\hat{\mathbf{V}}(\mathcal{L}, s) = \left(\frac{e^{sT_D} + e^{-sT_D}}{2} \right) \hat{\mathbf{V}}(0, s) - \left(\frac{e^{sT_D} - e^{-sT_D}}{2} \right) \mathbf{Z}_C \hat{\mathbf{I}}(0, s) \quad (9.10a)$$

$$\hat{\mathbf{I}}(\mathcal{L}, s) = - \left(\frac{e^{sT_D} - e^{-sT_D}}{2} \right) \mathbf{Z}_C^{-1} \hat{\mathbf{V}}(0, s) + \left(\frac{e^{sT_D} + e^{-sT_D}}{2} \right) \hat{\mathbf{I}}(0, s) \quad (9.10b)$$

Multiplying (9.10b) by \mathbf{Z}_C and adding and subtracting the equations gives

$$\hat{\mathbf{V}}(\mathcal{L}, s) + \mathbf{Z}_C \hat{\mathbf{I}}(\mathcal{L}, s) = e^{-sT_D} \hat{\mathbf{V}}(0, s) + e^{-sT_D} \mathbf{Z}_C \hat{\mathbf{I}}(0, s) \quad (9.11a)$$

$$\hat{\mathbf{V}}(\mathcal{L}, s) - \mathbf{Z}_C \hat{\mathbf{I}}(\mathcal{L}, s) = e^{sT_D} \hat{\mathbf{V}}(0, s) - e^{sT_D} \mathbf{Z}_C \hat{\mathbf{I}}(0, s) \quad (9.11b)$$

Observing once again the delay transform pair given in (8.43) of Chapter 8 gives the time-domain forms as

$$\mathbf{V}(\mathcal{L}, t) + \mathbf{Z}_C \mathbf{I}(\mathcal{L}, t) = \mathbf{V}(0, t - T_D) + \mathbf{Z}_C \mathbf{I}(0, t - T_D) \quad (9.12a)$$

$$\mathbf{V}(\mathcal{L}, t) - \mathbf{Z}_C \mathbf{I}(\mathcal{L}, t) = \mathbf{V}(0, t + T_D) - \mathbf{Z}_C \mathbf{I}(0, t + T_D) \quad (9.12b)$$

Time shifting (9.12b) and rearranging gives

$$\mathbf{V}(0, t) - \mathbf{Z}_C \mathbf{I}(0, t) = \mathbf{V}(\mathcal{L}, t - T_D) - \mathbf{Z}_C \mathbf{I}(\mathcal{L}, t - T_D) \quad (9.12c)$$

Define the vectors

$$\mathbf{E}_0(\mathcal{L}, t - T_D) = \mathbf{V}(\mathcal{L}, t - T_D) - \mathbf{Z}_C \mathbf{I}(\mathcal{L}, t - T_D) \quad (9.13a)$$

$$\mathbf{E}_{\mathcal{L}}(0, t - T_D) = \mathbf{V}(0, t - T_D) + \mathbf{Z}_C \mathbf{I}(0, t - T_D) \quad (9.13b)$$

Equations (9.12) become

$$\mathbf{V}(0, t) - \mathbf{Z}_C \mathbf{I}(0, t) = \mathbf{E}_0(\mathcal{L}, t - T_D) \quad (9.14a)$$

$$\mathbf{V}(\mathcal{L}, t) + \mathbf{Z}_C \mathbf{I}(\mathcal{L}, t) = \mathbf{E}_{\mathcal{L}}(0, t - T_D) \quad (9.14b)$$

Equations (9.13) after being time shifted become

$$\mathbf{E}_0(\mathcal{L}, t) = \mathbf{V}(\mathcal{L}, t) - \mathbf{Z}_C \mathbf{I}(\mathcal{L}, t) \quad (9.15a)$$

$$\mathbf{E}_{\mathcal{L}}(0, t) = \mathbf{V}(0, t) + \mathbf{Z}_C \mathbf{I}(0, t) \quad (9.15b)$$

Substituting (9.14) into (9.15) gives the terminal voltages in terms of the \mathbf{E} vectors as

$$\mathbf{V}(0, t) = \frac{1}{2} \mathbf{E}_{\mathcal{L}}(0, t) + \frac{1}{2} \mathbf{E}_0(\mathcal{L}, t - T_D) \quad (9.16a)$$

$$\mathbf{V}(\mathcal{L}, t) = \frac{1}{2} \mathbf{E}_0(\mathcal{L}, t) + \frac{1}{2} \mathbf{E}_{\mathcal{L}}(0, t - T_D) \quad (9.16b)$$

In order to incorporate the terminal constraints at the ends of the line, we describe the *resistive terminations* as generalized Thevenin equivalents:

$$\mathbf{V}(0, t) = \mathbf{V}_S(t) - \mathbf{R}_S \mathbf{I}(0, t) \quad (9.17a)$$

$$\mathbf{V}(\mathcal{L}, t) = \mathbf{V}_L(t) + \mathbf{R}_L \mathbf{I}(\mathcal{L}, t) \quad (9.17b)$$

Substituting these terminal relations into (9.15) and (9.14) gives

$$\mathbf{E}_{\mathcal{L}}(0, t) = 2 \mathbf{M}_S \mathbf{V}_S(t) + \Gamma_S \mathbf{E}_0(\mathcal{L}, t - T_D) \quad (9.18a)$$

$$\mathbf{E}_0(\mathcal{L}, t) = 2 \mathbf{M}_L \mathbf{V}_L(t) + \Gamma_L \mathbf{E}_{\mathcal{L}}(0, t - T_D) \quad (9.18b)$$

where we have defined, in the fashion for two-conductor lines, the $n \times n$ reflection coefficient matrices as

$$\Gamma_S = [\mathbf{R}_S - \mathbf{Z}_C][\mathbf{R}_S + \mathbf{Z}_C]^{-1} \quad (9.19a)$$

$$\Gamma_L = [\mathbf{R}_L - \mathbf{Z}_C][\mathbf{R}_L + \mathbf{Z}_C]^{-1} \quad (9.19b)$$

and the $n \times n$ voltage division coefficient matrices are defined as

$$\mathbf{M}_S = \mathbf{Z}_C[\mathbf{R}_S + \mathbf{Z}_C]^{-1} \quad (9.20a)$$

$$\mathbf{M}_L = \mathbf{Z}_C[\mathbf{R}_L + \mathbf{Z}_C]^{-1} \quad (9.20b)$$

The scheme is to discretize the time axis into N computation steps in each one-way time delay T_D as $\Delta t = T_D/N$ and then form the four $n \times N$ arrays $\mathbf{E}_0^{\text{old}}$, $\mathbf{E}_{\mathcal{L}}^{\text{old}}$, $\mathbf{E}_0^{\text{new}}$, and $\mathbf{E}_{\mathcal{L}}^{\text{new}}$. The N columns of these are associated with the time increment, and the n rows are associated with the particular conductor of the line. To begin the recursion algorithm, we assume an initially relaxed line and fill $\mathbf{E}_0^{\text{old}}$ and $\mathbf{E}_{\mathcal{L}}^{\text{old}}$ with zero entries. Then compute the entries in $\mathbf{E}_0^{\text{new}}$ and $\mathbf{E}_{\mathcal{L}}^{\text{new}}$ according to (9.18) and compute the terminal voltages from (9.16). Once all entries are filled for all N time increments for $0 \leq t \leq T_D$, write the entries in $\mathbf{E}_0^{\text{new}}$ and $\mathbf{E}_{\mathcal{L}}^{\text{new}}$ into $\mathbf{E}_0^{\text{old}}$ and $\mathbf{E}_{\mathcal{L}}^{\text{old}}$, respectively, and repeat the calculations for the N time increments in the next interval $T_D \leq t \leq 2T_D$. This is repeated to solve for the terminal voltages in blocks of time of length equal to the one-way line delay, T_D . This extension of Branin's method to MTLs is implemented in the FORTRAN program BRANIN.FOR described in Appendix A. The method implicitly assumes that all modes propagate with the same velocity so that it does not appear feasible to extend it to the lines in *inhomogeneous media*.

The recursive method can be solved in series form by recursively substituting (9.18) into (9.16) to give

$$\begin{aligned}
 \mathbf{V}(0, t) = & \mathbf{M}_S \mathbf{V}_S(t) + (\mathbf{1}_n + \Gamma_S) \{ \Gamma_L \mathbf{M}_S \mathbf{V}_S(t - 2T_D) \\
 & + (\Gamma_L \Gamma_S) \Gamma_L \mathbf{M}_S \mathbf{V}_S(t - 4T_D) \\
 & + (\Gamma_L \Gamma_S)^2 \Gamma_L \mathbf{M}_S \mathbf{V}_S(t - 6T_D) \\
 & + (\Gamma_L \Gamma_S)^3 \Gamma_L \mathbf{M}_S \mathbf{V}_S(t - 8T_D) + \dots \} \\
 & + (\mathbf{1}_n + \Gamma_S) \{ \mathbf{M}_L \mathbf{V}_L(t - T_D) \\
 & + (\Gamma_L \Gamma_S) \mathbf{M}_L \mathbf{V}_L(t - 3T_D) \\
 & + (\Gamma_L \Gamma_S)^2 \mathbf{M}_L \mathbf{V}_L(t - 5T_D) \\
 & + (\Gamma_L \Gamma_S)^3 \mathbf{M}_L \mathbf{V}_L(t - 7T_D) + \dots \}
 \end{aligned} \quad (9.21a)$$

$$\begin{aligned}
 \mathbf{V}(\mathcal{L}, t) = & \mathbf{M}_L \mathbf{V}_L(t) + (\mathbf{1}_n + \Gamma_L) \{ \Gamma_S \mathbf{M}_L \mathbf{V}_L(t - 2T_D) \\
 & + (\Gamma_S \Gamma_L) \Gamma_S \mathbf{M}_L \mathbf{V}_L(t - 4T_D) \\
 & + (\Gamma_S \Gamma_L)^2 \Gamma_S \mathbf{M}_L \mathbf{V}_L(t - 6T_D) \\
 & + (\Gamma_S \Gamma_L)^3 \Gamma_S \mathbf{M}_L \mathbf{V}_L(t - 8T_D) + \dots \} \\
 & + (\mathbf{1}_n + \Gamma_L) \{ \mathbf{M}_S \mathbf{V}_S(t - T_D) \\
 & + (\Gamma_S \Gamma_L) \mathbf{M}_S \mathbf{V}_S(t - 3T_D) \\
 & + (\Gamma_S \Gamma_L)^2 \mathbf{M}_S \mathbf{V}_S(t - 5T_D) \\
 & + (\Gamma_S \Gamma_L)^3 \mathbf{M}_S \mathbf{V}_S(t - 7T_D) + \dots \}
 \end{aligned} \quad (9.21b)$$

These reduce to the exact scalar results for a two-conductor line given in (8.14) of Chapter 8, but the order of multiplication of the matrices must be preserved here.

Equations (9.21) show that in order to eliminate reflections at the terminations, we must terminate the line in matched loads, that is, $\mathbf{R}_L = \mathbf{Z}_C$ and/or $\mathbf{R}_S = \mathbf{Z}_C$, in which case (9.19) become $\Gamma_L = \mathbf{0}_n$ and $\Gamma_S = \mathbf{0}_n$ where $\mathbf{0}_n$ is the $n \times n$ zero matrix with zeros in all positions. Therefore, in order to “match” an MTL, we must provide resistors *between all pairs of lines* [1]. It is not sufficient to simply attach resistors between each line and the reference conductor to eliminate reflections, as was the case for two-conductor lines. If the line is matched at the right end, that is, $\mathbf{R}_L = \mathbf{Z}_C$, then $\Gamma_L = \mathbf{0}_n$ and (9.21) become

$$\mathbf{V}(0, t) = \mathbf{M}_S \mathbf{V}_S(t) + (\mathbf{1}_n + \Gamma_S) \mathbf{M}_L \mathbf{V}_L(t - T_D) \quad (\mathbf{R}_L = \mathbf{Z}_C) \quad (9.21c)$$

and

$$\mathbf{V}(\mathcal{L}, t) = \mathbf{M}_L \mathbf{V}_L(t) + \Gamma_S \mathbf{M}_L \mathbf{V}_L(t - 2T_D) + \mathbf{M}_S \mathbf{V}_S(t - T_D) \quad (\mathbf{R}_L = \mathbf{Z}_C) \quad (9.21d)$$

and $\mathbf{M}_L = 2\mathbf{1}_n$. Suppose that the sources are only in the left termination, that is, $\mathbf{V}_L(t) = \mathbf{0}$. These results reduce to

$$\mathbf{V}(0, t) = \mathbf{M}_S \mathbf{V}_S(t) \quad (\mathbf{R}_L = \mathbf{Z}_C, \mathbf{V}_L(t) = \mathbf{0}) \quad (9.21e)$$

and

$$\mathbf{V}(\mathcal{L}, t) = \mathbf{M}_S \mathbf{V}_S(t - T_D) \quad (\mathbf{R}_L = \mathbf{Z}_C, \mathbf{V}_L(t) = \mathbf{0}) \quad (9.21f)$$

which simply says that the input voltages to the line are the “voltage-divided” portions of the sources in the left termination, $\mathbf{V}_S(t)$, and the output voltages at the right end of the line are those delayed by one line one-way delay T_D , which means that there are no reflections. The result in (9.21c) for the voltage at $z = 0$, $\mathbf{V}(0, t)$, is composed of two contributions. The source in the left termination, $\mathbf{V}_S(t)$, produces (9.21e), and the source in the right termination, $\mathbf{V}_L(t)$, is “voltage-divided” by \mathbf{M}_L , sent down to the source arriving there after one-time delay, reflected by Γ_S , added to the incident wave, and sent back down the line to the load where it is completely absorbed. Similarly, the result in (9.21d) for the voltage at $z = \mathcal{L}$, $\mathbf{V}(\mathcal{L}, t)$, is composed of two contributions. The source in the left termination, $\mathbf{V}_S(t)$, produces (9.21f), and the source in the right termination, $\mathbf{V}_L(t)$, is “voltage-divided” by \mathbf{M}_L , sent down to the source, reflected by Γ_S , and sent back down the line to the load arriving after two-time delays where it is completely absorbed.

9.1.2 Decoupling the MTL Equations

The primary technique used to determine the general form of the solution of the MTL equations for *sinusoidal, steady-state excitation* in Chapter 7 was to *decouple them with similarity transformations*. In the case of the general time-domain solution of *lossless lines*, the technique of decoupling the MTL equations in (9.1) or (9.2) via similarity transformations is again a useful technique that can always be used to affect the solution.

We define the similarity transformations to *mode voltages* and *currents* as

$$\mathbf{V}(z, t) = \mathbf{T}_V \mathbf{V}_m(z, t) \quad (9.22a)$$

$$\mathbf{I}(z, t) = \mathbf{T}_I \mathbf{I}_m(z, t) \quad (9.22b)$$

Substituting these into (9.1) gives

$$\frac{\partial}{\partial z} \mathbf{V}_m(z, t) = -\mathbf{T}_V^{-1} \mathbf{L} \mathbf{T}_I \frac{\partial}{\partial t} \mathbf{I}_m(z, t) \quad (9.23a)$$

$$\frac{\partial}{\partial z} \mathbf{I}_m(z, t) = -\mathbf{T}_I^{-1} \mathbf{C} \mathbf{T}_V \frac{\partial}{\partial t} \mathbf{V}_m(z, t) \quad (9.23b)$$

or for the uncoupled second-order equations in (9.2)

$$\frac{\partial^2}{\partial z^2} \mathbf{V}_m(z, t) = \mathbf{T}_V^{-1} \mathbf{L} \mathbf{C} \mathbf{T}_V \frac{\partial^2}{\partial t^2} \mathbf{V}_m(z, t) \quad (9.24a)$$

$$\frac{\partial^2}{\partial z^2} \mathbf{I}_m(z, t) = \mathbf{T}_I^{-1} \mathbf{C} \mathbf{L} \mathbf{T}_I \frac{\partial^2}{\partial t^2} \mathbf{I}_m(z, t) \quad (9.24b)$$

If we can choose a \mathbf{T}_V and a \mathbf{T}_I such that (9.23) or (9.24) are uncoupled, then we have the general form of the mode solutions as those of two-conductor lines of the previous chapter. This is always guaranteed for *lossless lines* as was shown in

Chapter 7 for sinusoidal excitation. For example, consider the coupled first-order equations in (9.23). Suppose we can find a \mathbf{T}_V and a \mathbf{T}_I such that they simultaneously diagonalize both \mathbf{L} and \mathbf{C} as

$$\mathbf{T}_V^{-1} \mathbf{L} \mathbf{T}_I = \mathbf{L}_m \quad (9.25a)$$

$$\mathbf{T}_I^{-1} \mathbf{C} \mathbf{T}_V = \mathbf{C}_m \quad (9.25b)$$

where \mathbf{L}_m and \mathbf{C}_m are *diagonal* as

$$\mathbf{L}_m = \begin{bmatrix} l_{m1} & 0 & \cdots & 0 \\ 0 & l_{m2} & \ddots & \vdots \\ \vdots & \ddots & \ddots & 0 \\ 0 & \cdots & 0 & l_{mn} \end{bmatrix} \quad (9.25c)$$

$$\mathbf{C}_m = \begin{bmatrix} c_{m1} & 0 & \cdots & 0 \\ 0 & c_{m2} & \ddots & \vdots \\ \vdots & \ddots & \ddots & 0 \\ 0 & \cdots & 0 & c_{mn} \end{bmatrix} \quad (9.25d)$$

Then the mode equations in (9.23) become

$$\frac{\partial}{\partial z} \mathbf{V}_m(z, t) = -\mathbf{L}_m \frac{\partial}{\partial t} \mathbf{I}_m(z, t) \quad (9.26a)$$

$$\frac{\partial}{\partial z} \mathbf{I}_m(z, t) = -\mathbf{C}_m \frac{\partial}{\partial t} \mathbf{V}_m(z, t) \quad (9.26b)$$

or

$$\begin{aligned} \frac{\partial}{\partial z} V_{m1}(z, t) &= -l_{m1} \frac{\partial}{\partial t} I_{m1}(z, t) \\ \frac{\partial}{\partial z} I_{m1}(z, t) &= -c_{m1} \frac{\partial}{\partial t} V_{m1}(z, t) \\ &\vdots \\ \frac{\partial}{\partial z} V_{mn}(z, t) &= -l_{mn} \frac{\partial}{\partial t} I_{mn}(z, t) \\ \frac{\partial}{\partial z} I_{mn}(z, t) &= -c_{mn} \frac{\partial}{\partial t} V_{mn}(z, t) \end{aligned} \quad (9.27)$$

These are the same equations as for *uncoupled, two-conductor lines* having characteristic impedances of

$$Z_{Cmi} = \sqrt{\frac{l_{mi}}{c_{mi}}} \quad (9.28)$$

and velocities of propagation of

$$v_{mi} = \frac{1}{\sqrt{l_{mi}c_{mi}}} \tag{9.29}$$

for $i = 1, 2, \dots, n$. Therefore, the solutions for these mode voltages and currents have the same general form as for the two-conductor line. The actual voltages and currents can be obtained from the forms of the mode voltages, and current solutions via (9.22). We now address the determination of the diagonalizing similarity transformation for the various classes of lines.

9.1.2.1 Lossless Lines in Homogeneous Media For this class of line, we have the important identity

$$\mathbf{LC} = \mathbf{CL} = \mu\varepsilon \mathbf{1}_n \tag{9.30}$$

where the surrounding *homogeneous* medium is characterized by permittivity ε and permeability μ . The similarity transformations that simultaneously diagonalize \mathbf{L} and \mathbf{C} as in (9.25) can be found in the following manner as shown in Chapter 7. Because \mathbf{L} is real and symmetric, a real, *orthogonal* transformation \mathbf{T} can be found such that

$$\mathbf{T}^t \mathbf{L} \mathbf{T} = \mathbf{L}_m \tag{9.31a}$$

where

$$\mathbf{L}_m = \begin{bmatrix} l_{m1} & 0 & \cdots & 0 \\ 0 & l_{m1} & \ddots & \vdots \\ \vdots & \ddots & \ddots & 0 \\ 0 & \cdots & 0 & l_{m1} \end{bmatrix} \tag{9.31b}$$

and the inverse of \mathbf{T} is its transpose that is denoted with the superscript t [10]:

$$\mathbf{T}^{-1} = \mathbf{T}^t \tag{9.31c}$$

Similarly, with the aid of the identity in (9.30) expressed as

$$\mathbf{C} = \mu\varepsilon \mathbf{L}^{-1} \tag{9.32}$$

we may form

$$\begin{aligned} \mathbf{T}^{-1} \mathbf{C} \mathbf{T}^{-1} &= \mathbf{T}^t \mathbf{C} \mathbf{T} \\ &= \mu\varepsilon \mathbf{T}^t \mathbf{L}^{-1} \mathbf{T} \\ &= \frac{1}{v^2} \mathbf{L}_m^{-1} \end{aligned} \tag{9.33}$$

where $v = 1/\sqrt{\mu\varepsilon}$. Comparing (9.31) and (9.33) to (9.25) shows that the transformations can be defined as

$$\mathbf{T}_I = \mathbf{T} \tag{9.34a}$$

$$\mathbf{T}_V = \mathbf{T} \tag{9.34b}$$

$$\mathbf{T}_I^{-1} = \mathbf{T}_V^{-1} = \mathbf{T}^t \tag{9.34c}$$

Therefore, the mode characteristic impedances in (9.28) are

$$Z_{Cmi} = v l_{mi} \tag{9.35}$$

and all modes have the same velocity of propagation:

$$v_{mi} = v = \frac{1}{\sqrt{\mu\varepsilon}} \tag{9.36}$$

For the special case of a three-conductor line, $n = 2$, the mode transformation is simple [10]:

$$\mathbf{T} = \begin{bmatrix} \cos \theta & -\sin \theta \\ \sin \theta & \cos \theta \end{bmatrix} \tag{9.37a}$$

where

$$\tan 2\theta = \frac{2l_{12}}{l_{11} - l_{22}} \tag{9.37b}$$

For $n \geq 3$, a numerical computer subroutine implementing, for example, the Jacobi method is used to obtain the orthogonal transformation [10]. Appendix A describes a FORTRAN subroutine, JACOBI . SUB, that accomplishes this reduction.

9.1.2.2 Lossless Lines in Inhomogeneous Media For this case we no longer have the identity in (9.30). However, we showed in Chapter 7 that because \mathbf{L} and \mathbf{C} are real, symmetric, and positive definite, we can find a transformation that simultaneously diagonalizes these matrices in the following manner. First, we find an orthogonal transformation that diagonalizes \mathbf{C} as

$$\mathbf{U}^t \mathbf{C} \mathbf{U} = \theta^2 \tag{9.38a}$$

where

$$\theta^2 = \begin{bmatrix} \theta_1^2 & 0 & \cdots & 0 \\ 0 & \theta_2^2 & \ddots & \vdots \\ \vdots & \ddots & \ddots & 0 \\ 0 & \cdots & 0 & \theta_n^2 \end{bmatrix} \tag{9.38b}$$

and

$$\mathbf{U}^{-1} = \mathbf{U}^t \quad (9.38c)$$

Since \mathbf{C} is positive definite, we can obtain the square root of θ^2 , θ , which is real and nonsingular and forms the product $\theta \mathbf{U}^t \mathbf{L} \mathbf{U} \theta$. Since this is real and symmetric, we can diagonalize it with another orthogonal transformation as

$$\mathbf{S}^t (\theta \mathbf{U}^t \mathbf{L} \mathbf{U} \theta) \mathbf{S} = \Lambda^2 \quad (9.39a)$$

where

$$\Lambda^2 = \begin{bmatrix} \Lambda_1^2 & 0 & \cdots & 0 \\ 0 & \Lambda_2^2 & \ddots & \vdots \\ \vdots & \ddots & \ddots & 0 \\ 0 & \cdots & 0 & \Lambda_n^2 \end{bmatrix} \quad (9.39b)$$

and

$$\mathbf{S}^{-1} = \mathbf{S}^t \quad (9.39c)$$

Define the matrix \mathbf{T} as

$$\mathbf{T} = \mathbf{U} \theta \mathbf{S} \quad (9.40)$$

The columns of \mathbf{T} can be normalized to a Euclidean length of unity as

$$\mathbf{T}_{\text{norm}} = \mathbf{T} \alpha \quad (9.41)$$

where α is the $n \times n$ diagonal matrix with entries

$$\alpha_{ii} = \frac{1}{\sqrt{\sum_{k=1}^n T_{ki}^2}} \quad (9.42a)$$

$$\alpha_{ij} = 0 \quad (9.42b)$$

The mode transformations in (9.22) that simultaneously diagonalize \mathbf{L} and \mathbf{C} as in (9.25) can then be defined as

$$\begin{aligned} \mathbf{T}_I &= \mathbf{U} \theta \mathbf{S} \alpha \\ &= \mathbf{T}_{\text{norm}} \end{aligned} \quad (9.43a)$$

$$\begin{aligned} \mathbf{T}_V &= \mathbf{U} \theta^{-1} \mathbf{S} \alpha^{-1} \\ &= \mathbf{T}_{\text{norm}}^{t^{-1}} \end{aligned} \quad (9.43b)$$

Also

$$\begin{aligned}\mathbf{T}_I^{-1} &= \alpha^{-1} \mathbf{S}^t \theta^{-1} \mathbf{U}^t \\ &= \mathbf{T}_V^t\end{aligned}\quad (9.44a)$$

$$\begin{aligned}\mathbf{T}_V^{-1} &= \alpha \mathbf{S}^t \theta \mathbf{U}^t \\ &= \mathbf{T}_I^t\end{aligned}\quad (9.44b)$$

Substituting (9.43) and (9.44) into (9.25) gives

$$\begin{aligned}\mathbf{T}_V^{-1} \mathbf{L} \mathbf{T}_I &= \alpha \mathbf{S}^t \theta \mathbf{U}^t \mathbf{L} \mathbf{U} \theta \mathbf{S} \alpha \\ &= \alpha \Lambda^2 \alpha\end{aligned}\quad (9.45a)$$

$$\begin{aligned}\mathbf{T}_I^{-1} \mathbf{C} \mathbf{T}_V &= \alpha^{-1} \mathbf{S}^t \theta^{-1} \mathbf{U}^t \mathbf{C} \mathbf{U} \theta^{-1} \mathbf{S} \alpha^{-1} \\ &= \alpha^{-2}\end{aligned}\quad (9.45b)$$

Comparing (9.45) and (9.25) shows that

$$\mathbf{L}_m = \alpha \Lambda^2 \alpha \quad (9.46a)$$

$$\mathbf{C}_m = \alpha^{-2} \quad (9.46b)$$

Since α and Λ are diagonal matrices, the mode characteristic impedances and velocities of propagation are given by

$$\begin{aligned}Z_{Cmi} &= \sqrt{\frac{l_{mi}}{c_{mi}}} \\ &= \alpha_{ii}^2 \Lambda_i\end{aligned}\quad (9.47)$$

and

$$\begin{aligned}v_{mi} &= \frac{1}{\sqrt{l_{mi} c_{mi}}} \\ &= \frac{1}{\Lambda_i}\end{aligned}\quad (9.48)$$

One can show that $\mathbf{Z}_C = \mathbf{T}_I^{t-1} \mathbf{Z}_{Cm} \mathbf{T}_I^{-1} = \mathbf{T}_V \mathbf{Z}_{Cm} \mathbf{T}_V^t$. The desired mode transformation matrices are

$$\begin{aligned}\mathbf{T}_V &= \mathbf{U} \theta^{-1} \mathbf{S} \alpha^{-1} \\ &= \mathbf{T}_{\text{norm}}^{t-1}\end{aligned}\quad (9.49a)$$

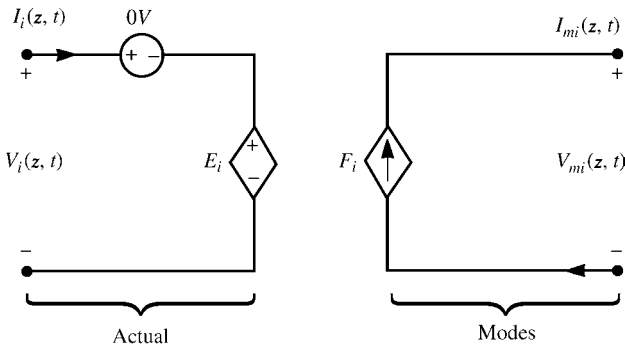
$$\begin{aligned}\mathbf{T}_I^{-1} &= \alpha^{-1} \mathbf{S}^t \theta^{-1} \mathbf{U}^t \\ &= \mathbf{T}_{\text{norm}}^{-1}\end{aligned}\quad (9.49b)$$

The above diagonalization is implemented in the FORTRAN subroutine `DIAG.SUB` described in Appendix A. This subroutine calls the FORTRAN subroutine `JACOBI.SUB` to compute the two orthogonal transformations required by `DIAG.SUB`.

9.1.2.3 Incorporating the Terminal Conditions via the SPICE Program Since we have uncoupled the equations via the mode transformation in the preceding sections, the mode voltages and currents are essentially associated with *n uncoupled, two-conductor transmission lines* as is illustrated in (9.27) whose general solutions are known. Again each general mode solution contains two undetermined constants so that there are a total of $2n$ undetermined constants. It remains to incorporate the terminal conditions at the two ends of the line in order to evaluate these $2n$ undetermined constants.

There are a number of ways of doing this. The most useful and simplest way is to utilize the exact time-domain model for a lossless, two-conductor line that exists in the SPICE code as shown in Figure 8.9 of Chapter 8 [A.2,A.3,B.19,11]. But each of these models relates only the n mode voltages and currents at the two ends of the line. In order to relate these mode quantities to the actual voltages and currents, we implement the mode transformations given in (9.22). These transformations can be implemented in the SPICE program through the use of controlled sources as illustrated in Figure 9.1. Writing the transformations in (9.22) out gives

$$\underbrace{\begin{bmatrix} V_1(z, t) \\ V_2(z, t) \\ \vdots \\ V_n(z, t) \end{bmatrix}}_{\mathbf{V}} = \underbrace{\begin{bmatrix} T_{V11} & T_{V12} & \cdots & T_{V1n} \\ T_{V21} & T_{V22} & \ddots & \vdots \\ \vdots & \ddots & \ddots & \vdots \\ T_{Vn1} & \cdots & \cdots & T_{Vnn} \end{bmatrix}}_{\mathbf{T}_V} \underbrace{\begin{bmatrix} V_{m1}(z, t) \\ V_{m2}(z, t) \\ \vdots \\ V_{mn}(z, t) \end{bmatrix}}_{\mathbf{V}_m} \tag{9.50a}$$



$$E_i = \sum_{k=1}^n [\mathbf{T}_V]_{ik} [\mathbf{V}_m]_k$$

$$F_i = \sum_{k=1}^n [\mathbf{T}_I^{-1}]_{ik} [\mathbf{I}]_k$$

FIGURE 9.1 Illustration of the use of controlled sources to implement the mode transformations.

$$\underbrace{\begin{bmatrix} I_1(z, t) \\ I_2(z, t) \\ \vdots \\ I_n(z, t) \end{bmatrix}}_{\mathbf{I}} = \underbrace{\begin{bmatrix} T_{I11} & T_{I12} & \cdots & T_{I1n} \\ T_{I21} & T_{I22} & \ddots & \vdots \\ \vdots & \ddots & \ddots & \vdots \\ T_{In1} & \cdots & \cdots & T_{Inn} \end{bmatrix}}_{\mathbf{T}_I} \underbrace{\begin{bmatrix} I_{m1}(z, t) \\ I_{m2}(z, t) \\ \vdots \\ I_{mn}(z, t) \end{bmatrix}}_{\mathbf{I}_m} \tag{9.50b}$$

Inverting (9.50b) gives

$$\mathbf{I}_m = \mathbf{T}_I^{-1} \mathbf{I} \tag{9.50c}$$

Hence, the rows of (9.50c) and 9.50c can be written as

$$V_i = \sum_{k=1}^n [\mathbf{T}_V]_{ik} [\mathbf{V}_m]_k \tag{9.50d}$$

$$I_{mi} = \sum_{k=1}^n [\mathbf{T}_I^{-1}]_{ik} [\mathbf{I}]_k \tag{9.50e}$$

where we denote the entries in the i th row and j th column of \mathbf{T}_V and \mathbf{T}_I^{-1} as $[\mathbf{T}_V]_{ij}$ and $[\mathbf{T}_I^{-1}]_{ij}$, respectively, and the entries in the i th rows of the vectors \mathbf{V}_m and \mathbf{I} are denoted as $[\mathbf{V}_m]_i$ and $[\mathbf{I}]_i$, respectively. The transformations in (9.50a) and (9.50c) can be implemented in SPICE using the controlled source representation illustrated in Figure 9.1. Zero-volt voltage sources are placed in each input to sample the current $I_i(z, t)$ for use in the controlled sources representing the transformation in (9.50e). The interior two-conductor mode lines having characteristic impedance Z_{Cmi} and time delay $T_{Di} = \mathcal{L}/v_{mi}$ are simulated with the existing two-conductor SPICE model as

$$\text{TXXX N1 0 N2 0 Z0} = Z_{Cmi} \quad \text{TD} = T_{Di}$$

as shown in Figure 9.2.

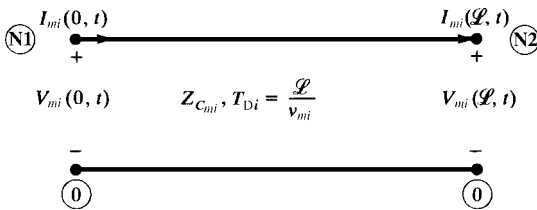


FIGURE 9.2 The two-conductor mode transmission lines.

The advantages of this method of implementing the terminal conditions are that the model for the line is independent of the terminations and any of the available device models in SPICE such as resistors, capacitors, inductors as well as the nonlinear models such as diodes and transistors can be called. Hence, the model is referred to as a *macromodel* of the line and also called a *2n-port model* of the line. The user need not redevelop the mathematical models of those devices in the terminations. The overall model of the line can be implemented as a subcircuit model in SPICE and the appropriate line terminations attached to the ports of this subcircuit. Thus, the solution implemented in this way in SPICE (or PSPICE) is *exact* within the time step discretization in the SPICE solution.

As an example of the implementation of this valuable technique, consider the example of three rectangular cross-section conductors (lands) on the surface of a printed circuit board (PCB) shown in Figure 9.3 that has been considered previously. This problem is that of an inhomogeneous medium, and we shall assume a lossless medium and perfect conductors so that the results of Section 9.1.2.2 will apply. The per-unit-length capacitance matrix was computed using the numerical technique described in Chapter 5 via the PCB.FOR program discussed in Appendix B using 50 divisions per land:

$$\mathbf{C} = \begin{bmatrix} 40.5985 & -20.2992 \\ -20.2992 & 29.7378 \end{bmatrix} \text{ pF/m}$$

The per-unit-length inductance matrix was computed from the capacitance matrix with the dielectric board removed, \mathbf{C}_0 , as

$$\mathbf{L} = \mu_0 \varepsilon_0 \mathbf{C}_0^{-1} = \begin{bmatrix} 1.10515 & 0.690613 \\ 0.690613 & 1.38123 \end{bmatrix} \mu\text{H/m}$$

Using SPICEMTL.FOR, the similarity transformations become

$$\mathbf{T}_V = \begin{bmatrix} 1.118 & 0.5 \\ -3.9 \times 10^{-6} & 1.0 \end{bmatrix}$$

and

$$\mathbf{T}_I^{-1} = \mathbf{T}_V^t = \begin{bmatrix} 1.118 & -3.9 \times 10^{-6} \\ 0.5 & 1.0 \end{bmatrix}$$

The mode characteristic impedances and propagation velocities are

$$\begin{aligned} Z_{Cm1} &= 109.445 \Omega \\ v_{m1} &= 1.80046 \times 10^8 \text{ m/s} \\ Z_{Cm2} &= 265.544 \Omega \\ v_{m2} &= 1.92251 \times 10^8 \text{ m/s} \end{aligned}$$

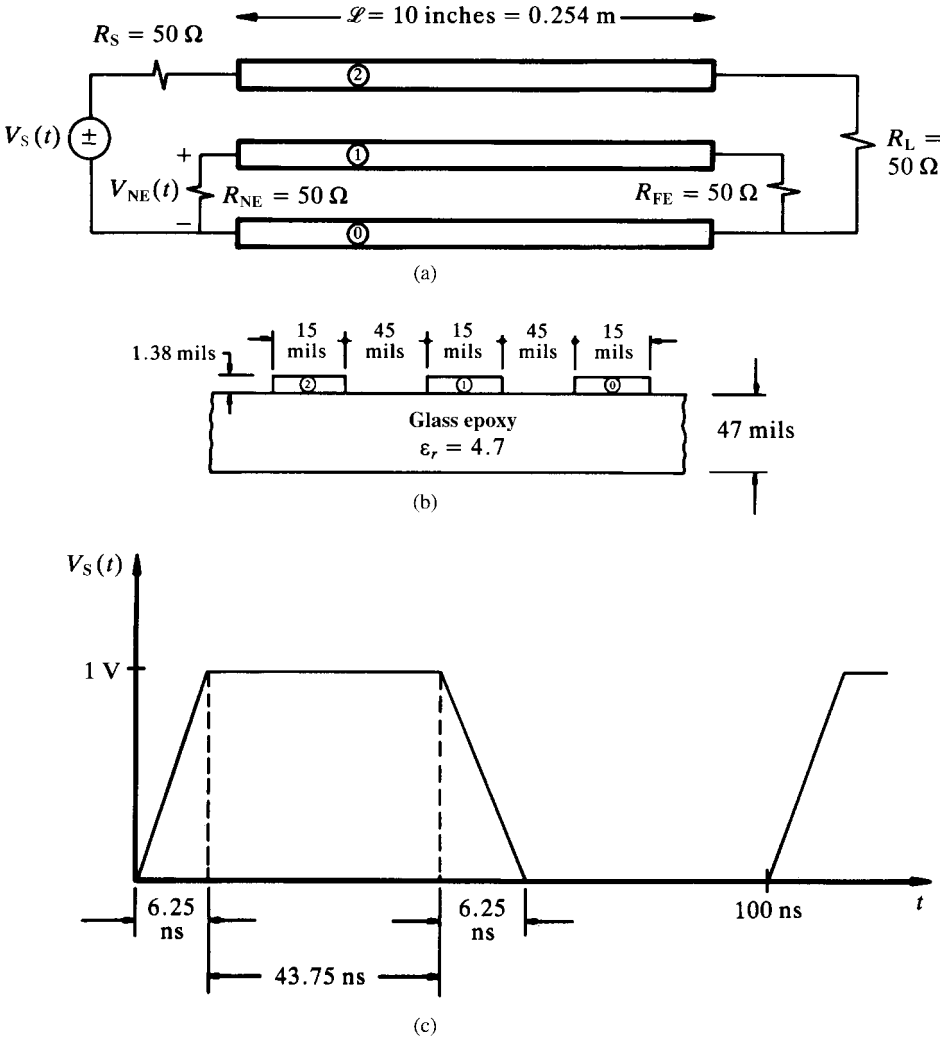


FIGURE 9.3 Example illustrating the generation of a SPICE model for coupled transmission lines: (a) longitudinal dimensions, (b) cross-sectional dimensions, and (c) the applied pulse train.

This gives the mode circuit one-way time delays as

$$\begin{aligned}
 T_{D1} &= 1.410753 \text{ ns} \\
 T_{D2} &= 1.321187 \text{ ns}
 \end{aligned}$$

The SPICE program (implemented on the personal computer version, PSPICE) is obtained from the circuit of Figure 9.4 as

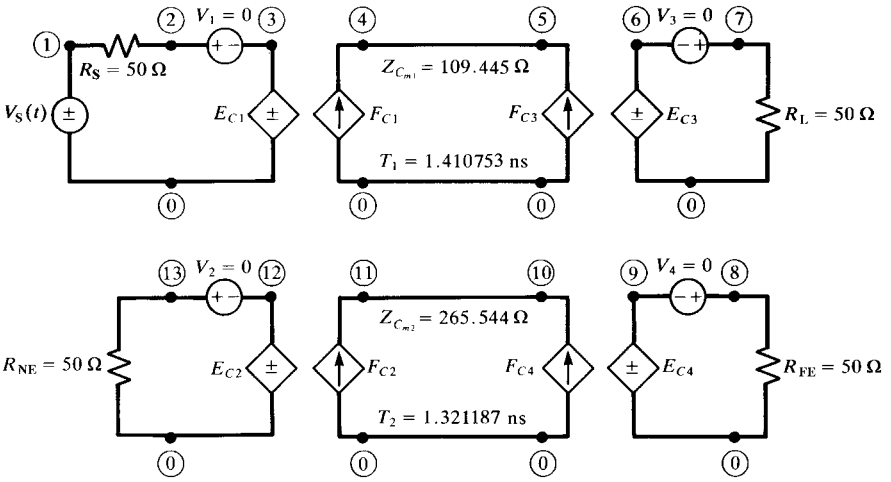


FIGURE 9.4 The SPICE model for the coupled line of Figure 9.3.

SPICE MTL MODEL

```

VS 1 0 PULSE(0 1 0 6.25N 6.25N 43.75N 100N)
RS 1 2 50
V1 2 3
RL 7 0 50
V3 7 6
RNE 13 0 50
V2 13 12
RFE 8 0 50
V4 8 9
EC1 3 0 POLY(2) (4,0) (11,0) 0 1.118 0.5
EC2 12 0 POLY(2) (4,0) (11,0) 0 -3.9E-6 1.0
EC3 6 0 POLY(2) (5,0) (10,0) 0 1.118 0.5
EC4 9 0 POLY(2) (5,0) (10,0) 0 -3.9E-6 1.0
FC1 0 4 POLY(2) V1 V2 0 1.118 -3.9E-6
FC2 0 11 POLY(2) V1 V2 0 0.5 1.0
FC3 0 5 POLY(2) V3 V4 0 1.118 -3.9E-6
FC4 0 10 POLY(2) V3 V4 0 0.5 1.0
T1 4 0 5 0 Z0=109.445 TD=1.410753N
T2 11 0 10 0 Z0=265.544 TD=1.321187N
.TRAN .1N 20N 0 .05N
.PRINT TRAN V(2) V(7) V(13) V(8)
.PROBE
.END
    
```

Comparisons with the experimentally obtained data will be shown in Section 9.3.2.

The method is implemented in the FORTRAN program `SPICEMTL.FOR` that is described in Appendix A. This code generates a SPICE subcircuit model. The user then imbeds this into a SPICE (PSPICE) program where the terminal constraints are added.

Another important advantage of the SPICE implementation of the solution is that the *frequency-domain* or *sinusoidal steady-state phasor solution* considered in Chapter 7 can also be obtained from this program with only a slight change in the control statements. These are to redefine the voltage source as

```
VS 1 0 AC 1
```

and redefine the control and print statements as

```
.AC DEC 50 10K 1000MEG
```

(which solves the frequency-domain circuit from 10 kHz to 1 GHz in steps of 50 per decade) and

```
.PRINT AC VM(2) VP(2) VM(7) VP(7) VM(13) VP(13) VM(8) VP(8)
```

where $VM(X)$ and $VP(X)$ denote the magnitude and phase, respectively, of the voltage at node X . Adding the `.PROBE` statement to this allows the plotting of the frequency response in a decibel plot. The remaining statements in the original time-domain program above are unchanged.

9.1.3 Lumped-Circuit Approximate Characterizations

One can also model the line using a lumped- Π or a lumped- T equivalent circuit so long as the line is electrically short at the highest significant frequency of the time-domain source waveform. These structures are shown for MTLs in Figure 7.6 of Chapter 7. For digital pulse waveforms having equal rise- and fall times τ_r , the highest significant frequency is approximately the bandwidth given earlier, $f_{\max} \cong 1/\tau_r$. The line length is one tenth of a wavelength at this frequency if the pulse rise-/fall time is approximately 10 times the line one-way delay or

$$\tau_r > 10 T_D$$

as was developed in Section 8.1.6.1 of Chapter 8. We saw that for MTLs there are n velocities of the modes. In order to determine whether the above criterion is satisfied, one should use the smaller of these mode velocities thereby guaranteeing that the condition will be satisfied at the larger mode velocities. However, in today's high-speed digital world, this criterion generally places impractically short-length limits on the PCB lands that can be modeled with one section. Other applications such as cables carrying signals with much lower spectral content perhaps can be feasibly modeled with lumped- Π or lumped- T sections. Again, for higher spectral content signals, dividing the line into several sections that are individually short at the highest frequency of the pulse waveform has been shown to not significantly increase the model accuracy to justify the inordinately large circuit that must be solved [B.15]. For lossless lines, one is better off simply using the SPICE subcircuit model generated by `SPICEMTL.FOR`.

9.1.4 The Time-Domain to Frequency-Domain (TDFD) Transformation Method

This method is identical for MTLs to that described in Section 8.1.7 of Chapter 8 for two-conductor lines. The only slight difference is that one must compute the single-input, single-output *frequency-domain transfer function* using a frequency-domain calculator such as MTL.FOR or using SPICEMTL.FOR to determine a MTL sub-circuit model, imbedding that generated model into a SPICE (PSPICE) program and using the .AC mode to compute this frequency-domain transfer function. Otherwise, there is no difference in its use for two-conductor lines or for MTLs. Once again, this method can incorporate line losses by including them in the frequency-domain transfer function (if MTL.FOR is used to generate it), which is a very straightforward process. However, the method suffers from the primary restriction that the line *and* its terminations must be *linear* since it uses the principle of superposition to return to the time domain.

9.1.5 The Finite-Difference, Time-Domain (FDTD) Method

The FDTD recursion relations were developed for a two-conductor line in the previous chapter. These are virtually unchanged for MTLs with only the use of matrix notation. Discretizing the derivatives in the MTL equations for a lossless line given in (9.1) using central differences [10,12] according to the scheme in Figure 8.17 gives

$$\frac{1}{\Delta z} \left[\mathbf{V}_{k+1}^{n+1} - \mathbf{V}_k^{n+1} \right] = -\frac{1}{\Delta t} \mathbf{L} \left[\mathbf{I}_k^{n+3/2} - \mathbf{I}_k^{n+1/2} \right] \tag{9.51a}$$

for $k = 1, 2, \dots, \text{NDZ}$ and

$$\frac{1}{\Delta z} \left[\mathbf{I}_k^{n+1/2} - \mathbf{I}_{k-1}^{n+1/2} \right] = -\frac{1}{\Delta t} \mathbf{C} \left[\mathbf{V}_k^{n+1} - \mathbf{V}_k^n \right] \tag{9.51b}$$

for $k = 2, \dots, \text{NDZ}$. The $n \times 1$ vectors \mathbf{I} and \mathbf{V} contain the line currents and line voltages, respectively, and we denote

$$\mathbf{V}_k^n \equiv \mathbf{V}((k - 1)\Delta z, n\Delta t) \tag{9.52a}$$

$$\mathbf{I}_k^n \equiv \mathbf{I}((k - 1/2)\Delta z, n\Delta t) \tag{9.52b}$$

Solving these gives the recursion relations for the interior points along the line as

$$\mathbf{I}_k^{n+3/2} = \mathbf{I}_k^{n+1/2} - \frac{\Delta t}{\Delta z} \mathbf{L}^{-1} \left(\mathbf{V}_{k+1}^{n+1} - \mathbf{V}_k^{n+1} \right) \tag{9.53a}$$

for $k = 1, 2, \dots, \text{NDZ}$ and

$$\mathbf{V}_k^{n+1} = \mathbf{V}_k^n - \frac{\Delta t}{\Delta z} \mathbf{C}^{-1} \left(\mathbf{I}_k^{n+1/2} - \mathbf{I}_{k-1}^{n+1/2} \right) \tag{9.53b}$$

for $k = 2, 3, \dots, \text{NDZ}$.

The second transmission-line equation given in Eq. (9.1b) is discretized at the source according to the scheme in Figure 8.18 as

$$\frac{1}{\Delta z/2} \left[\mathbf{I}_1^{n+1/2} - \frac{\mathbf{I}_S^{n+1} + \mathbf{I}_S^n}{2} \right] = -\frac{1}{\Delta t} \mathbf{C} \left[\mathbf{V}_1^{n+1} - \mathbf{V}_1^n \right] \quad (9.54a)$$

Similarly, the second transmission-line equation, (9.1b), is discretized at the load according to the scheme in Figure 8.18 as

$$\frac{1}{\Delta z/2} \left[\frac{\mathbf{I}_L^{n+1} + \mathbf{I}_L^n}{2} - \mathbf{I}_{\text{NDZ}}^{n+1/2} \right] = -\frac{1}{\Delta t} \mathbf{C} \left[\mathbf{V}_{\text{NDZ}+1}^{n+1} - \mathbf{V}_{\text{NDZ}+1}^n \right] \quad (9.54b)$$

In these relations, we denote the $n \times 1$ vectors of the currents at the source and at the load as \mathbf{I}_S and \mathbf{I}_L , respectively. Equations (9.54) are solved to give the recursion relations for the voltages at the source and the load:

$$\mathbf{V}_1^{n+1} = \mathbf{V}_1^n - \frac{2\Delta t}{\Delta z} \mathbf{C}^{-1} \mathbf{I}_1^{n+1/2} + \frac{\Delta t}{\Delta z} \mathbf{C}^{-1} \left[\mathbf{I}_S^{n+1} + \mathbf{I}_S^n \right] \quad (9.55a)$$

$$\mathbf{V}_{\text{NDZ}+1}^{n+1} = \mathbf{V}_{\text{NDZ}+1}^n + \frac{2\Delta t}{\Delta z} \mathbf{C}^{-1} \mathbf{I}_{\text{NDZ}}^{n+1/2} - \frac{\Delta t}{\Delta z} \mathbf{C}^{-1} \left[\mathbf{I}_L^{n+1} + \mathbf{I}_L^n \right] \quad (9.55b)$$

It should be pointed out that this method of obtaining collocated current and voltage relations in (9.54) at the source and the load was shown in Chapter 8 to yield the exact solution of a two-conductor line consisting of perfect conductors immersed in a lossless, homogeneous medium for the magic time step of $\Delta t = \Delta z/v$.

Assume that the multiconductor line has lumped terminal source and load representations that are resistive and are represented as generalized Thevenin equivalents:

$$\mathbf{V}(0, t) = \mathbf{V}_S(t) - \mathbf{R}_S \mathbf{I}(0, t) \quad (9.56a)$$

$$\mathbf{V}(\mathcal{L}, t) = \mathbf{V}_L(t) + \mathbf{R}_L \mathbf{I}(\mathcal{L}, t) \quad (9.56b)$$

Substituting these terminal representation of (9.56) into (9.55) yields the resulting FDTD recursion relations for the voltages at the source and at the load as

$$\mathbf{V}_1^{n+1} = \left[\frac{\Delta z}{\Delta t} \mathbf{R}_S \mathbf{C} + \mathbf{1}_n \right]^{-1} \left\{ \left[\frac{\Delta z}{\Delta t} \mathbf{R}_S \mathbf{C} - \mathbf{1}_n \right] \mathbf{V}_1^n - 2\mathbf{R}_S \mathbf{I}_1^{n+1/2} + \left(\mathbf{V}_S^{n+1} + \mathbf{V}_S^n \right) \right\} \quad (9.57a)$$

$$\begin{aligned} \mathbf{V}_{\text{NDZ}+1}^{n+1} = & \left[\frac{\Delta z}{\Delta t} \mathbf{R}_L \mathbf{C} + \mathbf{1}_n \right]^{-1} \left\{ \left[\frac{\Delta z}{\Delta t} \mathbf{R}_L \mathbf{C} - \mathbf{1}_n \right] \mathbf{V}_{\text{NDZ}+1}^n + 2\mathbf{R}_L \mathbf{I}_{\text{NDZ}}^{n+1/2} \right. \\ & \left. + \left(\mathbf{V}_L^{n+1} + \mathbf{V}_L^n \right) \right\} \end{aligned} \quad (9.57b)$$

These equations are implemented in the FORTRAN program FINDIF.FOR described in Appendix A. Again the time step Δt and the spatial discretization Δz must

satisfy the Courant condition

$$\Delta t \leq \frac{\Delta z}{v_{\max}} \quad (9.58)$$

in order to guarantee stability of the solution. For MTLs in inhomogeneous media that have n velocities of propagation of the modes, the Courant condition should be satisfied by the larger of the mode velocities thereby guaranteeing that it will be satisfied by the smaller mode velocities.

9.1.5.1 Including Dynamic and/or Nonlinear Terminations in the FDTD Analysis

Any lumped-element network can be completely characterized in a state-variable form [13, 14]. In the case of a linear network, this completely general formulation becomes

$$\frac{d}{dt}\mathbf{X}(t) = \mathbf{M}\mathbf{X}(t) + \mathbf{N}\mathbf{U}(t) \quad (9.59a)$$

with an associated output relation

$$\mathbf{Y}(t) = \mathbf{O}\mathbf{X}(t) + \mathbf{P}\mathbf{U}(t) + \mathbf{Q}\frac{d}{dt}\mathbf{U}(t) \quad (9.59b)$$

The vector \mathbf{X} contains the state variables of the lumped network. These are typically the inductor currents and capacitor voltages in that network or some subset of those variables. The vector \mathbf{U} contains the independent sources in the network (the inputs), and the vector \mathbf{Y} contains the designated outputs (currents and/or voltages) of the network. It should be emphasized that this formulation can characterize general linear networks that may contain such diverse conditions as inductor-current source cutsets and/or capacitor-voltage source loops as well as controlled sources of all types [13, 14].

Consider the recursion relations at the endpoints of the line given in (9.55a) and (9.55b). From these relations it is clear that we must configure the state-variable representations of the termination networks such that the outputs are the terminal currents \mathbf{I}_S and \mathbf{I}_L . The inputs for the state-variable representations must be the line voltages at the endpoints, \mathbf{V}_1 and $\mathbf{V}_{\text{NDZ}+1}$, as well as the independent sources within the termination networks. In order to accomplish this task, we will define the outputs in (9.59) as \mathbf{I}_S and \mathbf{I}_L and will partition the input vectors to yield

$$\frac{d}{dt}\mathbf{X}_S(t) = \mathbf{M}_S\mathbf{X}_S(t) + \mathbf{N}_1\mathbf{V}_1(t) + \mathbf{N}_S\mathbf{S}_S(t) \quad (9.60a)$$

$$\begin{aligned} \mathbf{I}_S(t) &= \mathbf{O}_S\mathbf{X}_S(t) + \mathbf{P}_1\mathbf{V}_1(t) + \mathbf{P}_S\mathbf{S}_S(t) \\ &+ \mathbf{Q}_1\frac{d}{dt}\mathbf{V}_1(t) + \mathbf{Q}_S\frac{d}{dt}\mathbf{S}_S(t) \end{aligned} \quad (9.60b)$$

$$\frac{d}{dt}\mathbf{X}_L(t) = \mathbf{M}_L\mathbf{X}_L(t) + \mathbf{N}_{\text{NDZ}+1}\mathbf{V}_{\text{NDZ}+1}(t) + \mathbf{N}_L\mathbf{S}_L(t) \quad (9.61a)$$

$$\begin{aligned} \mathbf{I}_L(t) = & \mathbf{O}_L \mathbf{X}_L(t) + \mathbf{P}_{\text{NDZ}+1} \mathbf{V}_{\text{NDZ}+1}(t) \\ & + \mathbf{P}_L \mathbf{S}_L(t) + \mathbf{Q}_{\text{NDZ}+1} \frac{d}{dt} \mathbf{V}_{\text{NDZ}+1}(t) + \mathbf{Q}_L \frac{d}{dt} \mathbf{S}_L(t) \end{aligned} \quad (9.61b)$$

where subscripts S and L refer to the networks at the source and load ends, respectively. The independent sources within the termination networks are denoted as \mathbf{S}_S and \mathbf{S}_L . Observe that in this state-variable characterization of the termination networks, the terminal voltages \mathbf{V}_1 and $\mathbf{V}_{\text{NDZ}+1}$ are treated as being independent voltage sources driving the terminations.

We now address the problem of interfacing the state-variable characterizations of the termination networks with the recursion relations for the attached line. We need to discretize the state-variable forms in (9.60) and (9.61). We will choose the implicit backward Euler method (also called the first-order Adams–Moulton algorithm) [13]. This method is absolutely stable regardless of time step size so long as the termination network itself is stable: a necessary assumption [13]. Because of this, the Courant stability condition on Δt given in (9.58) must be enforced only on the solution for the MTL portion of the system. The state-variable forms in (9.60) for the source termination network are discretized using the backward Euler method to yield [B.24]

$$\mathbf{X}_S^{n+1} = \mathbf{X}_S^n + \Delta t \left[\mathbf{M}_S \mathbf{X}_S^{n+1} + \mathbf{N}_1 \mathbf{V}_1^{n+1} + \mathbf{N}_S \mathbf{S}_S^{n+1} \right] \quad (9.62a)$$

$$\begin{aligned} \mathbf{I}_S^{n+1} = & \mathbf{O}_S \mathbf{X}_S^{n+1} + \mathbf{P}_1 \mathbf{V}_1^{n+1} + \mathbf{P}_S \mathbf{S}_S^{n+1} \\ & + \frac{1}{\Delta t} \mathbf{Q}_1 \left[\mathbf{V}_1^{n+1} - \mathbf{V}_1^n \right] + \frac{1}{\Delta t} \mathbf{Q}_S \left[\mathbf{S}_S^{n+1} - \mathbf{S}_S^n \right] \end{aligned} \quad (9.62b)$$

Solving (9.62a) for \mathbf{X}_S^{n+1} yields

$$[\mathbf{1} - \Delta t \mathbf{M}_S] \mathbf{X}_S^{n+1} = \mathbf{X}_S^n + \Delta t \mathbf{N}_1 \mathbf{V}_1^{n+1} + \Delta t \mathbf{N}_S \mathbf{S}_S^{n+1} \quad (9.63a)$$

$$\begin{aligned} \mathbf{I}_S^{n+1} = & \mathbf{O}_S \mathbf{X}_S^{n+1} + \mathbf{P}_1 \mathbf{V}_1^{n+1} + \mathbf{P}_S \mathbf{S}_S^{n+1} \\ & + \frac{1}{\Delta t} \mathbf{Q}_1 \left[\mathbf{V}_1^{n+1} - \mathbf{V}_1^n \right] + \frac{1}{\Delta t} \mathbf{Q}_S \left[\mathbf{S}_S^{n+1} - \mathbf{S}_S^n \right] \end{aligned} \quad (9.63b)$$

where $\mathbf{1}$ is the identity matrix with ones on the main diagonal and zeros elsewhere. Substituting (9.63b) into (9.55a) and combining with (9.63a) yields

$$\begin{aligned} & \left[\begin{array}{cc} \left(\frac{\Delta z}{\Delta t} \mathbf{C} - \mathbf{P}_1 - \frac{1}{\Delta t} \mathbf{Q}_1 \right) & -\mathbf{O}_S \\ -\Delta t \mathbf{N}_1 & \mathbf{1} - \Delta t \mathbf{M}_S \end{array} \right] \begin{bmatrix} \mathbf{V}_1^{n+1} \\ \mathbf{X}_S^{n+1} \end{bmatrix} \\ & = \left[\begin{array}{cc} \left(\frac{\Delta z}{\Delta t} \mathbf{C} - \frac{1}{\Delta t} \mathbf{Q}_1 \right) & \mathbf{0} \\ \mathbf{0} & \mathbf{1} \end{array} \right] \begin{bmatrix} \mathbf{V}_1^n \\ \mathbf{X}_S^n \end{bmatrix} + \left[\begin{array}{c} \left(\mathbf{P}_S + \frac{1}{\Delta t} \mathbf{Q}_S \right) \\ \Delta t \mathbf{N}_S \end{array} \right] \mathbf{S}_S^{n+1} \\ & + \left[\begin{array}{c} \mathbf{I}_S^n - \frac{1}{\Delta t} \mathbf{Q}_S \mathbf{S}_S^n - 2 \mathbf{I}_1^{n+1/2} \\ \mathbf{0} \end{array} \right] \end{aligned} \quad (9.64)$$

These simultaneous equations are solved for the new terminal voltages \mathbf{V}_1^{n+1} and state variables \mathbf{X}_S^{n+1} . Vectors \mathbf{S}_S^{n+1} and \mathbf{S}_S^n contain the independent lumped sources in the termination network all of which are readily evaluated at the appropriate time steps. Vectors \mathbf{V}_1^n , \mathbf{X}_S^n , $\mathbf{I}_1^{n+1/2}$, and \mathbf{I}_S^n are evaluated at the previous time step. Similarly, discretizing and combining (9.61) and (9.55b) yields the recursion relations for the load termination network as

$$\begin{aligned} & \left[\begin{array}{cc} \left(\frac{\Delta z}{\Delta t} \mathbf{C} + \mathbf{P}_{\text{NDZ}+1} + \frac{1}{\Delta t} \mathbf{Q}_{\text{NDZ}+1} \right) & \mathbf{O}_L \\ -\Delta t \mathbf{N}_{\text{NDZ}+1} & \mathbf{1} - \Delta t \mathbf{M}_L \end{array} \right] \begin{bmatrix} \mathbf{V}_{\text{NDZ}+1}^{n+1} \\ \mathbf{X}_L^{n+1} \end{bmatrix} \\ & = \left[\begin{array}{cc} \left(\frac{\Delta z}{\Delta t} \mathbf{C} + \frac{1}{\Delta t} \mathbf{Q}_{\text{NDZ}+1} \right) & \mathbf{0} \\ \mathbf{0} & \mathbf{1} \end{array} \right] \begin{bmatrix} \mathbf{V}_{\text{NDZ}+1}^n \\ \mathbf{X}_L^n \end{bmatrix} + \left[\begin{array}{c} \left(-\mathbf{P}_L - \frac{1}{\Delta t} \mathbf{Q}_L \right) \\ \Delta t \mathbf{N}_L \end{array} \right] \mathbf{S}_L^{n+1} \\ & \quad + \left[\begin{array}{c} -\mathbf{I}_L^n + \frac{1}{\Delta t} \mathbf{Q}_L \mathbf{S}_L^n + 2 \mathbf{I}_{\text{NDZ}+1}^{n+1/2} \\ \mathbf{0} \end{array} \right] \end{aligned} \quad (9.65)$$

All variables in the right-hand side of (9.65) are known.

In the case of resistive terminations, the generalized Thevenin equivalent representation in (9.56) is written as

$$\mathbf{I}_S = -\mathbf{G}_S \mathbf{V}_1 + \mathbf{G}_S \mathbf{V}_S \quad (9.66a)$$

$$\mathbf{I}_L = \mathbf{G}_L \mathbf{V}_{\text{NDZ}+1} - \mathbf{G}_L \mathbf{V}_L \quad (9.66b)$$

where $\mathbf{G}_S = \mathbf{R}_S^{-1}$ and $\mathbf{G}_L = \mathbf{R}_L^{-1}$. Hence, $\mathbf{X}_S = \mathbf{X}_L = \mathbf{0}$ so that

$\mathbf{M}_S = \mathbf{N}_1 = \mathbf{N}_S = \mathbf{O}_S = \mathbf{Q}_1 = \mathbf{Q}_S = \mathbf{0}$ and

$\mathbf{M}_L = \mathbf{N}_{\text{NDZ}+1} = \mathbf{N}_L = \mathbf{O}_L = \mathbf{Q}_{\text{NDZ}+1} = \mathbf{Q}_L = \mathbf{0}$ and $\mathbf{P}_1 = -\mathbf{G}_S$, $\mathbf{P}_S = \mathbf{G}_S$, $\mathbf{P}_{\text{NDZ}+1} = \mathbf{G}_L$, $\mathbf{P}_L = -\mathbf{G}_L$. Equations (9.64) and (9.65) reduce to [B.24]

$$\left(\frac{\Delta z}{\Delta t} \mathbf{C} + \mathbf{G}_S \right) \mathbf{V}_1^{n+1} = \left(\frac{\Delta z}{\Delta t} \mathbf{C} - \mathbf{G}_S \right) \mathbf{V}_1^n - 2 \mathbf{I}_1^{n+1/2} + \mathbf{G}_S \left(\mathbf{V}_S^{n+1} + \mathbf{V}_S^n \right) \quad (9.67a)$$

and

$$\begin{aligned} \left(\frac{\Delta z}{\Delta t} \mathbf{C} + \mathbf{G}_L \right) \mathbf{V}_{\text{NDZ}+1}^{n+1} & = \left(\frac{\Delta z}{\Delta t} \mathbf{C} - \mathbf{G}_L \right) \mathbf{V}_{\text{NDZ}+1}^n + 2 \mathbf{I}_{\text{NDZ}+1}^{n+1/2} \\ & \quad + \mathbf{G}_L \left(\mathbf{V}_L^{n+1} + \mathbf{V}_L^n \right) \end{aligned} \quad (9.67b)$$

If we premultiply (9.67a) with $\mathbf{R}_S = \mathbf{G}_S^{-1}$ and (9.67b) with $\mathbf{R}_L = \mathbf{G}_L^{-1}$, these are identical to those derived earlier and given in (9.57) for this special case.

The solution sequence is as follows. First, write the state-variable descriptions of the terminations as given in (9.60) and (9.61). Equations (9.64) and (9.65) are then

solved for the line voltages \mathbf{V}_1^{n+1} and $\mathbf{V}_{\text{NDZ}+1}^{n+1}$ and state variables of the termination networks \mathbf{X}_S^{n+1} and \mathbf{X}_L^{n+1} . Next the line voltages \mathbf{V}_k^{n+1} for $k = 2, \dots, \text{NDZ}$ are obtained from (9.53b). Finally, the currents are updated for $k = 1, \dots, \text{NDZ}$ via (9.53a). In order to insure stability of the solution for the lossless, single velocity case, the temporal and spatial discretizations should satisfy the Courant condition, which is $\Delta t \leq \Delta z/v$, where v is the velocity of propagation in the medium. We will assume that the similar condition applies to the multimode, multivelocity MTL case where v is the maximum of the velocities of the modes along the line. The above method can be similarly implemented for the case of nonlinear termination networks [B.24].

To compare the predictions of these models, we will investigate a three-conductor transmission line shown in Figure 9.5. Three conductors of rectangular cross section of width 5 mils and thickness 0.5 mils are separated by 5 mils and placed on one side of a silicon substrate having $\epsilon_r = 12$ and thickness 5 mils as shown in Figure 9.5(b). The total line length is 50 cm and is terminated as shown in Figure 9.5(a). The source is a 1-V trapezoidal pulse having a rise/fall time of $\tau_r = \tau_f = 100$ ps and pulse width of $\tau = 500$ ps. The per-unit-length inductance and capacitance matrices are computed as

$$\mathbf{L} = \begin{bmatrix} 0.805756 & 0.538771 \\ 0.538771 & 1.07754 \end{bmatrix} \mu\text{H/m}$$

$$\mathbf{C} = \begin{bmatrix} 117.791 & -58.8956 \\ -58.8956 & 71.8544 \end{bmatrix} \text{pF/m.}$$

These give mode velocities in the lossless case of $v_{m1} = 1.25809 \times 10^8$ m/s and $v_{m2} = 1.47934 \times 10^8$ m/s. The state-variable characterizations of the source and load given in (9.60) and (9.61) become

$$\mathbf{X}_S(t) = \mathbf{0}, \mathbf{M}_S = \mathbf{0}, \mathbf{N}_1 = \mathbf{0}, \mathbf{N}_S = \mathbf{0}, \mathbf{O}_S = \mathbf{0},$$

$$\mathbf{P}_1 = \begin{bmatrix} 1/R_{\text{NE}} & 0 \\ 0 & 1/R_S \end{bmatrix}, \mathbf{P}_S = \begin{bmatrix} 1/R_{\text{NE}} & 0 \\ 0 & 1/R_S \end{bmatrix},$$

$$\mathbf{Q}_1 = \mathbf{0}, \mathbf{Q}_S = \mathbf{0}, \mathbf{S}_S(t) = \begin{bmatrix} 0 \\ V_S(t) \end{bmatrix}$$

and

$$\mathbf{X}_L(t) = [i_L(t)], \mathbf{M}_L = [-R/L], \mathbf{N}_{\text{NDZ}+1} = [1/L \quad 0], \mathbf{N}_L = \mathbf{0},$$

$$\mathbf{O}_L = \begin{bmatrix} 1 \\ 0 \end{bmatrix}, \mathbf{P}_{\text{NDZ}+1} = \begin{bmatrix} 0 & 0 \\ 0 & 1/R_L \end{bmatrix}, \mathbf{P}_L = \mathbf{0}, \mathbf{Q}_{\text{NDZ}+1} = \begin{bmatrix} C & 0 \\ 0 & 0 \end{bmatrix}, \mathbf{Q}_L = \mathbf{0}$$

where $C = 100$ pF, $L = 1 \mu\text{H}$, $R = 10 \Omega$, $R_S = 50 \Omega$, $R_L = 50 \Omega$, and $R_{\text{NE}} = 5 \Omega$ and $i_L(t)$ is the inductor current. Observe that the capacitor produces a voltage source-capacitor loop with $[\mathbf{V}_{\text{NDZ}+1}]_1$. Hence, the coefficient of the derivative of

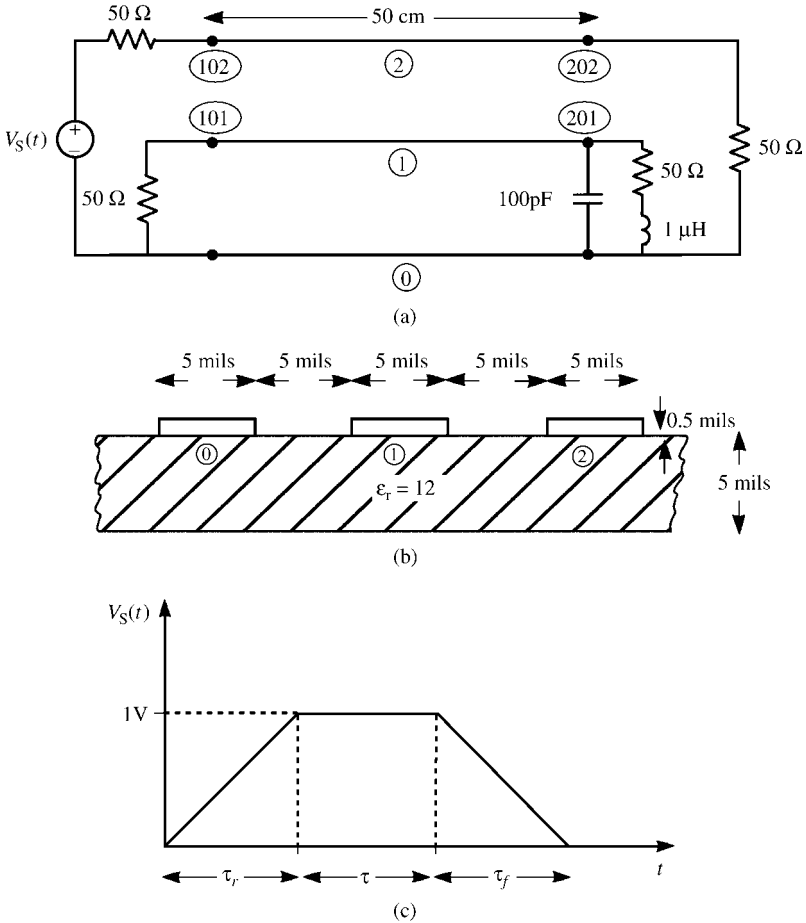


FIGURE 9.5 An example of a coupled line with dynamic loads: (a) longitudinal dimensions and loads, (b) cross-sectional dimensions, and (c) the applied pulse train.

V_{NDZ+1} in the terminal state-variable relation in (9.61b), Q_{NDZ+1} , is nonzero. We will compare the predictions of the SPICE (lossless) and the FDTD predictions. The FDTD spatial and temporal discretizations are denoted by

$$NDZ = \frac{\mathcal{L}}{\Delta z}$$

$$NDT = \frac{\text{final solution time}}{\Delta t}$$

Thus, the Courant stability criterion translates to

$$NDT \geq NDZ \times (\text{final solution time}) \times v/\mathcal{L}.$$

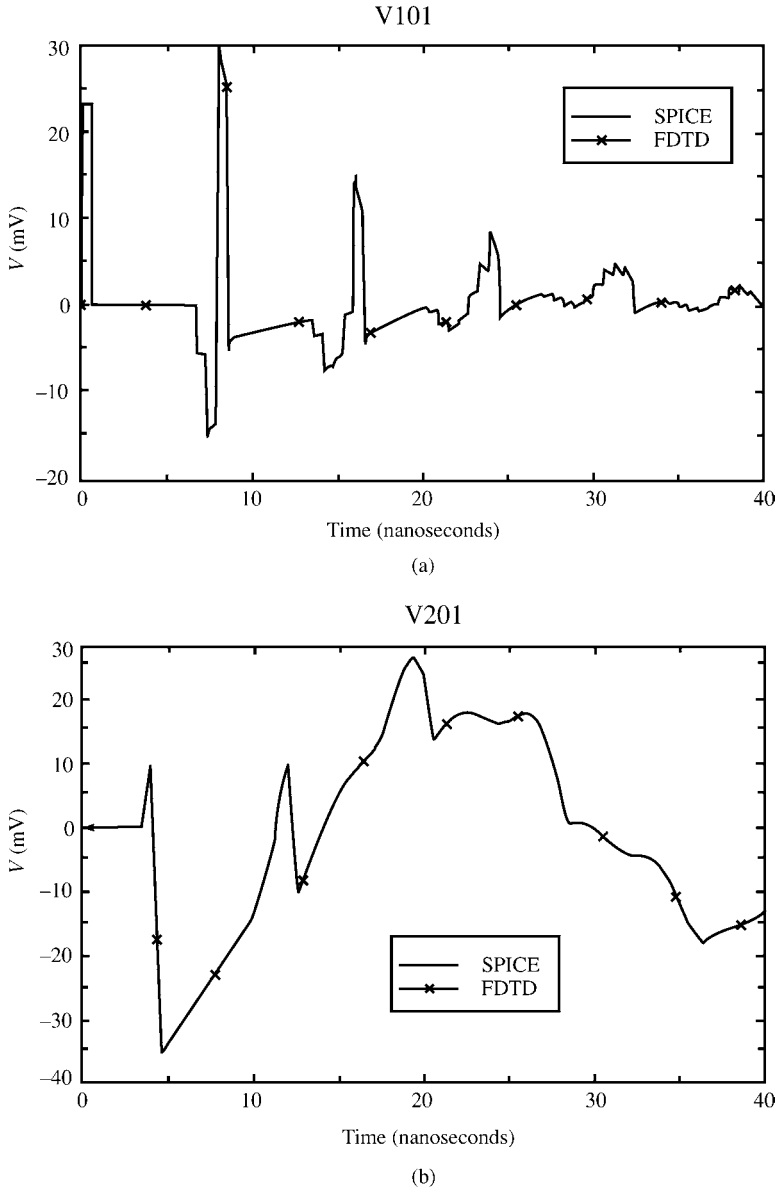


FIGURE 9.6 Predictions of the SPICE and FDTD models for the line of Figure 9.5: (a) V101 and (b) V201.

The bandwidth of the input pulse is on the order of $1/\tau_r = 10\text{GHz}$. The spatial discretization for the FDTD results is chosen so that each cell is $\lambda/10$ using the smaller of the mode velocities v_{m1} at $20\text{GHz} = 2 \times 1/\tau_r$, giving $\text{NDZ} = 795$. At the Courant limit of $\Delta t = \Delta z/v$ for this spatial discretization using the larger of the

mode velocities v_{m2} and a total solution time of 40 ns, we obtain a total number of time points of $NDT = 9410$. Figure 9.6(a) and (b) show the predictions for voltages across the ends of the receptor line. The FDTD predictions are compared to the SPICE predictions and give identical results as they should.

9.2 INCORPORATION OF LOSSES

Losses arise from either the nonzero conductivity and polarization loss of the surrounding medium or from imperfect conductors. Of the two mechanisms, the loss introduced by imperfect conductors is usually more significant than the loss due to the medium for typical transmission line structures and frequencies up to around 10 GHz. The resistance due to imperfect conductors is represented in the $n \times n$ per-unit-length resistance matrix \mathbf{R} . For lossy conductors, there is a $n \times n$ per-unit-length internal inductance matrix \mathbf{L}_i due to magnetic flux internal to the conductors. The frequency-dependent losses in the surrounding medium are contained in the $n \times n$ matrix \mathbf{G} and can be represented with the Debye model as discussed in Section 8.2.1.1 in the previous chapter. This is fairly straightforward for a homogeneous surrounding medium. For a lossy, inhomogeneous medium, incorporating losses in this fashion becomes tedious.

In the frequency domain, the MTL equations can be written as

$$\frac{d}{dz} \hat{\mathbf{V}}(z) = -[\hat{\mathbf{Z}}_i(\omega) + j\omega\mathbf{L}]\hat{\mathbf{I}}(z) \tag{9.68a}$$

$$\frac{d}{dz} \hat{\mathbf{I}}(z) = -[\mathbf{G}(\omega) + j\omega\mathbf{C}]\hat{\mathbf{V}}(z) \tag{9.68b}$$

where \mathbf{L} represents the external inductance, and the internal inductance is included in $\hat{\mathbf{Z}}_i(\omega) = \mathbf{R}(\omega) + j\omega\mathbf{L}_i(\omega)$. To obtain the time-domain results we represent the MTL equations with the Laplace transform as

$$\frac{d}{dz} \hat{\mathbf{V}}(z, s) = -[\hat{\mathbf{Z}}_i(s) + s\mathbf{L}]\hat{\mathbf{I}}(z, s) \tag{9.69a}$$

$$\frac{d}{dz} \hat{\mathbf{I}}(z, s) = -[\hat{\mathbf{G}}(s) + s\mathbf{C}]\hat{\mathbf{V}}(z, s) \tag{9.69b}$$

A common way of approximating the internal impedance term as discussed in the previous chapter is

$$\hat{\mathbf{Z}}_i(s) = \mathbf{A} + \mathbf{B}\sqrt{s} \tag{9.70}$$

This represents a reasonable approximation to the skin-effect behavior as can be seen if we substitute $s = j\omega$ to yield

$$\begin{aligned}\hat{\mathbf{Z}}_i(\omega) &= \mathbf{A} + \mathbf{B}\sqrt{j\omega} \\ &= \mathbf{A} + \mathbf{B}\sqrt{\pi}\sqrt{f}(1 + j)\end{aligned}\quad (9.71)$$

The $n \times n$ matrix \mathbf{A} represents the dc per-unit-length resistance matrix. The $n \times n$ matrix $\mathbf{B}\sqrt{\pi}\sqrt{f}(1 + j)$ represents the sum of the high-frequency per-unit-length resistance matrix and the high-frequency per-unit-length internal inductive reactance matrix. Hence, the entries in \mathbf{A} and \mathbf{B} are

$$[\mathbf{A}]_{ij} = [\mathbf{R}_{dc}]_{ij} \quad (9.72a)$$

$$[\mathbf{B}]_{ij}\sqrt{j\omega} = [\mathbf{R}_{hf}]_{ij} + j\omega[\mathbf{L}_{i,hf}]_{ij} = [\mathbf{R}_{dc}]_{ij}\sqrt{\frac{f}{f_0}}(1 + j) \quad (9.72b)$$

This assumes that the high-frequency resistance and internal inductive reactance of each conductor are equal. As we saw in Chapter 4, this is exact for isolated wires but is approximately true for conductors of rectangular cross section. This representation ignores the dc internal inductance of the conductors, which is typically dominated by the external inductance. The representation in (9.72b) also assumes that the break frequency f_0 , where the resistance and internal inductance transition from their dc behavior to their high-frequency \sqrt{f} behavior, is the same for all the conductors. This implicitly assumes that the conductors are identical. For example, an isolated wire transitions from its dc behavior to its high-frequency behavior when its radius equals two skin depths: $r_w = 2\delta$. If the conductors are not identical, this can be accommodated by putting the individual $\sqrt{f_0}$ break frequencies into the individual \mathbf{B} matrix terms giving the general representation in (9.71).

The Laplace transform representation in (9.69) translates in the time domain to

$$\frac{\partial}{\partial z}\mathbf{V}(z, t) = -\mathbf{Z}_i(t)*\mathbf{I}(z, t) - \mathbf{L}\frac{\partial}{\partial t}\mathbf{I}(z, t) \quad (9.73a)$$

$$\frac{\partial}{\partial z}\mathbf{I}(z, t) = -\mathbf{G}(t)*\mathbf{V}(z, t) - \mathbf{C}\frac{\partial}{\partial t}\mathbf{V}(z, t) \quad (9.73b)$$

where $*$ again denotes convolution, and the inverse Laplace transforms are denoted as

$$\hat{\mathbf{Z}}_i(s) \Leftrightarrow \mathbf{Z}_i(t) \quad (9.74a)$$

$$\hat{\mathbf{G}}(s) \Leftrightarrow \mathbf{G}(t) \quad (9.74b)$$

Using the Laplace transform identity given in the previous chapter:

$$\frac{1}{\sqrt{s}} \Leftrightarrow \frac{1}{\sqrt{\pi}} \frac{1}{\sqrt{t}} \quad (9.75)$$

the representation of the conductor internal impedance in (9.70) translates to

$$\hat{\mathbf{Z}}_i(s) = \mathbf{A} + \mathbf{B}\sqrt{s} \Leftrightarrow \mathbf{Z}_i(t) = \mathbf{A} + \frac{1}{\sqrt{\pi}} \mathbf{B} \frac{1}{\sqrt{t}} \frac{\partial}{\partial t} \quad (9.76)$$

Hence, the convolution becomes

$$\mathbf{Z}_i(t) * \mathbf{I}(z, t) \Leftrightarrow \mathbf{A} \mathbf{I}(z, t) + \frac{1}{\sqrt{\pi}} \mathbf{B} \left[\int_0^t \frac{1}{\sqrt{\tau}} \frac{\partial}{\partial(t-\tau)} \mathbf{I}(z, t-\tau) d\tau \right] \quad (9.77)$$

9.2.1 The Time-Domain to Frequency-Domain (TDFD) Method

This method of circumventing the convolution for lossy lines is essentially unchanged from previous descriptions except that the frequency-domain computation of the transfer function requires inclusion of the line losses. (See Section 8.2.2 of the previous chapter.) This is a very straightforward task and easily includes frequency-dependent losses. Simply compute the internal impedance at each frequency and include that in the solution for that frequency. Then recompute this for the next frequency and resolve for the transfer function (magnitude and phase) at that frequency and so on. The computer program `MTL.FOR` described in Appendix A provides this solution for lossy multiconductor lines, and the program `TIMEFREQ.FOR` recombines the processed Fourier frequency components of the time-domain input signal to indirectly give the time-domain response of the system. Once again, use of this method requires that the line terminations are *linear* since superposition was inherently used.

9.2.2 Lumped-Circuit Approximate Characterizations

Again, a common way of approximately representing the line is with a lumped-Pi or lumped-T equivalent circuit shown in Figure 7.6 of Chapter 7. The primary difficulty with these approximations is that they do not correctly process the high-frequency spectral components of the input signal because their validity is based on the assumption that they are electrically short at *all* frequencies of interest. Frequency-dependent losses such as the skin-effect losses in conductors can be simulated using the lumped-circuit models of the line impedances shown in Figure 8.50.

The FORTRAN code `SPICELPI.FOR` described in Appendix A for lossless lines generates a one-section, lumped-Pi SPICE subcircuit model. This can be then modified to include losses by adding either dc resistances or one of the skin-effect simulations in Figure 8.50. In this way only the line is modeled, and nonlinear loads can be handled in the CAD code in which this model is imbedded. This is a simple approximation but suffers from the lengthy computation time that a sufficiently large

circuit model requires to model the very high-frequency spectral components of the input signal [B.15].

9.2.3 The Finite-Difference, Time-Domain (FDTD) Method

The FDTD model for a lossy MTL is virtually identical to that for a lossy two-conductor line but with matrix notation. We will first formulate the FDTD recursion relations for a lossy line whose conductor loss parameters contained in \mathbf{R} and \mathbf{L}_i , and dielectric loss parameters contained in \mathbf{G} are frequency independent, that is, their dc values. The results can be obtained as in Section 8.2.3.1 but with matrix notation:

$$\begin{aligned} \mathbf{V}_k^{n+1} = & \left(\frac{\Delta z}{\Delta t} \mathbf{C} + \frac{\Delta z}{2} \mathbf{G} \right)^{-1} \left(\frac{\Delta z}{\Delta t} \mathbf{C} - \frac{\Delta z}{2} \mathbf{G} \right) \mathbf{V}_k^n \\ & - \left(\frac{\Delta z}{\Delta t} \mathbf{C} + \frac{\Delta z}{2} \mathbf{G} \right)^{-1} \left(\mathbf{I}_k^{n+1/2} - \mathbf{I}_{k-1}^{n+1/2} \right) \end{aligned} \quad (9.78a)$$

for $k = 2, 3, \dots, \text{NDZ}$ and

$$\begin{aligned} \mathbf{I}_k^{n+3/2} = & \left(\frac{\Delta z}{\Delta t} \mathbf{L} + \frac{\Delta z}{2} \mathbf{R} \right)^{-1} \left(\frac{\Delta z}{\Delta t} \mathbf{L} - \frac{\Delta z}{2} \mathbf{R} \right) \mathbf{I}_k^{n+1/2} \\ & - \left(\frac{\Delta z}{\Delta t} \mathbf{L} + \frac{\Delta z}{2} \mathbf{R} \right)^{-1} \left(\mathbf{V}_{k+1}^{n+1} - \mathbf{V}_k^{n+1} \right) \end{aligned} \quad (9.78b)$$

for $k = 1, 2, \dots, \text{NDZ}$. The terminal voltages are, for resistive terminations, in the form of a generalized Thevenin equivalent given in (9.56),

$$\begin{aligned} \mathbf{V}_1^{n+1} = & \left(\frac{\Delta z}{\Delta t} \mathbf{R}_S \mathbf{C} + \frac{\Delta z}{2} \mathbf{R}_S \mathbf{G} + \mathbf{1}_n \right)^{-1} \left\{ \left(\frac{\Delta z}{\Delta t} \mathbf{R}_S \mathbf{C} - \frac{\Delta z}{2} \mathbf{R}_S \mathbf{G} - \mathbf{1}_n \right) \mathbf{V}_1^n \right. \\ & \left. - 2 \mathbf{R}_S \mathbf{I}_1^{n+1/2} + \left(\mathbf{V}_S^{n+1} + \mathbf{V}_S^n \right) \right\} \end{aligned} \quad (9.79a)$$

and

$$\begin{aligned} \mathbf{V}_{\text{NDZ}+1}^{n+1} = & \left(\frac{\Delta z}{\Delta t} \mathbf{R}_L \mathbf{C} + \frac{\Delta z}{2} \mathbf{R}_L \mathbf{G} + \mathbf{1}_n \right)^{-1} \left\{ \left(\frac{\Delta z}{\Delta t} \mathbf{R}_L \mathbf{C} - \frac{\Delta z}{2} \mathbf{R}_L \mathbf{G} - \mathbf{1}_n \right) \right. \\ & \left. \times \mathbf{V}_{\text{NDZ}+1}^n + 2 \mathbf{R}_L \mathbf{I}_{\text{NDZ}}^{n+1/2} + \left(\mathbf{V}_L^{n+1} + \mathbf{V}_L^n \right) \right\} \end{aligned} \quad (9.79b)$$

Equations (9.78a) and (9.79) are solved first to obtain the line voltages, and then the line currents are updated using (9.78b).

We next obtain the recursion relations for the FDTD formulation that includes *frequency-dependent* conductor losses. Since the second transmission-line equation in (9.73b) contains the dielectric losses in \mathbf{G} , the voltage update equations for the

interior voltages of a lossless MTL in (9.53b) are unchanged for the case of a lossless medium, $\mathbf{G} = \mathbf{0}_n$ where $\mathbf{0}_n$ is the $n \times n$ zero matrix with zeros in every position:

$$\mathbf{V}_k^{n+1} = \mathbf{V}_k^n - \frac{\Delta t}{\Delta z} \mathbf{C}^{-1} \left(\mathbf{I}_k^{n+1/2} - \mathbf{I}_{k-1}^{n+1/2} \right) \quad (9.53b)$$

for $k = 2, 3, \dots, \text{NDZ}$. The terminal voltage update equations in (9.55) or in (9.57) for the generalized Thevenin equivalent characterization of the MTL terminations are also unchanged from the case of a lossless medium:

$$\mathbf{V}_1^{n+1} = \left[\frac{\Delta z}{\Delta t} \mathbf{R}_S \mathbf{C} + \mathbf{1}_n \right]^{-1} \left\{ \left[\frac{\Delta z}{\Delta t} \mathbf{R}_S \mathbf{C} - \mathbf{1}_n \right] \mathbf{V}_1^n - 2\mathbf{R}_S \mathbf{I}_1^{n+1/2} + \left(\mathbf{V}_S^{n+1} + \mathbf{V}_S^n \right) \right\} \quad (9.57a)$$

$$\mathbf{V}_{\text{NDZ}+1}^{n+1} = \left[\frac{\Delta z}{\Delta t} \mathbf{R}_L \mathbf{C} + \mathbf{1}_n \right]^{-1} \left\{ \left[\frac{\Delta z}{\Delta t} \mathbf{R}_L \mathbf{C} - \mathbf{1}_n \right] \mathbf{V}_{\text{NDZ}+1}^n + 2\mathbf{R}_L \mathbf{I}_{\text{NDZ}}^{n+1/2} + \left(\mathbf{V}_L^{n+1} + \mathbf{V}_L^n \right) \right\} \quad (9.57b)$$

Only the equation for updating the current given in (9.53a) that is derived from the first MTL equation in (9.73a) that contains the conductor losses needs to be changed.

In the case of a multiconductor line containing imperfect conductors, a virtually identical development to the two-conductor line result in (8.180) provides the current update equations for lossy conductors:

$$\begin{aligned} \mathbf{I}_k^{n+3/2} &= \mathbf{F}^{-1} \left(\mathbf{L} \frac{\Delta z}{\Delta t} - \mathbf{A} \frac{\Delta z}{2} + \mathbf{B} \frac{\Delta z}{\sqrt{\pi} \Delta t} Z_0(0) \right) \mathbf{I}_k^{n+1/2} \\ &\quad - \mathbf{F}^{-1} \mathbf{B} \frac{\Delta z}{\sqrt{\pi} \Delta t} \sum_{i=1}^{10} \Psi_i^n - \mathbf{F}^{-1} \left(\mathbf{V}_{k+1}^{n+1} - \mathbf{V}_k^{n+1} \right) \end{aligned} \quad (9.80a)$$

for $k = 1, \dots, \text{NDZ}$ where

$$\Psi_i^n = a_i e^{b_i} \left[\mathbf{I}_k^{n+1/2} - \mathbf{I}_k^{n-1/2} \right] + e^{b_i} \Psi_i^{n-1} \quad (9.80b)$$

and the a_i and b_i are again determined with the Prony method and are given in Table 8.2 of Chapter 8. The matrix \mathbf{F} is given by

$$\mathbf{F} = \left(\mathbf{L} \frac{\Delta z}{\Delta t} + \mathbf{A} \frac{\Delta z}{2} + \mathbf{B} \frac{\Delta z}{\sqrt{\pi} \Delta t} Z_0(0) \right) \quad (9.80c)$$

This replaces equation (9.53a) of the lossless line development. The details of the derivation are essentially the same as for the lossy, two-conductor line given in Section 8.2.3 of Chapter 8. This is implemented in the FORTRAN code FDTDLOSS.FOR that is described in Appendix A.

9.2.4 Representation of the Lossy MTL with the Generalized Method of Characteristics

In Section 9.1.2, we discussed representing a lossless MTL with the generalized method of characteristics [2]. Decoupling the MTL equations with similarity transformations is easily accomplished for lossless MTLs. The generalized method of characteristics derived for lossless MTLs can be extended to lossy MTLs in the following manner but the details become more tedious. Again, we attempt to decouple the MTL equations for lossy lines by converting to *modal* quantities with similarity transformations:

$$\hat{\mathbf{V}}(z, s) = \hat{\mathbf{T}}_V(s) \hat{\mathbf{V}}_m(z, s) \quad (9.81a)$$

$$\hat{\mathbf{I}}(z, s) = \hat{\mathbf{T}}_I(s) \hat{\mathbf{I}}_m(z, s) \quad (9.81b)$$

where we have denoted the line voltages and currents as their Laplace-transformed variables. Substituting these into the MTL equations for a lossy line given in (9.69) yields

$$\frac{d}{dz} \hat{\mathbf{V}}_m(z, s) = -\hat{\mathbf{T}}_V^{-1}(s) [\hat{\mathbf{Z}}_i(s) + s\mathbf{L}] \hat{\mathbf{T}}_I(s) \hat{\mathbf{I}}_m(z, s) \quad (9.82a)$$

$$\frac{d}{dz} \hat{\mathbf{I}}_m(z, s) = -\mathbf{T}_I^{-1}(s) [\hat{\mathbf{G}}(s) + s\mathbf{C}] \hat{\mathbf{T}}_V(s) \hat{\mathbf{V}}_m(z, s) \quad (9.82b)$$

where the internal impedances of the conductors are included as the sum of the resistances and internal inductances as $\hat{\mathbf{Z}}_i(s) = \hat{\mathbf{R}}(s) + s\hat{\mathbf{L}}_i(s)$. If we can determine mode transformations such that the equations are uncoupled as

$$\hat{\mathbf{T}}_V^{-1}(s) [\hat{\mathbf{Z}}_i(s) + s\mathbf{L}] \hat{\mathbf{T}}_I(s) = \hat{\mathbf{Z}}_m(s) \quad (9.83a)$$

$$\mathbf{T}_I^{-1}(s) [\hat{\mathbf{G}}(s) + s\mathbf{C}] \hat{\mathbf{T}}_V(s) = \hat{\mathbf{Y}}_m(s) \quad (9.83b)$$

where $\hat{\mathbf{Z}}_m(s)$ and $\hat{\mathbf{Y}}_m(s)$ are diagonal, then the modal MTL equations in (9.82) are decoupled as

$$\begin{aligned}
 \frac{d \hat{V}_{m1}(z, s)}{dz} &= -\hat{Z}_{m1}(s) \hat{I}_{m1}(z, s) \\
 \frac{d \hat{I}_{m1}(z, s)}{dz} &= -\hat{Y}_{m1}(s) \hat{V}_{m1}(z, s) \\
 &\vdots \\
 \frac{d \hat{V}_{mn}(z, s)}{dz} &= -\hat{Z}_{mn}(s) \hat{I}_{mn}(z, s) \\
 \frac{d \hat{I}_{mn}(z, s)}{dz} &= -\hat{Y}_{mn}(s) \hat{V}_{mn}(z, s)
 \end{aligned} \tag{9.84}$$

The mode voltages, $\hat{V}_{mi}(z, s)$, and mode currents, $\hat{I}_{mi}(z, s)$, are then represented with n separate, uncoupled, two-conductor, lossy lines. The diagonal per-unit-length impedance and admittance matrices for the modes in (9.83), $\hat{\mathbf{Z}}_m(s)$ and $\hat{\mathbf{Y}}_m(s)$, have entries $[\hat{\mathbf{Z}}_m(s)]_{ii} = \hat{Z}_{mi}(s)$ and $[\hat{\mathbf{Y}}_m(s)]_{ii} = \hat{Y}_{mi}(s)$ for $i = 1, \dots, n$ on the main diagonal and zeros elsewhere. Hence, the solutions for the modes are

$$\begin{aligned}
 \hat{V}_{m1}(z, s) &= e^{-\hat{\gamma}_{m1}(s)z} \hat{V}_{m1}^+(s) + e^{\hat{\gamma}_{m1}(s)z} \hat{V}_{m1}^-(s) \\
 \hat{I}_{m1}(z, s) &= \frac{1}{\hat{Z}_{Cm1}(s)} e^{-\hat{\gamma}_{m1}(s)z} \hat{V}_{m1}^+(s) - \frac{1}{\hat{Z}_{Cm1}(s)} e^{\hat{\gamma}_{m1}(s)z} \hat{V}_{m1}^-(s) \\
 &\vdots \\
 \hat{V}_{mn}(z, s) &= e^{-\hat{\gamma}_{mn}(s)z} \hat{V}_{mn}^+(s) + e^{\hat{\gamma}_{mn}(s)z} \hat{V}_{mn}^-(s) \\
 \hat{I}_{mn}(z, s) &= \frac{1}{\hat{Z}_{Cmn}(s)} e^{-\hat{\gamma}_{mn}(s)z} \hat{V}_{mn}^+(s) - \frac{1}{\hat{Z}_{Cmn}(s)} e^{\hat{\gamma}_{mn}(s)z} \hat{V}_{mn}^-(s)
 \end{aligned} \tag{9.85}$$

where the mode characteristic impedances and propagation constants are

$$\hat{Z}_{Cmi}(s) = \sqrt{\frac{\hat{Z}_{mi}(s)}{\hat{Y}_{mi}(s)}} \tag{9.86}$$

and

$$\hat{\gamma}_{mi}(s) = \sqrt{\hat{Z}_{mi}(s) \hat{Y}_{mi}(s)} \tag{9.87}$$

The solutions in (9.85) can be written in the matrix form as

$$\hat{\mathbf{V}}_m(z, s) = \mathbf{e}^{-\hat{\gamma}(s)z} \hat{\mathbf{V}}_m^+(s) + \mathbf{e}^{\hat{\gamma}(s)z} \hat{\mathbf{V}}_m^-(s) \tag{9.88a}$$

$$\hat{\mathbf{I}}_m(z, s) = \hat{\mathbf{Z}}_{Cm}^{-1}(s) \left[\mathbf{e}^{-\hat{\gamma}(s)z} \hat{\mathbf{V}}_m^+(s) - \mathbf{e}^{\hat{\gamma}(s)z} \hat{\mathbf{V}}_m^-(s) \right] \quad (9.88b)$$

where $\hat{\mathbf{Z}}_{Cm}$ is the $n \times n$ characteristic impedance matrix for the modes, which is diagonal with $[\hat{\mathbf{Z}}_{Cm}(s)]_{ii} = \hat{Z}_{Cmi}(s)$ on the main diagonal and zeros elsewhere, and $\mathbf{e}^{\pm\hat{\gamma}(s)}$ is an $n \times n$ diagonal matrix containing $[\mathbf{e}^{\pm\hat{\gamma}(s)}]_{ii} = e^{\pm\hat{\gamma}_{mi}(s)}$ on the main diagonal and zeros elsewhere. The $n \times 1$ vectors of undetermined constants, $\hat{\mathbf{V}}_m^\pm(s)$, have entries $[\hat{\mathbf{V}}_m^\pm(s)]_i = \hat{V}_{mi}^\pm(s)$ that are, in general, functions of s . Evaluating (9.88) at $z = 0$ and at $z = \mathcal{L}$ gives

$$\hat{\mathbf{V}}_m(0, s) = \hat{\mathbf{V}}_m^+(s) + \hat{\mathbf{V}}_m^-(s) \quad (9.89a)$$

$$\hat{\mathbf{Z}}_{Cm}(s)\hat{\mathbf{I}}_m(0, s) = \hat{\mathbf{V}}_m^+(s) - \hat{\mathbf{V}}_m^-(s) \quad (9.89b)$$

and

$$\hat{\mathbf{V}}_m(\mathcal{L}, s) = \mathbf{e}^{-\hat{\gamma}(s)\mathcal{L}} \hat{\mathbf{V}}_m^+(s) + \mathbf{e}^{\hat{\gamma}(s)\mathcal{L}} \hat{\mathbf{V}}_m^-(s) \quad (9.90a)$$

$$\hat{\mathbf{Z}}_{Cm}(s)\hat{\mathbf{I}}_m(\mathcal{L}, s) = \mathbf{e}^{-\hat{\gamma}(s)\mathcal{L}} \hat{\mathbf{V}}_m^+(s) - \mathbf{e}^{\hat{\gamma}(s)\mathcal{L}} \hat{\mathbf{V}}_m^-(s) \quad (9.90b)$$

Adding and subtracting (9.89) and (9.90) yields

$$\hat{\mathbf{V}}_m(0, s) - \hat{\mathbf{Z}}_{Cm}(s)\hat{\mathbf{I}}_m(0, s) = \hat{\mathbf{E}}_0(s) \quad (9.91a)$$

$$\hat{\mathbf{V}}_m(\mathcal{L}, s) + \hat{\mathbf{Z}}_{Cm}(s)\hat{\mathbf{I}}_m(\mathcal{L}, s) = \hat{\mathbf{E}}_{\mathcal{L}}(s) \quad (9.91b)$$

where

$$\hat{\mathbf{E}}_0(s) = \mathbf{e}^{-\hat{\gamma}(s)\mathcal{L}} \left[\hat{\mathbf{V}}_m(\mathcal{L}, s) - \hat{\mathbf{Z}}_{Cm}(s)\hat{\mathbf{I}}_m(\mathcal{L}, s) \right] \quad (9.92a)$$

$$\hat{\mathbf{E}}_{\mathcal{L}}(s) = \mathbf{e}^{-\hat{\gamma}(s)\mathcal{L}} \left[\hat{\mathbf{V}}_m(0, s) + \hat{\mathbf{Z}}_{Cm}(s)\hat{\mathbf{I}}_m(0, s) \right] \quad (9.92b)$$

We can therefore use all the techniques developed in Chapter 8 for two-conductor, lossy lines to model these uncoupled mode lines. The uncoupled mode line solutions in (9.91) and (9.92) can be represented as shown in Figure 9.7. Time-domain representations of the frequency-dependent individual mode characteristic impedances $Z_{Cmi}(s) \Leftrightarrow z_{Cmi}(t)$ as well as the propagation functions $e^{-\hat{\gamma}_{mi}(s)\mathcal{L}} \Leftrightarrow h_{mi}(t)$ can be obtained with the Pade method or the Prony method as described in Chapter 8. This allows the use of the recursive convolution method to evaluate the convolutions that are represented by products of functions of s . In some cases, these can be represented with lumped RLCG circuits [15]. Controlled sources can, as for lossless lines in the

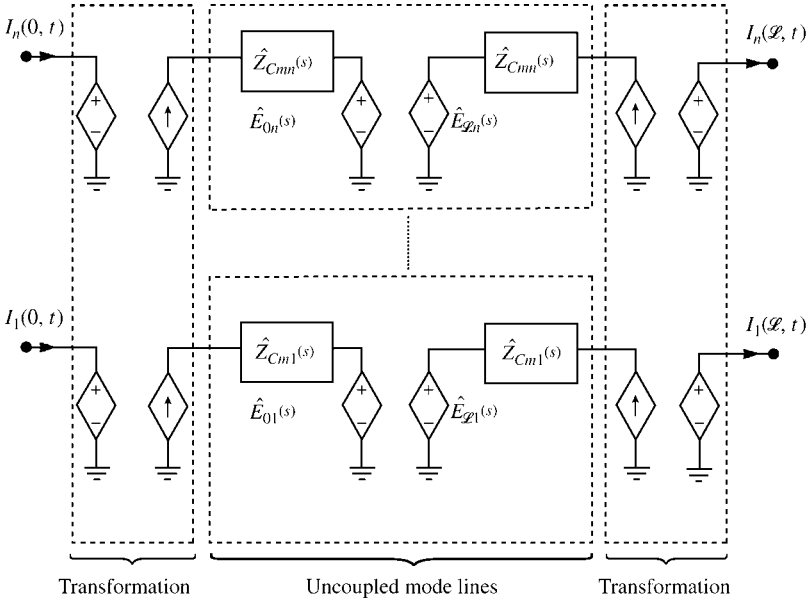


FIGURE 9.7 Illustration of the generalized method of characteristics for MTLs via decoupling.

earlier part of this chapter, be used to transform the mode voltages and currents from these uncoupled lines back to the actual line voltages and currents using (9.81) as illustrated in Figure 9.1. Hence, we can represent the lossy line and the transformations as shown in Figure 9.7.

This is very similar to the representation for the two-conductor lossless line shown in Figure 8.9 that was derived from the method of characteristics in Chapter 8 and produced the exact SPICE model of a two-conductor, lossless line. It is also used for a lossless MTL in Section 9.1.2 of this chapter. This representation is referred to in the literature as the generalized method of characteristics [15–27]. It should be noted that the vast majority of these works assume that the loss parameter matrices, \mathbf{R} , \mathbf{L}_i , and \mathbf{G} , are *constant matrices*, that is, independent of s and are therefore dc or low-frequency parameters. This is done to simplify the mathematics. But clearly, this is unrealistic since high-frequency skin-effect losses are neglected, as are the frequency-dependent losses in the surrounding dielectric medium. Incorporating the frequency-dependent losses of the conductors and dielectric medium obviously complicates the analysis rather severely but is a necessary, practical requirement. Investigation of the required relationship between $\hat{\mathbf{Z}}(\omega)$ and $\hat{\mathbf{Y}}(\omega)$ to ensure causality of the response is given in [28]. The method of numerical inversion of the Laplace transform is an alternative method of generating the time-domain functions and is discussed in [29–32]. Observe that a major difficulty with diagonalizing the MTL equations for a lossy line as in (9.83) is that, in general, *the mode transformations will be frequency dependent and*

will be functions of s ! Hence, the controlled sources in Figure 9.7 that implement the transformations back to actual line voltages and currents will represent convolutions. This presents a rather undesirable situation because we are faced with numerous convolutions when we convert the mode quantities back to actual line voltages and currents as in (9.81). Furthermore, it is difficult to compute the eigenvectors of a matrix (the columns of $\hat{\mathbf{T}}_V(s)$ and $\hat{\mathbf{T}}_I(s)$) when the matrix is a function of s . To henceforth simplify the notation, we will denote the mode transformations as $\hat{\mathbf{T}}_V(s) = \mathbf{T}_V$ and $\hat{\mathbf{T}}_I(s) = \mathbf{T}_I$ with the understanding that these will, in general, be frequency dependent for lossy MTLs.

To avoid these convolutions in the mode transformations, we try to obtain *frequency-independent* modal transformations. There are some special cases where we can obtain frequency-independent mode transformations thereby simplifying the equivalent circuit in Figure 9.7. The mode transformations will then be frequency independent and hence the parameters of the controlled sources representing them in Figure 9.7 will be constants. First we write out (9.83), substituting $\hat{\mathbf{Z}}_i(s) = \mathbf{R}(s) + s\mathbf{L}_i(s)$:

$$\mathbf{T}_V^{-1}\mathbf{R}(s)\mathbf{T}_I + s\mathbf{T}_V^{-1}\mathbf{L}_i(s)\mathbf{T}_I + s\mathbf{T}_V^{-1}\mathbf{L}\mathbf{T}_I = \hat{\mathbf{Z}}_m(s) \quad (9.93a)$$

$$\mathbf{T}_I^{-1}\mathbf{G}(s)\mathbf{T}_V + s\mathbf{T}_I^{-1}\mathbf{C}\mathbf{T}_V = \hat{\mathbf{Y}}_m(s) \quad (9.93b)$$

Hence, we must determine two $n \times n$ constant transformation matrices \mathbf{T}_V and \mathbf{T}_I that *simultaneously* diagonalize five matrices, \mathbf{R} , \mathbf{L}_i , \mathbf{L} , \mathbf{G} , and \mathbf{C} . Clearly, this is too much to expect. Now let us make some assumptions to allow the decoupling of the MTL equations and, in addition, give frequency-independent transformations. The first assumption is that the surrounding medium is *homogeneous*, for example, a stripline. For a *homogeneous medium*, we have the identities

$$\mathbf{G} = \frac{\sigma(s)}{\varepsilon(s)}\mathbf{C} \quad (9.94a)$$

$$\mathbf{C}\mathbf{L} = \mu \varepsilon(s)\mathbf{1}_n = \frac{1}{v^2}\mathbf{1}_n \quad (9.94b)$$

Next, we assume that the n conductors are identical leading to

$$\mathbf{R} = r_0(s)\mathbf{1}_n + r_{i0}(s)\mathbf{U}_n \quad (9.95a)$$

$$\mathbf{L}_i = l_i(s)\mathbf{1}_n + l_{i0}(s)\mathbf{U}_n \quad (9.95b)$$

where $r_0(s)$ and $l_{i0}(s)$ represent the resistance and internal inductance, respectively, of the reference conductor and $\mathbf{1}_n$ is the $n \times n$ identity matrix and \mathbf{U}_n is the $n \times n$ unit matrix with ones in all positions. (Note: For a reference conductor not of finite size such as a ground plane, spreading of the return current will cause the off-diagonal

terms to be unequal so that the forms in (9.95) will not apply.) The equations to be diagonalized in (9.93) reduce to

$$(r(s) + sl_i(s))\mathbf{T}_V^{-1}\mathbf{T}_I + (r_0(s) + sl_{i0}(s))\mathbf{T}_V^{-1}\mathbf{U}_n\mathbf{T}_I + \frac{1}{v^2}s\mathbf{T}_V^{-1}\mathbf{C}^{-1}\mathbf{T}_I = \hat{\mathbf{Z}}_m(s) \quad (9.96a)$$

$$\left(\frac{\sigma(s)}{\varepsilon(s)} + s\right)\mathbf{T}_I^{-1}\mathbf{C}\mathbf{T}_V = \hat{\mathbf{Y}}_m(s) \quad (9.96b)$$

Hence, we must simultaneously diagonalize two matrices \mathbf{U}_n and \mathbf{C} . In addition, the transformations must be such that $\mathbf{T}_V^{-1}\mathbf{T}_I$ is also diagonal. We can simultaneously diagonalize \mathbf{U}_n and \mathbf{C} because both are real, symmetric, and positive definite (see Section 9.1.2.2). However, the product of the transformation matrices $\mathbf{T}_V^{-1}\mathbf{T}_I$ is not diagonal. Hence, we must make the following assumptions:

1. n identical conductors ignoring loss in the reference conductor, that is, $r_0(s) = 0$ and $l_{i0}(s) = 0$ or
2. $n + 1$ identical conductors, that is, $r_0(s) = r(s)$ and $l_{i0}(s) = l_i(s)$.

In the first case, the equations in (9.96) become

$$(r(s) + sl_i(s))\mathbf{T}_V^{-1}\mathbf{1}_n\mathbf{T}_I + \frac{1}{v^2}s\mathbf{T}_V^{-1}\mathbf{C}^{-1}\mathbf{T}_I = \hat{\mathbf{Z}}_m(s) \quad (9.97a)$$

$$\left(\frac{\sigma(s)}{\varepsilon(s)} + 1\right)\mathbf{T}_I^{-1}\mathbf{C}\mathbf{T}_V = \hat{\mathbf{Y}}_m(s) \quad (9.97b)$$

The transformations can be found that diagonalize all matrices in (9.97) as the following shows. Since \mathbf{C} is a real, symmetric matrix, it can be diagonalized by an orthogonal transformation, as $\mathbf{T}^t\mathbf{C}\mathbf{T} = \Lambda$ where Λ is an $n \times n$ diagonal matrix and $\mathbf{T}^{-1} = \mathbf{T}^t$ where the superscript t denotes the transpose of the matrix (see Section 9.1.2.1). Hence, we can choose $\mathbf{T}_V = \mathbf{T}$ and $\mathbf{T}_I^{-1} = \mathbf{T}^t$ so that $\mathbf{T}_I^{-1}\mathbf{C}\mathbf{T}_V = \mathbf{T}^t\mathbf{C}\mathbf{T} = \Lambda$ is diagonal. The matrix $\mathbf{T}_V^{-1}\mathbf{C}^{-1}\mathbf{T}_I$, is automatically diagonalized: $\mathbf{T}_V^{-1}\mathbf{C}^{-1}\mathbf{T}_I = \left(\mathbf{T}_I^{-1}\mathbf{C}\mathbf{T}_V\right)^{-1} = \Lambda^{-1}$. Observe that $\mathbf{T}_V^{-1}\mathbf{1}_n\mathbf{T}_I = \mathbf{T}_V^{-1}\mathbf{T}_I = \mathbf{T}^t(\mathbf{T}^t)^{-1} = \mathbf{1}_n$ is also automatically diagonalized.

In the second case the equations in (9.96) become

$$(r(s) + sl_i(s))\mathbf{T}_V^{-1}(\mathbf{1}_n + \mathbf{U}_n)\mathbf{T}_I + \frac{1}{v^2}s\mathbf{T}_V^{-1}\mathbf{C}^{-1}\mathbf{T}_I = \hat{\mathbf{Z}}_m(s) \quad (9.98a)$$

$$\left(\frac{\sigma(s)}{\varepsilon(s)} + 1\right)\mathbf{T}_I^{-1}\mathbf{C}\mathbf{T}_V = \hat{\mathbf{Y}}_m(s) \quad (9.98b)$$

As \mathbf{C} and $(\mathbf{1}_n + \mathbf{U}_n)$ are symmetric matrices and \mathbf{C} is positive definite, the transformations can be found that simultaneously diagonalize these two matrices as

$\mathbf{T}_I^{-1}\mathbf{C}\mathbf{T}_V = \Lambda_1$ and $\mathbf{T}_V^{-1}(\mathbf{I}_n + \mathbf{U}_n)\mathbf{T}_I = \Lambda_2$ where Λ_1 and Λ_2 are diagonal matrices resulting in uncoupled mode equations (see Section 9.1.2.2). The matrix, $\mathbf{T}_V^{-1}\mathbf{C}^{-1}\mathbf{T}_I$, is again automatically diagonalized: $\mathbf{T}_V^{-1}\mathbf{C}^{-1}\mathbf{T}_I = \left(\mathbf{T}_I^{-1}\mathbf{C}\mathbf{T}_V\right)^{-1} = \Lambda_1^{-1}$.

Suppose, we assume that the n conductors are identical and that only the nearest neighbor coupling exists, that is, only adjacent lines are coupled. In addition, if the self-inductances are equal and the self-capacitances are equal, and if the mutual capacitances are equal and the mutual inductances are equal, then the \mathbf{C} and \mathbf{L} matrices are in the very special form as tridiagonal Toeplitz matrices, and we can choose the mode transformations to be identical as $\mathbf{T}_V = \mathbf{T}_I = \mathbf{M}$ and $\mathbf{M}^{-1} = \mathbf{M}^t$ where t denotes the transpose [33, 34]. If all of the above special conditions are satisfied, then the \mathbf{C} and \mathbf{L} matrices are of the very special form:

$$\mathbf{L} = \begin{bmatrix} l & l_m & 0 & 0 & 0 \\ l_m & l & l_m & 0 & 0 \\ 0 & l_m & l & l_m & 0 \\ 0 & 0 & l_m & l & l_m \\ 0 & 0 & 0 & l_m & l \end{bmatrix} \quad (9.99a)$$

$$\mathbf{C} = \begin{bmatrix} c & c_m & 0 & 0 & 0 \\ c_m & c & c_m & 0 & 0 \\ 0 & c_m & c & c_m & 0 \\ 0 & 0 & c_m & c & c_m \\ 0 & 0 & 0 & c_m & c \end{bmatrix} \quad (9.99b)$$

The coupled microstrip line is an example of this type of structure (although there exists coupling to some degree between all pairs of conductors). Furthermore, the entries in \mathbf{M} are independent of the entries in \mathbf{C} and \mathbf{L} for this type of structure and are given in [33, 34]. This is a very special case of symmetry and is very similar to the case of cyclic-symmetric structures discussed in Section 7.2.2.5 of Chapter 7. Hence, the \mathbf{C} and \mathbf{L} matrices may be simultaneously diagonalized as $\mathbf{M}^t\mathbf{L}\mathbf{M} = \Lambda_L$ and $\mathbf{M}^t\mathbf{C}\mathbf{M} = \Lambda_C$ where Λ_L and Λ_C are diagonal matrices. Although this seems to decouple the general case of lines in an *inhomogeneous* medium, decoupling of the MTL equations requires that the conductor impedance matrices be of the form $\mathbf{R} + s\mathbf{L}_i = (r + sl_i)\mathbf{I}_n$, which means that we must also assume that *all conductors are identical and neglect the loss in the reference conductor*. In this case

$$\mathbf{T}_V^{-1}[\mathbf{R} + s\mathbf{L}_i]\mathbf{T}_I = (r + sl_i)\mathbf{M}^{-1}\mathbf{M} = (r + sl_i)\mathbf{I}_n \quad (9.100)$$

Since \mathbf{C} is a tridiagonal Toeplitz form, assuming only the nearest neighbor coupling seems to imply that we may also assume that \mathbf{G} is a tridiagonal Toeplitz form. If that assumption is made, then the same \mathbf{M} will also diagonalize \mathbf{G} as

$$\begin{aligned} \mathbf{T}_I^{-1}\mathbf{G}\mathbf{T}_V &= \mathbf{M}^t\mathbf{G}\mathbf{M} \\ &= \Lambda_3 \end{aligned} \quad (9.101)$$

So if we assume (1) only nearest neighbor coupling, (2) all conductors are identical and neglect the loss in the reference conductor, and (3) special cross-sectional symmetry that yields the special forms of \mathbf{L} and \mathbf{C} in (9.99), then the MTL equations can be decoupled for an *inhomogeneous medium* with frequency-independent transformations. Furthermore, the transformations are general and are independent of the entries in \mathbf{L} and \mathbf{C} .

The case of cyclic-symmetric structures discussed in Section 7.2.2.5 of Chapter 7 is decoupleable by frequency-independent transformations. Frequency-independent transformations are given for these structures in Section 7.2.2.5. Cyclic-symmetric structures require that the n conductors be identical, for example, identical wire radii and insulation types and thicknesses as shown in Figure 7.1. The reference conductor can be different. Common cases are the case of two identical wires at the same height above a ground plane as shown in Figure 7.2(a) or the symmetrical microstrip line shown in Figure 7.2(b). For both of these structures, the impedance and admittance matrices have the form

$$\hat{\mathbf{Z}}(s) = \begin{bmatrix} \hat{Z}_s(s) & \hat{Z}_m(s) \\ \hat{Z}_m(s) & \hat{Z}_s(s) \end{bmatrix} \quad (9.102a)$$

$$\hat{\mathbf{Y}}(s) = \begin{bmatrix} \hat{Y}_s(s) & \hat{Y}_m(s) \\ \hat{Y}_m(s) & \hat{Y}_s(s) \end{bmatrix} \quad (9.102b)$$

The frequency-independent transformation that diagonalizes these is

$$\mathbf{T} = \mathbf{T}_V = \mathbf{T}_I = \frac{1}{\sqrt{2}} \begin{bmatrix} 1 & 1 \\ 1 & -1 \end{bmatrix} \quad (9.103a)$$

$$\mathbf{T}^{-1} = \mathbf{T}_V^{-1} = \mathbf{T}_I^{-1} = \frac{1}{\sqrt{2}} \begin{bmatrix} 1 & 1 \\ 1 & -1 \end{bmatrix} \quad (9.103b)$$

When none of the above special cases exist, the MTL equations including frequency-dependent losses cannot, in general, be decoupled with frequency-independent transformations. However, the method of characteristics developed earlier for lossless lines can be extended, using convolution, to the lossy line case to develop a $2n$ -port model of the lossy line. Consider the frequency-domain solution of the MTL equations given in (7.30) of Chapter 7 written in Laplace-transformed form substituting $j\omega = s$:

$$\hat{\mathbf{V}}(z, s) = \hat{\mathbf{T}}_V \left(\mathbf{e}^{-\hat{\gamma}(s)z} \hat{\mathbf{V}}_m^+ + \mathbf{e}^{\hat{\gamma}(s)z} \hat{\mathbf{V}}_m^- \right) \quad (9.104a)$$

$$\hat{\mathbf{I}}(z, s) = \hat{\mathbf{Y}}_C(s) \hat{\mathbf{T}}_V \left(\mathbf{e}^{-\hat{\gamma}(s)z} \hat{\mathbf{V}}_m^+ - \mathbf{e}^{\hat{\gamma}(s)z} \hat{\mathbf{V}}_m^- \right) \quad (9.104b)$$

The characteristic admittance matrix $\hat{\mathbf{Y}}_C(s)$ is the inverse of the characteristic impedance matrix and is given in (7.32) as $\hat{\mathbf{Y}}_C(s) = \hat{\mathbf{Y}}(s) \hat{\mathbf{T}}_V \hat{\gamma}^{-1}(s) \hat{\mathbf{T}}_V^{-1}$. The $n \times$

n matrix $\hat{\mathbf{T}}_V$ diagonalizes the product of the frequency-domain per-unit-length impedance and admittance matrices as $\hat{\mathbf{T}}_V^{-1} \hat{\mathbf{Z}}(s) \hat{\mathbf{Y}}(s) \hat{\mathbf{T}}_V = \hat{\gamma}^2(s)$ where the per-unit-length impedance and admittance matrices of the line are $\hat{\mathbf{Z}}(s) = \mathbf{R}(s) + s\mathbf{L}_i(s) + s\mathbf{L}$ and $\hat{\mathbf{Y}}(s) = \mathbf{G}(s) + s\mathbf{C}$. All matrices and vectors are, in general, frequency dependent, that is, functions of s . Multiplying (9.104b) by the characteristic impedance matrix, $\hat{\mathbf{Z}}_C(s) = \hat{\mathbf{Y}}_C^{-1}(s)$, evaluating at $z = 0$ and $z = \mathcal{L}$, and adding and subtracting the resulting equations gives

$$\hat{\mathbf{V}}(0, s) - \hat{\mathbf{Z}}_C(s) \hat{\mathbf{I}}(0, s) = \left[\hat{\mathbf{T}}_V \mathbf{e}^{-\hat{\gamma}(s)\mathcal{L}} \hat{\mathbf{T}}_V^{-1} \right] \left[\hat{\mathbf{V}}(\mathcal{L}, s) - \hat{\mathbf{Z}}_C(s) \hat{\mathbf{I}}(\mathcal{L}, s) \right] \quad (9.105a)$$

$$\hat{\mathbf{V}}(\mathcal{L}, s) + \hat{\mathbf{Z}}_C(s) \hat{\mathbf{I}}(\mathcal{L}, s) = \left[\hat{\mathbf{T}}_V \mathbf{e}^{-\hat{\gamma}(s)\mathcal{L}} \hat{\mathbf{T}}_V^{-1} \right] \left[\hat{\mathbf{V}}(0, s) + \hat{\mathbf{Z}}_C(s) \hat{\mathbf{I}}(0, s) \right] \quad (9.105b)$$

This gives the $2n$ -port equivalent circuit shown in Figure 9.8. Now, we convert to the time domain. Taking the inverse Laplace transform gives

$$\mathbf{V}(0, t) - \mathbf{z}_C(t) * \mathbf{I}(0, t) = \mathbf{h}(t) * [\mathbf{V}(\mathcal{L}, t) - \mathbf{z}_C(t) * \mathbf{I}(\mathcal{L}, t)] \quad (9.106a)$$

$$\mathbf{V}(\mathcal{L}, t) + \mathbf{z}_C(t) * \mathbf{I}(\mathcal{L}, t) = \mathbf{h}(t) * [\mathbf{V}(0, t) + \mathbf{z}_C(t) * \mathbf{I}(0, t)] \quad (9.106b)$$

where $\mathbf{z}_C(t) \Leftrightarrow \hat{\mathbf{Z}}_C(s)$ and $\mathbf{h}(t) \Leftrightarrow \hat{\mathbf{T}}_V \mathbf{e}^{-\hat{\gamma}(s)\mathcal{L}} \hat{\mathbf{T}}_V^{-1}$ and $*$ denotes convolution. This gives another form of the generalized method of characteristics (without the necessity for the mode transformations) as the convolutions of the time-domain characteristic impedance matrix $\mathbf{z}_C(t)$ and the time-domain delay matrix $\mathbf{h}(t)$ with port currents and voltages. The structure of this equivalent circuit in Figure 9.8 is virtually identical to that shown in Figure 8.9 for two-conductor lossless lines but with coupling between all lines. An alternative representation is obtained by premultiplying (9.105) by the characteristic admittance matrix $\hat{\mathbf{Y}}_C = \hat{\mathbf{Z}}_C^{-1}$ and rearranging to yield

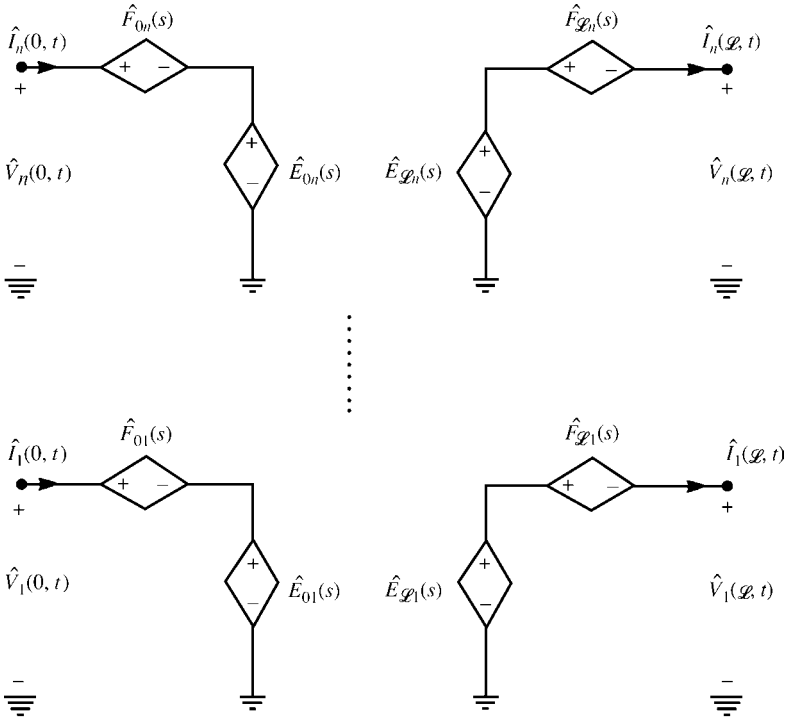
$$\hat{\mathbf{I}}(0, s) - \hat{\mathbf{Y}}_C(s) \hat{\mathbf{V}}(0, s) = \left[\hat{\mathbf{Y}}_C(s) \hat{\mathbf{T}}_V \mathbf{e}^{-\hat{\gamma}(s)\mathcal{L}} \hat{\mathbf{T}}_V^{-1} \hat{\mathbf{Z}}_C(s) \right] \left[\hat{\mathbf{I}}(\mathcal{L}, s) - \hat{\mathbf{Y}}_C(s) \hat{\mathbf{V}}(\mathcal{L}, s) \right] \quad (9.107a)$$

$$\hat{\mathbf{I}}(\mathcal{L}, s) + \hat{\mathbf{Y}}_C(s) \hat{\mathbf{V}}(\mathcal{L}, s) = \left[\hat{\mathbf{Y}}_C(s) \hat{\mathbf{T}}_V \mathbf{e}^{-\hat{\gamma}(s)\mathcal{L}} \hat{\mathbf{T}}_V^{-1} \hat{\mathbf{Z}}_C(s) \right] \left[\hat{\mathbf{I}}(0, s) + \hat{\mathbf{Y}}_C(s) \hat{\mathbf{V}}(0, s) \right] \quad (9.107b)$$

This gives the $2n$ -port equivalent circuit shown in Figure 9.9. Now, we convert to the time domain. Taking the inverse Laplace transform gives

$$\mathbf{I}(0, t) - \mathbf{y}_C(t) * \mathbf{V}(0, t) = \mathbf{f}(t) * [\mathbf{I}(\mathcal{L}, t) - \mathbf{y}_C(t) * \mathbf{V}(\mathcal{L}, t)] \quad (9.108a)$$

$$\mathbf{I}(\mathcal{L}, t) + \mathbf{y}_C(t) * \mathbf{V}(\mathcal{L}, t) = \mathbf{f}(t) * [\mathbf{I}(0, t) + \mathbf{y}_C(t) * \mathbf{V}(0, t)] \quad (9.108b)$$



$$\hat{F}_{0i}(s) = \sum_{k=1}^n [\hat{\mathbf{Z}}_C(s)]_{ik} [\hat{\mathbf{I}}(0, s)]_k$$

$$\hat{E}_{0i}(s) = \sum_{k=1}^n [\hat{\mathbf{T}}_V e^{-\hat{\gamma}z} \mathbf{T}_V^{-1}]_{ik} [\hat{\mathbf{V}}(z, s) - \hat{\mathbf{Z}}_C(s) \hat{\mathbf{I}}(z, s)]_k$$

$$\hat{F}_{zi}(s) = \sum_{k=1}^n [\hat{\mathbf{Z}}_C(s)]_{ik} [\hat{\mathbf{I}}(z, s)]_k$$

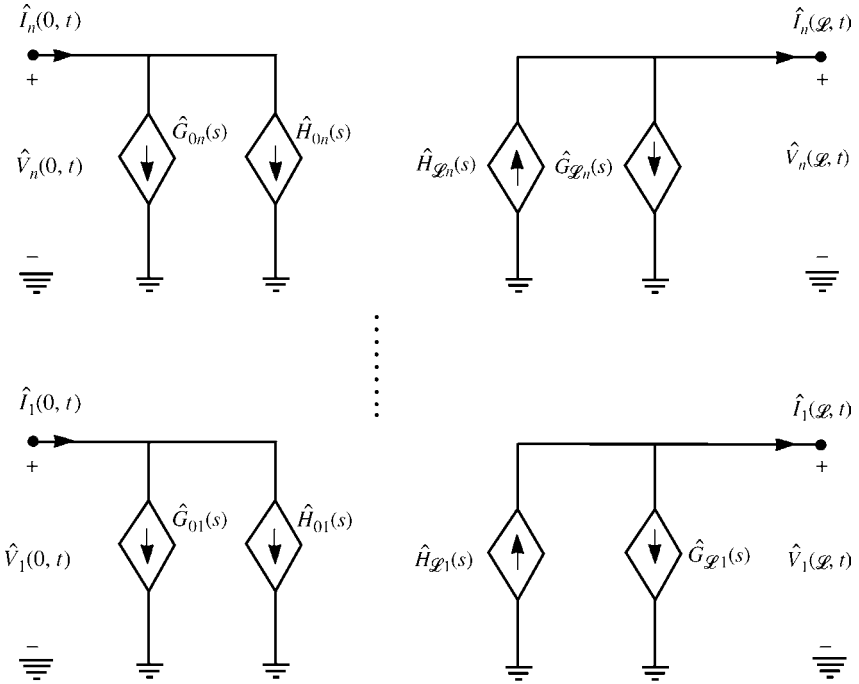
$$\hat{E}_{zi}(s) = \sum_{k=1}^n [\hat{\mathbf{T}}_V e^{-\hat{\gamma}z} \mathbf{T}_V^{-1}]_{ik} [\hat{\mathbf{V}}(0, s) + \hat{\mathbf{Z}}_C(s) \hat{\mathbf{I}}(0, s)]_k$$

FIGURE 9.8 An alternative form of the generalized method of characteristics.

where $\mathbf{y}_C(t) \Leftrightarrow \hat{\mathbf{Y}}_C(s)$ and $\mathbf{f}(t) \Leftrightarrow \hat{\mathbf{Y}}_C(s) \hat{\mathbf{T}}_V e^{-\hat{\gamma}(s)z} \hat{\mathbf{T}}_V^{-1} \hat{\mathbf{Z}}_C(s)$ and * denotes convolution. This gives another form of the generalized method of characteristics (without the necessity of mode transformations) as the convolutions of the time-domain characteristic admittance matrix $\mathbf{y}_C(t)$ and the time-domain delay matrix $\mathbf{f}(t)$ with port currents and voltages.

Alternative representations of these in terms of the transformation matrix $\hat{\mathbf{T}}_I$ that diagonalizes the product $\hat{\mathbf{Y}}(s) \hat{\mathbf{Z}}(s)$ as $\hat{\mathbf{T}}_I^{-1} \hat{\mathbf{Y}}(s) \hat{\mathbf{Z}}(s) \hat{\mathbf{T}}_I = \gamma^2$ are obtained from the representation in (7.25) of Chapter 7:

$$\hat{\mathbf{V}}(z, s) = \hat{\mathbf{Z}}_C(s) \hat{\mathbf{T}}_I \left(e^{-\hat{\gamma}(s)z} \hat{\mathbf{I}}_m^+ + e^{\hat{\gamma}(s)z} \hat{\mathbf{I}}_m^- \right) \tag{9.109a}$$



$$\hat{G}_{0i}(s) = \sum_{k=1}^n [\hat{\mathbf{Y}}_C(s)]_{ik} [\hat{\mathbf{V}}(0, s)]_k$$

$$\hat{H}_{0i}(s) = \sum_{k=1}^n [\hat{\mathbf{Y}}_C(s) \hat{\mathbf{T}}_V e^{-\hat{\gamma} \mathcal{L}} \hat{\mathbf{T}}_V^{-1} \hat{\mathbf{Z}}_C(s)]_{ik} [\hat{\mathbf{I}}(\mathcal{L}, s) - \hat{\mathbf{Y}}_C(s) \hat{\mathbf{V}}(\mathcal{L}, s)]_k$$

$$\hat{G}_{\mathcal{L}i}(s) = \sum_{k=1}^n [\hat{\mathbf{Y}}_C(s)]_{ik} [\hat{\mathbf{V}}(\mathcal{L}, s)]_k$$

$$\hat{H}_{\mathcal{L}i}(s) = \sum_{k=1}^n [\hat{\mathbf{Y}}_C(s) \hat{\mathbf{T}}_V e^{-\hat{\gamma} \mathcal{L}} \hat{\mathbf{T}}_V^{-1} \hat{\mathbf{Z}}_C(s)]_{ik} [\hat{\mathbf{I}}(0, s) + \hat{\mathbf{Y}}_C(s) \hat{\mathbf{V}}(0, s)]_k$$

FIGURE 9.9 An alternative form of the generalized method of characteristics.

$$\hat{\mathbf{I}}(z, s) = \hat{\mathbf{T}}_I \left(\mathbf{e}^{-\hat{\gamma}(s)z} \hat{\mathbf{I}}_m^+ - \mathbf{e}^{\hat{\gamma}(s)z} \hat{\mathbf{I}}_m^- \right) \tag{9.109b}$$

Eliminating the vectors of undetermined constants, $\hat{\mathbf{I}}_m^\pm$, as above gives

$$\hat{\mathbf{V}}(0, s) - \hat{\mathbf{Z}}_C(s) \hat{\mathbf{I}}(0, s) = \left[\hat{\mathbf{Z}}_C(s) \hat{\mathbf{T}}_I \mathbf{e}^{-\hat{\gamma}(s)\mathcal{L}} \hat{\mathbf{T}}_I^{-1} \hat{\mathbf{Z}}_C^{-1}(s) \right] [\hat{\mathbf{V}}(\mathcal{L}, s) - \hat{\mathbf{Z}}_C(s) \hat{\mathbf{I}}(\mathcal{L}, s)] \tag{9.110a}$$

$$\hat{\mathbf{V}}(\mathcal{L}, s) + \hat{\mathbf{Z}}_C(s) \hat{\mathbf{I}}(\mathcal{L}, s) = \left[\hat{\mathbf{Z}}_C(s) \hat{\mathbf{T}}_I \mathbf{e}^{-\hat{\gamma}(s)\mathcal{L}} \hat{\mathbf{T}}_I^{-1} \hat{\mathbf{Z}}_C^{-1}(s) \right] [\hat{\mathbf{V}}(0, s) + \hat{\mathbf{Z}}_C(s) \hat{\mathbf{I}}(0, s)]$$

(9.110b)

and, after multiplying by $\hat{\mathbf{Y}}_C = \hat{\mathbf{Z}}_C^{-1}$, alternatively

$$\hat{\mathbf{I}}(0, s) - \hat{\mathbf{Y}}_C(s)\hat{\mathbf{V}}(0, s) = \left[\hat{\mathbf{T}}_I e^{-\hat{\gamma}(s)\mathcal{L}} \hat{\mathbf{T}}_I^{-1} \right] \left[\hat{\mathbf{I}}(\mathcal{L}, s) - \hat{\mathbf{Y}}_C(s)\hat{\mathbf{V}}(\mathcal{L}, s) \right] \quad (9.111a)$$

$$\hat{\mathbf{I}}(\mathcal{L}, s) + \hat{\mathbf{Y}}_C(s)\hat{\mathbf{V}}(\mathcal{L}, s) = \left[\hat{\mathbf{T}}_I e^{-\hat{\gamma}(s)\mathcal{L}} \hat{\mathbf{T}}_I^{-1} \right] \left[\hat{\mathbf{I}}(0, s) + \hat{\mathbf{Y}}_C(s)\hat{\mathbf{V}}(0, s) \right] \quad (9.111b)$$

Using the methods in [B.25], it can be shown that

$$\hat{\mathbf{Z}}_C(s)\hat{\mathbf{T}}_I e^{-\hat{\gamma}(s)\mathcal{L}} \hat{\mathbf{T}}_I^{-1} \hat{\mathbf{Z}}_C^{-1}(s) = \hat{\mathbf{T}}_V e^{-\hat{\gamma}(s)\mathcal{L}} \hat{\mathbf{T}}_V^{-1} \quad (9.112a)$$

$$\hat{\mathbf{Y}}_C(s)\hat{\mathbf{T}}_V e^{-\hat{\gamma}(s)\mathcal{L}} \hat{\mathbf{T}}_V^{-1} \hat{\mathbf{Z}}_C(s) = \hat{\mathbf{T}}_I e^{-\hat{\gamma}(s)\mathcal{L}} \hat{\mathbf{T}}_I^{-1} \quad (9.112b)$$

This demonstrates (as expected) that (9.105) and (9.110) are equivalent as are (9.107) and (9.111), even though one set of equations involves $\hat{\mathbf{T}}_V$ and the other set of equations involves $\hat{\mathbf{T}}_I$. The article in [B.25] demonstrates the hazards in using quantities that involve *both* $\hat{\mathbf{T}}_V$ and $\hat{\mathbf{T}}_I$ rather than involving *only* $\hat{\mathbf{T}}_V$ or $\hat{\mathbf{T}}_I$. This has caused considerable confusion throughout the literature and the reader should be alert to these seemingly equivalent definitions. Many of the publications in the references use notation such as \mathbf{S}_i and \mathbf{S}_v when not only are these different from the above $\hat{\mathbf{T}}_V$ and $\hat{\mathbf{T}}_I$ but, even though it may be the case that $\mathbf{S}_v = \hat{\mathbf{T}}_V$, it also turns out that $\mathbf{S}_i \neq \hat{\mathbf{T}}_I$ and \mathbf{S}_i has an entirely different meaning.

9.2.5 Model Order Reduction (MOR) Methods

High-density interconnects in today's integrated circuits and digital systems contain an enormous number of coupled MTLs. The computational burden in using the above methods is becoming intractable. Hence, there is a need to reduce the order of the representation of these structures. These representations generally fit into the category of macromodels. Transfer functions of MTLs involve transcendental functions that have an infinite number of roots. Hence, these transfer functions will have an infinite number of poles making the inverse transforms impossible to compute. However, if we can represent these transfer functions with only a smaller, finite number of *dominant poles*, then the computational burden is reduced. This is generally referred to as Model Order Reduction or MOR. In this final section of the chapter, we will discuss some of the many MOR methods such as Pade approximations, asymptotic waveform evaluation or AWE, complex frequency hopping or CFH, and vector fitting or VF along with the synthesis of lumped equivalent circuits. The literature is rapidly expanding in terms of MOR techniques.

9.2.5.1 Pade Approximation of the Matrix Exponential The MTL equations in Laplace transform form for a lossy line are coupled, ordinary differential equations

given in (9.69) as

$$\frac{d}{dz} \hat{\mathbf{V}}(z, s) = -(\hat{\mathbf{Z}}_i(s) + s\mathbf{L}) \hat{\mathbf{I}}(z, s) \quad (9.69a)$$

$$\frac{d}{dz} \hat{\mathbf{I}}(z, s) = -(\hat{\mathbf{G}}(s) + s\mathbf{C}) \hat{\mathbf{V}}(z, s) \quad (9.69b)$$

where $\hat{\mathbf{Z}}_i(s) = \mathbf{R}(s) + s\mathbf{L}_i(s)$ is the internal impedance matrix for the conductor losses. These can be put into the so-called state-variable form as [13, 14]

$$\frac{d}{dz} \hat{\mathbf{X}}(z, s) = \hat{\mathbf{A}}(s) \hat{\mathbf{X}}(z, s) \quad (9.113a)$$

where $\hat{\mathbf{X}}(z, s)$ is a $2n \times 1$ vector containing the voltages and currents of the line as

$$\hat{\mathbf{X}}(z, s) = \begin{bmatrix} \hat{\mathbf{V}}(z, s) \\ \hat{\mathbf{I}}(z, s) \end{bmatrix} \quad (9.113b)$$

$\hat{\mathbf{A}}(s)$ is a $2n \times 2n$ matrix containing the line per-unit-length parameters as

$$\hat{\mathbf{A}}(s) = - \begin{bmatrix} \mathbf{0}_n & (\mathbf{R} + s\mathbf{L}) \\ (\mathbf{G} + s\mathbf{C}) & \mathbf{0}_n \end{bmatrix} \quad (9.113c)$$

and $\mathbf{0}_n$ is the $n \times n$ zero matrix with zeros in all positions. In the following, we will, for the purposes of economy of notation, not continue to place the caret over the transformed per-unit-length parameters nor indicate that they are functions of s . Nor will we explicitly show the separation of the internal impedance into the resistance and internal inductance. All of this is implied.

The solution to (9.113) is well known to be [A.2,13, 14]

$$\hat{\mathbf{X}}(\mathcal{L}, s) = \mathbf{e}^{\hat{\mathbf{A}}(s)\mathcal{L}} \hat{\mathbf{X}}(0, s) \quad (9.114)$$

where \mathcal{L} is the total line length. The $2n \times 2n$ matrix $\mathbf{e}^{\hat{\mathbf{A}}(s)\mathcal{L}}$ is referred to in the circuits and automatic controls literature as the *state-transition* matrix. In our vernacular, this is equivalent to the *chain-parameter* matrix:

$$\begin{bmatrix} \hat{\mathbf{V}}(\mathcal{L}) \\ \hat{\mathbf{I}}(\mathcal{L}) \end{bmatrix} = \underbrace{\mathbf{e}^{\hat{\mathbf{A}}(s)\mathcal{L}}}_{\hat{\Phi}(s, \mathcal{L})} \begin{bmatrix} \hat{\mathbf{V}}(0) \\ \hat{\mathbf{I}}(0) \end{bmatrix} \quad (9.115)$$

The state-transition or chain-parameter matrix has the following infinite series expansion [A.2,13, 14]

$$\mathbf{e}^{\hat{\mathbf{Z}}} = \mathbf{1}_n + \frac{1}{1!} \hat{\mathbf{Z}} + \frac{1}{2!} \hat{\mathbf{Z}}^2 + \frac{1}{3!} \hat{\mathbf{Z}}^3 + \dots \quad (9.116a)$$

and we denote the total line parameter matrix as

$$\hat{\mathbf{Z}} = \hat{\mathbf{A}}(s)\mathcal{L} \tag{9.116b}$$

In Section 8.2.6 of the previous chapter, we discussed using the Pade method how to approximate a function $F(s)$ as a rational function consisting of the ratio of N th order polynomials in s as

$$F(s) \cong F(0) \frac{1 + a_1s + \dots + a_Ns^N}{1 + b_1s + \dots + b_Ns^N} \tag{9.117}$$

where $F(0)$ is the dc response at $s = 0$. We can determine the $2N$ parameters in this representation, $a_1, \dots, a_N, b_1, \dots, b_N$, by matching it to a Maclaurin expansion about $s = 0$ as an infinite series in s :

$$F(s) = F(0) \left[1 + m_1s + m_2s^2 + \dots \right] \tag{9.118}$$

and the m_i are said to be the “moments” of $f(t)$. Equating (9.117) and (9.118) and multiplying both sides by the denominator gives

$$(1 + b_1s + \dots + b_Ns^N) \left(1 + m_1s + m_2s^2 + \dots \right) = 1 + a_1s + \dots + a_Ns^N \tag{9.119}$$

Matching powers of s gives the matrix equations given in equations (8.215) of Chapter 8:

$$\begin{bmatrix} m_1 & m_2 & m_3 & \dots & m_N \\ m_2 & m_3 & m_4 & \dots & m_{N+1} \\ m_3 & m_4 & m_5 & \dots & m_{N+2} \\ \vdots & \vdots & \vdots & \vdots & \vdots \\ m_N & m_{N+1} & m_{N+2} & \dots & m_{2N-1} \end{bmatrix} \begin{bmatrix} b_N \\ b_{N-1} \\ b_{N-2} \\ \vdots \\ b_1 \end{bmatrix} = - \begin{bmatrix} m_{N+1} \\ m_{N+2} \\ m_{N+3} \\ \vdots \\ m_{2N} \end{bmatrix} \tag{8.215a}$$

$$\begin{bmatrix} a_1 \\ a_2 \\ a_3 \\ \vdots \\ a_N \end{bmatrix} = \begin{bmatrix} 1 & 0 & 0 & \dots & 0 \\ m_1 & 1 & 0 & \dots & 0 \\ m_2 & m_1 & 1 & \dots & 0 \\ \vdots & \vdots & \vdots & \vdots & \vdots \\ m_{N-1} & m_{N-2} & m_{N-3} & \dots & 1 \end{bmatrix} \begin{bmatrix} b_1 \\ b_2 \\ b_3 \\ \vdots \\ b_N \end{bmatrix} + \begin{bmatrix} m_1 \\ m_2 \\ m_3 \\ \vdots \\ m_N \end{bmatrix} \tag{8.215b}$$

The b_i denominator coefficients for $i = 1, \dots, N$ can be obtained from (8.215a), and the a_i numerator coefficients for $i = 1, \dots, N$ can then be obtained from (8.215b). (See Section 8.2.6 of Chapter 8 for this development.) We can use this result to obtain a Pade representation of the chain-parameter matrix. Each entry in the $2n \times 2n$ chain-

parameter matrix is represented as a rational function of s as a ratio of polynomials in s :

$$\mathbf{e}^{\hat{\mathbf{Z}}} = \begin{bmatrix} F_{11}(s) & \cdots & F_{1(2n)}(s) \\ \vdots & \ddots & \vdots \\ F_{(2n)1}(s) & \cdots & F_{(2n)(2n)}(s) \end{bmatrix} \quad (9.120)$$

Rather than expanding the individual entries, we can obtain this in matrix form as

$$\hat{\mathbf{P}}(\hat{\mathbf{Z}}) \mathbf{e}^{\hat{\mathbf{Z}}} = \hat{\mathbf{Q}}(\hat{\mathbf{Z}}) \quad (9.121a)$$

or

$$\mathbf{e}^{\hat{\mathbf{Z}}} = \hat{\mathbf{P}}^{-1}(\hat{\mathbf{Z}}) \hat{\mathbf{Q}}(\hat{\mathbf{Z}}) \quad (9.121b)$$

Comparing (9.116a) to (9.118) indicates that the “moments” of the expansion will be in the form of factorials, that is, $m_i = 1/i!$. A closed-form solution for the Pade expansion polynomials can be obtained as powers of $\hat{\mathbf{Z}}$ [35–37]

$$\hat{\mathbf{Q}}(\hat{\mathbf{Z}}) = \sum_{k=0}^N \frac{(2N-k)!N!}{(2N)!k!(N-k)!} \hat{\mathbf{Z}}^k \quad (9.122a)$$

$$\hat{\mathbf{P}}(\hat{\mathbf{Z}}) = \sum_{k=0}^N \frac{(2N-k)!N!}{(2N)!k!(N-k)!} (-\hat{\mathbf{Z}})^k \quad (9.122b)$$

The general result for the orders of the numerator and denominator polynomials not being the same is given in [35–37]. In addition, it is shown in [36] that these representations and the associated model are passive. Passivity is a very important criterion for any simulation model and means that the system cannot generate more energy than it absorbs and that no passive termination on the system will make the system unstable. Recall from Chapter 8 that the Pade method may generate polynomials with unstable poles, that is, the denominator roots have positive real parts. For the above development, we are assured that no such instability will be generated. Furthermore, (9.122) gives a *closed-form result* for the expansions.

9.2.5.2 Asymptotic Waveform Evaluation (AWE) The AWE method is also a moment-matching technique [35–39]. The method seeks to expand the Laplace-transformed voltages and currents in power series in the Laplace transform variable s , that is, in terms of moments. By matching matrix coefficients of corresponding powers of s , the MTL equations are transformed into a series of differential equations that can be solved iteratively or interfaced with a conventional circuit simulator such as SPICE.

For example, the chain-parameter matrix can be solved this way by writing out (9.116a) as

$$\begin{aligned}
 \mathbf{e}^{\hat{\mathbf{Z}}} &= \mathbf{1}_n + \frac{1}{1!} \hat{\mathbf{Z}} + \frac{1}{2!} \hat{\mathbf{Z}}^2 + \frac{1}{3!} \hat{\mathbf{Z}}^3 + \dots \\
 &= \mathbf{1}_n + \frac{1}{1!} \left(\begin{bmatrix} \mathbf{0}_n & \mathbf{R} \\ \mathbf{G} & \mathbf{0}_n \end{bmatrix} + s \begin{bmatrix} \mathbf{0}_n & \mathbf{L} \\ \mathbf{C} & \mathbf{0}_n \end{bmatrix} \right) \\
 &\quad + \frac{1}{2!} \left(\begin{bmatrix} \mathbf{0}_n & \mathbf{R} \\ \mathbf{G} & \mathbf{0}_n \end{bmatrix} + s \begin{bmatrix} \mathbf{0}_n & \mathbf{L} \\ \mathbf{C} & \mathbf{0}_n \end{bmatrix} \right)^2 + \dots
 \end{aligned} \tag{9.123}$$

Expanding this and grouping terms that are associated with powers of s and comparing to a moment expansion as

$$\mathbf{e}^{\hat{\mathbf{Z}}} = \hat{\mathbf{F}}_0 + \hat{\mathbf{F}}_1 s + \hat{\mathbf{F}}_2 s^2 + \dots \tag{9.124}$$

gives recursion relations for the “moment matrices” $\hat{\mathbf{F}}_i$ [35].

Similarly, the transformed MTL equations in state-variable form given in (9.113) can be diagonalized as [41]

$$\underbrace{\begin{bmatrix} \hat{\mathbf{A}}(s) & \hat{\mathbf{B}}(s) \\ \hat{\mathbf{A}}(s) & -\hat{\mathbf{B}}(s) \end{bmatrix}}_{\hat{\mathbf{T}}(s)} \begin{bmatrix} \mathbf{0}_n & (\mathbf{R} + s\mathbf{L}) \\ \mathbf{G} + s\mathbf{C} & \mathbf{0}_n \end{bmatrix} = \begin{bmatrix} -\hat{\gamma} & \mathbf{0}_n \\ \mathbf{0}_n & \hat{\gamma} \end{bmatrix} \underbrace{\begin{bmatrix} \hat{\mathbf{A}}(s) & \hat{\mathbf{B}}(s) \\ \hat{\mathbf{A}}(s) & -\hat{\mathbf{B}}(s) \end{bmatrix}}_{\hat{\mathbf{T}}(s)} \tag{9.125}$$

where $\hat{\gamma}$ is the diagonal matrix of propagation constants and

$$\hat{\mathbf{A}}(s)(\mathbf{R} + s\mathbf{L})\hat{\mathbf{B}}^{-1}(s) = -\hat{\gamma} \tag{9.126a}$$

$$\hat{\mathbf{B}}(s)(\mathbf{G} + s\mathbf{C})\hat{\mathbf{A}}^{-1}(s) = -\hat{\gamma} \tag{9.126b}$$

or, in other words,

$$\hat{\mathbf{A}}(s)(\mathbf{R} + s\mathbf{L})(\mathbf{G} + s\mathbf{C})\hat{\mathbf{A}}^{-1}(s) = -\hat{\gamma}^2 \tag{9.127a}$$

$$\hat{\mathbf{B}}(s)(\mathbf{G} + s\mathbf{C})(\mathbf{R} + s\mathbf{L})\hat{\mathbf{B}}^{-1}(s) = \hat{\gamma}^2 \tag{9.127b}$$

From this we identify the modal transformation matrices of Chapter 7 as

$$\hat{\mathbf{A}}(s) = \hat{\mathbf{T}}_V^{-1} \tag{9.128a}$$

and

$$\hat{\mathbf{B}}(s) = \hat{\mathbf{T}}_V^{-1} \hat{\mathbf{Z}}_C(s) \tag{9.128b}$$

and $\hat{\mathbf{Z}}_C(s)$ is the characteristic impedance matrix. Hence, the solution of the first-order state-variable matrices in (9.114) becomes

$$\begin{bmatrix} \hat{\mathbf{V}}(\mathcal{L}, s) \\ \hat{\mathbf{I}}(\mathcal{L}, s) \end{bmatrix} = \begin{bmatrix} \hat{\mathbf{A}}(s) & \hat{\mathbf{B}}(s) \\ \hat{\mathbf{A}}(s) & -\hat{\mathbf{B}}(s) \end{bmatrix}^{-1} \begin{bmatrix} \mathbf{e}^{-\hat{\gamma}(s)\mathcal{L}} & \mathbf{0}_n \\ \mathbf{0}_n & \mathbf{e}^{-\hat{\gamma}(s)\mathcal{L}} \end{bmatrix} \begin{bmatrix} \hat{\mathbf{A}}(s) & \hat{\mathbf{B}}(s) \\ \hat{\mathbf{A}}(s) & -\hat{\mathbf{B}}(s) \end{bmatrix} \begin{bmatrix} \hat{\mathbf{V}}(0, s) \\ \hat{\mathbf{I}}(0, s) \end{bmatrix} \quad (9.129)$$

and the chain-parameter matrix has been generated. This gives the form of the solution that is identical to (9.107):

$$\hat{\mathbf{I}}(0, s) - \hat{\mathbf{Y}}_C(s)\hat{\mathbf{V}}(0, s) = \left[\hat{\mathbf{B}}^{-1}(s)\mathbf{e}^{-\hat{\gamma}(s)\mathcal{L}}\hat{\mathbf{B}}(s) \right] \left[\hat{\mathbf{I}}(\mathcal{L}, s) - \hat{\mathbf{Y}}_C(s)\hat{\mathbf{V}}(\mathcal{L}, s) \right] \quad (9.130a)$$

$$\hat{\mathbf{I}}(\mathcal{L}, s) + \hat{\mathbf{Y}}_C(s)\hat{\mathbf{V}}(\mathcal{L}, s) = \left[\hat{\mathbf{B}}^{-1}(s)\mathbf{e}^{-\hat{\gamma}(s)\mathcal{L}}\hat{\mathbf{B}}(s) \right] \left[\hat{\mathbf{I}}(0, s) + \hat{\mathbf{Y}}_C(s)\hat{\mathbf{V}}(0, s) \right] \quad (9.130b)$$

and $\hat{\mathbf{Y}}_C(s)$ is the characteristic admittance matrix. Hence, the solution is representable again in the form of the generalized method of characteristics as shown in Figure 9.9.

As an alternative to the use of Pade approximations to obtain the time-domain representations of $\hat{\mathbf{Y}}_C(s)$ and $\mathbf{e}^{-\hat{\gamma}(s)\mathcal{L}}$, we represent the various matrices in terms of moments about $s = 0$ as

$$\hat{\mathbf{A}}(s) = \mathbf{A}_0 + \mathbf{A}_1 s + \mathbf{A}_2 s^2 + \dots \quad (9.131a)$$

$$\hat{\mathbf{B}}(s) = \mathbf{B}_0 + \mathbf{B}_1 s + \mathbf{B}_2 s^2 + \dots \quad (9.131b)$$

$$\hat{\gamma}(s) = \gamma_0 + \gamma_1 s + \gamma_2 s^2 + \dots \quad (9.131c)$$

$$\hat{\mathbf{Y}}_C(s) = \mathbf{Y}_{C0} + \mathbf{Y}_{C1} s + \mathbf{Y}_{C2} s^2 + \dots \quad (9.131d)$$

Substituting these moment expansions into (9.125) gives a recursion relation for the moments as [41]

$$\begin{aligned} \begin{bmatrix} \mathbf{A}_k & \mathbf{B}_k \\ \mathbf{A}_k & -\mathbf{B}_k \end{bmatrix} \begin{bmatrix} \mathbf{0}_n & \mathbf{R} \\ \mathbf{G} & \mathbf{0}_n \end{bmatrix} + \begin{bmatrix} \mathbf{A}_{k-1} & \mathbf{B}_{k-1} \\ \mathbf{A}_{k-1} & -\mathbf{B}_{k-1} \end{bmatrix} \begin{bmatrix} \mathbf{0}_n & \mathbf{L} \\ \mathbf{C} & \mathbf{0}_n \end{bmatrix} \\ = \sum_{i=0}^k \begin{bmatrix} -\gamma_i & \mathbf{0}_n \\ \mathbf{0}_n & \gamma_i \end{bmatrix} \begin{bmatrix} \mathbf{A}_{k-1} & \mathbf{B}_{k-1} \\ \mathbf{A}_{k-1} & -\mathbf{B}_{k-1} \end{bmatrix} \end{aligned} \quad (9.132)$$

The moments of the characteristic admittance matrix can be obtained by substituting the moment expansion given in (9.131) into (9.128)

$$\hat{\mathbf{B}}(s)\hat{\mathbf{Y}}_C = \hat{\mathbf{A}}(s) \quad (9.133)$$

to yield the recursion relation [41]

$$\sum_{i=0}^k \mathbf{B}_i \mathbf{Y}_{C(k-i)} = \mathbf{A}_k \quad (9.134)$$

The moments of the propagation function $\mathbf{e}^{-\hat{\gamma}(s)\mathcal{L}}$ can be similarly obtained. The time-domain results can be put in a form allowing a recursive convolution scheme to be implemented and can be stenciled into the modified nodal admittance (MNA) matrix of SPICE [43].

9.2.5.3 Complex Frequency Hopping (CFH) The transfer functions of transmission lines involve transcendental functions and therefore have an infinite number of poles. However, not all of these poles need to be used in a macromodel of the line as shown in the pole plot in Figure 9.10. The horizontal axis is the real part of $s = \sigma + j\omega$ and the vertical axis is the imaginary part. For example, two real poles $s_1 = -1$ and $s_2 = -1000$ will have time-domain contributions in the response of e^{-t} and e^{-1000t} , respectively. The response due to the first pole $s_1 = -1$ will take a much longer time to decay to zero than the response to the second pole $s_2 = -1000$. Hence, poles that are further from the imaginary axis, $s = j\omega$, are less important in determining the time-domain response accurately. Conversely, the poles that are closer to the $s = j\omega$ axis are more important in obtaining an accurate time-domain response and are called the *dominant poles*. It is important to determine only the dominant poles in order to obtain an accurate time-domain macromodel.

The Pade approximation is accurate only in a region of convergence about the expansion point. For example, if we expand the function in moments about $s = 0$ as in (9.118)

$$F(s) = F(0) \left[1 + m_1 s + m_2 s^2 + \dots \right] \quad (9.118)$$

then the resulting Pade approximation in (9.117)

$$F(s) \cong F(0) \frac{1 + a_1 s + \dots + a_N s^N}{1 + b_1 s + \dots + b_N s^N} \quad (9.117)$$

gives a good approximation only in a region of convergence about $s = 0$ as illustrated in Figure 10. The method of CFH seeks to determine the other dominant poles by redetermining the expansions by moving the regions of convergence along the $s = j\omega$ axis as illustrated in Figure 10 [35, 44].

9.2.5.4 Vector Fitting In obtaining a solution to differential equations (ordinary or partial), we discretize the time axis into Δt intervals and recursively solve the equations. Performing a convolution generally requires the storage of all past time points, which is very burdensome in terms of memory requirements as well as computation

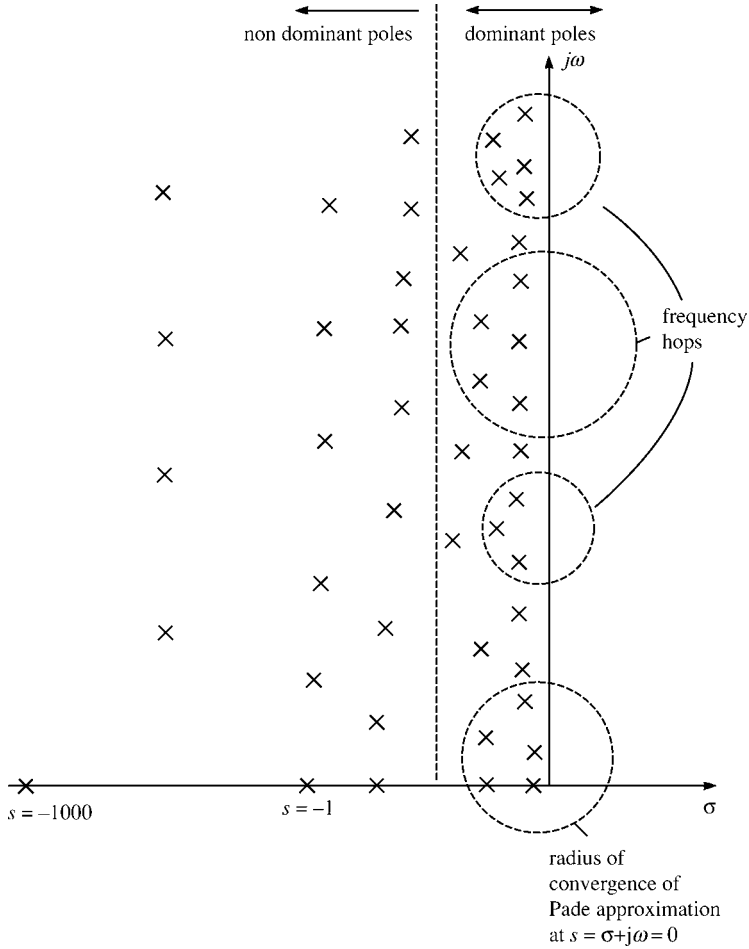


FIGURE 9.10 Illustration of the method of complex frequency hopping to determine the dominant poles.

time. In Section 8.2.3.4, we discussed the recursive convolution technique for evaluating convolution integrals, which avoids this problem. The recursive convolution method relies on representing the time-domain responses as the sum of exponential time functions such as

$$h(t) = \sum_{k=1}^N a_k e^{b_k t} \tag{9.135}$$

The recursive convolution scheme relies on the property of the exponential $e^{(a+b)} = e^a e^b$. For example, the convolution $h(t)*x(t)$ is evaluated as

$$\begin{aligned}
 [h(t)*x(t)]|_{t=t_i} &= \int_0^{t_i} \underbrace{ae^{b\tau}}_{h(\tau)} x(t_i - \tau) d\tau \\
 &= \int_0^{t_i-t_{i-1}} ae^{b\tau} x(t_i - \tau) d\tau + \int_{t_i-t_{i-1}}^{t_i} ae^{b\tau} x(t_i - \tau) d\tau \\
 &= \int_0^{\Delta t} ae^{b\tau} x(t_i - \tau) d\tau + e^{b\Delta t} \int_0^{t_{i-1}} ae^{b\zeta} x(t_{i-1} - \zeta) d\zeta \\
 &= \int_0^{\Delta t} ae^{b\tau} x(t_i - \tau) d\tau + e^{b\Delta t} y(t_{i-1})
 \end{aligned} \tag{8.192}$$

and we have used a change of variables, $\zeta = \tau - (t_i - t_{i-1}) = \tau - \Delta t$, in the second integral. Hence, the recursive convolution technique allows us to accumulate the values of the convolution at the previous time points as we proceed.

If we characterize a transfer function in the frequency domain in rational polynomial form as

$$F(s) = \frac{a_0 + a_1s + \cdots + a_Ns^N}{b_0 + b_1s + \cdots + b_Ns^N} \tag{9.136a}$$

it can be expanded using partial fractions as

$$F(s) = c_0 + \sum_{i=1}^N \frac{c_i}{s - p_i} \tag{9.136b}$$

where the p_i are the *poles* and the c_i are the *residues*. This becomes, in the time domain,

$$f(t) = c_0\delta(t) + \sum_{i=1}^N c_i e^{p_i t} \tag{9.137}$$

and hence, the recursive convolution scheme can be easily implemented. In order to determine the frequency-domain expansion in (9.136), we need to determine the dominant poles over the frequency range of interest and their residues as in (9.136b). The vector fitting method seeks to do this [45–47].

The vector fitting method uses an auxiliary undetermined rational function expanded as

$$\sigma(s) = 1 + \sum_{i=1}^N \frac{\tilde{c}_i}{s - \tilde{p}_i} \tag{9.138}$$

and an approximation to $F(s)$:

$$P(s) = c_0 + \sum_{i=1}^N \frac{c_i}{s - \tilde{p}_i} \tag{9.139}$$

In both these functions, we choose a set of starting poles \tilde{p}_i and write

$$P(s) = \sigma(s) F(s) \tag{9.140}$$

Writing this out yields

$$\underbrace{\left[c_0 + \sum_{i=1}^N \frac{c_i}{s - \tilde{p}_i} \right]}_{P(s)} = \underbrace{\left[1 + \sum_{i=1}^N \frac{\tilde{c}_i}{s - \tilde{p}_i} \right]}_{\sigma(s)} F(s) \tag{9.141a}$$

or

$$c_0 + \sum_{i=1}^N \frac{c_i}{s - \tilde{p}_i} - \sum_{i=1}^N \frac{\tilde{c}_i F(s)}{s - \tilde{p}_i} = F(s) \tag{9.141b}$$

Choosing M frequency points, $s_k = j\omega_k$, over the frequency range of interest to evaluate this gives M equations in the $2N + 1$ unknowns c_0, c_i, \tilde{c}_i in the form

$$\mathbf{A} \mathbf{X} = \mathbf{B} \tag{9.142a}$$

where

$$\underbrace{\begin{bmatrix} 1 & \frac{1}{s_1 - \tilde{p}_1} & \cdots & \frac{1}{s_1 - \tilde{p}_N} & -\frac{F(s_1)}{s_1 - \tilde{p}_1} & \cdots & -\frac{F(s_1)}{s_1 - \tilde{p}_N} \\ 1 & \frac{1}{s_2 - \tilde{p}_1} & \cdots & \frac{1}{s_2 - \tilde{p}_N} & -\frac{F(s_2)}{s_2 - \tilde{p}_1} & \cdots & -\frac{F(s_2)}{s_2 - \tilde{p}_N} \\ \vdots & \vdots & \vdots & \vdots & \vdots & \vdots & \vdots \\ 1 & \frac{1}{s_M - \tilde{p}_1} & \cdots & \frac{1}{s_M - \tilde{p}_N} & -\frac{F(s_M)}{s_M - \tilde{p}_1} & \cdots & -\frac{F(s_M)}{s_M - \tilde{p}_N} \end{bmatrix}}_{\mathbf{A}} \underbrace{\begin{bmatrix} c_0 \\ c_1 \\ \vdots \\ c_N \\ \tilde{c}_1 \\ \vdots \\ \tilde{c}_N \end{bmatrix}}_{\mathbf{X}} \tag{9.142b}$$

$$= \underbrace{\begin{bmatrix} F(s_1) \\ F(s_2) \\ \vdots \\ F(s_M) \end{bmatrix}}_{\mathbf{B}} \tag{9.142b}$$

matrix \mathbf{A} is $M \times (2N + 1)$, vector \mathbf{X} is of length $2N + 1$, and vector \mathbf{B} is of length M . Rewriting (9.140) as

$$F(s) = \frac{P(s)}{\sigma(s)} \tag{9.143}$$

shows the key fact about the vector fitting method: *the poles, p_i of $F(s)$ are the zeros of $\sigma(s)$!* Also observe that the initial estimates of the poles \tilde{p}_i *cancel out!* Hence, once (9.142) is solved for the N residues of $\sigma(s)$, $\tilde{c}_1, \dots, \tilde{c}_N$, the N zeros of $\sigma(s)$ can be determined by multiplying out (9.138) and then factoring the numerator polynomial. An alternative, more direct, method is to determine the N poles of $F(s)$, p_i , as the N *eigenvalues* of the $N \times N$ matrix [47, 48]

$$\mathbf{D} = \begin{bmatrix} (\tilde{p}_1 - \tilde{c}_1) & -\tilde{c}_2 & \cdots & -\tilde{c}_N \\ -\tilde{c}_1 & (\tilde{p}_2 - \tilde{c}_2) & \cdots & -\tilde{c}_N \\ \vdots & \vdots & \vdots & \vdots \\ -\tilde{c}_1 & \cdots & -\tilde{c}_{N-1} & (\tilde{p}_N - \tilde{c}_N) \end{bmatrix} \tag{9.144a}$$

as

$$|p_i \mathbf{1}_n - \mathbf{D}| = 0 \tag{9.144b}$$

where $||$ denotes the determinant of the enclosed matrix. These new poles are again used as the starting poles, and the process is repeated until the poles converge. The initial poles are typically chosen to be equally spaced, logarithmically, over the frequency range that we wish to characterize, and the real parts are chosen to be a factor of 100 smaller than the imaginary parts, that is, $\tilde{p}_i = \alpha_i + j\beta_i$ with $\beta_i = 100\alpha_i$, as recommended in [45].

If we choose the number of frequency points for the s_k , M , to be larger than the number of unknowns in \mathbf{X} , $2N+1$, (9.142) becomes an overdetermined set of equations, and the residues can be determined to minimize the error in a least-squares sense [49]. In a linear least-squares problem, we approximate a function as a linear combination of K basis functions $\phi_i(s)$ as

$$\tilde{F}(s) = \sum_{i=1}^K a_i \phi_i(s) \tag{9.145}$$

Matching this to the known values of the function at M points, s_j , where $M \geq K$ gives

$$\sum_{i=1}^K a_i \phi_i(s_j) = F(s_j) \quad \text{for } j = 1, \dots, M \quad (9.146)$$

This gives M equations in the K expansion coefficients, a_i , written in matrix form as

$$\mathbf{A}\mathbf{X} = \mathbf{B} \quad (9.147a)$$

where

$$[\mathbf{A}]_{ji} = \phi_i(s_j) \quad (9.147b)$$

$$[\mathbf{X}]_i = a_i \quad (9.147c)$$

$$[\mathbf{B}]_j = F(s_j) \quad (9.147d)$$

where \mathbf{A} is $M \times K$, \mathbf{X} is $K \times 1$, and \mathbf{B} is $M \times 1$. Then, we determine the a_i to minimize the square of the difference between $\tilde{F}(s)$ and the values of the function at the M points, s_j , as

$$\min \sum_{j=1}^M \left[F(s_j) - \sum_{i=1}^K a_i \phi_i(s_j) \right]^2 \quad (9.148)$$

To minimize this error, we differentiate (9.148) with respect to the a_i and set the result equal to zero giving K equations as

$$\sum_{j=1}^M \left[F(s_j) - \sum_{i=1}^K a_i \phi_i(s_j) \right] \phi_k(s_j) = 0 \quad \text{for } k = 1, \dots, K \quad (9.149)$$

This can be written as

$$\sum_{i=1}^K \alpha_{ki} a_i = \beta_k \quad \text{for } k = 1, \dots, K \quad (9.150a)$$

where

$$\alpha_{ki} = \sum_{j=1}^M \phi_k(s_j) \phi_i(s_j) \quad (9.150b)$$

$$\beta_k = \sum_{j=1}^M F(s_j) \phi_k(s_j) \quad (9.150c)$$

This can be written in matrix form as

$$[\mathbf{A}^t \mathbf{A}] \mathbf{X} = \mathbf{A}^t \mathbf{B} \quad (9.151)$$

where t denotes transpose and the entries in \mathbf{A} , \mathbf{X} , and \mathbf{B} are given in (9.147). The resulting equations in (9.151) are K equations in the K unknown expansion coefficients, a_i . To avoid roundoff error, the preferred method of solution for (9.151) is singular value decomposition (SVD) [49].

The equations in (9.142) are in the form of (9.147) where the $K \Rightarrow (2N + 1)$ $\phi_i(s_j)$ are

$$\phi_i(s_j) = 1, \frac{1}{s_j - \tilde{p}_i}, \dots, \frac{1}{s_j - \tilde{p}_i}, -\frac{F(s_j)}{s_j - \tilde{p}_i}, \dots, -\frac{F(s_j)}{s_j - \tilde{p}_i} \quad (9.152a)$$

and the $K \Rightarrow (2N + 1)$ a_i are

$$c_0, c_1, \dots, c_N, \tilde{c}_1, \dots, \tilde{c}_N \quad (9.152b)$$

and \mathbf{A} is $M \times (2N + 1)$, \mathbf{X} is $(2N + 1) \times 1$, and \mathbf{B} is $M \times 1$. The resulting equations in the least-square method in (9.151) are $2N + 1$ equations in the $2N + 1$ residues in (9.152b). The starting poles are chosen and (9.151) is solved for the residues of $\sigma(s)$ in (9.138), $\tilde{c}_1, \dots, \tilde{c}_N$. The new poles are obtained as the eigenvalues of (9.144). These are used for the new starting poles, and the process is repeated. After convergence, $F(s)$ is factored as in (9.136b), and the time-domain representation in terms of exponential functions is obtained as in (9.137). Any convolutions involving this function can then be evaluated using the method of recursive convolution.

An alternative to using the recursive convolution scheme is to synthesize lumped equivalent circuits to represent $F(s)$ thereby directly using programs such as SPICE to obtain the time-domain response of the system. Such representations of the frequency-domain factored form in (9.136b) are given in [50] using R, L, C elements and controlled sources.

9.3 COMPUTED AND EXPERIMENTAL RESULTS

The computed results are obtained for the time-domain responses of a three-wire ribbon cable (shown in cross section in Fig.7.10) and a three-land PCB (shown in cross section in Fig.7.13). The terminal configurations for both structures are shown in Figure 9.11. The conductors are numbered as shown in accordance with the numbering used to obtain the per-unit-length parameter matrices. A 50- Ω time-domain source produces an open-circuit voltage $V_S(t)$ that is in the form of a periodic trapezoidal

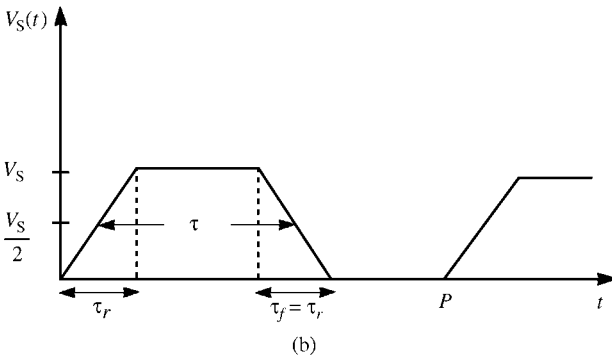
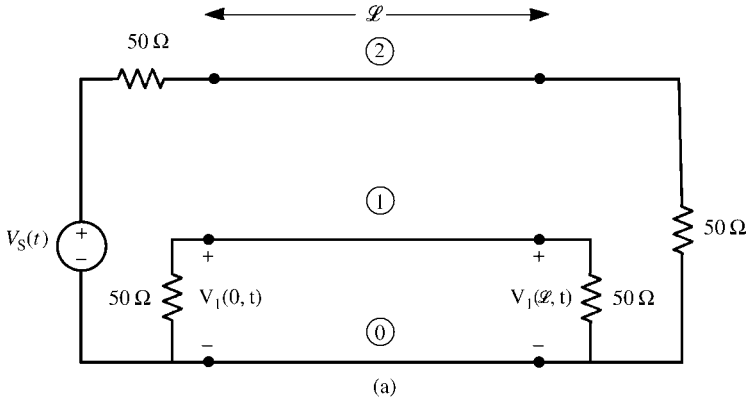


FIGURE 9.11 A three-conductor line for illustrating the predictions of various models: (a) terminal representations and (b) representation of the open-circuit voltage waveform of the source.

waveform having a 50 % duty cycle and equal rise and fall times with various values. The level of $V_S(t)$ will be 1 V in all cases. The source and load structure will be characterized with generalized Thevenin equivalents as

$$\mathbf{V}(0, t) = \mathbf{V}_S(t) - \mathbf{R}_S \mathbf{I}(0, t)$$

$$\mathbf{V}(\mathcal{L}, t) = \mathbf{R}_L \mathbf{I}(\mathcal{L}, t)$$

where

$$\mathbf{V}_S(t) = \begin{bmatrix} 0 \\ V_S(t) \end{bmatrix}$$

$$\mathbf{R}_S = \begin{bmatrix} 50 & 0 \\ 0 & 50 \end{bmatrix}$$

$$\mathbf{R}_L = \begin{bmatrix} 50 & 0 \\ 0 & 50 \end{bmatrix}$$

We will show the predictions of the lossless SPICE model, the lumped- Π approximate model, the TDFD transformation method, and the FDTD method. These will be compared with oscilloscope photographs of the experimentally obtained results.

9.3.1 Ribbon Cables

The cross section of the three-wire ribbon cable is shown in Figure 7.10 and the per-unit-length parameters are computed using RIBBON.FOR that is described in Appendix A and given in Chapter 5 as

$$\mathbf{L} = \begin{bmatrix} 0.7485 & 0.5077 \\ 0.5077 & 1.0154 \end{bmatrix} \mu\text{H/m}$$

$$\mathbf{C} = \begin{bmatrix} 37.432 & -18.716 \\ -18.716 & 24.982 \end{bmatrix} \text{pF/m}$$

The pulse rise/fall times are 20 ns and the line length is $\mathcal{L} = 2$ m. The mode velocities of propagation computed with SPICEMTL.FOR are $v_{m1} = 2.324 \times 10^8$ m/s and $v_{m2} = 2.5106 \times 10^8$ m/s giving one-way time delays of the modes of $T_{Dm1} = 8.606$ ns and $T_{Dm2} = 7.996$ ns. The characteristic impedances of the modes are $Z_{Cm1} = 91.96 \Omega$ and $Z_{Cm2} = 254.93 \Omega$.

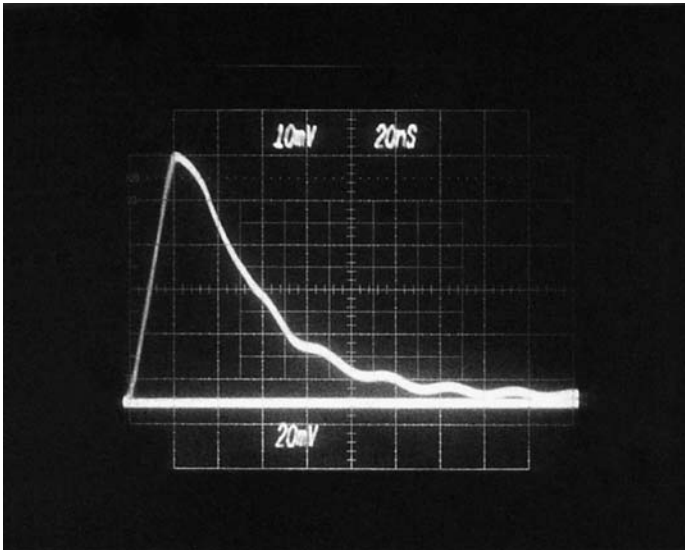


FIGURE 9.12 Oscilloscope photograph of the experimentally determined near-end crosstalk for the ribbon cable of Figure 7.10 and a pulse rise time of 20 ns.

Figure 9.12 shows an oscilloscope photograph of the near-end crosstalk voltage $V_1(0, t)$. The crosstalk waveform rises to a peak of around 110 mV. Figure 9.13(a) shows a comparison of the predictions of (a) SPICE using SPICEMTL.FOR to generate the PSPICE subcircuit model as described in Section 9.1.2, (b) one Pi section lumped model generated by SPICELPI.FOR to generate the PSPICE subcircuit model as described in Section 9.1.3, and (c) the Branin recursive solution model given in Section 9.1.1. All three models assume a lossless line and the Branin model also assumes a homogeneous medium. The SPICE model predicts the experimentally obtained waveform in Figure 9.12 very well. The peak voltage is also predicted to be 110 mV. The one-section lumped-Pi model predicts the general shape of the waveform, but there is some error around the peak. This is to be expected since the spectral content of the input pulse is on the order of $BW = 1/\tau_r = 50$ MHz. The line length of 2 m is on the order of $(1/2.3)\lambda$ at 50 MHz using the smaller of the mode velocities of $v_{m1} = 2.324 \times 10^8$ m/s. Branin's recursive solution method also predicts the general waveform shape but does not agree with the SPICE solution as it should. This is because, as discussed in Section 9.1.1, Branin's recursive solution as implemented in BRANIN.FOR requires that we assume a homogenous medium (logically free space). Figure 9.13(b) shows the comparison where we ignore the dielectric insulations and recompute the per-unit-length parameters and the resulting SPICE solution for free space surrounding the wires. The results are now identical as they should be.

Figure 9.14 shows the predictions of the TDFD prediction model described in Section 9.1.4. This model is implemented using TIMEFREQ.FOR. The values of the frequency-domain transfer function at the harmonics of the input pulse that are input to this program were computed, for a lossless line, using the SPICE code above to compute in the .AC mode. Various numbers of harmonics are used to recombine the sinusoidal components of the trapezoidal pulse train for a fundamental frequency of $f_0 = 1$ MHz. (Actually, it does not matter what repetition frequency is used so long as the response to the rising edge, which is shown in the figure, has died out sufficiently before the response to the trailing edge occurs.) The predictions using 100 and 50 harmonics are virtually identical to the exact SPICE results. The predictions using 10 and 20 harmonics are poor. The spectrum of the trapezoidal pulse train begins rolling off at -40 dB/decade above a frequency of $1/\pi \tau_r = 15.9$ MHz giving a bandwidth on the order of $1/\tau_r = 50$ MHz. Hence, we require at least 50 harmonics of the fundamental repetition frequency of $f_0 = 1$ MHz in order to capture the important spectral content.

Figure 9.15 shows the predictions of the FDTD model discussed in Section 9.1.5. This model is implemented using FINDIF.FOR for a lossless line. The line is discretized spatially into NDZ sections of length $\Delta z = \mathcal{L}/NDZ$. We chose $NDZ = 2$ so that each $\Delta z = 1$ m section length was on the order of $\Delta z < (1/5)\lambda$ at 50 MHz. The time discretization Δt must satisfy the Courant condition, that is,

$$NDT \geq NDZ \frac{v \times \text{final solution time}}{\mathcal{L}}$$

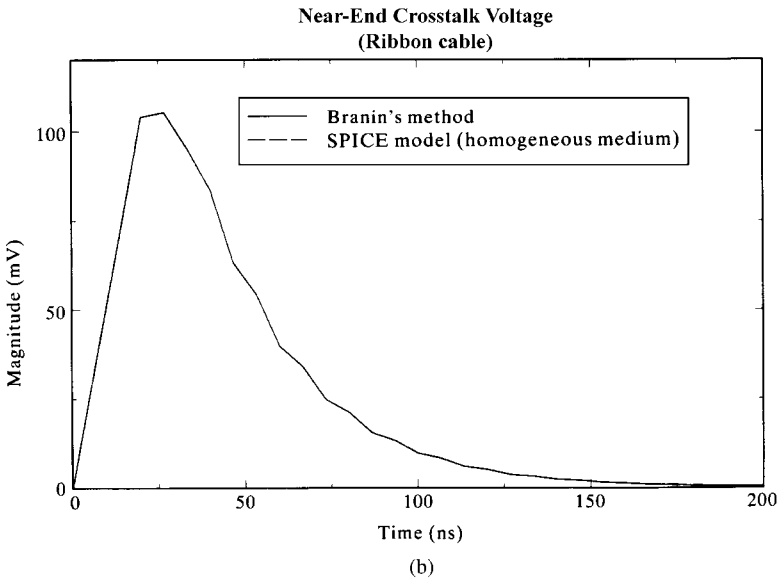
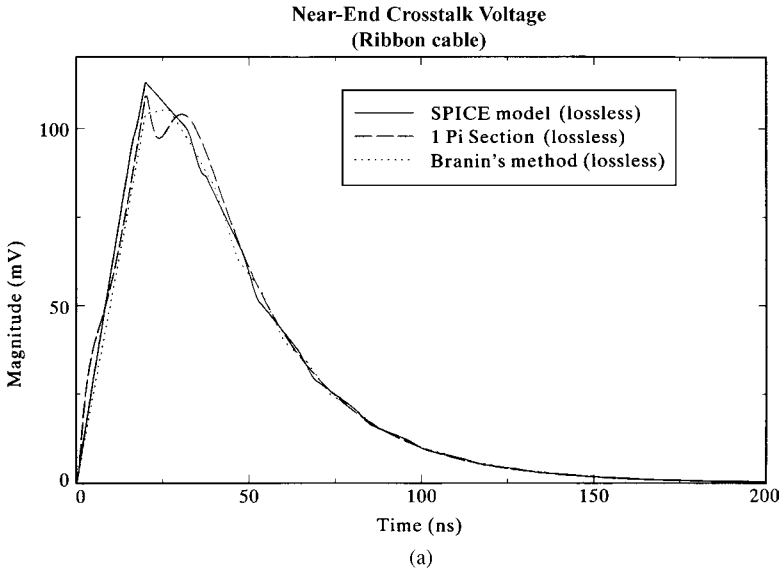


FIGURE 9.13 Comparison of the time-domain response of the near-end crosstalk of the lossless ribbon cable of Figure 7.10 determined (a) via the SPICE model, the lumped-Pi model, and Branin's series method implemented for a pulse rise time of 20 ns and (b) for a homogeneous medium.

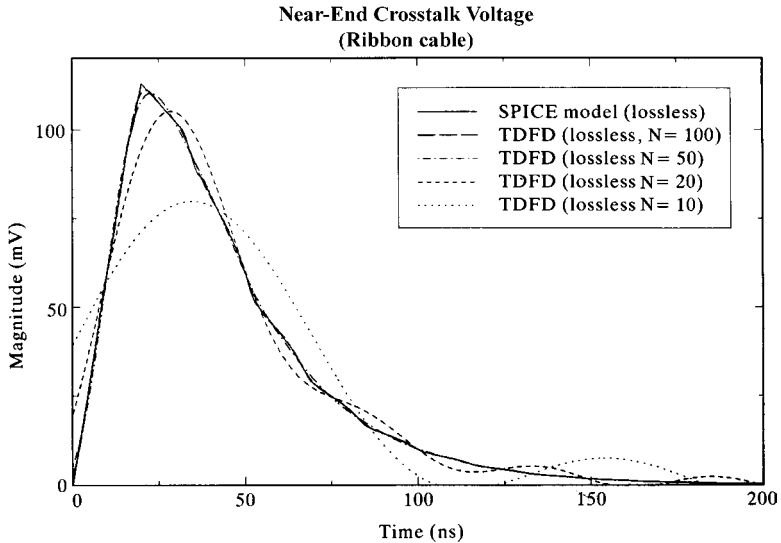


FIGURE 9.14 Comparison of the predictions of the SPICE model and the time-domain to frequency-domain transformation method for various numbers of harmonics for the lossless ribbon cable of Figure 7.10 for a pulse risetime of 20 ns.

For a final solution time of 200 ns, using the larger of the mode velocities, $v_{m2} = 2.5106 \times 10^8$ m/s, we obtain $NDT \geq 50$. The predictions for $NDZ = 2$ and $NDT = 50$ give reasonable correlation with the exact SPICE predictions. The results for $NDT = 500$ are also shown and are virtually identical to the exact SPICE results.

These lumped-Pi, TDFD, and FDTD predictions were repeated to include the line losses. The predictions for the lumped-Pi model including the dc resistances of the conductors are compared to the SPICE (lossless) predictions in Figure 9.16 for one and two Pi sections used to represent the 2-m line length. Both the one-Pi model and the two-Pi model show some error around the peak of the waveform with the one-Pi model showing more error as expected. (Later predictions of the TDFD and FDTD models including losses will show that the SPICE predictions for a lossless line are very close to the actual results when losses are included.) The radius of one of the #36 gauge strands is 2.5 mils giving a dc resistance of each wire (dividing the resistance of each strand by the number in parallel, 7) as 0.3888Ω . The frequency of onset of the \sqrt{f} increase is where the radius of a strand is equal to two skin depths or 4.3 MHz. Hence, using only the dc resistance in these lumped-Pi models will incur some poor predictions at the higher frequencies of the pulse spectrum.

Figure 9.17 shows the predictions of the TDFD and FDTD models as before but including the conductor losses. The lossy frequency-domain transfer function that is passed to the TDFD program, `TIMEFREQ.FOR`, was computed using `MTL.FOR`. The FDTD predictions including losses were obtained using `FDTDLOSS.FOR`. All

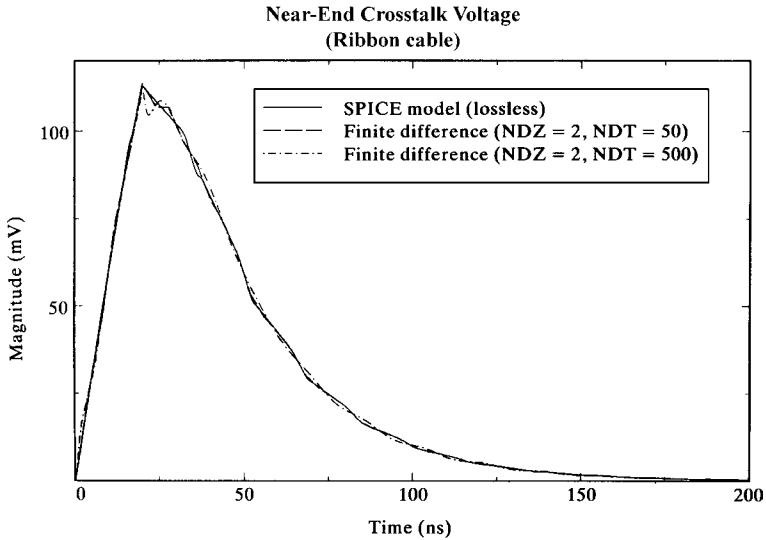


FIGURE 9.15 Comparison of the predictions of the SPICE model and the FDTD method for the lossless ribbon cable of Figure 7.10 for a pulse rise time of 20 ns.

models give approximately the same results, and the conductor losses appear to be inconsequential for this structure, line length, and pulse parameters. The losses give a dc offset during the time when the input pulse is in its 1-V steady state, which is referred to as common-impedance coupling. This level can be accurately predicted by modeling the line as simply its total dc resistances of 0.3888Ω as shown in the next chapter to be around 2 mV.

Figure 9.18 shows the predictions of the TDFD and FDTD models including losses for pulse rise/fall times of 1 ns. The bandwidth of the pulse is $1/\tau_r = 1 \text{ GHz}$. The TDFD program uses a repetition rate of $f_0 = 1 \text{ MHz}$, and hence 1000 harmonics are recombined in `TIMEFREQ.FOR`. The FDTD program breaks the 2-m line length into

$$\Delta z = \frac{1}{10} \frac{v_{m1}}{1 \text{ GHz}} = 2.32 \text{ cm}$$

sections giving $2 \text{ m}/\Delta z = 86$. Hence, we chose $\text{NDZ} = 100$. The magic time step is $\text{NDT} = 2511$. The results are shown in Figure 9.18 giving very good accuracy for both prediction methods. Again, the effect of the conductor losses is to give an offset of around 2 mV when the pulse is in its steady state of 1 V.

9.3.2 Printed Circuit Boards

The cross section of the three-land PCB is shown in Figure 7.13 and the per-unit-length parameters are computed using `PCB.FOR` that is described in Appendix A as

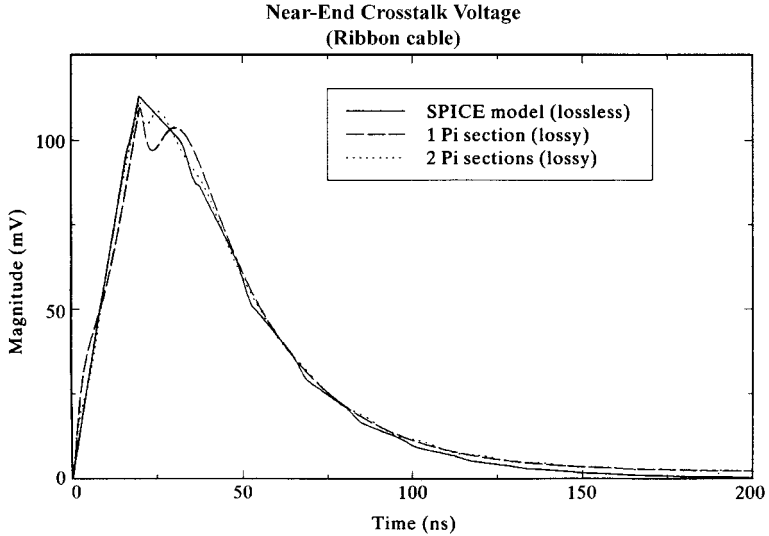


FIGURE 9.16 Comparison of the time-domain response of the near-end crosstalk of the ribbon cable of Figure 7.10 determined via the SPICE model (lossless) and the lumped-Pi model (dc losses included) using one and two sections to represent the line for a pulse rise time of 20 ns.

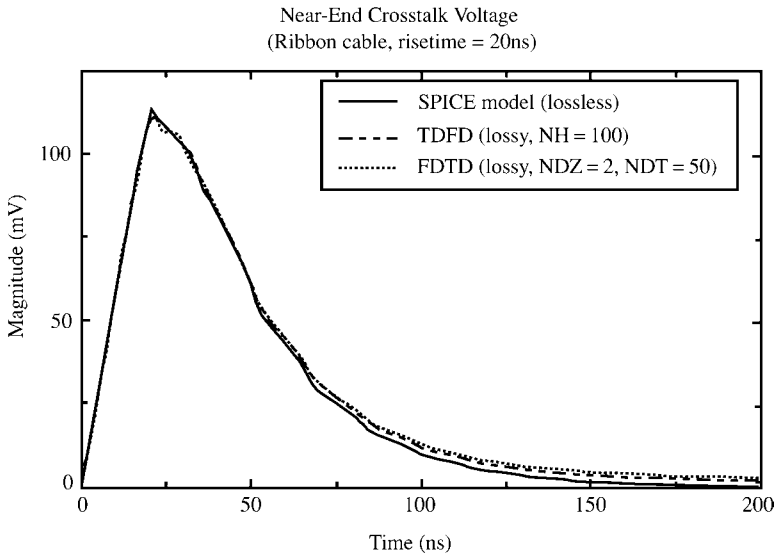


FIGURE 9.17 Comparison of the time-domain response of the near-end crosstalk of the ribbon cable of Figure 7.10 determined via the SPICE model (lossless), the time-domain to frequency-domain method (with skin effect losses), and the FDTD method (with skin effect losses) for a pulse rise time of 20 ns.

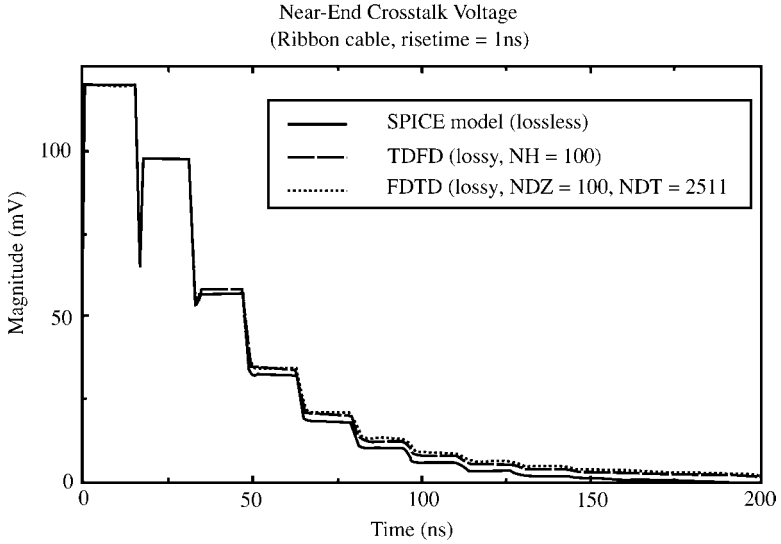


FIGURE 9.18 Comparison of the time-domain response of the near-end crosstalk of the ribbon cable of Figure 7.10 determined via the SPICE model (lossless), the time-domain to frequency-domain method (with skin effect losses), and the FDTD method (with skin effect losses) for a pulse rise time of 1 ns.

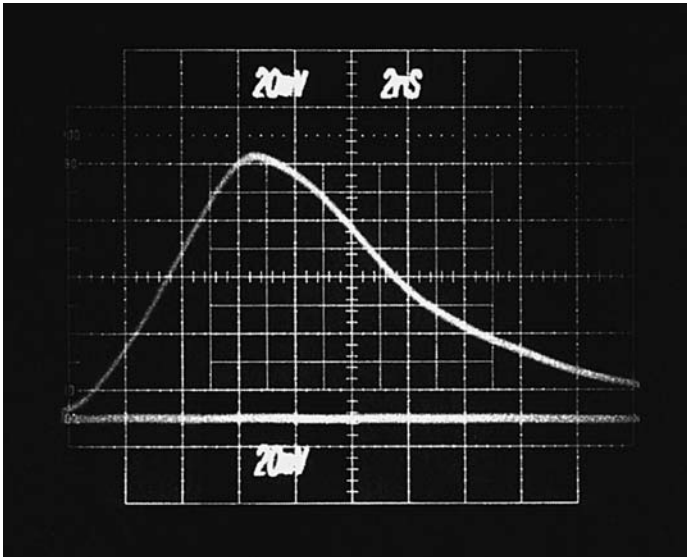


FIGURE 9.19 Oscilloscope photograph of the experimentally determined near-end crosstalk for the printed circuit board of Figure 7.13 and a pulse rise time of 6.25 ns.

$$\mathbf{L} = \begin{bmatrix} 1.10515 & 0.690613 \\ 0.690613 & 1.38123 \end{bmatrix} \mu\text{H/m}$$

$$\mathbf{C} = \begin{bmatrix} 40.5985 & -20.2992 \\ -20.2992 & 29.7378 \end{bmatrix} \text{pF/m}$$

The pulse rise-/fall times are 6.25 ns and the line length is $\mathcal{L} = 10 \text{ in.} = 0.254 \text{ m}$. The mode velocities of propagation computed with SPICEMTL.FOR are $v_{m1} = 1.8005 \times 10^8 \text{ m/s}$ and $v_{m2} = 1.9225 \times 10^8 \text{ m/s}$ giving one-way time delays of the modes of $T_{Dm1} = 1.4108 \text{ ns}$ and $T_{Dm2} = 1.3212 \text{ ns}$. The characteristic impedances of the modes are $Z_{Cm1} = 109.45 \Omega$ and $Z_{Cm2} = 265.54 \Omega$.

Figure 9.19 shows an oscilloscope photograph of the near-end crosstalk voltage, $V_1(0, t)$. The crosstalk waveform rises to a peak of around 95 mV. Figure 9.20 shows a comparison of the predictions of (a) SPICE using SPICEMTL.FOR to generate the PSPICE subcircuit model as described in Section 9.1.2, (b) one Pi section lumped model generated by SPICELPI.FOR to generate the PSPICE subcircuit model as described in Section 9.1.3, and (c) the Branin recursive solution model given in Section 9.1.1. All three models assume a lossless line and the Branin model also assumes a homogeneous medium. The SPICE model predicts the experimentally obtained waveform in Figure 9.19 very well. The peak voltage is also predicted to be 95 mV. The one-section lumped-Pi model predicts the general shape of the waveform but

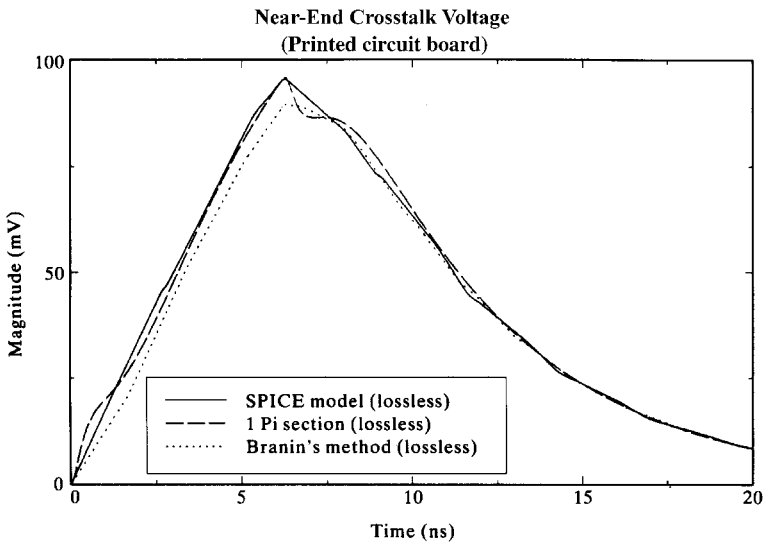


FIGURE 9.20 Comparison of the time-domain response of the near-end crosstalk of the lossless printed circuit board of Figure 7.13 determined via the SPICE model, the lumped-Pi model, and Branin's series method implemented for a pulse rise time of 6.25 ns and for a homogeneous medium.

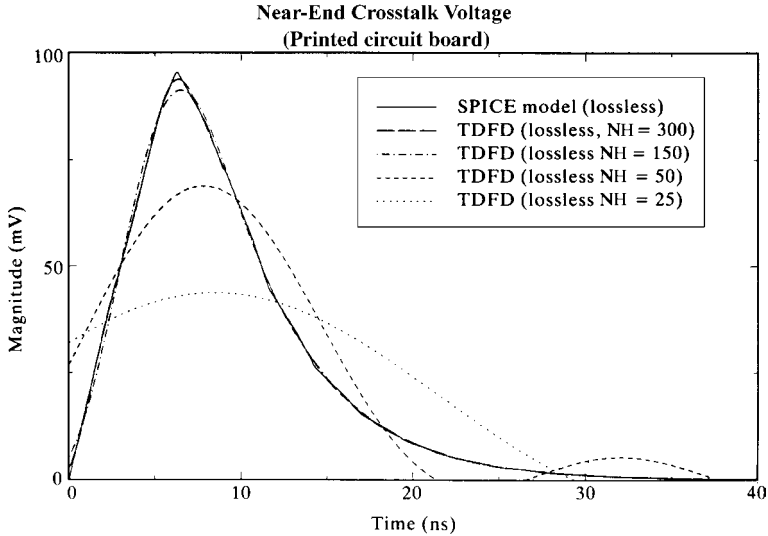


FIGURE 9.21 Comparison of the predictions of the SPICE model and the time-domain to frequency-domain transformation method for various numbers of harmonics for the lossless printed circuit board of Figure 7.13 for a pulse rise time of 6.25 ns.

there is some error particularly around the peak. This is to be expected since the spectral content of the input pulse is on the order of $BW = 1/\tau_r = 160$ MHz. The line length of .254 m is on the order of $(1/5)\lambda$ at 160 MHz using the smaller of the mode velocities of $v_{m1} = 1.8005 \times 10^8$ m/s. Branin's recursive solution method also predicts the general waveform shape but does not agree with the SPICE solution because, as discussed previously, it neglects the inhomogeneous surrounding medium.

Figure 9.21 shows the predictions of the TDFD prediction model described in Section 9.1.4. This model is implemented using `TIMEFREQ.FOR`. The values of the frequency-domain transfer function at the harmonics of the input pulse that are input to this program were computed, for a lossless line, using the SPICE code above to compute in the `.AC` mode. Various numbers of harmonics are used to recombine the sinusoidal components of the trapezoidal pulse train for a fundamental frequency of $f_0 = 1$ MHz. The predictions using 300 and 150 harmonics are virtually identical to the exact SPICE results. The predictions using 25 and 50 harmonics are poor. The spectrum of the trapezoidal pulse train begins rolling off at -40 dB/decade above a frequency of $1/\pi\tau_r = 51$ MHz giving a bandwidth on the order of $1/\tau_r = 160$ MHz. Hence, we require at least 160 harmonics of the fundamental repetition frequency of $f_0 = 1$ MHz in order to capture the important spectral content.

Figure 9.22 shows the predictions of the FDTD model discussed in Section 9.1.5. This model is implemented using `FINDIF.FOR` for a lossless line. The line is discretized spatially into NDZ sections of length $\Delta z = \mathcal{L}/NDZ$. We chose $NDZ = 2$

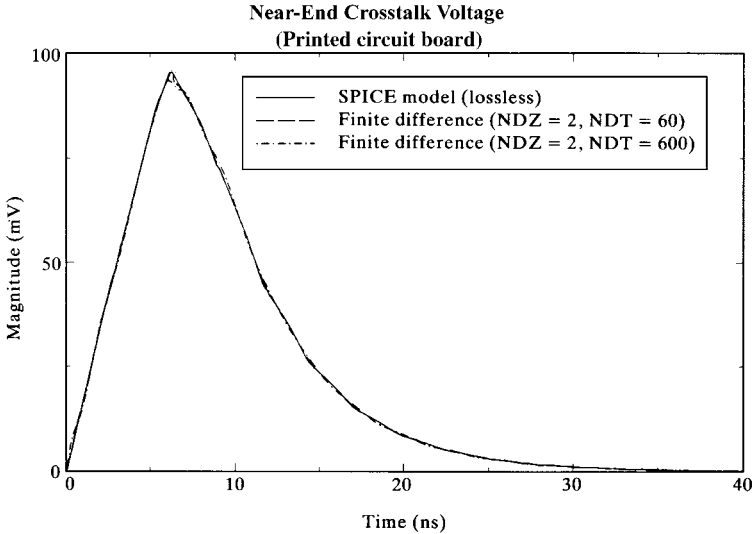


FIGURE 9.22 Comparison of the predictions of the SPICE model and the FDTD method for the lossless printed circuit board of Figure 7.13 for a pulse rise time of 6.25 ns.

so that each $\Delta z = 0.127$ m section length was on the order of $\Delta z < (1/10)\lambda$ at 160 MHz.. The time discretization Δt must satisfy the Courant condition, that is,

$$\text{NDT} \geq \text{NDZ} \frac{v \times \text{final solution time}}{\mathcal{L}}$$

For a final solution time of 40 ns, using the larger of the mode velocities, $v_{m2} = 1.9225 \times 10^8$ m/s, we obtain $\text{NDT} \geq 60$. The predictions for $\text{NDZ} = 2$ and $\text{NDT} = 60$ give reasonable correlation with the exact SPICE predictions. The results for $\text{NDT} = 600$ are also shown and are virtually identical to the exact SPICE results.

These lumped-Pi, TDFD, and FDTD predictions were repeated to include the line losses. The predictions for the lumped-Pi model including the dc resistances of the conductors are compared to the SPICE (lossless) predictions in Figure 9.23 for one and two Pi sections used to represent the 0.254 m line length. Both the one-Pi model and the two-Pi model show some error around the peak of the waveform with the one-Pi model showing more error as expected. (Later predictions of the TDFD and FDTD models including losses will show that the SPICE predictions for a lossless line are very close to the actual results when losses are included.) The dc resistance of each land (width of 15 mils and thickness of 1.38 mils) is 0.328Ω . The frequency of onset of the \sqrt{f} increase is approximated as where the thickness of each land is equal to two skin depths or 14.218 MHz. Hence, using only the dc resistance in these lumped-Pi models will incur some poor predictions at the higher frequencies of the pulse spectrum.

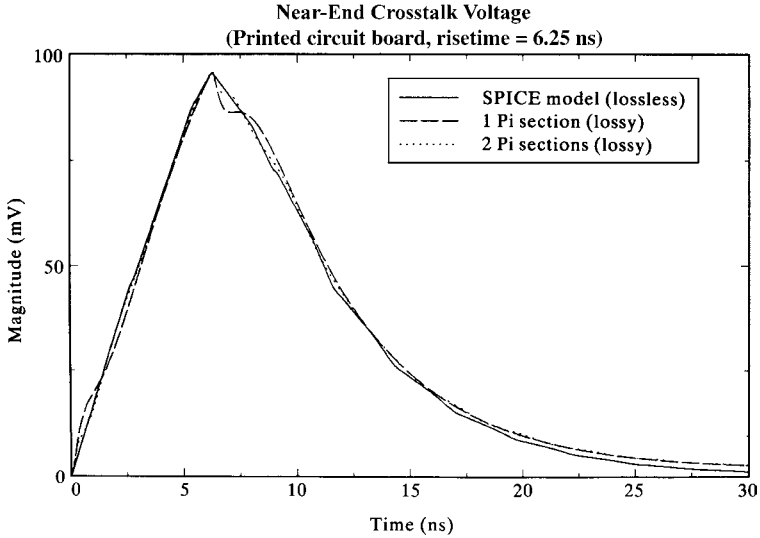


FIGURE 9.23 Comparison of the time-domain response of the near-end crosstalk of the printed circuit board of Figure 7.13 determined via the SPICE model (lossless) and the lumped-Pi model (dc losses included) using one and two sections to represent the line for a pulse rise time of 6.25 ns.

Figure 9.24 shows the predictions of the TDFD and FDTD models as before but including the conductor losses. The lossy frequency-domain transfer function that is passed to the TDFD program, TIMEFREQ.FOR, was computed using MTL.FOR. The FDTD predictions including losses were obtained using FDTDLOSS.FOR. All models give approximately the same results, and the conductor losses again appear to be inconsequential for this structure, line length, and pulse parameters. The losses again give a dc offset during the time when the input pulse is in its 1-V steady state, which is referred to as common-impedance coupling. This level can be accurately predicted by modeling the line as simply its total dc resistances of 0.328Ω as shown in the next chapter to be around 2 mV.

Figure 9.25 shows the predictions of the TDFD and FDTD models including losses for pulse rise/fall times of 50 ps. The bandwidth of the pulse is $1/\tau_r = 20 \text{ GHz}$. The TDFD program uses a repetition rate of $f_0 = 10 \text{ MHz}$, and hence 1000 harmonics are recombined in TIMEFREQ.FOR. The FDTD program breaks the 0.254-m line length into

$$\Delta z = \frac{1}{10} \frac{v_{m1}}{20\text{GHz}} = 0.9 \text{ mm}$$

sections giving $0.254 \text{ m}/\Delta z = 282$. Hence, we chose $\text{NDZ} = 280$. The magic time step is $\text{NDT} = 6358$. The results are shown in Figure 9.25 giving very good accuracy for both prediction methods. Again, the effect of the conductor

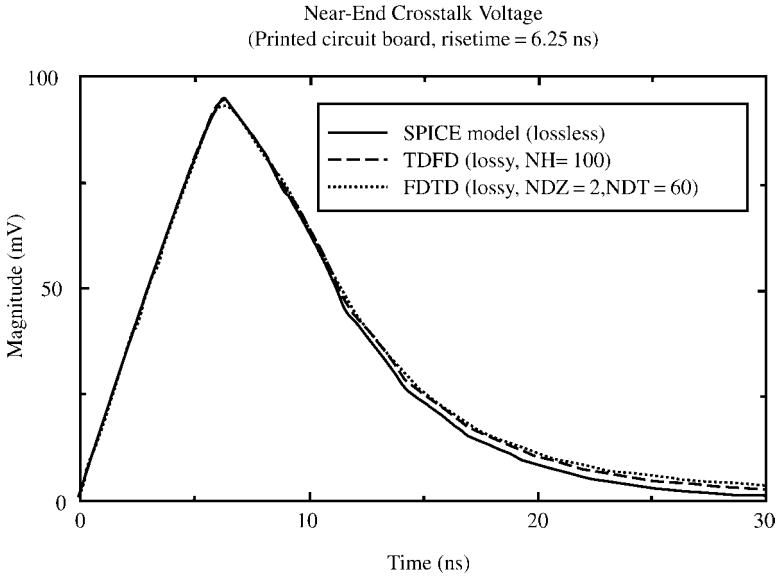


FIGURE 9.24 Comparison of the time-domain response of the near-end crosstalk of the printed circuit board of Figure 7.13 determined via the SPICE model (lossless), the time-domain to frequency-domain method (with skin effect losses), and the FDTD method (with skin effect losses) for a pulse rise time of 6.25 ns.

losses is to give an offset of around 2 mV when the pulse is in its steady state of 1 V.

PROBLEMS

- 9.1 Derive the recursive relations given in (9.21a) and (9.21b).
- 9.2 Consider a lossless two-conductor line that has $R_S = 300 \Omega$, $R_L = 60 \Omega$, $Z_C = 100 \Omega$, $v = 300 \text{ m}/\mu\text{s}$, $\mathcal{L} = 300 \text{ m}$, and $v_S(t) = 400u(t)$, where $u(t)$ is the unit step function. Sketch $V(0, t)$, $I(0, t)$, $V(\mathcal{L}, t)$, $I(\mathcal{L}, t)$ for $0 \leq t \leq 10 \mu\text{s}$. Do the results converge to the expected steady-state values? Confirm your results using PSPICE. [For voltage: $\Gamma_S = 1/2$, $\Gamma_L = -1/4$, $V_{\text{init}} = 100$. For current: $\Gamma_S = -1/2$, $\Gamma_L = 1/4$, $I_{\text{init}} = 1$. $V(0, t)_{\text{SS}} = V(\mathcal{L}, t)_{\text{SS}} = 66.67$, $I(0, t)_{\text{SS}} = I(\mathcal{L}, t)_{\text{SS}} = 1.11$]
- 9.3 Repeat Problem 9.2 for $R_L = 0$ (short-circuit load). Confirm your results using PSPICE. [For voltage: $\Gamma_S = 1/2$, $\Gamma_L = -1$, $V_{\text{init}} = 100$. For current: $\Gamma_S = -1/2$, $\Gamma_L = 1$, $I_{\text{init}} = 1$. $V(0, t)_{\text{SS}} = V(\mathcal{L}, t)_{\text{SS}} = 0$, $I(0, t)_{\text{SS}} = I(\mathcal{L}, t)_{\text{SS}} = 1.333$]
- 9.4 Repeat Problem 9.2 for $R_L = \infty$ (open-circuit load). Confirm your results using PSPICE. [For voltage: $\Gamma_S = 1/2$, $\Gamma_L = 1$, $V_{\text{init}} = 100$. For current:

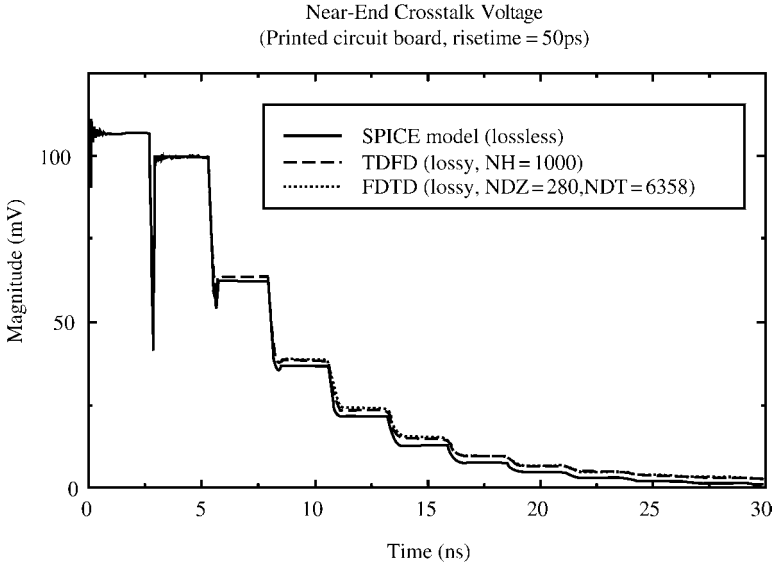


FIGURE 9.25 Comparison of the time-domain response of the near-end crosstalk of the printed circuit board of Figure 7.13 determined via the SPICE model (lossless), the time-domain to frequency-domain method (with skin effect losses), and the FDTD method (with skin effect losses) for a pulse rise time of 50 ps.

$$\Gamma_S = -1/2, \Gamma_L = -1, I_{init} = 1. V(0, t)_{SS} = V(\mathcal{L}, t)_{SS} = 400, I(0, t)_{SS} = I(\mathcal{L}, t)_{SS} = 0]$$

9.5 Confirm the diagonalization matrix for a real, symmetric matrix given in (9.37).

9.6 Determine the transformation \mathbf{T} that diagonalizes \mathbf{L} as $\mathbf{T}^t \mathbf{L} \mathbf{T} = \mathbf{L}_m$ where

$$\mathbf{L} = \begin{bmatrix} 5 & 1 \\ 1 & 3 \end{bmatrix} \mu\text{H/m}$$

$$[\mathbf{T}(1, 1) = \mathbf{T}(2, 2) = 0.92388, \mathbf{T}(1, 2) = -\mathbf{T}(2, 1) = -0.382683, \mathbf{L}_m(1, 1) = 5.414E - 6, \mathbf{L}_m(2, 2) = 2.586E - 6]$$

9.7 Determine the transformation \mathbf{T} that diagonalizes \mathbf{C} as $\mathbf{T}^t \mathbf{C} \mathbf{T} = \mathbf{C}_m$ where

$$\mathbf{C} = \begin{bmatrix} 10 & -5 \\ -5 & 15 \end{bmatrix} \text{pF/m}$$

$$[\mathbf{T}(1, 1) = \mathbf{T}(2, 2) = 0.85065, \mathbf{T}(1, 2) = -\mathbf{T}(2, 1) = -0.525731, \mathbf{C}_m(1, 1) = 6.90983E - 12, \mathbf{C}_m(2, 2) = 18.0902E - 12]$$

9.8 Determine the \mathbf{T}_V and \mathbf{T}_I that simultaneously diagonalize the \mathbf{L} and \mathbf{C} in Problems 9.6 and 9.7 as $\mathbf{T}_V^{-1} \mathbf{L} \mathbf{T}_I = \mathbf{L}_m$ and $\mathbf{T}_I^{-1} \mathbf{C} \mathbf{T}_V = \mathbf{C}_m$. [$\mathbf{T}_V(1, 1) = 0.745356, \mathbf{T}_V(1, 2) = -0.942809, \mathbf{T}_V(2, 1) = 0.745356, \mathbf{T}_V(2, 2) = 0.4714,$

$\mathbf{T}_I(1, 1) = 0.447214, \mathbf{T}_I(1, 2) = -0.707107, \mathbf{T}_I(2, 1) = 0.894427, \mathbf{T}_I(2, 2) = 0.707107, \mathbf{L}_m(1, 1) = 4.2E - 6, \mathbf{L}_m(2, 2) = 3.0E - 6, \mathbf{C}_m(1, 1) = 8.333E - 12, \mathbf{C}_m(2, 2) = 16.667E - 12]$

9.9 Determine the \mathbf{T}_V and \mathbf{T}_I that simultaneously diagonalize \mathbf{L} and \mathbf{C} as $\mathbf{T}_V^{-1}\mathbf{L}\mathbf{T}_I = \mathbf{L}_m$ and $\mathbf{T}_I^{-1}\mathbf{C}\mathbf{T}_V = \mathbf{C}_m$ where

$$\mathbf{L} = \begin{bmatrix} 3 & 1 \\ 1 & 2 \end{bmatrix} \text{ H/m}$$

$$\mathbf{C} = \begin{bmatrix} 5 & -3 \\ -3 & 4 \end{bmatrix} \text{ F/m}$$

$[\mathbf{T}_V(1, 1) = 1.10055, \mathbf{T}_V(1, 2) = 0.607046, \mathbf{T}_V(2, 1) = -0.1438, \mathbf{T}_V(2, 2) = 0.929182, \mathbf{T}_I(1, 1) = 0.837174, \mathbf{T}_I(1, 2) = 0.129561, \mathbf{T}_I(2, 1) = -0.546936, \mathbf{T}_I(2, 2) = 0.991571, \mathbf{L}_m(1, 1) = 1.7851, \mathbf{L}_m(2, 2) = 2.27372, \mathbf{C}_m(1, 1) = 7.0883, \mathbf{C}_m(2, 2) = 1.9117]$

9.10 Consider the three-conductor line shown in Figure P 9.10. The driven or generator conductor is a #20 gauge solid wire (radius 16 mils) and the pickup or receptor wire is a #28 gauge solid wire (radius 6.3 mils). The wires are separated by 1.5 cm and are suspended above an infinite, perfectly conducting ground

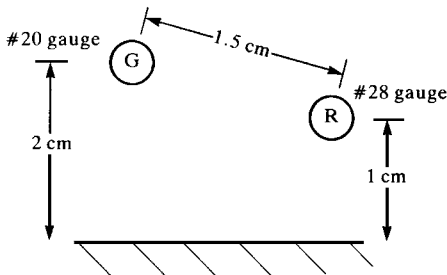
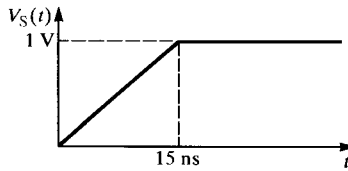
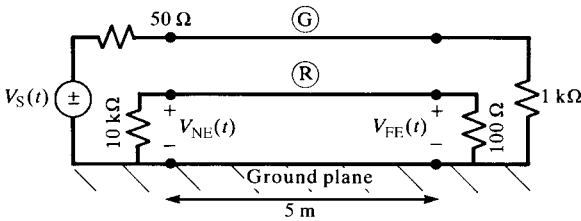


FIGURE P9.10

plane at heights of 2 cm and 1 cm as shown. The lines are terminated as shown and are driven by a ramp voltage source. Neglect all losses, assume a homogeneous medium, and compute and plot versus time the near-end and far-end coupled voltages, $V_{NE}(t)$ and $V_{FE}(t)$, by the following methods: (a) a PSPICE model using `SPICEMTL.FOR` to generate a PSPICE subcircuit model, (b) Branin's method using `BRANIN.FOR`, (c) the TDFD transformation method using `TIMEFREQ.FOR`, and (d) the FDTD method using `FINDIF.FOR`.

- 9.11** Recompute the SPICE results in Figure 9.6(a) and 9.6(b).
9.12 Verify the FDTD recursion relations in (9.78) and (9.79).
9.13 Verify the FDTD recursion relations in (9.53b), (9.57), and (9.80).
9.14 Verify the generalized method of characteristics results in (9.91) and (9.92).
9.15 Determine the transformation matrix that diagonalizes a 3×3 \mathbf{L} as $\mathbf{M}^t \mathbf{L} \mathbf{M}$ having the general Toeplitz form given in (9.99a).

$$\mathbf{M} = \begin{bmatrix} 1 & 1 & 1 \\ \frac{1}{2} & -\frac{1}{2} & -\frac{1}{\sqrt{2}} \\ \frac{1}{\sqrt{2}} & \frac{1}{\sqrt{2}} & 0 \\ \frac{1}{2} & -\frac{1}{2} & \frac{1}{\sqrt{2}} \end{bmatrix}$$

- 9.16** Show that the transformation matrices in (9.103) diagonalize the per-unit-length matrices in (9.102).
9.17 Derive the forms of the generalized method of characteristics given in (9.105), (9.107), (9.110), and (9.111).
9.18 Derive the result in (9.122).
9.19 Derive the Vector Fitting result in (9.142) and (9.144).
9.20 Derive the least-squares result in (9.151).
9.21 Using `BRANIN.FOR`, `SPICEMTL.FOR`, and `SPICELPI.FOR`, reproduce the results for the ribbon cable shown in Figure 9.13(a).
9.22 Using `SPICEMTL.FOR` and `TIMEFREQ.FOR`, reproduce the results for the ribbon cable shown in Figure 9.14.
9.23 Using `SPICEMTL.FOR` and `FINDIF.FOR`, reproduce the results for the ribbon cable shown in Figure 9.15.
9.24 Using `SPICEMTL.FOR`, `TIMEFREQ.FOR` (and `MTL.FOR`), and `FDTDLOSS.FOR`, reproduce the results for the ribbon cable shown in Figure 9.17.
9.25 Using `BRANIN.FOR`, `SPICEMTL.FOR`, and `SPICELPI.FOR`, reproduce the results for the PCB shown in Figure 9.20.
9.26 Using `SPICEMTL.FOR` and `TIMEFREQ.FOR`, reproduce the results for the PCB shown in Figure 9.21.
9.27 Using `SPICEMTL.FOR` and `FINDIF.FOR`, reproduce the results for the PCB shown in Figure 9.22.

- 9.28** Using SPICEMTL.FOR, TIMEFREQ.FOR (and MTL.FOR), and FDTDLOSS.FOR, reproduce the results for the PCB shown in Figure 9.24.

REFERENCES

- [1] H. Amemiya, Time domain analysis of multiple parallel transmission lines, *RCA Review*, **28**, 241–276, 1967.
- [2] F.Y. Chang, Transient analysis of lossless coupled transmission lines in inhomogeneous dielectric media, *IEEE Transactions on Microwave Theory and Techniques*, **18** (9), 616–626, 1970.
- [3] C.W. Ho, Theory and computer-aided analysis of lossless transmission lines, *IBM Journal of Research and Development*, **17**, 249–255, 1973.
- [4] K.D. Marx, Propagation modes, equivalent circuits, and characteristic terminations for multiconductor transmission lines with inhomogeneous dielectrics, *IEEE Transactions on Microwave Theory and Techniques*, **21** (7), 450–457, 1973.
- [5] H.W. Dommel and W. S. Meyer, Computation of electromagnetic transients, *Proceedings of IEEE*, **62** (7), 983–993, 1974.
- [6] A.J. Gruodis, Transient analysis of uniform resistive transmission lines in a homogeneous medium, *IBM Journal of Research and Development*, **23** (6), 675–681, 1979.
- [7] A.J. Gruodis and C. S. Chang, Coupled lossy transmission line characterization and simulation, *IBM Journal of Research and Development*, **25** (1) 25–41, 1981.
- [8] A.R. Djordjevic, T.S., Sarkar, and R.F. Harrington, Analysis of lossy transmission lines with arbitrary nonlinear terminal networks, *IEEE Transactions on Microwave Theory and Techniques*, **34** (6), 660–666, 1986.
- [9] A.R. Djordjevic, T.S. Sarkar, and R.F. Harrington, Time-domain response of multiconductor transmission lines, *Proceedings of IEEE*, **75** (6), 743–764, 1987.
- [10] A. Ralston, *A First Course in Numerical Analysis*, McGraw-Hill, New York, 1965.
- [11] V.K. Tripathi and J.B. Rettig, A SPICE model for multiple coupled microstrips and other transmission lines, *IEEE Transactions on Microwave Theory and Techniques*, **33** (12), 1513–1518, 1985.
- [12] M.N.O. Sadiku, *Numerical Techniques in Electromagnetics*, CRC Press, Boca Raton, FL, 1992.
- [13] L.O. Chua and P.M. Lin, *Computer Aided Analysis of Electronic Circuits: Algorithms and Computational Techniques*, Prentice-Hall, Englewood Cliffs, NJ, 1975.
- [14] B.J. Leon, *Lumped Systems*, Holt, Rinehart, and Winston, New York, 1968.
- [15] F.Y. Chang, Waveform relaxation analysis of RLCG transmission lines, *IEEE Transactions on Circuits and Systems*, **37** (11), 1394–1415, 1990.
- [16] F.-Y. Chang, The generalized method of characteristics for waveform relaxation analysis of lossy coupled transmission lines, *IEEE Transactions on Microwave Theory and Techniques*, **37** (12), 2028–2038, 1989.
- [17] V.K. Tripathi and A. Hill, Equivalent circuit modeling of losses and dispersion in single and coupled lines for microwave and millimeter-wave integrated circuits, *IEEE Transactions on Circuits and Systems*, **36** (2), 256–262, 1988.

- [18] N. Orhanovic, V.K. Tripathi, and P. Wang, Generalized method of characteristics for time domain simulation of multiconductor lossy transmission lines, *Proceedings of the IEEE Symposium on Circuits and Systems*, 2388–2391, 1990.
- [19] F.Y. Chang, Waveform relaxation analysis of nonuniform lossy transmission lines characterized with frequency-dependent parameters, *IEEE Transactions on Circuits and Systems*, **38** (12), 1484–1500, 1991.
- [20] F.Y. Chang, Relaxation simulation of transverse electromagnetic wave propagation in coupled transmission lines, *IEEE Transactions on Circuits and Systems*, **38** (8), 916–936, 1991.
- [21] C. Gordon, T. Blazek, and R. Mittra, Time-domain simulation of multiconductor transmission lines with frequency-dependent losses, *IEEE Transactions on Computer-Aided Design*, **11** (11), 1372–1387, 1992.
- [22] F.Y. Chang, Transient simulation of nonuniform coupled lossy transmission lines characterized with frequency-dependent parameters part II: Discrete-time analysis, *IEEE Transactions on Circuits and Systems*, **39** (11), 907–927, 1992.
- [23] S. Lin and E.S. Kuh, Transient simulation of lossy interconnects based on the recursive convolution formulation, *IEEE Transactions on Circuits and Systems-I: Fundamental Theory and Applications*, **39** (11), 879–892, 1992.
- [24] V.K. Tripathi and N. Orhanovic, Time-domain characterization and analysis of dispersive dissipative interconnects, *IEEE Transactions on Circuits and Systems*, **39** (11), 938–945, 1992.
- [25] J.I. Alonso, J.B. Borja, and F. Perez, A universal model for lossy and dispersive transmission lines for time domain CAD of circuits, *IEEE Transactions on Microwave Theory and Techniques*, **40** (5), 938–946, 1992.
- [26] J. Mao and Z. Li, Analysis of the time response of multiconductor transmission lines with frequency-dependent losses by the method of convolution characteristics, *IEEE Transactions on Microwave Theory and Techniques*, **40** (4), 637–644, 1992.
- [27] F.Y. Chang, Transient simulation of frequency-dependent nonuniform coupled lossy transmission lines, *IEEE Transactions on Components, Packaging, and Manufacturing Technology*, **17** (1), 3–14, 1994.
- [28] S. Grivet-Talocia, H.-M. Huang, A.E. Ruehli, F. Canavero, and I.M. Elfadel, Transient analysis of lossy transmission lines: An efficient approach based on the method of characteristics, *IEEE Transactions on Advanced Packaging*, **27** (1), 45–56, 2004.
- [29] K. Singhal and J. Vlach, Computation of the time-domain response by numerical inversion of the laplace transform, *Journal of Franklin Institute*, **299** (2), 109–126, 1975.
- [30] J.R. Griffith and M.S. Nakhla, Time-domain analysis of lossy coupled transmission lines, *IEEE Transactions on Microwave Theory and Techniques*, **38** (10), 1480–1487, 1990.
- [31] E.C. Chang and S. Kang, Computationally efficient simulation of a lossy transmission line with skin effect by using numerical inversion of laplace transform, *IEEE Transactions on Circuits and Systems-I: Fundamental Theory and Applications*, **39** (11), 861–868, 1992.
- [32] I. Maio and F.G. Canavero, Lossy transmission line response via numerical laplace transform inversion, *Proceedings of the 1994 International Symposium on Circuits and Systems*, **6**, 133–135, 1994.

- [33] F. Romeo and M. Santomauro, Time-domain simulation of n coupled transmission lines, *IEEE Transactions on Microwave Theory and Techniques*, **35** (2), 131–136, 1987.
- [34] D.S. Gao, A.T. Yang, and S.M. Kang, Modeling and simulation of interconnection delays and crosstalks in high-speed integrated circuits, *IEEE Transactions on Circuits and Systems*, **37** (1), 1–9, 1990.
- [35] R. Achar and M.S. Nakhla, Simulation of high-speed interconnects, *Proceedings of IEEE*, **89** (5), 693–728, 2001.
- [36] A. Dounavis, X. Li, M.S. Nakhla, and R. Achar, Passive closed-form transmission-line model for general purpose circuit simulators, *IEEE Transactions on Microwave Theory and Techniques*, **47** (12), 2450–2459, 1999.
- [37] A. Dounavis, R. Achar, and M.S. Nakhla, Efficient passive circuit models for distributed networks with frequency-dependent parameters, *IEEE Transactions on Advanced Packaging*, **23** (3), 382–392, 2000.
- [38] L.T. Pillage and R.A. Rohrer, Asymptotic waveform evaluation for timing analysis, *IEEE Transactions on Computer-Aided Design*, **9**, 352–366, 1990.
- [39] T.K. Tang, M.S. Nakhla, and R. Griffith, Analysis of lossy multiconductor transmission lines using the asymptotic waveform evaluation technique, *IEEE Transactions on Microwave Theory and Techniques*, **39** (12), 2107–2116, 1991.
- [40] T.K. Tang and M.S. Nakhla, Analysis of high-speed VLSI interconnects using the asymptotic waveform evaluation technique, *IEEE Transactions on Computer-Aided Design*, **11**, 341–352, 1992.
- [41] J.E. Bracken, V. Raghavan, and R.A. Rohrer, Interconnect simulation with asymptotic waveform evaluation (AWE), *IEEE Transactions on Circuits and Systems-I: Fundamental Theory and Applications*, **39** (11), 869–878, 1992.
- [42] E. Chiprout and M. Nakhla, *Asymptotic Waveform Evaluation and Moment Matching for Interconnect Analysis*, Kluwer, Boston, MA, 1993.
- [43] C.-W. Ho, A.E. Ruehli, and P.A. Brennan, The modified nodal approach to network analysis, *IEEE Transactions on Circuits and Systems*, **22** (6), 504–509, 1975.
- [44] E. Chiprout and M. Nakhla, Analysis of interconnected networks using complex frequency hopping, *IEEE Transactions on Computer-Aided Design*, **14**, 186–199, 1995.
- [45] B. Gustavsen and A. Semlyen, Rational approximation of frequency domain responses by vector fitting, *IEEE Transactions on Power Delivery*, **14** (3), 1052–1059, 1999.
- [46] M.S. Sarto, A. Scarlatti, and C.L. Holloway, On the use of fitting models for the time-domain analysis of problems with frequency-dependent parameters, *Proceedings of the 2001 IEEE International Symposium on Electromagnetic Compatibility*, Montreal, Canada, 580–593, August 13–17, 2001.
- [47] B. Gustavsen, Improving the pole relocating properties of vector fitting, *IEEE Transactions on Power Delivery*, **21** (3), 1587–1592, 2006.
- [48] B. Gustavsen and A. Semlyen, Simulation of transmission line transients using vector fitting and modal decomposition, *IEEE Transactions on Power Delivery*, **13** (2), 605–614, 1998.
- [49] W.H. Press, S.A. Teukolsky, W.T. Vetterling, and B.R. Flannery, *Numerical Recipes in Fortran: The Art of Scientific Computing*, 2nd edition, Cambridge University Press, New York, 1992.
- [50] G. Antonini, SPICE equivalent circuits of frequency-domain responses, *IEEE Transactions on Electromagnetic Compatibility*, **45** (3), 502–512, 2003.

10

LITERAL (SYMBOLIC) SOLUTIONS FOR THREE-CONDUCTOR LINES

The general solution of the transmission-line equations for a two-conductor line considered in Chapters 6 and 8 is simple enough that it can be obtained in *literal form*, that is, in terms of *symbols* for the line terminations and the line parameters such as characteristic impedance Z_C and the line one-way time delay T_D . For example, see Eqs. (6.39) and (6.70) of Chapter 6 and (8.14) of Chapter 8. This literal or symbolic solution gives considerable insight into how the various parameters affect the terminal voltages and currents. This advantage is similar to a transfer function that is useful in the design and analysis of electric circuits and automatic control systems [A.2]. In order to obtain the same insight from the numerical solution, we would need to perform a large set of computations with these parameters being varied over their range of anticipated values.

Chapters 7 and 9 have examined the solution of the MTL (multiconductor transmission line) equations for a general $(n + 1)$ -conductor line. This is so complex that it is not feasible to generate literal solutions, and the solution process must be accomplished with digital computer programs, that is, a numerical result is obtained. This numerical process does not reveal the general behavior of the solution. In other words, the only information we obtain is the solution for the specific set of input data, for example, line length, terminal impedance levels, source voltages, frequency, and so on. In order to understand the general behavior of the solution for a general $(n + 1)$ -conductor MTL, it would be helpful to have a *literal solution* for the induced crosstalk voltages in terms of the *symbols* for the line length, terminal impedances, per-unit-length capacitances and inductances, source voltage, and so on. From such

a result we could observe how changes in these parameters would affect the solution. Although highly desirable, such a literal solution is, in general, not feasible.

It is important to keep in mind that even though it may be *possible* to obtain a literal solution after laboriously manipulating the symbolic equations, any such result is worthless unless the result is simple enough to clearly and easily show what the mathematical result is telling us about the behavior of the system. There exist in the literature several symbolic results that are so complicated that no physical insight can be obtained. Hence, there is little value to going through the laborious symbolic solution, and one can obtain the same information included in these symbolic equations more easily by simply solving the transmission-line equations and incorporating the terminal constraints using numerical computer solutions. Hence, any symbolic result is useful only if it is simple enough to be interpretable.

Several transmission-line literal transfer functions for the prediction of crosstalk have been derived in the past for use in the frequency-domain analysis of microwave circuits [1–4] or for time-domain analysis of crosstalk in digital circuits [5–11]. All of these solutions assume that the line is a *three-conductor line*, that is, $n = 2$, with two signal conductors and a reference conductor. In addition, these results make the following assumptions about the line in order to simplify the derivation.

1. The line is *symmetric*, that is, the two signal conductors are identical in cross-sectional shape and the cross-sectional line dimensions are such that the self capacitances and inductances are identical, that is, $c_{11} = c_{22}$ and $l_{11} = l_{22}$. An example is the coupled microstrip where the two identical lands are at the same distance above the ground plane. For this case, the per-unit-length inductance and capacitance matrices are of the form

$$\mathbf{L} = \begin{bmatrix} l & l_m \\ l_m & l \end{bmatrix}, \quad \mathbf{C} = \begin{bmatrix} (c + c_m) & -c_m \\ -c_m & (c + c_m) \end{bmatrix}$$

2. The line is *weakly coupled*, that is, the effect of the induced signals in the receiving circuit on the driven circuit, that is, back interaction, is neglected (widely separated lines tend to satisfy this in an approximate fashion the wider the separation).
3. Both lines are *matched at both ends*, that is, the line is terminated at all four ports in the line characteristic impedances. The question of what is meant by the “line characteristic impedances” for an MTL will need to be clarified. For *weakly coupled* or widely separated lines, these approximate to the characteristic impedances of the isolated two-conductor lines.
4. The line is *lossless*, that is, the conductors are perfect conductors and the surrounding medium is lossless.

The obvious reason why these assumptions are used is to simplify the difficult manipulation of the *symbols* that are involved in the literal solution. The assumption of a symmetric line and the subsequent literal solution is referred to in the microwaves

literature as the *even-odd mode solution* [1–3]. However, the vast majority of the applications are not perfectly matched *at all four ports*. For example, consider a three-conductor line where each line with the reference conductor connects a CMOS driver and a CMOS receiver. The input to a CMOS inverter looks essentially capacitive. Since the characteristic impedances for lossless lines must be purely real, that is, resistive, these lines are severely mismatched at their load ends.

The purpose of this chapter is to derive the *literal or symbolic solution of the MTL equations for a three-conductor line and to incorporate the terminal constraints into this solution to yield explicit, symbolic equations for the crosstalk*. Both the frequency-domain and the time-domain solutions will be obtained. In addition, the derivations will not presume a symmetric line nor will they presume a “matched” line. The idea is to simply proceed through the usual solution steps that would be involved in a numerical solution but instead to use symbols for all quantities rather than numbers. First, we determine the general solution of the MTL equations for $n = 2$. This has generally already been done in earlier chapters. However, in order to simplify the solution, we will assume a *lossless line*, that is, we will assume perfect conductors in a lossless medium, $\mathbf{R} = \mathbf{0}$ and $\mathbf{G} = \mathbf{0}$. Next, we incorporate the terminal constraints into that general solution in order to give the desired literal solution. For a three-conductor line this last step, incorporation of the terminal conditions, involves the simultaneous solution of symbolic equations with, for example, Cramer’s rule and is quite tedious. It therefore does not appear to be feasible to extend this symbolic solution to lines consisting of more than three conductors. Even for a three-conductor line, the solution effort is so great that we must make another simplifying assumption. This primary assumption is to assume a *homogeneous surrounding medium* so that we may take advantage of the important identity for a homogeneous medium, $\mathbf{LC} = \mu\epsilon\mathbf{1}_2$. This identity essentially reduces the number of symbols and allows the consolidation of certain other groups of the per-unit-length symbols. Once the exact result has been derived for only the assumption of a lossless line in a homogeneous medium, we will then specialize this exact result to the case of *weak coupling* between the two circuits. This will verify the widely used approximate model referred to as the *inductive-capacitive coupling model* [A.3]. The solution for the general case of perfect conductors in a lossless but *inhomogeneous medium* is obtained in [B.30]. In order for that solution to be feasible to obtain, the assumption of *weak coupling* must be made at the outset.

The general statement of the problem is illustrated in Figure 10.1(a). The line consists of three *perfect conductors* immersed in a *lossless medium*. The *generator circuit* is composed of a generator conductor with the reference conductor. It is driven at the left end with an open-circuit source voltage $V_S(t)$ and source resistance R_S and is terminated at the right end in a load resistance R_L . The *receptor circuit* is composed of a receptor conductor and the reference conductor. It is terminated at the left or “near end” in a resistance R_{NE} and at the right or “far end” in a resistance R_{FE} . Although resistive terminations are used in the following developments, the frequency-domain phasor crosstalk results that we will obtain apply for complex-valued terminal impedances. The per-unit-length equivalent circuit is shown in Figure 10.1(b). From this, the MTL equations can be derived in the usual manner

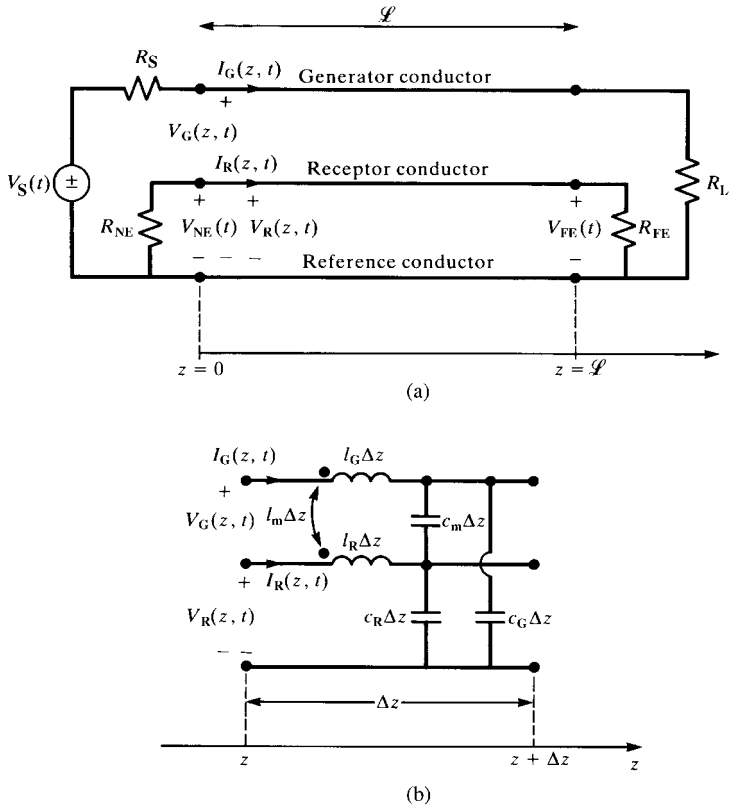


FIGURE 10.1 The three-conductor MTL: (a) line dimensions and terminal characterization and (b) the per-unit-length equivalent circuit.

and become

$$\frac{\partial}{\partial z} \mathbf{V}(z, t) = -\mathbf{L} \frac{\partial}{\partial t} \mathbf{I}(z, t) \tag{10.1a}$$

$$\frac{\partial}{\partial z} \mathbf{I}(z, t) = -\mathbf{C} \frac{\partial}{\partial t} \mathbf{V}(z, t) \tag{10.1b}$$

where

$$\mathbf{V}(z, t) = \begin{bmatrix} V_G(z, t) \\ V_R(z, t) \end{bmatrix} \tag{10.2a}$$

$$\mathbf{I}(z, t) = \begin{bmatrix} I_G(z, t) \\ I_R(z, t) \end{bmatrix} \tag{10.2b}$$

$$\mathbf{L} = \begin{bmatrix} l_G & l_m \\ l_m & l_R \end{bmatrix} \tag{10.2c}$$

$$\mathbf{C} = \begin{bmatrix} c_G + c_m & -c_m \\ -c_m & c_R + c_m \end{bmatrix} \tag{10.2d}$$

Subscripts G denote quantities associated with the generator circuit, whereas subscripts R denote quantities associated with the receptor circuit. The subscript m denotes the mutual quantity between the two circuits. The generalized Thevenin equivalent characterization of the terminations becomes

$$\mathbf{V}(0, t) = \mathbf{V}_S(t) - \mathbf{R}_S \mathbf{I}(0, t) \tag{10.3a}$$

$$\mathbf{V}(\mathcal{L}, t) = \mathbf{R}_L \mathbf{I}(\mathcal{L}, t) \tag{10.3b}$$

where

$$\mathbf{V}_S(t) = \begin{bmatrix} V_S(t) \\ 0 \end{bmatrix} \tag{10.4a}$$

$$\mathbf{R}_S = \begin{bmatrix} R_S & 0 \\ 0 & R_{NE} \end{bmatrix} \tag{10.4b}$$

$$\mathbf{R}_L = \begin{bmatrix} R_L & 0 \\ 0 & R_{FE} \end{bmatrix} \tag{10.4c}$$

Although we assume resistive terminations, the frequency-domain solution will allow complex-valued terminations. The objective is to obtain equations for the time-domain near-end and far-end crosstalk voltages: $V_{NE}(t) = V_R(0, t)$ and $V_{FE}(t) = V_R(\mathcal{L}, t)$.

10.1 THE LITERAL FREQUENCY-DOMAIN SOLUTION FOR A HOMOGENEOUS MEDIUM

In order to simplify the solution process, we assume that the surrounding medium is *homogeneous* and characterized by permittivity ϵ and permeability μ . Because of the assumption of a *homogeneous surrounding medium*, we have the important identity

$$\mathbf{LC} = \mu\epsilon \mathbf{1}_2 = \frac{1}{v^2} \mathbf{1}_2 \tag{10.5a}$$

or, by multiplying both sides by \mathbf{L}^{-1} ,

$$\underbrace{\begin{bmatrix} (c_G + c_m) & -c_m \\ -c_m & (c_R + c_m) \end{bmatrix}}_{\mathbf{C}} = \frac{1}{v^2} \underbrace{\begin{bmatrix} l_R & -l_m \\ -l_m & l_G \end{bmatrix}}_{\mathbf{L}^{-1}} \tag{10.5b}$$

where $v = 1/\sqrt{\mu\epsilon}$ is the velocity of propagation of the waves in the homogeneous medium. This identity gives the following relations between the per-unit-length

parameters:

$$l_G(c_G + c_m) = l_R(c_R + c_m) \tag{10.6a}$$

$$l_m(c_G + c_m) = l_R c_m \tag{10.6b}$$

$$l_m(c_R + c_m) = l_G c_m \tag{10.6c}$$

$$(c_G + c_m) = \frac{l_R}{v^2 (l_G l_R - l_m^2)} \tag{10.6d}$$

$$(c_R + c_m) = \frac{l_G}{v^2 (l_G l_R - l_m^2)} \tag{10.6e}$$

$$c_m = \frac{l_m}{v^2 (l_G l_R - l_m^2)} \tag{10.6f}$$

The frequency-domain MTL equations for sinusoidal steady-state excitation become

$$\frac{d}{dz} \hat{\mathbf{V}}(z) = -j\omega \mathbf{L} \hat{\mathbf{I}}(z) \tag{10.7a}$$

$$\frac{d}{dz} \hat{\mathbf{I}}(z) = -j\omega \mathbf{C} \hat{\mathbf{V}}(z) \tag{10.7b}$$

where the *phasor* line voltages and currents are

$$\hat{\mathbf{V}}(z) = \begin{bmatrix} \hat{V}_G(z) \\ \hat{V}_R(z) \end{bmatrix} \tag{10.8a}$$

$$\hat{\mathbf{I}}(z) = \begin{bmatrix} \hat{I}_G(z) \\ \hat{I}_R(z) \end{bmatrix} \tag{10.8b}$$

The phasor generalized Thevenin equivalent characterization of the terminations becomes

$$\hat{\mathbf{V}}(0) = \hat{\mathbf{V}}_S - \mathbf{R}_S \hat{\mathbf{I}}(0) \tag{10.9a}$$

$$\hat{\mathbf{V}}(\mathcal{L}) = \mathbf{R}_L \hat{\mathbf{I}}(\mathcal{L}) \tag{10.9b}$$

where

$$\hat{\mathbf{V}}_S = \begin{bmatrix} \hat{V}_S \\ 0 \end{bmatrix} \tag{10.10a}$$

$$\mathbf{R}_S = \begin{bmatrix} R_S & 0 \\ 0 & R_{NE} \end{bmatrix} \tag{10.10b}$$

$$\mathbf{R}_L = \begin{bmatrix} R_L & 0 \\ 0 & R_{FE} \end{bmatrix} \quad (10.10c)$$

The objective is to obtain equations for the phasor near-end and far-end crosstalk voltages: $\hat{V}_{NE} = \hat{V}_R(0)$ and $\hat{V}_{FE} = \hat{V}_R(\mathcal{L})$.

For this special case of perfect conductors in a lossless homogeneous medium, the MTL equations are decoupled as in Section 7.2.2.1 giving

$$\hat{\gamma} = j\omega\sqrt{\mu\epsilon}\mathbf{1}_2 \quad (10.11a)$$

$$\hat{\mathbf{T}}_I = \hat{\mathbf{T}}_V = \mathbf{1}_2 \quad (10.11b)$$

$$\hat{\mathbf{Z}}_C = v\mathbf{L} \quad (10.11c)$$

$$\hat{\mathbf{Y}}_C = v\mathbf{C} \quad (10.11d)$$

where $\mathbf{1}_2$ is the 2×2 identity matrix. The general solution of the MTL equations in terms of the chain-parameter matrix for this case becomes

$$\begin{bmatrix} \hat{\mathbf{V}}(\mathcal{L}) \\ \hat{\mathbf{I}}(\mathcal{L}) \end{bmatrix} = \begin{bmatrix} \hat{\Phi}_{11} & \hat{\Phi}_{12} \\ \hat{\Phi}_{21} & \hat{\Phi}_{22} \end{bmatrix} \begin{bmatrix} \hat{\mathbf{V}}(0) \\ \hat{\mathbf{I}}(0) \end{bmatrix} \quad (10.12)$$

where the chain-parameter submatrices for this case of perfect conductors in a lossless homogeneous medium simplify to (see Eqs. (7.115) of Chapter 7)

$$\hat{\Phi}_{11} = C\mathbf{1}_2 \quad (10.13a)$$

$$\hat{\Phi}_{12} = -j\omega\mathcal{L}S\mathbf{L} \quad (10.13b)$$

$$\hat{\Phi}_{21} = -j\omega\mathcal{L}S\mathbf{C} \quad (10.13c)$$

$$\hat{\Phi}_{22} = C\mathbf{1}_2 \quad (10.13d)$$

where

$$C = \cos(\beta\mathcal{L}) \quad (10.14a)$$

$$S = \frac{\sin(\beta\mathcal{L})}{\beta\mathcal{L}} \quad (10.14b)$$

and the phase constant is

$$\beta = \frac{\omega}{v} \quad (10.14c)$$

The terminal characterization in (10.9) is substituted into the chain-parameter matrix in (10.12) to give (see Eqs. (7.92) of Chapter 7)

$$[\hat{\Phi}_{11}\mathbf{R}_S + \mathbf{R}_L\hat{\Phi}_{22} - \hat{\Phi}_{12} - \mathbf{R}_L\hat{\Phi}_{21}\mathbf{R}_S]\hat{\mathbf{I}}(0) = [\hat{\Phi}_{11} - \mathbf{R}_L\hat{\Phi}_{21}]\hat{\mathbf{V}}_S \quad (10.15a)$$

$$[\hat{\Phi}_{11}\mathbf{R}_L + \mathbf{R}_S\hat{\Phi}_{22} - \hat{\Phi}_{12} - \mathbf{R}_S\hat{\Phi}_{21}\mathbf{R}_L]\hat{\mathbf{I}}(\mathcal{L}) = \hat{\mathbf{V}}_S \quad (10.15b)$$

Substituting the chain-parameter submatrices given in (10.13) into (10.15) gives

$$[C(\mathbf{R}_S + \mathbf{R}_L) + S(\mathbf{R}_L j\omega\mathbf{C}\mathcal{L}\mathbf{R}_S + j\omega\mathbf{L}\mathcal{L})]\hat{\mathbf{I}}(0) = [C\mathbf{1}_2 + S\mathbf{R}_L j\omega\mathbf{C}\mathcal{L}]\hat{\mathbf{V}}_S \quad (10.16a)$$

$$[C(\mathbf{R}_S + \mathbf{R}_L) + S(\mathbf{R}_S j\omega\mathbf{C}\mathcal{L}\mathbf{R}_L + j\omega\mathbf{L}\mathcal{L})]\hat{\mathbf{I}}(\mathcal{L}) = \hat{\mathbf{V}}_S \quad (10.16b)$$

Each of the equations in (10.16a) and (10.16b) are two simultaneous equations and once they are solved, the near-end and far-end crosstalk voltages are obtained from the second entries in these solution vectors as $\hat{V}_{NE} = \hat{V}_R(0) = -R_{NE}\hat{I}_R(0)$ and $\hat{V}_{FE} = \hat{V}_R(\mathcal{L}) = R_{FE}\hat{I}_R(\mathcal{L})$.

Equations (10.16) were solved in [B.6] in literal form via Cramer's rule to yield the following *exact* literal solutions for the near-end and far-end crosstalk voltages:

$$\hat{V}_{NE} = \frac{j\omega M_{NE} S}{\text{Den}} [C + j\omega T_D K_{NE} S] \hat{V}_S \quad (10.17a)$$

$$\hat{V}_{FE} = \frac{j\omega M_{FE} S}{\text{Den}} \hat{V}_S \quad (10.17b)$$

$$\text{Den} = C^2 + (j\omega)^2 S^2 \tau_G \tau_R P + j\omega CS (\tau_G + \tau_R) \quad (10.17c)$$

The various quantities in these equations are defined as [B.6]

$$M_{NE} = M_{NE}^{\text{IND}} + M_{NE}^{\text{CAP}} \quad (10.18a)$$

$$M_{FE} = M_{FE}^{\text{IND}} + M_{FE}^{\text{CAP}} \quad (10.18b)$$

where the *inductive coupling* coefficients are defined by

$$M_{NE}^{\text{IND}} = \frac{R_{NE}}{R_{NE} + R_{FE}} l_m \mathcal{L} \frac{1}{R_S + R_L} \quad (10.19a)$$

$$M_{FE}^{\text{IND}} = -\frac{R_{FE}}{R_{NE} + R_{FE}} l_m \mathcal{L} \frac{1}{R_S + R_L} \quad (10.19b)$$

and the *capacitive coupling* coefficients are defined by

$$M_{NE}^{\text{CAP}} = \frac{R_{NE} R_{FE}}{R_{NE} + R_{FE}} c_m \mathcal{L} \frac{R_L}{R_S + R_L} \quad (10.20a)$$

$$M_{FE}^{\text{CAP}} = M_{NE}^{\text{CAP}} \quad (10.20b)$$

The coupling coefficient between the two circuits is defined by

$$\begin{aligned} k &= \frac{l_m}{\sqrt{l_G l_R}} \\ &= \frac{c_m}{\sqrt{(c_G + c_m)(c_R + c_m)}} \end{aligned} \quad (10.21)$$

and the circuit characteristic impedances are defined by

$$\begin{aligned} Z_{CG} &= \sqrt{\frac{l_G}{(c_G + c_m)}} \\ &= v l_G \sqrt{1 - k^2} \\ &= \frac{1}{v(c_G + c_m)\sqrt{1 - k^2}} \end{aligned} \quad (10.22a)$$

$$\begin{aligned} Z_{CR} &= \sqrt{\frac{l_R}{(c_R + c_m)}} \\ &= v l_R \sqrt{1 - k^2} \\ &= \frac{1}{v(c_R + c_m)\sqrt{1 - k^2}} \end{aligned} \quad (10.22b)$$

where we have substituted (10.21) and the identities from (10.6d) and (10.6e). It should be pointed out that, as was previously determined, the line has a characteristic impedance *matrix*, and scalar characteristic impedances as defined above have no functional meaning. Here, we are merely defining terms that relate back and reduce to the scalar characteristic impedances of the two-conductor line. Observe that these definitions of each characteristic impedance do not simply involve just the self-capacitances of each circuit, c_G and c_R , but also contain the mutual capacitance c_m as $(c_G + c_m)$ and $(c_R + c_m)$. For weakly coupled lines ($k \ll 1$) these do indeed reduce to the scalar characteristic impedances of the isolated lines; $Z_{CG} \cong v l_G$ and $Z_{CR} \cong v l_R$. The relationships of the termination impedances to their associated characteristic impedances are important parameters. In order to highlight this dependency, the various ratios of termination impedance to the appropriate characteristic impedance are defined by

$$\begin{aligned} \alpha_{SG} &= \frac{R_S}{Z_{CG}}, & \alpha_{LG} &= \frac{R_L}{Z_{CG}} \\ \alpha_{SR} &= \frac{R_{NE}}{Z_{CR}}, & \alpha_{LR} &= \frac{R_{FE}}{Z_{CR}} \end{aligned} \quad (10.23)$$

The remaining quantities are defined in the following way. The coefficient K_{NE} in (10.17) is defined by

$$\begin{aligned}
 K_{NE} &= \frac{1}{\sqrt{1-k^2}} \left(\frac{Z_{CG}R_{FE} + Z_{CR}R_L}{Z_{CG}Z_{CR} + R_LR_{FE}} \right) \\
 &= \frac{1}{\sqrt{1-k^2}} \left(\frac{\alpha_{LG} + \alpha_{LR}}{1 + \alpha_{LG}\alpha_{LR}} \right)
 \end{aligned}
 \tag{10.24}$$

If only one line is matched at its load end, that is, $\alpha_{LG} = 1$ or $\alpha_{LR} = 1$, then $K_{NE} = 1/\sqrt{1-k^2}$ and for a weakly coupled line, $k \ll 1$, $K_{NE} \cong 1$. The circuit *time constants* are logically defined as

$$\begin{aligned}
 \tau_G &= \frac{l_G \mathcal{L}}{R_S + R_L} + (c_G + c_m)\mathcal{L} \frac{R_S R_L}{R_S + R_L} \\
 &= \frac{T_D}{\sqrt{1-k^2}} \left\{ \frac{1 + \alpha_{SG}\alpha_{LG}}{\alpha_{SG} + \alpha_{LG}} \right\}
 \end{aligned}
 \tag{10.25a}$$

$$\begin{aligned}
 \tau_R &= \frac{l_R \mathcal{L}}{R_{NE} + R_{FE}} + (c_R + c_m)\mathcal{L} \frac{R_{NE} R_{FE}}{R_{NE} + R_{FE}} \\
 &= \frac{T_D}{\sqrt{1-k^2}} \left\{ \frac{1 + \alpha_{SR}\alpha_{LR}}{\alpha_{SR} + \alpha_{LR}} \right\}
 \end{aligned}
 \tag{10.25b}$$

and the line one-way delay is denoted as

$$T_D = \frac{\mathcal{L}}{v}
 \tag{10.26}$$

and $v = 1/\sqrt{\mu \epsilon}$ for this homogeneous medium. If a line is matched at only one end, its time constant reduces to $T_D/\sqrt{1-k^2}$. In other words, $\tau_i = T_D/\sqrt{1-k^2}$ if $\alpha_{Si} = 1$ or if $\alpha_{Li} = 1$. In addition, if the line is weakly coupled, $k \ll 1$, the time constant reduces to $\tau_i \cong T_D$.

In terms of the ratios in (10.23), the factor P in Den in (10.17c) becomes

$$P = \left[1 - k^2 \frac{(1 - \alpha_{SG}\alpha_{LR})(1 - \alpha_{LG}\alpha_{SR})}{(1 + \alpha_{SG}\alpha_{LG})(1 + \alpha_{SR}\alpha_{LR})} \right]
 \tag{10.27}$$

The coupling coefficient is always less than unity, that is, $k < 1$. Hence, $P \cong 1$ if the line is *weakly coupled*, $k \ll 1$. There is another important case where P is identically unity, $P = 1$, and that occurs when the lines are matched at opposite ends, that is, $\alpha_{SG} = \alpha_{LR} = 1$ or $\alpha_{LG} = \alpha_{SR} = 1$, which occurs in *directional couplers* [1]. Hence, for these cases, the denominator of the expression in (10.17c) factors as

$$\text{Den} \cong (C + j\omega S \tau_G)(C + j\omega S \tau_R), \quad P \cong 1
 \tag{10.17c}$$

10.1.1 Inductive and Capacitive Coupling

The above results are an exact literal solution for the problem. No assumptions about symmetry or matched loads are used. Therefore, they cover a wider class of problems than have been considered in the past. Although they have been simplified by defining certain terms, they can be simplified further if we make the following assumptions. First, let us assume that *the line is electrically short at the frequency of interest*, that is, $\mathcal{L} \ll \lambda$. In this case, the terms C and S simplify to

$$\begin{aligned} C &= \cos(\beta \mathcal{L}) \\ &= \cos\left(2\pi \frac{\mathcal{L}}{\lambda}\right) \\ &\cong 1, \quad \mathcal{L} \ll \lambda \end{aligned} \tag{10.28a}$$

$$\begin{aligned} S &= \frac{\sin(\beta \mathcal{L})}{\beta \mathcal{L}} \\ &= \frac{\sin\left(2\pi \frac{\mathcal{L}}{\lambda}\right)}{2\pi \frac{\mathcal{L}}{\lambda}} \\ &\cong 1, \quad \mathcal{L} \ll \lambda \end{aligned} \tag{10.28b}$$

Further, let us assume that $\text{Den} \cong 1$ in (10.17c). This will be the case for a *weakly coupled line*, that is, $k \ll 1$, such that P in (10.27) is approximately unity, $P \cong 1$, and a *sufficiently small frequency* such that $\text{Den} \cong 1$ in (10.17c). Under these assumptions, the exact results in (10.17) simplify to

$$\hat{V}_{\text{NE}} \cong j\omega \left[\underbrace{\frac{R_{\text{NE}}}{R_{\text{NE}} + R_{\text{FE}}} l_{\text{m}} \mathcal{L} \frac{1}{R_{\text{S}} + R_{\text{L}}}}_{M_{\text{NE}}^{\text{IND}}} + \underbrace{\frac{R_{\text{NE}} R_{\text{FE}}}{R_{\text{NE}} + R_{\text{FE}}} c_{\text{m}} \mathcal{L} \frac{R_{\text{L}}}{R_{\text{S}} + R_{\text{L}}}}_{M_{\text{NE}}^{\text{CAP}}} \right] \hat{V}_{\text{S}} \tag{10.29a}$$

$$\hat{V}_{\text{FE}} \cong j\omega \left[\underbrace{-\frac{R_{\text{FE}}}{R_{\text{NE}} + R_{\text{FE}}} l_{\text{m}} \mathcal{L} \frac{1}{R_{\text{S}} + R_{\text{L}}}}_{M_{\text{FE}}^{\text{IND}}} + \underbrace{\frac{R_{\text{NE}} R_{\text{FE}}}{R_{\text{NE}} + R_{\text{FE}}} c_{\text{m}} \mathcal{L} \frac{R_{\text{L}}}{R_{\text{S}} + R_{\text{L}}}}_{M_{\text{FE}}^{\text{CAP}}} \right] \hat{V}_{\text{S}} \tag{10.29b}$$

These low-frequency results can be computed from the equivalent circuit of Figure 10.2(a). The terms depending on the per-unit-length mutual inductance l_{m} are referred to as the *inductive coupling contributions*, whereas the terms depending on the per-unit-length mutual capacitance c_{m} are referred to as the *capacitive coupling contributions*.

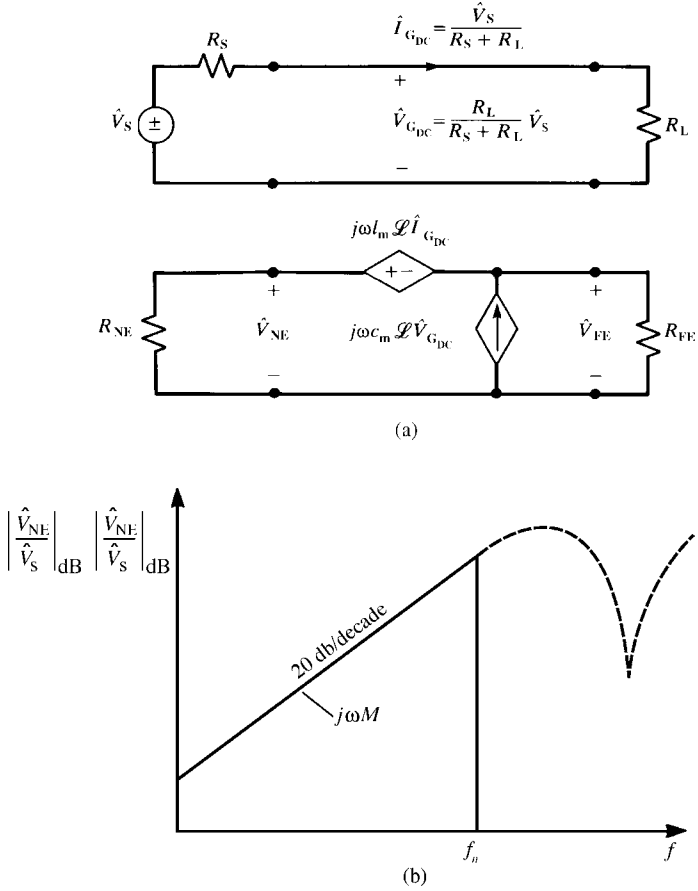


FIGURE 10.2 The frequency-domain inductive-capacitive low-frequency coupling model.

Observe that the low-frequency approximate results in (10.29) show that the crosstalk varies directly with frequency or 20 dB/decade as illustrated in Figure 10.2(b). The total coupling can be written as the sum of inductive coupling and capacitive coupling components as

$$\hat{V}_{NE} \cong \underbrace{j\omega M_{NE}^{IND}}_{\hat{V}_{NE}^{IND}} \hat{V}_S + \underbrace{j\omega M_{NE}^{CAP}}_{\hat{V}_{NE}^{CAP}} \hat{V}_S \tag{10.30a}$$

$$\hat{V}_{FE} \cong \underbrace{j\omega M_{FE}^{IND}}_{\hat{V}_{FE}^{IND}} \hat{V}_S + \underbrace{j\omega M_{FE}^{CAP}}_{\hat{V}_{FE}^{CAP}} \hat{V}_S \tag{10.30b}$$

Depending on the levels of the load impedances, the inductive coupling contribution may dominate the capacitive coupling contribution, or vice versa. This is illustrated

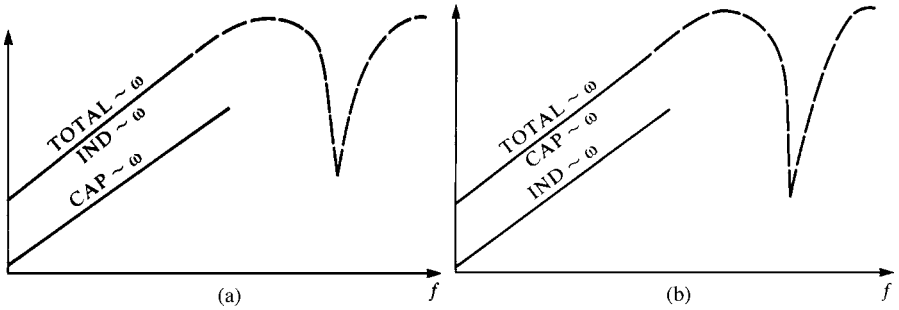


FIGURE 10.3 Illustration of the dominance of (a) inductive coupling for low-impedance terminations and (b) capacitive coupling for high-impedance terminations.

in Figure 10.3. If the termination impedances are much smaller than the line characteristic impedances, that is, *low-impedance loads*, then inductive coupling dominates. This is shown by substituting (10.19) and (10.20) into $M_{NE}^{IND} > M_{NE}^{CAP}$ and $M_{FE}^{IND} > M_{FE}^{CAP}$ to yield

$$\frac{R_{FE} R_L}{(l_m/c_m)} = \frac{R_{FE} R_L}{Z_{CG} Z_{CR}} < 1, \quad M_{NE}^{IND} > M_{NE}^{CAP} \tag{10.31a}$$

$$\frac{R_{NE} R_L}{(l_m/c_m)} = \frac{R_{NE} R_L}{Z_{CG} Z_{CR}} < 1, \quad M_{FE}^{IND} > M_{FE}^{CAP} \tag{10.31b}$$

We have written this result in terms of the line characteristic impedances by substituting the identity in (10.6f) along with (10.21) into (10.22). On the contrary, capacitive coupling dominates in the case of *high-impedance loads*, that is, $M_{NE}^{IND} < M_{NE}^{CAP}$ and $M_{FE}^{IND} < M_{FE}^{CAP}$. Thus, capacitive coupling dominates inductive coupling when the inequalities in (10.31) are reversed, that is, for high-impedance loads.

Although this approximation is valid only for a line that is electrically short and for a sufficiently small frequency, this separation of the total coupling into an inductive coupling and a capacitive coupling component provides considerable understanding of the crosstalk phenomena. In particular, it readily explains how shields and/or twisted pairs of wires will or will not reduce crosstalk [A.3].

10.1.2 Common-Impedance Coupling

The above derivation assumes that all three conductors are *perfect conductors* and the surrounding homogeneous medium is *lossless*. Losses can be ignored in many practical problems. However, there is a potentially significant contribution to crosstalk via imperfect conductors that occurs at the lower frequencies. This is referred to as *common-impedance coupling* and is contributed by the impedance of the reference conductor.

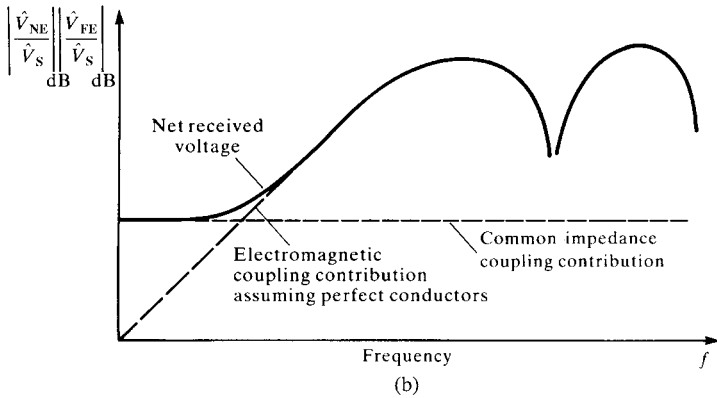
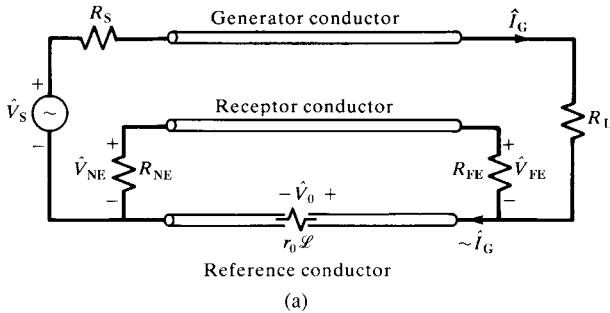


FIGURE 10.4 Illustration of common-impedance coupling due to a lossy reference conductor.

Figure 10.4 illustrates the problem. As the frequency of excitation is lowered, the crosstalk decreases directly with frequency. At some lower frequency, this contribution due to the electric and magnetic field interaction between the two circuits is dominated by the *common-impedance coupling component*. At a sufficiently low frequency, the current in the generator circuit, \hat{I}_G , returns predominantly in the reference conductor and can be computed from

$$\hat{I}_G \cong \frac{1}{R_S + R_L} \hat{V}_S \tag{10.32}$$

If we lump the per-unit-length resistance of the reference conductor, r_0 , as a total resistance, $R = r_0 \mathcal{L}$, then a voltage drop of

$$\hat{V}_0 = r_0 \mathcal{L} \hat{I}_G = \frac{r_0 \mathcal{L}}{R_S + R_L} \hat{V}_S \tag{10.33}$$

is developed across the reference conductor. This is voltage divided across the termination resistors of the receptor circuit to give

$$\hat{V}_{\text{NE}}^{\text{CI}} = \underbrace{\frac{R_{\text{NE}}}{R_{\text{NE}} + R_{\text{FE}}} r_0 \mathcal{L} \frac{1}{R_{\text{S}} + R_{\text{L}}}}_{M_{\text{NE}}^{\text{CI}}} \hat{V}_{\text{S}} \quad (10.34\text{a})$$

$$\hat{V}_{\text{FE}}^{\text{CI}} = - \underbrace{\frac{R_{\text{FE}}}{R_{\text{NE}} + R_{\text{FE}}} r_0 \mathcal{L} \frac{1}{R_{\text{S}} + R_{\text{L}}}}_{M_{\text{FE}}^{\text{CI}}} \hat{V}_{\text{S}} \quad (10.34\text{b})$$

In an approximate sense, we may simply combine these contributions with the inductive–capacitive coupling contributions in (10.30) to give the total as

$$\begin{aligned} \hat{V}_{\text{NE}} &\cong \hat{V}_{\text{NE}}^{\text{IND}} + \hat{V}_{\text{NE}}^{\text{CAP}} + \hat{V}_{\text{NE}}^{\text{CI}} \\ &= j\omega M_{\text{NE}}^{\text{IND}} \hat{V}_{\text{S}} + j\omega M_{\text{NE}}^{\text{CAP}} \hat{V}_{\text{S}} + M_{\text{NE}}^{\text{CI}} \hat{V}_{\text{S}} \end{aligned} \quad (10.35\text{a})$$

$$\begin{aligned} \hat{V}_{\text{FE}} &\cong \hat{V}_{\text{FE}}^{\text{IND}} + \hat{V}_{\text{FE}}^{\text{CAP}} + \hat{V}_{\text{FE}}^{\text{CI}} \\ &= j\omega M_{\text{FE}}^{\text{IND}} \hat{V}_{\text{S}} + j\omega M_{\text{FE}}^{\text{CAP}} \hat{V}_{\text{S}} + M_{\text{FE}}^{\text{CI}} \hat{V}_{\text{S}} \end{aligned} \quad (10.35\text{b})$$

This approximate inclusion of the impedance of the reference conductor at low frequencies was verified in [B.20] by deriving the exact chain-parameter matrix with the per-unit-length resistance of the reference conductor included.

10.2 THE LITERAL TIME-DOMAIN SOLUTION FOR A HOMOGENEOUS MEDIUM

To obtain the exact time-domain solution, we will assume $V_{\text{S}}(t) = 0$ for $t \leq 0$ and the line is initially relaxed: $\mathbf{V}(z, t) = \mathbf{I}(z, t) = \mathbf{0}$ for all $0 \leq z \leq \mathcal{L}$ and $t \leq 0$ [B.21]. In this case, the Laplace transform variable s can be substituted for $j\omega$ in the above frequency-domain exact solution. Substituting $j\omega \rightarrow s$ into (10.14a) and (10.14b) along with (10.14c) gives

$$j\omega S = j\omega \frac{\sin\left(\frac{\omega \mathcal{L}}{v}\right)}{\frac{\omega \mathcal{L}}{v}} \Rightarrow \frac{e^{sT_{\text{D}}} - e^{-sT_{\text{D}}}}{2T_{\text{D}}} \quad (10.36\text{a})$$

$$C = \cos\left(\frac{\omega \mathcal{L}}{v}\right) \Rightarrow \frac{e^{sT_{\text{D}}} + e^{-sT_{\text{D}}}}{2} \quad (10.36\text{b})$$

where again the line one-way time delay is

$$T_{\text{D}} = \frac{\mathcal{L}}{v} \quad (10.37)$$

Substituting these along with $j\omega \rightarrow s$ into (10.17) gives the *exact* Laplace-transformed time-domain solution:

$$V_{NE}(s) = \frac{M_{NE}}{X T_D} \left[\frac{(K_{NE} + 1) - 2K_{NE}e^{-2sT_D} + (K_{NE} - 1)e^{-4sT_D}}{1 + ae^{-2sT_D} + be^{-4sT_D}} \right] V_S(s) \quad (10.38a)$$

$$V_{FE}(s) = \frac{2M_{FE}}{X T_D} \left[\frac{e^{-sT_D} - e^{-3sT_D}}{1 + ae^{-2sT_D} + be^{-4sT_D}} \right] V_S(s) \quad (10.38b)$$

where

$$X = 1 + P \frac{\tau_G \tau_R}{T_D^2} + \frac{(\tau_G + \tau_R)}{T_D} \quad (10.39a)$$

$$a = \frac{2}{X} \left[1 - P \frac{\tau_G \tau_R}{T_D^2} \right] \quad (10.39b)$$

$$b = \frac{1}{X} \left[1 + P \frac{\tau_G \tau_R}{T_D^2} - \frac{(\tau_G + \tau_R)}{T_D} \right] \quad (10.39c)$$

and $V_S(s)$ is the Laplace transform of $V_S(t)$.

We now take the inverse Laplace transform of these results. Rewrite (10.38a) and (10.38b) as

$$\begin{aligned} & \left[1 + ae^{-2sT_D} + be^{-4sT_D} \right] V_{NE}(s) \\ &= \frac{M_{NE}}{X T_D} \left[(K_{NE} + 1) - 2K_{NE}e^{-2sT_D} + (K_{NE} - 1)e^{-4sT_D} \right] V_S(s) \end{aligned} \quad (10.40a)$$

$$\left[1 + ae^{-2sT_D} + be^{-4sT_D} \right] V_{FE}(s) = \frac{2M_{FE}}{X T_D} \left[e^{-sT_D} - e^{-3sT_D} \right] V_S(s) \quad (10.40b)$$

In order to obtain the inverse Laplace transform of this result, we recall the simple time-delay transform pair:

$$F(t \pm nT_D) \Leftrightarrow e^{\pm nsT_D} F(s) \quad (10.41)$$

Therefore, the exact time-domain expressions become

$$\begin{aligned} V_{NE}(t) = & -a V_{NE}(t - 2T_D) - b V_{NE}(t - 4T_D) + \frac{M_{NE}}{X T_D} [(K_{NE} + 1) V_S(t) \\ & - 2K_{NE} V_S(t - 2T_D) + (K_{NE} - 1) V_S(t - 4T_D)] \end{aligned} \quad (10.42a)$$

$$\begin{aligned} V_{FE}(t) = & -a V_{FE}(t - 2T_D) - b V_{FE}(t - 4T_D) \\ & + \frac{2M_{FE}}{X T_D} [V_S(t - T_D) - V_S(t - 3T_D)] \end{aligned} \quad (10.42b)$$

These equations can be solved recursively for the crosstalk voltages for an initially relaxed line, that is, $V_S(t) = V_{NE}(t) = V_{FE}(t) = 0$ for $t \leq 0$. The solutions are in terms of values of the source voltage at the present time, $V_S(t)$, and at various time delays prior to the present time: $V_S(t - T_D)$, $V_S(t - 2T_D)$, $V_S(t - 3T_D)$, and $V_S(t - 4T_D)$, as well as prior solutions at various time delays prior to the present time: $V_{NE}(t - 2T_D)$, $V_{NE}(t - 4T_D)$, $V_{FE}(t - 2T_D)$, and $V_{FE}(t - 4T_D)$.

10.2.1 Explicit Solution

Although the solution in (10.42) is exact, it requires knowledge of the solution at previous times that are multiples of the line one-way delay T_D . Thus, a recursive solution is required. In order to obtain a solution that depends only on $V_S(t)$, we recall the *time-shift* or *difference operator* D , where

$$D^m F(t) \equiv F(t + mT_D) \quad (10.43a)$$

$$D^{-m} F(t) \equiv F(t - mT_D) \quad (10.43b)$$

Using this time-shift operator along with (10.41) in (10.40) gives

$$\left[1 + aD^{-2} + bD^{-4}\right] V_{NE}(t) = \frac{M_{NE}}{X T_D} \left[(K_{NE} + 1) - 2K_{NE}D^{-2} + (K_{NE} - 1)D^{-4} \right] V_S(t) \quad (10.44a)$$

$$\left[1 + aD^{-2} + bD^{-4}\right] V_{FE}(t) = \frac{2M_{FE}}{X T_D} \left[D^{-1} - D^{-3} \right] V_S(t) \quad (10.44b)$$

Multiplying the equations by powers of D gives the transfer functions in terms of the time-shift operator D as

$$\begin{aligned} V_{NE}(t) &= \frac{M_{NE}}{X T_D} \left[\frac{(K_{NE} + 1) - 2K_{NE}D^{-2} + (K_{NE} - 1)D^{-4}}{1 + aD^{-2} + bD^{-4}} \right] V_S(t) \\ &= \frac{M_{NE}}{X T_D} \left[\frac{(K_{NE} + 1)D^4 - 2K_{NE}D^2 + (K_{NE} - 1)}{D^4 + aD^2 + b} \right] V_S(t) \end{aligned} \quad (10.45a)$$

$$\begin{aligned} V_{FE}(t) &= \frac{2M_{FE}}{X T_D} \left[\frac{D^{-1} - D^{-3}}{1 + aD^{-2} + bD^{-4}} \right] V_S(t) \\ &= \frac{2M_{FE}}{X T_D} \left[\frac{D^3 - D}{D^4 + aD^2 + b} \right] V_S(t) \end{aligned} \quad (10.45b)$$

These expressions can be inverted by carrying out the long division of the following basic problem:

$$\frac{1}{D^4 + aD^2 + b} = \alpha_0 D^{-4} + \alpha_1 D^{-6} + \alpha_2 D^{-8} + \alpha_3 D^{-10} + \alpha_4 D^{-12} + \alpha_5 D^{-14} + \alpha_6 D^{-16} + \dots \quad (10.46a)$$

where

$$\begin{aligned} \alpha_0 &= 1 \\ \alpha_1 &= -a \\ \alpha_2 &= a^2 - b \\ \alpha_3 &= -a^3 + 2ab \\ \alpha_4 &= a^4 - 3a^2b + b^2 \\ \alpha_5 &= -a^5 + 4a^3b - 3ab^2 \\ \alpha_6 &= a^6 - 5a^4b + 6a^2b^2 - b^3 \\ &\vdots \end{aligned} \quad (10.46b)$$

Substituting the results of (10.46) into (10.45) gives the time-domain crosstalk voltages in terms of $V_S(t)$ delayed by multiples of the one-way line delay T as

$$V_{NE}(t) = \frac{M_{NE}}{X T_D} [N_0 V_S(t) + N_2 V_S(t - 2T_D) + N_4 V_S(t - 4T_D) + \dots] \quad (10.47a)$$

$$V_{FE}(t) = 2 \frac{M_{FE}}{X T_D} [F_1 V_S(t - T_D) + F_3 V_S(t - 3T_D) + F_5 V_S(t - 5T_D) + \dots] \quad (10.47b)$$

where the constants are

$$\begin{aligned} N_0 &= \alpha_0 (K_{NE} + 1) \\ &= (K_{NE} + 1) \\ N_2 &= \alpha_1 (K_{NE} + 1) - 2\alpha_0 K_{NE} \\ &= -a(K_{NE} + 1) - 2K_{NE} \\ N_4 &= \alpha_2 (K_{NE} + 1) - 2\alpha_1 K_{NE} + \alpha_0 (K_{NE} - 1) \\ &= (a^2 - b)(K_{NE} + 1) + 2aK_{NE} + (K_{NE} - 1) \\ N_6 &= \alpha_3 (K_{NE} + 1) - 2\alpha_2 K_{NE} + \alpha_1 (K_{NE} - 1) \\ &= (2ab - a^3)(K_{NE} + 1) - 2(a^2 - b)K_{NE} - a(K_{NE} - 1) \\ &\vdots \end{aligned} \quad (10.48a)$$

and

$$\begin{aligned}
 F_1 &= (\alpha_0) \\
 &= 1 \\
 F_3 &= (\alpha_1 - \alpha_0) \\
 &= -a - 1 \\
 F_5 &= (\alpha_2 - \alpha_1) \\
 &= a^2 - b + a \\
 F_7 &= (\alpha_3 - \alpha_2) \\
 &= 2ab - a^3 - a^2 + b \\
 &\vdots
 \end{aligned} \tag{10.48b}$$

These final expressions give the explicit relationships for the crosstalk voltages as linear combinations of the source voltage delayed in time by various multiples of the line one-way delay T_D .

Some additional interesting forms of these expressions can be obtained by grouping terms of (10.48) to yield

$$\begin{aligned}
 V_{NE}(t) &= \frac{M_{NE}}{X T_D} \left(\begin{aligned} &\alpha_0[V_S(t) - V_S(t - 4T_D)] \\ &+ \alpha_1[V_S(t - 2T_D) - V_S(t - 6T_D)] \\ &+ \alpha_2[V_S(t - 4T_D) - V_S(t - 8T_D)] + \dots \end{aligned} \right) \\
 &+ K_{NE} \frac{M_{NE}}{X T_D} \left(\begin{aligned} &\alpha_0[V_S(t) - 2V_S(t - 2T_D) + V_S(t - 4T_D)] \\ &+ \alpha_1[V_S(t - 2T_D) - 2V_S(t - 4T_D) + V_S(t - 6T_D)] \\ &+ \alpha_2[V_S(t - 4T_D) - 2V_S(t - 6T_D) \\ &+ V_S(t - 8T_D)] + \dots \end{aligned} \right)
 \end{aligned} \tag{10.49a}$$

$$V_{FE}(t) = 2 \frac{M_{FE}}{X T_D} \left[\begin{aligned} &\alpha_0[V_S(t - T_D) - V_S(t - 3T_D)] \\ &+ \alpha_1[V_S(t - 3T_D) - V_S(t - 5T_D)] \\ &+ \alpha_2[V_S(t - 5T_D) - V_S(t - 7T_D)] + \dots \end{aligned} \right] \tag{10.49b}$$

10.2.2 Weakly Coupled Lines

The above time-domain solutions are exact but somewhat complicated. In this section, we will assume that the lines are weakly coupled, that is, $k \ll 1$. In this case, $P \cong 1$ in Den, in which case the above results simplify considerably. The quantities in (10.39) factor, for $P \cong 1$, as

$$X = \left(1 + \frac{\tau_G}{T_D} \right) \left(1 + \frac{\tau_R}{T_D} \right), \quad k \ll 1, P \cong 1, \tag{10.50a}$$

$$a = \frac{\left(1 - \frac{\tau_G}{T_D}\right)}{\left(1 + \frac{\tau_G}{T_D}\right)} + \frac{\left(1 - \frac{\tau_R}{T_D}\right)}{\left(1 + \frac{\tau_R}{T_D}\right)}, \quad k \ll 1, P \cong 1, \tag{10.50b}$$

$$b = \frac{\left(1 - \frac{\tau_G}{T_D}\right)\left(1 - \frac{\tau_R}{T_D}\right)}{\left(1 + \frac{\tau_G}{T_D}\right)\left(1 + \frac{\tau_R}{T_D}\right)}, \quad k \ll 1, P \cong 1, \tag{10.50c}$$

Assuming that the line is weakly coupled such that $\sqrt{1 - k^2} \cong 1$, the normalized time constants in (10.25) become

$$\frac{\tau_G}{T_D} \cong \frac{(1 + \alpha_{SG} \alpha_{LG})}{(\alpha_{SG} + \alpha_{LG})}, \quad k \ll 1 \tag{10.51a}$$

$$\frac{\tau_R}{T_D} \cong \frac{(1 + \alpha_{SR} \alpha_{LR})}{(\alpha_{SR} + \alpha_{LR})}, \quad k \ll 1 \tag{10.51b}$$

Now suppose that one of the ends of *each* line is matched; $\alpha_{SG} = 1$ or $\alpha_{LG} = 1$ and $\alpha_{SR} = 1$ or $\alpha_{LR} = 1$. In this case, the time constants in (10.25) become $\tau_G = T_D$ and $\tau_R = T_D$. The quantities X , a , and b in (10.50) become $X = 4$, $a = 0$, and $b = 0$. The coefficients in (10.46b) are zero except for $\alpha_0 = 1$. The near-end and far-end crosstalk expressions in (10.49) simplify to

$$V_{NE}(t) = \frac{M_{NE}}{4T_D} [V_S(t) - V_S(t - 4T_D)] + \frac{M_{NE} K_{NE}}{4T_D} [V_S(t) - 2V_S(t - 2T_D) + V_S(t - 4T_D)] \tag{10.52a}$$

$$V_{FE}(t) = \frac{M_{FE}}{2T_D} [V_S(t - T_D) - V_S(t - 3T_D)] \tag{10.52b}$$

If the line is matched at the load end of the generator circuit, $\alpha_{LG} = 1$, or at the load end of the receptor circuit, $\alpha_{LR} = 1$, then $K_{NE} = 1$ and (10.52) simplify to

$$V_{NE}(t) = \frac{M_{NE}}{2T_D} [V_S(t) - V_S(t - 2T_D)] \tag{10.53a}$$

$$V_{FE}(t) = \frac{M_{FE}}{2T_D} [V_S(t - T_D) - V_S(t - 3T_D)] \tag{10.53b}$$

There exist numerous electronic design handbooks and other publications that contain time-domain crosstalk prediction equations for three-conductor lines [5–11]. However, as pointed out previously, these invariably make the following assumptions:

1. The line is *weakly coupled*.
2. All ports are matched: $\alpha_{SG} = \alpha_{LG} = \alpha_{SR} = \alpha_{LR} = 1$.
3. Both circuits have identical cross sections, for example, two identical wires at the same height above a ground plane. Hence, $c_G = c_R$ and $l_G = l_R$.

These are very special restrictions that are generally not fulfilled in practical cases. For this special case where $R_S = R_L = R_{NE} = R_{FE} = Z_{CG} = Z_{CR} = Z_C$, M_{NE} and M_{FE} in (10.29) reduce to

$$M_{NE} = \frac{1}{4} \left[\frac{l_m \mathcal{L}}{Z_C} + Z_C c_m \mathcal{L} \right] \quad (10.54a)$$

$$M_{FE} = \frac{1}{4} \left[-\frac{l_m \mathcal{L}}{Z_C} + Z_C c_m \mathcal{L} \right] \quad (10.54b)$$

and the previously derived results in (10.53) reduce to

$$V_{NE}(t) = \frac{\mathcal{L}}{8T_D} \left[\frac{l_m}{Z_C} + c_m Z_C \right] [V_S(t) - V_S(t - 2T_D)] \quad (10.55a)$$

$$V_{FE}(t) = -\frac{\mathcal{L}}{8T_D} \left[\frac{l_m}{Z_C} - c_m Z_C \right] [V_S(t - T_D) - V_S(t - 3T_D)] = 0 \quad (10.55b)$$

For a homogeneous medium, using (10.6) and (10.22), $l_m/c_m = Z_C^2$ and the far-end crosstalk is (ideally) zero. For an inhomogeneous medium, the far-end crosstalk is not zero. These results are equivalent to results derived intuitively in [5–7]. Again, these results in (10.55) are restricted to lines that are (1) weakly coupled, (2) matched at all four ports, and (3) physically symmetric, that is, $l_G = l_R$ and $c_G = c_R$. The total of these conditions is very ideal and is not found in practical applications.

10.2.3 Inductive and Capacitive Coupling

In the frequency-domain solution, we observed that for a weakly coupled, electrically short line and for a sufficiently small frequency, the near-end and far-end crosstalk voltages reduce to (see (10.29))

$$\hat{V}_{NE}(j\omega) \cong j\omega M_{NE} \hat{V}_S(j\omega) \quad (10.56a)$$

$$\hat{V}_{FE}(j\omega) \cong j\omega M_{FE} \hat{V}_S(j\omega) \quad (10.56b)$$

The time-domain results can be obtained from these by substituting

$$j\omega \Rightarrow \frac{d}{dt} \quad (10.57)$$

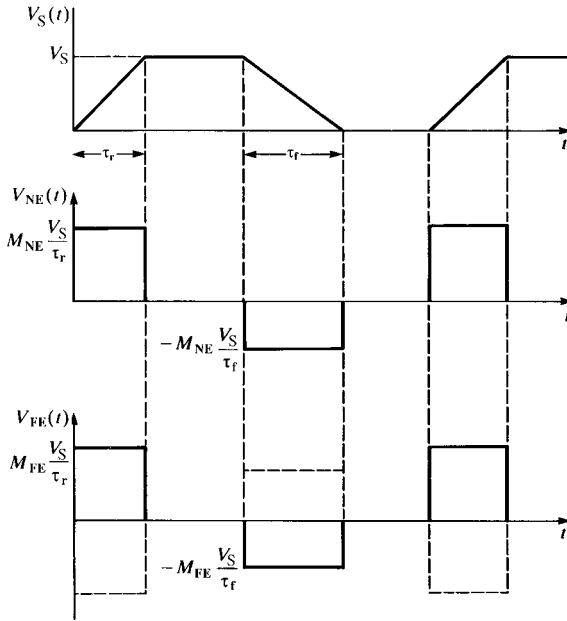


FIGURE 10.5 Illustration of near-end and far-end time-domain crosstalk predicted by the inductive-capacitive coupling model.

to give

$$V_{NE}(t) \cong M_{NE} \frac{d}{dt} V_S(t) \tag{10.58a}$$

$$V_{FE}(t) \cong M_{FE} \frac{d}{dt} V_S(t) \tag{10.58b}$$

For trapezoidal pulses representing, perhaps, digital clock or data signals, these results give crosstalk pulses occurring during the transitions of $V_S(t)$ with the levels of those pulses dependent on the slope or “slew rate” of $V_S(t)$ as illustrated in Figure 10.5. Substituting the definitions of M_{NE} and M_{FE} in (10.18) in terms of inductive and capacitive coupling contributions as given in (10.19) and (10.20) shows that this approximate time-domain crosstalk result can be computed from the equivalent circuit shown in Figure 10.6. Therefore, the time-domain crosstalk is the sum of an inductive coupling component and a capacitive coupling component.

The above time-domain result was obtained from the frequency-domain approximate result. In order for that frequency-domain result to be valid, the line must be electrically short at the highest significant sinusoidal frequency of excitation. Bounds on the spectrum of a periodic trapezoidal waveform representing a digital signal given in Chapter 1 are shown in Figure 10.7, where τ_r is the pulse rise time, and we assume that the rise time and fall time of the pulse are equal, $\tau_r = \tau_f$. Essentially, we require that the line be electrically short at the frequency components of

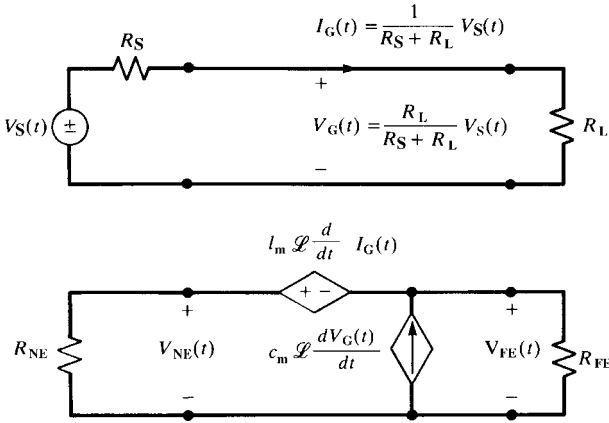


FIGURE 10.6 The time-domain inductive-capacitive coupling model.

the time-domain pulse waveform for frequencies up to some limit, f_{max} . We assume that the frequency components above this maximum frequency are decreasing in magnitude such that they do not substantially contribute to the pulse wave shape and hence incorrect processing of them by the time-domain model does not

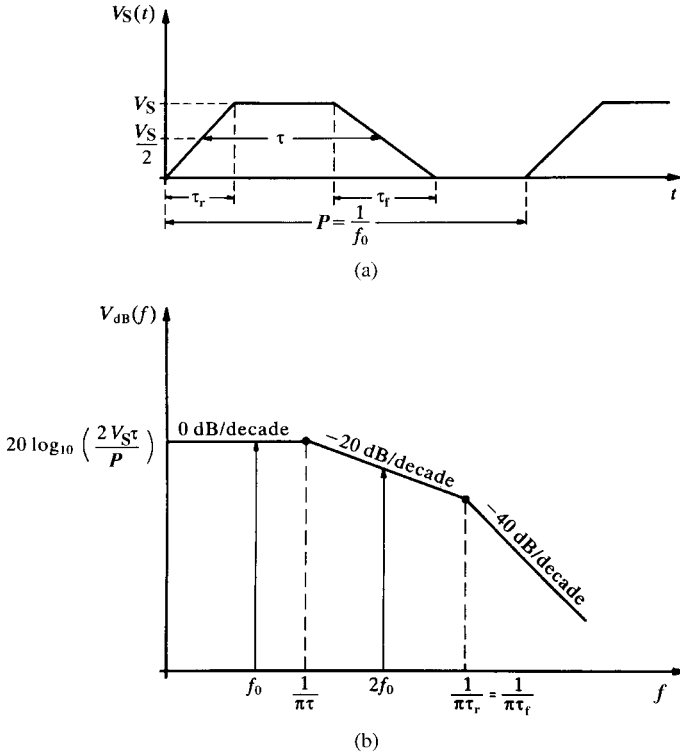


FIGURE 10.7 The frequency-domain representation of a periodic trapezoidal pulse train.

substantially introduce errors. For the trapezoidal waveform, the frequency components above the second break point, $f = 1/\pi \tau_r$, are rolling off at -40 dB/decade. In Chapter 1, we obtained a criterion for the bandwidth of a trapezoidal, digital waveform as $f_{\max} = 3(1/\pi \tau_r) \cong 1/\tau_r$. Hence, we assume that the above approximate model is valid for frequency components below this. This gives a time-domain criterion for the validity of the approximate model given in (10.58) and Figure 10.6. Hence, we require that

$$\begin{aligned} \mathcal{L} &< \frac{1}{10} \lambda_{\max} \\ &= \frac{1}{10} \frac{v}{f_{\max}} \\ &= \frac{1}{10} v \tau_r \end{aligned} \quad (10.59)$$

Rewriting this in terms of the line one-way delay, $T_D = \mathcal{L}/v$, gives the criterion for validity of the approximate time-domain model as

$$\tau_r > 10T_D \quad (10.60)$$

10.2.4 Common-Impedance Coupling

The effect of the impedance of the reference conductor can be handled in an approximate manner at the lower frequencies of the pulse by simply adding the common-impedance coupling term to the inductive–capacitive contributions in (10.58):

$$V_{\text{NE,FE}}(t) = \left[M_{\text{NE,FE}}^{\text{IND}} + M_{\text{NE,FE}}^{\text{CAP}} \right] \frac{dV_S(t)}{dt} + M_{\text{NE,FE}}^{\text{CI}} V_S(t) \quad (10.61)$$

where M_{NE} and M_{FE} are as given previously. The effect of common-impedance coupling is to add a scaled replica of $V_S(t)$ to the crosstalk resulting from inductive and capacitive coupling.

10.3 COMPUTED AND EXPERIMENTAL RESULTS

In this section, we will give some computed results comparing the predictions of the exact transmission-line model, the lumped-Pi model, and the inductive–capacitive coupling model developed in this chapter for three-conductor lines that were examined in the previous chapters. In all models, the conductors are considered to be lossless. For both structures, the SPICE subcircuit models were computed with the SPICEMTL.FOR, SPICELPI.FOR, and SPICELC.FOR computer programs described in Appendix A and combined into one SPICE program for ease of plotting of the results. The nodes at the input to the generator lines are designated as S1 (SPICE), S2 (lumped-Pi), and S3 (inductive–capacitive coupling model), whereas the nodes at the near end of the receptor circuit are designated as NE1 (SPICE), NE2 (lumped-Pi),

and NE3 (inductive–capacitive coupling model). The termination impedances are all 50Ω resistive, that is, $R_S = R_L = R_{NE} = R_{FE} = 50 \Omega$.

10.3.1 A Three-Wire Ribbon Cable

The first configuration is a three-wire ribbon cable considered in previous chapters. See Figure 7.10. The wires are #28 gauge stranded (7×36) and are separated by 50 mils. One of the outer wires is the reference conductor, and the line is of total length 2 m. The per-unit-length parameters were computed in Chapter 5 with the RIBBON.FOR computer program described in Appendix A. Figure 10.8 compares the

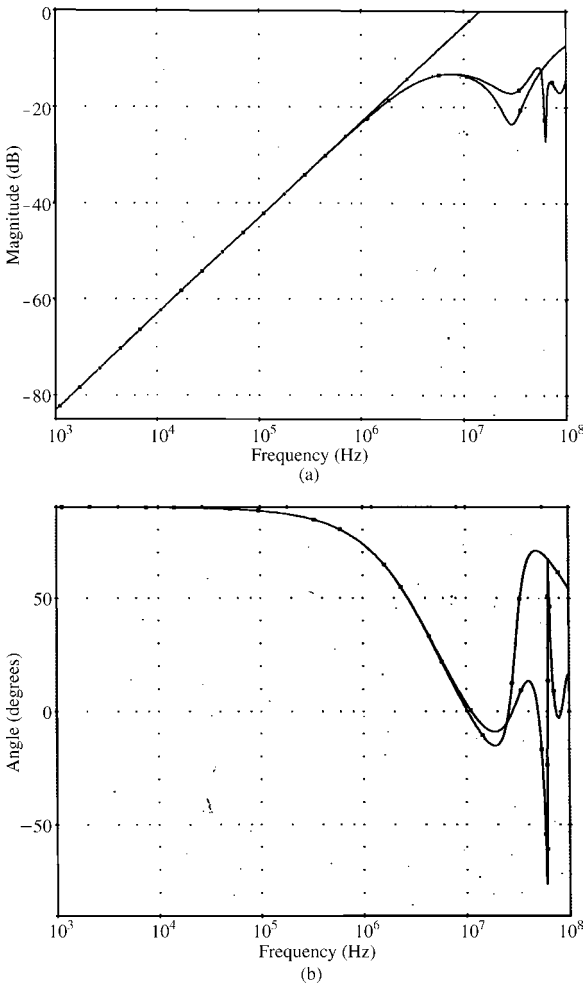


FIGURE 10.8 Illustration of the frequency response of the ribbon cable of Figure 7.10 via the SPICE model, one lumped-Pi section, and the inductive–capacitive coupling model: (a) magnitude and (b) phase.

frequency-domain predictions for all three models over the frequency range of 1 kHz to 100 MHz. The line is one wavelength (ignoring the dielectric insulations) at 150 MHz, so we may consider it to be electrically short for frequencies below, say, 15 MHz. The lumped-Pi model gives good predictions below 10 MHz, whereas the inductive–capacitive coupling model gives good predictions below 1 MHz. This shows that the simple inductive–capacitive coupling model can give adequate predictions for a significant frequency range so long as its basic limitations are observed.

Figure 10.9 shows the correlation between the three models for the time domain for the leading edge of the pulse. The source, $V_S(t)$, is a 1-MHz trapezoidal pulse train with 50% duty cycle. The trapezoidal pulses have 1 V magnitude with various rise times. The one-way time delay for the line (ignoring the dielectric insulations) is $T_D = \mathcal{L}/v = 6.67$ ns, so we should not expect the inductive–capacitive coupling model to give adequate predictions for rise times less than 70 ns. Figure 10.9(a) shows the predictions for $\tau_r = 60$ ns. The predictions of the lumped-Pi model compare well with those of the exact SPICE model. Figure 10.9(b) shows the predictions for $\tau_r = 120$ ns, and Figure 10.9(c) shows the predictions for $\tau_r = 240$ ns. Again, the predictions of the exact SPICE model and the lumped-Pi model correlate well. For the latter rise time of 240 ns, there is good agreement between the SPICE predictions and those of the inductive–capacitive coupling model for the peak crosstalk and $\tau_r = 36 T_D$.

Figure 10.10 shows oscilloscope photographs of the experimental results. For $\tau_r = 60$ ns in Figure 10.10(a), the measured peak voltage is 80 mV compared to a predicted value of 80 mV. For $\tau_r = 120$ ns in Figure 10.10(b), the measured peak voltage is 50 mV compared to a predicted value of 45 mV, and for $\tau_r = 240$ ns in Figure 10.10(c), the measured peak is 26 mV compared to a predicted value of 23 mV. Observe in the measured results that, while the pulse is in its quiescent state of 1 V, the crosstalk does not go to zero as predicted by the lossless model but appears to asymptotically approach a value on the order of 2.5 mV, as shown in Figure 10.10(c). This is a result of *common-impedance coupling*. The per-unit-length dc resistance of one wire is obtained by dividing the dc resistance of one of the #36 gauge strands by 7 (the number of strands in parallel) to give a total resistance of the 2-m-long reference wire as $r_0 \mathcal{L} = 0.389 \Omega$. Substituting this into (10.34a) gives a common-impedance coupling level of 1.94 mV.

10.3.2 A Three-Conductor Printed Circuit Board

The next configuration is a three-conductor printed circuit board also considered previously. See Figure 7.13. The conductors (lands) are 15 mils in width and have thicknesses of 1.38 mils (1 ounce copper). They are on one side of a 47-mil-thick glass epoxy board and have edge-to-edge separations of 45 mils. One of the outer lands is the reference conductor, and the line is of total length 10 in. = 0.254 m. The per-unit-length parameters were computed in Chapter 5 with the PCB.FOR computer program described in Appendix A. Figure 10.11 compares the frequency-domain predictions for all three models over the frequency range of 10 kHz to 1 GHz. The

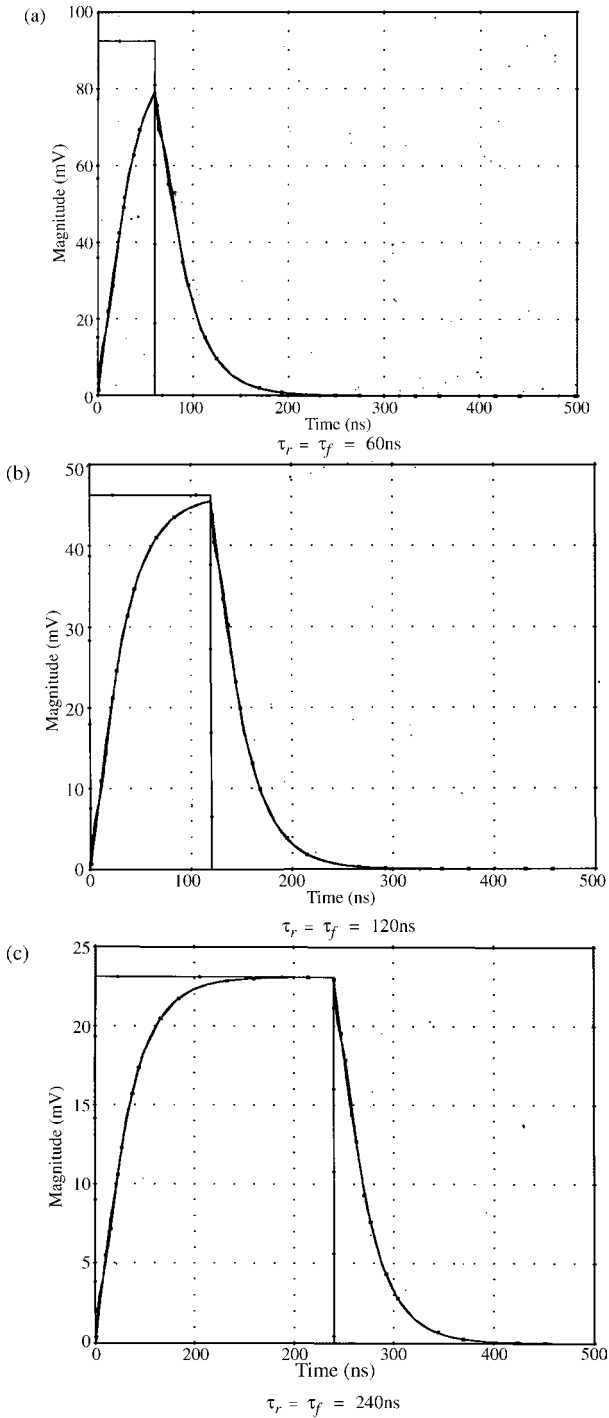
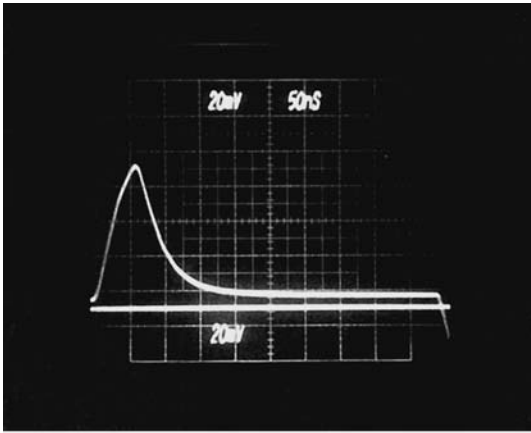
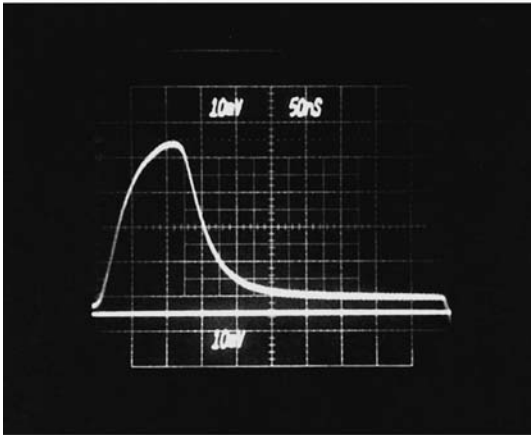


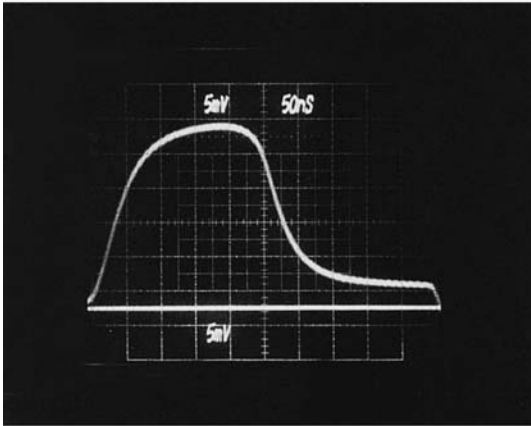
FIGURE 10.9 Illustration of the time-domain response of the ribbon cable of Figure 7.10 via the SPICE model, one lumped- Π section, and the inductive-capacitive coupling model for a rise/fall time of (a) 60 ns, (b) 120 ns, and (c) 240 ns.



(a)



(b)



(c)

FIGURE 10.10 The experimentally-determined time-domain response of the ribbon cable of Figure 7.10 for a rise/fall time of (a) 60 ns, (b) 120 ns, and (c) 240 ns.

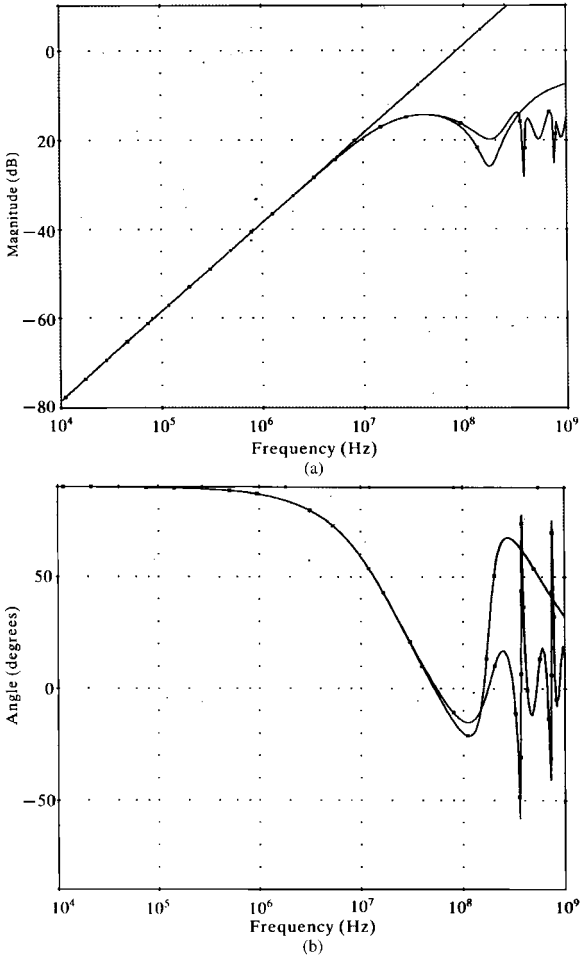


FIGURE 10.11 Illustration of the frequency response of the printed circuit board of Figure 7.13 via the SPICE model, one lumped-Pi section and the inductive–capacitive coupling model: (a) magnitude, and (b) phase.

line is one wavelength (assuming an effective relative permittivity as the average of the board and free space or $\epsilon'_r = (4.7 + 1)/2 = 2.85$) at 700 MHz, so we may consider it to be electrically short for frequencies below, say, 70 MHz. The lumped-Pi model gives good predictions below 100 MHz, whereas the inductive–capacitive coupling model gives good predictions below 10 MHz. This again shows that the simple inductive–capacitive coupling model can give adequate predictions for a significant frequency range so long as its basic limitations are observed.

Figure 10.12 shows the correlation between the three models for the time domain. The source, $V_S(t)$, is again a 1 - V, 1 - MHz trapezoidal pulse train with various rise times. The one-way time delay for the line is (assuming an effective relative

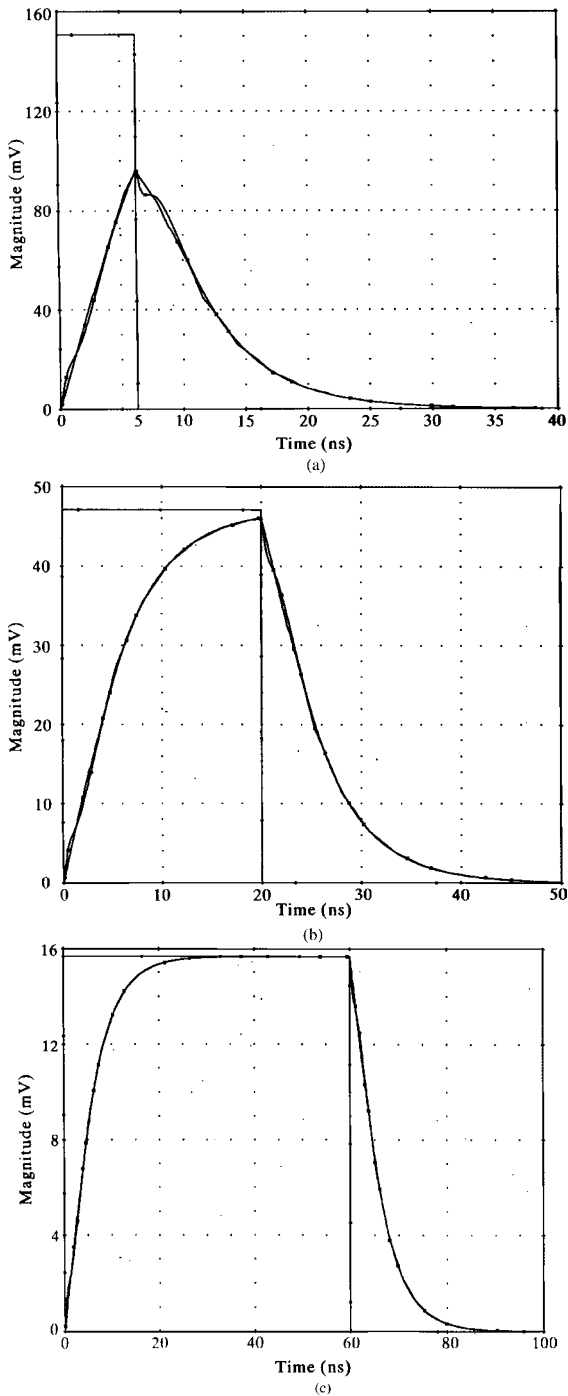
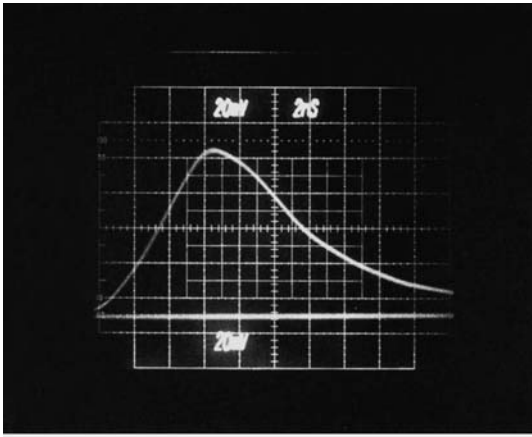
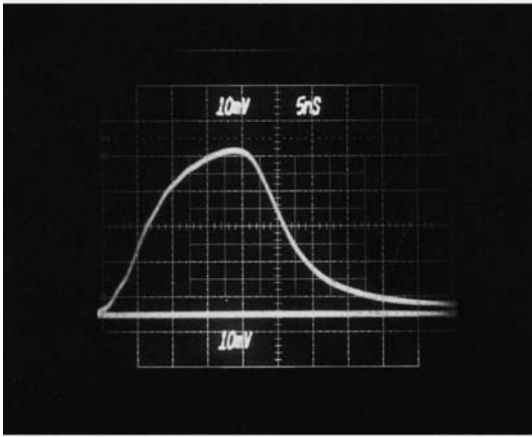


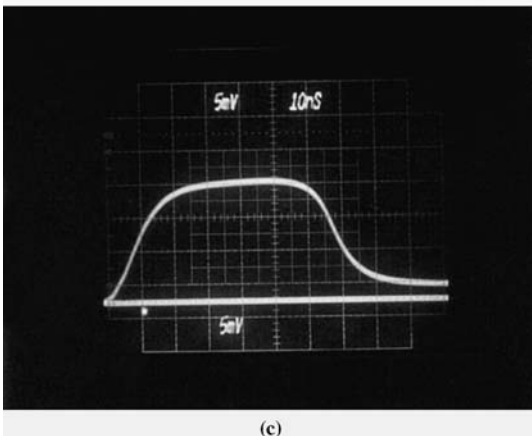
FIGURE 10.12 Illustration of the time-domain response of the printed circuit board of Figure 7.13 via the SPICE model, one lumped-Pi section, and the inductive-capacitive coupling model for a rise/fall time of (a) 6.25 ns, (b) 20 ns, and (c) 60 ns.



(a)



(b)



(c)

FIGURE 10.13 The experimentally-determined time-domain response of the printed circuit board of Figure 7.13 for a rise/fall time of (a) 6.25 ns, (b) 20 ns, and (c) 60 ns.

permittivity as the average of the board and free space or $\epsilon'_r = (4.7 + 1)/2 = 2.85$ $T_D = \mathcal{L}/v = 1.43$ ns, so we should not expect the inductive–capacitive coupling model to give adequate predictions for rise times less than 20 ns. Figure 10.12(a) shows the predictions for $\tau_r = 6.25$ ns. The predictions of the lumped-Pi model compare well with those of the SPICE model. Figure 10.12(b) shows the predictions for $\tau_r = 20$ ns, and Figure 10.12(c) shows the predictions for $\tau_r = 60$ ns. Again the predictions of the SPICE model and the lumped-Pi model are virtually identical. For the latter rise time of 60 ns, the inductive–capacitive coupling model gives excellent prediction of the peak crosstalk magnitude and $\tau_r = 70 T_D$.

Figure 10.13 shows oscilloscope photographs of the experimental results. For $\tau_r = 6.25$ ns in Figure 10.13(a), the measured peak voltage is 94 mV compared to a predicted value of 95 mV. For $\tau_r = 20$ ns in Figure 10.13(b), the measured peak voltage is 46 mV compared to a predicted value of 46 mV, and for $\tau_r = 60$ ns in Figure 10.13(c), the measured peak is 17.5 mV compared to a predicted value of 15.8 mV. Observe in Figure 10.13(c) that, again while the pulse is in its quiescent state of 1 V, the crosstalk does not go to zero as predicted by the lossless model but appears to asymptotically approach a value on the order of 2.5 mV, as shown in Figure 10.13. This shows that *common-impedance coupling* can be significant even for short conductors. The total dc resistance of one land is $r_0 \mathcal{L} = 0.3279 \Omega$. Substituting this into (10.34a) gives a common-impedance coupling level of 1.64 mV.

PROBLEMS

10.1 Show that the inverse of a 2×2 matrix

$$\mathbf{M} = \begin{bmatrix} a & b \\ c & d \end{bmatrix}$$

is

$$\mathbf{M}^{-1} = \frac{1}{ad - bc} \begin{bmatrix} d & -b \\ -c & a \end{bmatrix}$$

- 10.2** Solve, using Cramer's rule, Eqs. (10.16) to give the results in (10.17).
10.3 Derive the inductive–capacitive coupling model results in (10.29).
10.4 Demonstrate the results in (10.31).
10.5 Derive the Laplace transform solution in (10.38).
10.6 Derive the time-domain recursive solution in (10.42).
10.7 Derive the explicit time-domain solution in (10.47).
10.8 Demonstrate the relations in (10.50) and (10.51).
10.9 Obtain the simplified relations in (10.52)–(10.54).
10.10 Consider a problem consisting of three identical, bare wires wherein one of the wires serves as the reference conductor. The wires are #28 gauge stranded

wires (7×36) (radius 7.5 mils) and are arranged on the corners of an equilateral triangle so that the separations between each wire are 1 cm. The terminations are $R_S = 50 \Omega$, $R_L = 1k \Omega$, $R_{NE} = 300 \Omega$, and $R_{FE} = 100 \Omega$. If the total line length is 2 m, compute the near-end and far-end frequency-domain crosstalk (magnitude and angle) using (6.17) from 1 kHz to 100 MHz. Determine the coupling coefficient, the near-end and far-end crosstalk coefficients $M_{NE,FE}^{IND}$ and $M_{NE,FE}^{CAP}$, and the frequency where the line is 0.1λ long. Compare your results with those of the SPICE model, SPICEMTL.FOR, to show that (10.17) is correct.

- 10.11** For the structure of Problem 10.10, repeat the crosstalk calculations using the low-frequency, inductive–capacitive coupling model in (10.29). Verify your results using the SPICE model generated by SPICELC.FOR.
- 10.12** For the structure of Problem 10.10, assume that $V_S(t)$ is a 1-MHz periodic train of trapezoidal pulses with equal rise/fall times of 100 ns and a level of 1 V. Compute the time-domain near-end and far-end crosstalk using the iterative solution given in (10.42). Repeat these calculations for rise/fall times of 50 ns and 10 ns. Verify your results using the SPICE model generated by SPICEMTL.FOR.
- 10.13** Repeat Problem 10.12 using the low-frequency, inductive–capacitive coupling approximation given in (10.58). Verify your results using the SPICE model generated by SPICELC.FOR.
- 10.14** Determine the common-impedance coupling waveform for Problem 10.12.
- 10.15** Reproduce the results of Figures 10.8 and 10.9 using the SPICE models generated by SPICEMTL.FOR, SPICELPI.FOR, and SPICELC.FOR.
- 10.16** Reproduce the results of Figures 10.11 and 10.12 using the SPICE models generated by SPICEMTL.FOR, SPICELPI.FOR, and SPICELC.FOR.
- 10.17** Explain why you would expect to obtain the inductive–capacitive coupling models in the limit as the frequency goes to zero. [*Hint*: The current of the generator circuit produces a magnetic flux that links the receptor circuit. Now use Faraday’s law to determine the induced voltage in the receptor circuit and assume weak coupling between the lines. Similarly, the voltage of the generator circuit produces an electric field some of which terminates on the receptor conductor that induces a charge on that conductor.]

REFERENCES

- [1] L. Young, *Parallel Coupled Lines and Directional Couplers*, Artech House, Dedham, MA., 1972.
- [2] V.K. Tripathi, Asymmetric coupled transmission lines in an inhomogeneous medium, *IEEE Transactions on Microwave Theory and Techniques*, **23** (9), 731–739, 1975.
- [3] R. Speciale, Even- and odd-mode waves for nonsymmetrical coupled lines in nonhomogeneous media, *IEEE Transactions on Microwave Theory and Techniques*, **23** (11), 897–908, 1975.

- [4] J.C. Isaacs, Jr. and N.A. Strakhov, Crosstalk in uniformly coupled lossy transmission lines, *The Bell System Technical Journal*, **52** (1), 101–115, 1973.
- [5] W.R. Blood, Jr., *MECL System Design Handbook*, 4th edition, Motorola Semiconductor Products Inc., 1988.
- [6] A. Feller, H.R. Kaupp, and J.J. Digiacom, Crosstalk and reflections in high-speed digital systems, *Proceedings, Fall Joint Computer Conference*, 511–525, 1965.
- [7] J.A. DeFalco, Predicting crosstalk in digital systems, *Computer Design*, 69–75, June, 1973.
- [8] D.B. Jarvis, The effects of interconnections on high-speed logic circuits, *IEEE Transactions on Electronic Computers*, **12** (5), 476–487, 1963.
- [9] I. Catt, Crosstalk (noise) in digital systems, *IEEE Transactions on Electronic Computers*, **16** (6), 743–763, 1967.
- [10] A.J. Rainal, Transmission properties of various styles of printed wiring boards, *The Bell System Technical Journal*, **58** (5), 995–1025, 1979.
- [11] H. You and M. Soma, Crosstalk analysis of interconnection lines and packages in high-speed integrated circuits, *IEEE Transactions on Circuits and Systems*, **37** (8), 1019–1026, 1990.

11

INCIDENT FIELD EXCITATION OF TWO-CONDUCTOR LINES

In this chapter, we will examine the solution of the transmission-line equations for a two-conductor line that is excited by an external, incident electromagnetic field. This will represent, for example, airport surveillance radars and AM/FM radio station transmitters as well as near-field sources. We will provide a simple derivation of the transmission-line equations for the case of two-conductor lines and extend that in the next chapter to multiconductor transmission lines (MTLs). Once the transmission-line equations are derived and solved, the terminal constraints of the line are incorporated to give the solution for the terminal voltages and currents.

Incorporation of the effects of incident electromagnetic fields into the transmission line equations was considered for two-conductor lines in [1–5]. The transmission-line formulation for two-conductor lines has been compared to the full-wave method of moments (MoM) solution in [H.6,H.7] and to experimental results in [H.8]. A literal solution for the two-wire case was obtained in [H.9,H.11]. The formulation has also been adapted to twisted pairs [6] and to shielded cables [7]. The investigation of higher-order modes on these two-conductor lines was given in [8].

11.1 DERIVATION OF THE TRANSMISSION-LINE EQUATIONS FOR INCIDENT FIELD EXCITATION

The process of excitation of the line by an external, incident electromagnetic field can be thought of in the following way. The incident field induces currents and charges on the line conductors. These induced currents and charges in turn produce the scattered

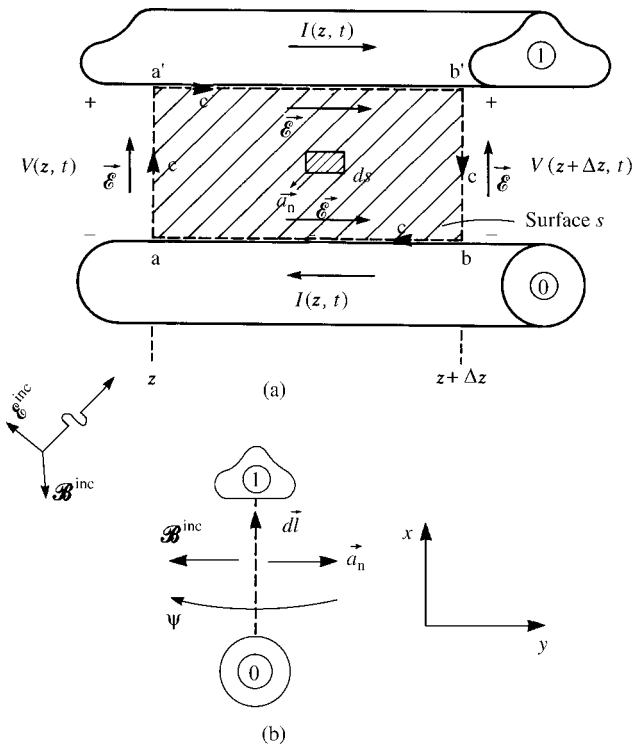


FIGURE 11.1 Definition of the contour for the derivation of the first transmission-line equation for incident field illumination.

field that, when combined with the incident field, satisfy the boundary conditions on the surfaces of the line conductors.

The derivation of the transmission-line equations for a two-conductor line that is excited by an incident field follows the same lines as in Chapter 2. For example, writing Faraday’s law around the contour of the flat surface between the two conductors as shown in Figure 11.1(a) gives

$$\int_a^{a'} \vec{E} \cdot d\vec{l} + \int_{a'}^{b'} \vec{E} \cdot d\vec{l} + \int_{b'}^b \vec{E} \cdot d\vec{l} + \int_b^a \vec{E} \cdot d\vec{l} = \frac{d}{dt} \psi_n \tag{11.1}$$

The total magnetic flux penetrating the flat surface is

$$\begin{aligned} \psi_n &= \int_s \mathcal{B}_n ds \\ &= \int_s \vec{\mathcal{B}} \cdot \vec{a}_n ds \end{aligned} \tag{11.2}$$

where the magnetic flux density is denoted as $\vec{\mathcal{B}}$ and the component that is normal to the flat surface and directed out of the page is denoted as \mathcal{B}_n . Note in Figure 11.1(b) that the unit normal to the surface, \vec{a}_n , is directed out of the page. Hence, because the direction of the contour c and the normal to the enclosed surface s are related by the right-hand rule, the usual minus sign on the right-hand side of Faraday’s law is absent in (11.1). For the case of incident field excitation, there are two components of the magnetic flux density. One component is referred to as the *scattered field* and is denoted as $\vec{\mathcal{B}}^{\text{scat}}$. The other component is due to the incident field and is denoted as $\vec{\mathcal{B}}^{\text{inc}}$. The total field is the sum of the scattered and incident components as

$$\vec{\mathcal{B}} = \vec{\mathcal{B}}^{\text{scat}} + \vec{\mathcal{B}}^{\text{inc}} \tag{11.3}$$

Hence, the total flux penetrating the surface is the combination of the two:

$$\begin{aligned} \psi_n &= \int_s \vec{\mathcal{B}} \cdot \vec{a}_n \, ds \\ &= \int_s \vec{\mathcal{B}}^{\text{scat}} \cdot \vec{a}_n \, ds + \int_s \vec{\mathcal{B}}^{\text{inc}} \cdot \vec{a}_n \, ds \end{aligned} \tag{11.4}$$

The line voltages are defined as

$$V(z, t) = - \int_a^{a'} \vec{\mathcal{E}}(x, y, z, t) \cdot d\vec{l} \tag{11.5a}$$

$$V(z + \Delta z, t) = - \int_b^{b'} \vec{\mathcal{E}}(x, y, z + \Delta z, t) \cdot d\vec{l} \tag{11.5b}$$

To allow for imperfect conductors, we again define the per-unit-length conductor resistance of each conductor as $r_1 \, \Omega/\text{m}$ and $r_0 \, \Omega/\text{m}$. Thus,

$$- \int_a^{a'} \vec{\mathcal{E}} \cdot d\vec{l} = - \int_a^{a'} \mathcal{E}_z \, dz = -r_1 \, \Delta z \, I(z, t) \tag{11.6a}$$

$$- \int_b^{a} \vec{\mathcal{E}} \cdot d\vec{l} = - \int_b^{a} \mathcal{E}_z \, dz = -r_0 \, \Delta z \, I(z, t) \tag{11.6b}$$

where, along the conductors, $\vec{\mathcal{E}} = \mathcal{E}_z \vec{a}_z$ and $d\vec{l} = dz \vec{a}_z$. The currents on the conductors are again defined as

$$I(z, t) = \oint_{c'} \vec{\mathcal{H}} \cdot d\vec{l} \tag{11.7}$$

where $\vec{\mathcal{B}} = \mu \vec{\mathcal{H}}$ and $\vec{\mathcal{H}}$ is the magnetic field intensity and contour c' is a contour just off the surface of and encircling the top conductor in the transverse plane as shown in Figure 11.2. Hence, (11.1) becomes

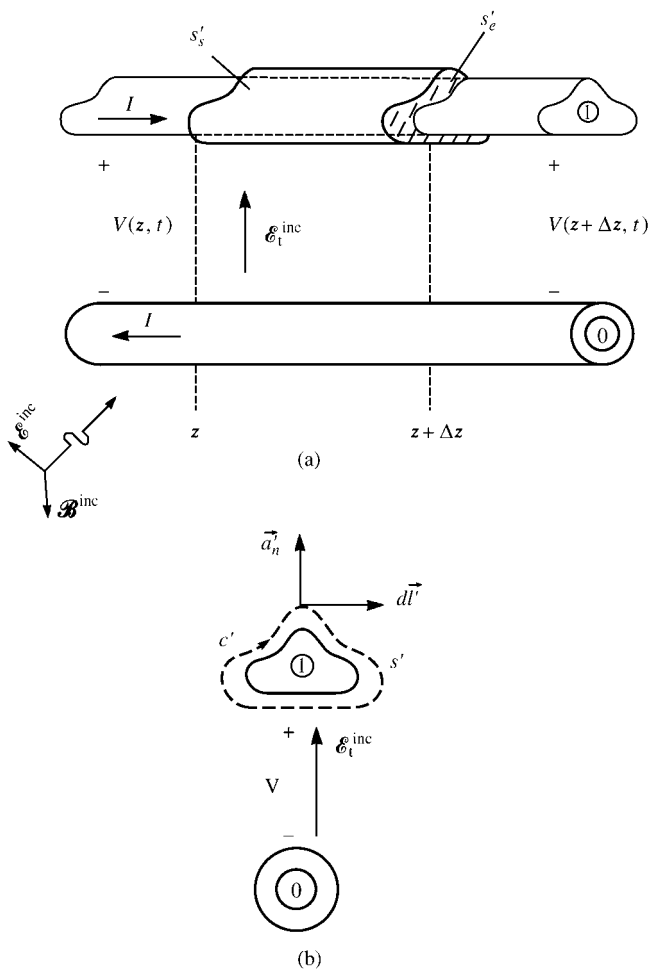


FIGURE 11.2 Definition of the surface for the derivation of the second transmission-line equation for incident field illumination.

$$\begin{aligned}
 & -V(z, t) + r_1 \Delta z I(z, t) + V(z + \Delta z, t) + r_0 \Delta z I(z, t) \\
 & = \frac{d}{dt} \int_s \vec{\mathcal{B}}^{\text{scat}} \cdot \vec{a}_n ds + \frac{d}{dt} \int_s \vec{\mathcal{B}}^{\text{inc}} \cdot \vec{a}_n ds
 \end{aligned} \tag{11.8}$$

Dividing both sides by Δz and rearranging gives

$$\begin{aligned}
 & \frac{V(z + \Delta z, t) - V(z, t)}{\Delta z} + r_1 I(z, t) + r_0 I(z, t) - \frac{1}{\Delta z} \frac{d}{dt} \int_s \vec{\mathcal{B}}^{\text{scat}} \cdot \vec{a}_n ds \\
 & = \frac{1}{\Delta z} \frac{d}{dt} \int_s \vec{\mathcal{B}}^{\text{inc}} \cdot \vec{a}_n ds
 \end{aligned} \tag{11.9}$$

The per-unit-length magnetic flux penetrating the flat surface that is due to the currents on the conductors is related to the per-unit-length inductance of the line, l , as

$$\begin{aligned}
 \psi & = - \lim_{\Delta z \rightarrow 0} \frac{1}{\Delta z} \int_s \vec{\mathcal{B}}^{\text{scat}} \cdot \vec{a}_n ds \\
 & = - \int_a^{a'} \vec{\mathcal{B}}^{\text{scat}} \cdot \vec{a}_n dl \\
 & = lI(z, t)
 \end{aligned} \tag{11.10}$$

Taking the limit of (11.9) as $\Delta z \rightarrow 0$ and substituting (11.10) gives the first transmission-line equation

$$\frac{\partial V(z, t)}{\partial z} + rI(z, t) + l \frac{\partial I(z, t)}{\partial t} = \frac{\partial}{\partial t} \int_a^{a'} \vec{\mathcal{B}}^{\text{inc}} \cdot \vec{a}_n dl \tag{11.11}$$

where the total per-unit-length resistance of the line is $r = r_1 + r_0$.

In order to derive the second transmission-line equation, consider placing a closed surface s' around the top conductor and just off that conductor as shown in Figure 11.2. This is the same surface used to define current in (11.7). The portion of the surface over the end caps is denoted as s'_e , whereas the portion over the sides is denoted as s'_s . Recall the continuity equation or equation of conservation of charge [A.1]:

$$\oiint_{s'} \vec{\mathcal{J}} \cdot d\vec{s}' = - \frac{\partial}{\partial t} Q_{\text{enc}} \tag{11.12}$$

Over the end caps we have

$$\iint_{s'_e} \vec{\mathcal{J}} \cdot d\vec{s}' = I(z + \Delta z, t) - I(z, t) \quad (11.13)$$

The total electric field is again the sum of a component that is due to the scattered field, which is denoted as $\vec{\mathcal{E}}^{\text{scat}}$, and the electric field of the incident wave, which is denoted as $\vec{\mathcal{E}}^{\text{inc}}$, as

$$\vec{\mathcal{E}} = \vec{\mathcal{E}}^{\text{scat}} + \vec{\mathcal{E}}^{\text{inc}} \quad (11.14)$$

and the voltage is defined in terms of the total field as

$$\begin{aligned} V(z, t) &= -\int_a^{a'} \vec{\mathcal{E}} \cdot d\vec{l} \\ &= -\int_a^{a'} \vec{\mathcal{E}}^{\text{scat}} \cdot d\vec{l} - \int_a^{a'} \vec{\mathcal{E}}^{\text{inc}} \cdot d\vec{l} \end{aligned} \quad (11.15)$$

Some derivations define a scattered voltage in terms of the scattered electric field. But that scattered voltage is not the total voltage in terms of which the terminal relations are defined. This has created considerable confusion in the past. So when we incorporate the terminal constraints at the ends of the line, we must use the total voltage given in (11.15). Again, we define the per-unit-length conductance g S/m between the two conductors as the ratio of the conduction current flowing between the two conductors in the transverse plane per unit of line length, I_t , to the voltage between the two conductors. Hence,

$$\begin{aligned} I_t(z, t) &= \underbrace{\lim}_{\Delta z \rightarrow 0} \frac{1}{\Delta z} \iint_{s'_s} \vec{\mathcal{J}} \cdot d\vec{s}' \\ &= -g \int_a^{a'} \vec{\mathcal{E}}^{\text{scat}} \cdot d\vec{l} \\ &= gV(z, t) + g \int_a^{a'} \vec{\mathcal{E}}^{\text{inc}} \cdot d\vec{l} \end{aligned} \quad (11.16)$$

Similarly, define the per-unit-length capacitance as

$$\underbrace{\lim}_{\Delta z \rightarrow 0} \frac{Q_{\text{enc}}}{\Delta z} = -c \int_a^{a'} \vec{\mathcal{E}}^{\text{scat}} \cdot d\vec{l}$$

$$= cV(z, t) + c \int_a^{a'} \vec{\mathcal{E}}^{\text{inc}} \cdot d\vec{l} \tag{11.17}$$

Substituting (11.13), (11.16), and (11.17) into (11.12) gives

$$\begin{aligned} I(z + \Delta z) - I(z) + g\Delta z V(z, t) + c\Delta z \frac{\partial V(z, t)}{\partial t} \\ = -g\Delta z \int_a^{a'} \vec{\mathcal{E}}^{\text{inc}} \cdot d\vec{l} - c \frac{\partial}{\partial t} \Delta z \int_a^{a'} \vec{\mathcal{E}}^{\text{inc}} \cdot d\vec{l} \end{aligned} \tag{11.18}$$

Dividing (11.18) by Δz and taking the limit as $\Delta z \rightarrow 0$ gives the second transmission-line equation

$$\frac{\partial I(z, t)}{\partial z} + gV(z, t) + c \frac{\partial V(z, t)}{\partial t} = -g \int_a^{a'} \vec{\mathcal{E}}^{\text{inc}} \cdot d\vec{l} - c \frac{\partial}{\partial t} \int_a^{a'} \vec{\mathcal{E}}^{\text{inc}} \cdot d\vec{l} \tag{11.19}$$

These transmission-line equations can also be derived from the per-unit-length equivalent circuit in Figure 11.3 as

$$\frac{\partial V(z, t)}{\partial z} + rI(z, t) + l \frac{\partial I(z, t)}{\partial t} = V_F(z, t) \tag{11.20a}$$

$$\frac{\partial I(z, t)}{\partial z} + gV(z, t) + c \frac{\partial V(z, t)}{\partial t} = I_F(z, t) \tag{11.20b}$$

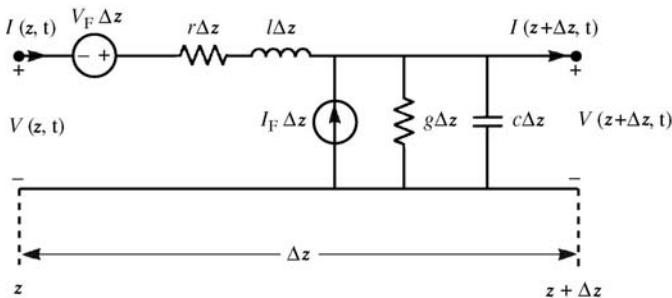


FIGURE 11.3 The per-unit-length equivalent circuit for a transmission-line with incident field illumination.

where the per-unit-length distributed sources due to the incident field, $V_F(z, t)$ and $I_F(z, t)$, are

$$V_F(z, t) = \frac{\partial}{\partial t} \int_a^{a'} \vec{\mathcal{B}}^{\text{inc}} \cdot \vec{a}_n dl \quad (11.21a)$$

and

$$I_F(z, t) = -g \int_a^{a'} \vec{\mathcal{E}}^{\text{inc}} \cdot d\vec{l} - c \frac{\partial}{\partial t} \int_a^{a'} \vec{\mathcal{E}}^{\text{inc}} \cdot d\vec{l} \quad (11.21b)$$

Thus, the *sources* are the component of the incident magnetic field *normal* to the circuit loop and the component of the incident electric field *transverse* to the line.

11.1.1 Equivalence of Source Representations

Observe that the equivalent per-unit-length voltage source in (11.21a) is in terms of the incident magnetic field, and the equivalent per-unit-length current source in (11.21b) is in terms of the incident electric field. Faraday's law can be used to relate these and give equivalent representations. Writing Faraday's law around the contour of the flat surface in Figure 11.1 gives, as $\Delta z \rightarrow 0$,

$$\begin{aligned} & -\frac{\partial}{\partial z} \int_a^{a'} \vec{\mathcal{E}}^{\text{inc}} \cdot d\vec{l} + \left[\mathcal{E}_z^{\text{inc}}(\text{conductor \#1}, z, t) - \mathcal{E}_z^{\text{inc}}(\text{reference conductor}, z, t) \right] \\ & = \frac{\partial}{\partial t} \int_a^{a'} \vec{\mathcal{B}}^{\text{inc}} \cdot \vec{a}_n dl \end{aligned} \quad (11.22)$$

Hence, the per-unit-length equivalent voltage source in (11.21a) can be equivalently written in terms of the incident electric field as

$$\begin{aligned} V_F(z, t) & = \left[\mathcal{E}_z^{\text{inc}}(\text{conductor \#1}, z, t) - \mathcal{E}_z^{\text{inc}}(\text{reference conductor}, z, t) \right] \\ & \quad - \frac{\partial}{\partial z} \int_a^{a'} \vec{\mathcal{E}}^{\text{inc}} \cdot d\vec{l} \end{aligned} \quad (11.23)$$

Therefore, we only need to know the components of the incident electric field that are (1) along the surfaces of the conductors, $\mathcal{E}_z^{\text{inc}}(\text{conductor \#1 or \#0}, z, t)$, and (2) transverse (perpendicular) to the line and between the two conductors to give $\int_a^{a'} \vec{\mathcal{E}}^{\text{inc}} \cdot d\vec{l}$.

11.2 THE FREQUENCY-DOMAIN SOLUTION

In the frequency domain, the time-domain transmission-line equations given in (11.20) become, by replacing $\partial/\partial t \Rightarrow j\omega$,

$$\frac{d\hat{V}(z)}{dz} + \underbrace{(r + j\omega l)}_{\hat{z}} \hat{I}(z) = \hat{V}_F(z) \tag{11.24a}$$

$$\frac{d\hat{I}(z)}{dz} + \underbrace{(g + j\omega c)}_{\hat{y}} \hat{V}(z) = \hat{I}_F(z) \tag{11.24b}$$

where the phasor sources are

$$\hat{V}_F(z) = j\omega \int_a^{d'} \vec{\hat{B}}^{\text{inc}} \cdot \vec{a}_n dl \tag{11.24c}$$

$$\hat{I}_F(z) = -\underbrace{(g + j\omega c)}_{\hat{y}} \int_a^{d'} \vec{\hat{E}}^{\text{inc}} \cdot d\vec{l} \tag{11.24d}$$

or, equivalently,

$$\begin{aligned} \hat{V}_F(z) = & \left[\hat{E}_z^{\text{inc}}(\text{conductor \#1}, z) - \hat{E}_z^{\text{inc}}(\text{reference conductor}, z) \right] \\ & - \frac{\partial}{\partial z} \int_a^{d'} \vec{\hat{E}}^{\text{inc}} \cdot d\vec{l} \end{aligned} \tag{11.24e}$$

where we denote the *phasor* incident fields as $\vec{\hat{B}}^{\text{inc}}$ and $\vec{\hat{E}}^{\text{inc}}$. The per-unit-length impedance and admittance are again $\hat{z} = r + j\omega l$ and $\hat{y} = g + j\omega c$, respectively.

11.2.1 Solution of the Transmission-Line Equations

The phasor transmission-line equations in (11.24a) and (11.24b) are coupled first-order ordinary differential equations and are in the same form as *state-variable equations* found in electric circuit analysis, automatic control system analyses, or other linear system analyses [A.2,B.1,H.1,9,10]. These *state-variable equations* are in the form

$$\frac{d}{dt} \mathbf{X}(t) = \mathbf{A}\mathbf{X}(t) + \mathbf{W}(t) \tag{11.25}$$

where t represents the variable *time*, $\mathbf{X}(t)$ is a vector of *state variables*, and $\mathbf{W}(t)$ is a vector of *forcing functions* that are the excitation for the linear system. The solution to these state-variable equations is [9,10]

$$\mathbf{X}(t) = \Phi(t - t_0)\mathbf{X}(t_0) + \int_{t_0}^t \Phi(t - \tau) \mathbf{W}(\tau) d\tau \quad (11.26a)$$

and the *state-transition matrix* is [9,10]

$$\begin{aligned} \Phi(t) &= \mathbf{e}^{\mathbf{A}t} \\ &= \mathbf{1}_n + \frac{t}{1!} \mathbf{A} + \frac{t^2}{2!} \mathbf{A}^2 + \frac{t^3}{3!} \mathbf{A}^3 + \dots \end{aligned} \quad (11.26b)$$

where $\mathbf{1}_n$ is the $n \times n$ identity matrix with 1s on the main diagonal and zeros elsewhere. This gives the solutions for the state variables of the system at some time t for the given initial conditions at time t_0 . The forcing functions affect the solution via a *convolution* term. The state-transition matrix has some very nice and very useful identities [9,10]:

$$\Phi(0) = \mathbf{1}_n \quad (11.27a)$$

$$\Phi^{-1}(t) = \Phi(-t) \quad (11.27b)$$

$$\Phi(t_1)\Phi(t_2) = \Phi(t_1 + t_2) \quad (11.27c)$$

All three identities follow from the definition of the state-transition matrix in (11.26b): $\Phi(0) = \mathbf{e}^{\mathbf{A}0} = \mathbf{1}_n$, $\Phi^{-1}(t) = \mathbf{e}^{-\mathbf{A}t} = \mathbf{e}^{\mathbf{A}(-t)} = \Phi(-t)$, and $\Phi(t_1 + t_2) = \mathbf{e}^{\mathbf{A}(t_1+t_2)} = \mathbf{e}^{\mathbf{A}t_1}\mathbf{e}^{\mathbf{A}t_2} = \Phi(t_1)\Phi(t_2)$.

We can make an analogy of these state-variable equations and their solution to that of the phasor transmission-line equations by replacing t in these state-variable equations with the distance variable for the transmission line, z , and writing the phasor transmission-line equations in (11.24) in matrix form as

$$\frac{d}{dz} \hat{\mathbf{X}}(z) = \hat{\mathbf{A}} \hat{\mathbf{X}}(z) + \hat{\mathbf{W}}(z) \quad (11.28a)$$

where

$$\hat{\mathbf{X}}(z) = \begin{bmatrix} \hat{V}(z) \\ \hat{I}(z) \end{bmatrix} \quad (11.28b)$$

$$\hat{\mathbf{A}} = \begin{bmatrix} 0 & -\hat{z} \\ -\hat{y} & 0 \end{bmatrix} \quad (11.28c)$$

$$\hat{\mathbf{W}}(z) = \begin{bmatrix} \hat{V}_F(z) \\ \hat{I}_F(z) \end{bmatrix} \quad (11.28d)$$

Hence, the solution to the phasor transmission-line equations in (11.28) can be obtained by analogy to the state-variable equations as

$$\hat{\mathbf{X}}(z) = \hat{\Phi}(z - z_0)\hat{\mathbf{X}}(z_0) + \int_{z_0}^z \hat{\Phi}(z - \tau) \underbrace{\begin{bmatrix} \hat{V}_F(\tau) \\ \hat{I}_F(\tau) \end{bmatrix}}_{\hat{\mathbf{W}}(\tau)} d\tau \quad (11.29a)$$

where the 2×2 chain-parameter matrix is defined as

$$\begin{aligned} \hat{\Phi}(z - z_0) &\equiv e^{\hat{\mathbf{A}}(z-z_0)} \\ &= \begin{bmatrix} \hat{\phi}_{11}(z - z_0) & \hat{\phi}_{12}(z - z_0) \\ \hat{\phi}_{21}(z - z_0) & \hat{\phi}_{22}(z - z_0) \end{bmatrix} \end{aligned} \quad (11.29b)$$

If we specialize this to a line of total length \mathcal{L} , then we let $z = \mathcal{L}$ and $z_0 = 0$ and obtain from (11.29)

$$\begin{bmatrix} \hat{V}(\mathcal{L}) \\ \hat{I}(\mathcal{L}) \end{bmatrix} = \hat{\Phi}(\mathcal{L}) \begin{bmatrix} \hat{V}(0) \\ \hat{I}(0) \end{bmatrix} + \int_0^{\mathcal{L}} \hat{\Phi}(\mathcal{L} - \tau) \begin{bmatrix} \hat{V}_F(\tau) \\ \hat{I}_F(\tau) \end{bmatrix} d\tau \quad (11.30a)$$

or, in expanded form,

$$\begin{bmatrix} \hat{V}(\mathcal{L}) \\ \hat{I}(\mathcal{L}) \end{bmatrix} = \begin{bmatrix} \hat{\phi}_{11}(\mathcal{L}) & \hat{\phi}_{12}(\mathcal{L}) \\ \hat{\phi}_{21}(\mathcal{L}) & \hat{\phi}_{22}(\mathcal{L}) \end{bmatrix} \begin{bmatrix} \hat{V}(0) \\ \hat{I}(0) \end{bmatrix} + \int_0^{\mathcal{L}} \begin{bmatrix} \hat{\phi}_{11}(\mathcal{L} - \tau) & \hat{\phi}_{12}(\mathcal{L} - \tau) \\ \hat{\phi}_{21}(\mathcal{L} - \tau) & \hat{\phi}_{22}(\mathcal{L} - \tau) \end{bmatrix} \begin{bmatrix} \hat{V}_F(\tau) \\ \hat{I}_F(\tau) \end{bmatrix} d\tau \quad (11.30b)$$

where $\hat{\Phi}(\mathcal{L})$ is the chain-parameter matrix of the line. The entries in the chain-parameter matrix, $\hat{\phi}_{ij}(\mathcal{L})$, are given, for a two-conductor line, in Eqs. (6.85) of Chapter 6:

$$\begin{aligned} \hat{\phi}_{11}(\mathcal{L}) &= \cosh(\hat{\gamma} \mathcal{L}) \\ &= \frac{e^{\hat{\gamma} \mathcal{L}} + e^{-\hat{\gamma} \mathcal{L}}}{2} \end{aligned} \quad (6.85a)$$

$$\begin{aligned} \hat{\phi}_{12}(\mathcal{L}) &= -\hat{Z}_C \sinh(\hat{\gamma} \mathcal{L}) \\ &= -\hat{Z}_C \frac{e^{\hat{\gamma} \mathcal{L}} - e^{-\hat{\gamma} \mathcal{L}}}{2} \end{aligned} \quad (6.85b)$$

$$\hat{\phi}_{21}(\mathcal{L}) = -\frac{1}{\hat{Z}_C} \sinh(\hat{\gamma} \mathcal{L})$$

$$= -\frac{1}{\hat{Z}_C} \frac{e^{\hat{\gamma}\mathcal{L}} - e^{-\hat{\gamma}\mathcal{L}}}{2} \quad (6.85c)$$

$$\begin{aligned} \hat{\phi}_{22}(\mathcal{L}) &= \cosh(\hat{\gamma}\mathcal{L}) \\ &= \frac{e^{\hat{\gamma}\mathcal{L}} + e^{-\hat{\gamma}\mathcal{L}}}{2} \end{aligned} \quad (6.85d)$$

The propagation constant is $\hat{\gamma} = \sqrt{\hat{z}\hat{y}} = \sqrt{(r + j\omega l)(g + j\omega c)}$ and the line characteristic impedance is $\hat{Z}_C = \sqrt{\hat{z}/\hat{y}} = \sqrt{(r + j\omega l)/(g + j\omega c)}$. Observe in (11.30) that the incident fields add a *convolution* term to the usual chain-parameter relation.

Because of the analogy of the phasor transmission-line equations to the state-variable formulation, the chain-parameter matrix $\hat{\Phi}(\mathcal{L})$ has some very nice and very useful identities. From the identities for the state-transition matrix in (11.27), we obtain

$$\hat{\Phi}(0) = \mathbf{1}_n \quad (11.31a)$$

$$\hat{\Phi}^{-1}(\mathcal{L}) = \Phi(-\mathcal{L}) \quad (11.31b)$$

$$\Phi(\mathcal{L}_1)\Phi(\mathcal{L}_2) = \Phi(\mathcal{L}_1 + \mathcal{L}_2) \quad (11.31c)$$

These identities are extraordinarily sensible since the chain-parameter matrix relates the voltage and current at the right end of a line to the voltage and current at the left end of the line. The first identity in (11.31a) essentially means that the voltage and current at one end of the line are equal to the voltage and current at the other end of the line for a *total line length of zero*. The second identity in (11.31b) essentially means that the voltage and current at the left end of the line, $z = 0$, are related to the voltage and current at the right end of the line, $z = \mathcal{L}$, by the chain-parameter matrix, and we have simply made a reversal in the axis variable, $z \Rightarrow -z$. The last identity in (11.31c) means that if we split a line into two consecutive sections each of length z_1 and z_2 where $z = z_1 + z_2$, then the chain-parameter matrix of the overall line that is of length $z = z_1 + z_2$ is the product of the chain-parameter matrices of each section.

The effects of the incident field can be written in terms of equivalent voltage and current sources. Writing (11.30) out for a transmission line of total length \mathcal{L} gives

$$\begin{bmatrix} \hat{V}(\mathcal{L}) \\ \hat{I}(\mathcal{L}) \end{bmatrix} = \hat{\Phi}(\mathcal{L}) \begin{bmatrix} \hat{V}(0) \\ \hat{I}(0) \end{bmatrix} + \begin{bmatrix} \hat{V}_{\text{FT}}(\mathcal{L}) \\ \hat{I}_{\text{FT}}(\mathcal{L}) \end{bmatrix} \quad (11.32)$$

where the total voltage and current sources, $\hat{V}_{\text{FT}}(\mathcal{L})$ and $\hat{I}_{\text{FT}}(\mathcal{L})$, are, according to (11.30),

$$\begin{bmatrix} \hat{V}_{\text{FT}}(\mathcal{L}) \\ \hat{I}_{\text{FT}}(\mathcal{L}) \end{bmatrix} = \int_0^{\mathcal{L}} \hat{\Phi}(\mathcal{L} - \tau) \begin{bmatrix} \hat{V}_{\text{F}}(\tau) \\ \hat{I}_{\text{F}}(\tau) \end{bmatrix} d\tau \quad (11.33a)$$

In expanded form, these total voltage and current sources become

$$\hat{V}_{\text{FT}}(\mathcal{L}) = \int_0^{\mathcal{L}} [\hat{\phi}_{11}(\mathcal{L} - \tau)\hat{V}_{\text{F}}(\tau) + \hat{\phi}_{12}(\mathcal{L} - \tau)\hat{I}_{\text{F}}(\tau)] d\tau \quad (11.33b)$$

$$\hat{I}_{\text{FT}}(\mathcal{L}) = \int_0^{\mathcal{L}} [\hat{\phi}_{21}(\mathcal{L} - \tau)\hat{V}_{\text{F}}(\tau) + \hat{\phi}_{22}(\mathcal{L} - \tau)\hat{I}_{\text{F}}(\tau)] d\tau \quad (11.33c)$$

According to (11.32), the equivalent circuit of the complete line can be viewed as an unexcited line along with the equivalent sources $\hat{V}_{\text{FT}}(\mathcal{L})$ and $\hat{I}_{\text{FT}}(\mathcal{L})$ located at $z = \mathcal{L}$ as illustrated in Figure 11.4(a).

We can also place equivalent sources at the left end of the line, $z = 0$. Premultiplying (11.32) by the inverse of the chain-parameter matrix and rearranging gives

$$\begin{aligned} \begin{bmatrix} \hat{V}(0) \\ \hat{I}(0) \end{bmatrix} &= \hat{\Phi}^{-1}(\mathcal{L}) \begin{bmatrix} \hat{V}(\mathcal{L}) \\ \hat{I}(\mathcal{L}) \end{bmatrix} - \hat{\Phi}^{-1}(\mathcal{L}) \begin{bmatrix} \hat{V}_{\text{FT}}(\mathcal{L}) \\ \hat{I}_{\text{FT}}(\mathcal{L}) \end{bmatrix} \\ &= \hat{\Phi}(-\mathcal{L}) \begin{bmatrix} \hat{V}(\mathcal{L}) \\ \hat{I}(\mathcal{L}) \end{bmatrix} - \begin{bmatrix} \hat{V}'_{\text{FT}}(\mathcal{L}) \\ \hat{I}'_{\text{FT}}(\mathcal{L}) \end{bmatrix} \\ &= \underbrace{\begin{bmatrix} \hat{\phi}_{11}(\mathcal{L}) & -\hat{\phi}_{12}(\mathcal{L}) \\ -\hat{\phi}_{21}(\mathcal{L}) & \hat{\phi}_{22}(\mathcal{L}) \end{bmatrix}}_{\hat{\Phi}(-\mathcal{L})} \begin{bmatrix} \hat{V}(\mathcal{L}) \\ \hat{I}(\mathcal{L}) \end{bmatrix} - \begin{bmatrix} \hat{V}'_{\text{FT}}(\mathcal{L}) \\ \hat{I}'_{\text{FT}}(\mathcal{L}) \end{bmatrix} \end{aligned} \quad (11.34)$$

where these equivalent voltage and current sources are defined as

$$\begin{aligned} \begin{bmatrix} \hat{V}'_{\text{FT}}(\mathcal{L}) \\ \hat{I}'_{\text{FT}}(\mathcal{L}) \end{bmatrix} &= \hat{\Phi}^{-1}(\mathcal{L}) \begin{bmatrix} \hat{V}_{\text{FT}}(\mathcal{L}) \\ \hat{I}_{\text{FT}}(\mathcal{L}) \end{bmatrix} \\ &= \hat{\Phi}(-\mathcal{L}) \begin{bmatrix} \hat{V}_{\text{FT}}(\mathcal{L}) \\ \hat{I}_{\text{FT}}(\mathcal{L}) \end{bmatrix} \end{aligned} \quad (11.35)$$

and we have used the identity for the inverse in (11.31b), $\hat{\Phi}^{-1}(\mathcal{L}) = \hat{\Phi}(-\mathcal{L})$, and have used the chain-parameter identities from (6.85) of $\hat{\phi}_{11}(-\mathcal{L}) = \hat{\phi}_{11}(\mathcal{L})$, $\hat{\phi}_{12}(-\mathcal{L}) = -\hat{\phi}_{12}(\mathcal{L})$, $\hat{\phi}_{21}(-\mathcal{L}) = -\hat{\phi}_{21}(\mathcal{L})$, and $\hat{\phi}_{22}(-\mathcal{L}) = \hat{\phi}_{22}(\mathcal{L})$. This gives the equivalent circuit of Figure 11.4(b) where the incident field sources are placed at the input to the line. We have reflected the sources at the right end of the line $z = \mathcal{L}$, $\hat{V}_{\text{FT}}(\mathcal{L})$ and $\hat{I}_{\text{FT}}(\mathcal{L})$, backward through the line to give the sources at the left end of the line $z = 0$, $\hat{V}'_{\text{FT}}(\mathcal{L})$ and $\hat{I}'_{\text{FT}}(\mathcal{L})$. These sources at the left end of

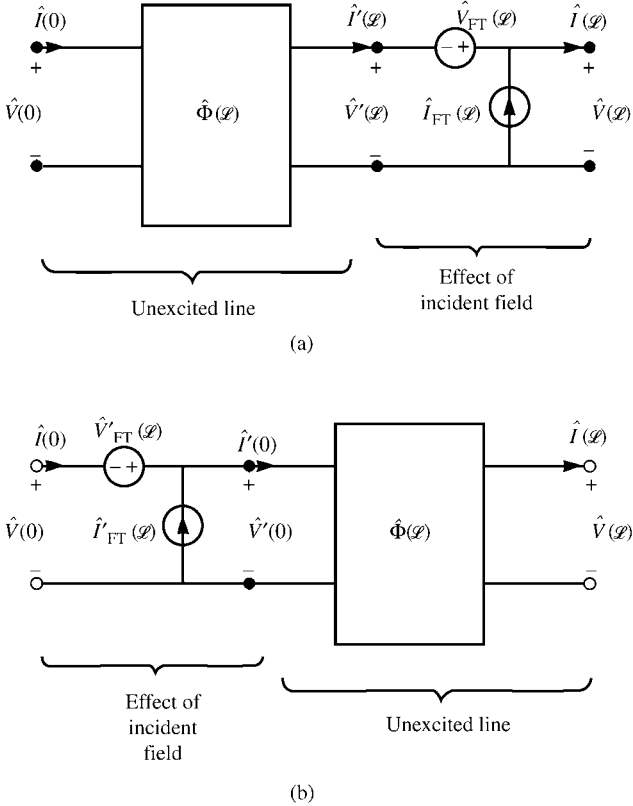


FIGURE 11.4 Illustration of the representation of a transmission line with incident field illumination as a two-port having lumped sources that represent the effects of the incident field.

the line can be written in a more direct form as

$$\begin{aligned}
 \begin{bmatrix} \hat{V}'_{FT}(\mathcal{L}) \\ \hat{I}'_{FT}(\mathcal{L}) \end{bmatrix} &= \hat{\Phi}^{-1}(\mathcal{L}) \int_0^{\mathcal{L}} \hat{\Phi}(\mathcal{L} - \tau) \begin{bmatrix} \hat{V}_F(\tau) \\ \hat{I}_F(\tau) \end{bmatrix} d\tau \\
 &= \int_0^{\mathcal{L}} \hat{\Phi}^{-1}(\mathcal{L}) \hat{\Phi}(\mathcal{L} - \tau) \begin{bmatrix} \hat{V}_F(\tau) \\ \hat{I}_F(\tau) \end{bmatrix} d\tau \\
 &= \int_0^{\mathcal{L}} \hat{\Phi}(-\tau) \begin{bmatrix} \hat{V}_F(\tau) \\ \hat{I}_F(\tau) \end{bmatrix} d\tau
 \end{aligned} \tag{11.36}$$

and we have used the chain-parameter matrix identity in (11.31c) to give $\hat{\Phi}(\mathcal{L} - \tau) = \hat{\Phi}(\mathcal{L})\hat{\Phi}(-\tau)$ or $\hat{\Phi}^{-1}(\mathcal{L})\hat{\Phi}(\mathcal{L} - \tau) = \hat{\Phi}(-\tau)$. Writing out (11.36) gives

$$\begin{aligned}
 \hat{V}'_{\text{FT}}(\mathcal{L}) &= \int_0^{\mathcal{L}} [\phi_{11}(-\tau)\hat{V}_{\text{F}}(\tau) + \phi_{12}(-\tau)\hat{I}_{\text{F}}(\tau)] d\tau \\
 &= \int_0^{\mathcal{L}} [\phi_{11}(\tau)\hat{V}_{\text{F}}(\tau) - \phi_{12}(\tau)\hat{I}_{\text{F}}(\tau)] d\tau \quad (11.37a)
 \end{aligned}$$

$$\begin{aligned}
 \hat{I}'_{\text{FT}}(\mathcal{L}) &= \int_0^{\mathcal{L}} [\phi_{21}(-\tau)\hat{V}_{\text{F}}(\tau) + \phi_{22}(-\tau)\hat{I}_{\text{F}}(\tau)] d\tau \\
 &= \int_0^{\mathcal{L}} [-\phi_{21}(\tau)\hat{V}_{\text{F}}(\tau) + \phi_{22}(\tau)\hat{I}_{\text{F}}(\tau)] d\tau \quad (11.37b)
 \end{aligned}$$

and we have again used the chain-parameter identities from (6.85) of $\hat{\phi}_{11}(-\tau) = \hat{\phi}_{11}(\tau)$, $\hat{\phi}_{12}(-\tau) = -\hat{\phi}_{12}(\tau)$, $\hat{\phi}_{21}(-\tau) = -\hat{\phi}_{21}(\tau)$, and $\hat{\phi}_{22}(-\tau) = \hat{\phi}_{22}(\tau)$.

11.2.2 Simplified Forms of the Excitations

The total voltage and current sources $\hat{V}_{\text{FT}}(\mathcal{L})$ and $\hat{I}_{\text{FT}}(\mathcal{L})$ given in (11.33), representing the effects of the incident field, can be simplified by using the definitions of the phasor distributed sources, $\hat{V}_{\text{F}}(\mathcal{L})$ and $\hat{I}_{\text{F}}(\mathcal{L})$, given in (11.24) and the properties of the chain-parameter submatrices given in (6.85). Substituting (11.24) into (11.33b) yields

$$\begin{aligned}
 \hat{V}_{\text{FT}}(\mathcal{L}) &= \int_0^{\mathcal{L}} [\hat{\phi}_{11}(\mathcal{L} - \tau)\hat{V}_{\text{F}}(\tau) + \hat{\phi}_{12}(\mathcal{L} - \tau)\hat{I}_{\text{F}}(\tau)] d\tau \\
 &= \int_0^{\mathcal{L}} \hat{\phi}_{11}(\mathcal{L} - \tau) \left[\begin{array}{c} \hat{E}_z^{\text{inc}}(\text{conductor \#1}, \tau) \\ -\hat{E}_z^{\text{inc}}(\text{reference conductor}, \tau) \end{array} \right] d\tau \\
 &\quad - \hat{\phi}_{11}(\mathcal{L} - \tau) \left[\frac{\partial}{\partial \tau} \int_a^{a'} \vec{E}^{\text{inc}} \cdot d\vec{l} \right] d\tau \\
 &\quad - \hat{\phi}_{12}(\mathcal{L} - \tau) \left[\int_a^{a'} \vec{E}^{\text{inc}} \cdot d\vec{l} \right] d\tau \quad (11.38)
 \end{aligned}$$

Using the chain rule for differentiation:

$$\frac{\partial}{\partial \tau} A(\tau) B(\tau) = A(\tau) \left[\frac{\partial}{\partial \tau} B(\tau) \right] + \left[\frac{\partial}{\partial \tau} A(\tau) \right] B(\tau) \quad (11.39)$$

we obtain

$$\begin{aligned}
 \hat{V}_{\text{FT}}(\mathcal{L}) = & \int_0^{\mathcal{L}} \hat{\phi}_{11}(\mathcal{L} - \tau) \left[\begin{array}{c} \hat{E}_z^{\text{inc}}(\text{conductor \#1}, \tau) \\ -\hat{E}_z^{\text{inc}}(\text{reference conductor}, \tau) \end{array} \right] d\tau \\
 & - \int_0^{\mathcal{L}} \frac{\partial}{\partial \tau} \left[\hat{\phi}_{11}(\mathcal{L} - \tau) \int_a^{a'} \vec{E}^{\text{inc}} \cdot d\vec{l} \right] d\tau \\
 & + \int_0^{\mathcal{L}} \underbrace{\left[\frac{\partial}{\partial \tau} \hat{\phi}_{11}(\mathcal{L} - \tau) - \hat{\phi}_{12}(\mathcal{L} - \tau) \hat{y} \right]}_{=0} \left[\int_a^{a'} \vec{E}^{\text{inc}} \cdot d\vec{l} \right] d\tau \quad (11.40)
 \end{aligned}$$

The last term of (11.40) is identically zero. To show this, we substitute the chain-parameter submatrices given in (6.85) into this last term to give

$$\begin{aligned}
 \frac{\partial}{\partial \tau} \hat{\phi}_{11}(\mathcal{L} - \tau) - \hat{\phi}_{12}(\mathcal{L} - \tau) \hat{y} &= \frac{\partial}{\partial \tau} \cosh(\hat{y}[\mathcal{L} - \tau]) + \hat{Z}_C \hat{y} \sinh(\hat{y}[\mathcal{L} - \tau]) \\
 &= [-\hat{y} + \hat{Z}_C \hat{y}] \sinh(\hat{y}[\mathcal{L} - \tau]) \\
 &= 0 \quad (11.41)
 \end{aligned}$$

since, from Chapter 6, $\hat{y} = \hat{Z}_C \hat{y}$ or $\sqrt{\hat{z}} \hat{y} = \sqrt{\frac{\hat{z}}{\hat{y}}}$. Hence,

$$\begin{aligned}
 \hat{V}_{\text{FT}}(\mathcal{L}) = & \int_0^{\mathcal{L}} \hat{\phi}_{11}(\mathcal{L} - \tau) \left[\begin{array}{c} \hat{E}_z^{\text{inc}}(\text{conductor \#1}, \tau) \\ -\hat{E}_z^{\text{inc}}(\text{reference conductor}, \tau) \end{array} \right] d\tau \\
 & - \underbrace{\hat{\phi}_{11}(0)}_1 \left[\int_a^{a'} \vec{E}^{\text{inc}} \cdot d\vec{l} \right] \Big|_{z=\mathcal{L}} + \hat{\phi}_{11}(\mathcal{L}) \left[\int_a^{a'} \vec{E}^{\text{inc}} \cdot d\vec{l} \right] \Big|_{z=0} \quad (11.42)
 \end{aligned}$$

Similarly, from (11.33c)

$$\begin{aligned}
 \hat{I}_{\text{FT}}(\mathcal{L}) = & \int_0^{\mathcal{L}} [\hat{\phi}_{21}(\mathcal{L} - \tau) \hat{V}_{\text{F}}(\tau) + \hat{\phi}_{22}(\mathcal{L} - \tau) \hat{I}_{\text{F}}(\tau)] d\tau \\
 = & \int_0^{\mathcal{L}} \hat{\phi}_{21}(\mathcal{L} - \tau) \left[\begin{array}{c} \hat{E}_z^{\text{inc}}(\text{conductor \#1}, \tau) \\ -\hat{E}_z^{\text{inc}}(\text{reference conductor}, \tau) \end{array} \right] d\tau \\
 & - \underbrace{\hat{\phi}_{21}(0)}_0 \left[\int_a^{a'} \vec{E}^{\text{inc}} \cdot d\vec{l} \right] \Big|_{z=\mathcal{L}} + \hat{\phi}_{21}(\mathcal{L}) \left[\int_a^{a'} \vec{E}^{\text{inc}} \cdot d\vec{l} \right] \Big|_{z=0} \quad (11.43)
 \end{aligned}$$

Thus, the simplified total voltage and current sources due to the incident field are

$$\begin{aligned} \hat{V}_{\text{FT}}(\mathcal{L}) = & \int_0^{\mathcal{L}} \hat{\phi}_{11}(\mathcal{L} - \tau) \left[\begin{array}{l} \hat{E}_z^{\text{inc}}(\text{conductor \#1}, \tau) \\ -\hat{E}_z^{\text{inc}}(\text{reference conductor}, \tau) \end{array} \right] d\tau \\ & - \left[\int_a^{a'} \vec{E}^{\text{inc}} \cdot d\vec{l} \right] \Big|_{z=\mathcal{L}} + \hat{\phi}_{11}(\mathcal{L}) \left[\int_a^{a'} \vec{E}^{\text{inc}} \cdot d\vec{l} \right] \Big|_{z=0} \end{aligned} \quad (11.44a)$$

and

$$\begin{aligned} \hat{I}_{\text{FT}}(\mathcal{L}) = & \int_0^{\mathcal{L}} \hat{\phi}_{21}(\mathcal{L} - \tau) \left[\begin{array}{l} \hat{E}_z^{\text{inc}}(\text{conductor \#1}, \tau) \\ -\hat{E}_z^{\text{inc}}(\text{reference conductor}, \tau) \end{array} \right] d\tau \\ & + \hat{\phi}_{21}(\mathcal{L}) \left[\int_a^{a'} \vec{E}^{\text{inc}} \cdot d\vec{l} \right] \Big|_{z=0} \end{aligned} \quad (11.44b)$$

The corresponding simplified results for $\hat{V}'_{\text{FT}}(\mathcal{L})$ and $\hat{I}'_{\text{FT}}(\mathcal{L})$ given in (11.37) are similarly derived as

$$\begin{aligned} \hat{V}'_{\text{FT}}(\mathcal{L}) = & \int_0^{\mathcal{L}} \hat{\phi}_{11}(\tau) \left[\begin{array}{l} \hat{E}_z^{\text{inc}}(\text{conductor \#1}, \tau) \\ -\hat{E}_z^{\text{inc}}(\text{reference conductor}, \tau) \end{array} \right] d\tau \\ & + \left[\int_a^{a'} \vec{E}^{\text{inc}} \cdot d\vec{l} \right] \Big|_{z=0} - \hat{\phi}_{11}(\mathcal{L}) \left[\int_a^{a'} \vec{E}^{\text{inc}} \cdot d\vec{l} \right] \Big|_{z=\mathcal{L}} \end{aligned} \quad (11.45a)$$

and

$$\begin{aligned} \hat{I}'_{\text{FT}}(\mathcal{L}) = & - \int_0^{\mathcal{L}} \hat{\phi}_{21}(\tau) \left[\begin{array}{l} \hat{E}_z^{\text{inc}}(\text{conductor \#1}, \tau) \\ -\hat{E}_z^{\text{inc}}(\text{reference conductor}, \tau) \end{array} \right] d\tau \\ & + \hat{\phi}_{21}(\mathcal{L}) \left[\int_a^{a'} \vec{E}^{\text{inc}} \cdot d\vec{l} \right] \Big|_{z=\mathcal{L}} \end{aligned} \quad (11.45b)$$

11.2.3 Incorporating the Line Terminations

Now that the general solution of the phasor transmission-line equations has been obtained, we will complete the remaining task in the solution: incorporating the line terminations into that general solution. In Chapter 7, we obtained that solution wherein

the sources were in the termination networks and were written in terms of a generalized Thevenin equivalent representation that specializes for a two-conductor line to

$$\hat{V}(0) = \hat{V}_S - \hat{Z}_S \hat{I}(0) \quad (7.87a)$$

$$\hat{V}(\mathcal{L}) = \hat{V}_L + \hat{Z}_L \hat{I}(\mathcal{L}) \quad (7.87b)$$

Substituting these into the chain-parameter matrix representation without incident field illumination gave the final solution in (7.92) that specializes for a two-conductor line to

$$[\hat{\phi}_{12} - \hat{\phi}_{11} \hat{Z}_S - \hat{Z}_L \hat{\phi}_{22} + \hat{Z}_L \hat{\phi}_{21} \hat{Z}_S] \hat{I}(0) = \hat{V}_L - [\hat{\phi}_{11} - \hat{Z}_L \hat{\phi}_{21}] \hat{V}_S \quad (7.92a)$$

and

$$\hat{I}(\mathcal{L}) = \hat{\phi}_{21} \hat{V}_S + [\hat{\phi}_{22} - \hat{\phi}_{21} \hat{Z}_S] \hat{I}(0) \quad (7.92b)$$

Once (7.92a) is solved for the current at $z = 0$, (7.92b) can be solved for the current at $z = \mathcal{L}$. Then the voltages can be obtained from the terminal relations in (7.87).

We now incorporate the incident field excitation of the line into the above solution where the excitation was only from lumped sources in the termination networks. This final step is very simple for incident field illumination because we can write the general solution in (11.32), by moving the total sources due to the incident field, $\hat{V}_{FT}(\mathcal{L})$ and $\hat{I}_{FT}(\mathcal{L})$, to the left-hand side, to give

$$\begin{bmatrix} \hat{V}'(\mathcal{L}) = [\hat{V}(\mathcal{L}) - \hat{V}_{FT}(\mathcal{L})] \\ \hat{I}'(\mathcal{L}) = [\hat{I}(\mathcal{L}) - \hat{I}_{FT}(\mathcal{L})] \end{bmatrix} = \hat{\Phi}(\mathcal{L}) \begin{bmatrix} \hat{V}(0) \\ \hat{I}(0) \end{bmatrix} \quad (11.46)$$

Hence, the chain-parameter matrix relates the voltage and current at $z = 0$ to the primed variables at $z = \mathcal{L}$, $\hat{V}'(\mathcal{L}) = [\hat{V}(\mathcal{L}) - \hat{V}_{FT}(\mathcal{L})]$ and $\hat{I}'(\mathcal{L}) = [\hat{I}(\mathcal{L}) - \hat{I}_{FT}(\mathcal{L})]$, as shown in Figure 11.4(a). Figure 11.4(a) shows that we may make the substitutions $\hat{V}(\mathcal{L}) = [\hat{V}'(\mathcal{L}) + \hat{V}_{FT}(\mathcal{L})]$ and $\hat{I}(\mathcal{L}) = [\hat{I}'(\mathcal{L}) + \hat{I}_{FT}(\mathcal{L})]$ in the terminal relations in (7.87) to give

$$\hat{V}(0) = \hat{V}_S - \hat{Z}_S \hat{I}(0) \quad (11.47a)$$

$$[\hat{V}'(\mathcal{L}) + \hat{V}_{FT}(\mathcal{L})] = \hat{V}_L + \hat{Z}_L [\hat{I}'(\mathcal{L}) + \hat{I}_{FT}(\mathcal{L})] \quad (11.47b)$$

or

$$\hat{V}(0) = \hat{V}_S - \hat{Z}_S \hat{I}(0) \quad (11.47a)$$

$$\hat{V}'(\mathcal{L}) = [\hat{V}_L - \hat{V}_{FT}(\mathcal{L}) + \hat{Z}_L \hat{I}_{FT}(\mathcal{L})] + \hat{Z}_L \hat{I}'(\mathcal{L}) \quad (11.47b)$$

Comparing (11.47) to (7.87) shows that we can modify (7.92) for incident field excitation by simply replacing \hat{V}_L with $[\hat{V}_L - \hat{V}_{FT}(\mathcal{L}) + \hat{Z}_L \hat{I}_{FT}(\mathcal{L})]$ and replacing $\hat{I}(\mathcal{L})$ with $\hat{I}'(\mathcal{L}) = [\hat{I}(\mathcal{L}) - \hat{I}_{FT}(\mathcal{L})]$. Hence, the final solution is

$$\begin{aligned}
 [\hat{Z}_S \hat{\phi}_{11} + \hat{Z}_L \hat{\phi}_{22} - \hat{\phi}_{12} - \hat{Z}_S \hat{Z}_L \hat{\phi}_{21}] \hat{I}(0) &= \underbrace{[\hat{\phi}_{11} - \hat{Z}_L \hat{\phi}_{21}] \hat{V}_S - \hat{V}_L}_{\text{due to lumped sources}} \\
 &+ \underbrace{[\hat{V}_{FT}(\mathcal{L}) - \hat{Z}_L \hat{I}_{FT}(\mathcal{L})]}_{\text{due to incident field}}
 \end{aligned}
 \tag{11.48a}$$

$$\hat{I}(\mathcal{L}) = \hat{I}_{FT}(\mathcal{L}) + \hat{\phi}_{21} \hat{V}_S + [\hat{\phi}_{22} - \hat{Z}_S \hat{\phi}_{21}] \hat{I}(0)
 \tag{11.48b}$$

These results can also be derived directly by substituting the terminal constraints, $\hat{V}(0) = \hat{V}_S - \hat{Z}_S \hat{I}(0)$ and $\hat{V}(\mathcal{L}) = \hat{V}_L + \hat{Z}_S \hat{I}(\mathcal{L})$, into (11.32).

Without any loss of generality, we will place the reference conductor at the origin of a rectangular coordinate system, $x = 0$ and $y = 0$, and place the other conductor on the x axis at $x = d$ as shown in Figure 11.5. Hence, the two conductors are separated by a distance d . The chain parameters for a two-conductor line become, for the most general case of a lossy line,

$$\hat{\phi}_{22}(\mathcal{L}) = \cosh(\hat{\gamma} \mathcal{L})
 \tag{11.49a}$$

$$\hat{\phi}_{12}(\mathcal{L}) = -\sinh(\hat{\gamma} \mathcal{L}) \hat{Z}_C
 \tag{11.49b}$$

$$\hat{\phi}_{21}(\mathcal{L}) = -\sinh(\hat{\gamma} \mathcal{L}) \hat{Z}_C^{-1}
 \tag{11.49c}$$

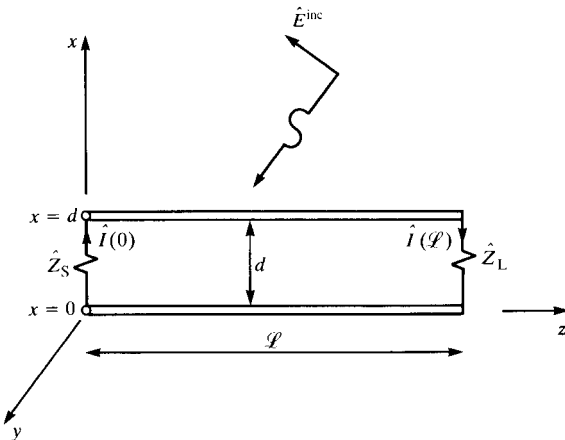


FIGURE 11.5 Orientation of the two-conductor line in the x - z plane for $y = 0$.

$$\hat{\phi}_{22}(\mathcal{L}) = \cosh(\hat{\gamma}\mathcal{L}) \quad (11.49d)$$

where the characteristic impedance is

$$\hat{Z}_C = \sqrt{\frac{r + j\omega l}{g + j\omega c}} \quad (11.50)$$

and the propagation constant is

$$\hat{\gamma} = \sqrt{(r + j\omega l)(g + j\omega c)} \quad (11.51)$$

Since the terminations are implicitly assumed to be *linear*, we will omit any lumped sources in them, that is, $\hat{V}_S = \hat{V}_L = 0$. The contributions to the terminal currents due to these lumped sources in the termination networks can be obtained with the results of Chapter 6 by superposition.

The total forcing functions due to the incident field given in (11.44) reduce to ($y = 0$)

$$\begin{aligned} \hat{V}_{\text{FT}}(\mathcal{L}) = & \int_0^{\mathcal{L}} \cosh(\hat{\gamma}(\mathcal{L} - \tau)) \left[\hat{E}_z^{\text{inc}}(x = d, z = \tau) - \hat{E}_z^{\text{inc}}(x = 0, z = \tau) \right] d\tau \\ & - \left[\int_0^d \hat{E}_x^{\text{inc}}(x, z = \mathcal{L}) dx \right] + \cosh(\hat{\gamma}\mathcal{L}) \left[\int_0^d \hat{E}_x^{\text{inc}}(x, z = 0) dx \right] \end{aligned} \quad (11.52a)$$

and

$$\begin{aligned} \hat{I}_{\text{FT}}(\mathcal{L}) = & - \int_0^{\mathcal{L}} \sinh(\hat{\gamma}(\mathcal{L} - \tau)) \hat{Z}_C^{-1} \left[\hat{E}_z^{\text{inc}}(x = d, z = \tau) - \hat{E}_z^{\text{inc}}(x = 0, z = \tau) \right] d\tau \\ & - \sinh(\hat{\gamma}\mathcal{L}) \hat{Z}_C^{-1} \left[\int_0^d \hat{E}_x^i(x, z = 0) dx \right] \end{aligned} \quad (11.52b)$$

The solution for the terminal current at the source end, $z = 0$, for the Thevenin equivalent representation of the terminations given in (11.48a) reduces to (for $\hat{V}_S = \hat{V}_L = 0$)

$$\begin{aligned} \hat{I}(0) = & \frac{\hat{V}_{\text{FT}}(\mathcal{L}) - \hat{Z}_L \hat{I}_{\text{FT}}(\mathcal{L})}{\hat{D}} \\ = & \frac{1}{\hat{D}} \int_0^{\mathcal{L}} \left[\cosh(\hat{\gamma}(\mathcal{L} - \tau)) + \sinh(\hat{\gamma}(\mathcal{L} - \tau)) \frac{\hat{Z}_L}{\hat{Z}_C} \right] \\ & \times \left[\hat{E}_z^{\text{inc}}(x = d, z = \tau) - \hat{E}_z^{\text{inc}}(x = 0, z = \tau) \right] d\tau \end{aligned}$$

$$\begin{aligned}
 & -\frac{1}{\hat{D}} \left[\int_0^d \hat{E}_x^{\text{inc}}(x, z = \mathcal{L}) dx \right] \\
 & + \frac{1}{\hat{D}} \left[\cosh(\hat{\gamma} \mathcal{L}) + \sinh(\hat{\gamma} \mathcal{L}) \frac{\hat{Z}_L}{\hat{Z}_C} \right] \left[\int_0^d \hat{E}_x^{\text{inc}}(x, z = 0) dx \right]
 \end{aligned} \tag{11.53a}$$

The corresponding expression for the current at $z = \mathcal{L}$ can be obtained by substituting the terminal constraints, $\hat{V}(0) = \hat{V}_S - \hat{Z}_S \hat{I}(0)$ and $\hat{V}(\mathcal{L}) = \hat{V}_L + \hat{Z}_S \hat{I}(\mathcal{L})$, into (11.34). This gives, in terms of the simplified sources $\hat{V}'_{\text{FT}}(\mathcal{L})$ and $\hat{I}'_{\text{FT}}(\mathcal{L})$ in (11.45) and for $\hat{V}_S = \hat{V}_L = 0$,

$$\begin{aligned}
 \hat{I}(\mathcal{L}) &= \frac{\hat{V}'_{\text{FT}}(\mathcal{L}) + \hat{Z}_S \hat{I}'_{\text{FT}}(\mathcal{L})}{\hat{D}} \\
 &= \frac{1}{\hat{D}} \int_0^{\mathcal{L}} \left[\cosh(\hat{\gamma} \tau) + \sinh(\hat{\gamma} \tau) \frac{\hat{Z}_S}{\hat{Z}_C} \right] \\
 &\quad \times \left[\hat{E}_z^{\text{inc}}(x = d, z = \tau) - \hat{E}_z^i(x = 0, z = \tau) \right] d\tau \\
 &\quad - \frac{1}{\hat{D}} \left[\cosh(\hat{\gamma} \mathcal{L}) + \sinh(\hat{\gamma} \mathcal{L}) \frac{\hat{Z}_S}{\hat{Z}_C} \right] \left[\int_0^d \hat{E}_x^i(x, z = \mathcal{L}) dx \right] \\
 &\quad + \frac{1}{\hat{D}} \left[\int_0^d \hat{E}_x^i(x, z = 0) dx \right]
 \end{aligned} \tag{11.53b}$$

The denominator in both expressions, \hat{D} , is

$$\hat{D} = \cosh(\hat{\gamma} \mathcal{L}) (\hat{Z}_S + \hat{Z}_L) + \sinh(\hat{\gamma} \mathcal{L}) \left(\hat{Z}_C + \frac{\hat{Z}_S \hat{Z}_L}{\hat{Z}_C} \right) \tag{11.53c}$$

These results agree with those obtained by Smith [2,5]. Once the terminal currents are obtained from (11.53), the terminal voltages can be obtained from $\hat{V}(0) = -\hat{Z}_S \hat{I}(0)$ and $\hat{V}(\mathcal{L}) = \hat{Z}_L \hat{I}(\mathcal{L})$. These results can be specialized to lossless lines by replacing $\cosh(\hat{\gamma} \mathcal{L}) \Rightarrow \cos(\beta \mathcal{L})$, $\sinh(\hat{\gamma} \mathcal{L}) \Rightarrow j \sin(\beta \mathcal{L})$, $\hat{Z}_C \Rightarrow Z_C = \sqrt{l/c}$, and $\beta = \omega \sqrt{lc}$.

11.2.4 Uniform Plane-Wave Excitation of the Line

A significant set of problems to which these results apply is the case of illumination of the line by a *uniform plane wave* from some distant source [A.1]. The radiated fields in the far field of a radiating structure are spherical waves that resemble, locally, uniform plane waves. This assumption also simplifies the evaluation of the sources in the above results.

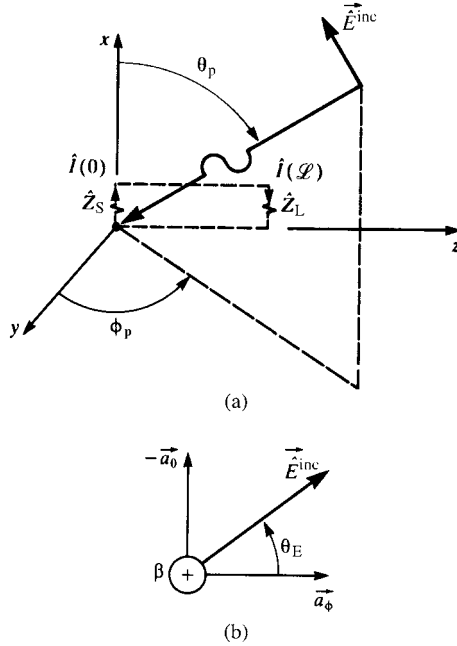


FIGURE 11.6 Definitions of the parameters characterizing the incident field as a uniform plane wave.

In order to characterize the frequency-domain response of the line, let us describe the incident uniform plane-wave angle of incidence and polarization with respect to a spherical coordinate system as illustrated in Figure 11.6. The propagation vector of the wave is incident on the origin of the coordinate system (the phase reference for the wave) at angles θ_p from the x axis and ϕ_p from the projection onto the y - z plane from the y axis as shown in Figure 11.6(a). The polarization of the electric field vector is described in terms of the relation to the unit vectors in the spherical coordinate system, \vec{a}_θ and \vec{a}_ϕ , as illustrated in Figure 11.6(b). In terms of these, the general expression for the phasor electric field vector can be written as [A.1]

$$\vec{E}^{\text{inc}} = \hat{E}_0 [e_x \vec{a}_x + e_y \vec{a}_y + e_z \vec{a}_z] e^{-j\beta_x x} e^{-j\beta_y y} e^{-j\beta_z z} \quad (11.54)$$

where the components of the incident electric field vector along the x , y , and z axes of the rectangular coordinate system describing the transmission line are [A.1]

$$\begin{aligned} e_x &= \sin \theta_E \sin \theta_p \\ e_y &= -\sin \theta_E \cos \theta_p \cos \phi_p - \cos \theta_E \sin \phi_p \\ e_z &= -\sin \theta_E \cos \theta_p \sin \phi_p + \cos \theta_E \cos \phi_p \end{aligned} \quad (11.55a)$$

and

$$e_x^2 + e_y^2 + e_z^2 = 1 \quad (11.55b)$$

The components of the phase constant along those coordinate axes are

$$\begin{aligned} \beta_x &= -\beta \cos \theta_p \\ \beta_y &= -\beta \sin \theta_p \cos \phi_p \\ \beta_z &= -\beta \sin \theta_p \sin \phi_p \end{aligned} \quad (11.56)$$

The phase constant is related to the frequency and properties of the medium as

$$\begin{aligned} \beta &= \omega \sqrt{\mu \varepsilon} \\ &= \frac{\omega}{v_0} \sqrt{\mu_r \varepsilon_r} \end{aligned} \quad (11.57)$$

where $v_0 = 1/\sqrt{\mu_0 \varepsilon_0}$ is the phase velocity in free space and the medium is characterized by $\varepsilon = \varepsilon_r \varepsilon_0$ and $\mu = \mu_r \mu_0$. Ordinarily, the medium in which the incident wave is propagating is free space with $\varepsilon_r = 1$ and $\mu_r = 1$. \hat{E}_0 is the complex amplitude of the sinusoidal wave. Although not needed, the magnetic field intensity vector of the incident wave is related to the electric field intensity vector by

$$\vec{H}^{\text{inc}} = \frac{1}{\eta} \vec{a}_\beta \times \vec{E}^{\text{inc}} \quad (11.58)$$

where \vec{a}_β is a unit vector in the direction of propagation. This gives

$$\vec{H}^{\text{inc}} = \frac{1}{\eta} \hat{E}_0 [h_x \vec{a}_x + h_y \vec{a}_y + h_z \vec{a}_z] e^{-j\beta_x x} e^{-j\beta_y y} e^{-j\beta_z z} \quad (11.59)$$

where the components of the incident magnetic field vector along the x , y , and z axes of the rectangular coordinate system describing the line are [A.1]

$$\begin{aligned} h_x &= -\cos \theta_E \sin \theta_p \\ h_y &= \cos \theta_E \cos \theta_p \cos \phi_p - \sin \theta_E \sin \phi_p \\ h_z &= \cos \theta_E \cos \theta_p \sin \phi_p + \sin \theta_E \cos \phi_p \end{aligned} \quad (11.60a)$$

and again

$$h_x^2 + h_y^2 + h_z^2 = 1 \quad (11.60b)$$

The intrinsic impedance is

$$\eta = \sqrt{\frac{\mu}{\varepsilon}} = 120\pi \sqrt{\frac{\mu_r}{\varepsilon_r}} \quad (11.61)$$

and $\eta_0 = \sqrt{\mu_0/\varepsilon_0} = 120\pi \cong 377 \Omega$ is the intrinsic impedance of free space.

The phasor sources due to the incident uniform plane wave in (11.53) can be easily evaluated in terms of the above results. The transverse or x electric field components in the plane of the conductors become, from (11.54) ($y = 0$),

$$\vec{\hat{E}}_T^{\text{inc}} = \hat{E}_0 e_x e^{-j\beta_x x} e^{-j\beta_z z} \vec{a}_x \quad (11.62)$$

Hence, the contribution from this component becomes

$$\begin{aligned} \int_a^{a'} \vec{\hat{E}}_T^{\text{inc}} \cdot d\vec{l} &= \int_{x=0}^d \hat{E}_0 e_x e^{-j\beta_x x} e^{-j\beta_z z} dx \\ &= \hat{E}_0 e_x e^{-j\beta_z z} \frac{(e^{-j\beta_x d} - 1)}{-j\beta_x} \\ &= j\hat{E}_0 \frac{d}{2} e_x e^{-j\beta_z z} e^{-j\beta_x \frac{d}{2}} \frac{\left(e^{-j\beta_x \frac{d}{2}} - e^{j\beta_x \frac{d}{2}} \right)}{\beta_x \frac{d}{2}} \\ &= \hat{E}_0 d e_x e^{-j\beta_z z} e^{-j\beta_x \frac{d}{2}} \left[\frac{\sin\left(\beta_x \frac{d}{2}\right)}{\beta_x \frac{d}{2}} \right] \end{aligned} \quad (11.63)$$

Similarly, the contributions from the longitudinal electric field components become

$$\begin{aligned} \hat{E}_z^{\text{inc}}(x = d, z) - \hat{E}_z^{\text{inc}}(x = 0, z) &= \hat{E}_0 e_z e^{-j\beta_z z} (e^{-j\beta_x d} - 1) \\ &= \hat{E}_0 e_z \beta_x \frac{d}{2} e^{-j\beta_z z} e^{-j\beta_x \frac{d}{2}} \frac{\left(e^{-j\beta_x \frac{d}{2}} - e^{j\beta_x \frac{d}{2}} \right)}{\beta_x \frac{d}{2}} \\ &= -j\beta_x \hat{E}_0 d e_z e^{-j\beta_z z} e^{-j\beta_x \frac{d}{2}} \left[\frac{\sin\left(\beta_x \frac{d}{2}\right)}{\beta_x \frac{d}{2}} \right] \end{aligned} \quad (11.64)$$

Therefore, the solutions for the terminal currents given in (11.53) become, for uniform plane-wave excitation,

$$\begin{aligned} \hat{I}(0) = & \frac{d\hat{E}_o}{\hat{D}} e^{-j\beta_x d/2} \left[\frac{\sin\left(\frac{\beta_x d}{2}\right)}{\frac{\beta_x d}{2}} \right] \left\{ -j\beta_x e_z \int_0^{\mathcal{L}} \right. \\ & \times \left[\cosh(\hat{\gamma}(\mathcal{L} - \tau)) + \sinh(\hat{\gamma}(\mathcal{L} - \tau)) \frac{\hat{Z}_L}{\hat{Z}_C} \right] e^{-j\beta_z \tau} d\tau \\ & \left. + e_x \left[\cosh(\hat{\gamma} \mathcal{L}) + \sinh(\hat{\gamma} \mathcal{L}) \frac{\hat{Z}_L}{\hat{Z}_C} - e^{-j\beta_z \mathcal{L}} \right] \right\} \end{aligned} \quad (11.65a)$$

and

$$\begin{aligned} \hat{I}(\mathcal{L}) = & \frac{d\hat{E}_o}{\hat{D}} e^{-j\beta_x d/2} \left[\frac{\sin\left(\frac{\beta_x d}{2}\right)}{\frac{\beta_x d}{2}} \right] \left\{ -j\beta_x e_z \int_0^{\mathcal{L}} \right. \\ & \times \left[\cosh(\hat{\gamma}\tau) + \sinh(\hat{\gamma}\tau) \frac{\hat{Z}_S}{\hat{Z}_C} \right] e^{-j\beta_z \tau} d\tau \\ & \left. + e_x \left[1 - \left(\cosh(\hat{\gamma} \mathcal{L}) + \sinh(\hat{\gamma} \mathcal{L}) \frac{\hat{Z}_S}{\hat{Z}_C} \right) e^{-j\beta_z \mathcal{L}} \right] \right\} \end{aligned} \quad (11.65b)$$

where, again,

$$\hat{D} = \cosh(\hat{\gamma} \mathcal{L}) (\hat{Z}_S + \hat{Z}_L) + \sinh(\hat{\gamma} \mathcal{L}) \left(\hat{Z}_C + \frac{\hat{Z}_S \hat{Z}_L}{\hat{Z}_C} \right) \quad (11.65c)$$

11.2.4.1 Special Cases The above results, although exact and general for uniform plane-wave excitation of two-conductor lines, are somewhat complicated. In this section, we will specialize those results to three special cases. These are illustrated in Figure 11.7.

The first case, illustrated in Figure 11.7(a), is referred to as *Endfire* excitation and has $\theta_p = 90^\circ$, $\phi_p = -90^\circ$, and $\theta_E = 90^\circ$. Thus, the wave is propagating in the $+z$ direction with the electric field polarized in the $+x$ direction. For this incidence and polarization,

$$\begin{aligned} e_x &= 1 \\ e_y &= 0 \\ e_z &= 0 \end{aligned} \quad (11.66a)$$

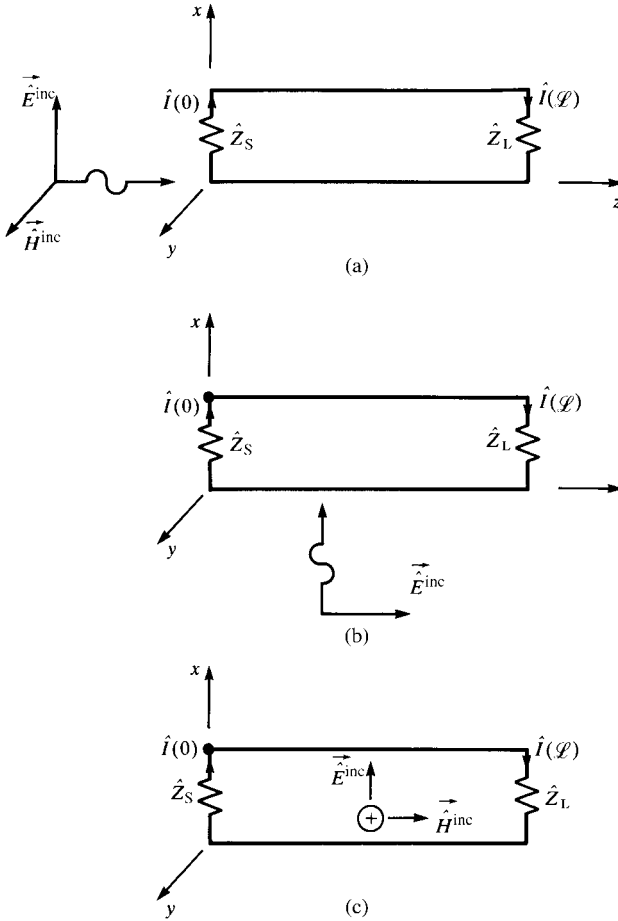


FIGURE 11.7 Three important cases of wave incidence: (a) *Endfire*, (b) *Sidefire*, and (c) *Broadside*.

and the components of the phase constant along those coordinate axes are

$$\begin{aligned} \beta_x &= 0 \\ \beta_y &= 0 \\ \beta_z &= \beta \end{aligned} \tag{11.66b}$$

as expected. The complete expression for the electric field vector is, from (11.54),

$$\vec{E}^{\text{inc}} = \hat{E}_0 e^{-j\beta z} \vec{a}_x \tag{11.67}$$

Substituting these into (11.65) and evaluating gives

$$\hat{I}(0) = \frac{d\hat{E}_0}{\hat{D}} \left[\cosh(\hat{\gamma} \mathcal{L}) + \sinh(\hat{\gamma} \mathcal{L}) \frac{\hat{Z}_L}{\hat{Z}_C} - \cos(\beta \mathcal{L}) + j \sin(\beta \mathcal{L}) \right] \tag{11.68a}$$

$$\hat{I}(\mathcal{L}) = \frac{d\hat{E}_o}{\hat{D}} \left[1 - \left(\cosh(\hat{\gamma} \mathcal{L}) + \sinh(\hat{\gamma} \mathcal{L}) \frac{\hat{Z}_S}{\hat{Z}_C} \right) (\cos(\beta \mathcal{L}) - j \sin(\beta \mathcal{L})) \right] \quad (11.68b)$$

and \hat{D} is given for this lossy case in (11.65c). For the case of a lossless line,

$$\hat{\gamma} = j\beta \quad (11.69a)$$

$$Z_C = \sqrt{\frac{l}{c}} \quad (11.69b)$$

and the results in (11.68) simplify to

$$\hat{I}(0) = j \frac{d\hat{E}_o}{\hat{D}} \sin(\beta \mathcal{L}) \left(1 + \frac{\hat{Z}_L}{Z_C} \right) \quad (11.70a)$$

$$\hat{I}(\mathcal{L}) = \frac{d\hat{E}_o}{2\hat{D}} \left(1 - \frac{\hat{Z}_S}{Z_C} \right) [1 - \cos(2\beta \mathcal{L}) + j \sin(2\beta \mathcal{L})] \quad (11.70b)$$

and \hat{D} becomes, from (11.65c), for a lossless line

$$\hat{D} = \cos(\beta \mathcal{L}) (\hat{Z}_S + \hat{Z}_L) + j \sin(\beta \mathcal{L}) \left(Z_C + \frac{\hat{Z}_S \hat{Z}_L}{Z_C} \right) \quad (11.70c)$$

The next case, illustrated in Figure 11.7(b), is referred to as *Sidefire* excitation and has $\theta_p = 180^\circ$, $\phi_p = 0^\circ$, and $\theta_E = 0^\circ$. Thus, the wave is propagating in the $+x$ direction with the electric field polarized in the $+z$ direction. For this incidence and polarization,

$$\begin{aligned} e_x &= 0 \\ e_y &= 0 \\ e_z &= 1 \end{aligned} \quad (11.71a)$$

and the components of the phase constant along those coordinate axes are

$$\begin{aligned} \beta_x &= \beta \\ \beta_y &= 0 \\ \beta_z &= 0 \end{aligned} \quad (11.71b)$$

as expected. The complete expression for the electric field vector is, from (11.54),

$$\vec{E}^{\text{inc}} = \hat{E}_o e^{-j\beta x} \vec{a}_z \quad (11.72)$$

Substituting these into (11.65) and evaluating gives

$$\hat{I}(0) = -j2 \frac{\hat{E}_o}{\hat{\gamma}\hat{D}} e^{-j\beta d/2} \sin\left(\frac{\beta d}{2}\right) \left(\frac{\hat{Z}_L}{\hat{Z}_C} (\cosh(\hat{\gamma}\mathcal{L}) - 1) + \sinh(\hat{\gamma}\mathcal{L}) \right) \quad (11.73a)$$

$$\hat{I}(\mathcal{L}) = -j2 \frac{\hat{E}_o}{\hat{\gamma}\hat{D}} e^{-j\beta d/2} \sin\left(\frac{\beta d}{2}\right) \left[\sinh(\hat{\gamma}\mathcal{L}) + (\cosh(\hat{\gamma}\mathcal{L}) - 1) \frac{\hat{Z}_S}{\hat{Z}_C} \right] \quad (11.73b)$$

and \hat{D} is given for this lossy case in (11.65c). For the case of a lossless line, these simplify to

$$\hat{I}(0) = -\frac{\hat{E}_o}{\hat{D}} d e^{-j\beta d/2} \left[\frac{\sin\left(\frac{\beta d}{2}\right)}{\frac{\beta d}{2}} \right] \left(\frac{\hat{Z}_L}{\hat{Z}_C} (\cos(\beta\mathcal{L}) - 1) + j \sin(\beta\mathcal{L}) \right) \quad (11.74a)$$

$$\hat{I}(\mathcal{L}) = -\frac{\hat{E}_o}{\hat{D}} d e^{-j\beta d/2} \left[\frac{\sin\left(\frac{\beta d}{2}\right)}{\frac{\beta d}{2}} \right] \left[j \sin(\beta\mathcal{L}) + (\cos(\beta\mathcal{L}) - 1) \frac{\hat{Z}_S}{\hat{Z}_C} \right] \quad (11.74b)$$

where \hat{D} for the lossless case is given by (11.70c).

The final case, illustrated in Figure 11.7(c), is referred to as *Broadside* excitation and has $\theta_p = 90^\circ$, $\phi_p = 0^\circ$, and $\theta_E = 90^\circ$. Thus, the wave is propagating in the $-y$ direction with the electric field polarized in the $+x$ direction. For this incidence and polarization,

$$\begin{aligned} e_x &= 1 \\ e_y &= 0 \\ e_z &= 0 \end{aligned} \quad (11.75a)$$

and the components of the phase constant along those coordinate axes are

$$\begin{aligned} \beta_x &= 0 \\ \beta_y &= -\beta \\ \beta_z &= 0 \end{aligned} \quad (11.75b)$$

as expected. The complete expression for the electric field vector is, from (11.54) ($y = 0$),

$$\vec{E}^{\text{inc}} = \hat{E}_o e^{j\beta y} \vec{a}_x = \hat{E}_o \vec{a}_x \quad (11.76)$$

Substituting these into (11.65) along with $y = 0$ and evaluating gives

$$\hat{I}(0) = \frac{d\hat{E}_o}{\hat{D}} \left(\cosh(\hat{\gamma}\mathcal{L}) - 1 + \sinh(\hat{\gamma}\mathcal{L}) \frac{\hat{Z}_L}{\hat{Z}_C} \right) \quad (11.77a)$$

$$\hat{\Gamma}(\mathcal{L}) = \frac{d\hat{E}_o}{\hat{D}} \left[1 - \cosh(\hat{\gamma}\mathcal{L}) - \sinh(\hat{\gamma}\mathcal{L}) \frac{\hat{Z}_S}{\hat{Z}_C} \right] \quad (11.77b)$$

and \hat{D} is given for this lossy case in (11.65c). For the case of a lossless line, these simplify to

$$\hat{\Gamma}(0) = \frac{d\hat{E}_o}{\hat{D}} \left(\cos(\beta\mathcal{L}) - 1 + j \sin(\beta\mathcal{L}) \frac{\hat{Z}_L}{\hat{Z}_C} \right) \quad (11.78a)$$

$$\hat{\Gamma}(\mathcal{L}) = \frac{d\hat{E}_o}{\hat{D}} \left[1 - \cos(\beta\mathcal{L}) - j \sin(\beta\mathcal{L}) \frac{\hat{Z}_S}{\hat{Z}_C} \right] \quad (11.78b)$$

where \hat{D} for the lossless case is given by (11.70c).

11.2.4.2 One Conductor Above a Ground Plane As a final application of the results for uniform plane-wave illumination of a two-conductor line, we consider the case of one conductor at a height h above an infinite, perfectly conducting ground plane as illustrated in Figure 11.8(a). This problem can be replaced with an equivalent problem by replacing the ground plane with images as illustrated in Figure 11.8(b). The image field can be viewed as the wave reflected by the ground plane, and the total incident field is the sum of the original field and the image or reflected field. Snell’s law provides that the angle of incidence and the angle of reflection are equal [A.1,H.4]. Thus, the fields can be written as

$$\vec{\hat{E}}^{\text{inc}} = \hat{E}_o \left[e_x^{\text{inc}} \vec{a}_x + e_y^{\text{inc}} \vec{a}_y + e_z^{\text{inc}} \vec{a}_z \right] e^{-j\beta_x x} e^{-j\beta_y y} e^{-j\beta_z z} \quad (11.79a)$$

$$\vec{\hat{E}}^{\text{ref}} = \hat{E}_o \left[e_x^{\text{ref}} \vec{a}_x + e_y^{\text{ref}} \vec{a}_y + e_z^{\text{ref}} \vec{a}_z \right] e^{j\beta_x x} e^{-j\beta_y y} e^{-j\beta_z z} \quad (11.79b)$$

At the position of the ground plane, $x = 0$, the boundary conditions on the electric field require that

$$e_z^{\text{ref}} = -e_z^{\text{inc}} \equiv -e_z \quad (11.80a)$$

$$e_y^{\text{ref}} = -e_y^{\text{inc}} \equiv -e_y \quad (11.80b)$$

$$e_x^{\text{ref}} = e_x^{\text{inc}} \equiv e_x \quad (11.80c)$$

Thus, the components of total field (incident plus reflected) can be written as (the y component is not needed)

$$\hat{E}_z^{\text{total}} = \hat{E}_z^{\text{inc}} + \hat{E}_z^{\text{ref}} = -j2\hat{E}_o e_z \sin(\beta_x x) e^{-j\beta_y y} e^{-j\beta_z z} \quad (11.81a)$$

$$\hat{E}_x^{\text{total}} = \hat{E}_x^{\text{inc}} + \hat{E}_x^{\text{ref}} = 2\hat{E}_o e_x \cos(\beta_x x) e^{-j\beta_y y} e^{-j\beta_z z} \quad (11.81b)$$

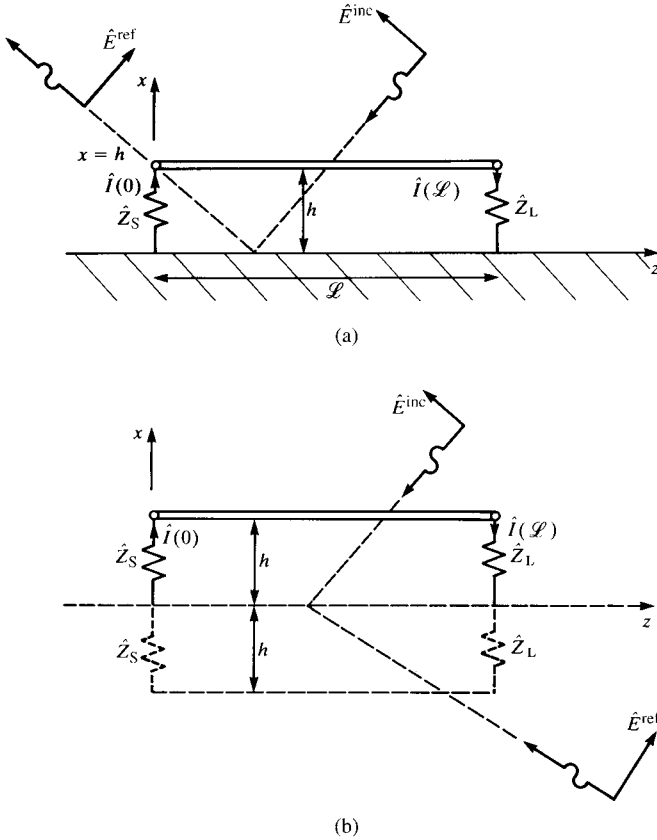


FIGURE 11.8 Replacement of a ground plane with images for incident field illumination. Equations (11.53) become ($y = 0$)

$$\hat{I}(0) = 2h \frac{\hat{E}_o}{\hat{D}} \frac{\sin(\beta_x h)}{\beta_x h} \left\{ -j\beta_x e_z \int_0^{\mathcal{L}} \left[\cosh(\hat{\gamma}(\mathcal{L} - \tau)) + \sinh(\hat{\gamma}(\mathcal{L} - \tau)) \frac{\hat{Z}_L}{\hat{Z}_C} \right] \times e^{-j\beta_z \tau} d\tau + e_x \left[\cosh(\hat{\gamma} \mathcal{L}) + \sinh(\hat{\gamma} \mathcal{L}) \frac{\hat{Z}_L}{\hat{Z}_C} - e^{-j\beta_z \mathcal{L}} \right] \right\} \quad (11.82a)$$

$$\hat{I}(\mathcal{L}) = 2h \frac{\hat{E}_o}{\hat{D}} \frac{\sin(\beta_x h)}{\beta_x h} \left\{ -j\beta_x e_z \int_0^{\mathcal{L}} \left[\cosh(\hat{\gamma} \tau) + \sinh(\hat{\gamma} \tau) \frac{\hat{Z}_S}{\hat{Z}_C} \right] \times e^{-j\beta_z \tau} d\tau + e_x \left[1 - \left(\cosh(\hat{\gamma} \mathcal{L}) + \sinh(\hat{\gamma} \mathcal{L}) \frac{\hat{Z}_S}{\hat{Z}_C} \right) e^{-j\beta_z \mathcal{L}} \right] \right\} \quad (11.82b)$$

Comparing (11.82) to (11.65), we see that the results for the case of a ground plane can be obtained from the case without a ground plane by (1) removing the factor $e^{-j\beta_x d/2}$ and (2) replacing d with $2h$: $d \Leftrightarrow 2h$. Of course, the characteristic impedance \hat{Z}_C in these expressions must be that of one conductor above a ground plane. In the case of a lossless line, the characteristic impedance is real and is one half the Z_C of two conductors that are separated by twice the height above ground (the image problem).

Again, if we restrict our consideration to the special cases shown in Figure 11.7, the results simplify. For the *Endfire* excitation, $\theta_p = 90^\circ$, $\phi_p = -90^\circ$, and $\theta_E = 90^\circ$. For this case, we obtain $e_x = 1$, $\beta_z = \beta$, and all others zero. The total field vector components become

$$\hat{E}_z^{\text{total}} = 0 \tag{11.83a}$$

$$\hat{E}_x^{\text{total}} = 2 \hat{E}_o e^{-j\beta z} \tag{11.83b}$$

This compares to the results without the ground plane given in (11.67):

$$\hat{E}_z = 0 \tag{11.84a}$$

$$\hat{E}_x = \hat{E}_o e^{-j\beta z} \tag{11.84b}$$

Therefore, we double (11.68) (replacing $d = 2h$), which gives

$$\hat{I}(0) = \frac{2h\hat{E}_o}{\hat{D}} \left[\cosh(\hat{\gamma} \mathcal{L}) + \sinh(\hat{\gamma} \mathcal{L}) \frac{\hat{Z}_L}{\hat{Z}_C} - \cos(\beta \mathcal{L}) + j \sin(\beta \mathcal{L}) \right] \tag{11.85a}$$

$$\hat{I}(\mathcal{L}) = \frac{2h\hat{E}_o}{\hat{D}} \left[1 - \left(\cosh(\hat{\gamma} \mathcal{L}) + \sinh(\hat{\gamma} \mathcal{L}) \frac{\hat{Z}_S}{\hat{Z}_C} \right) \left(\cos(\beta \mathcal{L}) - j \sin(\beta \mathcal{L}) \right) \right] \tag{11.85b}$$

and \hat{D} is given for this lossy case in (11.65c). For a lossless line, these simplify to

$$\hat{I}(0) = j \frac{2h\hat{E}_o}{\hat{D}} \sin(\beta \mathcal{L}) \left(1 + \frac{\hat{Z}_L}{\hat{Z}_C} \right) \tag{11.86a}$$

$$\hat{I}(\mathcal{L}) = \frac{h\hat{E}_o}{\hat{D}} \left(1 - \frac{\hat{Z}_S}{\hat{Z}_C} \right) [1 - \cos(2\beta \mathcal{L}) + j \sin(2\beta \mathcal{L})] \tag{11.86b}$$

where \hat{D} for the lossless case is given in (11.70c).

For the *Sidefire* excitation (propagating from above the ground plane in the $-x$ direction), $\theta_p = 0^\circ$, $\phi_p = 0^\circ$ and $\theta_E = 0^\circ$. For this case, we obtain $e_z = 1$, $\beta_x = -\beta$,

and all others zero. The total field vector components become

$$\hat{E}_z^{\text{total}} = j2\hat{E}_0 \sin(\beta x) \quad (11.87a)$$

$$\hat{E}_x^{\text{total}} = 0 \quad (11.87b)$$

This compares to the results without the ground plane given in (11.72):

$$\hat{E}_z = \hat{E}_0 e^{-j\beta x} \quad (11.88a)$$

$$\hat{E}_x = 0 \quad (11.88b)$$

Substituting (11.88) into (11.82) gives

$$\hat{I}(0) = j2h\beta \frac{\hat{E}_0}{\hat{\gamma}\hat{D}} \frac{\sin(\beta h)}{\beta h} \left(\frac{\hat{Z}_L}{\hat{Z}_C} (\cosh(\hat{\gamma}\mathcal{L}) - 1) + \sinh(\hat{\gamma}\mathcal{L}) \right) \quad (11.89a)$$

$$\hat{I}(\mathcal{L}) = j2h\beta \frac{\hat{E}_0}{\hat{\gamma}\hat{D}} \frac{\sin(\beta h)}{\beta h} \left[\sinh(\hat{\gamma}\mathcal{L}) + (\cosh(\hat{\gamma}\mathcal{L}) - 1) \frac{\hat{Z}_S}{\hat{Z}_C} \right] \quad (11.89b)$$

and \hat{D} is given for this lossy case in (11.65c). For a lossless line, these simplify to

$$\hat{I}(0) = 2h \frac{\hat{E}_0}{\hat{D}} \frac{\sin(\beta h)}{\beta h} \left(\frac{\hat{Z}_L}{Z_C} (\cos(\beta\mathcal{L}) - 1) + j \sin(\beta\mathcal{L}) \right) \quad (11.90a)$$

$$\hat{I}(\mathcal{L}) = 2h \frac{\hat{E}_0}{\hat{D}} \frac{\sin(\beta h)}{\beta h} \left[j \sin(\beta\mathcal{L}) + (\cos(\beta\mathcal{L}) - 1) \frac{\hat{Z}_S}{Z_C} \right] \quad (11.90b)$$

where \hat{D} for the lossless case is given in (11.70c).

For the *Broadside* excitation, $\theta_p = 90^\circ$, $\phi_p = 0^\circ$, and $\theta_E = 90^\circ$. For this case, we obtain $e_x = 1$, $\beta_y = -\beta$, and all others zero. The total field vector components become

$$\hat{E}_z^{\text{total}} = 0 \quad (11.91a)$$

$$\hat{E}_x^{\text{total}} = 2\hat{E}_0 \quad (11.91b)$$

This compares to the results without the ground plane given in (11.76):

$$\hat{E}_z = 0 \quad (11.92a)$$

$$\hat{E}_x = \hat{E}_o \quad (11.92b)$$

Therefore, we simply double the results in (11.77) and (11.78) and replace $d = 2h$ to give

$$\hat{I}(0) = \frac{2h \hat{E}_o}{\hat{D}} \left(\cosh(\hat{\gamma} \mathcal{L}) - 1 + \sinh(\hat{\gamma} \mathcal{L}) \frac{\hat{Z}_L}{\hat{Z}_C} \right) \quad (11.93a)$$

$$\hat{I}(\mathcal{L}) = \frac{2h \hat{E}_o}{\hat{D}} \left[1 - \cosh(\hat{\gamma} \mathcal{L}) - \sinh(\hat{\gamma} \mathcal{L}) \frac{\hat{Z}_S}{\hat{Z}_C} \right] \quad (11.93b)$$

and \hat{D} is given for this lossy case in (11.65c). For a lossless line,

$$\hat{I}(0) = \frac{2h \hat{E}_o}{\hat{D}} \left(\cos(\beta \mathcal{L}) - 1 + j \sin(\beta \mathcal{L}) \frac{\hat{Z}_L}{\hat{Z}_C} \right) \quad (11.94a)$$

$$\hat{I}(\mathcal{L}) = \frac{2h \hat{E}_o}{\hat{D}} \left[1 - \cos(\beta \mathcal{L}) - j \sin(\beta \mathcal{L}) \frac{\hat{Z}_S}{\hat{Z}_C} \right] \quad (11.94b)$$

where \hat{D} for the lossless case is given in (11.70c).

11.2.5 Comparison with Predictions of Method of Moments Codes

First we consider a lossless two-wire transmission line with uniform plane-wave excitation [H.7]. The wires have radii of 0.1 mm (0.0001 m), separations of 1 cm, and total length of 1 m. The terminations at each end are identical resistors, $\hat{Z}_S = \hat{Z}_L = R$, with three sets of values: $R = 552 \Omega$ (matched loads), $R = 50 \Omega$ (low-impedance loads), and $R = 10 \text{ k}\Omega$ (high-impedance loads). Three polarizations of the incident uniform plane wave are illustrated in Figure 11.7. The *Endfire* case has the wave propagating along the line (z) axis with the electric field vector lying in the plane of the line and polarized in the x directions: $\vec{E}^{\text{inc}} = 1e^{-j\beta z} \vec{a}_x$. The *Sidefire* case has the uniform plane wave propagating in the plane of the wires in the x direction perpendicular to them with the electric field vector polarized parallel to the wires in the z direction, $\vec{E}^{\text{inc}} = 1e^{-j\beta x} \vec{a}_z$. The *Broadside* case has the uniform plane wave propagating perpendicular to the plane of the line in the $-y$ direction with the electric field vector polarized in the plane of the wires in the x direction, $\vec{E}^{\text{inc}} = 1e^{j\beta y} \vec{a}_x$. Results for only certain polarizations, angles of incidence, and termination impedance values will be shown here. The reader is referred to [H.7] for more extensive numerical comparisons.

The numerical code used to give the baseline results is a method of moments (MoM) code developed at Ohio State University by J.H. Richmond [11,12]. It will

be referred to as OSMOM and uses piecewise sinusoidal expansion functions and a Galerkin technique. These features give this code exceptional accuracy. It is important to point out that the MoM method is a direct implementation of Maxwell's equations and, within numerical error, should provide "exact" solutions to compare with the transmission-line model predictions. Figure 11.9 shows the results for the *Endfire* case and low-impedance loads ($R = 50 \Omega$). Observe that the line is one wavelength long at 300 MHz, so we should expect to see nulls in the frequency response at multiples of 150 MHz. Figure 11.9(a) shows the magnitude of the frequency response, whereas Figure 11.9(b) shows the phase. Excellent correlation with the MoM results (OSMOM) is observed. Figure 11.10 shows the results for the *Sidefire* excitation and matched loads ($R = 552 \Omega$), whereas Figure 11.11 shows the results for the *Broadside* excitation and high-impedance loads ($R = 10 \text{ k}\Omega$). Excellent predictions of the transmission-line model are obtained for these orientations of the incident wave.

11.3 THE TIME-DOMAIN SOLUTION

In this last part of this chapter, we will extend the previous frequency-domain results to the time domain. In addition, we will develop a SPICE model for a lossless line and will also develop the finite-difference, time-domain (FDTD) solution method also for a lossless line.

11.3.1 The Laplace Transform Solution

In this section, we will transform the previous frequency-domain results using the Laplace transform and then inverse transform them to give the time-domain solution for a *lossless line*. The frequency-domain chain-parameter matrix relates the phasor voltage and current at one end of the line to the voltage and current at the other end as

$$\begin{bmatrix} \hat{V}(\mathcal{L}) \\ \hat{I}(\mathcal{L}) \end{bmatrix} = \hat{\Phi}(\mathcal{L}) \begin{bmatrix} \hat{V}(0) \\ \hat{I}(0) \end{bmatrix} + \begin{bmatrix} \hat{V}_{\text{FT}}(\mathcal{L}) \\ \hat{I}_{\text{FT}}(\mathcal{L}) \end{bmatrix} \quad (11.95a)$$

where the chain-parameter matrix is

$$\hat{\Phi}(\mathcal{L}) = \begin{bmatrix} \hat{\phi}_{11}(\mathcal{L}) & \hat{\phi}_{12}(\mathcal{L}) \\ \hat{\phi}_{21}(\mathcal{L}) & \hat{\phi}_{22}(\mathcal{L}) \end{bmatrix} \quad (11.95b)$$

The entries in the chain-parameter matrix for a *lossless line* are

$$\begin{aligned} \hat{\phi}_{11}(\mathcal{L}) &= \cos(\beta\mathcal{L}) \\ &= \frac{e^{j\beta\mathcal{L}} + e^{-j\beta\mathcal{L}}}{2} \end{aligned} \quad (11.96a)$$

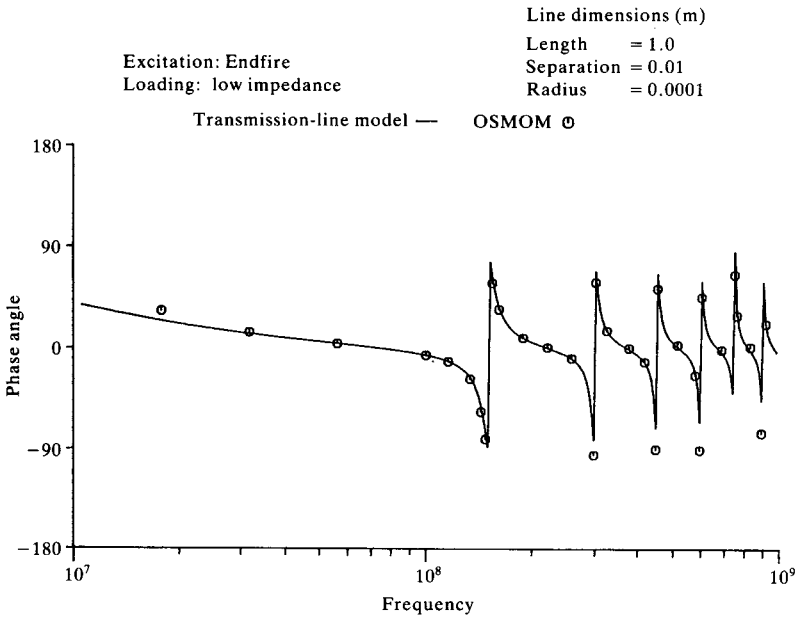
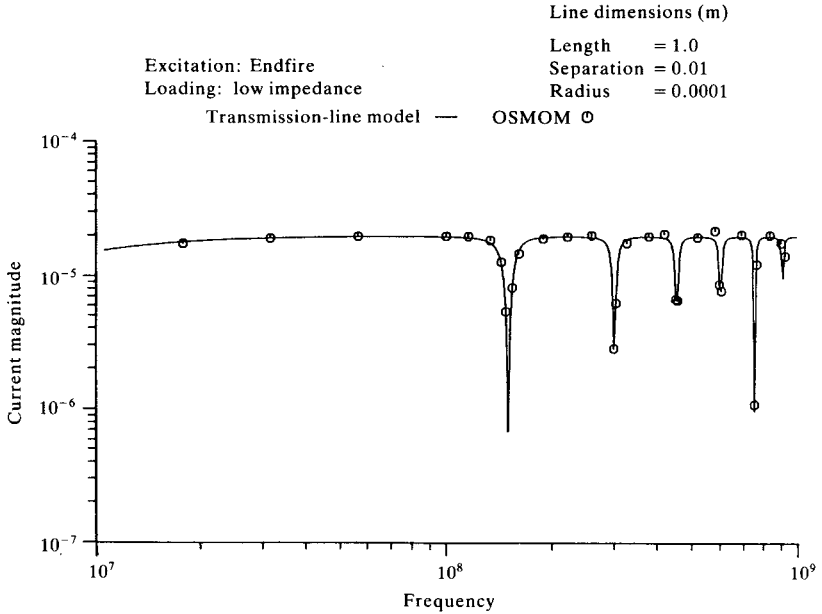


FIGURE 11.9 Comparison of the predictions of the transmission-line model and the method of moments for a two-wire line for *Endfire* illumination: (a) magnitude and (b) phase.

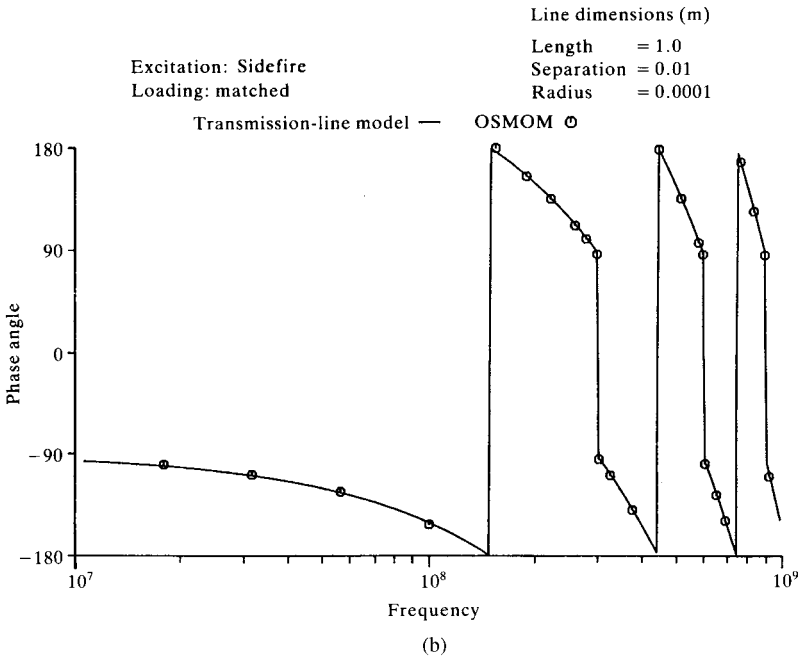
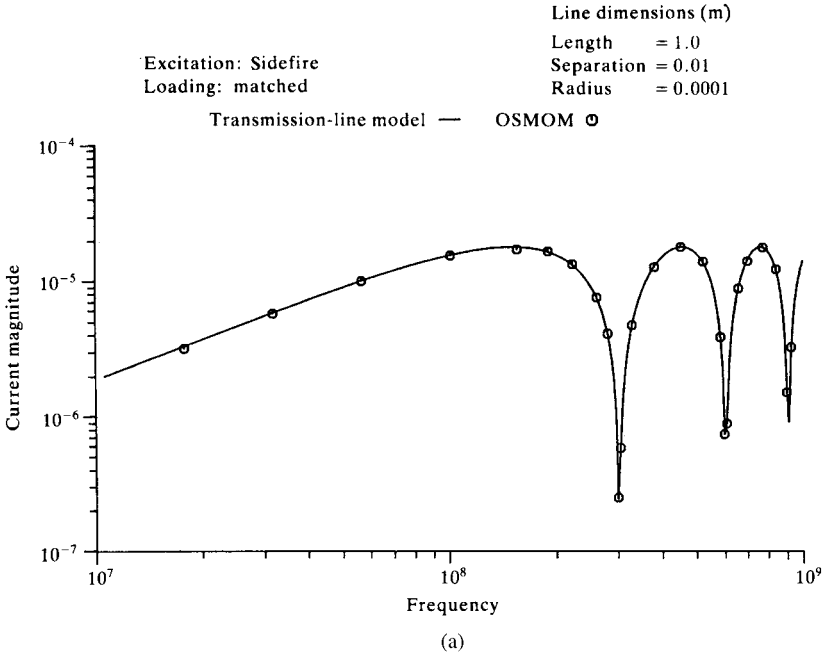
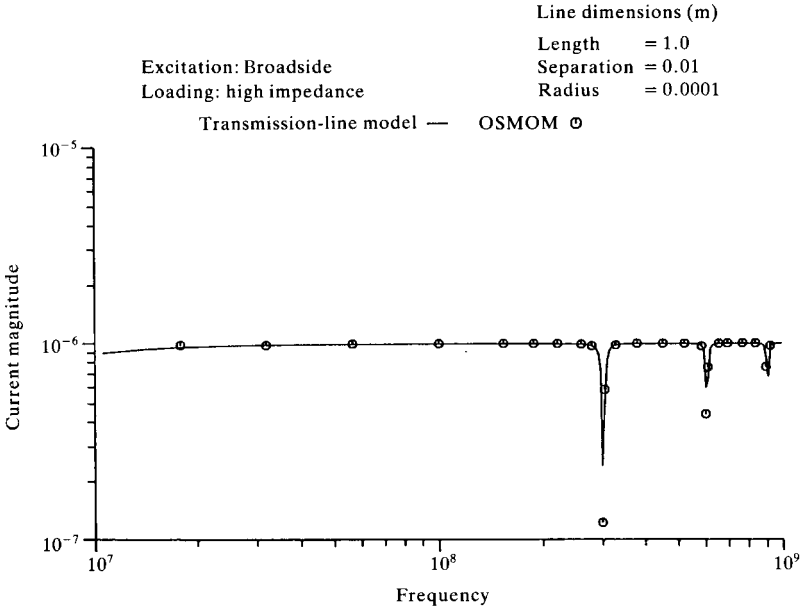
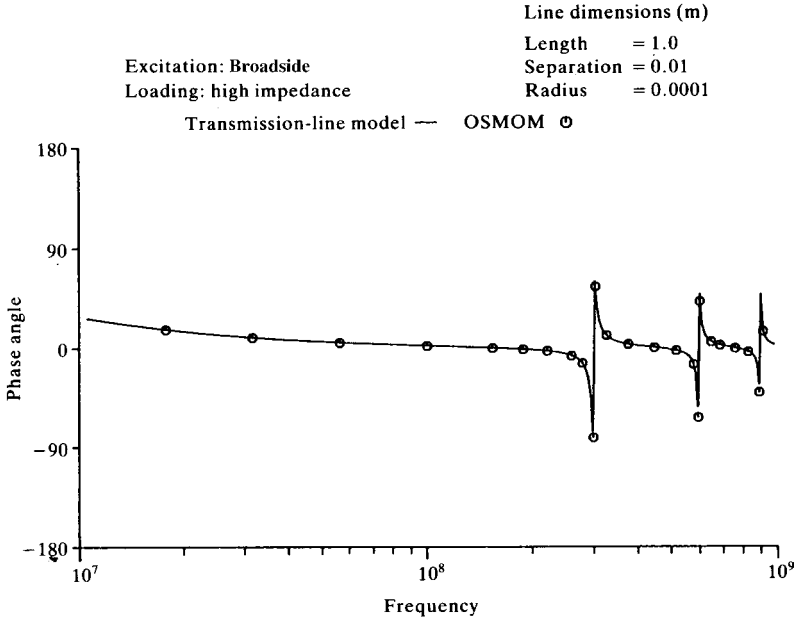


FIGURE 11.10 Comparison of the predictions of the transmission-line model and the method of moments for a two-wire line for *Sidefire* illumination: (a) magnitude and (b) phase.



(a)



(b)

FIGURE 11.11 Comparison of the predictions of the transmission-line model and the method of moments for a two-wire line for *Broadside* illumination: (a) magnitude and (b) phase.

$$\begin{aligned}\hat{\phi}_{12}(\mathcal{L}) &= -jZ_C \sin(\beta\mathcal{L}) \\ &= -Z_C \frac{e^{j\beta\mathcal{L}} - e^{-j\beta\mathcal{L}}}{2}\end{aligned}\quad (11.96b)$$

$$\begin{aligned}\hat{\phi}_{21}(\mathcal{L}) &= -j \frac{1}{Z_C} \sin(\beta\mathcal{L}) \\ &= -\frac{1}{Z_C} \frac{e^{j\beta\mathcal{L}} - e^{-j\beta\mathcal{L}}}{2}\end{aligned}\quad (11.96c)$$

$$\begin{aligned}\hat{\phi}_{22}(\mathcal{L}) &= \cos(\beta\mathcal{L}) \\ &= \frac{e^{j\beta\mathcal{L}} + e^{-j\beta\mathcal{L}}}{2}\end{aligned}\quad (11.96d)$$

The phase constant is

$$\beta = \omega\sqrt{lc} \quad (11.97)$$

the velocity of propagation is

$$\begin{aligned}v &= \frac{\omega}{\beta} \\ &= \frac{1}{\sqrt{lc}}\end{aligned}\quad (11.98)$$

and the characteristic impedance is

$$Z_C = \sqrt{\frac{l}{c}} \quad (11.99)$$

We can obtain the Laplace transform of these results by replacing $j\omega \Leftrightarrow s$, where s is the Laplace transform variable. In the course of doing so, we replace in the frequency-domain results above

$$e^{\pm j\beta\mathcal{L}} \Leftrightarrow e^{\pm sT_D} \quad (11.100)$$

where the one-way time delay of the line is

$$\begin{aligned}T_D &= \frac{\mathcal{L}}{v} \\ &= \frac{\beta}{\omega} \mathcal{L}\end{aligned}\quad (11.101)$$

Hence, we replace

$$j\beta\mathcal{L} = j\omega T_D \Leftrightarrow sT_D \quad (11.102)$$

The frequency-domain chain-parameter relations in (11.95) are Laplace transformed as

$$\hat{V}(\mathcal{L}, s) = \left(\frac{e^{sT_D} + e^{-sT_D}}{2} \right) \hat{V}(0, s) - Z_C \left(\frac{e^{sT_D} - e^{-sT_D}}{2} \right) \hat{I}(0, s) + \hat{V}_{\text{FT}}(\mathcal{L}, s) \quad (11.103a)$$

$$\begin{aligned} Z_C \hat{I}(\mathcal{L}, s) = & - \left(\frac{e^{sT_D} - e^{-sT_D}}{2} \right) \hat{V}(0, s) + Z_C \left(\frac{e^{sT_D} + e^{-sT_D}}{2} \right) \hat{I}(0, s) \\ & + Z_C \hat{I}_{\text{FT}}(\mathcal{L}, s) \end{aligned} \quad (11.103b)$$

where $\hat{V}(\mathcal{L}, s)$, $\hat{I}(\mathcal{L}, s)$, $\hat{V}(0, s)$, $\hat{I}(0, s)$, $\hat{V}_{\text{FT}}(\mathcal{L}, s)$, and $\hat{I}_{\text{FT}}(\mathcal{L}, s)$ denote the Laplace-transformed variables. We have multiplied the second equation by Z_C for reasons that will soon become apparent. Adding and subtracting (11.103a) and (11.103b) yields

$$\hat{V}(\mathcal{L}, s) - Z_C \hat{I}(\mathcal{L}, s) = e^{sT_D} [\hat{V}(0, s) - Z_C \hat{I}(0, s)] + [\hat{V}_{\text{FT}}(\mathcal{L}, s) - Z_C \hat{I}_{\text{FT}}(\mathcal{L}, s)] \quad (11.104a)$$

$$\hat{V}(\mathcal{L}, s) + Z_C \hat{I}(\mathcal{L}, s) = e^{-sT_D} [\hat{V}(0, s) + Z_C \hat{I}(0, s)] + [\hat{V}_{\text{FT}}(\mathcal{L}, s) + Z_C \hat{I}_{\text{FT}}(\mathcal{L}, s)] \quad (11.104b)$$

Multiplying (11.104a) by e^{-sT_D} and rearranging yields

$$\hat{V}(0, s) - Z_C \hat{I}(0, s) = e^{-sT_D} [\hat{V}(\mathcal{L}, s) - Z_C \hat{I}(\mathcal{L}, s)] - e^{-sT_D} \hat{V}^-(s) \quad (11.105a)$$

$$\hat{V}(\mathcal{L}, s) + Z_C \hat{I}(\mathcal{L}, s) = e^{-sT_D} [\hat{V}(0, s) + Z_C \hat{I}(0, s)] + \hat{V}^+(s) \quad (11.105b)$$

and we have written (11.105) in terms of the incident field sources as

$$\hat{V}^+(s) = \hat{V}_{\text{FT}}(\mathcal{L}, s) + Z_C \hat{I}_{\text{FT}}(\mathcal{L}, s) \quad (11.106a)$$

$$\hat{V}^-(s) = \hat{V}_{\text{FT}}(\mathcal{L}, s) - Z_C \hat{I}_{\text{FT}}(\mathcal{L}, s) \quad (11.106b)$$

We will find in the remaining results that the incident field sources, $\hat{V}_{\text{FT}}(\mathcal{L}, s)$ and $\hat{I}_{\text{FT}}(\mathcal{L}, s)$, always occur in combination as in (11.106) rather than individually.

We can derive an explicit Laplace transform solution for the terminal voltages by incorporating the terminal constraints:

$$\hat{V}(0, s) = -R_S \hat{I}(0, s) \quad (11.107a)$$

$$\hat{V}(\mathcal{L}, s) = R_L \hat{I}(\mathcal{L}, s) \quad (11.107b)$$

We have assumed resistive loads to make a literal solution feasible, but a later SPICE model will allow dynamic and/or nonlinear loads. Substituting these terminal constraints into (11.105) yields the terminal voltages as

$$\hat{V}(0, s) = \frac{e^{-sT_D} \Gamma_L \hat{V}^+(s) - e^{-sT_D} \hat{V}^-(s)}{[1 - \Gamma_S \Gamma_L e^{-2sT_D}]} \frac{R_S}{R_S + Z_C} \quad (11.108a)$$

$$\hat{V}(\mathcal{L}, s) = \frac{\hat{V}^+(s) - e^{-2sT_D} \Gamma_S \hat{V}^-(s)}{[1 - \Gamma_S \Gamma_L e^{-2sT_D}]} \frac{R_L}{R_L + Z_C} \quad (11.108b)$$

where the reflection coefficients are given by

$$\Gamma_S = \frac{R_S - Z_C}{R_S + Z_C} \quad (11.109a)$$

$$\Gamma_L = \frac{R_L - Z_C}{R_L + Z_C} \quad (11.109b)$$

The transformed equivalent sources $\hat{V}^+(s)$ and $\hat{V}^-(s)$ are obtained from the frequency-domain results in (11.52) by substituting, for a *lossless line*,

$$\cosh(\hat{\gamma} \mathcal{L}) \Rightarrow \cos(\beta \mathcal{L}) = \frac{e^{j\beta \mathcal{L}} + e^{-j\beta \mathcal{L}}}{2} \Leftrightarrow \frac{e^{sT_D} + e^{-sT_D}}{2} \quad (11.110a)$$

$$\sinh(\hat{\gamma} \mathcal{L}) \Rightarrow j \sin(\beta \mathcal{L}) = \frac{e^{j\beta \mathcal{L}} - e^{-j\beta \mathcal{L}}}{2} \Leftrightarrow \frac{e^{sT_D} - e^{-sT_D}}{2} \quad (11.110b)$$

to yield

$$\begin{aligned} \hat{V}^+(s) &= \hat{V}_{FT}(\mathcal{L}, s) + Z_C \hat{I}_{FT}(\mathcal{L}, s) = e^{-sT_D} \int_0^{\mathcal{L}} e^{s\tau/v} \\ &\times \left[\hat{E}_z^{\text{inc}}(x=d, z=\tau, s) - \hat{E}_z^{\text{inc}}(x=0, z=\tau, s) \right] d\tau + e^{-sT_D} \\ &\times \left[\int_0^d \hat{E}_x^{\text{inc}}(x, z=0, s) dx \right] - \left[\int_0^d \hat{E}_x^{\text{inc}}(x, z=\mathcal{L}, s) dx \right] \quad (11.111a) \end{aligned}$$

$$\begin{aligned} \hat{V}^-(s) &= \hat{V}_{FT}(\mathcal{L}, s) - Z_C \hat{I}_{FT}(\mathcal{L}, s) = e^{sT_D} \int_0^{\mathcal{L}} e^{-s\tau/v} \\ &\times \left[\hat{E}_z^{\text{inc}}(x=d, z=\tau, s) - \hat{E}_z^{\text{inc}}(x=0, z=\tau, s) \right] d\tau + e^{sT_D} \\ &\times \left[\int_0^d \hat{E}_x^{\text{inc}}(x, z=0, s) dx \right] - \left[\int_0^d \hat{E}_x^{\text{inc}}(x, z=\mathcal{L}, s) dx \right] \quad (11.111b) \end{aligned}$$

We now return to the time domain using the fundamental Laplace transform result [A.2]

$$e^{\pm sT_D} \hat{F}(s) \Leftrightarrow f(t \pm T_D) \quad (11.112)$$

The time-domain solution is obtained from the Laplace-transformed result in (11.108) by recognizing the basic result given in (11.112) as

$$V(0, t) - \Gamma_S \Gamma_L V(0, t - 2T_D) = [\Gamma_L V^+(t - T_D) - V^-(t - T_D)] \frac{R_S}{R_S + Z_C} \quad (11.113a)$$

$$V(\mathcal{L}, t) - \Gamma_S \Gamma_L V(\mathcal{L}, t - 2T_D) = [V^+(t) - \Gamma_S V^-(t - 2T_D)] \frac{R_L}{R_L + Z_C} \quad (11.113b)$$

The time forms of the equivalent incident field sources in (11.111), $V^+(t)$ and $V^-(t)$, are

$$\begin{aligned} V^+(t) = V_{FT}(\mathcal{L}, t) + Z_C I_{FT}(\mathcal{L}, t) = & \int_0^{\mathcal{L}} \left[\mathcal{E}_z^{\text{inc}} \left(x = d, z = \tau, t - T_D + \frac{\tau}{v} \right) \right. \\ & \left. - \mathcal{E}_z^{\text{inc}} \left(x = 0, z = \tau, t - T_D + \frac{\tau}{v} \right) \right] d\tau + \left[\int_0^d \mathcal{E}_x^{\text{inc}}(x, z = 0, t - T_D) dx \right] \\ & - \left[\int_0^d \mathcal{E}_x^{\text{inc}}(x, z = \mathcal{L}, t) dx \right] \end{aligned} \quad (11.114a)$$

$$\begin{aligned} V^-(t) = V_{FT}(\mathcal{L}, t) - Z_C I_{FT}(\mathcal{L}, t) = & \int_0^{\mathcal{L}} \left[\mathcal{E}_z^{\text{inc}} \left(x = d, z = \tau, t + T_D - \frac{\tau}{v} \right) \right. \\ & \left. - \mathcal{E}_z^{\text{inc}} \left(x = 0, z = \tau, t + T_D - \frac{\tau}{v} \right) \right] d\tau + \left[\int_0^d \mathcal{E}_x^{\text{inc}}(x, z = 0, t + T_D) dx \right] \\ & - \left[\int_0^d \mathcal{E}_x^{\text{inc}}(x, z = \mathcal{L}, t) dx \right] \end{aligned} \quad (11.114b)$$

The results in (11.113) are *implicit* relations in that the value of a solution variable, $V(0, t)$ or $V(\mathcal{L}, t)$, depends on the value two one-way line delays earlier, $V(0, t - 2T)$

or $V(\mathcal{L}, t - 2T)$. An explicit solution can be obtained with the *time-shift* or *difference operator* D , as was done in Chapter 8:

$$D^{\pm k} f(t) = f(t \pm kT_D) \quad (11.115)$$

Thus, the results in (11.108) become

$$V(0, t) = \frac{\Gamma_L D V^+(t) - D V^-(t)}{[D^2 - \alpha]} \frac{R_S}{R_S + Z_C} \quad (11.116a)$$

$$V(\mathcal{L}, t) = \frac{D^2 V^+(t) - \Gamma_S V^-(t)}{[D^2 - \alpha]} \frac{R_L}{R_L + Z_C} \quad (11.116b)$$

where

$$\alpha = \Gamma_S \Gamma_L \quad (11.116c)$$

Carrying out the long division giving

$$\frac{1}{D^2 - \alpha} = D^{-2} + \alpha D^{-4} + \alpha^2 D^{-6} + \dots \quad (11.117)$$

and substituting (11.115) gives

$$V(0, t) = \frac{R_S}{R_S + Z_C} \left\{ \Gamma_{\mathcal{L}} \left[V^+(t - T_D) + \alpha V^+(t - 3T_D) + \alpha^2 V^+(t - 5T_D) + \dots \right] - \left[V^-(t - T_D) + \alpha V^-(t - 3T_D) + \alpha^2 V^-(t - 5T_D) + \dots \right] \right\} \quad (11.118a)$$

$$V(\mathcal{L}, t) = \frac{R_L}{R_L + Z_C} \left\{ \left[V^+(t) + \alpha V^+(t - 2T_D) + \alpha^2 V^+(t - 4T_D) + \dots \right] - \Gamma_S \left[V^-(t - 2T_D) + \alpha V^-(t - 4T_D) + \alpha^2 V^-(t - 6T_D) + \dots \right] \right\} \quad (11.118b)$$

Thus, the terminal voltages are weighted sums of the functions produced by the incident field, $\hat{V}_{FT}(\mathcal{L}) \Leftrightarrow V_{FT}(\mathcal{L}, t)$ and $\hat{I}_{FT}(\mathcal{L}) \Leftrightarrow I_{FT}(\mathcal{L}, t)$, delayed in time by multiples of the line one-way delay T_D . Thus, the basic problem here is again to determine the frequency-domain to time-domain transformations of the functions representing the effect of the incident field given in (11.114). If the line is matched at both ends, $\Gamma_S = \Gamma_L = 0$, the results in (11.118) simplify to

$$V(0, t) = -\frac{R_S}{R_S + Z_C} V^-(t - T_D) \quad (11.119a)$$

$$V(\mathcal{L}, t) = \frac{R_L}{R_L + Z_C} V^+(t) \quad (11.119b)$$

11.3.2 Uniform Plane-Wave Excitation of the Line

Although the above results are valid for any time form of the incident field excitation, a useful form is that of a uniform plane wave considered earlier. Again consider a two-conductor line shown in Figure 11.5 with line conductors located in the x - z plane at $x = 0, y = 0$ and $x = d, y = 0$ and extending from $z = 0$ to $z = \mathcal{L}$. The frequency-domain forcing functions are given in (11.52). We consider a uniform plane wave incident on the line as shown in Figure 11.6 whose frequency-domain representation is, again,

$$\vec{E}^{\text{inc}}(x, y, z, \omega) = \hat{E}_o(\omega) [e_x \vec{a}_x + e_y \vec{a}_y + e_z \vec{a}_z] e^{-j\beta_x x} e^{-j\beta_y y} e^{-j\beta_z z} \quad (11.120)$$

where the components of the incident electric field vector along the $x, y,$ and z axes of the rectangular coordinate system describing the line are given in (11.55). The components of the phase constant along those coordinate axes are given in (11.56). In the time domain, (11.120) translates to [A.1]

$$\vec{\mathcal{E}}^{\text{inc}}(x, y, z, t) = [e_x \vec{a}_x + e_y \vec{a}_y + e_z \vec{a}_z] \mathcal{E}_o \left(t - \frac{x}{v_x} - \frac{y}{v_y} - \frac{z}{v_z} \right) \quad (11.121)$$

The time form of the electric field is denoted by $\mathcal{E}_o(t)$ where $\mathcal{E}_o(t) \Leftrightarrow \hat{E}_o(\omega)$, and the velocities of propagation along the axes are denoted by

$$\begin{aligned} v_x &= \frac{\omega}{\beta_x} = -\frac{v}{\cos \theta_p} \\ v_y &= \frac{\omega}{\beta_y} = -\frac{v}{\sin \theta_p \cos \phi_p} \\ v_z &= \frac{\omega}{\beta_z} = -\frac{v}{\sin \theta_p \sin \phi_p} \end{aligned} \quad (11.122)$$

The frequency-domain forcing functions, given in (11.52) and (11.111), become, for a lossless line,

$$\begin{aligned} \hat{V}^+(\omega) &= \hat{V}_{\text{FT}}(\mathcal{L}) + Z_C \hat{I}_{\text{FT}}(\mathcal{L}) \\ &= \hat{E}_o(\omega) d \left[\frac{\sin(\beta_x d/2)}{\beta_x d/2} \right] e^{-j\beta_x d/2} \left\{ \left[e_x + e_z \left(\frac{\beta_x}{\beta - \beta_z} \right) \right] \right. \\ &\quad \left. \times \left[e^{-j\beta \mathcal{L}} - e^{-j\beta_z \mathcal{L}} \right] \right\} \end{aligned} \quad (11.123a)$$

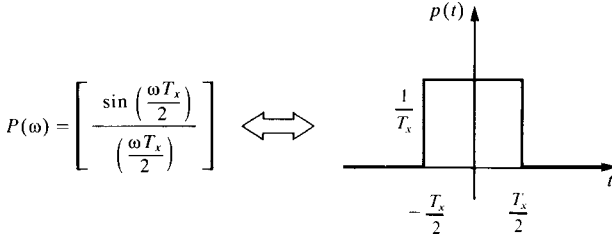


FIGURE 11.12 The pulse function representing the effect of propagation in the cross-sectional plane.

$$\begin{aligned} \hat{V}^-(\omega) &= \hat{V}_{\text{FT}}(\mathcal{L}) - Z_C \hat{I}_{\text{FT}}(\mathcal{L}) \\ &= \hat{E}_0(\omega) d \left[\frac{\sin(\beta_x d/2)}{\beta_x d/2} \right] e^{-j\beta_x d/2} \left\{ \left[e_x - e_z \left(\frac{\beta_x}{\beta + \beta_z} \right) \right] \right. \\ &\quad \left. \times [e^{j\beta \mathcal{L}} - e^{-j\beta \mathcal{L}}] \right\} \end{aligned} \tag{11.123b}$$

The time-domain forms can be obtained by first noting that the term in (11.123) can be written as

$$\begin{aligned} P(\omega) &= \left[\frac{\sin(\beta_x d/2)}{\beta_x d/2} \right] \\ &= \left[\frac{\sin\left(\pi f \frac{d}{v_x}\right)}{\pi f \frac{d}{v_x}} \right] \\ &= \left[\frac{\sin(\pi f T_x)}{\pi f T_x} \right] \end{aligned} \tag{11.124}$$

where the transit time delay of a wave propagating in the x direction between the two conductors is

$$T_x = \frac{d}{v_x} \tag{11.125}$$

The frequency-domain function $P(\omega)$ in (11.124) is equivalent, in the time domain, to the pulse function shown in Figure 11.12 [A.2,A.3]:

$$p(t) = \begin{cases} 0, & t < -\frac{T_x}{2} \\ \frac{1}{T_x}, & -\frac{T_x}{2} < t < \frac{T_x}{2} \\ 0, & t > \frac{T_x}{2} \end{cases} \tag{11.126}$$

Therefore, the frequency-domain forcing functions given in (11.123) transform to the time domain as a *convolution* of a time function and the pulse function in (11.126):

$$V^+(t) = d \left[e_x + e_z \left(\frac{\mathcal{L}}{d} \right) \frac{T_x}{(T_D - T_z)} \right] \times \left[\mathcal{E}_o \left(t - T_D - \frac{T_x}{2} \right) - \mathcal{E}_o \left(t - T_z - \frac{T_x}{2} \right) \right] * p(t) \quad (11.127a)$$

$$V^-(t) = d \left[e_x - e_z \left(\frac{\mathcal{L}}{d} \right) \frac{T_x}{(T_D + T_z)} \right] \times \left[\mathcal{E}_o \left(t + T_D - \frac{T_x}{2} \right) - \mathcal{E}_o \left(t - T_z - \frac{T_x}{2} \right) \right] * p(t) \quad (11.127b)$$

and we denote the convolution as

$$F(t) * p(t) = \int_{-\infty}^{\infty} F(\tau) p(t - \tau) d\tau \quad (11.128)$$

The transit time along the line of the z component of the wave propagation vector is

$$T_z = \frac{\mathcal{L}}{v_z} \quad (11.129)$$

and the time delay of the line is denoted in the usual fashion as

$$T_D = \frac{\mathcal{L}}{v} \quad (11.130)$$

In order for the transmission-line model to be a valid representation, the line cross sectional dimensions must be electrically small at the significant frequencies of the incident field waveform $\mathcal{E}_o(t)$. The phase velocity of propagation in the cross-sectional plane given in (11.122) is bounded by $v \leq v_x < \infty$. Hence, $(d/\mathcal{L})T_D \geq T_x \geq 0$. When the wave has no propagation component in the x direction, $\theta_p = \pm 90^\circ$, then $v_x = \infty$ and $T_x = 0$ and the function in (11.124) is unity, that is, $P(\omega)|_{v_x=\infty} = 1$. At the other extreme, when $\theta_p = 0^\circ, 180^\circ$ then $v_x = v$ and the function in (11.124) is

$$P(\omega) = \frac{\sin \left(\pi \frac{d}{\lambda} \right)}{\pi \frac{d}{\lambda}} .$$

Again, for the transmission-line model to be a valid representation, the line cross-sectional dimensions must be electrically small at the significant frequencies of the

incident field waveform $\mathcal{E}_o(t)$. Suppose that the conductor separation d is $1/10 \lambda$ at the highest significant frequency of the incident field waveform, $\mathcal{E}_o(t)$. In this case, $1 \geq P(\omega) \geq 0.984$. This is somewhat marginal for the transmission-line model to be applicable. So, suppose that the conductor separation d is $1/100 \lambda$ at the highest significant frequency of the incident field waveform $\mathcal{E}_o(t)$. In this case, $1 \geq P(\omega) \geq 0.99984$. Hence, for conditions on the line cross-sectional dimensions where the transmission-line model is applicable, $P(\omega) \cong 1$. When the line cross section is sufficiently small, electrically, over the spectrum of $\hat{E}_o(\omega)$ such that $P(\omega) \cong 1$, then the pulse function $p(t)$ approximates an impulse function:

$$p(t) \cong \delta(t) \quad \text{small } T_x \quad (11.131)$$

For this practical case, the time-domain functions in (11.127) simplify to

$$V^+(t) \cong d \left[e_x + e_z \left(\frac{\mathcal{L}}{d} \right) \frac{T_x}{(T_D - T_z)} \right] \left[\mathcal{E}_o \left(t - T_D - \frac{T_x}{2} \right) - \mathcal{E}_o \left(t - T_z - \frac{T_x}{2} \right) \right] \quad (11.132a)$$

$$V^-(t) \cong d \left[e_x - e_z \left(\frac{\mathcal{L}}{d} \right) \frac{T_x}{(T_D + T_z)} \right] \left[\mathcal{E}_o \left(t + T_D - \frac{T_x}{2} \right) - \mathcal{E}_o \left(t - T_z - \frac{T_x}{2} \right) \right] \quad (11.132b)$$

Observe that all the forcing function $\mathcal{E}_o(t)$ terms in (11.132a) and (11.132b) are delayed by $T_x/2$. In order to simplify the result, we will omit the terms $T_x/2$ from the delays in the incident waveform functions $\mathcal{E}_o(t)$ in (11.132). Once we obtain the solution for the terminal voltage and current waveforms using (11.132) with the terms $T_x/2$ removed, we can delay those solutions by $T_x/2$ to get back to this original solution. As a practical matter, the cross-sectional time delay $T_x/2$ will anyway be very small compared to the time frames of interest in a typical problem. For example, for a conductor separation of 10 cm and the wave propagating across the cross section, the time delay is $T_x = 0.33$ ns.

In the case of a conductor located at a height h above an infinite ground plane as illustrated in Figure 11.8, the above functions are easily modified. The *total* incident electric field (the incident field plus the field reflected from the ground plane) is given in the frequency domain in (11.81). The frequency-domain forcing functions given in (11.52) depend on the z and x components of the electric field. Substituting (11.81) ($x = h$ and $y = 0$) gives

$$\left[\hat{E}_z^{\text{total}}(h, z) - \underbrace{\hat{E}_z^{\text{total}}(0, z)}_0 \right] = \left[-j2\beta_x h \frac{\sin(\beta_x h)}{\beta_x h} \right] \hat{E}_o(\omega) e_z e^{-j\beta_z z} \quad (11.133)$$

This compares to the case with no ground plane given in (11.64):

$$[\hat{E}_z^i(d, z) - \hat{E}_z^i(0, z)] = \left[-j2\beta_x \frac{d \sin(\beta_x d/2)}{2 \beta_x d/2} e^{-j\beta_x d/2} \right] \hat{E}_o(\omega) e_z e^{-j\beta_z z} \quad (11.134)$$

Similarly,

$$\int_0^h \hat{E}_x^{\text{total}} dx = 2h \left[\frac{\sin(\beta_x h)}{\beta_x h} \right] \hat{E}_o(\omega) e_x e^{-j\beta_z z} \quad (11.135)$$

This compares to the case with no ground plane given in (11.63):

$$\int_0^d \hat{E}_x^i dx = 2 \left(\frac{d}{2} \right) \left[\frac{\sin(\beta_x d/2)}{\beta_x d/2} e^{-j\beta_x d/2} \right] \hat{E}_o(\omega) e_x e^{-j\beta_z z} \quad (11.136)$$

Therefore, to convert the previous frequency-domain results to the case of a ground plane, we simply remove the factor $e^{-j\beta_x d/2}$ and replace $d/2 \Leftrightarrow h$ in those results. The frequency-domain forcing functions given in (11.123) become

$$\begin{aligned} \hat{V}^+(\omega) &= \hat{V}_{\text{FT}}(\mathcal{L}) + Z_C \hat{I}_{\text{FT}}(\mathcal{L}) \\ &= 2\hat{E}_o(\omega) h \left[\frac{\sin(\beta_x h)}{\beta_x h} \right] \left\{ \left[e_x + e_z \left(\frac{\beta_x}{\beta - \beta_z} \right) \right] \left[e^{-j\beta \mathcal{L}} - e^{-j\beta_z \mathcal{L}} \right] \right\} \end{aligned} \quad (11.137a)$$

$$\begin{aligned} \hat{V}^-(\omega) &= \hat{V}_{\text{FT}}(\mathcal{L}) - Z_C \hat{I}_{\text{FT}}(\mathcal{L}) \\ &= 2\hat{E}_o(\omega) h \left[\frac{\sin(\beta_x h)}{\beta_x h} \right] \left\{ \left[e_x - e_z \left(\frac{\beta_x}{\beta + \beta_z} \right) \right] \left[e^{j\beta \mathcal{L}} - e^{-j\beta_z \mathcal{L}} \right] \right\} \end{aligned} \quad (11.137b)$$

Therefore, the time-domain forcing functions are again given by the convolutions in (11.127) as

$$V^+(t) = 2h \left[e_x + e_z \left(\frac{\mathcal{L}}{d} \right) \frac{T_x}{(T_D - T_z)} \right] [\mathcal{E}_o(t - T_D) - \mathcal{E}_o(t - T_z)] * p(t) \quad (11.138a)$$

$$V^-(t) = 2h \left[e_x - e_z \left(\frac{\mathcal{L}}{d} \right) \frac{T_x}{(T_D + T_z)} \right] [\mathcal{E}_o(t + T_D) - \mathcal{E}_o(t - T_z)] * p(t) \quad (11.138b)$$

and we denote

$$P(\omega) = \left[\frac{\sin(\beta_x h)}{\beta_x h} \right] \Leftrightarrow p(t) \quad (11.139)$$

Again, assuming that the line cross-sectional dimensions are electrically very small, we will ignore $p(t)$ and assume

$$V^+(t) \cong 2h \left[e_x + e_z \left(\frac{\mathcal{L}}{d} \right) \frac{T_x}{(T_D - T_z)} \right] [\mathcal{E}_o(t - T_D) - \mathcal{E}_o(t - T_z)] \quad (11.140a)$$

$$V^-(t) \cong 2h \left[e_x - e_z \left(\frac{\mathcal{L}}{d} \right) \frac{T_x}{(T_D + T_z)} \right] [\mathcal{E}_o(t + T_D) - \mathcal{E}_o(t - T_z)] \quad (11.140b)$$

The explicit time-domain series solution given for resistive loads in (11.118) can be used for this case of a ground plane without change except for the $V^+(t)$ and $V^-(t)$ functions.

11.3.3 A SPICE Equivalent Circuit

In this section, we will describe a simple model for computing the response of a lossless two-conductor transmission line to an incident uniform plane wave. This will be extended to the MTL case in the next chapter.

The frequency-domain chain parameters are given in (11.32):

$$\hat{V}(\mathcal{L}) = \hat{\phi}_{11}(\mathcal{L}) \hat{V}(0) + \hat{\phi}_{12}(\mathcal{L}) \hat{I}(0) + \hat{V}_{FT}(\mathcal{L}) \quad (11.32a)$$

$$\hat{I}(\mathcal{L}) = \hat{\phi}_{21}(\mathcal{L}) \hat{V}(0) + \hat{\phi}_{22}(\mathcal{L}) \hat{I}(0) + \hat{I}_{FT}(\mathcal{L}) \quad (11.32b)$$

Laplace transforming these and adding and subtracting them gives the Laplace transform results in (11.105) as

$$\hat{V}(0, s) - Z_C \hat{I}(0, s) = e^{-sT_D} [\hat{V}(\mathcal{L}, s) - Z_C \hat{I}(\mathcal{L}, s)] - e^{-sT_D} \hat{V}^-(s) \quad (11.105a)$$

$$\hat{V}(\mathcal{L}, s) + Z_C \hat{I}(\mathcal{L}, s) = e^{-sT_D} [\hat{V}(0, s) + Z_C \hat{I}(0, s)] + \hat{V}^+(s) \quad (11.105b)$$

Using the Laplace transform property in (11.112),

$$e^{\pm sT_D} \hat{F}(s) \Leftrightarrow f(t \pm T_D) \quad (11.112)$$

these become, in the time domain,

$$V(0, t) - Z_C I(0, t) = [V(\mathcal{L}, t - T_D) - Z_C I(\mathcal{L}, t - T_D)] - V^-(t - T_D) \quad (11.141a)$$

$$V(\mathcal{L}, t) + Z_C I(\mathcal{L}, t) = [V(0, t - T_D) + Z_C I(0, t - T_D)] + V^+(t) \quad (11.141b)$$

where $V^+(t)$ and $V^-(t)$ are given in (11.132) as

$$\begin{aligned}
 V^-(t - T_D) &= [V_{FT}(\mathcal{L}, t - T_D) - Z_C I_{FT}(\mathcal{L}, t - T_D)] \\
 &\cong d \left[e_x - e_z \left(\frac{\mathcal{L}}{v_x(T_z + T_D)} \right) \right] [\mathcal{E}_o(t) - \mathcal{E}_o(t - T_D - T_z)]
 \end{aligned} \tag{11.142a}$$

$$\begin{aligned}
 V^+(t) &= [V_{FT}(\mathcal{L}, t) + Z_C I_{FT}(\mathcal{L}, t)] \\
 &\cong d \left[e_x - e_z \left(\frac{\mathcal{L}}{v_x(T_z - T_D)} \right) \right] [E_o(t - T_D) - E_o(t - T_z)]
 \end{aligned} \tag{11.142b}$$

and, as discussed earlier, we have omitted the $T_x/2$ delay terms from the forcing functions in (11.132). Once we obtain the solution for the terminal voltage and current waveforms using (11.142) with the terms $T_x/2$ removed, we can delay those solutions by $T_x/2$ to get back to this original solution. As a practical matter, the cross-sectional time delay $T_x/2$ will anyway be very small compared to the time frames of interest in a typical problem.

Observe that these sources in (11.142) only require that we obtain delayed versions of $\mathcal{E}_o(t)$. This suggests the usual model of an unexcited line containing time-delayed voltage sources. The problem is that we do not have access to internal nodes of the usual SPICE transmission model so that we may add the sources in (11.142) in series with the ones already present according to (11.141). The remedy here is to simply build the model using ideal delay lines and controlled sources. Such a model is shown in Figure 11.13. The external terminals of the line are denoted as 101 and 201 with the 0 node being common. The controlled sources in that model are obtained as $V(2)$, $V(4)$ and

$$E_o(t) = -d \left[e_x - e_z \left(\frac{\mathcal{L}}{v_x(T_z + T_D)} \right) \right] [V(100) - V(6)] \tag{11.143a}$$

$$E_L(t) = d \left[e_x - e_z \left(\frac{\mathcal{L}}{v_x(T_z - T_D)} \right) \right] [V(5) - V(7)] \tag{11.143b}$$

where the usual SPICE designation for the voltage of node n is denoted as $V(n)$. The reader can observe that the circuit of Figure 11.13 with the controlled source parameters given in (11.143) yields Eqs. (11.141) and (11.142) and is therefore an exact representation. (The cross-sectional time delay terms $T_x/2$ have been omitted from the source functions in (11.143).) The characteristic impedances Z_{C1} , Z_{C2} , Z_{C3} , Z_{C4} , and Z_{C5} in the five auxiliary delay lines need not equal the characteristic impedances of the original line, Z_C , but each line must be appropriately matched to its chosen characteristic impedance to prevent reflections on that line and

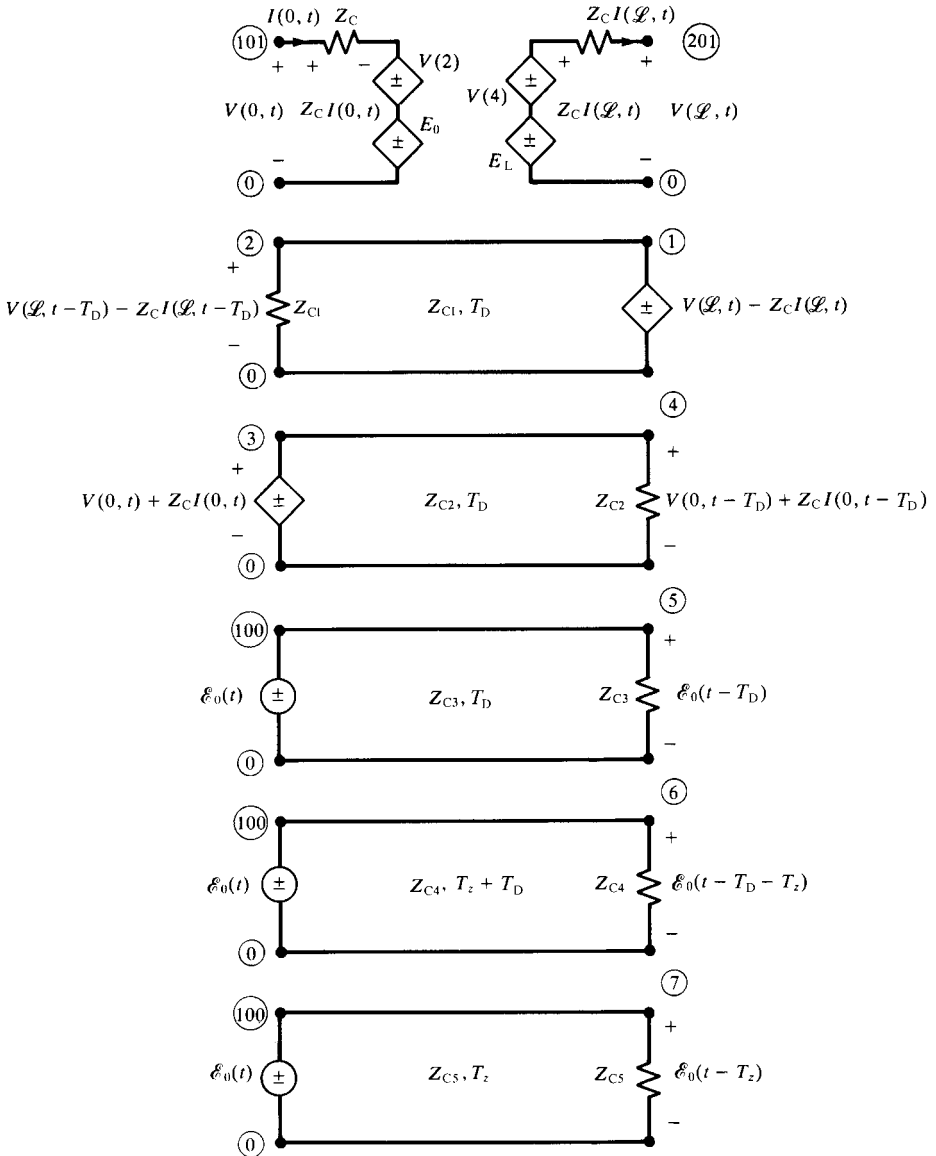


FIGURE 11.13 The SPICE model representing incident field illumination of a two-conductor line.

provide for an ideal delay. The velocities of propagation and line lengths (or equivalently the line time delays) must be as shown. Similarly, if the wave is propagating solely in the z direction, $T_z = \pm T_D$, then the e_z term in either (11.143a) or (11.143b) is removed since it also contains $v_x = \infty$. This basic model will be extended to the MTL case in the next chapter by decoupling the MTL equations.

This SPICE/PSPICE subcircuit model is generated with the FORTRAN program SPICEINC.FOR described in Appendix A.

11.3.4 The Time-Domain to Frequency-Domain (TDFD) Transformation

This method remains the same as before. First, we determine the Fourier coefficients of the time-domain source waveform, in this case for uniform plane-wave excitation, $\mathcal{E}_o(t)$. This is done for trapezoidal pulse trains representing digital signal waveforms within the FORTRAN program TIMEFREQ.FOR. Note that a uniform plane wave having a trapezoidal pulse train waveform is not a realistic waveform for a radiated signal from an antenna if its average value (dc) is nonzero. However, this program has not been changed from the case of lumped sources in the termination networks. We could eliminate the dc response by setting $H(0) = 0$ in the input data for TIMEFREQ.FOR. We simply need to determine the frequency-domain transfer function between $\mathcal{E}_o(t)$ and the desired terminal voltage or current, $\hat{V}(\mathcal{L})$, $\hat{I}(\mathcal{L})$, $\hat{V}(0)$, or $\hat{I}(0)$ at the harmonics of $\mathcal{E}_o(t)$. TIMEFREQ takes that frequency-domain transfer function and combines it with the Fourier coefficients of $\mathcal{E}_o(t)$, and adds them in time to produce the time domain terminal voltages or currents $V(\mathcal{L}, t)$, $I(\mathcal{L}, t)$, $V(0, t)$, or $I(0, t)$. We need to determine the frequency-domain transfer function at the harmonics of the basic repetition frequency that we chose for $\mathcal{E}_o(t)$, $f_0, 2f_0, 3f_0, \dots$ up to at least

$$f_{\max} = \frac{1}{\tau_r} \quad (11.144)$$

where τ_r is the pulse rise time that we assume is equal to the pulse fall time.

The frequency-domain transfer function for a lossless line at the desired harmonics of $\mathcal{E}_o(t)$ can be obtained by obtaining the SPICE subcircuit model with the FORTRAN program SPICEINC.FOR that implements the model of the previous section. Imbedding this subcircuit model into a SPICE/PSPICE program, attaching the terminations, and running it in the .AC mode generates this frequency response of the transfer function for sinusoidal sources, $\mathcal{E}_o(t) \Leftrightarrow \hat{E}_o = 1\angle 0^\circ$, of unit magnitude and zero phase angle.

The frequency-domain transfer function for a lossy or lossless line at the desired harmonics of $\mathcal{E}_o(t)$ can also be obtained using the FORTRAN program INCIDENT.FOR also described in Appendix A. This program is MTL.FOR modified for incident field excitation. Again, we use it to determine the transfer function for sinusoidal sources, $\mathcal{E}_o(t) \Leftrightarrow \hat{E}_o = 1\angle 0^\circ$, of unit magnitude and zero phase angle.

11.3.5 The Finite-Difference, Time-Domain (FDTD) Solution Method

The FDTD method of solution is virtually unchanged from the case of lumped source excitation in the terminal networks described in Chapters 8 and 9. First, consider the basic time-domain partial differential equations of a *lossless* line with incident field

excitation given in (11.20) as

$$\frac{\partial}{\partial z} V(z, t) + l \frac{\partial}{\partial t} I(z, t) = -\frac{\partial}{\partial z} E_T(z, t) + E_L(z, t) \quad (11.145a)$$

$$\frac{\partial}{\partial z} I(z, t) + c \frac{\partial}{\partial t} V(z, t) = -c \frac{\partial}{\partial t} E_T(z, t) \quad (11.145b)$$

The line cross-sectional dimensions are again contained in the per-unit-length parameters of l (inductance) and c (capacitance). The quantities $E_T(z, t)$ and $E_L(z, t)$ contain the components of the incident electric field that are transverse to the line and parallel to the line conductors, respectively, with the line conductors removed. The quantity $E_T(z, t)$ is

$$E_T(z, t) = \int_0^d \mathcal{E}_x^{\text{inc}}(x, z, t) dx \quad (11.146)$$

The quantity $E_L(z, t)$ is the difference between the longitudinal (z -directed) components of the incident electric field intensity vector along the position of conductor # 1 and along the position of the reference conductor (with those conductors absent):

$$E_L(z, t) = \mathcal{E}_z^{\text{inc}}(\text{conductor \#1}, z, t) - \mathcal{E}_z^{\text{inc}}(\text{reference conductor}, z, t) \quad (11.147)$$

We now specialize the results to the case of uniform plane-wave excitation of the line. The phasor results given in (11.63) and (11.64) are

$$\hat{E}_T(z, t) = \hat{E}_0 d e_x e^{-j\beta_z z} e^{-j\beta_x \frac{d}{2}} \left[\frac{\sin\left(\beta_x \frac{d}{2}\right)}{\beta_x \frac{d}{2}} \right] \quad (11.63)$$

and

$$\begin{aligned} \hat{E}_L(z, t) &= -j\beta_x \hat{E}_0 d e_z e^{-j\beta_z z} e^{-j\beta_x \frac{d}{2}} \left[\frac{\sin\left(\beta_x \frac{d}{2}\right)}{\beta_x \frac{d}{2}} \right] \\ &= -j\omega \hat{E}_0 d \frac{e_z}{v_x} e^{-j\beta_z z} e^{-j\beta_x \frac{d}{2}} \left[\frac{\sin\left(\beta_x \frac{d}{2}\right)}{\beta_x \frac{d}{2}} \right] \end{aligned} \quad (11.64)$$

We will omit the $\sin(\beta_x(d/2))/\beta_x(d/2)$ term and the $e^{-j\beta_x(d/2)}$ term for reasons discussed in Section 11.3.2. Hence, the time-domain result becomes

$$E_T(z, t) = d e_x \mathcal{E}_0 \left(t - \frac{z}{v_z} \right) \quad (11.148)$$

Similarly,

$$E_L(z, t) = -d \frac{e_z}{v_x} \frac{\partial}{\partial t} \mathcal{E}_o \left(t - \frac{z}{v_z} \right) \tag{11.149}$$

The forcing function terms on the right-hand side of (11.145) involve $(\partial/\partial z)E_T(z, t)$ and $(\partial/\partial t)E_T(z, t)$. First, we observe that

$$\frac{\partial}{\partial t} \mathcal{E}_o \left(t - \frac{z}{v_z} \right) = \frac{\partial \mathcal{E}_o \left(t - \frac{z}{v_z} \right)}{\partial \left(t - \frac{z}{v_z} \right)} \underbrace{\frac{\partial}{\partial t} \left(t - \frac{z}{v_z} \right)}_1 = \frac{\partial \mathcal{E}_o \left(t - \frac{z}{v_z} \right)}{\partial \left(t - \frac{z}{v_z} \right)} \tag{11.150}$$

and

$$\begin{aligned} \frac{\partial}{\partial z} \mathcal{E}_o \left(t - \frac{z}{v_z} \right) &= \frac{\partial \mathcal{E}_o \left(t - \frac{z}{v_z} \right)}{\partial \left(t - \frac{z}{v_z} \right)} \underbrace{\frac{\partial}{\partial z} \left(t - \frac{z}{v_z} \right)}_{-1/v_z} = -\frac{1}{v_z} \frac{\partial \mathcal{E}_o \left(t - \frac{z}{v_z} \right)}{\partial \left(t - \frac{z}{v_z} \right)} \\ &= -\frac{1}{v_z} \frac{\partial}{\partial t} E_o \left(t - \frac{z}{v_z} \right) \end{aligned} \tag{11.151}$$

Hence, the various derivatives in the time domain become

$$\begin{aligned} \frac{\partial}{\partial z} E_T(z, t) &= d e_x \frac{\partial}{\partial z} \mathcal{E}_o \left(t - \frac{z}{v_z} \right) \\ &= -d \frac{e_x}{v_z} \frac{\partial}{\partial t} \mathcal{E}_o \left(t - \frac{z}{v_z} \right) \end{aligned} \tag{11.152}$$

$$\frac{\partial}{\partial t} E_T(z, t) = d e_x \frac{\partial}{\partial t} \mathcal{E}_o \left(t - \frac{z}{v_z} \right) \tag{11.153}$$

Hence, the forcing function terms on the right-hand side of (11.145) become

$$-\frac{\partial}{\partial z} E_T(z, t) + E_L(z, t) = d \left(\frac{e_x}{v_z} - \frac{e_z}{v_x} \right) \frac{\partial}{\partial t} \mathcal{E}_o \left(t - \frac{z}{v_z} \right) \tag{11.154}$$

$$-c \frac{\partial}{\partial t} E_T(z, t) = -c d e_x \frac{\partial}{\partial t} \mathcal{E}_o \left(t - \frac{z}{v_z} \right) \tag{11.155}$$

In order to discretize these transmission-line equations, we divide the line axis into NDZ sections each of length Δz , as shown in Figure 11.14(b). Similarly, we

divide the total solution time into NDT segments of length Δt . To provide second-order accuracy of the discretization, we interlace the NDZ + 1 voltage points, $V_1, V_2, \dots, V_{\text{NDZ}}, V_{\text{NDZ}+1}$, and the NDZ current points, $I_1, I_2, \dots, I_{\text{NDZ}}$, as shown in Figure 11.14(a). Each voltage and adjacent current solution point is separated by $\Delta z/2$. In addition, the time points are also interlaced, and each voltage time point and adjacent current time point are separated by $\Delta t/2$.

Discretizing the derivatives in the transmission-line equations using second-order central differences according to the scheme in Figure 11.14(a) gives

$$\begin{aligned} & \frac{1}{\Delta z} \left[V_{k+1}^{n+1} - V_k^{n+1} \right] + \frac{1}{\Delta t} l \left[I_k^{n+3/2} - I_k^{n+1/2} \right] \\ &= \frac{d}{\Delta t} \left(\frac{1}{v_z} e_x - \frac{1}{v_x} e_z \right) \left[\mathcal{E}_o \left(t^{n+3/2} - \frac{(k-1/2)\Delta z}{v_z} \right) \right. \\ & \quad \left. - \mathcal{E}_o \left(t^{n+1/2} - \frac{(k-1/2)\Delta z}{v_z} \right) \right] \end{aligned} \quad (11.156a)$$

for $k = 1, 2, \dots, \text{NDZ}$ and

$$\begin{aligned} & \frac{1}{\Delta z} \left[I_k^{n+1/2} - I_{k-1}^{n+1/2} \right] + \frac{1}{\Delta t} c \left[V_k^{n+1} - V_k^n \right] = -c \frac{d}{\Delta t} e_x \left[\mathcal{E}_o \left(t^{n+1} - \frac{(k-1)z}{v_z} \right) \right. \\ & \quad \left. - \mathcal{E}_o \left(t^n - \frac{(k-1)z}{v_z} \right) \right] \end{aligned} \quad (11.156b)$$

for $k = 2, \dots, \text{NDZ}$, where we denote

$$V_k^n \equiv V((k-1)\Delta z, n\Delta t) \quad (11.157a)$$

$$I_k^n \equiv I((k-1/2)\Delta z, n\Delta t) \quad (11.157b)$$

The required recursion relations for the interior points on the line are obtained by solving Eqs. (11.156) giving

$$\begin{aligned} I_k^{n+3/2} &= I_k^{n+1/2} - \frac{\Delta t}{\Delta z} l^{-1} \left(V_{k+1}^{n+1} - V_k^{n+1} \right) \\ &+ d l^{-1} \left(\frac{1}{v_z} e_x - \frac{1}{v_x} e_z \right) \left[\mathcal{E}_o \left(t^{n+3/2} - \frac{(k-1/2)\Delta z}{v_z} \right) \right. \\ & \quad \left. - \mathcal{E}_o \left(t^{n+1/2} - \frac{(k-1/2)\Delta z}{v_z} \right) \right] \end{aligned} \quad (11.158a)$$

$$\begin{aligned} V_k^{n+1} &= V_k^n - \frac{\Delta t}{\Delta z} c^{-1} \left(I_k^{n+1/2} - I_{k-1}^{n+1/2} \right) \\ &- d e_x \left[\mathcal{E}_o \left(t^{n+1} - \frac{(k-1)z}{v_z} \right) - \mathcal{E}_o \left(t^n - \frac{(k-1)z}{v_z} \right) \right] \end{aligned} \quad (11.158b)$$

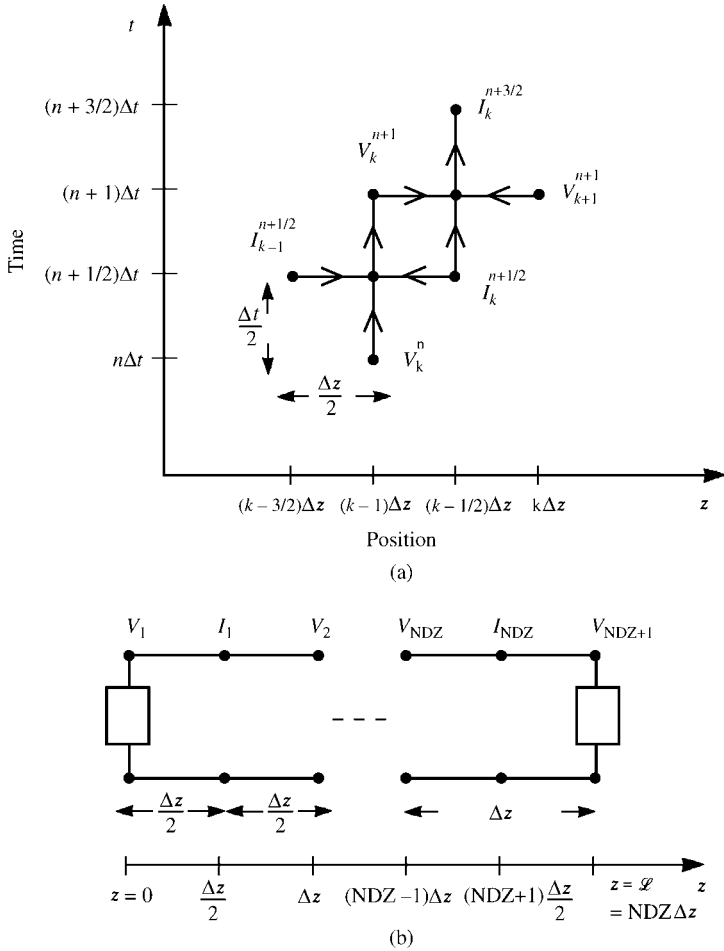


FIGURE 11.14 Spatial and temporal discretization of the two-conductor line for construction of the FDTD recursion relations.

Equations (11.158) are again solved in a leapfrog fashion. First, the voltages along the line are obtained, for a fixed time, from (11.158b) in terms of the previous solutions. Then, the currents are obtained from (11.158a) in terms of the voltages from (11.158b) as well as previously obtained values. The solution starts with an initially relaxed line having zero voltage and current values.

Next, consider the incorporation of the terminal conditions. The essential problem in incorporating the terminal conditions is that the FDTD voltages and currents at each end of the line, V_1, I_1 and V_{NDZ+1}, I_{NDZ} , are not collocated in space or time, whereas the terminal conditions relate the voltage and current at the same position and at the same time. We will denote the current at the source ($z = 0$) as I_S and the current

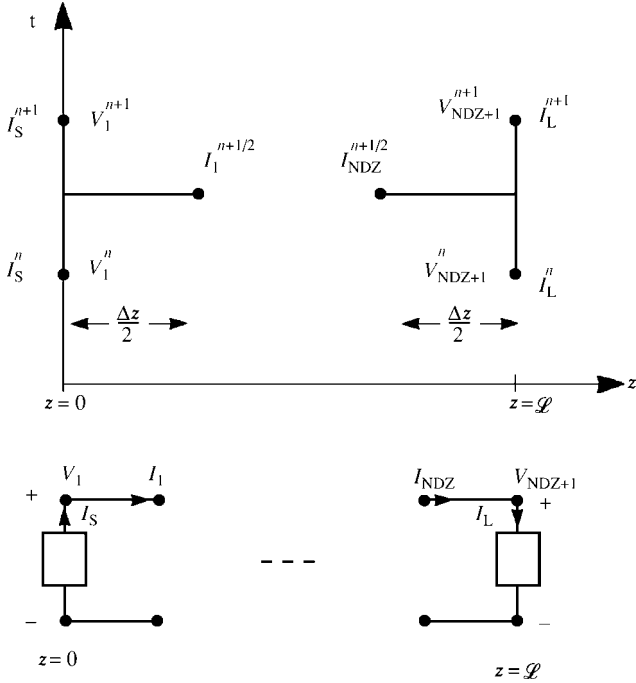


FIGURE 11.15 Spatial and temporal discretization of the two-conductor line at the source and the load ends.

at the load ($z = L$) as I_L as shown in Figure 11.15. The second transmission-line equation given in Eq. (11.145b) is discretized at the source as

$$\begin{aligned} \frac{1}{\Delta z/2} \left[I_1^{n+1/2} - \frac{(I_S^{n+1} + I_S^n)}{2} \right] + \frac{1}{\Delta t} c [V_1^{n+1} - V_1^n] \\ = -c \frac{d}{\Delta t} e_x \left[\mathcal{E}_o(t^{n+1}) - \mathcal{E}_o(t^n) \right] \end{aligned} \quad (11.159a)$$

Similarly, the second transmission-line equation, (11.145b), is discretized at the load as

$$\begin{aligned} \frac{1}{\Delta z/2} \left[\frac{(I_L^{n+1} + I_L^n)}{2} - I_{NDZ}^{n+1/2} \right] + \frac{1}{\Delta t} c [V_{NDZ+1}^{n+1} - V_{NDZ+1}^n] \\ - c \frac{d}{\Delta t} e_x \left[\mathcal{E}_o \left(t^{n+1} - \frac{L = NDZ \Delta z}{v_z} \right) - \mathcal{E}_o \left(t^n - \frac{L = NDZ \Delta z}{v_z} \right) \right] \end{aligned} \quad (11.159b)$$

Equations (11.159) are solved to give the recursion relations at the source and the load:

$$V_1^{n+1} = V_1^n - \frac{2\Delta t}{\Delta z} c^{-1} I_1^{n+1/2} + \frac{\Delta t}{\Delta z} c^{-1} \left[I_S^{n+1} + I_S^n \right] - d e_x \left[\mathcal{E}_o(t^{n+1}) - \mathcal{E}_o(t^n) \right] \quad (11.160a)$$

$$V_{\text{NDZ}+1}^{n+1} = V_{\text{NDZ}+1}^n + \frac{2\Delta t}{\Delta z} c^{-1} I_{\text{NDZ}}^{n+1/2} - \frac{\Delta t}{\Delta z} c^{-1} \left[I_{\mathcal{L}}^{n+1} + I_{\mathcal{L}}^n \right] - d e_x \left[\mathcal{E}_o \left(t^{n+1} - \frac{\mathcal{L} = \text{NDZ } \Delta z}{v_z} \right) - \mathcal{E}_o \left(t^n - \frac{\mathcal{L} = \text{NDZ } \Delta z}{v_z} \right) \right] \quad (11.160b)$$

In the case of resistive terminations, the terminal characterizations are written in terms of a generalized Thevenin equivalent as

$$V_1 = V_S - R_S I_S \quad (11.161a)$$

$$V_{\text{NDZ}+1} = V_L + R_L I_L \quad (11.161b)$$

Inverting these gives

$$I_S = -G_S V_1 + G_S V_S \quad (11.162a)$$

$$I_L = G_L V_{\text{NDZ}+1} - G_L V_L \quad (11.162b)$$

Substituting (11.162) into Eq. (11.160) gives the recursion relations for V_1 and $V_{\text{NDZ}+1}$:

$$V_1^{n+1} = \left(\frac{\Delta z}{\Delta t} R_S c + 1 \right)^{-1} \left\{ \left(\frac{\Delta z}{\Delta t} R_S c - 1 \right) V_1^n - 2R_S I_1^{n+1/2} + \left(V_S^{n+1} + V_S^n \right) - d e_x \frac{\Delta z}{\Delta t} R_S c \left[\mathcal{E}_o(t^{n+1}) - \mathcal{E}_o(t^n) \right] \right\} \quad (11.163a)$$

and

$$V_{\text{NDZ}+1}^{n+1} = \left(\frac{\Delta z}{\Delta t} R_L c + 1 \right)^{-1} \left\{ \left(\frac{\Delta z}{\Delta t} R_L c - 1 \right) V_{\text{NDZ}+1}^n + 2R_L I_{\text{NDZ}}^{n+1/2} + \left(V_L^{n+1} + V_L^n \right) - d e_x \frac{\Delta z}{\Delta t} R_L c \left[E_o \left(t^{n+1} - \frac{\mathcal{L} = \text{NDZ } \Delta z}{v_z} \right) - \mathcal{E}_o \left(t^n - \frac{\mathcal{L} = \text{NDZ } \Delta z}{v_z} \right) \right] \right\} \quad (11.163b)$$

and the voltages at the interior points are determined from (11.158b)

$$V_k^{n+1} = V_k^n - \frac{\Delta t}{\Delta z} c^{-1} \left(I_k^{n+1/2} - I_{k-1}^{n+1/2} \right) - d e_x \left[\mathcal{E}_o \left(t^{n+1} - \frac{(k-1)z}{v_z} \right) - \mathcal{E}_o \left(t^n - \frac{(k-1)z}{v_z} \right) \right] \quad (11.163c)$$

for $k = 2, 3, \dots, \text{NDZ}$. Equations (11.163) are first solved for the voltages and then the currents are determined from those voltages using (11.158a) as

$$I_k^{n+3/2} = I_k^{n+1/2} - \frac{\Delta t}{\Delta z} l^{-1} \left\{ (V_{k+1}^{n+1} - V_k^{n+1}) + d l^{-1} \left(\frac{1}{v_z} e_x - \frac{1}{v_x} e_z \right) \left[\mathcal{E}_o \left(t^{n+3/2} - \frac{(k-1/2)\Delta z}{v_z} \right) - \mathcal{E}_o \left(t^{n+1/2} - \frac{(k-1/2)\Delta z}{v_z} \right) \right] \right\} \quad (11.163d)$$

for $k = 1, 2, 3, \dots, \text{NDZ}$. Once again, for stability the position and time discretizations must satisfy the Courant conditions:

$$\Delta t \leq \frac{\Delta z}{v} \quad (11.164)$$

The FDTD method described in this section is implemented in the FORTRAN code FDTDINC.FOR that is described in Appendix A.

11.3.6 Computed Results

In order to illustrate the accuracy of models we have derived and to provide an understanding of the relationship between the time-domain parameters of the incident field waveform $\mathcal{E}_o(t)$, such as rise/fall time, we will consider the example shown in Figure 11.16(a). A wire of radius $r_w = 10$ mils and length $\mathcal{L} = 1$ m is suspended at a height of $h = 2$ cm above an infinite ground plane. The terminations are resistive with $R_S = 500 \Omega$ and $R_L = 1000 \Omega$. The incident uniform plane wave is incident from above, $\theta_E = 0^\circ$, $\theta_p = 0^\circ$, and $\phi_p = 0^\circ$, so that $e_x = 0$, $e_z = 1$, $v_x = -v$, and $v_z = \infty$. The time-domain waveform of the incident electric field $\mathcal{E}_o(t)$ is in the form of a trapezoidal periodic pulse train of repetition frequency 1 MHz and has a 1 V/m amplitude and a 50% duty cycle and various rise times. We will look at the time during the rise time of the pulse shown in Figure 11.16(b). The line characteristic impedance is $Z_C = 303.56 \Omega$, and the line one-way delay is $T_D = 3.33$ ns. We will consider three cases for the rise time: $\tau_r = 50$ ns, $\tau_r = 10$ ns, $\tau_r = 1$ ns. This will illustrate cases where the rise time is greater than or less than the line one-way delay. We will determine the induced voltage at the left end of the line, $V(0, t)$.

We will compare the predictions of four models: (1) the SPICE model described in the previous section and illustrated in Figure 11.13, (2) the series solution given

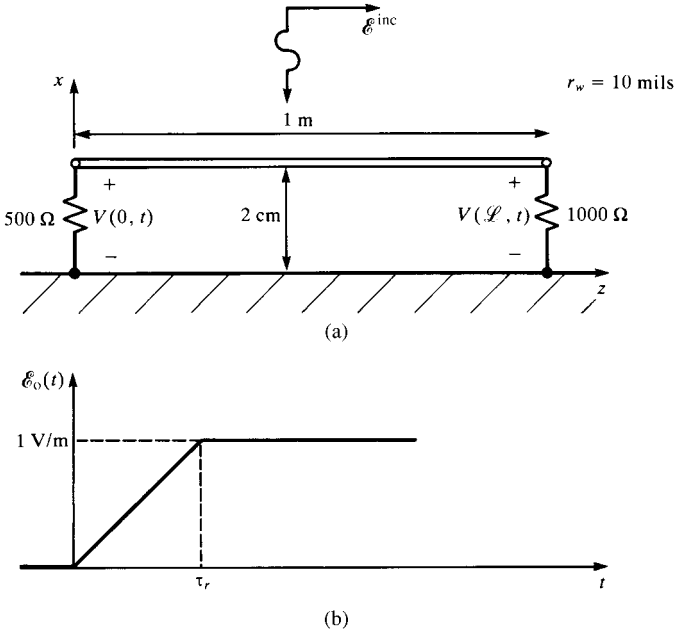


FIGURE 11.16 Characterization of a two-conductor line above a ground plane for illustration of numerical results.

by (11.118) using seven terms where $V^+(t)$ and $V^-(t)$ are given in (11.140), (3) the TDFD method, and (4) the FDTD method. For the SPICE model, the conductor separation d in (11.143) is replaced by $2h$ since the problem is above a ground plane for reasons discussed previously. The SPICE/PSPICE subcircuit model is generated with the FORTRAN code `SPICEINC.FOR`. The TDFD transformation technique simply views the problem as a two-port with $\mathcal{E}_o(t)$ as the input and $V(0, t)$ as the output. The incident waveform $\mathcal{E}_o(t)$ is modeled as a 1 MHz periodic trapezoidal waveform with equal rise and fall times. The frequency of this waveform is sufficiently long with respect to the transient behavior of the result that the response to the leading edge should be the same as to the actual waveform. The frequency-domain transfer function was computed at the various harmonics of the basic repetition rate of 1 MHz using the frequency-domain code `INCIDENT.FOR` described in Appendix A. It could also be computed using PSPICE by generating the SPICE subcircuit model using the FORTRAN code `SPICEINC.FOR` and running the code in the `.AC` mode. In fact, the author computed the frequency-domain transfer functions both ways and compared the results. Both codes gave virtually identical results. These values of the frequency-domain transfer functions at the various harmonics of 1 MHz were combined with the spectral amplitudes and phase angles of the periodic waveform $\mathcal{E}_o(t)$ using the code `TIMEFREQ.FOR`. The FDTD solution divides the line into NDZ discrete sections and the time variable into NDT divisions. The FDTD results were obtained with the `FDTDINC.FOR` code described in Appendix A.

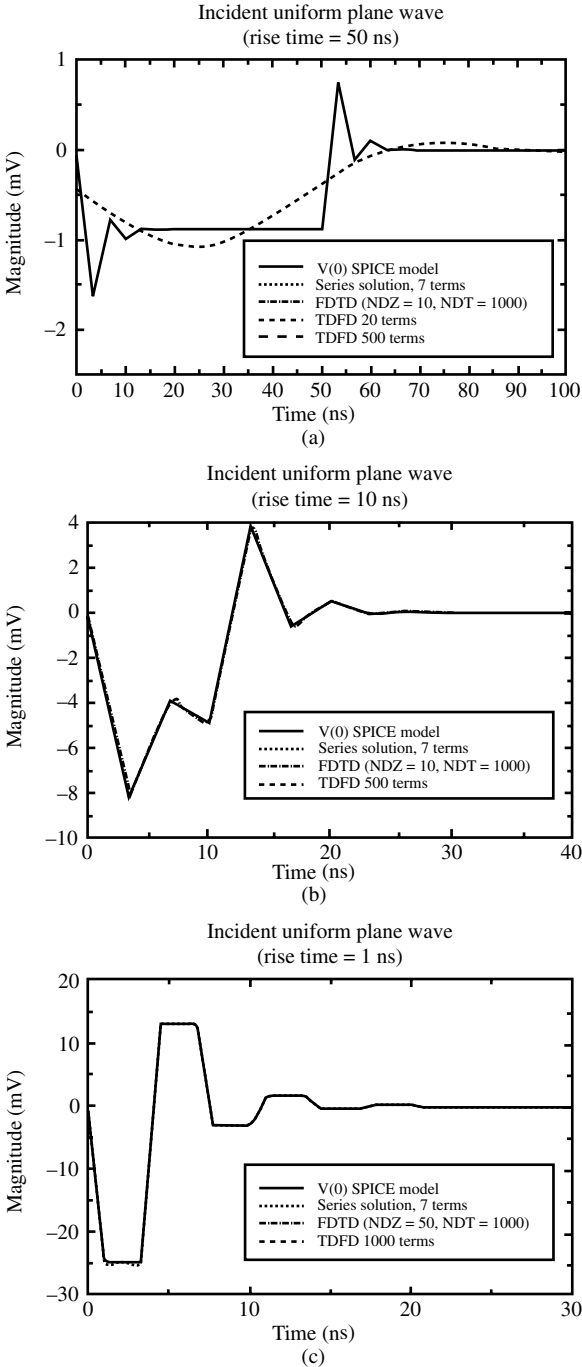


FIGURE 11.17 Predictions of the time-domain near-end voltage of the line of Figure 11.16 using the SPICE model, the series solution, the time-domain to frequency-domain transformation method, and the FDTD method for pulse rise times of (a) 50 ns, (b) 10 ns, and (c) 1 ns.

Figure 11.17(a) shows the result for a rise time of $\tau_r = 50$ ns. The SPICE model and the series result in (11.118) using seven terms give essentially the same results. The bandwidth of the input pulse $\mathcal{E}_o(t)$ is approximately $1/\tau_r = 20$ MHz. Hence, we may think we only need 20 harmonics for the TDFD method to give accurate results. Figure 11.17(a) shows that using only 20 harmonics (spectral content up to 20 MHz) gives a very poor representation of the output waveform. Looking at the SPICE result, we see why this is the case. The output waveform has regions where the rise/fall times are on the order of 3 ns! Hence, in order to reproduce the output pulse, it is this minimum rise/fall time that needs to be considered. Hence, the output waveform contains frequencies up to around $1/3$ ns = 333 MHz. Hence, we have used 500 harmonics, 1 MHz, 2 MHz, 3 MHz, . . . , 500 MHz, in the TDFD transformation method with `TIMEFREQ.FOR`. This gives excellent predictions. The FDTD method likewise requires the spatial discretization Δz to be electrically small at the highest spectral content of *the output pulse waveform* that is around 333 MHz! This requires that we choose $\text{NDZ} = 10$ in which case the cell lengths, $\Delta z = 0.1$ m, are $\lambda/9$ at 333 MHz. In order to satisfy the Courant stability condition in (11.164), it requires that

$$\text{NDT} > \text{NDZ} \times \text{final time} \times \frac{v}{\text{line length}} = 300$$

We will choose $\text{NDT} = 1000$ in order to satisfy the Courant condition and give sufficient detail in the solution. Observe that the FDTD method using the FORTRAN code `FDTDINC.FOR` described in Appendix A gives exceptionally good results.

Figure 11.17(b) shows the result for a rise time of $\tau_r = 10$ ns. The SPICE model and the series result in (11.118) using seven terms give essentially the same results. Again we see that the output waveform has regions where the rise/fall time of the waveform is on the order of 3 ns again. Hence, we choose 500 harmonics to be processed by the TDFD method using `TIMEFREQ.FOR`. Similarly, we choose $\text{NDZ} = 10$ and $\text{NDT} = 1000$ in the FDTD method using `FDTDINC.FOR`. Figure 11.17(b) shows that the FDTD, TDFD, and SPICE methods give virtually identical results.

Figure 11.17(c) shows the result for a rise time of $\tau_r = 1$ ns. The SPICE model and the series result in (11.118) using seven terms give essentially the same results. Observing the SPICE-predicted output waveform we see that it contains regions where the rise/fall times are on the order of 1 ns. Hence, the spectral content of the output waveform goes up to the order of 1 GHz. Hence, we use 1000 harmonics in the TDFD result and $\text{NDZ} = 50$ and $\text{NDT} = 1000$ in the FDTD result. This gives a subsection length of $\Delta z = 2$ cm, which is $\lambda/15$ at 1 GHz. Figure 11.17(c) shows that the FDTD, TDFD, and SPICE methods give virtually identical results.

PROBLEMS

- 11.1** Derive the transmission-line equations in (11.20) from the per-unit-length equivalent circuit in Figure 11.3.

- 11.2** Verify the equivalent source given in (11.23).
- 11.3** Verify that the solution to the state-variable equations in (11.25) is given by (11.26).
- 11.4** Verify the relations for the alternative sources given in (11.37).
- 11.5** Demonstrate the equivalence of the sources given in (11.44) and (11.45)).
- 11.6** Verify, by direct substitution, the terminal solutions in (11.48).
- 11.7** Verify the solutions for the terminal line currents given in (11.53).
- 11.8** Derive the relations for the components of the uniform plane wave given in (11.55) and the phase constants given in (11.56).
- 11.9** Verify the source terms in (11.63) and (11.64).
- 11.10** Verify the terminal current solutions for uniform plane-wave sources given in (11.65).
- 11.11** Verify the special cases given in (11.68), (11.73), and (11.77), and (11.77).
- 11.12** Verify the electric field relations for a conductor above a ground plane given in (11.81).
- 11.13** Verify the relations for the terminal currents given in (11.82).
- 11.14** Use SPICEINC . FOR to verify the results in Figures 11.9–11.11.
- 11.15** Verify the time-domain results in (11.105).
- 11.16** Verify (11.108).
- 11.17** Verify the recursive solution in (11.113).
- 11.18** Verify the series solution in (11.118).
- 11.19** Verify the relations in (11.140).
- 11.20** Verify the SPICE equivalent circuit in Figure 11.13.
- 11.21** Verify (11.154).
- 11.22** Demonstrate the FDTD recursion relations in (11.163).
- 11.22** Use SPICEINC . FOR, the series solution in (11.118), TIMEFREQ . FOR, and FDTDINC . FOR to verify the results in Figure 11.17.

REFERENCES

- [1] C.D. Taylor, R.S. Satterwhite, and C.W. Harrison, The response of a terminated two-wire transmission line excited by a nonuniform electromagnetic field, *IEEE Transactions on Antennas and Propagation*, **13**, 987–989, 1965.
- [2] A.A. Smith, Jr., A more convenient form of the equations for the response of a transmission line excited by nonuniform fields, *IEEE Transactions on Electromagnetic Compatibility*, **15**, 151–152, 1973.
- [3] K.S.H. Lee, Two parallel terminated conductors in external fields, *IEEE Transactions on Electromagnetic Compatibility*, **20**(2), 288–295, 1978.
- [4] S. Frankel, Forcing functions for externally excited transmission lines, *IEEE Transactions on Electromagnetic Compatibility*, **22**(3), 210, 1980.

- [5] A.A. Smith, *Coupling of External Electromagnetic Fields to Transmission Lines*, 2nd edition, Interference Control Technologies, Inc., 1987.
- [6] C.D. Taylor and J.P. Castillo, On the response of a terminated twisted-wire cable excited by a plane-wave electromagnetic field, *IEEE Transactions on Electromagnetic Compatibility*, **22**(1), 16–19, 1980.
- [7] E.F. Vance, *Coupling to Shielded Cables*, John Wiley & Sons, Inc., New York, 1978.
- [8] Y. Leviatan and A.T. Adams, The response of a two-wire transmission line to incident field and voltage excitation, including the effects of higher order modes, *IEEE Transactions on Antennas and Propagation*, **30**(5), 998–1003, 1982.
- [9] K. Ogata, *State Space Analysis of Control Systems*, Prentice-Hall, Englewood Cliffs, NJ, 1967.
- [10] C.T. Chen, *Linear System Theory and Design*, Holt, Rinehart, and Winston, New York, 1984.
- [11] J.H. Richmond, Radiation and scattering by thin-wire structures in the complex frequency domain, Interaction Notes, Note 202, Air Force Weapons Laboratory, Kirtland Air Force Base, Albuquerque, NM, May 1974.
- [12] J.H. Richmond, Computer program for thin-wire structures in a homogeneous conducting medium, Technical Report, NASA CR-2399, National Aeronautics and Space Administration, Washington, DC, 1974.

12

INCIDENT FIELD EXCITATION OF MULTICONDUCTOR LINES

The previous chapter was devoted to the analysis of two-conductor lines excited by an incident electromagnetic field that was generally in the form of a uniform plane wave. In this chapter, we will extend that analysis to multiconductor transmission lines (MTLs). Virtually all of the two-conductor line results in the previous chapter can be extended rather straightforwardly to the case of MTLs using matrix notation.

The derivation and solution of the MTL equations was considered in [H.1–H.5] and in [1–5]. A SPICE model for their solution was given in [H.10]. The MTL equations that we will obtain will be solved and the termination networks incorporated into that general solution in the usual fashion in order to determine the line currents *at the ends of the line*. The currents that are modeled with these MTL equations are, once again, *differential-mode* or *transmission-line currents* in that the sum of the currents directed in the $+z$ direction on all $n + 1$ conductors is *zero* at any line cross section. In other words, the differential-mode currents of n of the conductors “return” on the reference conductor. In addition to these differential-mode currents, there can exist certain common-mode or antenna-mode currents that are not modeled by the MTL equations, as discussed in Chapter 1 [6]. So at points along the line there will be a combination of both currents, only one component of which (the differential mode) will be modeled by the MTL equations that we will develop. If the MTL cross section is electrically small at the frequency of interest, the total current at the terminations is that predicted by the MTL equations. This is because, for a line with electrically small cross-sectional dimensions, we can surround each termination with

a closed surface (approximately a “node” in lumped-circuit analysis terminology), and Kirchoff’s current law shows that the total current entering this closed surface must be zero. Therefore, at the terminations of a line having electrically small cross-sectional dimensions, the total current at the terminations must sum to zero (differential-mode or transmission-line current) so that the common-mode current not predicted by the MTL equations must go to zero at the terminations and is therefore of no importance in predicting the terminal responses of an MTL [6]. This also applies to crosstalk on MTLs that have electrically small cross-sectional dimensions. Common-mode currents are important in modeling radiated emissions or for determining currents at some intermediate point along the line such as a folded dipole antenna. Therefore, the MTL equations we will obtain provide the complete prediction of the *terminal response* of an MTL that satisfies the necessary requirement of electrically small cross-sectional dimensions.

12.1 DERIVATION OF THE MTL EQUATIONS FOR INCIDENT FIELD EXCITATION

Consider an $(n + 1)$ -conductor uniform MTL where the conductors are parallel to the z axis as shown in Figure 12.1. In order to derive the first MTL equation, we again integrate Faraday’s law around the contour c_i between the reference conductor and the i th conductor enclosing surface s_i in the clockwise direction as shown in Figure 7.1:

$$\oint_{c_i} \vec{\mathcal{E}} \cdot d\vec{l} = \frac{d}{dt} \int_{s_i} \vec{\mathcal{B}} \cdot d\vec{s} \tag{12.1}$$

or

$$\int_a^{a'} \vec{\mathcal{E}}_t \cdot d\vec{l} + \int_{a'}^{b'} \vec{\mathcal{E}}_1 \cdot d\vec{l} + \int_{b'}^b \vec{\mathcal{E}}_t \cdot d\vec{l} + \int_b^a \vec{\mathcal{E}}_1 \cdot d\vec{l} = \frac{d}{dt} \int_{s_i} \vec{\mathcal{B}} \cdot \vec{a}_n ds \tag{12.2}$$

where $\vec{\mathcal{E}}_t$ is the transverse electric field in the x - y cross-sectional plane and $\vec{\mathcal{E}}_1$ is the longitudinal or z -directed electric field along the surfaces of the conductors. Observe that again the negative sign is absent from the right-hand side of Faraday’s law here because of the choice of the direction of the contour c_i and the normal \vec{a}_n to the enclosed surface s_i . Again, it is necessary to distinguish between *incident* and *scattered* field quantities. The incident field is that produced by the distant or nearby source *in the absence of the line conductors*. The scattered fields are produced by the currents and charges that are induced on the line conductors. The total field is the sum of a

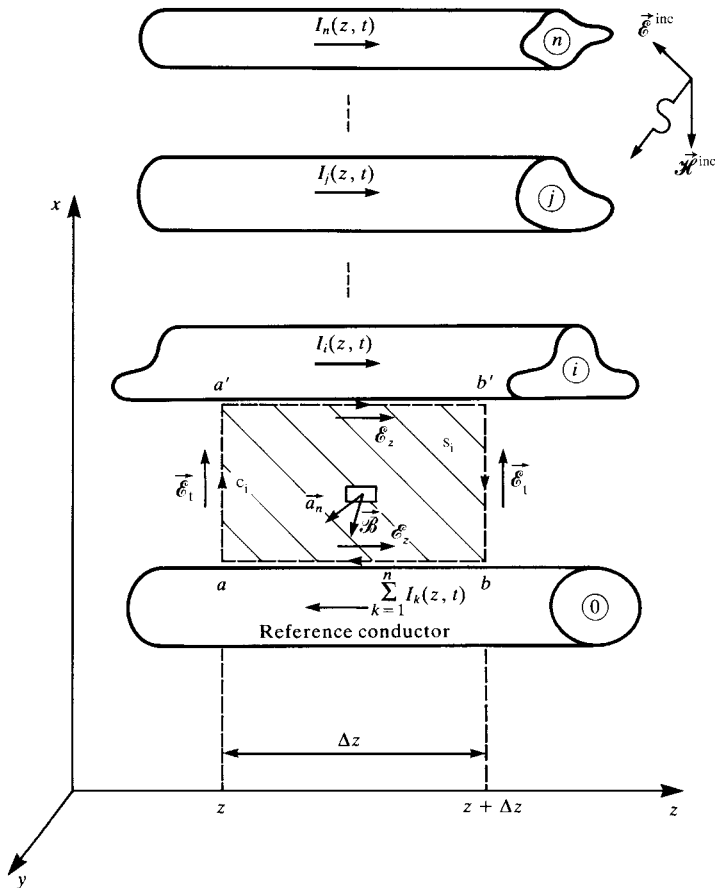


FIGURE 12.1 Definition of the contour for the derivation of the first MTL equation for incident field illumination.

scattered and an incident component as

$$\begin{aligned}
 \vec{\mathcal{E}}_t(x, y, z, t) &= \vec{\mathcal{E}}_t^{\text{inc}}(x, y, z, t) + \vec{\mathcal{E}}_t^{\text{scat}}(x, y, z, t) \\
 \vec{\mathcal{E}}_1(x, y, z, t) &= \vec{\mathcal{E}}_1^{\text{inc}}(x, y, z, t) + \vec{\mathcal{E}}_1^{\text{scat}}(x, y, z, t) \\
 \vec{\mathcal{B}}(x, y, z, t) &= \vec{\mathcal{B}}^{\text{inc}}(x, y, z, t) + \vec{\mathcal{B}}^{\text{scat}}(x, y, z, t)
 \end{aligned}
 \tag{12.3}$$

where superscript *inc* denotes *incident* and superscript *scat* denotes *scattered*. There are some important assumptions that need to be stated. First, we assume that the currents on the conductors are z directed. Therefore, the scattered magnetic fields will lie entirely in the transverse plane. Since there is no z -directed $\vec{\mathcal{B}}^{\text{scat}}$ field, Faraday's

law shows that we may uniquely define the *scattered voltage* between the *i*th conductor and the reference conductor independent of path in the transverse plane as

$$V_i^{\text{scat}}(z, t) = - \int_a^{a'} \vec{\mathcal{E}}_t^{\text{scat}} \cdot d\vec{l} \tag{12.4a}$$

$$V_i^{\text{scat}}(z + \Delta z, t) = - \int_b^{b'} \vec{\mathcal{E}}_t^{\text{scat}} \cdot d\vec{l} \tag{12.4b}$$

Second, because of the transverse nature of the scattered magnetic field, the scattered magnetic field can be related to the currents that produced it with the usual per-unit-length inductances as

$$\lim_{\Delta z \rightarrow 0} \frac{1}{\Delta z} \int_{s_i} \vec{\mathcal{B}}^{\text{scat}} \cdot \vec{a}_n ds = - [l_{i1} \quad \cdots \quad l_{ii} \quad \cdots \quad l_{in}] \begin{bmatrix} I_1(z, t) \\ \vdots \\ I_i(z, t) \\ \vdots \\ I_n(z, t) \end{bmatrix} \tag{12.5}$$

Again, we represent the imperfect conductors with per-unit-length resistances r_i . Although these will be functions of frequency due to skin effect, let us for the moment assume they are constant with the assurance that the frequency-domain result will handle this dependence. The *total* longitudinal fields are related to the currents on the conductors as

$$- \int_a^{b'} \vec{\mathcal{E}}_1 \cdot d\vec{l} = - \int_a^{b'} \mathcal{E}_z dz = -r_i \Delta z I_i(z, t) \tag{12.6a}$$

$$- \int_b^a \vec{\mathcal{E}}_1 \cdot d\vec{l} = - \int_b^a \mathcal{E}_z dz = -r_0 \Delta z \sum_{k=1}^n I_k(z, t) \tag{12.6b}$$

Substituting (12.3–12.6) into (12.2), dividing by Δz , and taking the limit as $\Delta z \rightarrow 0$ yields

$$\frac{\partial}{\partial z} V_i^{\text{scat}}(z, t) + [r_0 \quad \cdots \quad r_i + r_0 \quad \cdots \quad r_0] \begin{bmatrix} I_1(z, t) \\ \vdots \\ I_i(z, t) \\ \vdots \\ I_n(z, t) \end{bmatrix}$$

$$\begin{aligned}
 & + \frac{\partial}{\partial t} [l_{i1} \quad \cdots \quad l_{ii} \quad \cdots \quad l_{in}] \begin{bmatrix} I_1(z, t) \\ \vdots \\ I_i(z, t) \\ \vdots \\ I_n(z, t) \end{bmatrix} \\
 & = \frac{\partial}{\partial z} \int_a^{a'} \vec{\mathcal{E}}_t^{\text{inc}} \cdot d\vec{l} + \frac{\partial}{\partial t} \int_a^{a'} \vec{\mathcal{B}}^{\text{inc}} \cdot \vec{a}_n dl
 \end{aligned} \tag{12.7}$$

Repeating this for the other conductors and arranging in matrix form gives

$$\frac{\partial}{\partial z} \mathbf{V}^{\text{scat}}(z, t) + \mathbf{R} \mathbf{I}(z, t) + \mathbf{L} \frac{\partial}{\partial t} \mathbf{I}(z, t) = \begin{bmatrix} \vdots \\ \frac{\partial}{\partial z} \int_a^{a'} \vec{\mathcal{E}}_t^{\text{inc}} \cdot d\vec{l} + \frac{\partial}{\partial t} \int_a^{a'} \vec{\mathcal{B}}^{\text{inc}} \cdot \vec{a}_n dl \\ \vdots \end{bmatrix} \tag{12.8}$$

Observe that the voltages in this expression are the *scattered voltages* and not the *total voltages*.

The second MTL equation can similarly be derived as in Chapter 3 by enclosing the i th conductor with a closed surface as illustrated in Figure 12.2 applying the continuity equation:

$$\oint_{s'_i} \vec{\mathcal{J}} \cdot d\vec{s}' = -\frac{\partial}{\partial t} Q_{\text{enc}} \tag{12.9}$$

Over the end caps, we have

$$\iint_{s'_e} \vec{\mathcal{J}} \cdot d\vec{s}' = I_i(z + \Delta z, t) - I_i(z, t) \tag{12.10}$$

where s'_e is the surface over the end caps. Although there are some subtleties involved [1], we again define the per-unit-length conductance and capacitance matrices in terms of the *scattered voltages* as

$$I_{ii}(z, t) = \lim_{\Delta z \rightarrow 0} \frac{1}{\Delta z} \iint_{s'_e} \vec{\mathcal{J}} \cdot d\vec{s}' = \begin{bmatrix} -g_{i1} & \cdots & \sum_{k=1}^n g_{ik} & \cdots & -g_{in} \end{bmatrix} \begin{bmatrix} V_1^{\text{scat}}(z, t) \\ \vdots \\ V_i^{\text{scat}}(z, t) \\ \vdots \\ V_n^{\text{scat}}(z, t) \end{bmatrix} \tag{12.11}$$

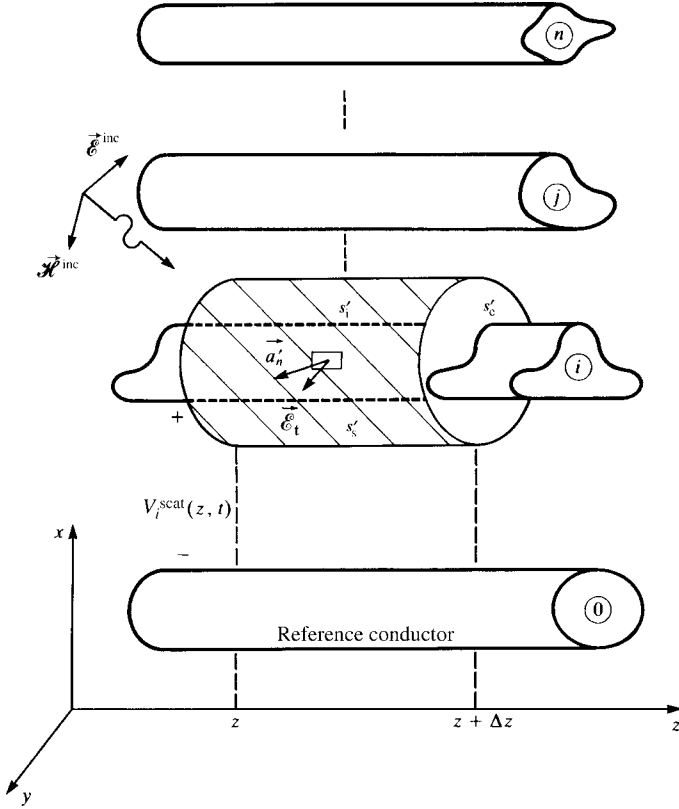


FIGURE 12.2 Definition of the surface for the derivation of the second MTL equation for incident field illumination.

where $I_{ij}(z, t)$ is the transverse conduction current between the i th conductor and all other conductors and s'_s is the surface of the sides. Also,

$$\lim_{\Delta z \rightarrow 0} \frac{Q_{enc}}{\Delta z} = \begin{bmatrix} -c_{i1} & \cdots & \sum_{k=1}^n c_{ik} & \cdots & -c_{in} \end{bmatrix} \begin{bmatrix} V_1^{scat}(z, t) \\ \vdots \\ V_i^{scat}(z, t) \\ \vdots \\ V_n^{scat}(z, t) \end{bmatrix} \quad (12.12)$$

Substituting (12.10–12.12) into (12.9), dividing both sides of this result by Δz , and taking the limit as $\Delta z \rightarrow 0$ yields the second MTL equation in matrix form as

$$\frac{\partial}{\partial z} \mathbf{I}(z, t) + \mathbf{G} \mathbf{V}^{scat}(z, t) + \mathbf{C} \frac{\partial}{\partial t} \mathbf{V}^{scat}(z, t) = \mathbf{0} \quad (12.13)$$

The above results are in terms of the *scattered voltages*. They can be placed in terms of the *total voltages* by writing the total voltages in terms of the total electric field as

$$V_i(z, t) = - \int_a^{a'} \vec{\mathcal{E}}_t \cdot d\vec{l} = V_i^{\text{scat}}(z, t) - \int_a^{a'} \vec{\mathcal{E}}_t^{\text{inc}} \cdot d\vec{l} \quad (12.14)$$

Substituting this into (12.8) and (12.13) gives the MTL equations in terms of the *total voltages* as

$$\frac{\partial}{\partial z} \mathbf{V}(z, t) + \mathbf{R} \mathbf{I}(z, t) + \mathbf{L} \frac{\partial}{\partial t} \mathbf{I}(z, t) = \frac{\partial}{\partial t} \begin{bmatrix} \vdots \\ \int_a^{a'} \vec{\mathcal{E}}_t^{\text{inc}} \cdot \vec{a}_n dl \\ \vdots \end{bmatrix} \quad (12.15a)$$

$$\frac{\partial}{\partial z} \mathbf{I}(z, t) + \mathbf{G} \mathbf{V}(z, t) + \mathbf{C} \frac{\partial}{\partial t} \mathbf{V}(z, t) = -\mathbf{G} \begin{bmatrix} \vdots \\ \int_a^{a'} \vec{\mathcal{E}}_t^{\text{inc}} \cdot d\vec{l} \\ \vdots \end{bmatrix} - \mathbf{C} \frac{\partial}{\partial t} \begin{bmatrix} \vdots \\ \int_a^{a'} \vec{\mathcal{E}}_t^{\text{inc}} \cdot d\vec{l} \\ \vdots \end{bmatrix} \quad (12.15b)$$

where the $n \times 1$ vectors of the n line voltages and currents are

$$\mathbf{V}(z, t) = \begin{bmatrix} V_1(z, t) \\ \vdots \\ V_i(z, t) \\ \vdots \\ V_n(z, t) \end{bmatrix} \quad (12.16a)$$

and

$$\mathbf{I}(z, t) = \begin{bmatrix} I_1(z, t) \\ \vdots \\ I_i(z, t) \\ \vdots \\ I_n(z, t) \end{bmatrix} \quad (12.16b)$$

12.1.1 Equivalence of Source Representations

Evidently, (12.15) again shows that incident electromagnetic fields modify the MTL equations by adding *sources* to the usual MTL equations. The MTL equations in terms of *total voltages* given in (12.15) can be written as

$$\frac{\partial}{\partial z} \mathbf{V}(z, t) + \mathbf{R} \mathbf{I}(z, t) + \mathbf{L} \frac{\partial}{\partial t} \mathbf{I}(z, t) = \mathbf{V}_F(z, t) \quad (12.17a)$$

$$\frac{\partial}{\partial z} \mathbf{I}(z, t) + \mathbf{G} \mathbf{V}(z, t) + \mathbf{C} \frac{\partial}{\partial t} \mathbf{V}(z, t) = \mathbf{I}_F(z, t) \quad (12.17b)$$

where

$$\mathbf{V}_F(z, t) = \frac{\partial}{\partial t} \begin{bmatrix} \vdots \\ \int_a^{a'} \vec{\mathcal{B}}^{\text{inc}} \cdot \vec{a}_n dl \\ \vdots \end{bmatrix} \quad (12.18a)$$

$$\mathbf{I}_F(z, t) = -\mathbf{G} \begin{bmatrix} \vdots \\ \int_a^{a'} \vec{\mathcal{E}}_t^{\text{inc}} \cdot d\vec{l} \\ \vdots \end{bmatrix} - \mathbf{C} \frac{\partial}{\partial t} \begin{bmatrix} \vdots \\ \int_a^{a'} \vec{\mathcal{E}}_t^{\text{inc}} \cdot d\vec{l} \\ \vdots \end{bmatrix} \quad (12.18b)$$

Thus, the *sources* are the component of the incident magnetic field *normal* to the *i*th circuit as shown in (12.18a) and the component of the incident electric field *transverse* to the *i*th circuit as shown in (12.18b). The *i*th *circuit* is the surface bounded by the *i*th conductor and the reference conductor between *z* and *z* + Δ*z*. These MTL equations can be derived from the per-unit-length equivalent circuit shown in Figure 12.3.

The equivalent per-unit-length sources in (12.18) are due to both the incident electric field and the incident magnetic field. These can be written in terms of only the incident electric field by recognizing that the transverse and longitudinal electric fields and the normal magnetic fields are related by Faraday's law. This can be shown by writing Faraday's law around the contour in terms of the *incident* fields, dividing both sides of the result by Δ*z*, and taking the limit as Δ*z* → 0 to give

$$\begin{aligned} -\frac{\partial}{\partial z} \int_a^{a'} \vec{\mathcal{E}}_t^{\text{inc}} \cdot d\vec{l} + \mathcal{E}_z^{\text{inc}}(\textit{i}th \textit{conductor}, z, t) \\ - \mathcal{E}_z^{\text{inc}}(\textit{reference conductor}, z, t) = \frac{\partial}{\partial t} \int_a^{a'} \vec{\mathcal{B}}^{\text{inc}} \cdot \vec{a}_n dl \end{aligned} \quad (12.19)$$

where $\mathcal{E}_z^{\text{inc}}(m\textit{th conductor}, z)$ is the longitudinal or *z*-directed *incident* electric field along the position of the *m*th conductor *with the conductor removed*. Substituting

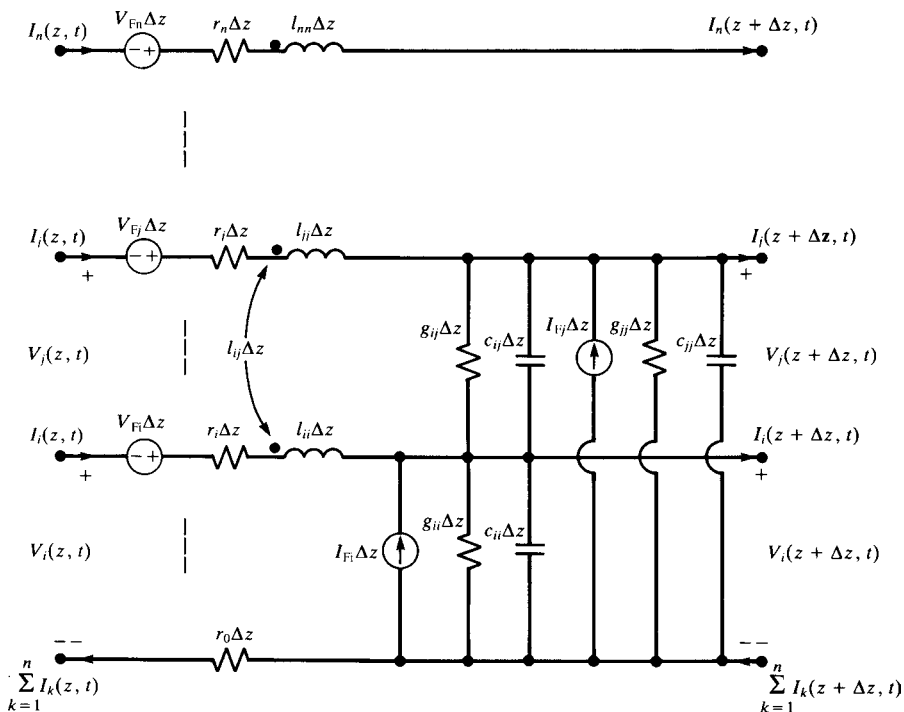


FIGURE 12.3 The per-unit-length equivalent circuit for an MTL with incident field illumination.

(12.19) into (12.18a) gives an alternate form of the source voltage as

$$\begin{aligned}
 \mathbf{V}_F(z, t) &= -\frac{\partial}{\partial z} \underbrace{\begin{bmatrix} \vdots \\ \int_a^{a'} \vec{\mathcal{E}}_t^{\text{inc}} \cdot d\vec{l} \\ \vdots \end{bmatrix}}_{\mathbf{E}_T} \\
 &+ \underbrace{\begin{bmatrix} \vdots \\ \mathcal{E}_z^{\text{inc}}(\textit{ith conductor}, z, t) - \mathcal{E}_z^{\text{inc}}(\textit{reference conductor}, z, t) \\ \vdots \end{bmatrix}}_{\mathbf{E}_L} \\
 &= -\frac{\partial}{\partial z} \mathbf{E}_T(z, t) + \mathbf{E}_L(z, t) \tag{12.20}
 \end{aligned}$$

12.2 FREQUENCY-DOMAIN SOLUTIONS

In the frequency domain, the phasor MTL equations become

$$\frac{d}{dz} \hat{\mathbf{V}}(z) = -\hat{\mathbf{Z}} \hat{\mathbf{I}}(z) + \hat{\mathbf{V}}_F(z) \tag{12.21a}$$

$$\frac{d}{dz} \hat{\mathbf{I}}(z) = -\hat{\mathbf{Y}} \hat{\mathbf{V}}(z) + \hat{\mathbf{I}}_F(z) \tag{12.21b}$$

where the $n \times n$ per-unit-length impedance and admittance matrices are

$$\hat{\mathbf{Z}} = \mathbf{R} + j\omega \mathbf{L} \tag{12.22a}$$

$$\hat{\mathbf{Y}} = \mathbf{G} + j\omega \mathbf{C} \tag{12.22b}$$

and the $n \times 1$ vectors of the incident field contributions are

$$\hat{\mathbf{V}}_F(z) = j\omega \begin{bmatrix} \vdots \\ \int_a^{a'} \vec{\hat{B}}^{\text{inc}} \cdot \vec{a}_n dl \\ \vdots \end{bmatrix} \tag{12.22c}$$

$$\hat{\mathbf{I}}_F(z) = -\hat{\mathbf{Y}} \begin{bmatrix} \vdots \\ \int_a^{a'} \vec{\hat{E}}_t^{\text{inc}} \cdot d\vec{l} \\ \vdots \end{bmatrix} \tag{12.22d}$$

where $\vec{\hat{B}}(x, y, z)$ and $\vec{\hat{E}}(x, y, z)$ denote the phasor fields. Alternatively, the forcing function $\hat{\mathbf{V}}_F(z)$ can be written in terms of the phasor incident electric field as in (12.20) as

$$\hat{\mathbf{V}}_F(z) = -\frac{\partial}{\partial z} \underbrace{\begin{bmatrix} \vdots \\ \int_a^{a'} \vec{\hat{E}}_t^{\text{inc}} \cdot d\vec{l} \\ \vdots \end{bmatrix}}_{\hat{\mathbf{E}}_T}$$

$$\begin{aligned}
 & + \underbrace{\left[\begin{array}{c} \hat{E}_z^{\text{inc}}(\textit{ith conductor}, z) - \hat{E}_z^{\text{inc}}(\textit{reference conductor}, z) \\ \vdots \\ \vdots \end{array} \right]}_{\hat{\mathbf{E}}_L} \\
 & = -\frac{\partial}{\partial z} \hat{\mathbf{E}}_T(z) + \hat{\mathbf{E}}_L(z) \quad (12.22e)
 \end{aligned}$$

Once again these can be written in state-variable form as a coupled set of first-order ordinary differential equations in matrix form as

$$\frac{d}{dz} \underbrace{\begin{bmatrix} \hat{\mathbf{V}}(z) \\ \hat{\mathbf{I}}(z) \end{bmatrix}}_{\hat{\mathbf{X}}(z)} = \underbrace{\begin{bmatrix} \mathbf{0} & -\hat{\mathbf{Z}} \\ -\hat{\mathbf{Y}} & \mathbf{0} \end{bmatrix}}_{\hat{\mathbf{A}}} \underbrace{\begin{bmatrix} \hat{\mathbf{V}}(z) \\ \hat{\mathbf{I}}(z) \end{bmatrix}}_{\hat{\mathbf{X}}(z)} + \begin{bmatrix} \hat{\mathbf{V}}_F(z) \\ \hat{\mathbf{I}}_F(z) \end{bmatrix} \quad (12.23)$$

Again, there are considerable advantages in writing the phasor MTL equations in this form as we showed in the previous chapter. In fact, drawing from the wealth of properties of the analogous solution for lumped linear systems, we can again immediately write the solution to these phasor MTL equations.

12.2.1 Solution of the MTL Equations

The solution to the phasor MTL equations given in (12.23) can again be immediately obtained by observing that they are directly analogous to the state-variable equations for lumped systems as was discussed in Chapter 11. Hence, the solution is again

$$\hat{\mathbf{X}}(z) = \hat{\Phi}(z - z_0) \hat{\mathbf{X}}(z_0) + \int_{z_0}^z \hat{\Phi}(z - \tau) \begin{bmatrix} \hat{\mathbf{V}}_F(\tau) \\ \hat{\mathbf{I}}_F(\tau) \end{bmatrix} d\tau \quad (12.24)$$

for $z \geq z_0$. Selecting $z = \mathcal{L}$ and $z = 0$ yields

$$\underbrace{\begin{bmatrix} \hat{\mathbf{V}}(\mathcal{L}) \\ \hat{\mathbf{I}}(\mathcal{L}) \end{bmatrix}}_{\hat{\mathbf{X}}(\mathcal{L})} = \underbrace{\begin{bmatrix} \hat{\Phi}_{11}(\mathcal{L}) & \hat{\Phi}_{12}(\mathcal{L}) \\ \hat{\Phi}_{21}(\mathcal{L}) & \hat{\Phi}_{22}(\mathcal{L}) \end{bmatrix}}_{\hat{\Phi}(\mathcal{L})} \underbrace{\begin{bmatrix} \hat{\mathbf{V}}(0) \\ \hat{\mathbf{I}}(0) \end{bmatrix}}_{\hat{\mathbf{X}}(0)} + \begin{bmatrix} \hat{\mathbf{V}}_{FT}(\mathcal{L}) \\ \hat{\mathbf{I}}_{FT}(\mathcal{L}) \end{bmatrix} \quad (12.25a)$$

where the total source voltages $\hat{\mathbf{V}}_{FT}(\mathcal{L})$ and $\hat{\mathbf{I}}_{FT}(\mathcal{L})$ are, according to (12.24),

$$\hat{\mathbf{V}}_{FT}(\mathcal{L}) = \int_0^{\mathcal{L}} [\hat{\Phi}_{11}(\mathcal{L} - \tau) \hat{\mathbf{V}}_F(\tau) + \hat{\Phi}_{12}(\mathcal{L} - \tau) \hat{\mathbf{I}}_F(\tau)] d\tau \quad (12.25b)$$

$$\hat{\mathbf{I}}_{\text{FT}}(\mathcal{L}) = \int_0^{\mathcal{L}} [\hat{\Phi}_{21}(\mathcal{L} - \tau)\hat{\mathbf{V}}_{\text{F}}(\tau) + \hat{\Phi}_{22}(\mathcal{L} - \tau)\hat{\mathbf{I}}_{\text{F}}(\tau)] dt \quad (12.25c)$$

and $\hat{\Phi}(\mathcal{L})$ is the $2n \times 2n$ chain-parameter matrix. From Chapter 7, the $n \times n$ chain-parameter submatrices are

$$\hat{\Phi}_{11}(\mathcal{L}) = \frac{1}{2}\hat{\mathbf{Y}}^{-1}\hat{\mathbf{T}}_I \left(\mathbf{e}^{\hat{\gamma}\mathcal{L}} + \mathbf{e}^{-\hat{\gamma}\mathcal{L}} \right) \hat{\mathbf{T}}_I^{-1}\hat{\mathbf{Y}} \quad (7.115a)$$

$$\hat{\Phi}_{12}(\mathcal{L}) = -\frac{1}{2}\hat{\mathbf{Y}}^{-1}\hat{\mathbf{T}}_I \hat{\gamma} \left(\mathbf{e}^{\hat{\gamma}\mathcal{L}} - \mathbf{e}^{-\hat{\gamma}\mathcal{L}} \right) \hat{\mathbf{T}}_I^{-1} \quad (7.115b)$$

$$\hat{\Phi}_{21}(\mathcal{L}) = -\frac{1}{2}\hat{\mathbf{T}}_I \left(\mathbf{e}^{\hat{\gamma}\mathcal{L}} - \mathbf{e}^{-\hat{\gamma}\mathcal{L}} \right) \hat{\gamma}^{-1}\hat{\mathbf{T}}_I^{-1}\hat{\mathbf{Y}} \quad (7.115c)$$

$$\hat{\Phi}_{22}(\mathcal{L}) = \frac{1}{2}\hat{\mathbf{T}}_I \left(\mathbf{e}^{\hat{\gamma}\mathcal{L}} + \mathbf{e}^{-\hat{\gamma}\mathcal{L}} \right) \hat{\mathbf{T}}_I^{-1} \quad (7.115d)$$

where $\hat{\mathbf{T}}_I^{-1}\hat{\mathbf{Y}}\hat{\mathbf{Z}}\hat{\mathbf{T}}_I = \hat{\gamma}^2$. According to (12.25a), the equivalent circuit of the complete line can be viewed as an unexcited line in series with the equivalent sources $\hat{\mathbf{V}}_{\text{FT}i}(\mathcal{L})$ and $\hat{\mathbf{I}}_{\text{FT}i}(\mathcal{L})$ located at $z = \mathcal{L}$, as illustrated in Figure 12.4.

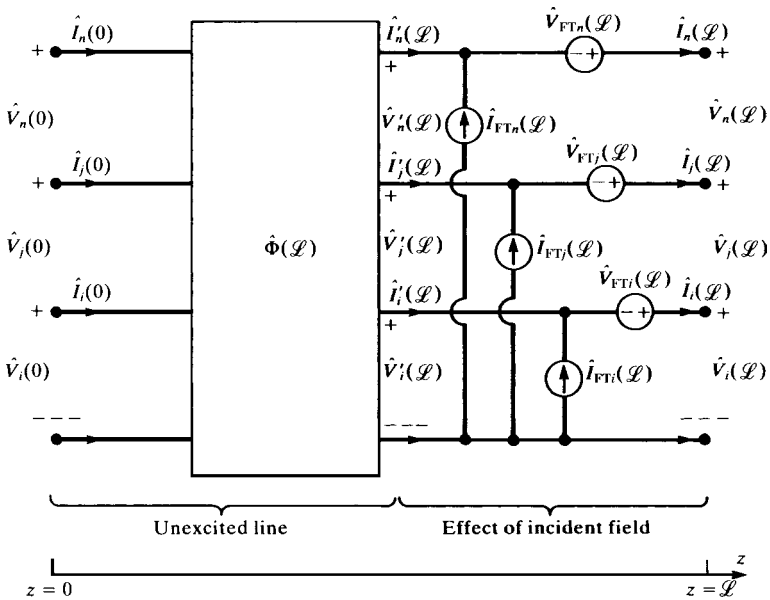


FIGURE 12.4 Illustration of the representation of an MTL with incident field illumination as a $2n$ -port having lumped sources that represent the effects of the incident field.

12.2.2 Simplified Forms of the Excitations

The total excitation source vectors due to the incident field, $\hat{\mathbf{I}}_{\text{FT}}(\mathcal{L})$ and $\hat{\mathbf{V}}_{\text{FT}}(\mathcal{L})$, in (12.25b) and (12.25c) can be simplified using the definitions of the phasor distributed sources, $\hat{\mathbf{I}}_{\text{F}}(z)$ and $\hat{\mathbf{V}}_{\text{F}}(z)$, given in (12.22d) and (12.22e) and the properties of the chain-parameter submatrices obtained in Section 7.5.3 of Chapter 7. The total forcing function $\hat{\mathbf{V}}_{\text{FT}}(\mathcal{L})$ given in (12.25b) becomes, by substituting $\hat{\mathbf{I}}_{\text{F}}(z)$ from (12.22d) and $\hat{\mathbf{V}}_{\text{F}}(z)$ from (12.22e),

$$\begin{aligned}
 \hat{\mathbf{V}}_{\text{FT}}(\mathcal{L}) &= \int_0^{\mathcal{L}} [\hat{\Phi}_{11}(\mathcal{L} - \tau) \hat{\mathbf{V}}_{\text{F}}(\tau) + \hat{\Phi}_{12}(\mathcal{L} - \tau) \hat{\mathbf{I}}_{\text{F}}(\tau)] d\tau \\
 &= \int_0^{\mathcal{L}} \hat{\Phi}_{11}(\mathcal{L} - \tau) \begin{bmatrix} \hat{E}_z^{\text{inc}}(i\text{th conductor}, \tau) - \hat{E}_z^{\text{inc}}(\text{reference conductor}, \tau) \\ \vdots \\ \vdots \end{bmatrix} d\tau \\
 &\quad - \int_0^{\mathcal{L}} \hat{\Phi}_{11}(\mathcal{L} - \tau) \frac{\partial}{\partial \tau} \begin{bmatrix} \vdots \\ \int_a^{a'} \vec{E}_t^{\text{inc}} \cdot d\vec{l} \\ \vdots \end{bmatrix} d\tau \\
 &\quad - \int_0^{\mathcal{L}} \hat{\Phi}_{12}(\mathcal{L} - \tau) \hat{\mathbf{Y}} \begin{bmatrix} \vdots \\ \int_a^{a'} \vec{E}_t^{\text{inc}} \cdot d\vec{l} \\ \vdots \end{bmatrix} d\tau
 \end{aligned} \tag{12.26}$$

Using the chain rule for differentiation:

$$\frac{\partial}{\partial \tau} [\mathbf{A}(\tau) \mathbf{B}(\tau)] = \mathbf{A}(\tau) \left[\frac{\partial}{\partial \tau} \mathbf{B}(\tau) \right] + \left[\frac{\partial}{\partial \tau} \mathbf{A}(\tau) \right] \mathbf{B}(\tau) \tag{12.27}$$

we obtain

$$\begin{aligned}
 \hat{\mathbf{V}}_{\text{FT}}(\mathcal{L}) &= \int_0^{\mathcal{L}} \hat{\Phi}_{11}(\mathcal{L} - \tau) \begin{bmatrix} \hat{E}_z^{\text{inc}}(i\text{th conductor}, \tau) - \hat{E}_z^{\text{inc}}(\text{reference conductor}, \tau) \\ \vdots \\ \vdots \end{bmatrix} d\tau \\
 &\quad - \int_0^{\mathcal{L}} \frac{\partial}{\partial \tau} \left\{ \hat{\Phi}_{11}(\mathcal{L} - \tau) \begin{bmatrix} \vdots \\ \int_a^{a'} \vec{E}_t^{\text{inc}} \cdot d\vec{l} \\ \vdots \end{bmatrix} \right\} d\tau
 \end{aligned}$$

$$+ \int_0^{\mathcal{L}} \underbrace{\left\{ \frac{\partial}{\partial \tau} \hat{\Phi}_{11}(\mathcal{L} - \tau) - \hat{\Phi}_{12}(\mathcal{L} - \tau) \hat{\mathbf{Y}} \right\}}_{=0} \begin{bmatrix} \vdots \\ \int_a^{a'} \vec{\hat{E}}_t^{\text{inc}} \cdot d\vec{l} \\ \vdots \end{bmatrix} d\tau \quad (12.28)$$

We now show that the last term in (12.28) is identically zero, that is,

$$\frac{\partial}{\partial \tau} \hat{\Phi}_{11}(\mathcal{L} - \tau) - \hat{\Phi}_{12}(\mathcal{L} - \tau) \hat{\mathbf{Y}} = 0 \quad (12.29)$$

This can easily be shown using the chain-parameter submatrix definitions given in (7.115) of Chapter 7:

$$\begin{aligned} \frac{\partial}{\partial \tau} \hat{\Phi}_{11}(\mathcal{L} - \tau) &= \frac{\partial}{\partial \tau} \left[\frac{1}{2} \hat{\mathbf{Y}}^{-1} \hat{\mathbf{T}}_I \left(\mathbf{e}^{\hat{\gamma}(\mathcal{L}-\tau)} + \mathbf{e}^{-\hat{\gamma}(\mathcal{L}-\tau)} \right) \hat{\mathbf{T}}_I^{-1} \hat{\mathbf{Y}} \right] \\ &= -\frac{1}{2} \hat{\mathbf{Y}}^{-1} \hat{\mathbf{T}}_I \hat{\gamma} \left(\mathbf{e}^{\hat{\gamma}(\mathcal{L}-\tau)} - \mathbf{e}^{-\hat{\gamma}(\mathcal{L}-\tau)} \right) \hat{\mathbf{T}}_I^{-1} \hat{\mathbf{Y}} \quad (12.30a) \end{aligned}$$

$$-\hat{\Phi}_{12}(\mathcal{L} - \tau) \hat{\mathbf{Y}} = \frac{1}{2} \hat{\mathbf{Y}}^{-1} \hat{\mathbf{T}}_I \hat{\gamma} \left(\mathbf{e}^{\hat{\gamma}(\mathcal{L}-\tau)} - \mathbf{e}^{-\hat{\gamma}(\mathcal{L}-\tau)} \right) \hat{\mathbf{T}}_I^{-1} \hat{\mathbf{Y}} \quad (12.30b)$$

Thus, the final result is

$$\begin{aligned} \hat{\mathbf{V}}_{\text{FT}}(\mathcal{L}) &= \int_0^{\mathcal{L}} \hat{\Phi}_{11}(\mathcal{L} - \tau) \begin{bmatrix} \vdots \\ \hat{E}_z^{\text{inc}}(\textit{ith conductor}, \tau) - \hat{E}_z^{\text{inc}}(\textit{reference conductor}, \tau) \\ \vdots \end{bmatrix} d\tau \\ &\quad - \underbrace{\hat{\Phi}_{11}(0)}_{\mathbf{1}_n} \begin{bmatrix} \vdots \\ \int_a^{a'} \vec{\hat{E}}_t^{\text{inc}} \cdot d\vec{l} \\ \vdots \end{bmatrix}_{z=\mathcal{L}} + \hat{\Phi}_{11}(\mathcal{L}) \begin{bmatrix} \vdots \\ \int_a^{a'} \vec{\hat{E}}_t^{\text{inc}} \cdot d\vec{l} \\ \vdots \end{bmatrix}_{z=0} \quad (12.31) \end{aligned}$$

where we have used the fact that $\hat{\Phi}_{11}(0) = \mathbf{1}_n$ and where $\mathbf{1}_n$ is the $n \times n$ identity matrix. In a similar fashion, we can show that

$$\hat{\mathbf{I}}_{\text{FT}}(\mathcal{L}) = \int_0^{\mathcal{L}} \hat{\Phi}_{21}(\mathcal{L}-\tau) \left[\begin{array}{c} \hat{E}_z^{\text{inc}}(i\text{th conductor } \tau) - \hat{E}_z^{\text{inc}}(\text{reference conductor } \tau) \\ \vdots \\ \vdots \end{array} \right] d\tau$$

$$- \underbrace{\hat{\Phi}_{21}(0)}_{\mathbf{0}} \left[\begin{array}{c} \vdots \\ \int_a^{a'} \vec{E}_t^{\text{inc}} \cdot d\vec{l} \\ \vdots \end{array} \right]_{z=\mathcal{L}} + \hat{\Phi}_{21}(\mathcal{L}) \left[\begin{array}{c} \vdots \\ \int_a^{a'} \vec{E}_t^{\text{inc}} \cdot d\vec{l} \\ \vdots \end{array} \right]_{z=0} \quad (12.32)$$

where we have used the property that $\hat{\Phi}_{21}(0) = \mathbf{0}$ (see Eq. (7.115c) of Chapter 7). These results show that the total forcing functions $\hat{\mathbf{V}}_{\text{FT}}(\mathcal{L})$ and $\hat{\mathbf{I}}_{\text{FT}}(\mathcal{L})$ depend on a *convolution* of one of the chain-parameter submatrices and the longitudinal incident electric field along the positions of the conductors (with the conductors removed), as well as the product of that chain-parameter submatrix and the integrals of the transverse incident electric field (with the conductors removed) that are evaluated at the left end of the line ($z = 0$) and at the right end of the line ($z = \mathcal{L}$).

12.2.3 Incorporating the Line Terminations

Now that the general solution of the phasor MTL equations has been obtained in terms of the chain-parameter matrix and the incident field forcing functions in (12.25), we next incorporate the terminal conditions to arrive at an explicit solution for the phasor line voltages and currents. Consider Figure 12.4. The voltages and currents at the right end of the unexcited line are denoted as $\hat{\mathbf{V}}'(\mathcal{L})$ and $\hat{\mathbf{I}}'(\mathcal{L})$. These are related to the actual desired voltages and currents, $\hat{\mathbf{V}}(\mathcal{L})$ and $\hat{\mathbf{I}}(\mathcal{L})$, as

$$\hat{\mathbf{V}}'(\mathcal{L}) = \hat{\mathbf{V}}(\mathcal{L}) - \hat{\mathbf{V}}_{\text{FT}}(\mathcal{L}) \quad (12.33a)$$

$$\hat{\mathbf{I}}'(\mathcal{L}) = \hat{\mathbf{I}}(\mathcal{L}) - \hat{\mathbf{I}}_{\text{FT}}(\mathcal{L}) \quad (12.33b)$$

Therefore, we can incorporate the effects of incident fields into the solution by replacing $\hat{\mathbf{V}}(\mathcal{L})$ and $\hat{\mathbf{I}}(\mathcal{L})$ in the equations for the terminal responses without incident field illumination given in Section 7.3 of Chapter 7 with $\hat{\mathbf{V}}(\mathcal{L}) - \hat{\mathbf{V}}_{\text{FT}}(\mathcal{L})$ and $\hat{\mathbf{I}}(\mathcal{L}) - \hat{\mathbf{I}}_{\text{FT}}(\mathcal{L})$! This is further confirmed by rewriting the general solution given in (12.25a) in terms of the chain-parameter matrix with sources. Rewriting this in the form of the chain-parameter relation without incident field illumination gives

$$\begin{bmatrix} \hat{\mathbf{V}}(\mathcal{L}) - \hat{\mathbf{V}}_{\text{FT}}(\mathcal{L}) \\ \hat{\mathbf{I}}(\mathcal{L}) - \hat{\mathbf{I}}_{\text{FT}}(\mathcal{L}) \end{bmatrix} = \begin{bmatrix} \hat{\Phi}_{11}(\mathcal{L}) & \hat{\Phi}_{12}(\mathcal{L}) \\ \hat{\Phi}_{21}(\mathcal{L}) & \hat{\Phi}_{22}(\mathcal{L}) \end{bmatrix} \begin{bmatrix} \hat{\mathbf{V}}(0) \\ \hat{\mathbf{I}}(0) \end{bmatrix} \quad (12.34)$$

Consider the terminal conditions written in the form of generalized Thevenin equivalents as

$$\hat{\mathbf{V}}(0) = \hat{\mathbf{V}}_S - \hat{\mathbf{Z}}_S \hat{\mathbf{I}}(0) \quad (12.35a)$$

$$\hat{\mathbf{V}}(\mathcal{L}) = \hat{\mathbf{V}}_L + \hat{\mathbf{Z}}_L \hat{\mathbf{I}}(\mathcal{L}) \quad (12.35b)$$

Making the substitutions given in (12.33) gives

$$\hat{\mathbf{V}}(0) = \hat{\mathbf{V}}_S - \hat{\mathbf{Z}}_S \hat{\mathbf{I}}(0) \quad (12.36a)$$

$$[\hat{\mathbf{V}}'(\mathcal{L}) + \hat{\mathbf{V}}_{\text{FT}}(\mathcal{L})] = \hat{\mathbf{V}}_L + \hat{\mathbf{Z}}_L [\hat{\mathbf{I}}'(\mathcal{L}) + \hat{\mathbf{I}}_{\text{FT}}(\mathcal{L})] \quad (12.36b)$$

or

$$\hat{\mathbf{V}}(0) = \hat{\mathbf{V}}_S - \hat{\mathbf{Z}}_S \hat{\mathbf{I}}(0) \quad (12.37a)$$

$$\hat{\mathbf{V}}'(\mathcal{L}) = [\hat{\mathbf{V}}_L - \hat{\mathbf{V}}_{\text{FT}}(\mathcal{L}) + \hat{\mathbf{Z}}_L \hat{\mathbf{I}}_{\text{FT}}(\mathcal{L})] + \hat{\mathbf{Z}}_L \hat{\mathbf{I}}'(\mathcal{L}) \quad (12.37b)$$

Observe that (12.37) shows we could modify the result derived in Chapter 7 for no incident field illumination given in (7.92) by replacing $\hat{\mathbf{V}}_L$ with $\hat{\mathbf{V}}_L - \hat{\mathbf{V}}_{\text{FT}}(\mathcal{L}) + \hat{\mathbf{Z}}_L \hat{\mathbf{I}}_{\text{FT}}(\mathcal{L})$ and $\hat{\mathbf{I}}(\mathcal{L})$ with $\hat{\mathbf{I}}(\mathcal{L}) - \hat{\mathbf{I}}_{\text{FT}}(\mathcal{L})$ to yield

$$\begin{aligned} & [\hat{\Phi}_{11} \hat{\mathbf{Z}}_S + \hat{\mathbf{Z}}_L \hat{\Phi}_{22} - \hat{\Phi}_{12} - \hat{\mathbf{Z}}_L \hat{\Phi}_{21} \hat{\mathbf{Z}}_S] \hat{\mathbf{I}}(0) \\ &= \underbrace{[\hat{\Phi}_{11} - \hat{\mathbf{Z}}_L \hat{\Phi}_{21}] \hat{\mathbf{V}}_S - \hat{\mathbf{V}}_L}_{\text{due to lumped sources}} + \underbrace{[\hat{\mathbf{V}}_{\text{FT}}(\mathcal{L}) - \hat{\mathbf{Z}}_L \hat{\mathbf{I}}_{\text{FT}}(\mathcal{L})]}_{\text{due to incident field}} \end{aligned} \quad (12.38a)$$

$$\hat{\mathbf{I}}(\mathcal{L}) = \hat{\mathbf{I}}_{\text{FT}}(\mathcal{L}) + \hat{\Phi}_{21} \hat{\mathbf{V}}_S + [\hat{\Phi}_{22} - \hat{\Phi}_{21} \hat{\mathbf{Z}}_S] \hat{\mathbf{I}}(0) \quad (12.38b)$$

Similarly, the alternative result given in (7.90) becomes

$$\begin{bmatrix} (\hat{\mathbf{Z}}_C + \hat{\mathbf{Z}}_S) \hat{\mathbf{T}}_I & (\hat{\mathbf{Z}}_C - \hat{\mathbf{Z}}_S) \hat{\mathbf{T}}_I \\ (\hat{\mathbf{Z}}_C - \hat{\mathbf{Z}}_L) \hat{\mathbf{T}}_I e^{-\hat{\gamma} \mathcal{L}} & (\hat{\mathbf{Z}}_C + \hat{\mathbf{Z}}_L) \hat{\mathbf{T}}_I e^{\hat{\gamma} \mathcal{L}} \end{bmatrix} \begin{bmatrix} \hat{\mathbf{I}}_m^+ \\ \hat{\mathbf{I}}_m^- \end{bmatrix} = \begin{bmatrix} \hat{\mathbf{V}}_S \\ \hat{\mathbf{V}}_L - \hat{\mathbf{V}}_{\text{FT}}(\mathcal{L}) + \hat{\mathbf{Z}}_L \hat{\mathbf{I}}_{\text{FT}}(\mathcal{L}) \end{bmatrix} \quad (12.39)$$

where the characteristic impedance matrix is $\hat{\mathbf{Z}}_C = \hat{\mathbf{Z}} \hat{\mathbf{T}}_I \hat{\gamma}^{-1} \mathbf{T}_I^{-1} = \hat{\mathbf{Y}}^{-1} \hat{\mathbf{T}}_I \hat{\gamma} \mathbf{T}_I^{-1}$. The solutions for the terminal voltages so obtained will be

$$\begin{aligned} \hat{\mathbf{V}}(0) &= \hat{\mathbf{Y}}^{-1} \hat{\mathbf{T}}_I \hat{\gamma} [\hat{\mathbf{I}}_m^+ + \hat{\mathbf{I}}_m^-] \\ &= \hat{\mathbf{Z}} \hat{\mathbf{T}}_I \hat{\gamma}^{-1} [\hat{\mathbf{I}}_m^+ + \hat{\mathbf{I}}_m^-] \end{aligned} \quad (12.40a)$$

$$\begin{aligned} \hat{\mathbf{V}}'(\mathcal{L}) &= \hat{\mathbf{V}}(\mathcal{L}) - \hat{\mathbf{V}}_{\text{FT}}(\mathcal{L}) \\ &= \hat{\mathbf{Y}}^{-1} \hat{\mathbf{T}}_I \hat{\gamma} \left[e^{-\hat{\gamma} \mathcal{L}} \hat{\mathbf{I}}_m^+ + e^{\hat{\gamma} \mathcal{L}} \hat{\mathbf{I}}_m^- \right] \\ &= \hat{\mathbf{Z}} \hat{\mathbf{T}}_I \hat{\gamma}^{-1} \left[e^{-\hat{\gamma} \mathcal{L}} \hat{\mathbf{I}}_m^+ + e^{\hat{\gamma} \mathcal{L}} \hat{\mathbf{I}}_m^- \right] \end{aligned} \quad (12.40b)$$

or

$$\begin{aligned}\hat{\mathbf{V}}(\mathcal{L}) &= \hat{\mathbf{V}}_{\text{FT}}(\mathcal{L}) + \hat{\mathbf{Y}}^{-1} \hat{\mathbf{T}}_I \hat{\gamma} \left[\mathbf{e}^{-\hat{\gamma} \mathcal{L}} \hat{\mathbf{I}}_m^+ + \mathbf{e}^{\hat{\gamma} \mathcal{L}} \hat{\mathbf{I}}_m^- \right] \\ &= \hat{\mathbf{V}}_{\text{FT}}(\mathcal{L}) + \hat{\mathbf{Z}} \hat{\mathbf{T}}_I \hat{\gamma}^{-1} \left[\mathbf{e}^{-\hat{\gamma} \mathcal{L}} \hat{\mathbf{I}}_m^+ + \mathbf{e}^{\hat{\gamma} \mathcal{L}} \hat{\mathbf{I}}_m^- \right]\end{aligned}\quad (12.40c)$$

The terminal constraints for the generalized Norton equivalent representation:

$$\hat{\mathbf{I}}(0) = \hat{\mathbf{I}}_S - \hat{\mathbf{Y}}_S \hat{\mathbf{V}}(0) \quad (12.41a)$$

$$\hat{\mathbf{I}}(\mathcal{L}) = -\hat{\mathbf{I}}_L + \hat{\mathbf{Y}}_L \hat{\mathbf{V}}(\mathcal{L}) \quad (12.41b)$$

become, substituting (12.33),

$$\hat{\mathbf{I}}(0) = \hat{\mathbf{I}}_S - \hat{\mathbf{Y}}_S \hat{\mathbf{V}}(0) \quad (12.42a)$$

$$\hat{\mathbf{I}}'(\mathcal{L}) = [-\hat{\mathbf{I}}_L - \hat{\mathbf{I}}_{\text{FT}}(\mathcal{L}) + \hat{\mathbf{Y}}_L \hat{\mathbf{V}}_{\text{FT}}(\mathcal{L})] + \hat{\mathbf{Y}}_L \hat{\mathbf{V}}'(\mathcal{L}) \quad (12.42b)$$

This shows that we can modify the equations developed for the generalized Norton equivalent in (7.97) of Chapter 7 by replacing the source $\hat{\mathbf{I}}_L$ with $\hat{\mathbf{I}}_L + \hat{\mathbf{I}}_{\text{FT}}(\mathcal{L}) - \hat{\mathbf{Y}}_L \hat{\mathbf{V}}_{\text{FT}}(\mathcal{L})$ and $\hat{\mathbf{V}}(\mathcal{L})$ with $\hat{\mathbf{V}}(\mathcal{L}) - \hat{\mathbf{V}}_{\text{FT}}(\mathcal{L})$ in those equations:

$$\begin{aligned}& [\hat{\Phi}_{22} \hat{\mathbf{Y}}_S + \hat{\mathbf{Y}}_L \hat{\Phi}_{11} - \hat{\Phi}_{21} - \hat{\mathbf{Y}}_L \hat{\Phi}_{12} \hat{\mathbf{Y}}_S] \hat{\mathbf{V}}(0) \\ &= \underbrace{[\hat{\Phi}_{22} - \hat{\mathbf{Y}}_L \hat{\Phi}_{12}] \hat{\mathbf{I}}_S + \hat{\mathbf{I}}_L}_{\text{due to lumped sources}} + \underbrace{[\hat{\mathbf{I}}_{\text{FT}}(\mathcal{L}) - \hat{\mathbf{Y}}_L \hat{\mathbf{V}}_{\text{FT}}(\mathcal{L})]}_{\text{due to incident field}}\end{aligned}\quad (12.43a)$$

$$\hat{\mathbf{V}}(\mathcal{L}) = \hat{\mathbf{V}}_{\text{FT}}(\mathcal{L}) + \hat{\Phi}_{12} \hat{\mathbf{I}}_S + [\hat{\Phi}_{11} - \hat{\Phi}_{12} \hat{\mathbf{Y}}_S] \hat{\mathbf{V}}(0) \quad (12.43b)$$

Similarly, the alternative result given in (7.95) in Chapter 7 becomes

$$\begin{aligned}& \begin{bmatrix} (\hat{\mathbf{Y}}_S \hat{\mathbf{Z}}_C + \mathbf{1}_n) \hat{\mathbf{T}} & (\hat{\mathbf{Y}}_S \hat{\mathbf{Z}}_C - \mathbf{1}_n) \hat{\mathbf{T}} \\ (\hat{\mathbf{Y}}_L \hat{\mathbf{Z}}_C - \mathbf{1}_n) \hat{\mathbf{T}} \mathbf{e}^{-\hat{\gamma} \mathcal{L}} & (\hat{\mathbf{Y}}_L \hat{\mathbf{Z}}_C + \mathbf{1}_n) \hat{\mathbf{T}} \mathbf{e}^{\hat{\gamma} \mathcal{L}} \end{bmatrix} \begin{bmatrix} \hat{\mathbf{I}}_m^+ \\ \hat{\mathbf{I}}_m^- \end{bmatrix} \\ &= \begin{bmatrix} \hat{\mathbf{I}}_S \\ \hat{\mathbf{I}}_{\mathcal{L}} + \hat{\mathbf{I}}_{\text{FT}}(\mathcal{L}) - \hat{\mathbf{Y}}_L \hat{\mathbf{V}}_{\text{FT}}(\mathcal{L}) \end{bmatrix}\end{aligned}\quad (12.44)$$

The solutions for the terminal voltages so obtained will again be given by (12.40).

The mixed termination representation results given in (7.98)–(7.101) in Chapter 7 are similarly obtained as

$$\begin{aligned}& \begin{bmatrix} (\hat{\mathbf{Z}}_C + \hat{\mathbf{Z}}_S) \hat{\mathbf{T}} & (\hat{\mathbf{Z}}_C - \hat{\mathbf{Z}}_S) \hat{\mathbf{T}} \\ (\hat{\mathbf{Y}}_L \hat{\mathbf{Z}}_C - \mathbf{1}_n) \hat{\mathbf{T}} \mathbf{e}^{-\hat{\gamma} \mathcal{L}} & (\hat{\mathbf{Y}}_L \hat{\mathbf{Z}}_C + \mathbf{1}_n) \hat{\mathbf{T}} \mathbf{e}^{\hat{\gamma} \mathcal{L}} \end{bmatrix} \begin{bmatrix} \hat{\mathbf{I}}_m^+ \\ \hat{\mathbf{I}}_m^- \end{bmatrix} \\ &= \begin{bmatrix} \hat{\mathbf{V}}_S \\ \hat{\mathbf{I}}_L + \hat{\mathbf{I}}_{\text{FT}}(\mathcal{L}) - \hat{\mathbf{Y}}_L \hat{\mathbf{V}}_{\text{FT}}(\mathcal{L}) \end{bmatrix}\end{aligned}\quad (12.45)$$

or

$$\begin{aligned}
 & [\hat{\Phi}_{21}\hat{\mathbf{Z}}_S + \hat{\mathbf{Y}}_L\hat{\Phi}_{12} - \hat{\Phi}_{22} - \hat{\mathbf{Y}}_L\hat{\Phi}_{11}\hat{\mathbf{Z}}_S] \hat{\mathbf{I}}(0) \\
 = & \underbrace{[\hat{\Phi}_{21} - \hat{\mathbf{Y}}_L\hat{\Phi}_{11}] \hat{\mathbf{V}}_S + \hat{\mathbf{I}}_L}_{\text{due to lumped sources}} + \underbrace{[\hat{\mathbf{I}}_{\text{FT}}(\mathcal{L}) - \hat{\mathbf{Y}}_L\hat{\mathbf{V}}_{\text{FT}}(\mathcal{L})]}_{\text{due to incident field}}
 \end{aligned} \tag{12.46a}$$

$$\hat{\mathbf{V}}(\mathcal{L}) = \hat{\mathbf{V}}_{\text{FT}}(\mathcal{L}) + \hat{\Phi}_{11}\hat{\mathbf{V}}_S + [\hat{\Phi}_{12} - \hat{\Phi}_{11}\hat{\mathbf{Z}}_S] \hat{\mathbf{I}}(0) \tag{12.46b}$$

and

$$\begin{bmatrix} (\hat{\mathbf{Y}}_S\hat{\mathbf{Z}}_C + \mathbf{1}_n) \hat{\mathbf{T}} & (\hat{\mathbf{Y}}_S\hat{\mathbf{Z}}_C - \mathbf{1}_n) \hat{\mathbf{T}} \\ (\hat{\mathbf{Z}}_C - \hat{\mathbf{Z}}_L) \hat{\mathbf{T}}\mathbf{e}^{-\hat{\gamma}\mathcal{L}} & (\hat{\mathbf{Z}}_C + \hat{\mathbf{Z}}_L) \hat{\mathbf{T}}\mathbf{e}^{\hat{\gamma}\mathcal{L}} \end{bmatrix} \begin{bmatrix} \hat{\mathbf{i}}_m^+ \\ \hat{\mathbf{i}}_m^- \end{bmatrix} = \begin{bmatrix} \hat{\mathbf{I}}_S \\ \hat{\mathbf{V}}_L - \hat{\mathbf{V}}_{\text{FT}}(\mathcal{L}) + \hat{\mathbf{Z}}_L\hat{\mathbf{I}}_{\text{FT}}(\mathcal{L}) \end{bmatrix} \tag{12.47}$$

or

$$\begin{aligned}
 & [\hat{\Phi}_{12}\hat{\mathbf{Y}}_S + \hat{\mathbf{Z}}_L\hat{\Phi}_{21} - \hat{\Phi}_{11} - \hat{\mathbf{Z}}_L\hat{\Phi}_{22}\hat{\mathbf{Y}}_S] \hat{\mathbf{V}}(0) \\
 = & \underbrace{[\hat{\Phi}_{12} - \hat{\mathbf{Z}}_L\hat{\Phi}_{22}] \hat{\mathbf{I}}_S - \hat{\mathbf{V}}_L}_{\text{due to lumped sources}} + \underbrace{[\hat{\mathbf{V}}_{\text{FT}}(\mathcal{L}) - \hat{\mathbf{Z}}_L\hat{\mathbf{I}}_{\text{FT}}(\mathcal{L})]}_{\text{due to incident field}}
 \end{aligned} \tag{12.48a}$$

$$\hat{\mathbf{I}}(\mathcal{L}) = \hat{\mathbf{I}}_{\text{FT}}(\mathcal{L}) + \hat{\Phi}_{22}\hat{\mathbf{I}}_S + [\hat{\Phi}_{21} - \hat{\Phi}_{22}\hat{\mathbf{Y}}_S] \hat{\mathbf{V}}(0) \tag{12.48b}$$

12.2.3.1 Lossless Lines in Homogeneous Media The above final equations for determining the terminal currents and voltages of the line are considerably simplified if we assume *lossless lines* in a *homogeneous medium*. For this case, the per-unit-length parameter matrices satisfy

$$\mathbf{R} = \mathbf{0} \tag{12.49a}$$

$$\mathbf{G} = \mathbf{0} \tag{12.49b}$$

$$\mathbf{L}\mathbf{C} = \mathbf{C}\mathbf{L} = \mu\varepsilon\mathbf{1}_n \tag{12.49c}$$

The chain parameters were derived in Chapter 7 and simplify to

$$\hat{\Phi}_{11} = \cos(\beta\mathcal{L})\mathbf{1}_n \tag{12.50a}$$

$$\begin{aligned}
 \hat{\Phi}_{12} &= -jv\sin(\beta\mathcal{L})\mathbf{L} \\
 &= -j\sin(\beta\mathcal{L})\hat{\mathbf{Z}}_C
 \end{aligned} \tag{12.50b}$$

$$\begin{aligned}
 \hat{\Phi}_{21} &= -jv\sin(\beta\mathcal{L})\mathbf{C} \\
 &= -j\sin(\beta\mathcal{L})\hat{\mathbf{Z}}_C^{-1}
 \end{aligned} \tag{12.50c}$$

$$\hat{\Phi}_{22} = \cos(\beta \mathcal{L}) \mathbf{1}_n \quad (12.50d)$$

where the characteristic impedance becomes real and is given by

$$\hat{\mathbf{Z}}_C = v \mathbf{L} \quad (12.51a)$$

$$\hat{\mathbf{Z}}_C^{-1} = v \mathbf{C} \quad (12.51b)$$

and the phase velocity of propagation in the surrounding homogeneous medium is

$$v = \frac{1}{\sqrt{\mu\varepsilon}} \quad (12.52)$$

The final equations to be solved for the terminal voltages simplify considerably for this assumption. For example, consider the generalized Thevenin equivalent characterization of the terminations given in (12.35). Substituting the simplified forms of the total forcing functions $\hat{\mathbf{V}}_{\text{FT}}(\mathcal{L})$ and $\hat{\mathbf{I}}_{\text{FT}}(\mathcal{L})$ given in (12.31) and (12.32) into (12.38) gives [H.2]

$$\begin{aligned} & [\cos(\beta \mathcal{L}) (\hat{\mathbf{Z}}_S + \hat{\mathbf{Z}}_L) + jv \sin(\beta \mathcal{L}) (\mathbf{L} + \hat{\mathbf{Z}}_L \mathbf{C} \hat{\mathbf{Z}}_S)] \hat{\mathbf{I}}(0) \\ &= [\cos(\beta \mathcal{L}) \mathbf{1}_n + jv \sin(\beta \mathcal{L}) \hat{\mathbf{Z}}_L \mathbf{C}] \hat{\mathbf{V}}_S - \hat{\mathbf{V}}_L \\ &+ \int_0^{\mathcal{L}} \{ \cos(\beta(\mathcal{L} - \tau)) \mathbf{1}_n + jv \sin(\beta(\mathcal{L} - \tau)) \hat{\mathbf{Z}}_L \mathbf{C} \} \\ &\times \left[\begin{array}{c} \vdots \\ \hat{E}_z^{\text{inc}}(\text{ith conductor}, \tau) - \hat{E}_z^{\text{inc}}(\text{reference conductor}, \tau) \\ \vdots \end{array} \right] d\tau \\ &- \left[\begin{array}{c} \vdots \\ \int_a^{a'} \vec{E}_t^{\text{inc}} \cdot d\vec{l} \\ \vdots \end{array} \right]_{z=\mathcal{L}} + \{ \cos(\beta \mathcal{L}) \mathbf{1}_n + jv \sin(\beta \mathcal{L}) \hat{\mathbf{Z}}_L \mathbf{C} \} \left[\begin{array}{c} \vdots \\ \int_a^{a'} \vec{E}_t^{\text{inc}} \cdot d\vec{l} \\ \vdots \end{array} \right]_{z=0} \end{aligned} \quad (12.53a)$$

and

$$\begin{aligned} \hat{\mathbf{I}}(\mathcal{L}) &= -jv \sin(\beta \mathcal{L}) \mathbf{C} \hat{\mathbf{V}}_S + [\cos(\beta \mathcal{L}) \mathbf{1}_n + jv \sin(\beta \mathcal{L}) \mathbf{C} \hat{\mathbf{Z}}_S] \hat{\mathbf{I}}(0) \\ &- \int_0^{\mathcal{L}} \{ jv \sin(\beta(\mathcal{L} - \tau)) \mathbf{C} \} \end{aligned}$$

$$\begin{aligned}
 & \times \left[\begin{array}{c} \hat{E}_z^{\text{inc}}(i\text{th conductor}, \tau) - \hat{E}_z^{\text{inc}}(\text{reference conductor}, \tau) \\ \vdots \\ \vdots \end{array} \right] d\tau \\
 & - \{ jv \sin(\beta \mathcal{L}) \mathbf{C} \} \left[\begin{array}{c} \vdots \\ \int_a^{a'} \vec{E}_t^{\text{inc}} \cdot d\vec{l} \\ \vdots \end{array} \right]_{z=0} \tag{12.53b}
 \end{aligned}$$

The generalized Norton equivalent representation in (12.43) as well as the mixed representations in (12.46) and (12.48) simplifies in a similar fashion.

12.2.4 Lumped-Circuit Approximate Characterizations

If the line is electrically short at the frequency of the incident field, then the usual lumped-circuit approximate circuits are adequate to characterize the line. For example, the per-unit-length equivalent circuit in Figure 12.3 as well as the MTL equations shows that the lumped-Pi and lumped-T circuits in Figure 7.6 of Chapter 7 can be modified to incorporate the effects of incident fields by simply multiplying the per-unit-length phasor voltage and current sources created by the incident field by the total line length, thus inserting the phasor voltage sources $\hat{V}_{Fi} \mathcal{L}$ in series with each line self-inductance and inserting the phasor current sources $\hat{I}_{Fi} \mathcal{L}$ in parallel to each line self-capacitance. Since the line must be electrically short for the lumped-circuit approximation to be valid, and the cross-sectional dimensions must be electrically small for the TEM assumption to be valid, the phasor fields do not vary significantly over the line. Thus, the *per-unit-length* phasor voltage and current sources, $\hat{\mathbf{I}}_F(z)$ in (12.22d) and $\hat{\mathbf{V}}_F(z)$ in (12.22e), can be approximately evaluated at any convenient location on the line, say, at the center of the line. These are then multiplied by the total line length to give the lumped sources in the model. Lumped-Pi and lumped-T circuits are illustrated in Figure 12.5.

12.2.5 Uniform Plane-Wave Excitation of the Line

A significant set of problems to which these results apply is the case of illumination of the line by a *uniform plane wave* from some distant source [A.1]. The radiated fields in the far field of a radiating structure are spherical waves that resemble, locally, uniform plane waves. This assumption also simplifies the evaluation of the sources in the above results.

In order to characterize the frequency-domain response of the line, let us again describe the incident uniform plane-wave angle of incidence and polarization with respect to a spherical coordinate system as illustrated in Figure 12.6. The propagation vector of the wave is incident on the origin of the coordinate system (the phase

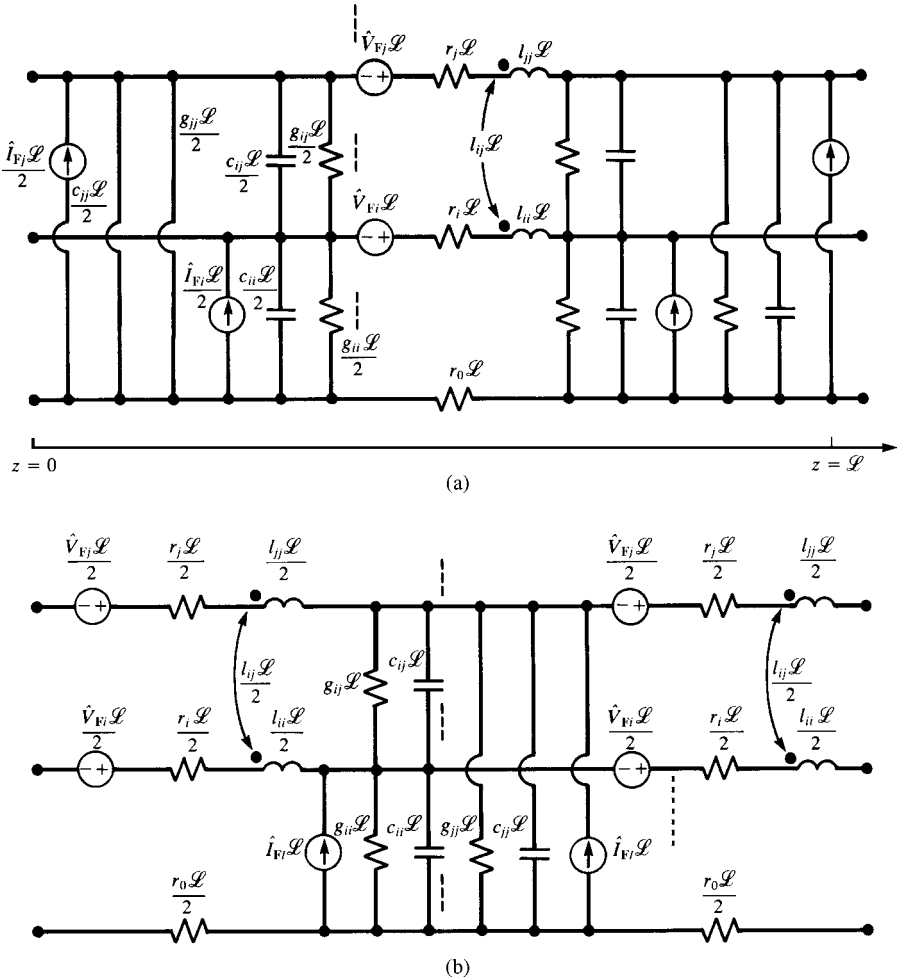


FIGURE 12.5 Adaptation of the lumped-Pi and lumped-T approximate equivalent circuits for incident field excitation.

reference for the wave) at angles θ_p from the x axis and ϕ_p from the projection onto the y - z plane from the y axis, as shown in Figure 12.6(a). The polarization of the electric field vector is described in terms of the relation to the unit vectors in the spherical coordinate system, \vec{a}_θ and \vec{a}_ϕ , as illustrated in Figure 12.6(b). In terms of these, the general expression for the phasor electric field vector can be written as [A.1]

$$\vec{E}^{\text{inc}} = \hat{E}_0 [e_x \vec{a}_x + e_y \vec{a}_y + e_z \vec{a}_z] e^{-j\beta_x x} e^{-j\beta_y y} e^{-j\beta_z z} \quad (12.54)$$

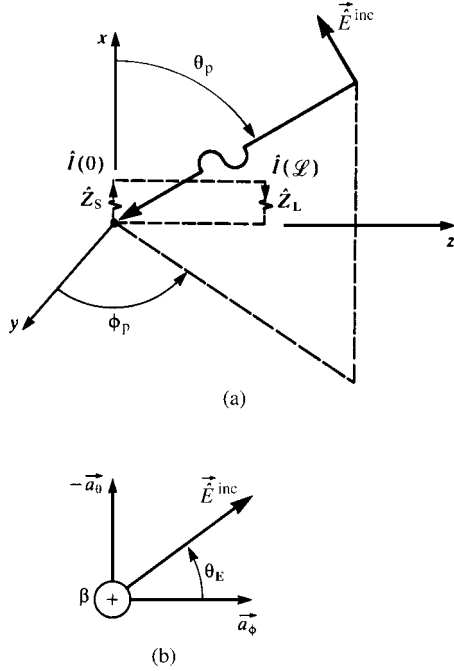


FIGURE 12.6 Definitions of the parameters characterizing the incident field as a uniform plane wave.

where the components of the incident electric field vector along the x , y , and z axes of the rectangular coordinate system describing the line are [A.1]

$$\begin{aligned}
 e_x &= \sin \theta_E \sin \theta_p \\
 e_y &= -\sin \theta_E \cos \theta_p \cos \phi_p - \cos \theta_E \sin \phi_p \\
 e_z &= -\sin \theta_E \cos \theta_p \sin \phi_p + \cos \theta_E \cos \phi_p
 \end{aligned}
 \tag{12.55a}$$

and

$$e_x^2 + e_y^2 + e_z^2 = 1
 \tag{12.55b}$$

The components of the phase constant along those coordinate axes are

$$\begin{aligned}
 \beta_x &= -\beta \cos \theta_p \\
 \beta_y &= -\beta \sin \theta_p \cos \phi_p \\
 \beta_z &= -\beta \sin \theta_p \sin \phi_p
 \end{aligned}
 \tag{12.56}$$

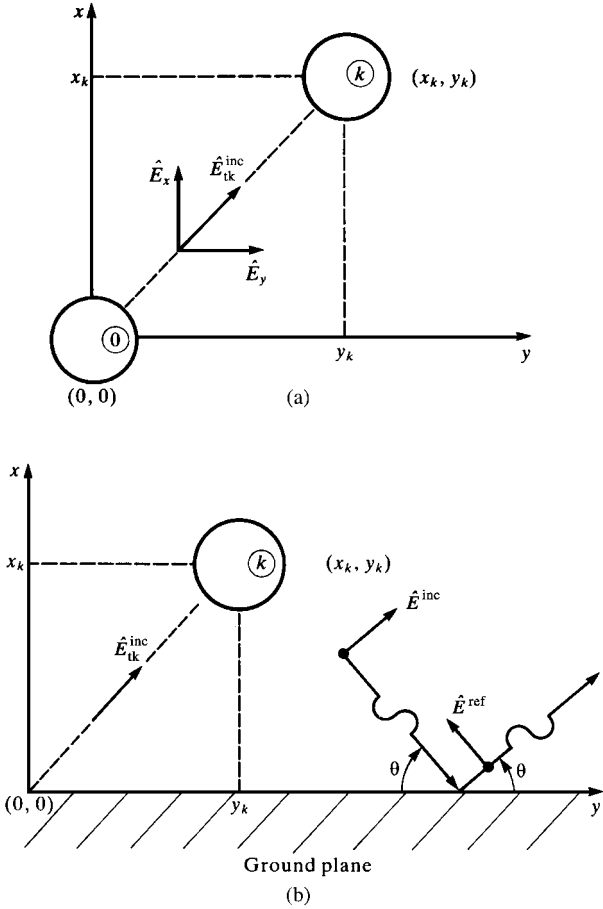


FIGURE 12.7 Derivation of the contributions to the equivalent sources due to the transverse component of the incident electric field for (a) a $(n + 1)$ -wire line and (b) n wires above a ground plane.

The phase constant is related to the frequency and properties of the medium as

$$\begin{aligned} \beta &= \omega \sqrt{\mu \epsilon} \\ &= \frac{1}{v_0} \sqrt{\epsilon_r \mu_r} \end{aligned} \tag{12.57}$$

where $v_0 = 1/\sqrt{\mu_0 \epsilon_0}$ is the phase velocity in free space and the medium is characterized by permeability $\mu = \mu_0 \mu_r$, and permittivity $\epsilon = \epsilon_0 \epsilon_r$. \hat{E}_0 is the complex amplitude of the sinusoidal wave.

If the reference conductor is placed at the origin of the coordinate system, $x = 0$, $y = 0$, as shown in Figure 12.7(a), the transverse field contributions in (12.22e) can be written in terms of the cross-sectional coordinates of the k th conductor (x_k , y_k) using the general form of the incident field in (12.54) as

$$\begin{aligned}
 \hat{E}_{\text{Tk}}(\mathcal{L}) &= \int_a^{a'} \vec{E}_{\text{tk}}^{\text{inc}} \cdot d\vec{l} \\
 &= \hat{E}_0 \int_0^{d_k} \left(e_x \frac{x_k}{d_k} + e_y \frac{y_k}{d_k} \right) e^{-j\beta_z \mathcal{L}} e^{-j \left(\beta_x \frac{x_k}{d_k} + \beta_y \frac{y_k}{d_k} \right) \rho} d\rho \\
 &= \hat{E}_0 [e_x x_k + e_y y_k] e^{-j\beta_z \mathcal{L}} \frac{[e^{-j(\beta_x x_k + \beta_y y_k)} - 1]}{-j(\beta_x x_k + \beta_y y_k)} \\
 &= \hat{E}_0 [e_x x_k + e_y y_k] \frac{\sin(\psi_k)}{\psi_k} e^{-j\psi_k} e^{-j\beta_z \mathcal{L}} \quad (12.58a)
 \end{aligned}$$

where $d_k = \sqrt{x_k^2 + y_k^2}$ is the straight-line distance between the reference conductor and the k th conductor in the transverse plane and

$$\psi_k = \frac{(\beta_x x_k + \beta_y y_k)}{2} \quad (12.58b)$$

Similarly, the contributions due to the longitudinal field in (12.22e) are

$$\begin{aligned}
 \hat{E}_{\text{Lk}}(z) &= \hat{E}_z^{\text{inc}}(x_k, y_k, z) - \hat{E}_z^{\text{inc}}(0, 0, z) \\
 &= \hat{E}_0 e_z e^{-j\beta_z z} [e^{-j(\beta_x x_k + \beta_y y_k)} - 1] \\
 &= -j(\beta_x x_k + \beta_y y_k) \hat{E}_0 e_z \frac{\sin(\psi_k)}{\psi_k} e^{-j\psi_k} e^{-j\beta_z z} \quad (12.59)
 \end{aligned}$$

Substituting the expressions for the chain-parameter submatrices given in Chapter 7:

$$\hat{\Phi}_{11}(\mathcal{L}) = \frac{1}{2} \hat{\mathbf{Y}}^{-1} \hat{\mathbf{T}} \left(\mathbf{e}^{\hat{\gamma} \mathcal{L}} + \mathbf{e}^{-\hat{\gamma} \mathcal{L}} \right) \hat{\mathbf{T}}^{-1} \hat{\mathbf{Y}} \quad (12.60a)$$

$$\hat{\Phi}_{21}(\mathcal{L}) = -\frac{1}{2} \hat{\mathbf{T}} \hat{\gamma}^{-1} \left(\mathbf{e}^{\hat{\gamma} \mathcal{L}} - \mathbf{e}^{-\hat{\gamma} \mathcal{L}} \right) \hat{\mathbf{T}}^{-1} \hat{\mathbf{Y}} \quad (12.60b)$$

into the expressions for $\hat{\mathbf{V}}_{\text{FT}}(\mathcal{L})$ given in (12.31) and $\hat{\mathbf{I}}_{\text{FT}}(\mathcal{L})$ given in (12.32) yields

$$\begin{aligned} \hat{\mathbf{V}}_{\text{FT}}(\mathcal{L}) = & \int_0^{\mathcal{L}} \frac{1}{2} \hat{\mathbf{Y}}^{-1} \hat{\mathbf{T}} \left(\mathbf{e}^{\hat{\gamma}(\mathcal{L}-\tau)} + \mathbf{e}^{-\hat{\gamma}(\mathcal{L}-\tau)} \right) \hat{\mathbf{T}}^{-1} \hat{\mathbf{Y}} \begin{bmatrix} \vdots \\ \hat{E}_{\text{L}k}(\tau) \\ \vdots \end{bmatrix} d\tau \\ & - \begin{bmatrix} \vdots \\ \hat{E}_{\text{T}k}(\mathcal{L}) \\ \vdots \end{bmatrix} + \frac{1}{2} \hat{\mathbf{Y}}^{-1} \hat{\mathbf{T}} \left(\mathbf{e}^{\hat{\gamma}\mathcal{L}} + \mathbf{e}^{-\hat{\gamma}\mathcal{L}} \right) \hat{\mathbf{T}}^{-1} \hat{\mathbf{Y}} \begin{bmatrix} \vdots \\ \hat{E}_{\text{T}k}(0) \\ \vdots \end{bmatrix} \end{aligned} \tag{12.61}$$

and

$$\begin{aligned} \hat{\mathbf{I}}_{\text{FT}}(\mathcal{L}) = & - \int_0^{\mathcal{L}} \frac{1}{2} \hat{\mathbf{T}} \hat{\gamma}^{-1} \left(\mathbf{e}^{\hat{\gamma}(\mathcal{L}-\tau)} - \mathbf{e}^{-\hat{\gamma}(\mathcal{L}-\tau)} \right) \hat{\mathbf{T}}^{-1} \hat{\mathbf{Y}} \begin{bmatrix} \vdots \\ \hat{E}_{\text{L}k}(\tau) \\ \vdots \end{bmatrix} d\tau \\ & - \frac{1}{2} \hat{\mathbf{T}} \hat{\gamma}^{-1} \left(\mathbf{e}^{\hat{\gamma}\mathcal{L}} - \mathbf{e}^{-\hat{\gamma}\mathcal{L}} \right) \hat{\mathbf{T}}^{-1} \hat{\mathbf{Y}} \begin{bmatrix} \vdots \\ \hat{E}_{\text{T}k}(0) \\ \vdots \end{bmatrix} \end{aligned} \tag{12.62}$$

Observe that the evaluation of these forcing functions requires that we evaluate the following $n \times 1$ vectors:

$$\hat{\mathbf{M}}^{\pm} = \int_0^{\mathcal{L}} \left(\mathbf{e}^{\hat{\gamma}(\mathcal{L}-\tau)} \pm \mathbf{e}^{-\hat{\gamma}(\mathcal{L}-\tau)} \right) \hat{\mathbf{T}}^{-1} \hat{\mathbf{Y}} \begin{bmatrix} \vdots \\ \hat{E}_{\text{L}k}(\tau) \\ \vdots \end{bmatrix} d\tau \tag{12.63}$$

and

$$\hat{\mathbf{N}}^{\pm} = \left(\mathbf{e}^{\hat{\gamma}\mathcal{L}} \pm \mathbf{e}^{-\hat{\gamma}\mathcal{L}} \right) \hat{\mathbf{T}}^{-1} \hat{\mathbf{Y}} \begin{bmatrix} \vdots \\ \hat{E}_{\text{T}k}(0) \\ \vdots \end{bmatrix} \tag{12.64}$$

The entries in these vectors become, in terms of the results in (12.58) and (12.59),

$$\begin{aligned} [\hat{\mathbf{M}}^{\pm}]_i = & \hat{E}_o e_z \left\{ e^{\gamma_i \mathcal{L}} \frac{[1 - e^{-(\gamma_i + j\beta_z)\mathcal{L}}]}{(\gamma_i + j\beta_z)} \pm e^{-\gamma_i \mathcal{L}} \frac{[e^{(\gamma_i - j\beta_z)\mathcal{L}} - 1]}{(\gamma_i - j\beta_z)} \right\} \\ & \times \sum_{k=1}^n \left\{ -j (\beta_x x_k + \beta_y y_k) \frac{\sin(\psi_k)}{\psi_k} e^{-j\psi_k} [\hat{\mathbf{T}}^{-1} \hat{\mathbf{Y}}]_{ik} \right\} \end{aligned} \tag{12.65}$$

where ψ_k is given by (12.58b) and

$$[\hat{\mathbf{N}}^\pm]_i = \hat{E}_0 \left\{ e^{\gamma_i \mathcal{L}} \pm e^{-\gamma_i \mathcal{L}} \right\} \times \sum_{k=1}^n \left\{ [e_x x_k + e_y y_k] \frac{\sin(\psi_k)}{\psi_k} e^{-j\psi_k} [\hat{\mathbf{T}}^{-1} \hat{\mathbf{Y}}]_{ik} \right\} \quad (12.66)$$

The forcing functions in (12.61) and (12.62) become

$$\hat{\mathbf{V}}_{\text{FT}}(\mathcal{L}) = \frac{1}{2} \hat{\mathbf{Y}}^{-1} \hat{\mathbf{T}} \hat{\mathbf{M}}^+ - \begin{bmatrix} \vdots \\ \hat{E}_{\text{Tk}}(\mathcal{L}) \\ \vdots \end{bmatrix} + \frac{1}{2} \hat{\mathbf{Y}}^{-1} \hat{\mathbf{T}} \hat{\mathbf{N}}^+ \quad (12.67)$$

and

$$\hat{\mathbf{I}}_{\text{FT}}(\mathcal{L}) = -\frac{1}{2} \hat{\mathbf{T}} \hat{\gamma}^{-1} \hat{\mathbf{M}}^- - \frac{1}{2} \hat{\mathbf{T}} \hat{\gamma}^{-1} \hat{\mathbf{N}}^- \quad (12.68)$$

These results can be extended to the case where the reference conductor is an infinite, perfectly conducting ground plane as illustrated in Figure 12.7(b). The total incident field is the sum of the incident field (with the ground plane and the other conductors removed) and the reflected field. Snell’s law shows that the angles of incidence and reflection are the same [A.1]. Similarly, continuity of the tangential electric fields at the surface of the ground plane gives constraints on the y and z components of the electric field. Thus, the incident and reflected (at the ground plane) fields are given by [A.1, H.1]

$$\vec{E}^{\text{inc}} = \hat{E}_0 [e_x \vec{a}_x + e_y \vec{a}_y + e_z \vec{a}_z] e^{-j\beta_x x} e^{-j\beta_y y} e^{-j\beta_z z} \quad (12.69a)$$

$$\vec{E}^{\text{ref}} = \hat{E}_0 [e_x \vec{a}_x - e_y \vec{a}_y - e_z \vec{a}_z] e^{j\beta_x x} e^{-j\beta_y y} e^{-j\beta_z z} \quad (12.69b)$$

Thus, the total fields are

$$\hat{E}_x^{\text{Total}} = \hat{E}_x^{\text{inc}} + \hat{E}_x^{\text{ref}} = 2 \hat{E}_0 e_x \cos(\beta_x x) e^{-j\beta_y y} e^{-j\beta_z z} \quad (12.70a)$$

$$\hat{E}_y^{\text{Total}} = \hat{E}_y^{\text{inc}} + \hat{E}_y^{\text{ref}} = -2 j \hat{E}_0 e_y \sin(\beta_x x) e^{-j\beta_y y} e^{-j\beta_z z} \quad (12.70b)$$

$$\hat{E}_z^{\text{Total}} = \hat{E}_z^{\text{inc}} + \hat{E}_z^{\text{ref}} = -2 j \hat{E}_0 e_z \sin(\beta_x x) e^{-j\beta_y y} e^{-j\beta_z z} \quad (12.70c)$$

Thus, the entries in the vectors in (12.63) and (12.64) become

$$[\hat{\mathbf{M}}^\pm]_i = -2 j \hat{E}_0 e_z \left\{ e^{\gamma_i \mathcal{L}} \frac{[1 - e^{-(\gamma_i + j\beta_z)\mathcal{L}}]}{(\gamma_i + j\beta_z)} \pm e^{-\gamma_i \mathcal{L}} \frac{[e^{(\gamma_i - j\beta_z)\mathcal{L}} - 1]}{(\gamma_i - j\beta_z)} \right\}$$

$$\times \sum_{k=1}^n \left\{ \left[\beta_x x_k \frac{\sin(\beta_x x_k)}{\beta_x x_k} e^{-j\beta_y y_k} \right] \left[\hat{\mathbf{T}}^{-1} \hat{\mathbf{Y}} \right]_{ik} \right\} \quad (12.71)$$

and

$$\begin{aligned} [\hat{\mathbf{N}}^\pm]_i &= \hat{E}_o \left\{ e^{j\gamma \mathcal{L}} \pm e^{-j\gamma \mathcal{L}} \right\} \times \sum_{k=1}^n \left\{ [e_x x_k + e_y y_k] \left[\frac{\sin(\psi_k^+)}{\psi_k^+} \right] e^{-j\psi_k^+} \right. \\ &\quad \left. + [e_x x_k - e_y y_k] \left[\frac{\sin(\psi_k^-)}{\psi_k^-} \right] e^{j\psi_k^-} \right\} \left[\hat{\mathbf{T}}^{-1} \hat{\mathbf{Y}} \right]_{ik} \end{aligned} \quad (12.72a)$$

where

$$\psi_k^\pm = \frac{\beta_x x_k \pm \beta_y y_k}{2} \quad (12.72b)$$

and

$$\begin{aligned} \hat{E}_{\text{Tk}}(\mathcal{L}) &= \hat{E}_o [e_x x_k + e_y y_k] \left[\frac{\sin(\psi_k^+)}{\psi_k^+} \right] e^{-j\psi_k^+} e^{-j\beta_z \mathcal{L}} \\ &\quad + \hat{E}_o [e_x x_k - e_y y_k] \left[\frac{\sin(\psi_k^-)}{\psi_k^-} \right] e^{j\psi_k^-} e^{-j\beta_z \mathcal{L}} \end{aligned} \quad (12.73)$$

These results are substituted into the equations for the terminal voltages for the generalized Thevenin equivalent characterization of the terminal networks given in (12.39) and (12.40) and implemented in the FORTRAN program `INCIDENT.FOR`, which is described in Appendix A.

12.3 THE TIME-DOMAIN SOLUTION

We next will extend the frequency-domain methods of the previous sections to develop the time-domain solutions for MTLs that are excited by external electromagnetic fields that are incident on the line. We will concentrate on *lossless lines*. The primary solution method will be to uncouple the MTL equations via similarity transformations. This yields n uncoupled two-conductor lines that can be modeled using all of the techniques of the previous chapter. In particular, a simple SPICE model will be developed. In addition, there are several other direct methods that will be discussed: lumped-circuit approximate models, the time-domain to frequency-domain (TDFD) transformation, and the finite-difference, time-domain (FDTD) method.

12.3.1 Decoupling the MTL Equations

Diagonalization of the MTL equations as in Chapter 9 is a viable method of solution for lossless lines. Consider the MTL equations for a lossless line:

$$\frac{\partial}{\partial z} \mathbf{V}(z, t) = -\mathbf{L} \frac{\partial}{\partial t} \mathbf{I}(z, t) + \mathbf{V}_F(z, t) \tag{12.74a}$$

$$\frac{\partial}{\partial z} \mathbf{I}(z, t) = -\mathbf{C} \frac{\partial}{\partial t} \mathbf{V}(z, t) + \mathbf{I}_F(z, t) \tag{12.74b}$$

In a fashion similar to the techniques of Chapters 7 and 9, define the transformation to *mode* quantities as

$$\mathbf{V}(z, t) = \mathbf{T}_V \mathbf{V}_m(z, t) \tag{12.75a}$$

$$\mathbf{I}(z, t) = \mathbf{T}_I \mathbf{I}_m(z, t) \tag{12.75b}$$

Substituting these into (12.74) gives

$$\frac{\partial}{\partial z} \mathbf{V}_m(z, t) = -\mathbf{L}_m \frac{\partial}{\partial t} \mathbf{I}_m(z, t) + \mathbf{V}_{Fm}(z, t) \tag{12.76a}$$

$$\frac{\partial}{\partial z} \mathbf{I}_m(z, t) = -\mathbf{C}_m \frac{\partial}{\partial t} \mathbf{V}_m(z, t) + \mathbf{I}_{Fm}(z, t) \tag{12.76b}$$

where \mathbf{L}_m and \mathbf{C}_m are the $n \times n$ matrices

$$\mathbf{L}_m = \mathbf{T}_V^{-1} \mathbf{L} \mathbf{T}_I \tag{12.77a}$$

$$\mathbf{C}_m = \mathbf{T}_I^{-1} \mathbf{C} \mathbf{T}_V \tag{12.77b}$$

and the incident field forcing functions for the *modes* become

$$\mathbf{V}_{Fm}(z, t) = \mathbf{T}_V^{-1} \mathbf{V}_F(z, t) \tag{12.78a}$$

$$\mathbf{I}_{Fm}(z, t) = \mathbf{T}_I^{-1} \mathbf{I}_F(z, t) \tag{12.78b}$$

If \mathbf{T}_V and \mathbf{T}_I can be chosen such that \mathbf{L}_m and \mathbf{C}_m are *diagonal* matrices as

$$\begin{aligned} \mathbf{L}_m &= \mathbf{T}_V^{-1} \mathbf{L} \mathbf{T}_I \\ &= \begin{bmatrix} l_{m1} & 0 & \cdots & \cdots & 0 \\ 0 & \ddots & \ddots & \ddots & \vdots \\ \vdots & \ddots & l_{mi} & \ddots & \vdots \\ \vdots & \ddots & \ddots & \ddots & 0 \\ 0 & \cdots & \cdots & 0 & l_{mn} \end{bmatrix} \end{aligned} \tag{12.79a}$$

$$\begin{aligned}
 \mathbf{C}_m &= \mathbf{T}_I^{-1} \mathbf{C} \mathbf{T}_V \\
 &= \begin{bmatrix} c_{m1} & 0 & \cdots & \cdots & 0 \\ 0 & \ddots & \ddots & \ddots & \vdots \\ \vdots & \ddots & c_{mi} & \ddots & \vdots \\ \vdots & \ddots & \ddots & \ddots & 0 \\ 0 & \cdots & \cdots & 0 & c_{mn} \end{bmatrix} \quad (12.79b)
 \end{aligned}$$

then (12.76) represent n uncoupled sets of two-conductor lines, each with incident field excitation through elements of the vectors $\mathbf{V}_{Fm}(z, t)$ and $\mathbf{I}_{Fm}(z, t)$. Once the solution to these uncoupled two-conductor lines has been obtained, we return to the original variables via the transformations given in (12.75). Hence, the basic solution technique utilizes the solution for a field-illuminated lossless two-conductor line that was obtained in the previous chapter.

As discussed in Chapters 7 and 9, a suitable transformation can be found that simultaneously diagonalizes \mathbf{L} and \mathbf{C} . This transformation is obtained by first determining a real orthogonal transformation \mathbf{U} that diagonalizes \mathbf{C} as

$$\mathbf{U}^t \mathbf{C} \mathbf{U} = \theta^2 \quad (12.80)$$

where θ^2 is a diagonal matrix and \mathbf{U}^t denotes the *transpose* of \mathbf{U} . Since \mathbf{C} is real and symmetric, this can always be done. Furthermore, since \mathbf{C} is positive definite, all elements of θ^2 are real and positive so that we can form the square root of that matrix, θ , which is also diagonal and will have real elements on its main diagonal and zeros elsewhere. Next, find a real orthogonal transformation \mathbf{S} such that

$$\mathbf{S}^t (\theta \mathbf{U}^t \mathbf{L} \mathbf{U} \theta) \mathbf{S} = \Lambda^2 \quad (12.81)$$

where Λ^2 is again a *diagonal* matrix with real, positive elements on its diagonal as

$$\Lambda^2 = \begin{bmatrix} \Lambda_1^2 & 0 & \cdots & \cdots & 0 \\ 0 & \ddots & \ddots & \ddots & \vdots \\ \vdots & \ddots & \Lambda_i^2 & \ddots & \vdots \\ \vdots & \ddots & \ddots & \ddots & 0 \\ 0 & \cdots & \cdots & 0 & \Lambda_n^2 \end{bmatrix} \quad (12.82)$$

This is always possible since the matrix in parentheses, $(\theta \mathbf{U}^t \mathbf{L} \mathbf{U} \theta)$, is real and symmetric. Define an $n \times n$ matrix \mathbf{T} as

$$\mathbf{T} = \mathbf{U} \theta \mathbf{S} \quad (12.83)$$

Normalizing the columns of \mathbf{T} to unity length gives

$$\mathbf{T}_{\text{norm}} = \mathbf{T} \alpha \tag{12.84}$$

where α is an $n \times n$ diagonal matrix. We define the above transformations as

$$\begin{aligned} \mathbf{T}_I &= \mathbf{T}_{\text{norm}} \\ &= \mathbf{U} \theta \mathbf{S} \alpha \end{aligned} \tag{12.85}$$

$$\mathbf{T}_V = \mathbf{U} \theta^{-1} \mathbf{S} \alpha^{-1} \tag{12.86}$$

The transformations \mathbf{T}_V and \mathbf{T}_I are related as

$$\begin{aligned} \mathbf{T}_V \mathbf{T}_I^t &= \mathbf{U} \theta^{-1} \mathbf{S} \alpha^{-1} \alpha \mathbf{S}^t \theta \mathbf{U}^t \\ &= \mathbf{1}_n \end{aligned} \tag{12.87a}$$

where $\mathbf{1}_n$ is the $n \times n$ identity matrix, and we have used the identities $\mathbf{S}^{-1} = \mathbf{S}^t$ and $\mathbf{U}^{-1} = \mathbf{U}^t$ for these orthogonal transformations. Hence,

$$\mathbf{T}_V^{-1} = \mathbf{T}_I^t \tag{12.87b}$$

We can directly show that these transformations simultaneously diagonalize \mathbf{L} and \mathbf{C} by writing

$$\begin{aligned} \mathbf{T}_V^{-1} \mathbf{L} \mathbf{T}_I &= \alpha \underbrace{\mathbf{S}^t \theta \mathbf{U}^t \mathbf{L} \mathbf{U} \theta \mathbf{S}}_{\Lambda^2} \alpha \\ &= \alpha^2 \Lambda^2 \end{aligned} \tag{12.88a}$$

and

$$\begin{aligned} \mathbf{T}_I^{-1} \mathbf{C} \mathbf{T}_V &= \alpha^{-1} \mathbf{S}^t \theta^{-1} \underbrace{\mathbf{U}^t \mathbf{C} \mathbf{U}}_{\theta^2} \theta^{-1} \mathbf{S} \alpha^{-1} \\ &= \alpha^{-2} \end{aligned} \tag{12.88b}$$

or $\mathbf{T}_V^{-1} \mathbf{C}^{-1} \mathbf{T}_I = \alpha^2$. Comparing (12.88) to (12.79) we see that

$$l_{mi} = \alpha_i^2 \Lambda_i^2 \tag{12.89a}$$

and

$$c_{mi} = \alpha_i^{-2} \tag{12.89b}$$

The basic idea is to determine the frequency-domain solution and then to transform that to the time domain. From Chapter 7, the matrix of propagation constants in the

frequency-domain result is

$$\begin{aligned}
 \hat{\gamma}^2 &= \hat{\mathbf{T}}_I^{-1} \hat{\mathbf{Y}} \hat{\mathbf{Z}} \hat{\mathbf{T}}_I \\
 &= -\omega^2 \mathbf{T}_I^{-1} \mathbf{C} \mathbf{L} \mathbf{T}_I^{-1} \\
 &= -\omega^2 \underbrace{\mathbf{T}_I^{-1} \mathbf{C} \mathbf{T}_V}_{\alpha^{-2}} \underbrace{\mathbf{T}_V^{-1} \mathbf{L} \mathbf{T}_I}_{\alpha^2 \Lambda^2} \\
 &= -\omega^2 \Lambda^2
 \end{aligned} \tag{12.90}$$

Also from Chapter 7, the characteristic impedance is real and becomes

$$\begin{aligned}
 \mathbf{Z}_C &= \hat{\mathbf{Y}}^{-1} \hat{\mathbf{T}}_I \hat{\gamma} \hat{\mathbf{T}}_I^{-1} \\
 &= \mathbf{C}^{-1} \mathbf{T}_I \Lambda \mathbf{T}_I^{-1}
 \end{aligned} \tag{12.91}$$

From the decoupled equations in (12.76) and (12.79), the mode characteristic impedances and velocities of propagation become, using (12.89),

$$\begin{aligned}
 Z_{Cmi} &= \sqrt{\frac{l_{mi}}{c_{mi}}} \\
 &= \alpha_i^2 \Lambda_i
 \end{aligned} \tag{12.92}$$

$$\begin{aligned}
 v_{mi} &= \frac{1}{\sqrt{l_{mi} c_{mi}}} \\
 &= \frac{1}{\Lambda_i}
 \end{aligned} \tag{12.93}$$

Hence, the modal characteristic impedance matrix is diagonal as

$$\begin{aligned}
 \mathbf{Z}_{Cm} &= \alpha^2 \Lambda \\
 &= \underbrace{\mathbf{T}_V^{-1} \mathbf{C}^{-1} \mathbf{T}_I}_{\alpha^2} \Lambda \\
 &= \mathbf{T}_V^{-1} \underbrace{\mathbf{C}^{-1} \mathbf{T}_I \Lambda \mathbf{T}_I^{-1}}_{\mathbf{Z}_C} \mathbf{T}_I \\
 &= \mathbf{T}_V^{-1} \mathbf{Z}_C \mathbf{T}_I
 \end{aligned} \tag{12.94}$$

The frequency-domain chain-parameter matrix relates the phasor voltages and currents at one end of the line to those at the other end as

$$\hat{\mathbf{V}}(\mathcal{L}) = \hat{\Phi}_{11}(\mathcal{L}) \hat{\mathbf{V}}(0) + \hat{\Phi}_{12}(\mathcal{L}) \hat{\mathbf{I}}(0) + \hat{\mathbf{V}}_{FT}(\mathcal{L}) \tag{12.95a}$$

$$\hat{\mathbf{I}}(\mathcal{L}) = \hat{\Phi}_{21}(\mathcal{L}) \hat{\mathbf{V}}(0) + \hat{\Phi}_{22}(\mathcal{L}) \hat{\mathbf{I}}(0) + \hat{\mathbf{I}}_{FT}(\mathcal{L}) \tag{12.95b}$$

where the total forcing functions are given by

$$\hat{\mathbf{V}}_{\text{FT}}(\mathcal{L}) = \int_0^{\mathcal{L}} [\hat{\Phi}_{11}(\mathcal{L} - \tau) \hat{\mathbf{V}}_{\text{F}}(\tau) + \hat{\Phi}_{12}(\mathcal{L} - \tau) \hat{\mathbf{I}}_{\text{F}}(\tau)] d\tau \quad (12.96a)$$

$$\hat{\mathbf{I}}_{\text{FT}}(\mathcal{L}) = \int_0^{\mathcal{L}} [\hat{\Phi}_{21}(\mathcal{L} - \tau) \hat{\mathbf{V}}_{\text{F}}(\tau) + \hat{\Phi}_{22}(\mathcal{L} - \tau) \hat{\mathbf{I}}_{\text{F}}(\tau)] d\tau \quad (12.96b)$$

and the chain-parameter submatrices are, for a lossless line,

$$\hat{\Phi}_{11}(\mathcal{L}) = \frac{1}{2} \mathbf{C}^{-1} \mathbf{T}_I \left(\mathbf{e}^{j\omega \Lambda \mathcal{L}} + \mathbf{e}^{-j\omega \Lambda \mathcal{L}} \right) \mathbf{T}_I^{-1} \mathbf{C} \quad (12.97a)$$

$$\begin{aligned} \hat{\Phi}_{12}(\mathcal{L}) &= -\frac{1}{2} \mathbf{C}^{-1} \mathbf{T}_I \Lambda \left(\mathbf{e}^{j\omega \Lambda \mathcal{L}} - \mathbf{e}^{-j\omega \Lambda \mathcal{L}} \right) \mathbf{T}_I^{-1} \\ &= -\frac{1}{2} \underbrace{\mathbf{C}^{-1} \mathbf{T}_I \Lambda \mathbf{T}_I^{-1}}_{\mathbf{Z}_C} \mathbf{T}_I \left(\mathbf{e}^{j\omega \Lambda \mathcal{L}} - \mathbf{e}^{-j\omega \Lambda \mathcal{L}} \right) \mathbf{T}_I^{-1} \end{aligned} \quad (12.97b)$$

$$\begin{aligned} \hat{\Phi}_{21}(\mathcal{L}) &= -\frac{1}{2} \mathbf{T}_I \left(\mathbf{e}^{j\omega \Lambda \mathcal{L}} - \mathbf{e}^{-j\omega \Lambda \mathcal{L}} \right) \Lambda^{-1} \mathbf{T}_I^{-1} \mathbf{C} \\ &= -\frac{1}{2} \mathbf{T}_I \left(\mathbf{e}^{j\omega \Lambda \mathcal{L}} - \mathbf{e}^{-j\omega \Lambda \mathcal{L}} \right) \mathbf{T}_I^{-1} \underbrace{\mathbf{T}_I \Lambda^{-1} \mathbf{T}_I^{-1} \mathbf{C}}_{\mathbf{Z}_C^{-1}} \end{aligned} \quad (12.97c)$$

$$\hat{\Phi}_{22}(\mathcal{L}) = \frac{1}{2} \mathbf{T}_I \left(\mathbf{e}^{j\omega \Lambda \mathcal{L}} + \mathbf{e}^{-j\omega \Lambda \mathcal{L}} \right) \mathbf{T}_I^{-1} \quad (12.97d)$$

where $\mathbf{e}^{\pm j\omega \Lambda \mathcal{L}}$ are diagonal matrices with $e^{\pm j\omega \Lambda_i \mathcal{L}}$ on the main diagonals. Transforming to mode quantities yields

$$\hat{\mathbf{V}}_{\text{m}}(\mathcal{L}) = \hat{\Phi}_{\text{m}11}(\mathcal{L}) \hat{\mathbf{V}}_{\text{m}}(0) + \hat{\Phi}_{\text{m}12}(\mathcal{L}) \hat{\mathbf{I}}_{\text{m}}(0) + \hat{\mathbf{V}}_{\text{FTm}}(\mathcal{L}) \quad (12.98a)$$

$$\hat{\mathbf{I}}_{\text{m}}(\mathcal{L}) = \hat{\Phi}_{\text{m}21}(\mathcal{L}) \hat{\mathbf{V}}_{\text{m}}(0) + \hat{\Phi}_{\text{m}22}(\mathcal{L}) \hat{\mathbf{I}}_{\text{m}}(0) + \hat{\mathbf{I}}_{\text{FTm}}(\mathcal{L}) \quad (12.98b)$$

where the modal chain-parameter submatrices are

$$\begin{aligned} \hat{\Phi}_{\text{m}11}(\mathcal{L}) &= \mathbf{T}_V^{-1} \hat{\Phi}_{11}(\mathcal{L}) \mathbf{T}_V \\ &= \frac{1}{2} \left(\mathbf{e}^{j\omega \Lambda \mathcal{L}} + \mathbf{e}^{-j\omega \Lambda \mathcal{L}} \right) \end{aligned} \quad (12.99a)$$

$$\begin{aligned}\hat{\Phi}_{m12}(\mathcal{L}) &= \mathbf{T}_V^{-1} \hat{\Phi}_{12}(\mathcal{L}) \mathbf{T}_I \\ &= -\frac{1}{2} \underbrace{\alpha^2 \Lambda}_{\mathbf{Z}_{Cm}} \left(\mathbf{e}^{j\omega \Lambda \mathcal{L}} - \mathbf{e}^{-j\omega \Lambda \mathcal{L}} \right)\end{aligned}\quad (12.99b)$$

$$\begin{aligned}\hat{\Phi}_{m21}(\mathcal{L}) &= \mathbf{T}_I^{-1} \hat{\Phi}_{21}(\mathcal{L}) \mathbf{T}_V \\ &= -\frac{1}{2} \left(\mathbf{e}^{j\omega \Lambda \mathcal{L}} - \mathbf{e}^{-j\omega \Lambda \mathcal{L}} \right) \underbrace{\alpha^{-2} \Lambda^{-1}}_{\mathbf{Z}_{Cm}^{-1}}\end{aligned}\quad (12.99c)$$

$$\begin{aligned}\hat{\Phi}_{m22}(\mathcal{L}) &= \mathbf{T}_I^{-1} \hat{\Phi}_{22}(\mathcal{L}) \mathbf{T}_I \\ &= \frac{1}{2} \left(\mathbf{e}^{j\omega \Lambda \mathcal{L}} + \mathbf{e}^{-j\omega \Lambda \mathcal{L}} \right)\end{aligned}\quad (12.99d)$$

where we have used the identity $\mathbf{T}_V^{-1} \mathbf{C}^{-1} \mathbf{T}_I = \alpha^2$ and α^2 is a diagonal matrix. We have also used the fact that in the multiplication of diagonal matrices the order of multiplication can be interchanged. The total modal forcing functions due to the incident field become

$$\begin{aligned}\hat{\mathbf{V}}_{FTm}(\mathcal{L}) &= \mathbf{T}_V^{-1} \hat{\mathbf{V}}_{FT}(\mathcal{L}) \\ &= \int_0^{\mathcal{L}} \left[\hat{\Phi}_{m11}(\mathcal{L} - \tau) \mathbf{T}_I^t \hat{\mathbf{V}}_F(\tau) + \hat{\Phi}_{m12}(\mathcal{L} - \tau) \mathbf{T}_V^t \hat{\mathbf{I}}_F(\tau) \right] d\tau \\ &= \int_0^{\mathcal{L}} \left[\frac{1}{2} \left(\mathbf{e}^{j\omega \Lambda (\mathcal{L}-\tau)} + \mathbf{e}^{-j\omega \Lambda (\mathcal{L}-\tau)} \right) \mathbf{T}_I^t \hat{\mathbf{V}}_F(\tau) \right. \\ &\quad \left. - \frac{1}{2} \left(\mathbf{e}^{j\omega \Lambda (\mathcal{L}-\tau)} - \mathbf{e}^{-j\omega \Lambda (\mathcal{L}-\tau)} \right) \mathbf{Z}_{Cm} \mathbf{T}_V^t \hat{\mathbf{I}}_F(\tau) \right] d\tau\end{aligned}\quad (12.100a)$$

$$\begin{aligned}\hat{\mathbf{I}}_{FTm}(\mathcal{L}) &= \mathbf{T}_I^{-1} \hat{\mathbf{I}}_{FT}(\mathcal{L}) \\ &= \int_0^{\mathcal{L}} \left[\hat{\Phi}_{m21}(\mathcal{L} - \tau) \mathbf{T}_I^t \hat{\mathbf{V}}_F(\tau) + \hat{\Phi}_{m22}(\mathcal{L} - \tau) \mathbf{T}_V^t \hat{\mathbf{I}}_F(\tau) \right] d\tau \\ &= \int_0^{\mathcal{L}} \left[-\frac{1}{2} \left(\mathbf{e}^{j\omega \Lambda (\mathcal{L}-\tau)} - \mathbf{e}^{-j\omega \Lambda (\mathcal{L}-\tau)} \right) \mathbf{Z}_{Cm}^{-1} \mathbf{T}_I^t \hat{\mathbf{V}}_F(\tau) \right. \\ &\quad \left. + \frac{1}{2} \left(\mathbf{e}^{j\omega \Lambda (\mathcal{L}-\tau)} + \mathbf{e}^{-j\omega \Lambda (\mathcal{L}-\tau)} \right) \mathbf{T}_V^t \hat{\mathbf{I}}_F(\tau) \right] d\tau\end{aligned}\quad (12.100b)$$

where we have substituted, from (12.87), $\mathbf{T}_V^{-1} = \mathbf{T}_I^t$ and $\mathbf{T}_I^{-1} = \mathbf{T}_V^t$.

12.3.2 A SPICE Equivalent Circuit

We now obtain the time-domain version of the chain-parameter representation. As in the previous chapter, this will show how to construct a time-domain equivalent circuit that is implementable in the SPICE program. Substituting (12.99) into (12.98) yields

$$\begin{aligned}\hat{\mathbf{V}}_m(\mathcal{L}) &= \frac{1}{2} \left(\mathbf{e}^{j\omega\Lambda\mathcal{L}} + \mathbf{e}^{-j\omega\Lambda\mathcal{L}} \right) \hat{\mathbf{V}}_m(0) \\ &\quad - \frac{1}{2} \left(\mathbf{e}^{j\omega\Lambda\mathcal{L}} - \mathbf{e}^{-j\omega\Lambda\mathcal{L}} \right) \mathbf{Z}_{\text{Cm}} \hat{\mathbf{I}}_m(0) + \hat{\mathbf{V}}_{\text{FTm}}(\mathcal{L})\end{aligned}\quad (12.101a)$$

$$\begin{aligned}\mathbf{Z}_{\text{Cm}} \hat{\mathbf{I}}_m(\mathcal{L}) &= -\frac{1}{2} \left(\mathbf{e}^{j\omega\Lambda\mathcal{L}} - \mathbf{e}^{-j\omega\Lambda\mathcal{L}} \right) \hat{\mathbf{V}}_m(0) \\ &\quad + \frac{1}{2} \left(\mathbf{e}^{j\omega\Lambda\mathcal{L}} + \mathbf{e}^{-j\omega\Lambda\mathcal{L}} \right) \mathbf{Z}_{\text{Cm}} \hat{\mathbf{I}}_m(0) + \mathbf{Z}_{\text{Cm}} \hat{\mathbf{I}}_{\text{FTm}}(\mathcal{L})\end{aligned}\quad (12.101b)$$

Adding and subtracting these yields

$$\hat{\mathbf{V}}_m(0) - \mathbf{Z}_{\text{Cm}} \hat{\mathbf{I}}_m(0) = \mathbf{e}^{-j\omega\Lambda\mathcal{L}} \left[\hat{\mathbf{V}}_m(\mathcal{L}) - \mathbf{Z}_{\text{Cm}} \hat{\mathbf{I}}_m(\mathcal{L}) \right] + \hat{\mathbf{E}}_0(\mathcal{L}) \quad (12.102a)$$

$$\hat{\mathbf{V}}_m(\mathcal{L}) + \mathbf{Z}_{\text{Cm}} \hat{\mathbf{I}}_m(\mathcal{L}) = \mathbf{e}^{-j\omega\Lambda\mathcal{L}} \left[\hat{\mathbf{V}}_m(0) + \mathbf{Z}_{\text{Cm}} \hat{\mathbf{I}}_m(0) \right] + \hat{\mathbf{E}}_{\mathcal{L}}(\mathcal{L}) \quad (12.102b)$$

where

$$\hat{\mathbf{E}}_0(\mathcal{L}) = -\mathbf{e}^{-j\omega\Lambda\mathcal{L}} \left[\hat{\mathbf{V}}_{\text{FTm}}(\mathcal{L}) - \mathbf{Z}_{\text{Cm}} \hat{\mathbf{I}}_{\text{FTm}}(\mathcal{L}) \right] \quad (12.103a)$$

$$\hat{\mathbf{E}}_{\mathcal{L}}(\mathcal{L}) = \left[\hat{\mathbf{V}}_{\text{FTm}}(\mathcal{L}) + \mathbf{Z}_{\text{Cm}} \hat{\mathbf{I}}_{\text{FTm}}(\mathcal{L}) \right] \quad (12.103b)$$

Recognizing the basic time-delay transformation:

$$e^{\pm j\omega T} \hat{F}(\omega) \Leftrightarrow F(t - T) \quad (12.104)$$

these become, in the time domain,

$$\left[\mathbf{V}_m(0, t) - \mathbf{Z}_{\text{Cm}} \mathbf{I}_m(0, t) \right]_i = \left[\mathbf{V}_m(\mathcal{L}, t - T_i) - \mathbf{Z}_{\text{Cm}} \mathbf{I}_m(\mathcal{L}, t - T_i) \right]_i + \left[\mathbf{E}_0(t) \right]_i \quad (12.105a)$$

$$\left[\mathbf{V}_m(\mathcal{L}, t) + \mathbf{Z}_{\text{Cm}} \mathbf{I}_m(\mathcal{L}, t) \right]_i = \left[\mathbf{V}_m(0, t - T_i) + \mathbf{Z}_{\text{Cm}} \mathbf{I}_m(0, t - T_i) \right]_i + \left[\mathbf{E}_{\mathcal{L}}(t) \right]_i \quad (12.105b)$$

where we denote the entry in the i th row of a vector \mathbf{V} as $[\mathbf{V}]_i$, and the one-way time delay of the i th modal line is denoted by

$$\begin{aligned} T_i &= \frac{\mathcal{L}}{v_{mi}} \\ &= \Lambda_i \mathcal{L} \end{aligned} \quad (12.106)$$

The additional sources are

$$[\mathbf{E}_0(t)]_i = -[\mathbf{V}_{\text{FTm}}(\mathcal{L}, t - T_i) - \mathbf{Z}_{\text{Cm}} \mathbf{I}_{\text{FTm}}(\mathcal{L}, t - T_i)]_i \quad (12.107a)$$

$$[\mathbf{E}_{\mathcal{L}}(t)]_i = [\mathbf{V}_{\text{FTm}}(\mathcal{L}, t) + \mathbf{Z}_{\text{Cm}} \mathbf{I}_{\text{FTm}}(\mathcal{L}, t)]_i \quad (12.107b)$$

Equations (12.105) suggest the usual SPICE equivalent circuit for the modes where we add to it the sources due to the incident field, $[\mathbf{E}_0(t)]_i$ and $[\mathbf{E}_{\mathcal{L}}(t)]_i$. The transformation back to the actual line voltages and currents is accomplished with controlled sources that represent the mode transformations according to (12.75):

$$[\mathbf{V}(z, t)]_i = \sum_{k=1}^n \{ [\mathbf{T}_V]_{ik} [\mathbf{V}_m(z, t)]_k \} \quad (12.108a)$$

$$[\mathbf{I}_m(z, t)]_i = \sum_{k=1}^n \left\{ \left[\mathbf{T}_I^{-1} \right]_{ik} [\mathbf{I}(z, t)]_k \right\} \quad (12.108b)$$

as in Chapter 9. Thus, the only difference between the SPICE model derived for the case of the excitation in the terminal networks and this case wherein the excitation is via an incident field is the implementation of the sources due to that field given in (12.105) and (12.107).

Although the above is valid for any time-domain form of the incident field, we will now restrict our attention to uniform plane wave excitation of the line. The modal forcing functions in (12.103) become, using the equivalent form given in (12.31) and (12.32),

$$\begin{aligned} \hat{\mathbf{E}}_0(\mathcal{L}) &= -\mathbf{e}^{-j\omega \Lambda \mathcal{L}} \left[\hat{\mathbf{V}}_{\text{FTm}}(\mathcal{L}) - \mathbf{Z}_{\text{Cm}} \hat{\mathbf{I}}_{\text{FTm}}(\mathcal{L}) \right] \\ &= -\mathbf{e}^{-j\omega \Lambda \mathcal{L}} \left\{ \int_0^{\mathcal{L}} [\hat{\Phi}_{m11}(\mathcal{L} - \tau) - \mathbf{Z}_{\text{Cm}} \hat{\Phi}_{m21}(\mathcal{L} - \tau)] \mathbf{T}_I^t \hat{\mathbf{E}}_L(\tau) d\tau \right. \\ &\quad \left. + [\hat{\Phi}_{m11}(\mathcal{L}) - \mathbf{Z}_{\text{Cm}} \hat{\Phi}_{m21}(\mathcal{L})] \mathbf{T}_I^t \hat{\mathbf{E}}_T(0) - \mathbf{T}_I^t \hat{\mathbf{E}}_T(\mathcal{L}) \right\} \quad (12.109a) \\ &= -\int_0^{\mathcal{L}} \mathbf{e}^{-j\omega \Lambda \tau} \mathbf{T}_I^t \hat{\mathbf{E}}_L(\tau) d\tau \\ &\quad + \mathbf{e}^{-j\omega \Lambda \mathcal{L}} \mathbf{T}_I^t \hat{\mathbf{E}}_T(\mathcal{L}) - \mathbf{T}_I^t \hat{\mathbf{E}}_T(0) \end{aligned}$$

$$\begin{aligned}
 \hat{\mathbf{E}}_{\mathcal{L}}(\mathcal{L}) &= [\hat{\mathbf{V}}_{\text{FTm}}(\mathcal{L}) + \mathbf{Z}_{\text{Cm}} \hat{\mathbf{I}}_{\text{FTm}}(\mathcal{L})] \\
 &= \left\{ \int_0^{\mathcal{L}} [\hat{\Phi}_{\text{m11}}(\mathcal{L} - \tau) + \mathbf{Z}_{\text{Cm}} \hat{\Phi}_{\text{m21}}(\mathcal{L} - \tau)] \mathbf{T}_I^t \hat{\mathbf{E}}_{\text{L}}(\tau) d\tau \right. \\
 &\quad \left. + [\hat{\Phi}_{\text{m11}}(\mathcal{L}) + \mathbf{Z}_{\text{Cm}} \hat{\Phi}_{\text{m21}}(\mathcal{L})] \mathbf{T}_I^t \hat{\mathbf{E}}_{\text{T}}(0) - \mathbf{T}_I^t \hat{\mathbf{E}}_{\text{T}}(\mathcal{L}) \right\} \\
 &= \int_0^{\mathcal{L}} \mathbf{e}^{-j\omega \Lambda(\mathcal{L} - \tau)} \mathbf{T}_I^t \hat{\mathbf{E}}_{\text{L}}(\tau) d\tau \\
 &\quad - \mathbf{T}_I^t \hat{\mathbf{E}}_{\text{T}}(\mathcal{L}) + \mathbf{e}^{-j\omega \Lambda \mathcal{L}} \mathbf{T}_I^t \hat{\mathbf{E}}_{\text{T}}(0)
 \end{aligned} \tag{12.109b}$$

where $\hat{\mathbf{E}}_{\text{T}}$ denotes the vector of contributions from the *transverse* electric field and $\hat{\mathbf{E}}_{\text{L}}$ denotes the vector of contributions from the *longitudinal* electric field. If the reference conductor is placed at the origin of the coordinate system, $x = 0$, $y = 0$, as shown in Figure 12.7(a), the transverse field contributions can again be written in terms of the cross-sectional coordinates of the k th conductor (x_k , y_k) using the general form of the incident field in (12.54) as in (12.58)

$$\begin{aligned}
 [\hat{\mathbf{E}}_{\text{T}}(\mathcal{L})]_k &= \int_a^{d'} \vec{\hat{E}}_{\text{tk}}^{\text{inc}} \cdot d\vec{l} \\
 &= \hat{E}_0 [e_x x_k + e_y y_k] \frac{\sin(\psi_k)}{\psi_k} e^{-j\psi_k} e^{-j\beta_z \mathcal{L}}
 \end{aligned} \tag{12.110a}$$

where $d_k = \sqrt{x_k^2 + y_k^2}$ is the straight-line distance between the reference conductor and the k th conductor in the transverse plane and

$$\psi_k = \frac{(\beta_x x_k + \beta_y y_k)}{2} \tag{12.110b}$$

Similarly, the contributions due to the longitudinal field are given in (12.59) as

$$\begin{aligned}
 [\hat{\mathbf{E}}_{\text{L}}(z)]_k &= \hat{E}_z^{\text{inc}}(x_k, y_k, z) - \hat{E}_z^{\text{inc}}(0, 0, z) \\
 &= -j(\beta_x x_k + \beta_y y_k) \hat{E}_0 e_z \frac{\sin(\psi_k)}{\psi_k} e^{-j\psi_k} e^{-j\beta_z z}
 \end{aligned} \tag{12.111}$$

Denoting the cross-sectional time delay as

$$T_{xyk} = \frac{x_k}{v_x} + \frac{y_k}{v_y} \tag{12.112}$$

and

$$T_z = \frac{\mathcal{L}}{v_z} \quad (12.113)$$

along with the time delay of the modes:

$$T_i = \frac{\mathcal{L}}{v_{mi}} = \Lambda_i \mathcal{L} \quad (12.114)$$

(12.109) becomes

$$\begin{aligned} [\hat{\mathbf{E}}_0(\mathcal{L})]_i &= \hat{E}_o(\omega) \sum_{k=1}^n \left\{ \left[\frac{\sin(\psi_k)}{\psi_k} \right] [\mathbf{T}'_I]_{ik} \right. \\ &\quad \times [e_z T_{xyk} \mathcal{L} - (e_x x_k + e_y y_k) (T_i + T_z)] \\ &\quad \left. \times \frac{\left(e^{-j\omega \frac{T_{xyk}}{2}} - e^{-j\omega \left(T_i + T_z + \frac{T_{xyk}}{2} \right)} \right)}{(T_i + T_z)} \right\} \end{aligned} \quad (12.115a)$$

$$\begin{aligned} [\hat{\mathbf{E}}_{\mathcal{L}}(\mathcal{L})]_i &= \hat{E}_o(\omega) \sum_{k=1}^n \left\{ \left[\frac{\sin(\psi_k)}{\psi_k} \right] [\mathbf{T}^t_I]_{ik} \right. \\ &\quad \times [e_z T_{xyk} \mathcal{L} + (e_x x_k + e_y y_k) (T_i - T_z)] \\ &\quad \left. \times \frac{\left(e^{-j\omega \left(T_i + \frac{T_{xyk}}{2} \right)} - e^{-j\omega \left(T_z + \frac{T_{xyk}}{2} \right)} \right)}{(T_i - T_z)} \right\} \end{aligned} \quad (12.115b)$$

Again, recognizing the basic time delay transformation in (12.104), these sources transform to the time domain as

$$[\mathbf{E}_0(t)]_i = \sum_{k=1}^n \{ [e_z T_{xyk} \mathcal{L} - (e_x x_k + e_y y_k) (T_i + T_z)] [\mathbf{T}'_I]_{ik}$$

$$\times p_k(t) * \left. \frac{\mathcal{E}_o \left(t - \frac{T_{xyk}}{2} \right) - \mathcal{E}_o \left(t - T_i - T_z - \frac{T_{xyk}}{2} \right)}{(T_i + T_z)} \right\} \tag{12.116a}$$

$$[\mathbf{E}_{\mathcal{L}}(t)]_i = \sum_{k=1}^n \left\{ [e_z T_{xyk} \mathcal{L} + (e_x x_k + e_y y_k) (T_i - T_z)] [\mathbf{T}_I^t]_{ik} \right. \\ \left. \times p_k(t) * \frac{\mathcal{E}_o \left(t - T_i - \frac{T_{xyk}}{2} \right) - \mathcal{E}_o \left(t - T_z - \frac{T_{xyk}}{2} \right)}{(T_i - T_z)} \right\} \tag{12.116b}$$

where $p_k(t)$ is the pulse function for the k th conductor given by

$$p_k(t) = \begin{cases} 0, & t < -\frac{T_{xyk}}{2} \\ \frac{1}{T_{xyk}}, & -\frac{T_{xyk}}{2} < t < \frac{T_{xyk}}{2} \\ 0, & t > \frac{T_{xyk}}{2} \end{cases} \tag{12.117}$$

as illustrated in Figure 11.12 of Chapter 11 and $*$ denotes the *convolution* operation. Again, let us assume that the line cross-sectional dimensions are electrically small at the significant frequencies of the waveform $\mathcal{E}_o(t)$, so that $p_k(t)$ approximates an impulse:

$$p_k(t) \cong \delta(t) \tag{12.118}$$

Similarly, we will neglect the cross-sectional time delay in the expressions involving $\mathcal{E}_o(t)$, that is, we remove the $T_{xyk}/2$ terms for all k , so that the forcing functions simplify to

$$[\mathbf{E}_0(t)]_i = [\alpha_0]_i \left[\frac{\mathcal{E}_o(t) - \mathcal{E}_o(t - T_i - T_z)}{(T_i + T_z)} \right] \tag{12.119a}$$

$$[\mathbf{E}_{\mathcal{L}}(t)]_i = [\alpha_{\mathcal{L}}]_i \left[\frac{\mathcal{E}_o(t - T_i) - \mathcal{E}_o(t - T_z)}{(T_i - T_z)} \right] \tag{12.119b}$$

where the entries in the $n \times 1$ vectors α_0 and $\alpha_{\mathcal{L}}$ are given by

$$[\alpha_0]_i = \sum_{k=1}^n \left\{ [e_z T_{xyk} \mathcal{L} - (e_x x_k + e_y y_k) (T_i + T_z)] [\mathbf{T}_I^t]_{ik} \right\} \quad (12.120a)$$

$$[\alpha_{\mathcal{L}}]_i = \sum_{k=1}^n \left\{ [e_z T_{xyk} \mathcal{L} + (e_x x_k + e_y y_k) (T_i - T_z)] [\mathbf{T}_I^t]_{ik} \right\} \quad (12.120b)$$

Therefore, the modal expressions in (12.105) simplify to

$$\begin{aligned} [\mathbf{V}_m(0, t) - \mathbf{Z}_{Cm} \mathbf{I}_m(0, t)]_i &= [\mathbf{V}_m(\mathcal{L}, t - T_i) - \mathbf{Z}_{Cm} \mathbf{I}_m(\mathcal{L}, t - T_i)]_i \\ &\quad + [\alpha_0]_i \left[\frac{\mathcal{E}_o(t) - \mathcal{E}_o(t - T_i - T_z)}{(T_i + T_z)} \right] \end{aligned} \quad (12.121a)$$

$$\begin{aligned} [\mathbf{V}_m(\mathcal{L}, t) + \mathbf{Z}_{Cm} \mathbf{I}_m(\mathcal{L}, t)]_i &= [\mathbf{V}_m(0, t - T_i) + \mathbf{Z}_{Cm} \mathbf{I}_m(0, t - T_i)]_i \\ &\quad + [\alpha_{\mathcal{L}}]_i \left[\frac{\mathcal{E}_o(t - T_i) - \mathcal{E}_o(t - T_z)}{(T_i - T_z)} \right] \end{aligned} \quad (12.121b)$$

Equations (12.121) suggest the SPICE model shown in Figure 12.8. The external nodes are denoted as $10i$ (at $z = 0$) and $20i$ (at $z = \mathcal{L}$). Nodes $30i$, $40i$, $50i$, and $60i$ attach to controlled sources that implement the transformations between actual and mode quantities given in (12.108). The remainder of the network implements (12.121) for the i th mode. The five delay lines simulating (12.119) for each mode need not be terminated in the mode characteristic impedances but can be terminated in any characteristic impedance in order to remove reflections and give the desired ideal delay of $\mathcal{E}_o(t)$. If the wave has no propagation component in the z direction, $T_z = 0$, then the last two lines are removed from the model. If the wave has a component in the $+z$ direction, it may happen that $T_i = T_z$, in which case (12.119b) appears to be undefined. However, this term becomes

$$\left[\frac{\mathcal{E}_o(t - T_i) - \mathcal{E}_o(t - T_z)}{(T_i - T_z)} \right]_{T_z \rightarrow T_i} = -\frac{d}{dt} \mathcal{E}_o(t - T_i) \quad (12.122)$$

so that the last delay line is replaced as shown in Figure 12.9. Waves that have a component in the $-z$ direction may result in the last two delay lines having negative delays, which SPICE does not allow. Thus, we must restrict this model to positive T_z . For negative T_z , simply reverse the ends of the model.

The above results for $[\mathbf{E}_0(t)]_i$ and $[\mathbf{E}_{\mathcal{L}}(t)]_i$ for uniform plane wave excitation for a line over an infinite ground plane can similarly be obtained using (12.70). This

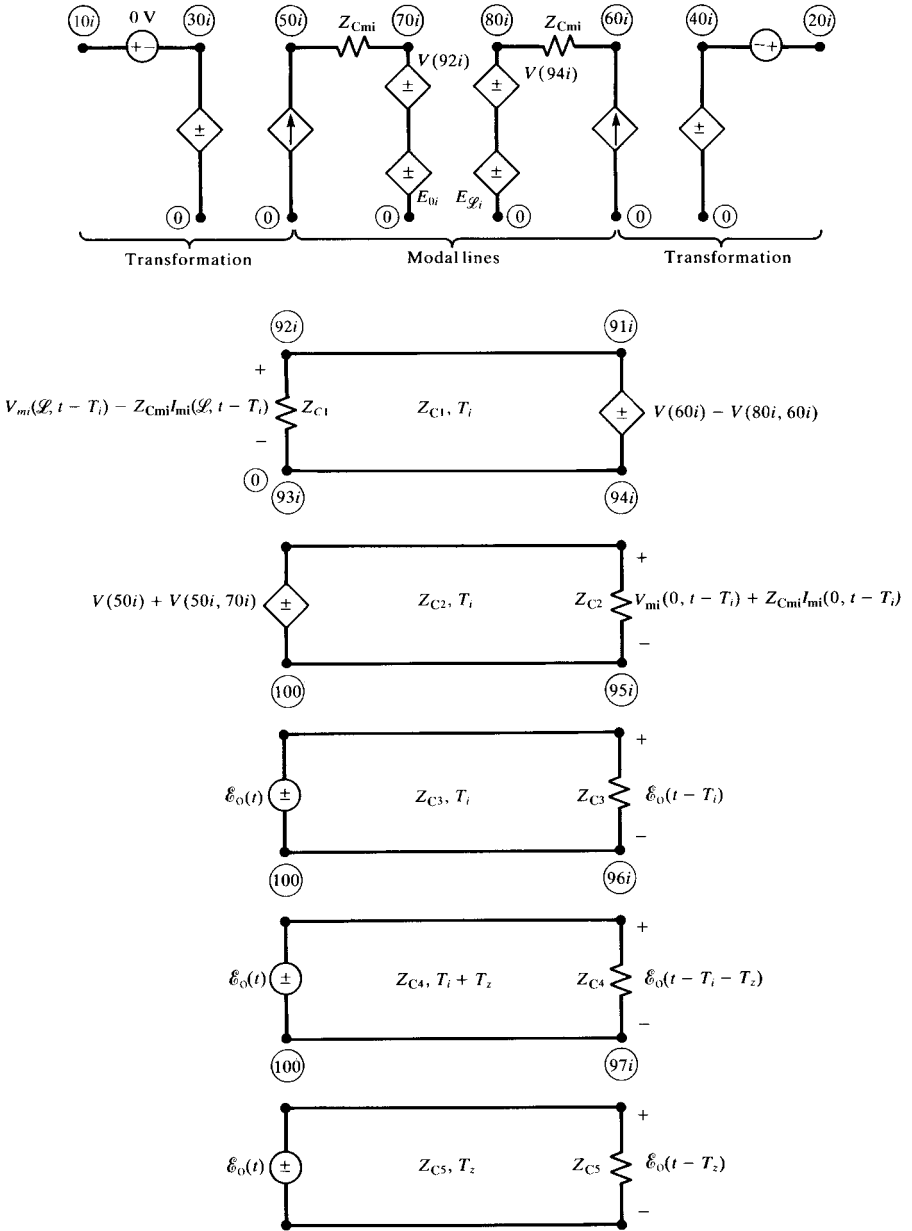


FIGURE 12.8 The SPICE model for an MTL with incident field illumination.

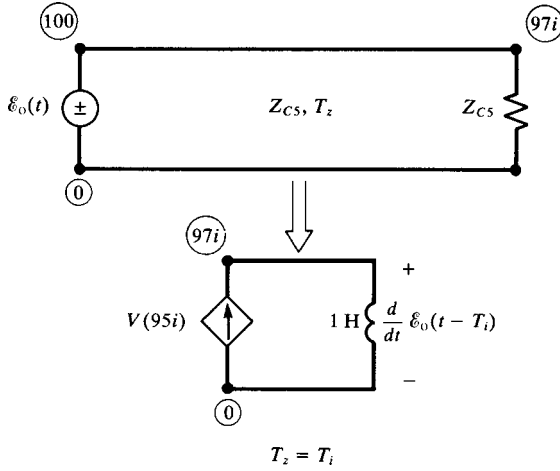


FIGURE 12.9 Replacement of one of the sources in Figure 12.8 for the special case where the propagation is solely in the z direction and the mode velocity equals that of the incident wave.

model is implemented via a SPICE subcircuit generated by the FORTRAN program SPICEINC.FOR described in Appendix A.

12.3.3 Lumped-Circuit Approximate Characterizations

The use of lumped-circuit approximations such as the lumped-Pi and lumped-T circuits parallels all of the previous such uses. The lumped-Pi and lumped-T circuits shown for the phasor frequency-domain solution in Figure 12.5 can be used directly for the time-domain solution by simply replacing the phasor sources $\hat{V}_{Fi} \mathcal{L}$ and $\hat{I}_{Fi} \mathcal{L}$ with their time-domain equivalents $V_{Fi} \mathcal{L}$ and $I_{Fi} \mathcal{L}$.

12.3.4 The Time-Domain to Frequency-Domain (TDFD) Transformation

Perhaps the most straightforward method of obtaining the time-domain response is to view the problem as a two-port with $\mathcal{E}_o(t)$ as the input and the desired terminal response voltage (or current) as the output. The magnitude and phase of $\mathcal{E}_o(t)$ can be obtained with the Fourier transform or can be approximated as a periodic waveform with a sufficiently long period. The frequency-domain transfer function for either a lossless or a lossy line can be obtained with the previous methods with the code INCIDENT.FOR described in Appendix A or, for a lossless line, with SPICEINC.FOR. The magnitudes of the spectral components of $\mathcal{E}_o(t)$ are multiplied by the magnitudes of the transfer function, and the phase angles of $\mathcal{E}_o(t)$ are added to the angles of the transfer function to produce the magnitude and phase of the response in the usual fashion. Then the inverse Fourier transform can be used to convert this back to the time domain.

The method is straightforward and can handle \sqrt{f} skin-effect losses (which INCIDENT.FOR can handle). However, it relies on superposition so that the two-port must be linear. This again means that the line terminations as well as the surrounding medium must be *linear*. Therefore, nonlinear loads as well as corona breakdown in lightning studies cannot be handled with this method.

12.3.5 The Finite-Difference, Time-Domain (FDTD) Solution Method

Another straightforward way of solving the MTL equations is with the FDTD method, which was described for two-conductor lines in the previous chapter. The space and time derivatives are discretized as Δz and Δt , respectively, giving a recursion relation in the form of a set of difference equations. The transmission-line equations in (12.74) become

$$\frac{\partial}{\partial z} \mathbf{V}(z, t) + \mathbf{L} \frac{\partial}{\partial t} \mathbf{I}(z, t) = -\frac{\partial}{\partial z} \mathbf{E}_T(z, t) + \mathbf{E}_L(z, t) \tag{12.123a}$$

$$\frac{\partial}{\partial z} \mathbf{I}(z, t) + \mathbf{C} \frac{\partial}{\partial t} \mathbf{V}(z, t) = -\mathbf{C} \frac{\partial}{\partial t} \mathbf{E}_T(z, t) \tag{12.123b}$$

where the $n \times 1$ vectors \mathbf{E}_T and \mathbf{E}_L are due to the transverse and longitudinal components of the incident electric field, respectively. These were given, in the frequency domain, for a uniform plane wave in (12.110) and (12.111). Thus (removing $\sin \psi_k / \psi_k$ and $e^{-j\psi_k}$)

$$\left[-\frac{\partial}{\partial z} \hat{\mathbf{E}}_T(z) + \hat{\mathbf{E}}_L(z) \right]_i = j\omega \left[\frac{1}{v_z} (e_x x_i + e_y y_i) - \left(\frac{x_i}{v_x} + \frac{y_i}{v_y} \right) e_z \right] \hat{E}_o(\omega) e^{-j\beta_z z} \tag{12.124}$$

This translates in the time domain to

$$-\frac{\partial}{\partial z} \mathbf{E}_T(z, t) + \mathbf{E}_L(z, t) = \left[\frac{1}{v_z} \mathbf{A}_T - \mathbf{A}_L \right] \frac{\partial}{\partial t} \mathcal{E}_o \left(t - \frac{z}{v_z} \right) \tag{12.125a}$$

where

$$\mathbf{A}_T = \begin{bmatrix} \vdots \\ (e_x x_i + e_y y_i) \\ \vdots \end{bmatrix} \tag{12.125b}$$

$$\mathbf{A}_L = \begin{bmatrix} \vdots \\ \left(\frac{x_i}{v_x} + \frac{y_i}{v_y} \right) e_z \\ \vdots \end{bmatrix} \tag{12.125c}$$

Similarly,

$$-\frac{\partial}{\partial t} \mathbf{C} \mathbf{E}_T(z, t) = -\mathbf{C} \mathbf{A}_T \frac{\partial}{\partial t} \mathcal{E}_o \left(t - \frac{z}{v_z} \right) \quad (12.126)$$

The voltage and current solution points are interlaced one-half cell apart as shown in Figure 11.14 of the previous chapter. Similarly, the voltage and current solution times are also interlaced one-half time step apart as shown in Figure 11.14. Using this scheme, the difference equations become

$$\begin{aligned} & \frac{1}{\Delta z} \left[\mathbf{V}_{k+1}^{n+1} - \mathbf{V}_k^{n+1} \right] + \frac{1}{\Delta t} \mathbf{L} \left[\mathbf{I}_k^{n+3/2} - \mathbf{I}_k^{n+1/2} \right] \\ &= \left[\frac{1}{v_z} \mathbf{A}_T - \mathbf{A}_L \right] \frac{1}{\Delta t} \left[\mathcal{E}_o \left(t^{n+3/2} - \frac{(k-1/2) \Delta z}{v_z} \right) \right. \\ & \quad \left. - \mathcal{E}_o \left(t^{n+1/2} - \frac{(k-1/2) \Delta z}{v_z} \right) \right] \end{aligned} \quad (12.127a)$$

for $k = 1, 2, \dots, \text{NDZ}$ and

$$\begin{aligned} & \frac{1}{\Delta z} \left[\mathbf{I}_k^{n+1/2} - \mathbf{I}_{k-1}^{n+1/2} \right] + \frac{1}{\Delta t} \mathbf{C} \left[\mathbf{V}_k^{n+1} - \mathbf{V}_k^n \right] \\ &= -\mathbf{C} \mathbf{A}_T \frac{1}{\Delta t} \left[\mathcal{E}_o \left(t^{n+1} - \frac{(k-1) \Delta z}{v_z} \right) \right. \\ & \quad \left. - \mathcal{E}_o \left(t^n - \frac{(k-1) \Delta z}{v_z} \right) \right] \end{aligned} \quad (12.127b)$$

for $k = 2, \dots, \text{NDZ}$, where

$$\mathbf{V}_k^n = \mathbf{V}((k-1) \Delta z, n \Delta t) \quad (12.128a)$$

$$\mathbf{I}_k^n = \mathbf{I}((k-1/2) \Delta z, n \Delta t) \quad (12.128b)$$

The required recursion relations can be obtained by solving (12.127) to give

$$\begin{aligned} \mathbf{I}_k^{n+3/2} &= \mathbf{I}_k^{n+1/2} - \frac{\Delta t}{\Delta z} \mathbf{L}^{-1} \left[\mathbf{V}_{k+1}^{n+1} - \mathbf{V}_k^{n+1} \right] \\ &+ \mathbf{L}^{-1} \left[\frac{1}{v_z} \mathbf{A}_T - \mathbf{A}_L \right] \left[\mathcal{E}_o \left(t^{n+3/2} - \frac{(k-1/2) \Delta z}{v_z} \right) \right. \\ & \quad \left. - \mathcal{E}_o \left(t^{n+1/2} - \frac{(k-1/2) \Delta z}{v_z} \right) \right] \end{aligned} \quad (12.129a)$$

$$\begin{aligned} \mathbf{V}_k^{n+1} = & \mathbf{V}_k^n - \frac{\Delta t}{\Delta z} \mathbf{C}^{-1} \left[\mathbf{I}_k^{n+1/2} - \mathbf{I}_{k-1}^{n+1/2} \right] \\ & - \mathbf{A}_T \left[\mathcal{E}_o \left(t^{n+1} - \frac{(k-1)\Delta z}{v_z} \right) - \mathcal{E}_o \left(t^n - \frac{(k-1)\Delta z}{v_z} \right) \right] \end{aligned} \quad (12.129b)$$

Next, consider the incorporation of the terminal conditions. The essential problem in incorporating the terminal conditions is again that the FDTD voltages and currents at each end of the line, \mathbf{V}_1 , \mathbf{I}_1 and $\mathbf{V}_{\text{NDZ}+1}$, \mathbf{I}_{NDZ} , are not collocated in space or time, whereas the terminal conditions relate the voltage and current at the same position and at the same time. We will denote the vector of currents at the source ($z = 0$) as \mathbf{I}_S and the vector of currents at the load ($z = \mathcal{L}$) as \mathbf{I}_L , as shown in Figure 11.15. The second transmission-line equation given in Eq. (12.123b) is discretized at the source as

$$\begin{aligned} \frac{1}{\Delta z/2} \left[\mathbf{I}_1^{n+1/2} - \frac{1}{2} \left(\mathbf{I}_S^{n+1} + \mathbf{I}_S^n \right) \right] + \frac{1}{\Delta t} \mathbf{C} \left[\mathbf{V}_1^{n+1} - \mathbf{V}_1^n \right] \\ = - \frac{1}{\Delta t} \mathbf{C} \mathbf{A}_T \left[\mathcal{E}_o \left(t^{n+1} \right) - \mathcal{E}_o \left(t^n \right) \right] \end{aligned} \quad (12.130a)$$

Similarly, the second transmission-line equation, (12.123b), is discretized at the load as

$$\begin{aligned} \frac{1}{\Delta z/2} \left[\frac{1}{2} \left(\mathbf{I}_L^{n+1} + \mathbf{I}_L^n \right) - \mathbf{I}_{\text{NDZ}}^{n+1/2} \right] + \frac{1}{\Delta t} \mathbf{C} \left[\mathbf{V}_{\text{NDZ}+1}^{n+1} - \mathbf{V}_{\text{NDZ}+1}^n \right] \\ = - \frac{1}{\Delta t} \mathbf{C} \mathbf{A}_T \left[\mathcal{E}_o \left(t^{n+1} - \frac{\mathcal{L} = \text{NDZ} \Delta z}{v_z} \right) - \mathcal{E}_o \left(t^n - \frac{\mathcal{L} = \text{NDZ} \Delta z}{v_z} \right) \right] \end{aligned} \quad (12.130b)$$

Equations (12.130) are solved to give the recursion relations at the source and the load:

$$\begin{aligned} \mathbf{V}_1^{n+1} = & \mathbf{V}_1^n - \frac{2\Delta t}{\Delta z} \mathbf{C}^{-1} \mathbf{I}_1^{n+1/2} + \frac{\Delta t}{\Delta z} \mathbf{C}^{-1} \left[\mathbf{I}_S^{n+1} + \mathbf{I}_S^n \right] \\ & - \mathbf{A}_T \left[\mathcal{E}_o \left(t^{n+1} \right) - \mathcal{E}_o \left(t^n \right) \right] \end{aligned} \quad (12.131a)$$

$$\begin{aligned} \mathbf{V}_{\text{NDZ}+1}^{n+1} = & \mathbf{V}_{\text{NDZ}+1}^n + \frac{2\Delta t}{\Delta z} \mathbf{C}^{-1} \mathbf{I}_{\text{NDZ}}^{n+1/2} - \frac{\Delta t}{\Delta z} \mathbf{C}^{-1} \left[\mathbf{I}_L^{n+1} + \mathbf{I}_L^n \right] \\ & - \mathbf{A}_T \left[\mathcal{E}_o \left(t^{n+1} - \frac{\mathcal{L} = \text{NDZ} \Delta z}{v_z} \right) - \mathcal{E}_o \left(t^n - \frac{\mathcal{L} = \text{NDZ} \Delta z}{v_z} \right) \right] \end{aligned} \quad (12.131b)$$

In the case of resistive terminations, the terminal characterizations are written in terms of a generalized Thevenin equivalent as

$$\mathbf{V}_1 = \mathbf{V}_S - \mathbf{R}_S \mathbf{I}_S \quad (12.132a)$$

$$\mathbf{V}_{\text{NDZ}+1} = \mathbf{V}_L + \mathbf{R}_L \mathbf{I}_L \quad (12.132b)$$

Inverting these gives

$$\mathbf{I}_S = -\mathbf{G}_S \mathbf{V}_1 + \mathbf{G}_S \mathbf{V}_S \quad (12.133a)$$

$$\mathbf{I}_L = \mathbf{G}_L \mathbf{V}_{\text{NDZ}+1} - \mathbf{G}_L \mathbf{V}_L \quad (12.133b)$$

Substituting (12.133) into Eq. (12.131) gives the recursion relations for \mathbf{V}_1 and $\mathbf{V}_{\text{NDZ}+1}$:

$$\begin{aligned} \mathbf{V}_1^{n+1} = & \left(\frac{\Delta z}{\Delta t} \mathbf{R}_S \mathbf{C} + \mathbf{1}_n \right)^{-1} \left\{ \left(\frac{\Delta z}{\Delta t} \mathbf{R}_S \mathbf{C} - \mathbf{1}_n \right) \mathbf{V}_1^n - 2 \mathbf{R}_S \mathbf{I}_1^{n+1/2} \right. \\ & + \left(\mathbf{V}_S^{n+1} + \mathbf{V}_S^n \right) \\ & \left. - \frac{\Delta z}{\Delta t} \mathbf{R}_S \mathbf{C} \mathbf{A}_T \left[\mathcal{E}_o \left(t^{n+1} \right) - \mathcal{E}_o \left(t^n \right) \right] \right\} \end{aligned} \quad (12.134a)$$

and

$$\begin{aligned} \mathbf{V}_{\text{NDZ}+1}^{n+1} = & \left(\frac{\Delta z}{\Delta t} \mathbf{R}_L \mathbf{C} + \mathbf{1}_n \right)^{-1} \left\{ \left(\frac{\Delta z}{\Delta t} \mathbf{R}_L \mathbf{C} - \mathbf{1}_n \right) \mathbf{V}_{\text{NDZ}+1}^n + 2 \mathbf{R}_L \mathbf{I}_{\text{NDZ}}^{n+1/2} \right. \\ & + \left(\mathbf{V}_L^{n+1} + \mathbf{V}_L^n \right) \\ & \left. - \frac{\Delta z}{\Delta t} \mathbf{R}_L \mathbf{C} \mathbf{A}_T \left[\mathcal{E}_o \left(t^{n+1} - \frac{\mathcal{L} = \text{NDZ} \Delta z}{v_z} \right) \right. \right. \\ & \left. \left. - \mathcal{E}_o \left(t^n - \frac{\mathcal{L} = \text{NDZ} \Delta z}{v_z} \right) \right] \right\} \end{aligned} \quad (12.134b)$$

and the voltages at the interior points are determined from (12.129b)

$$\begin{aligned} \mathbf{V}_k^{n+1} = & \mathbf{V}_k^n - \frac{\Delta t}{\Delta z} \mathbf{C}^{-1} \left[\mathbf{I}_k^{n+1/2} - \mathbf{I}_{k-1}^{n+1/2} \right] \\ & - \mathbf{A}_T \left[\mathcal{E}_o \left(t^{n+1} - \frac{(k-1) \Delta z}{v_z} \right) - \mathcal{E}_o \left(t^n - \frac{(k-1) \Delta z}{v_z} \right) \right] \end{aligned} \quad (12.134c)$$

for $k = 2, 3, \dots, \text{NDZ}$. Equations (12.134) are first solved for the voltages and then the currents are determined from those voltages using (12.129a) as

$$\begin{aligned} \mathbf{I}_k^{n+3/2} = & \mathbf{I}_k^{n+1/2} - \frac{\Delta t}{\Delta z} \mathbf{L}^{-1} \left[\mathbf{V}_{k+1}^{n+1} - \mathbf{V}_k^{n+1} \right] \\ & + \mathbf{L}^{-1} \left[\frac{1}{v_z} \mathbf{A}_T - \mathbf{A}_L \right] \left[\mathcal{E}_o \left(t^{n+3/2} - \frac{(k-1/2)\Delta z}{v_z} \right) \right. \\ & \left. - \mathcal{E}_o \left(t^{n+1/2} - \frac{(k-1/2)\Delta z}{v_z} \right) \right] \end{aligned} \quad (12.135)$$

for $k = 1, 2, 3, \dots, \text{NDZ}$. Once again, for stability the position and time discretizations must satisfy the Courant condition

$$\Delta t \leq \frac{\Delta z}{v_{i\text{MAX}}} \quad (12.136)$$

where $v_{i\text{MAX}}$ is the maximum of the mode velocities.

The above results can similarly be implemented for uniform plane wave excitation for a line over an infinite ground plane. This method is implemented in the FORTRAN program FDTDINC.FOR, which is described in Appendix A.

12.4 COMPUTED RESULTS

The computed results will compare the SPICE model using SPICEINC.FOR, the TDFD transformation using TIMEFREQ.FOR, and the FDTD model using FDTDINC.FOR. The structure is shown in Figure 12.10 and consists of a 2-m length of ribbon cable. The wire radii are 7.5 mils, the dielectric thicknesses are 10 mils, and the dielectric constant is 3.5. The wires have center-to-center separations of 50 mils. The middle wire is chosen as the reference conductor, and a uniform plane wave is incident in the z direction with the electric field polarized in the x direction. The per-unit-length parameter matrices of \mathbf{L} and \mathbf{C} were computed with RIBBON.FOR and are

$$\mathbf{L} = \begin{bmatrix} 0.7485 & 0.2408 \\ 0.2408 & 0.7485 \end{bmatrix} \mu\text{H/m}$$

and

$$\mathbf{C} = \begin{bmatrix} 24.982 & -6.266 \\ -6.266 & 24.982 \end{bmatrix} \text{pF/m}$$

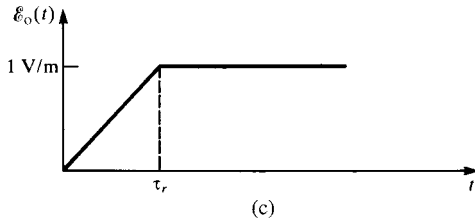
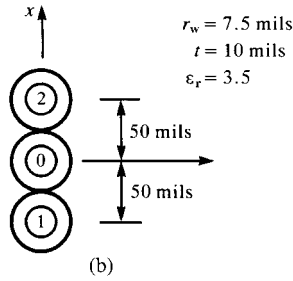
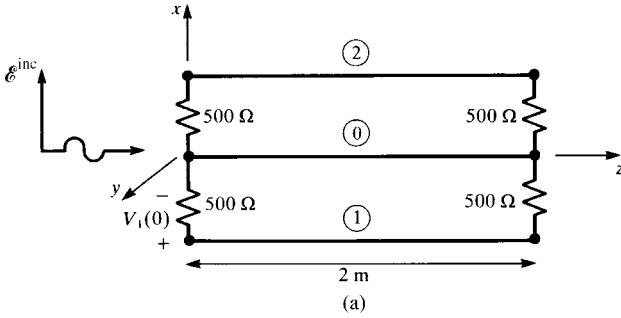


FIGURE 12.10 A three-wire ribbon cable with incident field excitation for illustrating numerical results.

The line is terminated in 500Ω resistors giving

$$\mathbf{R}_S = \mathbf{R}_L = \begin{bmatrix} 500 & 0 \\ 0 & 500 \end{bmatrix}$$

The time form of the incident electric field, $\mathcal{E}_o(t)$, is a ramp waveform rising to a level of 1 V/m with various rise times of $\tau_r = 100$ ns, 10 ns, and 1 ns. With regard to the diagram in Figure 12.6, $\theta_E = 90^\circ$, $\theta_p = 90^\circ$, and $\phi_p = -90^\circ$ giving $e_x = 1$, $e_y = e_z = 0$ and $\beta_x = \beta_y = 0$, $\beta_z = \beta_0$. We will compute and plot the voltage $V_1(0)$.

Figure 12.11(a) shows the results for the 100 ns rise time. All three models show excellent correlation. The $\mathcal{E}_o(t)$ waveform should have a bandwidth of

$BW = 1/\tau_r = 10$ MHz. However, the intent is to reproduce the induced waveform. The SPICE prediction shows a rise time of the output voltage $V_1(0)$ of roughly 20 ns. Hence, the induced waveform for $V_1(0)$ should have significant spectral content up to around $1/20$ ns = 50 MHz. The TDFD transformation simulated the $\mathcal{E}_o(t)$ waveform as a 1-MHz trapezoidal pulse with a 50% duty cycle and equal rise and fall times. The results were obtained using 100 harmonics to contain a spectrum up to 100 MHz. The FDTD results were obtained by discretizing the line into $NDZ = 5$ sections of length $\Delta z = \mathcal{L}/NDZ = 0.4$ m and the time into $NDT = 200$ time steps of $\Delta t = \text{final time}/NDT = 1$ ns. Hence, each section is $1/15 \lambda_0$ at 50 MHz. In order to satisfy the Courant condition, we should have, roughly, $NDT > NDZ \times \text{final time} \times v_0/\text{line length}$ giving $NDT > 150$, so we chose $NDT = 200$.

Figure 12.11(b) shows the results for the 10 ns rise time. All three models again show excellent correlation. The SPICE prediction shows a rise time of the output voltage $V_1(0)$ of roughly 10 ns. Hence, the induced waveform for $V_1(0)$ should have significant spectral content up to around $1/10$ ns = 100 MHz. The results were obtained using 500 harmonics to contain a spectrum up to 500 MHz. The FDTD results were obtained by discretizing the line into $NDZ = 10$ sections of length $\Delta z = \mathcal{L}/NDZ = 0.2$ m and the time into $NDT = 200$ time steps of $\Delta t = \text{final time}/NDT = 0.5$ ns. Hence, each section is $1/15 \lambda_0$ at 100 MHz. In order to satisfy the Courant condition, we should have, roughly, $NDT > NDZ \times \text{final time} \times v_0/\text{line length}$ giving $NDT > 150$, so we again chose $NDT = 200$.

Figure 12.11(c) shows the results for the 1 ns rise time. All three models again show excellent correlation. The SPICE prediction shows a rise time of the output voltage $V_1(0)$ of roughly 1 ns. Hence, the induced waveform for $V_1(0)$ should have significant spectral content up to around $1/1$ ns = 1 GHz. The TDFD transformation simulated the $\mathcal{E}_o(t)$ waveform as a 1-MHz trapezoidal pulse with a 50% duty cycle and equal rise and fall times. The results were obtained using 1000 harmonics to contain a spectrum up to 1 GHz. The FDTD results were obtained by discretizing the line into $NDZ = 100$ sections of length $\Delta z = \mathcal{L}/NDZ = 2$ cm and the time into $NDT = 1500$ time steps of $\Delta t = \text{final time}/NDT = 0.067$ ns. Hence, each section is $1/15 \lambda_0$ at 1 GHz. In order to satisfy the Courant condition, we should have, roughly, $NDT > NDZ \times \text{final time} \times v_0/\text{line length}$ giving $NDT > 1500$, so we chose $NDT = 1500$.

The SPICE model is not restricted to the time domain and can be used to give frequency-domain results although restricted to lossless lines. These are shown in Figure 12.12 from 1 kHz to 200 MHz. The results of the frequency-domain direct calculation with and without losses are obtained using the code `INCIDENT.FOR`. All three models give virtually identical results except around frequencies where the line is some multiple of a half wavelength.

The effect of losses on the time-domain results can be investigated by computing the results using the TDFD method using the `TIMEFREQ.FOR` program described in Appendix A. The frequency-domain transfer function is computed with and without losses using the program `INCIDENT.FOR`. The time-domain results for 1 ns rise time are compared in Figure 12.13 using 1000 harmonics of the 1 MHz waveform. The

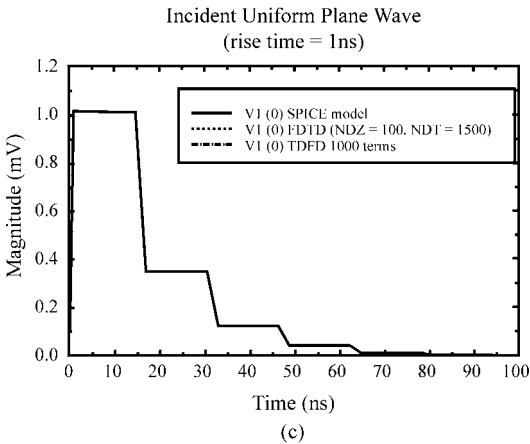
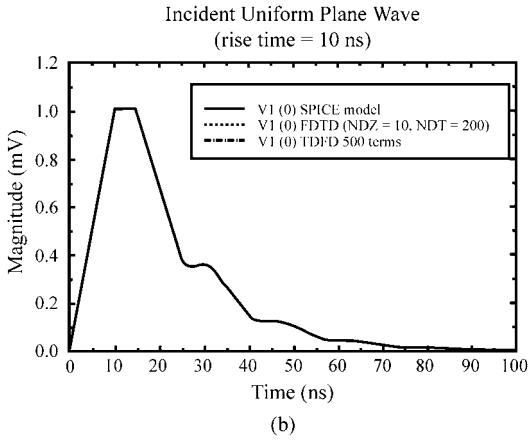
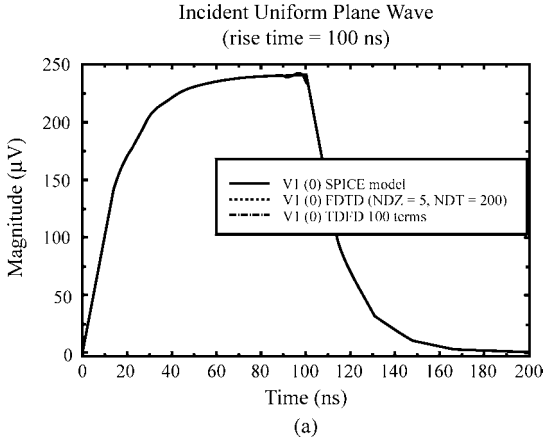


FIGURE 12.11 Predictions of the time-domain near-end voltage of the line of Figure 12.10 using the SPICE model, the time-domain to frequency-domain transformation method, and the FDTD method for pulse rise times of (a) 100 ns, (b) 10 ns, and (c) 1 ns.

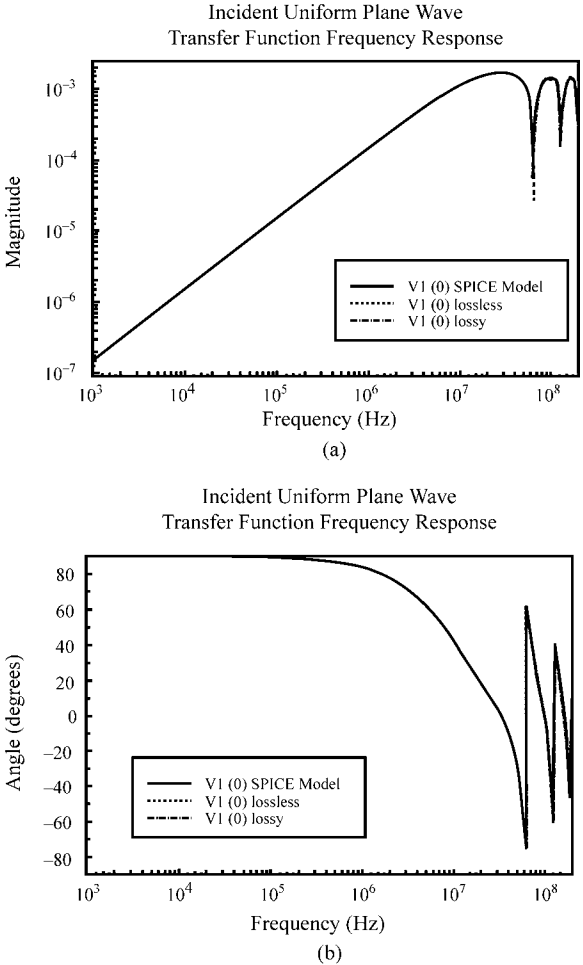


FIGURE 12.12 Predictions of the frequency response of the near-end voltage of the line of Figure 12.10 using the SPICE model, and the MTL model with and without losses: (a) magnitude and (b) phase.

SPICE prediction showed in Figure 12.11(c) a rise time of the output voltage $V_1(0)$ of roughly 1 ns. Hence, the induced waveform for $V_1(0)$ should have significant spectral content up to around $1/1 \text{ ns} = 1 \text{ GHz}$, so excellent predictions are to be expected. The results with and without losses are virtually identical. This is not to say that losses are always unimportant, but for the particular load impedance level, line dimensions and spectral content of the waveform used here, they are apparently not significant.

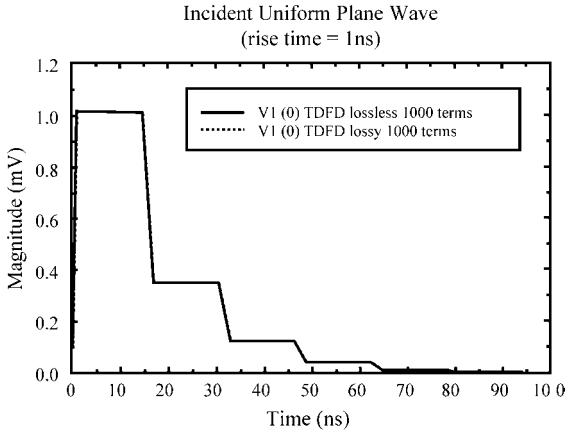


FIGURE 12.13 Predictions of the time-domain near-end voltage of the line of Figure 12.10 using the time-domain to frequency-domain transformation method with and without losses for a rise time of 1 ns.

PROBLEMS

- 12.1 Verify the equivalence in (12.20).
- 12.2 Verify the simplified forms of the excitation sources in (12.31) and (12.32).
- 12.3 Verify the solutions in (12.38), (12.39), and (12.43)–(12.48).
- 12.4 Verify the forms of the transverse and longitudinal excitations in (12.58) and (12.59).
- 12.5 Verify the results for \mathbf{M}^{\pm} and \mathbf{N}^{\pm} given in (12.65) and (12.66).
- 12.6 Verify the results for \mathbf{M}^{\pm} and \mathbf{N}^{\pm} for a ground plane given in (12.71) and (12.72).
- 12.7 Verify the results for the modal forcing functions in (12.100).
- 12.8 Verify the results for the SPICE sources in (12.116).
- 12.9 Verify the SPICE equivalent circuit shown in Figure 12.8.
- 12.10 Verify the MTL equations for plane-wave excitation given in (12.125) and (12.126).
- 12.11 Verify the FDTD recursion relations in (12.134) and (12.135).
- 12.12 Verify the computed results in Figures 12.11–12.13.

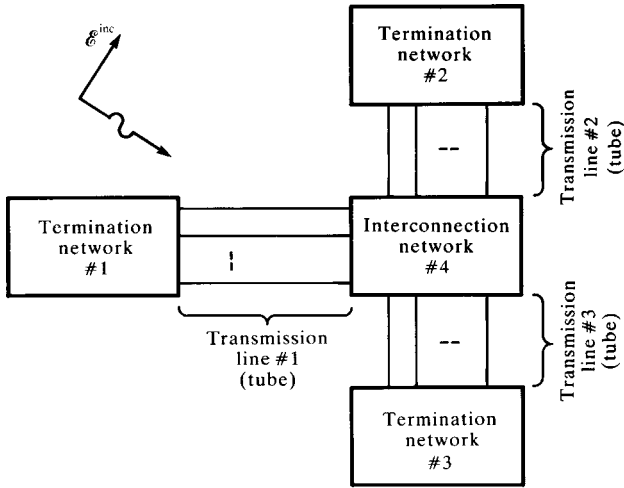
REFERENCES

- [1] A. K. Agrawal, H. J. Price, and S. H. Gurbaxani, Transient response of multiconductor transmission lines excited by a nonuniform electromagnetic field, *IEEE Transactions on Electromagnetic Compatibility*, **22**, 119–129, 1980.
- [2] F. M. Tesche, T. K. Liu, S. K. Chang, and D. V. Giri, Field excitation of multiconductor transmission lines, Technical Report AFWL-TR-78-185, Air Force Weapons Lab, Albuquerque, NM, February 1979.
- [3] G. W. Bechtold and D. J. Kozakoff, Transmission line mode response of a multiconductor cable in a transient electromagnetic field, *IEEE Transactions on Electromagnetic Compatibility*, **12**, 5–9, 1970.
- [4] G. E. Bridges and L. Shafai, Plane wave coupling to multiple conductor transmission lines above a lossy earth, *IEEE Transactions on Electromagnetic Compatibility*, **31** (1), 21–33, 1989.
- [5] C. W. Harrison, Generalized theory of impedance loaded multiconductor transmission lines in an incident field, *IEEE Transactions on Electromagnetic Compatibility*, **14**, 56–63, 1972.
- [6] F. M. Tesche, Plane wave coupling to cables, in: *Handbook of Electromagnetic Compatibility*, Academic Press, San Diego, CA, 1994.

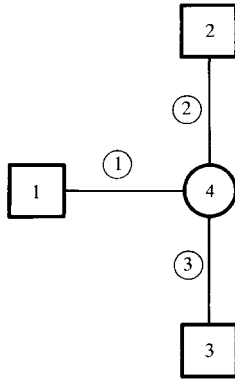
13

TRANSMISSION-LINE NETWORKS

The previous chapters of this book have considered the analysis of uniform transmission lines that have one important restriction: All $n + 1$ conductors are parallel to each other. Numerous practical configurations consist of interconnections of these types of lines as illustrated in Figure 13.1(a). These practical configurations will be referred to as *transmission-line networks*. Lines may end in *termination networks* or may be interconnected by *interconnection networks*. Each transmission line of the network will be referred to as a *tube* after [1–3]. A convenient way of describing the overall network is with a *graph* as illustrated in Figure 13.1(b) [1,2,4]. The transmission lines are represented with single lines or *branches* of the graph. The termination networks are defined as a node having only one tube incident on it and are represented by rectangles. The interconnection networks are defined as a node having more than one tube incident on it and are represented by circles. The excitation for the network may be in the form of lumped sources in the termination or interconnection networks or it may be due to either distributed excitation from an incident electromagnetic field or a point excitation along the line as with the direct attachment of a lightning stroke. Point excitation of a tube as in the case of a direct attachment of a lightning stroke can be handled by characterizing the segments of the tube to the left and right of the excitation point with any of the following models and treating the point excitation as an interconnection network between these tube subsegments. Lumped sources in this interconnection network then represent this point excitation at the junction. Distributed excitation must be included in the overall characterization of the tube as described in Chapters 11 and 12, whereas lumped sources within the termination/interconnection



(a)



(b)

FIGURE 13.1 Illustration of a transmission-line network: (a) tube and network definitions and (b) representation with a graph.

networks are included in their description. The purpose of this chapter is to examine methods for characterizing these types of interconnected lines.

Evidently, any method for characterizing this network seeks to (1) characterize each tube in some fashion as outlined in the previous chapters and (2) interconnect these tubes by enforcing the constraints on the line voltages and currents via Kirchhoff's laws and the element characteristics within the termination/interconnection networks. One obvious representation method is to use SPICE subcircuit models for the tubes developed in Chapters 8, 9, 11, and 12 and interconnect and/or terminate the nodes of those subcircuit models in the resulting SPICE code. This method is very straightforward using the program SPICEMTL.FOR or SPICEINC.FOR described

in Appendix A to provide the SPICE subcircuit models of each tube. The advantages of this method are that (1) it is straightforward to implement and (2) dynamic as well as nonlinear loading and elements within the termination/interconnection networks such as diodes and transistors are already available in the SPICE code and can be readily used to build the termination/interconnection networks to complete the overall characterization. So a wide variety of practical terminations can be analyzed without the need for developing either the models of complicated elements or the numerical integration routines to give a time-domain analysis. The disadvantage of this method is that it is so far applicable only to *lossless* lines.

An approximate method is to use lumped-circuit iterative models of each tube such as the lumped-Pi or lumped-T models and use any lumped-circuit analysis program such as SPICE to analyze the resulting interconnection. *Frequency-independent losses* can be incorporated into this result, but the method is restricted to tubes that are electrically short. Time-domain results can again be reasonably approximated if the rise/fall times of the source waveforms are sufficiently longer than the tube one-way delays.

It is also possible to construct an exact model of the line using the frequency-domain admittance or impedance parameter characterizations of each tube [4, 5]. These methods have the advantage of simple construction of the overall equations that are to be solved to give the tube terminal voltages and currents. Losses such as skin-effect losses that vary as \sqrt{f} can be included by simply determining the frequency response of the network and converting to the time domain with the time-domain to frequency-domain (TDFD) transformation.

With the exception of the SPICE subcircuit method, all methods ultimately must face the problem of the systematic interconnection of the tube models. Computer implementation of the interconnection of the tubes for a large network is not a simple task and must be designed so that a user can easily and unambiguously describe the interconnections to the resulting computer code. Of course, all standard lumped-circuit analysis codes such as SPICE must address this problem of systematic and unambiguous implementation of the element interconnections via user input to the code, and the characterization of transmission-line networks is similar in that respect. Characterization of the tubes via the admittance parameters as in [4] was designed so that a systematic interconnection process will be affected. Another method is the use of the *scattering parameters* for the tubes [1, 2]. This leads to the so-called BLT equations (apparently named for the authors). A similar modal decomposition method was described in [3].

All of the above methods must address both the frequency-domain and the time-domain analysis of the network. The time-domain analysis of the network can be obtained in the usual fashion using the TDFD transformation discussed earlier wherein the source waveform is decomposed into its spectral components and each component is passed through the previously computed frequency-domain transfer function. The time-domain result is the inverse Fourier transform of this. As before, the TDFD method can readily handle skin-effect losses that are difficult to characterize in the time domain, but it suffers from the fundamental restriction that the network must be linear, that is, the line and all terminations must be *linear*, since superposition is used.

13.1 REPRESENTATION OF LOSSLESS LINES WITH THE SPICE MODEL

Perhaps one of the more straightforward methods of characterizing and analyzing the crosstalk on transmission-line networks or the effect of incident fields is with the SPICE equivalent circuit developed in Chapters 8 and 9 or incident field illumination in Chapters 11 and 12. Each tube is characterized by its SPICE subcircuit model

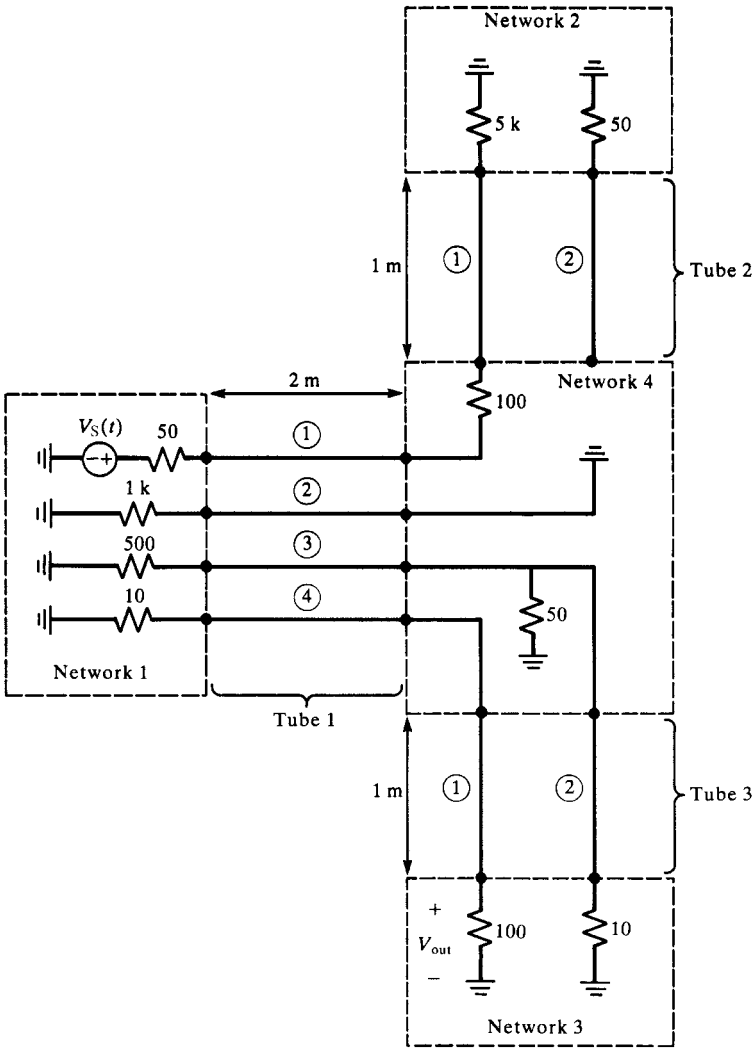


FIGURE 13.2 An example of a transmission-line network to illustrate and compare numerical results.

generated with the program SPICEMTL.FOR or SPICEINC.FOR described in Appendix A. These subcircuit models are then interconnected and the terminations added to produce the final SPICE model of the network. The method is straightforward using the above codes to generate the subcircuit models but is restricted to lossless tubes. Again, this method can handle, in a straightforward way, dynamic and/or nonlinear loads in the termination/interconnection networks.

In order to illustrate the methods of this chapter, we will use the example shown in Figure 13.2. The network consists of three tubes. Tube # 1 contains four wires, whereas tubes # 2 and # 3 contain two wires. All tubes will consist of bare wires above a ground plane as illustrated in Figure 13.3. Tube # 1 is of length 2 m and tubes # 2 and # 3 are of length 1 m. The cable is suspended 1 cm above an infinite, perfectly conducting ground plane, and the wires have radii of 7.5 mils. A source, $V_S(t)$, in network # 1 drives line # 1 of tube # 1. This source is in the form of a ramp waveform with a rise time of 1 ns as shown in Figure 13.3(c). The tubes are terminated in various resistive terminations at termination networks # 1, # 2, and # 3. Interconnection network # 4 contains a variety of terminations, open circuit, short circuit, series impedance,

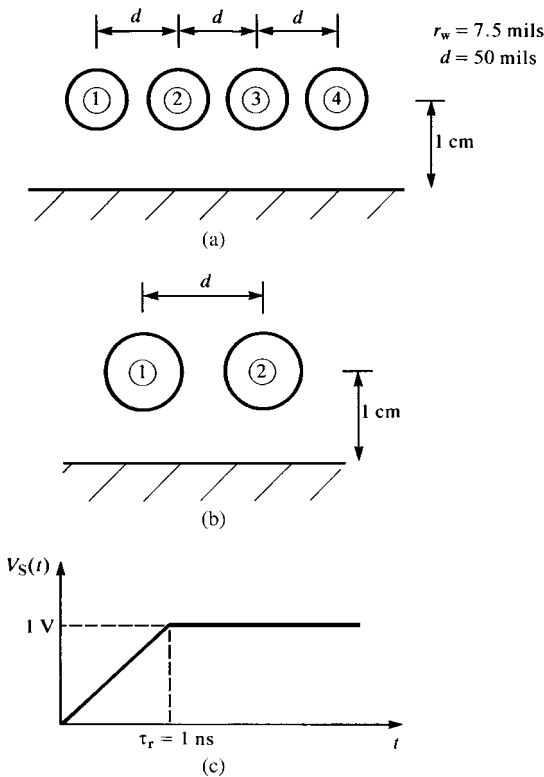


FIGURE 13.3 Cross-sectional dimensions of the tubes of the transmission-line network of Figure 13.2.

shunt impedance, and direct connection, to illustrate the versatility of the method. The desired output will be the voltage, $V_{out}(t)$, across the termination of wire # 1 of tube # 3 at termination network # 3. The graph of this transmission-line network is shown in Figure 13.1(b). Each termination or interconnection network has the number of that node included within the symbol. The number of each *tube* is noted on that branch of the graph.

Figure 13.4 illustrates the resulting construction of the overall SPICE network with node numbering. The SPICE subcircuit models of the tubes are constructed using SPICEMTL.FOR, and the per-unit-length parameters are computed using WIDSEPF.FOR.

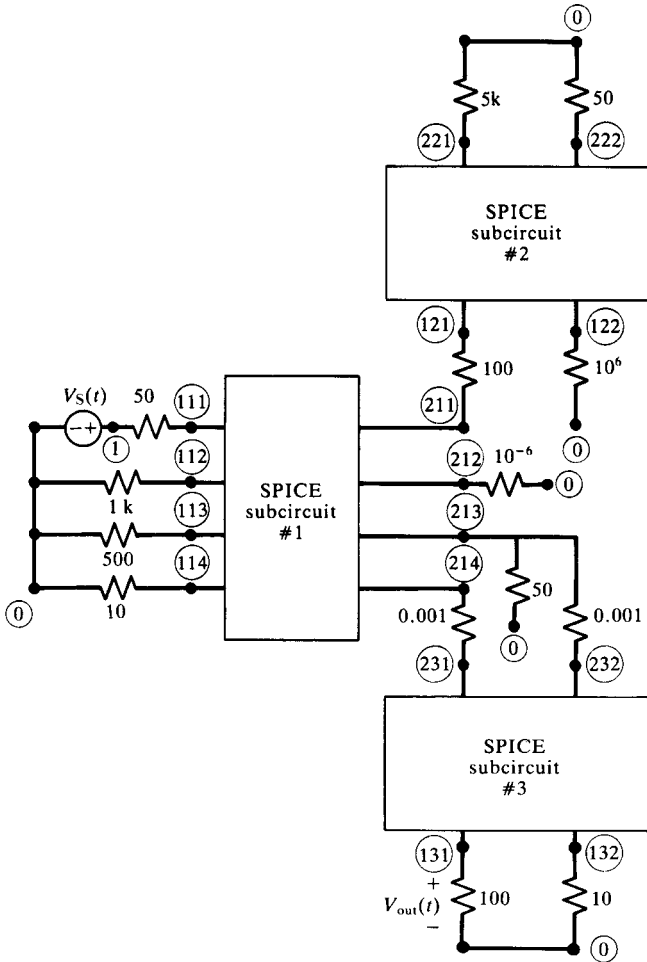


FIGURE 13.4 Illustration of the SPICE model of the transmission-line network of Figure 13.2.

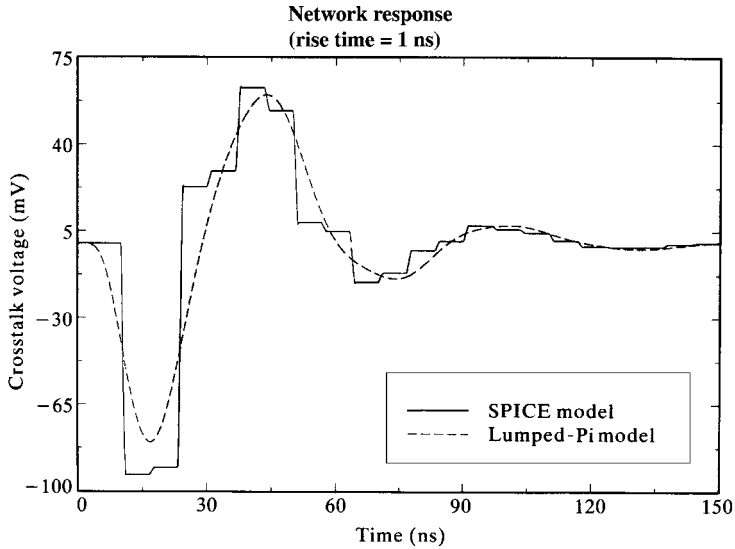


FIGURE 13.5 Comparison of crosstalk voltage at the termination of conductor # 1 of tube # 3 for the transmission-line network of Figure 13.2 for a rise time of 1 ns using the SPICE model and using one lumped-Pi section to represent each tube.

13.2 REPRESENTATION WITH LUMPED-CIRCUIT APPROXIMATE MODELS

The next method is to approximately characterize each tube with a lumped-circuit approximate structure such as a lumped-Pi structure. These characterizations are obtained using the `SPICELPI.FOR` code. The resulting overall SPICE model of the network is virtually identical to that of Figure 13.4 with the only exception being that the subcircuit models of the tubes are lumped-Pi structures. Figure 13.5 shows the comparison of the predictions of the output voltage, $V_{\text{out}}(t)$, obtained with the SPICE model of Figure 13.4 and the lumped-Pi structure using only one lumped-Pi section to represent each tube. The correlation is obviously very poor due to the fact that the tube one-way delays are on the order of 3 ns and 6 ns that are not significantly smaller than the waveform rise time of 1 ns. Figure 13.6 shows this correlation for a rise time of 100 ns, which is much better.

13.3 REPRESENTATION VIA THE ADMITTANCE OR IMPEDANCE $2n$ -PORT PARAMETERS

The use of the admittance parameters to characterize the tubes was described in [4]. This leads to a straightforward way of incorporating the termination and interconnection networks, since we essentially need to simply add admittances in order to construct the admittance matrix of the overall network.

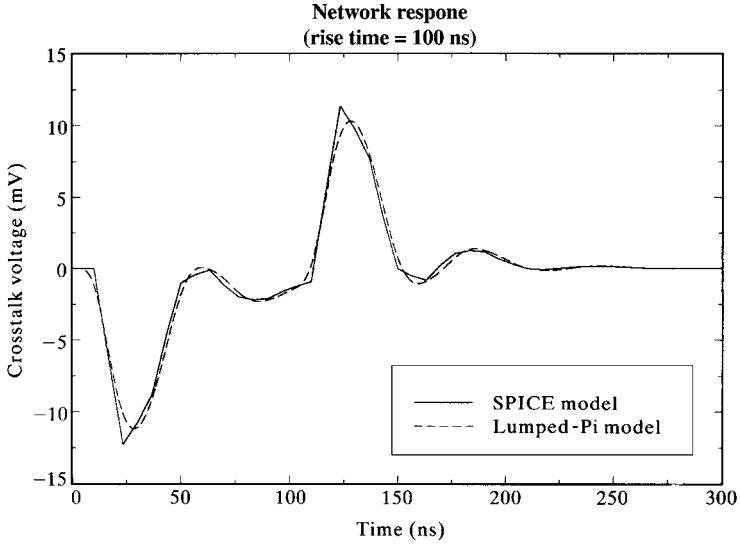


FIGURE 13.6 The predictions of Figure 13.5 for a rise time of 100 ns showing the adequacy of the lumped-Pi representation.

The frequency-domain chain parameters of a uniform line are

$$\hat{\mathbf{V}}(\mathcal{L}) = \hat{\Phi}_{11} \hat{\mathbf{V}}(0) + \hat{\Phi}_{12} \hat{\mathbf{I}}(0) + \hat{\mathbf{V}}_{\text{FT}} \tag{13.1a}$$

$$\hat{\mathbf{I}}(\mathcal{L}) = \hat{\Phi}_{21} \hat{\mathbf{V}}(0) + \hat{\Phi}_{22} \hat{\mathbf{I}}(0) + \hat{\mathbf{I}}_{\text{FT}} \tag{13.1b}$$

where $\hat{\mathbf{V}}_{\text{FT}}$ and $\hat{\mathbf{I}}_{\text{FT}}$ are due to any incident field excitation of the line. The frequency-domain admittance parameters are derived in Section 7.5.5 of Chapter 7 from these to yield

$$\hat{\mathbf{I}}(0) = \hat{\mathbf{Y}}_S \hat{\mathbf{V}}(0) + \hat{\mathbf{Y}}_M \hat{\mathbf{V}}(\mathcal{L}) + \hat{\mathbf{I}}_{S0} \tag{13.2a}$$

$$-\hat{\mathbf{I}}(\mathcal{L}) = \hat{\mathbf{Y}}_M \hat{\mathbf{V}}(0) + \hat{\mathbf{Y}}_S \hat{\mathbf{V}}(\mathcal{L}) + \hat{\mathbf{I}}_{SL} \tag{13.2b}$$

where

$$\begin{aligned} \hat{\mathbf{Y}}_S &= -\hat{\Phi}_{12}^{-1} \hat{\Phi}_{11} = -\hat{\Phi}_{22} \hat{\Phi}_{12}^{-1} \\ &= \hat{\mathbf{T}}_I \left[\mathbf{e}^{\hat{\gamma} \mathcal{L}} - \mathbf{e}^{-\hat{\gamma} \mathcal{L}} \right]^{-1} \left[\mathbf{e}^{\hat{\gamma} \mathcal{L}} + \mathbf{e}^{-\hat{\gamma} \mathcal{L}} \right] \hat{\mathbf{T}}_I^{-1} \hat{\mathbf{Y}}_C \end{aligned} \tag{13.3a}$$

$$\begin{aligned} \hat{\mathbf{Y}}_M &= \hat{\Phi}_{12}^{-1} \\ &= -2\hat{\mathbf{T}}_I \left[\mathbf{e}^{\hat{\gamma} \mathcal{L}} - \mathbf{e}^{-\hat{\gamma} \mathcal{L}} \right]^{-1} \hat{\mathbf{T}}_I^{-1} \hat{\mathbf{Y}}_C \end{aligned} \tag{13.3b}$$

$$\hat{\mathbf{I}}_{S0} = -\hat{\mathbf{Y}}_M \hat{\mathbf{V}}_{\text{FT}} \tag{13.3c}$$

$$\hat{\mathbf{I}}_{SL} = -\hat{\mathbf{Y}}_S \hat{\mathbf{V}}_{\text{FT}} - \hat{\mathbf{I}}_{\text{FT}} \tag{13.3d}$$

Observe that the currents are defined as directed *into each end of the tube*. The admittance parameters show that the tube is reciprocal as it should be. The various parameters in these are as defined in Chapter 7, where the per-unit-length impedance and admittance parameters are diagonalized as

$$\hat{\mathbf{T}}_I^{-1} \underbrace{(\mathbf{G} + j\omega \mathbf{C})}_{\hat{\mathbf{Y}}} \underbrace{(\mathbf{R}(f) + j\omega \mathbf{L})}_{\hat{\mathbf{Z}}} \hat{\mathbf{T}}_I = \hat{\gamma}^2 \tag{13.4}$$

and the characteristic admittance matrix is

$$\begin{aligned} \hat{\mathbf{Y}}_C &= \hat{\mathbf{Z}}_C^{-1} \\ &= \hat{\mathbf{T}}_I \hat{\gamma} \hat{\mathbf{T}}_I^{-1} \hat{\mathbf{Z}}^{-1} \\ &= \hat{\mathbf{T}}_I \hat{\gamma}^{-1} \hat{\mathbf{T}}_I^{-1} \hat{\mathbf{Y}} \end{aligned} \tag{13.5}$$

The only potential disadvantage to the admittance parameter description of the tubes is that the parameters do not exist for lossless lines and frequencies where the tube is a multiple of a half wavelength.

The tubes are characterized by the above admittance parameters with the following notation illustrated in Figure 13.7(a). Consider the i th tube connecting the j th network and the k th network at its endpoints. Denote the vector of currents and voltages at the ends of the tube as $\hat{\mathbf{I}}_i^j$, $\hat{\mathbf{V}}_i^j$, $\hat{\mathbf{I}}_i^k$, and $\hat{\mathbf{V}}_i^k$, where the subscript denotes the tube and the superscript denotes the network at that end:

$$\begin{array}{l} \hat{\mathbf{V}}_{\text{tube}}^{\text{termination/interconnection network}} \\ \hat{\mathbf{I}}_{\text{tube}}^{\text{termination/interconnection network}} \end{array}$$

The admittance parameters (13.2) and (13.3) become

$$\hat{\mathbf{I}}_i^j = \hat{\mathbf{Y}}_{Si} \hat{\mathbf{V}}_i^j + \hat{\mathbf{Y}}_{Mi} \hat{\mathbf{V}}_i^k + \hat{\mathbf{I}}_{Si}^j \tag{13.6a}$$

$$\hat{\mathbf{I}}_i^k = \hat{\mathbf{Y}}_{Mi} \hat{\mathbf{V}}_i^j + \hat{\mathbf{Y}}_{Si} \hat{\mathbf{V}}_i^k + \hat{\mathbf{I}}_{Si}^k \tag{13.6b}$$

where $\hat{\mathbf{I}}_{Si}^j$ accounts for the effects of the incident field incident on tube i referred to the end at network j , whereas $\hat{\mathbf{I}}_{Si}^k$ accounts for the effect of the incident field on tube i referred to the end at network k .

The characterization of the termination and interconnection networks must be general enough to include open and short circuits as well as lumped sources and impedances and direct connections within the termination/interconnection networks. A general way of characterizing these is in the form of a combination of generalized Thevenin and generalized Norton equivalents [4]. Consider characterizing the m th interconnection network that has the i th, j th, and k th tubes interconnected by it as illustrated in Figure 13.7(b). The tube voltages and currents can be

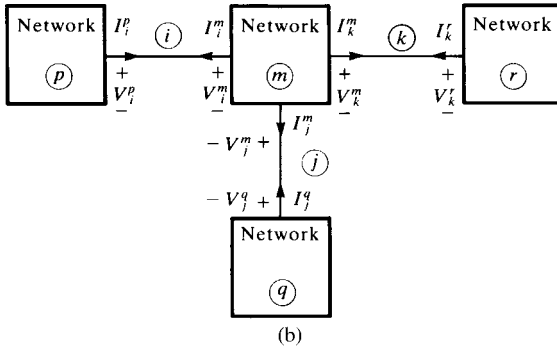
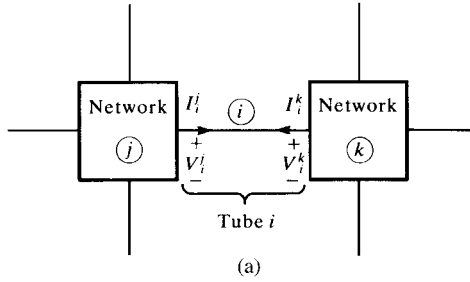


FIGURE 13.7 Definitions of the tube voltages and currents for (a) an individual tube and (b) and interconnection network.

interrelated as

$$\hat{Y}_i^m \hat{V}_i^m + \hat{Z}_i^m \hat{I}_i^m + \hat{Y}_j^m \hat{V}_j^m + \hat{Z}_j^m \hat{I}_j^m + \hat{Y}_k^m \hat{V}_k^m + \hat{Z}_k^m \hat{I}_k^m = \hat{P}^m \tag{13.7a}$$

The total number of equations in (13.7) equals the number of conductors incident at the termination/interconnection network (node). For the example of Figure 13.2 at interconnection network # 4, this is $4 + 2 + 2 = 8$. The equations in (13.7) are organized in the order of tube # 1, then tube # 2, and then tube # 3. Within each row, the conductors of that tube are ordered sequentially according to their number. Each row refers to the conductor of the tube attached to the network. For example, the third row of (13.7) is for conductor 3 of tube # 1, whereas the sixth row is for conductor # 2 of tube # 2 and the seventh row is for conductor # 1 of tube # 3. For a termination network such as the p th termination network in Figure 13.7, the representation is

$$\hat{Y}_i^p \hat{V}_i^p + \hat{Z}_i^p \hat{I}_i^p = \hat{P}^p \tag{13.7b}$$

The fact that this representation is completely general can be proven from the fact that it can be derived from a chain-parameter representation of the ports of the network, which always exists for any linear network. The representation in (13.7) has

the sole purpose of enforcing (1) Kirchhoff's voltage law (KVL), (2) Kirchhoff's current law (KCL), and (3) the element relations that are imposed by the particular interconnections within the interconnection network. Each row of (13.7) represents a specific KVL constraint or a KCL constraint and/or an element relation for the termination/interconnection network for which (13.7) is being written. All of the entries in that row are zero with the exception of the following. Figure 13.8 illustrates

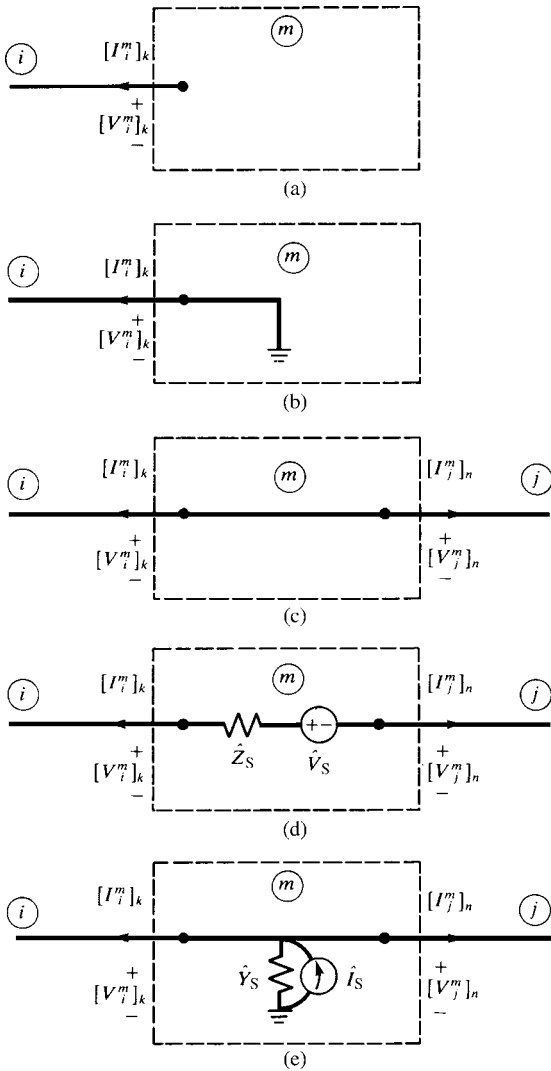


FIGURE 13.8 Illustration of the determination of the network characterizations for (a) an open circuit, (b) a short circuit, (c) a direct connection, (d) a Thevenin equivalent, and (e) a Norton equivalent.

some common examples. Figure 13.8(a) illustrates the k th conductor of the i th tube terminating in an open circuit within the m th network. The constraint here is that the current is zero:

$$[\hat{\mathbf{I}}_i^m]_k = 0 \quad (13.8)$$

Therefore, a 1 appears in the column of $\hat{\mathbf{Z}}_i^m$ corresponding to the current of that conductor (the k th conductor) of that tube in $\hat{\mathbf{I}}_i^m$ and all other entries in that row of (13.7) are zero. Figure 13.8(b) illustrates the k th conductor of the i th tube terminating in a short circuit within the m th network. The constraint here is that the voltage is zero:

$$[\hat{\mathbf{V}}_i^m]_k = 0 \quad (13.9)$$

Therefore, a 1 appears in the column of $\hat{\mathbf{Y}}_i^m$ corresponding to the voltage of that conductor of that tube in $\hat{\mathbf{V}}_i^m$ and all other entries in that row of (13.7) are zero. Figure 13.8(c) illustrates a direct connection between the k th conductor of tube i and the n th conductor of tube j within the m th network. The constraints here are that the voltage of the conductor of the i th tube and the voltage of the conductor of the j th tube are equal and the sum of the currents of the conductor of the i th tube and the conductor of the j th tube equals zero:

$$[\hat{\mathbf{V}}_i^m]_k - [\hat{\mathbf{V}}_j^m]_n = 0 \quad (13.10a)$$

$$[\hat{\mathbf{I}}_i^m]_k + [\hat{\mathbf{I}}_j^m]_n = 0 \quad (13.10b)$$

The first constraint is imposed by placing a 1 in the column of $\hat{\mathbf{Y}}_i^m$ corresponding to the voltage of that conductor of that tube in $\hat{\mathbf{V}}_i^m$ and by placing a -1 in the column of $\hat{\mathbf{Y}}_j^m$ corresponding to the voltage of that conductor of that tube in $\hat{\mathbf{V}}_j^m$, and all other entries in that row of (13.7) are zero. The second constraint is imposed by placing a 1 in the column of $\hat{\mathbf{Z}}_i^m$ corresponding to the current of that conductor of that tube in $\hat{\mathbf{I}}_i^m$ and by placing a 1 in the column of $\hat{\mathbf{Z}}_j^m$ corresponding to the voltage of that conductor of that tube in $\hat{\mathbf{I}}_j^m$, and all other entries in that row of (13.7) are zero. Multiple connections of conductors can similarly be handled. For example, consider the case of three conductors, k of tube i , n of tube j , and p of tube l , connected at a common point within the network. KCL requires that the sum of the currents at that interconnection equals zero:

$$[\hat{\mathbf{I}}_i^m]_k + [\hat{\mathbf{I}}_j^m]_n + [\hat{\mathbf{I}}_l^m]_p = 0 \quad (13.10c)$$

Similarly, KVL requires that the differences of two of the three pairs of the voltages that are interconnected equal zero:

$$[\hat{\mathbf{V}}_i^m]_k - [\hat{\mathbf{V}}_j^m]_n = 0, \quad [\hat{\mathbf{V}}_i^m]_k - [\hat{\mathbf{V}}_l^m]_p = 0 \quad (13.10d)$$

Figure 13.8(d) illustrates a series connection of an impedance and a lumped voltage source. The constraints are that the currents are equal and the voltages are related by the element relations:

$$[\hat{\mathbf{I}}_i^m]_k + [\hat{\mathbf{I}}_j^m]_n = 0 \tag{13.11a}$$

$$[\hat{\mathbf{V}}_i^m]_k - [\hat{\mathbf{V}}_j^m]_n + \hat{Z}_S [\hat{\mathbf{I}}_i^m]_k = \hat{V}_S \tag{13.11b}$$

The first constraint is imposed by placing a 1 in the column of $\hat{\mathbf{Z}}_i^m$ corresponding to the current of that conductor of that tube in $\hat{\mathbf{I}}_i^m$ and by placing a 1 in the column of $\hat{\mathbf{Z}}_j^m$ corresponding to the voltage of that conductor of that tube in $\hat{\mathbf{I}}_j^m$, and all other entries in that row of (13.7) are zero. The second constraint is imposed by placing a 1 in the column of $\hat{\mathbf{Y}}_i^m$ corresponding to the voltage of that conductor of that tube in $\hat{\mathbf{V}}_i^m$, placing a -1 in the column of $\hat{\mathbf{Y}}_j^m$ corresponding to the voltage of that conductor of that tube in $\hat{\mathbf{V}}_j^m$, placing \hat{Z}_S in the column of $\hat{\mathbf{Z}}_i^m$ corresponding to the current of that conductor of that tube in $\hat{\mathbf{I}}_i^m$, and placing \hat{V}_S in $\hat{\mathbf{P}}^m$ in the row corresponding to the equation being written, and all other entries in that row of (13.7) are zero. Figure 13.8(e) illustrates a parallel connection of an admittance and a lumped current source. The constraints are that the voltages are equal and the currents are related by the element relations:

$$[\hat{\mathbf{V}}_i^m]_k - [\hat{\mathbf{V}}_j^m]_n = 0 \tag{13.12a}$$

$$[\hat{\mathbf{I}}_i^m]_k + [\hat{\mathbf{I}}_j^m]_n + \hat{Y}_S [\hat{\mathbf{V}}_i^m]_k = \hat{I}_S \tag{13.12b}$$

The first constraint is imposed by placing a 1 in the column of $\hat{\mathbf{Y}}_i^m$ corresponding to the voltage of that conductor of that tube in $\hat{\mathbf{V}}_i^m$ and by placing a -1 in the column of $\hat{\mathbf{Y}}_j^m$ corresponding to the voltage of that conductor of that tube in $\hat{\mathbf{V}}_j^m$, and all other entries in that row of (13.7) are zero. The second constraint is imposed by placing a 1 in the column of $\hat{\mathbf{Z}}_i^m$ corresponding to the current of that conductor of that tube in $\hat{\mathbf{I}}_i^m$, placing a 1 in the column of $\hat{\mathbf{Z}}_j^m$ corresponding to the current of that conductor of that tube in $\hat{\mathbf{I}}_j^m$, placing \hat{Y}_S in the column of $\hat{\mathbf{Y}}_i^m$ corresponding to the voltage of that conductor of that tube in $\hat{\mathbf{V}}_i^m$, and placing \hat{I}_S in $\hat{\mathbf{P}}^m$ in the row corresponding to the equation being written, and all other entries in that row of (13.7) are zero.

The final element of the process is the combination of the admittance parameters of the tubes and the constraint relations imposed by the termination/interconnection networks. The objective here is to write these termination/interconnection constraints as a set of simultaneous (complex) equations in terms of only the voltages at the ends of the tubes that are also the voltages at the ports of the termination/interconnection networks. Hence, we wish to solve for the termination voltages (versus frequency). A simple example will illustrate that result. Consider the m th network interconnecting tubes i, j , and k as shown in Figure 13.7(b), where the i th tube connects to termination

network p at the other end, the j th tube connects to termination network q at the other end, and the k th tube connects to termination network r at the other end. The tube admittance characterizations at the m th end are

$$\hat{\mathbf{I}}_i^m = \hat{\mathbf{Y}}_{Si} \hat{\mathbf{V}}_i^m + \hat{\mathbf{Y}}_{Mi} \hat{\mathbf{V}}_i^p + \hat{\mathbf{I}}_{Si}^m \tag{13.13a}$$

$$\hat{\mathbf{I}}_j^m = \hat{\mathbf{Y}}_{Sj} \hat{\mathbf{V}}_j^m + \hat{\mathbf{Y}}_{Mj} \hat{\mathbf{V}}_j^q + \hat{\mathbf{I}}_{Sj}^m \tag{13.13b}$$

$$\hat{\mathbf{I}}_k^m = \hat{\mathbf{Y}}_{Sk} \hat{\mathbf{V}}_k^m + \hat{\mathbf{Y}}_{Mk} \hat{\mathbf{V}}_k^r + \hat{\mathbf{I}}_{Sk}^m \tag{13.13c}$$

The network characterization is given for the m th interconnection network in (13.7a). Substituting (13.13) into (13.7) gives

$$\begin{aligned} & [\hat{\mathbf{Y}}_i^m + \hat{\mathbf{Z}}_i^m \hat{\mathbf{Y}}_{Si}] \hat{\mathbf{V}}_i^m + [\hat{\mathbf{Y}}_j^m + \hat{\mathbf{Z}}_j^m \hat{\mathbf{Y}}_{Sj}] \hat{\mathbf{V}}_j^m + [\hat{\mathbf{Y}}_k^m + \hat{\mathbf{Z}}_k^m \hat{\mathbf{Y}}_{Sk}] \hat{\mathbf{V}}_k^m \\ & + \hat{\mathbf{Z}}_i^m \hat{\mathbf{Y}}_{Mi} \hat{\mathbf{V}}_i^p + \hat{\mathbf{Z}}_j^m \hat{\mathbf{Y}}_{Mj} \hat{\mathbf{V}}_j^q + \hat{\mathbf{Z}}_k^m \hat{\mathbf{Y}}_{Mk} \hat{\mathbf{V}}_k^r = \hat{\mathbf{P}}^m - \hat{\mathbf{Z}}_i^m \hat{\mathbf{I}}_{Si}^m - \hat{\mathbf{Z}}_j^m \hat{\mathbf{I}}_{Sj}^m - \hat{\mathbf{Z}}_k^m \hat{\mathbf{I}}_{Sk}^m \end{aligned} \tag{13.14a}$$

Similarly, for a termination network such as the p th termination network whose terminal characterization is given in Figure 13.7(b), the result is

$$[\hat{\mathbf{Y}}_i^p + \hat{\mathbf{Z}}_i^p \hat{\mathbf{Y}}_{Si}] \hat{\mathbf{V}}_i^p + \hat{\mathbf{Z}}_i^p \hat{\mathbf{Y}}_{Mi} \hat{\mathbf{V}}_i^m = \hat{\mathbf{P}}^p - \hat{\mathbf{Z}}_i^p \hat{\mathbf{I}}_{Si}^p \tag{13.14b}$$

This provides a simple rule for constructing the overall admittance matrix that can be solved for the voltages at the ends of each tube:

$$\underbrace{\begin{bmatrix} \vdots & \vdots \\ \vdots & [\hat{\mathbf{Y}}_i^m + \hat{\mathbf{Z}}_i^m \hat{\mathbf{Y}}_{Si}] & [\hat{\mathbf{Y}}_j^m + \hat{\mathbf{Z}}_j^m \hat{\mathbf{Y}}_{Sj}] & [\hat{\mathbf{Y}}_k^m + \hat{\mathbf{Z}}_k^m \hat{\mathbf{Y}}_{Sk}] & \vdots & [\hat{\mathbf{Z}}_i^m \hat{\mathbf{Y}}_{Mi}] & [\hat{\mathbf{Z}}_j^m \hat{\mathbf{Y}}_{Mj}] & [\hat{\mathbf{Z}}_k^m \hat{\mathbf{Y}}_{Mk}] & \vdots \\ \vdots & \vdots \end{bmatrix}}_{\hat{\mathbf{Y}}_T} \times \underbrace{\begin{bmatrix} \vdots \\ \hat{\mathbf{V}}_i^m \\ \hat{\mathbf{V}}_j^m \\ \hat{\mathbf{V}}_k^m \\ \vdots \\ \hat{\mathbf{V}}_i^p \\ \hat{\mathbf{V}}_i^q \\ \hat{\mathbf{V}}_i^r \\ \vdots \end{bmatrix}}_{\hat{\mathbf{V}}_T} = \underbrace{\begin{bmatrix} \vdots \\ \hat{\mathbf{P}}^m - \hat{\mathbf{Z}}_i^m \hat{\mathbf{I}}_{Si}^m - \hat{\mathbf{Z}}_j^m \hat{\mathbf{I}}_{Sj}^m - \hat{\mathbf{Z}}_k^m \hat{\mathbf{I}}_{Sk}^m \\ \vdots \end{bmatrix}}_{\hat{\mathbf{P}}_T} \tag{13.15}$$

As an example, consider the transmission-line network in Figure 13.2 with graph shown in Figure 13.1(b). The admittance matrix becomes

$$\begin{bmatrix} (\hat{Y}_1^1 + \hat{Z}_1^1 \hat{Y}_{S1}) & \hat{Z}_1^1 \hat{Y}_{M1} & 0 & 0 & 0 & 0 \\ 0 & 0 & (\hat{Y}_2^2 + \hat{Z}_2^2 \hat{Y}_{S2}) & \hat{Z}_2^2 \hat{Y}_{M2} & 0 & 0 \\ 0 & 0 & 0 & 0 & (\hat{Y}_3^3 + \hat{Z}_3^3 \hat{Y}_{S3}) & \hat{Z}_3^3 \hat{Y}_{M3} \\ \hat{Z}_1^4 \hat{Y}_{M1} & (\hat{Y}_1^4 + \hat{Z}_1^4 \hat{Y}_{S1}) & \hat{Z}_2^4 \hat{Y}_{M2} & (\hat{Y}_2^4 + \hat{Z}_2^4 \hat{Y}_{S2}) & \hat{Z}_3^4 \hat{Y}_{M3} & (\hat{Y}_3^4 + \hat{Z}_3^4 \hat{Y}_{S3}) \end{bmatrix} \times \begin{bmatrix} \hat{V}_1^1 \\ \hat{V}_1^4 \\ \hat{V}_2^1 \\ \hat{V}_2^4 \\ \hat{V}_3^3 \\ \hat{V}_3^4 \end{bmatrix} = \begin{bmatrix} \hat{P}^1 \\ \hat{P}^2 \\ \hat{P}^3 \\ \hat{P}^4 \end{bmatrix}$$

Numbering each conductor of each tube as shown gives the following. First, we examine termination network # 1. The constraints are

$$\begin{aligned} [\hat{V}_1^1]_1 &= V_S(t) - 50 [\hat{I}_1^1]_1 \\ [\hat{V}_1^1]_2 &= -1k [\hat{I}_1^1]_2 \\ [\hat{V}_1^1]_3 &= -500 [\hat{I}_1^1]_3 \\ [\hat{V}_1^1]_4 &= -10 [\hat{I}_1^1]_4 \end{aligned}$$

Therefore,

$$\hat{Y}_1^1 = \begin{bmatrix} 1 & 0 & 0 & 0 \\ 0 & 1 & 0 & 0 \\ 0 & 0 & 1 & 0 \\ 0 & 0 & 0 & 1 \end{bmatrix}, \hat{Z}_1^1 = \begin{bmatrix} 50 & 0 & 0 & 0 \\ 0 & 1k & 0 & 0 \\ 0 & 0 & 500 & 0 \\ 0 & 0 & 0 & 10 \end{bmatrix}, \hat{P}^1 = \begin{bmatrix} V_S(t) \\ 0 \\ 0 \\ 0 \end{bmatrix}$$

The number of equations equals the number of conductors incident on this node: 4. Similarly, termination networks # 2 and # 3 are characterized by

$$\begin{aligned} [\hat{V}_2^2]_1 &= -5k [\hat{I}_2^2]_1 \\ [\hat{V}_2^2]_2 &= -50 [\hat{I}_2^2]_2 \end{aligned}$$

and

$$\begin{aligned} [\hat{V}_3^3]_1 &= -100 [\hat{I}_3^3]_1 \\ [\hat{V}_3^3]_2 &= -10 [\hat{I}_3^3]_2 \end{aligned}$$

Hence, the termination network characterizations in (13.7b) become

$$\hat{\mathbf{Y}}_2^2 = \begin{bmatrix} 1 & 0 \\ 0 & 1 \end{bmatrix}, \hat{\mathbf{Z}}_2^2 = \begin{bmatrix} 5k & 0 \\ 0 & 50 \end{bmatrix}, \hat{\mathbf{P}}^2 = \begin{bmatrix} 0 \\ 0 \end{bmatrix}$$

and

$$\hat{\mathbf{Y}}_3^3 = \begin{bmatrix} 1 & 0 \\ 0 & 1 \end{bmatrix}, \hat{\mathbf{Z}}_3^3 = \begin{bmatrix} 100 & 0 \\ 0 & 10 \end{bmatrix}, \hat{\mathbf{P}}^3 = \begin{bmatrix} 0 \\ 0 \end{bmatrix}$$

The number of equations equals the number of conductors incident on each node: 2. Interconnection network # 4 has the following constraints. KVL imposes

$$\begin{aligned} [\hat{\mathbf{V}}_1^4]_1 - [\hat{\mathbf{V}}_2^4]_1 &= -100 [\hat{\mathbf{I}}_1^4]_1 \\ [\hat{\mathbf{V}}_1^4]_2 &= 0 \\ [\hat{\mathbf{V}}_1^4]_3 - [\hat{\mathbf{V}}_3^4]_2 &= 0 \\ [\hat{\mathbf{V}}_1^4]_4 - [\hat{\mathbf{V}}_3^4]_1 &= 0 \end{aligned}$$

KCL imposes

$$\begin{aligned} [\hat{\mathbf{I}}_1^4]_1 + [\hat{\mathbf{I}}_2^4]_1 &= 0 \\ [\hat{\mathbf{I}}_1^4]_3 + [\hat{\mathbf{I}}_3^4]_2 &= -\frac{1}{50} [\hat{\mathbf{V}}_1^4]_3 \\ [\hat{\mathbf{I}}_1^4]_4 + [\hat{\mathbf{I}}_3^4]_1 &= 0 \\ [\hat{\mathbf{I}}_2^4]_2 &= 0 \end{aligned}$$

Observe that the total number of constraint equations for network # 4 equals the total number of conductors incident on that node: $4 + 2 + 2 = 8$. This requirement must always be met for any set of constraint equations for a termination/interconnection network. The interconnection network characterizations in (13.7a) become

$$\hat{\mathbf{Y}}_1^4 = \begin{bmatrix} 1 & 0 & 0 & 0 \\ 0 & 1 & 0 & 0 \\ 0 & 0 & 1 & 0 \\ 0 & 0 & 0 & 1 \\ 0 & 0 & 0 & 0 \\ 0 & 0 & 1/50 & 0 \\ 0 & 0 & 0 & 0 \\ 0 & 0 & 0 & 0 \end{bmatrix}, \hat{\mathbf{Z}}_1^4 = \begin{bmatrix} 100 & 0 & 0 & 0 \\ 0 & 0 & 0 & 0 \\ 0 & 0 & 0 & 0 \\ 0 & 0 & 0 & 0 \\ 1 & 0 & 0 & 0 \\ 0 & 0 & 1 & 0 \\ 0 & 0 & 0 & 1 \\ 0 & 0 & 0 & 0 \end{bmatrix}$$

$$\hat{\mathbf{Y}}_2^4 = \begin{bmatrix} -1 & 0 \\ 0 & 0 \\ 0 & 0 \\ 0 & 0 \\ 0 & 0 \\ 0 & 0 \\ 0 & 0 \\ 0 & 0 \end{bmatrix}, \hat{\mathbf{Z}}_2^4 = \begin{bmatrix} 0 & 0 \\ 0 & 0 \\ 0 & 0 \\ 0 & 0 \\ 1 & 0 \\ 0 & 0 \\ 0 & 0 \\ 0 & 1 \end{bmatrix}$$

$$\hat{\mathbf{Y}}_3^4 = \begin{bmatrix} 0 & 0 \\ 0 & 0 \\ 0 & -1 \\ -1 & 0 \\ 0 & 0 \\ 0 & 0 \\ 0 & 0 \\ 0 & 0 \end{bmatrix}, \hat{\mathbf{Z}}_3^4 = \begin{bmatrix} 0 & 0 \\ 0 & 0 \\ 0 & 0 \\ 0 & 0 \\ 0 & 0 \\ 0 & 1 \\ 1 & 0 \\ 0 & 0 \end{bmatrix}$$

and

$$\hat{\mathbf{P}}^4 = \begin{bmatrix} 0 \\ 0 \\ 0 \\ 0 \\ 0 \\ 0 \\ 0 \\ 0 \end{bmatrix}$$

The predictions of this model with and without losses are compared for a pulse rise time of 1 ns in Figure 13.9. The predictions of the TDFD transformation are obtained by first determining the frequency-domain transfer function with this model at the spectral harmonics of the input using the above method. The resulting spectral components of the output voltage are combined using `TIMEFREQ.FOR` giving $V_{out}(t)$. The predictions of the SPICE model in Figure 13.5 and those for this admittance parameter characterization using the TDFD conversion to the time domain for a lossless line are identical. The ramp waveform of Figure 13.3(c) is modeled as a trapezoidal waveform with identical $\tau_r = 1$ ns rise and fall times and a 1-MHz repetition rate. This is decomposed into its spectral components and combined with the frequency-domain transfer function computed with the above admittance parameter model at 1000 harmonics. The bandwidth of this pulse is on the order of $BW = 1/\tau_r = 1$ GHz. Hence, the excellent correlation with the SPICE results are expected. The frequency-dependent losses of the conductors were also included in the transfer function and the results recomputed and shown in Figure 13.9 using 1000 harmonics. The wire losses have a minor effect on the output voltage waveshape, which is probably due to the fact that the common ground plane losses are omitted. Figure 13.10 shows the frequency response of the transfer function obtained with this method with

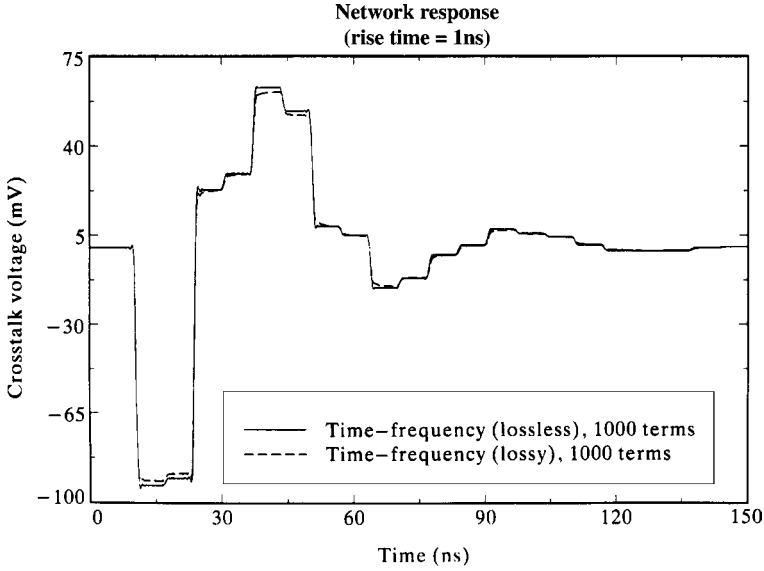


FIGURE 13.9 Comparison of crosstalk voltage at the termination of conductor # 1 of tube # 3 for the transmission-line network of Figure 13.2 for a rise time of 1 ns using the time-domain to frequency-domain transformation with and without losses.

and without losses. This further confirms that the wire losses have little effect in this problem.

The admittance parameters are not, of course, the only way of characterizing the tubes. The dual is the impedance parameter characterization:

$$\hat{\mathbf{V}}(0) = \hat{\mathbf{Z}}_S \hat{\mathbf{I}}(0) + \hat{\mathbf{Z}}_M (-\hat{\mathbf{I}}(\mathcal{L})) + \hat{\mathbf{V}}_{S0} \tag{13.16a}$$

$$\hat{\mathbf{V}}(\mathcal{L}) = \hat{\mathbf{Z}}_M \hat{\mathbf{I}}(0) + \hat{\mathbf{Z}}_S (-\hat{\mathbf{I}}(\mathcal{L})) + \hat{\mathbf{V}}_{SL} \tag{13.16b}$$

The chain parameters in (13.1) can be manipulated to yield

$$\begin{aligned} \hat{\mathbf{Z}}_S &= -\hat{\phi}_{21}^{-1} \hat{\phi}_{22} = -\hat{\phi}_{11} \hat{\phi}_{21}^{-1} \\ &= \hat{\mathbf{Z}}_C \hat{\mathbf{T}}_I [\mathbf{e}^{\hat{\gamma} \mathcal{L}} - \mathbf{e}^{-\hat{\gamma} \mathcal{L}}]^{-1} [\mathbf{e}^{\hat{\gamma} \mathcal{L}} + \mathbf{e}^{-\hat{\gamma} \mathcal{L}}] \hat{\mathbf{T}}_I^{-1} \end{aligned} \tag{13.17a}$$

$$\begin{aligned} \hat{\mathbf{Z}}_M &= -\hat{\phi}_{21}^{-1} \\ &= 2\hat{\mathbf{Z}}_C \hat{\mathbf{T}}_I [\mathbf{e}^{\hat{\gamma} \mathcal{L}} - \mathbf{e}^{-\hat{\gamma} \mathcal{L}}]^{-1} \hat{\mathbf{T}}_I^{-1} \end{aligned} \tag{13.17b}$$

$$\hat{\mathbf{V}}_{S0} = \hat{\mathbf{Z}}_M \hat{\mathbf{V}}_{FT} \tag{13.17c}$$

$$\hat{\mathbf{V}}_{SL} = \hat{\mathbf{V}}_{FT} + \hat{\mathbf{Z}}_S \hat{\mathbf{I}}_{FT} \tag{13.17d}$$

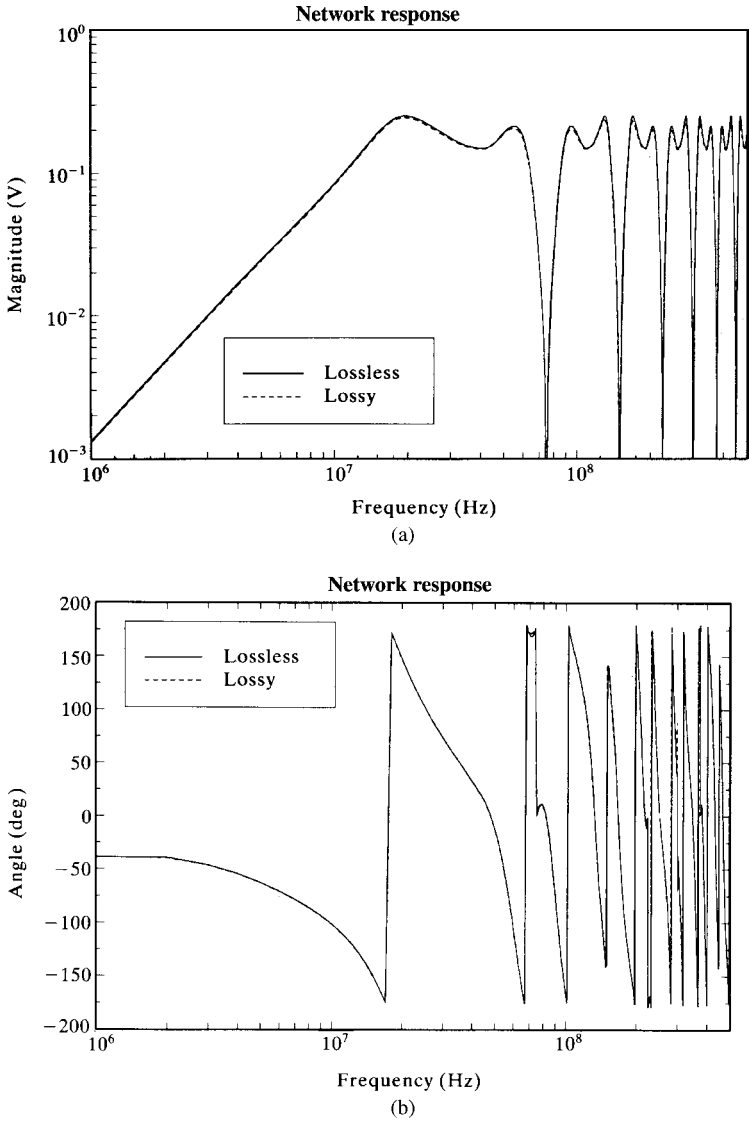


FIGURE 13.10 The frequency-domain crosstalk voltage at the termination of conductor # 1 of tube # 3 for the transmission-line network of Figure 13.2 with and without losses: (a) magnitude and (b) phase.

The overall matrix to be solved can be obtained by substituting (13.16) for the tubes connected to node m that is characterized by (13.7) to give

$$\hat{\mathbf{Z}}_T \hat{\mathbf{I}}_T = \hat{\mathbf{P}}_T \tag{13.18}$$

This result has the same form as (13.14) and (13.15) with the following substitutions:

$$\hat{\mathbf{Y}}_i^m \Rightarrow \hat{\mathbf{Z}}_i^m \tag{13.19a}$$

$$\hat{\mathbf{Z}}_i^m \Rightarrow \hat{\mathbf{Y}}_i^m \tag{13.19b}$$

$$\hat{\mathbf{Y}}_{Si} \Rightarrow \hat{\mathbf{Z}}_{Si} \tag{13.19c}$$

$$\hat{\mathbf{Y}}_{Mi} \Rightarrow \hat{\mathbf{Z}}_{Mi} \tag{13.19d}$$

$$\hat{\mathbf{I}}_{Si}^m \Rightarrow \hat{\mathbf{V}}_{Si}^m \tag{13.19e}$$

$$\hat{\mathbf{V}}_i^m \Rightarrow \hat{\mathbf{I}}_i^m \tag{13.19f}$$

With the impedance parameters we solve for the currents incident on the nodes, $\hat{\mathbf{I}}_i^m$.

13.4 REPRESENTATION WITH THE BLT EQUATIONS

An alternative to the above methods is the use of the *scattering parameter* representation of the tubes [1,2,3]. Consider a tube having *lumped excitation* at some point, $z = \tau$, along its length illustrated in Figure 13.11. These lumped excitations may represent point sources such as the direct attachment of a lightning stroke or can be extended to include distributed incident field excitation, as we will show. The general frequency-domain solution of the MTL (multiconductor transmission line) equations for this tube can be written as in Chapter 7 for the tube segments to the left and right of the sources as

$$\hat{\mathbf{V}}(z) = \hat{\mathbf{Z}}_C \hat{\mathbf{T}}_I \left[e^{-\hat{\gamma}z} \hat{\mathbf{I}}_L^+ + e^{\hat{\gamma}z} \hat{\mathbf{I}}_L^- \right] \tag{13.20a}$$

$$\hat{\mathbf{I}}(z) = \hat{\mathbf{T}}_I \left[e^{-\hat{\gamma}z} \hat{\mathbf{I}}_L^+ - e^{\hat{\gamma}z} \hat{\mathbf{I}}_L^- \right] \tag{13.20b}$$

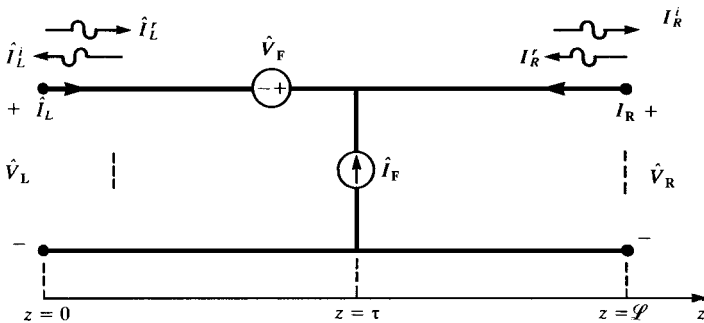


FIGURE 13.11 Determination of the scattering parameters for a tube having lumped excitation at a point on the tube.

for $0 \leq z < \tau$ and

$$\hat{\mathbf{V}}(z) = \hat{\mathbf{Z}}_C \hat{\mathbf{T}}_I \left[\mathbf{e}^{-\hat{\gamma}z} \hat{\mathbf{I}}_R^+ + \mathbf{e}^{\hat{\gamma}z} \hat{\mathbf{I}}_R^- \right] \quad (13.21a)$$

$$\hat{\mathbf{I}}(z) = \hat{\mathbf{T}}_I \left[\mathbf{e}^{-\hat{\gamma}z} \hat{\mathbf{I}}_R^+ - \mathbf{e}^{\hat{\gamma}z} \hat{\mathbf{I}}_R^- \right] \quad (13.21b)$$

for $\tau < z \leq \mathcal{L}$. The subscripts on the undetermined constant vectors, L and R, represent the left and right segments, respectively. The characteristic impedance matrix is the inverse of the characteristic admittance matrix given in (13.5), and the propagation matrix is determined as in (13.4). Evaluating these at $z = \tau$ yields

$$-\hat{\mathbf{Z}}_C \hat{\mathbf{T}}_I \left[\mathbf{e}^{-\hat{\gamma}\tau} \hat{\mathbf{I}}_L^+ + \mathbf{e}^{\hat{\gamma}\tau} \hat{\mathbf{I}}_L^- \right] + \hat{\mathbf{Z}}_C \hat{\mathbf{T}}_I \left[\mathbf{e}^{-\hat{\gamma}\tau} \hat{\mathbf{I}}_R^+ + \mathbf{e}^{\hat{\gamma}\tau} \hat{\mathbf{I}}_R^- \right] = \hat{\mathbf{V}}_F \quad (13.22a)$$

$$-\hat{\mathbf{T}}_I \left[\mathbf{e}^{-\hat{\gamma}\tau} \hat{\mathbf{I}}_L^+ - \mathbf{e}^{\hat{\gamma}\tau} \hat{\mathbf{I}}_L^- \right] + \hat{\mathbf{T}}_I \left[\mathbf{e}^{-\hat{\gamma}\tau} \hat{\mathbf{I}}_R^+ - \mathbf{e}^{\hat{\gamma}\tau} \hat{\mathbf{I}}_R^- \right] = \hat{\mathbf{I}}_F \quad (13.22b)$$

Adding and subtracting these yields

$$\hat{\mathbf{I}}_L^+ - \hat{\mathbf{I}}_R^+ = -\frac{1}{2} \mathbf{e}^{\hat{\gamma}\tau} \hat{\mathbf{T}}_I^{-1} \hat{\mathbf{Z}}_C^{-1} [\hat{\mathbf{V}}_F + \hat{\mathbf{Z}}_C \hat{\mathbf{I}}_F] \quad (13.23a)$$

$$\hat{\mathbf{I}}_L^- - \hat{\mathbf{I}}_R^- = -\frac{1}{2} \mathbf{e}^{-\hat{\gamma}\tau} \hat{\mathbf{T}}_I^{-1} \hat{\mathbf{Z}}_C^{-1} [\hat{\mathbf{V}}_F - \hat{\mathbf{Z}}_C \hat{\mathbf{I}}_F] \quad (13.23b)$$

The currents at the line endpoints can be logically decomposed into *incident* and *reflected* waves by evaluating (13.20b) at $z = 0$ and (13.21b) at $z = \mathcal{L}$ as

$$\hat{\mathbf{I}}_L = \hat{\mathbf{I}}(0) = \hat{\mathbf{I}}_L^i + \hat{\mathbf{I}}_L^r \quad (13.24a)$$

$$\hat{\mathbf{I}}_R = -\hat{\mathbf{I}}(\mathcal{L}) = \hat{\mathbf{I}}_R^i + \hat{\mathbf{I}}_R^r \quad (13.24b)$$

where

$$\hat{\mathbf{I}}_L^r = \hat{\mathbf{T}}_I \hat{\mathbf{I}}_L^+ \quad (13.25a)$$

$$\hat{\mathbf{I}}_L^i = -\hat{\mathbf{T}}_I \hat{\mathbf{I}}_L^- \quad (13.25b)$$

$$\hat{\mathbf{I}}_R^i = -\hat{\mathbf{T}}_I \mathbf{e}^{-\hat{\gamma}\mathcal{L}} \hat{\mathbf{I}}_R^+ \quad (13.25c)$$

$$\hat{\mathbf{I}}_R^r = \hat{\mathbf{T}}_I \mathbf{e}^{\hat{\gamma}\mathcal{L}} \hat{\mathbf{I}}_R^- \quad (13.25d)$$

where superscripts i and r denote *incident* and *reflected*, respectively. This is a sensible designation if we designate the incident wave as the portion incoming at the termination and the reflected wave as the portion outgoing from the junction and also observe that a component containing $\mathbf{e}^{-\hat{\gamma}z}$ is traveling to the right and a component containing $\mathbf{e}^{\hat{\gamma}z}$ is traveling to the left. To conform with the results of the previous

section, the tube currents are directed into the tube at both ends. Combining (13.23) and (13.25) yields the reflected components in terms of the incident quantities as

$$\hat{\mathbf{I}}_L^r = - \left(\hat{\mathbf{T}}_I \mathbf{e}^{\hat{y} \mathcal{L}} \hat{\mathbf{T}}_I^{-1} \right) \hat{\mathbf{I}}_R^i - \frac{1}{2} \left(\hat{\mathbf{T}}_I \mathbf{e}^{\hat{y} \tau} \hat{\mathbf{T}}_I^{-1} \right) \left[\hat{\mathbf{I}}_F + \hat{\mathbf{Z}}_C^{-1} \hat{\mathbf{V}}_F \right] \quad (13.26a)$$

$$\hat{\mathbf{I}}_R^r = - \left(\hat{\mathbf{T}}_I \mathbf{e}^{\hat{y} \mathcal{L}} \hat{\mathbf{T}}_I^{-1} \right) \hat{\mathbf{I}}_L^i - \frac{1}{2} \left(\hat{\mathbf{T}}_I \mathbf{e}^{\hat{y}(\mathcal{L}-\tau)} \hat{\mathbf{T}}_I^{-1} \right) \left[\hat{\mathbf{I}}_F - \hat{\mathbf{Z}}_C^{-1} \hat{\mathbf{V}}_F \right] \quad (13.26b)$$

(There are sign differences between these results and those of [1–3] due to our choice of the total currents as being directed into the tube at both ends.) In matrix notation, these become

$$\begin{bmatrix} \hat{\mathbf{I}}_L^r \\ \hat{\mathbf{I}}_R^r \end{bmatrix} = \hat{\mathbf{R}} \begin{bmatrix} \hat{\mathbf{I}}_L^i \\ \hat{\mathbf{I}}_R^i \end{bmatrix} + \hat{\mathbf{I}}_T \quad (13.27)$$

where the *tube propagation matrix* $\hat{\mathbf{R}}$ is

$$\hat{\mathbf{R}} = \begin{bmatrix} \mathbf{0} & \hat{\mathbf{\Gamma}} \\ \hat{\mathbf{\Gamma}} & \mathbf{0} \end{bmatrix} \quad (13.28a)$$

with entries

$$\hat{\mathbf{\Gamma}} = -\hat{\mathbf{T}}_I \mathbf{e}^{\hat{y} \mathcal{L}} \hat{\mathbf{T}}_I^{-1} \quad (13.28b)$$

The current source vector due to the lumped sources at $z = \tau$ is

$$\hat{\mathbf{I}}_T = \begin{bmatrix} -\frac{1}{2} \left(\hat{\mathbf{T}}_I \mathbf{e}^{\hat{y} \tau} \hat{\mathbf{T}}_I^{-1} \right) \left[\hat{\mathbf{I}}_F + \hat{\mathbf{Z}}_C^{-1} \hat{\mathbf{V}}_F \right] \\ -\frac{1}{2} \left(\hat{\mathbf{T}}_I \mathbf{e}^{\hat{y}(\mathcal{L}-\tau)} \hat{\mathbf{T}}_I^{-1} \right) \left[\hat{\mathbf{I}}_F - \hat{\mathbf{Z}}_C^{-1} \hat{\mathbf{V}}_F \right] \end{bmatrix} \quad (13.29a)$$

In the case of distributed excitation such as the case for incident field illumination of the tube, the source vector simply becomes

$$\hat{\mathbf{I}}_T = \int_0^{\mathcal{L}} \begin{bmatrix} -\frac{1}{2} \left(\hat{\mathbf{T}}_I \mathbf{e}^{\hat{y} \tau} \hat{\mathbf{T}}_I^{-1} \right) \left[\hat{\mathbf{I}}_F(\tau) + \hat{\mathbf{Z}}_C^{-1} \hat{\mathbf{V}}_F(\tau) \right] \\ -\frac{1}{2} \left(\hat{\mathbf{T}}_I \mathbf{e}^{\hat{y}(\mathcal{L}-\tau)} \hat{\mathbf{T}}_I^{-1} \right) \left[\hat{\mathbf{I}}_F(\tau) - \hat{\mathbf{Z}}_C^{-1} \hat{\mathbf{V}}_F(\tau) \right] \end{bmatrix} d\tau \quad (13.29b)$$

The total voltages and currents at the left end of the tube become, by evaluating (13.20) at $z = 0$ and substituting (13.25a) and (13.25b),

$$\hat{\mathbf{V}}(0) = \hat{\mathbf{V}}_L = \hat{\mathbf{Z}}_C \left(\hat{\mathbf{I}}_L^r - \hat{\mathbf{I}}_L^i \right) \quad (13.30a)$$

$$\hat{\mathbf{I}}(0) = \hat{\mathbf{I}}_L = \hat{\mathbf{I}}_L^r + \hat{\mathbf{I}}_L^i \quad (13.30b)$$

Similarly, the total voltages and currents at the right end of the tube become, by evaluating (13.21) at $z = \mathcal{L}$ and substituting (13.25c) and (13.25d),

$$\hat{\mathbf{V}}(\mathcal{L}) = \hat{\mathbf{V}}_R = \hat{\mathbf{Z}}_C \left(\hat{\mathbf{I}}_R^r - \hat{\mathbf{I}}_R^i \right) \quad (13.31a)$$

$$-\hat{\mathbf{I}}(\mathcal{L}) = \hat{\mathbf{I}}_R = \hat{\mathbf{I}}_R^r + \hat{\mathbf{I}}_R^i \quad (13.31b)$$

Observe that, as in the case of the admittance parameters, the total currents are defined as being *directed into the tubes* at both ends. The *incident* components are defined as being the components traveling out of the tubes or into the network attached to that end. The *reflected* components are similarly defined as being the components traveling into the tubes or out of the network attached to that end. Hence, the origin of the names *incident* and *reflected*, with respect to the network or node at which the end of the tube is incident.

These results can be derived in an alternative manner from the chain-parameter matrix representation of the line with incident field illumination. Substituting the chain-parameter matrix of the line given in (12.25) of Chapter 12 into (13.30) and (13.31), we obtain (13.26). This gives the current source vector in (13.29b) in terms of the total incident field vectors, $\hat{\mathbf{I}}_{FT}$ and $\hat{\mathbf{V}}_{FT}$, developed in Chapter 12 and given in (12.25) as

$$\hat{\mathbf{I}}_T = \begin{bmatrix} -\frac{1}{2} \hat{\mathbf{T}}_T e^{\hat{\gamma} \mathcal{L}} \hat{\mathbf{T}}_T^{-1} [\hat{\mathbf{I}}_{FT} + \hat{\mathbf{Y}}_C \hat{\mathbf{V}}_{FT}] \\ -\frac{1}{2} [\hat{\mathbf{I}}_{FT} - \hat{\mathbf{Y}}_C \hat{\mathbf{V}}_{FT}] \end{bmatrix} \quad (13.32)$$

We next form the *junction scattering matrix* for node m , $\hat{\mathbf{S}}_m$, which relates the reflected and incident current components at node m as

$$\hat{\mathbf{I}}_m^r = \hat{\mathbf{S}}_m \hat{\mathbf{I}}_m^i \quad (13.33)$$

The number of equations here equals the total number of conductors incident on that node. First, consider a *termination node* where only one tube is incident as shown in Figure 13.12. Suppose that the network contains no lumped sources and is

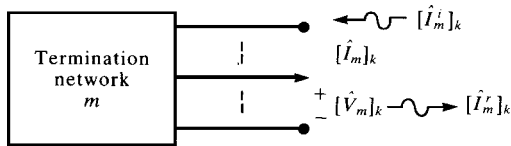


FIGURE 13.12 Definitions of incident and scattered waves for determining the scattering parameters of a termination network.

characterized by a generalized Thevenin equivalent as

$$\begin{aligned} \hat{V}_m &= -\hat{Z}_m \hat{\mathbf{I}}_m \\ &= -\hat{Z}_m [\hat{\mathbf{I}}_m^r + \hat{\mathbf{I}}_m^i] \end{aligned} \tag{13.34}$$

(Recall that the total currents are defined as being directed into the tube ends and are therefore directed out of the termination networks.) The relations for the voltage and current at the end of the tube that is incident on this node are

$$\hat{V}_m = \hat{Z}_{Cm} [\hat{\mathbf{I}}_m^r - \hat{\mathbf{I}}_m^i] \tag{13.35}$$

Solving (13.34) and (13.35) yields the *current scattering matrix*:

$$\hat{\mathbf{S}}_m = -(\hat{Z}_m + \hat{Z}_{Cm})^{-1} (\hat{Z}_m - \hat{Z}_{Cm}) \tag{13.36}$$

This has a direct parallel to the scalar *current reflection coefficient* for a two-conductor line [A.1].

The next form of the scattering matrix is for an interconnection network wherein there are two or more tubes incident. In the admittance parameter representation of the previous section, we characterized these in a general sense as a combination of generalized Thevenin and generalized Norton equivalents so that series and parallel impedances and excitation sources could be included. The formulation of the BLT equations in [1–3] has the excitation sources as lumped or distributed sources along the tubes due to incident fields. We will derive the BLT equations with that assumption although we will later modify them for the more general case of lumped sources within the networks. Thus, the interconnection networks will simply have (1) conductors directly connected, (2) conductors terminated in short circuits, and (3) conductors terminated in open circuits as shown in Figure 13.13. First consider the direction connection of several conductors as shown in Figure 13.13(a). This is characterized as

$$C_I \hat{\mathbf{I}}_m = \mathbf{0} \tag{13.37a}$$

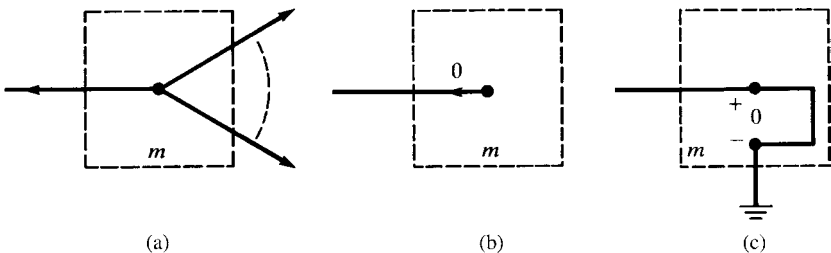


FIGURE 13.13 Interconnection networks: (a) direct connection, (b) open circuit, and (c) short circuit.

$$\mathbf{C}_V \hat{\mathbf{V}}_m = \mathbf{0} \quad (13.37b)$$

where $\hat{\mathbf{I}}_m$ contains the total currents of the conductors incident on the m th node and $\hat{\mathbf{V}}_m$ contains the voltages of those conductors. The first relation in (13.37a) enforces KCL at the connection so that for each connection a 1 appears in the columns of \mathbf{C}_I corresponding to the currents of $\hat{\mathbf{I}}_m$ for the conductors that are connected. The second condition in (13.37b) enforces KVL at the connection so that for n conductors connected, there are $n-1$ equations enforcing $\hat{V}_a - \hat{V}_b = 0$ for $n-1$ pairs of the voltages. Thus, a 1 appears in the column of \mathbf{C}_V corresponding to the voltage of the pair in $\hat{\mathbf{V}}_m$ and a -1 appears in the column of \mathbf{C}_V corresponding to the other voltage of the pair in $\hat{\mathbf{V}}_m$. The second situation is an open circuit as illustrated in Figure 13.13(b). Enforcing KCL requires that we place a 1 in the column of \mathbf{C}_I corresponding to the current of $\hat{\mathbf{I}}_m$ that is constrained to zero by the open circuit. The third constraint is a short circuit illustrated in Figure 13.13(c). Enforcing KVL requires that we place a 1 in the column of \mathbf{C}_V corresponding to the voltage of $\hat{\mathbf{V}}_m$ that is constrained to zero by the short circuit. The sum of the row dimensions of \mathbf{C}_I and \mathbf{C}_V must equal the total number of conductors incident on the node. The scattering matrix for this interconnection node can now be formulated. Decomposing the total currents and voltages into their incident and reflected components gives

$$-\mathbf{C}_I \hat{\mathbf{I}}_m^r = \mathbf{C}_I \hat{\mathbf{I}}_m^i \quad (13.38a)$$

$$\mathbf{C}_V \hat{\mathbf{Z}}_{Cm} \hat{\mathbf{I}}_m^r = \mathbf{C}_V \hat{\mathbf{Z}}_{Cm} \hat{\mathbf{I}}_m^i \quad (13.38b)$$

where $\hat{\mathbf{Z}}_{Cm}$ contains the characteristic impedance matrices of the tubes incident on the node on the main diagonal and zeros elsewhere. Solving (13.38) yields the scattering matrix of the interconnection node as

$$\hat{\mathbf{S}}_m = \left[\begin{array}{c} -\mathbf{C}_I \\ \mathbf{C}_V \hat{\mathbf{Z}}_{Cm} \end{array} \right]^{-1} \left[\begin{array}{c} \mathbf{C}_I \\ \mathbf{C}_V \hat{\mathbf{Z}}_{Cm} \end{array} \right] \quad (13.39)$$

Arranging the tube characterizations for all tubes in the network and the scattering matrix representations for all nodes in the network yields the overall characterization

$$\hat{\mathbf{I}}_T^r = \hat{\mathbf{R}}_T \hat{\mathbf{I}}_T^i + \hat{\mathbf{I}}_{TT} \quad (13.40a)$$

$$\hat{\mathbf{I}}_T^r = \hat{\mathbf{S}}_T \hat{\mathbf{I}}_T^i \quad (13.40b)$$

The overall tube propagation matrix $\hat{\mathbf{R}}_T$ is $2n_T \times 2n_T$, where n_T is the total number of conductors in the overall transmission-line network and has the individual tube characterization matrices given in (13.27) on the main diagonal and zeros elsewhere. Similarly, the overall junction scattering matrix $\hat{\mathbf{S}}_T$ is $2n_T \times 2n_T$ and contains the individual scattering matrices for the interconnection and termination networks on the main diagonal and zeros elsewhere. Combining (13.40) gives

$$\left(\hat{\mathbf{S}}_T - \hat{\mathbf{R}}_T \right) \hat{\mathbf{I}}_T^i = \hat{\mathbf{I}}_{TT} \quad (13.41)$$

which are referred to as the BLT (Baum, Liu, and Tesche) equations. The total currents can be obtained by writing

$$\hat{\mathbf{I}}_T = \hat{\mathbf{I}}_T^i + \hat{\mathbf{I}}_T^r \tag{13.42}$$

Solving (13.40) and (13.42) simultaneously gives the total currents as

$$\hat{\mathbf{I}}_T = [\mathbf{1} + \hat{\mathbf{S}}_T] [\hat{\mathbf{S}}_T - \hat{\mathbf{R}}_T]^{-1} \hat{\mathbf{I}}_{TT} \tag{13.43}$$

This formulation can be extended to include series and parallel impedances and lumped sources in the termination/interconnection networks. In order to provide that extension, consider the general characterization of the m th termination/interconnection node illustrated in Figure 13.7(b) and given in (13.7a):

$$\hat{\mathbf{Y}}_i^m \hat{\mathbf{V}}_i^m + \hat{\mathbf{Z}}_i^m \hat{\mathbf{I}}_i^m + \hat{\mathbf{Y}}_j^m \hat{\mathbf{V}}_j^m + \hat{\mathbf{Z}}_j^m \hat{\mathbf{I}}_j^m + \hat{\mathbf{Y}}_k^m \hat{\mathbf{V}}_k^m + \hat{\mathbf{Z}}_k^m \hat{\mathbf{I}}_k^m = \hat{\mathbf{P}}^m \tag{13.7a}$$

This can be written in matrix form as

$$[\hat{\mathbf{Y}}_i^m \quad \hat{\mathbf{Y}}_j^m \quad \hat{\mathbf{Y}}_k^m] \begin{bmatrix} \hat{\mathbf{V}}_i^m \\ \hat{\mathbf{V}}_j^m \\ \hat{\mathbf{V}}_k^m \end{bmatrix} + [\hat{\mathbf{Z}}_i^m \quad \hat{\mathbf{Z}}_j^m \quad \hat{\mathbf{Z}}_k^m] \begin{bmatrix} \hat{\mathbf{I}}_i^m \\ \hat{\mathbf{I}}_j^m \\ \hat{\mathbf{I}}_k^m \end{bmatrix} = \hat{\mathbf{P}}^m \tag{13.44}$$

The currents and voltages can be decomposed into incident and reflected components according to (13.31) as

$$\hat{\mathbf{V}}_i^m = \hat{\mathbf{Z}}_{Ci} (\hat{\mathbf{I}}_i^{mr} - \hat{\mathbf{I}}_i^{mi}) \tag{13.45a}$$

$$\hat{\mathbf{I}}_i^m = \hat{\mathbf{I}}_i^{mr} + \hat{\mathbf{I}}_i^{mi} \tag{13.45b}$$

and likewise for tube j and tube k . Substituting (13.45) into (13.44) yields

$$\begin{bmatrix} \hat{\mathbf{I}}_i^{mr} \\ \hat{\mathbf{I}}_j^{mr} \\ \hat{\mathbf{I}}_k^{mr} \end{bmatrix} = \hat{\mathbf{S}}_m \begin{bmatrix} \hat{\mathbf{I}}_i^{mi} \\ \hat{\mathbf{I}}_j^{mi} \\ \hat{\mathbf{I}}_k^{mi} \end{bmatrix} + \hat{\mathbf{I}}_S^m \tag{13.46}$$

where

$$\hat{\mathbf{S}}_m = -\{[\hat{\mathbf{Z}}_i^m \quad \hat{\mathbf{Z}}_j^m \quad \hat{\mathbf{Z}}_k^m] + [\hat{\mathbf{Y}}_i^m \quad \hat{\mathbf{Y}}_j^m \quad \hat{\mathbf{Y}}_k^m] \hat{\mathbf{Z}}_{Cm}\}^{-1} \times \{[\hat{\mathbf{Z}}_i^m \quad \hat{\mathbf{Z}}_j^m \quad \hat{\mathbf{Z}}_k^m] - [\hat{\mathbf{Y}}_i^m \quad \hat{\mathbf{Y}}_j^m \quad \hat{\mathbf{Y}}_k^m] \hat{\mathbf{Z}}_{Cm}\} \tag{13.47a}$$

and the collection of characteristic impedance matrices of the tubes incident on the termination/interconnection network is

$$\hat{\mathbf{Z}}_{Cm} = \begin{bmatrix} \hat{\mathbf{Z}}_{Ci} & \mathbf{0} & \mathbf{0} \\ \mathbf{0} & \hat{\mathbf{Z}}_{Cj} & \mathbf{0} \\ \mathbf{0} & \mathbf{0} & \hat{\mathbf{Z}}_{Ck} \end{bmatrix} \tag{13.47b}$$

The current source vector is

$$\hat{\mathbf{I}}_S^m = \{ [\hat{\mathbf{Z}}_i^m \quad \hat{\mathbf{Z}}_j^m \quad \hat{\mathbf{Z}}_k^m] + [\hat{\mathbf{Y}}_i^m \quad \hat{\mathbf{Y}}_j^m \quad \hat{\mathbf{Y}}_k^m] \hat{\mathbf{Z}}_{Cm} \}^{-1} \hat{\mathbf{P}}^m \quad (13.47c)$$

For example, consider the case of a termination network (only one tube incident on the node) and a generalized Thevenin representation of this network:

$$\underbrace{\mathbf{1}}_{\hat{\mathbf{Y}}_i^m} \hat{\mathbf{V}}_i^m + \underbrace{\hat{\mathbf{Z}}_m}_{\hat{\mathbf{Z}}_i^m} \hat{\mathbf{I}}_i^m = \underbrace{\hat{\mathbf{V}}_{Sm}}_{\hat{\mathbf{P}}^m} \quad (13.48)$$

The above representation becomes

$$\hat{\mathbf{S}}_m = -\{ \hat{\mathbf{Z}}_m + \hat{\mathbf{Z}}_{Ci} \}^{-1} \{ \hat{\mathbf{Z}}_m - \hat{\mathbf{Z}}_{Ci} \} \quad (13.49a)$$

$$\hat{\mathbf{I}}_S^m = \{ \hat{\mathbf{Z}}_m + \hat{\mathbf{Z}}_{Ci} \}^{-1} \hat{\mathbf{V}}_{Sm} \quad (13.49b)$$

Thus, the scattering parameter representation in (13.33) has been modified to include lumped sources in the termination/interconnection networks. In the case of an interconnection network containing only short circuits, open circuits, and/or direct connections, this representation becomes

$$[\hat{\mathbf{Y}}_i^m \quad \hat{\mathbf{Y}}_j^m \quad \hat{\mathbf{Y}}_k^m] = \begin{bmatrix} \mathbf{0} \\ \mathbf{C}_V \end{bmatrix} \quad (13.50)$$

and

$$[\hat{\mathbf{Z}}_i^m \quad \hat{\mathbf{Z}}_j^m \quad \hat{\mathbf{Z}}_k^m] = \begin{bmatrix} \mathbf{C}_I \\ \mathbf{0} \end{bmatrix} \quad (13.51)$$

where \mathbf{C}_V and \mathbf{C}_I were originally defined in (13.37). Substituting (13.50) and (13.51) into (13.47a) yields (13.39).

The tube characterizations in (13.27) remain unchanged. Thus, the overall representation of the network is of the form in (13.40):

$$\hat{\mathbf{I}}_T^r = \hat{\mathbf{R}}_T \hat{\mathbf{I}}_T^i + \hat{\mathbf{I}}_{TT} \quad (13.52a)$$

$$\hat{\mathbf{I}}_T^r = \hat{\mathbf{S}}_T \hat{\mathbf{I}}_T^i + \hat{\mathbf{I}}_{ST} \quad (13.52b)$$

where $\hat{\mathbf{S}}_T$ is $2n_T \times 2n_T$ and contains the individual scattering matrices given in (13.47a) on the main diagonal and zeros elsewhere, and $\hat{\mathbf{I}}_{ST}$ is $2n_T \times 1$ and contains the $\hat{\mathbf{I}}_S^m$ in (13.47c). In a fashion similar to the earlier derivation, we obtain the general form of the BLT equations for the total tube currents as

$$\hat{\mathbf{I}}_T = [\mathbf{1} + \hat{\mathbf{S}}_T] [\hat{\mathbf{S}}_T - \hat{\mathbf{R}}_T]^{-1} \hat{\mathbf{I}}_{TT} - [\mathbf{1} + \hat{\mathbf{R}}_T] [\hat{\mathbf{S}}_T - \hat{\mathbf{R}}_T]^{-1} \hat{\mathbf{I}}_{ST} \quad (13.53)$$

For example, consider the two-conductor line shown in Figure 6.1 of Chapter 6 (without incident field illumination). The total tube propagation matrix $\hat{\mathbf{R}}_T$ is simply (13.28) since there is only one tube and becomes

$$\hat{\mathbf{R}}_T = \begin{bmatrix} 0 & -e^{\hat{y} \mathcal{L}} \\ -e^{\hat{y} \mathcal{L}} & 0 \end{bmatrix}$$

Writing (13.44) at the source and at the load gives

$$\underbrace{1}_{\hat{y}_1^S} \hat{V}_1^S + \underbrace{\hat{Z}_S}_{\hat{z}_1^S} \hat{I}_1^S = \underbrace{\hat{V}_S}_{\hat{p}^S}$$

$$\underbrace{1}_{\hat{y}_1^L} \hat{V}_1^L + \underbrace{\hat{Z}_L}_{\hat{z}_1^L} \hat{I}_1^L = \underbrace{0}_{\hat{p}^L}$$

Thus, the scattering matrices at the source and the load in (13.47a) become

$$\hat{S}_S = -[\hat{Z}_S + \hat{Z}_C]^{-1} [\hat{Z}_S - \hat{Z}_C] = -\hat{\Gamma}_S$$

$$\hat{S}_L = -[\hat{Z}_L + \hat{Z}_C]^{-1} [\hat{Z}_L - \hat{Z}_C] = -\hat{\Gamma}_L$$

where $\hat{\Gamma}_S$ and $\hat{\Gamma}_L$ are the *voltage reflection coefficients* at the source and the load, respectively. The *current reflection coefficients* are the negatives of these [A.1]. Thus, the overall scattering matrix is

$$\hat{\mathbf{S}}_T = \begin{bmatrix} -\hat{\Gamma}_S & 0 \\ 0 & -\hat{\Gamma}_L \end{bmatrix}$$

Also, the current source vectors in (13.47c) become

$$\hat{I}_S^S = (\hat{Z}_S + \hat{Z}_C)^{-1} \hat{V}_S$$

$$\hat{I}_S^L = (\hat{Z}_L + \hat{Z}_C)^{-1} 0$$

so that the overall current source vector becomes

$$\hat{\mathbf{I}}_{ST} = \begin{bmatrix} \hat{Z}_S + \hat{Z}_C & 0 \\ 0 & \hat{Z}_L + \hat{Z}_C \end{bmatrix}^{-1} \begin{bmatrix} \hat{p}^S \\ \hat{p}^L \end{bmatrix} = \begin{bmatrix} \frac{\hat{V}_S}{(\hat{Z}_S + \hat{Z}_C)} \\ 0 \end{bmatrix}$$

Forming the BLT equation in (13.53) for the total currents yields

$$\begin{aligned}
 \begin{bmatrix} \hat{\Gamma}_1^S \\ \hat{\Gamma}_1^L \end{bmatrix} &= - [\mathbf{1} + \hat{\mathbf{R}}_T] [\hat{\mathbf{S}}_T - \hat{\mathbf{R}}_T]^{-1} \hat{\mathbf{I}}_{ST} \\
 &= - \begin{bmatrix} 1 & -e^{\hat{\gamma} \mathcal{L}} \\ -e^{\hat{\gamma} \mathcal{L}} & 1 \end{bmatrix} \begin{bmatrix} -\hat{\Gamma}_S & e^{\hat{\gamma} \mathcal{L}} \\ e^{\hat{\gamma} \mathcal{L}} & -\hat{\Gamma}_L \end{bmatrix}^{-1} \begin{bmatrix} 1 \\ 0 \end{bmatrix} \frac{\hat{V}_S}{(\hat{Z}_S + \hat{Z}_C)} \\
 &= \frac{1}{1 - \hat{\Gamma}_S \hat{\Gamma}_L e^{-2\hat{\gamma} \mathcal{L}}} \begin{bmatrix} 1 - \hat{\Gamma}_L e^{-2\hat{\gamma} \mathcal{L}} \\ (\hat{\Gamma}_L - 1) e^{-\hat{\gamma} \mathcal{L}} \end{bmatrix} \frac{\hat{V}_S}{(\hat{Z}_S + \hat{Z}_C)}
 \end{aligned}$$

Recalling that $\hat{\Gamma}_1^S = \hat{\Gamma}(0)$ and $\hat{\Gamma}_1^L = -\hat{\Gamma}(\mathcal{L})$, these results are identical to those derived in Chapter 6 and given in Eqs. (6.40b) and (6.41b).

The time-domain solution can be obtained from this formulation by first using the BLT equations to obtain the frequency-domain transfer function and then using the TDFD transformation method as before. Again, that technique for obtaining the time-domain solution assumes linear loads and tubes since superposition is implicitly used.

13.5 DIRECT TIME-DOMAIN SOLUTIONS IN TERMS OF TRAVELING WAVES

With the exception of the SPICE solution method, the above solution methods concentrated on the frequency-domain solution of transmission-line networks. The time-domain solution can be obtained from this solution via the TDFD technique, which is very straightforward and has been used on numerous occasions. Of course, the TDFD technique requires *linear terminations*. In this final section, we briefly investigate the direct time-domain solution via the traveling waves existing on the various tubes of the network.

To begin the discussion, consider a tandem connection of two-conductor lines having a discontinuity as shown in Figure 13.14(a). Each line is characterized by a characteristic impedance Z_{Ci} and time delay T_{Di} . Lossless lines and resistive terminations are assumed to simplify the discussion. The frequency-domain solutions on each line are of the form

$$\hat{V}_i(z) = \hat{V}_i^+ e^{-j\beta_i z} + \hat{V}_i^- e^{j\beta_i z} \quad (13.54a)$$

$$\hat{I}_i(z) = \frac{1}{Z_{Ci}} \hat{V}_i^+ e^{-j\beta_i z} - \frac{1}{Z_{Ci}} \hat{V}_i^- e^{j\beta_i z} \quad (13.54b)$$

in accordance with the general solution of the transmission-line equations for each tube. The discontinuity may be characterized as before with a form of *voltage scattering* parameter matrix that relates the incident and reflected voltage waves at that point as illustrated in Figure 13.14(b). The incident waves are the portions of (13.45a) that are incoming at the junction, $\hat{V}_1^+ e^{-j\beta_1 \mathcal{L}_1}$ and $\hat{V}_2^- e^{j\beta_2 \mathcal{L}_1}$. The reflected waves are the portions of (13.54a) that are outgoing at the junction, $\hat{V}_1^- e^{j\beta_1 \mathcal{L}_1}$ and $\hat{V}_2^+ e^{-j\beta_2 \mathcal{L}_1}$.

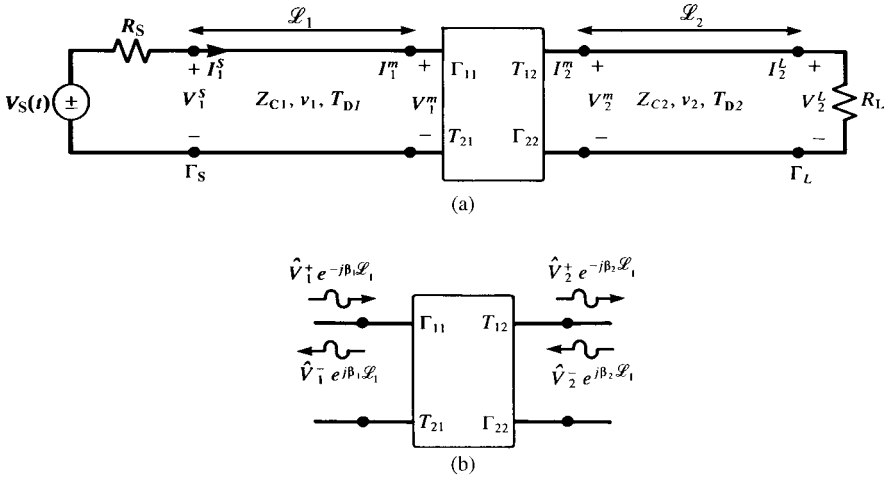


FIGURE 13.14 Determination of the scattering parameters at the junction of two different two-conductor lines: (a) line configuration and (b) definition of incident and reflected voltage waves at the junction.

Hence we may write

$$\underbrace{\begin{bmatrix} \hat{V}_1^- e^{j\beta_1 L_1} \\ \hat{V}_2^+ e^{-j\beta_2 L_1} \end{bmatrix}}_{\hat{V}^{\text{reflected}}} = \begin{bmatrix} \Gamma_{11} & T_{12} \\ T_{21} & \Gamma_{22} \end{bmatrix} \underbrace{\begin{bmatrix} \hat{V}_1^+ e^{-j\beta_1 L_1} \\ \hat{V}_2^- e^{j\beta_2 L_1} \end{bmatrix}}_{\hat{V}^{\text{incident}}} \quad (13.55)$$

The Γ_{ii} elements are the *voltage reflection coefficients* and the T_{ij} elements are the *voltage transmission coefficients*. Figure 13.15 illustrates the determination of these parameters for various discontinuities. Consider the direct connection shown in Figure 13.15(a). The voltages and currents must be continuous. Equating Eqs. (13.54) for the left and right sections and putting them in the form of (13.55) yields

$$\Gamma_{11} = \frac{Z_{C2} - Z_{C1}}{Z_{C2} + Z_{C1}}, \quad T_{12} = \frac{2Z_{C1}}{Z_{C2} + Z_{C1}} \quad (13.56a)$$

$$T_{21} = \frac{2Z_{C2}}{Z_{C1} + Z_{C2}}, \quad \Gamma_{22} = \frac{Z_{C1} - Z_{C2}}{Z_{C1} + Z_{C2}} \quad (13.56b)$$

This result is directly analogous to the case of a uniform plane wave incident at an interface between two media [A.1]. It is a sensible result for the following reason. In the time domain, the wave incident from line # 1 “sees” an impedance at the junction equal to the characteristic impedance of line # 2 since it has not arrived at the termination of line # 2 and therefore line # 2 appears infinite in length. So the reflection coefficient can be calculated as though line # 1 is terminated in the

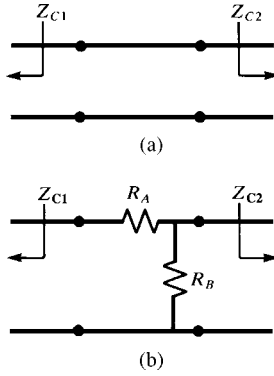


FIGURE 13.15 Illustration of the simplified determination of the scattering parameters for (a) a direct connection and (b) a resistive interconnection network.

characteristic impedance of line # 2. The transmission coefficient is easily calculated from the reflection coefficients since the total voltage incident on the junction from line # 1 is the sum of the incident and reflected waves on that line that, because of the direct connection, must equal the transmitted voltage or $(1 + \Gamma_{11}) = T_{21}$. In a similar fashion, $(1 + \Gamma_{22}) = T_{12}$.

The BLT equations can be easily formed for this network although their solution is best suited to computer implementation. The overall tube propagation matrix is

$$\hat{\mathbf{R}}_T = \begin{bmatrix} 0 & -e^{j\beta_1 \mathcal{L}_1} & 0 & 0 \\ -e^{j\beta_1 \mathcal{L}_1} & 0 & 0 & 0 \\ 0 & 0 & 0 & -e^{j\beta_2 \mathcal{L}_2} \\ 0 & 0 & -e^{j\beta_2 \mathcal{L}_2} & 0 \end{bmatrix}$$

Writing (13.7) at the source, the junction, and the load gives

$$\underbrace{\begin{bmatrix} 1 & -1 \\ 0 & 0 \end{bmatrix}}_{\hat{\mathbf{Y}}^m} \underbrace{\begin{bmatrix} \hat{V}_1^m \\ \hat{V}_2^m \end{bmatrix}}_{\hat{\mathbf{V}}^m} + \underbrace{\begin{bmatrix} 0 & 0 \\ 1 & 1 \end{bmatrix}}_{\hat{\mathbf{Z}}^m} \underbrace{\begin{bmatrix} \hat{I}_1^m \\ \hat{I}_2^m \end{bmatrix}}_{\hat{\mathbf{I}}^m} = \underbrace{\begin{bmatrix} 0 \\ 0 \end{bmatrix}}_{\hat{\mathbf{P}}^m}$$

$$\underbrace{1}_{\hat{Y}_1^S} \hat{V}_1^S + \underbrace{R_S}_{\hat{Z}_1^S} \hat{I}_1^S = \underbrace{\hat{V}_S}_{\hat{P}^S}$$

$$\underbrace{1}_{\hat{Y}_1^L} \hat{V}_1^L + \underbrace{R_L}_{\hat{Z}_1^L} \hat{I}_1^L = \underbrace{0}_{\hat{P}^L}$$

where m designates the “middle node” (the junction). The junction scattering matrices are obtained from (13.47a) as

$$\begin{aligned} \hat{\mathbf{S}}_S &= -(R_S + Z_C)^{-1} (R_S - Z_C) = -\Gamma_S \quad \hat{\mathbf{I}}_S^S = (R_S + Z_C)^{-1} \hat{V}_S \\ \hat{\mathbf{S}}_m &= -\left\{ \begin{bmatrix} 0 & 0 \\ 1 & 1 \end{bmatrix} + \begin{bmatrix} 1 & -1 \\ 0 & 0 \end{bmatrix} \begin{bmatrix} Z_{C1} & 0 \\ 0 & Z_{C2} \end{bmatrix} \right\}^{-1} \left\{ \begin{bmatrix} 0 & 0 \\ 1 & 1 \end{bmatrix} \right. \\ &\quad \left. - \begin{bmatrix} 1 & -1 \\ 0 & 0 \end{bmatrix} \begin{bmatrix} Z_{C1} & 0 \\ 0 & Z_{C2} \end{bmatrix} \right\} \\ &= -\begin{bmatrix} Z_{C1} & -Z_{C2} \\ 1 & 1 \end{bmatrix}^{-1} \begin{bmatrix} -Z_{C1} & Z_{C2} \\ 1 & 1 \end{bmatrix} \\ &= \begin{bmatrix} -\Gamma_{11} & -T_{21} \\ -T_{12} & -\Gamma_{22} \end{bmatrix} \\ \hat{\mathbf{S}}_L &= -(R_L + Z_C)^{-1} (R_L - Z_C) = -\Gamma_L \quad \hat{\mathbf{I}}_S^S = (R_L + Z_C)^{-1} 0 \end{aligned}$$

Thus, the overall scattering matrix becomes

$$\hat{\mathbf{S}}_T = \begin{bmatrix} -\Gamma_S & 0 & 0 & 0 \\ 0 & -\Gamma_{11} & -T_{21} & 0 \\ 0 & -T_{12} & -\Gamma_{22} & 0 \\ 0 & 0 & 0 & -\Gamma_L \end{bmatrix}$$

These reflection and transmission coefficients are the negative of the voltage reflection and transmission coefficients in (13.56) because we are considering currents and because of the current directions at the junctions (into the tubes). Additionally, the current transmission coefficients are $\frac{Z_{C2}}{Z_{C1}} T_{12} = T_{21}$ and $\frac{Z_{C1}}{Z_{C2}} T_{21} = T_{12}$ in the same fashion as uniform plane waves [A.1]. The total current source vector is

$$\hat{\mathbf{I}}_{ST} = \begin{bmatrix} 1 \\ 0 \\ 0 \\ 0 \end{bmatrix} \frac{\hat{V}_S}{(R_S + Z_C)}$$

The BLT equations are then formed from (13.53) with $\hat{\mathbf{I}}_{TT} = \mathbf{0}$ (no incident field illumination).

Figure 13.15(b) shows a connection consisting of a resistive network. For the above reasons, we may similarly determine

$$\Gamma_{11} = \frac{R_2 - Z_{C1}}{R_2 + Z_{C1}}, \quad T_{12} = \frac{2R_1}{Z_{C2} + R_1} \frac{Z_{C1}}{R_A + Z_{C1}} \tag{13.57a}$$

$$T_{21} = \frac{R_B || Z_{C2}}{R_A + R_B || Z_{C2}} \frac{2R_2}{R_2 + Z_{C1}}, \quad \Gamma_{22} = \frac{R_1 - Z_{C2}}{R_1 + Z_{C2}} \tag{13.57b}$$

where

$$R_1 = R_B || (R_A + Z_{C1}), \quad R_2 = R_A + R_B || Z_{C2} \tag{13.57c}$$

Determination of these is very similar to the case of plane waves normally incident on a boundary [A.1]. The notation $A || B$ denotes the parallel combination of two resistances as $A || B = AB/(A + B)$.

In the time domain, the source initially “sees” a termination of Z_{C1} so that the voltage wave sent out is, by voltage division,

$$V(t) = \frac{Z_{C1}}{R_S + Z_{C1}} V_S(t) \tag{13.58}$$

This wave travels down line # 1 reaching the discontinuity at one time delay of T_{D1} , where $\Gamma_{11} V(t - T_{D1})$ is reflected and $T_{21} V(t - T_{D1})$ is transmitted across the junction. The reflected portion arrives at the source at $2T_{D1}$ where a portion of it, $\Gamma_S \Gamma_{11} V(t - 2T_{D1})$, is sent back toward the junction where a portion of it is reflected, $\Gamma_{11} \Gamma_S \Gamma_{11} V(t - 3T_{D1})$, and a portion is transmitted, $T_{21} \Gamma_S \Gamma_{11} V(t - 3T_{D1})$, and so on. Meanwhile, the portion of the original wave that was transmitted across the junction, $T_{21} V(t - T_{D1})$, arrives at the load where it is reflected as $\Gamma_L T_{21} V(t - T_{D1} - T_{D2})$. This is sent back to the junction where a portion of it, $\Gamma_{22} \Gamma_L T_{21} V(t - T_{D1} - 2T_{D2})$, is reflected back toward the load and a portion, $T_{12} \Gamma_L T_{21} V(t - T_{D1} - 2T_{D2})$, is transmitted across the junction onto line # 1. This process of continued reflections and transmissions continues, and the total voltage at any point on either line is the sum of the total waves at that point and time. Clearly, the line voltages will be linear combinations of the initial transmitted wave, $V(t)$, delayed in time by various sums of multiples of the line delays T_{D1} and T_{D2} . A lattice diagram can be constructed as described in Chapter 6 to aid in determining these total voltages but the process is clearly very complicated owing to the multitude of reflections and transmissions. If either line is terminated in its characteristic impedance, the summation is simplified considerably, and a series solution can be developed [A.3]. But for completely mismatched lines, the summation is tedious.

A symbolic solution can be obtained if we use the time-shift or difference operator as before:

$$D_i^{\pm k} f(t) = f(t \pm kT_{Di})$$

in the BLT equations of (13.53). Thus,

$$\mathbf{R}_T(D) = \begin{bmatrix} 0 & -D_1 & 0 & 0 \\ -D_1 & 0 & 0 & 0 \\ 0 & 0 & 0 & -D_2 \\ 0 & 0 & -D_2 & 0 \end{bmatrix}$$

The BLT equations in (13.53) with $\hat{\mathbf{I}}_{TT} = \mathbf{0}$ (no incident field illumination) can be written as

$$[\mathbf{R}_T(D) - \mathbf{S}_T][\mathbf{R}_T(D) + \mathbf{1}]^{-1} \mathbf{I}_T(t) = \mathbf{I}_{ST}(t)$$

and $[\mathbf{R}_T(D) + \mathbf{1}]^{-1}$ is simple to obtain. However, the literal solution of the BLT equations is very tedious even for this simple case. If we substitute a previously described SPICE model for each line, the summation of these waves is taken care of and nonresistive loads can be considered. A direct time-domain summation of the traveling waves was implemented using the scattering parameters of the termination/interconnection networks in [3] but, once again, keeping track of all the incident/reflected waves on the line is a very tedious task because of the multiple reflections/transmissions and the different mode velocities on each tube.

13.6 A SUMMARY OF METHODS FOR ANALYZING MULTICONDUCTOR TRANSMISSION LINES

If one is willing to forego losses, then the simplest and most accurate solution method for transmission-line networks is to use `SPICEMTL.FOR` or `SPICEINC.FOR` to build SPICE subcircuit models for the tubes and then imbed them in an overall SPICE circuit model where the termination networks as well as the interconnection networks are attached. This method is extraordinarily simple to implement and, in addition, it will handle nonlinear terminations such as diodes, transistors, and so on in the termination/interconnection networks. The author strongly recommends this method of analyzing lossless transmission-line networks. Including losses of the tubes is the only challenging problem left. However, the admittance parameter method can be used to incorporate losses and the TDFD method can be used to return to the time domain. The only disadvantage of this method is that the termination/interconnection networks must be linear, since superposition is used to return to the time domain. In addition, the FDTD method using a state-variable characterization of the termination/interconnection networks can handle transmission-line networks that have losses as well as nonlinear terminations [B.27, B.29].

These remarks also apply to single tube networks that we studied for the first 12 chapters of this text. This long journey in the study of methods for analyzing MTLs can therefore be summarized as follows. For lossless lines, the solution process is virtually trivial: generate SPICE/PSPICE subcircuit models with `SPICEMTL.FOR` or `SPICEINC.FOR` and then imbed these into an overall SPICE program where the terminations are attached. If losses of the lines (conductor and/or dielectric) must be included in the analysis, then we have a choice of several methods: (1) The time-domain to frequency-domain (TDFD) method where losses are included in the frequency-domain transfer function at the harmonics of the input source, (2) the finite-difference, time-domain (FDTD) method where losses are included in the numerical evaluation of the convolution integral via the Prony method, for example, or (3) for electrically short lines, modeling the line with a lumped-Pi or lumped-T equivalent circuit but the losses must be frequency-independent. The lumped-Pi and lumped-T approximate circuit models require that the per-unit-length resistances and internal inductances of the conductors be their dc values and the conductance must be frequency independent since frequency-dependent elements

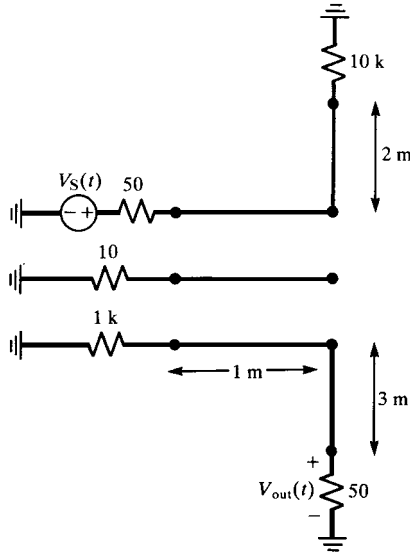


FIGURE P13.11

are not readily modelable directly in the time domain in lumped circuit models. There are, however, some equivalent circuits that tend to mimic frequency-dependent behavior of these elements to some degree. (See Figure 8.50).

PROBLEMS

- 13.1 Derive the admittance parameters given in (13.3).
- 13.2 Derive the admittance parameter relation for a transmission-line network given in (13.15) and for the problem in Figure 13.2.
- 13.3 Derive the impedance parameters given in (13.17).
- 13.4 Derive the relations given in (13.26) and (13.27).
- 13.5 Derive the scattering parameter relation for a termination network given in (13.36).
- 13.6 Derive the scattering parameter relation for an interconnection network given in (13.39).
- 13.7 Derive the BLT equations given in (13.41) and in (13.43).
- 13.8 Derive the scattering parameter matrix and current source vector given for the general case in (13.47).
- 13.9 Derive the BLT equations for the general case given in (13.53).
- 13.10 For the tandem connection of two-conductor lines shown in Figure 13.14, derive series expressions for the time-domain source and load voltages in

terms of delayed source voltage waveforms for a matched load on line # 2, that is, $R_L = Z_{C2}$.

- 13.11** Consider the transmission-line network shown in Figure P13.11. All conductors are # 20 gauge wires ($r_w = 16$ mils) at a height of 1 cm above a ground plane. Solve for the voltage $V_{out}(t)$ where $V_S(t)$ is a 10-MHz trapezoidal pulse train with rise/fall times of 1 ns and 50% duty cycle. Compute this using (a) the SPICE model, (b) the lumped-Pi model, (c) the admittance parameter model, (d) the impedance parameter model, and (e) the BLT equations.

REFERENCES

- [1] C. E. Baum, T. K. Liu, F. M. Tesche, and S. K. Chang, *Numerical results for multiconductor transmission-line networks*, *Interaction Note 322*, Air Force Weapons Laboratory, Albuquerque, NM, September 1977.
- [2] C. E. Baum, T. K. Liu, and F. M. Tesche, *On the analysis of general multiconductor transmission-line networks*, *Interaction Note 350*, Air Force Weapons Laboratory, Albuquerque, NM, November 1978.
- [3] A. K. Agrawal, H. K. Fowles, L. D. Scott, and S. H. Gurbaxani, Application of modal analysis to the transient response of multiconductor transmission lines with branches, *IEEE Transactions on Electromagnetic Compatibility*, **21**(3), 256–262, 1979.
- [4] C. R. Paul, Analysis of electromagnetic coupling in branched cables, *Proceedings of the 1979 IEEE International Symposium on Electromagnetic Compatibility*, San Diego, CA, August 1979.
- [5] J. L. Allen, Time-domain analysis of lumped-distributed networks, *IEEE Transactions on Microwave Theory and Techniques*, **27**(11), 890–896, 1979.
- [6] F. M. Tesche and T. K. Liu, *User manual and code description for QV7TA: a general multiconductor transmission-line analysis code*, *Interaction Application Memos*, Memo 26, LuTech, Inc., August 1978.
- [7] A. R. Djordjevic and T. K. Sarkar, Analysis of time response of lossy multiconductor transmission line networks, *IEEE Transactions on Microwave Theory and Techniques*, **35**(10), 898–907, 1987.

PUBLICATIONS BY THE AUTHOR CONCERNING TRANSMISSION LINES

A. BOOKS

- [A.1] *Introduction to Electromagnetic Fields, 2nd edition*, McGraw-Hill, New York, 1987 (with S.A. Nasar).
- [A.2] *Analysis of Linear Circuits*, McGraw-Hill, New York, 1989.
- [A.3] *Introduction to Electromagnetic Compatibility, 2nd edition*, John Wiley Interscience, New York, 2006.
- [A.4] *Essential Engineering Equations*, CRC Press, Boston, MA, 1991 (with S.A. Nasar).
- [A.5] *Fundamentals of Electric Circuit Analysis*, John Wiley & Sons, Inc., New York, 2001.
- [A.6] *Electromagnetics for Engineers: with Applications to Digital Systems and Electromagnetic Interference*, John Wiley & Sons, Inc., New York, 2004.
- [A.7] *Handbook of Electromagnetic Compatibility*, Chapter 2, Part II, “Crosstalk”, Chapter 3, Part II, “Radiated and conducted emissions”, Appendix, “Effect of interspersed grounds”, Academic Press, 1995.
- [A.8] *Encyclopedia of RF and Microwave Engineering*, John Wiley Interscience, Hoboken, NY, 2005, “Electromagnetic compatibility”, pp.1137–1151, “Coupled transmission lines”, pp. 863–882.
- [A.9] *Analysis of Multiconductor Transmission Lines*, 1st edition, John Wiley Interscience, Hoboken, NY, 1994.

B. GENERAL

- [B.1] On uniform multimode transmission lines, *IEEE Transactions on Microwave Theory and Techniques*, **21**(8), 556–558, 1973.

- [B.2] Useful matrix chain parameter identities for the analysis of multiconductor transmission lines, *IEEE Transactions on Microwave Theory and Techniques*, **23**(9), 756–760, 1975.
- [B.3] Comments on ‘On the properties of the product of the impedance and admittance matrices of three-conductor transmission lines’, *Proceedings of IEEE*, **63**(12), 1720, 1975.
- [B.4] Application of multiconductor transmission line theory to the prediction of cable coupling — vol. I — multiconductor transmission line theory, Technical Report, Rome Air Development Center, Griffiss AFB, New York, RADC-TR-76-101, April 1976 (A025028).
- [B.5] Applications of multiconductor transmission line theory to the prediction of cable coupling — Vol. VII — Digital computer programs for the analysis of multiconductor transmission lines, Technical Report, Rome Air Development Center, Griffiss AFB, New York, RADC-TR-76-101, July 1977 (A046662).
- [B.6] Solution of the transmission line equations for three-conductor lines in homogeneous media, *IEEE Transactions on Electromagnetic Compatibility*, **20**(1), 216–222, 1978.
- [B.7] Analysis of electromagnetic coupling in branched cables, *IEEE International Symposium on Electromagnetic Compatibility*, San Diego, CA, October 1979.
- [B.8] Design of wire routing for EMC, *1979 IEEE International Symposium on Electromagnetic Compatibility*, San Diego, CA, October 1979.
- [B.9] A probabilistic approach to wire coupling interference prediction, *4th Symposium and Technical Exhibition on Electromagnetic Compatibility*, Zurich, Switzerland, March 1981.
- [B.10] Adequacy of low-frequency, crosstalk prediction models, *4th Symposium and Technical Exhibition on Electromagnetic Compatibility*, Zurich, Switzerland, March 1981.
- [B.11] Computation of crosstalk in a multiconductor transmission line, *IEEE Transactions on Electromagnetic Compatibility*, **23**(4), 352–358, 1981.
- [B.12] On the superposition of inductive and capacitive coupling in crosstalk prediction models, *IEEE Transactions on Electromagnetic Compatibility*, **24**(3), 335–343, 1982.
- [B.13] Coupling to transmission lines: an overview, *1983 International Symposium and Technical Exhibition on Electromagnetic Compatibility*, Zurich, Switzerland, March 1983.
- [B.14] A simple technique for estimating crosstalk, *1983 IEEE International Symposium on Electromagnetic Compatibility*, Washington, DC, August 1983.
- [B.15] Lumped model approximations of transmission lines: effect of load impedances on accuracy, Technical Report, Rome Air Development Center, Griffiss AFB, New York, RADC-TR-82-286, vol. IV E, August 1984 (with W.W. Everett III).
- [B.16] Estimation of crosstalk in three-conductor transmission lines, *IEEE Transactions on Electromagnetic Compatibility*, **26**(4), 182–192, 1984.
- [B.17] Lumped circuit modeling of transmission lines, *1985 IEEE International Symposium on Electromagnetic Compatibility*, Wakefield, MA, August, 1985 (with L. Monroe).
- [B.18] Sensitivity of crosstalk to variations in wire position in cable bundles, *1987 International Symposium and Technical Exhibition on Electromagnetic Compatibility*, Zurich, Switzerland, 1987.
- [B.19] A Simple SPICE model for coupled transmission lines, *1988 IEEE International Symposium on Electromagnetic Compatibility*, Seattle, WA, September 1988.
- [B.20] Derivation of common impedance coupling from the transmission-line equations, *IEEE Transactions on Electromagnetic Compatibility*, **34**(3), 315–319, 1992.

- [B.21] Literal solutions for time-domain crosstalk on lossless transmission lines, *IEEE Transactions on Electromagnetic Compatibility*, **34**(4), 433–444, 1992.
- [B.22] Incorporation of terminal constraints in the FDTD analysis of transmission lines, *IEEE Transactions on Electromagnetic Compatibility*, **36**(2), 85–91, 1994.
- [B.23] Finite-difference, time-domain analysis of lossy transmission lines, *IEEE Transactions on Electromagnetic Compatibility*, **38**(1), 15–24, 1996 (with J.A. Roden, W.T. Smith and S.D. Gedney).
- [B.24] FDTD analysis of lossy, multiconductor transmission lines terminated in arbitrary loads, *IEEE Transactions on Electromagnetic Compatibility*, **38**(3), 1–12, 1996 (with A. Orlandi).
- [B.25] Decoupling the multiconductor transmission line equations, *IEEE Transactions on Microwave Theory and Techniques*, **44**(8), 1429–1440, 1996.
- [B.26] State-variable characterization of transmission Line terminations for FDTD analysis, *1996 International Symposium on Electromagnetic Compatibility*, Santa Clara, CA, August 1996 (with A. Orlandi).
- [B.27] Analysis of multiconductor transmission lines networks: state-variable characterization of junctions and terminations, *1998 International Symposium on Electromagnetic Compatibility*, Rome, Italy, September 1998 (with M. Baccala and A. Orlandi).
- [B.28] An improved method of modeling lossy transmission lines in finite-difference, time-domain analysis, *1999 IEEE International Symposium on Electromagnetic Compatibility*, Seattle, WA, August 1999, (with G. Antonini and A. Orlandi).
- [B.29] An efficient characterization of interconnected multiconductor transmission line networks, *IEEE Transactions on Microwave Theory and Techniques*, **48**(3), 466–470, 2000 (with A. Orlandi).
- [B.30] Solution of the transmission-line equations under the weak-coupling assumption, *IEEE Transactions on Electromagnetic Compatibility*, **44**(3), 413–423, 2002.

C. PER-UNIT-LENGTH PARAMETERS

- [C.1] *Computation of the capacitance matrix for dielectric-coated wires*, Technical Report, Rome Air Development Center, Griffiss AFB, New York, RADC-TR-74-59, March 1974 (with J.C. Clements).
- [C.2] Two-dimensional systems of dielectric-coated, cylindrical conductors, *IEEE Transactions on Electromagnetic Compatibility*, **17**(4), 238–248, 1975 (with J.C. Clements and A.T. Adams).
- [C.3] Applications of multiconductor transmission line theory to the prediction of cable coupling — Vol. II — Computation of the capacitance matrices for ribbon cables, Technical Report, Rome Air Development Center, Griffiss AFB, New York, RADC-TR-76-101, April 1976 (with A.E. Feather) (A025029).
- [C.4] Computation of the transmission line inductance and capacitance matrices from the generalized capacitance matrix, *IEEE Transactions on Electromagnetic Compatibility*, **18**(4), 175–183, 1976 (with A.E. Feather).
- [C.5] Application of moment methods to the characterization of ribbon cables, *Computers and Electrical Engineering*, **4**, 173–184, 1977 (with A.E. Feather).

- [C.6] Application of moment methods to the characterization of ribbon cables, *International Symposium on Innovative Numerical Analysis in Applied Engineering Science*, Paris, France, May 1977 (with A.E. Feather).
- [C.7] Reference potential terms in static capacitance calculations via the method of moments, *IEEE Transactions on Electromagnetic Compatibility*, **20**(1), 267–269, 1978.
- [C.8] Moment method calculation of the per-unit-length parameters of cable bundles, *1994 IEEE International Symposium on Electromagnetic Compatibility*, Chicago, IL, August 1994 (with J.S. Savage and W.T. Smith).
- [C.9] Internal impedance of conductors of rectangular cross section, *1998 International Symposium on Electromagnetic Compatibility*, Denver, CO, August 1998 (with A. Orlandi and G. Antonini).
- [C.10] Internal impedance of conductors of rectangular cross section, *IEEE Transactions on Microwave Theory and Techniques*, **47**(7), 979–985, 1999 (with G. Antonini and A. Orlandi).
- [C.11] Comments on ‘Internal Impedance of Conductors of Rectangular Cross Section’, Reply, *IEEE Transactions on Microwave Theory and Techniques*, **49**(8), 1512–1513, 2001 (with G. Antonini and A. Orlandi).

D. CABLE HARNESSSES

- [D.1] Sensitivity of multiconductor cable coupling to parameter variations, *1974 IEEE International Symposium on Electromagnetic Compatibility*, San Francisco, California, July 16–18, 1974.
- [D.2] Applications of multiconductor transmission line theory to the prediction of cable coupling — Vol. III — Prediction of crosstalk in random cable bundles, Technical Report, Rome Air Development Center, Griffiss AFB, New York, RADC-TR-76-101, February 1977 (A038316).
- [D.3] Sensitivity of crosstalk to variations in wire position in cable bundles, *1987 International Symposium and Technical Exhibition on Electromagnetic Compatibility*, Zurich, Switzerland, 1987.
- [D.4] Sensitivity of crosstalk to variations in wire position in cable bundles, *1987 IEEE International Symposium on Electromagnetic Compatibility*, Atlanta, GA, September 1987.

E. RIBBON CABLES

- [E.1] Applications of multiconductor transmission line theory to the prediction of cable coupling — Vol. IV — Prediction of crosstalk in ribbon cables, Technical Report, Rome Air Development Center, Griffiss AFB, New York, RADC-TR-76-101, February 1978 (A053548).
- [E.2] Prediction of crosstalk in ribbon cables: comparison of model predictions and experiment results, *IEEE Transactions on Electromagnetic Compatibility*, **20**(3), 394–406, 1978.
- [E.3] Prediction of crosstalk in ribbon cables, *IEEE International Symposium on Electromagnetic Compatibility*, Atlanta, GA, June 1978.

F. SHIELDED WIRES

- [F.1] Effect of pigtailed on coupling to shielded wires, *IEEE International Symposium on Electromagnetic Compatibility*, San Diego, CA, October 1979.
- [F.2] Applications of multiconductor transmission line theory to the prediction of cable coupling — Vol. VIII — Prediction of crosstalk involving braided-shield cables, Technical Report, Rome Air Development Center, Griffiss AFB, New York, RADC-TR-76-101, August 1980.
- [F.3] Effect of pigtailed on crosstalk to braided-shield cables, *IEEE Transactions on Electromagnetic Compatibility*, **22**(3), 161–172, 1980.
- [F.4] Transmission-line modeling of shielded wires for crosstalk prediction, *IEEE Transactions on Electromagnetic Compatibility*, **23**(4) 345–351, 1981.
- [F.5] SHIELD — A digital computer program for computing crosstalk between shielded cables, Technical Report, Rome Air Development Center, Griffiss AFB, New York, RADC-TR-82-286, vol. IV B, November 1982.
- [F.6] SHIELD — A digital computer program for the prediction of crosstalk to shielded cables, *1983 International Symposium and Technical Exhibition on Electromagnetic Compatibility*, Zurich, Switzerland, March 1983.
- [F.7] Prediction of crosstalk in flatpack, coaxial cables, Technical Report, Rome Air Development Center, Griffiss AFB, New York, RADC-TR- 82-286, vol. IV F, December, 1984 (with W.E. Beech).
- [F.8] Prediction of crosstalk in flatpack, coaxial cables, (with W.E. Beech), *1984 IEEE International Symposium on Electromagnetic Compatibility*, San Antonio, Texas, April 1984.
- [F.9] Literal solution of the transmission-line equations for shielded wires, *1990 IEEE International Symposium on Electromagnetic Compatibility*, Washington, DC, August 1990 (with B.A. Bowles).
- [F.10] Symbolic solution of the multiconductor transmission-line equations for lines containing shielded wires, *IEEE Transactions on Electromagnetic Compatibility*, **33**(3), 149–162, 1991 (with B.A. Bowles).

G. TWISTED PAIRS OF WIRES

- [G.1] Applications of multiconductor transmission line theory to the prediction of cable coupling — Vol. V — Prediction of crosstalk involving twisted wire pairs, Technical Report, Rome Air Development Center, Griffiss AFB, New York, RADC-TR-76-101, February 1978 (A053559).
- [G.2] Prediction of crosstalk in twisted pairs of wires: A simplified, low-frequency model, *IEEE International Symposium on Electromagnetic Compatibility*, Atlanta, GA, June 1978.
- [G.3] Prediction of crosstalk involving twisted pairs of wires, Part I, A transmission line model for twisted wire pairs, *IEEE Transactions on Electromagnetic Compatibility*, **21**(2), 92–105, 1979 (with J.A. McKnight).

- [G.4] Prediction of crosstalk involving twisted pairs of wires, Part II, A simplified, low-frequency prediction model, *IEEE Transactions on Electromagnetic Compatibility*, **21**(2), 105–114, 1979 (with J.A. McKnight).
- [G.5] Coupling to twisted-pair transmission lines, *4th Symposium and Technical Exhibition on Electromagnetic Compatibility*, Zurich, Switzerland, March 1981.
- [G.6] Crosstalk in balanced, twisted-pair circuits, *1981 IEEE International Symposium on Electromagnetic Compatibility*, Boulder, CO, August 1981 (with M.B. Jolly).
- [G.7] Crosstalk in twisted-wire circuits, Technical Report, Rome Air Development Center, Griffiss AFB, New York, RADC-TR-82-286, vol. IV C, November 1982 (with M.B. Jolly).
- [G.8] Sensitivity of crosstalk in twisted-pair circuits to line twist, *IEEE Transactions on Electromagnetic Compatibility*, **24**(3), 359–364, 1982 (with M. Jolly).
- [G.9] Sensitivity of coupling to balanced, twisted pair lines to line twist, *1983 International Symposium and Technical Exhibition on Electromagnetic Compatibility*, Zurich, Switzerland, March 1983 (with D. Koopman).
- [G.10] Prediction of crosstalk in balanced, twisted pair circuits, Technical Report, Rome Air Development Center, Griffiss AFB, New York, RADC-TR-82-286, vol. IV D, August 1984 (with D. Koopman).

H. EFFECTS OF INCIDENT FIELDS

- [H.1] Efficient numerical computation of the frequency response of cables illuminated by an electromagnetic field, *IEEE Transactions on Microwave Theory and Techniques*, **22**(4), 454–457, 1974.
- [H.2] Frequency response of multiconductor transmission lines illuminated by an incident electromagnetic field, *1975 IEEE International Symposium on Electromagnetic Compatibility*, San Antonio, TX, October 1975.
- [H.3] Frequency response of multiconductor transmission lines illuminated by an incident electromagnetic field, *IEEE Transactions on Electromagnetic Compatibility*, **18**(4), 183–190, 1976.
- [H.4] Applications of multiconductor transmission line theory to the prediction of cable coupling — vol. VI — A digital computer program for determining terminal currents induced in a multiconductor transmission line by an incident electromagnetic field, Technical Report, Rome Air Development Center, Griffiss AFB, New York, RADC-TR-76-101, February 1978 (A053560).
- [H.5] WIRE: a digital computer program for determining terminal currents induced on a multiconductor transmission line by an incident electromagnetic field, *1978 National Aerospace and Electronics Convention*, Dayton, OH, May 1978.
- [H.6] Coupling of electromagnetic fields to transmission lines, *1981 IEEE International Symposium on Electromagnetic Compatibility*, Boulder, CO, August 1981 (with R.T. Abraham).
- [H.7] Coupling of electromagnetic fields onto transmission lines: a comparison of the transmission line model and the method of moments, Technical Report, Rome Air Development, Griffiss AFB, New York, RADC-TR-82-286, vol. IV A, November 1982 (with R.T. Abraham).

- [H.8] Coupling of electromagnetic fields to transmission lines, *1982 IEEE International Symposium on Electromagnetic Compatibility*, Santa Clara, CA, September 1982 (with D.F. Herrick).
- [H.9] Bounds on currents induced in transmission lines by incident fields, *1984 IEEE SOUTH-EASCON*, Louisville, KY, April 1984 (with D.R. Bush).
- [H.10] A SPICE model for multiconductor transmission lines excited by an incident electromagnetic field, *IEEE Transactions on Electromagnetic Compatibility*, **36**(4), 342–354, 1994.
- [H.11] Literal solutions for the time-domain response of a two-conductor transmission line excited by an incident electromagnetic field, *IEEE Transactions on Electromagnetic Compatibility*, **37**(2), 241–251, 1995.

I. PRINTED CIRCUIT BOARDS

- [I.1] Modeling crosstalk on printed circuit boards, Technical Report, Rome Air Development Center, Griffiss AFB, New York, RADC-TR-85-107, July 1985 (with W.W. Everett, III).
- [I.2] Printed circuit board EMC, *1985 International Symposium and Technical Exhibition on Electromagnetic Compatibility*, Zurich, Switzerland, March 1985.
- [I.3] Printed circuit board crosstalk, *1985 IEEE International Symposium on Electromagnetic Compatibility*, Wakefield, MA, August 1985 (with W.W. Everett, III).
- [I.4] Modeling and prediction of ground shift on printed circuit boards, *1986 IERE Symposium on Electromagnetic Compatibility*, University of York, England, September 1986.
- [I.5] Modeling of printed circuit boards for the prediction of crosstalk and ground drop, *IBM Journal of Research and Development*, **33**(1), 1989.

J. POWER TRANSMISSION LINES

- [J.1] Solutions of the transmission line equations for lossy conductors and imperfect earth, *Proceedings of IEE (London)*, **122**(2), 177–182, 1975.
- [J.2] A modal decomposition for power transmission lines with imperfect earth return, *Proceedings of IEE (London)*, **124**(7), 647–648, 1977.

APPENDIX A

DESCRIPTION OF COMPUTER SOFTWARE

Several FORTRAN computer programs that implement the methods described in this text have been developed. The codes can be downloaded from the Wiley FTP site at ftp://ftp.wiley.com/public/sci_tech_med/multiconductor_transmission/

This appendix gives a description of those codes. The programs are written in standard FORTRAN 77 language. A conscious attempt was made to use rudimentary FORTRAN programming commands so that the codes would be compilable with a wide variety of FORTRAN compilers on a large number of platforms. The codes use certain arrays to store information. These array dimensions are determined by the total number of conductors of the transmission line and other solution properties and are stored in parameters at the beginning of the code. An example is the parameter MSIZE:

```
PARAMETER(MSIZE = 99)
```

The user needs only to change these parameters for the program to handle larger numbers of conductors in the line and can recompile the source code (XXXXXX . FOR) to obtain an executable code (XXXXXX . EXE). Each uncompiled source code (XXXXXX . FOR) contains at the beginning a brief description of the code, the array dimensions, and the names and contents of the required input files and the name of the resulting output file.

The codes fall into two distinct categories: those that compute the per-unit-length parameters of inductance and capacitance and those that solve the MTL equations and incorporate the terminal conditions. The codes that determine the per-unit-length

parameters are WIDSESEP.FOR, which implements the wide-separation approximations for wires, RIBBON.FOR for considering ribbon cables, PCB.FOR for considering lands on printed circuit boards, MSTRP.FOR for considering coupled microstrip structures, and STRPLINE.FOR for considering coupled stripline structures. All of these codes require an input file (XXXXX.IN) that contains the two-dimensional, cross-sectional dimensions and material characteristics of the line. These files are called WIDSESEP.IN, RIBBON.IN, PCB.IN, MSTRP.IN, and STRPLINE.IN, respectively. The output of all these programs is the file PUL.DAT. The upper triangle of the per-unit-length parameter inductance, L , and capacitance, C , matrices are stored by rows in this file with the inductance matrix given first followed by the capacitance matrix. The input data are printed at the end of these files but are not read by the programs that subsequently use these per-unit-length data. When one of these per-unit-length parameter codes is run, its output overwrites the present contents of PUL.DAT. The sample outputs of each of these codes are included at the above FTP site and are named XXXXX.OUT. There is no such output for these per-unit-length parameter programs: the output file PUL.DAT is simply renamed XXXXX.OUT and as stored as a sample of that program's PUL.DAT output.

The remaining codes solve the MTL equations and incorporate the terminal conditions to give the solutions for the line voltages and/or currents. These codes are further subdivided into those for the frequency-domain solution and those for the time-domain solution. Each of these codes requires one or more input files that are described at the beginning of the code listings. For example, the code SPICEMTL.FOR requires the input files SPICEMTL.IN and PUL.DAT. The file PUL.DAT is the output of the codes WIDSESEP.FOR, RIBBON.FOR, PCB.FOR, MSTRP.FOR, or STRPLINE.FOR. The user may alternatively provide his/her per-unit-length data from other sources. The output file of SPICEMTL.FOR is simply SPICEMTL.OUT. The output files generally contain either the magnitude and phase of the line voltages and/or currents at each frequency or the line voltages and/or currents at each time step. There is one exception to this: The programs SPICEMTL.FOR, SPICELPI.FOR, SPICELC.FOR, and SPICEINC.FOR provide as output a SPICE subcircuit that models the MTL on a port basis.

The input data for each code appear as one item per line in the appropriate file. These data are in a free field format. The READ statements in the calling program are in an unformatted type:

```
READ(5,*)
```

Each data item appears in a separate line of the input file followed in that line with several blank spaces and an = sign followed by descriptive remarks. The annotation (in the input and output files) of = ***** simply describes the data entry preceding the = sign to the user and is not read by the calling program. In order for this to function properly, *at least one blank space must appear between the data item and the = sign*. This is in the same format in both the input and output files and anticipates that the subsequent program that may use this output file has unformatted reads such as READ (5,*).

A.1 PROGRAMS FOR THE CALCULATION OF THE PER-UNIT-LENGTH PARAMETERS

In this section, we describe three codes for the calculation of the entries in the per-unit-length inductance matrix, \mathbf{L} , and capacitance matrix, \mathbf{C} : `WIDSESEP.FOR`, which implements the wide-separation approximations for wires, `RIBBON.FOR` for ribbon cables, `PCB.FOR` for printed circuit boards, `MSTRP.FOR` for coupled microstrip structures, and `STRPLINE.FOR` for coupled striplines. The output of these codes is the file `PUL.DAT` that contains the upper triangles of these matrices with the inductance matrix given first followed by the capacitance matrix.

A.1.1 Wide-Separation Approximations for Wires: `WIDSESEP.FOR`

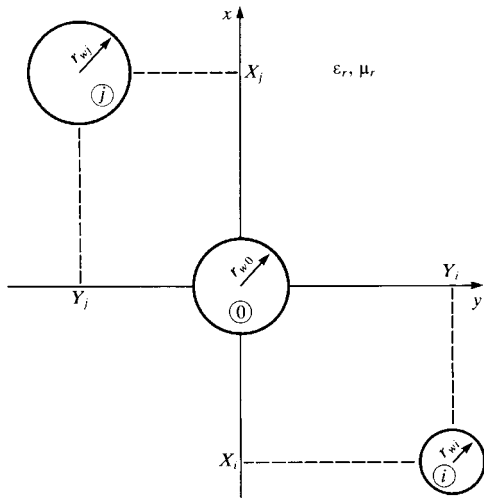
Required input files: `WIDSESEP.IN`

Output file: `PUL.DAT`

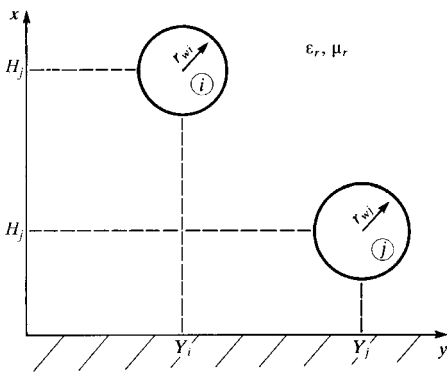
The code computes the entries in the per-unit-length inductance matrix, \mathbf{L} , for three configurations of widely spaced wires in a homogeneous medium described in Section 5.2.1: (a) $(n + 1)$ wires (5.23), (b) n wires above an infinite, perfectly conducting ground plane (5.25), and (c) n wires within an overall circular, cylindrical shield (5.26). The per-unit-length capacitance matrix is obtained from $\mathbf{C} = \mu_0 \mu_r \varepsilon_0 \varepsilon_r \mathbf{L}^{-1}$ where μ_r and ε_r are the relative permeability and permittivity, respectively, of the homogeneous medium surrounding the wires. These structures are depicted in Figure A.1. The first data parameter in `WIDSESEP.IN` is the number of wires, n (exclusive of the reference conductor). The relative permittivity and relative permeability of the surrounding homogeneous medium are the next input parameters. The type of structure is input to `WIDSESEP.IN` by the reference conductor parameter: 1 = wire, 2 = ground plane, and 3 = overall shield. The remaining parameters describe the wire radii and their cross-sectional positions.

The first case, n wires with another wire as the reference wire, is depicted in Figure A.1(a). The reference wire is located at the origin of a rectangular coordinate system. The input data in `WIDSESEP.IN` are (1) the number of wires, n (exclusive of the reference wire), (2) the reference conductor type (type = 1), (3) the relative permittivity and permeability of the surrounding homogeneous medium, (4) the radius of the reference wire (in mils), and (5) the radii of the other wires (in mils) along with their x coordinates (in meters) and y coordinates (in meters). The last group is input sequentially for each wire: $r_{w1}, x_1, y_1, r_{w2}, x_2, y_2, \dots, r_{wn}, x_n, y_n$.

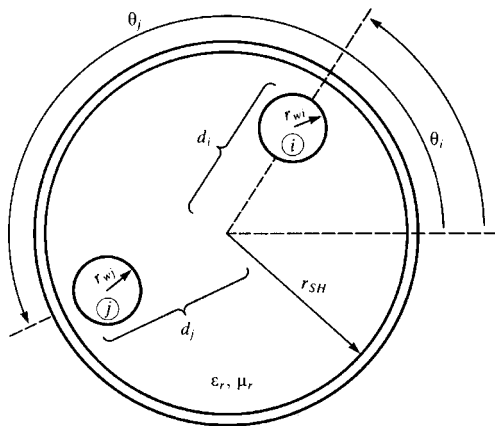
The second case, n wires above an infinite ground plane as the reference conductor, is depicted in Figure A.1(b). The ground plane forms the y coordinate axis ($x = 0$) of a rectangular coordinate system. The input data in `WIDSESEP.IN` are (1) the number of wires, n , (2) the reference conductor type (type = 2), (3) the relative permittivity and permeability of the surrounding homogeneous medium, and (4) the radii of the other wires (in mils) along with their x coordinates (height above ground) (in meters) and y coordinates (in meters). The last group is again input sequentially for each wire: $r_{w1}, h_1, y_1, r_{w2}, h_2, y_2, \dots, r_{wn}, h_n, y_n$.



(a)



(b)



(c)

FIGURE A.1 Cross-sectional configurations of wire lines for the WIDSEEP.FOR FORTRAN program input data: (a) $n + 1$ wires, (b) n wires above a ground plane, and (c) n wires within a cylindrical shield.

The last case, n wires within an overall shield of radius r_{SH} as the reference conductor, is depicted in Figure A.1(c). The input data in `WIDSESEP.IN` are (1) the number of wires, n , (2) the reference conductor type (type = 3), (3) the relative permittivity and permeability of the surrounding homogeneous medium, (4) the (interior) radius of the shield (in mils), and (5) the radii of the other wires (in mils) along with their distances from the shield center, d_i , (in mils) and their angular locations, θ_i , (in degrees). The last group is again input sequentially for each wire: $r_{w1}, d_1, \theta_1, r_{w2}, d_2, \theta_2, \dots, r_{wn}, d_n, \theta_n$.

The entries in the upper triangle of the per-unit-length inductance and capacitance matrices are output to `PUL.DAT`. The last items in `PUL.DAT` simply restate the input parameters to insure that the correct problem was solved. These are not read by the subsequent application program.

A.1.2 Ribbon Cables: `RIBBON.FOR`

Required input files: `RIBBON.IN`

Output file: `PUL.DAT`

Consider the general N -wire ribbon cable shown in Figure A.2. The line consists of N identical, dielectric-insulated wires. The wire radii are denoted in the code as `RW`, the insulation thicknesses are denoted by `TD`, and the identical adjacent wire spacings are denoted as `S`. The relative permittivity of the insulation is denoted by `ER` in the code. These input data are contained in `RIBBON.IN`. The results of the computation are contained in the output file `PUL.DAT`. The last items in `PUL.DAT` simply restate the input parameters to insure that the correct problem was solved. These are not read by the subsequent application program.

The structure of the main program `RIBBON.FOR` is as follows. Utilizing Tables 5.2 and 5.3, we can write the matrix that satisfies the boundary conditions: (1) the potentials of a conductor at points on that conductor due to all charge distributions in the system are set equal to the potential of that conductor, and (2)

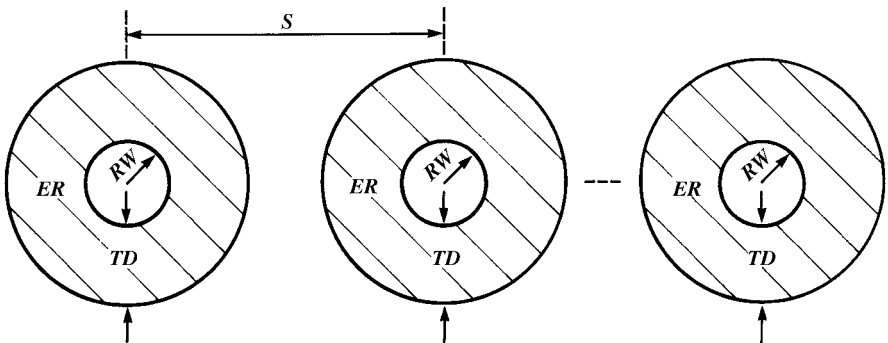


FIGURE A.2 Cross-sectional definition of the ribbon cable parameters for the `RIBBON.FOR` FORTRAN program input data.

the components of the electric flux density vector $\mathbf{D} = \epsilon \mathbf{E}$ that are normal to the dielectric–free-space boundary at points on that boundary are continuous across the boundary. This corresponds to the matrix equation (5.44) of Chapter 5 that becomes of the form

$$\begin{bmatrix} \mathbf{D}_{11} & \mathbf{D}_{12} \\ \mathbf{D}_{21} & \mathbf{D}_{22} \end{bmatrix} \begin{bmatrix} \mathbf{A} \\ \mathbf{A}' \end{bmatrix} = \begin{bmatrix} \Phi \\ \mathbf{0} \end{bmatrix} \tag{A.1}$$

Expanding these gives

$$\mathbf{D}_{11}\mathbf{A} + \mathbf{D}_{12}\mathbf{A}' = \Phi \tag{A.2a}$$

$$\mathbf{D}_{21}\mathbf{A} + \mathbf{D}_{22}\mathbf{A}' = \mathbf{0} \tag{A.2b}$$

The first set in (A.2a) enforces the potentials on the conductors, and the second set in (A.2b) enforces the continuity of the normal components of the electric flux density vector across the dielectric–free-space boundary. We will assume that *the number of Fourier expansion functions around the conductor–dielectric boundary and around the dielectric–free-space boundary is equal*. The number of expansion coefficients around each of these two boundaries is denoted as NF. The $(N \cdot \text{NF}) \times 1$ vector \mathbf{A} contains the Fourier expansion coefficients for the free and bound charge around the conductor–dielectric boundary. Similarly, the $(N \cdot \text{NF}) \times 1$ vector \mathbf{A}' contains the Fourier expansion coefficients for the bound charge around the dielectric–free-space boundary. The $(N \cdot \text{NF}) \times 1$ vector Φ contains the potentials of the conductors at the matchpoints on those conductors. The $(N \cdot \text{NF}) \times 1$ zero vector $\mathbf{0}$ results from the satisfaction of the continuity of the normal components of the electric flux density vector across the dielectric–free-space boundary. The submatrices \mathbf{D}_{11} , \mathbf{D}_{12} , \mathbf{D}_{21} , and \mathbf{D}_{22} are $(N \cdot \text{NF}) \times (N \cdot \text{NF})$. Because of the repetitive nature of the ribbon cable structure, these submatrices have a special form:

$$\mathbf{D}_{11} = \begin{bmatrix} \mathbf{A}_1 & \mathbf{A}_2 & \cdots & \mathbf{A}_N \\ \mathbf{A}_{-2} & \mathbf{A}_1 & \ddots & \vdots \\ \vdots & \ddots & \ddots & \mathbf{A}_2 \\ \mathbf{A}_{-N} & \cdots & \mathbf{A}_{-2} & \mathbf{A}_1 \end{bmatrix} \tag{A.3}$$

and \mathbf{D}_{12} , \mathbf{D}_{21} , and \mathbf{D}_{22} have a similar structure. This simplifies the fill time for (A.1). In order to avoid a singular solution matrix in (A.1), the matchpoints are chosen from the following scheme [C.3,C.4]. On each conductor–dielectric interface and each dielectric–free-space interface, the NF matchpoints are separated by the angle

$$\theta = \frac{2\pi}{\text{NF}} \tag{A.4a}$$

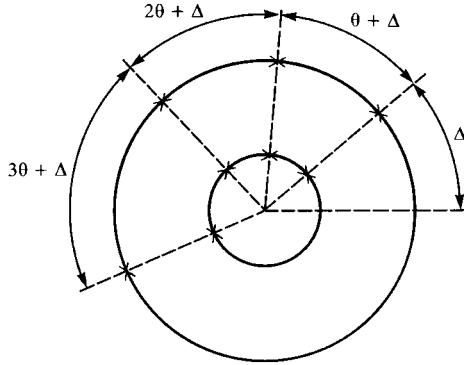


FIGURE A.3 Illustration of the scheme for rotating the match points of a ribbon cable to avoid singular solution matrices.

These are rotated by an angle

$$\Delta = \frac{\pi}{2NF} \tag{A.4b}$$

as illustrated in Figure A.3.

The matrix equations in (A.1) or (A.2) are solved as

$$\mathbf{A} = \left[\mathbf{D}_{11} - \mathbf{D}_{12} \mathbf{D}_{22}^{-1} \mathbf{D}_{21} \right]^{-1} \Phi \tag{A.4a}$$

$$\mathbf{A}' = -\mathbf{D}_{22}^{-1} \mathbf{D}_{21} \mathbf{A} \tag{A.4b}$$

Once these are solved, the total free charge on each conductor and the elements of the generalized capacitance matrix are obtained according to (5.48). The transmission-line capacitance matrix \mathbf{C} is obtained from the generalized capacitance matrix according to the algorithm given in (5.21) for the chosen reference conductor. The generalized capacitance matrix *with the dielectric removed* is computed by computing the free charge with the dielectric removed:

$$\mathbf{A} = \mathbf{D}_{11}^{-1} \Phi \tag{A.5}$$

and the transmission-line capacitance matrix \mathbf{C}_0 is computed for the chosen reference conductor. The transmission-line inductance matrix is computed according to

$$\mathbf{L} = \mu_0 \epsilon_0 \mathbf{C}_0^{-1} \tag{A.6}$$

The upper triangle of \mathbf{C} and \mathbf{L} are printed out to the file PUL.DAT with \mathbf{L} printed first. Observe the numbering of the conductors illustrated in Figure A.4. The conductors to the left of the reference conductor are numbered sequentially from left to right and the remaining conductors to the right of the reference conductor are also numbered

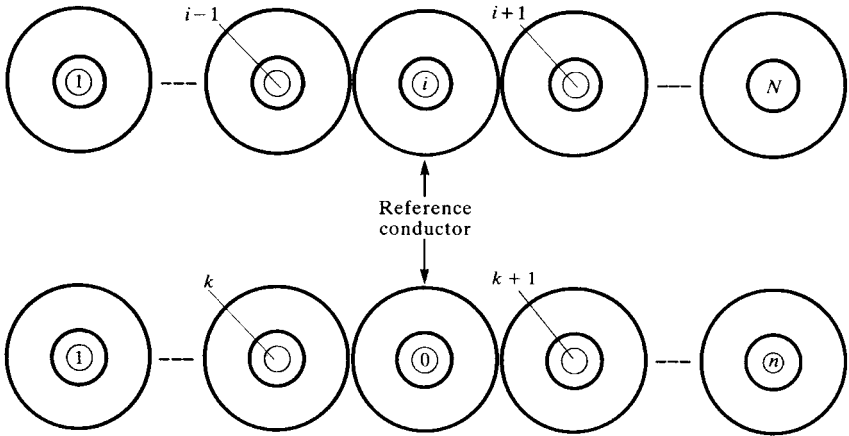


FIGURE A.4 Illustration of the numbering scheme for determining the transmission-line capacitance matrix from the generalized capacitance matrix for a ribbon cable.

sequentially. This numbering is critical to observe when one generates the entries of the matrices and vectors of the terminal characterization as with a generalized Thevenin equivalent in the programs that use these data.

The inversion of the above real-valued matrices is accomplished with a standard Gauss–Jordan subroutine, **GAUSSJ**, which is supplied as a part of the code **RIBBON.FOR**. This subroutine was taken with permission from W.H. Press, B.P. Flannery, S.A. Teukolsky, and W.T. Vetterling, *Numerical Recipes, The Art of Scientific Computing*, Cambridge University Press, NY, 1989 ([1]).

A.1.3 Printed Circuit Boards: PCB.FOR

Required input files: **PCB.IN**

Output file: **PUL.DAT**

This code determines the entries in the per-unit-length inductance and capacitance matrices **L** and **C** for an *N*-land PCB illustrated in Figure A.5 and described in Section 5.3.1.1. The problem that is solved is a special case wherein all lands have

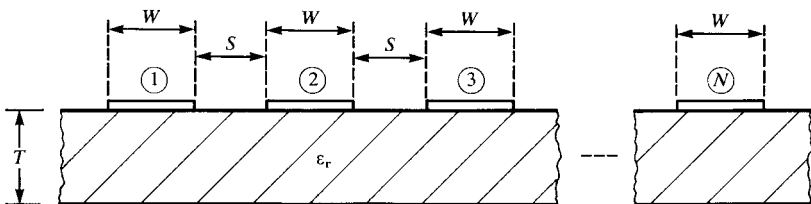


FIGURE A.5 Cross-sectional definition of the printed circuit board parameters for the **PCB.FOR** FORTRAN program input data.

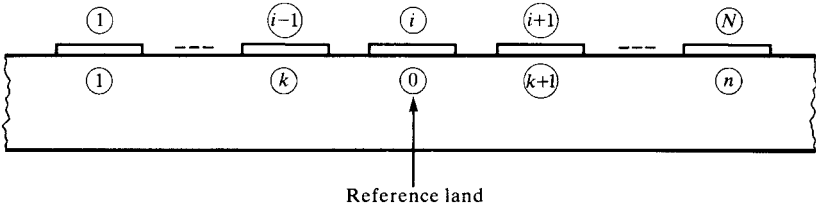


FIGURE A.6 Illustration of the numbering scheme for determining the transmission-line capacitance matrix from the generalized capacitance matrix for a PCB.

the same width of W and identical edge-to-edge separations S . The board has thickness T and relative permittivity ϵ_r . The lands are numbered from left to right as shown. The generalized capacitance matrix for the structure is first solved using the results for potential given in Section 5.3.1.1 of Chapter 5. One of the input data parameters provided in PCB.IN is the number of the desired reference land as illustrated in Figure A.6. The code then solves for the transmission-line capacitance matrix from the generalized capacitance matrix based on the desired reference conductor. The code first solves for the capacitance matrix with the board removed and replaced with free space C_0 from which the transmission-line inductance matrix is obtained as $L = \mu_0 \epsilon_0 C_0^{-1}$. Then the capacitance matrix with the board present, C , is determined.

The matrix given in (5.60) of Chapter 5 relating the charge distributions over the land subsections to the potentials of the lands is formed and inverted as in (5.61). From this result the generalized capacitance matrix is formed as in (5.62). Then the algorithm in (5.21) is used to obtain the entries in the transmission-line capacitance matrices C and C_0 for the chosen reference land. For both cases, the matrix equation to be solved has, because of the assumption of identical land widths and edge-to-edge spacing, the following structure:

$$\begin{bmatrix} \mathbf{A}_1 & \mathbf{A}_2 & \cdots & \mathbf{A}_N \\ \mathbf{A}_2^t & \mathbf{A}_1 & \ddots & \vdots \\ \vdots & \ddots & \ddots & \mathbf{A}_2 \\ \mathbf{A}_N^t & \cdots & \mathbf{A}_2^t & \mathbf{A}_1 \end{bmatrix} \begin{bmatrix} \sigma_1 \\ \sigma_2 \\ \vdots \\ \sigma_N \end{bmatrix} = \begin{bmatrix} \Phi_1 \\ \Phi_2 \\ \vdots \\ \Phi_N \end{bmatrix} \tag{A.7}$$

where t denotes the transpose of the matrix, σ_i contains the unknown levels of the charge distributions (assumed constant) of each subsection of the i th land, and Φ_i contains the potentials of the subsections of the i th land.

The upper triangle of the per-unit-length inductance matrix is printed to PUL.DAT followed by the upper triangle of the per-unit-length capacitance matrix. These data are used by all subsequent analysis codes. Additionally, the per-unit-length capacitance matrix with the board removed, C_0 , is printed to PUL.DAT but is not used by the analysis codes. And finally, the problem parameters are printed to PUL.DAT so that the user can insure that the problem solved is as desired. The inversion

of (A.7) is again performed using the Gauss–Jordan subroutine that was used in `RIBBON.FOR`.

A.1.4 Coupled Microstrip Structures: `MSTRP.FOR`

Required input files: `MSTRP.IN`

Output file: `PUL.DAT`

This code determines the $n \times n$ per-unit-length transmission line capacitance and inductance matrices \mathbf{C} and \mathbf{L} consisting of n equal-width lands with identical separations on a dielectric substrate with a ground plane on the opposite side as illustrated in Figure A.7 and described in Section 5.3.1.2. This code is useful in simulating a printed circuit board that has one or more inner planes that are buried at various distances within the board. Essentially, it simulates the surface of the PCB where the traces are located and the innerplane closest to that surface. Since we assume a board of infinite width, the remaining innerplanes are of no consequence since they are isolated in this calculation from the surface lands by the first innerplane. This code also simulates many other microstrip structures that are used in microwave circuits.

The construction of this code requires two simple modifications of the previous code `PCB.FOR`. The first modification is that the generalized capacitance matrix computed in the code `PCB.FOR` is the transmission-line capacitance matrix for the microstrip structures. This is because the voltages of the n lands of the microstrip structure are taken *with respect to the ground plane*. It can be shown that these voltages are essentially the absolute potentials computed in the generalized capacitance matrix [B.4]. Therefore, the first modification of the code `PCB.FOR` is to simply remove the computations that determine the transmission-line capacitance matrices from the generalized capacitance matrices.

The second modification of the code `PCB.FOR` is to determine the absolute potential of a infinitesimal line charge on the surface of an dielectric sheet having a ground plane on the opposite side. This basic subproblem was solved for the PCB having no ground plane in Chapter 3 by imaging across the two dielectric surfaces as shown in

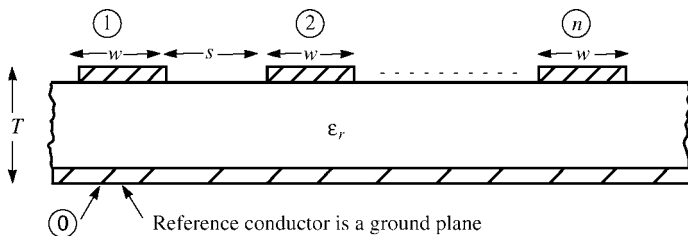


FIGURE A.7 Cross-sectional definition of the coupled microstrip line parameters for the `MSTRP.FOR` FORTRAN program input data.

Figure 5.27(b) resulting in

$$\begin{aligned} \phi(d) &= -\frac{q}{4\pi\epsilon_0}(1-k)\ln[d^2] - \frac{q}{4\pi\epsilon_0}(1-k^2)\sum_{n=1}^{\infty}k^{(2n-1)}\ln\left[d^2+(2nt)^2\right] \\ &= -\frac{q}{4\pi\epsilon_0\epsilon_{\text{reff}}}\ln[d^2] - \frac{q}{4\pi\epsilon_0\epsilon_{\text{reff}}}(1+k)\sum_{n=1}^{\infty}k^{(2n-1)}\ln\left[d^2+(2nt)^2\right] \end{aligned} \tag{5.76}$$

In the case of the microstrip structure, we image the line charge across the top dielectric surface and across the ground plane and obtain in a similar fashion as shown in Figure 5.33:

$$\begin{aligned} \phi(d) &= -\frac{(1-k)q}{4\pi\epsilon_0}\ln[d^2] - \frac{(1-k^2)q}{4\pi\epsilon_0}\sum_{n=1}^{\infty}(-1)^nk^{(n-1)}\ln\left[d^2+(2nt)^2\right] \\ &= -\frac{q}{4\pi\epsilon_0\epsilon_{\text{reff}}}\ln[d^2] - \frac{q}{4\pi\epsilon_0\epsilon_{\text{reff}}}(1+k)\sum_{n=1}^{\infty}(-1)^nk^{(n-1)}\ln\left[d^2+(2nt)^2\right] \end{aligned} \tag{5.84}$$

Comparing (5.76) and (5.84), we see that the code PCB.FOR can be simply modified to analyze the microstrip structures by replacing in all summations

$$\underbrace{\sum_{n=1}^{\infty}k^{(2n-1)}}_{\text{PCB.FOR}} \Leftrightarrow \underbrace{\sum_{n=1}^{\infty}(-1)^nk^{(n-1)}}_{\text{MSTRP.FOR}} \tag{A.8}$$

There is one additional difference. In the case of PCB.FOR with the dielectric removed (replaced with free space) $k = 0$ and the summation is zero. In the case of microstrip structures, MSTRP.FOR, the first term of the summation is nonzero for $k = 0$, that is, with the dielectric removed. This term represents the image across the ground plane and is present even with the dielectric removed.

A.1.5 Coupled Stripline Structures: STRPLINE.FOR

Required input files: STRPLINE.IN

Output file: PUL.DAT

This code determine the $n \times n$ per-unit-length transmission line capacitance and inductance matrices **C** and **L** for n equal-width lands with identical separations within a homogeneous, dielectric substrate with ground planes on both sides as illustrated in Figure A.8 and described in Section 5.3.1.3. This code is useful in simulating a printed circuit board that has one or more inner planes that are buried at various distances within the board. The lands are assumed to be at an equal distance above

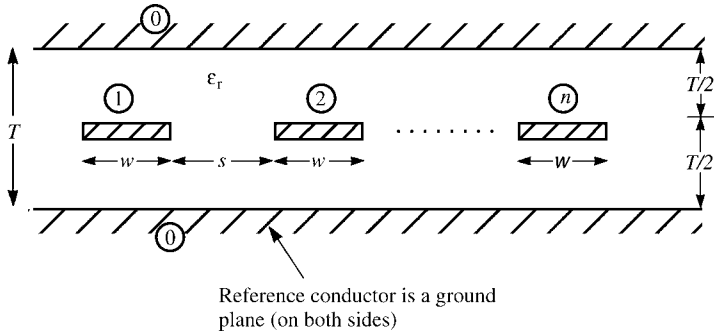


FIGURE A.8 Cross-sectional definition of the coupled stripline parameters for the STRPLINE.FOR FORTRAN program input data.

and below the two ground planes. Again, the voltages of the n lands of the microstrip structure are taken *with respect to the ground plane*.

A.2 FREQUENCY-DOMAIN ANALYSIS

One code, MTL.FOR, serves to determine the frequency-domain response of an MTL. Depending on the input data, one can consider lossless or lossy lines as well as homogeneous media or inhomogeneous media. The lossy description of the conductors is contained in MTL.IN, and the inhomogeneity of the surrounding medium is determined by the per-unit-length parameters contained in PUL.DAT.

A.2.1 General: MTL.FOR

Required input files: MTL.IN, PUL.DAT, FREQ.IN
 Output file: MTL.OUT

The program forms the per-unit-length impedance and admittance matrices:

$$\hat{\mathbf{Z}} = \mathbf{R}(f) + j\omega\mathbf{L} \tag{A.9a}$$

$$\hat{\mathbf{Y}} = j\omega\mathbf{C} \tag{A.9b}$$

where the entries in \mathbf{R} , \mathbf{L} , and \mathbf{C} are given in (3.12), (3.11c), and (3.24). The entries in the upper diagonal of \mathbf{L} and \mathbf{C} are read from PUL.DAT. The entries in \mathbf{R} are input data from MTL.IN. These are given for each conductor as (1) the dc resistance r_{dc} and (2) the break frequency f_0 where the resistance transitions to a \sqrt{f} skin-effect frequency dependence as $r_{hf} = r_{dc}\sqrt{f/f_0}$. The per-unit-length internal inductances of the conductors are also included in \mathbf{L}_i and are determined from these data according to the scheme given in (8.137) in Section 8.2.1.3 assuming that the high-frequency resistance and internal inductive reactance are equal, $r_{hf} = \omega l_{i,hf}$, and that they both transition at the same frequency, f_0 . If no conductor loss is desired, set the dc

resistance to zero, and if no skin-effect dependence is desired, set f_0 larger than the largest analysis frequency. The analysis frequencies are read from the file `FREQ.IN`. The code determines the eigenvalues γ and eigenvectors \mathbf{T} of \mathbf{YZ} as in (7.35). The entries in the generalized Thevenin equivalent characterizations of the terminations as in (7.87) are read from the file `MTL.IN`. Incorporating these into the general solution in (7.86) gives the $2n \times 2n$ matrix to solve (7.90) for the $2n$ undetermined constants in the vectors \mathbf{I}_m^\pm .

The eigenvectors and eigenvalues of \mathbf{YZ} are determined using the International Mathematical and Statistical Libraries (IMSL) version 9.2 subroutine `EIGCC` [2]. Equation (7.90) is solved using the IMSL subroutine `LEQT1C`.

A.3 TIME-DOMAIN ANALYSIS

Four time-domain analysis codes are included. These implement the time-domain to frequency-domain (TDFD) transformation (`TIMEFREQ.FOR`), Branin's recursive solution method extended (for a homogeneous medium) to MTLs (`BRANIN.FOR`), the finite-difference, time-domain (FDTD) method for lossless lines (`FINDIF.FOR`), and the finite-difference, time-domain (FDTD) method for lossy lines (`FDTD-LOSS.FOR`).

A.3.1 Time-Domain to Frequency-Domain Transformation: `TIMEFREQ.FOR`

Required input files: `TIMEFREQ.IN`, `MTLFREQ.DAT`

Output file: `TIMEFREQ.OUT`

This code determines the time-domain response of the MTL using the TDFD transformation described in Sections 8.1.7, 8.2.2, 9.1.4, and 9.2.1. The input signal is assumed to be a periodic pulse train with trapezoidal pulses. The Fourier series of this input signal is given by (1.121), and the coefficients are given by (1.126). The input file `TIMEFREQ.IN` contains the number of harmonics used, the pulse level, the repetition frequency of the pulse train, the duty cycle, the pulse rise/fall time, and the final solution time. In addition, the dc level of the transfer function, $H(0)$, is input and multiplied by the dc level of the input spectrum, c_0 , to give the dc level of the output spectrum. The input file `MTLFREQ.DAT` contains the frequency-domain transfer function (magnitude and phase) at each of the desired harmonics of the input signal. These can be computed (a) for a lossless line using `PSPICE` in the `.AC` mode and the lossless transmission-line subcircuit model generated by `SPICEMTL.FOR` or (b) for a lossy (or lossless) line using the frequency-domain analysis code `MTL.FOR` that was described in the previous section. The program combines these data to compute the time-domain response according to (1.124).

A.3.2 Branin's Method Extended to Multiconductor Lines: `BRANIN.FOR`

Required input files: `BRANIN.IN`, `VSVL.IN`, `PUL.DAT`

Output file: `BRANIN.OUT`

This code implements the recursive solution of Branin's method extended to MTLs *for a homogeneous medium* as described in Section 9.1.1. Equations (9.18) are solved recursively. The source and load voltage waveforms in $V_S(t)$ and $V_L(t)$ in the generalized Thevenin equivalent representation of the terminations in (9.17) are described in a piecewise linear fashion in the input file `VSVL.IN`. The *resistive* entries in the matrices \mathbf{R}_S and \mathbf{R}_L in (9.17) are input data in the file `BRANIN.IN`. These are assumed to be symmetric and the upper triangles of these are input. It is implicit in this method that the surrounding medium is homogeneous (for which \mathbf{L} and \mathbf{C} were computed).

A.3.3 Finite Difference-Time Domain Method: **FINDIF.FOR**

Required input files: `FINDIF.IN`, `VSVL.IN`, `PUL.DAT`
 Output file: `FINDIF.OUT`

This code implements the FDTD method for a *lossless line* described in Section 9.1.5. Equations (9.53) and (9.57) are solved recursively. The discretizations of position and time are contained in `FINDIF.IN`. The *resistive* entries in the matrices \mathbf{R}_S and \mathbf{R}_L in the generalized Thevenin equivalent characterizations of the terminations are also the input data in the file `FINDIF.IN`. The source and load input voltages are described versus time in a piecewise linear manner in the input file `VSVL.IN`.

A.3.4 Finite-Difference-Time-Domain Method: **FDTDLOSS.FOR**

Required input files: `FDTDLOSS.IN`, `VSVL.IN`, `PUL.DAT`
 Output file: `FDTDLOSS.OUT`

This code implements the FDTD method for *lossy lines* described in Section 9.2.3. It is essentially identical to `FINDIF.FOR` with the addition of the discrete convolution for the dc and skin-effect losses (resistance and internal inductance) described in Section 8.2.3. Equations (9.53), (9.57), and (9.80) are solved recursively. The discretizations of position and time are contained in `FDTDLOSS.IN` along with the dc resistance and skin-effect transition frequencies of the conductors according to the scheme described in Section 8.2.3 of Chapter 8. The *resistive* entries in the matrices \mathbf{R}_S and \mathbf{R}_L in the generalized Thevenin equivalent characterizations of the terminations are also input data in the file `FDTDLOSS.IN`. The source and load input voltages are described in a piecewise linear manner in the input file `VSVL.IN`.

A.4 SPICE/PSPICE SUBCIRCUIT GENERATION PROGRAMS

This section describes three FORTRAN codes that generate SPICE/PSPICE subcircuit models that implement the SPICE method (`SPICEMTL.FOR`), the lumped-Pi model (`SPICELPI.FOR`), and the low-frequency, inductive-capacitive model (`SPICELC.FOR`).

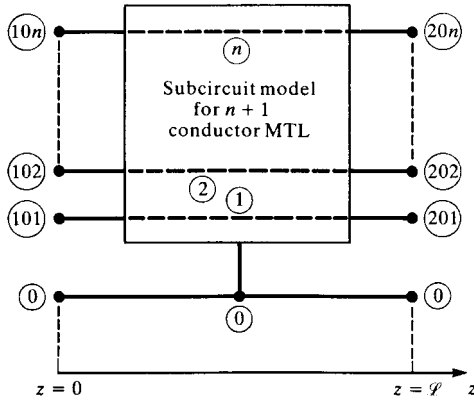


FIGURE A.9 Terminal node numbering scheme for the SPICE subcircuit models generated by the FORTRAN programs SPICEMTL.FOR and SPICELPI.FOR models.

A.4.1 General Solution, Lossless Lines: SPICEMTL.FOR

Required input files: SPICEMTL.IN, PUL.DAT

Output file: SPICEMTL.OUT

This code implements the exact SPICE model described in Section 9.1.2. The line is assumed to be lossless but the surrounding medium may be inhomogeneous as determined by the per-unit-length parameters in PUL.DAT. The per-unit-length inductance and capacitance matrices are read from PUL.DAT and diagonalized as in Section 9.1.2 using the subroutines DIAG and JACOBI. A subcircuit model is developed with the node numbering as 101, 102, ..., 10n for the nodes of conductors 1, 2, ..., n at $z = 0$ and 201, 202, ..., 20n for the nodes of conductors 1, 2, ..., n at $z = L$ as illustrated in Figure A.9. This subcircuit model can then be incorporated into a SPICE/PSPICE program. The total number of conductors, $n + 1$, and the total line length are specified in the input file SPICEMTL.IN. Note that the resulting SPICE/PSPICE code can also handle frequency-domain solutions by replacing the .TRAN run instruction with the .AC instruction.

A.4.2 Lumped-Pi Circuit, Lossless Lines: SPICELPI.FOR

Required input files: SPICELPI.IN, PUL.DAT

Output file: SPICELPI.OUT

This code implements a SPICE subcircuit for the lumped-Pi model of an MTL described in Sections 7.4, 9.1.3, and 9.2.2. The line is again assumed to be lossless but the surrounding medium may be inhomogeneous as determined by the per-unit-length parameters in PUL.DAT. The per-unit-length inductance and capacitance matrices are read from PUL.DAT. A subcircuit model is again developed with the node numbering as before as 101, 102, ..., 10n for the nodes of conductors 1, 2, ..., n at $z = 0$ and 201, 202, ..., 20n for the nodes of conductors 1, 2, ..., n at $z = L$

as is illustrated in Figure A.9. This subcircuit model can then be incorporated into a SPICE/PSPICE program. The total number of conductors, $n + 1$, and the total line length are specified in the input file `SPICELPI.IN`. Conductor losses can be incorporated by adding additional nodes and the appropriate line resistances and internal inductances or frequency-dependent models for them as described in Section 9.2.2.

A.4.3 Inductive-Capacitive Coupling Model: `SPICELC.FOR`

Required input files: `SPICELC.IN`

Output file: `SPICELC.OUT`

This code implements the low-frequency, inductive-capacitive coupling model described in Section 10.1.1 for a three-conductor line. The line is assumed to be lossless but the surrounding medium may be inhomogeneous as determined by the per-unit-length mutual inductance and mutual capacitance parameters in `SPICELC.IN`. This input file also specifies the total line length. Figure A.10 shows the SPICE model that is developed. A subcircuit model, shown in Figure A.11, is developed with the node numbering as S, NE for the two nodes of conductors 1, 2 at $z = 0$ and L, FE for the nodes of conductors 1, 2 at $z = \mathcal{L}$. This subcircuit model can then be incorporated into a SPICE/PSPICE program.

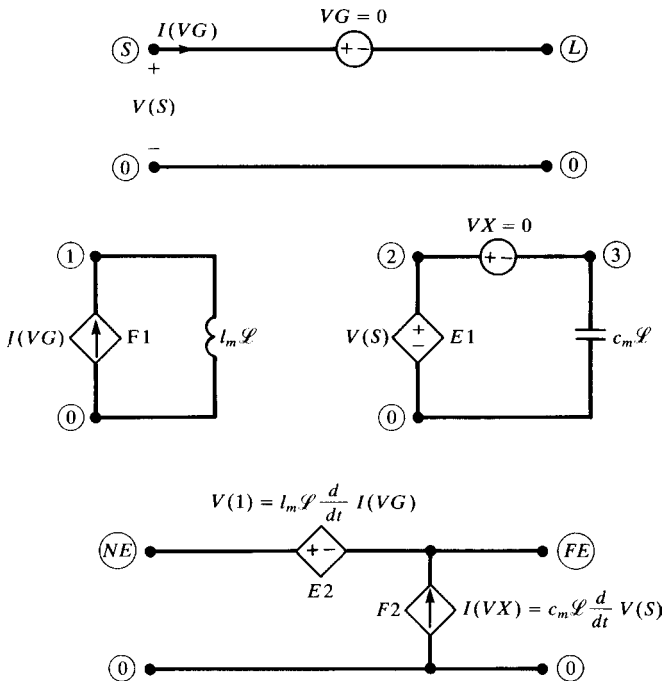


FIGURE A.10 The SPICE subcircuit model generated by the code `SPICELC.FOR`.

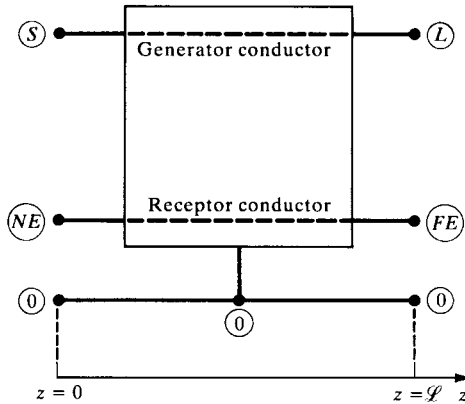


FIGURE A.11 The node numbering scheme for the SPICE subcircuit model generated by the code SPICELC.FOR.

A.5 INCIDENT FIELD EXCITATION

A.5.1 Frequency-Domain Program: INCIDENT.FOR

Required input files: INCIDENT.IN, PUL.DAT, FREQ.IN

Output file: INCIDENT.OUT

This code determines the frequency-domain response of a general MTL to a single frequency, uniform plane wave. Two types of line structures are provided for: an $n + 1$ conductor MTL and n conductors above an infinite, perfectly conducting ground plane. The terminations are characterized by generalized Thevenin equivalents. Lumped voltage sources can also be included in these terminations. Equations (12.39) are solved for the vectors of undetermined constants in the general solution, and the terminal voltages are obtained from equations (12.40). The forcing functions due to a uniform plane-wave incident field $\hat{\mathbf{V}}_{\text{FT}}(\mathcal{L})$ and $\hat{\mathbf{I}}_{\text{FT}}(\mathcal{L})$ are determined from equations (12.61)–(12.68). Essentially, the program MTL.FOR described earlier was modified to include the incident field sources.

The code requires the input files INCIDENT.IN, PUL.DAT, and FREQ.IN. The file PUL.DAT is as before and gives the usual per-unit-length parameters of the line. The file FREQ.IN is also the same as for the program MTL.FOR and gives the solution frequencies sequentially. The file INCIDENT.IN describes (in this order) (1) the total number of conductors $n + 1$, (2) the total line length, (3) the line type (1 = no ground plane and 2 = ground plane), (4) the output conductor for the terminal solution voltages, (5) the incident uniform plane-wave description ($\hat{\mathbf{E}}_0$, θ_E , θ_P , and ϕ_P with reference to Figure A.12), (6) the conductor cross-sectional coordinates (sequentially according to Figure A.13), (7) the dc resistances and skin-effect break frequencies (for the reference conductor and sequentially for the other n conductors) as described for MTL.FOR, and (8) the generalized Thevenin equivalent characterizations for the terminations as described for MTL.FOR. The output file INCIDENT.OUT gives the termination solution voltages for the chosen output conductor (with respect to the

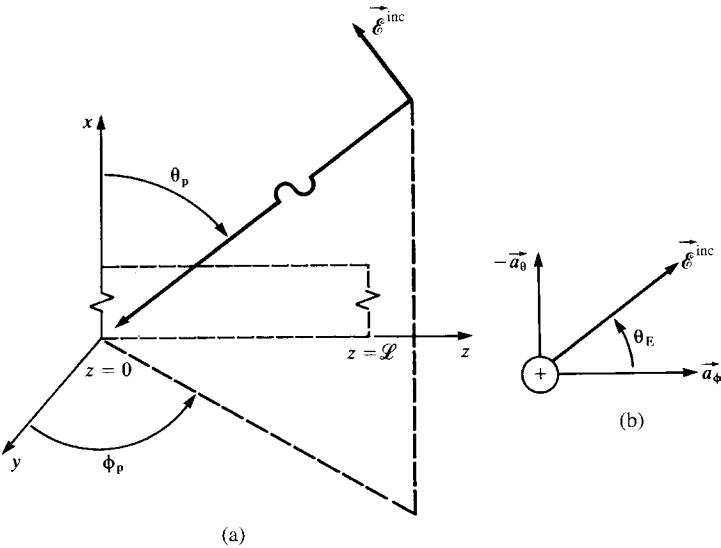


FIGURE A.12 Definition of (a) the angles of incidence and (b) polarization of the electric field for an incident uniform plane wave for the codes `INCIDENT.FOR`, `SPICEINC.FOR`, and `FDTDINC.FOR`.

reference conductor) sequentially for each solution frequency in `FREQ.IN`. These can be used in the previously described code, `TIMEFREQ.FOR` to compute the time-domain response to a uniform plane wave that has a periodic, trapezoidal waveform.

A.5.2 SPICE/PSPICE Subcircuit Model: `SPICEINC.FOR`

Required input files: `SPICEINC.IN`, `PUL.DAT`

Output file: `SPICEINC.OUT`

This code generates a `SPICE/PSPICE` subcircuit model for an $n + 1$ conductor MTL excited by a uniform plane wave. The input file `SPICEINC.IN` contains the total number of conductors, the line length, the line type (1 = no ground plane and 2 = ground plane), the incident wave polarization and propagation direction with reference to Figure A.12 (θ_E , θ_p , and ϕ_p), and the cross-sectional conductor locations with reference to Figure A.13 ($X(i)$, $Y(i)$). The cross-sectional coordinates are entered sequentially as the last items in this input file. The other input file is the usual `PUL.DAT` that contains the per-unit-length parameters. The output file `SPICEINC.OUT` contains the `SPICE` subcircuit model. The external nodes are labeled as in `SPICEMTL` and are shown in Figure A.14. The code implements the model shown in Figure 12.8. The external nodes at $z = 0$ are denoted as 101, 102, ..., 10n and the external nodes at $z = L$ are denoted as 201, 202, ..., 20n. One additional node 100 is external to which the time waveform source of the incident wave $\mathcal{E}_0(t)$ is attached. The code is restricted to ϕ_p positive, that is, components of the propagation vector in

the $+z$ direction. For propagation directions giving a component in the $-z$ direction, simply reverse the line.

A.5.3 Finite-Difference, Time-Domain (FDTD) Model: FDTDINC.FOR

Required input files: FDTDINC.IN, PUL.DAT, E0.IN

Output file: FDTDINC.OUT

This code implements the FDTD method contained in equations (12.134) and (12.135) of Chapter 12. The input file FDTDINC.IN contains the total number of conductors, the line length, the line type (1 = no ground plane and 2 = ground plane), the incident wave polarization and propagation direction with reference to Figure A.12 ($\theta_E, \theta_p, \phi_p$), the cross-sectional conductor locations with reference to Figure A.13

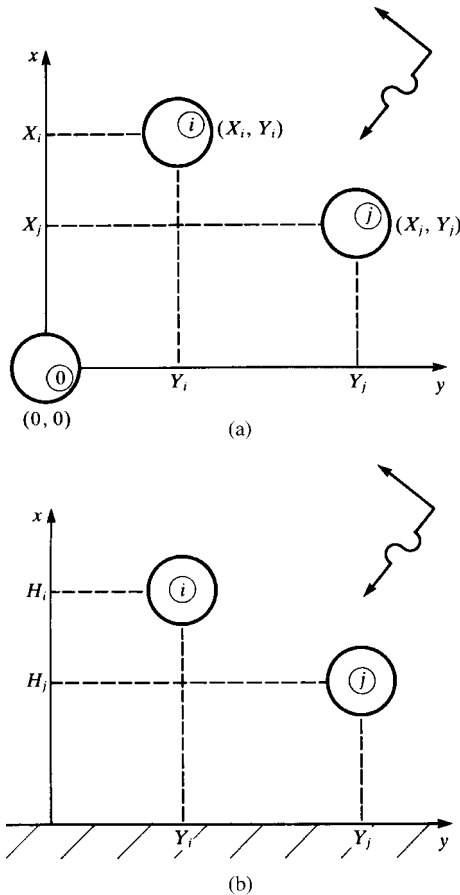


FIGURE A.13 Definition of the cross-sectional dimensions for input data to the codes INCIDENT.FOR, SPICEINC.FOR, and FDTDINC.FOR for (a) $n + 1$ wires and (b) n wires above a ground plane.

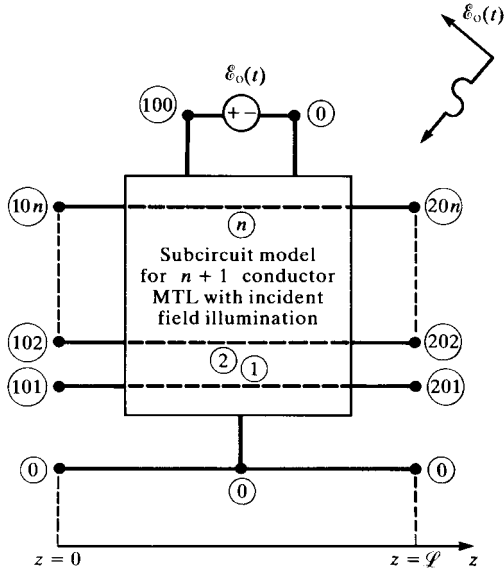


FIGURE A.14 Node numbering for the SPICE subcircuit model generated by the code SPICEINC.FOR.

$(X(i), Y(i))$, the number of line position cells, NDZ, the number of time discretizations, NDT, the final solution time, the print solution index, the output conductor for the terminal voltages, and the line terminations in the form of a generalized Thevenin equivalent without sources ($\mathbf{R}_S, \mathbf{R}_L, \mathbf{V}_S = \mathbf{0}$, and $\mathbf{V}_L = \mathbf{0}$). The input file PUL.DAT contains the usual per-unit-length parameters. The input file E0.IN contains a piecewise linear specification of $\mathbf{E}_o(t)$ versus time. The output file FDTDINC.OUT contains the solution at the discrete time steps at the endpoints of the chosen output conductor.

REFERENCES

- [1] W.H. Press, S.A. Teukolsky, W.T. Vetterling, and B.P. Flannery, *Numerical Recipes in FORTRAN: The Art of Scientific Computing*, 2nd edition, Cambridge University Press, 1992.
- [2] Visual Numerics, Inc., 9990 Richmond Ave., Suite 400, Houston, TX 77042-4548.

APPENDIX B

A SPICE (PSPICE) TUTORIAL

This is a brief summary of the SPICE, or its personal computer version PSPICE, electric circuit analysis program. SPICE is an acronym for *simulation program with integrated-circuit emphasis*. The original SPICE computer program was developed to analyze complex electric circuits, particularly integrated circuits. It was developed at the University of California at Berkeley in the early 1970s. Since it was developed under U.S. government funding, it is not proprietary and can be freely copied, used, and distributed. We will discuss the most common and widely available SPICE2, version G6 code, which was written in FORTRAN. This was written for use on large mainframe computers of the time. In the 1980s, the MicroSim Corporation developed a personal computer version of SPICE called PSPICE. A number of important modifications were made particularly in the plotting of data via the .PROBE function. Since then a number of commercial firms have modified and developed their own PC versions' but essentially the core engine is that of the original SPICE code. The MicroSim version of PSPICE was acquired by the OrCAD Corporation, now Cadence Design Systems. A windows-based version is available free from www.orcad.com. The latest is the version 10.0 called OrCAD Capture, which contains the primary simulation code PSPICE A/D. The OrCAD Capture program was originally called Schematic in the MicroSim version. A number of books [1–5] detail the use of SPICE and PSPICE.

There are two methods of entering and executing a PSPICE program. The first method is the direct method, which is described here, where one enters the program code using a ASCII text editor (supplied with PSPICE). Then this text file is run using the PSpice A/D section of the program, and the output is examined with the text editor.

The second method is the schematic method (now called Capture), where the user “draws” the circuit diagram directly on the screen and then executes this program. The direct method is generally the most rapid method of solving a problem. The schematic (capture) method has the advantage of visually seeing whether the circuit components are connected as intended but is a bit more time-consuming than the direct method for the simple problems in this textbook because numerous windows and drop-down menus must be navigated.

Once the PSPICE program has been installed on your computer, the following is a description of how you can input your program, run it, and examine the output. The various selections are underlined. In the following, we will discuss the MicroSim version 8. The method of accessing PSPICE and inputting data in the OrCAD version 10 is very similar. Although there are several ways of doing this, the simplest way is to use the *design manager*. To load this, you click or select the following in this sequence:

1. Start
2. Programs
3. MicroSim Eval 8
4. Design Manager

The direct method is to simply type in the PSPICE program using the *TextEdit* feature. To enter this and prepare the program, we select the following in this sequence:

1. TextEdit (lower button on the vertical toolbar on the left).
2. Type the program.
3. Save the program as XXX.cir or XXX.in and close it.
4. Select PSpice A/D (second button on the vertical toolbar on the left).
5. Click on file, open, and select the previously stored file. The program will automatically run and the output will be stored in file XXX.out.
6. Click on File, and run probe in order to plot waveforms.
7. Recall the *TextEdit* program and select file, open XXX.out. Examine the output, which is self-explanatory.

B.1 CREATING THE SPICE OR PSPICE PROGRAM

SPICE and PSPICE write the node voltage equations of an electric circuit [1]. One node, the reference node for the node voltages, is designated the zero (0) node. All circuits must contain a zero node. The other nodes in the circuit are labeled with numbers or letters. For example, a node may be labeled 23, or it may be labeled FRED. The voltages with respect to the reference (zero) node are positive at the node and denoted as $V(N1)$, $V(N2)$ as shown in Figure B.1. The general structure of any SPICE or PSPICE program is as follows:

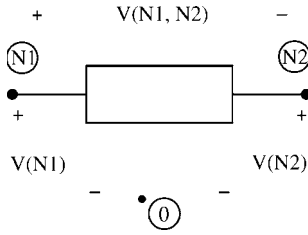


FIGURE B.1 Node voltage and element voltage notation in the SPICE (PSPICE) circuit analysis program.

1. Title
2. Circuit Description
3. Execution Statements
4. Output Statements
5. .END

The first line of the SPICE program is the title and is not processed by SPICE. It is simply written on the output and on any plots. A comment line is started with an asterisk (*) and is also not processed by the program. A line may be continued with a plus sign (+) at the beginning of the following line. The next set of lines, circuit description, describes the circuit elements and their values and tells SPICE how they are connected together to form the circuit. The next set of lines is the execution statements that tells SPICE what type of analysis is to be run: dc sources (.DC), sinusoidal steady state or phasor analysis (.AC), or the full time-domain analysis consisting of the transient and steady-state solution (.TRAN). The next set of statements, output statements, tells SPICE what output is desired. The results can be printed to a file with the .PRINT statement or can be plotted with the .PROBE feature. Finally, all programs must end with the .END statement. Actually, the items 2–4 can appear in any order in the program, but the program must begin with a title statement and end with the .END statement.

B.2 CIRCUIT DESCRIPTION

The basic elements and their SPICE descriptions are shown in Figure B.2. Figure B.2a shows the independent voltage source. It is named starting with the letter V and then any other letters. For example, a voltage source might be called VFRED. It is connected between nodes N1 and N2. It is very important to note that the source is assumed positive at the first-named node. The current through the voltage source is designated as I(VXXX) and is assumed to flow from the first-named node to the last-named node. The source type can be either dc for which we append the term DC *magnitude*, or a sinusoid for which we append the term AC *magnitude phase (degrees)*. A time-domain waveform is described by several functions that we will

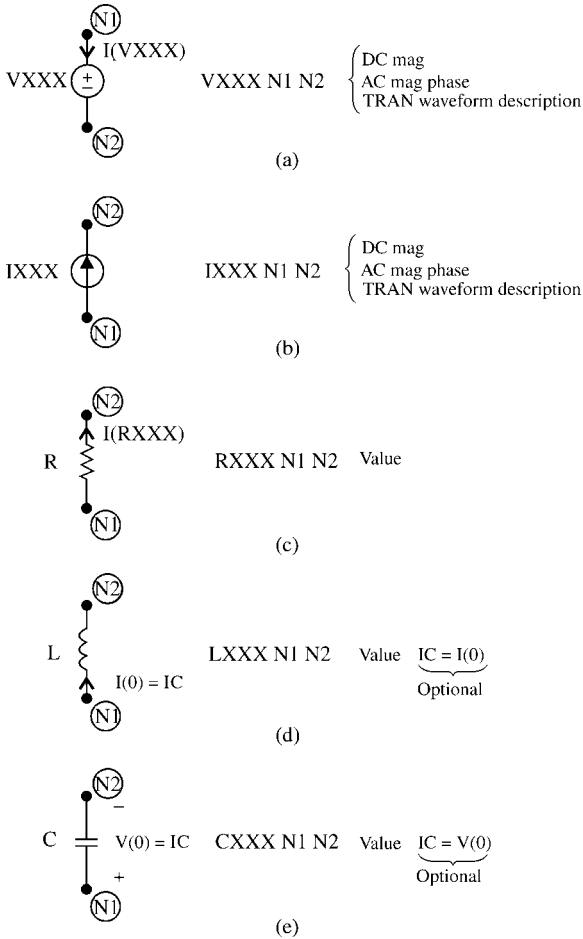


FIGURE B.2 Coding convention for (a) the independent voltage source, (b) the independent current source, (c) the resistor, (d) the inductor, and (e) the capacitor.

describe later and these descriptions are appended (without the word TRAN). The independent current source is shown in Figure B.2b. Its name starts with the letter I followed by any other letters. For example, a current source might be designated as ISAD. The current of the source is assumed to flow from the first-named node to the last-named mode. The types of sources are the same as for the voltage source.

The resistor is shown in Figure B.2c, and its name starts with the letter R, for example, RHAPPY. The current through the resistor is designated as I(RXXX) and is assumed to flow from the first-named node to the last-named node. SPICE does not allow elements with zero values. Hence, a resistor whose value is 0Ω (a short circuit) may be represented as having a value of $1E8$ (1×10^{-8}) or any other suitably small value. Similarly, an open circuit may be designated as a resistor having a value

of 1E8 or any other suitably large value. SPICE does not allow “floating nodes,” that is, nodes with no connection. Also, SPICE requires that every node have a dc path to ground.

The inductor is shown in Figure B.2d and is designated with the letter L, for example, LTOM. The current through the inductor as well as the initial inductor current at $t = 0^+$, $I(0)$ is assumed to flow from the first-named node to the last-named node. The initial condition can be specified at the end of the statement with $IC = I(0)$. The capacitor is shown in Figure B.2e and is designated by the letter C, for example, CME. The initial voltage across the capacitor at $t = 0^+$, $V(0)$ can be specified at the end of the statement with $IC = V(0)$, and this voltage is assumed to be positive at the first-named node.

All numerical values can be specified in powers of 10 and written in exponential format, for example, $2 \times 10^{-5} = 2E - 5$ or specified by using standard multipliers using standard specified engineering notation:

| Multiplier | SPICE symbol |
|-------------------|--------------|
| 10^9 (giga) | G |
| 10^6 (mega) | MEG |
| 10^3 (kilo) | K |
| 10^{-3} (milli) | M |
| 10^{-6} (micro) | U |
| 10^{-9} (nano) | N |
| 10^{-12} (pico) | P |

For example, 1 m Ω is written as 1M, 1 k Ω is written as 1K, 3 mH is written as 3M, 5 μ F is written as 5U, 2 nH is written as 2N, and 7 pF is written as 7P. A 3-F capacitor should not be written as 3F since F stands for femto = 10^{-15} . SPICE makes no distinction between uppercase and lowercase letters. Hence, we could write 1m, 1k, 3m, 5n, 2n, and 7p.

The four types of controlled sources, G, E, F, and H are shown in Figure B.3 along with their descriptions. The polarities of voltages and the currents through the elements conform to the previous rules governing these in terms of the first- and last-named nodes on their description statements. For a current-controlled source F or H, the controlling current may be through an independent voltage source. Often we insert a 0-V source to sample the current. Some more recent versions of PSPICE allow the specification of the current through any element as a controlling current, but it is always a simple matter to insert a 0-V voltage source.

Figure B.4 shows how to specify mutual inductance. First, the self-inductances that are coupled are specified as before. The mutual inductance is specified in terms of its coupling coefficient:

$$K = \frac{M}{\sqrt{L_1 L_2}}$$

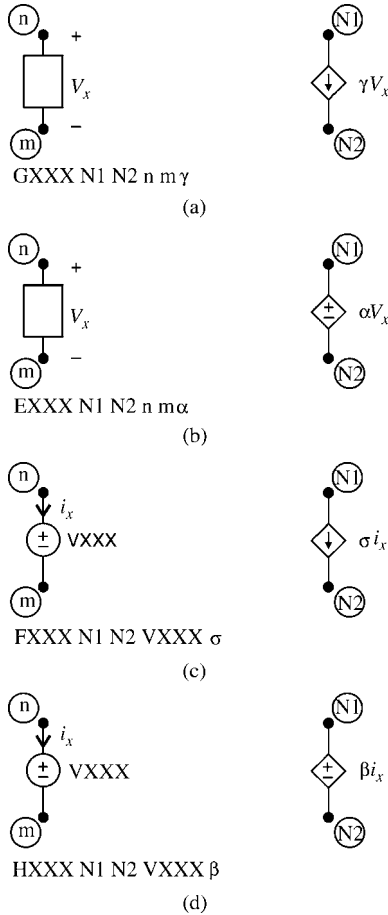


FIGURE B.3 Coding convention for (a) the voltage-controlled current source, (b) the voltage-controlled voltage source, (c) the current-controlled current source, and (d) the current-controlled voltage source.

In order to keep the polarities correct, define the self-inductances so that the dots are on the first-named nodes; otherwise, a negative coupling coefficient may need to be specified.

Figure B.5 shows the last important element, the transmission line (lossless), which we will use extensively. There are many ways to specify the important parameters for the line, but the one shown in the figure is the most widely used; specify the characteristic impedance of the line and the line's one-way time delay.

Figure B.6 shows how to specify the important time-domain waveforms. Figure B.6a shows the PWL (piecewise-linear) waveform where straight lines are drawn between pairs of points that are specified by their time location and their value. Observe that the function holds the last specified value, V4 in the figure.

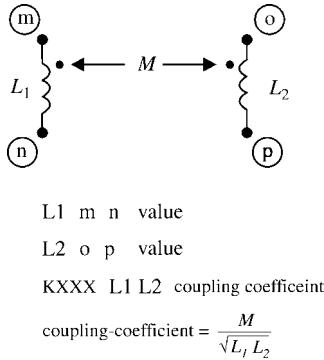


FIGURE B.4 Coding convention for mutual inductance between two coupled inductors.

Figure B.6b shows the periodic pulse waveform. The function specifies a trapezoidal waveform that repeats periodically with period PER (the reciprocal is the fundamental frequency of the waveform). Note that the pulse width P_w is not specified between the 50% points of the pulse as convention. The sinusoidal function is specified by

```
SIN (V0 Va [[Freq [[Td [[Df [[Phase]]]]]]]])
```

which gives the waveform

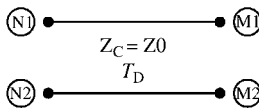
$$x(t) = V_0 + V_a \sin \left(2\pi \left(\text{Freq}(t - T_d) + \frac{\text{Phase}}{360} \right) \right) e^{-(t - T_d) D_f}$$

Hence, to specify the general sinusoidal waveform

$$x(t) = A \sin(n\omega_0 t + \theta)$$

we would write

```
SIN(0 A nf 0 0 θ)
```



```
TXXX N1 N2 M1 M2 Z0 = value TD = value
```

FIGURE B.5 Coding convention for the two-conductor lossless transmission line.

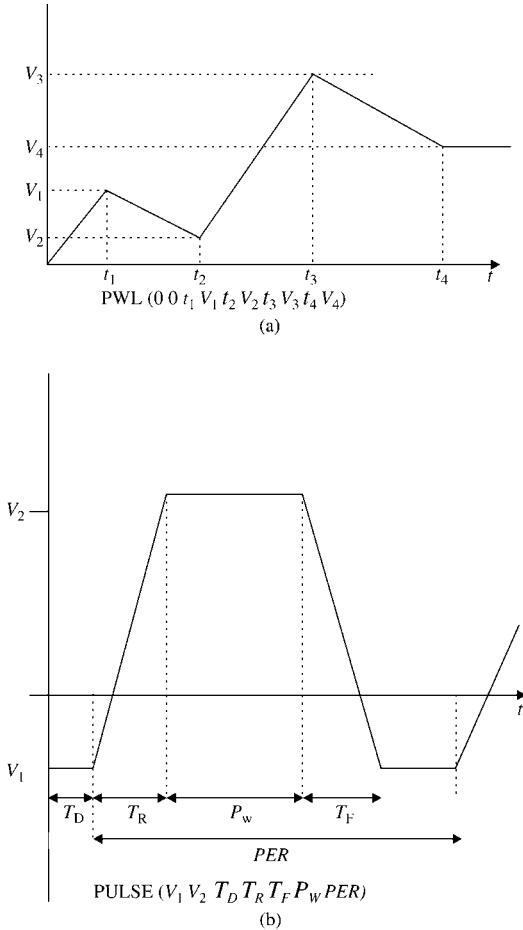


FIGURE B.6 Coding convention for the important source waveforms: (a) the piecewise-linear waveform and (b) the pulse source waveform (periodic).

B.3 EXECUTION STATEMENTS

There are three types of solutions: dc, sinusoidal steady state or phasor, and the full time-domain solution (so-called transient, although it contains both the transient and the steady-state parts of the solution).

The dc solution is specified by

```
.DC V,IXXX start_value end_value increment
```

where V,IXXX is the name of a dc voltage or current source in the circuit whose value is to be swept. For example, to sweep the value of a dc voltage source VFRED from

1 to 10 V in increments of 2 V and solve the circuit for each of these source values, we would write

```
.DC VFRED 1 10 2
```

If no sweeping of any source is desired, then we simply choose one dc source in the circuit and iterate its value from the actual value (5 V) to the actual value and use any nonzero increment. For example

```
.DC VFRED 5 5 1
```

The sinusoidal steady-state or phasor solution is specified by

```
.AC {LIN, DEC, OCT} points start_frequency end_frequency
```

where LIN denotes a linear frequency sweep from *start_frequency* to *end_frequency*, and *points* is the total number of frequency points. DEC denotes a log sweep of the frequency where the frequency is swept logarithmically from the *start_frequency* to the *end_frequency* and *points* is the number of frequency points per decade. OCT is a log sweep by octaves where *points* is the number of frequency points per octave.

The time-domain solution is obtained by specifying

```
.TRAN print_step end_time [no_print_time  
[step_ceiling]] [UIC]
```

SPICE solves the time-domain differential equations of the circuit by discretizing the time variable and solving the equations in a bootstrapping manner. The first item *print_step* governs when an output is requested. Suppose that the discretization used in the solution is every 2 ms. We might not want to see (in the output generated by the .PRINT statement) an output at every 2 ms but only at every 5 ms. Hence, we might set the *print_step* time as 5M. The *end_time* is the final time for which the solution is obtained. The remaining parameters are optional. The analysis always starts at $t = 0$. But we may not wish to see a printout of the solution (in the output generated by the .PRINT statement) until after some time has elapsed. If so, we would set the *no_print_time* to this starting time. SPICE and PSPICE have a very sophisticated algorithm for determining the minimum time step size Δt for discretization of the differential equations in order to get a valid solution. The default maximum step size is $end_time/50$. However, there are some cases where we want the step size to be smaller than what SPICE would allow in order to increase the accuracy of the solution. This is frequently the case when we use SPICE in the analysis of transmission lines. The *step_ceiling* is the maximum time step size that will be used. Although this gives longer run times, there are cases where we need to do this to generate the required accuracy. The last item UIC means that SPICE is to use the initial capacitor voltage

or inductor current specified on these element lines with the `IC =` command. In a transient analysis, SPICE will compute the initial conditions. If some other initial conditions are required, then we should set these and specify `UIC` on the `.TRAN` statement. For example

```
.TRAN 0.1N 20N 0 0.01N
```

would command SPICE to do a time-domain (transient analysis) for times from 0 to 20 ns, print out a solution at every 0.1 ns, start printing the output file at $t = 0$, and use a time discretization time step no larger than 0.01 ns.

B.4 OUTPUT STATEMENTS

The output statements are either for printing a file with the `.PRINT` statement or producing a plotted graph of any waveform with the `.PROBE` statement. The `.PRINT` statement has three forms depending on the type of analysis being run. For a DC analysis

```
.PRINT DC V(X) I(R)
```

prints the dc solution for the voltage of node `X` with respect to the reference node, and `I(R)` prints the dc solution for current through resistor `R` (defined from the first-named node to the last-named node on the specification statement for resistor `R`). For a sinusoidal steady-state analysis (phasor solution)

```
.PRINT AC VM(NI) VP(NI) IM(RFRED) IP(RFRED)
```

prints the magnitude and phase of node voltages and currents, where the magnitude and phase of the node voltage at node `NI` are `VM(NI)` and `VP(NI)`, respectively. For the currents through a resistor `RFRED`, the magnitude is `IM(RFRED)` and the phase is `IP(RFRED)`. For the time domain or the so-called transient analysis, the print statement is

```
.PRINT TRAN V(NI) I(RFRED)
```

and prints the solutions at all print solution time points for the voltage at node `NI` with respect to the reference node and the current through resistor `RFRED` (defined from the first-named node to the last-named node on the specification statement for resistor `RFRED`).

In addition, the `.FOUR` statement computes the expansion coefficients for the (one-sided) complex exponential form of the Fourier series (magnitude and phase):

```
.FOUR f0 [output_variable(s)]
```

The `.FOUR` command can be used only in a `.TRAN` analysis. The fundamental frequency of the *periodic* waveform to be analyzed is denoted as $f_0 = 1/P$ where P is the period of the waveform. The *output_variable(s)* are the desired voltage or current waveforms to be analyzed, for example, `V(2)`, `I(R1)`. The phase results are with reference to a sine form of the series:

$$x(t) = c_0 + \sum_{n=1}^{\infty} 2|c_n| \sin(n\omega_0 t + \angle c_n + 90^\circ)$$

Hence, when one compares the coefficients $c_n = |c_n| \angle c_n$ computed by hand to those computed with `.FOUR`, one must add 90° to the hand-calculated phases. There is an important consideration in using the `.FOUR` command. The portion of the waveform that is analyzed to give the Fourier expansion coefficients is the last portion of the solution time of length one period $1/f_0 = P$. In other words, SPICE determines the coefficients from the waveform between `end.time-[1/f0]` and `end.time`. Hence, `end.time` on the `.TRAN` command should be at least one period long. In situations where the solution has a transient portion at the beginning of the solution interval and we want to determine the Fourier coefficients for the steady-state solution, we would run the analysis for several periods to ensure that the solution has gotten into steady state. For example, consider an input signal that is periodic with a period of 2 ns or a fundamental frequency of 500 MHz. An output voltage at, for example, node 4 would also have this periodicity but would have a transient period of some five time constants, say, 5 ns. The following commands would be used to obtain the Fourier coefficients of the steady-state response of the node voltage at node 4:

```
.TRAN 0.1N 20N
.FOUR 500MEG V(4)
```

This would compute the solution for the voltage waveform at node 4 from $t = 0$ to $t = 20$ ns. Since the period (the inverse of 500 MHz) is specified as 2 ns, the portion of the waveform from 18 to 20 ns would be used to compute the Fourier coefficients for the waveform. If we wanted to compute the Fourier coefficients for the initial part of the waveform including the transient, we would specify

```
.TRAN 0.1N 2N
```

which would run for only one period.

All printed output statements are directed to a file named `XXXX.OUT` if the input file is named `XXXX.IN` or `XXXX.CIR`. Plotting waveforms is the greatest enhancement of PSPICE over the original SPICE. This is invoked by simply placing the `.PROBE` statement in the list. No additional parameters are required. PSPICE stores all variables at all solution timepoints and waits for the user to specify which to plot.

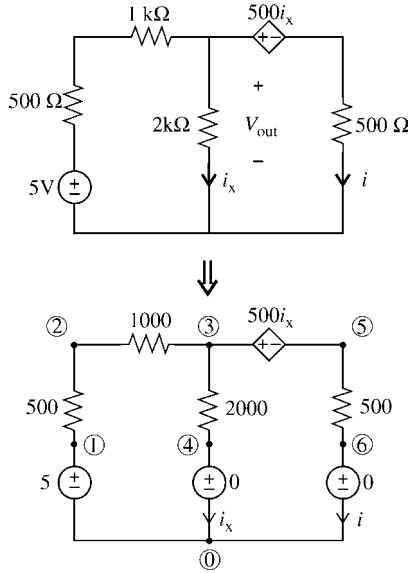


FIGURE B.7 Example B.1.

B.5 EXAMPLES

In this brief tutorial, we have shown the basic commands that one can use to solve the vast majority of electric circuit analysis problems. We have conscientiously tried to minimize the detail and purposely not shown all the possible options in order to simplify the learning. However, there are a myriad of options that can simplify many computations and the reader should consult the references.

Example B.1 Use PSpice to compute the voltage V_{out} and the current I in the circuit of Figure B.7.

Solution: The PSpice coding diagram with nodes numbered is shown in Figure B.7. Zero-volt voltage sources are inserted to sample the current i_x and I . The PSpice program is

```

EXAMPLE B.1
VS 1 0 DC 5
R1 1 2 500
R2 2 3 1K
R3 3 4 2K
VTEST1 4 0 DC 0
HSOURCE 3 5 VTEST1 500
R4 5 6 500
VTEST2 6 0 DC 0
.DC VS 5 5 1
*THE CURRENT I IS I (VTEST2) AND THE VOLTAGE VOUT IS
    
```

```
+V(3) OR V(3, 4)
.PRINT DC V(3) I(VTEST2)
.END
```

The result is $I = I(VTEST2) = 1.875E-3$ and the voltage $v_{out} = V(3) = 1.250E0$.
Example B.2 Use PSPICE to plot the frequency response of the band-pass filter shown in Figure B.8a.

Solution: The nodes are numbered on the circuit diagram, and the PSPICE program is

```
EXAMPLE B.2
VS 1 0 AC 1 0
RES 3 0 100
LIND 1 2 159U
CAP 2 3 1.6P
.AC DEC 50 1MEG 100MEG
.PROBE
*THE MAGNITUDE OF THE OUTPUT IS VM(3) AND THE PHASE
+IS VP(3)
.END
```

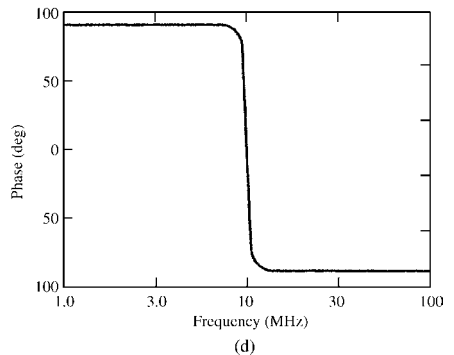
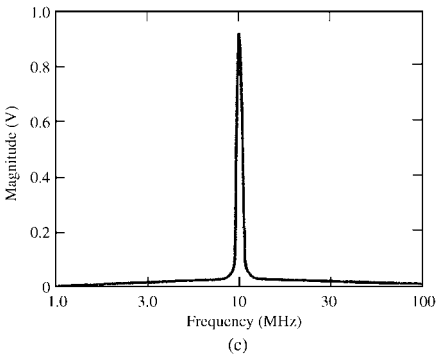
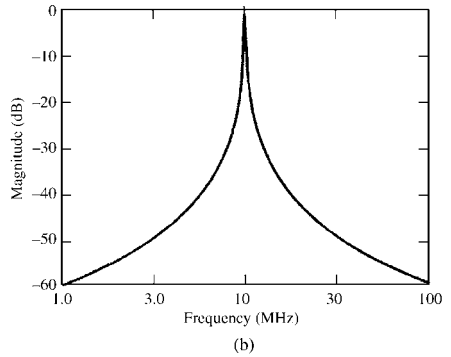
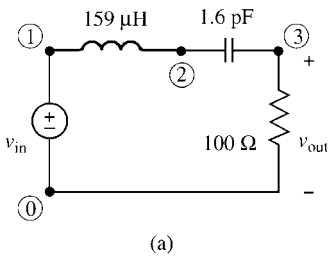


FIGURE B.8 Example B.2.

The magnitude of the voltage is plotted in Figure B.8b in decibels using $VDB(3)$, which means

$$VDB(3) = 20 \log_{10} VM(3)$$

Figure B.8c shows what we get if we request $VM(3)$: the data are highly compressed outside the band-pass region. The phase is plotted in Figure B.8d. The resonant frequency is 10 MHz. The phase is $+90^\circ$ below the resonant frequency because of the dominance of the capacitor in this range and is -90° above the resonant frequency, due to the dominance of the inductor in this range.

Example B.3 Use PSPICE to plot the inductor current for $t > 0$ in the circuit of Figure B.9a. The circuit immediately before the switch opens, that is, at $t = 0^-$, shown in Figure B.9b, from which we compute the initial voltage of the capacitor as 4 V and the initial current of the inductor as 2 mA. The PSPICE diagram with nodes numbered is shown in Figure B.9c, and the PSPICE program is

Example B.3

```
IS 0 1 DC 10M
R 1 2 2K
VTEST 2 3
L 3 0 10M IC=2M
C 1 0 100P IC=4
.TRAN .05U 50U 0 .05U UIC
*THE INDUCTOR CURRENT IS I(VTEST) OR I(L)
.PROBE
.END
```

We have chosen to solve the circuit out to 50 μs and have directed PSPICE to use a solution time step no larger than 0.05 μs as well as to use the initial conditions given for the inductor and capacitor. The result is plotted using PROBE in Figure B.9e. The result starts at 2 mA, the initial inductor current, and eventually converges to the steady-state value of 10 mA, which can be confirmed by replacing the inductor with a short circuit and the capacitor with an open circuit in the $t > 0$ circuit as shown in Figure B.9d.

B.6 THE SUBCIRCUIT MODEL

SPICE (PSPICE) has a handy way of utilizing models of devices in several places in a SPICE program without having to redescribe these models at every place of usage. This is similar to the subroutine in FORTRAN. It is called the SUBCKT model. For example, suppose we have developed an extensive model of, say, an Op Amp or an MTL. The model might have, for example, four external nodes that we have named 101, 102, 201, and 202, as illustrated in Figure B.10. The nodes internal to the model are unique to this model and bear no resemblance to the nodes of the SPICE program into which this model is to be imbedded (perhaps at several locations). However, the

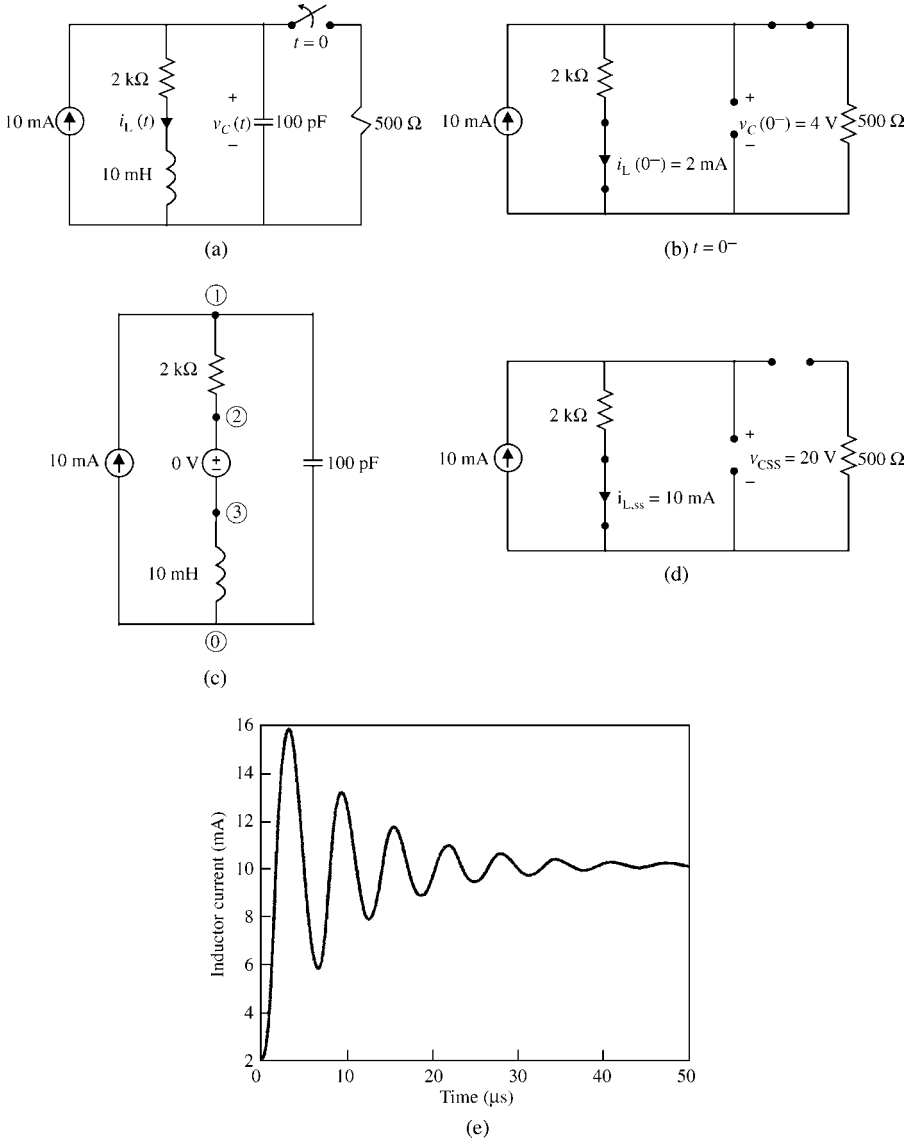


FIGURE B.9 Example B.3.

zero (0) or universal ground node is the only node that is common with the main program. The subcircuit model description is

```
.SUBCKT MTL 101 102 201 202
. . . .
. . . .
.ENDS MTL
```

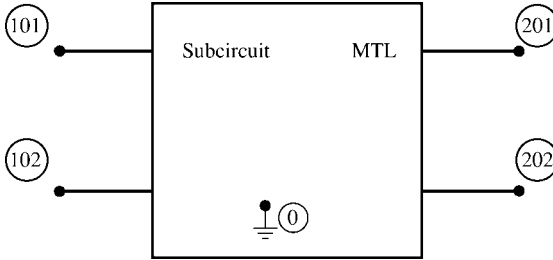


FIGURE B.10 Definition of terminal nodes for a subcircuit model.

where MTL is the name of the subcircuit, and its external nodes are denoted as 101, 102, 201, and 202. The subcircuit model ends with `.ENDS` and the name of the subcircuit model, MTL. These node numbers are unique to the subcircuit, *but their ordering is important*. The call statement in the SPICE program is formatted as

```
XMTL S NE L FE MTL
```

Hence, the nodes of the subcircuit are attached to the external nodes of the main SPICE model as $S = 101$, $NE = 102$, $L = 201$, and $FE = 202$. The subcircuit must end with the statement

```
.ENDS MTL
```

REFERENCES

- [1] CR. Paul, *Fundamentals of Electric Circuit Analysis*, John Wiley & Sons, Inc., New York, 2001.
- [2] PW. Tuinenga, *SPICE: A Guide to Simulation and Analysis Using PSPICE*, 3rd edition, Prentice-Hall, Englewood Cliffs, NJ, 1995.
- [3] A. Vladimirescu, *The SPICE Book*, John Wiley & Sons, Inc., New York, 1994.
- [4] R. Conant, *Engineering Circuit Analysis with PSpice and Probe*, McGraw-Hill, New York, 1993.
- [5] JW. Nilsson and SA. Riedel, *Introduction to PSpice Manual for Electric Circuits Using OrCad Release 9.1*, 4th edition, Prentice-Hall, Englewood Cliffs, NJ, 2000.

INDEX

Index Terms

Links

| | | | |
|-------------------------------|-----|-----|-----|
| MTL equations | | | |
| for lossy MTLs | 494 | | |
| .AC | 762 | | |
| .DC | 761 | | |
| .FOUR | 763 | | |
| .PRINT | 762 | 763 | |
| .SUBCKT | | | |
| SPICE subcircuit model | 767 | | |
| .TRAN | 762 | | |
| Ampere's law | 9 | 113 | 132 |
| | 136 | | |
| A | | | |
| antenna currents | 45 | 638 | |
| asymptotic waveform expansion | | | |
| (AWE) | 513 | | |
| attenuation constant | 17 | 259 | |
| average power flow | | | |
| on a MTL | 332 | | |
| average power flow | | | |
| on a two-conductor line | 258 | | |

Index Terms

Links

B

| | | | |
|--------------------------------|-----|-----|-----|
| backward Euler method | 489 | | |
| balanced wire lines | 311 | | |
| bandwidth | | | |
| of digital waveforms | 54 | | |
| basis functions | | | |
| in MoM techniques | 191 | | |
| BLT equations | | | |
| for transmission-line networks | 709 | | |
| bound charge | 130 | 181 | |
| BRANIN.FOR | 472 | 746 | 524 |
| BRANIN.OUT | 746 | | |
| broadside illumination | 602 | | |

C

| | | | |
|--------------------------------|-----|-----|--|
| cable harnesses | 304 | 729 | |
| capacitance | | | |
| per unit length | 22 | 77 | |
| capacitance matrix | | | |
| per unit length | 98 | 164 | |
| causal time function | 83 | | |
| Cayley-Hamilton theorem | | | |
| for multiplying matrices | 275 | | |
| central difference | 225 | | |
| chain parameter matrix | | | |
| for lossy, two-conductor lines | 451 | | |

Index Terms

Links

| | | |
|---------------------------------------|-----|-----|
| chain parameter matrix | | |
| MTLs, incident field excitation | 648 | |
| chain parameter matrix | 511 | |
| chain parameters | | |
| of MTL with incident field excitation | 697 | |
| chain parameters | | |
| two-conductor lines | 271 | |
| chain-parameter matrix | | |
| of a MTL | 315 | |
| chain-parameter matrix | | |
| solutions for a MTL | 318 | |
| chain-parameter matrix | | |
| two-conductor lines, incident field | | |
| excitation | 585 | |
| chain-parameter matrix identities | | |
| of a MTL | 316 | |
| chain-parameter matrix identities | 322 | 323 |
| chain-parameter matrix properties | | |
| of a MTL | 319 | |
| characteristic equation | 287 | |
| characteristic impedance | 244 | |
| characteristic impedance | | |
| for lossless, three-conductor line | 549 | |
| coaxial transmission line | 43 | |
| coefficients of potential | 165 | |
| common impedance coupling | | |
| time domain | 564 | |

Index Terms

Links

| | | | |
|--------------------------------------|-----|-----|-----|
| common-impedance coupling | | | |
| frequency domain (phasor form) | 553 | | |
| common-mode currents | 45 | | |
| complex frequency hopping (CFH) | 458 | 515 | |
| complex permittivity | 131 | 132 | 148 |
| | 167 | 409 | |
| conductance | | | |
| per unit length | 22 | 76 | |
| conductance matrix | | | |
| per unit length | 98 | 103 | 165 |
| conduction current | 75 | 96 | 136 |
| conductivity | | | |
| effective | 131 | | |
| conductivity | | | |
| of the medium | 130 | | |
| conductor impedance | | | |
| representing frequency-dependent | | | |
| losses | 494 | | |
| conservation of charge | 75 | 96 | |
| convolution integral | 48 | 80 | |
| convolution with frequency-dependent | | | |
| losses | 416 | | |
| coupled microstrip lines | 211 | | |
| coupled striplines | 219 | | |
| coupling coefficient | | | |
| for lossless, three-conductor line | 549 | | |
| coupling coefficient | 758 | | |

Index Terms

Links

| | | |
|---|-----|-----|
| Courant stability condition | 385 | |
| current scattering matrix | 713 | |
| cyclic-symmetric structures | 299 | |
| D | | |
| Debye model | | |
| for representing losses in the medium | 410 | |
| decoupling the MTL equations | | |
| frequency domain (phasor form) | 286 | |
| decoupling the MTL equations | | |
| lossless lines in homogeneous media | 476 | |
| decoupling the MTL equations | | |
| lossless lines in inhomogeneous media | 477 | |
| decoupling the MTL equations | | |
| lossy conductors in homogeneous media | 294 | |
| decoupling the MTL equations | | |
| perfect conductors in homogeneous media | 293 | |
| decoupling the MTL equations | | |
| perfect conductors in inhomogeneous media | 297 | |
| decoupling the MTL equations | 474 | 664 |
| del operator | 9 | |
| DIAG.SUB | 480 | 747 |
| difference operator | 359 | 722 |

Index Terms

Links

| | | | |
|---|-----|-----|----|
| differential-mode currents | 45 | 638 | |
| diffusion equation | 136 | 137 | |
| displacement current | 22 | 75 | 96 |
| | 136 | | |
| dominant poles | 510 | 516 | |
| duty cycle | | | |
| of digital waveforms | 53 | | |
| dynamic line terminations | 488 | | |
| E | | | |
| E0.IN | 752 | | |
| effective relative permittivity | | | |
| microstrip | 146 | | |
| effective relative permittivity | | | |
| PCB | 147 | | |
| effects of incident fields | 731 | | |
| effects of line discontinuities | 400 | | |
| EIGCC.SUB | 745 | | |
| Eigenvalues | 287 | 292 | |
| eigenvectors | 287 | 292 | |
| endfire illumination | 599 | | |
| equivalent circuit of transmission line | | | |
| per unit length | 77 | 99 | |
| Euler's identity | 81 | | |
| even-odd mode solution | 543 | | |
| even-odd mode transformation | 306 | | |

Index Terms

Links

F

| | | | |
|---|-----|-----|-----|
| far end | 543 | | |
| Faraday's law | 9 | 71 | 137 |
| | 576 | 639 | |
| FDTDINC.FOR | 632 | 633 | 635 |
| | 683 | 752 | |
| FDTDINC.IN | 752 | | |
| FDTDINC.OUT | 752 | | |
| FDTDLOSS.FOR | 438 | 442 | 527 |
| | 532 | 746 | |
| FDTDLOSS.OUT | 746 | | |
| FINDIF.FOR | 526 | 531 | 746 |
| FINDIF.OUT | 746 | | |
| finite difference approximations | 380 | | |
| finite difference techniques | 223 | | |
| finite element (FEM) techniques | 229 | | |
| finite-difference, time-domain (FDTD) transformation | | | |
| for a two-conductor line | 380 | | |
| finite-difference, time-domain (FDTD) transformation | | | |
| for lossy MTLs | 496 | | |
| finite-difference, time-domain (FDTD) transformation | | | |
| for MTLs | 486 | | |
| finite-difference, time-domain (FDTD) transformation | | | |

Index Terms

Links

| | | |
|--|-----|-----|
| finite-difference (<i>Cont.</i>) | | |
| frequency-dependent losses | 428 | |
| finite-difference, time-domain (FDTD) | | |
| transformation | | |
| frequency-independent losses | 424 | |
| finite-difference, time-domain (FDTD) | | |
| transformation | | |
| incident field excitation | 625 | |
| finite-difference, time-domain (FDTD) | | |
| transformation | | |
| recursion relations | | |
| for a two-conductor line | 383 | |
| finite-difference, time-domain (FDTD) | | |
| transformation | 679 | |
| Fourier series | | |
| of digital waveforms | 53 | |
| Fourier series | 50 | |
| Fourier series representation | | |
| of charge distribution around a wire | 176 | |
| Fourier transform | 50 | 81 |
| FR4 | | |
| in PCBs | 132 | 262 |
| free charge | 182 | |
| free field format | 734 | |
| FREQ.IN | 744 | 748 |
| frequency domain | 47 | |
| frequency-dependent losses in the medium | | |
| representing in the time domain | 409 | |

Index Terms

Links

| | |
|---|-----|
| frequency-dependent losses of the conductors representing in the frequency domain | 416 |
| frequency-dependent losses of the conductors representing in the time domain | 411 |

G

| | | | |
|---|-----|-----|-----|
| Gauss' law | 11 | 228 | 114 |
| | 116 | | |
| GAUSSJ.SUB | 740 | | |
| generalized capacitance matrix for three-wire ribbon cable | 187 | | |
| generalized capacitance matrix | 167 | | |
| generalized method of characteristics for lossy MTLs | 498 | | |
| generalized method of characteristics | 451 | | |
| generalized Norton equivalent of terminations of a MTL | 309 | | |
| generalized Thevenin equivalent of the terminations of a MTL | 307 | | |
| generator circuit | 543 | | |
| graph of a transmission-line network | 690 | | |
| graphical time-domain solution for a two-conductor line | 347 | | |

H

| | | | |
|--------------------|-----|--|--|
| Hermitian matrix | 292 | | |
| higher-order modes | 38 | | |

Index Terms

Links

| | | | |
|-----------------------------------|-----|-----|-----|
| Hilbert transform | 83 | | |
| homogeneous medium | 35 | | |
| hyperdominant matrix | 108 | 109 | |
| I | | | |
| impulse response | 48 | | |
| incident field | 639 | | |
| incident field excitation | | | |
| frequency-domain (phasor form) | | | |
| solution | 594 | | |
| incident field excitation | | | |
| SPICE equivalent circuit | | | |
| incident field excitation | | | |
| time-domain solution | 614 | | |
| incident waves | 710 | | |
| INCIDENT.FOR | 625 | 633 | 678 |
| | 679 | 685 | 748 |
| INCIDENT.OUT | 748 | | |
| incremental inductance rule | 149 | | |
| inductance | | | |
| internal | 101 | | |
| inductance | | | |
| per unit length | 23 | 75 | |
| inductance matrix | | | |
| per unit length | 93 | 94 | 103 |
| | 161 | | |
| inductive and capacitive coupling | | | |
| frequency domain (phasor form) | 551 | 543 | |

Index Terms

Links

inductive and capacitive coupling

time domain 561

input impedance

to a two-conductor line 247

input impedance matrix

for a MTL 330

internal impedance

PCB land 151

internal inductance 79

intrinsic impedance 14

J

JACOBI.SUB 477 480 747

junction scattering matrix 712

K

Kronig-Kramers relations 85 131 411

L

lands 8

Laplace transform solution

for a two-conductor line 369

least squares, method of 433 520

Laplace's equation 11 110 198

224

LEQTIC.SUB 745

literal solution for lossless,

three-conductor line

Index Terms

Links

| | | | |
|--------------------------------------|-----|-----|-----|
| literal solution (<i>Cont.</i>) | | | |
| frequency domain (phasor form) | 541 | 548 | |
| literal solution for lossless, | | | |
| three-conductor line | | | |
| time domain | 555 | | |
| literal solution for lossless, three | | | |
| -conductor line | | | |
| time domain, weakly coupled lines | 559 | | |
| loss tangent | 131 | 261 | 410 |
| losses | | | |
| frequency dependent | 79 | 101 | |
| lossy line | 36 | | |
| lumped-circuit approximate models | | | |
| for a two-conductor line | 374 | | |
| lumped-circuit approximate models | | | |
| validity of | 376 | | |
| lumped-circuit approximations | | | |
| MTLs, incident field excitation | 657 | 678 | |
| lumped-circuit approximations | | | |
| of a lossy, two-conductor line | 448 | | |
| lumped-circuit approximations | | | |
| of MTLs | 485 | | |
| lumped-circuit approximations | 496 | | |
| lumped-circuit models | | | |
| two-conductor lines | 266 | | |
| lumped-circuit representations | | | |
| of a MTL | 313 | | |

Index Terms

Links

| M | | | |
|-----------------------------------|-----|-----|-----|
| macromodels | 451 | | |
| magic time step | 386 | | |
| match points | 184 | | |
| matched line | | | |
| for a MTL | 331 | | |
| matched line | 247 | | |
| matrix exponential | 316 | 320 | 511 |
| matrix hyperbolic cosine | 320 | | |
| matrix hyperbolic sine | 321 | | |
| matrix pencil method | 435 | | |
| Maxwell's equations | 9 | | |
| method of characteristics | | | |
| for a two-conductor line | 362 | | |
| Method of images | 118 | | |
| method of images for dielectric | | | |
| boundaries | 201 | | |
| method of moments (MoM) | 190 | 607 | |
| method of symmetrical components, | 304 | | |
| microstrip line | 8 | | |
| mixed representation | | | |
| of terminations of a MTL | 311 | | |
| mode transformations | | | |
| incorporating with the | | | |
| SPICE program | 480 | | |
| mode voltages and currents | 474 | | |
| model order reduction (MOR) | 510 | | |

Index Terms

Links

| | | | |
|--|-----|-----|-----|
| modes | 8 | | |
| moments | 456 | 512 | 514 |
| | 515 | | |
| MSTRP.FOR | 211 | 214 | 216 |
| | 734 | 735 | 742 |
| MSTRP.IN | 734 | 742 | |
| MTL equations | | | |
| frequency-domain (phasor form) | 102 | 284 | 285 |
| MTL equations | | | |
| frequency-domain solution | 289 | | |
| MTL equations | | | |
| incident field excitation, phasor form | 647 | | |
| MTL equations | | | |
| time-domain form | 100 | 101 | 102 |
| MTL equations | 93 | | |
| MTL.FOR | 441 | 496 | 527 |
| | 532 | 744 | |
| MTL.OUT | 744 | | |
| MTLFREQ.DAT | 745 | | |
| multipliers | 758 | | |
| N | | | |
| near end | 543 | | |
| node voltages | 755 | | |
| nonuniform lines | 33 | | |
| nonuniform MTLs | | | |
| approximating with chain | | | |
| parameters | 323 | | |
| normal matrix | 293 | | |

Index Terms

Links

Norton equivalent

MTLs, incident field excitation 654

O

orthogonal transformation

three-conductor lines 477

orthogonal transformation 293 476

orthonormal 302

P

Pade approximation 510 516

Pade methods

for two-conductor lines 455

parallel matching for signal integrity 395

parallel-plate transmission line 38

partial element equivalent

circuit (PEEC) 149

partial inductance 149

passivity 513

PCB, FOR 209 214 336

566 734 735

741 743

PCB.IN 734

permeability of free space 8

permittivity of free space 8

per-unit-length capacitance

coaxial cable 129

Index Terms

Links

| | | |
|-------------------------------|-----|-----|
| per-unit-length capacitance | | |
| microstrip | 147 | |
| per-unit-length capacitance | | |
| one wire above a ground | | |
| plane | 126 | 127 |
| per-unit-length capacitance | | |
| PCB | 148 | |
| per-unit-length capacitance | | |
| stripline | 146 | |
| per-unit-length capacitance | | |
| two-wire line | 121 | 124 |
| per-unit-length conductance | | |
| coaxial cable | 129 | |
| per-unit-length conductance | | |
| one wire above a ground plane | 128 | |
| per-unit-length conductance | | |
| two-wire line | 126 | |
| per-unit-length inductance | | |
| coaxial cable | 129 | |
| per-unit-length inductance | | |
| microstrip | 146 | |
| per-unit-length inductance | | |
| one wire above a ground plane | 127 | |
| per-unit-length inductance | | |
| PCB | 147 | |
| per-unit-length inductance | | |
| stripline | 145 | |
| per-unit-length inductance | | |

Index Terms

Links

| | | | |
|---|-----|-----|-----|
| per-unit (<i>Cont.</i>) | | | |
| two-wire line | 121 | 126 | 127 |
| per-unit-length internal inductance | | | |
| wires | 142 | | |
| per-unit-length parameter matrices | | | |
| properties of | 103 | 104 | |
| per-unit-length resistance | | | |
| wires | 142 | | |
| phase constant | 15 | | |
| phase constant | 259 | | |
| phase velocity | 16 | | |
| phase velocity | 244 | | |
| phase velocity | 259 | | |
| phasor | 15 | | |
| point matching | | | |
| in MoM techniques | 194 | | |
| Poisson's equation | 190 | | |
| polarization loss | 131 | | |
| positive definite matrix | 107 | | |
| potential functions | 10 | | |
| potential of constant charge distribution | | | |
| on a flat strip | 197 | | |
| power transmission lines | 732 | | |
| printed circuit board (PCB) | | | |
| computed results, frequency | | | |
| domain | 336 | | |
| printed circuit board (PCB) | | | |
| computed results, time domain | 529 | | |

Index Terms

Links

| | | | |
|---------------------------------------|-----|-----|-----|
| printed circuit board (PCB) | 2 | 8 | 732 |
| computed results, frequency domain | 336 | | |
| printed circuit board (PCB) | | | |
| computed results, time domain | 529 | | |
| printed circuit board (PCB) | 2 | 8 | 732 |
| Prony's method | 432 | | |
| propagation constant | 17 | | |
| proximity effect | | | |
| closely-spaced wires | 125 | 176 | |
| PUL.DAT | 734 | 735 | 737 |
| | 741 | 742 | 744 |
| | 746 | 747 | 748 |
| | 751 | 752 | |
| PULSE | | | |
| pulse source specification | 760 | | |
| pulse expansion method | | | |
| in MoM techniques | 191 | | |
| PWL | | | |
| piecewise-linear source specification | 759 | | |
| Q | | | |
| quadratic form | 107 | 231 | |
| quasi-TEM mode | 5 | 37 | |
| R | | | |
| radiated emissions | 46 | | |
| receptor circuit | 543 | | |

Index Terms

Links

| | | | |
|---|-----|-----|-----|
| recursive convolution | 437 | 517 | |
| recursive solution for MTLs | 469 | | |
| reference conductor | 5 | | |
| reflected waves | 710 | | |
| reflection coefficient | 246 | 260 | |
| reflection coefficient matrix for a MTL | 329 | | |
| reflection coefficients for a two-conductor line | 347 | | |
| resistance matrix per unit length | 94 | 95 | |
| ribbon cable incident field excitation | 683 | | |
| ribbon cables computed results | 187 | | |
| ribbon cables computed results, frequency domain | 333 | | |
| ribbon cables computed results, time domain | 523 | | |
| ribbon cables | 729 | | |
| RIBBON.FOR | 176 | 187 | 333 |
| | 523 | 565 | 734 |
| | 735 | 737 | 740 |
| RIBBON.IN | 734 | 737 | |

S

| | | | |
|-------------------|-----|-----|--|
| scattered field | 577 | 639 | |
| scattered voltage | 640 | | |

Index Terms

Links

| | | | |
|--------------------------------------|-----|-----|-----|
| scattering parameters | 692 | 709 | |
| series matching for signal integrity | 394 | | |
| series solution for MTLs | 473 | | |
| series time-domain solution | | | |
| for a two-conductor line | 358 | | |
| shielded wires | 730 | | |
| shielded wires with pigtailed | | | |
| approximating with chain parameters | 275 | | |
| sidefire illumination | 601 | | |
| signal integrity | 393 | | |
| similarity transformations | 286 | 292 | |
| SIN | | | |
| sinusoidal source specification | 760 | | |
| singular-value-decomposition (SVD) | | | |
| method | 435 | 521 | |
| skin depth | 101 | 411 | |
| skin effect | 59 | 79 | 449 |
| spectrum | | | |
| of digital waveforms | 53 | | |
| SPICE equivalent circuit | | | |
| MTLs, incident field excitation | 671 | | |
| SPICE transmission-line model | 759 | | |
| SPICE(PSPICE) | | | |
| transmission-line model | 251 | | |
| SPICE(PSPICE) equivalent circuit | | | |
| for a two-conductor, lossless line | 366 | | |
| SPICEINC.FOR | 625 | 678 | 683 |
| | 691 | 694 | 723 |

Index Terms

Links

| | | | |
|---|-----|-----|-----|
| | 734 | 751 | |
| SPICEINC.IN | 751 | | |
| SPICEINC.OUT | 751 | | |
| SPICELC.FOR | 564 | 734 | 748 |
| SPICELC.OUT | 748 | | |
| SPICELPI.FOR | 450 | 496 | 524 |
| | 530 | 564 | 696 |
| | 734 | 747 | 748 |
| SPICELPI.OUT | 748 | | |
| SPICEMTL.FOR | 485 | 523 | 524 |
| | 530 | 564 | 691 |
| | 694 | 695 | 723 |
| | 734 | 747 | |
| SPICEMTL.IN | 734 | | |
| SPICEMTL.OUT | 747 | | |
| square root of a matrix | 319 | | |
| state variable characterization of terminal networks | 488 | | |
| state-transition matrix | 584 | | |
| state-variable equations analogy of the phasor MTL equations to | 315 | | |
| state-variable equations | 511 | 583 | 648 |
| static fields | 10 | | |
| stripline | 8 | | |
| STRPLINE.FOR | 219 | 222 | 734 |
| | 735 | 744 | |
| STRPLINE.IN | 734 | 744 | |

Index Terms

Links

| | | | |
|--|-----|-----|-----|
| surface impedance | 138 | 139 | |
| symmetric line | 542 | | |
| T | | | |
| TE mode | 40 | | |
| TEM mode of propagation | 8 | | |
| Thevenin equivalent | | | |
| MTLs, incident field excitation | 652 | | |
| Thevenin equivalent | | | |
| of terminations | 249 | | |
| Thevenin equivalent | | | |
| two-conductor lines, incident field | | | |
| excitation | 592 | | |
| time constants | | | |
| for lossless, three-conductor line | 550 | | |
| time domain | 47 | | |
| time-domain to frequency-domain (TDFD) | | | |
| transformation | | | |
| for MTLs | 486 | | |
| time-domain to frequency-domain (TDFD) | | | |
| transformation | | | |
| incident field excitation | 625 | | |
| time-domain to frequency-domain (TDFD) | | | |
| transformation | | | |
| MTLs, incident field excitation | 678 | | |
| time-domain to frequency-domain (TDFD) | | | |
| transformation | 56 | 376 | 422 |
| | 496 | | |

Index Terms

Links

| | | | |
|-------------------------------------|-----|-----|-----|
| TIMEFREQ.FOR | 56 | 58 | 59 |
| | 379 | 441 | 496 |
| | 524 | 529 | 531 |
| | 532 | 534 | 625 |
| | 633 | 635 | 683 |
| | 706 | 745 | |
| TIMEFREQ.IN | 745 | | |
| TIMEFREQ.OUT | 745 | | |
| TM mode | 41 | | |
| Toeplitz matrices | 504 | | |
| transfer function | 49 | | |
| transmission-line equations | | | |
| for a two-conductor line | 345 | | |
| transmission-line equations | | | |
| MTLs, incident field excitation | 644 | 645 | |
| transmission-line equations | | | |
| phasor form | 80 | | |
| transmission-line equations | | | |
| phasor form | 242 | 259 | |
| transmission-line equations | | | |
| two-conductor lines | 23 | | |
| transmission-line equations | | | |
| two-conductor lines, incident field | | | |
| excitation | 581 | | |
| transmission-line equations | | | |
| two-conductor lines, incident field | | | |
| excitation | 583 | | |
| transmission-line networks | | | |

Index Terms

Links

| | | |
|------------------------------------|-----|-----|
| transmission (<i>Cont.</i>) | | |
| representation with a SPICE model | 693 | |
| transmission-line networks | | |
| representation with admittance | | |
| parameters | 696 | |
| transmission-line networks | | |
| representation with lumped-circuit | | |
| models | 696 | |
| transmission-line networks | 690 | |
| transverse electromagnetic (TEM) | 4 | |
| traveling waves | 245 | 346 |
| tube propagation matrix | 711 | |
| tubes | | |
| of a transmission-line network | 690 | |
| twisted pair lines | | |
| approximating with chain | | |
| parameters | 275 | |
| twisted pairs of wires | 730 | |
| U | | |
| uniform lines | 7 | |
| uniform plane wave excitation | | |
| frequency domain (phasor | | |
| form) | 595 | 657 |
| uniform plane wave excitation | | |
| time-domain | 617 | |
| unit vectors | 9 | |

Index Terms

Links

V

| | |
|---------------------------------------|-----|
| vector fitting (VF) | 517 |
| velocity of propagation of free space | 8 |
| voltage reflection coefficients | 719 |
| voltage standing wave ratio (VSWR) | 257 |
| voltage transmission coefficients | 719 |
| VSVL.IN | 746 |

W

| | | | |
|--|-----|-----|-----|
| wavelength | 16 | | |
| waves | | | |
| backward-traveling | 14 | | |
| waves | | | |
| forward-traveling | 14 | | |
| weakly-coupled line | 542 | | |
| when is matching required for signal integrity? | 399 | | |
| wide separation approximations | | | |
| for wires | 735 | | |
| WIDSESEP.FOR | | | |
| for three-wire ribbon cable | 188 | | |
| WIDSESEP.FOR | 172 | 695 | 734 |
| | 735 | | |
| WIDSESEP.IN | 734 | 735 | 736 |
| | 737 | | |

Index Terms

Links

| | | | |
|--------------------------------|-----|-----|-----|
| wide-separation approximations | | | |
| for wires | 171 | | |
| wide-separation approximations | | | |
| for inductance matrix | | | |
| n wires above a ground plane | 173 | | |
| wide-separation approximations | | | |
| for inductance matrix | | | |
| n wires within a shield | 175 | 176 | |
| wide-separation approximations | | | |
| for inductance matrix | | | |
| n+1 wires | 173 | | |
| wires | | | |
| fundamental subproblems for | 113 | 115 | 118 |
| wires | 5 | | |
| Y | | | |
| Y parameters | | | |
| two-conductor lines | 277 | | |
| Y-parameter matrix | | | |
| for a MTL | 324 | | |
| Z | | | |
| Z parameters | | | |
| two-conductor | | | |
| lines | 276 | | |
| Z-parameter matrix | | | |
| for a MTL | 324 | | |